IAEA-TECDOC-1889
COMPANION CD-ROM

EDITORIAL NOTE

This publication has been prepared from the original material as submitted by the contributors and has not been edited by the editorial staff of the IAEA. The views expressed remain the responsibility of the contributors and do not necessarily represent the views of the IAEA or its Member States.

Neither the IAEA nor its Member States assume any responsibility for consequences which may arise from the use of this publication. This publication does not address questions of responsibility, legal or otherwise, for acts or omissions on the part of any person.

The use of particular designations of countries or territories does not imply any judgement by the publisher, the IAEA, as to the legal status of such countries or territories, of their authorities and institutions or of the delimitation of their boundaries.

The mention of names of specific companies or products (whether or not indicated as registered) does not imply any intention to infringe proprietary rights, nor should it be construed as an endorsement or recommendation on the part of the IAEA.

The IAEA has no responsibility for the persistence or accuracy of URLs for external or third party Internet web sites referred to in this publication and does not guarantee that any content on such web sites is, or will remain, accurate or appropriate.

For further information on this publication, please contact:

Nuclear Fuel Cycle and Materials Section
International Atomic Energy Agency
Vienna International Centre
PO Box 100
1400 Vienna, Austria
Email: Official.Mail@iaea.org

Enquiries should be addressed to the IAEA Publishing Section at:

Marketing and Sales Unit, Publishing Section
International Atomic Energy Agency
Vienna International Centre
PO Box 100
1400 Vienna, Austria
fax: +43 1 26007 22529
tel.: +43 1 2600 22417
email: sales.publications@iaea.org
www.iaea.org/publications

FUEL MODELLING IN ACCIDENT CONDITIONS (FUMAC)
IAEA, VIENNA, 2019
IAEA-TECDOC-1889 (COMPANION CD-ROM)
ISBN 978–92–0–163919–6
ISSN 1011–4289

Produced by the IAEA in Austria
December 2019

FUEL MODELLING IN ACCIDENT CONDITIONS (FUMAC)

Final Report of a Coordinated Research Project (CRP) (2014–2018)

ANNEX II:

COUNTRY REPORTS FROM PARTICIPANTS

INTERNATIONAL ATOMIC ENERGY AGENCY
VIENNA, 2019

CONTENTS

ACCIDENT CONDITION MODELS IN THE DIONISIO 2.0 CODE

A. SOBA, M. LEMES, E. GOLDBERG, M. LOZA, M. CAZADO, M.E. GONZALEZ, A. DENIS
Sección Códigos y Modelos, Gerencia Ciclo del Combustible Nuclear,
Comisión Nacional de Energía Atómica,
Avenida General Paz 1499, 1650 San Martín, Provincia de Buenos Aires, Argentina.
E-mail: (soba@cnea.gov.ar) (corresponding author)

Abstract

This document summarizes the work carried out with the DIONISIO code in the frame of the FUMAC Research Project.

The more challenging task implied in the proposal of expanding the application range of fuel simulation codes to accident conditions is the depiction of the fuel rod environment. It can exhibit a wide variety of thermal-hydraulic conditions substantially different to those existing under normal operation, thus affecting heat removal from the rod. But a detailed description of the different regimes the coolant may exhibit is an enormous work that constitutes the specific purpose of the thermal-hydraulic codes. Several famous and reliable codes exist that perform this task. Nevertheless, and without attempting to solve the complete problem in its many details, a subroutine was developed for the DIONISIO code that performs a simplified analysis of the coolant in a PWR, restricted to the more representative situations. Keeping the focus on the simulation of fuel behavior, the thermal-hydraulic modulus is intended to provide to the code the boundary conditions necessary to reproduce accident situations. Empirical expressions have also been incorporated to the subroutine dedicated to accidents, that predict ballooning and burst phenomena. Experiments of the FUMAC database, in addition to several of the FUMEX II and III data sets, have been simulated with DIONISIO using the LOCA subroutines.

Moreover, due to the fast cladding oxidation and the associated dissociation of water molecules that can take place under accident conditions, the hydrogen content in the cladding material can exhibit a considerable increase. This can trigger severe material damage during a sudden rod cooling. Due to its importance regarding materials safety criteria, a modulus dedicated to hydrogen uptake simulation was developed and is presently under intensive examination.

1. INTRODUCTION

The DIONISIO code describes most of the phenomena occurring in a PWR/PHWR fuel rod in normal operation conditions. To take into consideration the axial variation of reactor linear power and coolant temperature, the rod is divided into a user defined number of segments. In every time step and for each axial section, a complete description of the local system variables is obtained by solving the tightly-coupled, non-linear differential equations accounting for the thermal and mechanical behavior. Then, the temperature and stress-strain distributions in the complete rod are obtained as step-like functions of the axial coordinate. With respect to the gas inventory, the code evaluates the amount of gas released by each rod segment and then that released by the whole rod. The composition of the gas mixture in the gap and its thermal conductivity are recalculated in every time step. The internal rod pressure is evaluated with the ideal gas law using the total number of gas atoms in the free volume within the rod and the average temperature in the total void volume in the rod (gap and dishings in all the segments, and plenum). The elongation of every individual pellet and the corresponding cladding are added up to obtain the total elongation of the pellet stack and the rod. DIONISIO 2.0 is nowadays a code able to simulate a fuel rod in extended burnup conditions. Particularly, in the high burnup range the inventory of the more relevant isotopes and the microstructure at the pellet periphery are described.

The code results have been compared with some 34 experiments published in the IAEA data base, covering more than 380 fuel rods irradiated up to average burnup levels of 40-60 MWd/kgU. The results of these comparisons are quite satisfactory and reveal the good quality of the simulations. They were performed within the frame of the IAEA Research Project FUMEX III. The diverse models have been explained in detail in a number of papers [1]–[5].

In the frame of the Research Project FUMAC the application range of the code was expanded to conditions typical of Loss of Coolant Accidents (LOCA). To this end, a new module able to reproduce the thermal-hydraulic conditions in the coolant was developed. This module is intended to give account of the numerous parameters that govern the heat exchange between the fuel rod and the coolant in accident situations, thus providing the boundary conditions necessary to simulate the fuel rod behavior during a fast excursion, particularly in such a determinant aspect as the thermal behavior.

The code simulates a vertical channel, typical of a PWR or BWR fuel element, containing one fuel rod. Scenarios like forced single-phase (water or vapor) convection or double-phase flow, including departure from nucleate boiling (DNB) are taken into consideration. The model adopted analyzes and quantifies the coolant behavior in terms of the system pressure and coolant velocity. Moreover, models to describe mechanical problems occurring in accidental situations, like ballooning and burst, are also included.

A separate testing plan was first followed, which consisted in comparing the predictions of the new thermal-hydraulic module with specific codes in different flow regimes. Then it was included as a subroutine of the DIONISIO code and its results were compared with available experimental data. It is seen that the predictive ability of the general code has improved with the introduction of the heat transfer coefficients corresponding to the different patterns that can be encountered in the coolant flow.

In accident conditions, due to the fast cladding oxidation and the associated dissociation of water molecules, a considerable increase of the hydrogen content in the cladding material takes place. This can give origin to severe material damage during a sudden rod cooling. The model considered in the present work [6] assumes two different mechanisms of hydrogen capture. One of them is the chemical reaction with the H2 present in the coolant; the other one assumes fast diffusion of H+ through the oxide layer, where it discharges at the oxide-metal interface, by capture of one e- proceeding from the oxidation reaction [7].

2. MODELS AND PARAMETERS INVOLVED

2.1. Mechanical aspects

The simulation of off-normal operation conditions imposes the need of incorporating diverse mechanical models to the code, specific for these conditions. At the present time, a model to predict clad failure (burst stress) and its localization, and another of cladding creep to evaluate clad ballooning have been recently included in the code. These subroutines are turned on if accidental conditions are met.

Cladding failure is assumed to occur when the hoop stress exceeds the burst stress, σ_B. The empirical correlation [8, 9].

$$\sigma_B = C_1\, exp(-C_2 T)\, exp(-(C_0 W_{fO})^2) \quad (1)$$

was adopted as cladding burst criterion, where C_0, C_1 and C_2 are constants whose values for Zircaloy (Zry) in the single-phase domains α and β are listed in Table 1. T is the absolute temperature and W_{fO} is the total weight fraction of oxygen picked up in high temperature metal-water reactions.

For the effective cladding creep rate the correlation [9].

$$\frac{d\varepsilon}{dt} = C_3\, exp\left(-\frac{C_4}{T}\right) exp(-C_5 W_{fO})\sigma_{VM}^n \quad (2)$$

was adopted. It is valid when the cladding material is in the pure α or β phase; W_{fO} is the excess oxygen weight fraction in the cladding metal layer and σ_{VM} is the von Mises stress. The constants C_3, C_4, C_5 and n adopt the values listed in Table 1when the Zry cladding material is in the single phase domains (α or β). For the two-phase (α+β) region, the creep rate is calculated as an average of both single-phase rates weighed with the volume fractions of both phases.

TABLE 1. VALUES OF THE CONSTANTS USED IN CORRELATIONS (1) AND (2), IN PURE A OR B PHASES

Constants	Pure α-Zr	Pure β-Zr
C_0	1052.63	1052.63
C_1 (N cm^{-2})	8.3×10^4	2.3×10^5
C_2 (K^{-1})	0.001	0.003
C_3 (s^{-1} N^{-n} cm^{2n})	1.4523×10^{-8}	2.1751×10^{-7}
C_4 (K)	38487.0	17079.0
C_5	342.0	0.0
n	5.89	3.78

2.2. Thermal-hydraulic conditions

The temperature distribution in each axial segment of the fuel-cladding system is solved in DIONISIO by means of the heat exchange equation in cylindrical symmetry. The boundary conditions are provided by the coolant exchange regime.

2.2.1. Flow regimes and heat transfer ranges

Different possible heat transfer conditions and coolant flow patterns can arise along the axis of a PWR channel in a large and intermediate break LOCA [10]–[12]. They are schematically shown in Fig. 1(a). An experimental image corresponding to an electrically heated rod is also shown in Fig. 1(b) where the different coolant flow regimes and heat transfer modes can be appreciated [13].

In steady-state conditions and also in the first phase of a LOCA, heat removal is carried out by forced convection of a single-phase turbulent flow of liquid water.

In the subcooled nucleate boiling region the mean water temperature is slightly below and the wall temperature is a little above the saturation temperature. The liquid immediately adjoining the hot wall is overheated giving rise to nucleation of water vapor bubbles on the wall. In this stream pattern, which is described as bubbly flow, the water flow breaks the bubbles off the wall provoking the rupture of the boundary layer; the flow changes from laminar to turbulent thus enhancing the heat removal from the rod while the bubbles condense in the subcooled liquid region [9].

When the saturation temperature is reached in the whole channel, the heat removal regime is described as nucleate boiling. The bubbles continuously created on the cladding wall migrate towards the bulk but do not condense any longer. They coalesce giving rise to a pattern which is described as slug flow. These large bubbles provoke displacement of water from the channel center towards the layers closer to the cladding. Heat transfer in this region is still quite efficient [6].

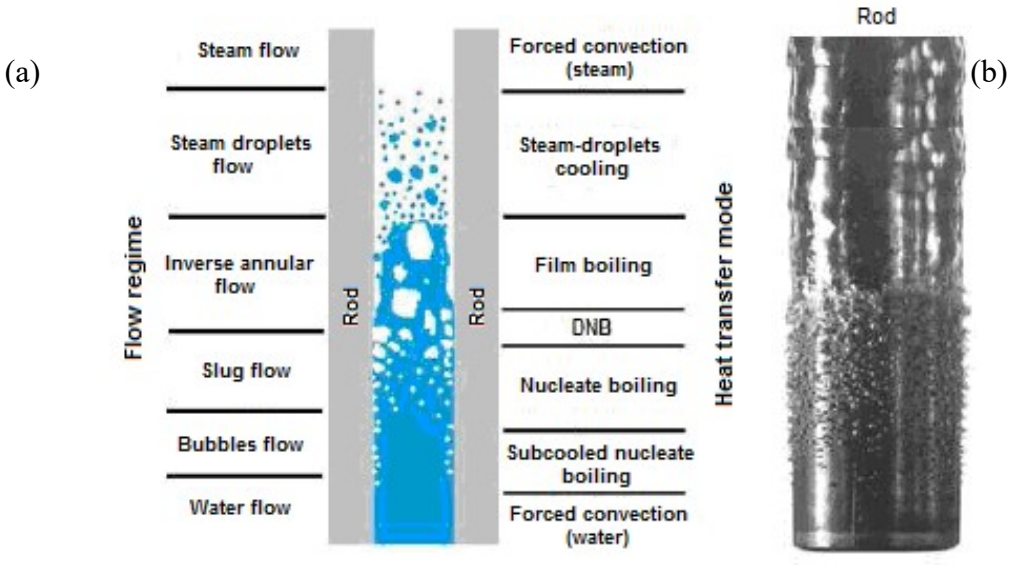

FIG. 1. (a) Heat transfer an flow configurations with high heat flux [10]; (b) image of the distribution of convective boiling around a heated rod [13].

The maximum heat flux that can be removed is called critical heat flux (CHF). It represents the thermal limit at which the boiling regime changes during heating. At this point the vapor bubbles abruptly form a film on the heating surface that thermally insulates the heater from the liquid [14]. If the generated heat flux exceeds this level, the heated surface can no longer hold the contact with the liquid and a boiling crisis occurs, associated with a drastic decrease of the heat transfer coefficient [15]. The transition from nucleate boiling to film boiling is characterized by the change from bubbles or slug flow to inverse annular flow. Due to the high heat flux density, the liquid water detaches from the cladding wall giving rise to the formation of a thin vapor layer next to the wall, through which the heat has to be removed by conduction. This phenomenon is described as departure from nucleate boiling (DNB).

For heat flux values higher than the CHF, a steam-droplets (mist) flow is established. In an even higher heat flux range, the droplets are finally evaporated in the channel center. The heat transfer coefficient shows a sudden decrease also in this region. The vapor is overheated due to continuous heat addition and pressure decrease. The flow pattern in this range is turbulent vapor.

2.2.2. Calculation of the critical heat flux

The CHF is a major limit for reactor safety since if the heat flux through the cladding is higher than this value, the cladding wall temperature will rapidly increase. A number of empirical correlations and physical models have been proposed during the past decades to calculate the CHF in terms of the mass flow, pressure, temperature, working power, as well as the fuel element geometry, mainly the hydraulic diameter. The adoption in several recent works of a table of CHF values is based on its higher accuracy and more extended range of application [15].

Nevertheless, in this work the Bowring correlation [13]:

$$q_{cr}^{"} = \frac{A - B h_{fg} X_t}{C} \tag{3}$$

is used to determine the CHF, indicated as $q_{cr}^{"}[W/m^2]$. It is given in terms of the latent heat of vaporization $(h_{fg}[J/kgK])$ and the mass fraction of vapor in the coolant (X_t); the parameters A, B and C are expressed in terms of the hydraulic diameter, the mass flow through the channel $(G[kg/m^2 s])$ and the system pressure. X_t is obtained with the Levy correlation [16]

in terms of the equilibrium mass fraction, the fraction of subcooled vapor, the enthalpies of the coolant and the saturated liquid, the temperatures of the coolant and the cladding and the specific heat of the liquid.

For $G > 271$ kg/m^{2}s or voids fraction higher than 80%, q''_{cr} is calculated with the Zuber correlation:

$$q''_{cr} = 743 \cdot F_g F_{sub} h_{fg} \sqrt{\rho[\sigma g(\rho_f - \rho_g)^{0.25}]} \quad (4)$$

in terms of the densities of liquid and vapor ($\rho_{f,g}$ [kg/m^3]); F_g and F_{sub} are correction factors for the extended void fraction range and for bulk subcooloed fluid conditions, respectively, and g is the acceleration of gravity.

Additionally, the code evaluates the 'departure from nucleate boiling ratio'. This parameter, briefly indicated as DNBR, is the ratio of the heat flux needed to cause departure from nucleate to the actual local heat flux of a fuel rod. A high value of DNBR reveals a wide safety range, i.e. it indicates that in the working conditions the CHF is not reached.

2.2.3. Calculation of the heat transfer coefficient

The models generally used to predict the heat transfer coefficient quantify the rate of energy exchange between the solid surface and the fluid under different conditions. The present work assumes that the subcooled flow regime can be divided into the following steps:

— Forced single-phase convection – sub-cooled boiling;
— Saturated nucleate boiling;
— Post-critical transition boiling;
— Post-critical film boiling;
— Forced single-phase convection to superheated vapor.

Additional modes can be encountered in severe transients which are also described in the literature. Nevertheless, since the objective of DIONISIO is the simulation of the fuel behavior, the thermal-hydraulic analysis included in it is restricted to the five modes listed above.

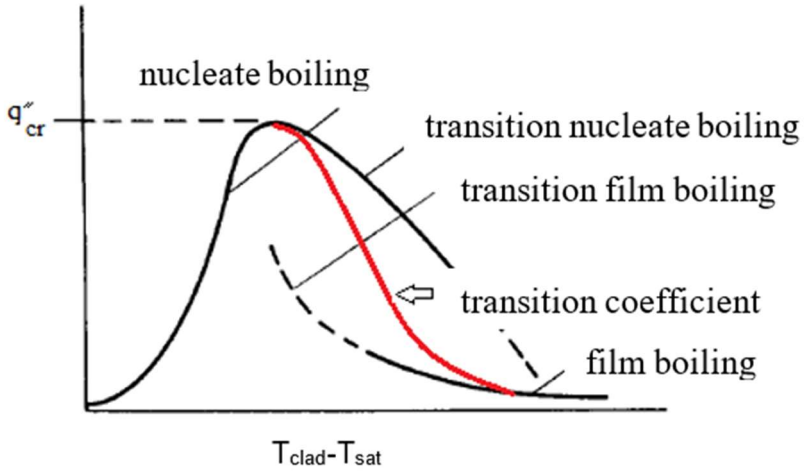

FIG. 2. Heat flux vs. overheating for different transfer regimes.

In the nucleate boiling regime, the Thom correlation [16, 18] expresses the heat flux as the sum of two terms, one giving the contribution of nucleate boiling and the other of single phase convection.

In the post-critical zone, heat is transferred through the film formed between the cladding and the coolant. The correlation proposed by Miropolskij [10, 19] is used in this work to represent this regime.

The transition between nucleate boiling and film boiling is expressed by a coefficient represented in Fig. 2. obtained in the present work as an average between the nucleate and film boiling coefficients in the transition range, following the criterion proposed by Ramu et al. [20]. The fluid temperature is assumed to be higher than the saturation temperature and the fluid is assumed a single phase vapor.

2.3. High temperature oxide growth

In normal operation conditions, in which the coolant temperature is in the range 250°C–400°C, the Zircaloy cladding material exists in hexagonal close packed (hcp) structure, which contains interstitial oxygen. It is usually indicated as α-Zr(O) phase. As stated by the model described in MATPRO [21] the oxide (ZrO_2) layer that develops on the external surface grows according to different rate laws, depending on the layer thickness. The change is assumed to be due to the morphological modification that takes place in the oxide layer when it thickens. Within that model, the transition thickness, δ^{trans}, is given by a temperature dependent, Arrhenius-type expression.

For pre-transition layers, the oxide is assumed to grow according to a cubic rate law, i.e. the increase of the oxide thickness, $\Delta\delta^{ox}$, experienced during the time interval Δt is proportional to $(\Delta t)^{1/3}$. Instead, for $\delta > \delta^{trans}$, a linear law is assumed for the growth rate, i.e. $\Delta\delta^{ox}$ is proportional to Δt .

In the high temperature range, $T > 900$°C, achievable in accident conditions, the Cathcart-Pawel [22] model is accepted. It assumes a parabolic rate law for the oxide layer growth, i.e. $\Delta\delta^{ox}$ proportional to $(\Delta t)^{1/2}$.

For the intermediate temperature range, an interpolation formula is adopted in the present work.

2.4. High temperature hydrogen uptake and release

The model adopted to simulate high temperature hydrogen behavior assumes two distinct uptake and release mechanisms: direct reaction with molecular H_2 and absorption of H^+ through the oxide layer [6], [23]–[25], [32].

The fuel rod is divided into a number of axial segments to perform the balance of the hydrogen content in the liquid and vapor phases of the coolant and also in the solid phases present in the outer cladding surface in contact with the coolant.

Due to the intensive oxidation in the high temperature range typical of accident conditions, the molar fraction of vapor next to the cladding is lower than that in the bulk. Then, the oxide layer growth rate depends on the flux of H_2O arriving from the bulk. A vapor phase volume V_g is assumed to correspond to each axial rod segment, i. Given a constant upstream vapor flow Q, the balance in the segment is [26]:

$$V_g C_g \frac{dy_i}{dt} = Q(y_{i-1} - y_i) - A_c \dot{w} \tag{5}$$

where $C_g = p_{tot}/RT$ (mol/cm^3) is the gas concentration in segment i, p_{tot} (atm) is the total pressure in the system, R is the gas constant and T (K) is the gas temperature, A_c (cm^2) is the lateral cladding area exposed to the vapor, Q (mol/s) is the molar flux rate of vapor, y_i and y_s are the vapor fractions in the bulk and the surface, respectively, k_g (cm/s) is the mass transfer

coefficient of H_2O and $\dot{w}$ is the oxygen absorption rate per unit area through the oxide layer. Then,

$$\dot{w} = k_g C_g (y_i - y_s) \tag{6}$$

The gas composition (C_s) on the cladding surface at a given temperature determines the O/Zr fraction. $C_s = 2.00$ in a vapor saturated atmosphere, but in steam starved conditions y_s can be quite low and then $C_s < 2$. When C_s reaches the value $C_a = 1.985,$ which is the lower concentration limit in Zirconia, the oxide dissolves and the cladding metal becomes exposed to the atmosphere.

When the oxide layer is present, the oxygen diffusion rate through the oxide is governed by the vapor flux through the gas layer: The gas composition (C_s) on the cladding surface at a given temperature determines the O/Zr fraction. $C_s = 2.00$ in a vapor saturated atmosphere, but in steam starved conditions y_s can be quite low and then $C_s < 2$. When C_s reaches the value $C_a = 1.985,$ which is the lower concentration limit in Zirconia, the oxide dissolves and the cladding metal becomes exposed to the atmosphere.

When the oxide layer is present, the oxygen diffusion rate through the oxide is governed by the vapor flux through the gas layer:

$$\dot{w} = \rho_{ox} D_O^{(ox)} (C_s - C_a)/\delta \tag{7}$$

where $\rho_{ox} = 0.047$ (mol/cm^3) is the molar density of Zr in ZrO_2, $D_O^{(ox)} = 33.3\exp(-42418/\mathrm{RT})$ (cm^2/s) is the diffusion coefficient of Oxygen in the oxide [6] and δ is the oxide layer thickness [5]. Equations (6) and (7) yield the conditions on the cladding surface. Taking into account that, even with a small vapor fraction in the coolant, the concentration in the oxide is very close to stoichiometry, $C_s \approx 2$, then y_s can be calculated as:

$$y_s = y_i - D_O^{(ox)} \rho_{ox} (2 - C_a)/k_g C_g \, \delta \tag{8}$$

As long as y_s remains positive, the oxygen absorption is controlled by diffusion in the solid phase and the flux will be given by (7) with $C_s = 2$. In case (8) predicts a negative value for y_s , then the uptake rate will be controlled by the flux given by (6) assuming $y_s = 0$ and the surface concentration by:

$$C_s = C_a + k_g C_g y_i \delta / D_O^{(ox)} \rho_{ox} \tag{9}$$

Starting from y_s and C_s, the partial pressures $P_{H_2O}(\mathrm{s})$, $P_{H_2}(\mathrm{s})$, $P_{O_2}(\mathrm{s})$ of the gaseous components on the cladding surface are obtained [5].

On the oxide/gas interface equilibrium conditions are assumed for the chemical reactions of oxygen and hydrogen: dissociation of H_2O, H_2 and O_2 molecules, dissolution of O, dissolution of H either as neutral atoms or as protons. The following constants are taken: for the dissociation of water, $k = exp(-6.61 + 29600/T)$ [26]; for Oxygen dissolution, $\beta = \sqrt{2\exp(2 - 68000/T)}$ [27]; for the Sievert´s coefficient K_S^{ox}, that given by [28] and for protons dissolution, $\gamma = \sqrt{1/(1.6865 \cdot 10^8 - 2.27005 \cdot 10^7 \cdot \log(T))}$.

Finally, considering the equilibrium equations and the chemical reactions mentioned above, the expression of the concentration of protons on the surface of the oxide is derived [32]:

$$\left(2k\beta^{1/2} C_{H^+}^3 / \gamma \, P_{H_2O}(S)\right) + C_{H^+}^2 - \gamma^{1/2} P_{H_2}^{1/2}(s) = 0 \tag{10}$$

The mass transfer through the oxide layer is evaluated assuming that its thickness is much smaller than that of the cladding. Hence the diffusion problem can be reduced to one dimension: the radius. The Hydrogen flux in the oxide can be represented by [6, 32]

$$J_H^{(ox)} = \frac{D_H^{(ox)} \partial C_H}{\partial r} \approx \frac{D_{H^+}^{(ox)} \Delta C_{H^+}}{\delta(t)} + \frac{D_H^{(ox)} \Delta C_H}{\delta(t)} \tag{11}$$

where $D_{H^+}^{(ox)}$ and $D_H^{(ox)}$ are the diffusion coefficients of protons and neutral hydrogen in the oxide, respectively in (cm^2/s), $\Delta C_{H^+} = C_{H^+}(s) - C_{H^+}(i)$ is the protons concentration variation between the oxide surface (s) and the oxide/metal interface (i), and similarly for neutral H: ΔC_H; $\delta(t)$ is the oxide thickness in cm [6, 32].

The diffusion coefficient of protons at high temperatures was fitted to experimental determinations [29]

$$D_{H^+}^{(ox)} = 4 \cdot 10^{-4} \exp\left(-7.2496 \cdot \frac{10^3}{T}\right) \tag{12}$$

If thermodynamic equilibrium is assumed at the oxide/metal interface, the following relation holds between the protons concentration at the interface, $C_{H^+}(i)$, the electrons in the oxide, $C_e(i)$, and the hydrogen in the $\alpha - Zr$ phase of the metal, $C_H(m)$, all of them in (mol/ cm^3) [6, 32]:

$$C_{H^+}(i) C_e(i) = \left(\gamma^{1/2}/k_s^{\alpha}\right) C_H(\mathrm{m}) \tag{13}$$

where k_s^{α} is the Sieverts coefficient in $\alpha - Zr$ [30]. The neutrality condition at the interface is represented by

$$\begin{aligned} C_e(i) &= 2C_v(i) \\ C_v(i) + C_{H^+}(i) &= C_{H^+}(i) + 2\chi_b \rho_{ox} \end{aligned} \tag{14}$$

where $\rho_{ox} = 4.7 \cdot 10^{-2}$ mol/cm^3 is the molar oxide and $\chi_b = 0.015$ is a stoichiometric parameter for the high temperature range [26]. From (13) the protons concentration in the oxide next to the oxide/metal interface is given by

$$C_{H^+}(i) + C_{H^+}^2(i)/2\chi_b \rho_{ox_v} = \lambda C_H(m) \tag{15}$$

To calculate the H concentration at the interface, we have:

$$C_H(i) = \lambda_* C_H(m) \tag{16}$$

with $\lambda_* = K_S^{ox}/k_s^{\alpha}$ [32]. Eqs (15) and (16) determine the boundary condition of the hydrogen diffusion problem in $\alpha - Zr$ in one dimension. The balance equation, that takes into account the external oxidation of the cladding, is [32]:

$$\frac{d(l_m C_H(m))}{dt} = J_H^{(ox)} - \frac{d(\delta(t)(C_{H^+}(s) - C_{H^+}(i)))}{2dt} \tag{17}$$

where l_m is the cladding thickness in cm.

The model assumes a limiting oxide layer thickness which acts as a barrier for the diffusion of neutral hydrogen, as proposed by Park and Olander [31]. This thickness is

considered in [23, 32] to be approximately 1~2 μm. For oxide layers thicker than this value, the neutral hydrogen diffusion is neglected in comparison with proton diffusion.

The total hydrogen H_{tot} (g/cm^2) produced by vapor dissociation is assumed to be related to the oxygen cladding uptake O_v (g/cm^2)

$$H_{tot} = (1/8)\, O_v \tag{18}$$

O_v is obtained from the oxide growth model at high temperature [3, 5], already incorporated to the accident module.

The amount of H captured by the cladding is not superior to [6],

$$C_H^{(m)}(max) = (\phi/\theta)\,(D_O^{(ox)}\Delta C_O/\delta(t)K_2)^{1/4} \tag{19}$$

with K_2 = 75 cm/s and

$$\phi = 1.86 - 3.18(T/1000) + 1.38\left(\frac{T}{1000}\right)^2 \tag{20}$$

$$\theta = 6.56 - 10.97(T/1000) + 4.63(T/1000)^2 \tag{21}$$

The released amount, H_l, is the difference between produced and captured

3. VALIDATION

All the models were subjected to a number of examinations. Firstly, separate ideal tests were performed imposing different sets of conditions typical of accident situations. Some of them were published [5] and were also presented in the FUMAC meetings. Table 2 summarizes the experiments and codes used to perform the separate testing of each model as well as the comparisons carried out with DIONISIO after including and interconnecting the new accident modulus.

TABLE 2. EXPERIMENTS AND CODES

Experimental data / code to be compared	Characteristics of the test performed
COBRA-IV [33]	Thermal-hydraulic code used to test the module under normal operation condition.
ATHLET Mod 1.1 Cycle [46] Simulation of breaks and transients in PWRs and BWRs including beyond design basis accidents.	Comparison of accident cases in PWR/BWR scenarios
RELAP5 Mod 3.1 Models the coupled behavior of the reactor coolant system and the core for loss-of-coolant and operational transients [47]	Comparison of accident cases in PWR/BWR scenarios
SOCRAT [34] Thermal-hydraulic predictions and general fuel code participant of the FUMAC project.	Comparison of the thermal-hydrahulic and mechanical predictions of DIONISIO.
DAKOTA [35] Statistical environment devoted to the investigation of uncertainty and sensitivity analysis of software packages.	Testing of the sensitivity and uncertainty of the whole module.
IAEA-SPE-4	Testing of the thermal-hydrahulic behavior of the module.

TABLE 2. EXPERIMENTS AND CODES

Experimental data / code to be compared	Characteristics of the test performed
Several experiments were performed in the PMK-2 facility [44, 45]	
IFA 650-1, 650-2. Experiment series performed at Halden to re-examine the traditional safety criteria for LOCA accidents, included in the FUMEX III data base [36]–[38]	Testing of the thermal-hydrahulic and oxide growth models; mechanical models are also tested in IFA 650-2
IFA 650-9, 650-10, 650-11	Testing of the thermal-hydrahulic and mechanical models and the general response of the whole module.
PUZRY [39] Performed at the AEKY facility to study and compare the mechanical properties of the cladding materials	Comparison of the mechanical model.
NRC LOCA test program Performed at Studsvik to investigate the strength and ductility of HBu rods after ballooning, rupture, oxidation and quench [40]	Comparison of the mechanical model.
QUENCH-L0/L1 experiment Performed at the QUENCH facility in the forced convection mode (relevant for LOCA accidents) [41, 42]	Comparison of the whole module, especially to test the hydrogen uptake/release model.
CORA-15, Part of the severe fuel damage program. Provides information on the failure mechanisms of LWR fuel in the high temperature range [43].	Comparison of the mechanical model. Testing of the hydrogen uptake/release model.

Some results obtained with DIONISIO with the accident modulus incorporated are shown here below.

3.1. Comparison with predictions of ATHLET and RELAP5 for PMK-2 experiements

Several experiments were performed in the PMK-2 facility (in Budapest) between 1984 and 1993. The device is a scaled model of the Paks NPP, designed to extend the data base for VVER-type power plants, to investigate the processes following small and medium size breaks (of 1% to 22%) in the primary circuit and also to test the thermal-hydraulic simulation codes in these conditions. The system consists of 19 fuel rods distributed in a hexagon, containing UO_2 pellets in Zry claddings. The experiments were organized by the International Atomic Energy Agency (IAEA) in cooperation with the Atomic Energy Research Institute (AEKI) of the Hungarian Academy of Sciences. These experiments were also aimed at investigating the capability of thermal-hydraulic codes for modeling natural circulation phenomena in these reactors. The results of the experiments are compared with the predictions of ATHLET and RELAP-5 [44, 45].

The computer code ATHLET Mod 1.1 Cycle A was developed by GRS as an advanced best estimate code for the simulation of breaks and transients in PWRs and BWRs including beyond design basis accidents [46]. The RELAP5 Mod 3.1 code models the coupled behavior of the reactor coolant system and the core for loss-of-coolant and operational transients [47].

The DIONISIO code was compared with some of these experiments. In this work the comparison with the fourth experiment of the Standard Problem Exercises (IAEA-SPE-4) is presented. The test, which was performed in April 1993, started from full power and nominal operation conditions: core power 658 kW, primary circuit pressure 12.43 MPa, coolant flow 5.1 kg/s, core inlet temperature 263°C. To perform the simulation with DIONISIO of the accidental sequence the rod length is divided into 10 axial segments in such a way that the ninth segment coincides quite well with the location of one of the thermocouples, placed 30 cm below the top of the rod, which had a length of 250 cm. In Fig. 3(a) the coolant flow rate and pressure during the experiment are shown together with the pressure curve fitted as input for DIONISIO. Figure 3(b) shows the temperature recorded during the experiment along with the predictions of RELAP5, ATHLET and DIONISIO. The coolant temperature at the bottom of the rod reported in the experiment is compared with the values simulated by DIONISIO corresponding to the first rod segment. The coolant flow drop that starts at about 1000 s is responsible for the steep temperature increase observed in Fig. 3(b) that ceases when the coolant flow is reestablished. The good agreement with the experimental records reached with DIONISIO can be appreciated.

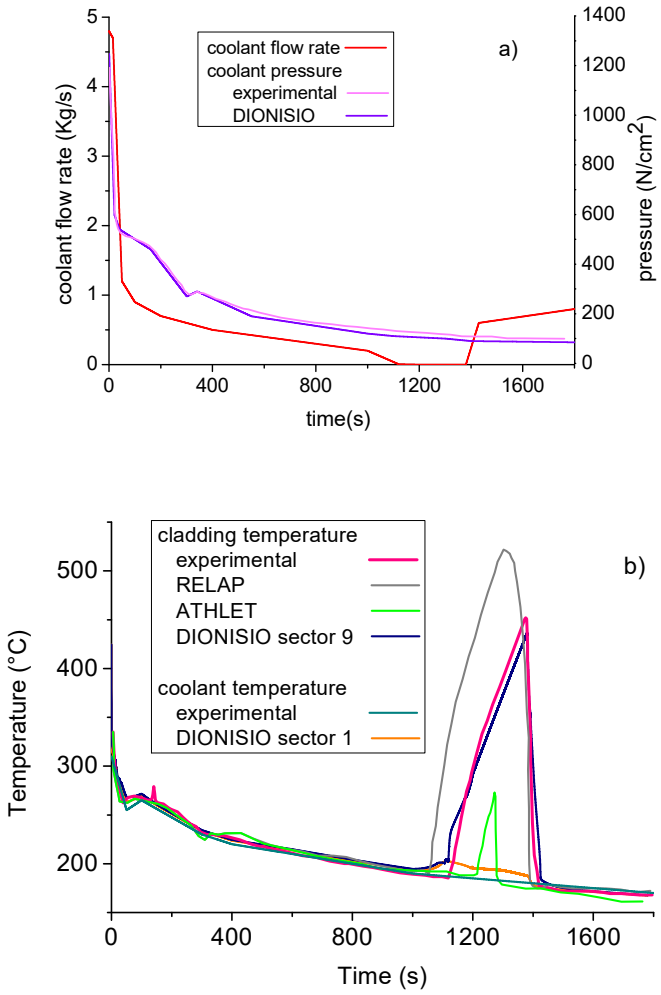

FIG. 3. (a) Coolant flow rate and pressure during the experiment; (b) Comparison between measured cladding temperature[1].

[1] The predictions of RELAP, ATHLET and DIONISIO, also between the measured coolant temperature at the inlet and the prediction of DIONISIO in sector 1.

3.2. Comparison with data of the PUZRY experiments

The PUZRY experiments [39] were performed at the AEKY facility. The data, compiled in the Experimental Database of E110 Claddings under Accident Conditions, are available to the FUMAC members. In particular, the PUZRY experiments were designed to study and compare the mechanical properties of the cladding materials. They consist of 31 Zry-4 tubes 5 cm long treated at constant temperature with linearly incremented internal pressure.

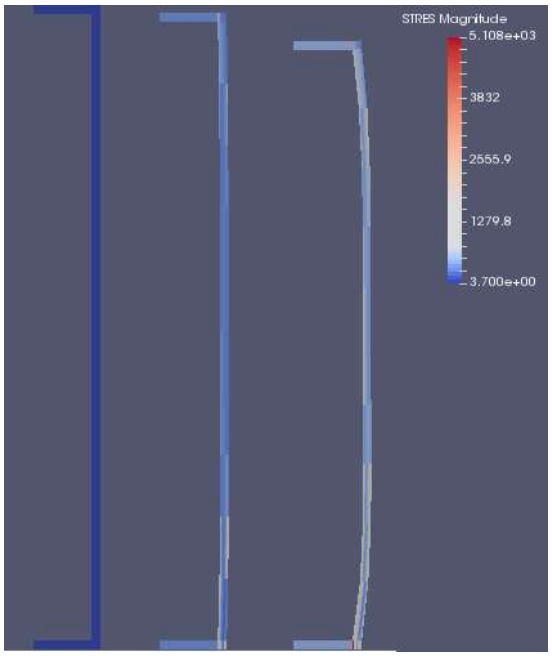

FIG. 4. Deformation of PUZRY-12 at different times: 0.0, 60.0 and 80.0 s.

To reproduce this type of experiment, a new working scheme was developed in DIONISIO. It consists in meshing a domain constituted by a tube, with cylindrical symmetry and user defined dimensions. The internal and external pressures as well as the temperature are allowed to vary with time. The thermal-mechanical problem is thus solved.

Figure 4. shows the initially non-deformed tube of the PKZRY-12 experiment and the deformation simulated for 60 s and 80 s after pressure rise initiation. The experimental time for burst was 79.62 s.

In Fig. 5. the experimental time for burst and that predicted by DIONISIO are compared for the 31 mini-rods of the test. The perfect agreement line, along with those indicating a departure of ±10% are also drawn to make evident the precision of the results. It is observed that the cases corresponding to low pressure increase rate, indicated with red squares, depart some more from the ideal agreement line.

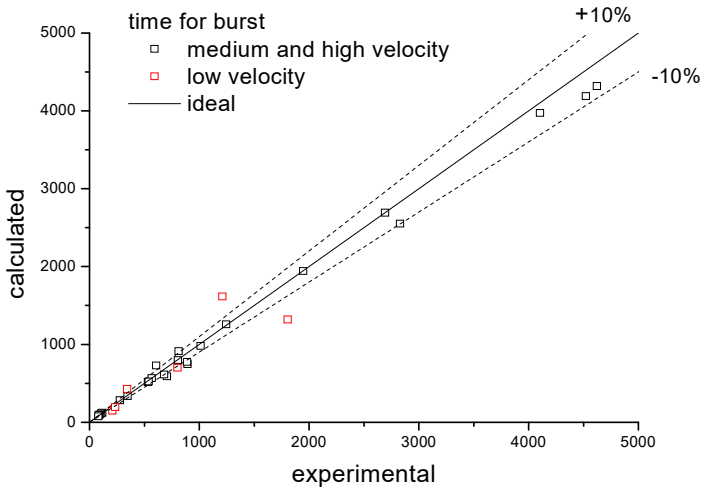

FIG. 5. Time for burst of the 31-mini rods of Zry with incremental internal pressure. The red points correspond to the cases with low velocity.

3.3. QUENCH experiments

The QUENCH-L0 experiment was the first of a series of fifteen tests carried out in the QUENCH facility [41]. This experiment was performed in the forced convection mode (relevant for LOCA accidents); the coolant was a mixture of superheated steam with argon which acted as a carrier gas. Twenty one instrumented rods were internally heated with tungsten heaters connected to copper electrodes. Two DC-generators were used for two groups of rods connected in parallel: 10 internal rods with high electric power and 11 external rods with low electric power.

In order to reproduce LOCA scenarios, the fuel rods were loaded with inner pressures of 35, 40, 45, 50, and 55 bar, respectively [42]. The purpose was to investigate the influence of the pressure on the involved processes. The experimental determinations and DIONISIO predictions of pressure evolution are show in Fig. 6. Burst occurrence is evidenced by the sharp pressure decrease. It is recognized that the rods subjected to higher pressure, i.e., at higher temperature, fail before than those at lower power but no significant difference in time for burst is visible in connection with the initial internal pressure.

According to the experimental determinations, burst occurs in the temperature range 776–850ºC. DIONISIO predicts a quite similar range: 789–850ºC. But some differences are recognized in the burst axial position: the experimental determinations show that the burst occurs between 930 and 1100 mm while DIONISIO locates the burst in the range 600–700 mm. This difference could be explained by the calculation procedure used in DIONISIO, which includes dividing the rod in axial segments. This can lead to a more dispersed temperature range within which is the maximum.

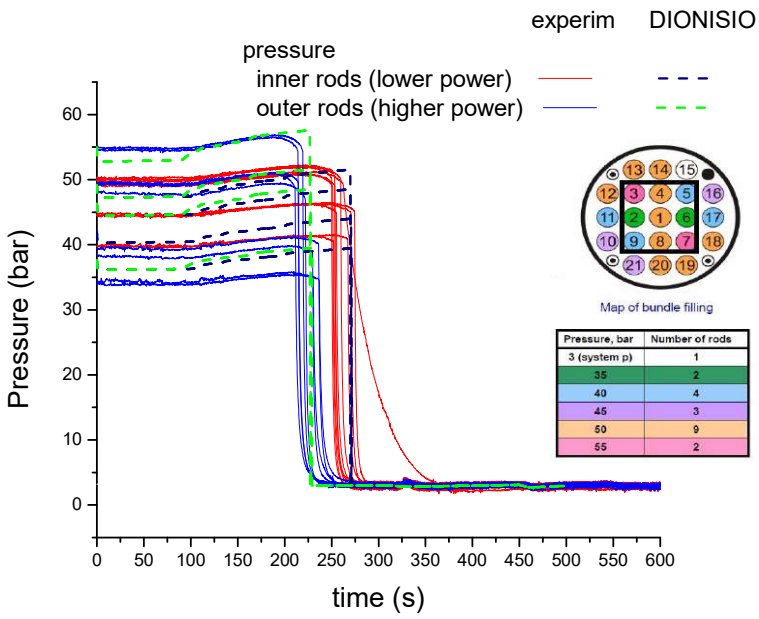

FIG. 6. Internal pressure of the inner and outer rods vs. time in the QUENCH-L0 experiments.

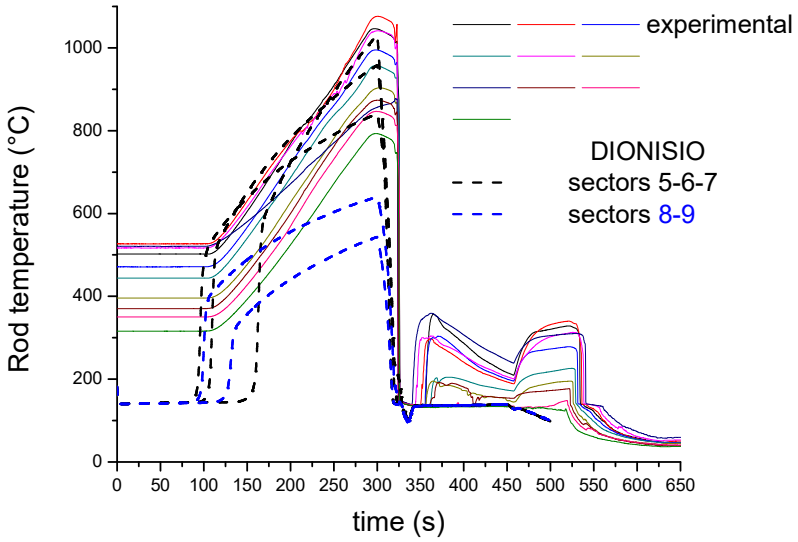

FIG. 7. Experimental and predicted cladding temperature in selected sectors vs. time.

Figure 7 shows the temperature evolution in different rod sectors. They are numbered from bottom to top of the rod in such a way that sectors 5–7 correspond to the middle, while sectors 8 and 9 are located next to the top of the rod. Power supply is drastically reduced and cooling is increased after rod bursting, which is recognized in the fast temperature drop. However, the remnant heat provokes the evaporation of the entrained water and a further temperature increase is observed which is counteracted by a second injection of vapor accompanied by argon. This process occurs twice, as can be appreciated in the tail of the experimental curves. But this sequence is not accounted for by the simulation with DIONISIO, which assumes that the process is over after the first drop.

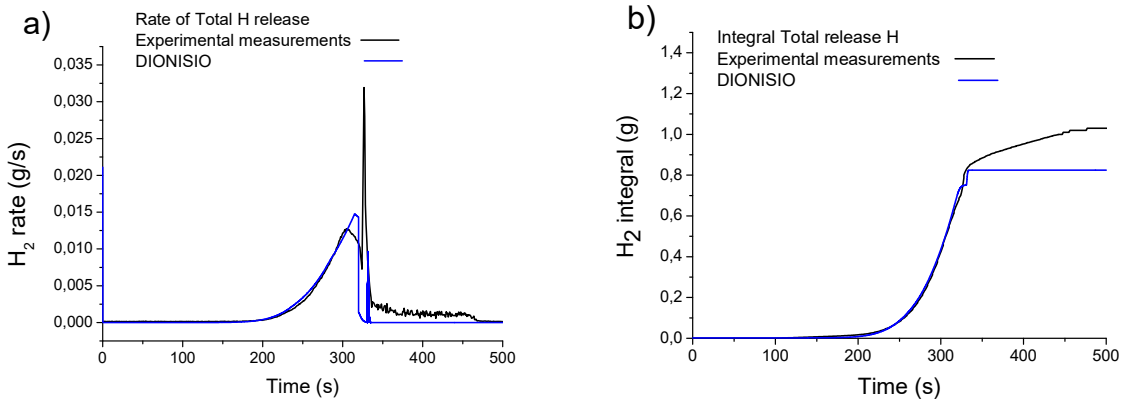

FIG. 8. Hydrogen release, experimental and predicted by DIONISIO; (a) Instantaneous release rate, (b) Accumulated amount of hydrogen released.

Fig 8 shows the preliminary results of hydrogen release obtained with DIONISIO, which are compared with the experimental data. Fig 8 (a) gives the instantaneous release rate (g/s) and Fig. (b) gives the accumulated amount of released hydrogen. The fast temperature drop is reflected in a sudden release of hydrogen, which is observed in the experiment and in the simulated curve. A certain disagreement between both is recognized at the end of the curve which can be originated by the mismatch in temperature already described in connection with Fig. 7. Moreover, the experimental predictions are referred to the whole bundle but the calculations in DIONISIO were made for one rod (identified as rod 4) and the result were then extended to the whole bundle. This fact can be responsible for a certain degree of disagreement.

3.4. IFA-650 experiments

As an example, results of the IFA 650-11 experiment are presented. In Fig. 9. The comparison of the predictions of DIONISIO with those of SOCRAT and with the experimental determinations of the cladding temperature obtained with thermocouples located at three axial positions, vs. time after accident initiation in IFA 650-10. The times for occurrence of blowdown, ballooning, burst and scram can be appreciated.

As a further test of the newly developed thermal-hydraulic (Th-H) subroutine, the IFA 650-11 experiment was reproduced with DIONISIO in two different conditions. In one case, the predictions of this subroutine were used; in the other one, the outputs of SOCRAT were taken as boundary conditions (BC) for DIONISIO. Fig 10 shows the comparison between the measured internal rod pressure and both types of calculations. A similar presentation is given in Fig. 11 for the elongation. The excellent agreement between both simulations of the thermal-hydraulic conditions can be appreciated. The agreement is also good with respect to the measured values of pressure and elongation.

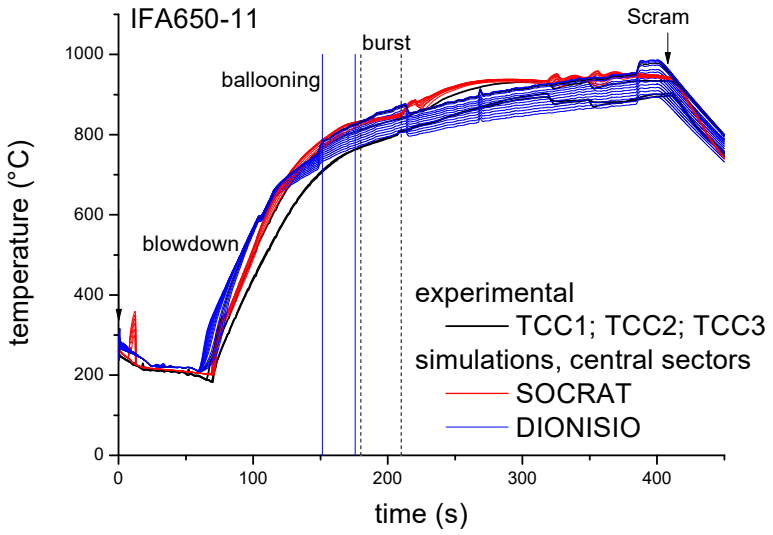

FIG. 9. Comparison between calculated and measured cladding temperature at three axial positions vs. time after accident initiation in IFA 650-11. Predicted and measured ballooning and burst times as well as the scram are also indicated. Superimposed are also the predictions of SOCRAT.

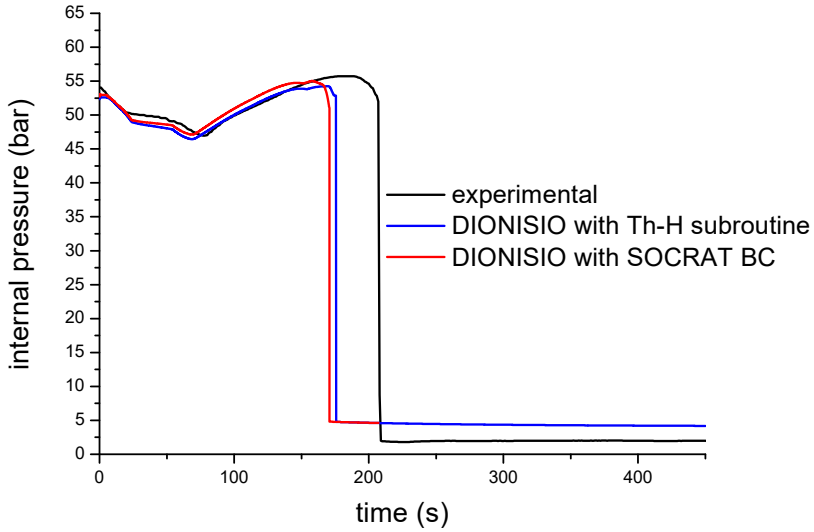

FIG. 10. Comparison between calculated and measured internal rod pressure. The simulations with DIONISIO were made with the thermal-hydraulic subroutine and with the boundary conditions provided by SOCRAT.

The temperature of the plenum plays a role in the mechanical response of the cladding since it determines the internal gas pressure and, hence, determines ballooning and burst occurrence. Fig. 12 shows the comparison between measured and simulated values of the plenum temperature in experiment IFA 650-11. Also here the results of the simulations carried out with DIONISIO, obtained with the thermal-hydraulic subroutine and with the boundary conditions provided by SOCRAT are represented. The difference between measured and calculated temperature values (of about 90°C) can be considered as acceptable, taking into consideration the wide error margins of the experimental determinations. Moreover, they reflect

in a narrow discrepancy between measurements and calculations of the internal rod pressure, as can be appreciated in Fig. 10.

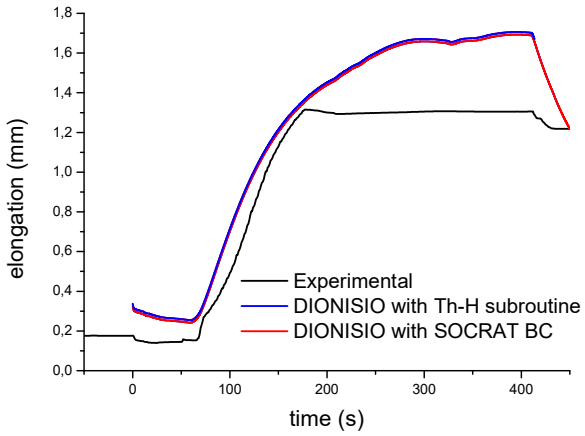

FIG. 11. Comparison between calculated and measured axial cladding elongation in IFA 650-11. The simulations with DIONISIO were made with the thermal-hydraulic subroutine and with the boundary conditions provided by SOCRAT.

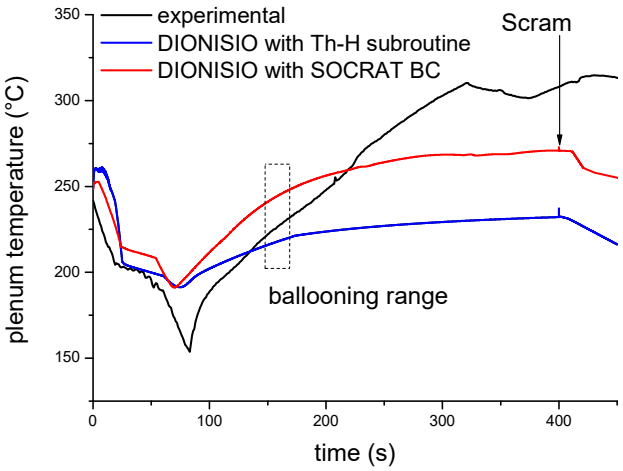

FIG. 12. Comparison between experimental and simulated values of the plenum temperature in IFA 650-11. The simulations with DIONISIO were made with the thermal-hydraulic subroutine and with the boundary conditions provided by SOCRAT.

3.5. Discussion and Conclusions

The degree of development presently achieved with the thermal-hydraulic model reported here allows analyzing and quantifying a considerable number of parameters involved in the rod evolution. Accumulated and released heat, temperature distribution in the rod, particularly on its external surface, temperature of the fluid in the cooling channel, vapor mass and volume fractions in the coolant, pressure and coolant flow drop, among others are evaluated not only in normal operation conditions but also in accidental conditions, particularly those described as LOCA events.

The fast variations and the extreme conditions experienced by the fuel rod in this type of accident may cause severe rod damage. Safety reasons indicate the importance of building accurate simulation tools. However, these rapid transients are precisely the cause of some of

the more challenging difficulties encountered in the simulations since the general system conditions are definitely far from equilibrium.

The strategy of dividing the rod length into segments, solving the various physical and chemical issues in one representative pellet subjected to the locally averaged conditions of the segment, then extending the results to the whole segment and finally coupling all the segments to reach a description for the entire rod has proved to be effective and quite accurate, particularly in the simulation of normal irradiation conditions. Nevertheless, in accidental conditions, this calculation scheme tends to produce a systematic underestimation of creep and cladding growth. The reason for this relies on the assumption of small strains implied in the model. To overcome this limitation a different scheme valid for large strains is presently under development.

In spite of the approximations implied in the thermal-hydraulic subroutine and its relative simplicity, the results it produces agree quite well with the available experimental data and with the results of specific codes, thus providing the adequate boundary conditions necessary to simulate the fuel behavior.

The development of the model to describe the capture and release of hydrogen in a wide range of scenarios is almost finished. The comparisons with experimental data available in the literature give a good agreement. It will be incorporated to DIONISIO in the near future as a new subroutine.

At the present moment a relocation model based on the density changes of the fuel pile is under construction and will be also included in the DIONISIO LOCA section. The model is not intended to predict the change in the geometry of the rod, but it can provide the temperature profile modification and changes in oxide and hydrogen uptake (or release) in the densified zone.

A model to describe quench experiments was also included. Nevertheless, some aspects are still under development; it will include a fracture module appropriate to predict cracks propagation through the cladding wall up to burst occurrence.

In summary, the activities programmed for the whole contract have been successfully accomplished.

REFERENCES

[1] SOBA A., DENIS A., DIONISIO 2.0: New version of the code for simulating a whole nuclear fuel rod under extended irradiation, Nucl. Eng. and Des. 292 (2015) 213–221.

[2] SOBA A., DENIS A., ROMERO L., VILLARINO E., SARDELLA F., A high burn-up model developed for the DIONISIO code, J. Nucl. Mater., Vol. 433, Issues 1–3 (2013) 160–166

[3] SOBA A., LEMES M., DENIS A., An empirical formulation to describe the evolution of the high burnup structure, J. Nucl. Mater., 456 (2015) 174–181.

[4] SOBA A., LEMES M., GONZÁLEZ M.E., DENIS A., ROMERO L., Simulation of the behaviour of nuclear fuel under high burnup conditions, Ann. Nucl. Energy. 70 (2014) 147–156.

[5] LEMES M., SOBA A., DAVERIO H., DENIS A., Inclusion of models to describe severe accident conditions in the fuel simulation code DIONISIO, Nucl. Eng. and Des. 315 (2017) 1–10.

[6] VESHCHUNOV M.S., BERDYSHEV A.V., Modelling of hydrogen absorption by zirconium alloys during high temperature oxidation in steam, J. Nucl. Mater. 255 (1998) 250–262.

[7] COX B., Adv. Corrosion Sci. Technol., 5 (1976) 173.

[8] ROSINGER H.E., A model to predict the failure of Zircaloy-4 fuel sheathing during postulated LOCA conditions, J. Nucl. Mater.120,1 (1984) 41–54.

[9] MANNGARD T., JERNKVIST L.O., MASSIH A., Evaluation of Loss-of-Coolant Accident Simulation Tests with the Fuel Rod Analysis Code FRAPTRAN-1.4. Quantum Technologies AB, Report TR11-008V1 (2011).
[10] Vojtek I., Heat Transfer Processes During Intermediate and Large Break Loss-Of-Coolant Accidents (LOCAs), International Agreement Report, U.S. Nuclear Regulatory Commission (1986).
[11] MOCHIZUKI, H., Thermal Hydraulics in Nuclear Reactors, International graduate course, Tokyo Institute of Technology, (2009).
[12] ODAR F., Assessment of the TRAC-M Codes Using Flecht-Seaset Reflood and Steam Cooling Data, U.S. Nuclear Regulatory Commission, (2001).
[13] TODREAS N.E., KAZIMI M.S., Nuclear Systems I, Thermal Hydraulic Fundamentals, Massachusetts Institute of Technology, (1990).
[14] COLLIER J.G., THOME J.R., Convective Boiling and Condensation, Clarendon Press, (1994).
[15] CHEN Y., An Overview of Heat Transfer Phenomena, Chapter 9: Critical Heat Flux in Subcooled Flow Boiling of Water, (2012).
[16] LEVY S., Forced convection subcooled boiling, Prediction of vapor volumetric fraction, Int. J. of Heat and Mass Transfer, 10 (1967) 951-965.
[17] FRAPTRAN 1.4: A Computer Code for the Transient Analysis of Oxide Fuel Rods, (2011).
[18] TONG L.S., WEISMAN J., Thermal Analysis of Pressurized Water Reactors, American Nuclear Society, (1966).
[19] KOLEV N.I., Multiphase Flow Dynamics 2, Thermal and Mechanical Interactions, Springer-Verlag Berlin Heidelberg, (2005).
[20] RAMU K., WEISMAN J., Transition Flow Boiling Heat Transfer to Water in a Vertical Annulus, Nucl. Eng. and Des., 40 (1977) 285–295.
[21] HAGRMAN, D.L., REYMANN, G.A., MATPRO Version 11—Handbook of materials properties for use in the analysis of light water reactor fuel behavior. In: NUREG/CR-0497, TREE-1280, Idaho National Engineering Lab., Idaho Falls (1979).
[22] CATHCART J. V., PAWEL R. E., MCKEE R. A., DRUSCHEL R. E., YUREK, G. J., CAMPBELL, J. J., JURY, S. H., Zirconium metal-water oxidation kinetics IV. Reaction rate studies ORNL/NUREG-17 (1977).
[23] VESHCHUNOV, M.S., SHESTAK, V.E., Modeling of Zr alloy burst cladding internal oxidation and secondary hydriding under LOCA conditions, J. Nucl. Mater., 461, (2015) 129–142.
[24] COX, B., Mechanisms of Hydrogen Absorption by Zirconium Alloys, Atomic Energy of Canada Limited, AECL (Report), (January 1985).
[25] ADAMSON, R., GARZAROLLI, F., COX, B., STRASSER, A., RUDLING, P., Corrosion Mechanisms in Zirconium Alloys, Advanced Nuclear Technology International, Skultuna, Sweden (2007).
[26] OLANDER, D.R., Materials chemistry and transport modelling for severe accident analysis in light-water reactors I: External cladding oxidation, Nucl. Eng. and Des., 148(2–3) (1994) 253–271.
[27] WANG, W., OLANDER, D.R., Thermochemistry of the U-0 and Zr-0 Systems', (1992).
[28] MOALEM, M., OLANDER, D. R. (1991) 'The high-temperature solubility of hydrogen in pure and oxygen-containing Zircaloy', J. Nucl. Mater., 178(1), 61–72.
[29] GROSSE, M., 'Kinetics of hydrogen absorption and release in zirconium alloys during steam oxidation', Oxidation of Metals, 70(3–4) (2008) 149–162.
[30] STEINBRÜCK, M., Hydrogen absorption by zirconium alloys at high temperatures, J. Nucl. Mater., 334(1) (2004) pp. 58–64.

[31] PARK, K., OLANDER, D.R., Hydrogen dissolution in and release from nonmetals: III Tetragonal Zirconia, J. Am. Ceram. Soc. 74, 1 (1991) 72–77.
[32] VESHCHUNOV, M., SHESTAK, V., Models for hydrogen uptake and release kinetics by zirconium alloys at high temperatures, Nucl. Eng. and Des. 252 (2012) 96–107.
[33] WEBB, B.J., COBRA-IV PC: A Personal Computer Version of COBRA-IV-I for Thermal-Hydraulic Analysis of Rod Bundle Nuclear Fuel Elements and Cores, PNL-6476, (1988).
[34] Short Information on the Results of IFA-650.9, IFA-650.10 and IFA-650.11, Calculations with SOCRAT code. Internal FUMAC Technical Note, v2.
[35] ADAMS, B., et al., A Multilevel Parallel Object-Oriented Framework for Design Optimization, Parameter Estimation, Uncertainty Quantification, and Sensitivity Analysis: Version 6.4 User's Manual. SAND2014-4633, (2016).
[36] LESTINEN, V., KOLSTAD, E., WIESENACK, W., LOCA testing at Halden, Trial runs in IFA-650, Nuclear Safety Research Conference Washington, (2003).
[37] LESTINEN, V., LOCA testing at Halden, first experiment IFA-650.1 HWR-762, (2004).
[38] EK, M., LOCA testing at Halden; the second experiment IFA-650.2, HWR-813, (2005).
[39] PEREZ-FERÓ, E., et al., Experimental Database of E110 claddings under accident conditions. EK-FL-2011-744-01/04, (2012).
[40] NUCLEAR ENERGY AGENCY, Report on Fuel Fragmentation, Relocation and Dispersal, Nuclear Safety, NEA/CSNI/R (2016)16., (2016).
[41] STUCKERT, J., GROßE, M., RÖSSGER, C., STEINBRÜCK, M., WALTER, M., Results of the LOCA reference bundle test QUENCH-L0 with Zircaloy-4 claddings, Karlsruher Institut für Technologie, (2011).
[42] HOLLANDS, T. BALS, C., AUSTREGESILO, H., Simulation of QUENCH-L0 with ATHLET-CD, International Quench Workshop, November, (2011).
[43] SEPOLD, L., HAGEN, S., HOFMANN, P., SCHANZ, G. Behavior of AgInCd Absorber Material in Zry/ UO_2 Fuel Rod Simulator Bundles Tested at High Temperatures in the CORA Facility, Report FZKA 7448, (2009).
[44] SZABADOS, L., et al., two phase flow behavior during a medium size cold leg LOCA test on PMK-2 (IAEA SPE-4), KFKl Atomic Energy Research Institute, Budapest, Hungary (1995).
[45] EZSÖL, GY., Simulation of a small cold-leg-break experiment at the PMK-2 test facility using the RELAP-5 and ATHLET codes, (1996).
[46] GLAESER, H., Validation and uncertainty analysis of the ATHLET thermal-hydraulic computer code, Nuclear Society of Slovenia 2nd Regional Meeting, Nuclear Energy in Central Europe, Portoroz, Slovenia, (1995).
[47] RELAP5/MOD3 Code Manual, NUREG/CR-5535 INEL-95/0174 Vol. 5, Rev. 1, 1995.

QUALIFICATION OF FRAPCON/ FRAPTRAN CODES FOR LOCA FUEL BEHAVIOUR MODELLING AND SAFETY EVALUATION: TRACTEBEL CONTRIBUTION TO FUMAC PROJECT (2014-2017)

JINZHAO ZHANG* (CSI), ADRIEN DETHIOUX, THOMAS DRIEU, CHRISTOPHE SCHNEIDESCH
Tractebel (ENGIE)
Avenue Ariane 7, 1200 Brussels, Belgium
jinzhao.zhang@tractebel.engie.com

Abstract

As part of the Tractebel contribution to the IAEA FUMAC project, Tractebel has used the updated FRAPTRAN-TE-1.5 code for simulation of selected Halden LOCA tests IFA-650.9 and IFA-650.10, together with the improvement in the thermal hydraulic modelling by using the imposed thermal hydraulic boundary conditions from SOCRAT calculations and in the thermal boundary conditions (axial power profile, plenum temperature). In particular, the impacts of the model improvements such as the Quantum Technologies' axial relocation model and errors corrections in the adapted FRAPTRAN-TE-1.5 version on the calculation results were identified and discussed. In addition, the statistical uncertainty and sensitivity analysis has been performed on the FRAPTRAN-TE-1.5 modelling of the selected Halden LOCA test IFA-650.10. First, uncertainty parameters in fuel rod manufacturing data, operation and test boundary conditions, physical properties and key models were identified, with their ranges and distributions defined. The DAKOTA tool has been used to sample these parameters 200 times and generate corresponding input models for FRAPTRAN-TE-1.5. After running these 200 cases, the relevant output parameters were collected, the lower and upper bounds were determined by using the order statistics. The objective is to verify if the uncertainties on the predicted key uncertainty parameters (cladding temperature, plenum gas pressure, cladding radius and elongation) well bound the measured data during the test. Finally, the important input uncertainty parameters were identified through the partial rank correlation coefficients obtained by the global sensitivity analysis.

1. INTRODUCTION

The DIONISIO code describes most of the phenomena occurring in a PWR/PHWR fuel rod in normal operation conditions. To take into consideration the axial variation of reactor linear power and coolant temperature, the rod is divided into a user defined number of segments. In every time step and for each axial section, a complete description of the local system variables is obtained by solving the tightly-coupled, non-linear differential equations accounting for the thermal and mechanical behavior. Then, the temperature and stress-strain distributions in the complete rod are obtained as step-like functions of the axial coordinate. With respect to the gas inventory, the code evaluates the amount of gas released by each rod segment and then that released by the whole rod. The composition of the gas mixture in the gap and its thermal conductivity are recalculated in every time step. The internal rod pressure is evaluated with the ideal gas law using the total number of gas atoms in the free volume within the rod and the average temperature in the total void volume in the rod (gap and dishings in all the segments, and plenum). The elongation of every individual pellet and the corresponding cladding are added up to obtain the total elongation of the pellet stack and the rod. DIONISIO 2.0 is nowadays a code able to simulate a fuel rod in extended burnup conditions. Particularly, in the high burnup range the inventory of the more relevant isotopes and the microstructure at the pellet periphery are described.

The code results have been compared with some 34 experiments published in the IAEA data base, covering more than 380 fuel rods irradiated up to average burnup levels of 40-60 MWd/kgU. The results of these comparisons are quite satisfactory and reveal the good quality

of the simulations. They were performed within the frame of the IAEA Research Project FUMEX III. The diverse models have been explained in detail in a number of papers [1-5].

In the frame of the Research Project FUMAC the application range of the code was expanded to conditions typical of Loss of Coolant Accidents (LOCA). To this end, a new module able to reproduce the thermal-hydraulic conditions in the coolant was developed. This module is intended to give account of the numerous parameters that govern the heat exchange between the fuel rod and the coolant in accident situations, thus providing the boundary conditions necessary to simulate the fuel rod behavior during a fast excursion, particularly in such a determinant aspect as the thermal behavior.

The code simulates a vertical channel, typical of a PWR or BWR fuel element, containing one fuel rod. Scenarios like forced single-phase (water or vapor) convection or double-phase flow, including departure from nucleate boiling (DNB) are taken into consideration. The model adopted analyzes and quantifies the coolant behavior in terms of the system pressure and coolant velocity. Moreover, models to describe mechanical problems occurring in accidental situations, like ballooning and burst, are also included.

A separate testing plan was first followed, which consisted in comparing the predictions of the new thermal-hydraulic module with specific codes in different flow regimes. Then it was included as a subroutine of the DIONISIO code and its results were compared with available experimental data. It is seen that the predictive ability of the general code has improved with the introduction of the heat transfer coefficients corresponding to the different patterns that can be encountered in the coolant flow.

In accident conditions, due to the fast cladding oxidation and the associated dissociation of water molecules, a considerable increase of the hydrogen content in the cladding material takes place. This can give origin to severe material damage during a sudden rod cooling. The model considered in the present work [6] assumes two different mechanisms of hydrogen capture. One of them is the chemical reaction with the H2 present in the coolant; the other one assumes fast diffusion of H+ through the oxide layer, where it discharges at the oxide-metal interface, by capture of one e- proceeding from the oxidation reaction [7].

The project FUMAC (Fuel Modelling in Accident Conditions) has been launched by IAEA as a new Coordinated Research Project (CRP). It has started in 2014 and will end in 2018.

The objectives of the CRP are:

— Analysis and better understanding of fuel behaviour in accident conditions, including Fukushima accident;
— Collection of well checked results of accident simulation experiments, and share of experience in the organizations of Member States;
— Identification of best practices in the application of physical models and computer codes used in different Member States for modelling of fuel in accident conditions, and enhancement of predictive capacities of these models and codes.

The project FUMAC is a continuation of the FUMEX III project [1] with the focus on the modelling of fuel behaviour in design basis and severe accidents that is particularly demanding after the Fukushima accidents. In particular, it will focus on the scenario of a Loss-Of-Coolant Accident (LOCA).

The CRP FUMAC is planned under the IAEA Nuclear Safety Action Plan with the well-proven organizational approach used in the recent CRP FUMEX-III, which presumes cross-comparisons of computer codes used in different Member States and close collaboration with the NEA/OECD and the joint NEA-IAEA International Fuel Performance Experiments (IFPE) Database. Selected sets of accident simulation experimental results, provided by CRP members, will be integrated into the IFPE Database and used for codes verification. The codes involved can range from fuel performance codes (e.g. TRANSURANUS or FRAPTRAN) to system or

severe accident codes (e.g. TRACE or MELCOR) as well as multi-physics codes (e.g. BISON, ALCYONE).

Tractebel is participating in the simulation of the integral (single rod) LOCA tests, and possibly some separate effect clad tests. Tractebel will use the USNRC fuel performance code, FRAPTRAN-1.5, with the following proposed work-plan:

- Perform selected benchmark cases on the fuel behaviours during LOCA using the available or modified fuel rod codes FRAPCON/FRAPTRAN;
- Compare against data provided by the IAEA and OECD/NEA, and/or other code calculation results;
- If necessary and feasible, couple with other codes such as system thermal hydraulic codes (RELAP or TRACE), in order to improve the thermal hydraulic modelling;
- Perform statistical uncertainty and sensitivity analysis for the selected cases with DAKOTA software;

This final report summarizes the Tractebel contribution, conclusions and recommendations, as well as other detailed information requested by IAEA to prepare the FUMAC project final report.

2. CONTRIBUTION FROM TRACTEBEL

2.1. Contribution during the 1st phase of the project (2014-2016)

Two selected Halden PWR LOCA Tests IFA-650.9 & 10 were first modelled with FRAPTRAN-1.5

- It is important to specify appropriate thermal hydraulic boundary conditions;
- The weaknesses of the relevant models in FRAPTRAN-1.5 were identified.

Deliverables:

- DDN/4NT/377789/000/00: FUMAC Interim report 1: Review of FRAPTRAN code for LOCA fuel behaviour modelling and safety evaluation;
- DDN/4NT/433919/000/00: FUMAC Interim report No. 2: Preliminary assessment of FRAPTRAN code for LOCA fuel behaviour modelling and safety evaluation;
- Jinzhao Zhang, Adrien Dethioux, Laurence Oury, Christoph Schneidesch, "FRAPTRAN 1.5 Modelling of the Halden LOCA Tests IFA650.9 and 10: Scoping Parametric Studies and Perspectives," Enlarged Halden Programme Group Meeting, Sandefjord, Norway, 8th – 13th May, 2016. (Public).

An axial fuel relocation as developed by QT was implemented, and relevant model uncertainty multipliers were identified and implemented in a TE version of the FRAPTRAN 1.5 code.

Deliverables:

- Jinzhao Zhang, “Code modification requirements specifications (CMRS) for extension and adaptation of FRAPTRAN-1.5 for LOCA fuel behaviour modelling,” Internal report FUELROD/4DO/0437004/000/00, Tractebel Engineering, Brussels, Belgium, February 2016. (Public);
- Lars Olof Jernkvist, “The FRAPTRAN-TE-1.5 computer program”, Report TR16-001, Quantum Technologies AB, March 2016.

Status report and recommendations to IAEA.

Deliverables:

- Jinzhao Zhang, Adrien Dethioux, Laurence Oury, Christoph Schneidesch, “Tractebel Contribution to FUMAC: FRAPTRAN 1.5 Modelling of the Halden LOCA Tests IFA-

650.9 and 10", IAEA FUMAC 2nd Research Coordination Meeting, Vienna, Austria, May 30 – June 2, 2016;
— Jinzhao Zhang, "FUMAC: Proposal for Uncertainty Analysis," IAEA FUMAC 2nd Research Coordination Meeting, Vienna, Austria, May 30 – June 2, 2016.

2.2. Contribution during the 2nd phase of the project (2016-2017)

Preparation of Specifications for Uncertainty Analysis on Modelling of the Halden LOCA Test IFA-650.10

Deliverables:

— DDN/4NT/520044/000/00: IAEA FUMAC CRP - Specifications for Uncertainty Analysis on Modelling of the Halden LOCA Test IFA-650.10. (Public)

Assessment of the model improvements in the TE version of the FRAPTRAN-1.5 code with the 2 selected Halden PWR LOCA Tests IFA-650.9 & 10.

— Refining the FRAPTRAN input models
— Consideration of the axial power distribution
— Choice of the appropriate properties and models;
— Use of the T/H boundary conditions from system T/H code calculations (SOCRAT);
— Verification of the improvements to FRAPTRAN-1.5 modelling of fuel behaviours under LOCA.

To perform sensitivity and uncertainty analysis using the DAKOTA tool

— to identify the most important parameters (fuel data, models and experimental conditions) to be considered
— to quantify the uncertainties of fuel data, models and experimental conditions on the predicted results

Final report to IAEA (this report).

Deliverables:

— DDN/4NT/544355/000/00: FUMAC Interim report No. 3: Assessment of FRAPTRAN code for LOCA fuel behaviour modelling and safety evaluation.
— DDN/4NT/559449/000/00: FUMAC Interim report No. No. 4: Statistical Uncertainty and Sensitivity Analysis on the FRAPTRAN-TE-1.5 Modelling of the Halden LOCA Tests IFA-650.9 and IFA650.10.
— Jinzhao Zhang, Adrien Dethioux, Thomas Drieu, Bernard Quivy, Christophe Schneidesch, "Statistical Uncertainty and Sensitivity Analysis on the FRAPTRAN-TE-1.5 Modelling of the Halden LOCA Tests IFA-650.9 and IFA650.10," Enlarged Halden Programme Group Meeting (EHPG2017), Lillehammer, Norway, September 24-29, 2017. (Public).

3. MODEL IMPROVEMENTS IN FRAPTRAN-TE-1.5

FRAPTRAN code is a fuel rod transient analysis code, designed to calculate the thermal and mechanical behaviour of LWR single fuel rod during fast reactor power and coolant transients, e.g. hypothetical accident and operation transients such as reactivity accidents (RIA) or loss-of-coolant accidents (LOCA), and power oscillations without scram.

The latest version is FRAPTRAN-1.5. It has been released in May 2014. The code is described in [6] and the integral assessment in [7].

The fuel behaviours during LOCAs have been extensively studied during the last decades [2]. Recent LOCA tests, performed in Halden, Norway, and Studsvik, Sweden, have revived

interest in the fuel relocation and dispersion phenomena, since the test results suggest that high burnup fuel pellets may pulverize into very fine fragments, with a higher potential for axial relocation and subsequent dispersal, than observed for low to medium burnup fuel in early tests. This issue is a current research area, which is being addressed by the Working Group on Fuel Safety (WGFS) of the Nuclear Energy Agency (NEA) Committee on the Safety of Nuclear Installations (CSNI). It is also identified as a key issue in the ongoing IAEA coordinated research project FUMAC.

In a recent project funded by the Swedish Radiation Safety Authority (SSM), Quantum Technologies AB developed a computational model for axial fuel relocation under LOCA [14]. The relocation model has been fully integrated with an in-house SSM/QT-version of the fuel rod analysis program FRAPTRAN 1.5. In contrast to earlier relocation models for fuel rod analysis programs (such as the one developed by SCK•CEN [12]), the model considers thermal feedback effects from the fuel relocation. It also uses submodels to estimate the packing fraction and effective thermal conductivity of particle beds formed by crumbled fuel in ballooned regions of the fuel rod, based on the estimated state of fragmentation and pulverization of the fuel pellets. Models in the SSM/QT-version of FRAPTRAN 1.5, including the fuel relocation model, were validated against recent LOCA tests in Halden and Studsvik [16].

Tractebel has used FRAPTRAN-1.5 to simulate the selected Halden LOCA tests, and has found that FRAPTRAN-1.5 is able to well simulate the cladding burst and corrosion behaviour, with imposed measure cladding temperature. However, the current version of FRAPTRAN-1.5 is unable to well simulate some other phenomena like the axial relocation.

In the FUMAC project, Tractebel intends to improve and use the FRAPTRAN-1.5 code for better simulation of the fuel behaviours during LOCA, including the axial relocation. TE has reviewed the capability of FRAPTRAN-1.5 and made the preliminary assessment for LOCA simulation. The preliminary scoping parametric analyses recommended improving certain models in FRAPTRAN-1.5, in particular the heat transfer boundary conditions and the axial relocation model [17].

Therefore, Tractebel requests the Quantum Technologies to implement their model in the Tractebel version of FRAPTRAN-1.5 [18], in order to perform further model validation and improvements.

The extensions and adaptations in the FRAPTRAN-TE-1.5 code are documented in the Quantum Technologies report [19]. They mainly consist in three parts:

- Introduction of the QT axial fuel relocation model, and integration of the model with the thermal solution model in FRAPTRAN-1.5 [14];
- Corrections of observed errors in the algorithms and source code of the original (PNNL) version of FRAPTRAN-1.5 [15];
- Introduction of additional input to FRAPTRAN-1.5 to enable uncertainty analyses by statistic methods. The additional input allows the user to impose variations on about thirty model parameters and material properties as requested in [17].

The correctness of the code changes has been verified by comparing calculated results with simple analytical solutions. In addition, FRAPTRAN-TE-1.5 has also been validated against three LOCA simulation experiments in the Halden IFA-650 series of tests. The results of this testing are summarized, and recommendations for further testing and for using different modelling options in FRAPTRAN-TE-1.5 program are given, based on the test results [16].

4. FRAPTRAN MODELLING OF HALDEN LOCA TESTS IFA-650.9 AND IFA-650.10

4.1. FRAPTRAN modelling assumptions

In order to simulate the fuel rod conditions before the LOCA tests, FRAPCON input models are built to generate initial conditions for FRAPTRAN analysis.

In both FRAPCON and FRAPTRAN input models, most of the data are set according to the specifications of IFA-650 tests or the code manual recommended values. The test rodlet data and conditions are summarized in the following table:

TABLE 1. SUMMARY OF THE TEST RODLE DATA AND CONDITIONS

Fuel rodlet design data	IFA-650.9	IFA-650.10
Rod outer diameter (mm)	10.75	9.50
Rod inner diameter (mm)	9.3	8.36
Pellet diameter (mm)	9.13	8.19
Stack length (mm)	480	440
Plenum free volume (cm^3)	19.0	17.0
Pellet height (mm)	8.0	13.78
Dish radius (mm)	3.965	3
Dish depth (mm)	0.25	0.32
UO_2 Enrichment (%)	3.50	4.49
Pellet density (%TD)	95.2	95.32
Pellet roughness (μm)	2.0	2
Expected density increase (kg/m^3)	98.64	98.64
Cladding type	Duplex Zry-4	Zry-4
Cladding heat treatment	SRA	SRA
Cladding cold work	0.5	0.5
Cladding roughness (μm)	1.0	1
Rod pitch (mm)	12.6	12.6
Fuel rodlet initial state		
Fuel average burnup (Mwd/kgU)	89.9	61
Oxide thinkness (μm)	8.0	30
Hydrogen concentration (wppm)	30	150-220
Fill gas pressure at 295 K (MPa)	4.0	4.0
Test conditions	IFA-650.9	IFA-650.10
Rodlet initial LHGR (kW/m)	2.60	1.37
Peak cladding temperture (K)	1475	1114
Hearter initial LHGR (kW/m)	1.6	1.2
Coolant initial pressure (MPa)	15.5	15.5
Coolant initial inlet temperature (°C)	287	287
Coolant initial mass flux (kg/m^2s)	0	0
Fast flux (n/m^2s per kW/m)	$4 \cdot 10^{16}$	$4 \cdot 10^{16}$

The results of the FRAPCON calculation with refabricated rodlet FRAPCON-3.5 input model are compared with available measured data, in particular the rod average burnup, oxidation and hydrogen concentration, as shown in the following table.

TABLE 2. PREDICTED ROD STATE AFTER PRE-IRRADIATION

	IFA650.9	IFA650.10
Rod average burnup (MWd/kgU)	90.5 (89.9)	61.06 (61.0)
Oxide thickness (μm)	9 (8)	22 (30)
Hydrogen concentration (wppm)	47 (30)	184 (150–220)

The refabricated rodlet FRAPTRAN-TE-1.5 initialization file is the output of FRAPCON-3.5 input model which contained gas data from the initial father rod and subsequent Fission Gas Release (FGR) history data. The number of moles of new gas mixture and the relative amount of each gas species in the refabricated rodlet are adapted to match the calculated and measured initial rod internal pressure (4.0 MPa).

The default options in FRAPTRAN-TE-1.5 are selected for most of the models, namely:

— The FRACAS-I rigid pellet model (finite difference model) for fuel rod mechanical response (mechan=2);
— The default “gasflo” model, allowing to evaluate the gas flow between the plenum and the balloon, considering the reduction of the flow section between the fuel and the pellet when the gap gets closed at high burn-up.

The Massih model for Fission Gas Release.

— The Cathcart-Pawel (C-P) model for high temperature oxidation.
— The non-protective initial oxide layer option [13].

In the reference case (P0), the following specific model options are made:

— The default BALON2 high temperature clad failure model based on empirical strain and stress limits for the burst (pitch value > 0) is activated;
— The axial relocation model is deactivated.

The re-fabricated rodlet have the same number of nodalization: 45 radial nodes and 40 axial nodes for both in FRAPCON and FRAPTRAN (about 15 mm per node).

During the test, the rod power is set constant, and the axial power profile in the rodlet is nearly symmetric, with an axial peak to average power factor of 1.04–1.05.

The “Heat” option is selected, the axial coolant temperatures and coolant-cladding heat transfer coefficient as calculated by SOCRAT code [20] are imposed as boundary conditions, and FRAPTRAN will calculate the cladding temperatures. The clad to coolant heat transfer coefficients are determined from the SOCRAT calculated total heat flux (radiative + convective), namely HTC = Qtot / (Tclad – Tcool), for each axial node. For simplicity, only 3 pairs of the SOCRAT calculated thermal hydraulic conditions are imposed at bottom, mid and top of the test rod, consistent with the cladding temperature measurements. The coolant channel is simulated by 3 zones (each for 15 axial nodes of the fuel rod); each corresponds to the imposed coolant temperature and heat transfer coefficient.

The external plenum is modelled and the external plenum gas temperature history is considered equal to the coolant temperature calculated by SOCRAT at the external plenum elevation.

A steady-state period of at least 100 s is imposed for the simulations: the LOCA transient is assumed to occur at 100 s and to end after the scram time at 600 s.

The maximum time step is 0.1 s during the steady-state and 0.001 s during the transient.

4.2. Parametric studies

In the parametric study (P1), the 'noball' option is used, which will deactivate the default ballooning model (BALON2). The code will predict rupture when the cladding effective plastic strain exceeds the instability strain.

In the second parametric study (P2), the "axial relocation" option model is used, together with the 'noball' option that deactivates the default ballooning model (BALON2). The calibrated axial relocation model associated parameters are in the following table:

TABLE 3. SUMMARY OF THE RELOCATION MODEL RELATED PARAMETERS FOR IFA-650.9 AND -650.10

Parameters	IFA650.9	IFA650.10
Sigburststrain	1.0	0.45
Sigcladanneal	0.15	0.1
Sigcladyieldstress	1.05	1.30
Packing fraction	0.72	0.72

In the third parametric study (P3), the FEA model will be used (P2+FEA), instead of the default FRACAS I model.

4.3. Results for Halden LOCA Test IFA-650.9

The results of comparison between calculated and measured fuel rod pressure for IFA-650.9 are presented in **Error! Reference source not found.**. While the different modelling choices for the calculation show limited impact, a clear divergence is observed between calculations and the measure. The more plausible explanation to this divergence is the inability of FRAPTRAN to model pressure gradients. Axial gas flow may be partially obstructed in the fuel rod leading to a higher plenum pressure (the rod internal pressure is measured in the plenum). This can also explain the delayed cladding rupture after the beginning of the ballooning.

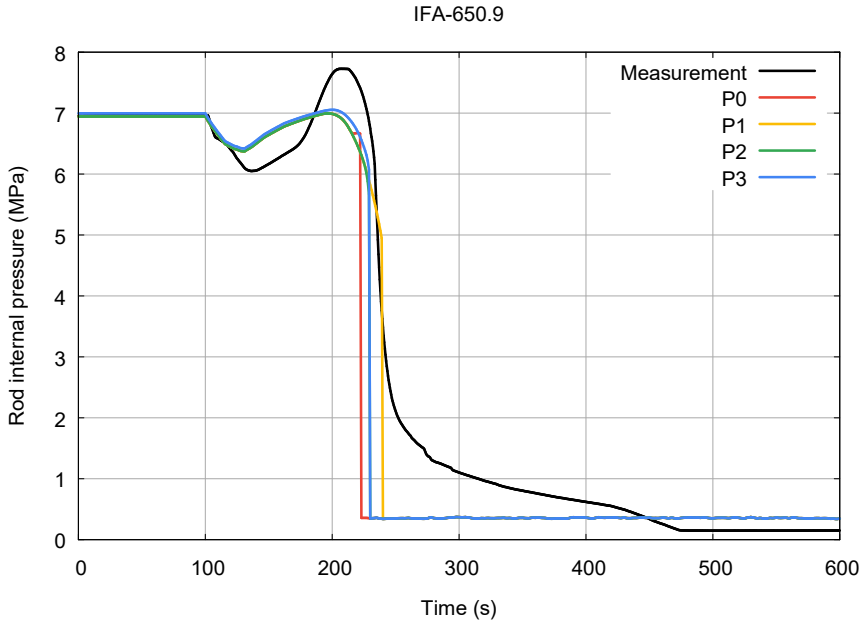

FIG. 1. IFA-650.9 - Rod internal pressure.

A comparison of measured and calculated cladding surface temperature histories is presented in Fig. 2 and in Fig. 3, respectively corresponding to the lower part (elevation 100mm – TCC1) and the upper part (elevation 415mm – TCC2) of the fuel rod.

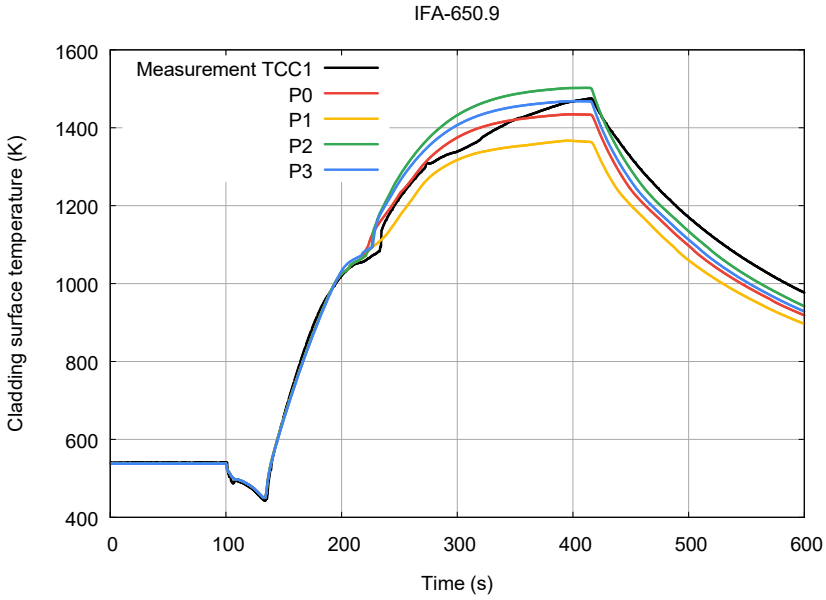

FIG. 2. IFA-650.9 - Cladding surface temperature at elevation 100 mm.

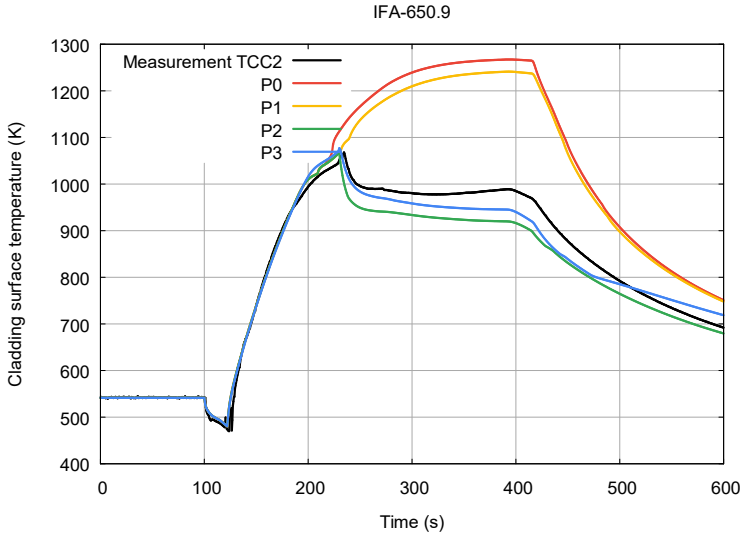

FIG. 3. IFA-650.9 - Cladding surface temperature at elevation 415 mm.

The Figs show that, up to 225 s, an excellent agreement is observed between the measured and calculated results. After 225 s – time of rupture, a clear deviation is observed between the calculated cases with the relocation model activated and the ones without relocation model. In the lower part of the fuel rod, a slight increase of the cladding temperature is observed for case with relocation. In the upper part of the fuel rod, an important temperature drop is observed due to the relocation of the fuel downward the rod. As expected, this phenomenon is correctly predicted only by cases P2 and P3 for which the relocation model is activated.

Fig 4 represents the equivalent cladding reacted as a function of the elevation at the end of the test. No measurements are available for this parameter. The important peak at burst elevation seems to cause numerical errors when the FRACAS-1 model is used. As the cladding failed at this elevation, it is difficult to state that it is incorrect. Only the FEA model seems stable enough to provide a realistic value of the equivalent cladding reacted at this location. In addition, the benefit of the relocation model can be observed here. The absence of fuel at the top following its relocation induce a lower equivalent cladding reacted.

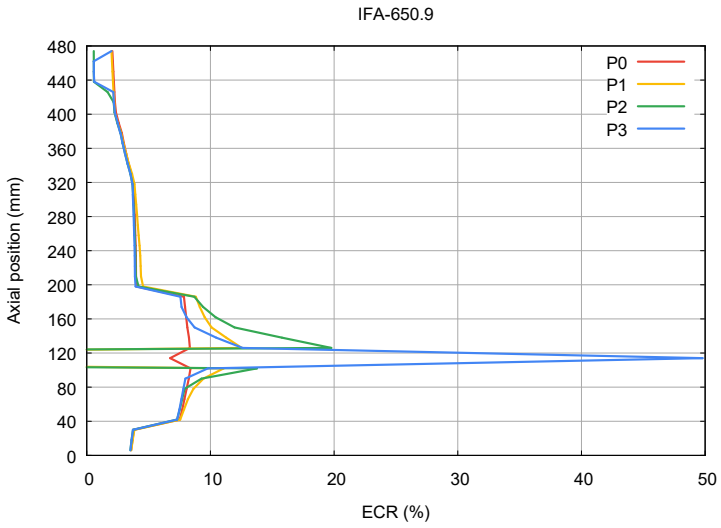

FIG. 4. IFA-650.9 - Equivalent cladding reacted.

Figure 5 represents the axial variation of the cladding outer surface radius at the end of the test.

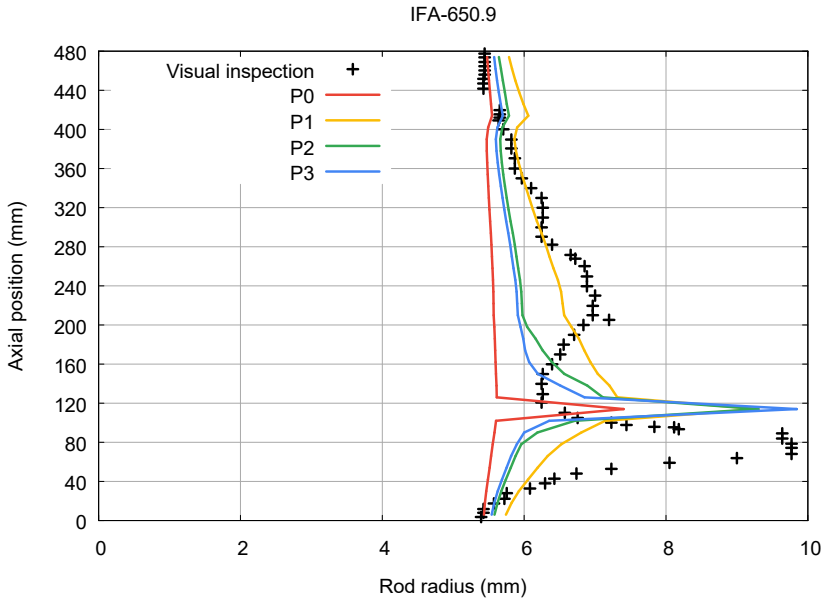

FIG. 5. IFA-650.9 - Rod radius.

The visual inspection of the fuel rod shows that, in addition to the main deformation at the burst location, a second smaller ballooning occurred approximately at mid-height of the fuel rod. This information tends to confirm the observations based on the rod internal pressure – the assumption of pressure gradient due to partial obstruction of gas flow inside the rod. The calculation results confirm also that, as FRAPTRAN does not consider any pressure gradient, it is unable to predict the second ballooning. In addition, if the pressure gradient capability was to be added in FRAPTRAN, a more precise description of the boundary conditions might be required to predict correctly the second ballooning. Indeed, in the present calculations, the boundary conditions are described at three axial elevations while at least 15 might be necessary to predict such a gradient.

The comparison of the modelling choices shows a good prediction of the cladding radius change of the main ballooning as long as the default model BALON is deactivated.

The cladding total hoop strain (Fig. 6) is another good indicator of the cladding radius deformation. The cladding total hoop stress (Fig. 7) shows that the FEA predict a more important pressure applied on the cladding at burst elevation. This reflects the more localized deformation observed previously.

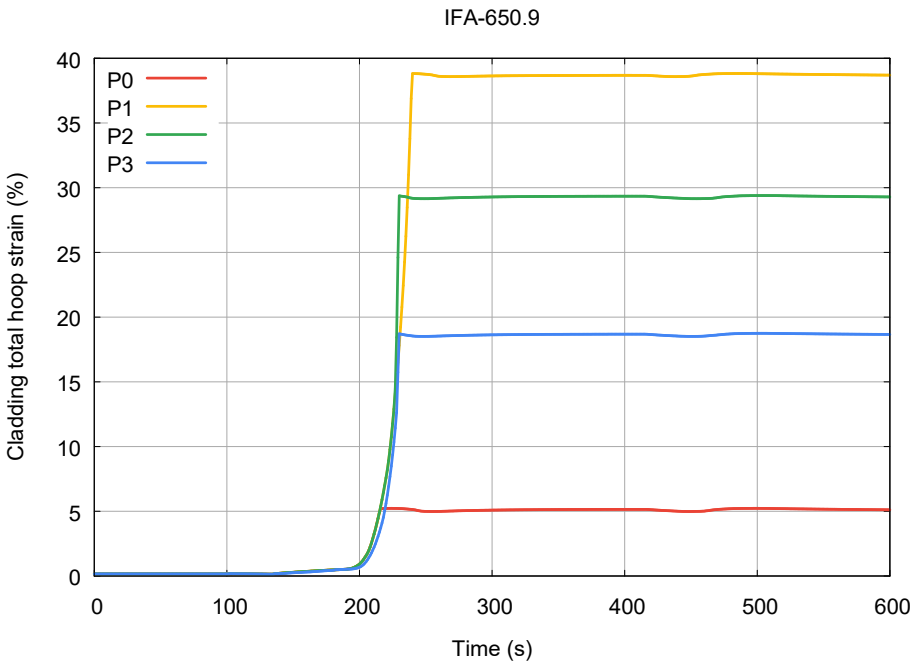

FIG. 6. IFA-650.9 - Cladding total hoop strain at burst elevation.

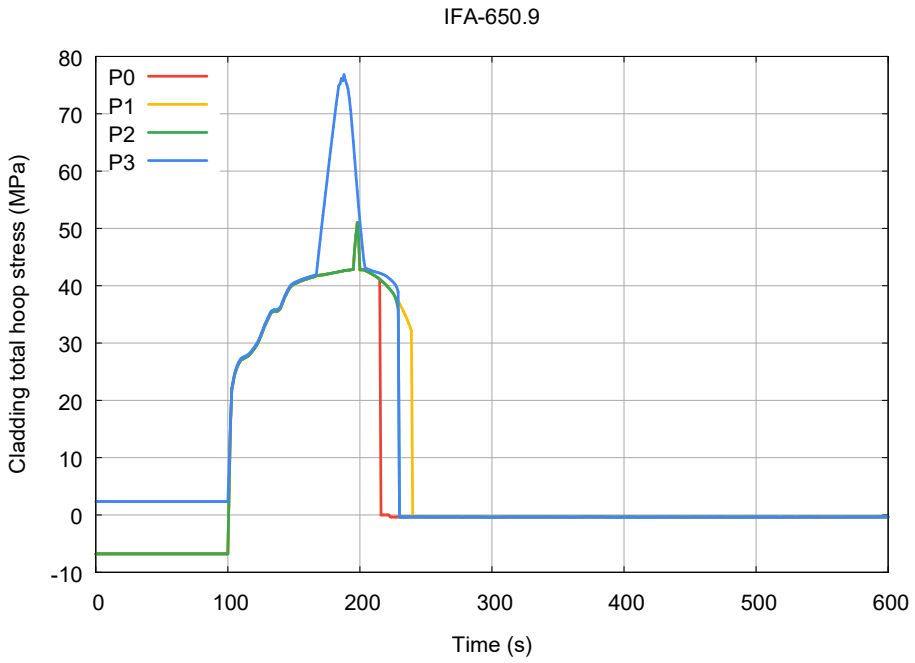

FIG. 7. IFA-650.9 - Cladding total hoop stress at burst elevation.

Figure 8 presents the evolution of the cladding elongation during the test. It shows that the evolution of the cladding elongation is correctly predicted only if either the BALON model or the FEA model is activated. As the BALON model is incompatible with the axial relocation option, this indicates that we should always use the FEA model instead of the FRACAS-1 model if we intend to use the relocation option.

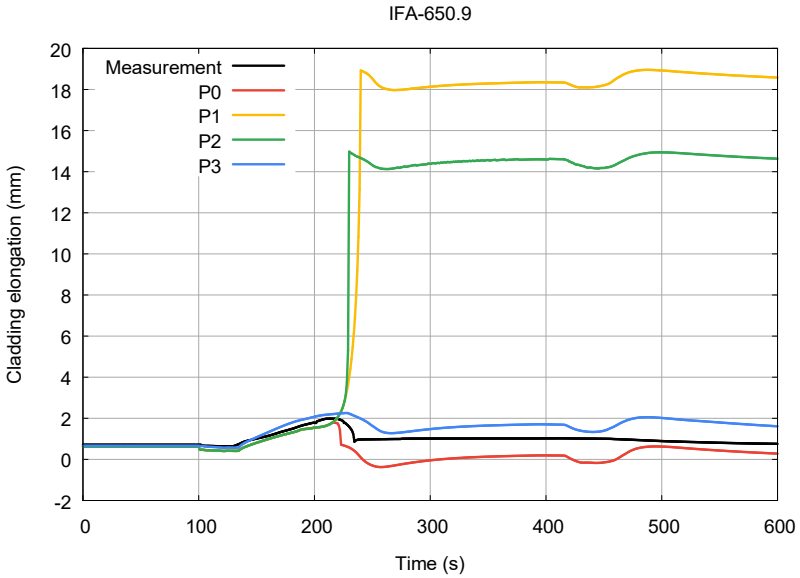

FIG. 8. IFA-650.9 - Cladding elongation.

4.4. Results for Halden LOCA Test IFA-650.10

The comparison between the calculated and the measured rod internal pressure is presented in Fig. 9. The first phase is well predicted by FRAPTRAN simulations. However, in all the simulations, the cladding rupture occurs 25 s later than the measurement. The residual pressure indicated by the measurements is about 1.2 MPa. This is due to mechanical constraints in the pressure sensor. The pressure drops to the coolant pressure (0.4 MPa). This is well predicted by the calculations.

By comparing the different calculation options, no case is clearly identified to have better results. Only the case P0, using the BALON model seems to have a better shape just before the pressure drop.

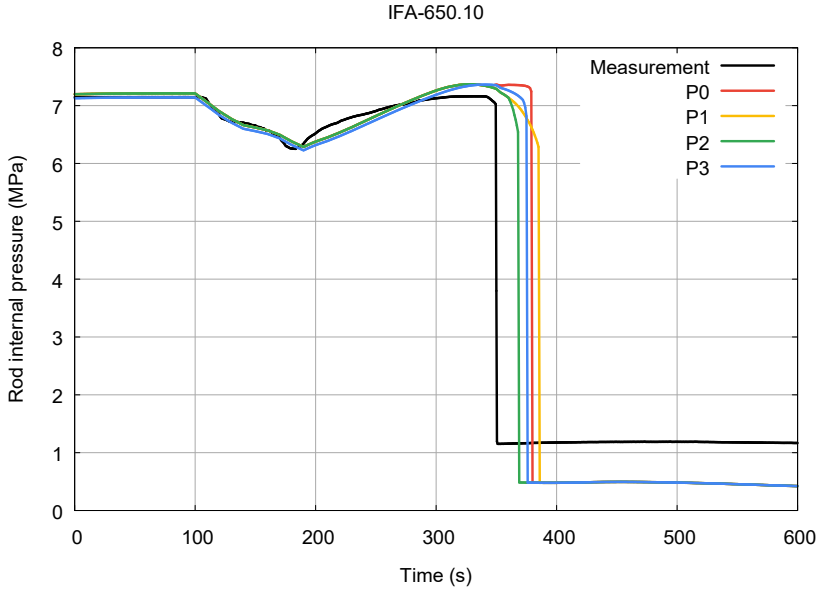

FIG. 9. IFA-650.10 - Rod internal pressure.

In Fig. 10 and Fig. 11, the cladding surface temperatures are presented as a function of time at elevations of, respectively, 95 mm (TCC1) and 361mm (TCC2).

At elevation 95 mm, the calculated temperatures under-predict slightly the measured temperature. However, the shape of curve indicate tends to indicate a correct calculated behaviour.

At elevation 361mm, the results are in better agreement with the measurement. The only discrepancy is observed for the temperature drop after 525 s.

As there is almost no relocation in this case, no differences are observed between the calculated cases.

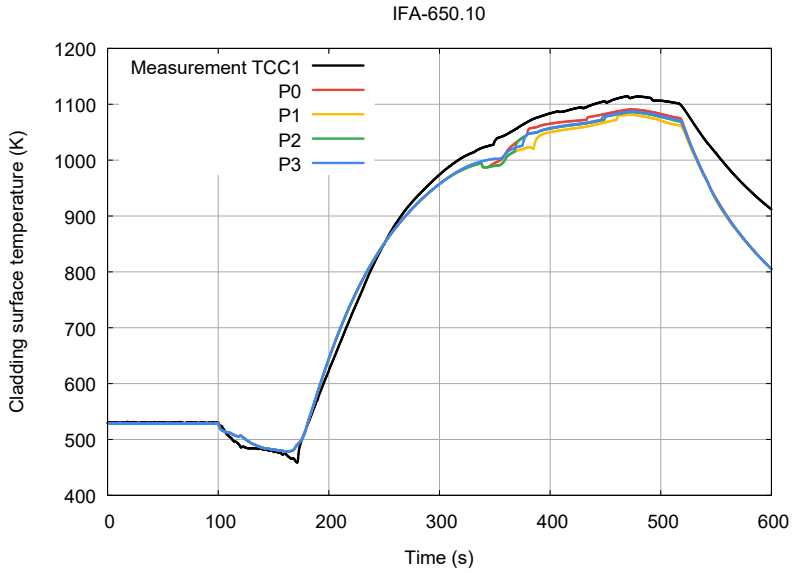

FIG. 10. IFA-650.10 - Cladding surface temperature at elevation 95 mm.

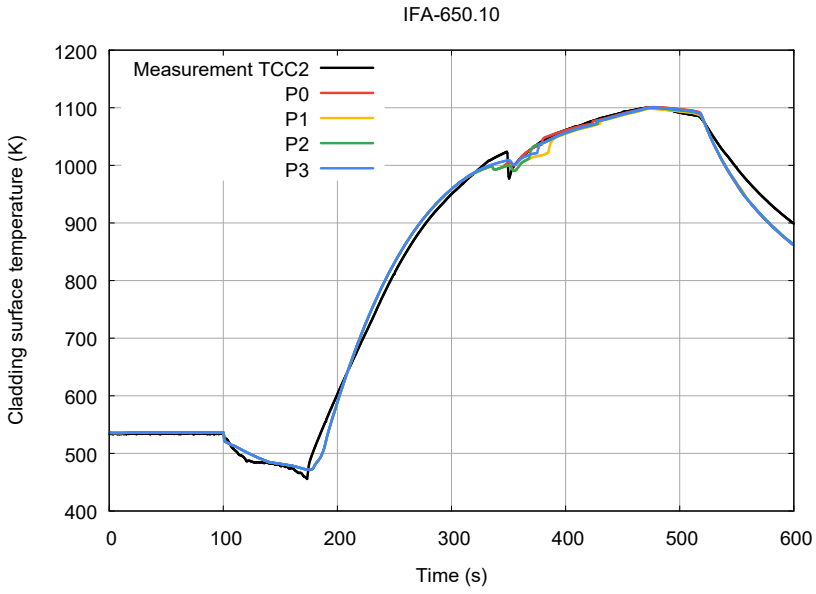

FIG. 11. IFA-650.10 - Cladding surface temperature at elevation 361 mm.

The equivalent cladding reacted at the end of the test is presented as a function of the axial elevation in Fig. 12. As for IFA-650.9, no measurements were done for this parameter. The effect of the use of the relocation model can be observed here. Indeed, the 3 cases using the relocation model present higher ECR at the burst elevation. The use of the FEA model, however, tends to reduce this effect. The results obtained by use of the FEA seem to be more reliable. As seen in IFA-650.9, FEA is much more stable than FRACAS-1 in case of ballooning.

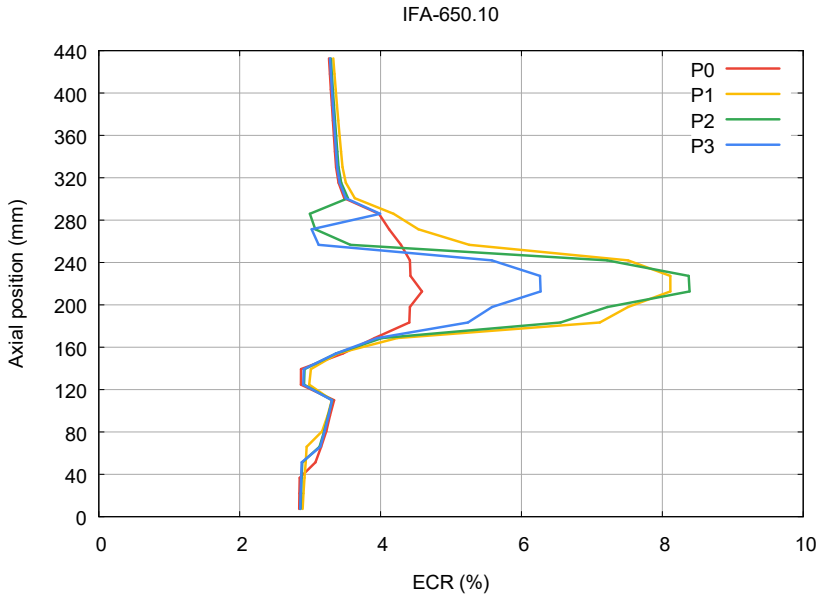

FIG. 12. IFA-650.10 - Equivalent cladding reacted.

The rod diameter at the end of the test as a function of the axial elevation is presented in Fig. 13. The comparison of the calculated results to the visual inspection show that, despite a slight shift of the predicted elevation of ballooning occurrence, the calculations present a good prediction of the size of the ballooning.

The main difference observed between the calculations is the width of the balloon. In this case, the FRACAS-1 model seems to present better predictions than the FEA model. However, the FEA model offers more progressive deformation over the entire rod, which is more realistic.

Concerning the cladding total hoop strain and stress (Fig. 14 and Fig. 15), the observations made for case IFA-650.9 remain valid.

As for test rod IFA-650.9, the cladding elongation is reasonably well predicted only if either the BALON model or the FEA model is activated (Fig. 16). However, for this test, FRACAS-1 is unable to predict the correct behaviour of the cladding elongation after the pressure drop (~ 375 s). On the other hand, the FEA model presents more realistic result.

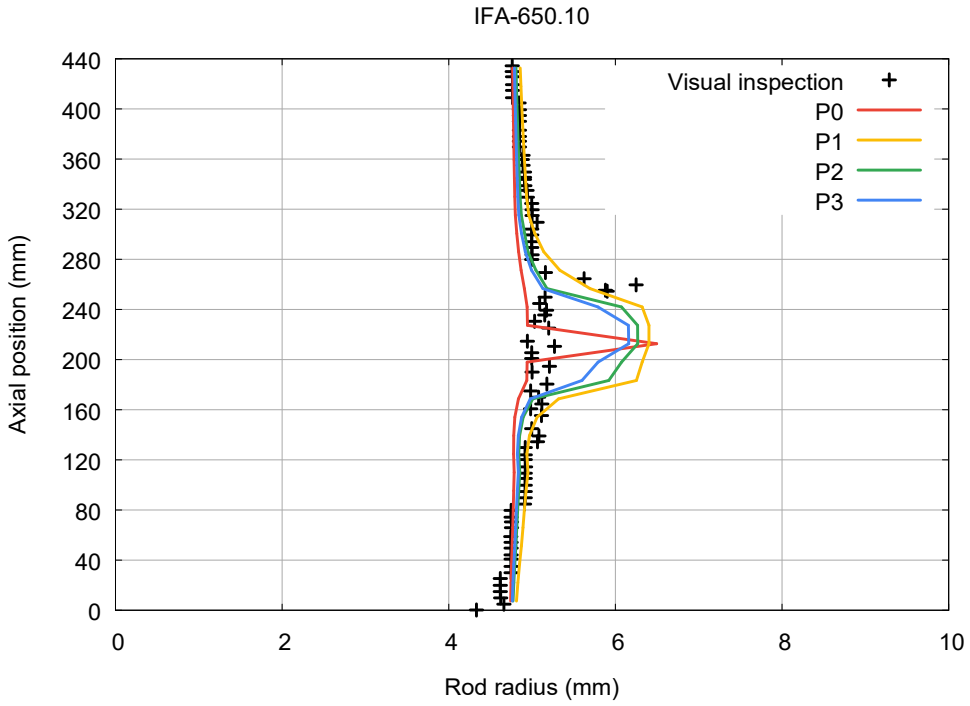

FIG. 13. IFA-650.10 - Rod radius.

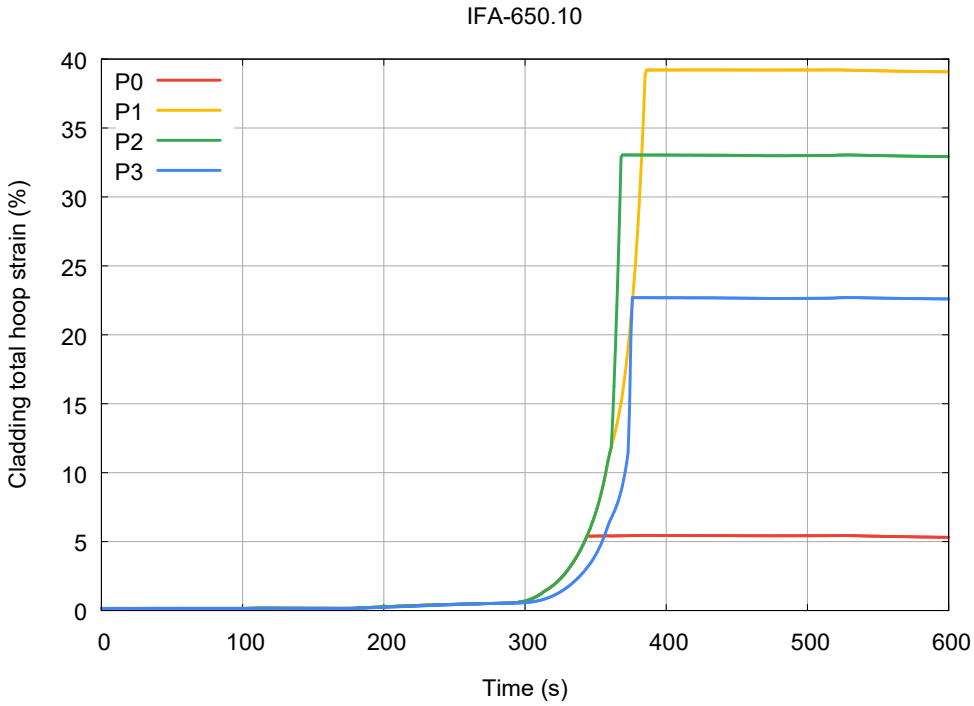

FIG. 14. IFA-650.10 - Cladding total hoop strain.

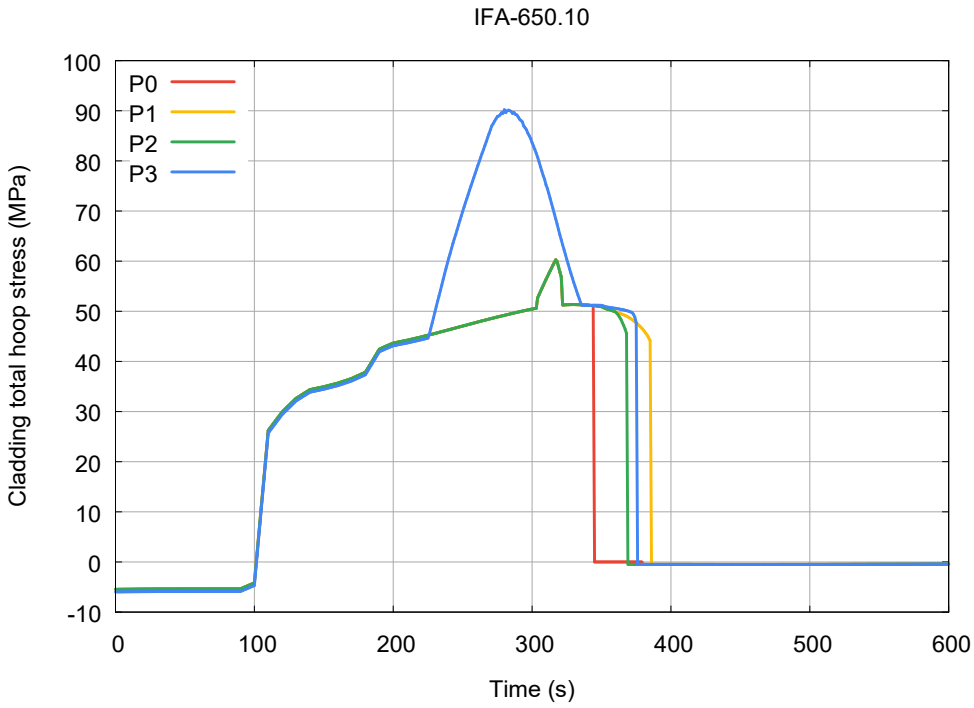

FIG. 15. IFA-650.10 - Cladding total hoop stress.

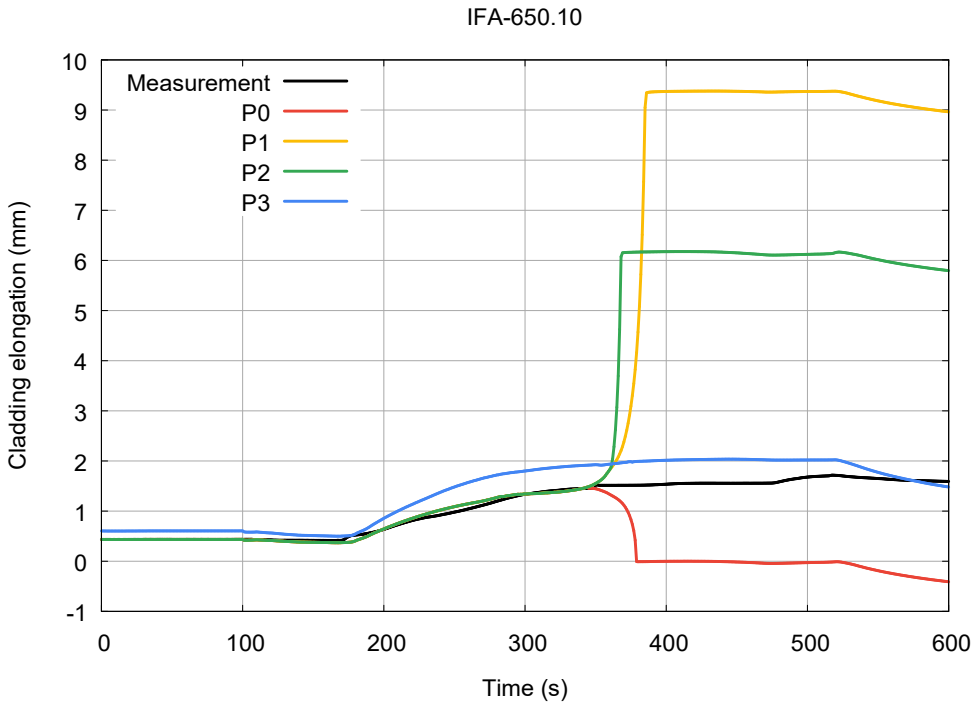

FIG. 16. IFA-650.10 - Cladding elongation.

4.5. Conclusion

The two selected Halden PWR rod LOCA tests, IFA-650.9 and IFA-650.10, are simulated using the adapted FRAPTRAN-TE-1.5 code.

The thermal boundary conditions (axial power profile, external plenum gas temperature) are improved according to the specifications, and the thermal hydraulic modelling by using the imposed thermal hydraulic boundary conditions from SOCRAT calculations.

These two experiments are modelled using different major options of FRAPTRAN-TE-1.5:

- With/without axial relocation model;
- With/without ballooning model;
- Mechanical model: FRACAS-1 or FEA.

The results show that:

- The rod pressure evolution of IFA-650.9 was not well predicted;
- The double-ballooning in IFA-650.9 was not well predicted;
- The relocation model + FEA gave better prediction on the mechanical behaviour.

However, our parametric studies give more insights:

- The default mechanical model (FRACAS-I) with ballooning model under predicts the ballooning but predicts better the rupture behaviour;
- The default mechanical model (FRACAS-I) with non-ballooning model over predicts the ballooning but predicts later rupture behaviour;
- The default mechanical model (FRACAS-I) with non-ballooning and relocation model predicts better the cladding temperatures (in particular for IFA-650.9), the ballooning and rupture behaviour (in particular IFA-650.10);
- Only the FEA model predicts better the cladding elongation.

The following conclusions are speculations, which may need to be verified:

- The gas temperature model (=imposed SOCRAT coolant temperature) seems appropriate.
- The measured rod pressure evolution for IFA-650.9 may be questionable due to the ‘double ballooning’ and significant relocation (gas flow within rodlet?).
- The absence of double ballooning in IFA650.9 may be attributed to the rough T/H boundary conditions: A refined nodalization of the T/H boundary conditions (e.g., 6 or 12 nodes) may be helpful (see SOCRAT’s prediction [20])

5. STATISTICAL UNCERTAINTY AND SENSITIVITY ANALYSIS FOR IFA-650.10

5.1. Specifications and Implementation

The specifications for the statistical uncertainty and sensitivity analysis are given in details in reference [21] for Halden LOCA test IFA-650.10 (without significant axial fuel relocation).

TABLE 4. SUMMARY OF THE UNCERTAINTY PARAMETERS FOR IFA-650.10.

Input uncertainty parameter	Distribution				
	Mean	Standard Deviation	Type	Lower bound	Upper bound
Cladding outside diameter (mm)	9.50	0.01	Normal	9.48	9.52
Cladding inside diameter (mm)	8.36	0.01	Normal	8.34	8.38
Pellet outside diameter	8.2	0.01	Normal	8.18	8.22
Fuel theoretical density (kg/m3 at 20 °C)	10457	50	Normal	10357	10557
U^{235} enrichment (%)	4.487	0.05	Normal	4.387	4.587
Filling gas pressure (MPa)	4.0	0.05	Normal	3.9	4.1
Relative power during base irradiation	1	0.01	Normal	0.98	1.02
Relative power during test	1	0.025	Normal	0.95	1.05
Test rod power profile	1	0.01	Normal	0.98	1.02
Cladding temperature (°C)	1	10	-	T-20	T+20
Coolant temperature (°C)	1	5	-	T-10	T+10
Clad-to-Coolant heat transfer coefficient (Same Coef. applied for all flow regimes)	1	0.125	Normal	0.75	1.25
Fuel thermal conductivity model	1.00	5%	Normal	0.90	1.10
Clad thermal conductivity model	1.00	5%	Normal	0.90	1.10
Fuel thermal expansion model	1.00	5%	Normal	0.90	1.10
Clad thermal expansion model	1.00	5%	Normal	0.90	1.10
Fuel densification model	1.00	5%	Normal	0.90	1.10
Fuel solid swelling model	1.00	5%	Normal	0.90	1.10
Fuel gaseous swelling model	1.00	5%	Normal	0.90	1.10
Clad Yield stress	1.00	5%	Normal	0.90	1.10
Fuel heat capacity	1.00	1.5%	Normal	0.97	1.03
Cladding heat capacity	1.00	1.5%	Normal	0.97	1.03
Cladding elastic modulus	1.00	5%	Normal	0.90	1.10
Cladding corrosion model during steady-state operation	1.00	12.5%	Normal	0.75	1.25
Cladding hydrogen pickup fraction during steady-state operation	1.00	15%	Normal	0.7	1.30
Cladding oxidation model at high temperature	1.00	15%	Normal	0.7	1.30
Thermal conductivity of the oxide layer	1.00	10%	Normal	0.80	1.20
Fission gas release (or gas diffusion coefficient)	1.00	25%	Normal	0.50	1.50
Gap gas conductivity	1.00	12.5%	Normal	0.75	1.25
Fuel/cladding emissivity	1.00	5%	Normal	0.90	1.10
Fuel radial relocation	1.00	10%	Normal	0.80	1.20
Fuel fragment packing fraction (if applicable)	1.00	10%	Normal	0.80	1.20

TABLE 4. SUMMARY OF THE UNCERTAINTY PARAMETERS FOR IFA-650.10.

Input uncertainty parameter	Distribution				
	Mean	Standard Deviation	Type	Lower bound	Upper bound
Cladding strain threshold for fuel mobility (if applicable)	1.00	10%	Normal	0.80	1.20
Cladding Meyer hardness	1.00	5%	Normal	0.90	1.10
Cladding annealing	1.00	5%	Normal	0.90	1.10
Cladding burst criteria	1.00	10%	Normal	0.80	1.20
Cladding burst strain criteria	1.00	10%	Normal	0.80	1.20
Plenum gas temperature (°C)	–	5	–	T-10	T+10

The same specifications are adapted for Halden LOCA test IFA-650.9 (with significant axial fuel relocation).

The following deviations from the specification are implemented:

(a) The following input uncertainties are not implemented:

- Uncertainties related to the cladding temperature, as the coolant temperature is used as boundary condition. However, the uncertainties related to the coolant temperature and the heat transfer coefficient are implemented;
- The uncertainty on coolant pressure has been added, but is shown to have no significant impact.

(b) Calibrated axial relocation model associated parameters.

The same calibrated parameters as IFA-650.9 in Table 2 are used in the calculation.

- Clad annealing factor is set to 0.15 instead of 1.00;
- Clad yield stress factor is set to 1.05 instead of 1.00;
- The packing fraction is set to 0.72 instead of 1.00;
- The uncertainty for the calibrated parameters in Table 3 are not modified.

Two cases are performed:

(c) In the reference case (P0), the following specific model options are made:

- The default BALON2 high temperature clad failure model based on empirical strain and stress limits for the burst (pitch value > 0) is activated;
- The axial relocation model is deactivated.

(d) In the parametric study (P1):

- The default BALON2 high temperature clad failure model based on empirical strain and stress limits for the burst (pitch value > 0) is deactivated;
- The axial relocation model is activated.

The maximum time step is 0.1 s during the steady-state and 0.001 s during the transient and 0.0002 s during the burst period. Short time steps have been made necessary for the uncertainty studies, due to the decreased stability of some calculations.

5.2. Reference case without axial relocation model (P0)

5.2.1. Uncertainty analysis results

The FRAPTRAN-TE-1.5 calculation results of the first 200 successful runs are collected, and the 5th and 196th ranks are chosen to estimate the upper/lower (95%/5%) uncertainty bounds (LB, UB) of the output parameter of interest. The reference case results (Best-Estimate or BE) are also presented, using all input parameters at their mean (or nominal) values. The calculated reference, upper and lower bounds are compared with the available measured data (Experimental) in the following Figures.

— Rod internal pressure (MPa)

As the reference rod internal pressure agrees remarkably well with the experimental data, it is also well bounded by the uncertainties. The pressure is a little underestimated just after the blowdown, but both burst instant and peak pressure are well predicted. This confirms that the thermal aspects are well modelled by FRAPTRAN. Since the fuel axial relocation and deformation are known to be much weaker in this test, the weaknesses in the mechanical deformation models and lack of axial relocation model have no consequences on the pressure.

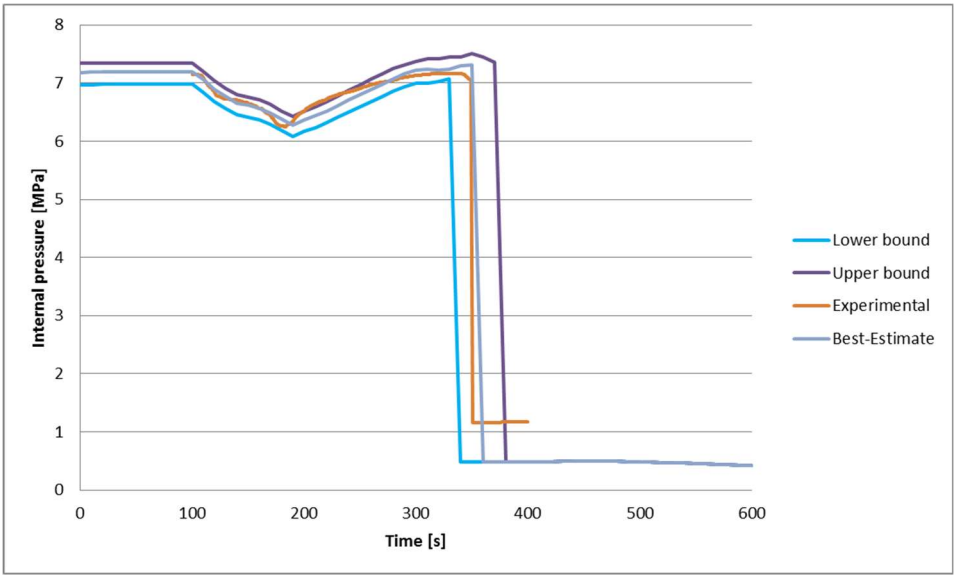

FIG. 17. IFA-650.10 - Rod internal pressure.

— Clad outer surface temperature (K)

Since the location of the calculated cladding surface temperature at burst node is not precisely the one of the measurements, the results are different from those in Fig. 10 and Fig. 11. In the heatup phase of this calculation, the cladding outer surface temperature is above the experimental data, even when the uncertainties are accounted.

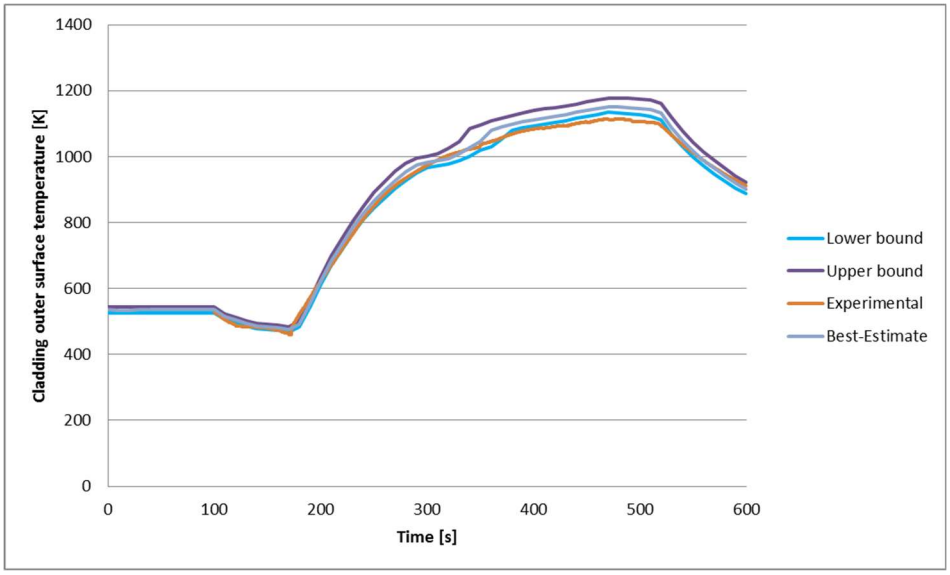

FIG. 18. IFA-650.10 - Clad temperature.

— Clad elongation (mm)

The predicted clad elongation has large initial uncertainty, which nearly disappears with blowdown. The difference could be due to that the definition of the starting points are different in the calculations and in the experiment. A correction would probably be useful, but would be difficult to determine as it depends on certain uncertain parameters.

The trend from blowdown to burst is well represented. However, same as shown in Fig. 16, with BALON2 model being activated, FRACAS-1 is unable to correctly predict the behaviour of the cladding elongation after the burst (the FEA model seems do a better job, but is not used in this case). The uncertainty band follow the same trend as the reference case. This shows that the mechanical deformation model is not sufficiently good and shall be improved. Those improvements can be on the use of the code (calibration, input data, meshing...) or the modification of the models (improved ballooning model, or use of FEA).

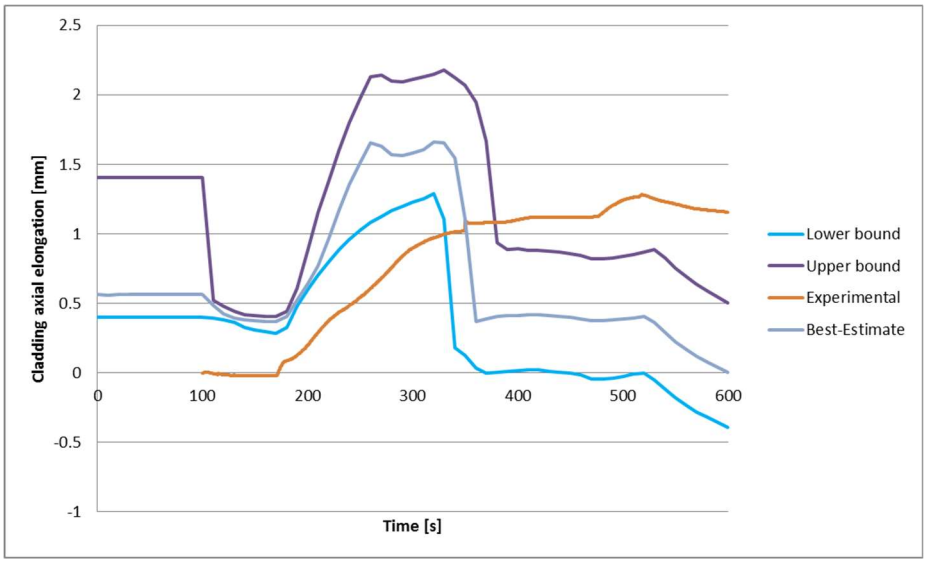

FIG. 19. IFA-650.10 - Clad elongation.

— Clad strain (%)

The uncertainties on the cladding diameter are rather weak, except for in the bottom part. This means that there are more phenomena of interest occurring in that bottom part, leading to

larger uncertainties. The fact that the uncertainty analysis does not cover the experimental data confirms that the models used are not adequate for all phenomena. Indeed, the axial fuel relocation model might have been used to predict a sufficiently large balloon at the correct place (see P1).

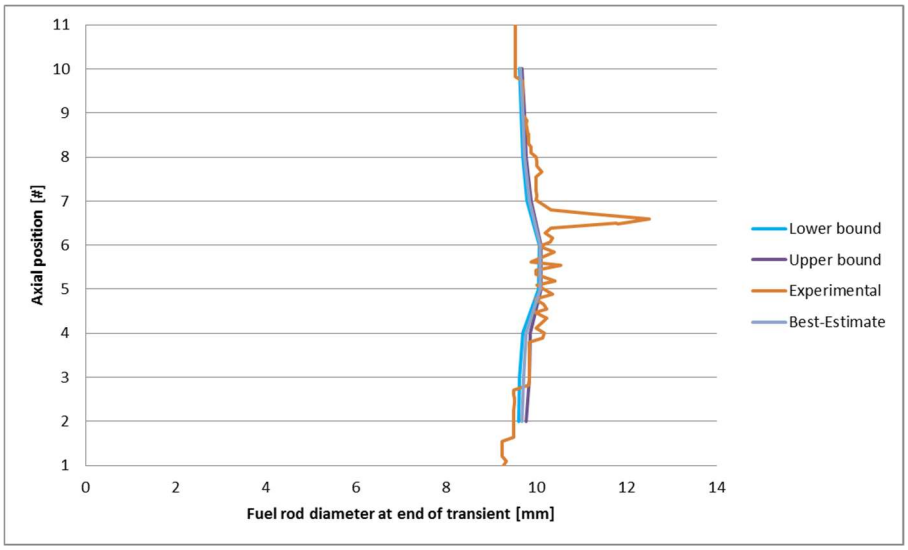

FIG. 20. IFA-650.10 - Clad strain.

5.2.2. Sensitivity analysis results

The global sensitivity analysis is a powerful tool to identify the most influential input parameters on each output parameter of interest. They can be identified by using various sensitivity indices like correlation coefficients and well-defined significance thresholds. As the fuel rod codes like FRAPTRAN have very complex models, and there are certain interactions between input parameters, the correlation coefficients can only be considered as qualitative and relative index for screening the non-important input parameters.

In the current work, the partial Rank Correlation coefficients (PRCCs) are used and arbitrary significance thresholds of 0.25 and 0.5 are chosen for identification of the influence (PRCC > 0.25 for Mediate effect, in orange, or PRCC > 0.5 for High effect, in green) of the input parameters on the output parameter, although specific guidance and interpretation of the significance depends on the number of samples, number of variables, and analysis tolerance. Note also that the PRCCs for each output parameter of interest as a function of all the input parameters change during the transient. For simplicity, only the PRCCs at their maximum absolute values are presented for each output, as shown in the following Table 5.

It can be observed that the following input parameters are of mediate or high importance:

- Fuel rod geometry;
- Applied power and coolant temperature during the test;
- Models related to fuel and clad heat transfer (including thermal conductivity and heat capacity, gap conductivity), at the exception of the cladding heat capacity, oxide thermal conductivity and fuel/cladding emissivity;
- Models related to thermal expansion and swelling;
- Cladding Yield stress, annealing;
- Models related to clad corrosion;
- Plenum gas temperature.

TABLE 5. PARTIAL RANK CORRELATION COEFFICIENTS (PRCC) AT THEIR MAXIMUM FOR IFA-650.10 (P0 - WITHOUT RELOCATION MODEL)

Input uncertainty parameter	RIP	TFC	TFO	TCI	TCO	TOL	ECR	DCO	CES	ECT	EFT
Cladding outside diameter (mm)	18%	9%	12%	13%	12%	11%	83%	19%	83%	17%	8%
Cladding inside diameter (mm)	70%	63%	64%	50%	50%	6%	82%	81%	90%	79%	50%
Pellet outside diameter	65%	56%	60%	40%	40%	7%	17%	83%	77%	79%	43%
Fuel theoretical density (kg/m3 at 20 °C)	10%	39%	36%	38%	38%	9%	9%	13%	10%	15%	21%
U^{235} enrichment (%)	10%	10%	12%	12%	12%	9%	8%	11%	12%	11%	14%
Filling gas pressure (MPa)	98%	15%	30%	28%	28%	8%	17%	35%	92%	26%	11%
Relative power during base irradiation	10%	8%	9%	9%	9%	6%	10%	7%	8%	10%	9%
Relative power during test	53%	94%	93%	94%	94%	52%	54%	80%	33%	39%	84%
Test rod power profile	10%	25%	7%	8%	7%	11%	8%	85%	9%	10%	6%
Cladding temperature (°C)											
Coolant temperature (°C)	39%	95%	96%	100%	100%	58%	60%	73%	27%	87%	90%
Clad-to-Coolant heat transfer coefficient	85%	100%	98%	99%	99%	90%	91%	96%	64%	77%	94%
Fuel thermal conductivity model	16%	80%	26%	29%	29%	14%	15%	10%	7%	44%	42%
Clad thermal conductivity model	11%	9%	8%	44%	8%	9%	8%	7%	5%	9%	4%
Fuel thermal expansion model	18%	19%	17%	13%	13%	8%	17%	51%	43%	61%	99%
Clad thermal expansion model	11%	11%	12%	14%	15%	7%	6%	96%	19%	97%	9%
Fuel densification model	24%	36%	38%	18%	18%	7%	10%	61%	51%	54%	35%
Fuel solid swelling model	25%	40%	41%	24%	24%	11%	16%	62%	55%	60%	31%
Fuel gaseous swelling model	39%	38%	38%	24%	24%	10%	11%	65%	56%	61%	30%
Clad Yield stress	44%	25%	59%	67%	66%	15%	37%	77%	36%	55%	21%
Fuel heat capacity	20%	69%	67%	69%	69%	14%	13%	31%	16%	17%	48%
Cladding heat capacity	6%	15%	19%	20%	20%	7%	9%	7%	6%	9%	14%
Cladding elastic modulus	10%	9%	9%	11%	11%	9%	7%	13%	17%	10%	13%
Cladding corrosion model during steady-state operation	10%	11%	29%	22%	22%	100%	100%	21%	57%	15%	11%
Cladding hydrogen pickup fraction during steady-state operation	11%	10%	10%	7%	7%	11%	6%	10%	6%	11%	11%
Cladding oxidation model at high temperature	13%	7%	7%	18%	18%	83%	84%	10%	11%	11%	4%
Thermal conductivity of the oxide layer	6%	5%	5%	10%	10%	8%	8%	7%	7%	6%	6%
Fission gas release (or gas diffusion coefficient)	8%	5%	7%	6%	10%	9%	9%	9%	13%	9%	2%
Gap gas conductivity	17%	59%	91%	48%	47%	15%	17%	47%	14%	19%	44%
Fuel/cladding emissivity	8%	7%	19%	13%	13%	9%	7%	17%	11%	10%	10%
Fuel radial relocation	10%	6%	8%	17%	15%	8%	8%	6%	7%	7%	8%
Fuel fragment packing fraction (if applicable)	14%	7%	7%	10%	10%	12%	12%	8%	6%	12%	11%
Cladding strain threshold for fuel mobility (if applicable)	12%	4%	5%	15%	15%	15%	13%	8%	10%	15%	8%
Cladding Meyer hardness	8%	11%	11%	16%	16%	9%	9%	13%	12%	7%	4%
Cladding annealing	65%	51%	79%	82%	82%	28%	56%	90%	47%	63%	35%
Cladding burst criteria	9%	4%	9%	5%	5%	7%	5%	14%	9%	10%	6%
Cladding burst strain criteria	6%	10%	9%	10%	9%	5%	12%	10%	11%	6%	5%
Plenum gas temperature (°C)	95%	5%	16%	23%	23%	9%	13%	21%	86%	15%	12%

On the contrary, the following parameters appear to have only low importance:

- Enrichment and mother rod filling pressure,
- Relative power during base irradiation,
- Fission gas release,
- Fuel radial relocation,
- Clad heat capacity, elastic modulus, and Mayer hardness,
- Relocation related parameters (fuel fragmentation fraction, Strain threshold for fuel mobility),
- Burst stress and strain criteria.

The non-significance of some parameters is astonishing. Indeed, without relocation model, the ballooning and burst are predicted by the BALON2 model. Ballooning model BALON2 calculates the extent and shape of the localized large cladding deformation (ballooning) that occurs between the time that the cladding effective strain exceeds the instability strain and the time of cladding rupture. In particular, the BALON2 model predicts failure (burst) in the ballooning node when the cladding true hoop stress exceeds an empirical limit that is a function of cladding temperature, or when the predicted cladding permanent hoop strain exceeds the strain limit that is a function of cladding temperature. It is expected that there should be at least an impact of the “cladding burst stress criteria” or “cladding burst strain criteria”.

However, we must not forget the limitations of the correlation coefficients. Indeed, the impacts could be non-linear and non-monotonic and thus not captured by the correlation coefficients. Another explanation would be that those parameters affect only the burst time, but not the other parameters. This would make their effect harder to notice. Additional efforts would be necessary to investigate those questions by plotting and displaying flyspecks or extracting and studying the burst instants. An alternative approach is to use other sensitivity indices such as Sobol’s.

In summary, based on the current sensitivity study results, the important parameters can be identified in the following Table 7.

TABLE 6. IMPORTANCE RANKING OF EACH PARAMETER FOR IFA-650.10 (P0 - WITHOUT RELOCATION MODEL)

Input uncertainty parameter	Fuel Thermal +RIP	Clad thermal +ECR	Fuel/Clad Mechanical	Overall
Cladding outside diameter (mm)	L	H	H	H
Cladding inside diameter (mm)	H	H	H	H
Pellet outside diameter	H	M	H	H
Fuel theoretical density (kg/m3 at 20 °C)	M	M	L	M
U^{235} enrichment (%)	L	L	L	L
Filling gas pressure (MPa)	H	M	H	H
Relative power during base irradiation	L	L	L	L
Relative power during test	H	H	H	H
Test rod power profile	M	L	H	H
Cladding temperature (°C)	H	H	H	H
Coolant temperature (°C)	H	H	H	H
Clad-to-Coolant heat transfer coefficient	H	H	H	H
Fuel thermal conductivity model	H	M	M	H
Clad thermal conductivity model	L	M	L	M
Fuel thermal expansion model	H	L	H	H
Clad thermal expansion model	H	L	H	H
Fuel densification model	M	L	H	H
Fuel solid swelling model	M	L	H	H
Fuel gaseous swelling model	M	L	H	H
Clad Yield stress	H	H	H	H
Fuel heat capacity	H	H	M	H
Cladding heat capacity	L	L	L	L
Cladding elastic modulus	L	L	L	L
Cladding corrosion model during steady-state operation	L	H	H	H
Cladding hydrogen pickup fraction during steady-state operation	L	L	L	L
Cladding oxidation model at high temperature	L	H	H	H
Thermal conductivity of the oxide layer	L	L	L	L
Fission gas release (or gas diffusion coefficient)	L	L	L	L
Gap gas conductivity	H	M	M	H
Fuel/cladding emissivity	L	L	L	L
Fuel radial relocation	L	L	L	L
Fuel fragment packing fraction (if applicable)	L	L	L	L
Cladding strain threshold for fuel mobility (if applicable)	L	L	L	L
Cladding Meyer hardness	L	L	L	L
Cladding annealing	H	H	H	H
Cladding burst criteria	L	L	L	L
Cladding burst strain criteria	L	L	L	L
Plenum gas temperature (°C)	H	L	H	H

5.3. Parametric case with axial relocation model (P1)

5.3.1. Uncertainty analysis results

Results (BE, LB, UB) for comparing cases P1 and Experiment for all the requested results are given in the following Figs.

— Rod internal pressure (MPa)

The only significant difference with reference case P0 is that the pressure evolution at burst is smoother, but this is coming from the best-estimate case and not linked to the uncertainties. The conclusion is not affected.

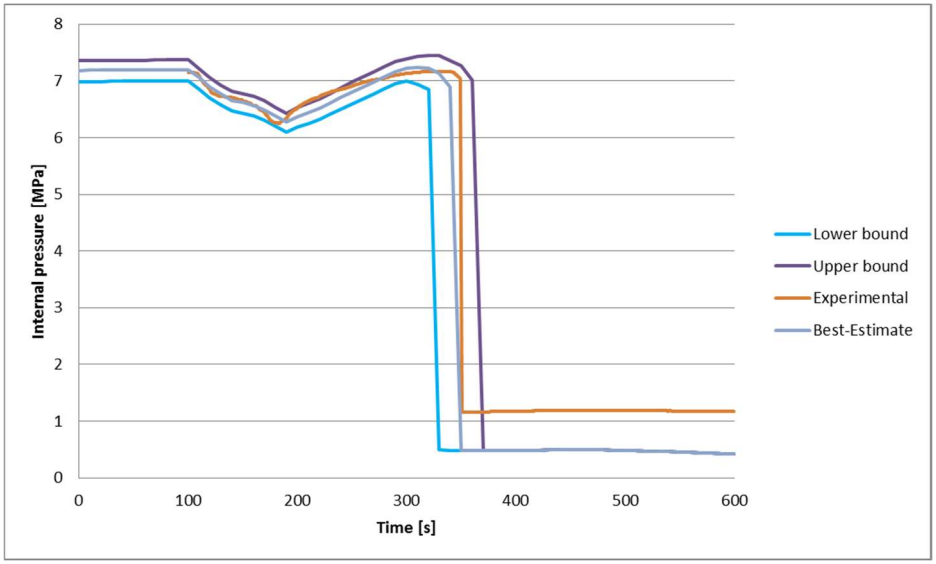

FIG. 21. IFA-650.10 – Rod internal pressure.

— Clad temperature (K)

The situation is the same as reference case P0, but the overestimation is worse and the uncertainties larger. This is due to the consideration of axial relocation in the calculation. Indeed, it is suspected that some small axial relocations occurred during the test but were not detected in the 3 cladding temperature measurements. Tractebel recommends for more precise measurements in the future LOCA tests.

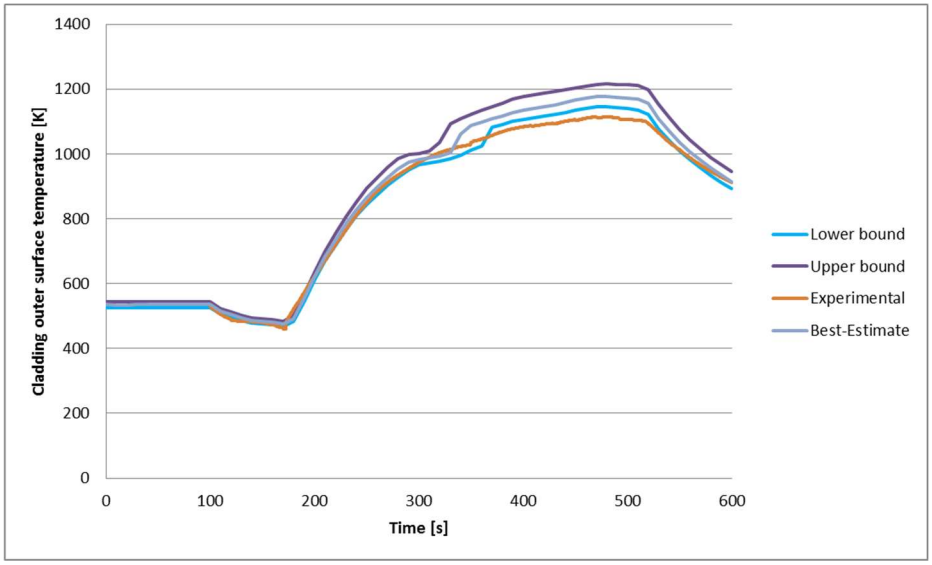

FIG. 22. IFA-650.10 - Clad temperature.

— Clad elongation (mm)

The measurements are overestimated by far and this confirms the need to work on the mechanical deformation models. Use of FEA may also improve the prediction.

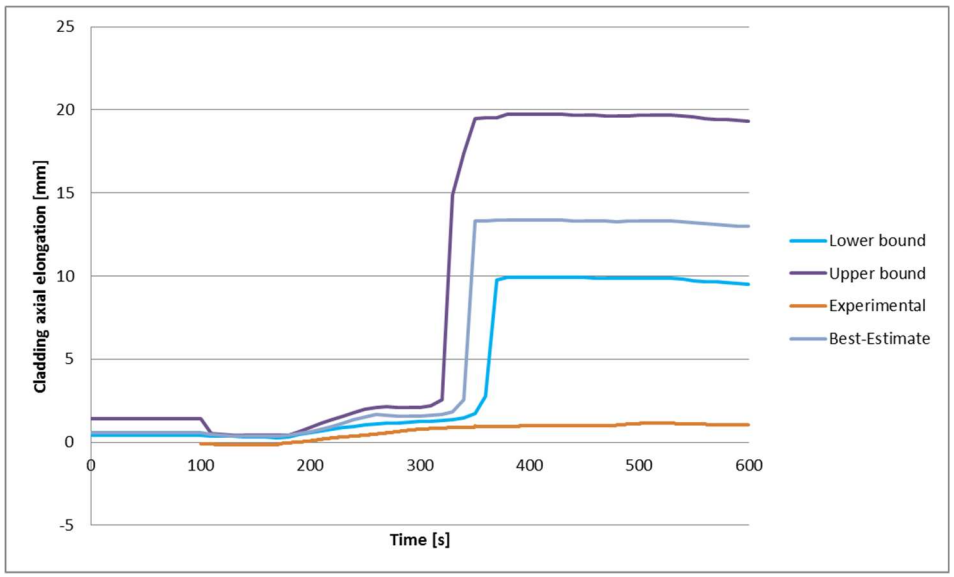

FIG. 23. IFA-650.10 - Clad axial elongation.

— Clad strain (%)

There is now a balloon of the appropriate radial size, but of exaggerated axial size. This confirms the results on the oversized elongation, but also the choice of the axial relocation model.

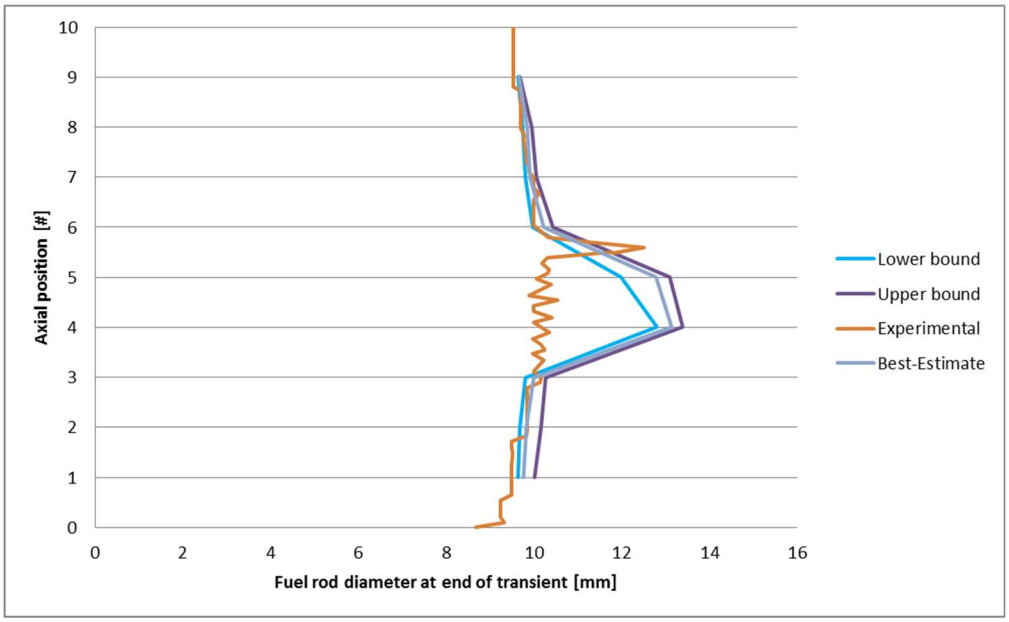

FIG. 24. IFA-650.10 - Clad strain.

5.3.2. Sensitivity analysis results

The PRCCs at their maximum absolute values are presented for each output, as shown in the following table.

The results are quite like the reference case P0, but show significant impacts of the axial relocation related parameters (clad yield stress, fuel fragment packing ratio and clad annealing).

The following significant impacts are observed on:

— The rod internal pressure (RIP) by the gap geometry, filling gas pressure, test conditions (transient power, coolant temperature, coolant to clad HTC), plenum gas temperature, and

axial relocation related parameters (clad yield stress, fuel fragment packing ratio and clad annealing);

- The fuel temperatures (TFC, TFO) by gap and fuel geometry, test conditions, fuel related properties and models (fuel density, thermal conductivity, densification, swelling, heat capacity), gap conductivity, axial relocation related parameters;
- The cladding temperatures (TCI, TCO) by the test conditions, the fuel heat capacity, and axial relocation related parameters;
- The total oxidation layer (TOL) or cladding equivalent reacted (ECR) by clad geometry, axial power profile, test conditions, steady-state corrosion, high temperature oxidation, and axial relocation related parameters;
- The cladding diameter (DCO) by gap geometry, test conditions, axial power profile, densification models, gas gap conductivity, and axial relocation related parameters;
- The cladding effective stress (CES) by fuel rod geometry, fill gas pressure, clad to coolant HTC, swelling models, steady-state corrosion and plenum gas temperature;
- The cladding and fuel elongation (ECT and EFT) by clad/fuel geometry, test conditions, fuel/clad related properties and models (fuel thermal conductivity, densification, swelling, fuel/clad thermal expansion), and axial relocation related parameters.

TABLE 7. PARTIAL RANK CORRELATION COEFFICIENTS (PRCC) AT THEIRMAXIMUM FOR IFA-650.10 (P1 - WITH RELOCATION MODEL)

Input uncertainty parameter	RIP	TFC	TFO	TCI	TCO	TOL	ECR	DCO	CES	ECT	EFT
Cladding outside diameter (mm)	18%	8%	8%	12%	11%	6%	82%	20%	83%	9%	9%
Cladding inside diameter (mm)	72%	62%	63%	50%	52%	9%	82%	82%	92%	81%	52%
Pellet outside diameter	63%	56%	61%	42%	42%	5%	21%	82%	75%	79%	44%
Fuel theoretical density (kg/m3 at 20 °C)	11%	42%	40%	41%	41%	6%	9%	12%	10%	16%	23%
U^{235} enrichment (%)	9%	7%	7%	10%	10%	11%	8%	7%	12%	12%	10%
Filling gas pressure (MPa)	97%	16%	24%	30%	30%	6%	27%	33%	93%	21%	13%
Relative power during base irradiation	10%	14%	16%	12%	12%	10%	12%	15%	9%	11%	13%
Relative power during test	58%	95%	94%	94%	94%	55%	49%	82%	35%	44%	82%
Test rod power profile	8%	25%	24%	24%	24%	15%	69%	78%	15%	11%	12%
Cladding temperature (°C)											
Coolant temperature (°C)	52%	95%	96%	100%	100%	47%	48%	73%	34	85%	89%
Clad-to-Coolant heat transfer coefficient	88%	99%	98%	98%	98%	85%	79%	96%	59%	74%	93%
Fuel thermal conductivity model	15%	79%	26%	31%	30%	19%	18%	8%	10%	46%	37%
Clad thermal conductivity model	11%	13%	10%	43%	10%	8%	7%	11%	12%	8%	13%
Fuel thermal expansion model	17%	18%	18%	15%	15%	8%	17%	50%	38%	59%	98%
Clad thermal expansion model	11%	13%	13%	16%	16%	14%	10%	46%	17%	97%	11%
Fuel densification model	24%	35%	35%	19%	19%	9%	7%	60%	48%	53%	37%
Fuel solid swelling model	23%	38%	39%	23%	23%	9%	10%	63%	54%	61%	26%
Fuel gaseous swelling model	36%	41%	41%	32%	31%	4%	10%	63%	53%	60%	31%
Clad Yield stress	63%	40%	60%	70%	69%	16%	55%	81%	37%	55%	26%
Fuel heat capacity	24%	72%	68%	70%	70%	12%	16%	31%	21%	12%	47%
Cladding heat capacity	4%	18%	21%	22%	22%	11%	11%	7%	9%	9%	18%
Cladding elastic modulus	7%	9%	13%	15%	15%	10%	10%	15%	12%	9%	16%
Cladding corrosion model during steady-state operation	20%	12%	17%	21%	21%	100%	100%	31%	56%	20%	20%
Cladding hydrogen pickup fraction during steady-state operation	6%	13%	17%	16%	17%	10%	9%	14%	7%	8%	12%
Cladding oxidation model at high temperature	19%	11%	18%	18%	18%	77%	74%	17%	16%	19%	13%

TABLE 7. PARTIAL RANK CORRELATION COEFFICIENTS (PRCC) AT THEIRMAXIMUM FOR IFA-650.10 (P1 - WITH RELOCATION MODEL)

Input uncertainty parameter	RIP	TFC	TFO	TCI	TCO	TOL	ECR	DCO	CES	ECT	EFT
Thermal conductivity of the oxide layer	8%	10%	9%	12%	12%	10%	12%	12%	13%	14%	6%
Fission gas release (or gas diffusion coefficient)	9%	6%	11%	11%	11%	9%	12%	10%	12%	12%	5%
Gap gas conductivity	26%	55%	31%	48%	47%	14%	46%	57%	17%	15%	29%
Fuel/cladding emissivity	14%	8%	11%	8%	8%	5%	7%	13%	14%	13%	10%
Fuel radial relocation	16%	12%	14%	21%	20%	6%	14%	12%	12%	8%	18%
Fuel fragment packing fraction (if applicable)	55%	62%	95%	95%	95%	73%	79%	59%	41%	47%	68%
Cladding strain threshold for fuel mobility (if applicable)	13%	11%	12%	19%	17%	15%	5%	10%	11%	13%	10%
Cladding Meyer hardness	10%	14%	14%	16%	15%	11%	7%	18%	10%	9%	12%
Cladding annealing	73%	60%	78%	81%	81%	37%	58%	89%	46%	57%	37%
Cladding burst criteria	19%	5%	11%	8%	8%	10%	11%	20%	11%	11%	6%
Cladding burst strain criteria	8%	7%	16%	18%	15%	11%	10%	9%	9%	11%	11%
Plenum gas temperature (°C)	95%	14%	15%	27%	27%	7%	19%	21%	88%	19%	12%

It is clear that the clad, gap and fuel geometry, test conditions (power, coolant temperatures and clad-to-coolant heat transfer coefficients) and axial relocation related parameters (clad yield stress, fuel fragment packing fraction and clad annealing) are important for nearly all output parameters. This means that a good simulation of the fuel behaviours in Halden LOCA tests need a better characterisation of the test rods, better measurements or calculations of the thermal hydraulic boundary conditions, and a realistic axial relocation model.

The relevant fuel related properties and models (fuel thermal conductivity, densification, swelling, heat capacity, thermal expansion) are also important for predicting fuel thermal and mechanical behaviour.

The relevant cladding related properties and models (cladding Yield stress, thermal expansion, steady-state corrosion and high temperature oxidation), fuel densification/swelling and gap conductivity are also important for predicting cladding thermal and mechanical behaviour.

The plenum gas temperature is also important for predicting the rod internal pressure and cladding stress.

Note also that the following test rod data, properties or models are shown to have weak effect (PRCC < 0.25) on all the output parameter of interest for the current FRAPTRAN-TE-1.5 simulation:

- U^{235} enrichment;
- Relative power during base irradiation;
- Cladding heat capacity,
- thermal conductivity;
- elastic modulus;
- Meyer hardness;
- Fuel/cladding emissivity, radial relocation;
- Fission gas release during transient;
- Thermal conductivity of the oxide layer;
- Cladding hydrogen pick up fraction during base irradiation;
- Cladding strain threshold for fuel mobility;
- Cladding burst stress or strain criteria.

The discussion about the certain parameters for the reference case P0 remains valid here, related to cladding strain threshold for fuel mobility, and cladding burst stress or strain criteria.

In summary, based on the current sensitivity study results, the important parameters can be identified as in the following Table 8.

TABLE 8. IMPORTANT RANKING OF EACH PARAMETER FOR IFA-650.10 (P1 - WITH RELOCATION MODEL)

Input uncertainty parameter	Fuel Thermal +RIP	Clad thermal +ECR	Fuel/Clad Mechanical	Overall
Cladding outside diameter (mm)	L	H	H	H
Cladding inside diameter (mm)	H	H	H	H
Pellet outside diameter	H	M	H	H
Fuel theoretical density (kg/m3 at 20 °C)	M	M	L	M
U^{235} enrichment (%)	L	L	L	L
Filling gas pressure (MPa)	H	M	H	H
Relative power during base irradiation	L	L	L	L
Relative power during test	H	H	H	H
Test rod power profile	L	H	H	H
Cladding temperature (°C)				
Coolant temperature (°C)	H	H	H	H
Clad-to-Coolant heat transfer coefficient	H	H	H	H
Fuel thermal conductivity model	H	M	M	H
Clad thermal conductivity model	L	M	L	M
Fuel thermal expansion model	L	L	H	H
Clad thermal expansion model	L	L	H	H
Fuel densification model	M	L	H	H
Fuel solid swelling model	M	L	H	H
Fuel gaseous swelling model	M	L	H	H
Clad Yield stress	H	H	H	H
Fuel heat capacity	H	H	M	H
Cladding heat capacity	L	L	L	L
Cladding elastic modulus	L	L	L	L
Cladding corrosion model during steady-state operation	L	H	H	H
Cladding hydrogen pickup fraction during steady-state operation	L	L	L	L
Cladding oxidation model at high temperature	L	H	H	H
Thermal conductivity of the oxide layer	L	L	L	L
Fission gas release (or gas diffusion coefficient)	L	L	L	L
Gap gas conductivity	H	M	H	H
Fuel/cladding emissivity	L	L	L	L
Fuel radial relocation	L	L	L	L
Fuel fragment packing fraction (if applicable)	H	H	H	H
Cladding strain threshold for fuel mobility (if applicable)	L	L	L	L
Cladding Meyer hardness	L	L	L	L
Cladding annealing	H	H	H	H
Cladding burst criteria	L	L	L	L
Cladding burst strain criteria	L	L	L	L
Plenum gas temperature (°C)	H	M	H	H

6. CONCLUSIONS AND RECOMMENDATIONS

During the first phase of FUMAC, selected Halden LOCA tests (IFA-650.9 and IFA-650.10) have been simulated and scoping parametric studies have been performed using the USNRC version of FRAPTRAN-1.5. The objective was to identify the potential improvements to FRAPTRAN-1.5 models for LOCA fuel behaviours modelling.

It was concluded that:

(a) The FRAPTRAN-1.5 code prediction of the fuel behaviours in the LOCA tests depends strongly on local thermal hydraulic boundary conditions.
(b) The FRAPTRAN-1.5 heat transfer models need further validation with more appropriate inlet thermal hydraulic boundary conditions. As an alternative, local thermal hydraulic boundary conditions calculated with a system thermal hydraulic code should be used.
(c) The uncertainties related to the plenum gas temperature and other properties and models (initial radial deformation, gap conductance, ballooning and burst, etc.), as well as the lack of a fuel axial relocation model also play a role in the differences with the calculated results.

During the second phase of FUMAC, the two selected Halden LOCA tests IFA-650.9 and IFA-650.10 have been simulated using the updated version of FRAPTRAN-TE-1.5, to improve FRAPTRAN-1.5 for LOCA fuel behaviour modelling. In addition, uncertainty and sensitivity analysis has been performed on the FRAPTRAN-TE-1.5 simulation of the IFA-650.10 test.

It was concluded that:

(d) The updated version of FRAPTRAN-TE-1.5 can well simulate the LOCA fuel thermal behaviours as observed in the Halden LOCA tests IFA-650.9 and IFA-650.10, using adequate thermal hydraulic boundary conditions and the axial relocation model.

— The SOCRAT calculated coolant temperatures are higher than the measured heater temperatures, particularly in case of significant axial relocation (Case IFA-650.9).
— The FRAPTRAN-TE-1.5 plenum gas temperature model based on the SOCRAT calculated coolant temperatures fails to well predict the rod internal pressure for IFA650.9, but enables to well predict the rod internal pressure for IFA650.10. This This can be attributed to the inability of FRAPTRAN to model pressure gradients due to the possible axial gas transportation from the plenum to the ballooned and burst region in FRAPTRAN-TE-1.5, in case of significant axial relocation (Case IFA-650.9).
— The FRAPTRAN-TE-1.5 axial relocation model developed by Quantum Technologies can simulate the cladding temperature variations due to relocation, using the calibrated model parameters.

(e) The updated version of FRAPTRAN-TE-1.5 fails to well simulate the LOCA fuel mechanical deformation as observed in the Halden LOCA tests IFA-650.9 and IFA-650.10, using the default FRACAS-I model.

— The ballooning and burst models may need to be improved.
— The finite element analysis (FEA) of the cladding helps to improve the mechanical calculation.
(f) The uncertainty analysis on FRAPTRAN-TE-1.5 simulation of the IFA-650.10 test confirms that the FRAPTRAN-TE-1.5 thermal models, axial relocation model, the heat transfer boundary conditions and gas temperature model are adequate for simulating the thermal behaviour of the Halden LOCA tests, and their impacts can be well considered by statistical uncertainty analysis. However, the mechanical models for the cladding deformation still need to be improved for simulating the Halden LOCA tests, and only after that the statistical uncertainty analysis can help to improve the coverage of the experimental data.
(g) The sensitivity analysis on the FRAPTRAN-TE-1.5 simulation of the IFA-650.10 test helps to identify the most influential input fuel rod data, test conditions, physical properties or models. However, when considering the parameters that are only important in one of the case or a few instants, only enrichment, clad yield stress, clad elastic modulus,

and fission gas release model have low correlation coefficients and are expected to have low importance. The parameters related to the axial relocation model (when applied) are also important. However, the situation of strain threshold for fuel mobility and burst criteria is more dubious, as they have low correlation coefficients, but should be of importance according to the physics and the modelling. More detailed analysis is needed to examine this, e.g., by considering the scatter plots or using other sensitivity indices (such as Sobol's).

In conclusion, substantial progress has been made in achieving the FUMAC project objectives and the agreed work plan for Tractebel.
The following recommendations can be made:

- Further improvements or validation should be made to FRAPTRAN code for LOCA fuel mechanical behaviour modelling: the ballooning and burst models, the finite element analysis model for cladding, and if possible the axial gas transportation model.
- Further improvements could be made to FRAPTRAN code for LOCA fuel rod to coolant heat transfer modelling: this may be overcome by coupling with a system thermal hydraulic code, using a refined nodding scheme.
- The QT's axial fuel relocation model could be improved by obtaining a unique set of model related parameters based on all available Halden LOCA tests with significant fuel relocation.
- More detailed uncertainty and sensitivity analysis should be performed after the code improvements.

It is recommended to perform the above work in the continuation of the FUMAC project. Finally, it is recommended to apply the validated FRAPTRAN code to development of an efficient fuel performance and safety evaluation methodology for new or advanced technology fuel design assessment and licensing. This would enhance the sustainability of nuclear technology and ensure the diversification of fuel supply.

REFERENCES

[1] INTERNATIONAL ATOMIC ENERGY AGENCY, Improvement of Computer Codes Used for Fuel Rod Behaviour Simulation (FUMEX-III), TECDOC-1697, IAEA, Vienna (2013).

[2] NUCLEAR ENERGY AGENCY, ORGANISATION FOR ECONOMIC CO-OPERATION AND DEVELOPMENT, Nuclear Fuel Behaviour in Loss-Of-Coolant Accident (LOCA) Conditions, State-of-the-Art Report, NEA no. 6846, (2009).

[3] MASSIH A.R., Review of experimental data for modelling LWR fuel cladding behaviour under loss of coolant accident conditions, SKI Report 2007:14, (2007).

[4] NUCLEAR ENERGY AGENCY, Safety Significance of the Halden IFA-650 LOCA Test Results, OECD/NEA/CSNI/R(2010)5, (2010).

[5] NUCLEAR ENERGY AGENCY, Benchmark calculations on HALDEN IFA-650 LOCA test results, OECD/NEA/CSNI/R(2010)6, (2010).

[6] U.S. NUCLEAR REGULATORY COMMISSION, FRAPTRAN 1.5: A Computer Code for the Transient Analysis of Oxide Fuel Rods, Vol. 1, NUREG/CR-7023, Revision 1, (2014).

[7] U.S. NUCLEAR REGULATORY COMMISSION, FRAPTRAN 1.5: Integral assessment, Vol. 2, NUREG/CR-7023, Revision 1, (2014).

[8] MANNGARD. T., MASSIH A. R., Modelling and Simulation of Reactor Fuel Cladding under Loss-Of-Coolant Accident Conditions, J. Nucl. Sci. Technol., Vol. 48, Issue 1, (2011) 39–49.

[9] JERNKVIST, L. O., Implementation of Models for Cladding High Temperature Metal-Water Reactions, Phase Transformation, Creep and Failure in the FRAPTRAN-1.4 computer program, SSM2012-510, report TR10-005V2, 2012.

[10] MANNGARD, T., MASSIH A., STENGARD J. O., Evaluation of the Halden IFA-650 loss-of-coolant accident experiments 2, 3 and 4, SSM2014:18, (2014).

[11] JERNKVIST, L. O., MASSIH A. R., and ALVESTAV A., Axial Relocation of Fragmented and Pulverized Fuel and its Effects on Fuel Rod Heat Load During LOCAs, Top Fuel 2015, Paper A0059, (2015).

[12] GOVERS, K., and VERWERFT, M., Simulation of ballooning and relocation in the Halden LOCA tests with FRAPTRAN, EHPG meeting (2014).

[13] GOVERS K., and VERWERFT M., An insight on fuel fragmentation, relocation and dispersal during loss-of-coolant accidents from computer simulations, Top Fuel 2015, paper A0185, (2015).

[14] JERNKVIST L. O., and MASSIH, A. R., "Models for axial relocation of fragmented and pulverized fuel pellets in distending fuel rods and its effects on fuel rod heat load," SSM research report 2015:37, Swedish Radiation Safety Authority (SSM), Stockholm, Sweden (2015).

[15] JERNKVIST, L. O., "Observed and corrected errors in source code and algorithms of FRAPTRAN-1.5", Report TR15-002V2, Quantum Technologies AB, (2016).

[16] JERNKVIST, L.O., MASSIH, A.R., ALVESTAV, A., Computational assessment of axial fuel relocation in Halden IFA-650 LOCA tests. In Proceedings of Enlarged Halden Program Group Meeting, Sandefjord, Norway, OECD Halden Reactor Project, (2016).

[17] ZHANG, J., DETHIOUX, A., OURY, L., SCHNEIDESCH, C., "FRAPTRAN 1.5 Modelling of the Halden LOCA Tests IFA650.9 and 10: Scoping Parametric Studies and Perspectives," Enlarged Halden Programme Group Meeting, Sandefjord, Norway, (8th–13th May 2016).

[18] ZHANG, J., "Code modification requirements specifications (CMRS) for extension and adaptation of FRAPTRAN-1.5 for LOCA fuel behaviour modelling," Internal report FUELROD/4DO/0437004/000/00, Tractebel, (2016).

[19] JERNKVIST, L. O., "The FRAPTRAN-TE-1.5 computer program", Report TR16-001, Quantum Technologies AB, (2016).

[20] KISELEV, A. E., "Short Information on the Results of IFA-650.9, IFA-650.10 and IFA-650.11 Calculations with SOCRAT code", Technical Note, version 2, IBRAE, December 2016.

[21] ZHANG J., "IAEA FUMAC CRP - Specifications for Uncertainty Analysis on Modelling of the Halden LOCA Test IFA-650.10," Internal report DDN/4NT/520044/000/00, Tractebel, (2017).

DEVELOPMENT AND APPLICATION OF MODIFIED FUEL PERFORMANCE CODE BASED ON STAINLESS STEEL AS CLADDING UNDER STEADY STATE, TRANSIENT AND ACCIDENT CONDITIONS

ALFREDO ABE*, ANTONIO TEIXEIRA E SILVA*, CLAUDIA GIOVEDI+, CAIO MELO+, DANIEL DE SOUZA GOMES*, RAFAEL RONDON MUNIZ+
*Instituto de Pesquisas Energéticas e Nucleares - IPEN/CNEN-BRAZIL
Avenida Prof. Lineu Prestes 2242, Cidade Universitária – São Paulo – Brazil.
+ Escola Politécnica – Universidade de São Paulo LABRISCO
Avenida Prof. Mello Moraes 2231, Cidade Universitária – São Paulo – Brazil.

Abstract

The IPEN/CNEN proposal for FUMAC-CRP was to modified fuel performance codes (FRAPCON and FRAPTRAN) in order to assess the behavior of fuel rod using stainless steel as cladding and compare to zircaloy cladding performance under steady state and accident condition. The IFA 650-9, IFA-650-10 and UFA-650-11experiments were modelled to perform the LOCA accident simulation considering the original cladding and compared to stainless steel cladding.

1. INTRODUCTION

The nuclear fuel behaviour under accidental conditions is a main concern during the fuel design process, especially for safety analysis. In particular, the most challenging design basis accidents (DBA) such as loss of coolant accident (LOCA) and reactivity initiated accident (RIA) have been investigated experimentally in order to quantify properly the safety criteria associated to the fuel rod and those experiments allow the verification of capabilities of fuel performance codes. The FUMAC CRP is aiming at analysis of fuel behaviour under normal and off normal condition considering the capabilities of fuel performance code to simulate the experiments dedicated to LOCA accident condition. Several set of LOCA experimental data were made available to the participants in order to address different fuel parameters by means of codes simulations, furthermore some sensitivity and uncertainties analysis were addressed. The IPEN/CNEN proposal for FUMAC-CRP was to investigate the stainless steel cladding performance under same conditions as zircaloy cladding fuel. The comparison could contribute to verify the stainless steel cladding performance under accident condition.

2. ACTIVITIES PERFORMED

The CRP initial activities start with introductory studies and literature surveys associated to the LOCA accident such as phenomena, license safety criteria, experiments performed, simulation of accident using several codes and their results [1]–[9]. The initial activities performed illustrate how challenging is the analysis of LOCA accident and still open issues associated to the fuel performance codes to reproduce adequately the experimental results.
The following activities had been performed at first year of CRP:

- Experiments data and description made available were evaluated in order to select the most appropriated experiments for simulation;
- Experimental data were proper retrieved from selected experiment data file;
- FRAPCON [10] and FRAPTRAN [11] codes input data and modelling were addressed;
- Simulation of selected experiments using original version of FRAPCON and FRAPTRAN codes were performed;
- Preliminary results evaluation and analysis were carried out;
- FRAPCON and FRAPTRAN codes were modified in order to consider stainless steel as cladding material;

— Initial verification of implemented modification in FRAPCON and FRAPTRAN codes were performed;
— Simulations of selected experiments using modified version (stainless steel cladding) of FRAPCON and FRAPTRAN were conducted, and;
— Preliminary results evaluation and comparison with zircaloy cladding were performed.

Those activities listed above were conducted during 2015/2016 and some obtained results were presented at 2nd RCM Meeting. At final phase (2016/2017) of the CRP, following activities were conducted:

— FRAPTRAN subroutine modification,
— Sensitivity and Uncertainties assessment, and
— Obtained results compilation and analysis.

Those activities were conducted during 2016/2017 and obtained results will be presented at 3rd RCM Meeting.

2.1. Experimental Data Assessment and Codes Simulation

The experimental data of LOCA experiments were made available to the participants of the CRP with additional HWR reports (Halden Technical Report) and Data Sheet Description. The selected experimental data are from IFA-650.9, IFA-650.10 and IFA50.11 experiments, and all data were retrieved from experimental data files and plotted (see Fig. 1 to 8) in order to verify the behaviour and trends.

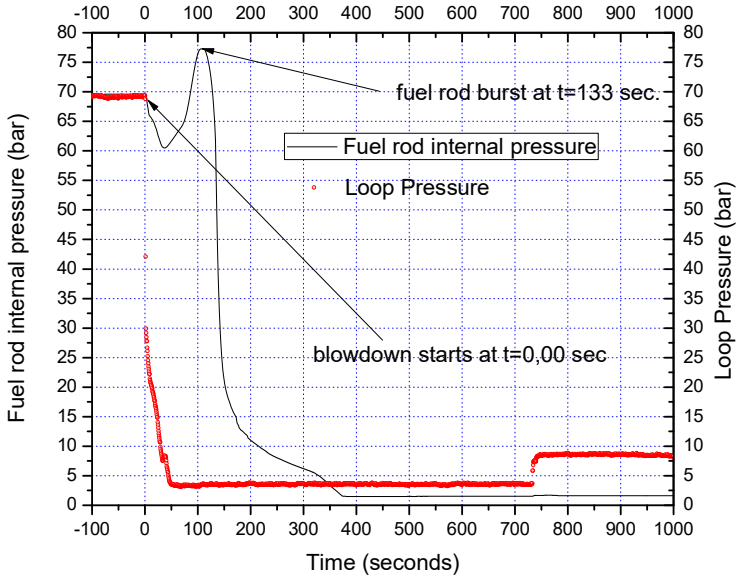

FIG. 1. Experimental data (loop and fuel internal pressure) from IFA-650.9.

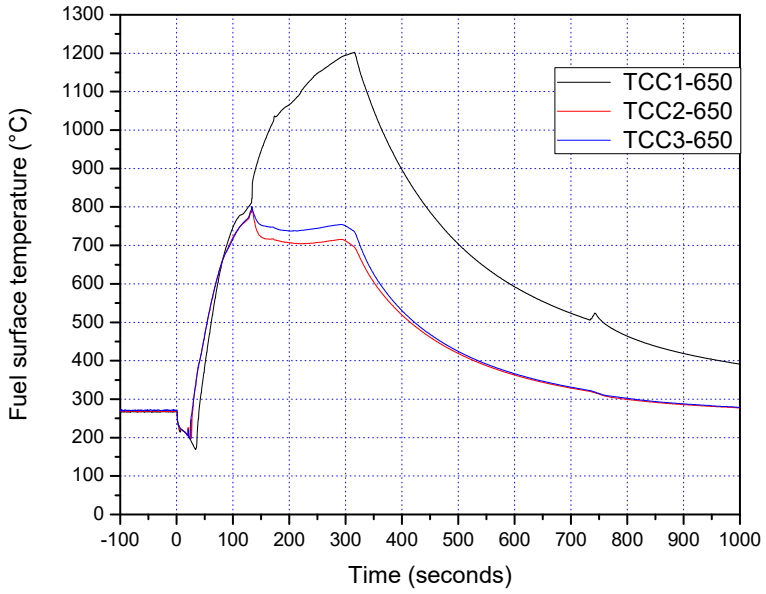

FIG. 2. Experimental data (Thermocouple) from IFA-650.9.

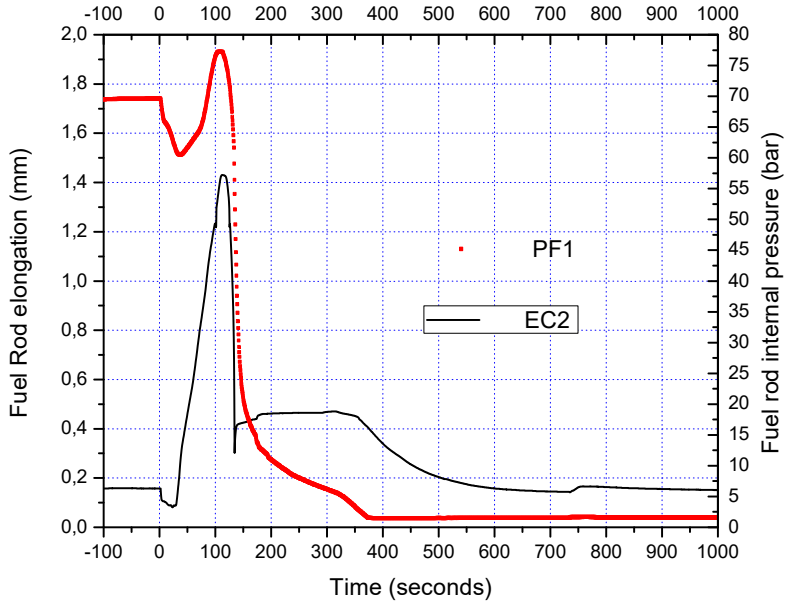

FIG. 3. Experimental data (Fuel internal pressure and clad elongation) from IFA-650.9.

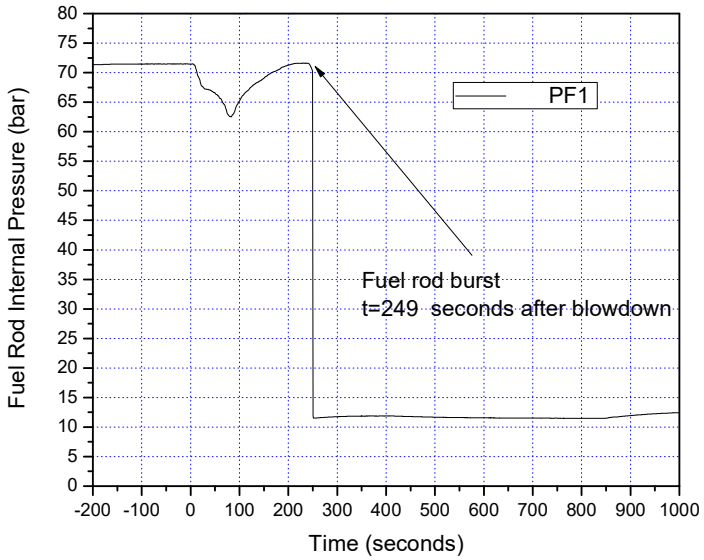

FIG. 4. Experimental data (Fuel internal pressure) from IFA-650.10.

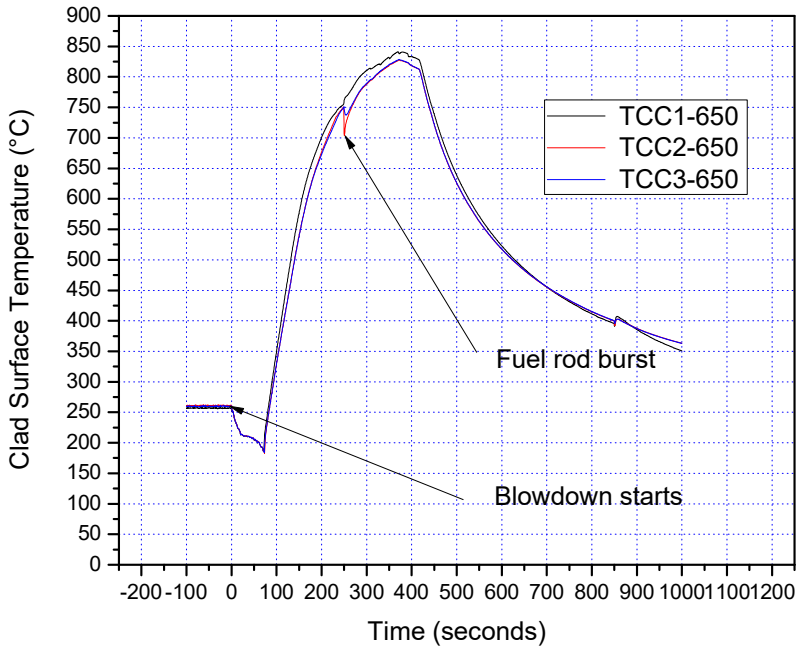

FIG. 5. Experimental data (Thermocouple) from IFA-650.10.

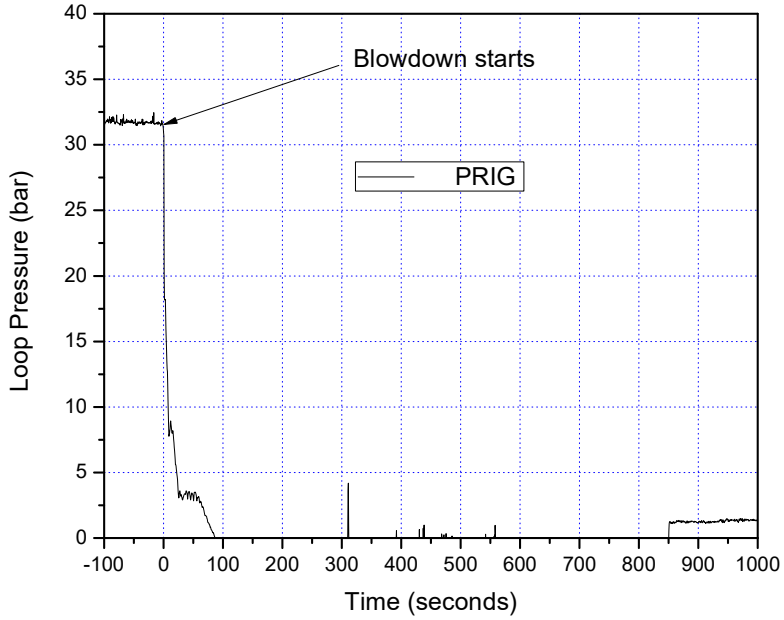

FIG. 6. Experimental data (Loop Pressure) from IFA-650.10.

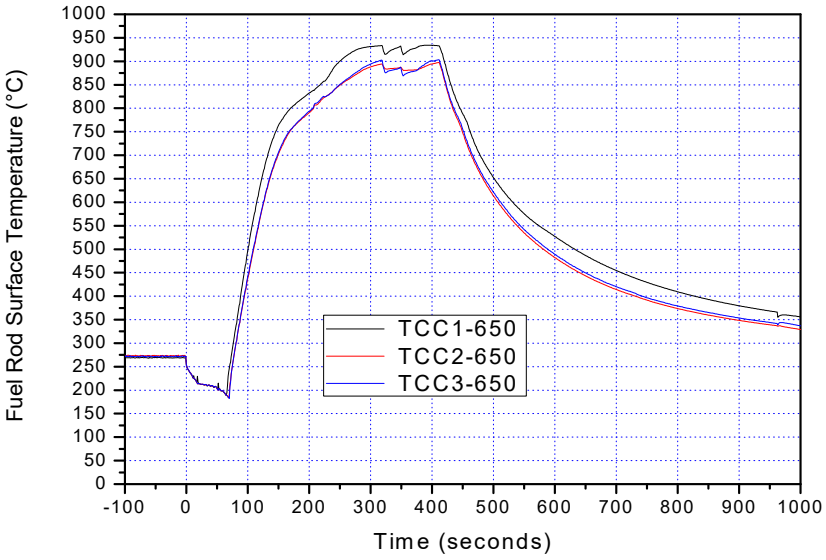

FIG. 7. Experimental data (Thermocouple) from IFA-650.11.

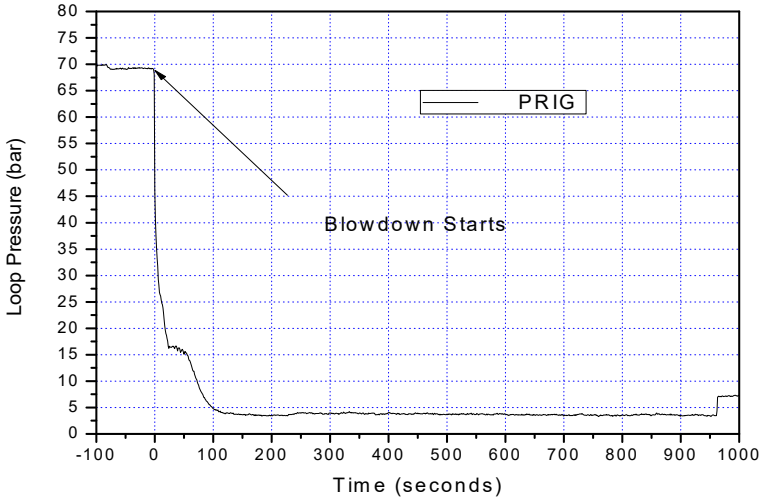

FIG. 8. Experimental data (Loop Pressure) from IFA-650.11.

The input data for FRAPCON and FRAPTRAN codes were prepared using information available from the technical reports made available.

The FRAPCON code required data as fuel geometry, composition and irradiation condition (power profile) were taken from HALDEN Data Sheet QA-F-702 and HWR-917 technical reports for the experiment IFA-650.09.

The FRAPCON code required data as fuel geometry, composition and irradiation condition were taken from HALDEN Data Sheet IFA-650.10 and HWR-974 technical reports for the experiment IFA-650.10.

The FRAPCON code required data as fuel geometry, composition and irradiation condition were taken from HALDEN Data Sheet IFA-650.11 and HWR-976 technical reports for the experiment IFA-650.11.

2.2. Preliminary results for Zircaloy cladding

The base irradiation (burnup accumulation) simulations using FRAPCON code (original version) were performed in order to address some fuel parameters (fission gas release, temperature, pressure, hoop stress, etc.) related to base irradiation. Additionally, the FRAPCON simulation creates an initialization file to be utilized in the FRAPTRAN calculation (LOCA simulation). As example of some results obtained from FRAPCON code (base irradiation), the following Figs 9, 10 and 11 present the fuel centerline temperature as function of burnup level obtained for base irradiation of IFA-650.09, IFA-650.10 and IFA-650.11 cases.

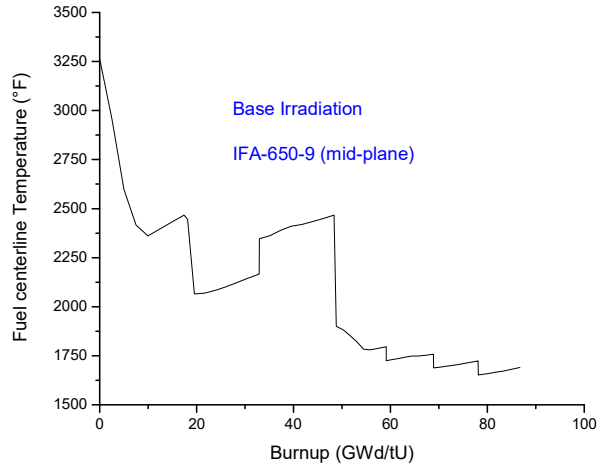

FIG. 9. Fuel Centerline as function of Burnup (IFA-650.09).

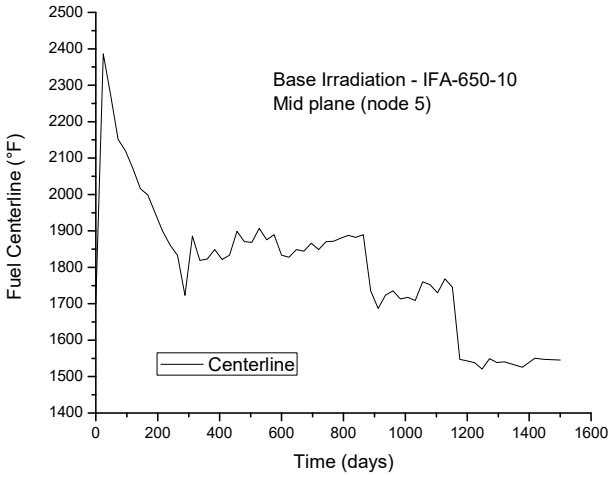

FIG. 10. Fuel Centerline as function of Burnup (IFA-650.10).

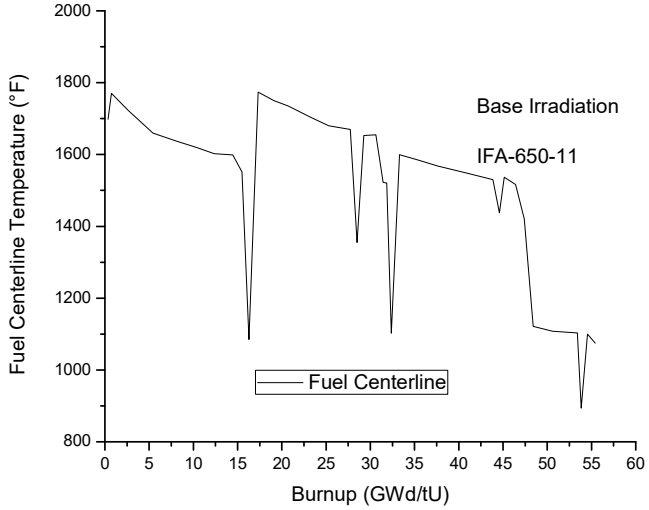

FIG. 11. Fuel Centerline as function of Burnup (IFA-650.11).

Others fuel parameters such as internal pressure evolution, fission gas release fraction (%), plenum gas temperature, clad temperature profile, gap thickness, clad strain, hoop stress, and others were also evaluated for each IFA case, and those results were presented at 2° RCM.

The transient/accident simulations were performed using FRAPTRAN code (original version), which is an analytical code applied to calculate fuel rod behaviour when power or coolant boundary conditions, or both, are changing quite fast. The FRAPTRAN code calculates power, fuel and cladding temperatures, cladding elastic and plastic stress and strain, cladding oxidation, and fuel rod gas pressure as function of time. The fuel parameters that are slowly varying with time (burnup), such as fuel densification and swelling, and cladding creep and irradiation growth are not calculated by FRAPTRAN code. Those parameters are read from a file generated by FRAPCON code during the steady state simulation.

All required input data were taken from same technical reports already mentioned before. Additional required data (temperature and pressure as function of time) were taken from experimental data file.

The time length for LOCA experiment simulation (IFA series) was considered 100 s before the blowdown phase and up to reactor SCRAM, so the fuel rod burst time was properly considered, others input data were prepared according to FRAPTRAN User´s Manual.

As example of obtained results from FRAPTRAN code, the following Fig. 12 to 14 present the fuel rod pressure evolution during the LOCA for IFA-650.09, IFA-650.10 and IFA-650.11 cases, respectively.

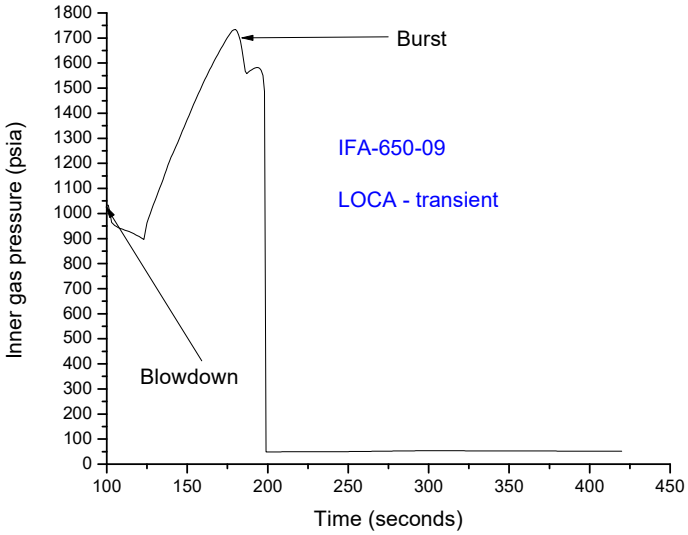

FIG. 12. Inner gas pressure during the LOCA simulation (IFA-650.09).

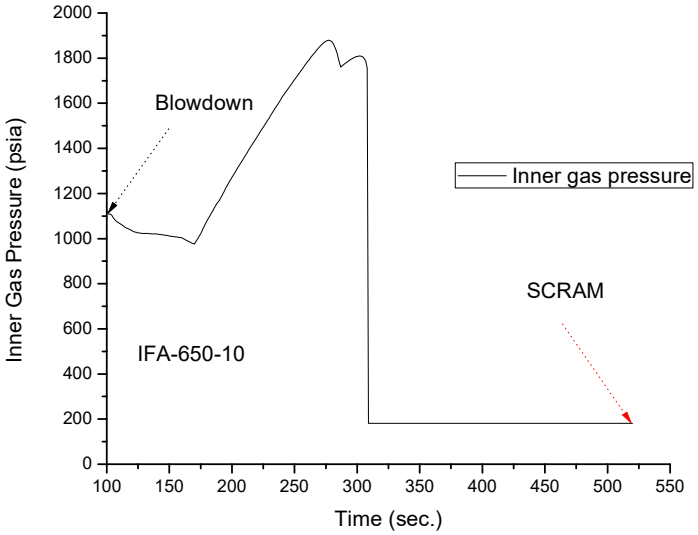

FIG. 13. Inner gas pressure during the LOCA simulation (IFA-650.10).

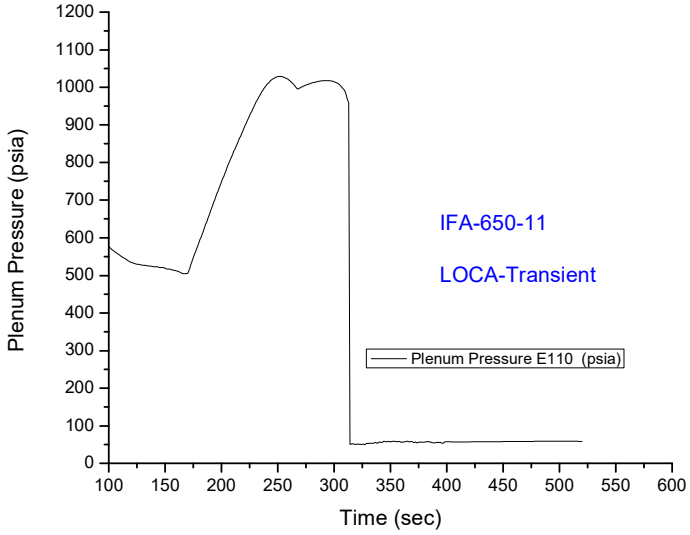

FIG. 14. Plenum gas pressure during the LOCA simulation (IFA-650.11).

2.3. FRAPCON and FRAPTRAN codes modification for stainless steel cladding

The IPEN contribution for FUMAC-CRP was to perform assessment and analysis considering stainless steel as cladding material. After Fukushima Daiichi nuclear accident, the ATF (Accident Tolerant Fuel) became a very important issue. In this context, the IPEN/CNEN (Brazil) has presented a proposal to modify the FRAPCON/FRAPTRAN codes in order to consider iron (Fe) based alloys as cladding material. Originally, FRAPCON/FRAPTRAN codes consider only zirconium based alloys as cladding material (Zircaloy-2, Zircaloy-4, M5, Zirlo, Improved Zirlo, and E110).

Existing material properties in the FRAPCON code was considered in modular subroutines that define material properties (thermal and mechanical) for temperatures ranging from room temperature to temperatures above melting and for fuel rod-average burnup levels between 0 and 62 gigawatt-days per metric ton of uranium. Each subroutine defines only a single material property: fuel thermal conductivity as a function of fuel temperature, fuel density, and burnup; fuel thermal expansion as a function of fuel temperature; and the cladding stress-strain relation as a function of cladding temperature, strain rate, cold work, hydride content, and fast neutron fluence.

In order to perform modification properly, initially all subroutines related to material properties were clearly identified. After verification of existing information in the specific subroutine related to material properties, the modification was performed replacing zirconium alloy data for stainless steel data. Some material properties for stainless steel were not available in the open literature, in that case, the material properties were not changed at all. Additional details can be found in the reference [12]: Revisiting Stainless Steel as PWR Fuel Rod Cladding after Fukushima Daiichi Accident, published in Journal of Energy and Power Engineering 8 (2014).

Some qualitative and quantitative comparisons were performed in other to verify the modifications implemented in the FRAPCON (stainless steel version) code. The FRAPTRAN code modification approach was the same as FRAPCON code and the verification was in process at that time (2016).

Specifically, for IFA experiment series simulations, the mechanical properties related to hoop strain and stress of cladding were not changed, due to that, the cladding burst failure should not be reliable and revision was planned for the future simulation (third year).

According to FRAPTRAN code documentation (User Manual), the BALON2 subroutine calculates the extent and shape of the localized large cladding deformation that occurs between the time that the cladding effective strain exceeds the instability strain and the time of cladding rupture. The BALON2 model predicts failure in the ballooning node when the cladding true hoop stress exceeds an empirical limit that is a function of temperature. The empirical limit was not changed in this work due to lack of burst data for iron based alloys. The limit adopted in this work was taken from the FRAPTRAN – User´s Manual, specifically the Fig. 2.18 (True hoop stress at burst as function of temperature).

2.4. Preliminary results for Stainless Steel cladding

The obtained results from FRAPCON/FRAPTRAN modified version were compared to original version of both codes (FRAPCON and FRAPTRAN) for zirconium based alloy.

The preliminary results are presented in Table 1 (base irradiation) and Table 2 (LOCA condition).

The base irradiation has shown similar results, main difference should be associated to heat transfer coefficient (zirconium alloy and Fe alloy). The material property difference cause an increase of fuel pellet temperature and high fission gas release, consequently slightly high internal fuel rod pressure.

TABLE 1. BASE IRRADIATION RESULTS FROM FRAPCON (ORIGINAL VERSION) AND FRAP-SS-IPEN (MODIFIED VERSION FOR AISI-348)

Parameters	IFA-650.09		IFA-650.10		IFA-650.11	
	Zircaloy	Stainless Steel	Zircaloy	Stainless Steel	E110	Stainless Steel
Maximum rod internal pressure (PSIA)	1376	1390	1231	1231	645	631
Fission gas release (%)	13.81	14.13	0.16	2.35	1.94	1.94
Maximum fuel centerline temperature (°F)	3267	3293	2397	2534	1782	1845

The result (see Table 2) obtained for LOCA simulation, somehow were not in good agreement due to ballooning (maximum circumferential strain data), the IFA-650.10 results for stainless steel were higher than zirconium alloy, others cases (IFA-650.09 and IFA-650.11) exhibited different trend. The mechanical ballooning model in the FRAPTRAN (BALON2) was not modified for the stainless steel code version due to that, the results are not consistent as expected. The assessment of ballooning model for stainless steel was in progress at that time.

TABLE 2. LOCA-TRANSIENT RESULTS FROM FRAPTRAN (ORIGINAL VERSION) AND FRAPT-SS-IPEN (MODIFIED VERSION FOR AISI-348)

Parameters	IFA-650.09		IFA-650.10		IFA-650.11	
	Zircaloy	Stainless Steel	Zircaloy	Stainless Steel	E110	Stainless Steel
Burst (sec)	99	134	109	110	258	267
Rod burst at elevation (ft)	0.787	0.787	0.722	0.722	0.787	0.787
Clad ballooning - maximum circumferential strain (%)	31.25	30.58	74.66	87.71	38.83	30.94

TABLE 2. LOCA-TRANSIENT RESULTS FROM FRAPTRAN (ORIGINAL VERSION) AND FRAPT-SS-IPEN (MODIFIED VERSION FOR AISI-348)

Parameters	IFA-650.09		IFA-650.10		IFA-650.11	
	Zircaloy	Stainless Steel	Zircaloy	Stainless Steel	E110	Stainless Steel
plenum gas pressure (PSIA)	48.68	49.73	181.4	181.4	58.15	56.62
plenum gas temperature (F)	1333	1476	1282	1284	1581	1599

Figures 15 to 17 present internal pressure evolution during the LOCA accident, obtained considering iron alloy and zirconium alloy for IFA-650.9, IFA-650.10, and IFA-650.11, respectively.

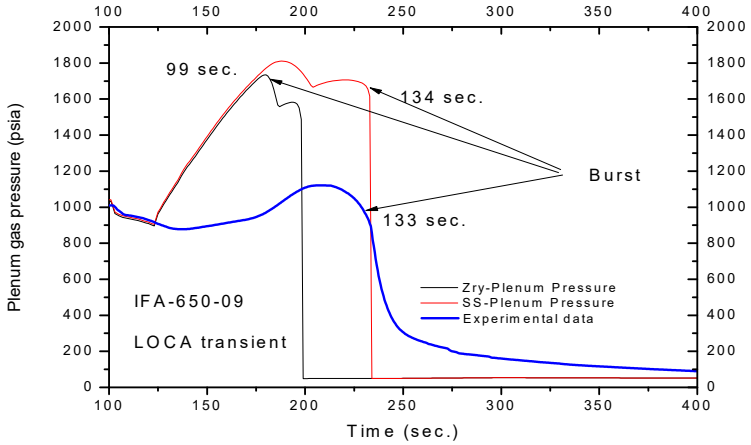

FIG. 15. Internal pressure evolution (plenum) during the LOCA transient (IFA-650.09).

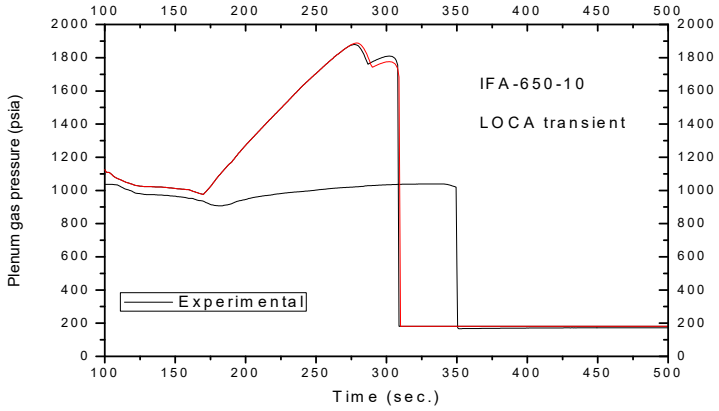

FIG. 16. Internal pressure evolution (plenum) during the LOCA transient (IFA-650.10).

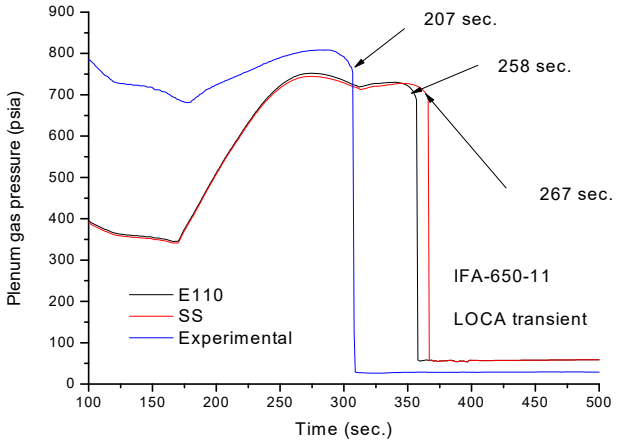

FIG. 17. Internal pressure evolution (plenum) during the LOCA transient (IFA-650.11).

According to recent publication: Cladding burst behavior of Fe-based alloys under LOCA [13], the stainless steel (Fe alloy) hoop stress parameter as function of temperature is higher than zirconium alloy (Fig. 4 of mentioned publication).

The mechanical model related to ballooning was detailed investigated in order to modify properly the subroutines associated to the burst calculations.

2.5. Review of FRAPCON and FRAPTRAN codes modification for stainless steel Cladding

The results obtained from the FRAPTRAN code modification and additional information from literature shown clearly that results might not be consistent. In order to verify better the burst phenomena, the subroutines dedicated to burst were verified in deep.

Considering that, the FRAPTRAN code shares with FRAPCON some subroutines related to the cladding, part of the modifications already implemented in the modified version of FRAPCON code for AISI 348 (stainless steel), could be utilized to change the FRAPTRAN code. Then, the modification of FRAPTRAN was reviewed step by step, initially the following subroutines from FRAPCON code were used in the FRAPTRAN: CCP, CELMOD, CSHEAR, CMHARD, CTHEXP, CTHCON, ZOEMIS, and ZOTCON. The subroutines related to mechanical properties of cladding such as stress and strain evaluation during the transient of cladding were identified in the CMLIMT [14] and CKMN subroutines, which calculate the limits of mechanical strain and the plastic strain for the cladding, respectively.

The modification was performed introducing in the code the data related to the burst stress as function of temperature for AISI-304 (stainless steel) obtained from Ref. [13], according to the equation 1:

$$ctstrt = (599.98 - 0.73269 \cdot T_C + 0.0002143 \cdot T_C^2) \cdot 10^6 \quad (1)$$

where:

$ctstrt$	is the tangential component of real stress at burst (in Pa);
T_C	is the temperature (in °C).

The stress-strain behavior in the FRAPTRAN code is described using two different correlations based on stress [8]. The deformation in the elastic region is described by the Hooke´s law as shown in equation 2:

$$\sigma = E\varepsilon \quad (2)$$

where:

σ is the stress;
E is the modulus of elasticity; and
ε is the strain.

The elastic strain is described by a power law

$$\sigma = K\varepsilon^{n}\left(\frac{\dot{\varepsilon}}{10^{-3}}\right)^{m} \quad (3)$$

where:

K is the strength coefficient;
n is the strain hardening exponent;
m is the strain rate sensitivity constant; and
$\dot{\varepsilon}$ is the strain rate.

From Eqs (2) and (3) was obtained the stress-strain curve with yield strength (YS), ultimate tensile strength (UTS), and uniform elongation (EU) for the studied material.

The coefficient K and the exponent n in equation 3 as function of temperature for stainless steel were obtained from Ref. [15].

The value for the constant m was not available for stainless steel, the m value was kept the same of the zircaloy, considering that the open literature shows that m values for metals are about 0.1 to 0.2. Those modifications were implemented and a verification of the modified version was performed using another LOCA experiment (IFA-650.5). The obtained results have shown qualitatively a better agreement with expected for stainless steel. Furthermore, IFA-650-10 experiment was verified and compared to previous modification, where the elasto-plastic deformation was not properly addressed; it is clearly that modification implemented represent better the deformation (Fig. 19).

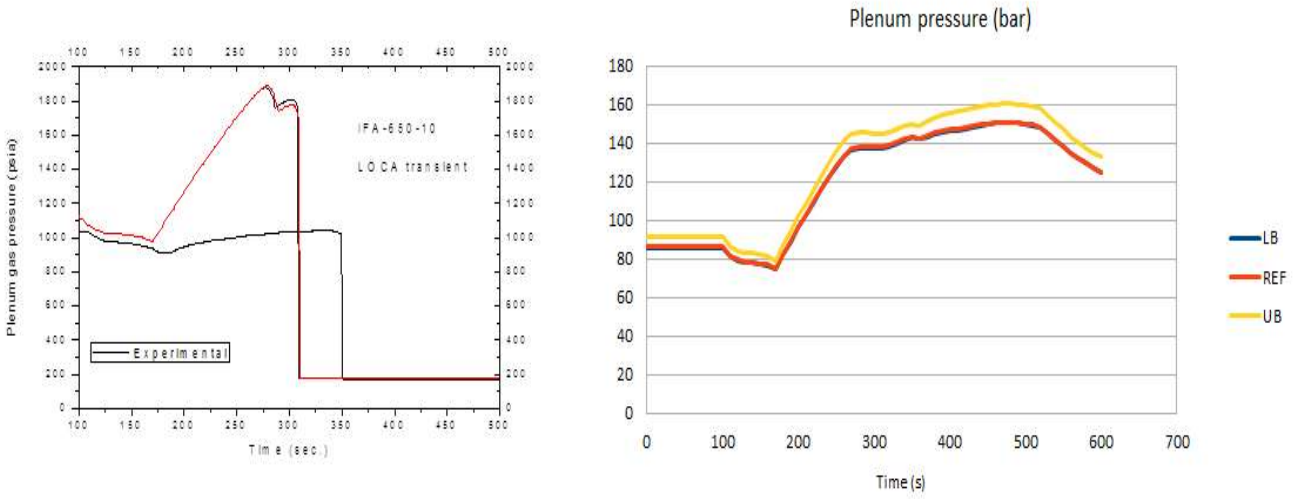

FIG. 18. Plenum pressure (IFA-650-10) evolution, left picture represent preliminary results before elasto-plastic implementation in the FRAPTRAN, right picture is after elasto-plastic properties of stainless steel implement in the FRAPTRAN.

2.6. Sensitivity and Uncertainties Assessment and Analysis for IFA-650.10 Considering Zircaloy and stainless steel cladding

The uncertainty and sensitivity assessment was conducted mostly according to Technical Specification (see Annex I). The IPEN/CNEN approach to perform the sensitivity analysis was slightly different compared to Technical Specification, mainly EXCEL spreadsheet was considered as a tool to assist in statistical analysis instead of DAKOTA package. The statistical distribution (normal) was applied for each one of the fuel fabrication/design parameters and for fuel models (physical properties) utilized in the fuel performance code (FRAPCON) models. The coupled (FRAPCON and FRAPTRAN) simulation was performed by means of script (GNU-OCTAVE), where all inputs files were generated and the results from outputs files were extracted automatically. The obtained results were statistically treated using EXCEL spreadsheet (Pearson Correlation) and some transient results were gathered in standard spreadsheet format as suggested by Dr. J. Zhang. The codes FRAPCON and FRAPTRAN applied to perform the assessment were the original version (as released by NRC for zirconium alloy) and a modified version (including material properties of AISI-348 cladding).

The IFA-650.10 experiment was modelled properly for steady state condition (FRAPCON) and transient (FRAPTRAN) condition taking into account the experimental data (temperature and pressure profile). Thermo-hydraulics calculation data from SOCRATES code were not considered.

Initially, a set of simulations was performed considering 200 (two hundred) runs (FRAPCON and FRAPTRAN), where fuel fabrication/design parameters were considered, such as: cladding thickness, gap thickness, fuel pellet outside diameter, U^{235} enrichment, fuel theoretical density and rod gas-gap fill pressure. The statistical distribution (normal) and tolerance interval (upper and lower bounds) for each fuel fabrication/design parameter were considered as suggested in the Technical Specification. Additionally, following fuel models (physical properties) embedded in the FRAPCON code were addressed: fuel thermal conductivity, fuel thermal expansion coefficient, cladding axial growth model, cladding creep model, fuel swelling model, fission gas release model, cladding corrosion and, cladding hydrogen pickup. The statistical distribution (normal) was considered as well as correspondent standard deviation for each fuel model (physical properties) as suggested in the Technical Specification. Moreover, suggested uncertainties in the boundary condition were not addressed because only the experimental data were taken into account for modelling the transient simulation. As the irradiation conditions (steady state) are explicitly simulated, the uncertainties in the initial states of the fuel rod will be propagated from steady state to transient simulation.

The IFA-650.10 experiment was addressed also considering stainless steel as cladding material and all others data were not changed, including irradiation condition and transient boundary condition.

After all simulations, the main outcomes are Pearson Correlation and some specific behavior and trends presented in the set of curves. Some extract of results presented in the Technical Report of sensitivity and uncertainties assessments are presented below.

TABLE 3. PEARSON CORRELATION FOR EACH FUEL FABRICATION PARAMETER FOR IFA-650.10.

Fabrication/design tolerance	Fission gas release	Maximum Plenum pressure	Peak fuel centerline temperature
dco	-0.02	0.10	-0.07
thkcld	0.01	0.01	-0.50
thkgap	0.28	0.13	0.99
enrch	0.05	0.08	-0.02
den	-0.87	-0.19	-0.04
fgpav	0.12	0.94	-0.15

*200 cases (normal distribution)

Table 3 shows the results obtained from FRAPCON (original version) considering the fuel fabrication parameters: cladding thickness (thkclad), gap thickness (thkgap), fuel pellet outside diameter (dco), U^{235} enrichment (enrch), fuel theoretical density (den), rod gas-gap fill pressure (fgpav). The results have shown that there are three strong Pearson correlation related to fuel fabrication parameters, as can be seen for fuel density and fission gas release, fuel rod fill gas pressure and maximum plenum pressure, gap thickness and fuel centerline temperature. The Pearson correlation outcome agrees with the expected results. As gap thickness increases, the heat transfer from fuel surface to clad surface will be degraded, consequently the fuel centerline temperature will increase. The higher initial fill rod gas pressure will produce higher final plenum pressure.

The following fuel model uncertainty parameters were addressed: fuel thermal conductivity (sigftc), fuel thermal expansion coefficient (sigftex), cladding axial growth (siggro), cladding creep (sigcreep), fuel swelling (sigswell), fission gas release (sigfgr), cladding corrosion (sigcor) and cladding hydrogen pickup (sigh2). Table 4 shows the results of Pearson Correlation due to the fuel models.

TABLE 4. PEARSON CORRELATION FOR EACH FUEL MODEL FOR IFA-650.10.

Fuel model	Fission gas release	Maximum Plenum pressure	Peak fuel centerline temperature
sigftc	NA	0.03	-0.55
sigftex	NA	0.04	-0.84
sigfgr	NA	0.07	-0.04
sigswell	NA	0.02	0.03
sigcreep	NA	-0.11	-0.07
siggro	NA	-0.10	-0.04
sigcor	NA	-0.04	0.17
sigh2	NA	-0.95	0.00

*200 cases (normal distribution)

It can be seen from Table 4, that there are three strong Pearson Correlation (PRC > 5.0) related to fuel model as can be seen for fuel thermal expansion coefficient, fuel thermal conductivity and, cladding hydrogen pickup, all correlations are negative.

The initial assessment have shown as each set of parameters (fuel fabrication and fuel model) are correlated taking into account isolated contribution and combination. The fuel fabrication parameters are more strong correlated to final results in the steady state simulation. As steady state condition at the end of irradiation somehow will propagate to transient simulation, it can be expected that, existing correlation somehow will contribute to the transient results.

After steady state simulations, transient simulations were addressed considering combined approach (fuel fabrication and fuel model) uncertainties due to the finding obtained in the first assessment (steady state simulation). According to Technical, the transient simulation results should be selected at specific phenomena time window in order to verify the existing correlation with the input parameters. The results selected to verify the correlation are related to thermal and mechanical behavior of fuel and cladding: Plenum Pressure, Fuel Centerline Temperature, Fuel Surface Temperature, Cladding Inner Temperature, Cladding Outer Temperature, Cladding Hoop Strain, Cladding Effective Stress, Cladding Radial Strain, Cladding Axial Elongation, Fuel Stack Elongation, Fuel Energy, and Fuel Surface Displacement. The phenomena time windows are: beginning of blowdown (100 s), end of blowdown (110 s), before burst (300 s), after burst (320 s) and, end of simulation (600 s).

The following tables (Tables 5, 6 and 7) present the Pearson Correlation results at beginning of blowdown.

TABLE 5. PEARSON CORRELATION* FOR TRANSIENT SIMULATION AT BEGINNING OF BLOWDOWN (T=100 S) FOR IFA-650.10.

Parameter	Plenum Pressure	Fuel Center Temperature	Fuel Surface Temperature	Clad Inner Temperature
dco	0.12	-0.08	-0.07	-0.02
thkcld	0.44	0.06	0.05	0.04
thkgap	-1.00	0.28	0.22	-0.03
enrch	-0.02	0.79	-0.20	0.33
den	-0.03	-0.47	-0.46	0.36
fgpav	0.11	0.16	0.12	-0.01
sigftc	-0.03	0.04	-0.03	0.02
sigftex	-0.03	0.00	-0.01	0.00
sigfgr	-0.11	0.00	0.05	0.03
sigswell	-0.07	-0.01	0.03	0.02
sigcreep	-0.02	0.04	0.00	0.03
siggro	-0.08	0.04	0.10	0.02
sigcor	0.02	0.01	-0.02	0.12
sigh2	-0.05	0.07	0.00	-0.02

*Nomenclature:

High correlation (grey color): PRC > 0.50 (absolute value)
Medium correlation (yellow color): 0.25 < PRC < 0.50 (absolute value)
Low correlation (white color): PRC < 0.25 (absolute value)

TABLE 6. PEARSON CORRELATION* FOR TRANSIENT SIMULATION AT BEGINNING OF BLOWDOWN (T=100 S) FOR IFA-650.10.

Parameter	Cladding Outer Temperature	Cladding Hoop Strain	Cladding Effective Stress	Cladding radial Strain
dco	0.00	-0.12	-0.12	0.12
thkcld	0.00	-0.44	-0.44	0.44
thkgap	0.00	1.00	1.00	-1.00
enrch	0.00	0.02	0.02	-0.03
den	0.00	0.03	0.04	-0.03
fgpav	0.00	-0.11	-0.11	0.11

TABLE 6. PEARSON CORRELATION* FOR TRANSIENT SIMULATION AT BEGINNING OF BLOWDOWN (T=100 S) FOR IFA-650.10.

Parameter	Cladding Outer Temperature	Cladding Hoop Strain	Cladding Effective Stress	Cladding radial Strain
sigftc	0.00	0.03	-0.01	-0.03
sigftex	0.00	0.03	-0.01	-0.03
sigfgr	0.00	0.11	0.07	-0.11
sigswell	0.00	0.07	0.02	-0.08
sigcreep	0.00	0.02	-0.03	-0.02
siggro	0.00	0.08	0.03	-0.08
sigcor	0.00	-0.02	-0.06	0.02
sigh2	0.00	0.05	0.03	-0.06

*Nomenclature:

High correlation (grey color): PRC > 0.50 (absolute value)
Medium correlation (yellow color): 0.25 < PRC < 0.50 (absolute value)
Low correlation (white color): PRC < 0.25 (absolute value)

TABLE 7. PEARSON CORRELATION* FOR TRANSIENT SIMULATION AT BEGINNING OF BLOWDOWN (T=100 S) FOR IFA-650.10.

Parameter	Cladding Axial Elongation	Fuel Stack Elongation	Fuel energy	Fuel Surface Displacement
dco	-0.08	-0.08	-0.05	-0.12
thkcld	0.06	0.06	0.09	-0.44
thkgap	0.28	0.28	0.33	1.00
enrch	0.79	0.79	0.46	0.03
den	-0.48	-0.48	-0.73	0.03
fgpav	0.16	0.16	0.17	-0.11
sigftc	0.05	0.05	0.03	0.03
sigftex	0.00	0.00	-0.02	0.03
sigfgr	0.00	0.00	-0.01	0.11
sigswell	-0.01	-0.01	-0.01	0.07
sigcreep	0.04	0.04	0.03	0.02
siggro	0.04	0.04	0.05	0.08
sigcor	0.02	0.02	0.02	-0.02
sigh2	0.07	0.07	0.05	0.05

*Nomenclature:

High correlation (grey color): PRC > 0.50 (absolute value)
Medium correlation (yellow color): 0.25 < PRC < 0.50 (absolute value)
Low correlation (white color): PRC < 0.25 (absolute value)

The following Figs 19 to 24 present the trend curves considering reference case (RF) bounding by lower (LB) and upper (UB) limits. Those Figures are also presented in the specific Technical Report regarding sensitivity and uncertainties assessment.

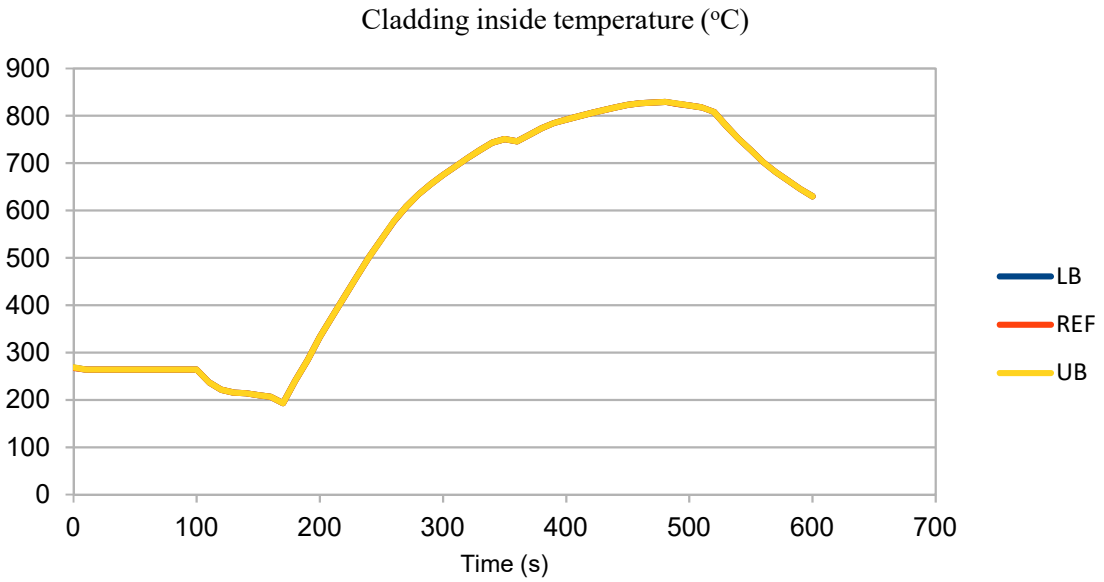

FIG. 19. Cladding inside temperature profile during the transient.

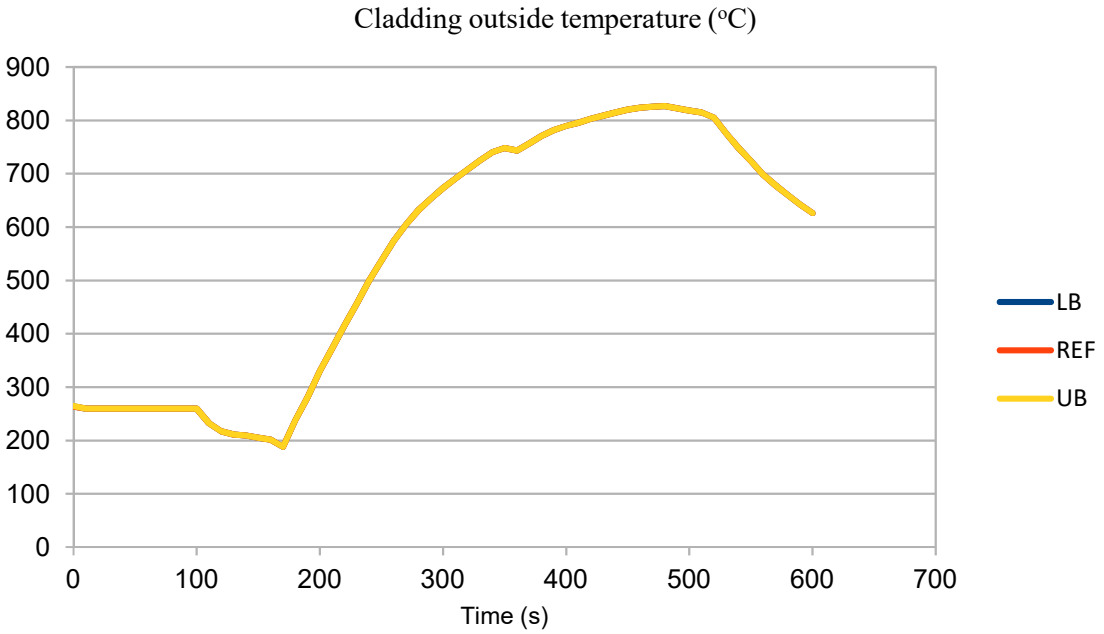

FIG. 20. Cladding outside temperature profile during the transient.

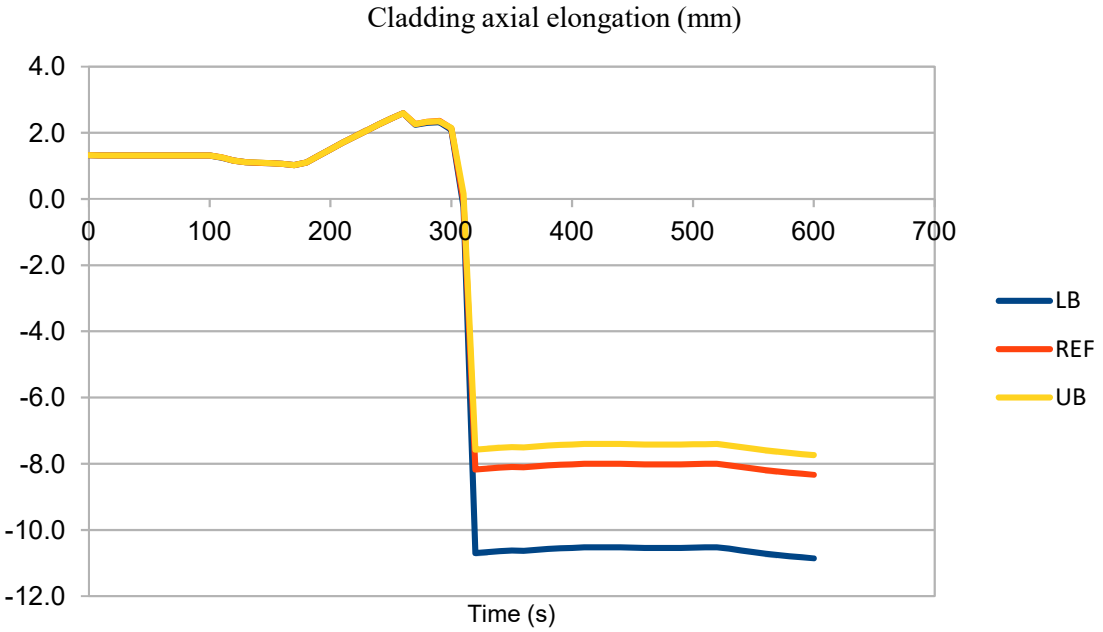

FIG. 21. Cladding axial elongation during the transient.

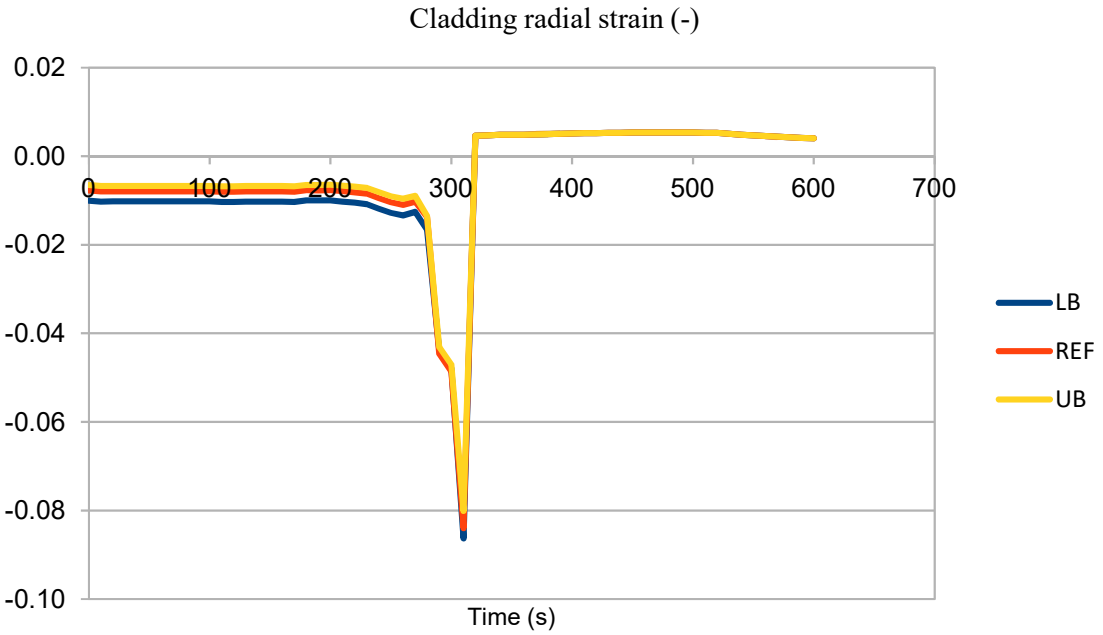

FIG. 22. Cladding radial strain during the transient.

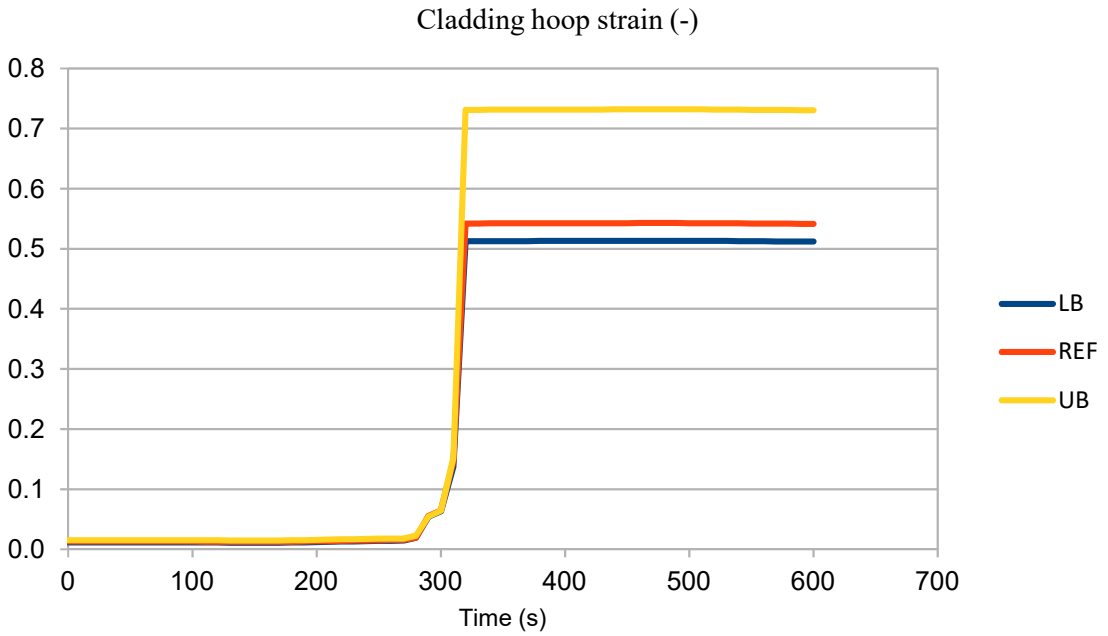

FIG. 23. Cladding hoop strain during the transient.

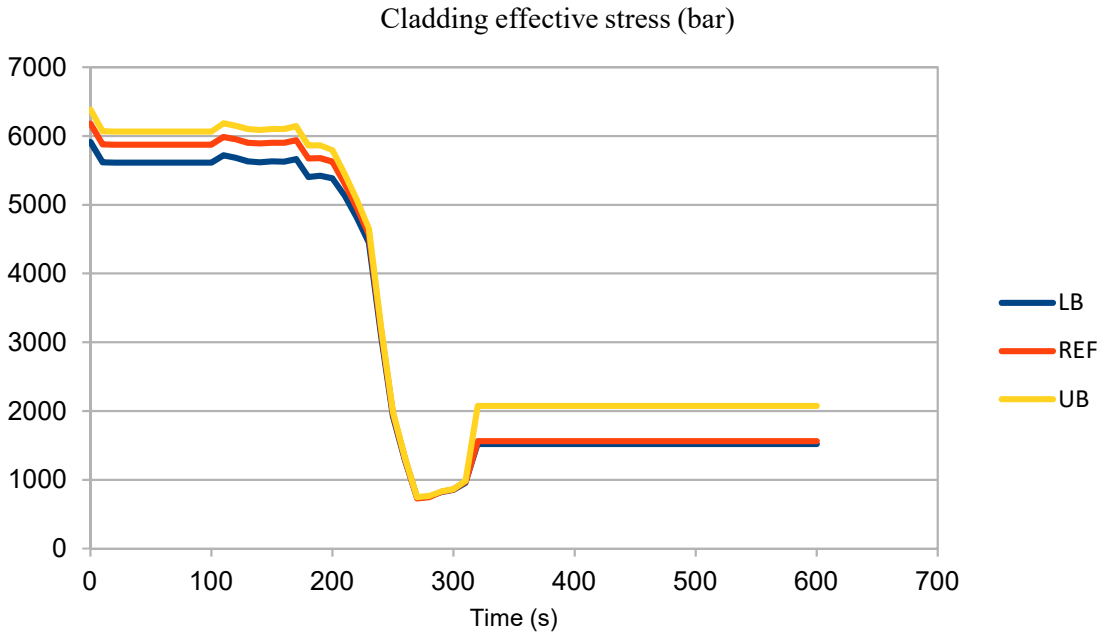

FIG. 24. Cladding effective stress during the transient.

The stainless steel assessment was carried out using the same approach as zircaloy cladding. Only the fuel cladding material was changed in the modelling, all others fuel data and boundary conditions were kept as original IFA-650.10. As example, Table 8 presents the results (Person Correlation) obtained for stainless steel.

TABLE 8. PEARSON CORRELATION FOR EACH FUEL FABRICATION PARAMETER AND FUEL MODEL (STAINLESS STEEL AS CLADDING).

Fuel model and fuel fabrication tolerance	Fission gas release	Maximum plenum pressure	Peak fuel centerline temperature
dco	-0.10	-0.01	-0.08
thkcld	-0.52	-0.35	-0.50
thkgap	0.98	0.78	0.97
enrch	-0.02	0.04	-0.02
den	-0.03	-0.15	-0.08
fgpav	-0.18	0.45	-0.14

*200 cases (normal distribution)

The following Figs. 25 to 30 present the trend curves obtained for stainless steel cladding considering reference case (RF) bounding by lower (LB) and upper (UB) limits for each one of the transient results selected for analysis. Those Figures were taken from specific Technical Report (already delivered) of Sensitivity and Uncertainties Assessment.

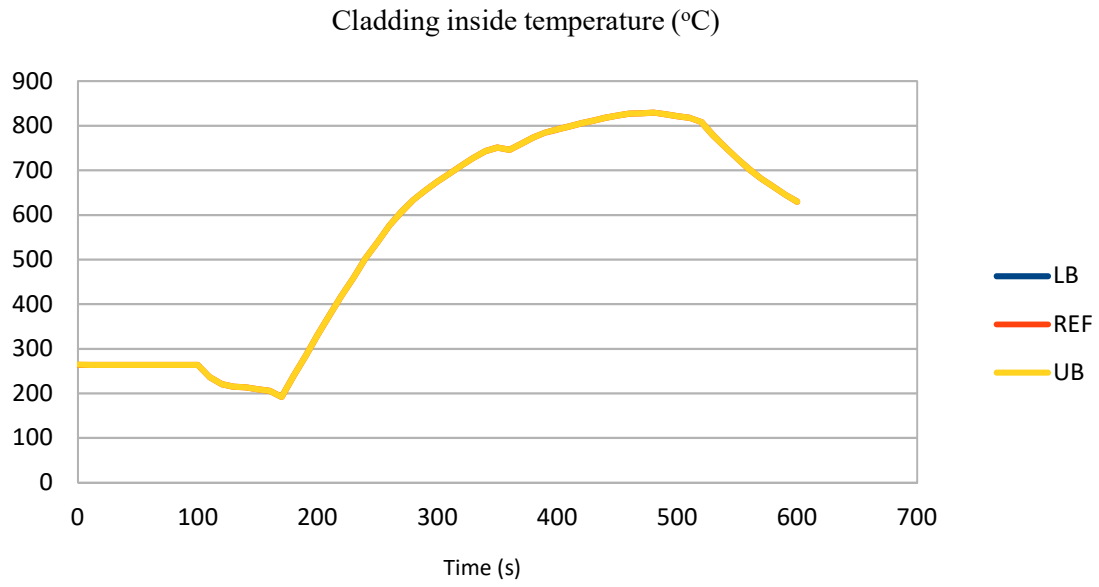

FIG. 25. Cladding (stainless steel) inside temperature profile during the transient.

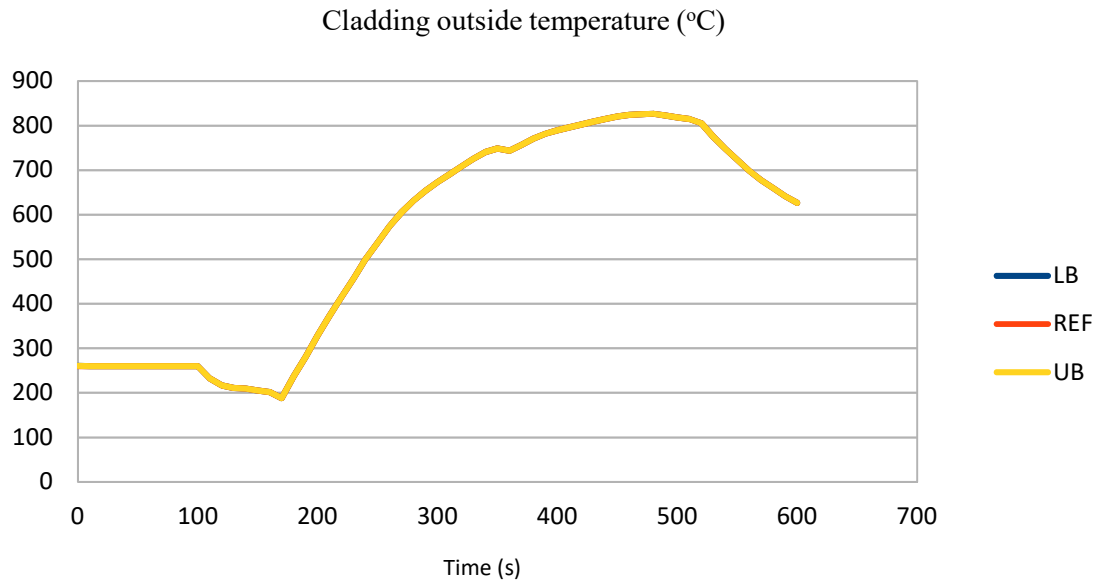

FIG. 26. Cladding (stainless steel) outside temperature profile during the transient.

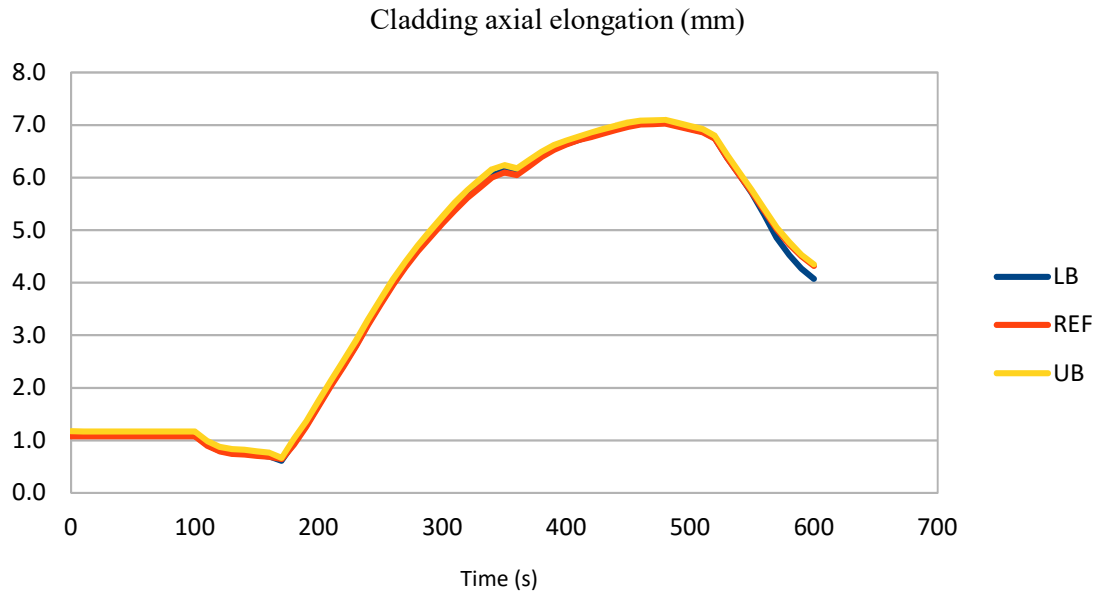

FIG. 27. Cladding (stainless steel) axial elongation profile during the transient.

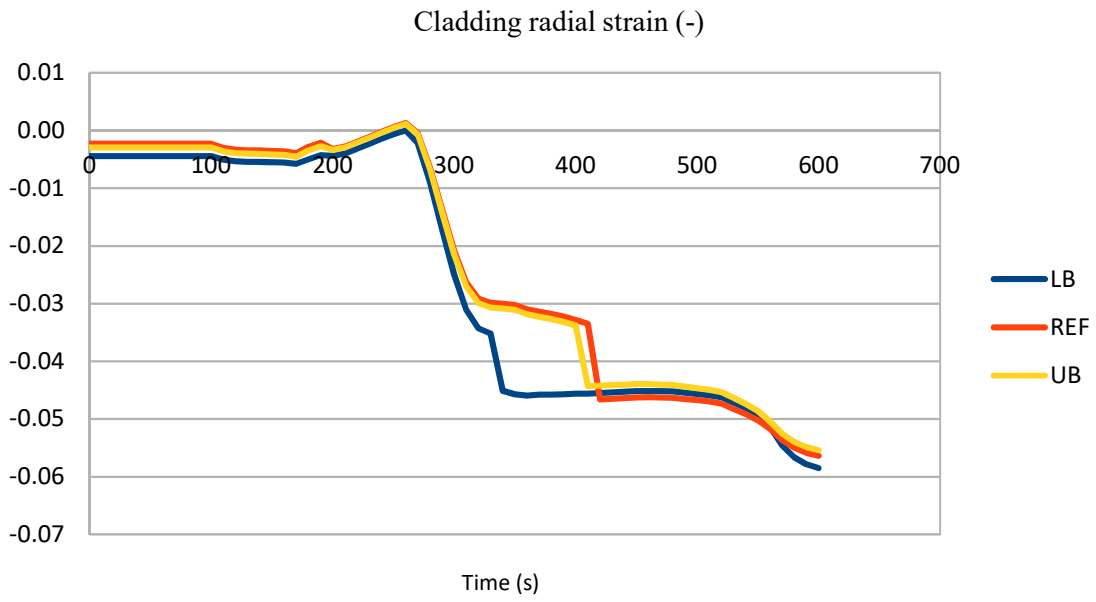

FIG. 28. Cladding (stainless steel) radial strain profile during the transient.

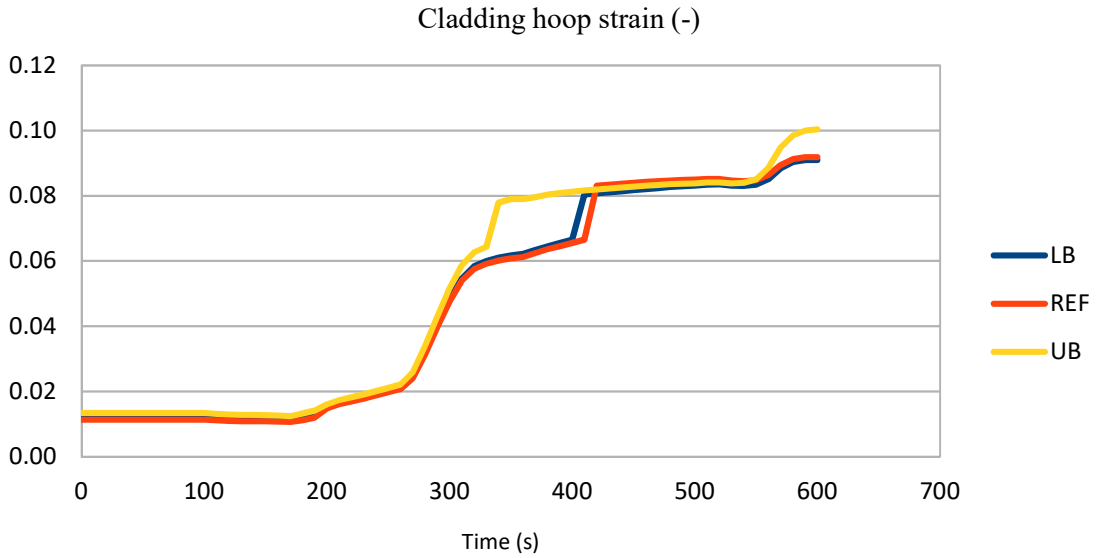

FIG. 29. Cladding (stainless steel) hoop strain profile during the transient.

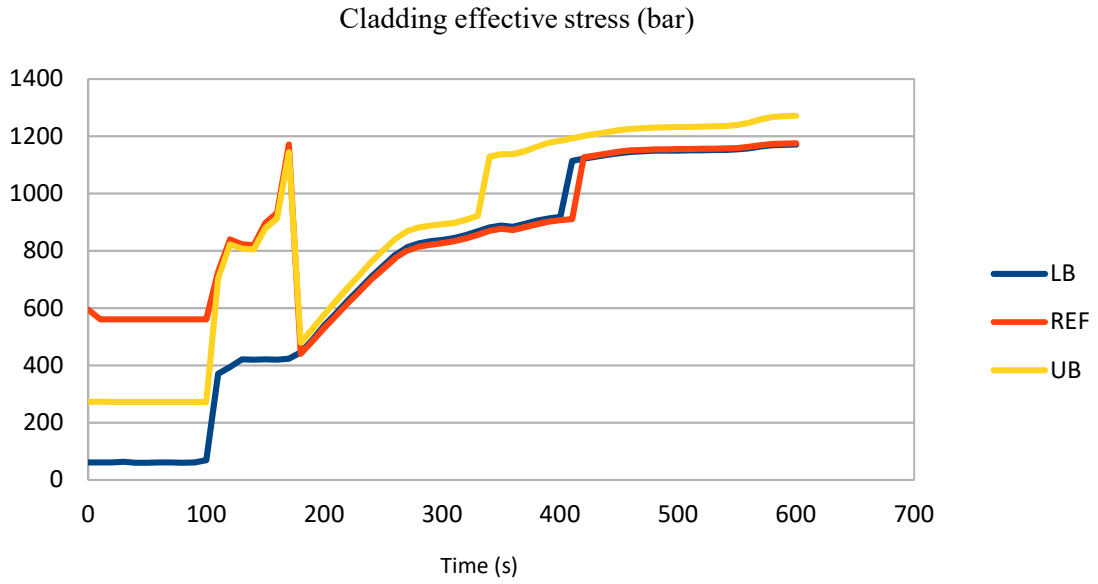

FIG. 30. Cladding (stainless steel) effective stress profile during the transient.

3. ANALYSIS AND CONCLUSIONS

One of the challenging design basis accidents for water cooled reactors is the loss of coolant (LOCA) caused by the failure of a large coolant pipe. More specifically, for the PWR reactor the initiating event of the design basis accident is the double-ended guillotine break of one of the large coolant pipes between the reactor vessel and the main circulation pump. In order to mitigate the consequences of this event, it is mandatory that all reactors must have an emergency core cooling systems in order to keep the fuel cooled efficiently and a coolable geometry through all phases of the accident. The requirement associated to coolable geometry and structural integrity is very challenging issue for fuel rod with zirconium alloy as cladding.

In the LOCA event there are at least two ways in that coolable geometry of the reactor core could be compromised: fuel clad ballooning which can lead to partial blockage of the fuel assembly channel and loss of cladding integrity during the emergency cooling system actuation (quench and loading associated after quench). The U.S. NRC (American Nuclear Regulatory Commission) address the issue considering requirement for peak cladding temperature (PCT < 1204°C) and a maximum cladding oxidation of ECR < 17%.

Before discussing the criteria associated to coolability and their implication is important to review some aspects of Zircaloy as fuel cladding material. During the sixties (1960´s), zircaloy became the standard material for cladding materials in Light Water Reactors (LWR), Zircaloy-2 in BWR cores and Zircaloy-4 in PWR cores. However, besides the fuel assemblies, most of the structural components remained to be made from stainless steel or Ni-alloys. Later, the use of zircaloy for other fuel components occurred mainly after the eighties (1980s). Due to corrosion detected in the current zircaloy, an optimized Zircaloy-4 was developed at Siemens named PCA-Zircaloy (with PCA for 'Prime Candidate Alloy') mainly for PWR reactor and other designers/vendors were following with improved Zircaloy-4 cladding material, such as: AFA 2G-Cladding by Framatome/Fragema, OPTINTM by ABB and "Improved Zircaloy-4" from Westinghouse.

The improvement knowledge obtained during the optimization of zircaloy gives a new generation of zirconium material cladding for PWR, called "Duplex Cladding". Others different composition were made available in order to increase the corrosion resistance, such as M5, M4, HPA-4 (Siemens), ZIRLO (Westinghouse), HANA (KNFC), E635 and E110(Russia). These are the alloys currently utilized and some of them have substantial operational experience in

commercial PWRs and performance data from experiments (in-pile tests) performed under operational and accident condition.

Nowadays, the new alloys mentioned above are currently utilized and level of burnup increase compared at a time when the acceptance criteria was stablished. The aim of the criteria was to ensure some margin of ductility would remain in the zircaloy cladding when subject to quench process and therefore the reactor core could remain essentially intact and keep some condition for long term cooling. Furthermore, such criteria (PCT and ECR) include some conservatism degree due to lack of data related to oxidation embrittlement. Later, in 1988 the NRC considered that there are sufficient experimental data to quantify the degree of conservatism associated to the current criteria and amended the requirements of 10CFR50.46 Appendix K for the use of best-estimate models, including the Cathcart-Pawel oxidation correlation, therefore somehow these regulations would reflect the improved understanding of the phenomena that occurs during the LOCA transient.

Currently, many experimental data have shown that different factors can influence cladding embrittlement during a LOCA event; several important variables can influence and contributes including initial pre-transient hydrogen content, breakaway oxidation, inner surface oxygen uptake. Moreover, some others contribution are not clearly well-understood.

The CRP FUMAC was an excellent opportunity to address and verify how existing fuel performance code can simulate properly the LOCA event considering experiment performed specifically for LOCA evaluation, such as IFA-650 experiments series, CORA from KIT, NRC-STUDVIK and others.

Moreover, verify the sensitivity and uncertainties related to fuel parameters (fabrication, models, boundary condition, etc.) that could affect and/or have some correlation to the fuel cladding integrity.

The objective proposed by IPEN/CNEN (Brazil) was accomplished considering the investigation performed using stainless steel as cladding. The most important outcome of the CRP-FUMAC participation is the performance of stainless steel during the accident of loss of coolant, the fuel cladding integrity was preserved during all steps of the LOCA event, furthermore after Fukushima accident and all research related to ATF fuel, the iron based alloy can be a very promising candidate, especially stainless steel.

REFERENCES

[1] PARSONS, P.D., HINDLE, E.D., MANN, C.A., “PWR Fuel Behaviour in Design Basis Accident Conditions. A State-of-the-Art Report by the Task Group on Fuel Behaviour of CSNI Principal Working Group No 2”, Committee on the Safety of Nuclear Installations, OECD-NEA, NEA/CSNI-129, (1986).

[2] U.S. NUCLEAR REGULATORY COMMISSION, “Acceptance Criteria for Emergency Core Cooling Systems for Light-Water Nuclear Power Reactors”, 10 CFR 50.46, USA.

[3] CHUNG, H.M. “Fuel Behavior under Loss-of-Coolant-Accident Situations”, Nucl. Eng. Technol. , Vol. 37, 327 (2005).

[4] HESSON, J.C. et al., Laboratory Simulations of Cladding-Steam Reactions Following Loss-of-Coolant Accidents in Water-Cooled Power Reactors, Argonne National Laboratory, ANL-7609 (1970).

[5] MASSIH, A.R., Transformation Kinetics of Zirconium Alloys under Non-Isothermal Conditions, J. Nucl. Mater., Vol. 384, (2009) 330–335.

[6] NAGASE, F., FUKETA, T., Investigation of Hydride Rim Effect on Failure of Zircaloy-4 Cladding with Tube Burst Test. J. Nucl. Sci. Technol., Vol. 42, (2005) 58.

[7] UDAGAWA, Y., NAGASE, F., FUKETA, T., Effect of Cooling History on Cladding Ductility under LOCA Conditions, J. Nucl. Sci. Technol., Vol. 43, (2006) 844.

[8] M. Ek, “LOCA Testing at Halden, the Third Experiment IFA-650.3”, OECD Halden Reactor Project, HWR-785, (2005).
[9] MANNGARD, T., STENGARD, J., Evaluation of the Halden IFA-650 Loss-of-Coolant Accident Experiments 5, 6 and 7, 2014:19 ISSN:2000–0456, Swedish Radiation Safety Authority, Sweden (2014).
[10] GEELHOOD, K. J., LUSCHER, W.G., FRAPCON-3.5: A Computer Code for the Calculation of Steady-State, Thermal-Mechanical Behavior of Oxide Fuel Rods for High Burnup, Vol. 1, Rev.1, NUREG/CR-7022, (2014).
[11] GEELHOOD, K. J., LUSCHER, W.G., CUTA. J. M., FRAPTRAN-1.5: A Computer Code for the Transient Analysis of Oxide Fuel Rods, Vol. 1 Rev.1, NUREG/CR-7023, U.S. Nuclear Regulatory Commission (2014).
[12] KULA, A., GIOVEDI, C., TEIXEIRA, A., GOMES, D.S., Revisiting Stainless Steel as PWR Fuel Rod Cladding after Fukushima Daiichi Accident, J. Energ. Eng., Vol. 8, (2014) 973–980.
[13] MASSEY, C.P., TERRANI, K.A., DRYEPONDT, S.N., PINT, B.A., J. Nucl. Mater., 470, (2016) 128–138.
[14] HAGRMAN, D.L., “Code Development and Analysis Program Cladding Mechanical Limits (CMLIMT)”, Report prepared by EG&G - IDAHO CDAP-TR-056.
[15] DESU, R. K., et al., “Mechanical Properties of Austenitic Stainless Steel 304L and 316L at Elevated Temperatures,” J. Mater. Res. Technol., 5, (2016) 13–20.

FUEL ROD BEHAVIOUR MODELLING AND SAFETY EVALUATION BY TRANSURANUS CODE: HALDEN LOCA TESTS IFA-650

S. BONEVA, M. MANOLOVA, N. MIHAYLOV, ML. MITEV
Instutute for Nuclear Research and Nuclear Energy,
Bulgarian Academy of Sciences
72, Tzarigradsko schaussee Blvd.
1784 Sofia, Bulgaria

Abstract

This paper summarizes the work performed by the Institute for Nuclear Research and Nuclear Energy (INRNE, BAS) – Sofia, Bulgaria in the IAEA's Coordinated Research Project "Fuel Modelling in Accident Conditions (FUMAC)". The IFA 650 LOCA experiments in Halden are integral in-pile tests on fuel behaviour under simulated LOCA conditions. Two cases from the Halden LOCA experiments are the subject of this analysis: IFA650.11 - test with WWER fuel, manufactured by JSC TVEL and pre-irradiated up to 56 MWd/kgU in the Loviisa NPP (Finland). The cladding material was the Zr alloy E110. IFA650.10 LOCA experiment is a test on PWR fuel behaviour, pre-irradiated up to 60MWd/kgU. The modified version of the TRANSURANUS code with incorporated specific LOCA models was applied and predicted fuel behaviour was analysed and compared. Applying the Monte-Carlo technique, TRANSURANUS code allowed statistical variations of large number of input quantities to be simulated according to Gaussian distribution. Results of the calculation with nominal value of input parameters and with sufficient large number of Monte-Carlo simulations are enclosed in this report as well.

1. INTRODUCTION

The present paper presents the research work, done at the Institute for Nuclear Research and Nuclear Energy (INRNE, BAS) – Sofia, Bulgaria in the frame of the IAEA's Coordinated Research Project "T12028", entitled "Fuel Modelling in Accident Conditions (FUMAC)".

According to the work program of the project INRNE had to analyze the fuel performance of WWER rods included into the CRP FUMAC by means of the TRANSURANUS code. INRNE team made code predictions for any optional WWER cases that are available within the FUMAC framework. In particular, attention is given to experiments that provide support for verification and validation of the TRANSURANUS (WWER version) code for design-basis accidents (DBA) simulations at the initial stage of a severe accident, when the cylindrical fuel rod geometry is still preserved.

Most of on-going experiments with nuclear fuel and developments of fuel performance codes lie in the field of DBA conditions as applicable for loss-of-coolant and reactivity-initiated accidents (LOCA and RIA). The behaviour of in-core materials, especially of fuel cladding, in extreme high temperature and corrosive environments is among the primary factors that define accident evolution. The simulation tools are developed and validated on the OECD/NEA and IAEA data base. The IAEA CRP "Fuel Modelling in Accident Condition" (FUMAC) supports different Member States in their efforts to develop reliable tools for modelling of fuel behaviour during accidents. This task is tackled by share of experimental data and comparison of modelling predictions acquired with different computer codes.

TRANSURANUS code is one of the most powerful computer codes [1] for assessing fuel performance developed to high level of reliability at the Modeling Group of the European Commission Institute for Transuranium Elements in Karlsruhe, Germany. Reactor Physics Laboratory in INRNE-BAS gained experience with this code and the new version developed [2] in order to simulate design basic accident (DBA) conditions. Last two version of the code were used to simulate Halden LOCA experiments in the frame of CRP FUMAC. The Halden LOCA experiments IFA650.2 with fresh nuclear fuel and IFA650.11 with WWER fuel were

simulated by version v1m1j14, officially released between users. The new TRANSURANUS version v1m1j17 with developed and implemented models for transient fission gas bevahiour, double sided cladding oxidation after burst of the rod, H-uptake and accounting for effects on mechanical cladding properties was implemented for simulation of the IFA650.10 and IFA650.11. The calculations were performed for base irradiation as well as for the LOCA test irradiation, using restart option of TRANSURANUS code for account rod cutting and refilling. The calculations were done with two different models of thermo-hydraulic boundary conditions and code predictions were analyzed and compared.

Applying the Monte-Carlo technique, TRANSURANUS code allowed statistical variation of large number of input quantities to be simulated according to normal (Gaussian) distribution. Using the new developed version of TRANSURANUS code [3] the statistical uncertainty analysis of case IFA650.10 was performed. Uncertainties in fuel rod operation and test boundary conditions as well as material properties of the fuel and cladding were considered. Impact of realistic input uncertainties has been tested for the output parameters specified in the FUMAC recommendations. Results of the calculation with nominal value of input parameters and with sufficient large number of Monte-Carlo simulations are enclosed in this report.

2. OECD HALDEN REACTOR PROJECT - LOCA TESTING

The IFA 650 LOCA experiments in Halden are integral in-pile tests on fuel behaviour under simulated LOCA conditions. The IFA 650 test rig is designed for a single fuel rod. The test section is located inside a test channel in the Halden research reactor and is connected to the external Heavy Water High Pressure loop [4]. The rig is cooling by natural circulation. The rod is surrounded by an annular flow channel, which is separated from the outer annular channel by an electrically heated shroud. One fuel rod is located in a standard high-pressure flask, which was connected to a heavy water loop and a blow down system. Heating was provided from the fuel pellets and from the heater surrounding the fuel rod. The heater was used to simulate the heat from the adjacent rods. The cladding temperature was controlled by the rod and heater power. The experimental goal was to produce cladding ballooning and burst and to achieve a peak cladding temperature. The rod power can be controlled by varying the additional heating and by changing the reactor power. The test rig instrumentation consists of two heater thermocouples, two inlet and outlet coolant thermocouples, a flow meter, three self-powered vanadium neutron detectors (ND) and two fast response cobalt neutron detectors (NDs). The two embedded heater thermocouples are located above and below the axial mid height of the fuel rod. The volume flow rate is measured in the external loop. The axial power distribution can be observed by the three vanadium NDs, which are located at three elevations.

The test conditions were planned to meet the following primary objectives: to maximize the ballooning size to promote fuel relocation and to evaluate its possible effect on the cladding temperature and oxidation; to investigate the extent (if any) of “secondary transient hydriding” on the inner side of the cladding around the burst region.

The Halden LOCA test project covers both fuel rods with fresh fuel and pre-irradiated rods up to high burnup during steady-state normal operation.

The goal of our study is:

— To study TRANSURANUS code predictions of WWER fuel rods under off-normal conditions (LOCA);
— To demonstrate the TRANURANUS capabilities for statistical analysis of fuel performance simulations.

The calculations were done for base irradiation as well as for the test irradiation, using restart option of TRANSURANUS code for account rod cutting and refilling. The Halden LOCA tests analyzed are: IFA-650.2 one fresh fuel rod, tight-gap and pressurized PWR fuel rod with Zr-4 cladding; IFA650.10 – pre-irradiated PWR up to 61 MWd/kgU, cladding of Zy-

4 + boundary conditions (BC) determined by means of multi-physics/dimensional tools, SOCRAT modelling + uncertainty analysis: IFA650.11 with pre-irradiated WWER fuel rod, cladding Zr1%Nb alloy and two models of BC.

3. OECD HALDEN REACTOR PROJECT - LOCA TESTING AT THE SECOND EXPERIMENT IFA-650.2

In IFA-650.2 test one fresh PWR fuel rod with tight-gap, high inner pressure (4MPa (RT) and Zry-4 cladding was located in a standard high-pressure flask, which was connected to a heavy water loop and a blow down system [5].

The IFA-650.2 post calculation the normal operation and natural convection parts were modelled using standard TRANSURANUS options for these cases. The post experimental calculations of the blow down and dry out phase are based on thermo-hydraulic boundary conditions calculated with the ATHLET code [6] and data obtained from the experiment itself. As thermo-hydraulic boundary condition the calculated outer cladding temperature was used as TRANSURANUS input. The values for plenum temperature, system pressure and linear heat generation were taken from the measurements. The average coolant outlet temperature was chosen as plenum temperature.

The time of cladding burst could be recognized by the cladding extensometer records as well as the drop of inner pin pressure. The comparison of calculated cladding elongation and extensometer data is presented on Fig. 1 and shows an acceptable accuracy of TRASURANUS prediction.

A good indicator of rod failure is the drop of inner pin pressure. Coolant pressure after start of the blow down and calculated inner pin pressure for the same time period are presented on the Fig. 2. Measured rod pressure is also presented in Fig. 2.

Next two pictures present the comparison of the time dependence cladding elongation and inner rod pressure of IFA650.2 LOCA test.

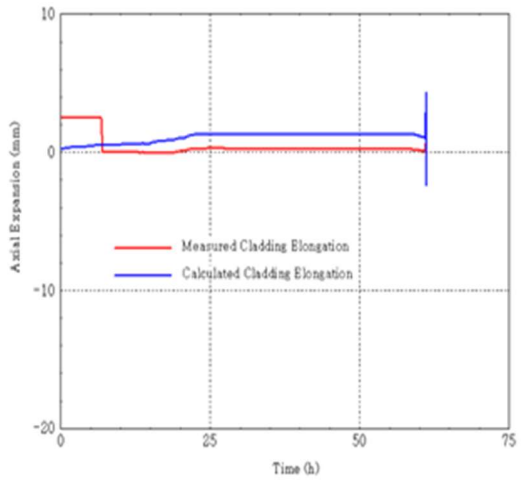

FIG. 1. Cladding Elongation, calculated and measured.

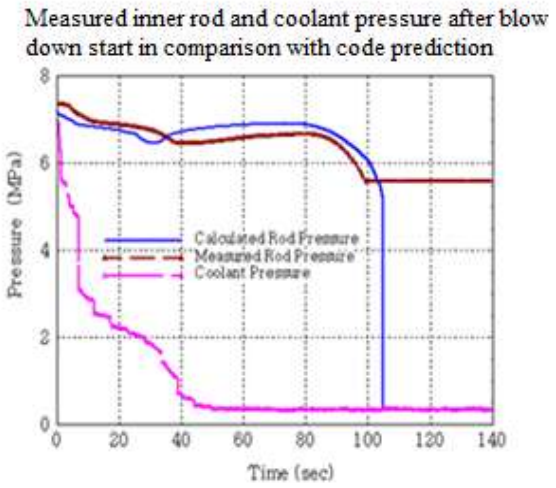

FIG. 2. Gap Pressure comparison after blow down start.

Durin the experiment the pressure transducer stuck at 5.6 MPa after rod rupture but the time of burst could be compared. The calculated inner pin pressure underestimated in the blow down phase and overestimated in the dry out phase. The difference between the calculated inner pin pressure and the measured data might be caused by a not well known plenum temperature used in the calculation.

4. OECD HALDEN REACTOR PROJECT - LOCA TESTING AT THE ELEVENTH EXPERIMENT IFA-650.11

4.1. Description of the experiment

IFA650.11 is the test with WWER fuel, manufactured by JSC TVEL and pre-irradiated up to 56 MWd/kgU in the WWER Loviisa NPP (Finland) [7] The test segment (length of 480mm) was cut from a standard WWER fuel rod. The rod was filled with a gas mixture of 95% Ar and 5%He at 3 MPa (RT). Argon was chosen to simulate the fission gases. The rod plenum volume (free gas volume) was made relatively large in order to maintain stable pressure conditions until cladding burst. The total free gas volume of ~16–17 cm^3 was practically all located in the plenum, outside the heated region. The cladding material was the Zr alloy E110 and the pellet bore diameter 1.50 mm. The main fuel rod parameters as well as the surrounding conditions are presented in the Table 1.

TABLE 1. IFA650.11. FUEL PARAMETERS

Description	Value
Burnup	56.0 (MWd/kgU)
Active fuel length	480 (mm)
Enrichment	3.6 (wt% U^{235})
Fuel density	10.64 (g/cm^3)
Fuel diameter	7.55 mm
Pellet centre hole	1.484 (mm)
Cycles	4
Cladding material	Zr1%Nb
Clad outer diameter	9.13 (mm)
Cladding thickness	0.679 (mm)
Oxide thickness, irradiated, mean	5 (μm)
Filling gas / Pressure	95% Ar+5% He/ 3MPa (RT)
Free volume (as designed)	16 (cm^3)

Prior to the test during normal operation (25 days), the rig was connected to the loop and forced circulation flow, the system pressure was set to 7MPa. Shortly before the test about 3 min, the rig was disconnected from the loop and flow separator enabled natural convection flow in it. When blow down started the channel pressure decreased to 4MPa and the rig was practically emptied of water in 70 s. The heat-up phase started – ballooning and burst (207 s after blow down). The test was ended by reactor scram.

4.2. IFA 650.11 LOCA test - TRANSURANUS simulation

The LOCA extension of the fuel performance code TRANSURANUS is designed to calculate both steady state part of the fuel rod life with appropriate models and transient. In the transient LOCA part of the calculation some cladding mechanics have to be treated either with special LOCA models or they have to be switched off. The rod re-fabrication requires the input modifications. When the assumed time of the LOCA event is reached, the calculation is stopped

and the steady state models are replaced by the transient mode and special LOCA models. For the change from steady state model to LOCA models and the data manipulation e.g. to simulate the re-fabrication, the TRANSURANUS restart option and restart data modification modules are used. Using the re-start mode of the code the plenum volume (height), inner gas amount, gas composition and rod pressure are adjusted at the moment of the restart according the test data.

The LOCA test IFA 650.11 with pre-irradiated WWER fuel was of special interest for our work. The IFA650.11 case was simulated using restart option of the code, with two versions of TRANSURANUS code (v1m1j14 and v1m1j17). Version (j17) developed in the frame of CRP FUMAC [3] includes new options for the LOCA-modelling: the corrosion model is changed and it considers oxidation both on the outside and on the inside of cladding after rod burst incl. spalling, hydrogen uptake is considered; some of the material properties of the fuel are refined.

Halden test IFA650.11 was simulated using two models of the boundary conditions (BC) during LOCA phase of the test:

— The axial distribution of rod outer cladding temperature was created using the measured cladding temperature from the Halden TFDB database. The cladding temperature was measured at two points in axial direction of the rod, but there aren't any data about axial profile and the position of peak cladding temperature. Cladding temperature was modelled by using the measured data at two points and assuming a parabolic temperature profile with the peak clad temperature at elevation 150 mm. The thermo-hydraulic behaviour in test period was calculated using the mass flow rate and the coolant inlet temperature data as done in the steady state part. The data for plenum temperature (thermocouple TCC3, placed on the outside surface at axial midplane of the plenum) were prescribed at the last (11th) small node of fuel;
— More accurate way to simulate the thermo-hydraulic (T/H) environment during LOCA test is to calculate it by means of multi-physics/dimensional tools and used it as input data for the LOCA part of the TRANSURANUS calculation. The recently release T/H data for Halden LOCA tests calculated by SOCRAT code are applied and new simulation of IFA650.11 was performed by new version of TRANSURANUS code (J17).

As is pointed out in the [8], a reasonable agreement between thermocouple records and calculated cladding temperature in the case IFA650.11 was performed with 15% reduction of total rod power. In this new simulation the linear heat rate, coolant pressure, cladding outside temperature and upper plenum temperature are prescribed in input file of TRANSURANUS code according results of SOCRAT code calculations.

To choose suitable for this case model, the following considerations had to be taken into account. Fuel rod was modelled with 10 equidistant slices and 1 thin slice which attributed plenum temperatures. Linear heat rate and the fast neutron flux are simulated with axial profile. The model options comprised the standard TRANSURANUS recommendations for simulation of WWER fuel rods. UO_2 material properties were modelled by standard TRANSURANUS models for LWR. Standard Zr1%Nb cladding material correlations, models and options for the TRANSURANUS version v1m1j14 were selected.

The simulation with new version (j17) takes into account the new oxidation model as well. The base irradiation (4cycles in Loviisa WWER 440, Bu=56MWd/kgU) was modeled in of these two TRANSURANUS simulations (applied versions v1m1j14 and v1m1j17) without any differences. The base irradiation power history is slightly simplified (no axial profile) because the tested rod (480mm long) is a small part of the whole rod irradiated in WWER. Using the restart mode of TRANSURANUS the rod re-fabrication was accounted – new filling gas (95%Ar and 5%He) and 3MPa inner rod pressure and large plenum volume of 17cm^3. The

rod free gas volume was made relatively large in order to maintain stable pressure conditions until cladding burst. The total free gas volume of ~16–17 cm^3 was practically all located in the plenum, outside the heated region.

The predictions according two models of boundary conditions during LOCA test are very similar and were compared with the data from Halden TFDB database. The TRANSURANUS calculations performed with two TU versions show the main difference at place of burst and oxide layer thickness according the new model of oxidation and new axial distribution of the outer cladding temperature (see Fig. 3 and Fig. 4).

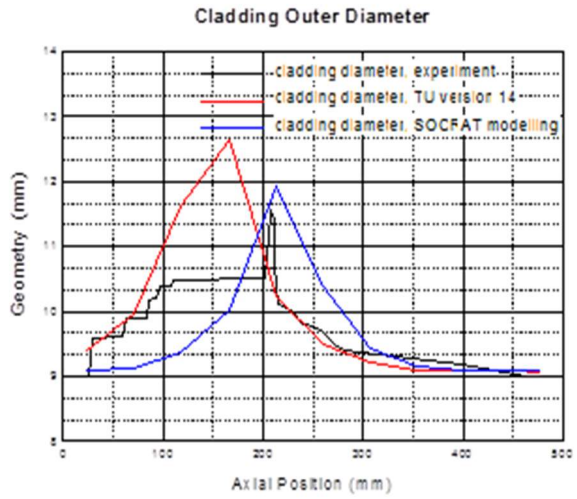

FIG. 3. Clad outer diameter after LOCA test.

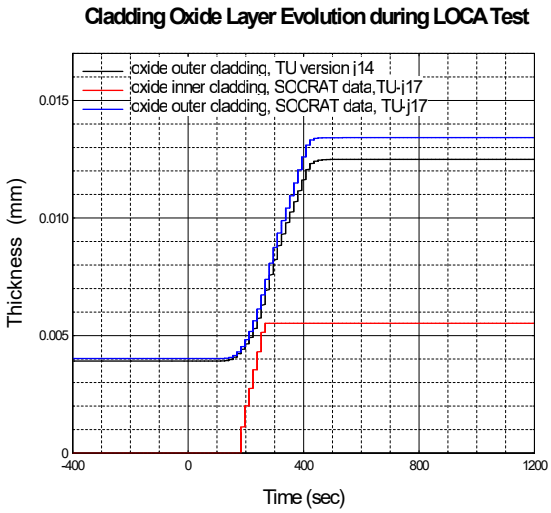

FIG. 4. Oxide layer according two models.

According the Halden data the time of start of blow down phase is set to zero. The results for the place of rod burst and cladding outer diameter change according these two models are compared with the experimental data. The difference in the predicted place of burst was expected in accordance with different axial distribution of the prescribed cladding temperature in two applied models. The difference of the results of cladding oxidation is caused to the double side oxidation model, developed and incorporated in the last version of TRANSURANUS code. Some results are presented below as a demonstration of the TRANSURANUS LOCA test simulations with different T/H boundary conditions

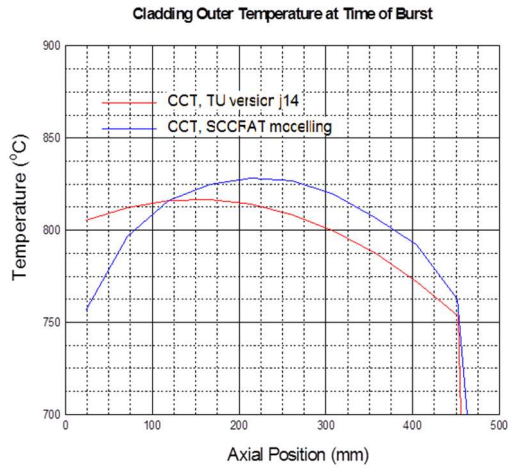

FIG. 5. Comparison of Cladding Outer temp. (axial) according two models.

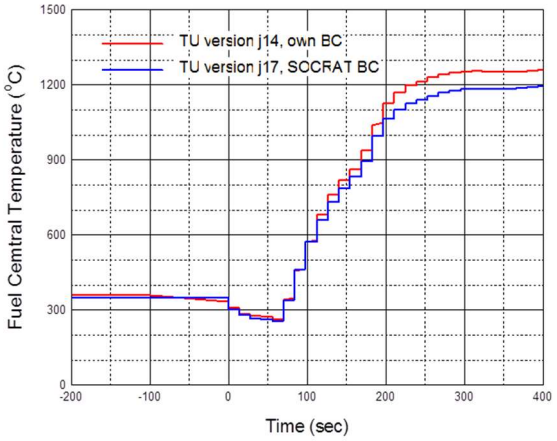

FIG. 6. Fuel Central Temperature during LOCA phase.

An indicator of rod failure is the drop of inner pin pressure. Calculated inner pin pressure is compared with the pressure transducer records on the Fig. 7. Coolant pressure after start of the blow down and calculated inner pin pressure for the same time period are presented below. Measured rod and coolant pressure is presented on the Fig. 7 as well.

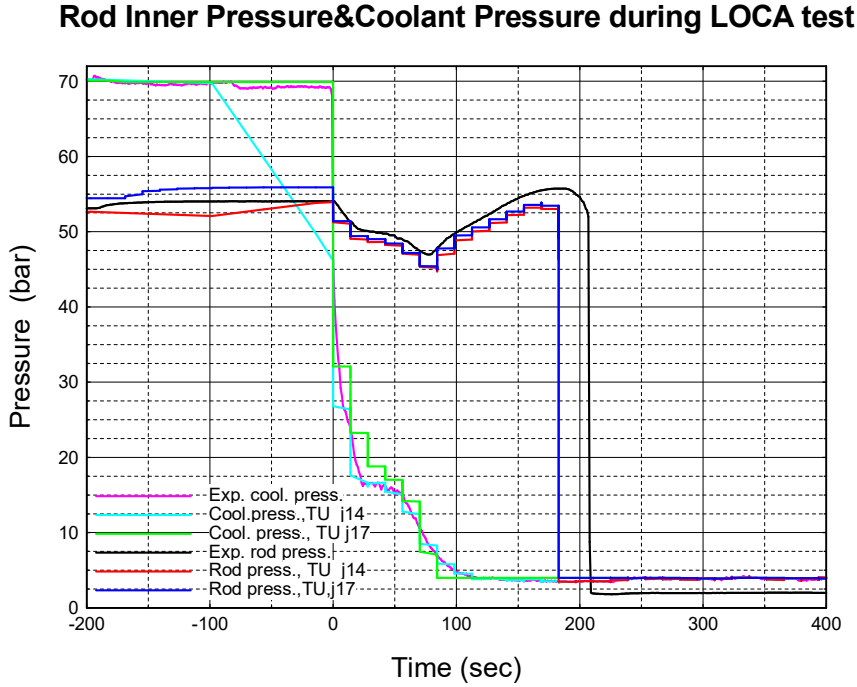

FIG. 7. Comparison of rod inner pressure and coolant pressure measured and simulated according two models.

Despite the observed difference in the predicted location of the rupture, the predicted time of burst according two different models of BC is the same, 183 s after blow-down. For these two simulations two cladding failure criterions were chosen: ICIFaiL=1, overstress is assumed if the average true tangential stress was larger than the failure stress calculated by the material property and ICIFail=4, failure is assumed if the tangential stress or the tangential strain limit is achieved. Nevertheless the time of burst is 183 s in two cases.

As is noted in [7] the deformation of the rod started to occur 183 s after blow-down when the rod pressure reached its maximum value. Cladding burst occurred ~207 s after the end of

the blow down. The burst time is recognizable regarding the drop of the internal pressure signal. In our simulation probably the failure criterion has to be refined.

5. UNCERTAINTY ANALYSIS. HALDEN LOCA TEST IFA650.10

5.1. Short description of the IFA650.10 experiment and TRANSURANUS model

The detailed description of IFA-650.10 can be found in [5]. The test segment was cut from a standard PWR fuel rod which had been irradiated in the PWR Gravelines 5 during five cycles up to burnup of 60MWd/kgU.

The LOCA test started with steady state operation at high power in the rig, it was connected to the outer loop and forced circulation flow. Nuclear power calibration is done during this period. Shortly before the start of the LOCA test, power is decreased to test level and the heater is turn on. Time of blow-down start is taken 0 s. The cladding burst, detected by pressure transducer is at ~ 249 s. Target peak cladding temperature was 850°C. Slight clad ballooning and burst were detected in-pile and verified by the gamma scanning performed at Halden.

The test fuel rod was modelled by a steady state simulation of the base in-reactor irradiations. In both steady state and transient fuel rod input models were set according to the specifications of IFA-650.10 tests (PWR fuel and Zircaloy 4 cladding). The thermo-hydraulic boundary conditions calculated from SOCRAT [8], are used in the TRANSURANUS input file: the coolant temperature and appropriate it axial distribution; the power in the fuel stack (average LHR and axial distribution); pin inner pressure and coolant pressure are prescribed too.

The TRANSURANUS prediction of the time of burst according the inner pin pressure is 251 s after blow-down and the pressure evolution during LOCA test is presented on the Fig. 8.

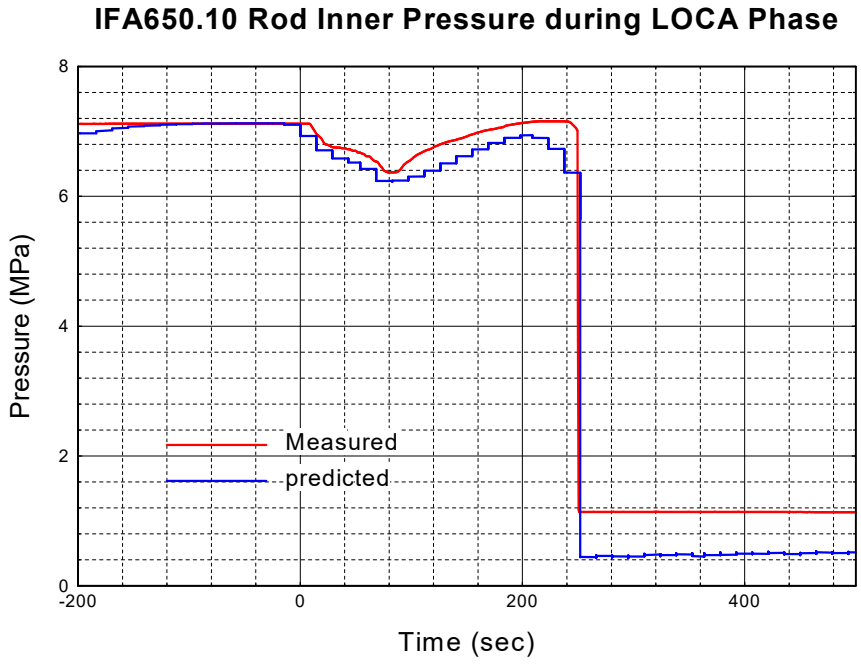

FIG. 8. Rod inner pressure during LOCA phase of IFA650.10 test compared with pressure transducer records.

The agreement between measured and predicted time of burst is acceptable and it was checked by the statistical tool of TU.

The cladding outer diameter after rod burst is presented in the next Fig. 9.

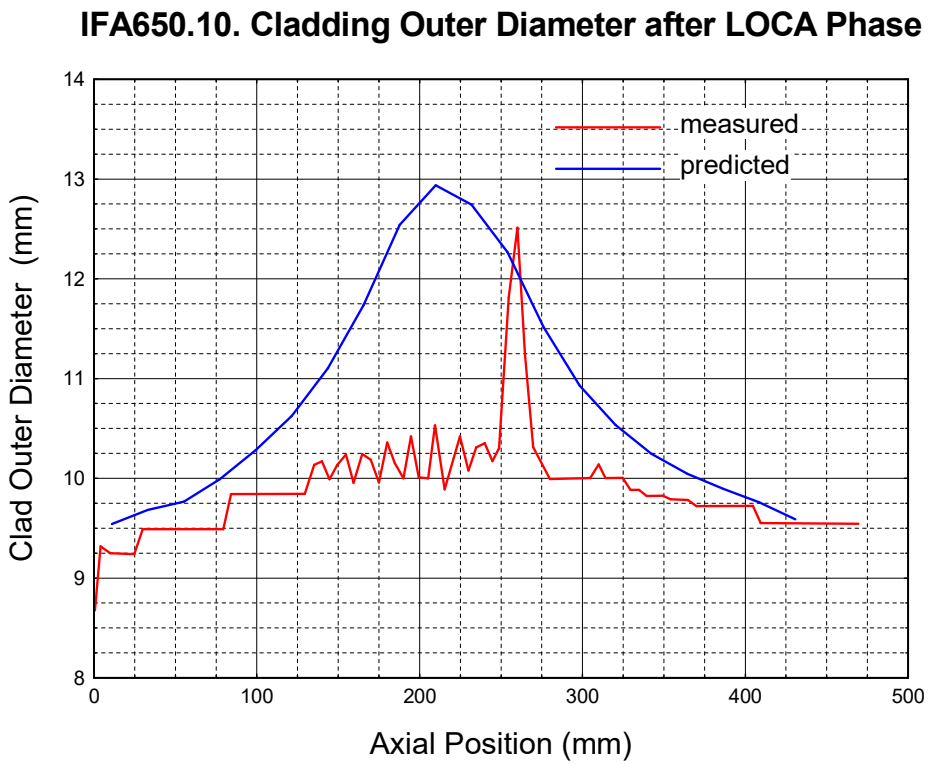

FIG. 9. IFA650.10 LOCA test. Outer cladding diameter comparison.

The place of rod burst is compared with measured ones as well. A reasonable agreement between predicted and measured values of these two parameters is observed.

5.2.TRANSURANUS capabilities for statistical analyses of fuel performance simulations.

Applying the Monte-Carlo technique, already the first versions of TRANSURANUS allowed statistical variations of a large number of input quantities to be simulated according to normal (Gaussian) distributions [9]. The corresponding code input options cover the fuel rod geometry at beginning of life, all prescribed time-dependent quantities (e.g. linear heat rate and coolant or cladding outside temperatures) as well as all material properties (e.g. thermal conductivity, creep) that are applied in the code for fuel, cladding and coolant. By introducing additional types of input distributions (uniform, log-normal) as well as by allowing user-defined lower and upper bounds of the input quantities the code capabilities were extended. The applications to WWER fuel were outlined in [10].

In the frame of the FUMAC project statistical uncertainty analysis of the above mentioned LOCA experiment IFA650.10 with pre-irradiated PWR UO_2 fuel was performed. Uncertainties in fuel rod operation and test boundary conditions, e.g. time dependent prescribed quantities as linear heat rate, coolant temperature and inner pin pressure as well as material properties of the fuel and cladding were considered. The input parameters as well as the information related to their uncertainties are provided in the Table 2. For each of uncertainty parameters, it includes a mean value, a standard deviation (σ) and a type of distribution. A normal distribution has been assigned for simplicity to all the considered input parameters.

TABLE 2. SPECIFICATION FOR UNCERTAINTY ANALYSIS ON MODELLING OF THE HALDEN IFA650.10 LOCA TEST.

Input uncertainty parameter	Mean	Standart deviation	Type of distribution
Operation & test boundary conditions			
Relative power during base irradiation	1	0.01	Normal
Relative power during test	1	0.02	Normal
Coolant temperature - base	1	0.01	Normal
Coolant temperature - test	1	0.2	Normal
Inner pin pressure - base	1	0.0125	Normal
Inner pin pressure - test	1	0.025	Normal
Model Parameters			Normal
Gap conductance	1	0.125	Normal
Minimum porosity at the end of thermal and irradiation induced densification	1	0.05	Normal
Eff. diffusion coefficient	1	0.25	Normal
Corrosion rate	1	0.15	Normal
Material Properties of the Fuel			Normal
Fuel Swelling	1	0.05	Normal
Fuel Thermal Strain	1	0.05	Normal
Fuel Thermal Conductivity	1	0.05	Normal
Fuel Specific Heat	1	0.015	Normal
Fuel density	1	0.0048	Normal
Fuel Emissivity	1	0.05	Normal
Material Properties of the Cladding			Normal
Clad Elasticity Module	1	0.05	Normal
Clad Thermal Strain	1	0.05	Normal
Clad Thermal Conductivity	1	0.05	Normal
Clad Yield Stress	1	0.05	Normal
Clad Burst Stress	1	0.1	Normal
Clad Specific Heat	1	0.015	Normal
Clad Emissivity	1	0.05	Normal
Clad Rupture Strain	1	0.05	Normal

The impact of realistic input uncertainties has been tested for the output parameters specified in the [11]:

— Fuel rod internal pressure;

— Cladding inner side temperature;
— Cladding surface temperature;
— Fuel centreline temperature;
— Fuel surface temperature;
— Cladding outsider oxidation layer thickness;
— Equivalent cladding reacted (ECR);
— Cladding outside diameter;
— Cladding effective stress.

Results for the mean value of the listed parameters over time were obtained. The results uncertainty due to the varied input parameters was evaluated by means of fractional frequency.

5.2.1. Fuel Central Temperature

Graphical representation of FCT results from the Monte Carlo calculations at burst node for the time of LOCA start is shown in Fig. 10 and Fig. 11 below. The mean value and the upper and lower boundaries at 5% and 95% correspondingly are presented. Results for the mean value of the FCT over time were obtained and shown as well.

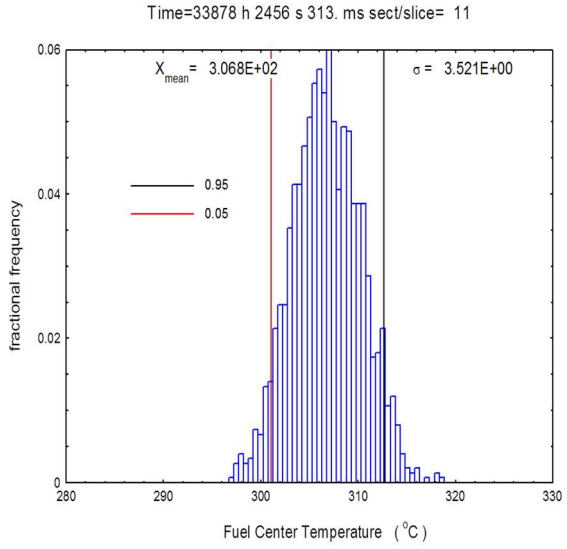

FIG. 10. FCT at time of LOCA start.

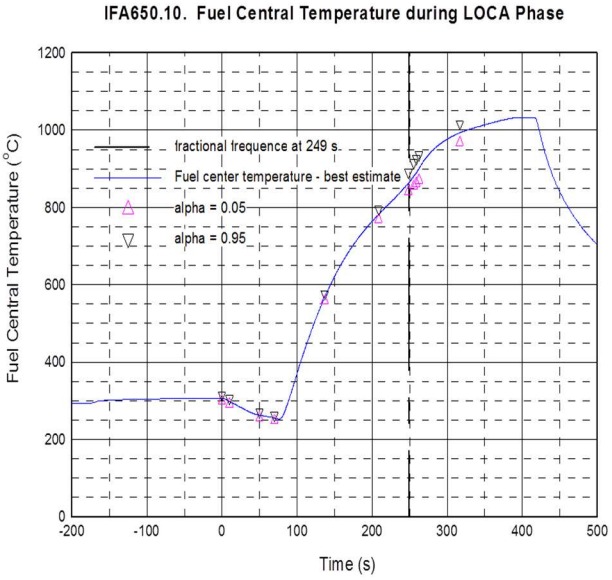

FIG. 11. Mean value and its boundaries over time.

5.2.1. Outer cladding Diameter

Outer cladding diameter evolution during time of LOCA test is assessed and presented on the Fig. 12 together with its 5% and 95% boundary conditions.

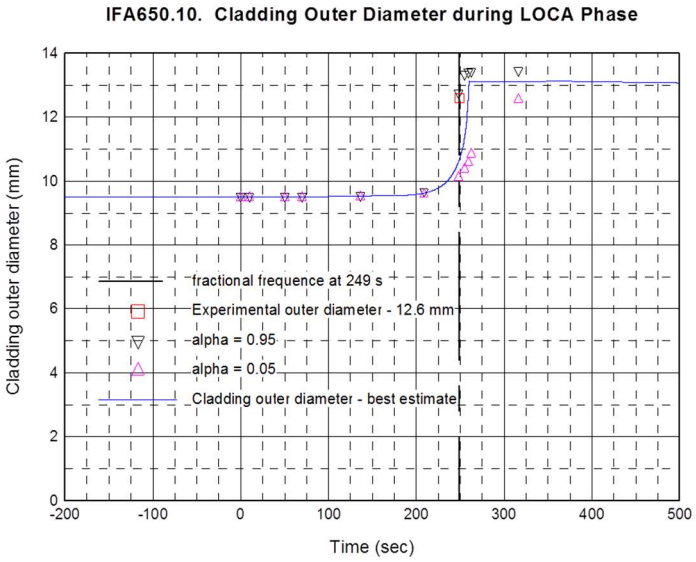

FIG. 12. Cladding Outer Diameter v/s time of LOCA process.

The results show that during transient (time of burst) a great uncertainty in some of the fuel parameters as cladding diameter and rod inner pressure have to be expected as shown in Fig. 13.

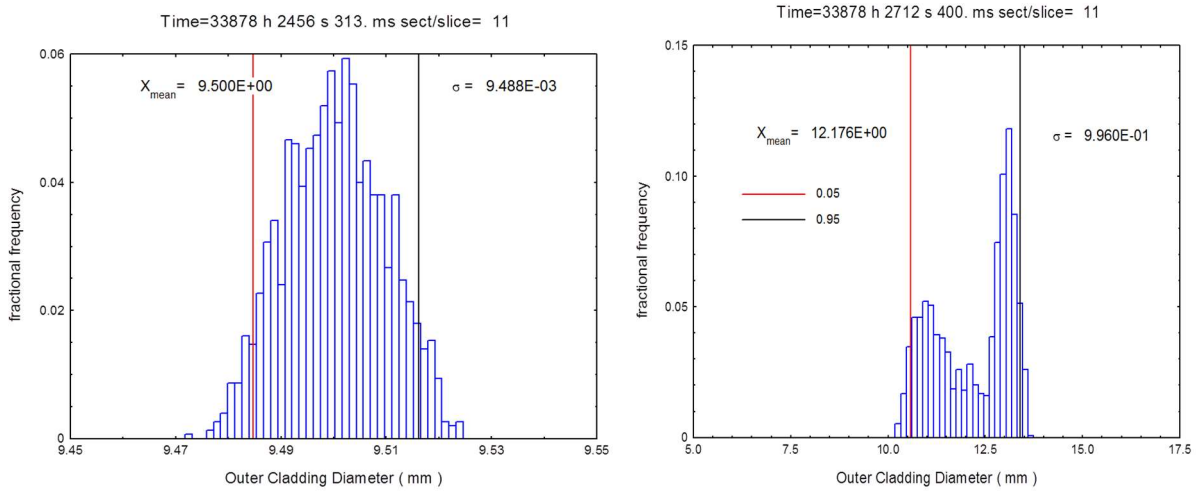

FIG. 13. Fractional Frequency of outer cladding diameter at time of LOCA start as well as the time of burst.

6. CONCLUSIONS

Halden LOCA test IFA650.11 with pre-irradiated WWER fuel was of special interest for our work. Comparison of the fuel performance behavior predictions according two code versions and two models of thermo-hydraulic conditions are of great importance for the good qualification of the team.

The uncertainty of input parameters that impact most on the code predictions have to be carefully evaluated. Further precise analyses on the uncertainty sources are necessary in order to better predict the fuel behaviour under transient conditions.

REFERENCES

[1] LASSMANN, K., The TRANSURANUS Code - Past, Present and Future (Review Article), ITU Activity Report 2001 - EUR 20252, ISBN 92-894-3639-5, 2001, p. 16, http://itu.jrc.cec.eu.int/annual_reports/annual_report_2001/index.htm.

[2] VAN UFFELEN, P., et al., Extending the application range of a fuel performance code from normal operating to design basis accident conditions, J. Nucl. Mater. 383 (2008) 137.

[3] VAN UFFELEN P., et al., Developments of the TRANSURANUS code in the frame of the FUMAC Project, Proc. Of 11th Int. Conference of WWER Fuel Performance, Modelling and Experimental Support, Vol.1, 26.09-03.10.2015, Varna, Bulgaria, 2015 (267–275).

[4] LESTINEN, V., KOLSTAD, E., WIESENACK, W., LOCA testing at Halden, Trial runs in IFA-650, OECD Halden Reactor Project, Nuclear Safety Research Conference Washington, (October 20th– 22nd, 2003).

[5] LAVOIL, A., LOCA Testing at Halden, the Tenth Experiment IFA-650.10, HWR-974, OECD Halden Reactor Project, (2010).

[6] SPYKMAN, G., MAERTENS, D., BOUR, D., Blind and post calculation of the Halden LOCA experiments with the Transuranus LOCA Extension, P. Van Uffelen (Ed.), Proceedings of International workshop–Towards nuclear fuel modelling in the various reactor types across Europe, Institute for Transuranium Elements, Karlsruhe, (25–26 June, 2007).

[7] LAVOIL, A., Loca Testing at Halden, the VVER Fuel Experiment IFA-650.11, OECD Halden Reactor Project, HWR-976.

[8] KISELEV A., Short Information on the Results of IFA-650.9, IFA-650.10 and IFA-650.11 Calculations with SOCRAT code, Technical Note, version 3, IBRAE RAN, (2016).

[9] LASSMANN, K., O'CARROLL, C., VAN DE LAAR, J., Probabilistic fuel rod analyses using the TRANSURANUS code, Technical Committee Meeting on Water Reactor Fuel Element Modelling at High Burnup and Experimental Support, International Atomic Energy Agency, (1997).

[10] SCHUBERT, A., VAN DE LAAR, J., ELENKOV, D., The Statistics Version of TRANSURANUS, Recent Developments and Applications to WWER Fuel, 4th International Conference on WWER Fuel Performance, Modelling and Experimental Support, Albena, Bulgaria (1–5 October, 2001), 293–298.

[11] ZHANG, J., IAEA FUMAC CRP- Specifications for Uncertainty Analysis on Modelling of the Halden LOCA Test IFA650.10, published on the http://nucleus.iaea.org/sites/nefw-projects/fumaccrp/Lists/Team%20Discussion/AllItems.aspx.

DEVELOPMENT OF FTPAC CODE AND APPLICATION ON SAFETY PERFORMANCE RESEARCH UNDER LOCA CONDITION

ZHI-JIE HAN, SHENG CHEN, SONG-TAO JI
Reactor Engineering and Technology Research Division, China Institute of Atomic Energy
P.O. Box 275-64, Beijing, 102413, P.R. China
Email: mr_hanzhijie@163.com , chens09@163.com , st_ji@sina.cn

Abstract

Fuel performance analysis code is an important method to simulate the safety behavior under accident conditions. This document describes the FTPAC (Fuel Transient Performance Analysis Code) developed by China Institute of Atomic Energy. FTPAC v1.0 was used to calculate the performance of single light water reactor fuel rod during accident conditions. It is consisted of capabilities of thermal distribution, mechanical deformation and plenum pressure history prediction. The large deformation model is updated in FTPAC for LOCA accident condition.

1. INTRODUCTION

Nuclear fuel rods are key components in the reactor, which is the first barrier to the escape of radioactivity. If the cladding does not crack, rupture, or melt during a reactor transient, the radioactive fission products are contained within the fuel rod. So fuel rod behavior, especially the integrity of cladding, plays an important role in reactor safety during transient and hypothetical accidents conditions. That development and application of computer codes related to fuel performance analysis is of great significance [1] .

Because of major advantages in increasing burn-up of fuel rod, new cladding alloys have developed and proposed in China. The performance of new type of Zircaloy-clad fuel rod under loss of coolant accident LOCA condition is an important aspect to be specified. In recognition of this, LOCA-related behavior of the new type of cladding is being actively investigated in China Institute of Atomic Energy (CIAE).

The cladding oxidation under LOCA condition results in significant degradation in microstructure and it contributes to the cladding brittleness, which can lead to the fragmentation of the fuel rods under thermal and mechanical loads. The separation oxidation tests have been carried out to simulate high temperature steam oxidation of new type of Zircaloy-cladding. Integral tests that consist of single rod and rod bundle are also being performed to simulate ballooning and burst of cladding in order to evaluate the strength and deformation of new type of cladding as well as coolant flow blockage under LOCA condition [2] .

The proposed research project of CIAE in FUMAC CRP is summarized as follow:

- The new type zirconium cladding safety performance research under LOCA condition;
- Transient performance code development and validation;
- Assessment of safety criterion under LOCA condition for new zirconium cladding.

This report gives a very brief overview of the research project.

2. CODE DESCRIPTION

FTPAC is designed for transient conditions to analyze the behavior of Light Water Reactor fuel rods. It deals with quasi-independent one dimension thermal-mechanical problems. The axial slices are independent of each other, and at each discretized elevation, thermal and mechanical performance are predicted by coupling the temperature, deformation, and gas pressure calculation.

FTPAC consists of models calculating the behavior of LWR fuel rods under transient conditions, which simulate the following processes [3]:

— Heat conduction from fuel pellet to coolant through gas gap-cladding and cladding coolant;
— Fuel pellet cladding deformation;
— Fuel rod gas pressure history;
— Cladding oxidation evolution.

Each phenomenon associate specific models used to solve for the variables. So the analysis models included in FTPAC composed of:

— Thermal model: this model is included to calculate the temperature history of a fuel rod as a function of time dependent fuel rod power and coolant boundary conditions, which is based on finite volume method;
— Mechanical model: this model calculates the deformation of fuel rod and stress applied to the cladding by the mechanical interaction of the fuel and cladding, by the gas pressure inside the rod, and by the pressure of the external coolant. The use of slip coefficient can simulate the sliding between pellet and cladding when there is contact;
— Fuel rod gas pressure model: this model is for computing gas pressure history according to the assumption of gas inside the rod behaves as a perfect gas;
— Oxidation model: the code has an oxidation model to calculate the oxidation degree of cladding and amount of heat generated by cladding oxidation.

2.1. Deformation model

Fuel pellet deformation is used to calculate the fuel stack length change and fuel radial displacement. The cladding deformation analysis in FTPAC consists of a small deformation analysis which is based on the assumption that the cladding retains its cylindrical shape during deformation and a large deformation analysis. The total strain composed of three separate parts. The first one is an isotropic deformation induced by the temperature. It is a function of temperature and thermal expansion coefficient. The second one is an isotropic linear elasticity strain based on the Hooke's law. The last one is plastic strain associated to the stress-strain curve of cladding material.

2.1.1. Slip coefficient for PCMI

If the fuel pellet and cladding is in contact, there will be pellet-cladding mechanical interaction (PCMI), and the fuel deformation model will apply a driving force to the cladding deformation model. In this situation calculation for cladding strain are made using a thin cylindrical shell with prescribed external pressure and a prescribed radial displacement of its inside surface. The prescribed displacement is obtained from the fuel thermal expansion model. Moreover, because slippage is assumed between pellet-cladding, the axial elongation of cladding is obtain from axial expansion of fuel pellet concerned with the slip coefficient.

$$\Delta\varepsilon_z^{clad} = F_{slip} \cdot \Delta\varepsilon_z^{clad} \tag{1}$$

When fuel pellet-cladding is in contact, the slip coefficient is calculated to decide the extent of cladding elongation transmitted by axial expansion of fuel pellet stack.

According to the defining, the value of slip coefficient is between zero and 1. The larger the contact pressure is, the bigger the slip coefficient is, smaller the contact pressure is. The smaller the contact pressure is, the smaller the slip coefficient is. When the fuel-cladding interfacial pressure is less than or equal to the internal gas pressure, even if there is contact, the

fuel and cladding is “unlocked”. So the relative pressure (force) fuel pellet driving on cladding is:

$$\frac{\ln(P_{int})-\ln(P_{gas})}{\ln(P_{int})} \tag{2}$$

The elongation of cladding under this driving force associated with friction factor, interface area between fuel pellet and cladding. So the slip coefficient is:

$$F_{slip} = a + b \cdot \frac{\ln(P_{int})-\ln(P_{gas})}{\ln(P_{int})} \tag{3}$$

The parameter b is a function of friction factor and interface area between fuel pellet and cladding.

2.2.2. Ballooning model

After the cladding deformation has been calculated based on small deformation assumption, a check is made to determine whether or not the cladding ballooning model should be used. If the cladding effective plastic strain is greater than the cladding instability strain, the ballooning model is used to calculate the localized large deformation of cladding. Large deformation model calculates the extent and shape of the cladding ballooning node. Another ballooning model is added to FTPAC code recently by coupling with ABAQUS [4]. The coupled code calculation framework is as Fig. 1.

Deformation and stresses under large deformation condition in the cladding are calculated using the ABAQUS model which considers the cladding to be a thick cylindrical shell loaded with specified internal and external pressures and a prescribed uniform temperature [5]. The deformation result of ballooning model is fed back to the main program FTPAC used for subsequent calculation.

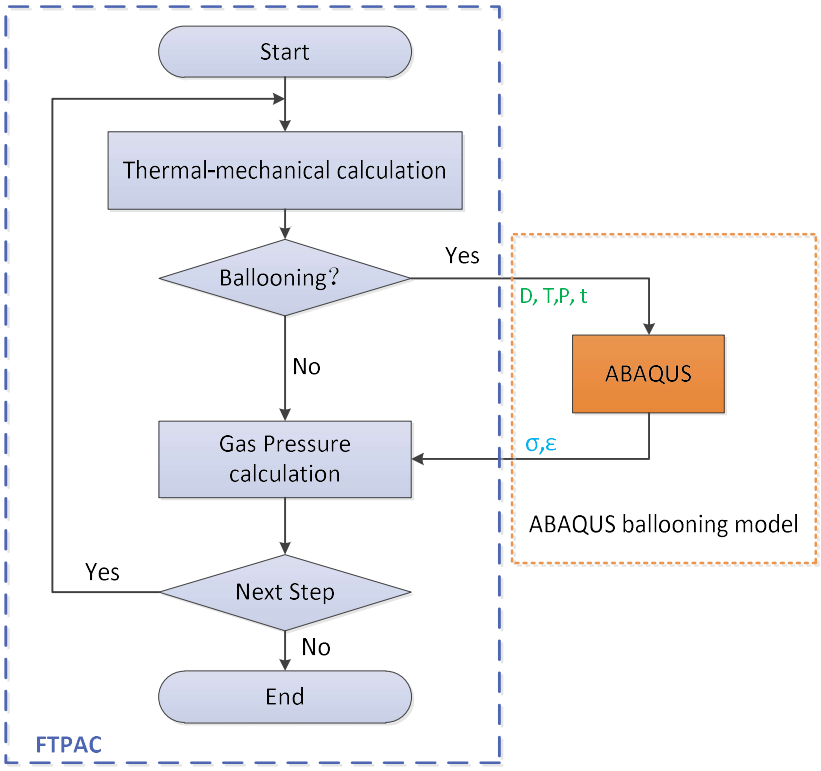

FIG. 1. The calculation framework of FTPAC coupled to ABAQUS.

2.2. Oxidation model

The cladding-steam reaction is modelled by means of kinetic correlations for both the oxygen mass gain and the ZrO2 layer thickness growth:

$$\frac{dK}{dt} = \frac{1}{K} A \exp(-\frac{B}{RT}). \quad (4)$$

The relation for a new type of Zircaloy is developed at CIAE by means of separate high temperature oxidation tests.

2.3. Code assessment

A few experiments were selected to demonstrate the specific models in FTPAC are working correctly. The selected tests were the IFA-432, FA-513, IFA-507, NSRR and CABRI experiments [6]. The experiments data is used to compare against the FTPAC prediction as a function of time.

These comparisons between code prediction and experiment data in Fig. 2 to Fig. 4 provide evidence that the basic models in FTPAC are operating acceptably. The primary results shows that the FTPAC can be used to simulate transient behavior of LWR fuel rod, and gives reasonable agreement in temperature, deformation and gas pressure prediction. And the application of slip coefficient is more suitable for simulating the sliding between pellet and cladding when they are contact.

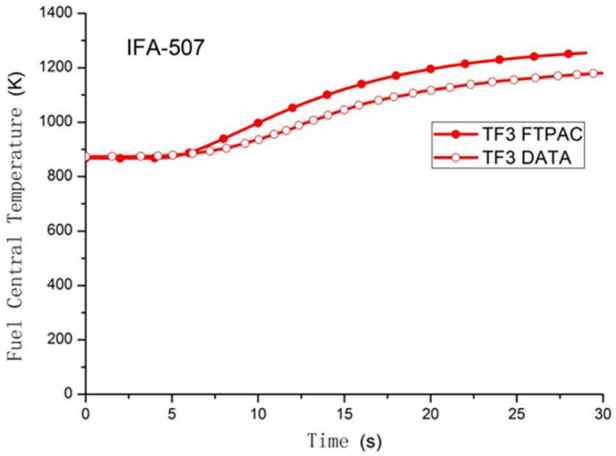

FIG. 2. Temperature history of IFA-507.

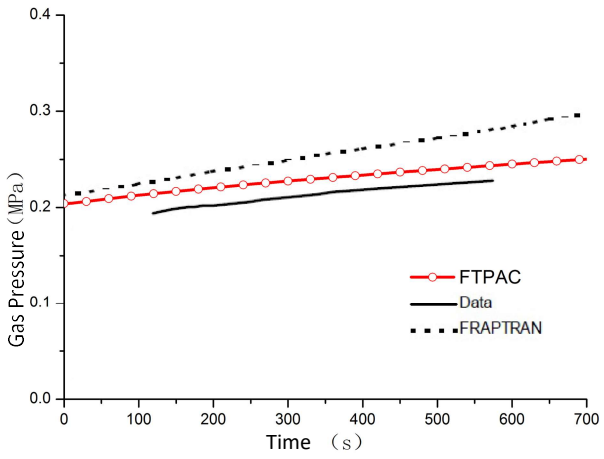

FIG. 3. Gas pressure history of IFA-513.

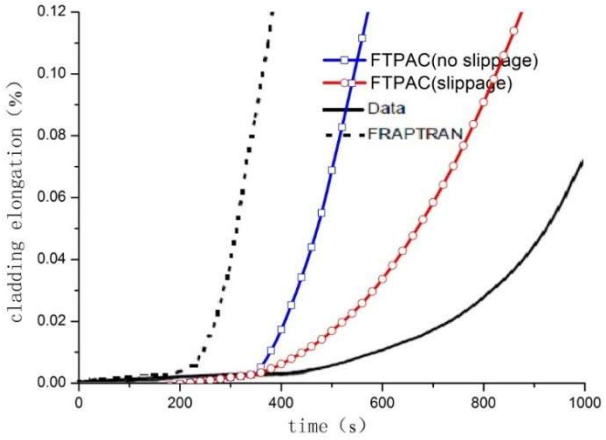

FIG. 4. Cladding elongation of IFA-432 rod.

3. CODE APPLICATION

3.1. IFA-650.2, 9, 10

The LOCA experiments in Halden are integral in-pile tests on fuel behaviour under simulated LOCA conditions. High and medium burnup fuel rods, which have been irradiated in commercial reactors, will be used. The Halden experiments will focus on effects that are different from those studied in out-of-reactor tests. FTPAC was used to analyze several cases including IFA-650.2, IFA-650.9, IFA-650.10 [7]–[9].

In simulation for the above LOCA case, the cladding temperature and coolant pressure are set according to the experiment measured data in FTPAC, with exception of IFA-650.9 and IFA-650.10 tests for which calculation results of SOCRAT were used.

3.1.1. Time of cladding burst

According to the test measuring variables and code calculation, the comparison of the two is shown in the Table 1. The predicted burst time is earlier than measured data for IFA 650.2 and IFA 650.9. And the results show reasonable agreement for IFA 650.10. The difference may come from the effect of burn-up on cladding creep property.

TABLE 1. COMPARISON OF BURST TIME BETWEEN EXPERIMENT AND FTPAC CALCULATION

Burst Time	Experiment	FTPAC
IFA-650.2	99s	89.81s
IFA-650.9	133s	80.48s
IFA-650.10 （PWR）	249s	267.45s
IFA-650.10（SOCRAT）	249s	250.16s

3.1.2. Cladding deformation

Photographs taken of the IFA-650.2 rod in the PIE shows the burst was situated 2 cm below the rod middle point. The increase in cladding diameter was ~40% in the vicinity of the burst, ~22% at 10 cm distance from the lower end, and ~7% at 10 cm form the upper end of the rod.

The FTPAC code results show that the burst occurred at node 6th (10 nodes in all) from bottom, about 0–5cm above the middle point. And the hoop strain is 38% at burst node.

3.1.3. Rod internal pressure

The comparison of rod internal pressure of IFA-650.10 is shown in Fig. 5. After cladding temperature increase, the calculated rod plenum pressure is higher than measured data, which is because of the higher plenum temperature prediction (Fig. 6).

According to the design of test rod, the rod plenum volume (free gas volume) was made relatively large in order to maintain stable pressure conditions until cladding burst. The total free gas volume of was thus practically all located in the plenum, outside the heated region. But the sudden increasing of plenum temperature with the cladding temperature changes in FTPAC simulating during heat up phase leading to the gas pressure reached the maximum fuel rod pressure.

After remodeling the LOCA test by specifying the plenum temperature, the result of plenum pressure is more reasonable before the cladding burst. It is shown in Fig. 7.

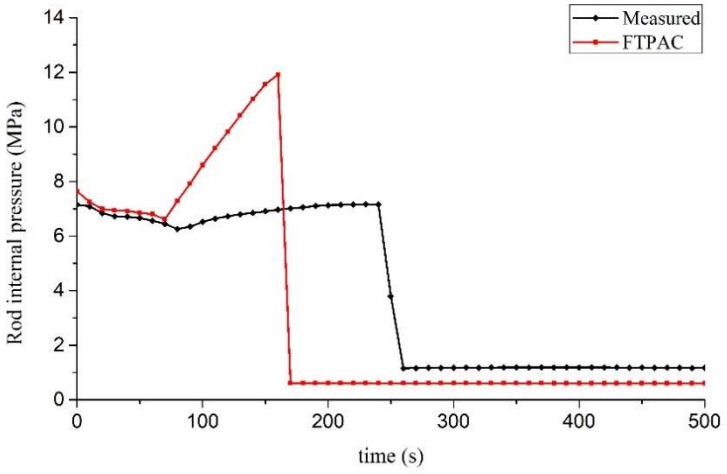

FIG. 5. Fig Fuel rod internal gas pressure of IFA-650.10.

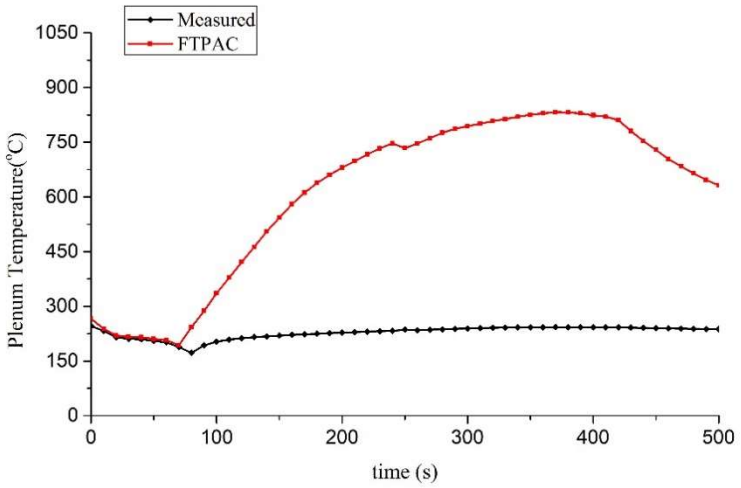

FIG. 6. Plenum temperature history of IFA-650.10.

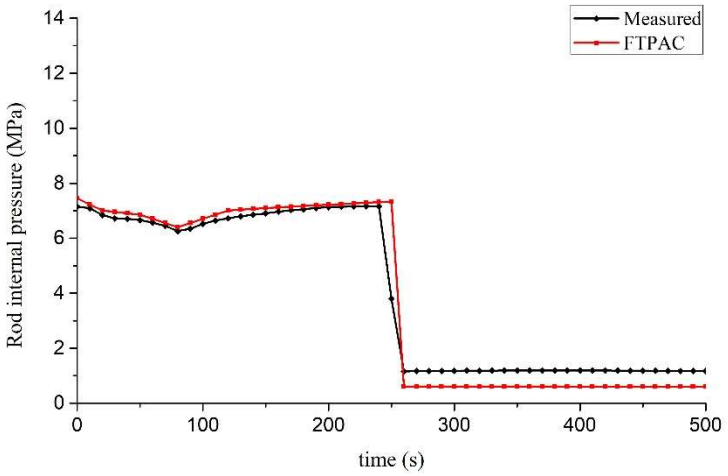

FIG. 7. Updated plenum temperature history of IFA-650.10.

3.2. QUENCH ROD L1

The overall objective of QUENCH-L1 bundle experiment is the investigation of ballooning, burst and secondary hydrogen uptake of the cladding under representative design based accident conditions, as well as to check the embrittlement criteria by means of detailed mechanical post-test investigations [10].

The ABAQUS model is used for calculating cladding burst in QUENCH-L1 bundle experiment and six rod is selected. Internal and external pressures and a prescribed temperature of cladding are specified in the calculation. The results are shown in Table 2.

TABLE 2. THE COMPARISON OF EXPERIMENT DATA AND RESULTS BY ABAQUS MODEL

Rod #	Burst time (s)	
	Exp.	Cal.
2	57.2	47
4	55.2	38
7	59.8	52
11	67.6	71

TABLE 2. THE COMPARISON OF EXPERIMENT DATA AND RESULTS BY ABAQUS MODEL

Rod #	Burst time (s)	
	Exp.	Cal.
15	54.4	53
19	83.6	74

4. UNCERTAINTY AND SENSITIVITY ANALYSIS

A statistical uncertainty and sensitivity analysis (UASA) tool, DAKOTA [11, 12] is used to accomplish the UASA of the fuel performance codes FTPAC and IFA-650.10 (for PWR) is chosen as the case. In order to complete the code coupling between DAKOTA and performance analysis code, there have to be several scripts which relay information from output files and store them into another file [13]. A flowchart showing how the different scripts and codes are coupled with DAKOTA and FTAPC is shown in Fig. 8. According to the specifications, sample number is chosen to 200.

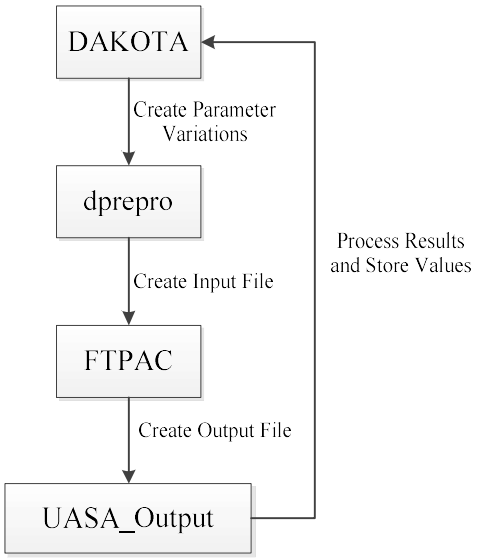

FIG. 8. Flowchart of analysis.

4.1. List of input uncertainty parameters

Some recommended parameters have been discarded with respect to the capabilities of FTPAC [14]. Details are listed below:

Some parameters related to base irradiation are discarded because of the absence of the ability to simulate long-term steady-state operation in FTPAC, such as relative power during base irradiation, cladding corrosion model and cladding hydrogen pickup fraction during steady-state operation.

Due to the simplification of the FTPAC model, the effect of some parameters has not been taken into account, including U^{235} enrichment (%), fuel densification model, fuel solid swelling model, fuel gaseous swelling model, thermal conductivity of the oxide layer, fission gas release (or gas diffusion coefficient) and so on.

The thermal-hydraulic boundary condition is obtained by specifying cladding temperature in this case, so the analysis of coolant temperature and clad-to-coolant heat transfer coefficient is not available. Finally, the input uncertainty parameters for uncertainty and sensitivity analysis and their ranges and distributions are defined in Table 3.

TABLE 3. LIST OF INPUT UNCERTAINTY PARAMETERS FOR STATISTICAL UNCERTAINTY ANALYSIS FOR IFA650.10.

Input uncertainty parameter	Distribution					Importance Ranking (H, M, L)		
	Mean	Standard Deviation	Type	Lower bound	Upper bound	Fuel Thermal Behaviour	Clad Thermal Behaviour	Mechanical Behaviour
1. fuel rod design/manufacturing data								
Cladding outside diameter (mm)	9.50	0.01	Normal	9.48	9.52	L	L	H
Cladding inside diameter (mm)	8.36	0.01	Normal	8.34	8.38	H	L	H
Pellet outside diameter	8.2	0.01	Normal	8.18	8.22	H	L	M
Fuel theoretical density (%T.D. at 20 °C) (convert kg/m^3 to %T.D. with 10980 kg/m^3)	95.237	0.455	Normal	94.326	96.148	L	L	L
Filling gas pressure (MPa)	4.0	0.05	Normal	3.9	4.1	L	L	H
2. Operation and test boundary conditions								
Relative power during test	1	0.025	Normal	0.95	1.05	H	L	L
Cladding temperature (°C)	–	10	Normal	T-20	T+20	H	M	H
3. Physical Properties/Key models (Mult. Coef.)								
Fuel thermal conductivity model	1.00	5%	Normal	0.90	1.10	H	L	L
Clad thermal conductivity model	1.00	5%	Normal	0.90	1.10	L	L	L
Fuel thermal expansion model	1.00	5%	Normal	0.90	1.10	M	L	L
Clad thermal expansion model	1.00	5%	Normal	0.90	1.10	M	L	H
Clad Yield stress	1.00	5%	Normal	0.90	1.10	H	H	H
Fuel heat capacity	1.00	1.5%	Normal	0.97	1.03	L	L	L
Cladding heat capacity	1.00	1.5%	Normal	0.97	1.03	L	L	L
Cladding elastic modulus	1.00	5%	Normal	0.90	1.10	L	L	M
Cladding oxidation model at high temperature	1.00	15%	Normal	0.7	1.30	L	H	L
Gap gas conductivity	1.00	12.5%	Normal	0.75	1.25	H	L	L
Fuel/cladding emissivity	1.00	5%	Normal	0.90	1.10	M	L	L

TABLE 3. LIST OF INPUT UNCERTAINTY PARAMETERS FOR STATISTICAL UNCERTAINTY ANALYSIS FOR IFA650.10.

Input uncertainty parameter	Distribution					Importance Ranking (H, M, L)		
	Mean	Standard Deviation	Type	Lower bound	Upper bound	Fuel Thermal Behaviour	Clad Thermal Behaviour	Mechanical Behaviour
Fuel radial relocation	1.00	10%	Normal	0.80	1.20	L	L	L
Cladding Meyer hardness	1.00	5%	Normal	0.90	1.10	L	L	L
Cladding annealing	1.00	5%	Normal	0.90	1.10	L	L	L
Cladding burst criteria	1.00	10%	Normal	0.80	1.20	L	L	L
Cladding burst strain criteria	1.00	10%	Normal	0.80	1.20	L	L	L
Plenum gas temperature (°C)	–	5	Normal	T-10	T+10	L	L	H

4.2. Uncertainty analysis results

Figure 9a. to 9k. give the lower and upper bounds (min and max) associated with all the time trend of output parameters. The results of the calculation with the nominal value of the input parameters, also called reference calculation (ref) are provided in the figures too. Most of them are under 10% except the deformation of cladding.

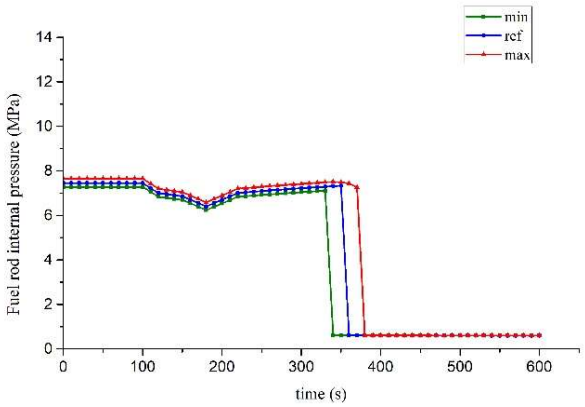

a. Fuel rod internal pressure (RIP)

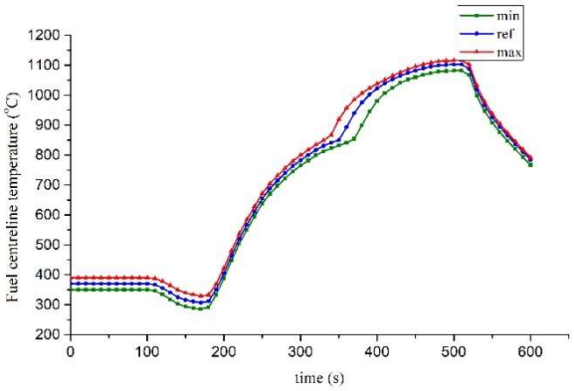

b. Fuel centerline temperature(TFc)

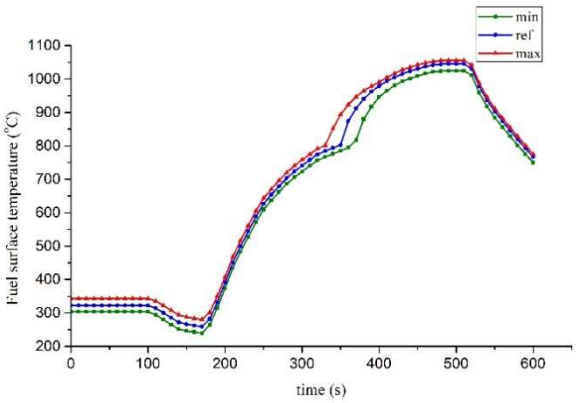

c. Fuel surface temperature (TFo)

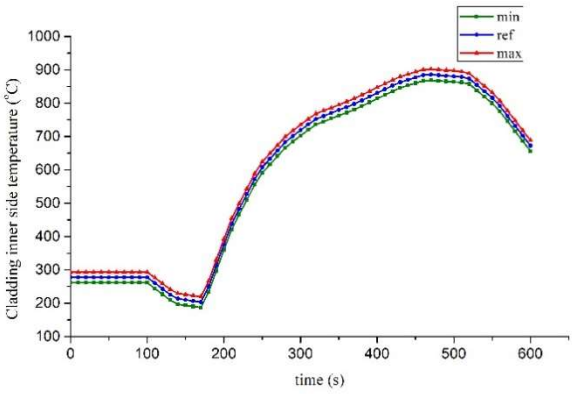

d. Cladding inner side temperature (TCi)

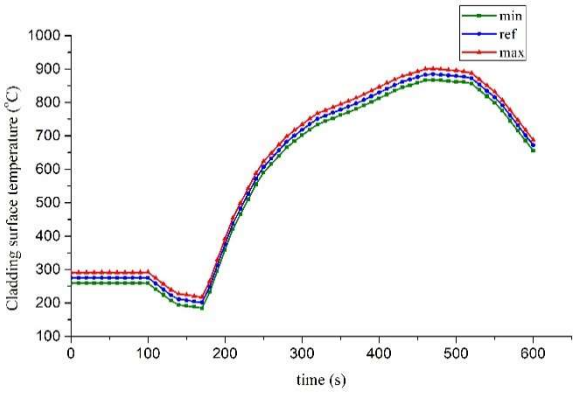

e. Cladding surface temperature (TCo)

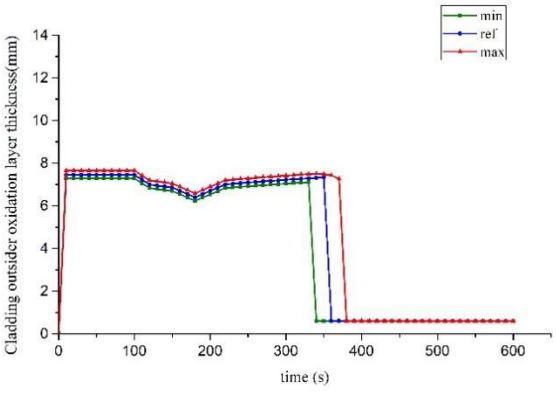

f. Cladding outsider oxidation layer thickness (TOL)

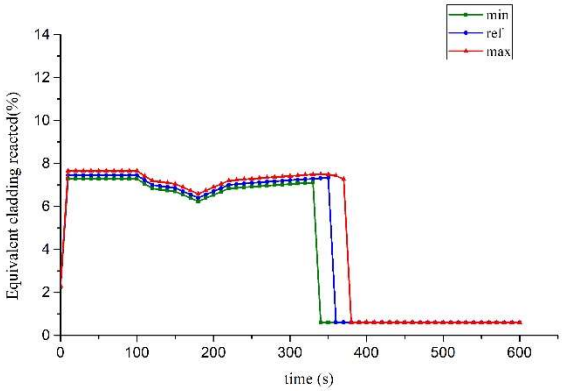

g. Equivalent cladding reacted (ECR)

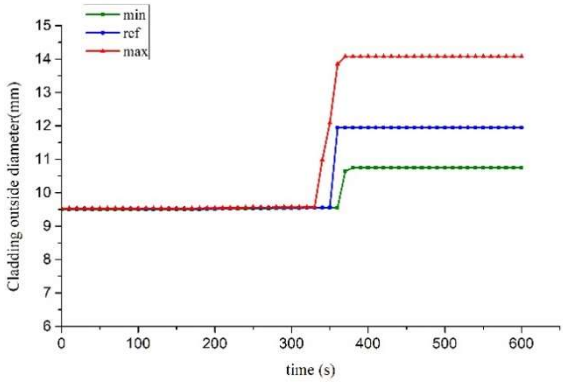

h. Cladding outside diameter (DCo)

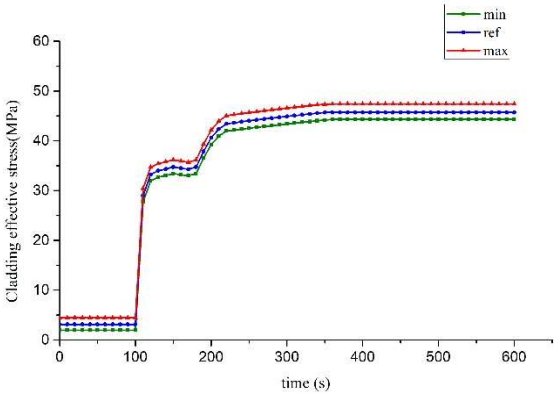

i. Cladding effective stress (CES)

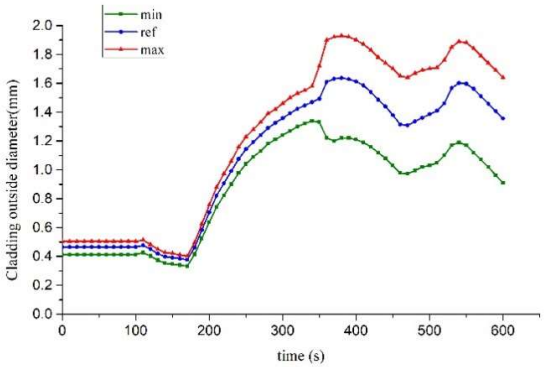

j. Cladding elongation (ECT)

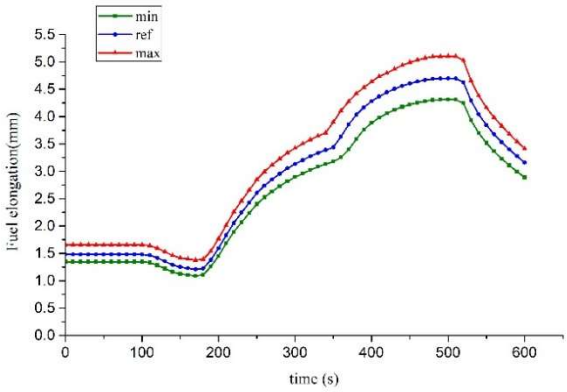

k. Fuel elongation (EFT)

FIG. 9. Uncertainty analysis results.

4.3. Sensitivity analysis results

Sensitivity analysis is done together with the statistical uncertainty analysis based on the 200 code runs previously. The partial rank correlation coefficients (PRCC) and partial correlation coefficients (PCC) at special times defined in the specifications are obtained.
The relative importance of each input parameter is given in the last column of Table 5 based on the max absolute value of PRCC of the concerned output parameter vs. each of the input uncertainty. It should be noted that the thresholds for measuring the importance (H, M or L) are defined as follows:

— H (High): absolute value of correlation coefficients ≥ 0.5;

— M (Medium): 0.5 > absolute value of correlation coefficients > 0.25;
— L (Low): absolute value of correlation coefficients ≤ 0.25.

According to the results, the clad thermal behaviour (cladding surface temperatures and oxidation layer thickness) are highly sensitive to cladding temperature and oxidation model at high temperature. The gap gas conductivity and filling gas pressure are the most influential parameter on fuel thermal behavior(fuel pellet centreline and surface temperature) and clad mechanical behavior(cladding diameter, effective stress) respectively.

5. CONCLUSION

The facilities for high temperature steam oxidation and integral tests have been built to investigate the oxidation kinetics and ballooning, burst behavior of new type of zircaloy-cladding. The facilities consist of high temperature furnace and inner electric heater to heat up the short specimen. The oxidation tests with the temperature from around 800℃ to 1200℃ have been carried out to assess the embrittlement of new type zircaloy-cladding against the existing criteria .

A single rod code FTPAC is under development for simulating light water reactor fuel rod transient behavior at CIAE. FTPAC consists of kinds of models calculating the behavior of LWR fuel rods, such as thermal, mechanical, fuel rod gas pressure and oxidation model. Another ballooning model is added to FTPAC code recently by coupling ABAQUS. Some validations are performed and the results show that FTPAC separate model work correctly.

The application of FTPAC for calculating the LOCA cases including IFA-650.2, IFA-650.9, IFA650.10 and QUENCH Rod L1 indicates that code prediction is reasonable for specific parameters, but further modification and verification are required for large deformation model. The uncertainty analysis result shows that most of maximum deviations are below 10% and the sensitivity analysis gives the most influential parameters on fuel and clad behaviour simulations.

More high temperature oxidation tests including various pre-hydrogen contents are foreseen to be conducted in coming years. More integral tests will also be performed to study ballooning and burst of cladding. The study on breakaway oxidation mechanism has also been planned. Along with the experiments, the creep model in ABAQUS used by FTPAC for simulating ballooning and burst of cladding would be further developed.

REFERENCES

[1] CHUNG, H.M., Fuel Behavior Under Loss-of-Coolant Accident Situations. Nucl. Eng. Technol. , Vol. 37, Issue 4 (2005) 327–362.

[2] ERBACHER, F.J., LEISTIKOW, S., A Review of Zircaloy Fuel Cladding Behavior in a Loss-of-Coolant Accident, KfK 3973, Kernforschungszentrum Karlsruhe (1985).

[3] GEELHOOD, K.J., LUSCHER W.G., CUTA, J.M., FRAPTRAN-1.5: A Computer Code for the Transient Analysis of Oxide Fuel Rods, U.S. Nuclear Regulatory Commission (2014).

[4] WILLIAMSON R.L., et al., Modelling of LOCA Tests with the BISON Fuel Performance Code[R]. Idaho National Laboratory (INL), Idaho Falls, ID (United States), (2016).

[5] ROSINGER H.E., NEITZEL H.J., ERBACHER F.J., Development of a Burst Criterion For Zircaloy Fuel Cladding Under LOCA Conditions, KfK 2893, Kernforschungszentrum Karlsruhe, (1980).

[6] GEELHOOD, K.J., LUSCHER, W.G., FRAPTRAN-1.5: Integral Assessment. Vol. 2, Rev. 1, NUREG/CR-7023, U.S. Nuclear Regulatory Commission (2014).

[7] MIRKKA EK, LOCA Testing at Halden; the Second Experiment IFA-650.2, Institutt for Energiteknikk, OECD Halden Reactor Project (2005).
[8] DU CHOMONT F.B., LOCA Testing At Halden, the Ninth Experiment IFA-650.9, OECD Halden Reactor Project, (2009).
[9] LAVOIL, A., LOCA Testing at Halden, The Tenth Experiment IFA-650.10, OECD Halden Reactor Project, (2010).
[10] STUCKERT, J., GROßE, M., RÖSSGER, C., STEINBRÜCK, M., WALTER, M., Results of the LOCA reference bundle test QUENCH-L1 with Zircaloy-4 claddings, SR-7651, Kernforschungszentrum Karlsruhe (2015).
[11] ADAMS B.M., et al., A Multilevel Parallel Object-Oriented Framework for Design Optimization, Parameter Estimation, Uncertainty Quantification, and Sensitivity Analysis: Version 6.5 User's Manual[Z], SAND2014-4633.
[12] ADAMS, B.M., et al. Ibid., SAND (2014–2015).
[13] BLYTH. T.S., Fuel Performance Code Benchmark For Uncertainty Analysis in Light Water Reactor Modeling [D], the Pennsylvania State University (2012)
[14] ZHI-JIE, H., SONG-TAO, J., YING-CHAO Z., Validation and Application of Fuel Transient Fuel Performance Analysis code FTPAC, Atomic Energy Science and Technology (2014).

SIMULATION OF FUEL ROD LOCA BEHAVIOR TESTS IFA-650.9/10/11 WITH FRAPCON & FRAPTRAN CODE

XIE YIRAN, REN QISEN*, CHENG MENGTENG, ZHANG YONGDONG
ATF R&D Department,
China Nuclear Power Technology Research Institute (CNPRI)
4F, Science and Technology Building, No.1001, Shangbuzhong Rd,
Shenzhen, 518031, P.R. China
Email: renqisen@cgnpc.com.cn

Abstract

Fuel rod represents the ultimate danger in accident conditions. Typically, fuel rod behavior in accident conditions is one of the main concerns in nuclear industry. Fuel performance analysis code can help us to observe the behavior of fuel rod under different conditions and obtain the information that hard to be achieved from experiments. Meanwhile, the validation and assessment coordinated with experiments are of great interest for improving the prediction reliability of the code. In this report, in order to better understand fuel rod behavior under LOCA condition and assess the predictive ability of the FRAPCON/FRAPTRAN codes, simulations of IFA-650.9/10/11 Halden experiments are performed. Feasibility on code prediction of fuel rod performance during steady/transient state are assessed, and results indicate that the FRAPCON/FRAPTRAN codes predict the fuel rod behavior well under LOCA condition in general.

1. INTRODUCTION

Fuel rod behavior under accident conditions is complicated and becomes one of the main concerns in nuclear industry. Particularly, safety criteria for loss-of-coolant accident (LOCA) used at present are based on the LOCA experiments conducted mainly with fresh fuel rod in the 1970s. With the modifications in fuel design, cladding material and burnup level, validation of the criteria is needed to be reassessed. Recent years, several LOCA experiments were carried out in Halden reactor. For the IFA-650.9, 10, 11 experiments, high burnup fuel rods which were pre-irradiated in commercial reactors are used. Computer simulation, as a method of great importance in fuel rod behavior analysis, needs the validation and assessment to improve its prediction reliability. FRAPCON/FRAPTRAN, developed by Pacific Northwest national laboratory, is the codes that calculate the steady-state/ transient-state response of traditional light-water reactor fuel rods. In this report, simulations of IFA-650.9, 10, 11 Halden experiments are performed with FRAPCON/FRAPTRAN to better understand fuel rod behavior under LOCA condition and assess the predictive ability of the codes.

2. DESCRIPTION OF IFA-650 RIG AND TEST RODS

The information on IFA-650 rig and tested fuel rods is provided in [1]–[3]. The test rods used in IFA-650.9–11. Halden experiments were segments cut from the standard PWR or VVER fuel rod of different burnup. Table 1 summarizes the main characteristics of the test rods. After the re-fabrication, the rod plenum volume was made relatively large so as to maintain stable pressure conditions until cladding burst.

The test rod was located in the center of the rig and surrounded by an electrical heater inside the flask for simulating the LOCA conditions and investigating the fuel rod performance [1]. Both rod and heater powers influence the cladding temperature.

TABLE 1. MAIN CHARACTERISTICS OF THE TEST RODS

	The test rods used in IFA-650.9–11.		
	IFA-650.9	IFA-650.10	IFA-650.11
Reactor type	PWR	PWR	VVER
Burnup (MWd/kgU)	89.9	61	56
Stack length (mm)	480	440	480
Enrichment (wt% U^{235})	3.5	4.49	3.6
Fuel density, (% of T.D.)	95	95.32	97
Fuel Diameter (mm)	9.13	8.21	7.55
Fuel length (mm)	8	10	10
Cladding type	DX Zr2.5Nb (duplex) Zry-4 (base)	Zry-4	E110
Cladding outer diameter (mm)	10.75	9.5	9.13
Cladding inner diameter (mm)	9.3	8.36	7.77
Plenum volume (cm^3)	19	16-17	16-17
Gas pressure (RT) (bar)	40	40	30

3. SIMULATION OF IFA-650.9

3.1. Initial and boundary condition

For the steady state simulation, power history was determined by the given pre-test irradiation history as shown in Fig. 1. Axial power profiles were set to be uniform all along the fuel rod. Table 2 presents the nodalization of fuel rod.

For the transient state simulation, data for power history and axial power profiles come from the experiment data provided (also see Part I, Section 2.2.). The data file calculated by SOCRAT[2] contains the boundary conditions for the benchmarks: evolutions of the cladding and coolant temperatures, heat transfer rates by convection and radiation in 26 nodes, coolant inlet/outlet pressure, temperatures of phases (gas, fluid), void fraction, and flow rates of the fluid and the gas mixture components (steam, hydrogen, argon and helium), etc. For the calculation with FRAPTRAN, thermal hydraulic boundary conditions are described with the coolant pressure, temperature and clad to coolant heat transfer coefficients (HTC), as shown in Figs 2–4.

TABLE 2. NODALIZATION (STEADY & TRANSIENT STATES).

Node	1	2	3	4	5
Axial Elevation (mm)	26.667	80	133.33	186.67	240
Node	6	7	8	9	
Axial Elevation (mm)	293.33	346.67	400	453.33	

[2] Refer to Simulation of Initial and Boundary Conditions with SOCRAT code for benchmarks based on IFA-650.10 and IFA-650.11 tests, by Dolganov et al. in this Annex.

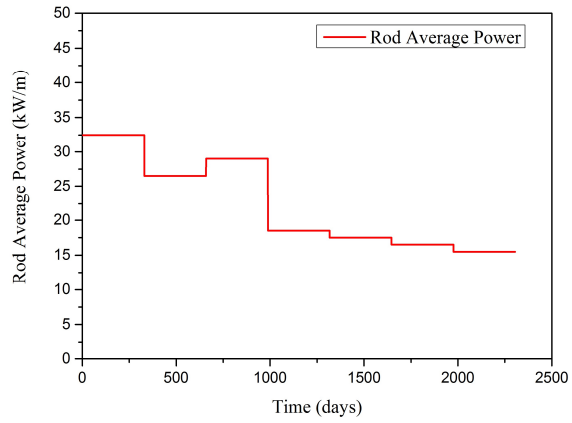

FIG. 1. Rod average power history of pre-irradiation.

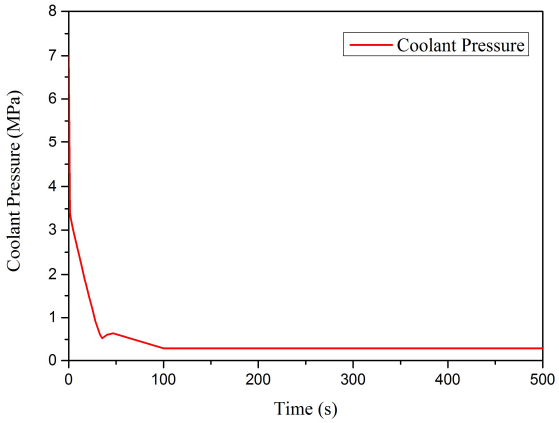

FIG. 2. Coolant pressure history of transient condition.

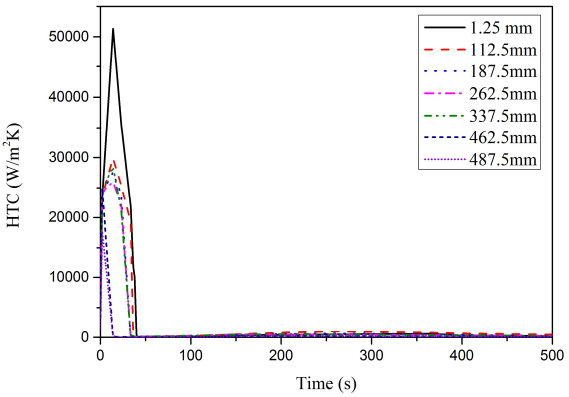

FIG. 3. Heat transfer coefficient history of transient condition.

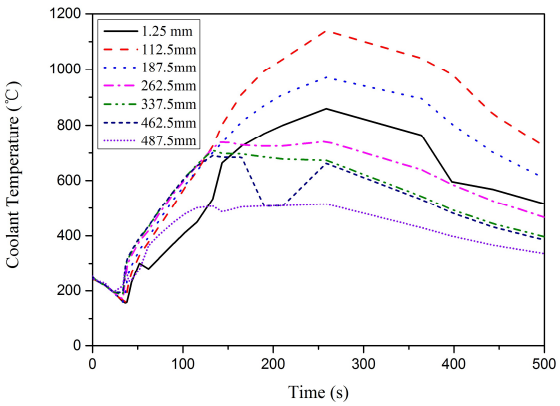

FIG. 4. Coolant temperature history of transient condition.

3.2. Steady state simulation results

As shown in Figs 5–7, during normal operation, fuel temperature, rod pressure and cladding temperature do not change significantly. By comparison with Fig. 1, it is found that the fuel and cladding temperatures as well as the rod pressure change with rod power. The increase/decrease of rod power leads to the increase/decrease of the fuel and cladding temperature and rod pressure.

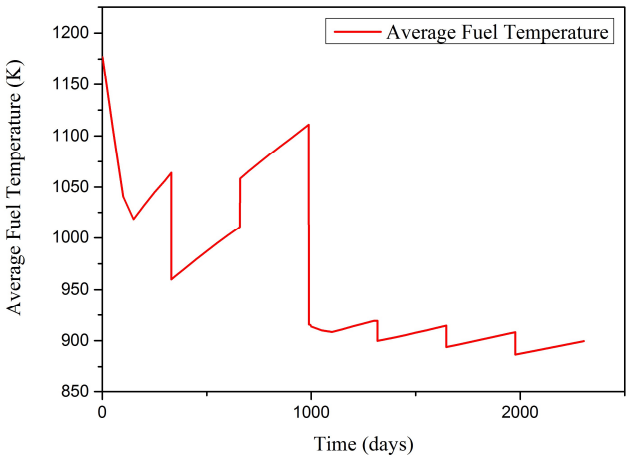

FIG. 5. Variation of average fuel temperature during normal operation

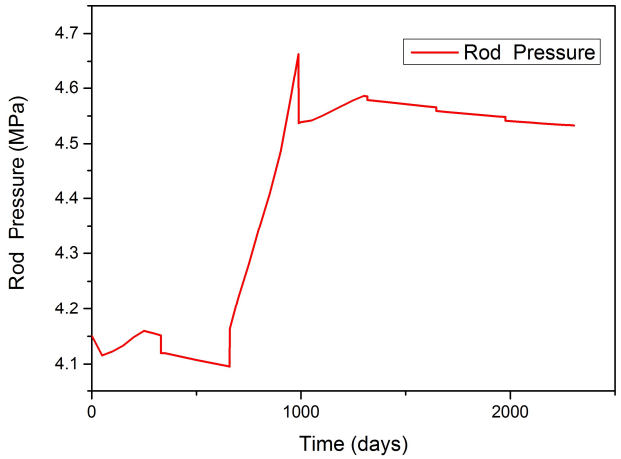

FIG. 6. Variation of rod pressure during normal operation.

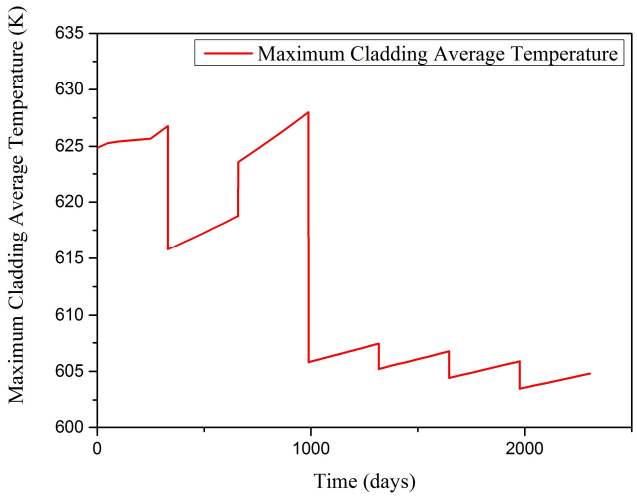

FIG. 7. Variation of maximum cladding average temperature during normal operation.

3.3. LOCA condition simulation results

Table 3 shows the overall comparison of FRAPTRAN calculated results and corresponding measured values. It implies that FRAPTRAN predicts failure to occur before it

was actually measured; but the predicted maximum rod pressure and its corresponding cladding hoop stress as well as cladding failure temperature are close to the measured value.

TABLE 3. OVERALL COMPARISON OF FRAPTRAN CALCULATED RESULTS AND CORRESPONDING MEASURED VALUES

	Measured	FRAPTRAN
Cladding deformation start time (s)	106	78
Cladding failure time (s)	133	87
Maximum rod pressure (MPa)	7.73	7.08
Maximum rod pressure corresponding hoop stress (MPa)	47.2	47.1
Cladding failure temperature (K)	1083	1066.7

Figure 8 illustrates the comparison of measured and calculated rod pressure. The sudden decrease of rod pressure indicates the failure of fuel rod. For the IFA tests, the total free volume of gas was practically all located in the plenum, outside the heated region [4]. FRAPTRAN can model an external plenum, and the external plenum gas temperature data is imposed as initial condition. However, the predicted plenum gas temperature is higher than the measured values, as shown in Fig. 9. The reasons is that in FRAPTRAN, there are two options for defining the plenum gas temperature:

— Assume the gas temperature to be 260.9 K higher than the axial local coolant temperature;
— A more detailed model to concern the interactions between the plenum gas and the top pellet surface, hold-down spring, and cladding wall.

In these temperature calculation processes, the input plenum gas temperature hasn't been used. The input plenum gas temperature history is only used for defining the sum of volume over temperature terms in gas gap pressure equation [5]. Difference in plenum gas temperature might cause the deviation of other parameters.

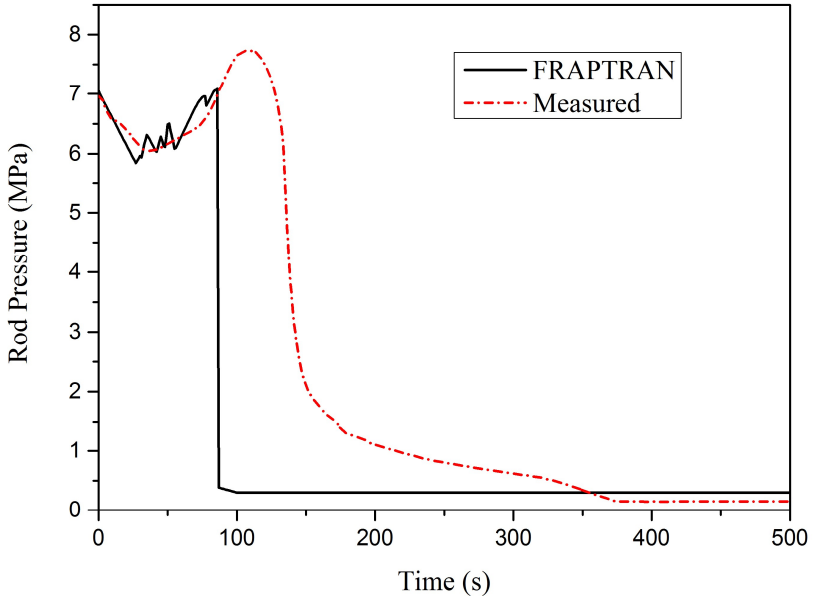

FIG. 8. Variation of rod pressure during LOCA.

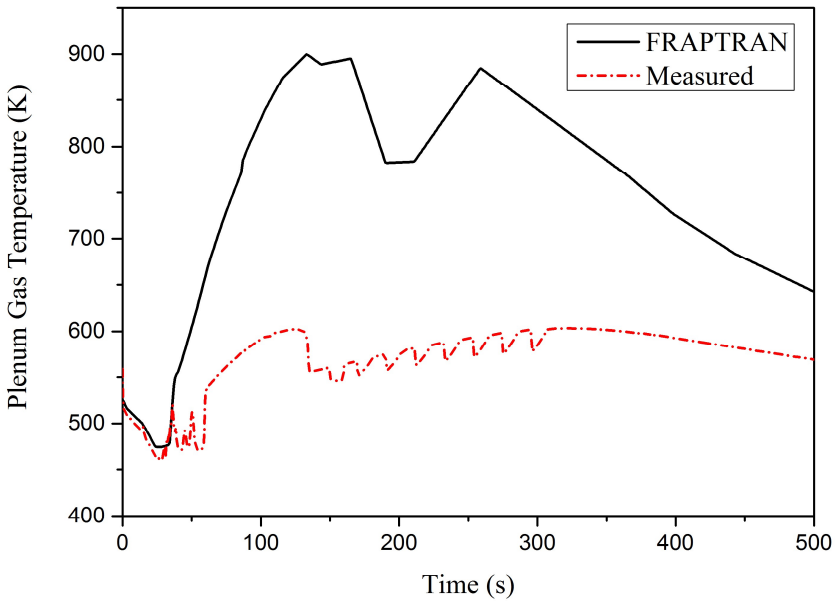

FIG. 9. Variation of plenum gas temperature during LOCA.

Figure 10 illustrates the comparison of measured and predicted cladding outside temperature. The predicted cladding outside temperature shows similar trend with the measured values. The little difference can be accounted by the difference in nodalization and the simplification of the models. Besides, using the thermal properties of light water to replace those of heavy water might have some effect on the results.

Due to the loss of cooling ability, cladding temperature increase significantly, and until the spray water accumulate to a certain level, cladding temperature decrease gradually. In IFA test, spray was applied as 0.5s pulses every 20s after detection of the cladding burst. In the simulation, the cooling effect of spray is modeling by the variation of coolant boundary condition and the start time is the same as the test.

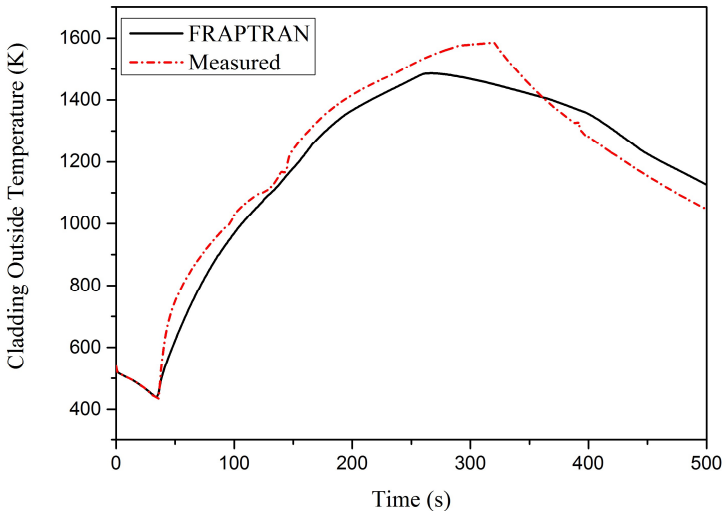

FIG. 10. Variation of cladding outside temperature during LOCA.

Figure 11 illustrates the comparison of measured and predicted cladding elongation. The predicted cladding elongation shows similar trend with the measured values, but is about 0.5mm higher than the measured values. After the blow-down of coolant, the cladding elongation increases rapidly. When the cladding is about to burst, cladding elongation decreases suddenly to a lower value.

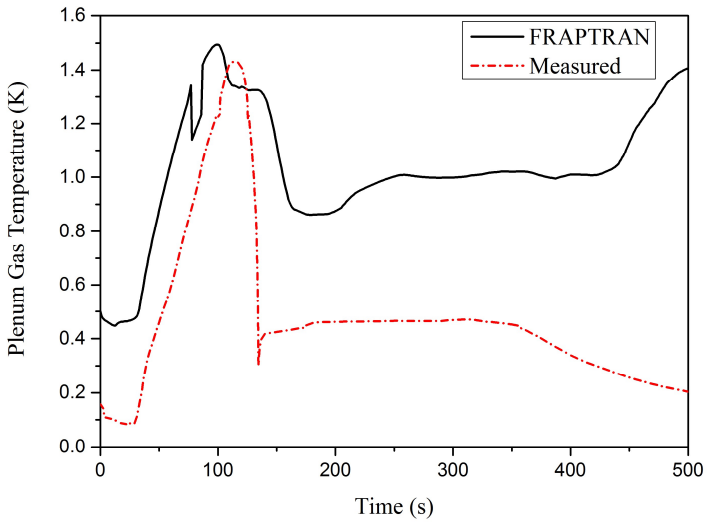

FIG. 11. Variation of cladding elongation during LOCA.

Figure 12 illustrates the comparison of measured and predicted cladding outer diameter. It implies that FRAPTRAN underestimates the change of cladding outer diameter, but the variation change is correct. The measured results indicate that cladding ballooning occurred in two portions of the rod while the predicted result show that cladding ballooning occurred only on the upper part of the rod. This difference is due to the calculation method of FRAPTRAN. Once the ballooning has been predicted in one node, no further strain calculations would be performed for any nodes, the further calculation focuses only on the ballooning node. Thus, it could only predict the primary ballooning.

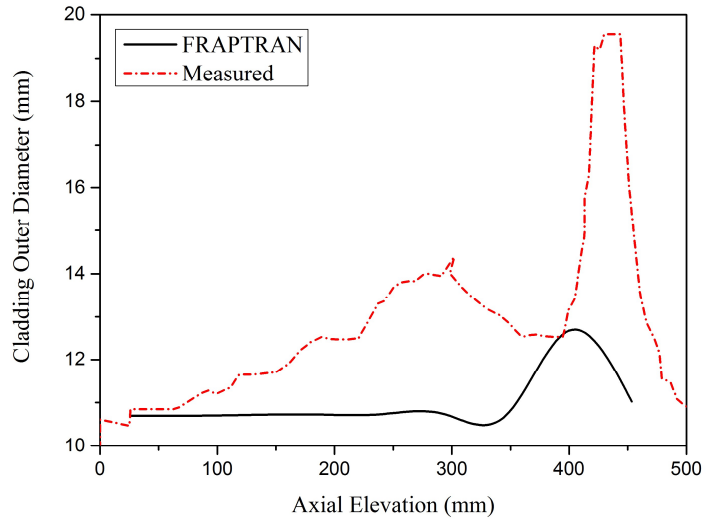

FIG. 12. Variation of cladding outer diameter during LOCA.

4. SIMULATION OF IFA-650.10

4.1. Initial and boundary conditions

Power history of steady state was determined by the given pre-test irradiation history, as shown Fig. 13. Axial power profiles were set to be uniform all along the fuel rod. Table 4 presents the nodalization of fuel rod.

For the transient state simulation, data for power history and axial power profiles come from the experiment data provided. The data file calculated by SOCRAT contains the boundary

conditions for the benchmarks[3]. Thermal hydraulic boundary conditions in FRAPTRAN are described with the coolant pressure, temperature and clad to coolant heat transfer coefficients (HTC), as shown in Figs 14–16. The heat transfer coefficients were derived with the cladding and coolant temperature, as well as the heat transfer rates by convection and radiation. The uncertainty of LHGR measurement (4%) was taken into account.

TABLE 4. NODALIZATION (STEADY AND TRANSIENT STATES)

Node	1	2	3	4	5
Axial Elevation (mm)	24.5	73.5	122.5	171.5	220.5
Node	6	7	8	9	
Axial Elevation (mm)	269.5	318.5	367.5	416.5	

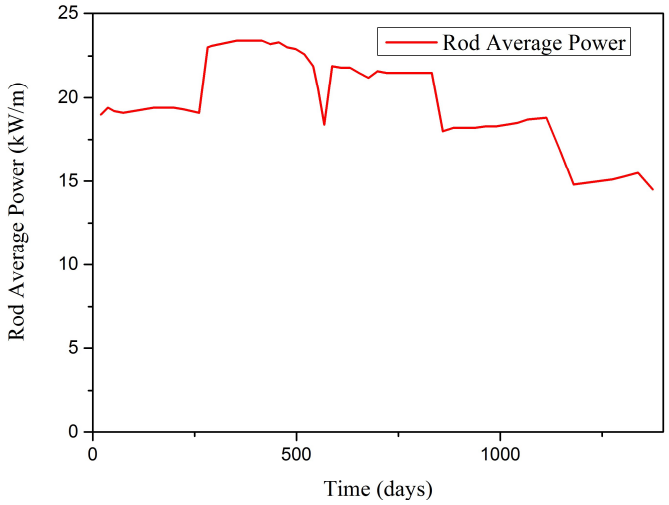

FIG. 13. Rod average power history of pre-irradiation.

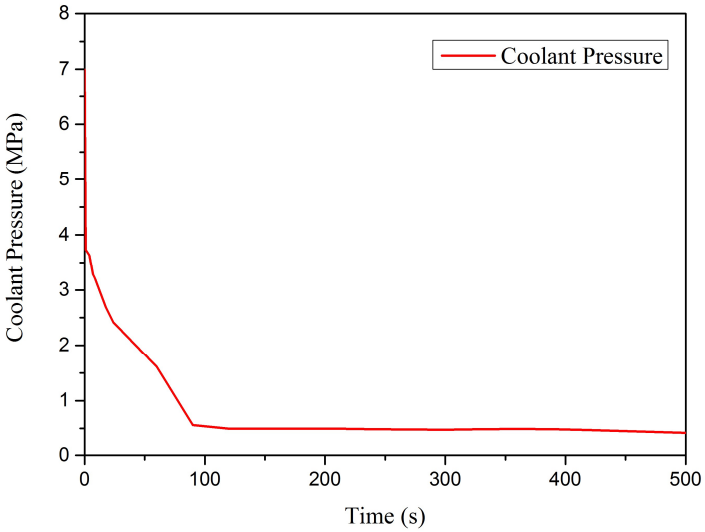

FIG. 14. Coolant pressure history of transient condition.

[3] Refer to Simulation of Initial and Boundary Conditions with SOCRAT code for benchmarks based on IFA-650.10 and IFA-650.11 tests, by Dolganov et al. in this Annex.

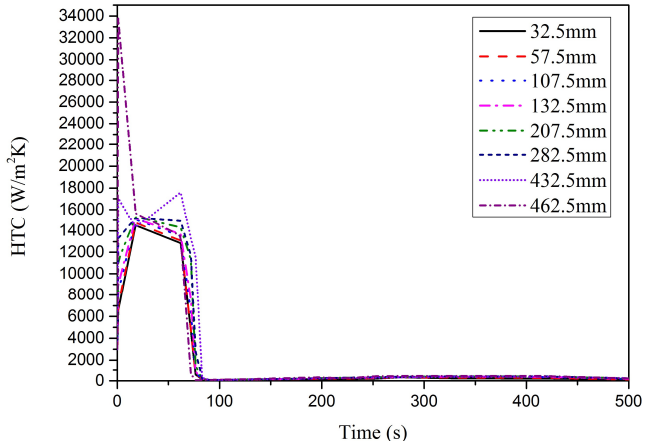

FIG. 15. Heat transfer coefficient history of transient condition.

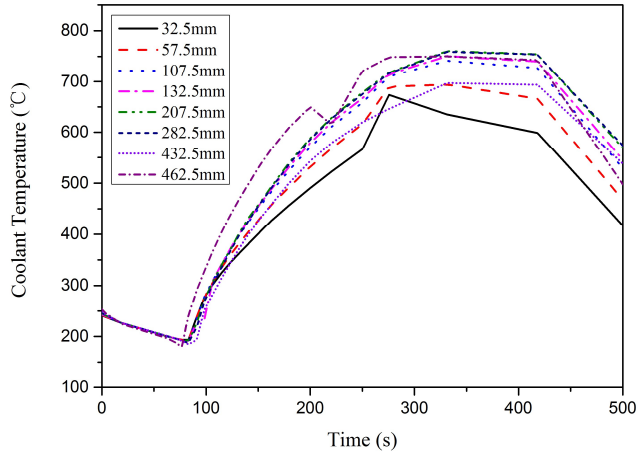

FIG. 16. Coolant temperature history of transient condition.

4.2. Steady state simulation results

Similar as the results of 650.9, during normal operation, fuel temperature, rod pressure and cladding temperature change with rod power, as shown in Figs 17–18.

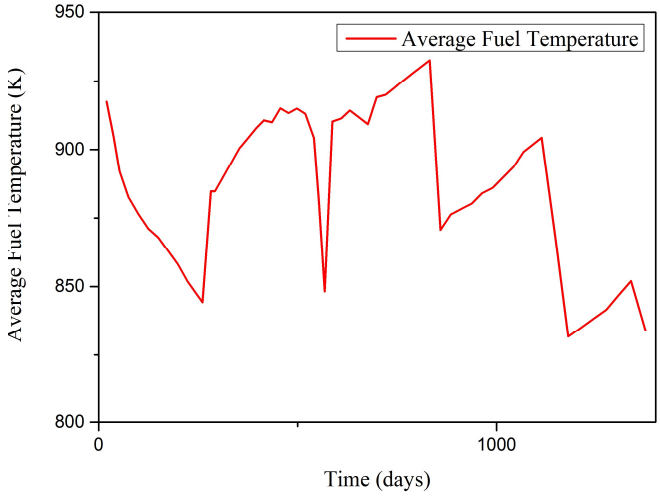

FIG. 17. Variation of average fuel temperature during normal operation.

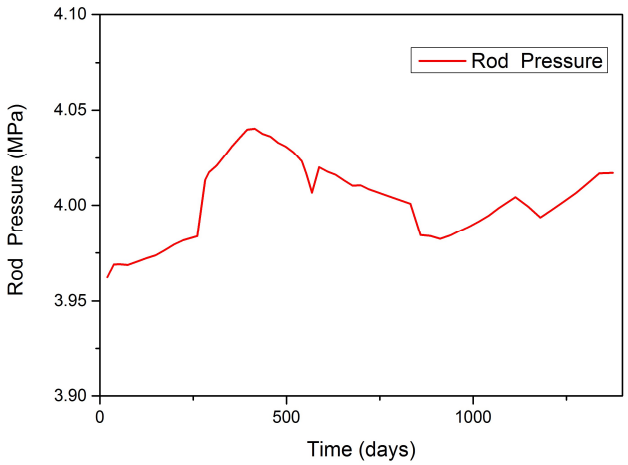

FIG. 18. Variation of rod pressure during normal operation.

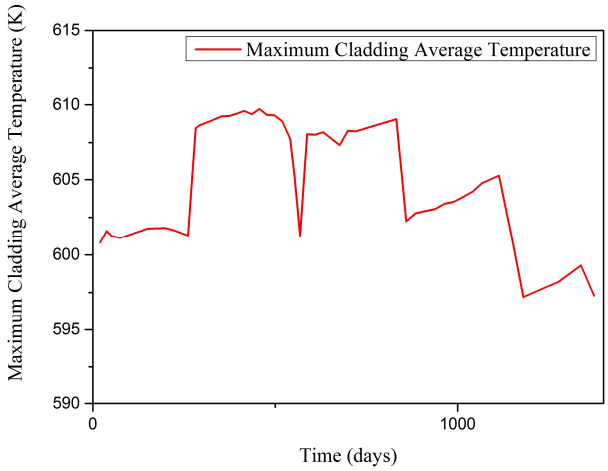

FIG. 19. Variation of maximum cladding average temperature during normal operation.

4.3. LOCA condition simulation results

Table 5 shows the overall comparison of FRAPTRAN calculated results and corresponding measured values. The failure time predicted by FRAPTRAN is close to the measured one and the predicted maximum rod pressure and its corresponding cladding hoop stress approach to the measured value.

TABLE 5. OVERALL COMPARISON OF FRAPTRAN CALCULATED RESULTS AND CORRESPONDING MEASURED VALUES

	Measured	FRAPTRAN
Cladding deformation start time (s)	228	211
Cladding failure time (s)	249	233
Maximum rod pressure (MPa)	7.16	7.00
Maximum rod pressure corresponding hoop stress (MPa)	49	48.6
Cladding failure temperature (K)	1028	944.7

Figure 20 illustrates the comparison of measured and simulated rod pressure. The sudden decrease of rod pressure indicates the failure of fuel rod. For the IFA test, the plenum which contains the total free gas in the fuel rod, is located outside the heated region, so during the LOCA event, the plenum gas temperature changes slightly, as presented in Fig. 21.

Consequently, the measured rod pressure raises little. As case 650.9, an external plenum is concerned, variation of rod pressure shows similar trend as the measured one, but plenum gas temperature is still higher than the measured one. Difference of the plenum gas temperature is due to the calculation model of FRAPTRAN.

After the burst of cladding, the phenomenon that the measured pressure is higher than the predicted one is similar to the results calculated with SOCRAT. It is probably due to the coolant boundary condition used.

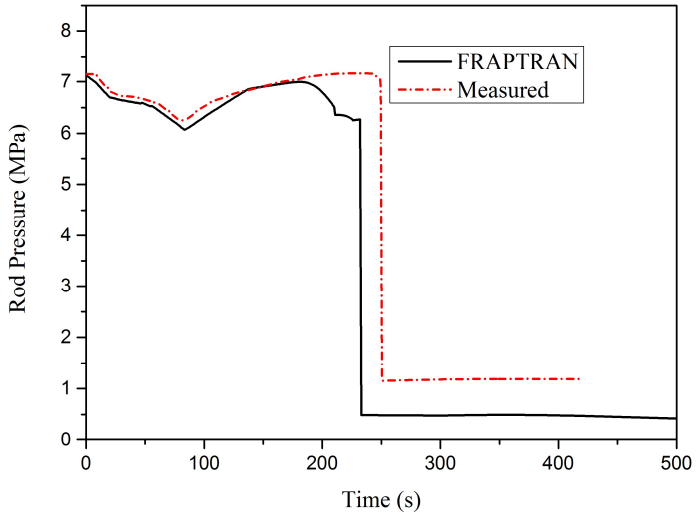

FIG. 20. Variation of rod pressure during LOCA.

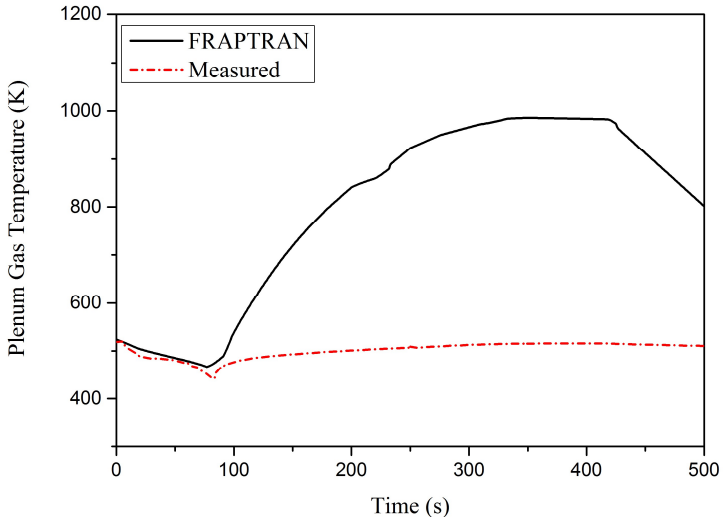

FIG. 21. Variation of plenum gas temperature during LOCA.

Figure 22 illuustrates the comparison of measured and simulated cladding outside temperature. The predicted cladding outside temperature shows similar trend with the measured values. Difference in nodalization and the simplification of the models as well as the replacement of thermal properties of heavy water by those of light water might account for the deviation of the measured and predicted value.

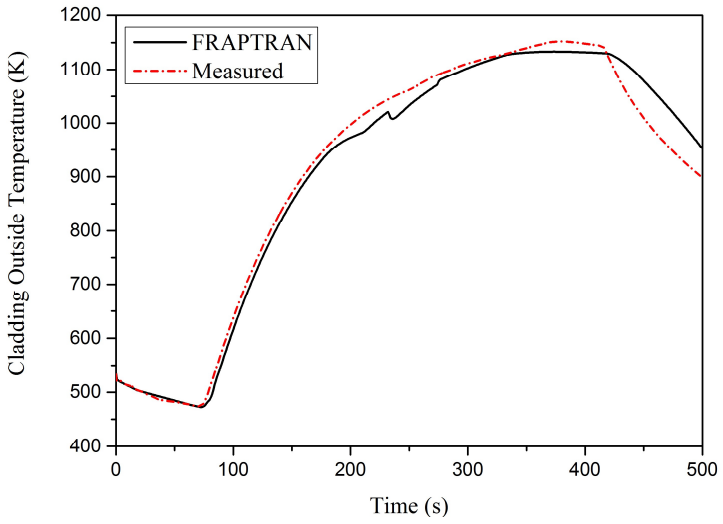

FIG. 22. Variation of cladding outside temperature during LOCA.

Figure 23 illustrates the comparison of measured and predicted cladding outer diameter. The predicted axial variation of cladding outer diameter shows similar trend with the measured one. Deviation of the ballooning node may be accounted by the difference in nodalization of boundary conditions.

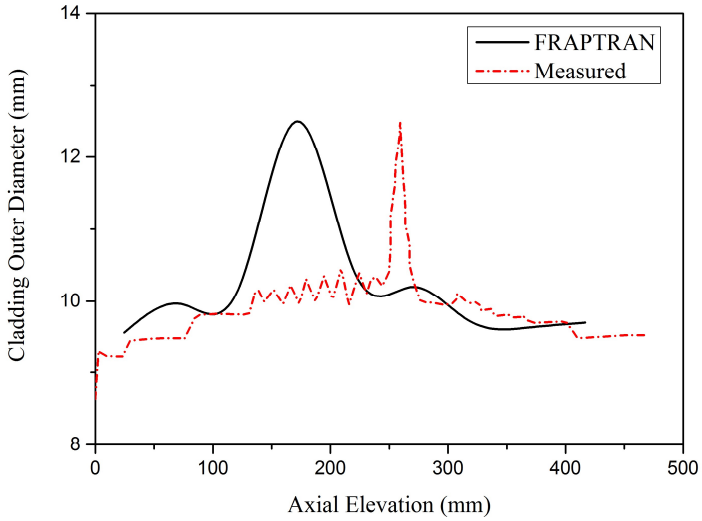

FIG. 23. Variation of cladding outer diameter during LOCA.

5. SIMULATION OF IFA-650.11

5.1.Initial and boundary condition

Steady state power history was determined by the given pre-test irradiation history as shown in Fig. 24. Axial power profiles were set to be uniform all along the fuel rod. Table 6 presents the nodalization of fuel rod.

For the transient state simulation, data for power history and axial power profiles come from the experiment data provided[4]. The data file contains the boundary conditions for the benchmarks. Thermal hydraulic boundary conditions used in FRAPTRAN are described with

[4] Refer to Simulation of Initial and Boundary Conditions with SOCRAT code for benchmarks based on IFA-650.10 and IFA-650.11 tests, by Dolganov et al. in this Annex.

the coolant pressure, temperature and clad to coolant heat transfer coefficients, as shown in Figs 25–27. The heat transfer coefficients were derived with the cladding and coolant temperature, as well as the heat transfer rates by convection and radiation. LHGR was set equal to 71% of nominal values based on the rod power recalibration[5].

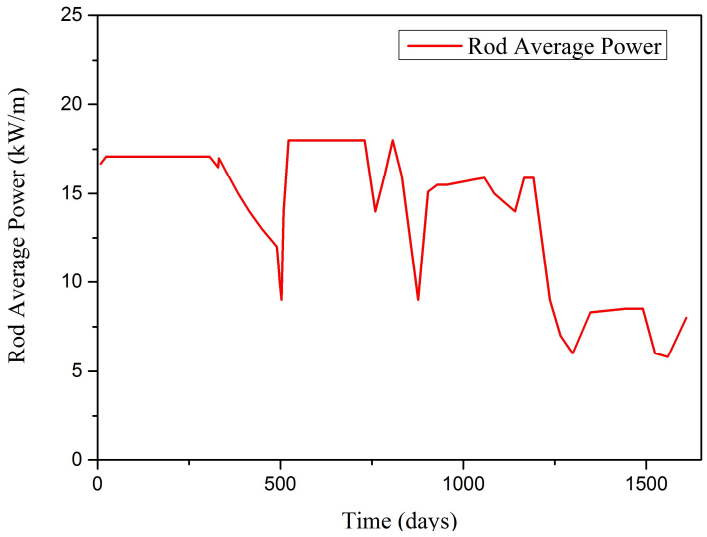

FIG. 24. Rod average power history of pre-irradiation.

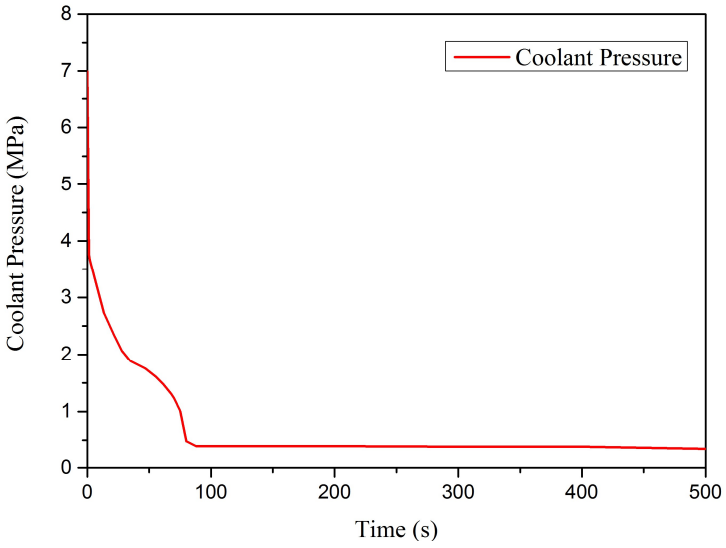

FIG. 25. Coolant pressure history of transient condition.

[5] Refer to Simulation of Initial and Boundary Conditions with SOCRAT code for benchmarks based on IFA-650.10 and IFA-650.11 tests, by Dolganov et al. in this Annex.

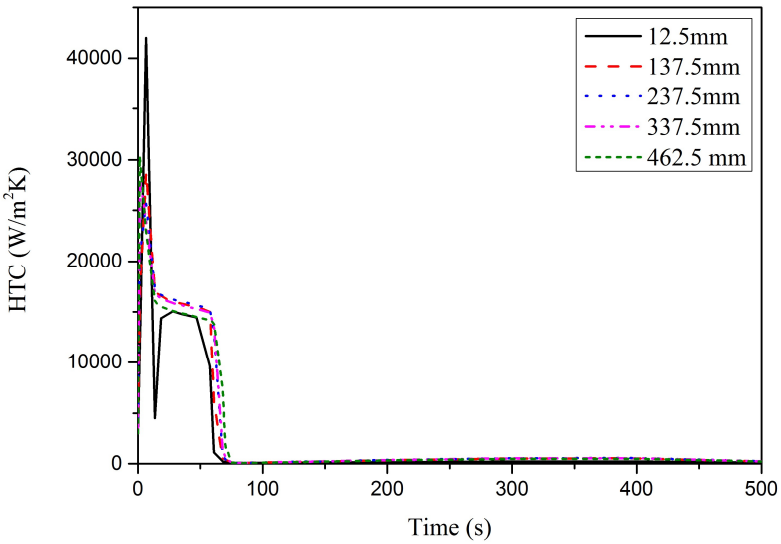

FIG. 26. Heat transfer coefficient history of transient condition.

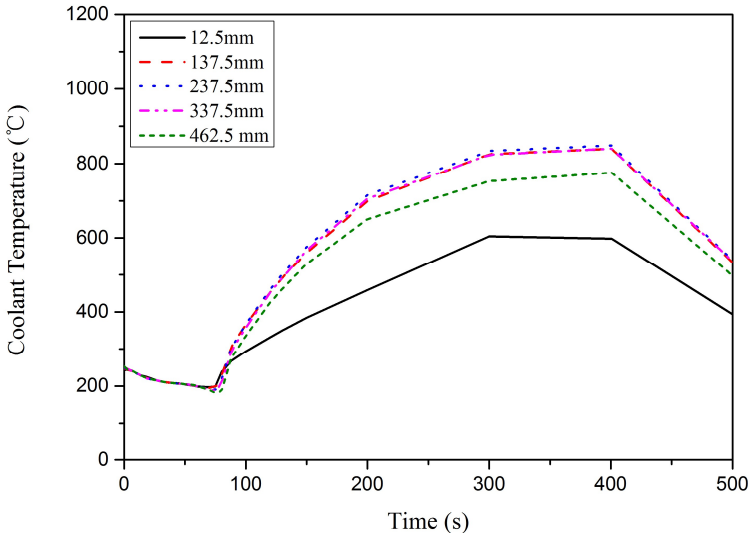

FIG. 27. Coolant temperature history of transient condition.

TABLE 6. NODALIZATION (STEADY & TRANSIENT STATES).

Node	1	2	3	4	5
Axial Elevation (mm)	26.667	80	133.33	186.67	240
Node	6	7	8	9	
Axial Elevation (mm)	293.33	346.67	400	453.33	

5.2.Steady state simulation results

Similar to the results of 650.9 and 650.10, during normal operation, fuel temperature, rod pressure and cladding temperature change with rod power, as shown in Figs 28–30.

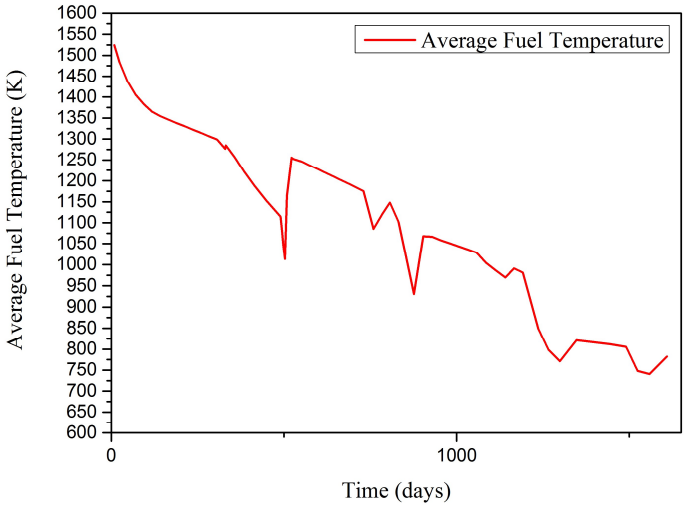

FIG. 28. Variation of average fuel temperature during normal operation.

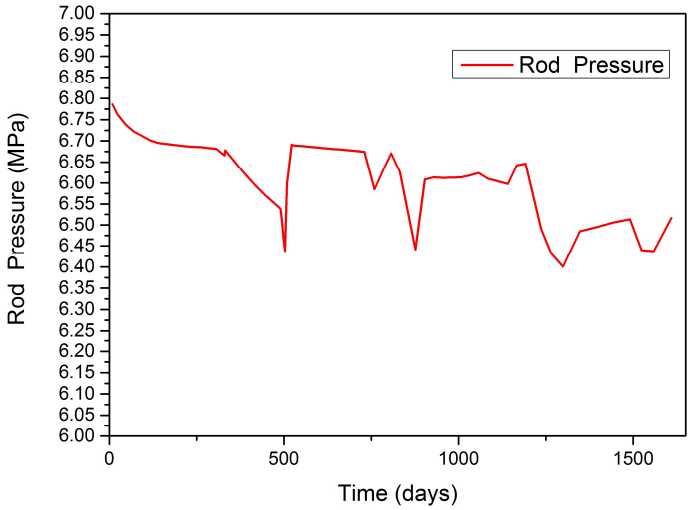

FIG. 29. Variation of rod pressure during normal operation.

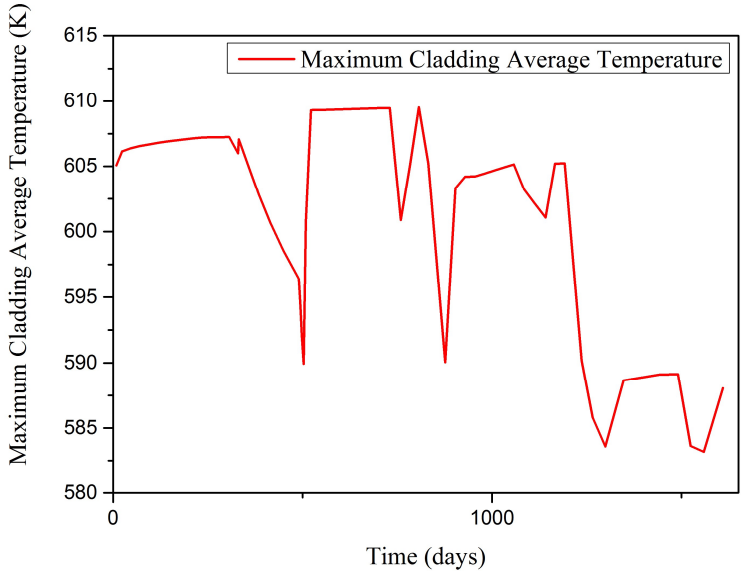

FIG. 30. Variation of cladding average temperature during normal operation.

5.3.LOCA condition simulation results

Table 7 shows the overall comparison of FRAPTRAN calculated results and corresponding measured values. In this case, failure time predicted by FRAPTRAN is a little later than the measured failure time and the predicted maximum rod pressure and its corresponding cladding hoop stress as well as the cladding failure temperature approach to the measured value.

TABLE 7. OVERALL COMPARISON OF FRAPTRAN CALCULATED RESULTS AND CORRESPONDING MEASURED VALUES

	Measured	FRAPTRAN
Cladding deformation start time (s)	183	212
Cladding failure time (s)	207	217
Maximum rod pressure (MPa)	5.57	5.36
Maximum rod pressure corresponding hoop stress (MPa)	29.5	29.0
Cladding failure temperature (K)	1112	1075.4

Figure 31 and Fig. 32 present the comparison between the FRAPTRAN predicted value and measured value of rod pressure, plenum gas temperature, respectively. The variation trend of the predicted plenum pressure matches well with the measured value. For the plenum temperature, similar phenomenon to that in 650.9 and 650.10 was observed.

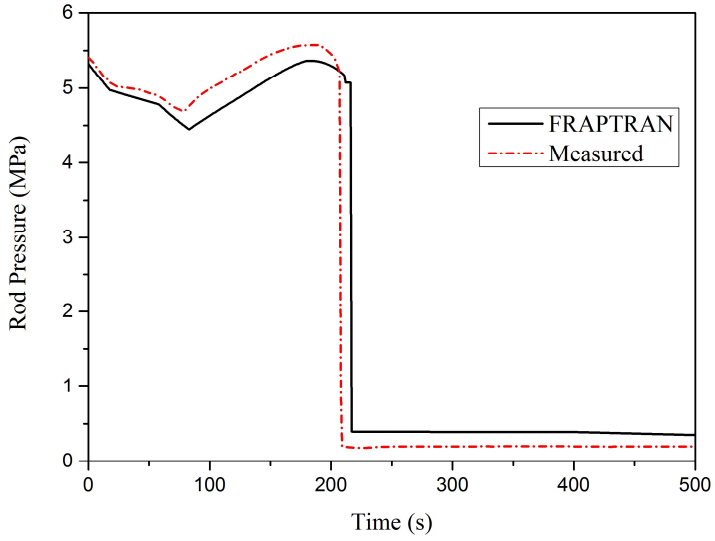

FIG. 31. Variation of rod pressure during LOCA.

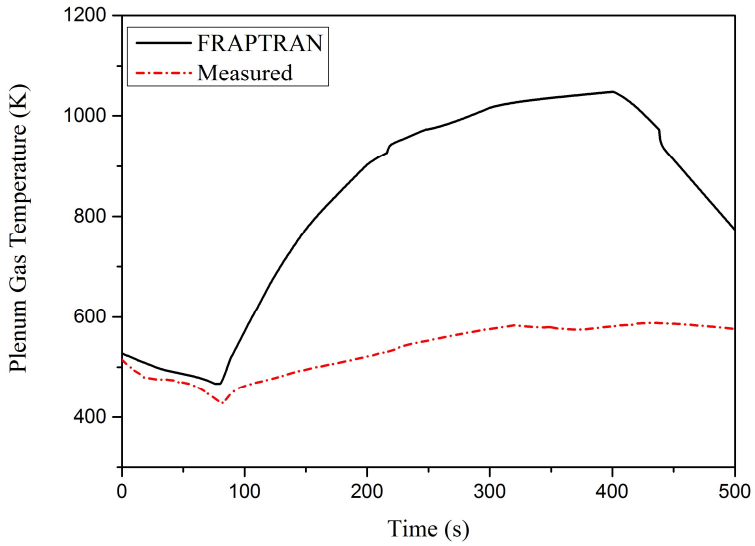

FIG. 32. Variation of plenum gas temperature during LOCA.

Figure 33 illustrates the comparison of measured and simulated cladding outside temperature. The predicted cladding outside temperature shows similar trend with the measured values. Deviation can be explained by the same reason as in the cases 650.9 and 650.10.

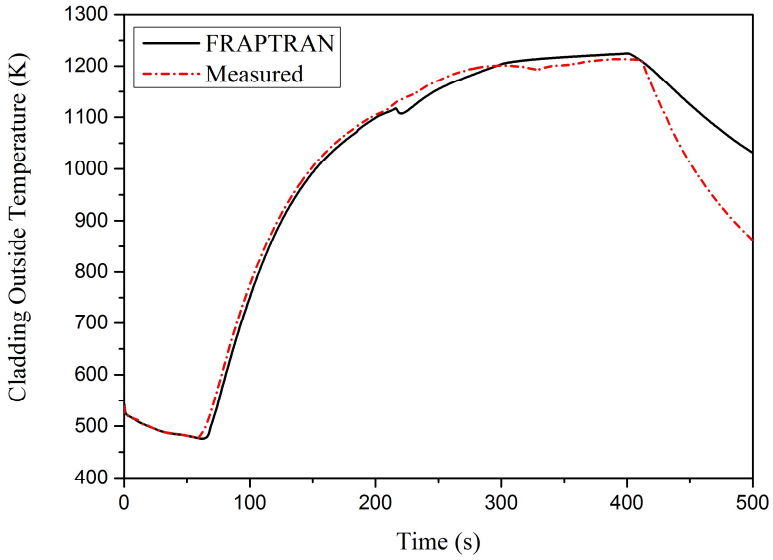

FIG. 33. Variation of cladding outside temperature during LOCA.

Figure 34 illustrates the comparison of measured and predicted cladding outer diameter. The predicted axial variation of cladding outer diameter shows similar trend with the measured one.

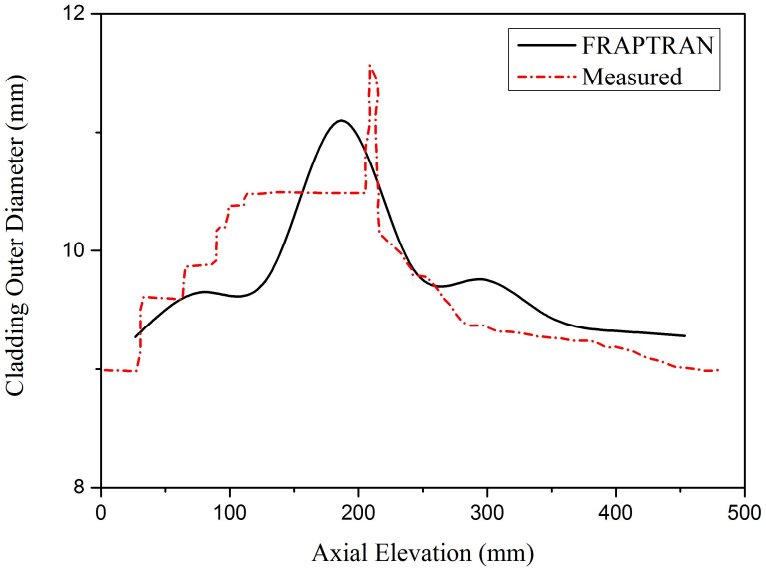

FIG. 34. Variation of cladding outer diameter during LOCA.

6. CONCLUSION

With the simulation of Halden fuel rod LOCA behavior tests IFA-650.9, 10, 11 using FRAPCON/FRAPTRAN, evaluation of integrated performance of fuel rod under LOCA condition is performed. Cladding temperature, cladding outer diameter variation, rod internal pressure as well as cladding failure are well predicted. Due to its very high burnup, significant fuel relocation and the complicated thermal hydraulic boundary condition, the IFA-650.9 case is rather complex. Consequently, deviations between the predicted and measured results are relatively large. In addition, even though the FRAPTRAN can model an external plenum volume, the plenum gas temperature calculation model have not yet been updated to concern the external plenum volume. Thus, large deviation of plenum gas temperature between predicted and measured value is observed. Moreover, feasibility of FRAPCON/FRAPTRAN codes for predicting fuel rod performance during steady/transient state has been assessed. Due to the simulations of FRAPCON/FRAPTRAN concern only the single fuel rod, but not the entire system loop, this will probably cause some deviation between predicted and measured values. Generally, FRAPCON/FRAPTRAN predict well the fuel rod behavior under LOCA condition. For further study, potential improvement could be made to FRAPTRAN cladding failure model and plenum gas temperature calculation model to enhance the predict ability and accurate the analysis results.

REFERENCES

[1] DU CHOMONT F.B, LOCA Testing at HALDEN, the Ninth Experiment IFA-650.9, Report on OECD HALDEN Reactor Project No. HWR-917, (2009).

[2] LAVOIL, A., LOCA Testing at HALDEN, the Tenth Experiment IFA-650.10, Report on OECD HALDEN Reactor Project No. HWR-974, (2010).

[3] LAVOIL, A., LOCA Testing at HALDEN, the VVER Fuel Experiment IFA-650.11, Report on OECD HALDEN Reactor Project No. HWR-976, (2010).

[4] GEELHOOD, K.J., LUSCHER, W.G., FRAPTRAN-2.0: Integral Assessment, DE-AC05-76RL01830, Vol. 2, Rev. 2, PNNL-19400, U.S. Department of Energy under Contract (2016).

[5] GEELHOOD, K.J., LUSCHER, W.G., CUTA, J.M., IA Porter, FRAPTRAN-2.0: A Computer Code for the Transient Analysis of Oxide Fuel Rods, under Contract DE-AC05-76RL01830 Initial and boundary conditions for IFA-650.10 and IFA-650.11

calculations with SOCRAT code. Vol. 1, Rev. 2, PNNL-19400, U.S. Department of Energy (2016).

FUEL BEHAVIOUR UNDER LOCA CONDITIONS ESTIMATED WITH FRAPTRAN

J. HEIKINHEIMO, V. TULKKI, J. KÄTTÖ, T. IKONEN, H. LOUKUSA
VTT Technical Research Centre of Finland Ltd
Kivimiehentie 3, Espoo, P.O. Box 1000
FI-02044 VTT, Finland
Email: janne.heikinheimo@vtt.fi

Abstract

Objective of this work was to improve the fuel behaviour codes' capability to predict the behaviour of the fuel in accident conditions. Especially for LOCA modelling, the description of the thermal hydraulic behaviour is of great importance. Both the FRAPTRAN-GENFLO code and the FINIX module (if coupled with a thermal hydraulic code) are capable of advanced treatment of the coupling between the fuel and thermal hydraulic behaviours. During the CRP FUMAC several new versions of FRAPTRAN (1.5, 2.0) were taken into use and tested at VTT. Some irregular behaviour of the ballooning model was observed in the AEKI test simulations. Otherwise, the simulations of the experimental tests IFA-650.10, IFA-650.11, and Studsvik 192 were able to predict quite accurately the observations in the experiments. The original plan was to implement LOCA-relevant models to VTT's own FINIX code and then run benchmark simulations with it. However, due to resource issues and expert turnover this was not achieved during this time period.

1. INTRODUCTION

VTT aims at the improvement of the expertise and the computer codes used for prediction of nuclear fuel behaviour in accident conditions. This goal is promoted via participation in the CRP FUMAC. The VTT-modified FRAPCON fuel performance code was to be used for steady state calculations. Transient calculations was to be performed with two codes, FRAPTRAN-GENFLO and FINIX. FRAPTRAN-GENFLO uses the FRAPTRAN fuel performance code with the FEM mechanical model coupled with the general purpose thermal hydraulics code GENFLO. FINIX is VTT's in-house transient fuel behaviour module designed for easy integration into thermal hydraulics, reactor physics, and other codes in multiphysics simulations.

Objective of the work was to improve the fuel behaviour codes' capability to predict the behaviour of the fuel in accident conditions. Especially for LOCA modelling, the description of the thermal hydraulic behaviour is of great importance. Both the FRAPTRAN-GENFLO code and the FINIX module (if coupled with a thermal hydraulic code) are capable of advanced treatment of the coupling between the fuel and thermal hydraulic phenomena. However, model development in both and code development in the case of FINIX are necessary, and planned to take place within and parallel to the FUMAC project.

We anticipated that as the outcome from FUMAC we would have established and strengthened collaborations and information exchange between participants. This would lead to improvements in the models and in understanding the physical phenomena that arise in accident condition fuels. The exercise was expected to reveal specific objectives for code and model development, which would be investigated and improvements implemented in the most important areas. In addition, we anticipated that the FUMAC project would expand the amount of available experimental data, leading to more possibilities in validating the numerical tools.

2. CODES USED

2.1. FRAPTRAN AND FRAPTRAN-GENFLO

During the CRP FUMAC, new versions of FRAPCON and FRAPTRAN were published. In this work FRAPTRAN-1.4, 1.5 and 2 were used. The final submitted results were obtained using FRAPTRAN-2 using FUMAC boundary conditions, this report details also the earlier simulations performed during the CRP FUMAC.

FRAPTRAN is a single-rod transient fuel performance code developed by PNNL for U.S.NRC [1]. It has been coupled with the thermal hydraulics code GENFLO, developed at VTT [2, 3].

GENFLO is a fast running program due to its non-iterative solution model of the thermal hydraulics equations. The coupled code has been verified against the experimental results from the Halden project IFA-650 LOCA tests [4]. The solution principles and models used during the LOCA are based on the SMABRE code developed at VTT [5]. The coupled code, FRAPTRAN-GENFLO, has been previously applied in the works of Arkoma et al. [6, 7].

2.2. FINIX

The design philosophy in FINIX development has been to provide a sufficient model for fuel rod simulations that is simple, computationally light, and easy to couple with other codes, such as neutronics, reactor dynamics, thermal hydraulics, and system codes. The direct code-to-code coupling is often a laborious task when highly specialized software is involved. Therefore, the flexibility of the interface has been prioritized in the FINIX design. FINIX can be integrated to the main simulation code at the source code level, which reduces the data transfer between the codes and allows the host code to access FINIX functions and data structures. In order to reduce user's need for fuel-specific knowledge, FINIX has an internal database for different kinds of fuels. This enables the uploading of required simulation parameters just based on the desired fuel rod type.

FINIX has been initially designed for a transient modelling, but recently models for the steady-state modelling has been included. Compared to the full-featured fuel performance codes, such as FRAPTRAN [1], TRANSURANUS [8], and BISON [9], FINIX emphasizes flexibility and the requirements of the host code in favour of the fuel performance modelling. For example, many of the features less important to the host code, such as irradiation growth, are currently not considered in FINIX. However, the coupling between the mechanical behaviour of the gap and the radial heat transfer is modelled as in references [10–12].

During the time of the FUMAC CRP, models for irradiation effects and a new steady state temperature solver have been implemented in FINIX. The models for irradiation effects include a fission gas release model, basic swelling and densification and cladding creep models. The fission gas release model in FINIX combines the intragranular model of Forsberg and Massih [13] with the Pastore et al. [14] model for intergranular behaviour. Swelling and densification models are simple correlations from MATPRO and FRAPCON, and implemented cladding creep models are the Limbäck-Andersson [15] or the FRAPCON [16] model. With these new models, the capability of FINIX to model long irradiation periods has improved significantly. Current developments include also improvements in computation time. These are preconditions for accurately simulating accident conditions, however, due to time and personnel constrains there was no resources to implement the LOCA-relevant models during 2015–17 period.

No model in FINIX has been fitted to integral experiments, so differences to experimental data can be found from FINIX calculations and the models retain their mechanistic nature. Comparisons to some experimental results especially with regards the fission gas release

modelling have been performed, but a thorough validation of the module will be performed in 2018.

3. PHASE I: RESULTS AND DISCUSSION

3.1 AEKI ballooning tests

3.1.1. Simulation description

The PUZRY ballooning tests were calculated by using a coupled code FRAPTRAN-GENFLO. The code consists of the VTT modified version of FRAPTRAN-1.4 and the thermal hydraulics code GENFLO, version 22. In these tests there were no need for thermal hydraulics calculations, and therefore the functionalities of GENFLO were not used. Detailed information about the PUZRY experiment can be found in the publication by Perez-Feró et al. [17].

The cladding was divided to 10 axial nodes and 4 radial nodes. There were no fuel pellets inside the cladding, but in FRAPTRAN at least two radial nodes in the fuel pellet had to be given. In addition, a very small value, 10^{-10} m, was set for the fuel pellet diameter.

The tube specimens were pressurized at a constant temperature. In FRAPTRAN this temperature was set for the plenum and cladding. In VTT modified version of FRAPTRAN-1.4 the plenum temperature can be given as an input by selecting *PlenumTemp=3* in the *$model* data block. The cladding temperature can be set to the desired value by using the *heat* option in the *$boundary* data block. Here the coolant temperature is set to the target value and a very high value is used for the heat transfer coefficient.

In FRAPTRAN it is possible to give the rod internal pressure history as a boundary condition. This can be done in the $model data block by setting *prescri=1* and entering values for the keyword *gasphs*. Only 10 data pairs can be given to describe the internal pressure history, which will limit the keyword use in more complicated situations. The current pressure at each time step is found by linear interpolation. In PUZRY experiments the pressure increases linearly, and therefore the limit did not cause problems in this case. However, when the rod internal pressure is given as an input, it is not possible to use option *mechan=1* in the *$model* data block, which selects the FEA mechanical model. Therefore the rod mechanical behaviour is modelled with the FRACAS-I model.

A major limitation in the calculations is the fact that without code modifications it is not possible to restrict the cladding axial or radial movement by external constraints. In this case Zircaloy-4 plugs are welded at the top and bottom of the tubes. In reality the plugs restrict the cladding radial movement at these locations, but currently their effect cannot be taken into account.

3.1.2. Simulation results

The illustration of the main simulation results are listed in table 1, where we used a time step of 0.1 s. The relative errors in the simulated burst pressures and times were 0-20%. We observed that the length of the time step in the simulations has a significant effect on the aforementioned parameters. In FRAPTRAN input instructions [1] the recommended time step size for a large break loss of coolant accident during blowdown is 0.2 s. In a reactivity initiated accident during the power pulse the recommended time step size is 10 μs.

When FRAPTRAN calculates the cladding deformation with the FRACAS-I model, it checks whether or not it should begin to use the cladding ballooning model. The cladding ballooning model, called BALON2, is used to calculate the localized non-uniform straining of the cladding. Once FRAPTRAN changes from the FRACAS-I model to BALON2 model, FRACAS-I no longer calculates further cladding deformation. The BALON2 model uses two criteria to check if the cladding burst has occurred. The first criterion is based on the cladding

hoop stress, while the second criterion is based on the cladding permanent hoop strain. The cladding burst is calculated to occur, if the cladding hoop stress exceeds an empirical limit, or if the cladding permanent hoop strain exceeds a temperature dependent strain limit given in the FRAPTRAN user manual [1].

As mentioned in the previous section, the effect of the end plugs on the axial and radial movement of the cladding have not been taken into account in the calculations. Therefore the mechanical deformations of the tubes cannot be simulated correctly. Consequently, the pressure increase leads to equal radial deformation in each node, until the ballooning model starts to calculate rod ballooning in one random node. For some reason FRAPTRAN does not update the tube volume during the simulation.

TABLE 1. SIMULATION RESULTS FOR THE PUZRY BALLOONING TESTS WITH A 0.1 S TIME STEP SIZE.

No.	Temperature (°C)	Simulated burst pressure (MPa)	Measured burst pressure (MPa)	Relative error in burst pressure (%)	Simulated burst time (s)	Measured burst time (s)	Relative error in burst time (%)	Simulated hoop stress at burst location (MPa)
26	700	8.76	10.705	-18.2	717.6	888.8	-19.3	123.3
30	800	6.05	7.351	-17.7	222.7	275.7	-19.2	101.0
18	900	3.11	2.789	11.5	264.6	233.7	13.2	40.0
8	1000	0.86	0.990	-13.1	98.8	116.7	-15.3	14.4
10	1100	0.75	0.753	-0.4	91.8	92.0	-0.2	13.4
12	1200	0.69	0.678	1.8	82.0	80.0	2.5	11.4

3.2. IFA-650.11 tests

3.2.1. Simulation description

The base irradiation period of the Loviisa rod used in the Halden LOCA test was calculated with the VTT-modified steady-state code FRAPCON-3.4. The LOCA test performed at the Halden reactor was calculated with the coupled code FRAPTRAN-GENFLO. The code consists of the VTT modified version of FRAPTRAN-1.4 and the thermal hydraulics code GENFLO, version 22. More information about the experiment in Halden can be found in reference [18].

The rod simulation was performed in four steps: the first two steps were performed to calculate the base irradiation history of the Loviisa rod, and the two latter steps were performed to calculate the LOCA test.

In the first step the base irradiation history was calculated with FRAPCON for the whole Loviisa rod, labelled as ‘j13’. From this calculation one can get the coolant temperature history at the bottom of the segmented rod, labelled as “segment 3”. This is the segment that was used in the LOCA test. From this calculation one can also get the rod internal pressure at the end of the irradiation that is needed in the second step.

In the second step the base irradiation history was calculated again, but this time for the segment 3 of the rod j13. The coolant inlet temperature history, that is required as an input, was calculated in the previous step. Also, the plenum length of the segment was varied until the calculated rod internal pressure was equal to that calculated in the previous step for the whole rod at the end of the irradiation period. The result of this step is a FRAPCON generated restart file that will be further modified in the next step.

In the third step a zero-power stand-alone FRAPTRAN simulation was performed for the instrumented rod. In this step the coolant pressure and enthalpy were set so that the calculated coolant temperature was 20 °C. The restart file produced in step 2 was further modified so that

the fill gas composition was equal to that of the instrumented rod. In addition, the fill gas mole amount given in the restart file was varied until the calculated fill gas pressure was equal to that of the instrumented rod fill gas pressure. The result of this step is a modified restart file that is needed in the actual LOCA simulation in the last step.

The actual LOCA simulation was calculated with FRAPTRAN-GENFLO. The GENFLO code was originally developed for calculating the thermal hydraulics of a whole BWR reactor core during severe transients. The coupled version of GENFLO used in this work, however, is used for calculating the coolant boundary conditions in one subchannel containing one fuel rod. FRAPTRAN-GENFLO is optimized for Halden LOCA tests and validated against several tests in IFA-650 series, including VVER tests IFA-650.6 and IFA-650.11 [19]. The selection of some parameters in GENFLO input, such as cladding and heater emissivities, is based on the experience gained from these previous simulations.

The cladding mechanical behaviour was calculated with the FEA-model developed at VTT [20], as recommended by Stengård [21]. In previous Halden LOCA simulations the FRAPTRAN original mechanical model FRACAS and the model for ballooning were considered unsatisfactory, while the FEA model produced generally better predictions for the cladding deformation and rupture time [21]. It was noticed that with some input parameter combinations the convergence in the simulation cannot be achieved with the FEA model. To achieve the convergence, the following parameter-value combinations were used: *frcoef=0* and *irefine=2*. In the former assignment the Coulomb friction coefficient has been set to zero, while the latter assignment means that no mesh refinement is used with FEA model in case of ballooning.

In Halden IFA-650 tests most of the total free gas volume is located outside the heated region. This would cause problems in a stand-alone FRAPTRAN simulation because the code is designed for simulating nuclear fuel behaviour in a set-up similar to a commercial reactor. FRAPTRAN-GENFLO, however, is designed for set-ups like the Halden test rig, which makes it possible to calculate the plenum temperature more reliably. The plenum temperature is calculated by GENFLO by selecting *PlenumTemp=2* in FRAPTRAN input file.

3.2.2. Simulation results

After blowdown at 0 s both the measured and calculated fill gas pressures start to decrease, as can be seen in Fig. 1. The pressure decrease occurs because the evaporating coolant provides additional cooling for the rod. This additional cooling is provided as long as the rig pressure is high enough compared to the dump tank pressure, and there is high enough coolant flow from the rig to the tank. The rig is completely emptied of water at ~70 s, after which the measured plenum temperature starts to rise due to the rise in cladding temperatures. At this point, however, there is no substantial rise in calculated plenum pressure, and shortly before the rod burst the difference between measured and calculated plenum pressures is almost 1 MPa. FRAPTRAN-GENFLO simulation suggests that the time to rod burst is 197.7 s, while the measured time to burst was 207 s. The rod burst can be detected from Fig. 3: the burst occurs when the fill gas pressure drops suddenly to coolant pressure at 0.1 MPa.

The reason for the differences between the calculated and measured plenum pressures can be seen in Fig. 2, which shows the measured and calculated plenum temperatures. After the rig has been emptied, the measured plenum temperature rises quickly, while the calculation suggests that there is a relatively large delay in plenum temperature rise. After 300 s both the measured and calculated plenum temperatures start to fluctuate, but the calculated fluctuation is more pronounced than the measured.

Figure 3 shows the measured and calculated cladding temperatures at different axial elevations. Cladding thermocouple TCC1 was located 9.5 cm above the fuel stack bottom, and cladding thermocouple TCC3 8 cm below the top of the fuel stack. As can be seen in the figure,

the point at which the cladding temperatures start to rise is predicted quite accurately. Also, the early heat-up phase is predicted relatively well, especially for the lower thermocouple. After the rod burst the differences between the calculated and measured temperatures start to increase, and cladding temperatures are clearly overestimated, for TCC3 ~150 K and for TCC1 ~130 K. The largest differences between measured and calculated temperatures, however, occur after the rod burst, and therefore the overestimation does not significantly affect the rod deformation calculation or the burst time prediction. The calculated clad average temperature at the burst location in the middle of the rod was 1198.2 K.

The calculated maximum cladding outer diameter is 11.2 mm, while the measured maximum diameter is 11.6 mm. The calculated burst location is 216 mm above the bottom of the fuel stack, while the measured burst location is ~205 mm above the bottom of the stack. The burst location and size are therefore quite well predicted. The cladding elongation, on the other hand, was not predicted well. The measured cladding elongation at 1000 s was 1.13 mm, while the calculated value was -7.01 mm. The cladding oxide layer thickness is probably overestimated, because the measured cladding temperatures were lower than the calculated.

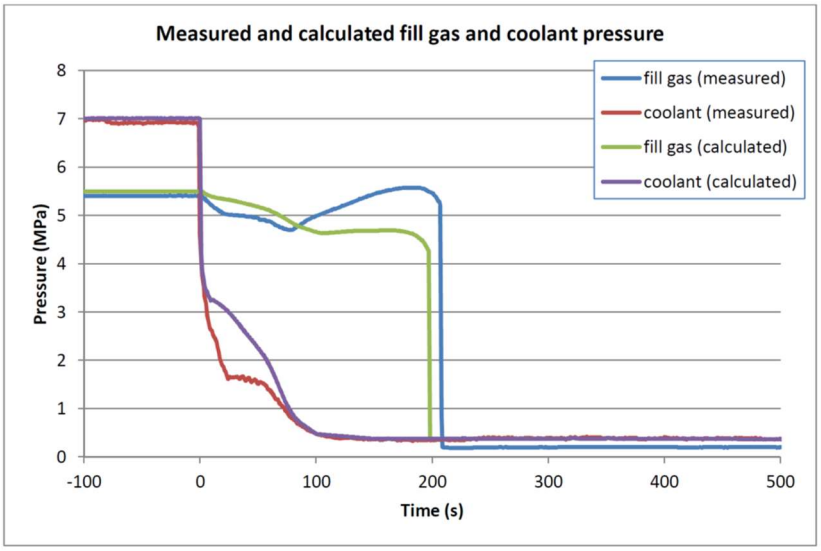

FIG. 1. Measured and calculated fill gas and coolant pressures.

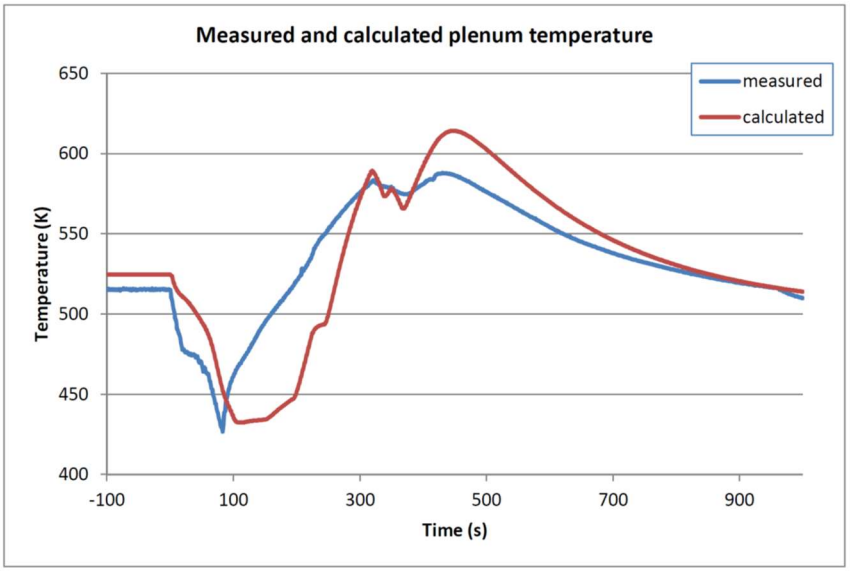

FIG. 2. Measured and calculated plenum temperature.

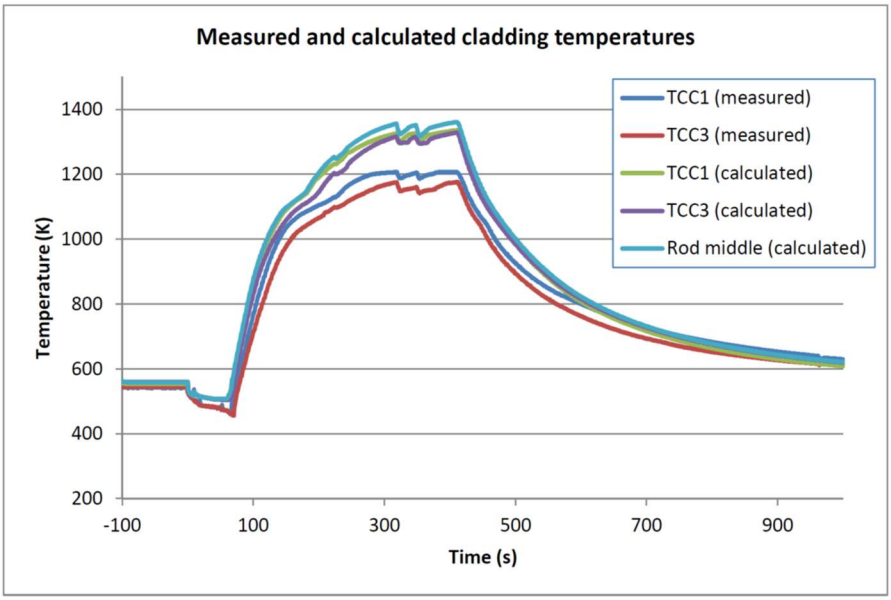

FIG. 3. Measured and calculated cladding temperatures.

4. PHASE II: RESULTS AND DISCUSSION

4.1. Simulation description

In order to better compare the LOCA results obtained with the different fuel performance codes, the participants used in the second phase the same preset boundary conditions for thermal hydraulic conditions calculated with the integral code SOCRAT [22]. In the simulations we used FRAPCON-4.0 for determination of the initial state of the rods at the beginning before the LOCA and FRAPTRAN-2.0 for the LOCA calculations. VTT modifications has been implemented in the codes [23].

In phase II, we simulated the Halden experiments IFA-650.10 and IFA-650.11 [18]– [24]. In the IFA-650.10 experiment, a PWR fuel segment at a burnup of 61 MWd/kgU was placed in the LOCA test rig. The simulations were similar as in section 4.2.1 with the exception of applying preset boundary conditions for thermal hydraulics. The preset boundary conditions for FRAPTRAN included cladding heat transfer coefficients, bulk coolant temperature, and plenum temperature.

We also simulated Studsvik test 192 where a sample has been cut from a Westinghouse PWR UO_2 fuel rod. The test segment with an active length of about 0.30 m was placed inside a quartz tube and externally heated by infrared radiation without nuclear heating. Majority of the total free gas volume was located in the plenum outside the heated region. In the test, the studied segment balloons and bursts when it is heated in flowing steam in atmospheric pressure. The preset boundary conditions for FRAPTRAN included cladding surface temperatures and plenum temperature.

4.2. Simulation results

In the IFA-650 benchmark tests, a simulation starts at the time moment t = –300 s of experimental time. The following initial conditions have been used to match the test data:

- Temperature of the rod is 300 K;
- Gas mixture of 95 vol-% Ar and 5 vol-% He at a pressure of 3MPa/4MPa (IFA-650.11/IFA-650.10) and temperature of 300 K are set in the rod free volume;
- Temperature/pressure of the coolant in the loop and the flask is 235 °C/7 MPa;
- Environment outside the flask is heavy water at a temperature of 229 °C and pressure of 3.4 MPa.

Prescribed benchmark conditions on the heat source has been obtained from the CRP FUMAC.

4.2.1. IFA-650.10 test

IFA-650.10 LOCA simulations resulted the cladding temperature and inner gas pressure illustrated in figures 4 and 5. The time of failure occurred in the simulations at 269 s while the measured value was 249 s. The burst location and rod outer diameter are presented in Fig. 6: the simulated location is 220 mm above the bottom of the rod while the measured location is 260 mm and the simulated rod outer diameter is 15.0 mm while the measured value is 12.5 mm.

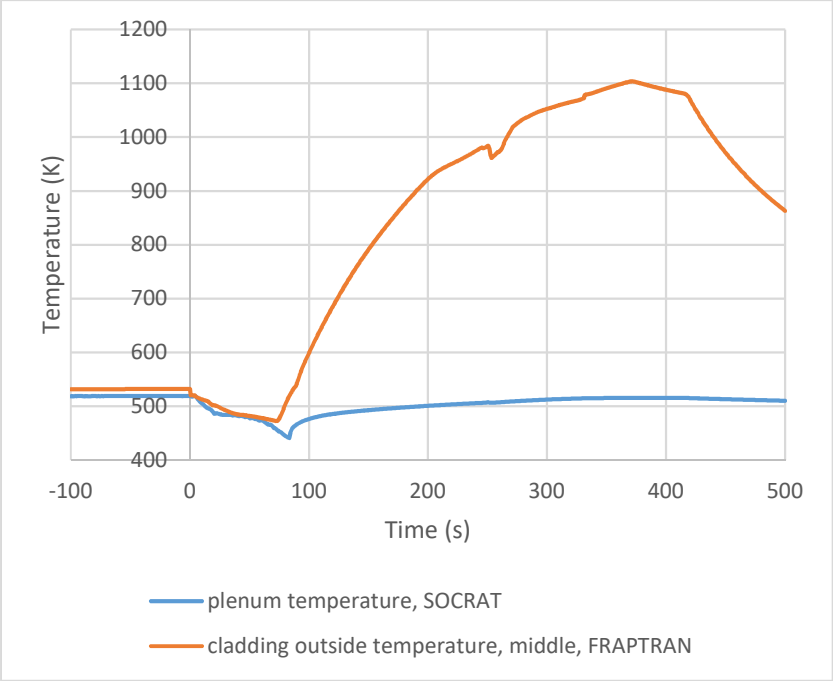

FIG. 4. Cladding and plenum temperature in IFA-650.10 simulations with predetermined boundary conditions.

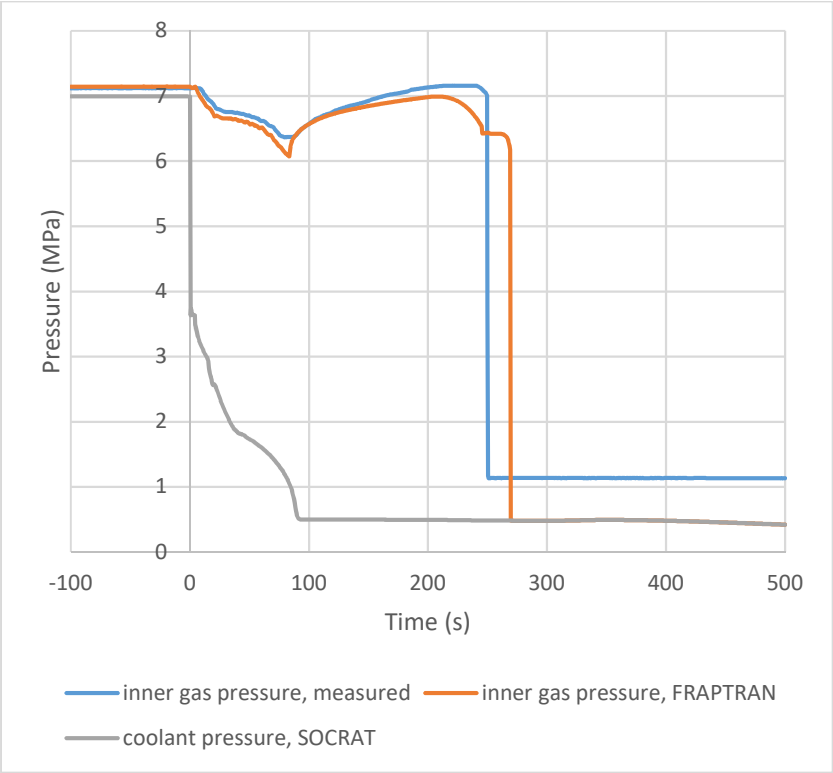

FIG. 5. Rod inner gas and coolant pressure in IFA-650.10 simulations with predetermined boundary conditions.

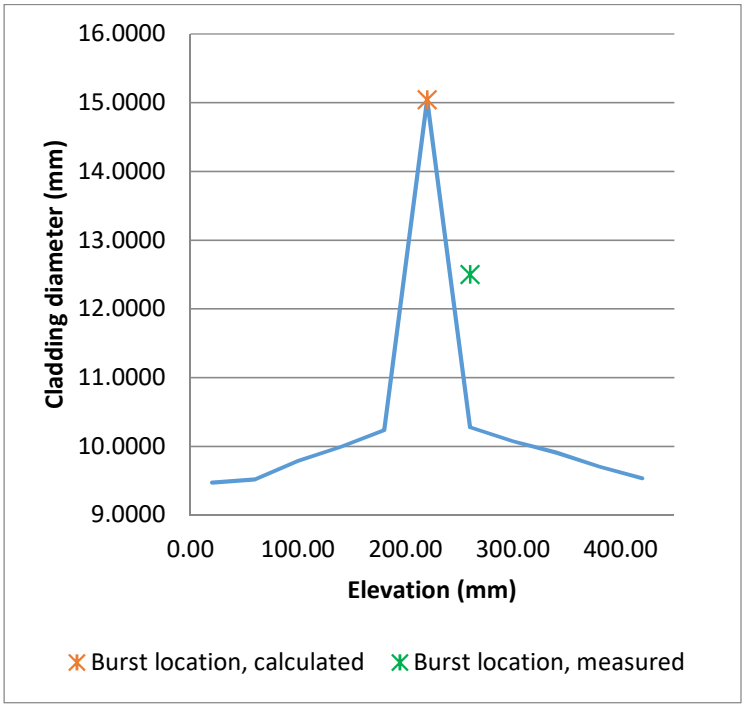

FIG. 6. Calculated cladding outer diameter and burst location in IFA-650.10 simulations with predetermined boundary conditions.

4.2.2. IFA-650.11 test

IFA-650.11 LOCA simulations resulted the cladding temperature and inner gas pressure illustrated in Figures 7 and 8. The time of failure occurred in the simulations at 221 s while the

measured value was 207 s. The burst location and rod outer diameter are presented in Fig. 9: the simulated location is 240 mm above the bottom of the rod while the measured location is 205 mm and the simulated rod outer diameter is 11.3 mm while the measured value is 11.6 mm.

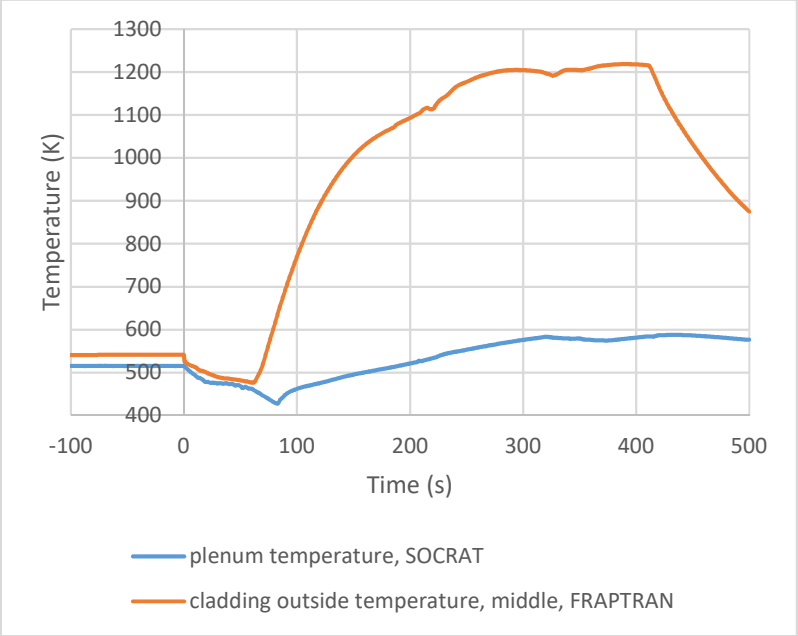

FIG. 7. Cladding and plenum temperature in IFA-650.11 simulations with predetermined boundary conditions.

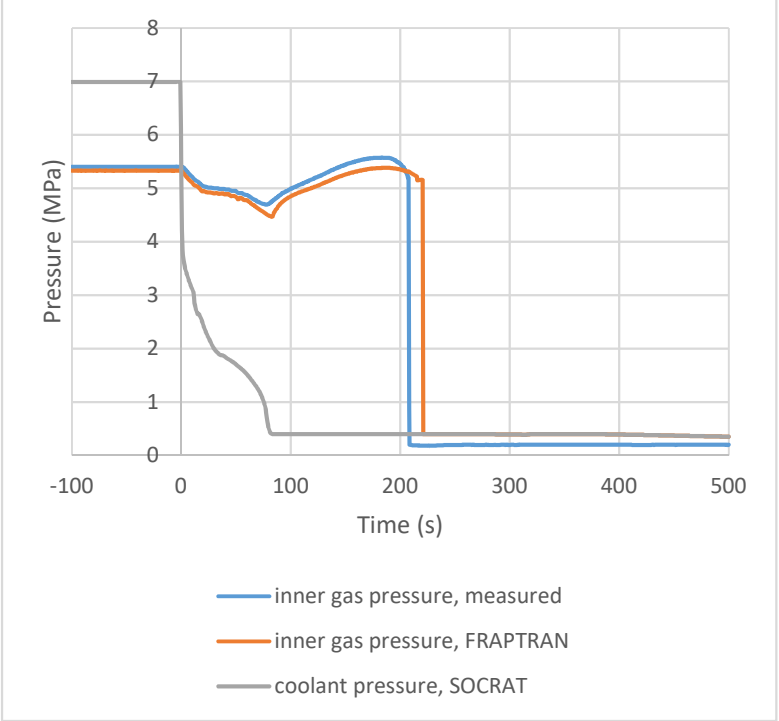

FIG. 8. Rod inner gas and coolant pressure in IFA-650.11 simulations with predetermined boundary conditions.

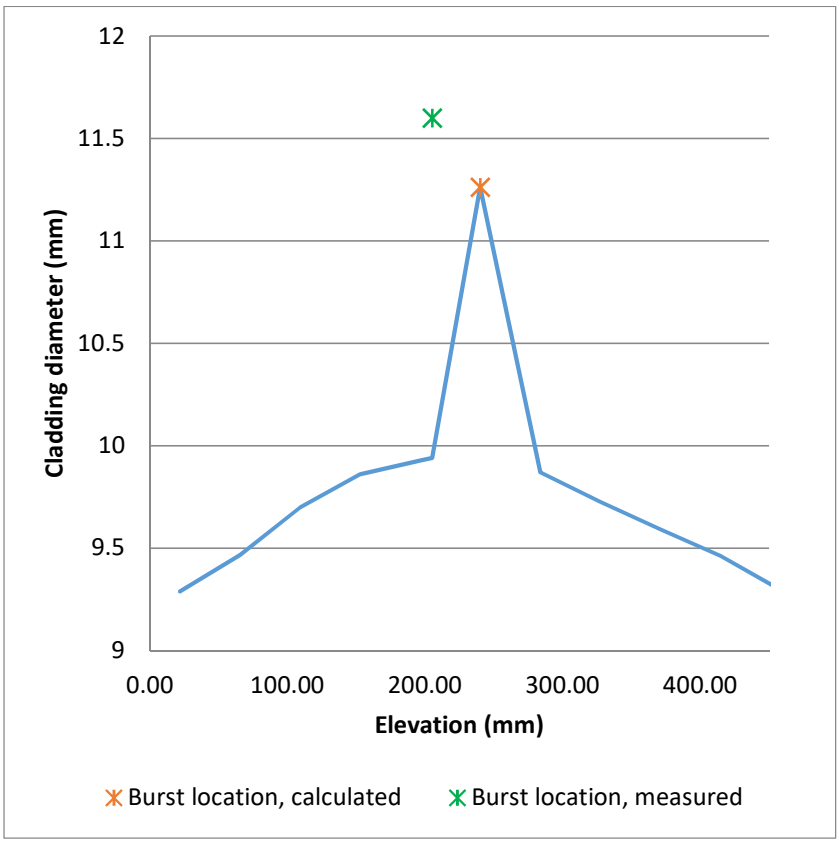

FIG. 9. Calculated cladding outer diameter and burst location in IFA-650.11 simulations with predetermined boundary conditions.

4.2.3. Studsvik 192 test

The similar kind of simulations were performed to the Studsvik 192 LOCA test as for the IFA-650 tests. Cladding temperature and inner gas pressure illustrated in figures 10 and 11. The time of failure occurred in the simulations at 84 s while the measured value was 81 s. The burst location and rod outer diameter are presented in Fig. 12: the simulated location is 150 mm above the bottom of the rod while the measured location is 205 mm and the simulated rod outer diameter is 28.9 mm while the measured value is 16.4 mm.

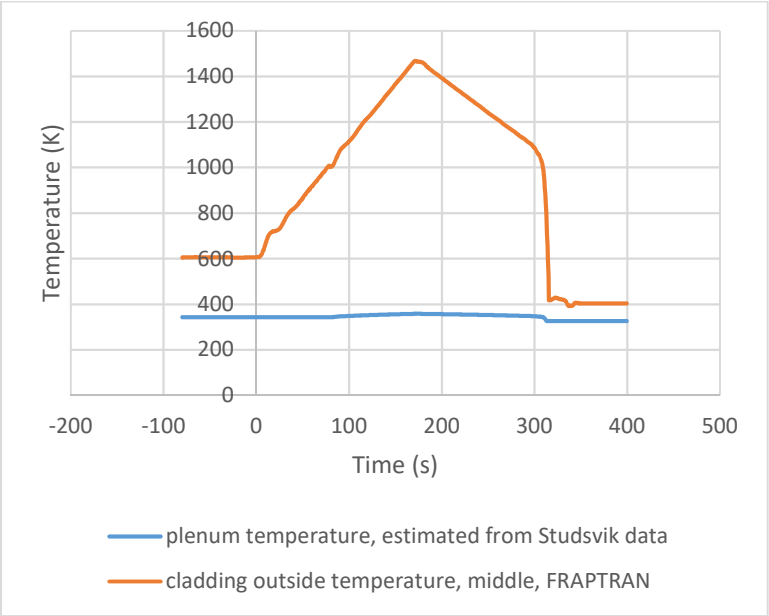

FIG. 10. Cladding and plenum temperature in Studsvik 192 simulations with predetermined boundary conditions.

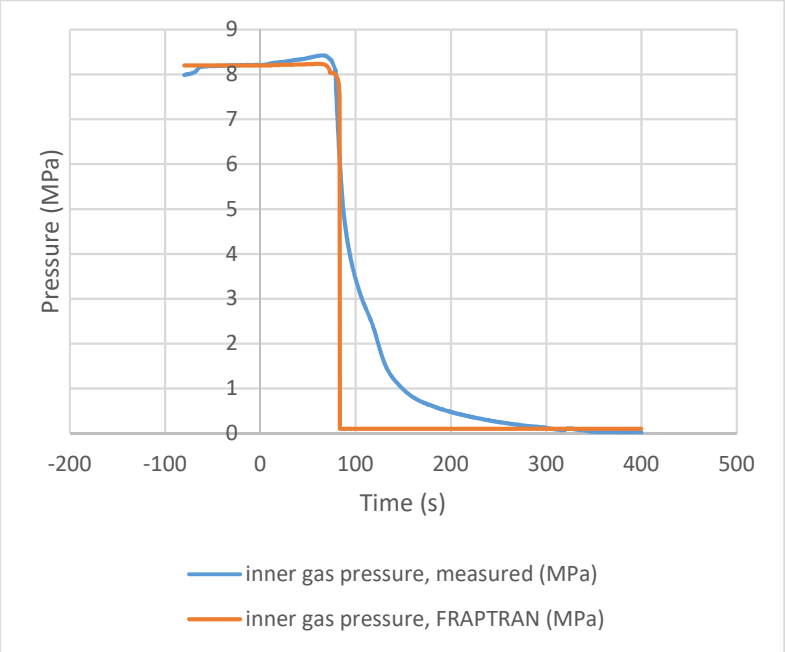

FIG. 11. Rod inner gas pressure in Studsvik 192 simulations with predetermined boundary conditions.

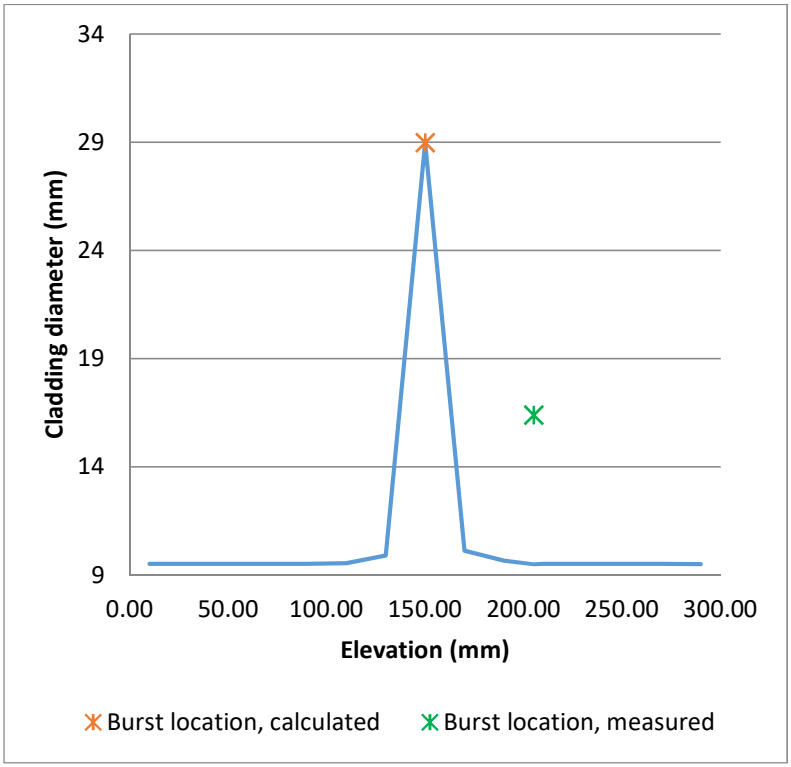

FIG. 12. Calculated cladding outer diameter and burst location in Studsvik 192 simulations with predetermined boundary conditions.

5. CONCLUSIONS AND RECOMMENDATIONS

The following was performed within the VTT's FUMAC work:

(a) FRAPTRAN-GENFLO

- Was used to perform the calculations in the first phase of the FUMAC project;
- Consists of a VTT-modified version of FRAPTRAN-1.4 that is coupled to a thermal hydraulics code GENFLO;
- FRAPTRAN calculates the thermal and mechanical behaviour of a single fuel rod in transient and accident conditions, while GENFLO calculates the coolant conditions around the fuel rod.

(b) FRAPTRAN-2.0

- Was used to perform the calculations in the second phase of the FUMAC project;
- Calculates the thermal and mechanical behaviour of a single fuel rod in transient and accident conditions; coolant conditions must be given as a boundary condition.

(c) FINIX

- Light-weight module for calculating the thermal and mechanical behaviour of a fuel rod;
- Designed for multiphysics calculations;
- Was further developed during the project but is not yet ready for LOCA simulations.

During the CRP FUMAC several new versions of FRAPTRAN (1.5, 2) were taken into use and tested at VTT. Some irregular behaviour of the ballooning model was observed in the AEKI test simulations that were reported to the developer. The original plan was to implement LOCA-relevant models to VTT's own FINIX code and the run the benchmark simulations with it, but due to resource issues and expert turnover this was not achieved during this time period.

REFERENCES

[1] GEELHOOD, K.J., LUSCHER, W.G., BEYER, C.E., CUTA, J.M., FRAPTRAN 1.4: A Computer Code for the Transient Analysis of Oxide Fuel Rods, NUREG/CR-7023, Vol. 1, PNNL-19400, (2011).

[2] HÄMÄLÄINEN, A., STENGÅRD, J.O., MIETTINEN, J., KYRKI-RAJAMÄKI, R., Coupled Code FRAPTRAN – GENFLO for Analysing Fuel Behaviour During PWR and BWR Transients and Accidents. In proceeding of: Technical Committee meeting, 10–14 September 2001, Halden, Norway, IAEA-TECDOC-1320, (2001).

[3] Miettinen, J., Hämäläinen, A., GENFLO—A General Thermal Hydraulic Solution for Accident Simulation. VTT Research Notes 2163, ISBN 951-38-6083-3, ISSN 1455-0865 (2002).

[4] ORGANISATION FOR ECONOMIC CO-OPERATION AND DEVELOPMENT, NUCLEAR ENERGY AGENCY, Benchmark Calculations on Halden IFA-650 LOCA Test Results, NEA/CSNI/R(2010)6 (2010).

[5] MIETTINEN, J., Thermohydraulic Model SMABRE for Light Water Reactor Simulations. Thesis for the degree of Licentiate of Technology, Helsinki University of Technology (2000).

[6] ARKOMA, A., IKONEN, T., Sensitivity analysis of local uncertainties in large break loss-of-coolant accident (LB-LOCA) thermo-mechanical simulations. Nucl. Eng. Des., Vol. 305, (2016) 293–302,.

[7] ARKOMA, A., HÄNNINEN, M., RANTAMÄKI, K., KURKI, J., AND HÄMÄLÄINEN, A., Statistical analysis of fuel failures in large break loss-of-coolant accident (LBLOCA) in EPR type nuclear power plant. Nucl. Eng. Des., Vol. 285, (2015) 1–14.

[8] Lassmann, K., Transuranus: A Fuel Rod Analysis Code Ready For Use, J. Nucl. Mater. Vol. 188, (1992) 295–302.

[9] Williamson R.L. et al., Multidimensional multiphysics simulation of nuclear fuel behavior, J. Nucl. Mater. Vol. 423, (2012) 149–163.

[10] Rohde, U., The modeling of fuel rod behaviour under RIA conditions in the code DYN3D, Ann. Nucl. Energy. Vol. 28, (2001) 1343.

[11] U.S. NUCLEAR REGULATORY COMMISSION, RELAP5/MOD3.3 Code Manual,Volume I: Code Structure, System Models, and Solution Methods, Nuclear Safety Division, Technical Report, Vol. 1, Rev. 4, NUREG-CR-5535, Information Systems Laboratories, Idaho Falls (2010).

[12] IKONEN, T., FINIX Fuel Behavior Model and Interface for Multiphysics Applications. Code Documentation for Version 0.13.9, VTT-R-06563-13, VTT Technical Research Centre of Finland, (2013). http://virtual.vtt.fi/virtual/montecarlo/download/VTT-R-06563-13.pdf.

[13] HERMANSSON, P. AND MASSIH, A. R., An effective method for calculation of diffusive flow in spherical grains. J. Nucl. Mater., Vol. 304, (2002) 204–211.

[14] PASTORE, G., LUZZI, L., DI MARCELLO, V., AND VAN UFFELEN, P., Physics-based modelling of fission gas swelling and release in UO2 applied to integral fuel rod analysis. Nucl. Eng. Des., Vol. 256, (2013) 75–86.

[15] LIMBÄCK, M. AND ANDERSSON, T.A, Model for Analysis of the Effect of Final Annealing on the In- and Out-of-Reactor Creep Behavior of Zircaloy Cladding. In Zirconium in the Nuclear Industry, 11th International Symposium, ASTM, (1996) 448–468.

[16] GEELHOOD, K. Implementing primary creep calculations during stress changes and reversals in the fuel performance code FRAPCON-3, in TopFuel, Charlotte, NC, ANS, (2013) 188–194.

[17] PEREZ-FERÓ, E. et al., Experimental database of E110 claddings exposed to accident conditions, J. Nucl. Mater. Vol. 397, Issues 1–3, (2010) 48–54,.
[18] LAVOIL, A., LOCA Testing at Halden, The VVER Fuel Experiment IFA-650.11. HWR-976. OECD Halden Reactor Project, 2010.
[19] STENGÅRD, J., The VVER LOCA Test IFA-650.6 Post Test Calculations with FRAPTRAN-GENFLO. Research Report VTT-R-10275-07. VTT Technical Research Centre of Finland, Espoo, Finland (2008).
[20] KNUUTILA, A., Improvement on FRAPCON3/FRAPTRAN Mechanical Modelling. Research Report VTT-R-11337-06. VTT Technical Research Centre of Finland, Espoo, Finland (2006).
[21] STENGÅRD, J., The VVER LOCA Test IFA-650.11 Post Test Calculations with FRAPTRAN-GENFLO. Customer Report VTT-CR-04155-12. VTT Technical Research Centre of Finland, Espoo, Finland (2012).
[22] BOLSHOV L., STRIZHOV V., "SOCRAT – the system of codes for realistic analysis of severe accidents," in: Proc. ICAPP'06, USA, June 2006, Paper 6439.
[23] IKONEN, T., VTT's modifications to the FRAPCON-4.0 code. Research Report VTT-R-00119-17. VTT Technical Research Centre of Finland, Espoo, Finland, 2017.
[24] LAVOIL, A., LOCA testing at Halden, The tenth experiment IFA-650.10, HWR-974, OECD Halden Reactor Project, (2010).

FUEL SIMULATION OF LOCA TESTS USING ALCYONE FUEL PERFORMANCE CODE

A. BOULORÉ, C. STRUZIK
CEA/DEN/Cadarache, Fuel Research Department
13108 Saint-Paul-lez-Durance, FRANCE

1. INTRODUCTION

CEA is developing the ALCYONE fuel performance code in the PLEIADES software environment. This code is dedicated to normal, off-normal and accident conditions such as RIA and LOCA. The objectives and motivations for CEA to participate to the FUMAC CRP were first to improve the validation of this fuel performance code in order to contribute to the interpretation of integral experiments based on single rod LOCA tests, but also to extend CEA's knowledge of LOCA fuel modelling through scientific exchanges.

In a first place, as ALCYONE is dedicated to the simulation of the behavior of one single rod, the experiments of interest for CEA in this project were the following ones:

— IFA 650.2, 650.9 and 650.10;
— Studsvik tests 192 and 198.

As the work progressed, partial conclusions and uncertainty analysis lead us to limit the studied cases to one of each type of experiment:

— IFA 650.10;
— Studsvik tests 192.

Specific developments of the fuel performance code for the LOCA conditions have been done regarding cladding behavior modelling, fission gas release and stress evaluation in the pellet before and during the tests.

ALCYONE 1D simulations of the state of the fuel rod before LOCA test have been performed and compared to the experimental data available.

The LOCA tests have also been simulated using as far as possible the boundary conditions provided to the project participants (for example the outer cladding temperature calculated with the SOCRAT code for IFA 650.10). The results have been compared to the experimental results. As agreed with the other participants, uncertainty quantification and sensitivity analysis has also been performed following the recommendations issued by the project Consultant Team.

2. CONCLUSIONS AND RECOMMENDATIONS

Some improvements have been done in the ALCYONE fuel performance code to better assess the fuel behavior in LOCA conditions.

The simulation of IFA650.10 and Studsvik 192 test have been done successfully until the cladding burst with ALCYONE. The calculated results are in relative good agreement with the experimental data, especially if we consider the uncertainties on boundary conditions.

This is the main conclusion of the second part of the work about uncertainty quantification and sensitivity analysis. As it has already been discussed in the first part of the project, the boundary conditions, especially the cladding temperature during the tests, have a major influence on the results of the simulation. Sensitivity analysis using PRCC quantifies this point.

So as far as boundary conditions are not very precisely known, burst time cannot be estimated more precisely than ± 10–15 s.

As recommendation and for future work, a precise quantification of the uncertainties on the boundary conditions of such experiments should be done in cooperation with the organizations that perform the experiments. In fact the specifications for the UQ/SA gave an uncertainty of ± 20°C on the cladding temperature, but it is probably an arbitrary value.

For future work, it would be interesting to integrate a fuel fragmentation/relocation model in ALCYONE in order to be able to perform the simulation until the end of the experiment. Cladding oxidation during the experiment also has to be represented.

The experimental cladding profile measured after the test in IFA650.10 (Fig. 6) shows that there are probably 3D effects in the pellet-cladding interaction. The sticking between the cladding and the pellet has to be considered particularly in 3D simulations.

3. ALCYONE CODE AND ITS IMPROVEMENTS

3.1. Presentation of ALCYONE fuel performance code

ALCYONE [1] is a multi-dimensional fuel performance code co-developed in the PLEIADES [2] platform by the CEA, EDF and AREVA. It is dedicated to the modeling of the in-reactor behavior of PWR fuel rods during normal (base irradiation) and off-normal (power ramps and accidental situations) operating conditions and incorporates three calculation schemes. A one-dimensional reference scheme, based on a one-dimensional axi-symmetric description of the fuel element associated to a discrete axial decomposition of the fuel rod in stacked independent fuel slices, is used to study the behavior of the complete fuel rod [3]. A two-dimensional scheme which describes Pellet-Cladding Interaction (PCI) at the mid-pellet plane of a pellet fragment is available to assess precisely stress concentration in the cladding near a pellet crack tip [4]. A three-dimensional model of the complete pellet fragment and overlying cladding is also of interest when detailed studies of PCI at pellet–pellet interfaces are required [5]. The different schemes use the Finite Element (FE) code Cast3M to solve the thermo-mechanical problem and share the same physical material models at each node or integration points of the FE mesh. Figure 1 presents the flows chart of ALCYONE 1D. On this figure the different tests of convergence loops are identified in blue, the models in the thermo-physical loop are in beige and the other models are in green if they are calculated before the thermo physical loop or in grey pink if after.

Base irradiation code result has been extensively validated on PWR rods (UO_2 and MOX fuel up to 80 GW·d/tM, cladding Zry-4 or M5) irradiated in the frame of the French survey program. Power ramp tests performed in MTR are used to validate the behavior of the fuel rod in case of power transient regime. Calculated results are confronted to experimental values at different scales, from overall measurements on the whole rod such as overall fission gas release or geometrical changes to the local measurements on the fuel pellet by SIMS and EPMA. Moreover, fuel temperature calculations are validated specifically on MTR experiments which present a thermocouple in the fuel center [3].

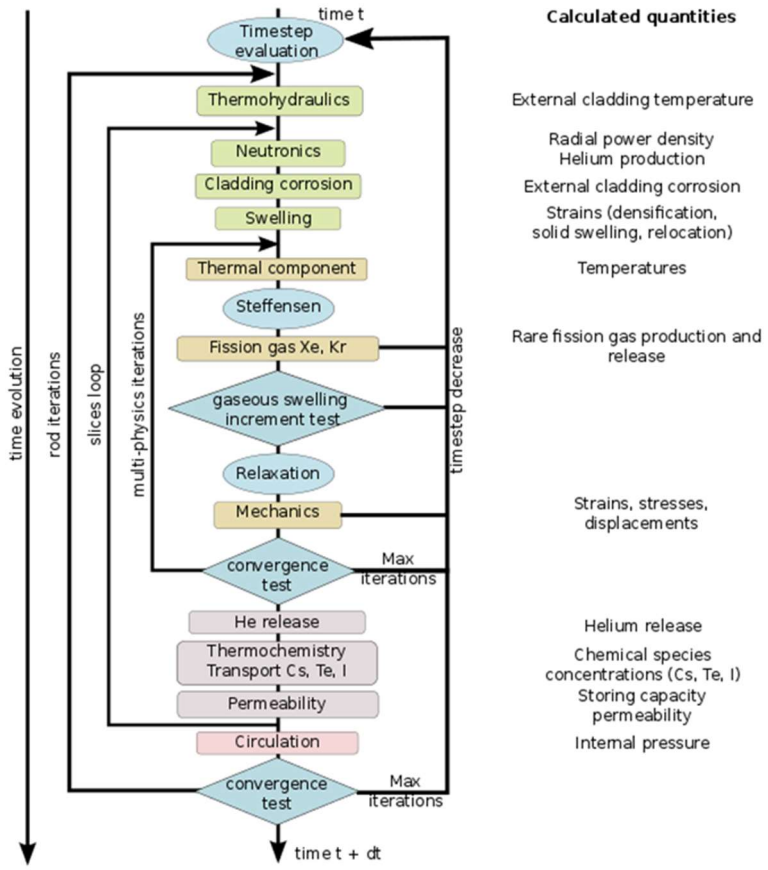

FIG. 1. ALCYONE flow chart.

Up to now, LOCA studies have been performed using 1.5 D scheme. For LOCA transient analysis, ALCYONE is not able to calculate the cladding temperature evolution with time, so this information has to be provided as input data. Nevertheless, the coupling of ALCYONE [6] with the system code CATHARE will be available in a near future. For the LOCA studies point of view, the evaluation of the rod internal pressure is crucial. To do so, it is necessary to have a good description of the fuel at the end of base irradiation. Then, it is essential to have a correct evolution of the differnt components of the free volume (plenum, gap, …) and of the fission gas behavior. On the other hand, the evaluation of the quantity of fuel which could be fractured in fine pieces during the accident phase (i.e. at least the fuel zone which are restructured (HBS) or in restructuration) is also important. This description is done by two fission gas models CARACAS [7] or MARGARET [8] (more phenomenological). Both models describe the fission gas production, release and swelling and also the HBS formation. In the grain, dissolved gas, nanometric bubbles, precipitated bubbles (up to 0.1µm) are considered; the gas atom diffusion and bubbles diffusion are modelled. Trapping of gas atom by bubbles is taken into account. On the grain boundary gas is considered to be precipitated into bubbles and the release could happen by inter-connection of bubbles or fracture by overpressure on a weakened grain boundary. In each point of the pellet, the fraction of HBS is calculated by the balance between defaults accumulation due to fission spike and thermal recovery. These entire phenomena are very sensitive to fuel temperature, fission rate and local stresses.

3.2. Cladding Behaviour Modelling

The EDGAR model [1] describes the viscoplastic behaviour of a zirconium alloy tube under a pressure imposed loading and at high temperature (more than 950 K). This model also

gives the phase fractions evolution (2 phases are considered: alpha and beta and a mixed transition domain, alpha + beta).

This model was classically identified as a relationship between the internal pressure and the diameter. Finite strains were taken into account by computing the Cauchy stress. Roughly, for a pressurised tube in 1D, the tangential stress can be approximated by the formulation Pd/2e, where P, d and e are respectively the pressure applied on the cladding, the current diameter and the thickness of the tube.

For its introduction into ALCYONE, the EDGAR model has been turned into a constitutive law suitable for a mechanical analysis: basically, the EDGAR model appears as a modified Norton viscoplastic behaviour with the total strain being split into an elastic and a viscoplastic part. The viscoplastic strain is then traceless which, for small strains, guarantees that the cladding deformation is isochoric (no volume change), as it is classically assumed, based on experimental facts, in metal plasticity and viscoplasticty.

Using the EDGAR model established as a point model in a Finite Element 3D calculation tool like ALCYONE requests some adaptations. A particular care had to be taken to find a proper finite strain framework. We thus modified both our mechanical analysis and our definition of the mechanical constitutive equations [2]. The mechanical analysis is still performed on the undeformed geometry. The stress tensor is then the first Piola-Kirchhoff stress. The geometrical non-linearity of the mechanical problems is then held by the boundary conditions which can be easily changed in 1D analysis.

The mechanical behaviour is expressed in the logarithmic strain framework proposed by Miehe et al [3]. This lagrangian framework (all tensors are defined in the reference configuration) has very appealing features:

— It is based on energetic considerations. It introduces a new stress measure which is the dual of the logarithmic strain. Mechanical constitutive equations are automatically objective and do not suffer from discrepancies arising in classical hypoelastic approaches;
— The dual stress is the Kirchhoff stress in 1D. As the viscoplastic flow of zirconium alloys is supposed isochoric, the Kirchhoff stress is very close to the Cauchy stress, which is consistent with the EDGAR model identification;
— The classical partition of strain still holds. This feature comes from the fact that the trace of strain is directly linked to the change of volume: a traceless flow is isochoric. This means that the constitutive equations can be written as "in small strain". Introduction in 1D analysis is straight-forward and only consists in a pre- and post-processing of the mechanical behaviour integration subroutine.

Those points are discussed in details in a dedicated paper [2]. Once those changes were made, the EDGAR experiments were simulated using ALCYONE to validate this implementation.

3.3. Stress distribution in the pellet

The 1D code generally considers that for a solid pellet, the radial displacement of the central point is not authorised. This hypothesis has no impact in hot conditions during base irradiation or power ramp regime. Indeed, the radial stress is in a compressive state in the whole pellet, due to the thermal gradient and that is all the more true when the fuel to cladding gap is closed.

In case of LOCA, the thermal gradient is significantly lower, and the gap is calculated open (even if at very high burn up, the gap, strictly speaking, is closed between cladding and fuel due to internal zirconia layer, but a reopening occurs inside the pellet at about hundred microns from the edge). Then the calculated radial stress tends to be in a tensile state in the central part of the pellet if the hypothesis of the central node blockage is done. This induces

wrong input data for fission gas behaviour modelling. We have then decided to consider that the central point of the pellet is able to move radially.

Figure 2 presents stress distribution in the pellet when the gap is open in the cold conditions at the end of a base irradiation with the two hypotheses. During a LOCA, stresses distribution is likely to be in the same shape, as the thermal gradient remains low in the fuel pellet. Nevertheless, the actual value of the stress level depends on the fission gas swelling contribution and then on the base irradiation power history.

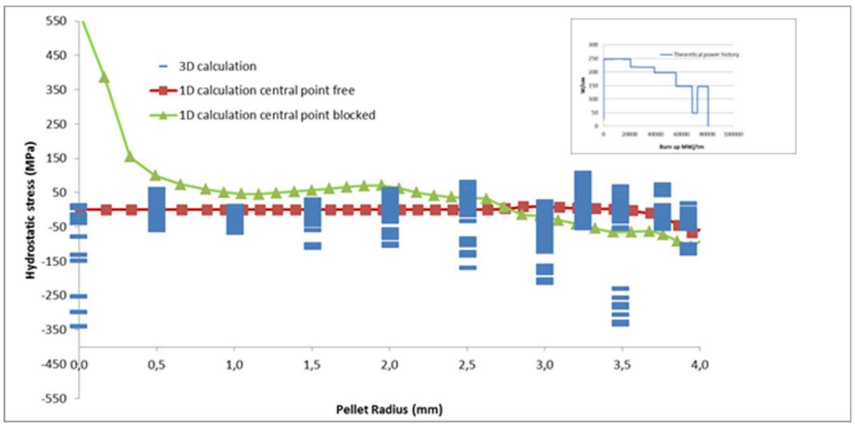

FIG. 2. Hydrostatic stresses distribution in the pellet at room temperature.

3.4. Fission gas release

The fission gas model used in the ALCYONE calculations is CARACAS [7], which considers the following fission gas populations:

- Nanometric intragranular bubbles;
- Precipitated intragranular bubbles;
- Intergranular bubbles;
- Rim structure formation and rim bubbles evolution.

This model is validated in base irradiation conditions and power ramp conditions for UO_2 up to 70 GWd/tM.

During the first part of the LOCA transient, fuel temperature remains low enough to affect only the intergranular gas. A specific criterion for intergranular fracturation initiation has been developed. It is based on the evaluation of stress applied to grain boundary resulting from macroscopic hydrostatic stress and from stress induced by over-pressurized intergranular bubbles (tensile stress). If the tensile stress on the grain boundary induced by intergranular bubbles is higher than the grain boundary yield stress, partial or total fracturation of the grain boundaries is supposed to be possible. This allows fission gas release.

We also assume that grain boundary yield stress is reduced by irradiation (fission gas atoms dissolved on the grain boundary).

This criterion depends on first order on the amount of fission gas precipitated into bubbles after base irradiation (thus before transient), and so on the initial state of the fuel and the distribution of fission gas between the different populations.

It has to be mentioned that this model has been developed to make most of the intergranular gas available for release in transient conditions. Even if the model results in a fraction of opened grain boundaries, it must not be used for now to evaluate a fuel fragment average size. The total fraction of opened grain boundaries being between 10 and 50%, it would result in very fine fragmentation (a few grains) which is not always observed, and particularly has not been observed in the IFA-650.10 experiment.

4. MODELLED CASES AND MODELLING RESULTS

4.1. IFA-650.10

The father rod is a UO_2 rod with a SRA Zircaloy-4 cladding, irradiated during five annual cycle up to 57 MWd/kgU (rod average) under moderate power conditions (average liner heat rate used without taken into account the gamma power generated in the coolant: 175 W/cm, 219 W/cm, 214 W/cm,184 W/cm,145 W/cm). At the end of irradiation on the tested part of the rod, the corrosion layer thickness calculated is around 30 to 40 µm and the calculated hydrogen content around 250 ppm. The fission gas release calculated for the whole rod is 3.8% and the distribution of gas on the pellet radius is presented in Fig. 3. The calculated rim extension is about 200 µm and a significant intragranular precipitation is calculated in the central part of the pellet.

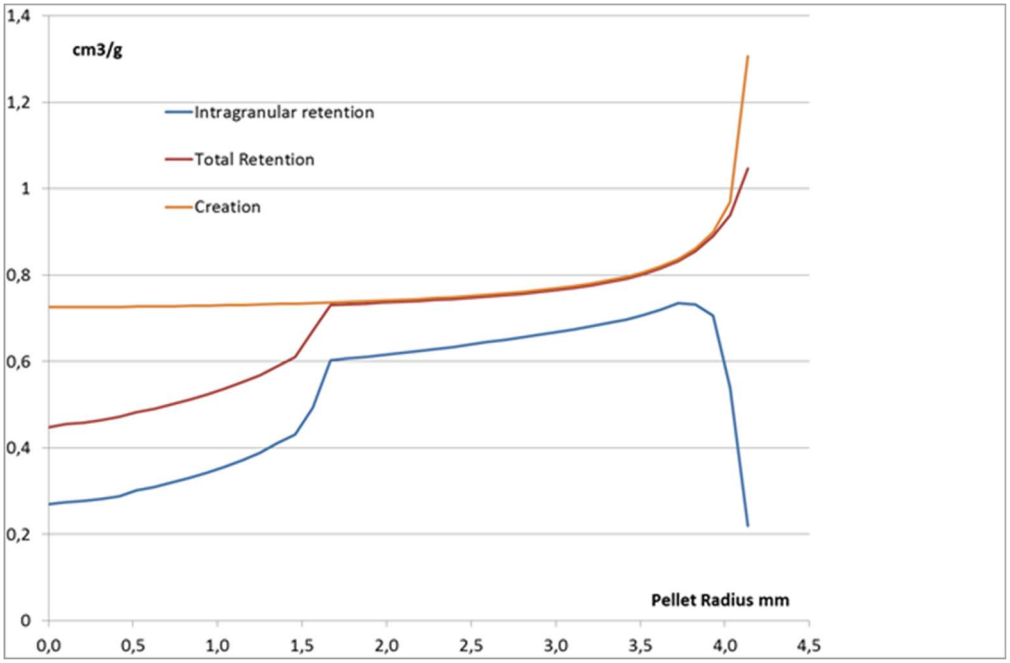

FIG. 3. Fission gas distribution at the end of the base irradiation (IFA650.10).

This experiment has been performed in the IFA650 device, the HWR report in [12] presents the experiment:

The test was carried out using low fission power 14 W/cm (rod average, this value was provided by the Halden Project). The heater surrounding the rod was operating at 12 W/cm it was used for simulating the heat from adjacent rods.

The fill gas pressure was 40 bar (RT). The target peak cladding temperature was 850 °C, and the hold time was ~169 s (from burst to scram). Rod overpressure at hot temperature was about 70 bar. Cladding failure occurred ~249 s after blow-down at ~755°C. The average cladding temperature increase rate during the heat-up was around 5°C/s. The results from the in-pile measurements and the gamma scanning indicate modest deformations and negligible fuel relocation.

The whole instrumentation of the experiment gives a large amount of valuable data which are used to build the input data for calculation. Nevertheless, it remains difficult to evaluate the temperature axial profile of the cladding, even with the use of fine thermohydraulic modelling. The following assumptions have been made:

— The coolant temperature is close to the saturation temperature;
— Plenum temperature is fixed from measurement (TCP);

— Initial free volume is 17 cm^3 and initial pressure is imposed at 40 bars.

About the cladding outer temperature profile during the experiment, two different sets of assumptions have been made:

(a) The temperature difference between the coolant and the cladding is proportional to the fissile power. Then, available measurements at two levels of the fissile rod (TCC1 (95 mm/bfc), TCC2 & TCC3 (360 mm/bfc)) allow the cladding temperature calculation for the whole rod and it is exact at the two TC levels. This set is mentioned as 'ALCYONE boundary conditions' in the following.
(b) The cladding temperature profile provided by SOCRAT calculations.

The calculation of the transient is done with the hypothesis of free communication for the gases between plenum and fissile part of the rod, the gap is calculated open during all the transient phase (even if the outer part of the pellet is likely to be stuck on the cladding and the "gap" opened only in the internal part of the pellet), and then instantaneous equilibrium of pressure in the whole rod is assumed.

The evolution of Zircaloy-4 properties with temperature is taken into account. In the first part of the work which consists in deterministic simulations of the IFA650.10 experiment with different sets of boundary conditions (cf. 5.1), the considered creep behaviour and phase transformation laws are the ones of the 'fresh' material. For the determination of the uniform strain limit at failure we consider the value recommended for irradiated material.

But in the second part of the work (uncertainty quantification and sensitivity analysis, cf. 6), the law considered for the cladding is the law of irradiated material, because uncertainty on hydrogen pickup fraction during steady-state irradiation had to be taken into account.

The calculation is done considering transient condition to evaluate the thermal exchanges. Cladding burst is not calculated directly by ALCYONE but determined by post-processing the calculated internal pressure, cladding radius and cladding temperature. The possibility of the grain boundary fracturation due to the gas bubble action is tested.

4.2. Studsvik 192 LOCA test

The father rod is a UO_2 rod with a ZIRLO cladding, irradiated up to 71 MWd/kgU (rod average) at high linear heat rate [13]. As the ZIRLO behavior law is not available in ALCYONE, the 'fresh' Zry-4 law is considered for the cladding.

The total fission gas release measured for this rod is about 10%, and the calculation with ALCYONE results in 6.4%. The calculated high burn-up structure extension is at least of 500 μm because of the high average burnup of the whole rod.

As the thermal loading of this rod is quite important (high average linear heat rate), the zone where Intragranular bubbles are precipitated extends to 2.5mm from the centre of the pellet. This is larger than what is calculated for the father rod of IFA650.10 experiment.

Same as for IFA650.10 experiment, the outer cladding axial temperature profile is imposed (given in the data sheet) in the data file. So is the initial inner pressure in the rodlet.

The plenum temperature is imposed during the experiment, and it is assumed that all the different components of the free volume of the rodlet are connected (plenum, gap, open porosity…) so that the pressure in the rod is uniform during all the experiment.

5. RESULTS AND DISCUSSION

5.1. IFA650.10

Figure 4 and Fig. 5 present the evolution of axial cladding elongation and pressure. Up to burst time, the agreement between the experiment results and calculation is rather good, but both boundary conditions sets delay a little the burst time compared to the experiment. This result validates the hypothesis of perfect communication of the gases between the plenum and the free volumes of the rod for this case (fast plenum depressurization).

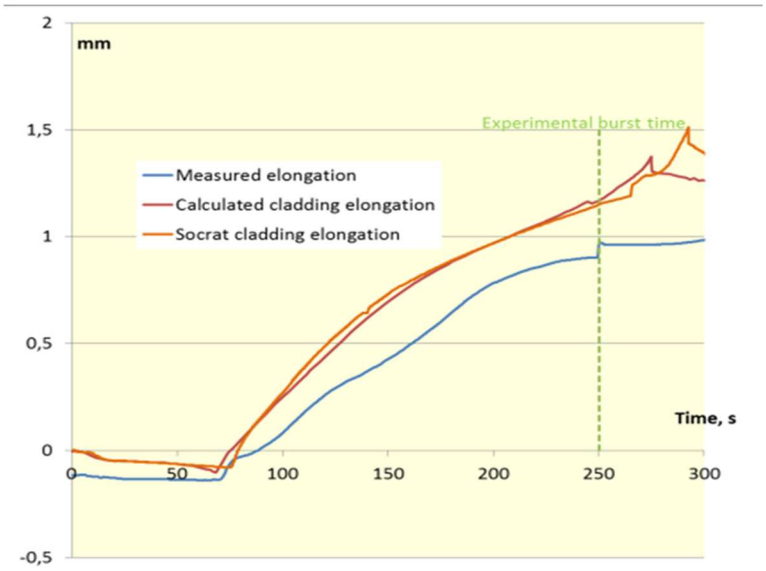

FIG. 4. Cladding elongation evolution.

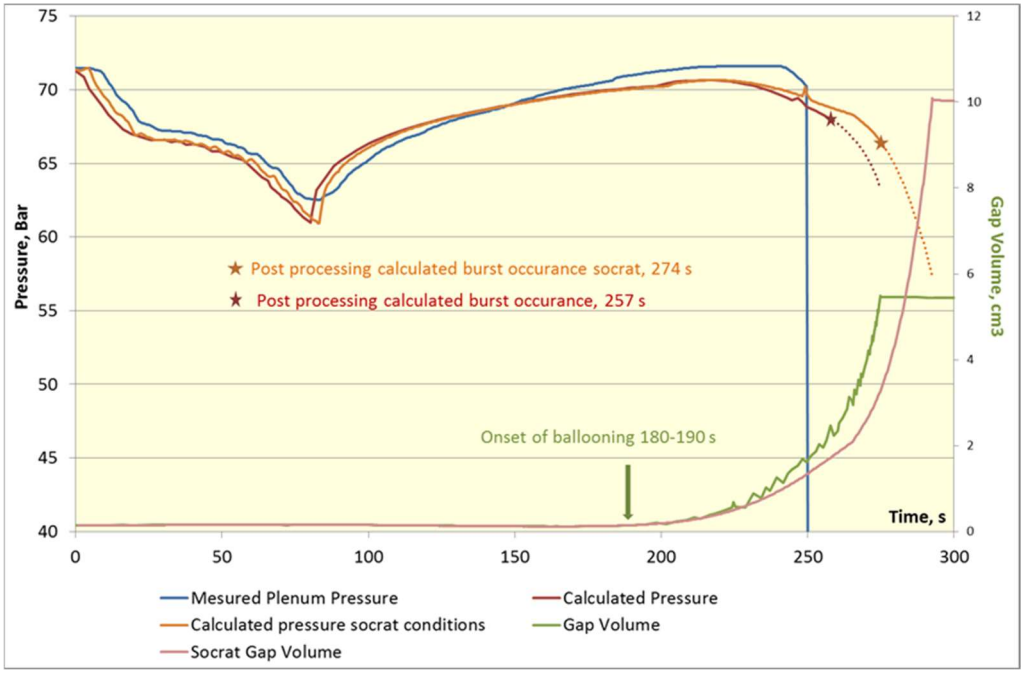

FIG. 5. Rod pressure evolution.

Figure 6 presents the cladding diameter calculated at burst time, two times are considered: the experimental burst time and the calculated one. It appears that the tendency is correct (calculated diameter is slightly underestimated compared to the two measured diameters). With

the SOCRAT thermal-hydraulic boundary conditions, the rod diameter is underestimated at experimental burst time. Also a little depletion of the rod profile is calculated at 2502 mm, and this result has to be related to the provided boundary conditions where this little depletion exists.

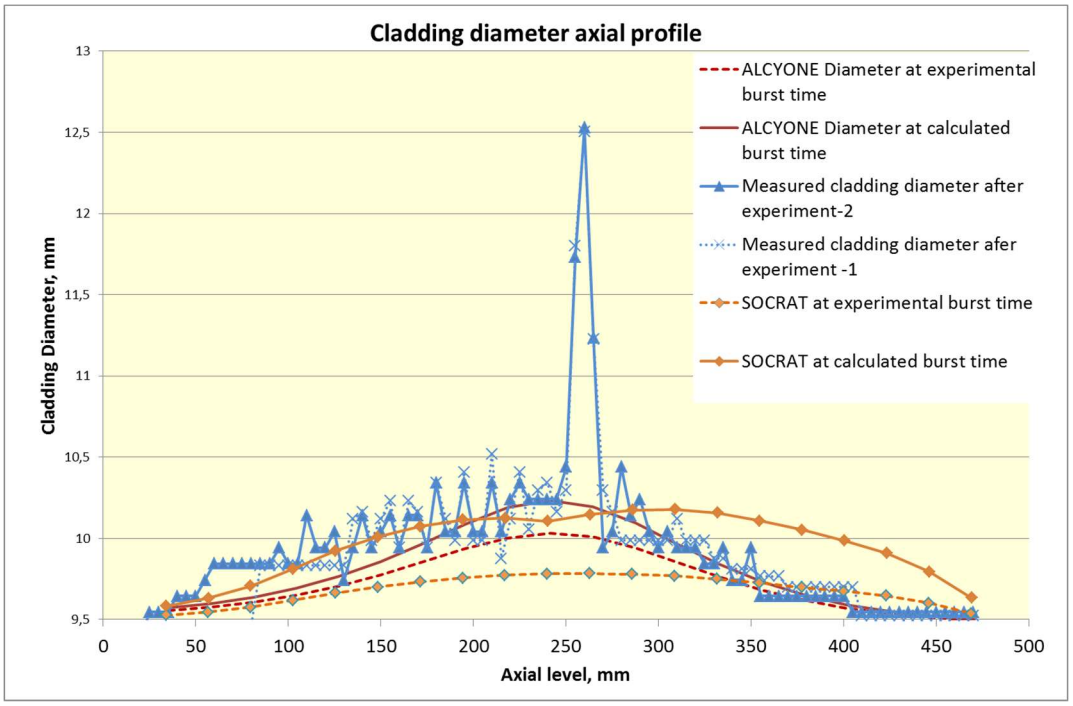

FIG. 6. Cladding diameter at burst time.

Fuel fragmentation due to the over-pressurized intergranular bubbles occurs in the simulation in the HBS zones (outer parts of the pellet) and in some central parts. Fuel fragmentation also occurs after the burst of the cladding which leads to a fast decrease of the inner pressure of the rod.

The amount of gas released during the test is about 8 cm^3, and it has a negligible effect on the evolution of the pressure during the test.

The parameters of the fragmentation model still have to be calibrated, to better assess the quantification of fuel fragmentation after burst. Results of this fragmentation model will provide inputs for a proper fuel fragment relocation model.

5.2. Studsvik 192 loca test

Figure 7 presents the calculated evolution of the pressure in the rodlet and the cladding temperature evolution during the test. The calculated time of burst is a little bit delayed compared to the experiment (about 20 s later). In the calculation, burst occurs for a cladding temperature higher of 100°C than the temperature at experimental burst. This can be explained by the fact that the real cladding of the experiment is irradiated ZIRLO, whereas we use the mechanical behavior law of the fresh Zry-4.

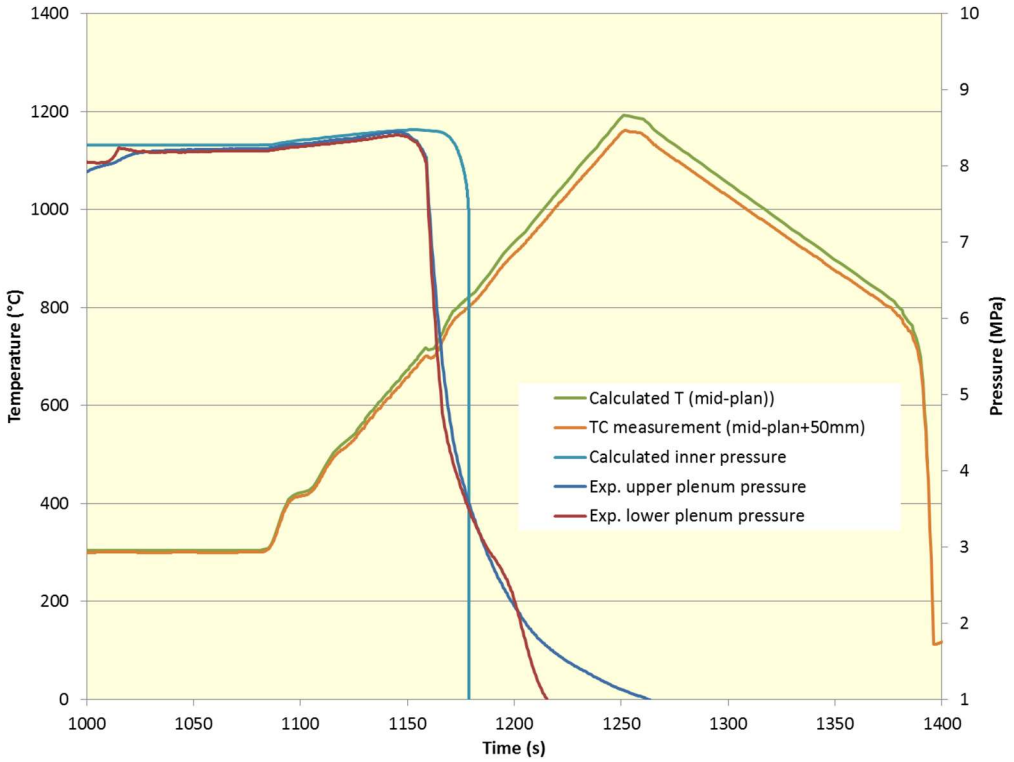

FIG. 7. Rod pressure evolution (Studsvik 192 test).

But the cladding profile calculated just before burst is in a good agreement with the measured cladding profiles after the test (Fig. 8).

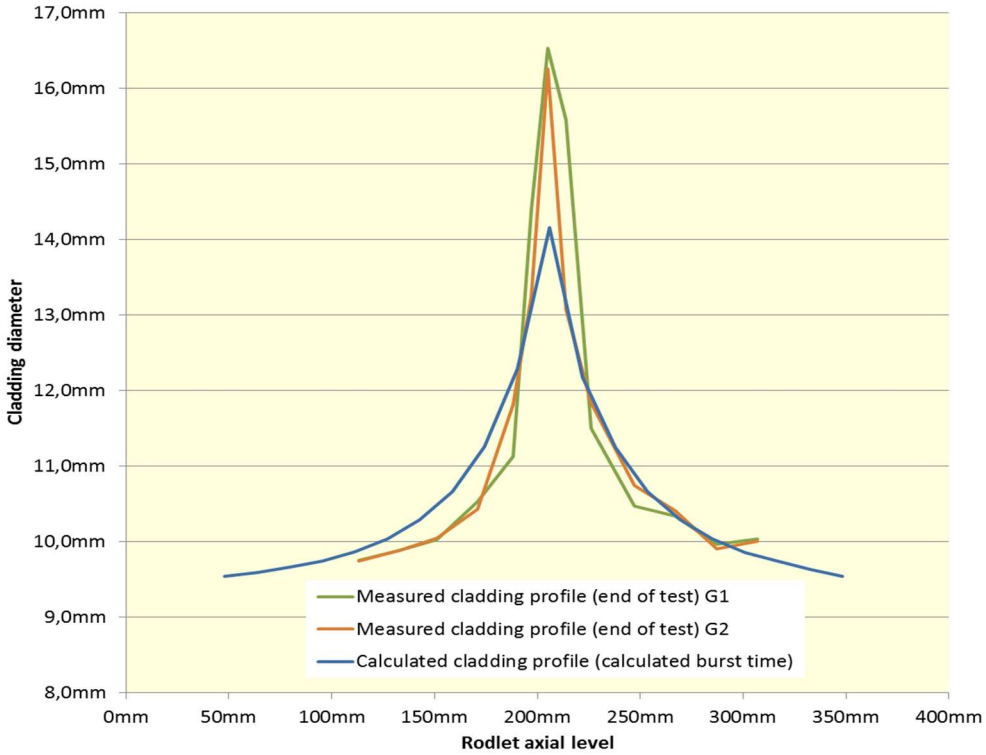

FIG. 8. Cladding profile after test (Studsvik 192 test).

Fuel fragmentation before burst occurs only in high burnup structure zones (edge of the pellet). But after burst, because of the fast decrease of the pressure in the rod, intergranular

fragmentation occurs after burst in the simulation in HBS zones and central zones of the pellet as shown on Fig. 9.

The fragmentation criterion is based on the calculation of the stress applied on the grain boundary due to the overpressurized intergranular bubbles. So it is closely related to the amount of gas on the grain boundary (in bubbles in the CARACAS model) at the end of the steady-state irradiation and to the fraction of bubbles interconnected to the free volume of the rod.

But as the fission gas model is based on the description of an average grain of the microstructure with spherical shape, the fractured grain boundary ratio cannot be used to quantify a fuel fragment size. In its current development state, the "fragmentation model" can only be used as a fission gas release mechanism.

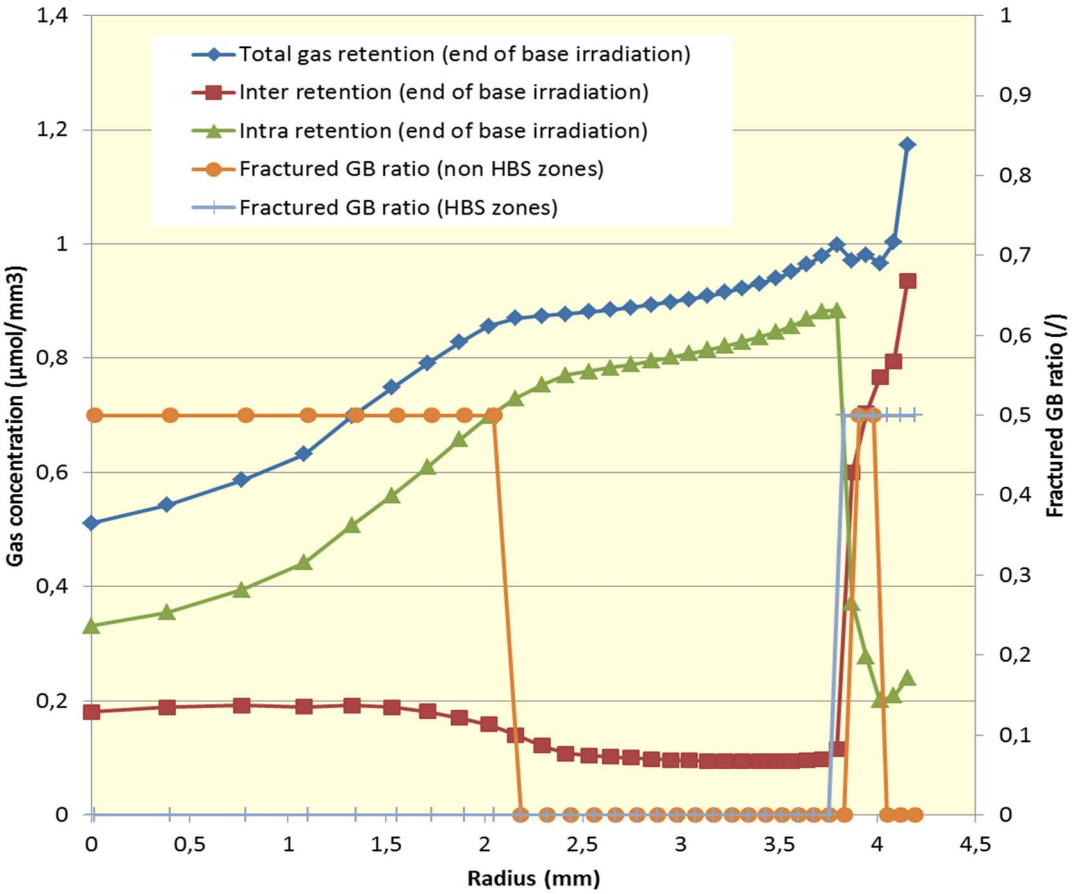

FIG. 9. Fuel fragmentation and fission gas distribution (Studsvik 192 test).

6. UNCERTAINTY QUANTIFICATION AND SENSITIVITY ANALYSIS OF CASE IFA650.10

In the specification document for the UQ/SA of IFA650.10 experiment, the uncertainty on hydrogen pickup fraction during steady-state irradiation of the rod has to be taken into account. So, instead of considering a behaviour law of "fresh" Zry-4, we consider in this part of the work a behaviour law of irradiated Zry-4 cladding. The available law corresponds to a cladding with 600 ppm hydrogen, whereas the cladding of IFA650.10 rodlet contains around 300 ppm hydrogen. Nevertheless, our formulation which describes the phase transformation is a continuous function of the hydrogen content.

The reference calculation with these new assumptions is a bit different from the calculation results obtained in the first part with "fresh" Zry-4 cladding properties (Fig. 10). The cladding diameter at burst time is higher than in the first set of simulation because the creep

rate of irradiated cladding is higher than for fresh Zry-4. It is much higher than the experiment probably because the behaviour law used is for Zry-4 with 600ppm hydrogen whereas the cladding of IFA650.10 experiment only contains 300 wppm hydrogen. So the creep rate is probably overestimated.

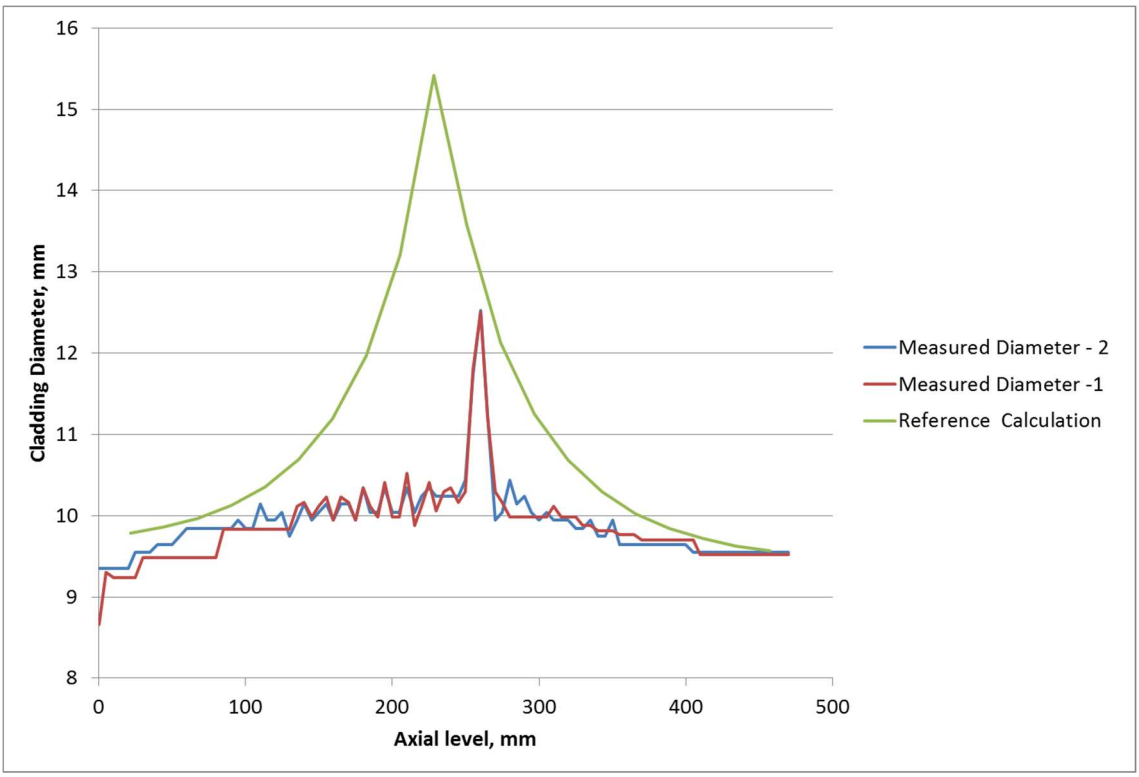

FIG. 10. Cladding diameter at burst time with irradiated Zry-4 cladding properties.

UQ/SA has been performed using the URANIE software [14] developed by CEA/DEN. 200 simulations have been performed on a simple random sampling design of experiment generated following the specifications of the project [15].

The following input parameters and data have not been taken into account in the uncertainty analysis:

- Test rod power profile;
- Clad to coolant heat transfer coefficient (cladding temperature imposed);
- Fuel solid swelling model;
- Fuel gaseous swelling model;
- Cladding oxidation model at high temperature (model not available in ALCYONE);
- Thermal conductivity of the oxide layer (oxide layer conductivity not taken into account in ALCYONE);
- Fission gas release;
- Gap gas conductivity (parameter not accessible in input file);
- Fuel radial relocation (not relevant);
- Fuel fragment packing (not relevant);
- Cladding strain threshold for fuel mobility (not relevant);
- Cladding Meyer hardness (not relevant).

At the moment, ALCYONE is only able to model the behaviour of the rod until the burst of the cladding. After that, models of fuel fragmentation, fuel relocation, gas release are not

available. So all the parameters regarding the behaviour of the rod after burst are not taken into account.

We also chose deliberately not to consider fission gas release model and fuel swelling models in the uncertainty quantification problem, because they are not independent from the uncertainty on material properties.

To be more precise, fission gas release model has been calibrated using a deterministic function for thermal conductivity. If the considered thermal conductivity had been different (+5% for example), the fission gas release model would have been calibrated differently on the same experimental database. So FGR model and thermal conductivity are correlated in terms of random variables.

Figure 10 shows for each of the 200 simulations, the calculated rod diameter as a function of the calculated Burst Time. There is apparently no correlation between those two quantities. The range for calculated burst time is between 320 and 345 s, and the range for the maximum rod diameter is between 14 and 17 mm.

In Fig. 11, the evolution of the calculated inner pressure in the rod during the test is plotted for all the 200 simulations. Until the cladding burst, the standard deviation of the pressure stays constant. It increases around the burst, due to the scattering of the balloon volume, represented by the maximum rod diameter (Fig. 12).

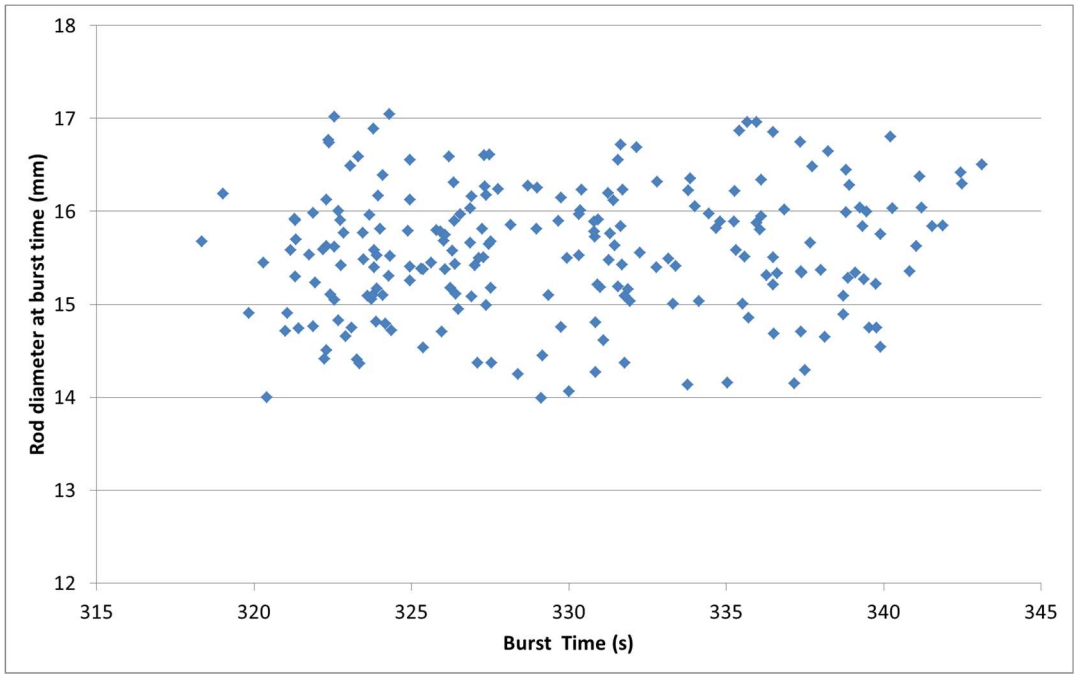

FIG. 11. Calculated rod diameter at Burst time.

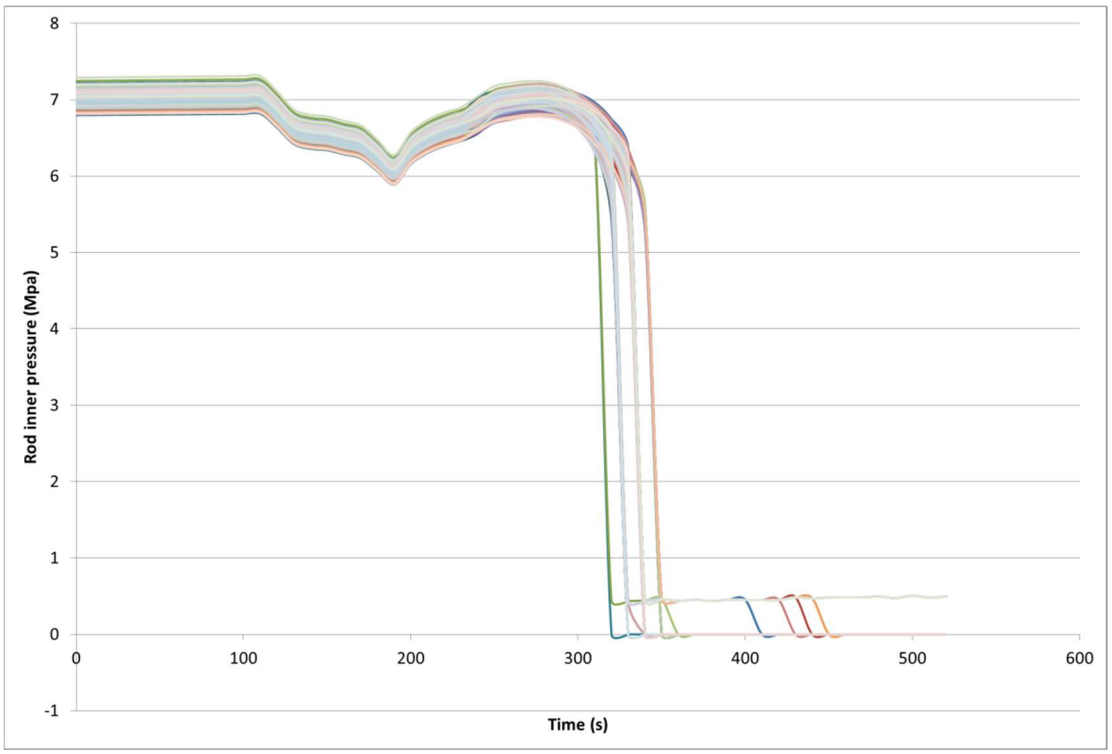

FIG. 12. Scattering of the evolution of the inner rod pressure during test.

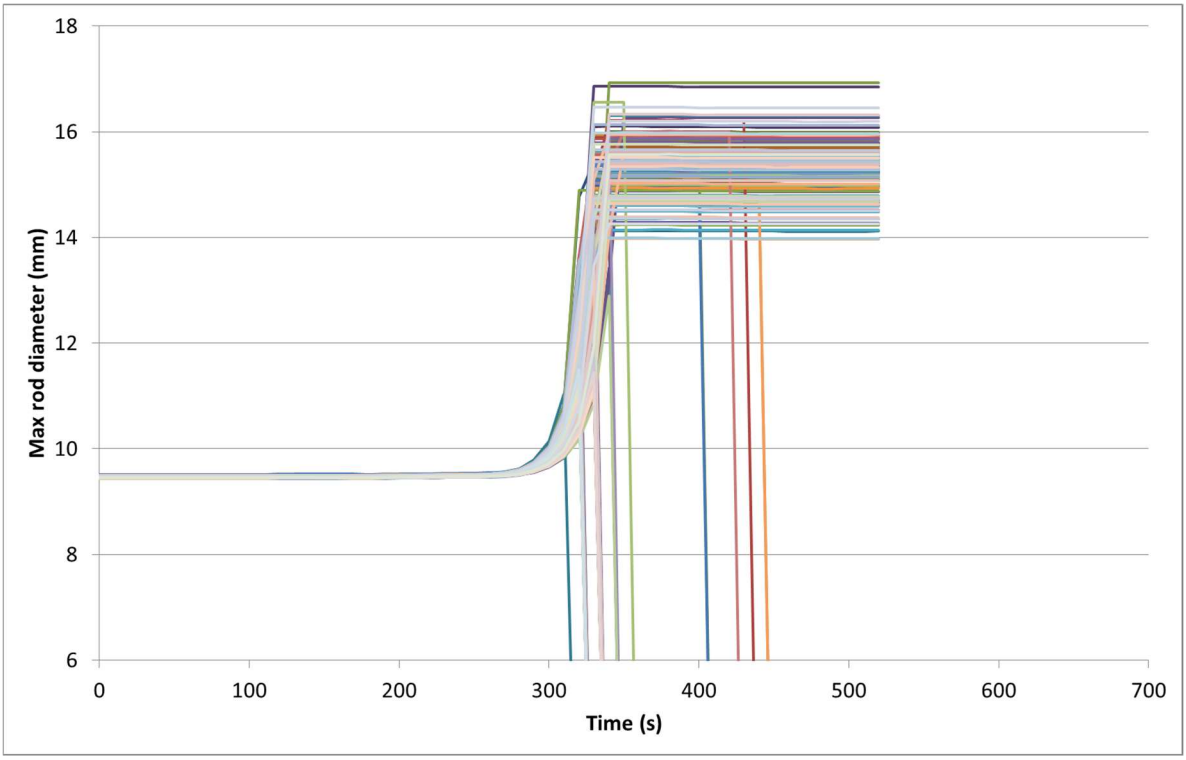

FIG. 13. Scattering of the evolution of the maximum rod diameter during test.

Once the uncertainty quantification is performed, it is important to know which inputs are responsible for this scattering of the outputs. As requested in the specification document, Partial Rank Correlation Coefficients are used as sensitivity indices. As ALCYONE is only qualified until the cladding burst, we only performed sensitivity analysis until about 310 s.

Most of the requested outputs are very sensitive to the uncertainty on cladding outer temperature, which is what was expected from the first set of calculations.

In this report, it is interesting to add some results about burst time and maximum cladding strain at burst. Burst time is very sensitive to the uncertainty on cladding outer temperature (Fig. 13) and maximum cladding deformation is sensitivity practically only to the cladding burst criteria uncertainty (Fig. 14).

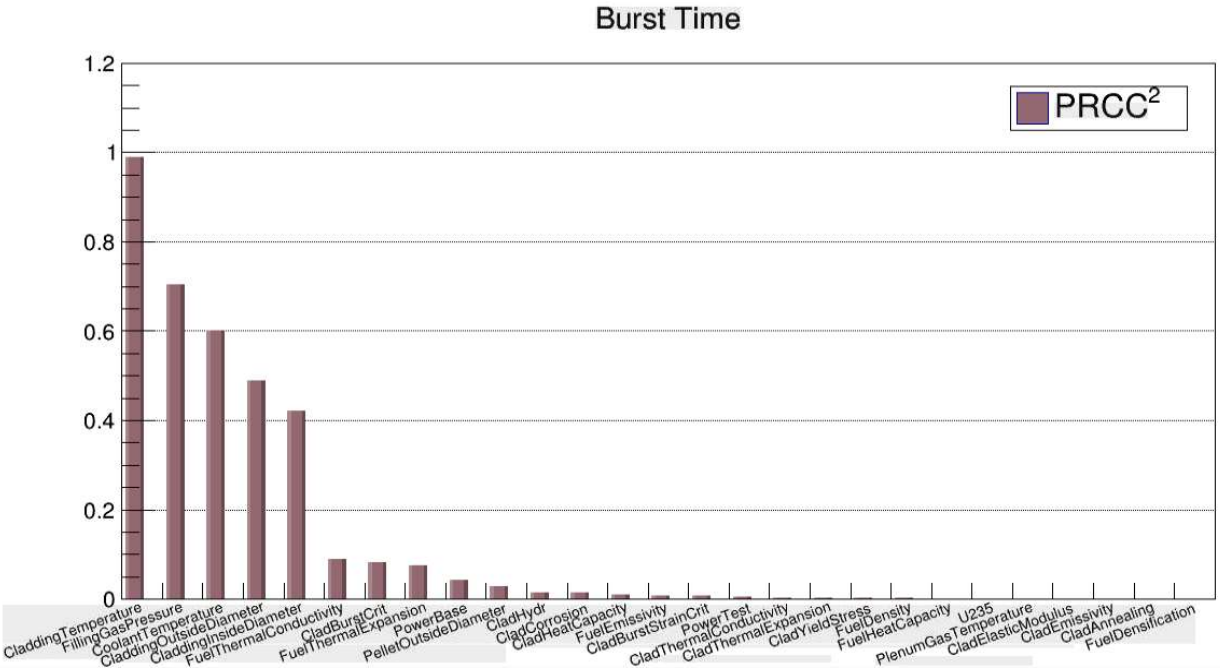

FIG. 14. Sensitivity analysis of Burst Time.

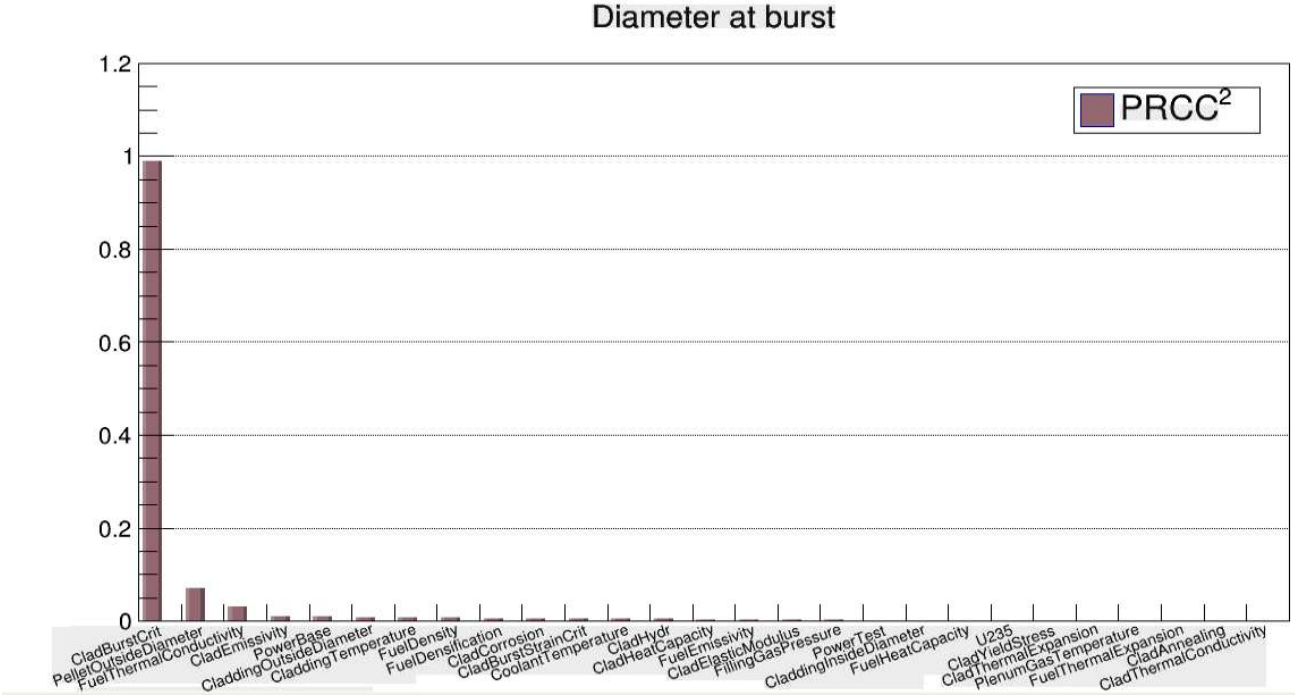

FIG. 15. Sensitivity analysis of Diameter at burst.

REFERENCES

[1] MARELLE, V. et al., Thermo-mechanical modeling of PWR fuel with ALCYONE. in proceedings of Top Fuel 2011, Chengdu, China, (2011).

[2] MARELLE, V. et al., New developments in ALCYONE 2.0 fuel performance code. in proceedings of Top Fuel Boise Idaho USA, (2016).
[3] STRUZIK, C. et al., Validation of fuel performance CEA code ALCYONE, scheme 1D, on extensive data base. in proceedings of Top Fuel 2012, Manchester, United Kingdom, (2012).
[4] SERCOMBE, J. et al., Stress concentration during pellet cladding interaction: Comparison of closed-form solutions with 2D(r,theta) finite element simulations. Nucl. Eng. Des. 260, 175 (2013).
[5] MICHEL, B. et al., 3D fuel cracking modelling in pellet cladding mechanical interaction. Engineering Fracture Mechanics 75, 3581 (2008).
[6] MARELLE, V., Validation of PLEIADES/ALCYONE 2.0 fuel performance code. WRFPM2017, Jeju Island Corea, (2017).
[7] JOMARD, G. et al., CARACAS: an industrial model for the description of fission gas behavior in LWR-UO2 fuel. in Proceedings WRFPM 2014, Sendaï (Japan), (2014).
[8] NOIROT, L. et al., MARGARET: A comprehensive code for the description of fission gas behavior. Nucl. Eng. and Des. Vol. 241, (2011).
[9] FORGERON, T. et al., "Experiment and modeling of advanced fuel rod cladding behavior under LOCA conditions: Alpha-beta phase transformation kinetics and EDGAR methodology". Zirconium in the Nuclear Industry: Twelfth International Symposium. ASTM International (2000).
[10] HELFER, T. Extension of monodimensional fuel performance codes to finite strain analysis using a Lagrangian logarithmic strain framework. Nucl. Eng. and Des. Vol. 288 (2015) 75–81
[11] MIEHE, C. APEL, N. and LAMBRECHT, M., "Anisotropic additive plasticity in the logarithmic strain space: modular kinematic formulation and implementation based on incremental minimization principles for standard materials". Comput. Method. Appl. M., Vol. 191, (2002) 47–48.
[12] LAVOIL, A., HWR 974, LOCA Testing experiment at Halden. The tenth experiment IFA650-10.
[13] FLANAGAN, M., ASKJELJUUNG, P. , US NRC NUREG 2160, August 2013, Post test examination, Results from integral, High burn up, fueled LOCA tests at Studsvik Nuclear Laboratory (2013).
[14] GAUDIER, F., "URANIE: The CEA/DEN Uncertainty and Sensitivity platform". Procedia Social and Behavioral Sciences 2 (2010) 7660–7661.
[15] ZHANG, J., "IAEA FUMAC CRP – Specifications for Uncertainty Analysis on Modelling of the Halden LOCA Test IFA-650.10".

RESULTS OF THE CORA-15 BUNDLE TEST WITH PRESSURIZED RODS

J. STUCKERT
Karlsruhe Institute of Technology (KIT)
Hermann-von-Helmholtz-Platz 1, 76344 Eggenstein-Leopoldshafen, Germany
e-mail: juri.stuckert@kit.edu

Abstract

In the CORA-15 bundle test with electrical heating the fuel rod simulators (heated and unheated) were pressurized to 6.0 MPa at temperature of about 300 °C. During the transient, all rods underwent ballooning and burst. Burst occurred within 150 s in the temperature bandwidth between about 700 and 800 °C. The mostly probable burst elevation is the elevation 750 mm. During the temperature escalation above 1800 °C, Zr melt formed in the gap between ZrO_2 and UO_2 was relocated partially inside the gap to lower bundle elevations and partially penetrated through the failed ZrO_2 layer into the space between rods. The resulting melt of the fuel rod interaction, containing mainly U, Zr, O is solidified between 400 and 550 mm. The maximum bundle blockage (almost 100%) was observed at the top of the Inconel grid spacer (500 mm). The maximum hydrogen release rate of 210 mg/s was measured on the end of the transient (4800 s). The total hydrogen release was 145 ± 15 g.

1. INTRODUCTION

As a further step after the small scale single rod and 3×3 rod bundle tests in the NIELS facility [1], partially also engaged by the TMI-2 accident, the CORA facility was designed and erected in the FR2 reactor containment. It was intended to study the main processes occurring during a severe fuel damage accident in larger fuel rod bundles with prototypic materials so that the heterogeneous structure of a water reactor can be simulated. Due to its size, CORA should allow experiments under more realistic conditions than in smaller test facilities (single rods).

An overview of the tests is given in Table 1. Two reflood tests were performed for PWR configuration, CORA-12 [2] and CORA-13 [3] and one for BWR environment CORA-17 [4]. CORA tests, terminated by flooding with water (quenching) from the bottom, show an unexpected increase of the hydrogen source term. A detailed description of a typical CORA experiment can be found in Refs [5] and [6].

Sometimes, a more detailed knowledge of the degradation phase is necessary and for that purpose, the damage progression diagrams were developed [6, 7]. The damage progression started from the centre of the bundle, initiated by eutectic interactions at the Inconel spacer progressing downward until termination of the test at 4800 s. Rivulets and droplets can clearly be distinguished by observations through the specially installed quartz windows. With such an observation, processes releasing both types of melt can be identified as described in detail by Hering [6, 7].

TABLE 1. CORA TEST MATRIX

No	Date	Max clad T, °C	Absor-ber	Other test conditions	H_2 release, g	H_2O con-sumed,
2	Aug. 6,1987	2000	–	$U0_2$ refer. Inconel spacer	–	–
3	Dec. 3,1987	2400	–	$U0_2$ refer. high temperature	–	–
5	Feb. 26,1988	2000	AgInCd	PWR-absorber	–	–
12	June 9,1988	2000	AgInCd	Quenching	–	–
16	Nov. 14,1988	2000	B_4C	BWR-absorber	167	76
15	March 2, 1989	2000	AgInCd	Rods with internal pressure	180	27

TABLE 1. CORA TEST MATRIX

No	Date	Max clad T, °C	Absor-ber	Other test conditions	H_2 release, g	H_2O con-sumed,
17	June 29,1989	2000	BWR B_4C	Quenching	250 (126 quench)	14 (before reflood)
9	Nov. 9,1989	2000	AgInCd	10 bar system pressure	159	30
7	Feb. 22, 1990	2000	AgInCd	57-rod bundle, slow cooling	114	17
18	June 21, 1990	2000	B_4C	59-rod bundle, slow cooling	106	60
13	Nov. 15, 1990	2200	AgInCd	Quenching; OECD/ISP	210	19 (before reflood)
29	Apr. 11, 1991	2000	AgInCd	Pre-oxidized	225 (after pre-oxidation)	38
31	July 25, 1991	2000	B_4C	Slow initial heat-up (≈ 0.3 K/s)	205	21
30	Oct. 30, 1991	2000	AgInCd	Slow initial heat-up (≈ 0.2 K/s)	194	27
28	Feb. 25, 1992	2000	B_4C	Pre-oxidized	104 (after pre-oxidation)	79
10	July 16, 1992	2000	AgInCd	Cold lower end; 2 g/s steam	180	19
33	Oct. 1, 1992	2000	B_4C	Dry core conditions, no steam	84	
W1	Feb. 18, 1993	2000		WWER-test	96	23
W2	Apr. 21, 1993	2000	B_4C	WWER-test with absorber	75	

2. DESCRIPTION OF THE TEST FACILITY

In the axial cross section of Fig. 1 the main components of the CORA facility are shown schematically. The general scheme of the test section is given in Fig. 2. The test rods were arranged within the CORA-15 bundle as shown in the schematic cross section of Fig. 3, 16 of the 25 fuel rods were electrically heated by using tungsten pins as heater elements. The heated rods (fuel rod simulators) were filled with annular UO_2 pellets whereas the unheated rods contained full UO_2 pellets of the same outer diameter. Composition characteristics of the CORA-15 bundle are presented in Table 2.

Irrespective of the bundle configurations, the dimensions and materials for components outside the shroud insulation are the same for all bundle tests. The bundle is composed of unheated and electrically heated rods (simulators), and of absorber rods. The heated and unheated rods are mounted at the upper bundle flange and kept in place laterally by three grid spacers. To cool the copper electrodes water pools are used at both ends of the simulators. The quench cylinder (not used in CORA-15), filled with water for bundle flooding, is situated below the test section and can be raised over the bundle up to 1.0 m. To allow the quench cylinder lifting, the fluid has to enter the bundle from the side at the lower end of the heated zone (steam inlet).

The CORA shroud, a Zircaloy liner with about 20 mm thick ZrO_2 fibre insulation at the outside surrounds the bundle. This fibre insulation extends only up to 1.0 m, and above this elevation - in the upper electrode zone - the shroud is not insulated in order to prevent the electrodes made of molybdenum and copper from melting. For optical on-line inspection, the shroud has several observation holes that, however, allow the fluid to penetrate into the annular gap outside of the shroud. Separated by this annular gap, the high temperature shield (HTS) reduces radial heat losses. It is composed of several layers of fibre insulation, made of zirconia and alumina oxides. In the off-gas system above the test section, devices to condense steam and to measure the fluid components are located.

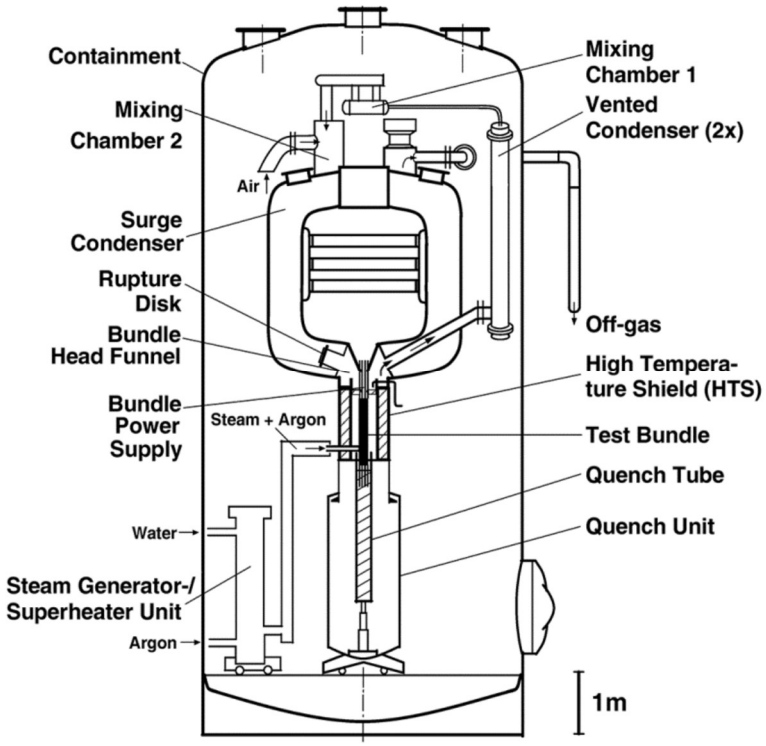

FIG. 1. Main components of the CORA facility.

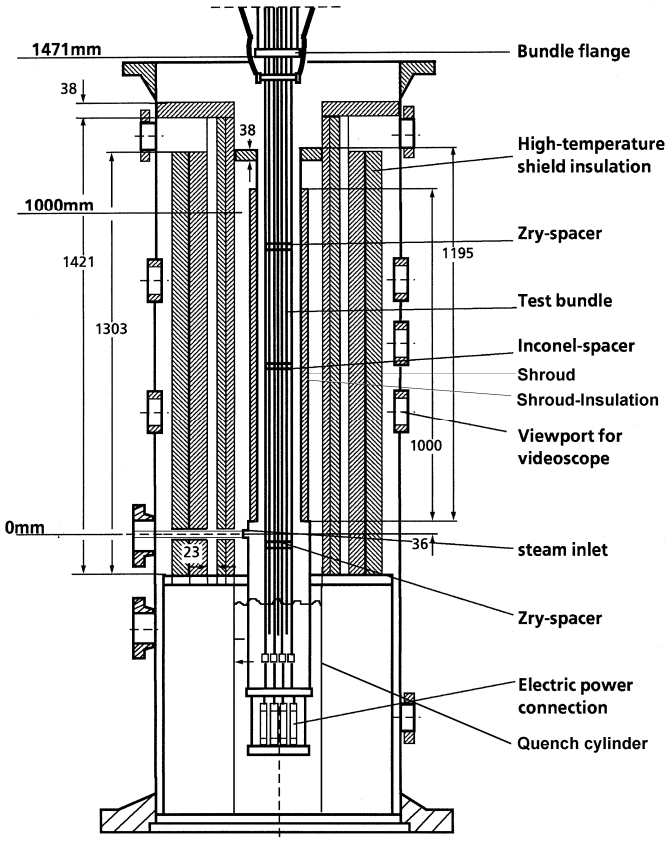

FIG. 2. CORA: Schematics of the test section. Apart from the test section, the Fig. includes the upper and lower fuel rod bundle connectors, the HTS, and the containment.

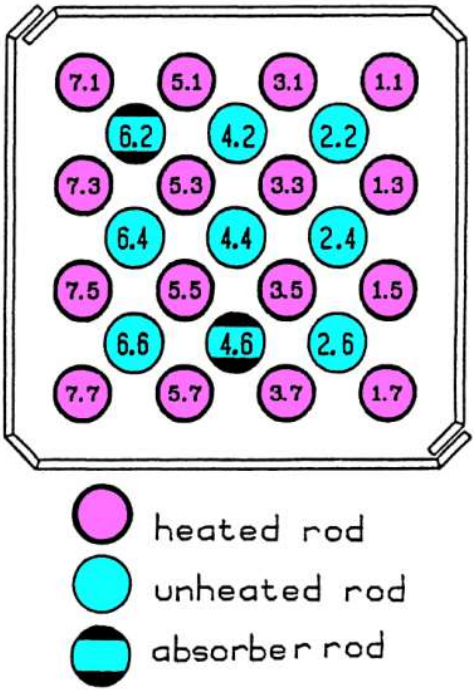

FIG. 3. Cross section of CORA-15 bundle, top view.

In the tests, the fuel rod bundle was heated electrically at initial heat-up of 0.2 to 1 K/s in a mixture of steam and argon flow. Maximum temperatures of about 2700 K were attained. At the end of a test, the hot fuel rod bundle was either slowly cooled down by argon (CORA-15), or it was rapidly cooled by raising the quench cylinder to simulate flooding the reactor core from the bottom.

The fuel rod bundle could be observed by on-line optical inspection with several video systems along the test section. The instrumentation also allowed tracking the hydrogen source term. Based on these data, detailed analyses on melt relocation and damage progression could be made. The facility is described in detail in [6] and [8]. Many details on the CORA-15 test could be found in [9]. In the meanwhile, the CORA facility has been dismantled due to safety requirements.

TABLE 2. DESIGN CHARACTERISTICS OF THE CORA-15 BUNDLE

Characteristics			Values
Bundle size			25 rods
Number of heated rods			16
Pitch			14.3 mm
Rod outside diameter			10.75 mm
Cladding material			Zircaloy-4
Cladding thickness			0.725 mm
Rod length			2175 mm
Heated length			1000 mm
Fuel pellets		Heated rods	UO_2 annular pellets
		Unheated rods	UO_2 full pellets
U^{235} enrichment			0.2 %
Pellet outer diameter (nominal)			9.1 mm
Heater material			Tungsten (W)
Heater diameter			6 mm
Grid spacer	Material		Zircaloy-4, Inconel 718
	Length		Zry 42 mm; Inconel 38 mm
	Location	Lower (Zry)	-5 mm
		Centre (Inc.)	+496 mm
		Top (Zry)	+880 mm
Shroud		material	Zircaloy-4
		wall thickness	1.2 mm
		outside dimensions	86 × 86 mm
		elevation	36 mm–1236 mm
		insulation material	ZrO_2 fibre
		insulation thickness	20 mm
Absorber rod		number of rods	2
		material and composition	80Ag, 15In, 5Cd (wt.%)
		cladding	stainless steel
		cladding OD	10.2 mm
		cladding ID	8.85 mm
		length	1489 mm
		elevation	-189 mm to +1300 mm
Absorber rod guide tube		material	Zircaloy-4
		OD	13.8 mm
		wall thickness of tube	0.8 mm

3. TEST BUNDLE INSTRUMENTATION

The test section was instrumented with thermocouples (W/Re and NiCr/Ni type thermocouples) and two-colour pyrometers to measure steam temperature, rod cladding temperature, shroud temperature, and insulation temperature. The high-temperature thermocouples were made of W5Re/W26Re wires, insulated with HfO_2 and sheathed in Ta/Zry duplex tubing. For the positions at lower temperatures K-type thermocouples with Inconel sheath were installed. The axial positions of the thermocouples can be taken from Fig. 4. For unheated rods, the thermocouples were installed in pellet centres; for heated rods - at the cladding outer surface.

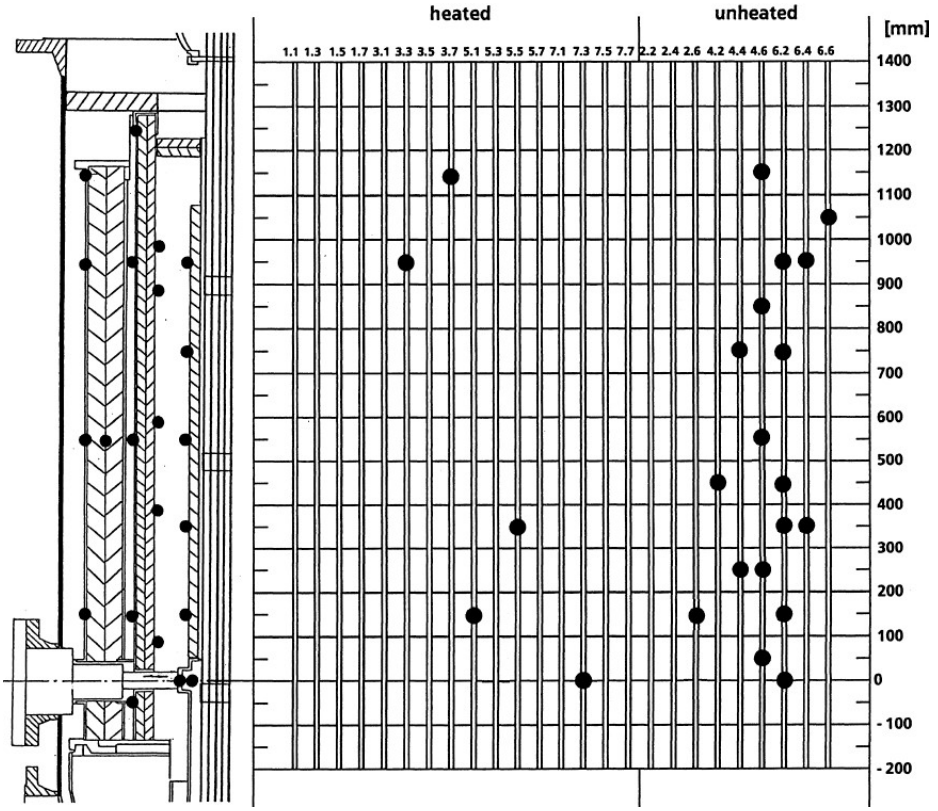

FIG. 4. CORA-15: positions of thermocouples.

The thermocouple measurement accuracies are:

— At bundle elevations between 0 and 500 mm (NiCr/Ni thermocouples): ± 2 K (up to 600 K), ± 0.005·T K (above 600 K);
— At bundle elevations between 600 and +1300 mm (W/Re thermocouples): ± 5 K (up to 700 K), ± 0.01·T K (above 700 K).

Six videoscopes were used in tests to observe the materials behaviour and the relocation of material during transient testing: at 30° (500 mm), 120° (400, 600, 800 mm), 120° (700 mm), 300° (900 mm).

The operational data, e.g. voltage, current, electric power, pressure, and temperatures were recorded by a data acquisition system as were the temperatures of the test section. The hydrogen produced during the test by the steam/Zr reaction is usually measured at two different positions:

— Immediately above the test section (1st mass spectrometer, data not included into the data set); and then

— In the mixing chamber after condenser (continuous on-line measurement with including of measurements results into the data set).

To dilute the gas taken at the location above the test section a dilution chamber with flow meters was installed. The off-gas mixtures which contain hydrogen among other gases are being transported to the spectrometers via capillary tubes. Two quadrupole mass spectrometers of the type Leybold PQ 100 were used. The ion currents representing the concentrations of the respective gases are determined. From these data the mass production rate of hydrogen as well as of the other gases is calculated with the ratio of the partial pressure of the particular gas and that one of argon (carrier gas) and multiplied by the argon flow rate through the test bundle.

4. TEST CONDUCT AND RESULTS OF ONLINE MEASUREMENTS

In the CORA experiments the test sequence can be distinguished in the following phases:

— Pre-heating: 0000–3000 s (argon only);
— Heat-up: 3000–3900 s (argon + steam);
— Escalation: 3900–4900 s (argon + steam);
— Cool-down: ≈ 4900 s (argon only).

During the preheating phase argon of about 500 °C enters the test bundle with a flow rate of 8 ± 0.2 g/s. Between 3000 s and 4700 s the electric power is increased from 6 to 28 kW to achieve the initial heat-up rate of 1 K/s. At 3300 s within the test a constant flow of superheated steam of 6 g/s is established in addition to the argon flow. In the escalation phase, i.e. starting from about 1100 °C the slow temperature rise is followed by a rapid increase caused by the increased electric power input and the additional energy from the exothermal zirconium - steam reaction. The contribution of this exothermal heat to the total energy input is generally between 30 and 40% for different CORA bundle tests. The CORA-15 test was terminated by power reduction (slow cooldown without quenching).

The power input history for the CORA-15 test is provided together with the coolant data as argon flow, steam flow (provided as mass flow of the injected water into the evaporator), and system pressure is depicted in Fig. 5. Readings of thermocouples at different elevations during transient are presented in Fig. 6.

In CORA-15 the fuel rod simulators (heated and unheated) were pressurized to 6.0 MPa before electrical power switch on. All rods underwent ballooning and burst during the subsequent transient (Fig. 7). The ballooning duration started at about 650 °C and lasted about 100 s. The sequence of the burst for the individual rods is presented in Table 3. Burst occurred within 150 s (from 3500 to 3650 s) in the temperature bandwidth between about 700 to 800 °C. These temperatures were registered between elevations 350 and 950 mm. The hottest elevation during the burst time period was the elevation 750 mm. It could be suggested that it was the burst axial position of the majority of rods.

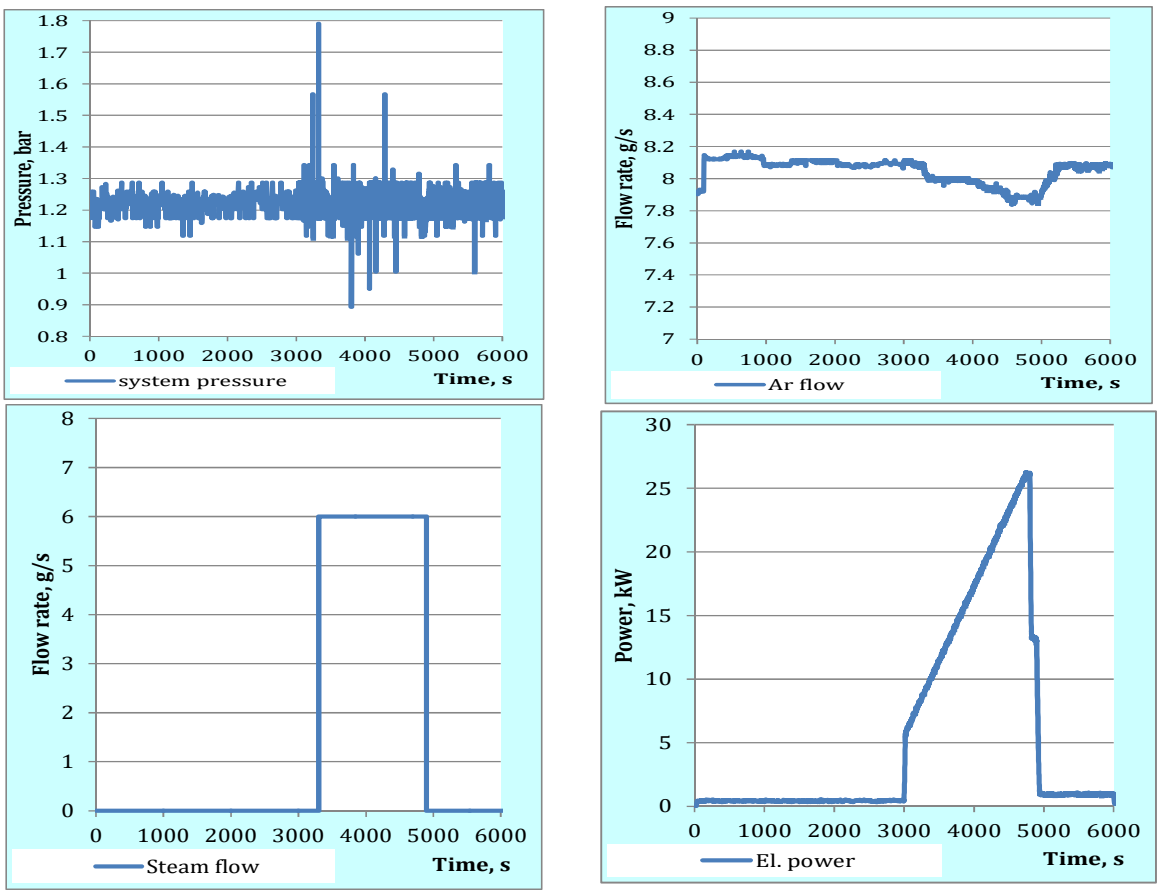

FIG. 5. System pressure, argon flow, steam flow and electrical power of CORA-15.

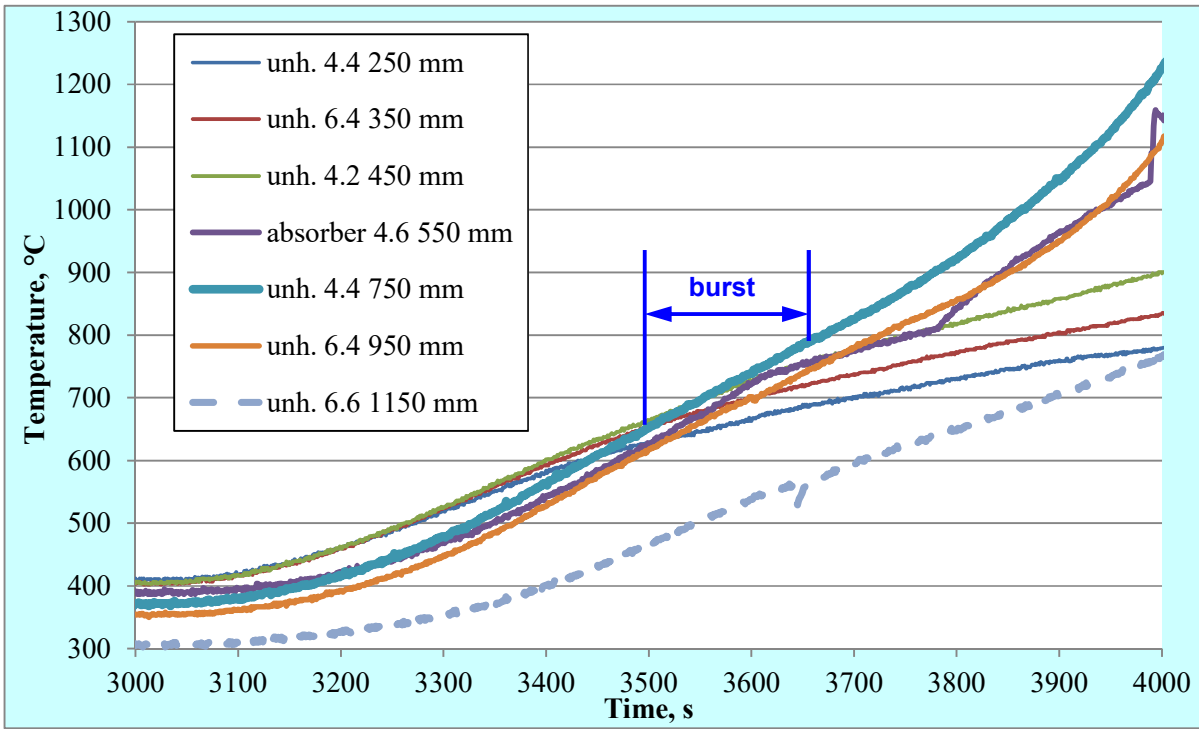

FIG. 6. Readings of thermocouples at different elevations during transient.

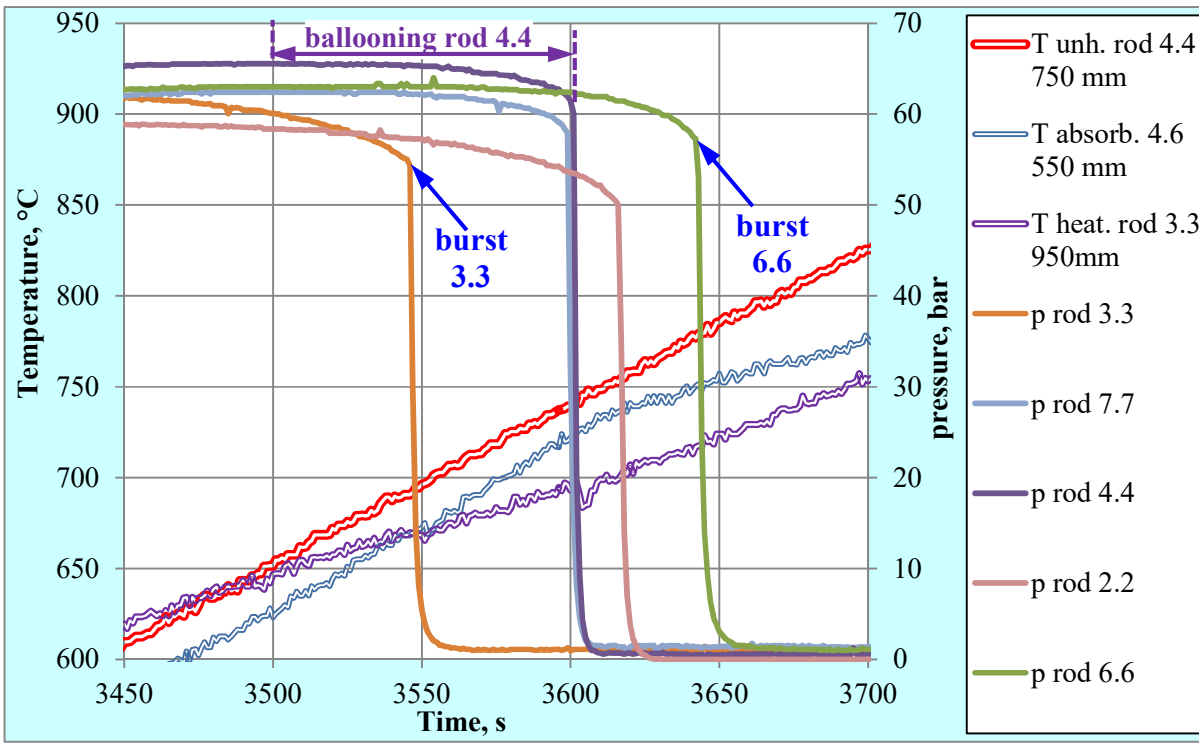

FIG. 7. Ballooning and burst (readings of pressure transducers).

TABLE 3. BURST TIMES

Rod	5.1	3.3	3.5	1.3	5.5	5.3	2.4	3.1	1.1
Time (s)	3493.8	3547.8	3561.5	3562.1	3562.7	3564.2	3565.1	3570.2	3579.4
Rod	7.5	7.3	1.5	5.7	7.7	7.1	4.4	3.7	6.4
Time (s)	3579.5	3585.1	3588.7	3588.9	3593.9	3600.8	3600.9	3602.0	3602.2
Rod	4.2	2.2	1.7	2.6	6.6	–	–	–	–
Time (s)	3604.0	3616.3	3617.8	3624.8	3644.5	–	–	–	–

The readings of thermocouples during the test at different elevations are provided with Fig. 8. This figure showers also the readings of two pyrometers installed at elevations 690 and 890 mm and oriented to the bundle through holes in fiber insulation and shroud. Significant oscillations of thermocouple and pyrometer readings are connected to the Zry melt onset at T > 1760 °C. It could be suggested that after these incidences the thermocouples were failed or shifted to lower elevations. However, the comparison of thermocouple and pyrometer data at 750 and 950 mm shows very similar behavior after oscillation occurrences. So, it can indicate the correctness of thermocouple readings also during the cooling stage.

The maximum temperature reached in the test amounts to about 2000 °C. The temperatures of absorber rod and pertinent guide tube show basically the same behaviour as the unheated or heated rods. A difference in CORA-15 compared to experiments without internal rod pressure can be found for the temperature escalation process. In CORA-15 the escalation developed in the upper half of the bundle only. Usually the escalation also takes place in the lower half of the bundle, down to about 150 mm. In CORA-15 the temperature in the lower part was insufficient to trigger a temperature escalation.

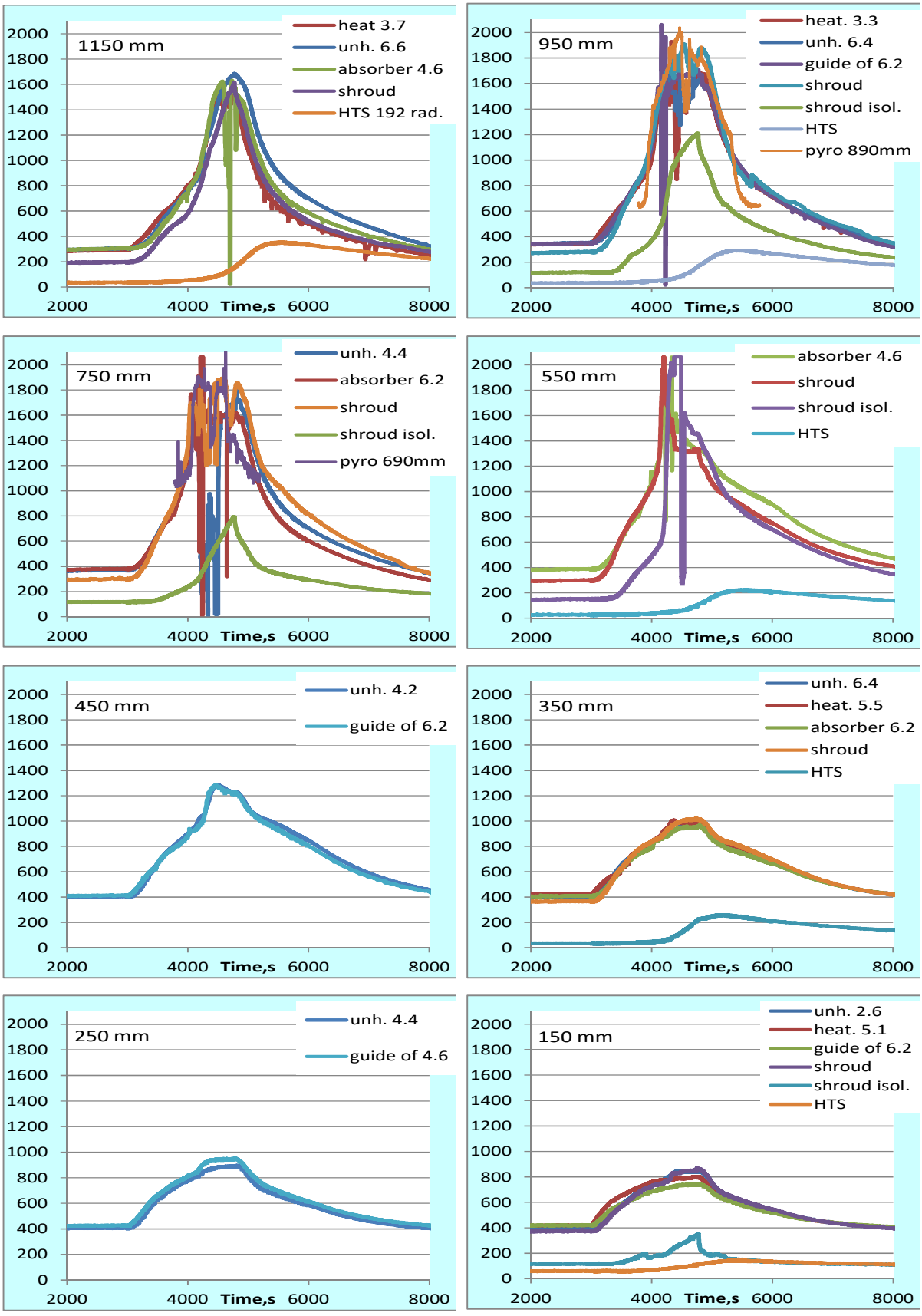

FIG. 8. Thermocouple (and pyrometer) readings at different elevations of CORA-15 (temperature in °C).

The measured hydrogen data for the test CORA-15 are given in Fig. 9. They are derived from the ion current obtained from the gas probes 1) at the outlet of the test section (before condenser) and 2) at the outlet of the mixing chamber (after condenser). Both mass spectrometers indicate the maximum of the hydrogen release rate about 210 mg/s on the end of the transient. There is some time shift of the readings of the second mass spectrometer due to its larger remoteness from the bundle outlet. The total hydrogen release on the end of the test was 180 g according to the first mass spectrometer (installed before condenser) and 145 g according to the second mass spectrometer (installed after condenser). The data of the second spectrometer are more reliable due to absence of condensable gases (steam) at the measurement point. Due to problems with the pre-test calibration of spectrometers, the following measurement errors concerning the total hydrogen value could be estimated: ±20% for the first spectrometer and ±10% for the second mass spectrometer.
Based on the accumulated H_2 productions the oxidation energy is determined as about 27 MJ. Its percentage amounts to 45% of the total energy input (electric supply plus exothermal energy). Also on the basis of the total H_2 generation the percentage of zirconium oxidation was calculated (about 75%). This percentage is an integral value and does not reflect local differences. The fraction of steam consumed during the transient (heat-up) phase, was calculated (27%). The result, too, is an integral (average) value that is based on the total amount of H_2, the steam flow rate, and the time at temperature above 1400 °C.

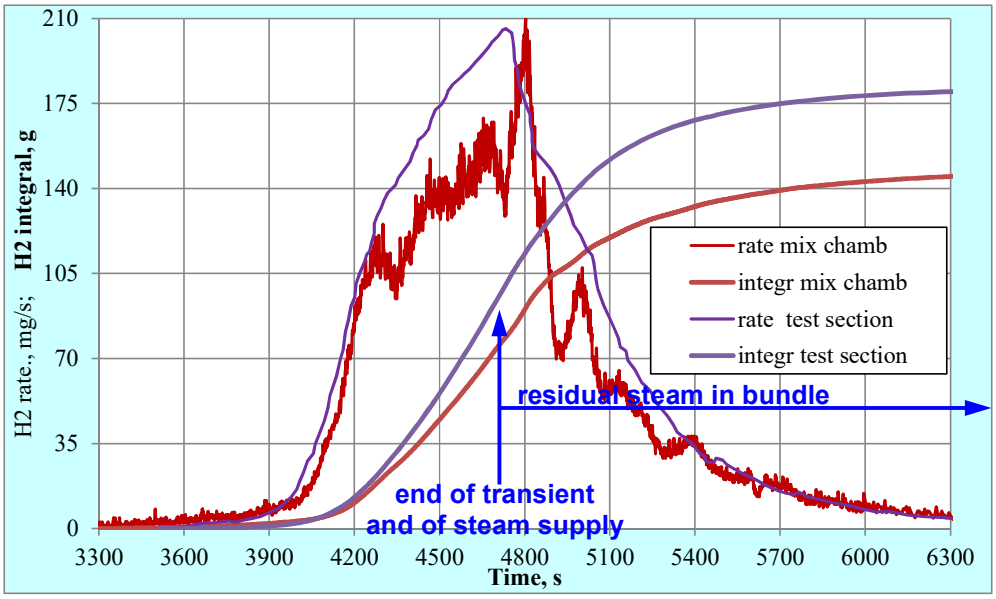

FIG. 9. Hydrogen production during CORA-15; results of two mass spectrometers: 1)Purple curve: before condenser (total hydrogen release 180 g), 2) Red curve:after condenser (total hydrogen release 145 g).

In presence of PWR absorber material (Ag, In, Cd) the sequence of failure starts with the release, relocation and re-solidification of the (Ag, In, Cd) melt. The melt release occurred at about 1350 °C (elevation ≈ 800 mm, time point 3988 s) for the rod #4.6 and at 1290 °C (elevation 750 mm, time point 4025 s) for the rod #6.2 (Fig. 10).

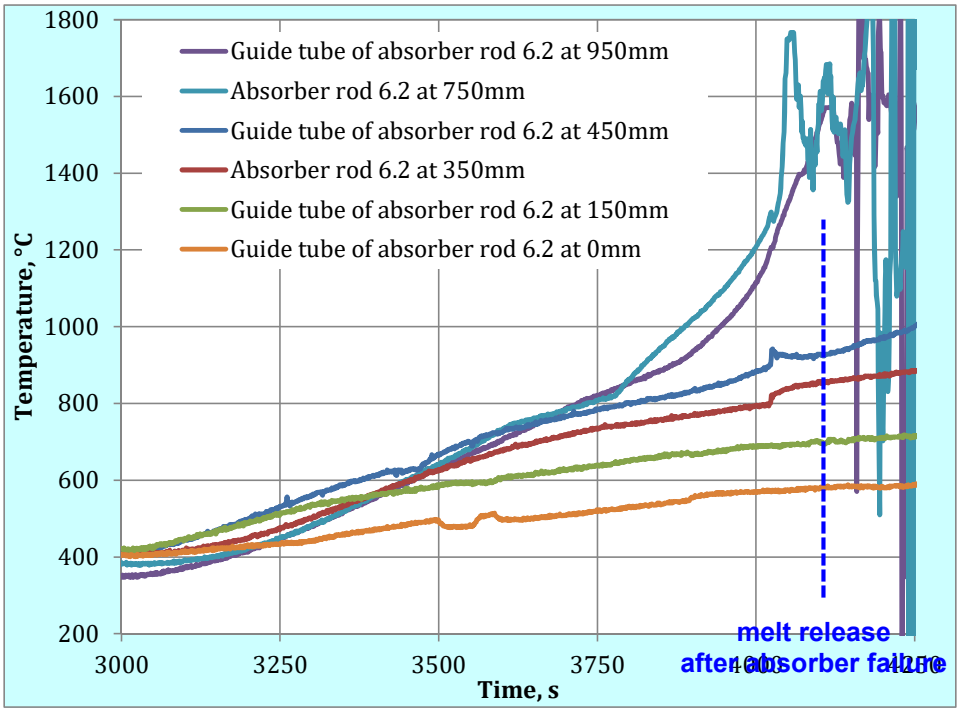

FIG. 10. Reaction of thermocouples of the rod #6.2 on the absorber melt release and relocation.

5. POST-TEST INVESTIGATIONS

In test CORA-15 escalation took place only in the upper half of the bundle. The posttest appearance confirms the result indicated by the temperature recordings. So, melting and relocation of material took place only in the upper half of the bundle as can be seen in the view from outside the bundle as well as from the vertical and horizontal cross sections (Figs. 12 and 14). The behavior of the bundle might be explained by a different response of the heater resistance in the upper and the lower part of the bundle. Once the temperature increases in the upper part above 550 mm, an escalation is triggered in this part while the rods stay cool in the lower part where the heater resistance is kept at a relative constant value. (The total energy fed into the heated rods is constant). In the lower part the temperature reached was too low to start an escalation. The behavior is a consequence of cladding ballooning at elevation above 550 mm which changes the heat transfer (in the heated rods) from the heater and pellets to cladding.

The absorber melt release occurred between 1290 and 1350 °C at elevations between 750 and 800 mm. Most of the melt reacts with the Zircaloy cladding and guide tube by liquefying the zirconium components, forming a metallic melt of the type (Ag, In, Zr). Due to its zirconium content this melt is capable of dissolving UO_2 as low as 1250 °C, i.e. clearly below the melting point of Zircaloy (1760 °C). During the temperature escalation above 1800 °C, Zr melt formed in the gap between ZrO_2 and UO_2 penetrated partially through the failed ZrO_2 layer into the space between rods. The resulting melt can be significantly oxidized, what was detected by single effect tests [10] and observed in many bundle tests [11]. Based on these results, the mechanistic model of the molten pool oxidation [12] and the model for melt blockage (slug) relocation with concurrent oxidation [13] were developed[6]. In the CORA-15 test, the oxidized melt was solidified between 400 and 550 mm. A partial flow channel blockage occurred at

[6] Refer to Implementation of The Molten U-Zr-O SLUG (blockage) relocation model into the SFPR code, by Veshchunov, M. S., et al. in this report.

elevations between 200 and 600 mm, i.e. below and upper the central grid spacer located at 496 mm (Fig. 11).

Metallographical investigations showed negligible oxidized cladding up to elevation of about 350 mm. The claddings were completely oxidized between elevations 480 and 1000 mm (Fig. 13). Larger cladding portions are missing. However, the pellet stacks of the full-pellet rods are kept in place.

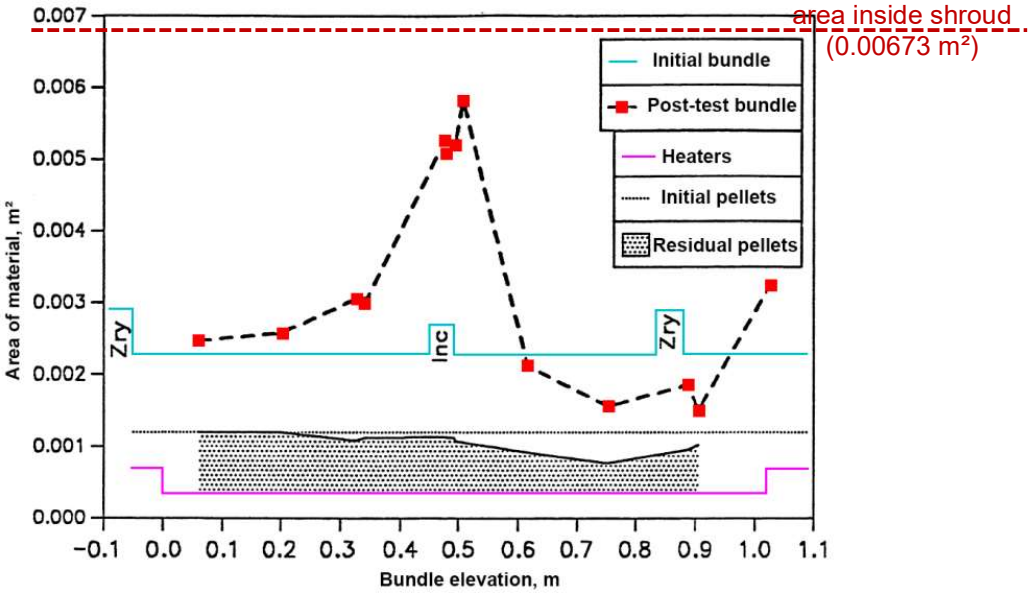

FIG. 11. material relocation and bundle blockage.

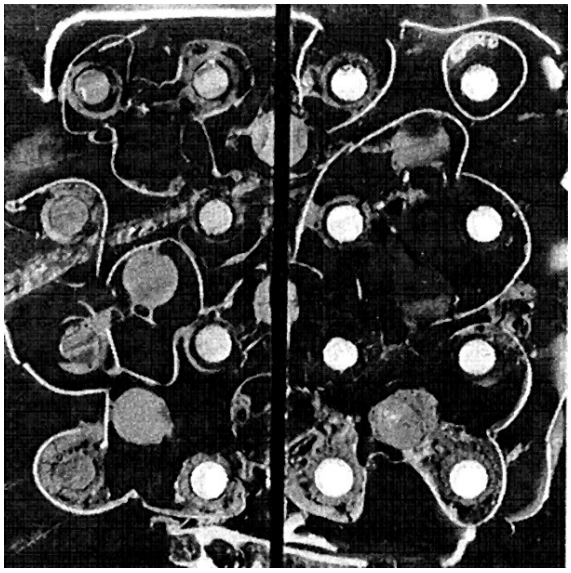

615 mm

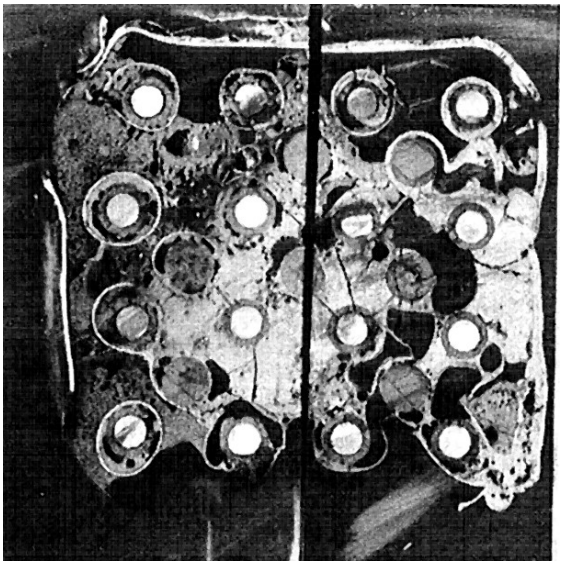

508 mm

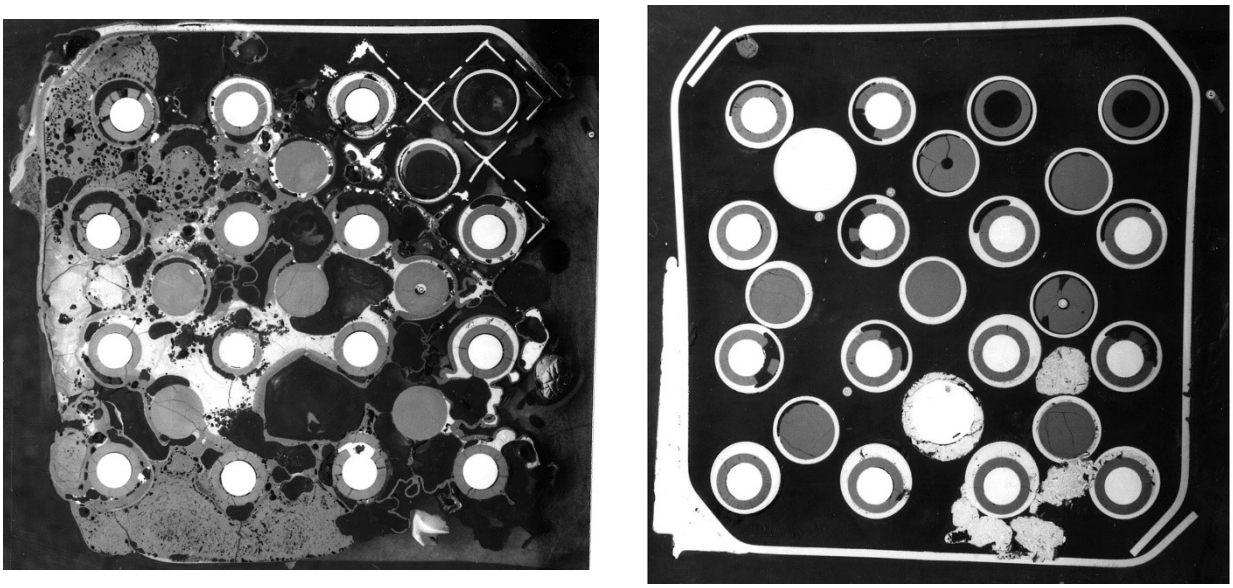

480 mm 328 mm

FIG. 12. Horizontal cross sections of CORA-15.

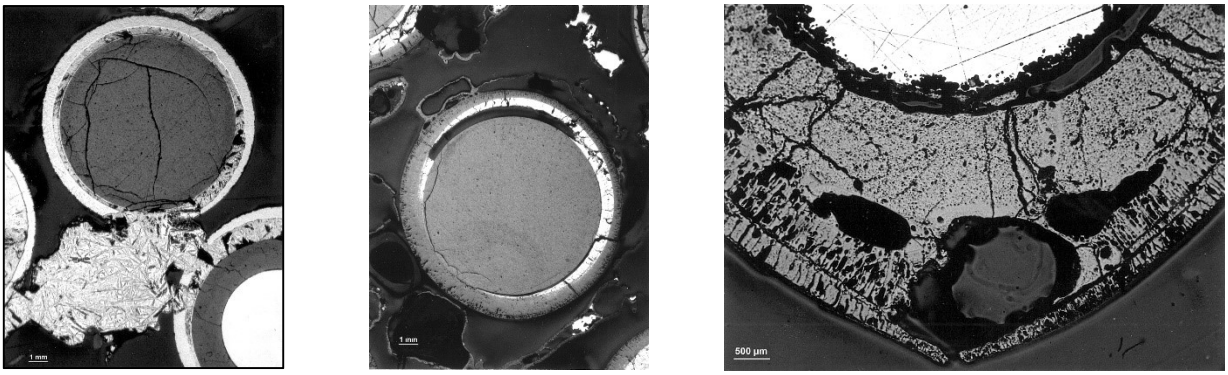

328 mm, rods 2.6 (unh.) and 1.7: min oxidised clad

495 mm, rod 2.2: completely oxidised clad

891 mm, rod 5.1: completely oxidised clad

FIG. 13. CORA-15 bundle elevations between 300 and 100 mm: cladding oxidation.

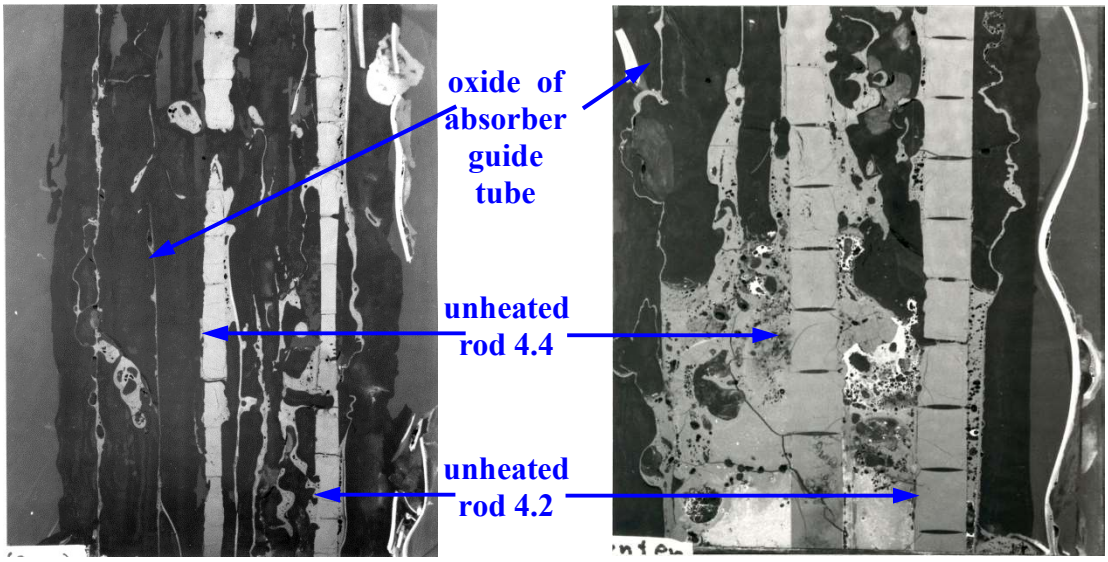

FIG. 14. Vertical cross section: melt between remnants of guide tube and pellet remnants for 617 to 752 mm (left) and 510 to 615 mm (right)

6. SUMMARY AND CONCLUSIONS

The CORA-15 bundle test was performed under transient conditions typical for many CORA-PWR tests with bundle containing two Ag/In/Cd neutron absorber rods. Unlike other CORA bundles, all heated and unheated fuel rod simulators (16 + 7 correspondingly) were filled with helium and pressurized to 6.0 MPa before transient. During the transient, all rods underwent ballooning and burst. Ballooning progressed during about 100 s. Bursts occurred within 150 s (between 3500 and 3650 s) in the temperature bandwidth between about 700 and 800 °C. The mostly probable burst elevation is the bundle elevation 750 mm (the hottest elevation during the burst period).

During the further heat-up, temperature escalation due to the zirconium-steam reaction starts at elevations 550…950 mm at temperature of about 1100 °C. In presence of PWR absorber material (Ag, In, Cd) the sequence of failure starts with the release, relocation and re-solidification of the (Ag, In, Cd) melt. The absorber melt release occurred between 1290 and 1350 °C at elevations between 750 and 800 mm. Most of the melt reacts with the Zircaloy cladding and guide tube by liquefying the zirconium components, forming a metallic melt of the type (Ag, In, Zr). Due to its zirconium content this melt is capable of dissolving UO_2 as low as 1250 °C, i.e. clearly below the melting point of Zircaloy (1760 °C).

During the temperature escalation above 1800 °C, Zr melt formed in the gap between ZrO_2 and UO_2 was relocated partially inside the gap to lower bundle elevations and partially penetrated through the failed ZrO_2 layer into the space between rods. The resulting melt of the fuel rod interaction, containing mainly U, Zr, O, relocated downwards as slug and solidified between 400 and 550 mm according to its solidus temperature as a large lump of porous structure. The maximum bundle blockage (almost 100%) was observed at the top of the Inconel grid spacer (about 500 mm). The (Ag, In, Cd) absorber melt with the much lower solidus temperature solidified down at the lower elevation of about 150 mm.

Post-test investigations showed negligible oxidized cladding up to elevation of about 350 mm. The claddings were completely oxidized between elevations 480 and 1000 mm. The maximum hydrogen release rate of 210 mg/s was measured on the end of the transient (4800 s). The total hydrogen release was 145 ± 15 g.

Based on the CORA-15 experimental data, the benchmark on the test modeling by computer ATHLET-CD and SOCRAT was performed. Corresponding descriptions of code applications are represented in Section 2.5.2 and 2.5.3; the comparison of simulation results is to find in Section 4.5.

Furthermore, in the framework of the FUMAC project was shown that the implementation of the slug model in the single-channel SFPR code (IBRAE) demonstrates the possibility of extending the fuel codes to severe accidents, on the one hand, and the possibility of using them in the form of a stand-alone module in integral codes, on the other hand. It is very important from the point of view of development of modern technology of new generation of multi-physical codes, one of the most important development principles of which is their modular structure.

REFERENCES

[1] HAGEN, S., KAPULLA, H., MALAUSCHEK, H., WALLENFELS, K. P., BUESCHER, B., Temperature Escalation in PWR Fuel Rod Simulator Bundles due to the Zircaloy/Steam Reaction: Post-Test Investigations of Bundle Test ESBU-2A, Kernforschungszentrum Karlsruhe, KfK-3789, November 1986, https://publikationen.bibliothek.kit.edu/270023528/3813102.

[2] HAGEN, S., HOFMANN, P., NOACK, V., SCHANZ, G., SCHUMACHER, G., SEPOLD, L., Results of SFD Experiment CORA-13 (OECD International Standard

Problem 31), Kernforschungszentrum Karlsruhe, KfK-5054, February 1993, https://publikationen.bibliothek.kit.edu/270033715/3813473.

[3] FIRNHABER, M., TRAMBAUER, K., HAGEN, S., HOFMANN, P., OECD/NEA-CSNI International Standard Problem No. 31. CORA-13 Experiment on Severe Fuel Damage, Gesellschaft für Reaktorsicherheit, Cologne, GRS-106, Juli 1993 / Kernforschungszentrum Karlsruhe, KfK 5287, July 1993, http://www.nea.fr/html/nsd/docs/1993/csni-r1993-17.pdf.

[4] HAGEN, S., HOFMANN, P., NOACK, V., SEPOLD, L. SCHANZ, G., SCHUMACHER, G., Comparison of the Quench Experiments CORA-12, CORA-13, CORA-17, Forschungszentrum Karlsruhe, FZKA 5679, August 1996, https://publikationen.bibliothek.kit.edu/270039707/3813575.

[5] MINATO, K., HERING, W, HAGEN, S., Zircaloy Oxidation and Cladding Deformation in PWR-specific CORA Experiments, Kernforschungszentrum Karlsruhe, KfK 4827, 1991, https://publikationen.bibliothek.kit.edu/270030844/3813433.

[6] HERING, W., Interpretation und Modellierung des Experimentes CORA mit dem erweiterten Kernschmelz-Code SCDAP/MOD1, Dissertation, University of Stuttgart, IKE 2-100, 1993.

[7] HERING, W., MINATO, K., NAGASE, F., Global Analysis of Bundle Behavior in Pressurized Water Reactor Specific CORA Experiments, Nuclear Technology, 102, April 1993, 100–115, http://www.ans.org/pubs/journals/nt/a_34806.

[8] HERING, W., HOFMANN, P., Material Interactions during Early-Phase Core Melt Progression, Festschrift Energie-Technik-Umwelt, Prof. Dr. Unger, RUB Bochum, May 1994.

[9] SEPOLD, L., HAGEN, S., HOFMANN, P., SCHANZ, G., Behavior of AgInCd absorber material in Zry/UO_2 fuel rod simulator bundles tested at high temperatures in the CORA facility. Scientific report FZKA-7448, January 2009, https://publikationen.bibliothek.kit.edu/270074441/3815428.

[10] VESHCHUNOV, M. S.; STUCKERT, J.; BERDYSHEV, A.V., Modelling of Zr-O and U-Zr-O melts oxidation and new crucible tests. Scientific report FZKA-6792, December 2002, https://publikationen.bibliothek.kit.edu/270053667/3814311.

[11] HASTE, T., STEINBRÜCK, M., BARRACHIN, M., DE LUZE, O., GROSSE, M., STUCKERT, J., A comparison of core degradation phenomena in the CORA, QUENCH, Phébus SFD and Phébus FP experiments. Nucl. Eng. Des., Volume 283, March 2015, Pages 8-20, DOI: 10.1016/j.nucengdes.2014.06.035.

[12] VESHCHUNOV, M. S., BOLDYREV, A. V., SHESTAK, V. E. Modelling the formation and oxidation of molten pools. Ann. Nucl. Energy., Volume 61, November 2013, Pages 54-62, DOI: 10.1016/j.anucene.2013.03.046.

[13] VESHCHUNOV, M. S., SHESTAK, V. E., Model for melt blockage (slug) relocation and physico-chemical interactions during core degradation under severe accident conditions, Nucl. Eng. Des., Volume 238, Issue 12, December 2008, Pages 3500-3507, DOI: 10.1016/j.nucengdes.2008.08.012.

RESULTS OF THE LOCA REFERENCE BUNDLE TEST QUENCH-L1 WITH ZIRCALOY-4 CLADDINGS

J. STUCKERT, M. GROßE, M. STEINBRÜCK, M. WALTER
Karlsruhe Institute of Technology (KIT)
Hermann-von-Helmholtz-Platz 1, 76344 Eggenstein-Leopoldshafen, Germany
e-mail: juri.stuckert@kit.edu

Abstract

The QUENCH-L1 bundle experiment with Zircaloy-4 cladding tubes was defined as reference test for the QUENCH-LOCA test series. The overall objective of this bundle test series is the investigation of ballooning, burst and secondary hydrogen uptake of the cladding under representative design based accident conditions, as well as to check the embrittlement criteria by means of detailed mechanical post-test investigations. The QUENCH-L1 test bundle contained 21 electrically heated fuel rod simulators made of as-received Zircaloy-4 claddings. Each rod was separately pressurized with krypton gas using an initial pressure of 55 bar for all rods. The transient phase with heating up from 570 °C to 1100 °C lasted 90 s. The decreasing yield strength and increasing ductility of the heated claddings with increasing temperature resulted in a progressive ballooning and consequent burst of all rods during the transient. The duration of the slow cooling phase was about 120 s. The test was terminated by water quenching. Post-test investigations showed maximal strain values between 25 and 45% at cladding positions with oxidation degree corresponding to 2% ECR measured in the burst region. Neutron radiography investigations of inner cladding tubes showed elevated concentrations of absorbed hydrogen close to the burst positions in band shaped cladding regions formed at the boundary of inner oxidised zone (so called secondary hydriding). Tensile tests on the cladding tubes with higher hydrogen content showed, that all these tubes failed not at the hydrogen band but in the centre of the burst opening (excluding the cladding of the centre rod, which could not be tested since it already has broken in the regions of the hydrogen bands above and below the burst opening during the manual withdrawal of heaters).

1. INTRODUCTION

Under the licensing procedures for pressurized water reactors (PWR) evidence must be given that the impacts of all pipe ruptures hypothetically occurring in the primary loop and implying a loss of coolant can be controlled. The double-ended break of the main coolant line between the main coolant pump and the reactor pressure vessel is considered to constitute the design basis for the emergency core cooling system (ECCS) in a loss-of-coolant accident (LOCA). The break of a main coolant line leads to the loss of coolant in the primary circuit of a PWR and the decrease in system pressure from 15.5 MPa to eventually around 0.32 MPa (boiling point, corresponding to 135 °C). Consequently, the remaining coolant in the core as well as the emergency cooling water fed into the reactor core evaporate, the temperature of the fuel elements rises and the fuel rods start to balloon since they contain pressurized filling gas and fission gas products. At temperatures above 700 °C, the load within the metallic cladding wall reaches a critical value and the most ballooned section finally bursts.

Upon rupture of the reactor coolant line the reactor is shut down. However, as the production of decay heat will be continued, reliable sustainment of the reactor core rod geometry and long-term emergency cooling of the core are required. To retain the core rod geometry it should be established the acceptable limit of cladding embrittlement, which is increased during oxidation in steam. The current LOCA criteria and their safety goals are applied worldwide with minor modifications since the NRC release in 1973 [1, 2]. The criteria are given as limits on peak cladding temperature ($T_{PCT} \leq 1200$ °C) and on oxidation level ECR (equivalent cladding reacted) calculated as a percentage of cladding oxidized (ECR ≤ 17% using the Baker-Just oxidation correlation). These two rules constitute the criterion of cladding

embrittlement due to oxygen uptake and, according to the RSK (Reactor Safety Commission) Guidelines, are included in the current German LOCA criteria, too [3].

The results elaborated worldwide in the 1980's on the Zircaloy-4 (Zry-4) cladding tubes behavior (oxidation, deformation and bundle coolability) under LOCA conditions constitute a reliable data base and an important input for the safety assessment of LWRs. With respect to the LOCA conditions for German LWRs, different off-pile [4]–[6], the FR2 in-pile [7] single rod as well as the REBEKA bundle tests [8, 9] were performed. It was concluded that the ECC-criteria established by licensing authorities are conservative and that the coolability of an LWR and the public safety can be maintained in a LOCA [10]. In-pile test data (with burn-up up to 35 MWd/kgU) were consistent with the out-of-pile data and did not indicate an influence of the nuclear environment on cladding deformation.

Due to major advantages in fuel-cycle costs, optimised reactor operation, and waste management, the current trend in the nuclear industry is to increase fuel burn-up. At high burn-up, fuel rods fabricated from conventional Zry-4 often exhibit significant oxidation, hydriding, and oxide spallation. Thus, fuel vendors have developed and proposed the use of new cladding alloys, such as Duplex DX-D4, M5, ZIRLO and other. Therefore, it is important to verify the safety margins for high burn-up fuel and fuel claddings with advanced alloys. In recognition of this, LOCA-related behaviour of new types of cladding is being actively investigated in several countries [11, 12]. Due to long cladding hydriding period for the high fuel burn-up, post-quench ductility is not only influenced by oxidation, it is also significantly depending on the hydrogen concentration. Consequently, the 17% ECR limit is inadequate to ensure post-quench ductility at hydrogen concentrations higher than ≈500 wppm [13]. Due to so-called secondary hydriding (during oxidation of inner cladding surface after burst), which was firstly observed in JAERI [14], the hydrogen content can reach 4000 wppm in cladding regions around burst [15].

Particularly to investigate the influence of the secondary hydriding phenomena on the applicability of the embrittlement criteria for the German nuclear reactors, it was decided to perform the QUENCH-LOCA bundle test series in the QUENCH facility of KIT, supported by the association of the German utilities (VGB) [16]. Additionally, the QUENCH-LOCA bundle tests could support experiments performed in-pile and in-cell, respectively, e.g. single-rod tests OECD SCIP-2 [17]. Compared to single-rod experiments, bundle tests have the advantage to study the mutual interference of rod ballooning among fuel rod simulators as well as to take into account the local coolant channel blockages in this more realistic arrangement.

The first test QUENCH-L0 was performed with Zry-4 cladding tubes not pre-oxidised on 22.07.2010 as commissioning test and terminated with reflood immediately after the transient phase [18, 19]. The QUENCH-L1 test was performed on 02.02.2012 as reference test, using a similar bundle compared to the QUENCH-L0 test but including a cool-down phase between transient and reflood.

2. DESCRIPTION OF THE TEST FACILITY

The QUENCH facility was constructed 1997 at KIT for investigation of the so-called hydrogen source term during reflood, i.e. of the measurement of hydrogen release during the reflood of an overheated reactor core. Since then 17 bundle tests were successfully performed under severe accident conditions and 7 bundle tests under LOCA conditions.

The test section is enclosed by safety containment with a wall thickness of 5.6 mm and an inner diameter of 801.8 mm. The facility can be operated in two modes: a forced-convection mode and a boil-off mode. In the forced-convection mode (relevant for QUENCH-LOCA-1) superheated steam from the steam generator and superheater together with argon as a carrier gas enter the test bundle at the bottom (Fig. 1).

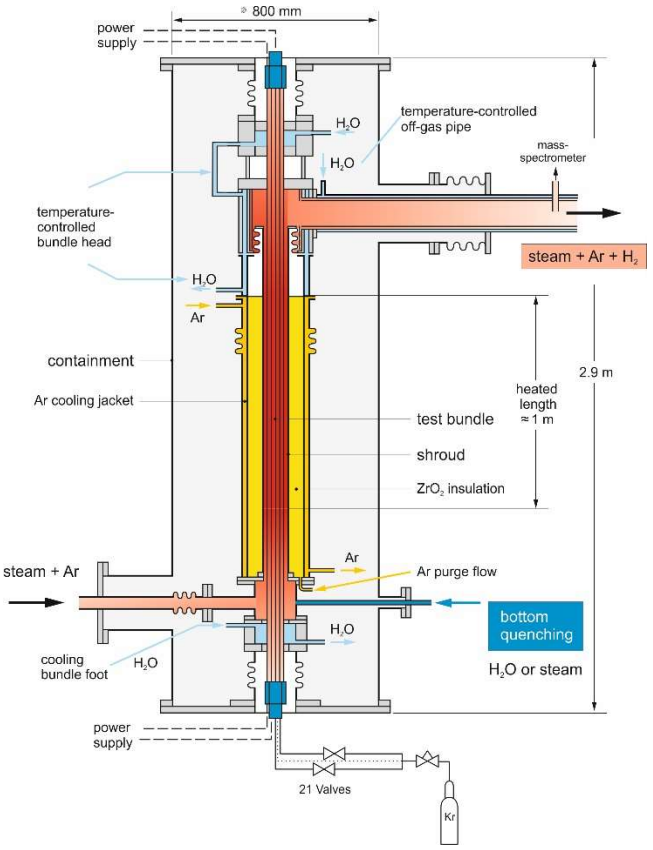

FIG. 1. QUENCH test section with flow lines.

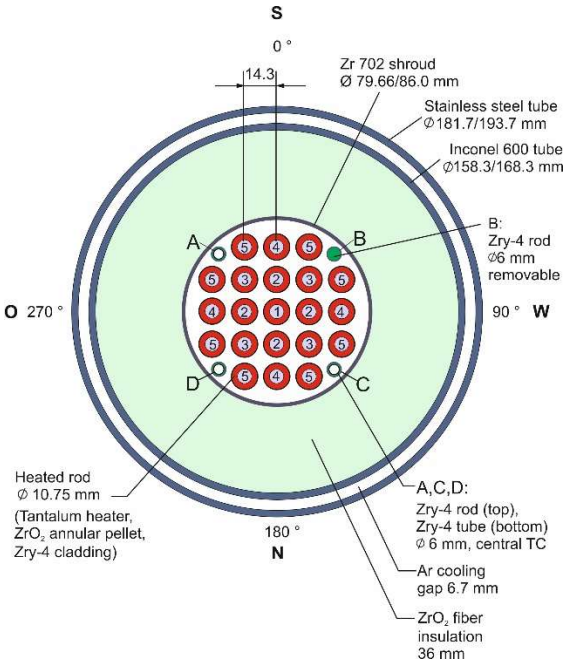

FIG. 2. Fuel rod simulator bundle (cross section, top view).

The system pressure in the test section for the QUENCH-LOCA test is about 0.3 MPa. The argon, steam and hydrogen produced in the zirconium-steam reaction flow upward inside the bundle and from the outlet at the top through a water-cooled off-gas pipe to the condenser where the remaining steam is separated from the non-condensable gases argon and hydrogen. The water cooling circuits for bundle head and off-gas pipe are temperature-controlled to guarantee that the steam/gas temperature is high enough so that condensation at the test section outlet and inside the off-gas pipe can be avoided. The temperature at the bundle head is kept at 348 K, and the flow rate of the cooling water is ≈ 250 g/s. The off-gas pipe consists of a water-cooled inner pipe with a countercurrent flow and a flow rate of ≈370 g/s. The water inlet temperature is controlled at 393 K. Between the off-gas pipe and inner cooling jacket there is stagnant off-gas. The main dimensions of the tubes that make up the off-gas pipe are:

— Inner pipe: Outer diameter 139.7 mm, wall thickness 4.5 mm, total length 3256 mm, (material- stainless steel);
— Inner cooling jacket: Outer diameter 154 mm, wall thickness 2 mm, (material- stainless steel);
— Outer cooling jacket: Outer diameter 168.3 mm, wall thickness 5 mm, (material- stainless steel).

The quenching water is injected into the bundle through a separate line marked ‘bottom quenching’ in Fig. 1. The design characteristics of the test bundle are given in Table 1. The test bundle is made up of 21 fuel rod simulators, each with a length of approximately 2.5 m, and of four corner rods (see cross section in Fig. 2). The bundle is surrounded by a shroud, which has two functions:

— The shroud acts as steam and gas guide tube;

— It simulates an adiabatic surrounding of the reactor core. The consideration of heated rod claddings, corner rods and shroud, manufactured from similar zirconium alloys, results in the surface of 30.6 effective rod simulators.

TABLE 1. DESIGN CHARACTERISTICS OF THE QUENCH-L1 TEST BUNDLE

QUENCH-L1 Test Bundle		
Bundle type		PWR
Bundle size		21 heated rods
Effective number of rods	(considering surface of heated rods, shroud and corner rods)	30.6 rods (21 + 7.4 from shroud + 2.2 from corner rods)
Pitch		14.3 mm
Coolant channel area		29.65 cm^2
Hydraulic diameter		11.5 mm
Rod outside diameter		10.75 mm
Cladding material		Zircaloy-4
Cladding thickness		0.725 mm
Rod length	(Elevations)	2480 mm (-690 to 1790 mm)
Internal rod pressure	(Gas)	5.5 MPa abs.; rod#10: 4.6 MPa due to leakage before heating; (Kr)
Material of middle heater		Tantalum (Ta)
	Surface roughness	Ra=1.6 µm
Length of middle heater		1024 mm
Diameter of middle heater		6 mm
Annular pellet	Material	ZrO_2;Y_2O_3-stabilized
	Dimensions	∅ 9.15/6.15 mm; L=11 mm
	Surface roughness	Ra=0.3 µm
Pellet stack		0 mm to ≈1020 mm
Corner rod (4)	Material	Zircaloy-4
	Instrumented (A, C, D)	tube ∅ 6x0.9 (bottom: -1140 mm)
	not instrumented (B)	rod ∅ 6 mm (top: +1300 mm)
		rod ∅ 6 mm (-1350 to +1155 mm)
Grid spacer	Material	Zircaloy-4, Inconel 718
	Length	Zircaloy: 42 mm, Inconel: 38 mm
	Sheet thickness	0.5 mm
	Elevation of lower edge	Incon.: -100 mm; Zry: 150, 550, 1050, 1410 mm
Shroud	Material	Zirconium 702 (flange: Zry-4)
	Wall thickness	3.17 mm
	Outside diameter	86.0 mm
	Length (extension)	1600 mm (-300 mm to 1300 mm)
Shroud insulation	Material	ZrO_2 fiber
	Insulation thickness	≈36 mm
	Elevation	-300 to ≈1000 mm
Mo-heater and Cu-electrodes	Length of upper parts	766 mm (576 Mo, 190 mm Cu)
	Length of lower parts	690 mm (300 Mo, 390 mm Cu)
	Outer diameter:	
	Prior to coating	8.6 mm
	After coating with ZrO_2	9.0 mm
	Coating surface roughness	Ra=6-12 µm
	Borehole of Cu-electrodes	diameter 2 mm, length 96 mm
Cooling jacket	Material: inner/outer tube	Inconel 600 (2.4816) / SS (1.4571)
	Inner tube	∅ 158.3 / 168.3 mm
	Outer tube	∅ 181.7 / 193.7 mm

The fuel rod simulators (Fig. 3) are held in their positions by five grid spacers, four of Zry-4, and one of Inconel 718 in the lower bundle zone. This bundle design is applied with a pitch of 14.3 mm. All test rods are heated electrically over a length by central heaters. The Zry-4 cladding of the fuel rod simulator has an outside diameter of 10.75 mm and a wall thickness of 0.725 mm (see also Table 1).

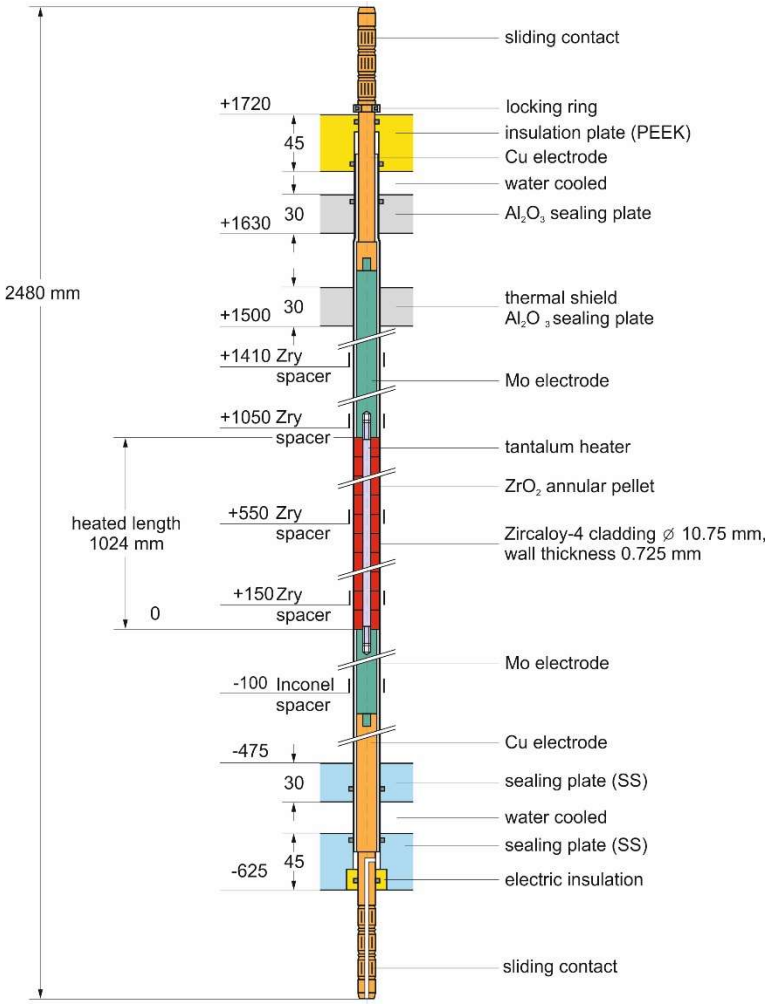

FIG. 3. Heated fuel rod simulator.

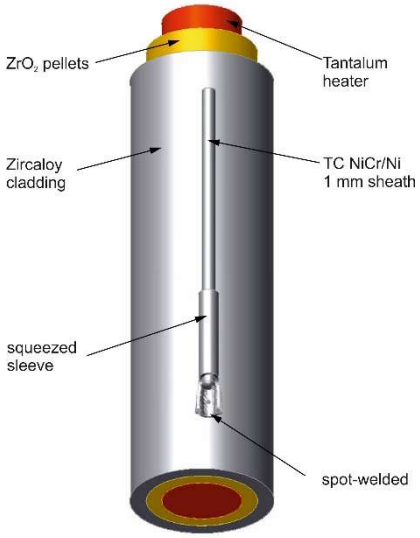

FIG. 4. Concept for TC fastening at the test rod.

Tantalum heating elements of 6 mm diameter are installed in the center of rods. Ta heaters were used for the first time in the QUENCH-L1 experiment. Their higher electrical resistance in comparison to tungsten results in higher maximum heating rates, especially during the first transient phase and hence to a more prototypical test conduct. These heaters are surrounded by annular yttria-stabilized ZrO_2 pellets. The physical properties of the ZrO_2 pellets are described in TABLE 2.

TABLE 2. MAIN CHARACTERISTICS OF THE ZRO_2 PELLET MATERIAL, YTTRIA-STABILIZED (TYPE FZY)

Property	Data
Density	5.5-5.8 g/cm^3
Elastic modulus	165 GPa
Specific heat at 20 °C	400 J/kg K
Thermal conductivity at 100 °C	2.5 W/m K
Linear expansion, 20-1000 °C	10.5 x 10^{-6}/K

The tantalum heaters (chemically clean tantalum) are connected serially to molybdenum heater (chemically clean molybdenum) and then to copper electrode (material 2.1293 with Cr 0.8, Zr 0.08 and balance Cu) at each end of the heater. The molybdenum and copper parts are joined by high-frequency/high-temperature brazing under vacuum (2x10^{-3} mbar) using an

AuNi 18 powder (particle size <105 μm). The average electrical resistance of 6.5 mΩ for the rod heating system, combined of Ta heater and Mo-(Cu alloy) parts, was not changed after the test. For electrical insulation the surfaces of Mo and Cu parts are plasma-coated with 0.2 mm ZrO_2. To protect the copper electrodes and the O-ring-sealed wall penetrations against excessive heat they are water-cooled (lower and upper cooling chambers filled with circulated demineralized water). The copper electrodes are connected to the DC electric power supply by means of special sliding contacts at the top and bottom of the bundle. The total heating power is limited by a maximal current of 7200 A and voltage of 9 V. Two DC-generators were used for two groups of rods connected in parallel: 1) 10 internal rods: #1 – #9 and rod #15; 2) 11 external rods: #10 – #14 and #16 – #21. The electric resistance of a single heater increases significantly with temperature. The additional resistance of the external electric circuit between the axial end of the single heater and the connection to the generator (sliding contacts, cables, and bolts) is 3.75 mΩ for the inner rod group and 4.05 mΩ for the outer rod group. These values can be taken as constant because the external electric circuit remains at ambient temperature throughout the experiment.

The lower boundary for the lower cooling chamber is a sealing plate made of stainless steel with plastic inlays for electrical insulation, sealed toward the system by O-shaped rings. The upper boundary of the lower cooling chamber is a sealing plate of stainless steel. An insulation plate made of plastic (PEEK) forms the top of the upper cooling chamber, and a sealing plate of Al_2O_3, functioning as a heat-protection shield, is the lower boundary of the upper cooling chamber.

In the region below the upper Al_2O_3 plate the copper electrode is connected firmly to the cladding. This is done by rotary swaging the cladding onto the electrode. In the swaging region a sleeve of boron nitride is put between electrode and cladding for electrical insulation. The axial position of the fuel rod simulator in the test bundle is fixed by a groove and a locking ring in the top Cu electrodes. Referred to the test bundle the fixing point of the fuel rod simulators is located directly above the upper edge of the upper insulation plate. So, during operation the fuel rod simulators are allowed to expand downwards. Clearance for expansion of the test rods is provided in the region of the lower sealing plate. Also in this region, relative movement between cladding and internal heater/electrode can take place.

The test bundle is surrounded by a 3.17 mm thick shroud (79.66 mm ID) made of Zr 702 with a 36 mm thick ZrO_2 fiber insulation with porosity of 92% (thermal properties are given in TABLE 3) and an annular cooling jacket made of Inconel 600 (inner tube) and stainless steel (outer tube). The annulus between shroud and cooling jacket was filled (after several cycles of degasing) with stagnant argon of 0.22 MPa and was connected to a flow-controlled argon feeding system in order to prevent steam access to the annulus after possible shroud failure. The 6.7 mm annulus of the cooling jacket is cooled by an argon flow. Above the heated zone, i.e. above the 1024 mm elevation there is no ZrO_2 fiber insulation to allow for higher radial heat losses. This region of the cooling jacket is cooled by a water flow. Both the lack of ZrO_2 insulation above the heated region and the water cooling force the axial temperature maximum downward.

TABLE 3. THERMAL PROPERTIES OF ZIRCONIA FIBER INSULATING

Temperature (K)	366	673	1073	1373	1673	1923	2644
Thermal conductivity W/(m*K)		0.08	0.11	0.14	0.19	0.24	
Specific heat capacity J/(kg*K)	544						754

Insertion of four corner rods avoids an atypically large flow cross section at the outer positions and hence helps to obtain a rather uniform radial temperature profile.

The fuel rod simulators were separately pressurized. The gas supply system for individual pressurization of rods consists of pressure controller, 21 valves, 21 pressure transducers, and 21 justified compensation volumes for setting of original volume value of 31.5 cm^3 (the

compensation is needed because of the absence of empty plenums inside the rod simulators). The gas supply is connected with capillary tubes (with inner diameter 1 mm, length ca. 1.2 m) to each rod at its lower end with drilled copper electrode. The gas gap under the cladding is: 0.15 mm in the region of Cu/Mo parts and 0.075 mm in the region of Ta-heater/ZrO2-pellets. Before gas filling the rods and gas supply system were evacuated. At the beginning of experiment, the fuel rod simulators were backfilled with Kr gas to 20 bar. Then, before the transient, they were separately pressurized to the target pressure of 55 bar.

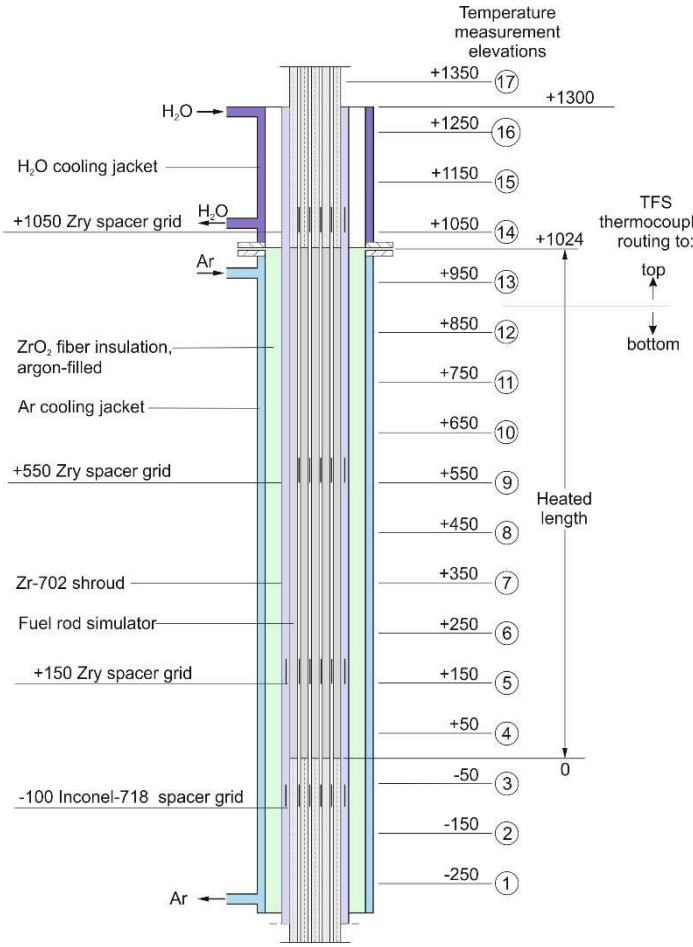

FIG. 5. Axial temperature measurement locations in the QUENCH-L1 test section.

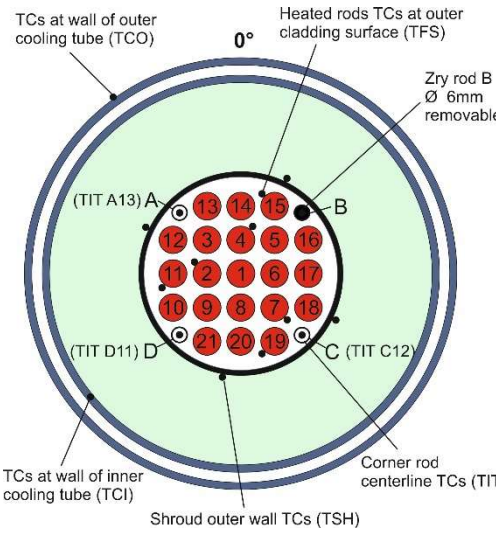

FIG. 6. Test bundle; TC instrumentation and rod designation (top view).

3. TEST BUNDLE INSTRUMENTATION

The test bundle was instrumented with sheathed thermocouples (TC) attached to the rod claddings (Fig. 4) at 17 different elevations between -250 mm and 1350 mm and at different orientations according to Fig. 5 and Fig. 6. The NiCr/Ni thermocouples (1 mm diameter, stainless steel sheath 1.4541 (X6CrNiTi18-10), MgO insulation) are used for temperature measurement of rod cladding and shroud outer surfaces. The TC tip is held in place by a Zr ferrule welded to the surface. The cables of the thermocouples from the -250 mm to the 850 mm level leave the test section at the bottom of the test section whereas those of the TCs above 850 mm are routed out on the top of the test section to prevent TC cables to pass the hot zone. The thermocouples attached to the outer surface of the rod claddings are designated “TFS” for all heated rods.

The shroud thermocouples (designation “TSH”) are mounted at the outer surface between -250 mm and 1250 mm. The thermocouples that are installed inside the Zry-4

instrumentation rods at the three corner positions of the bundle (positions A, C and D) are designated “TIT”. The thermocouples of the cooling jacket are installed inside the wall of the inner cooling tube (from -250 mm to 1150 mm, designation “TCI”). The distribution of the thermocouples along the bundle is shown in TABLE 4. No failed thermocouples were detected during the test. Accuracy of thermocouples: ± 2 K (up to 600 K).

The flow rates of noble gases (Ar, Kr) are regulated with the BRONKHORST flow controllers. Steam and water flows are controlled with the SIEMENS flow controllers. Numerous pressure transmitters from WIKA measure absolute and differential pressures along the gas supply system, at inlet and outlet of the test section.

TABLE 4. QUENCH-L1: ROD THERMOCOUPLE POSITIONS

Elevation (mm)	-250	-150	-50	50	150	250	350	450	550	650	750	850	950	1050	1150	1250	1350
Rod /Elevation	1	2	3	4	5	6	7	8	9	10	11	12	13	14	15	16	17
1																	
2										X	X	X	X	X	X		
3																	
4						X	X	X	X	X	X	X	X	X	X		
5																	
6																	
7	X	X	X	X	X	X	X	X	X	X	X	X	X	X	X	X	X
8																	
9																	
10																	
11							X	X	X	X	X	X	X	X	X	X	
12																	
13																	
14																	
15									X	X	X	X	X	X	X		
16																	
17																	
18																	
19										X	X	X	X	X	X		
20																	
21																	
Number per elevation	1	1	1	1	1	2	3	3	4	6	6	6	6	6	6	2	1

TFS (rod surface), indicated in table above	**56**	
TIT (inside corner rods)	***3***	TCs to bundle bottom ◄——► TCs to bundle top
TSH (outer shroud surface)	***13***	
Total quantity of bundle and shroud NiCr/Ni thermocouples	***72***	

3.1. Gas measurement system

The outlet gases (Ar, released hydrogen and residual steam) are analyzed by a Balzers mass spectrometer (MS) “GAM 300”. Due to its location at the off-gas pipe in the facility the mass spectrometer responds almost immediately (less than 10 s). The “BALZERS GAM 300” is a completely computer-controlled quadrupole MS with an 8 mm rod system which allows reliable quantitative measurement of gas concentrations down to about 10 ppm. For the MS

measurement a sampling tube is inserted in the off-gas pipe located approx. 2.7 m downstream from the test section outlet. It has several holes at different elevations to guarantee that the sampling of the gas to be analyzed is representative. To avoid steam condensation in the gas pipes between the sampling position and the MS the temperature of the gas at the MS inlet is controlled by heating tapes to about 150 °C (the upper operating temperature of the MS inlet valves). This allows the MS to analyze the steam production rate. Besides, the concentrations of the following species were continuously measured by the mass spectrometer during all test phases: argon, hydrogen, steam, nitrogen, oxygen, and krypton. The fuel rod simulators are filled with krypton which can be used as an indicator for a cladding failure. Additionally, the MS is used to control the atmosphere in the facility, e.g., to monitor the gas composition at the beginning of the test.

The temperature and pressure of the analyzed gas are measured near the inlet valve of the MS. The MS is calibrated for gas with well-defined argon/gas mixtures and for steam with mixtures of argon and steam supplied by a BRONKHORST controlled evaporator mixing (CEM) device. The MS off-gas is released into the atmosphere because the amount of sampling gas taken out of the system is negligible. A heated measuring gas pump was used to ensure a continuous flow of the steam-gas mixture from the off-gas pipe to the mass spectrometer.

For the MS the gas mass flow rate is calculated by referring the measured gas concentration to the known argon mass flow rate according to Eq. (1):

$$\dot{m}_{gas} = \frac{M_{gas}}{M_{Ar}} \cdot \frac{C_{gas}}{C_{Ar}} \cdot \dot{m}_{Ar} \tag{1}$$

with M representing the molecular masses, C the concentrations in vol% and $\dot{m}$ the mass flow rates of the corresponding gases.

4. DATA ACQUISITION AND PROCESS CONTROL

A LabView-based control and data acquisition system is used in the QUENCH facility. Data acquisition, data storage, online visualization as well as process control, control engineering and system protection are accomplished by three computer systems that are linked in a network. The data acquisition system allows recording of about 200 measurement channels at a maximum frequency of 25 Hz per channel. The experimental data and the date and time of the data acquisition are stored as raw data in binary format. After the experiment the raw data are converted into SI units and stored as ASCII data.

For process control, a system flow chart with the most important actual measurement values is displayed on the computer screen. Furthermore, the operating mode of the active components (pumps, steam generator, superheater, DC power system, valves) is indicated. Blocking systems and limit switches ensure safe plant operation. Operating test phases, e.g. heating or quenching phases, are pre-programmed and can be started on demand during the experiment. The parameter settings of the control circuits and devices can be modified online. Online visualization allows to observe and to document the current values of selected measurement positions in the form of tables or plots. Eight diagrams with six curves each can be displayed as graphs. This means that altogether 48 measurement channels can be selected and displayed online during the course of the experiment.

The data of the main data acquisition system and of the mass spectrometers are stored on two computers. Both computers are synchronized. The data of the main acquisition system are stored at a frequency of 5 Hz. The mass spectrometer data are recorded at a frequency of approx. 1 Hz during the entire test.

5. TEST CONDUCT AND RESULTS OF ONLINE MEASUREMENTS

The test procedure was based on pre-test calculations performed by the Paul Scherrer Institute (PSI, Villigen) using the SCDAP/RELAP5 and IBRAE (Moscow) using the SOCRAT code systems. According to the planned LOCA scenario, the transient phase should be performed with 8 K/s followed by slow cool-down phase and quenching.

The sequence of the test events is represented in TABLE 5. The experiment started (Fig. 7) by stabilizing the bundle conditions with an application of electrical bundle power of 3.5 kW (corresponding to a linear heat rate of ≈1 W/cm) in argon - superheated steam mixture (with rates of 6 g/s argon and 2 g/s steam, or specific rates 0.2 g/s/(effective rod) and 0.07 g/s/(effective rod) correspondingly) resulting in maximum bundle temperatures of 800 K.

TABLE 5. QUENCH-L1; SEQUENCE OF EVENTS

Time (s)	Event
-3248 (11:00:00; 02.02.2012)	Start data recording, Tmax = TFS 4/13 = 839 K, el. power at 3.49 kW. L701 = 1438 mm. L 501 = -405 mm. System pressure 3 bar. Ar 6 g/s, superheated steam 2 g/s.
-2260… -2170	Pressurization of rods from 15 to 55 bar.
0	Start of transient with max electrical power increase rate.
2; 4	Electrical power 32; 43 kW.
36…58	Sequential onset of ballooning for rods pressurized to 55 bar.
55…87	Sequential onset of burst for rods from inner rod #4 to peripherical rod #10.
87	Switch of the electrical power from max 58.65 kW to decay heat of 3.5 kW. Initiation of rapid steam supply line (50 g/s) additionally to carrier argon (6 g/s). Switch-off of slow steam supply (2 g/s). Tmax = TFS 4/12 = 1345 K.
91	Cladding surface temperature maximum reached. Maximal hydrogen production rate. Tmax = TFS 4/12 = 1373 K.
91…209	Cool-down of bundle in steam. Decrease of TFS 4/12 reading from 1373 K to 1023 K.
212	Initiation of quench water supply. Switch-off of steam supply. Switch of argon to bundle top supply.
212…221	Increase of bundle temperatures to ≈1073 K due to switch-off of the steam cooling.
237	Maximal quench rate (about 100 g/s) reached.
247…293	Wetting of cladding surface thermocouples (TFS) at elevations between -250 and 1350 mm at temperatures between 484 (TFS 7/1) and 858 K (TFS 7/12).
270…305	Maximal water evaporation rate (about 25 g/s).
351	Bundle completely filled with water (collapsed water level L 501 = 1307 mm)
417	Electrical power switched off. Tmax = TFS 15/15 = 333 K
1688 (12:22:20)	End of data recording. L 501 = 1289 mm

The transient was initiated by rapidly increasing the electrical power to 43 kW (linear heat rate ≈9 W/cm) followed by steady increase to 59 kW (linear heat rate ≈13 W/cm) within 63 s and stayed at that level for the rest of the transient (until 87 s). During this period the temperatures increased from their initial values to a maximum in excess of 1300 K, as planned. Due to limitation of the maximal electrical current of the DC generators the average heating rate of 5.7 K/s was realised. Fig. 8 shows the history of maximum temperature at each elevation.

The axial temperature profile in the bundle has a pronounced maximum between 850 and 1050 mm (Fig. 9). There is also a radial temperature gradient due to two reasons: 1) radial heat flux to the shroud, 2) electrical power supplied to internal rod group was higher than the power for external group because both DC generators reached current limit (~3600 A) but electrical resistance of 11 external rods connected in parallel is lower than for 10 internal rods.

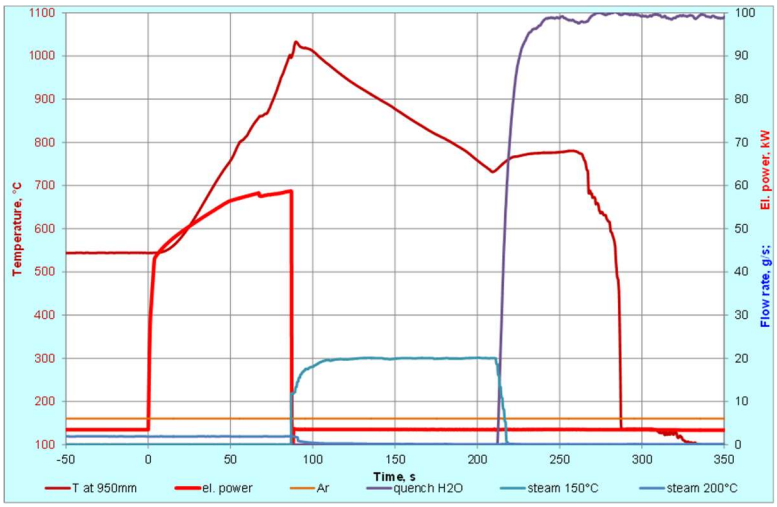

FIG. 7. QUENCH-L1 test scenario.

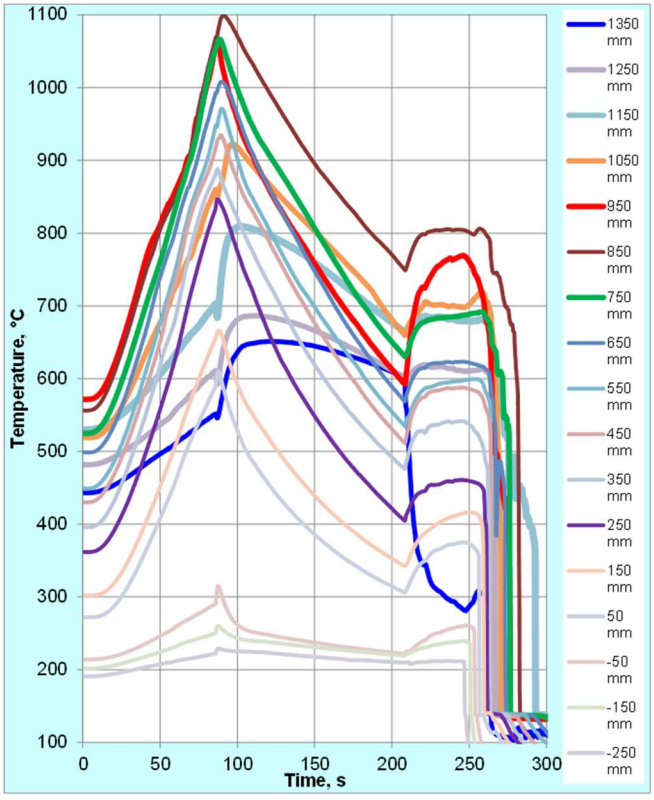

FIG. 8. Maximal cladding temperatures at different elevations.

According to the later measurements during the tests QUENCH-L2…-L5, the tangential temperature gradient across a rod was between 30 and 70 K on the burst onset [20]. As a consequence, according to the REBEKA criterion [8], a smaller ballooning strain could be expected for claddings with larger temperature gradient. Significant radial temperature difference can be developed during the transient not only due to global radial temperature gradient across the bundle (heat loss through the shroud), but due to non-coaxial positioning of

pellets and cladding [4]. For each rod, the highest cladding temperature is achieved at the contact between pellet and cladding (absence of gas gap with relatively low heat conductivity). The temperature difference between this contact position and opposite cladding side increased during the 3D ballooning process, due to the increase of the gas gap at the cold side whereas no gas gap formed at the hot side.

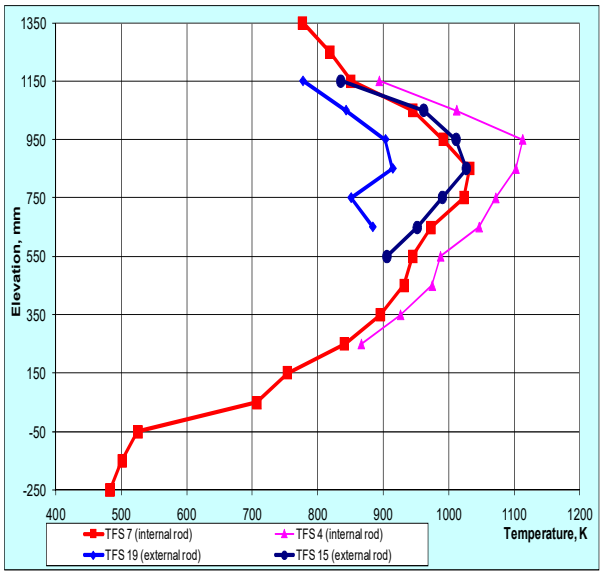

FIG. 9. Axial and radial temperature distribution on time of the first burst for selected rods.

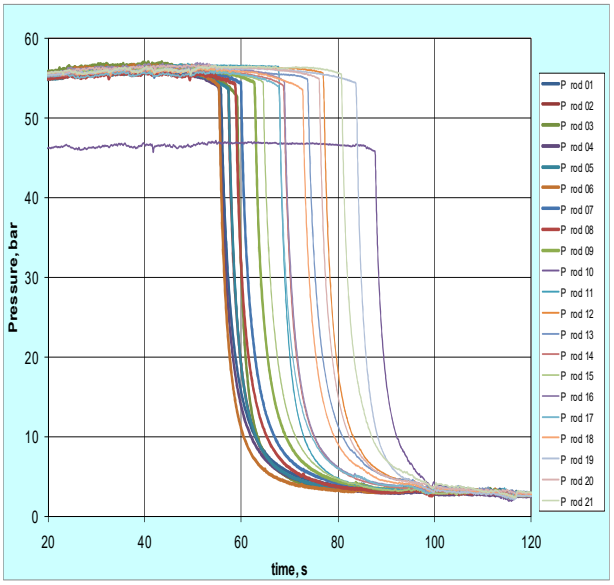

FIG. 10. Pressure changing during heating phase; ballooning and burst.

The experiment continued with power decrease to 3.5 kW at 87 s to simulate decay heat and injection of steam at a nominal of 20 g/s. There was an initial minor temporary increase in temperatures at some locations, but this phase was mostly steady cooling to about 900 K. The cooling phase was followed by 100 g/s water injection at 207 s. There was a period of about 40 s while the lower volume was being filled during which time the temperatures increased somewhat in the absence of significant fluid flow. The first quench occurred at the bottom of the bundle at 246 s. Quenching progressed readily toward the top (indicated by wetting of thermocouples at different elevations), and the first quench in the ballooned region occurred at 266 s. Complete quench was achieved at 293 s.

The decreased yield strength and increased ductility of claddings during the transient phase resulted in a progressive ballooning and consequent burst of all of the pressurized rods (Table 6). The first burst occurred 55 s after initiation of the transient phase at about 1154 K at rod #4. All 21 pressurized rods failed within 32 s (Fig. 10). The individual rod failures were indicated by internal pressure readings and precisely correlated with krypton peaks measured in the off-gas pipe by mass spectrometer. The Kr release indicates failure of inner and outer rod groups. The first failed rod was the inner rod #4, the last one was the peripherical rod #10. The temperature range for bursts is estimated from thermocouple readings to be between 1074 and 1169 K. Significant rod bending due to limited axial thermal expansion was observed. Due to this bending there are mechanical contacts between some rods at hottest elevations.

6. POST-TEST EXAMINATION

6.1. Visual observations

After the test, the bundle was dismounted and all rods were inspected separately. The radial burst positions of rods correspond to the hottest rod region and are directed mostly to the bundle centre (Fig. 11): bundle periphery is relative cold due to heat loss through the shroud). Several burst openings were directed not to the bundle centre due to rod internal temperature gradient. All bursts are axially located between 800 and 980 mm (Fig. 12). The measured burst lengths are between 8 (rod #4) and 33 mm (rod #12). No global blockage was formed due to the variation of the axial ballooning positions. The average linear burst opening parameters (Table 6): width 4.2 ± 2.6 mm, length: 15 ± 6 mm.

TABLE 6. QUENCH-L1: BURST PARAMETERS

Rod	Burst time, s	Interpolated burst T, K	Burst azimuthal	Burst middle	Burst width,	Burst length,	Burst area,
1	55.6	1169	45	900	–	13	–
2	57.2	1132	45	907	2.4	17	30
3	59	1118	190	968	3.0	13	25
4	55.2	1154	210	982	2.5	8	14
5	57.2	1104	270	966	12.8	24	198
6	55.2	1110	315	952	4.3	12	30
7	59.8	1074	350	953	2.8	12	20
8	58.6	1132	350	908	1.5	13	11
9	62.6	1162	45	909	7.8	20	110
10	87.6	1143	64	943	3.0	12	24
12	76.8	1092	130	807	5.6	33	126
13	73.6	1147	135	946	4.8	15	40
14	68.6	1154	156	947	3.4	11	24
15	64.4	1159	190	945	4.3	14	35
16	68.8	1156	225	946	5.0	17	42
17	67.6	1104	270	848	2.3	10	18
18	72.6	1081	316	967	2.9	11	17
19	83.6	1163	354	941	4.3	13	22
20	76	1105	20	886	4.3	25	92
21	80.6	1140	15	900	2.0	10	17
Average	–	1130 ± 30	–	–	4.2 ± 2.6	15 ± 6	–

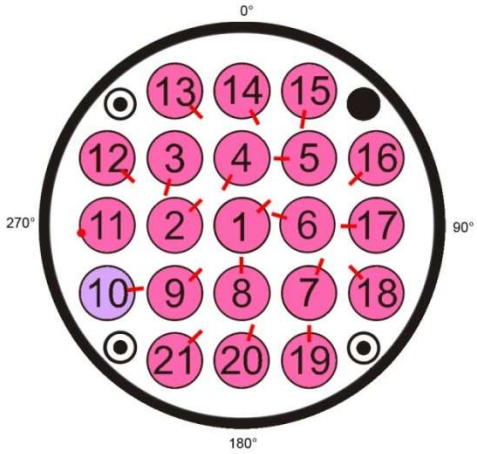

FIG. 11. Circumferential positions of bursts: predominant orientation to bundle center.

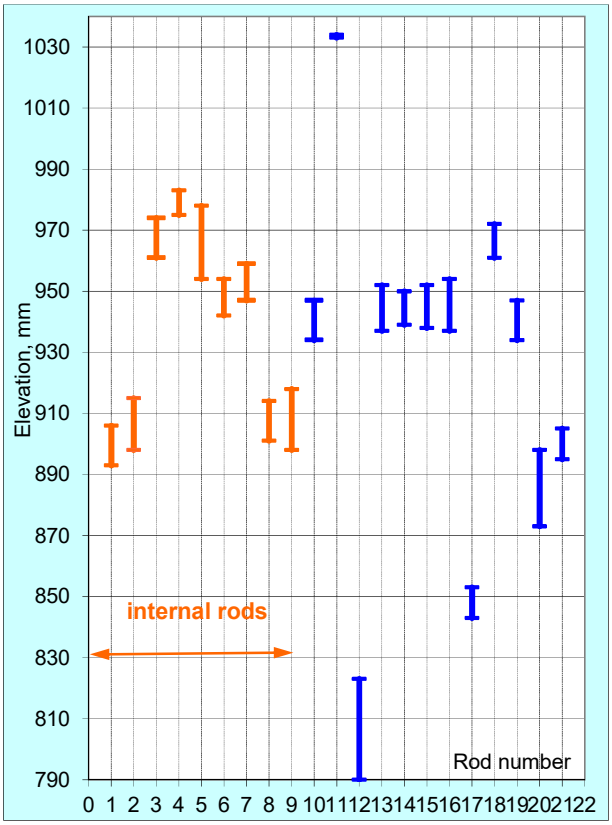

FIG. 12. Axial positions of burst openings: scattering between elevations 800 and 980 mm.

6.2. Profilometry of claddings with laser scanner

6.2.1. Linear laser scanning

The profilometry of rods was performed with a Linear Laser Scanner. It was custom built by ANT Antriebstechnik GmbH for quantifying the deformations produced on the rods as a result of the QUENCH LOCA experiments. The ballooned parts of the bundle rods submitted to LOCA scenarios acquire a variety of shapes and sizes due to different temperature conditions. Therefore a precise method to detect the local variations in diameter along the rod was required.

6.2.2. Main characteristics of the measuring device and procedures

The measuring mechanism is based upon photocells which compare the amount of laser light blocked by the rod in relation to the portion of light that reaches the sensors. The equipment is mounted vertically and supported on a wall of the experimental hall in order to minimize the effects of shocks and vibrations propagated by the floor. The rod to be measured is placed vertically and linked to a stepper motor which is responsible for the precise turning of the rod according to a given number of measurements that should be made each 360°. A resolution of 0.25° is provided. The laser scanner itself moves a predetermined length up or down the driving rails in order to cover a specific section of the examined rod. The smallest vertical step is 100 μm and the maximum length which the scanner can handle is 2000 mm.

Automatic settings allow the scanner to work for many hours without the need of supervision. On the other hand, for safety reasons and because of mechanical limitations, the data gathering is quite slow. A total of approximately 5700 points are measured each hour. This means that a scanning of a 1500 mm rod section takes roughly 4 days considering a measurement every 1 mm and 1°.

All data generated can be processed in various ways in order to determine different information. For instance, it allows the exact location and orientation of each burst, determination of radial strain, calculation of cross-section area reduction and thus blockage. Also, a digital 3D rendered image is generated as a record and for further analysis.

6.2.3. Results of the scans

The evaluation of the scans can be divided into azimuthal and longitudinal analysis. The analysis of azimuthal plots clearly shows the orientation of the bursts and also gives an idea on the not symmetrical shape of the ballooned cladding. It was revealed that the bursts were oriented mostly to the center of the bundle, mainly because of the radial thermal gradient which was established in the test section. The shape of the bursts vary widely, neither size nor symmetry have any apparent correlation to burst temperature.

Also based on these scans, the minimal and maximal diameters as well as the circumferential strains at the burst position can be determined (Table 7). The difference in the maximal and minimal diameters at the burst position is significant due to cladding deformation during burst. The maximal diameter was observed in the burst plane, the minimal one – in the perpendicular plane. It should be mentioned that immediately before the burst the situation was oppositely: the maximal diameter was measured in the plane perpendicular to the burst plane. Figure 13 illustrates this circumstance for the rod #6 (rod with more prototypical small bending). The dashed curves show middle and lowest elevation of the burst opening. The neighboring elevations lower the burst evident the maximal diameter in the plane perpendicular to the burst. It could be seen noticeable ovality of ballooned claddings with difference D_{max}-$D_{max}-D_{min} \geq 0.5$ mm at distances up to 10 mm outside of burst opening. It shows the preferable direction of the cladding extension in the plane perpendicular to burst.

The strain values at the burst elevation include the burst opening widths. There is a clear correlation of the burst mean location and the temperature distribution on the longitudinal axis. Maximum strain of 62% (not prototypical due to significant bending) was observed on the inner rod #5, minimum strain of 20% was observed on the outer rod #17. Without take into account strong bended rods, the average strain was about 30±6%.

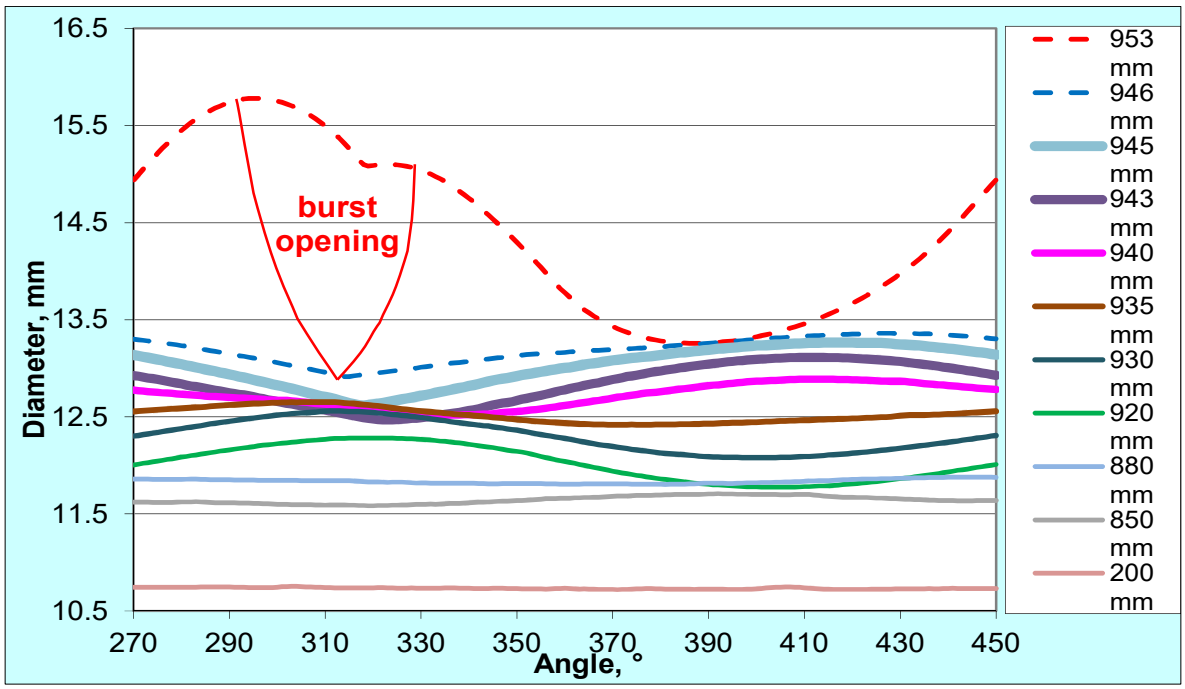

FIG. 13. Azimuthal cladding diameter variation at elevations immediately below the burst.

TABLE 7. QUENCH-L1, STRAIN PARAMETERS AT BURST MIDDLE

Rod #	Initial p, bar	Burst p, bar	Max D mm	At azimuth°	Min D mm	At azimuth°	Circumferential strain, %
2	54.5	53.8	15.2	63	11.6	146	23.7
3	54.8	52.6	16.1	154	13.8	256	36.3
4	54.8	53.9	14.7	31	13.0	124	28.9
5	54.6	53.6	18.6	226	16.0	348	61
6	55.1	54	15.8	295	13.3	208	33.9
7	54.4	55.1	14.7	143	12.5	234	24.8
8	54.3	54.2	14.5	206	12.2	270	21.3
9	54.7	54.3	16.7	257	13.2	158	40.6
10	45.5	45.7	14.7	77	12.4	157	26.1
12	55.1	55.6	15.3	82	11.6	142	27.5
13	54.4	54.9	15.4	125	12.9	51	34.1
14	54.9	54	16.4	141	13.8	245	39.3
15	54.9	54.4	15.7	205	13.2	100	34.5
16	55	54.5	15.6	243	13.1	317	34.1
17	54.2	54	13.5	257	12.4	180	20.1
18	54.5	53.5	15	306	12.8	226	28.8
19	54.5	50.7	15.3	340	13.2	258	31.5
20	55.3	54.8	16.9	249	14.6	307	44.9
21	54.7	55.5	15.2	247	12.5	187	26.7

Fig. 14 shows axial distribution of strain for the rod #4. The maximal strain at the burst position (982 mm) includes the burst opening width. This width should be subtracted from the measured cladding perimeter to obtain the maximal circumferential strain “before burst” Fig. 15 illustrates decrease of corrected strain for the rod #15, which has more prototypical smaller

rod bending. To comparison with modelling results, the averaged cladding diameter could be used, which can be recalculated from the strain. The maximal recalculated diameter for the rod #4 would be 13.87 mm (with consideration of burst opening) or 13.07 mm (corrected value after subtraction of the opening width). The last value is larger than average diameter of 12.9 mm measured immediately below and above the burst opening.

It is worth to notice that for many rods besides the main strain maximum some of the claddings have a second (or sometimes even third) strain maximum located ≈ 100 mm (or ≈ 200 mm) below or above main maximum i.e. the ballooning was initiated at many axial locations inside the hot zone before cladding was burst.

For all rods the cladding deformation starts at elevations about 250 mm and ends at 1250 mm. The part of the cladding which suffered more than 5% strain is usually smaller than 185 mm. This high strain section is not symmetrically distributed around the burst and is located with 75% on the lower levels of the burst.

The blockage is obtained by the sum of the cross-section of the rods along their lengths and subtracted from the void between bundle and shroud. Since the burst locations are scattered between elevations 800 and 980 mm, the blockage was not too significant. The maximum blockage occurs at 950 mm and reaches 24% of area reduction. If, hypothetically, all burst were located at the same level, the blockage would be 46%.

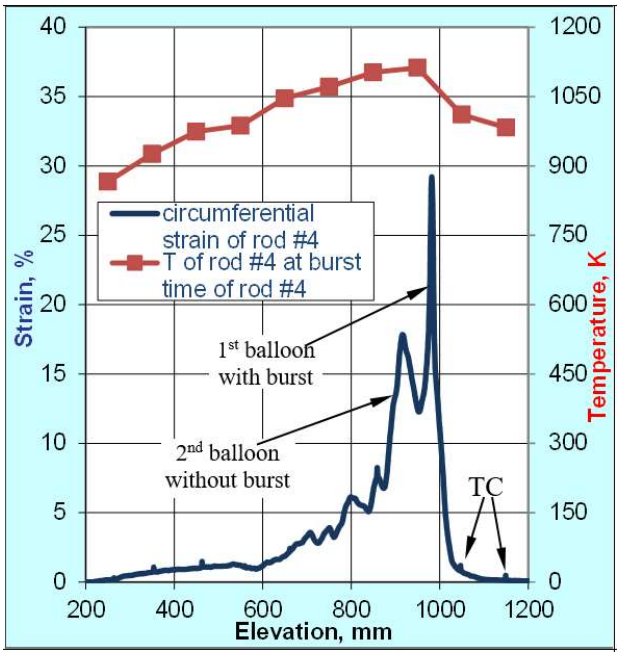

FIG. 14. QUENCH-L1, Rod #4; longitudinal circumferential strain changing.

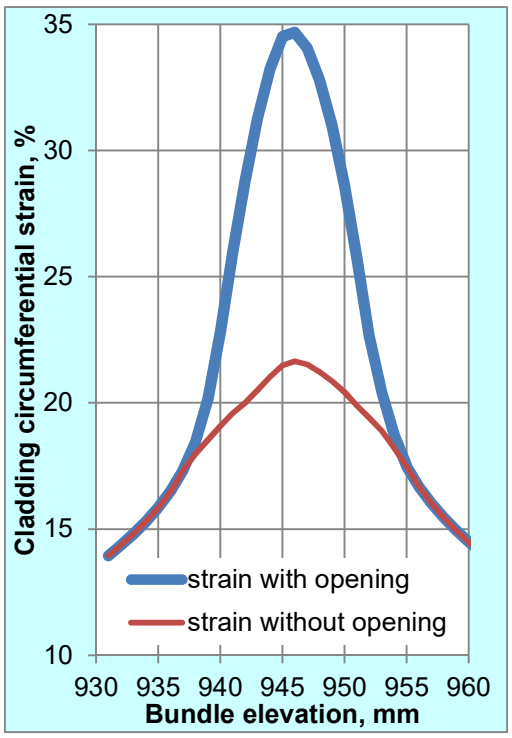

FIG. 15. QUENCH-L1, Rod #15; circumferential strain at burst.

6.3. Eddy current measurement of oxidation degree

Before cutting of cladding tubes for further investigations, the oxidation degree of each cladding was measured with the eddy current measurement device ISOSCOPE FMP30 from Helmut Fischer GmbH. The device was calibrated with two plastic foils of 24.3 and 99.3 µm thicknesses, which were disposed to the surface of as-received Zry-4 tube. At least 20 circumferential measurements at each axial position were used to achieve the averaged result. The axial step was 20 mm. The device shows distance between the gauge and internal metallic layer; i.e. the measured value corresponds to the sum of the thicknesses of ZrO_2 and α-Zr(O) layers. The comparison of eddy current results with metallographic results confirms this fact. The measurements were performed for seven inner and nine outer rods.

The measurements illustrate clearly the existence of radial temperature gradient: the inner rod group is more oxidized than the outer group of rods. This radial temperature gradient causes also azimuthal difference in oxidation of each rod: the side of cladding oriented to the central (hottest) rod is more oxidized than the cladding side oriented to shroud (Fig. 16). Irregular thickness changings were observed inside of the axial zone with the pronounced ballooning of gas loaded tubes due to deviation of cladding thickness from this parameter for the original calibration sample. The most oxidized region is between 750 and 950 mm, what corresponded to the axial temperature profile.

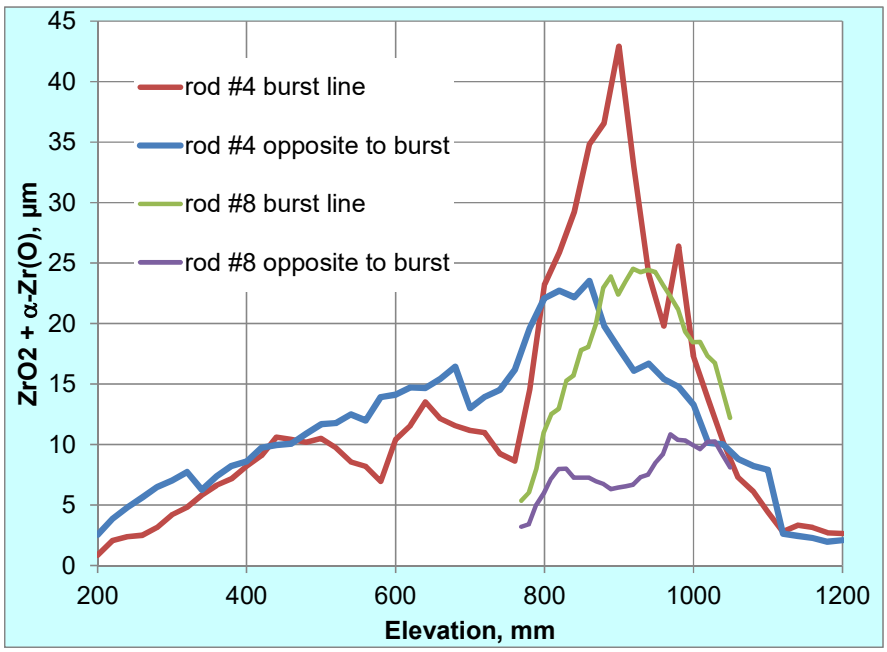

FIG. 16. QUENCH-L1: results of eddy-current measurements of axial layer thickness distribution for two opposite sides of rods #4 and #8.

6.4. Optical observation of outer cladding surfaces

First observations of burst positions were performed immediately after the test by means of the OLYMPUS videoscope. The camera of videoscope (diameter 6 mm, total cable length 9 m) was introduced through the bundle bottom at positions of withdrawn corner rods (Fig. 17).

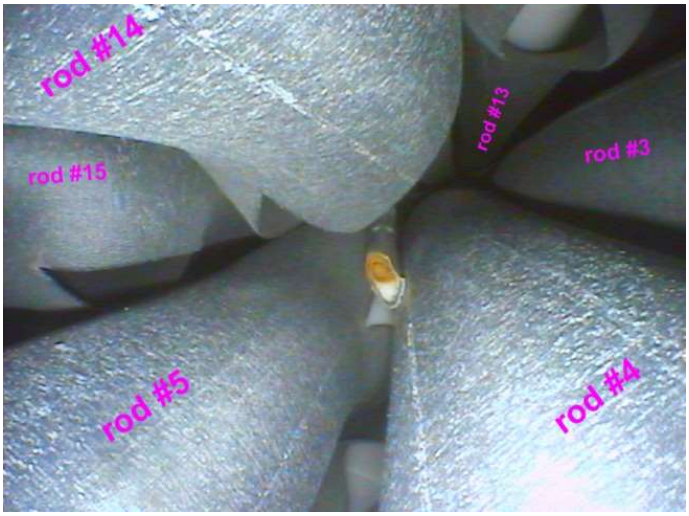

FIG. 17. Post-test bundle investigation by videoscope at position of withdrawn corner rod A, elevation 950 mm: TC TFS 4/13.

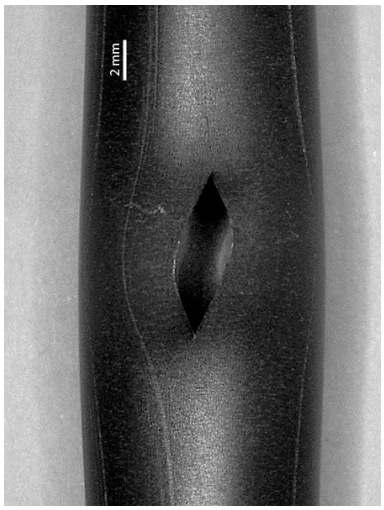

FIG. 18. Burst opening of rod #4.

Observations of cladding surface were performed with a Keyence digital microscope equipped with a macroscopic objective. The form of burst opening and the overview of oxidized cladding surface near to opening of rod #4 are shown in Fig. 18. The oxidized cladding surface is covered with a network of crossed longitudinal cracks developed during the ballooning process and penetrated the ZrO_2 and α-Zr(O) layers (Fig. 19). Large scale cells of crack network are located near to the burst opening (about 20 cracks/mm), whereas small scale cells are typical for the cladding side opposite to burst. The cell size changed not only circumferentially, but

also longitudinally: cell size decreased with increase of the distance to the burst location (about 40 cracks/mm). The cracks are disappeared practically at distances between 50 and 60 mm from the burst position – accordingly to the axial positions of sharp strain decrease. The cell size strongly depends on strain: the higher the strain the larger are the cells.

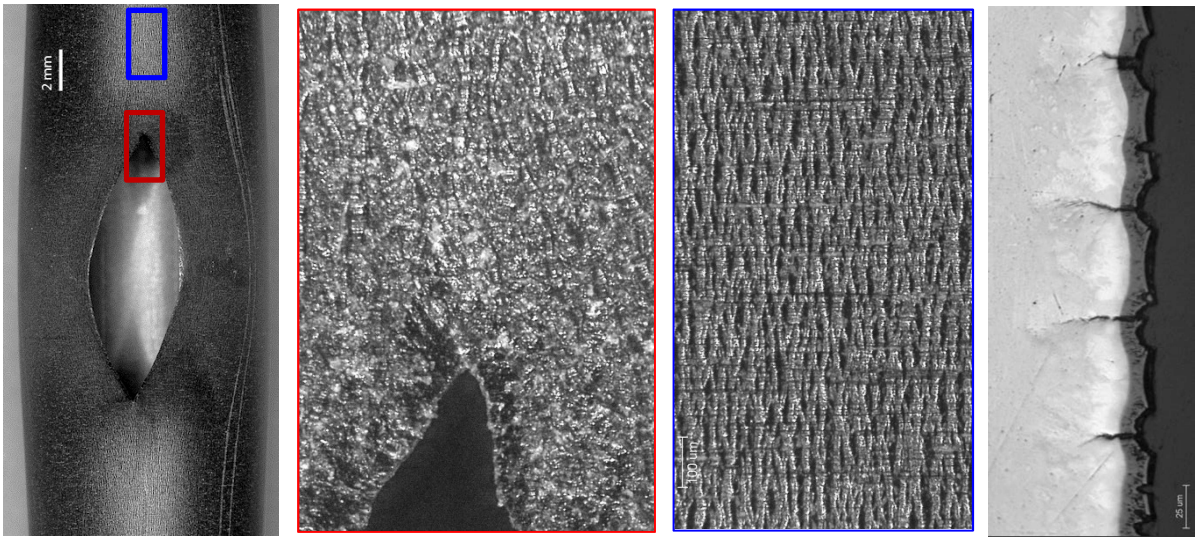

FIG. 19. Surface structure around burst opening. Burst opening of rod #19 (left): surface "bark" structures at elevations 940 (red) and 955 mm (blue). Surface cracks inside cladding of rod #5 of the QUENCH-L3 test.

6.5. Metallographic examination

The metallographic investigation of the cross cladding sections at the elevation of the burst middle evidences oxide layer growth at the outer cladding surface as well as oxidation of the inner surface. The averaged maximal outer oxide thickness of 15 µm and corresponding α-Zr(O) thickness of 16 µm were measured for inner bundle rods. The thickness of the oxide layer at inner cladding surface decreases axially. If around the burst opening the oxide layer thickness reaches 12…25 µm, only very thin oxide layer (less 3 µm) were found at distances 30…50 mm from the burst middle (Fig. 20). According to the radiography observations, the hydrogen bands were formed at these positions with very thin oxide layers.

Addition to oxidation measurements, metallography and radiography showed thinning of cladding wall thickness around burst opening. These observations were confirmed by continuous ultra sound scanning of claddings: cladding wall thinning from 725 to 350 µm due to ballooning was observed at the burst side along 50 mm below and above burst opening.

The internal cladding oxidation is caused by steam penetration through the burst opening. It can be assumed that the hydrogen, released during the oxidation of the inner cladding surface, propagated in the gap between cladding and pellet up to boundary of the inner oxidised region. Outside of this region there is no more barrier for the absorption of hydrogen by the metal, and this internally oxidised region should be surrounded by hydrided zones. This assumption was confirmed by neutron radiography.

By optical microscopy, no zirconium hydrides were detected even inside the hydride zones. Probably reasons:

— Hydrogen is partially dissolved in the metallic matrix;
— Hydrides are quite small.

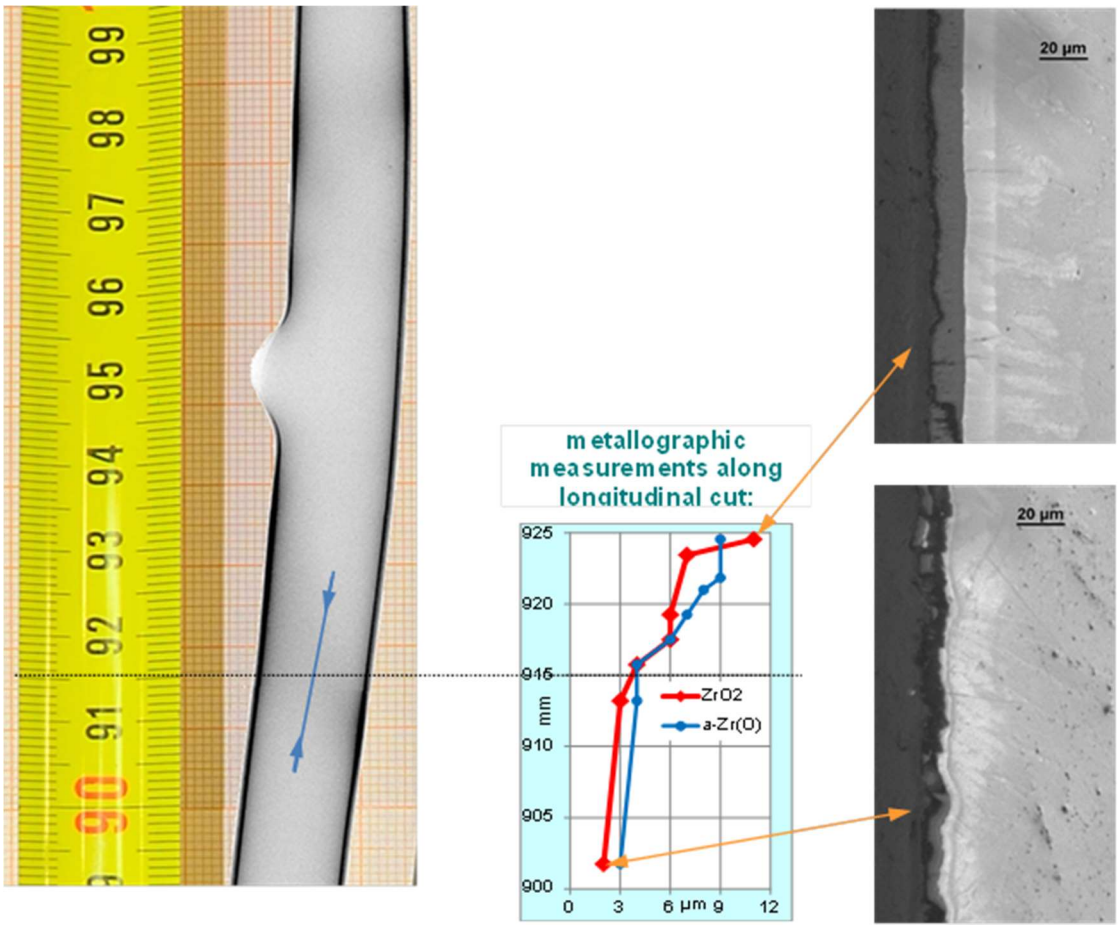

FIG. 20. QUENCH-L1; Axial distribution of inner oxidation in region of secondary hydrogenation for rod #6 at azimuth 25°: oxide layer thicknesses at the position and above hydrogen band detected by neutron radiography.

6.6. Analysis of absorbed hydrogen by means of neutron radiography and tomography

6.6.1. Basic principles

Neutron radiography is a powerful tool for the determination of hydrogen concentration and distribution in zirconium alloys [21]–[24]. Hydrogen can be quantitatively and non-destructively determined with a spatial resolution of at least 25 µm. The method was applied for the post-test hydrogen analysis of selected QUENCH-L1 cladding tubes.

Firstly, a short introduction into neutron radiography will be given. The sample is positioned into a parallel neutron beam. The intensity distribution behind the sample is measured for each pixel. From the intensity the transmission T can be calculated:

$$T(x,y) = \frac{I(x,y) - I_B(x,y)}{I_0(x,y) - I_B(x,y)} \tag{2}$$

where x and y are the coordinates of the pixel position. I, I_0 and I_B are the intensities behind and before the sample and the background intensity, respectively. From the neutron transmission the total macroscopic neutron cross section Σ_{total} can be calculated:

$$\Sigma_{total}(x,y) = \frac{-\ln(T(x,y))}{s(x,y)} \tag{3}$$

where s is the neutron path length through the material. The total macroscopic neutron cross section is the sum of the total microscopic cross section σ of the isotopes i multiplied with their number density N:

$$\Sigma_{total}(x,y) = \sum_i \sigma_i \cdot N_i = \underbrace{N_{Zry}(x,y)\overline{\sigma_{Zry}}}_{\Sigma_{sample\,as\,received}} + N_o(x,y)\sigma_o + N_H(x,y)\sigma_H \quad (4)$$

In the case of steam oxidation of cladding materials it can be assumed that only the amount of oxygen and hydrogen is changed whereas the amount of zirconium and the alloying elements is not influenced significantly.

In order to reconstruct the specimen three-dimensionally, radiography projections have to be taken from different orientations. According to the sampling theorem, the number n of projections is connected with the resolution d and the radius R of the object circle that fully encompasses the object formed by the rotating of the sample:

$$n = \sqrt{2\pi}\frac{R}{d} \quad (5)$$

6.6.2. Technique

The neutron radiography measurements were performed in two beam times at the ICON facility at the Swiss neutron source SINQ at Paul Scherrer Institute Villigen. The investigations were performed applying the so called micro-tomography setup providing the highest resolution (pixel size 13.7 µm). The field of view is 28mm×28 mm. The samples were scanned through the field of view with a step width of 20 mm. Exposure times of 300 s were applied. The specimens were measured horizontally.

The neutron tomography experiments were performed at the ConRad facility at the Berlin Neutron Scattering Centre (BENSC) of the Helmholtz Zentrum Berlin. 601 projections were measured with a pixel size of 44 µm and an illumination time of 60 s. In order to fit the detector resolution to the sampling theorem and save measurement time, the number of image pixels was reduced. 2×2 pixels were transformed into one. The specimens were investigated vertical oriented.

6.6.3. Results of radiography

The radiography measurements were performed from September 16 – 21, 2012. The investigations comprise measurements of all rods of the QUENCH-L1 test. Firstly, the calibration of the correlation between hydrogen concentration and total macroscopic neutron cross section was performed for the experimental setup applied. Calibration specimens were produced by annealing of Zry-4 cladding tube segments in argon/hydrogen atmosphere with different hydrogen partial pressures at various temperatures. The hydrogen uptake of calibration samples was determined by measurement of the weight gain. From the slope of the curve the calibration was determined:

$$\frac{H}{Zr} = \frac{\Sigma_{total} - 0.21\ cm^{-1}}{1.9541\ cm^{-1}} \quad (6)$$

Figure 21 shows the radiographs taken from internal rods. For the inner rods, not only the bended hydrogen enriched bands known from the QUENCH-L0 test were found but also hydrogen enrichments directly at the burst opening. The hydrogen enrichments are more blurred and show less contrast to the neighboring regions, compared to the bands found in rods of the QUENCH-L0 test.

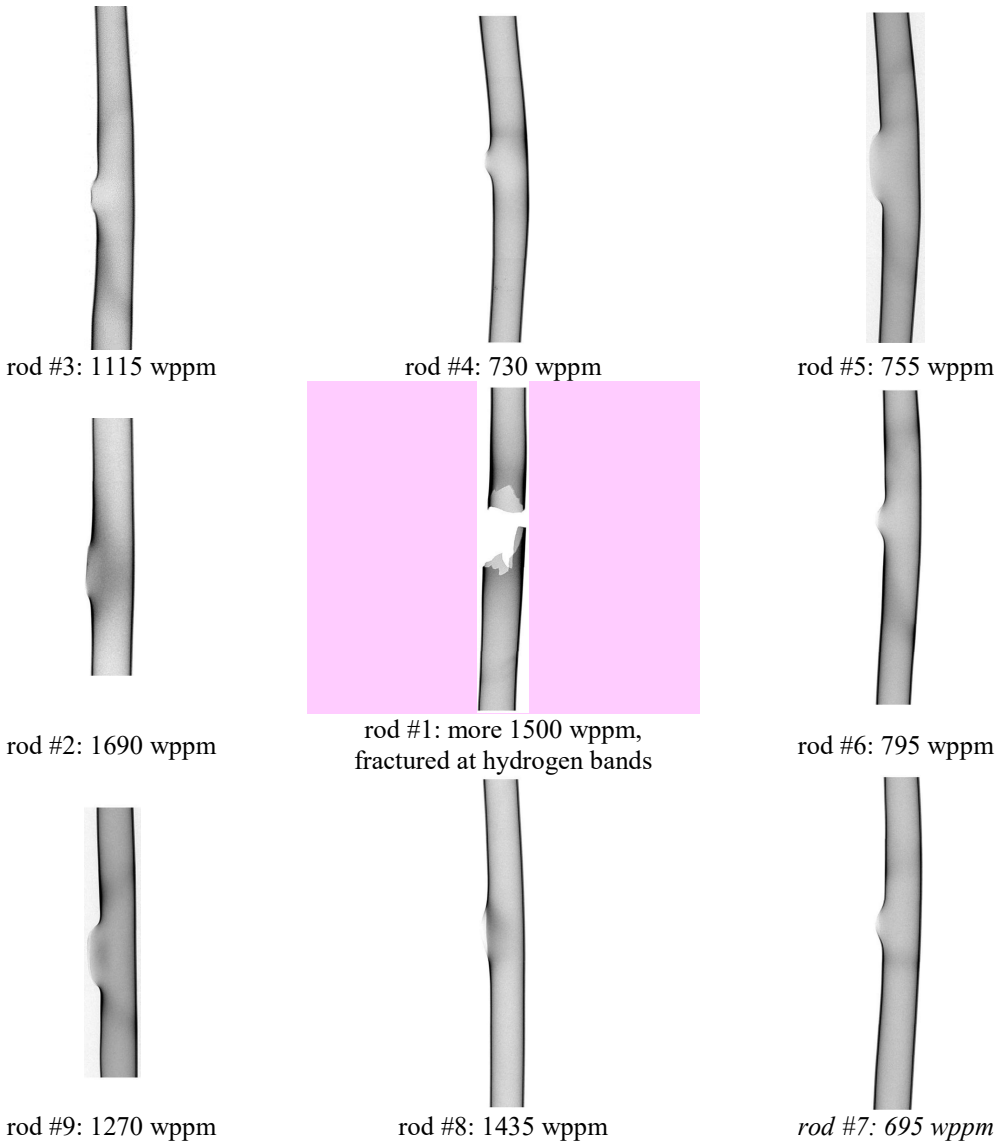

FIG. 21. QUENCH-L1; Hydrogen bands on neutron radiographs of inner rods and maximum hydrogen content.

6.6.4. Results of tomography

The tomography measurements were performed from June 18 – 22, 2013. For the experimental setup applied the following correlation was determined:

$$\frac{H}{Zr} = \frac{\Sigma_{total} - 0.2375\ cm^{-1}}{2.4914\ cm^{-1}} \tag{7}$$

The reasons for the difference between Eqs (6) and (7) are different neutron spectra of the SINQ and the Berlin research reactor and different wavelength efficiencies of the two detector systems applied at PSI and BENSC, respectively.

Figure 22 shows the results of tomography evaluation for the rod #2. On the basis of evaluation of each cladding cross section (slice with thickness of 44 μm), two curves are established: for local slice hydrogen maximum (with linear size of about 100 μm) and average slice hydrogen content.

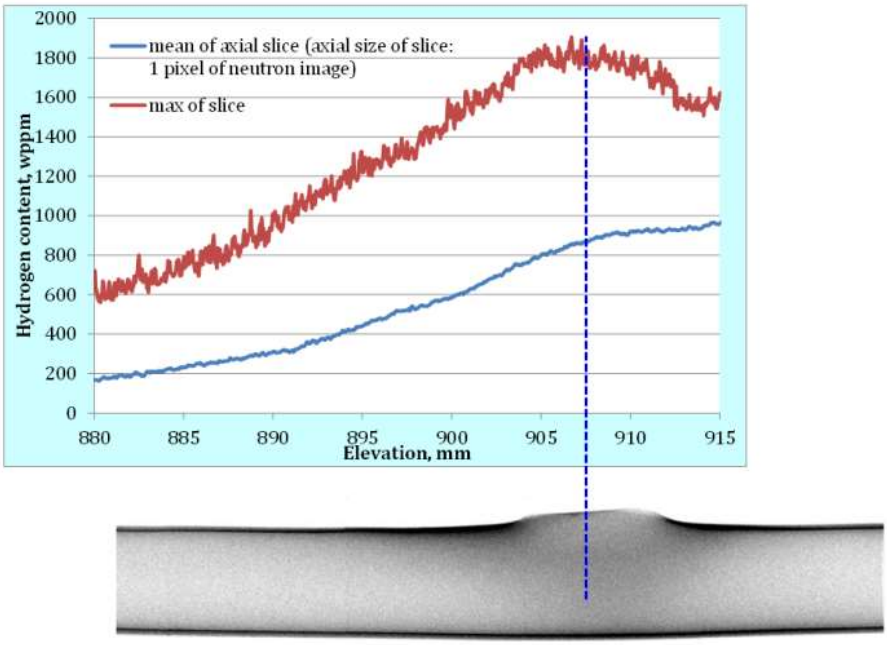

FIG. 22. Axial distribution of the hydrogen along the clad #2 (tomography results for each axial slice of 44 µm).

Table 8 gives the maximal hydrogen concentrations determined. The radiography data were determined for local area of 25×25 µm² (area of double pixel.). In contrast to the neutron imaging results obtained for the QUENCH-L0 test, no clear dependence of the hydrogen concentration and the burst time can be found. The reasons can be:

— The shorter time interval in which the burst of the inner rods of the QUENCH-L1 test occurred; and
— Different temperature histories during the cool-down phase.

However, a comparison between inner and peripheral rods of both tests gives a hint that hydrogen enrichments are formed if the temperature exceeds 1273 K.

TABLE 8. QUENCH-L1, HYDROGEN ABSORBED BY SECONDARY HYDROGENATION (RESULTS OF N^0-RADIO- AND TOMOGRAPHY)

Rod #	Radiography: Absolute local maximum, (wppm)	Tomography: Averaged for one cladding cross section (cross section thickness: 1 pixel), (wppm)
2	1800	980
3	1115	
4	730	
5	755	
6	795	
7	695	
8	1435	
9	1270	

6.6.5. Conclusions of the neutron radiography and tomography

Neutron radiography and tomography give new information about the secondary hydrogen uptake during LOCA scenarios, not yet obtained by other methods. Spatial resolutions of about 25 and about 50 µm were achieved in the radiography and the tomography

investigations, respectively. Hydrogen is distributed in sloped and bended bands in regions close to the burst position and directly at the burst opening. According to metallographic investigations, positions of hydrogen containing bands correspond to boundaries of inner oxide regions observed by the metallographic investigations. For the formation of significant hydrogen enrichments temperatures above 1273 K seem to be needed. This means that the enrichments are only formed if the tetragonal phase of the zirconium oxide is stable. According to the neutron radiography results, the maximum hydrogen concentration of about 1800 wppm was reached. The calculated average value for one cladding slice of rod #2 could be useful for comparison with results of hot extraction methodic usually performed with cut out cladding rings. However, the hydrogen absorption directly around the burst opening observed for rod #2 is not prototypical situation as was shown in later QUENCH-LOCA bundle tests performed without axial limitation of rod thermal expansion and therefore without strong rod bending [20]; usually the hydrogen will be absorbed inside declined bands above the burst opening and sometimes inside axial spots below opening. Also the mechanistic model developed by IBRAE for secondary cladding hydriding shows formation of hydrogen peaks at about 15 mm above and below burst opening under conditions of the QUENCH-LOCA-0 bundle test [25].

6.7. X-Ray diffractometry

X-ray diffractometry (XRD) analysis was applied to investigate the phases existing in the tested rods including possibly precipitated hydrides. A Seifert C3000 equipped with a Meteor 1D linear detector and a MZ4 goniometer was used. As commonly applied in this technique, a monochromatic radiation corresponding to the copper CuKα emission line was used (E = 8047 eV, λ= 0.154 nm). The objective of crystallographic diffraction was to identify crystalline components in a sample by a search/match method [26]. Since the X-ray diffraction pattern of a pure substance is very characteristic, the powder diffraction method can be used for identification and quantification of polycrystalline phases. Additionally, the areas under the peak are related to the amount of each phase present in the sample. However, the method can fail if, for instance, one of the crystalline phases is strongly texturized, the grain size of a phase is less than a few microns or if the lattice is strongly disturbed. The CIF files (Crystallographic Information File) for inorganic compounds ("Inorganic Crystal Structure Database") can be consulted at the "Fachinformationszentrum Karlsruhe" (FIZ) and also at the JCPDS files.

Each of the four samples investigated were arranged as short longitudinal sections that were axially cut out from rods #3, 4, 5 and 9 (at the hydrogen enriched zones). The X-rays reach a maximum depth of about 15 μm, so that the most important factor is a sufficient probe area which should also be flat [27]. In all of the obtained diffraction patterns solely metallic zirconium was detected. The agreement with the JCPDS card 05-0665, corresponding to pure metallic zirconium, revealed to fit almost perfectly, despite the presence of 1.5 wt% tin and the intrinsic crystallographic texture of the samples extracted from the rods. Only small and wide peak at 2Θ = 55.2° could indicate small content of ε-hydrides.

The following line shifts between the pattern obtained from the as-received specimen and the specimen from the hydrogen enriched zone were observed: 0.08° (rod #3 with 1115 wppm hydrogen), 0° (rod #4 with 730 wppm), 0.02° (rod #5 with 755 wppm) and 0.06° (rod #9 with 1270 wppm hydrogen). This indicates that hydrogen is at least partially dissolved in the α-Zr lattice. A raw estimation gives less of 300 wppm dissolved hydrogen for rod #3.

The detection limit of the applied laboratory diffractometer is about 2 vol%. A raw estimation shows that this detection limit corresponds to a hydrogen concentration less than 370 wppm for hydrogen bonded in zirconium hydrides. This is a factor of about 4 lower than the results obtained by neutron radiography. The discrepancy can be explained by 1) partial solution of hydrogen in the lattice, and/or 2) a low grain size and/or a strong lattice distortion of the hydrides.

Whereas the integral intensity of Bragg lines depends on the chemical position, the crystalline structure, the volume fraction and the texture of the phase, the width of the reflection is determined by the crystallite size and lattice distortion. According to Scherrer's formula, the line broadening due to low grain size $\Delta B \sim \lambda/L$ becomes noticeable for grain sizes less than L~100 nm. From the metallography investigations it is known that no hydrides are visible by optical microscope (visibility limit ~1 µm). Therefore, the results of both methods, XRD and metallography are consistent and give hints that the size of the hydrides, if existent, is very small. However, both methods are not appropriate in this case to deliver information on the existence, size and structure of zirconium hydrides. Therefore it is intended to apply other methods like neutron small-angle scattering of specimens loaded with deuterium and Electron Backscatter Diffraction (EBSD) to get more information on the status of hydrogen in zirconium additionally to solid solution indicated with XRD.

6.8. Mechanical tests

To determine the residual strength and ductility of QUENCH-LOCA tested claddings, particularly to identify the embrittlement in dependence of the different quench test conditions, tensile tests on relevant cladding sections were performed at room temperature. Four inner rods (#4, #6, #7, #9) and nine outer rods (#12–#19) were tested. Previously, the mechanical properties of the axially homogeneous hydrogenated Zircaloy-4 claddings were investigated in 2010 during the single rod test series [28].

6.8.1. Tensile test set-up

The tensile tests were carried out using an universal testing machine from INSTRON (type 4505, 50 kN load cell), equipped with specially developed grip holders. The experiments were performed displacement-controlled with a displacement rate of 4 mm/min at room temperature (RT). To clamp the tubes without deforming their end sections, exact fitting end plugs were mounted. Since a quench tested cladding usually shows an inhomogeneous ZrO_2/ α-Zr(O) layer thickness along the main tube axis, the specimens were optically subdivided with paint markers to determine both the global and the local axial elongation during a test by using a CCD-camera measurement system. The initial gauge length l_0 of a specimen in general was 1000 mm and a sample was prepared in that way, that the ballooning section was positioned in the axial center. To increase the resolution of the optical measurement device, two cameras were used for the tests. However, with respect to a central position of the ballooning section, particularly the specimens which revealed a strongly warped shape after the QUENCH test, had to be cut to a measuring length of 250 mm (# 4, #6, #7, #17, #18, #20) in order to replace the heating rod as well as all ceramic pellets. For these samples, only one camera was used during an experiment. The strain was calculated from the captured pictures by using the Digital Image Correlation and Tracing program provided by MATLAB [29, 30] and the stress was calculated by using average values of the measured initial inner and outer diameters from the ends of a tube.

6.8.2. Results of the tensile tests

The experiments showed that in contrast to QUENCH-L0 all tensile tested claddings failed in the centre of the burst opening by brittle fracture (compare Fig. 22). This failure behavior is caused by stress concentrations, based on discontinuities like buckles or small cross cracks at the crack edges of the burst openings. The failure due to hydrogen embrittlement was observed only for the rod #1, which was ruptured along two hydrogen bands during handling (see Fig. 23).

Compared to the QUENCH-LOCA-0 test it is as well remarkable, that almost every cladding had to be straightened at the beginning of the tensile test, since nearly all samples

revealed a more or less pronounced warped initial shape. One was observed that the most warped samples exhibit both lower strength and lower ductility at fracture. This behavior might be explained by higher superimposed tensile stresses in the region of the burst opening, resulting from the bending moment, necessary to straighten the samples. In general, the strength at fracture of the QUENCH tested cladding varies between 310…530 MPa, and the elongation at fracture varies between 0.3 and 8.3 %. Fig. 24 shows tensile test results for two QUENCH-L1 claddings as well as the influence of annealing on decrease of the yield and ultimate strengths.

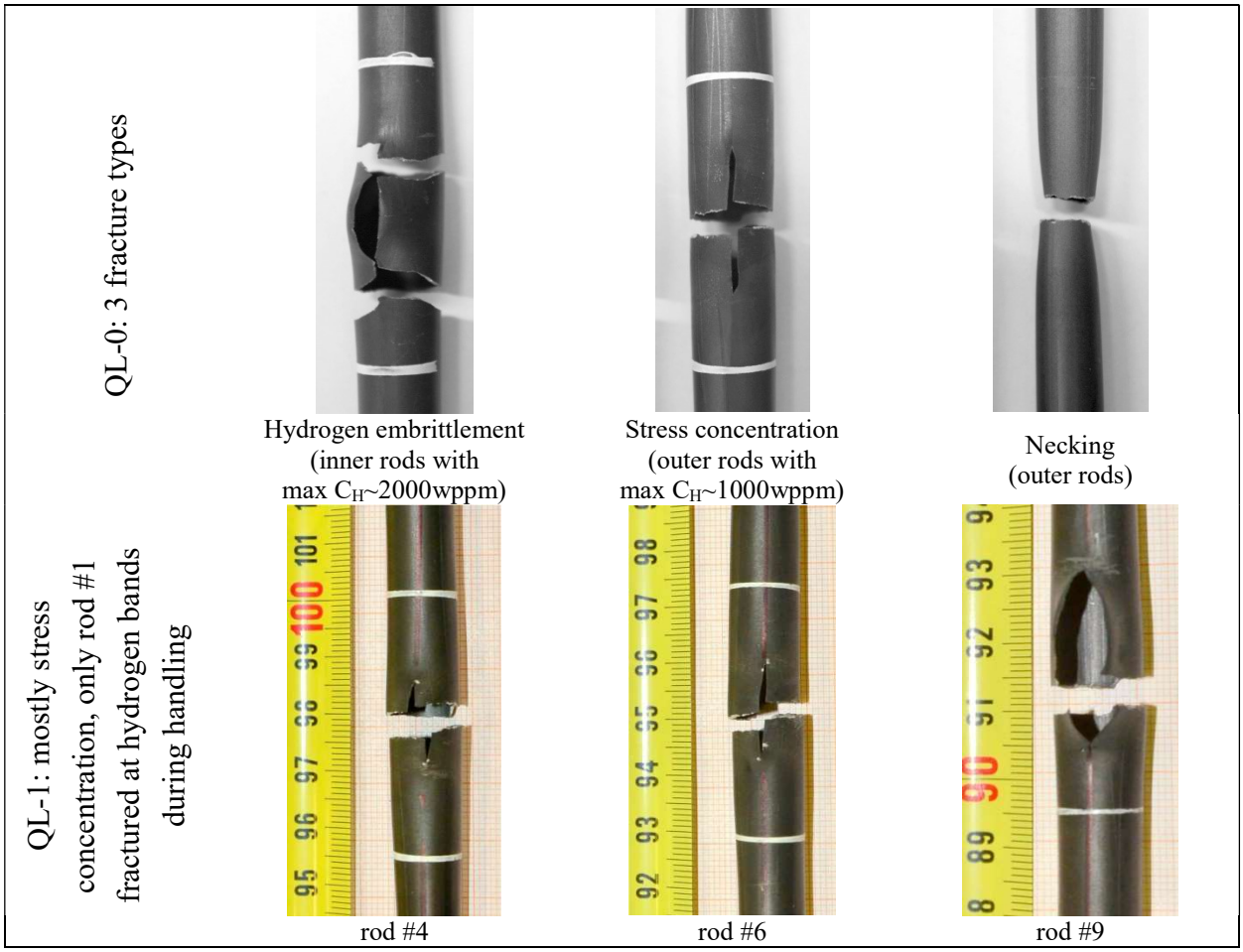

FIG. 23. QUENCH-L0 and QUENCH-L1; fracture modes, occurred in tensile tests.

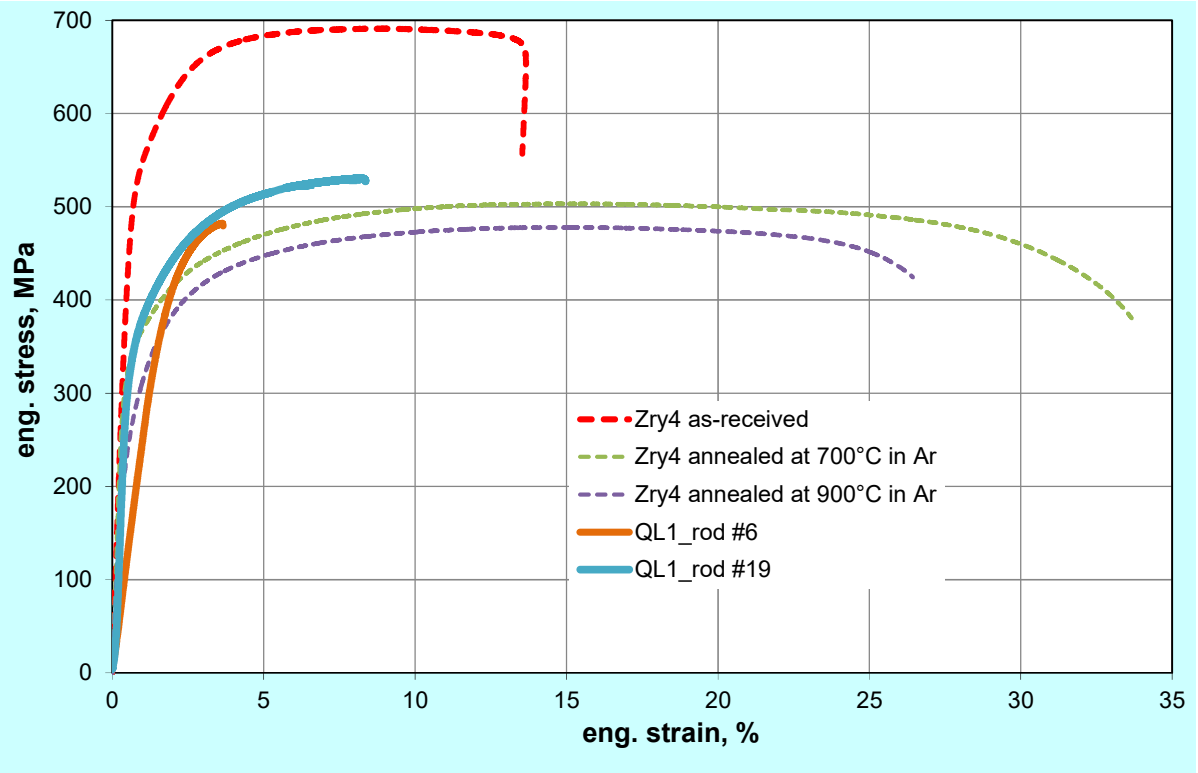

FIG. 24. Results of tensile tests at room temperature with QUENCH-LOCA-1 claddings #6 and #19 failed by stress concentration as well as as-received and annealed Zircaloy-4 claddings failed by necking.

7. SUMMARY AND CONCLUSIONS

Test QUENCH-LOCA-1 (QUENCH-L1) with electrically heated bundle (center Ta heaters inside each of 21 rods) was performed according to a temperature/time-scenario typical for a LBLOCA in a German PWR with maximal heat-up rate of 7 K/s, the cooling phase lasted 120 s and terminated with 3.3 g/s/(effective rod) water flooding. The maximal temperature of 1373 K was reached at the end of the heat-up phase at elevation 850 mm (for reference test QUENCH-L0 with lower heat up rate - at 950 mm).

According to ultra sound scanning of claddings, the cladding wall thinning from 725 to 350 µm due to ballooning was observed at the burst side along 50 mm below and above burst openings.

The cladding burst occurred at temperatures between 1074 and 1169 K with average value of 1130 ± 30 K (for QUENCH-L0 - between 1123 K and 1223 K). The inner rod pressures relief to the system pressure during less of 40 s (similar to QUENCH-L0). The average linear burst opening parameters are: width 4.2 ± 2.6 mm, length: 15 ± 6 mm. The opening sizes are quite small for release of usual pellet fragments.

Strong rod bending up to 23 mm was observed for several rods (the reason was the limited axial expansion of heaters). Without take into account strong bended rods, the average cladding strain at the burst opening was about 30 ± 6% including burst opening width (or about 20 ± 5% only for cladding perimeter without opening).

The maximum blockage ratio of cooling channel (24%) was observed at elevation 950 mm (similar blockage of QUENCH-L0 was observed at 990 mm). If, hypothetically, all burst would located at the same level, the blockage would be 46% - still enough for bundle coolability (which should be up to 90% blockage achievable according to the REBEKA tests). Similar to QUENCH-L0, the oxide layer thickness on the inner cladding surface was measured up to 25 µm at burst elevations and less 2 µm at hydrogenated bands.

No hydrogen bands around the burst openings were observed by means of neutron radiography for outer rods. Local maximum hydrogen content in cladding cross-section areas of about 25×25 μm² inside hydrogen bands of inner rods varied between 700 and 1800 wppm. It is comparable with values predicted by the SVECHA/QUENCH mechanistical code. No linear zirconium hydrides were detected, instead the hydride domains with sizes less of 30 μm were observed. Concentration of hydrogen dissolved in matrix estimated as < 300 wppm.

During quenching, following the high-temperature phase, no fragmentation of claddings was observed (residual strengths or ductility is sufficient).

During tensile tests at room temperature, all from thirteen tested claddings were fractured due to stress concentration at the burst position – similar to rods of the QUENCH-L0 bundle with hydrogen concentration < 1500 wppm. The central rod (rod #1) was destroyed brittle at the hydrogen bands during pulling out of its heater with hand.

REFERENCES

[1] U.S. ATOMIC ENERGY COMMISSION, Rule-Making Hearing, Opinion of the Commission, Docket No. RM-50-1, (28 December, 1973).

[2] HACHE G., CHUNG H. M., "The History of LOCA Embrittlement Criteria," NUREG/CP-0172, (2001) 205–237, https://www.nrc.gov/reading-rm/doc-collections/nuregs/conference/cp0172/

[3] RSK-Leitlinien für Druckwasserreaktoren. Original Version (3rd edition of 14 October 1981) with amendments of 15.11.1996.) http://www.rskonline.de/sites/default/files/reports/rsklldwr1996.pdf

[4] HOFMANN, P., RAFF. S., Verformungsverhalten von Zircaloy-4-Hüllrohren unter Schutzgas im Temperaturbereich zwischen 600 und 1200°C. Wissenschaftliche Berichte, KFK-3168, Karlsruhe, (1981). https://publikationen.bibliothek.kit.edu/270016057/3812276

[5] SCHMIDT, L., LEHNING, H., PIEL. D., Berstversuche an Zircaloy-Huellrohren unter kombinierter mechanisch-chemischer Beanspruchung (FABIOLA). In: Projekt Nukleare Sicherheit. Jahresbericht 1982. KfK-3350, S. 4200/69-4200/70, (1983). https://publikationen.bibliothek.kit.edu/270019106/3812628

[6] MARKIEWICZ, M. E., ERBACHER. F. J., Experiments on Ballooning in Pressurized and Transiently Heated Zircaloy-4 Tubes. Wissenschaftliche Berichte, KFK-4343, Karlsruhe, (1988). https://publikationen.bibliothek.kit.edu/270025905/3813281

[7] KARB, E. H., PRÜSSMANN, M., SEPOLD, L., HOFMANN, P., SCHANZ. G., LWR Fuel Rod Behavior in the FR2 ln-pile Tests Simulating the Heatup Phase of a LOCA. Final Report. Wissenschaftliche Berichte, KFK-3346, Karlsruhe, (1983). https://publikationen.bibliothek.kit.edu/270018525/3812543

[8] WIEHR, K., REBEKA-Bündelversuche Untersuchungen zur Wechselwirkung zwischen aufblähenden Zircaloyhüllen und einsetzender Kernnotkühlung. Abschlußbericht. Wissenschaftliche Berichte, KFK-4407, Karlsruhe, (1988). https://publikationen.bibliothek.kit.edu/270026029/3813291

[9] ERBACHER, F. J., NEITZEL, H. J., WIEHR. K., Cladding Deformation and Emergency Core Cooling of a Pressurized Water Reactor in a LOCA. Summary Description of the REBEKA Program. Wissenschaftliche Berichte, KFK-4781, Karlsruhe, (1990). https://publikationen.bibliothek.kit.edu/270029557/3813416

[10] ERBACHER, F. J., LEISTIKOW. S., A Review of Zircaloy Fuel Cladding Behavior in a Loss-of-Coolant Accident. Wissenschaftliche Berichte, KFK-3973, Karlsruhe, (1985). https://publikationen.bibliothek.kit.edu/270021792/3812948

[11] BRACHET, J.C., et al., Hydrogen Content, Preoxidation, and Cooling Scenario Effects on Post-Quench Microstructure and Mechanical Properties of Zircaloy-4 and M5 Alloys in LOCA Conditions. J. ASTM Intl., Vol. 5, No. 5 (2008). Available online as JAI101116 at www.astm.org.
[12] CHUTO, T., NAGASE F., AND FUKETA. T., High Temperature Oxidation of Nb-containing Zr Alloy Cladding in LOCA Conditions. Nucl. Eng. Technol., Vol.41, No.2, March 2009.
[13] CHUNG, H.M., Fuel Behavior under Loss-of-Coolant Accident Situations. Nucl. Eng. Technol. , Vol. 37 No.4, August 2005.
[14] UETSUKA, H., FURUTA T., AND KAWASAKI. S., Zircaloy-4 Cladding Embrittlement due to Inner Surface Oxidation under Simulated Loss-of-Coolant Condition. J. Nucl. Sci. Technol., 18[9], (1981) 705–717.
[15] BILLONE, M., YAN, Y., BURTSEVA, T., DAUM, R., SCOTT. H., Cladding Embrittlement During Postulated Loss-of-Coolant Accidents, NUREG/CR-6967, (2008). https://www.nrc.gov/docs/ML0821/ML082130389.pdf
[16] STUCKERT, J., GROSSE, M., RÖSSGER, C., KLIMENKOV, M., STEINBRÜCK, M., WALTER. M., QUENCH-LOCA program at KIT on secondary hydriding and results of the commissioning bundle test QUENCH-L0. Nucl. Eng. Des., Vol. 255 (2013), 185–201. DOI:10.1016/j.nucengdes.2012.10.024.
[17] NUCLEAR ENERGY AGENCY, NEA Studsvik Cladding Integrity Project – Phase 2, http://www.oecd-nea.org/jointproj/scip-2.html
[18] STUCKERT, J., GROSSE, M., RÖSSGER, C., STEINBRÜCK, M., WALTER. M., Results of the commissioning bundle test QUENCH-L0 performed under LOCA conditions. KIT Scientific Reports, KIT-SR 7571 (March 2013).
[19] GROSSE, M., STUCKERT, J., STEINBRÜCK, M., KAESTNER, A., Secondary hydriding during LOCA – Results from the QUENCH-L0 test, J. Nucl. Mater. 420 (2012) 575–582. doi:10.1016/j.jnucmat.2011.11.045.
[20] STUCKERT, J., GROSSE, M., RÖSSGER, C., STEINBRÜCK, M., WALTER, M., The QUENCH-LOCA Experimental Program. Final report. KIT Scientific Reports, KIT SR 7740 (2017).
[21] GROSSE, M., KÜHNE, G., STEINBRÜCK, M., LEHMANN, E., VONTOBEL, P., STUCKERT, J., Determination of the hydrogen uptake of steam-oxidised zirconium alloys by means of quantitative analysis of neutron radiographs. J. Phys.: Condens. Matter 20 (2008), 104263.
[22] GROSSE. M., LEHMANN. E., STEINBRUECK. M., KÜHNE. G., STUCKERT. J., Influence of oxide layer morphology on hydrogen concentration in tin and niobium containing zirconium alloys after high temperature steam oxidation. J. Nucl. Mater. Vol. 385 (2009), 339.
[23] STUCKERT. J., BIRCHLEY. J., GROSSE. M., JAECKEL. B., STEINBRÜCK. M., Experimental and calculation results of the integral reflood test QUENCH-14 with M5 cladding tubes. Ann. Nucl. Energy., 37S.1036-47, (2010). DOI:10.1016/j.anucene.2010.04.015.
[24] GROSSE, M., VAN DEN BERG, M., GOULET C., LEHMANN, E., SCHILLINGER. B., In-situ neutron radiography investigations of hydrogen diffusion and absorption in zirconium alloys. Nuclear Instruments and Methods in Physics Research Section A: Accelerators, Spectrometers, Detectors and Associated Equipment, Volume 651, Issue 1, (2011) 253–257.
[25] VESHCHUNOV, M.S., SHESTAK, V.E., Modeling of Zr alloy burst cladding internal oxidation and secondary hydriding under LOCA conditions. J. Nucl. Mater. 461 (2015)129–142. DOI: 10.1016/j.jnucmat.2015.03.006.

[26] WARREN, M.R., BHATTACHARYA. D.K., γ Zr-Hydride precipitate in irradiated massive δ Zr-Hydride. J. Nucl. Mater. 56 (1975), 121–123.
[27] PARK, Y.S., HA, Y.K., HAN, S.H., JEE, K.Y., KIM. W.H., Changes in chemical structure of oxidation reaction layers of Zircaloy-4 and Ti by micro X-ray diffractometry. Journal of Nuclear Materials 372 (2008) 59–65.
[28] STUCKERT, J., GROSSE, M., WALTER, M., Mechanical properties of pre-hydrogenated (600 – 5000 wppm) cladding segments. 16th International QUENCH-Workshop, Karlsruhe, November, ISBN 978-3-923704-74-3 (2010).
[29] EBERL, C., GIANOLA, D.S., HEMKER, K. J., Mechanical Characterization of Coatings Using Microbeam Bending and Digital Image Correlation Techniques. Experimental Mechanics, Vol. 50, Issue 1, (2010) 85–97.
[30] EBERL, C., GIANOLA, D.S., HEMKER. K.J., Mechanical Characterization of Coatings Using Microbeam Bending and Digital Image Correlation Techniques. Experimental Mechanics, Vol. 50, Issue 1, (2010) 85–97.

POST-TEST SIMULATION OF CORA TEST 15 WITH ATHLET-CD

H. AUSTREGESILO, CH. BALS, TH. HOLLANDS
Gesellschaft für Anlagen und Reaktorsicherheit (GRS) gGmbH
P.O. Box 1221, 85738 Garching, Germany
Email: Henrique.Austregesilo@grs.de

Abstract

As an in-kind contribution to the FUMAC activity, a post-test calculation of CORA Test 15 has been performed with the GRS system code ATHLET-CD, using as far as possible the same code input parameters and modeling options as for the simulation of a similar experiment, CORA-13, object of an OECD/NEA international standard problem (ISP-31). In general, for both tests a good agreement between calculated and measured data with respect to the evolution of cladding temperatures has been obtained, with a slight overestimation at the bottom and a slight underestimation at the top of the active bundle. The effect of the pressurized rods in Test 15 has been taken adequately into account by the code. The calculated rupture time, the elevation and the cladding temperatures at burst are within the experimental ranges. The hydrogen production has been calculated within the uncertainty of the measured data, with an overestimation of the generation rate for Test 15 during the phase of oxidation excursion. One main discrepancy of the calculated results is related to the missing modeling of melt retention due to the spacer grids, leading to a shift of the blockage profile and to an overestimation of the temperatures at elevations below the spacer grids.

1. INTRODUCTION

The CORA experimental program at the Karlsruhe Institute of Technology (KIT, formerly KfK - Kernforschungszentrum Karlsruhe) was conducted between 1987 and 1993 [1]. Its main objective was to investigate the integral behavior of typical light water reactors (LWR) fuel bundles under severe accident conditions. The decay heat was simulated by electrical heating. The test bundles contained all materials normally used in LWR fuel elements: pellets, cladding, grid spacers, absorber rods and guide tubes were typical to those of commercial LWRs concerning their composition and radial dimensions.

A total of 19 tests have been performed in the CORA facility. Seven of them are included in the validation matrix of the German severe accident code ATHLET-CD: 4 of 6 BWR bundle tests, 2 of 2 VVER bundle tests, but only one of eleven PWR bundle test, namely Test 13. This experiment is well documented and was applied for an OECD/NEA International Standard Problem (ISP-31) [2].

The experiment CORA-15 was conducted in a similar configuration as CORA-13 [3]. For both tests, the PWR-typical bundle consisted of 16 heated, 7 unheated and two absorber rods. The absorber material (Ag 80%, In 15%, Cd 5%) was sheathed in stainless steel and surrounded by a Zry-4 guide tube. The bundle was surrounded by a Zry-4 shroud, which in turn was surrounded by an insulating layer of ZrO_2 fiber. The general test procedure of Test 15 was also similar to CORA-13 and consisted of three main phases (Fig. 1): a gas pre-heating phase (0-3000 s), a transient heat-up phase (3000 – 4900 s) with a power increase from 6 to 27 kW and a steam flow rate of 6 g/s, and a cooling phase after 4900 s. An argon flow rate of 8 g/s was maintained during the whole test duration. The main differences with respect to Test 13 consisted in the use of pressurized rods, slightly different shroud geometry and no quenching with water during the cooling phase.

In the frame of the FUMAC activity, Test CORA-13 has been recalculated using the most recent version of the code ATHLET-CD. Afterwards, the input data set has been adapted for CORA-15 (initial and boundary conditions), using the same nodalization and as far as possible

the same modeling options. The simulation of CORA-15 has been complemented by some additional sensitivity studies concerning the cladding rupture model options.

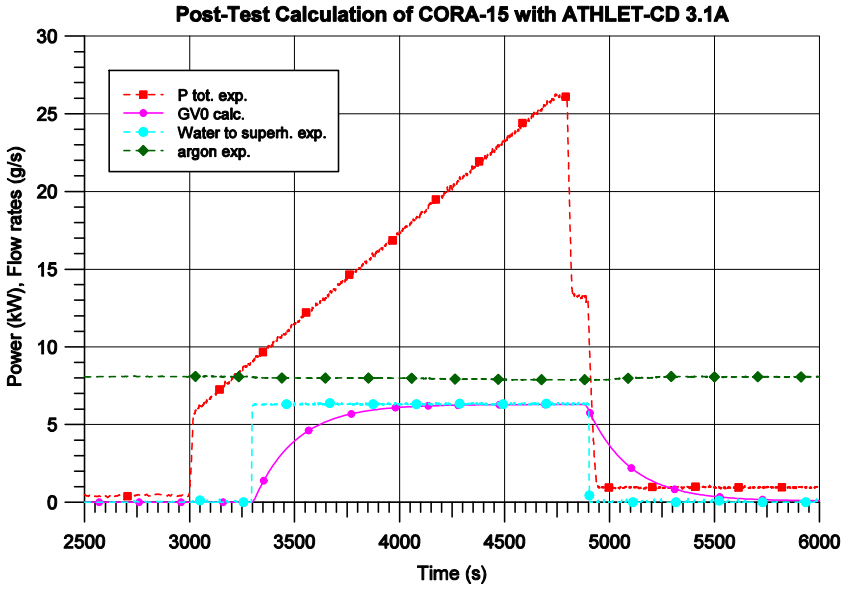

FIG. 1. Main boundary conditions for test CORA-15.

2. SHORT DESCRIPTION OF THE CODE ATHLET-CD

The system code ATHLET-CD (Analysis of THermal-hydraulics of LEaks and Transients with Core Degradation) [4] describes the reactor coolant system thermal-hydraulic response during severe accidents, including core damage progression as well as fission product and aerosol behavior, to calculate the source term for containment analyses, and to evaluate accident management measures. It is developed by GRS in cooperation with IKE, University of Stuttgart. ATHLET-CD includes also the aerosol and fission product transport code SOPHAEROS, developed by IRSN, and is coupled with the GRS code COCOSYS for modeling thermal-hydraulics and iodine behavior in the containment.

The code structure is highly modular to include a manifold spectrum of models and to offer an optimum basis for further development (Fig. 2). ATHLET-CD contains the original ATHLET models for comprehensive simulation of the thermal-hydraulics in the reactor coolant system. The ATHLET code comprises a thermo-fluid-dynamic module, a heat transfer and heat conduction module, a neutron kinetics module, a general control simulation module, and a general-purpose solver of differential equation systems called FEBE. The thermo-fluid-dynamic module is based on a six-equation model, with fully separated balance equations for liquid and vapor, complemented by mass conservation equations for up to 5 different non-condensable gases and by a boron tracking model. Alternatively, a five-equation model, with a mixture momentum equation and a full-range drift-flux formulation for the calculation of the relative velocity between phases is also available. Specific models for pumps, valves, separators, mixture level tracking, critical flow etc. are also included in ATHLET.

The rod module ECORE consists of models for fuel rods, absorber rods (AgInCd and B_4C) and for the fuel assemblies including BWR canisters and absorbers. It describes mechanical rod behavior (ballooning), Zr-alloy and B_4C oxidation (Arrhenius-type rate equations), Zr-UO_2 dissolution and melting of metallic and ceramic components. Melt relocation (candling) is simulated by rivulets with constant velocity and cross-section, starting from the node of rod failure. The models allow oxidation, freezing, re-melting, re-freezing and melt accumulation due to blockage formation. Feedback to the thermal-hydraulics considers

steam starvation and blockage formation. Besides convective heat transfer, energy can be exchanged by radiation amongst fuel rods and to surrounding core structures.

The release of fission products is modeled by rate equations or by a diffusion model within the module FIPREM. The transport and retention of fission products and aerosols in the reactor coolant system are simulated by the module SOPHAEROS. For the simulation of debris bed a specific model MEWA can be applied, with its own thermal-hydraulic equation system, coupled to the ATHLET fluid-dynamics on the outer boundaries of the debris bed. The transition of the simulation of the core zones from ECORE to MEWA depends on the degree of degradation in the zone. Finally the code also comprises late phase models for core slumping, melt pool behavior in the lower plenum and vessel failure within the module AIDA.

The code validation is based on integral tests and separate effect tests, as proposed by the CSNI validation matrices, and covers thermal-hydraulics, bundle degradation as well as release and transport of fission products and aerosols. They include out-of-pile bundle experiments performed in the CORA and in the QUENCH facility as well as in-pile experiments performed in the PHÉBUS or in the LOFT facility. The TMI-2 accident is used to assess the code for reactor applications.

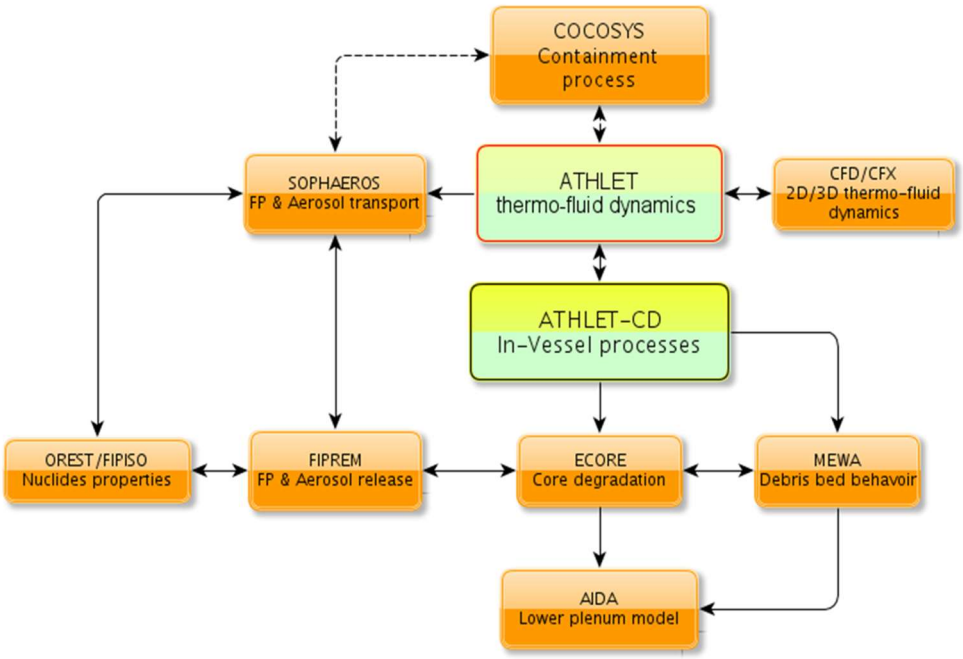

FIG. 2. Modular structure of the system code ATHLET-CD.

3. POST-TEST CALCULATIONS OF CORA PWR TESTS 13 AND 15

3.1. ATHLET-CD Input Data for the CORA facility

The input model for the CORA facility (Fig. 3) comprises among others the bundle fluid channel, composed by two parallel fluid channels connected via cross flow junctions, and subdivided into 13 axial nodes (10 nodes within the heated length). The rod bundle is simulated within the code module ECORE by four concentric rings, an inner ring (ROD1) containing the central unheated rod, a second ring containing four heated rods (ROD2), a third ring containing six unheated rods and two absorber rods (ROD3) and an outer ring with twelve heated rods (ROD4). In addition, the spacer grids, the shroud with its ZrO_2 thermal insulation, and the outer jacket with the three-layer high temperature shield have been simulated.

The argon and steam flows, as well the quenching by water in Test CORA-13 have been simulated by fill junctions at the bottom of the bundle.

For the simulation of both CORA tests, input parameters and modeling options as recommended by the code user's manual [4] have been applied. For the calculation of Zr oxidation at higher temperatures, however, the correlation of Urbanic-Heidrick has been used instead of the correlation of Prater-Courtright normally applied for the calculation of QUENCH experiments. Table 1 summarizes the main code input parameters concerning the calculation of Zr oxidation and rod melt and relocation.

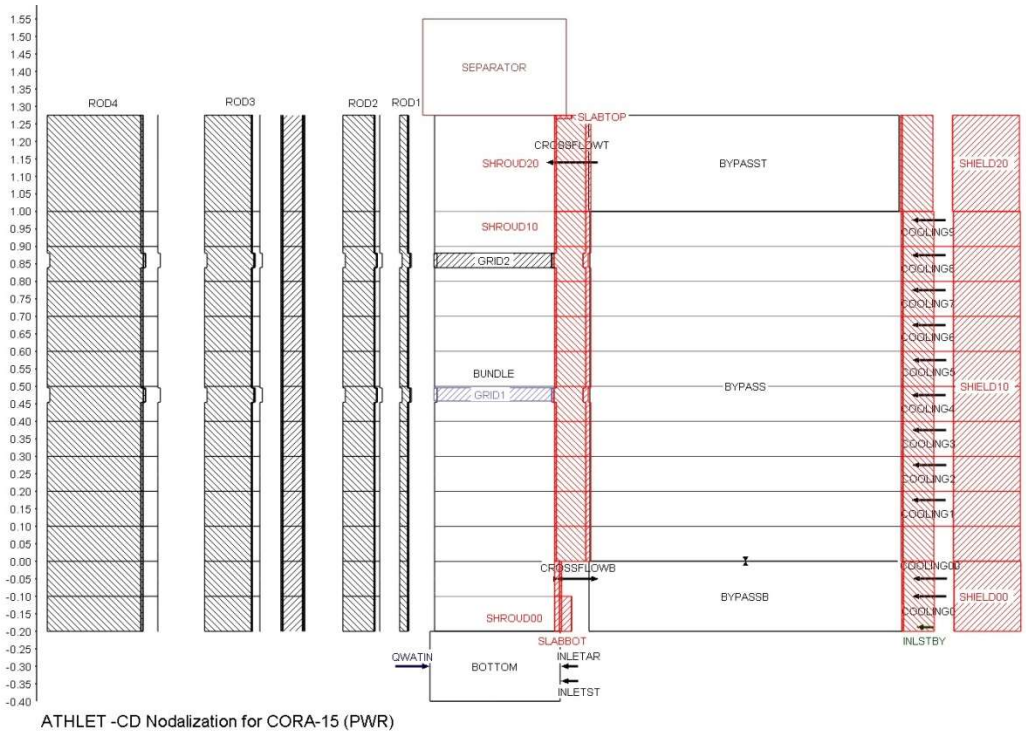

FIG. 3. ATHLET-CD nodalization for the CORA facility.

For the external resistance per heated rod, which takes into account the voltage drop across the sliding contacts at the rod extremities as well as at the wires connecting the sliding contacts to power supply, a value of 4 mΩ (3.5 mΩ for CORA-15) has been used.

The calculations have been performed using the most recent code version ATHLET-CD 3.1A.

TABLE 1. INPUT PARAMETERS AND MODELING OPTIONS

Parameter	CORA-13	CORA-15
Channel flow area (due to slightly different shroud)	0.00527 m^2	0.00460 m^2
Zr oxidation correlation	Cathcart (T < 1800 K) Urbanic-Heidrick (T > 1900 K)	Cathcart (T<1800 K) Urbanic-Heidrick (T>1900 K)
Melting temperature of metallic cladding	2200 K	2200 K
Lower clad failure temperature (low cladding oxidation)	2200 K	2200 K
Upper clad failure temperature (high cladding oxidation)	2400 K	2400 K
Minimum oxide layer thickness for upper failure temp	0.3 mm	0.3 mm
Melt relocation velocity	1 mm/s	0.5 mm/s

TABLE 1. INPUT PARAMETERS AND MODELING OPTIONS

Parameter	CORA-13	CORA-15
Maximum effective oxide layer thickness (bundle/shroud)	0.1 mm	no limit
Upper limit of relative steam availability	0.3	0.5
External resistance per heated rod	4 mΩ	3.5 mΩ

3.2. MAIN results of CORA-13 simulation

Some of the main results of the post-test calculation of Test CORA-13 are depicted in the Figs. 4 to 7. Figs. 4 and 5 show the calculated (solid lines) and measured (dashed lines) temperatures of cladding, shroud, shroud isolation and thermal shield at the elevations 350 mm and 750 mm from the bottom of the active fuel. The bundle temperatures are satisfactorily reproduced by the code. However, the cladding temperatures at the bottom of active bundle (< 150 mm) were slightly overestimated in comparison to the experiment.

As shown in Fig. 6, the total hydrogen production (blue line) was calculated within the uncertainty of the experimental data (dashed line). The contribution of the oxidation of fuel rods to the total H_2 production (about 50%) is also shown in this picture. Finally Fig. 7 compares the calculated steam/argon temperatures at elevation 750 mm with the measured ones.

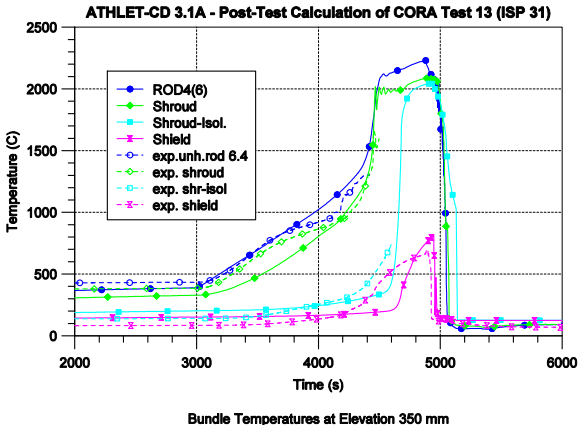

FIG. 4. Bundle temperatures at 350 mm.

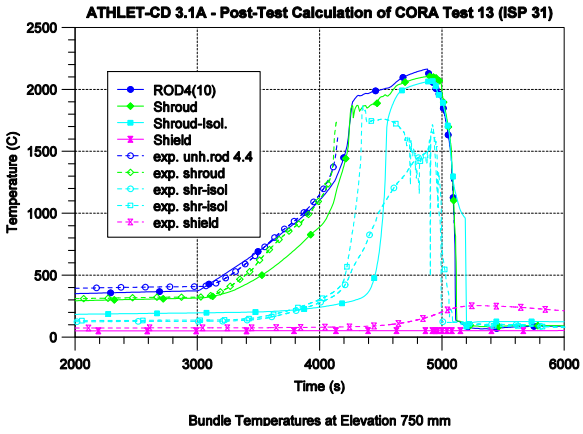

FIG. 5. Bundle temperatures at 750 mm.

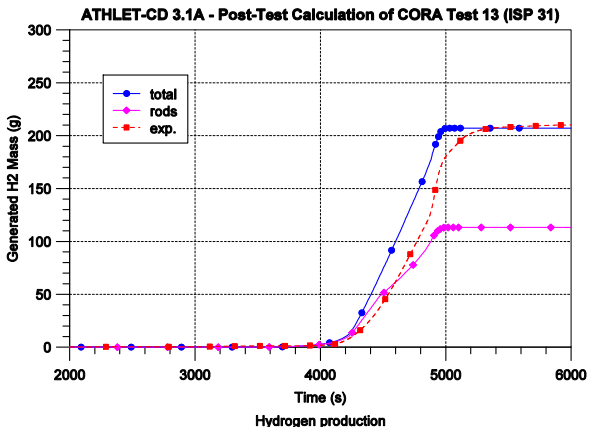

FIG. 6. Hydrogen production.

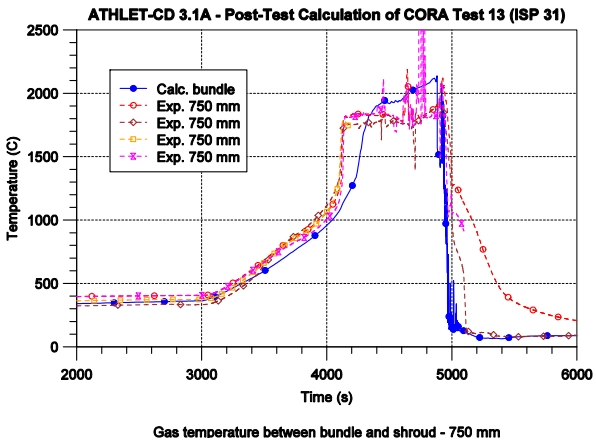

FIG. 7. Gas temperatures at 750 mm.

3.3. Main results of CORA-15 simulation

The main results of the simulation of CORA-15 with ATHLET-CD are summarized in the Figs. 8 to 13. As shown in Fig. 8, there is a satisfactory agreement between calculation and experiment concerning mechanical rod behavior, including ballooning and cladding rupture. The calculated rupture times, the rupture elevation and the corresponding cladding temperatures are within the experimental ranges. Additional sensitivity studies with the variation of the rod failure model options in ATHLET-CD yielded quite similar results. The best agreement with the experiment was achieved with the simple failure criterion based on maximum strain. A similar outcome was obtained from the simulation of the bundle test QUENCH-L0 [5], with pressurized rods with internal pressures between 35 and 55 bar.

Figures 9 to 11 depict the calculated (solid lines) and the measured (dashed lines) bundle temperatures at different axial elevations. The code overestimates the bundle temperatures at the lower bundle regions (Fig. 9) due to melt relocation below the spacer grid elevation (450 mm). At higher elevations, a good agreement between calculated and measured temperatures up to the start of melt relocation has been achieved. Since several thermocouples failed during this phase (and were probably dislocated to lower elevations), the measured temperatures in the cooling phase are questionable.

Figures 12 and 13 show the calculated hydrogen production and the corresponding generation rate, respectively. Figure 12 also depicts the contributions of cladding oxidation (about 65%) and of melt oxidation (about 3.8%) to the total H_2 generation. The code seems to overestimate the hydrogen generation rate during the bundle heat-up phase, between 4000 and 4500 sec (Fig. 13), mostly due to the shroud oxidation.

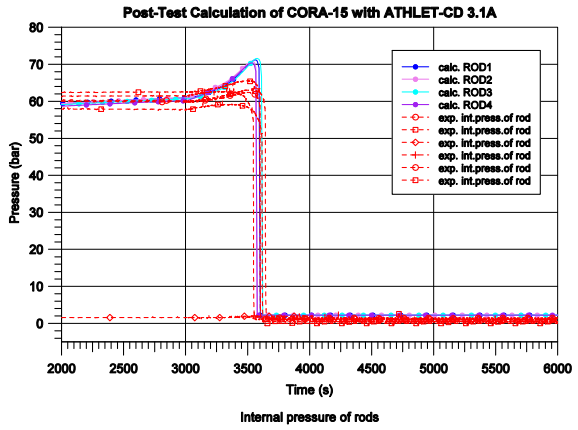

FIG. 8. Internal rod pressures.

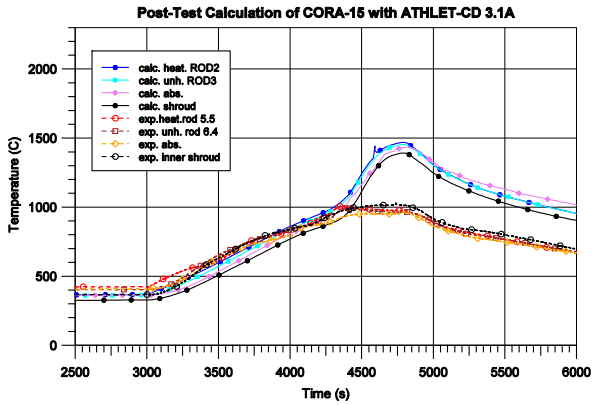

FIG. 9. Bundle temperatures at 350 mm.

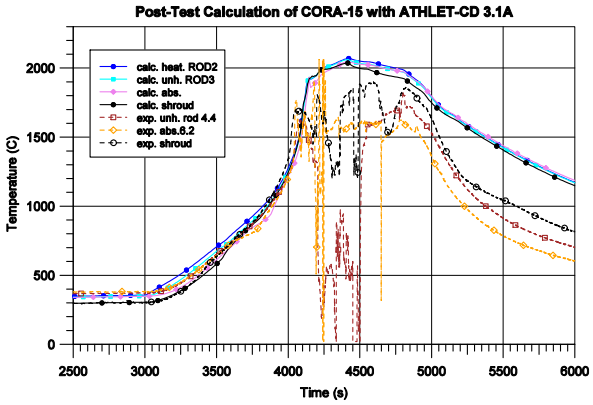

FIG. 10. Bundle temperatures at 750 mm.

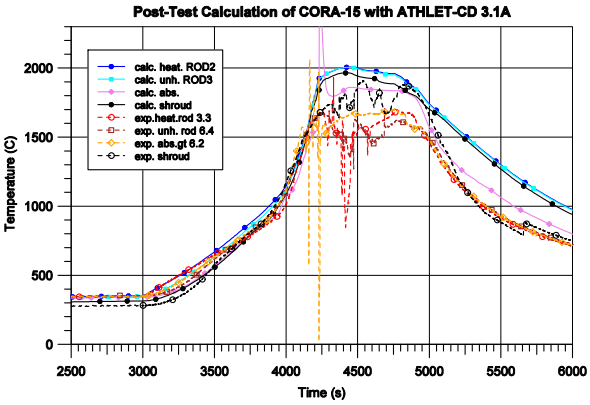

FIG. 11. Bundle temperatures Bundle temperatures at 950 mm.

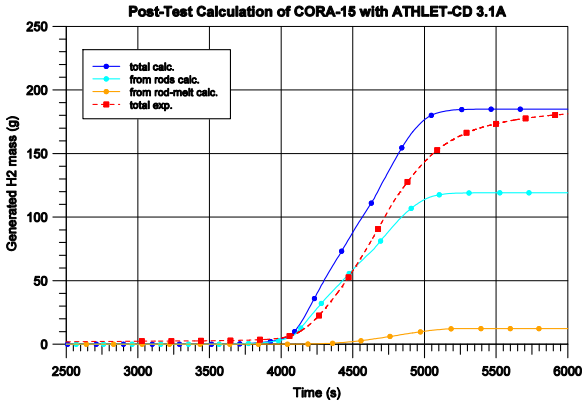

FIG. 12. Total hydrogen production.

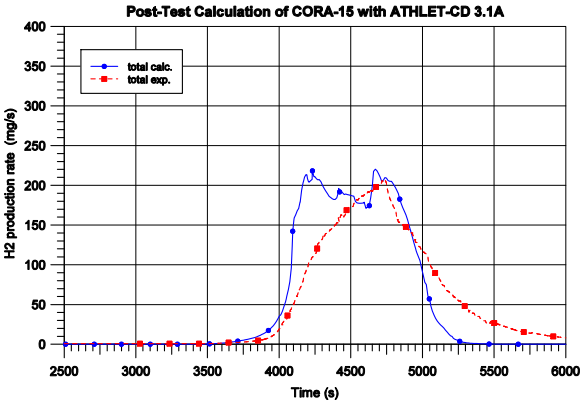

FIG. 13. Hydrogen generation rate.

4. SUMMARY AND CONCLUSIONS

The most recent ATHLET-CD code version has been applied for the simulation of the CORA Tests 13 and 15, with basically the same input data set and modeling options. In general, a good agreement between calculated and measured data with respect to the evolution of cladding temperatures has been obtained for both tests, with a slight overestimation at the bottom and a slight underestimation at the top of the active bundle.

The effect of the pressurized rods in Test 15 has been taken adequately into account by the code. The calculated rupture time, the elevation and the cladding temperatures at burst are within the experimental ranges. The hydrogen production has been calculated within the uncertainty of the measured data, with an overestimation of the generation rate for Test 15 during the phase of oxidation excursion between 4000 and 4500 s.

One main discrepancy of the calculated results is related to the lacking modeling of melt retention due to the spacer grids, leading to a shift of the blockage profile and an overestimation of the temperatures at elevations below the spacer grids in Test 15.

ACKNOWLEDGEMENT

The development and validation of ATHLET-CD are sponsored by the German Federal Ministry for Economic Affairs and Energy (BMWi)

REFERENCES

[1] HOFMANN, P. et al. Chemical-physical behaviour of light water reactor core components tested under severe reactor accident conditions in the CORA facility, Nucl. Tech. Vol. 118 (1992) 131–145.

[2] FIRNHABER, M. et al. ISP-31 – OECD/NEA-CSNI International Standard Problem No. 31 – CORA-13 Experiment on Severe Fuel Damage, GRS Report GRS-106, KfK 5287, NEA/CSNI/R(93) (1993).

[3] SEPOLD, L. et al., Behavior of AgInCd absorber material in ZRy/UO_2 fuel rod simulator bundles tested at high temperatures in the CORA facility, Forschungszentrum Karlsruhe, Report FZKA 7448, (2008).

[4] AUSTREGESILO, H. et al., ATHLET-CD 3.1A – User's Manual, GRS Report GRS-P-4/Vol. 1, (2016).

[5] HOLLANDS, T. et al., Simulation of QUENCH-L0 with ATHLET-CD, Proc. of the 17th International QUENCH Workshop, Karlsruhe (2011).

FINAL REPORT FOR THE DEVELOPMENT AND APPLICATION OF THE TRANSURANUS CODE FOR THE FUMAC PROJECT

P. VAN UFFELEN, A. SCHUBERT, J. VAN DE LAAR
European Commission, Joint Research Centre, Directorate for Nuclear Safety and Security,
Hermann-von-Helmholtz Platz 1,
D-76344 Eggenstein-Leopoldshafen
Germany
E-mail: Paul.Van-Uffelen@ec.europa.eu (corresponding author)

Abstract

This is the final report of the JRC for the fifth round robin exercise organised by the IAEA for the LWR fuel rod behaviour codes. In the wake of the accident in Fukushima in 2011, the IAEA has setup the Nuclear Safety Action Plan aiming at enhancing safety of nuclear reactor operation. As one of many contributions, a new fuel modelling co-ordinated research project Fuel Modelling under Accident Conditions (CRP FUMAC) has been launched. In the frame of the research agreement between the IAEA and JRC for FUMAC, it has been agreed to consider model development, material properties improvements and validation of the TRANSURANUS fuel performance code for assessing fuel behaviour under design basis accidents and the initial phase of severe accidents. The model improvements considered deal with cladding behaviour such as double sided oxidation, hydrogen production and uptake, and transient fission gas release. This report summarises the code changes, the results and outlines the topics for future work.

1. INTRODUCTION

This is the fifth round robin exercise organised by the IAEA for the LWR fuel rod behaviour codes, and the JRC has contributed to all of them. The last exercise was organised in 2008-2012, and included one design basis accident case representing a reactivity initiated accident and one loss of coolant accident with fresh fuel.

In the wake of the accident in Fukushima in 2011, the IAEA has setup the Nuclear Safety Action Plan aiming at enhancing safety of nuclear reactor operation. As one of many contributions, a new fuel modelling co-ordinated research project Fuel Modelling under Accident Conditions (CRP FUMAC) has been launched. It focuses on accident conditions in the light of the Fukushima accident, and is performed in close collaboration with the NEA/OECD on the joint International Fuel Performance Experimental (IFPE) database.

In the frame of the research agreement between the IAEA and JRC for FUMAC, it has been agreed to consider model development, material properties improvements and validation of the TRANSURANUS fuel performance code for assessing fuel behaviour under design basis accidents and the initial phase of severe accidents. The model improvements considered are in line with the perspectives outlined in the final report of the JRC for FUMEX-III and deal with cladding behaviour such as double sided oxidation, hydrogen production and uptake, and transient fission gas release. This report summarises the code changes, the results and outlines the topics for future work that will be discussed with the other participants during the 3rd and final RCM.

2. MAIN CODE DEVELOPMENTS AND CHANGES

The fuel rod behaviour was simulated with standard options of the TRANSURANUS code. Unless stated otherwise, all cases are run with identical models and identical parameters. The most important model improvements and changes that were implemented in the TRANSURANUS code in the course of this CRP are briefly outlined in the following.

2.1. Cladding developments

Thanks to a clearly defined mechanical and mathematical framework as well as a consistent modelling, the TRANSURANUS fuel performance code has been able to cope with normal, off-normal and accidental operating conditions right from the beginning. Despite the fact that the numerical solution techniques enable handling of non-steady-state conditions, and as such provide an ideal framework for a code to handle all conditions, some of the phenomena important for design basis accidents (DBA) were not incorporated. As a first step towards this goal, a project was launched in order to extend the TRANSURANUS code capabilities to LOCA conditions [1]. More recently, the safety criteria for DBA are being revised [2]. One of the criteria deals with the cladding oxidation and hydriding.

The zirconium – steam reaction during loss of coolant accidents (LOCA) is a remarkable phenomenon from the safety point of view, as it is highly exothermic, results in hydrogen production and considerably influences the mechanical strength of the cladding and other structural elements made of zirconium alloys. In order to control the cladding embrittlement, the temperature excursion and the hydrogen generation during design basis accidents (DBA), the current international safety standards limit the equivalent cladding reacted (ECR) between 15 % and 18 %, the peak cladding temperature (PCT) to 1200 °C and the cumulative zirconium oxidation in the core to 1 %. Therefore, the correct simulation of the high temperature oxidation of the cladding and the verification of the fulfilment of the above criteria are essential in a comprehensive safety analysis.

The high-temperature oxidation model of the TRANSURANUS fuel performance code is based on parabolic kinetic correlations for both the ZrO_2 layer thickness growth and the oxygen mass gain and on a numerical solution adequate to simulate the cladding oxidation under temperature transients. However, the inner-side oxidation of the cladding tubes due to steam inflow after rod burst is not simulated in the previous version of the TRANSURANUS code, though it may have an important role in the verification of the DBA acceptance criteria, since unoxidized metal surface and thin cladding wall at the ballooned region may result in considerably larger local oxidation rate. Furthermore, it has been suggested to impose the consideration of two-sided oxidation [3]–[5]. Therefore, the application of the TRANSURANUS code in fuel licensing analyses has necessitated the model extension for the inner-side cladding oxidation for a ruptured fuel rod. The model improvement concerns:

- The ECR computation considering additional mass gain due to inner side oxidation;
- Additional heat generation rate;
- ZrO_2 layer increase at the inner side of the cladding;
- Account for the larger reaction surface of ballooned cladding; and
- Consider the breakaway oxidation or oxide spalling (provided on input by the user).

The Zr-steam reaction in light water reactors (LWR) under accident conditions results in a heavy oxidation of the fuel rod claddings as well as an intensive hydrogen production. The formed hydrogen gas is partly released into the steam atmosphere and partly absorbed by the Zr cladding. This absorption is also an exothermic reaction and the produced heat is not negligible in comparison with the oxidation heat. Moreover, it accelerates the cladding embrittlement, which may lead to fuel rupture at the moment of core quenching. However, hydrogen uptake can also occur in a later phase of the LOCA when there is a hydrogen-rich atmosphere (i.e. under steam starvation). This means that the cladding can become brittle at an oxidation level even below 17%.

The hydrogen content must also include that absorbed during normal operating conditions. To this end, a model based on experimental data for both Zry-2 and Zry-4 hase been developed and implemented [5-7]. For DBA conditions as a first step, a simple model that describes the hydrogen absorption of Zr1%Nb cladding alloy under LOCA conditions has been developed on the basis of experimental data from MTA EK: appropriate correlations of

hydrogen solubility in Zr1%Nb and absorption kinetics are introduced for both steam oxidation and gaseous hydriding [8]. In line with the high temperature oxidation model, the content of hydrogen uptake is computed incrementally with a quasi-stationary approach. The stand-alone model has been rewritten in fortran95 and is being extended to Zry materials and is being assessed independently in collaboration with CIAE, before implementation in the TRANSURANUS code. This work has been delayed by administrative issues in Germany and China.

Finally, for transient stresses applied in the cladding (below the yield strength), fuel performance codes usually consider secondary creep, and sometimes also primary creep, using a strain hardening rule. In the one-dimensional mechanical model of the TRANSURANUS the non-elastic strain components are calculated incrementally in time. The increments of the equivalent creep are defined through a non-linear function of the equivalent stress. More precisely, this relation is described by means of a Norton power equation that actually represents secondary creep. Primary creep has been introduced in the TRANSURANUS code when developing a specific version for optimized Zirlo for Westinghouse. Nevertheless, as was pointed out recently by V. Tullki [9], modelling of primary creep in zircaloy cladding during load drop can be challenging and pointed out shortcomings of the strain hardening rule on the basis of some creep data from Halden. Tulkki suggested an alternative approach, which has been tested in the TRANSURANUS code in the frame of the FUMAC project. The current version of this non-stationary creep model works, however, without automatic time-step control and the limited amount of experimental data did not enable a proper fitting. Therefore this approach still needs further refinement. In the meantime, however, a more elaborate cladding creep model for E110 has been implemented and validated [10]–[12], which includes primary creep.

3. FUEL DEVELOPMENTS

In addition to the cladding behaviour during accident conditions, also the fuel must be considered. Specific model improvements considered for TRANSURANUS in the frame of FUMAC deal with the high burnup structure and fission gas behaviour under transient conditions.

The first model for the high burnup structure (HBS) was implemented in TRANSURANUS on the basis of EPMA data of JRC [13]. Following recent developments to describe the onset of the high burnup structure better on the basis of both local temperature and burnup values [14], more experimental data have become available at JRC for the more precise description of the hardness and Young's modulus of high burnup fuel, the HBS pore size distribution and its evolution during irradiation. The measured radial profiles suggest a close relationship between the hardness and Young's modulus, and extend the range of available data in high burnup LWR fuels. The experimental data also hint at the possibility of using micro-hardness as local probe for the variation of the Young's modulus in the pellet periphery, where direct measurements by means of acoustic microscopy are challenging [15].

As a second step towards the mechanistic modelling of the HBS in the TRANSURANUS code, a model has been developed to describe the pore size evolution in the HBS during normal operation, and the corresponding progression of the mechanical properties [16]–[19]. As a third step, a semi-empirical model has been developed to describe the formation of the HBS, which embraces the polygonisation/recrystallization process concomitant with the depletion of intra-granular fission gas. For this purpose, we performed grain-size measurements on samples at radial positions in which the restructuring was incomplete. Based on these new experimental data, we inferred an exponential reduction of the average grain size with local effective burnup, paired with a simultaneous depletion of intra-granular fission gas driven by diffusion [20].

Another important phenomenon deals with the abrupt fission gas release that can appear along with the fragmentation of the fuel at high burnup. For this purpose, two contributions

have developed for the TRANSURANUS code. The first deals with the grain boundary cracking and has been developed in collaboration with INL and POLIMI [21]–[22]. The second deals with abrupt release from the high burnup structure (HBS) during LOCA conditions [23].

The substantial release of fission gas during temperature transients (burst release) can be critical during both operational reactor transients and (design-basis) accidents. A purely diffusion-based model cannot explain the rapid kinetics of the process. Therefore a recent model for transient fission gas release in oxide fuel has been developed, considering grain-face separations or micro-cracking [24]. In fact, the micro-cracking phenomenon has been implemented in the TRANSURANUS code in two different models for fission gas behaviour, albeit in a different manner. The former model represents an empirical approach [25]–[26], whereas the latter is a more mechanistic model that couples the gaseous swelling and release consistently and has been developed in collaboration with POLIMI and INL [27].

In parallel, to the micro-cracking along the grain boundaries, an empirical model for release from the High Burnup Structure (HBS) has been implemented in the conventional fission gas treatment of the code that describes the HBS in a simplified manner [23].

In order to consolidate the transient release modelling in TRANSURANUS, both the conventional and the mechanistic models are being revisited in collaboration with INL and POLIMI [28]. The aim is to consider the transient release of the HBS pores consistently with the model for HBS evolution as mentioned above, in order to be able to reproduce the out-of-pile experiments of JRC [29], and ultimately the integral release values from in-pile experiments considered in the frame of FUMAC.

4. GENERAL CODE DEVELOPMENTS

4.1. Plenum Temperature model

The plenum temperature is an important parameter in the calculation of LWR fuel rod internal pressure, since the plenum volume contains over 40% of the total free volume in typical LWR fuel design. In many fuel performance codes the plenum temperature is, however, determined in a simple and empirical manner. There is a concern about whether such a simple method can properly reflect the temperature variation during fast transients and accident conditions. Therefore, a stand-alone COMSOL model and a two-zone model for the calculation of plenum gas temperature were developed in order to improve the accuracy of the average gas temperature and internal pressure under both steady-state and transient conditions [30] in the frame of a collaboration with NPIC, and has been implemented in the FUPAC and TRANSURANUS codes. Considering that the gas temperature near the top surface of pellets was significantly higher than that in other areas of the plenum, a two-zone model was developed and compared with a COMSOL model. In addition, the COMSOL model has been applied to design an experiment that should enable an experimental validation of the plenum temperature model at the JRC.

4.2. Extended Monte Carlo analysis

The most relevant capabilities for statistical analyses of fuel performance simulations were established in the earlier URANUS code [31]. Applying the Monte-Carlo technique, already the first versions of TRANSURANUS allowed statistical variations of a large number of input quantities to be simulated according to normal (Gaussian) distributions [32]. The corresponding code input options cover the fuel rod geometry at beginning of life, all prescribed time-dependent quantities (e.g. linear heat rate and coolant or cladding outside temperatures) as well as all material properties (e.g. thermal conductivity, creep) that are applied in the code for fuel, cladding and coolant. After 2000, these capabilities were extended by introducing additional types of input distributions (uniform, log-normal, Cauchy) and by allowing user-defined lower and upper bounds of the input quantities to be set. Typical applications to fuel used in VVER reactors were outlined in [33].

In the course of the ESSANUF project which ran in parallel with the FUMAC project, the statistics options of TRANSURANUS have been further extended to the following input quantities [5]:

- The athermal fission gas release rate;
- The effective fission gas diffusion coefficient;
- The threshold burnup for fission gas release from the high-burnup structure (hbs);
- The growth rate of the cladding oxidation layer.

First tests have been made in the frame of the FUMAC project by probabilistic simulations for IFA-650.10 as indicated below.

5. MAIN RESULTS FROM THE SIMULATIONS

During the first research co-ordination meeting in Karlsruhe, it has been agreed to consider for the code benchmark both representative separate-effect cladding tests from MTA-EK, in-pile and out-of-pile single-rod tests from the OECD Halden reactor project and Studsvik respectively, as well as out-of-pile bundle tests from KIT. In addition, it had been agreed to consider also an uncertainty/sensitivity analysis, and the list of output variables for the comparison of the different codes had been established as well.

At the second research co-ordination meeting, it has been agreed to limit the uncertainty analysis to one single case (IFA-650.10), and to carry out a second series of calculations for IFA-650.10 and IFA-650.11 with imposed boundary conditions obtained from IBRAE by means of the SOCRAT code.

The JRC has carried out all cases suggested, except for IFA-650.9 (including axial relocation and dispersal of fuel) and CORA-15 (including loss of fuel rod geometry due to melting) because these exceptional cases cannot be handled by the TRANSURANUS fuel rod performance code. Furthermore, the case IFA650.2 had been analysed successfully in the previous code benchmark FUMEX-III [34] and is therefore not included here for the sake of conciseness.

In the following sections, we provide an overview of the main results from the TRANSURANUS code in order to corroborate our conclusions and perspectives for future work. The more detailed results will be provided separately in electronic form to the IAEA in order to prepare the common final technical document for FUMAC.

5.1. Simulation of MTA-EK single rods effects case

As first set of experimental data for FUMAC, we have considered the out-of-pile single rod separate-effect tests under conditions that are representative for loss of coolant conditions as indicated in Table 1.The experiments considered short cladding tubes (outer diameter= 10.73 mm, length=50 mm) submitted to a linear increasing pressure at constant temperature until rupture occurred. The participants from the FUMAC CRP have agreed to carry out a selected number of these isothermal ballooning tests (at high pressure increase rate), which are marked in the table as well. Nevertheless, the JRC has simulated all cases provided. The comparison of the predicted burst times versus measured values is shown in Fig. 1.

The online measured temperature and internal gas pressure have been provided on input to the TRANSURANUS code. It should be pointed out that in cases 1, 11 and 20 the pressure increase has been extrapolated linearly in order to ensure clad failure at the end of the experiment.

TABLE 1. SUMMARY OF EXPERIMENTAL CONDITIONS AND RESULTS FOR SINGLE ROD BALLOONING TESTS UNDER LOCA CONDITIONS CARRIED OUT AT MTA EK

No.	T	p	time	dp/dt
	°C	(bar)	(s)	(bar/s)
1	1201.3	3.41	531.9	0.0064
2	1154.4	3.7	566	0.0065
3	1102.1	3.83	607.8	0.0063
4	1053.2	4.38	705.3	0.0062
5	997.9	5.02	810.7	0.0062
6	950.5	8.73	1805.4	0.0048
7	952.9	15.8	208.2	0.0759
8*	1001	8.9	116.7	0.0763
9	1051.6	7.45	104.7	0.0712
10*	1102.6	6.53	92	0.071
11	1149.8	6.03	84.1	0.0717
12*	1197.7	5.78	80	0.0723
13	698.8	88.83	2828	0.0314
14	702.2	106.16	892.4	0.119
15	802.1	63.18	538.4	0.1173
16	750.3	83.06	678.5	0.1224
17	850.1	39.79	342.3	0.1162
18*	900.2	26.89	233.7	0.1151
19	900.6	19.51	801.3	0.0243
20	849.7	27.22	1211.1	0.0225
21	800.8	45.3	2693.3	0.0168
22	749.9	60.8	4105.1	0.0148
23	748.6	72.58	1011.8	0.0717
24	698.8	80.75	4522.2	0.0179
25	698.3	79.78	4623.5	0.0173
26*	698.4	106.05	888.8	0.1193
27	801.4	48.18	1946	0.0248
28	800	52.94	1244.7	0.0425
29	799.9	57.95	804.5	0.072
30*	800.4	72.51	275.7	0.263
31	800.4	67.88	346.2	0.1961

The cases indicated with an asterisk (*) have been selected for the FUMAC CRP.

The comparison of the predicted versus the measured times of burst for all cases is depicted in Fig. 1. The TRANSURANUS predictions have been made with two different failure criteria: iclfail =1 corresponds to the tangential stress criterion, whereas iclfail=4 corresponds to a combination of the stress and the tangential strain failure limit (40% engineering strain).

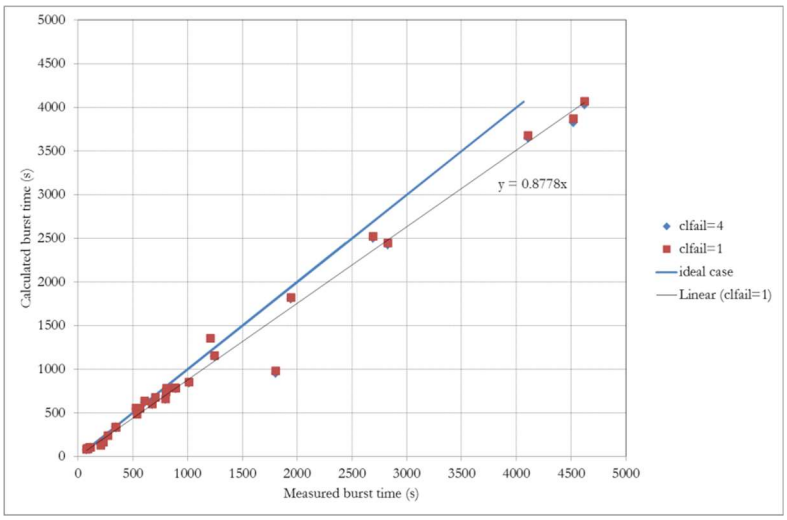

FIG. 1. Summary of the predicted time to burst (s) by means of TRANSURANUS (with two options for clad failure, see text) versus the measured values for the isothermal ballooning tests of MTA EK.

The results are in line with previous simulations of similar clad ballooning experiments [1, 35, 36]. Considering the range of experimental parameters, it is thus fair to conclude that the predictions of time to cladding failure for these additional cases are slightly conservative but satisfactory. Also the reduction of the burst time as a function of the temperature is well reproduced, as illustrated in Fig. 2. The cladding failure criterion has only a small influence on the predicted time to burst because the ballooning that leads to burst occurs suddenly and very rapidly. What is much more affected, hence subject to much larger uncertainty, is the strain after failure. Nevertheless, it should be underlined that the scatter of both the measured and predicted cladding strains is far more important. It has already been pointed out in previous papers that such strains should be considered very carefully since they may exceed the range of acceptability of the models that rely on the small strain approximation. Finally, it should also be mentioned that the strains obtained from out-of-pile bundle tests (e.g. QUENCH-LOCA tests) are typically smaller than those observed in single rod experiments, which has been attributed in part to the azimuthal temperature gradient along the cladding by Erbacher et al. [37].

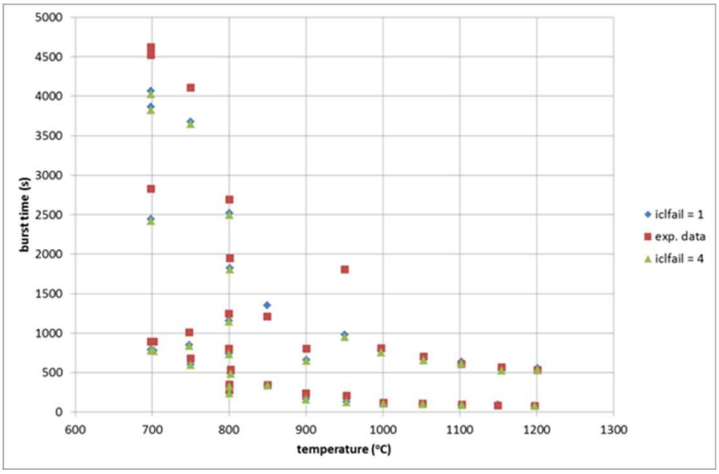

FIG. 2. Measured burst times (s) compared with values calculated by means of the TRANSURANUS code with two clad failure criteria (iclfail=1, iclfail=4) as a function of the test temperature (°C).

5.2. Simulation of QUENCH LOCA case L1

Four fuel rod simulators from the QUENCH-L1 test were considered for simulation. Their selection was made based on:

— Their position in the test bundle (internal group rod 4 and rod 7 and external group rod 14 and rod 19); and
— On the basis of the thermocouple (TC) instrumentation (see Table 8 from Reference [38]).

The TRANSURANUS code enables to simulate experiments without fuel, thus only the cladding by using the ifall = 1 option for the analysis of a cladding burst test. This option has been selected in view of the particular experimental setup with electrical heating and isolating pellets in QUENCH-LOCA, together with the on-line internal gas pressure control. The internal gas pressure has therefore also been provided on input via the input variable WERT(21) in accordance with the experimental values provided in the excel table, albeit in a simplified form as shown in Fig. 3.

Another aspect of the simulations regards the outer cladding temperature. It was set equal to the coolant temperature by means of option ialpha = 2. Therefore, the coolant temperature was prescribed via the input variable WERT (9), the values used being the experimental data for each analysed rod.

According to [38], the deformation starts at elevations about 250 mm and ends at 1250 mm for all rods. In view of this, the TRANSURANUS results were obtained for this portion from each rod. More precisely, the fuel rod simulated by TRANSURANUS started at an elevation of 100 mm and was divided in 13 equal axial slices up to a maximum elevation of 1400 mm.

All the analysed fuel rods were internally pressurized at around 55 bar (see Fig. 3) and the coolant pressure was averaged between the pressure measured at the test section inlet and outlet.

The results obtained with TRANSURANUS code are briefly presented by comparison with the experimental measurements. The burst parameters, as burst time and burst elevation, can be seen in Table 2.

TABLE 2. QUENCH-LOCA L1 BURST PARAMETERS

Rod Number	Burst time, s		Burst T, K		Burst elevation, mm	
	Exp	TU	Exp (interpolated)	TU	Exp	TU
4	55.2	63.2	1154	1145	978±4	950±50
7	59.8	76.0	1074	1147	953±6	850±50
14	68.6	82.9	1154	1150	945±7	950±50
19	83.6	85.8	1163	1152	941±7	850±50

Despite a slight systematic over-prediction by the code, measured and calculated burst times are in reasonable agreement both in absolute terms as well as in terms of the trends observed, when taking into consideration several factors:

— There is a spread on the axial temperature profiles (see for example Figs. 40-42 in [38]);
— There is a radial temperature gradient in the bundle [38];
— The observed bending of the fuel rods (related to azimuthal temperature variations) is not simulated by the TRANSURANUS fuel rod performance code;
— The observed clad ballooning is not symmetric, although the fuel rod performance code treats an axisymmetric problem that is typical for a so-called 1.5D code.

In order to assess the effect of some known uncertainties, a few additional calculations have been carried out. More precisely, we have assessed the impact of a ±10% spread on the

cladding temperatures as illustrated in Fig. 4, corresponding to the order of magnitude indicated in Figs 41-42 of [38].

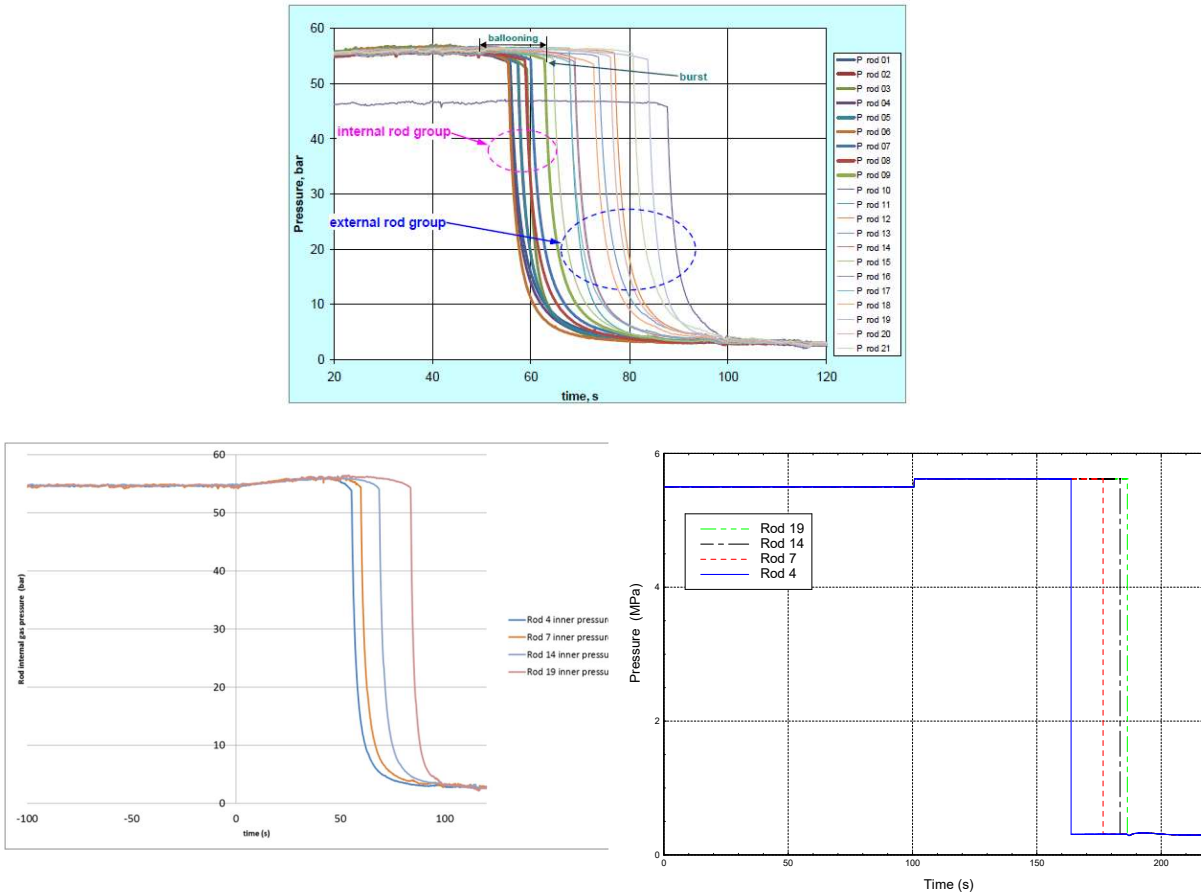

FIG. 3. Internal rod pressure evolutions: measured (left) and calculated (right).

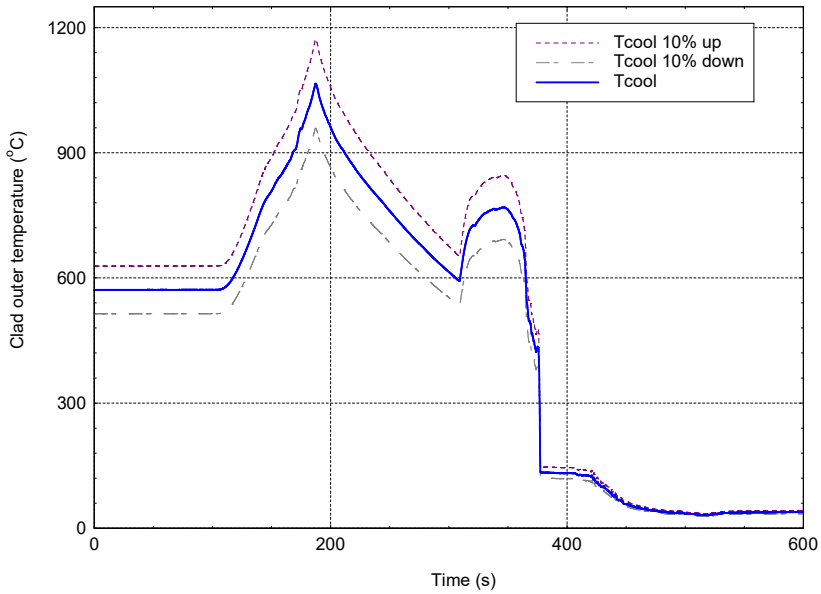

FIG. 4. Clad outer temperature of rod 4 at an axial elevation of 950 mm from the bottom of the fuel rod as a function of time.

The effect of the coolant temperature variations of 10% on the burst time shown in Fig. 5 is consistent with the spread of the burst time observed in the internal rod group in Fig. 3 underlining the strong impact of the coolant temperature on the burst time.

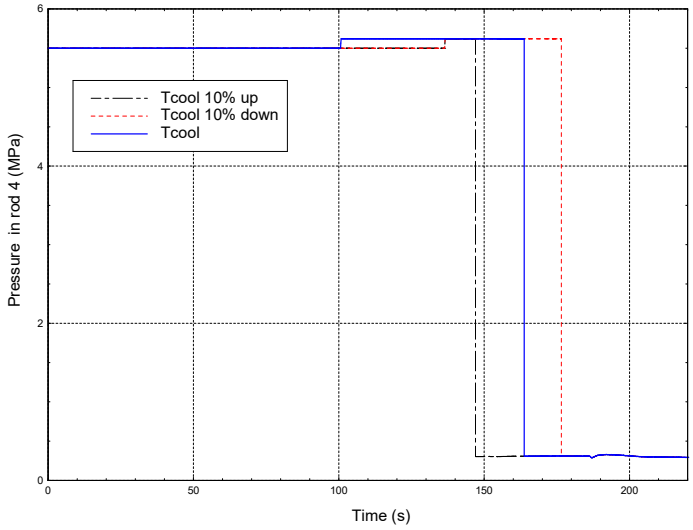

FIG. 5. Effect of coolant temperature on inner burst time in rod 4.

The axial distributions of the tangential strains calculated with the code at the end of the experiment are depicted below along with the measurements. In general there is a strong correlation between the burst mean location and the temperature distribution along the longitudinal axis, and there is a large uncertainty on the strains because of the instability associated with the ballooning and burst.

The results are reasonable and quite encouraging, but again we have made some parametric study for a more complete analysis of the outcome. More precisely we have tested for Rod 4 the impact of (see Fig. 6).

- The rupture criterion: iclfail = 1, 2, 3 or 4 (standard);
- The large strain versus small strain approximation (standard);
- The coolant temperature : 10% variation as used above; and
- The corrosion model : baker-just (nr 49) versus cathcart-pawel (nr 41, standard).

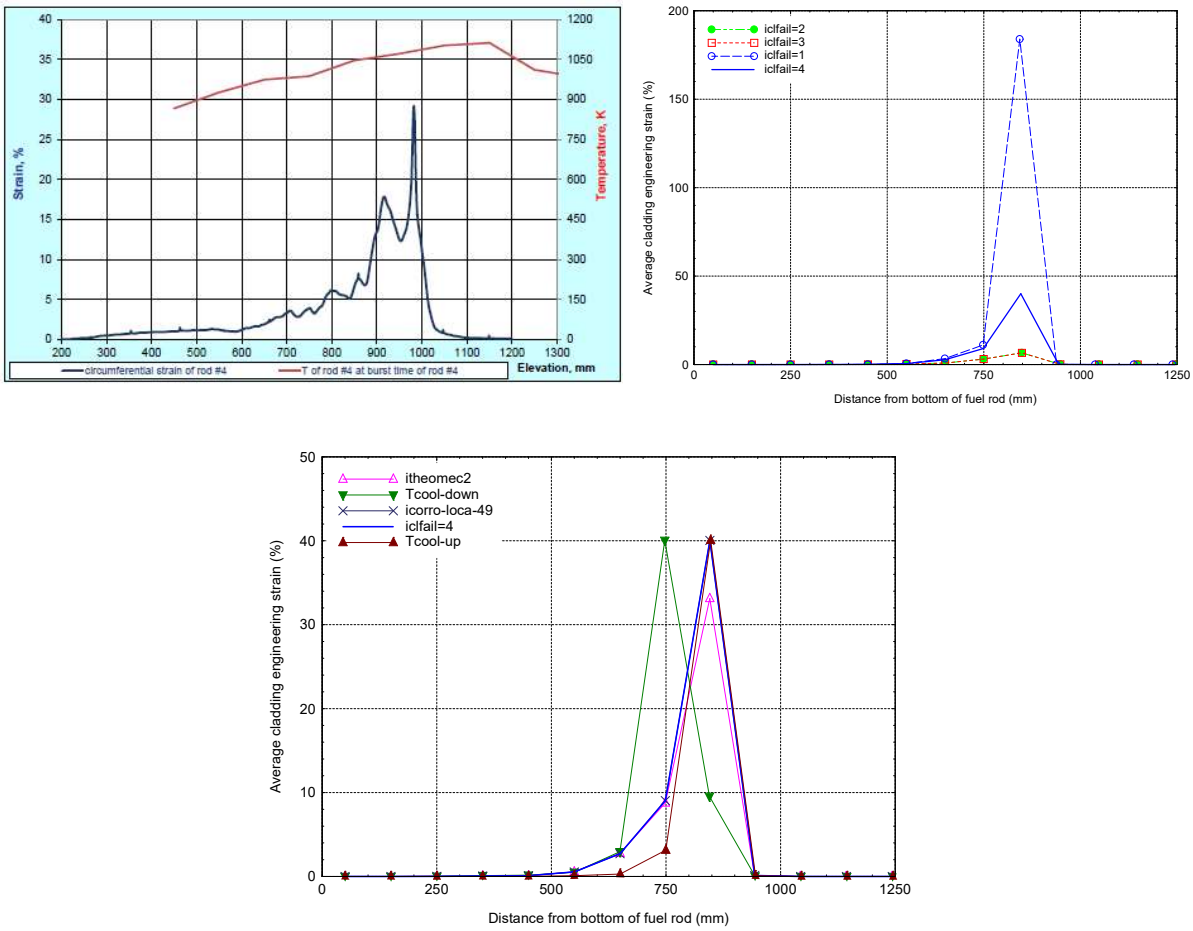

FIG. 6. Comparison between measurements (Upper left) and TRANSURANUS predictions for circumferential strain as a function of axial position at the end of the experiment for rod #4, including a parametric study.

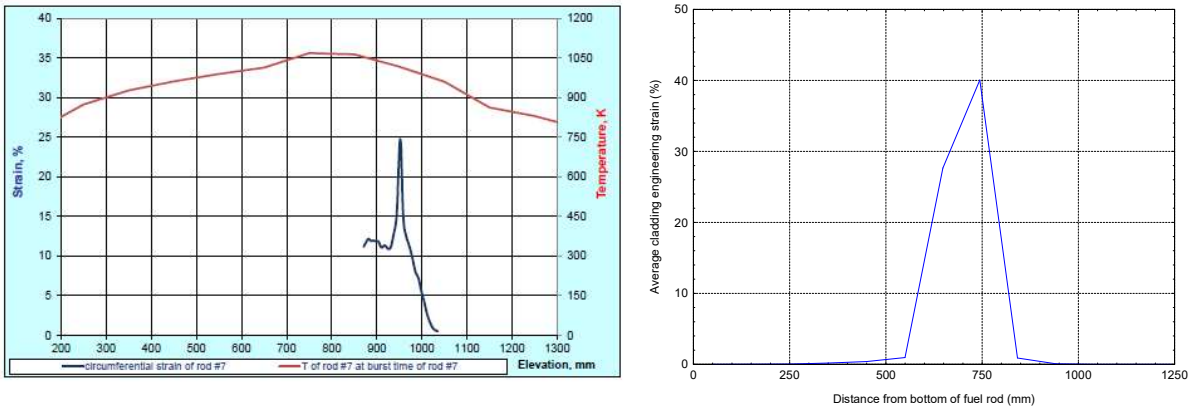

FIG. 7. Comparison between measurements (left) and TRANSURANUS predictions for circumferential strain as a function of axial position at the end of the experiment for rod #7.

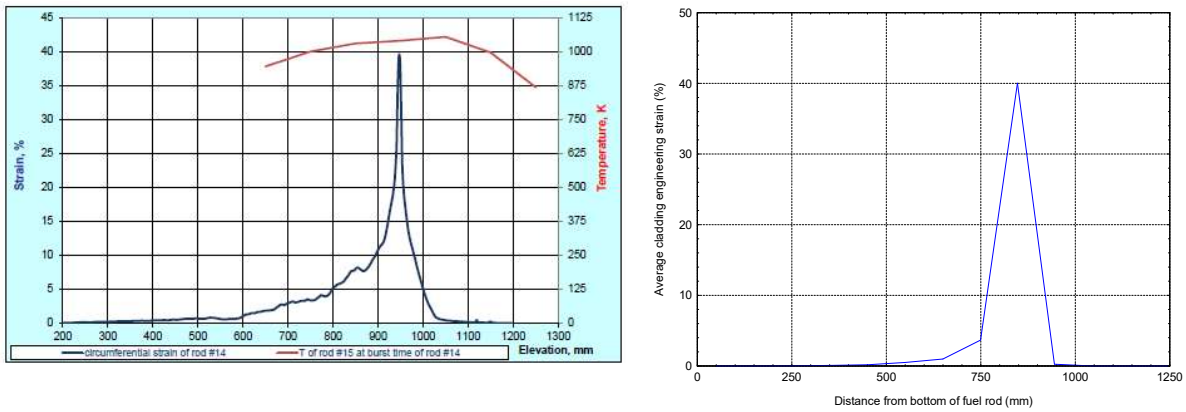

FIG. 8. Comparison between measurements (left) and TRANSURANUS predictions for circumferential strain as a function of axial position at the end of the experiment for rod #14.

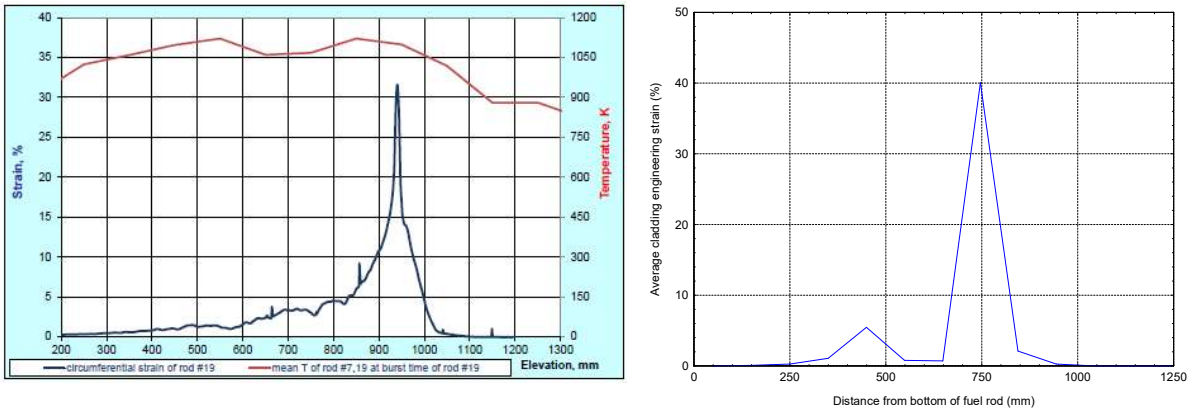

FIG. 9. Comparison between measurements (left) and TRANSURANUS predictions for circumferential strain as a function of axial position at the end of the experiment for rod #19.

It should be pointed out in Fig. 9, that the double bump in the permanent tangential deformation is directly resulting from the cladding temperature axial profile evolution.

Regarding the oxidation degree of cladding, the TRANSURANUS predictions illustrated in Fig. 10, show that the internal rod group (rod #4, rod #7) is more oxidized than the outer group of rods (rod #14, rod #19) as observed in the experiment because of the radial coolant temperature profile in the bundle. Taking into account that the values obtained with the TRANSURANUS code for the oxidized layer thickness are only for the ZrO_2 while the experimental values represent a sum of the thickness of ZrO_2 and α–Zr(O), and the large experimental scatter, it is fair to conclude that the values obtained with the code are close to the measured values of ZrO_2.

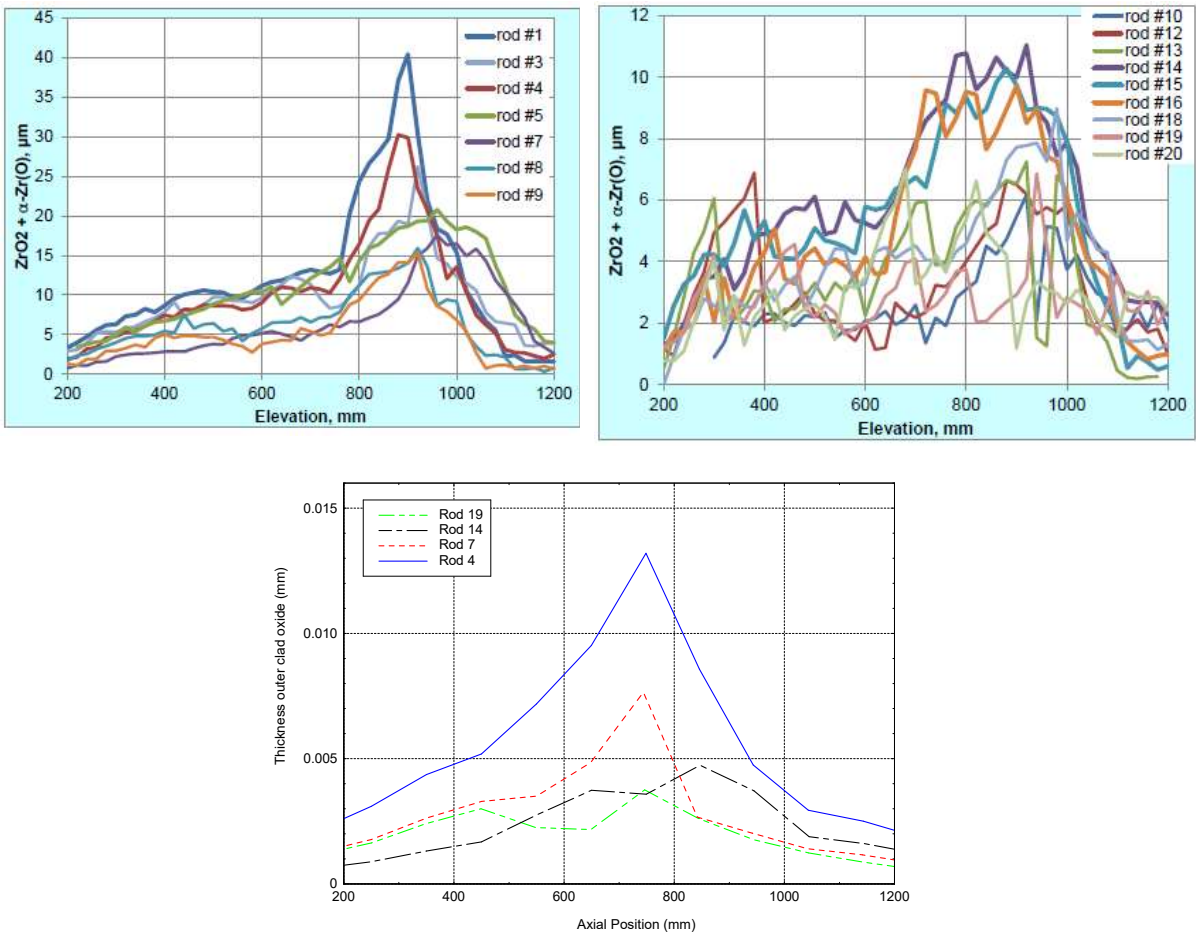

FIG. 10. Axial oxide layer thickness profiles after the experiment predicted by TRANSURANUS.

As a conclusion, the code results are in a reasonable agreement with the measurements regarding the studied parameters.

5.3. Simulation of the Studsvik cases 192 and 198

The two rodlets under consideration are modelled by means of TRANSURANUS as fuel rod segments as follows. The outer diameter of the rodlets is inferred from the pre-test profilometry and the given oxide layer thickness to consider cladding creep during base irradiation. However, given the lack of information about the latter, only the LOCA test could be performed with fresh fuel and Zircaloy (opt ZIRLO properties are confidential and results are not shown here for the sake of conciseness).

The upper and lower plenum are not modelled as usual with one single volume because of the pipes, plugs and adapters attached to the rodlets as indicated in Fig. 11. Instead of a plenum, the void volume of the pipes, plugs and adapters are modelled as fuel-free cladding with the appropriate diameters and lengths in order to model the changing temperatures of the void volumes as good as possible.

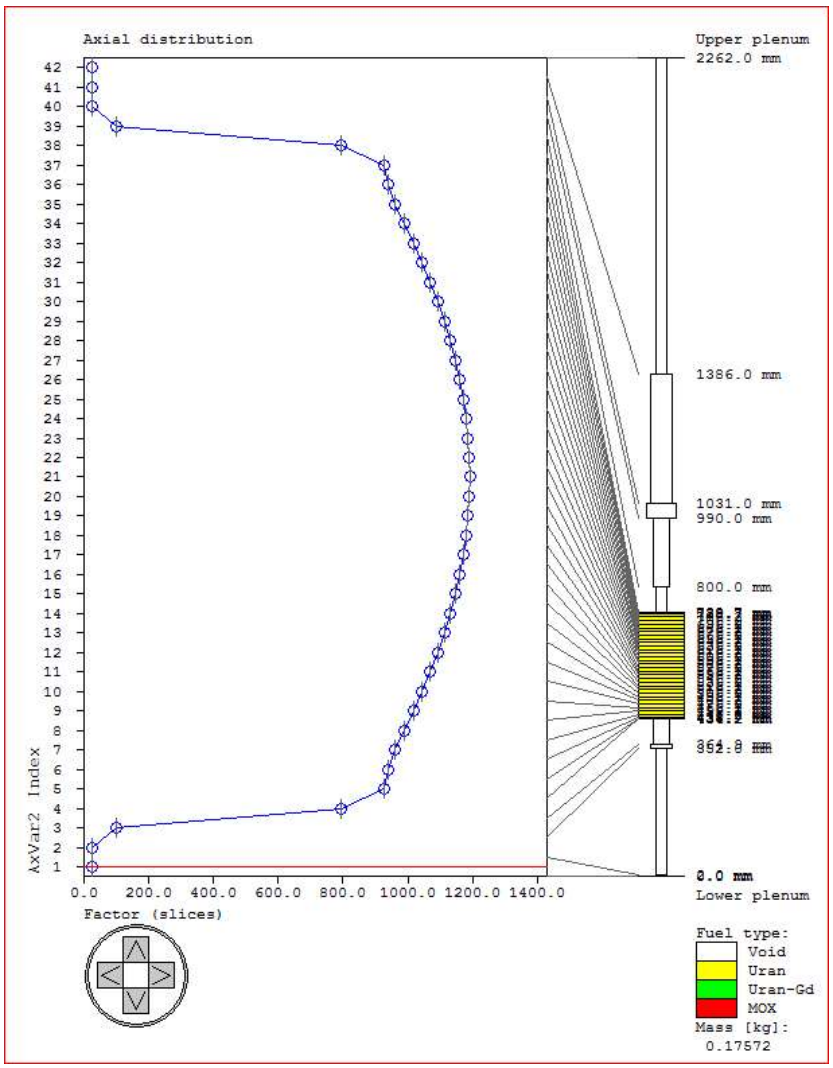

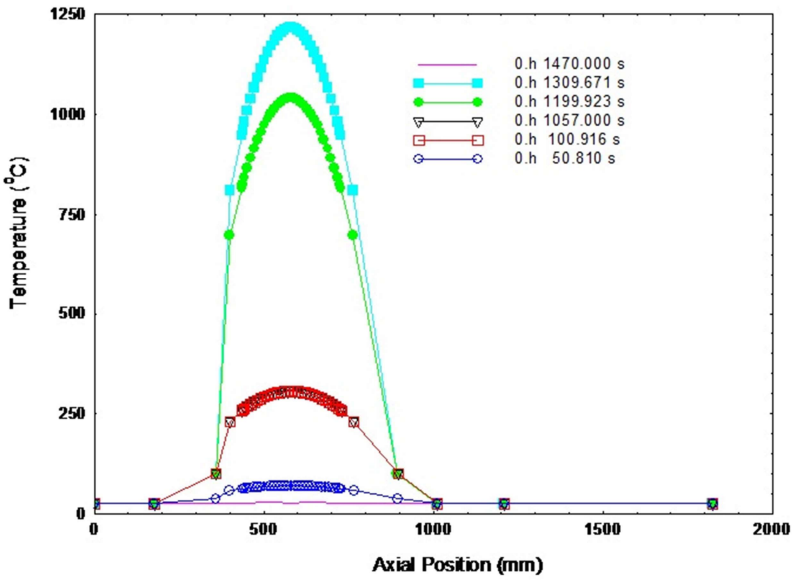

FIG. 11. Schematic representation of the experimental setup and the corresponding axial temperature profiles adopted for simulating the LOCA tests in Studsvik. by means of TRANSURANUS.

The calculations rely on the outer cladding temperature as external boundary condition. The axial temperature distribution approaches provided to the FUMAC participants are not used directly since they were not applicable to model the axial temperature profile for distances greater than 150 mm from the rodlet mid plane. Accordingly, the following approach was developed using parabolic functions (illustrated in the right part of Fig. 11):

— The temperature of the void volume far away from the heater is set to ambient temperature (25 °C);
— The temperature of the void volume close to the heater is set to the steam condensing temperature (100 °C);
— The temperature of the void volume close to the fuel stack is interpolated together with the fuel stack, and the temperature of the cladding is inferred from the experimental data using a parabolic fitting as illustrated in Fig. 11.

5.3.1. Results for rodlet 192

The inner rod pressure evolution during the LOCA tests in Studsvik for rodlet 192 is shown in Fig. 12. It can be seen that the failure time is somewhat over-predicted (1159 s measured versus 1176 s calculated). Moreover, it is shown that the uncertainty on the coolant temperature (i.e. clad outer temperature) by about 5% has an important impact, which is line with the other simulations of TRANSURANUS in FUMAC for QUENCH LOCA, the MTA EK cases and the uncertainty analysis for IFA-650.10. The over-prediction can be due to different reasons: the use of zircaloy properties without hydrogen (fresh material) instead of opt ZIRLO, the lacking contribution from fission gas release in high burnup fuel, etc.

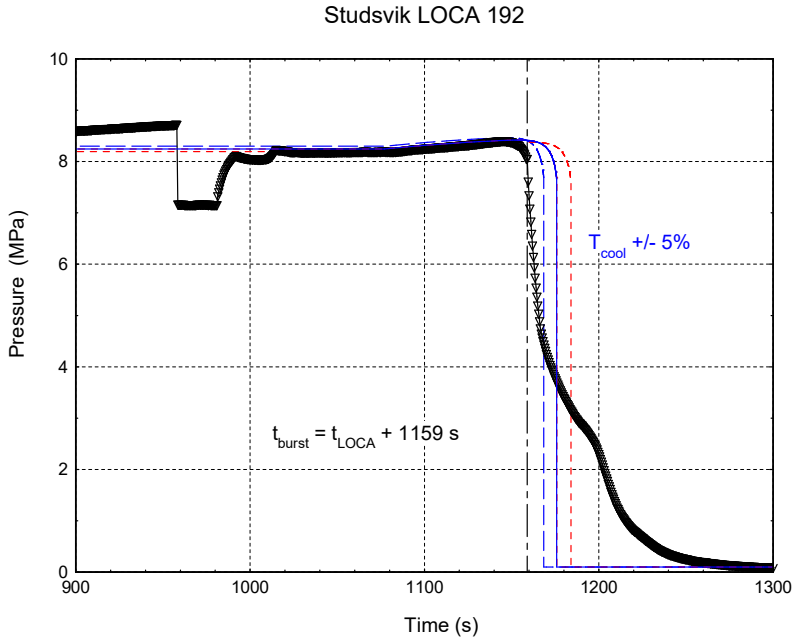

FIG. 12. Inner gas pressure evolution during LOCA test of rodlet 192 in Studsvik by means of the TRANSURANUS code.

Another difference between the measured and calculated evolution of the inner pressure is observed once the failure occurs. More precisely, the slower release kinetics from the rod observed in the experiments can be attributed to the small gap in the high burnup fuel. A model that specifically addresses the kinetics of the axial gas pressure evolution in a rod is therefore under development, and should enable a better reproduction of the pressure evolution after rod failure, provide that we obtain the necessary data for the simulation.

The corresponding cladding deformation obtained by means of the TRANSURANUS code during the LOCA test of rodlet 192 is depicted in Fig. 13. The effect of the failure criterion has a much larger effect on the resulting clad deformation after failure in comparison with the effect of the coolant temperature uncertainty of 5%. Similar to what has been observed in other FUMAC cases, it is also observed that the tangential strain criterion (Iclfail=4) leads to a much smaller deformation in comparison with the tangential stress criterion.

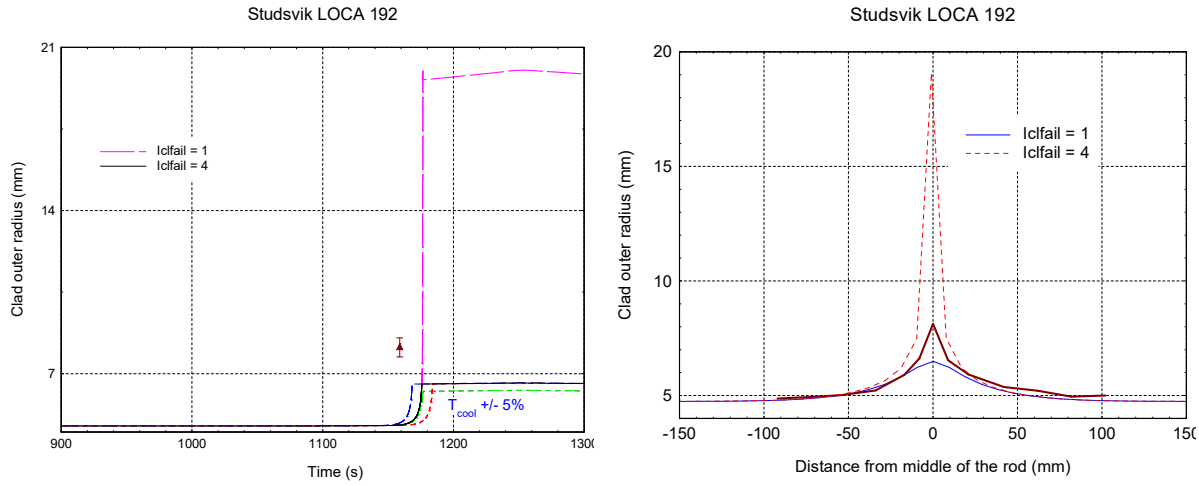

FIG. 13. Radial cladding deformation predicted by means of the TRANSURANUS code as function of time (s) during the LOCA test of rodlet 192 (left), and as a function of the axial position at the end of the test (right). The left figure also contains the measured cladding outer radius at the end of the test.

5.3.2. Results for rodlet 198

The inner rod pressure evolution during the LOCA tests in Studsvik for rodlet 198 is shown in Fig. 14. It can be seen that the failure time is somewhat over-predicted (1138 s measured versus 1156 s calculated), and that the uncertainty on the coolant temperature (i.e. clad outer temperature) by about 5% has an important impact as well. The slight over-prediction can be due the same reasons enumerated above.

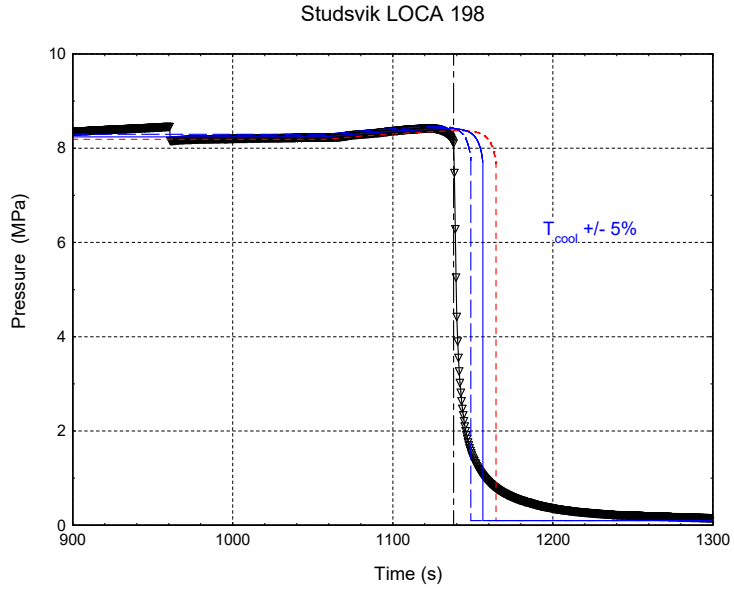

FIG. 14. Inner gas pressure evolution during LOCA test of rodlet 198 in Studsvik by means of the TRANSURANUS code.

The corresponding cladding deformation obtained by means of the TRANURANUS code during the LOCA test of rodlet 198 is shown in Fig. 15.

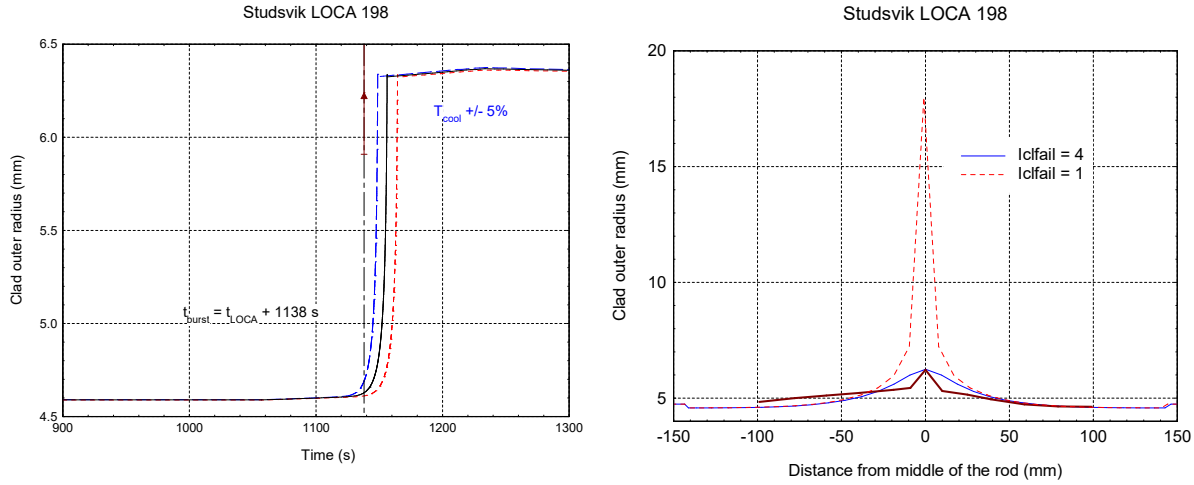

FIG. 15. Radial cladding deformation predicted by means of the TRANSURANUS code as function of time (s) during the LOCA test of rodlet 198 (left), and as a function of the axial position at the end of the test (right). The left figure also contains the measured cladding outer radius at the end of the test.

More information about the base irradiation and fuel characteristics are needed is order to enable a better prediction, and to deepen the analysis.

5.4. Simulation of IFA-650.11

The LOCA experiments in Halden are integral in-pile single pin tests on fuel behaviour under simulated LOCA conditions aiming at the critical analysis of existing safety criteria for new materials and higher discharge burn-up values. The simulation of the base irradiation and the subsequent LOCA test for each rod could be carried out by means of the automatic restart option of the TRANSURANUS code.

Table 5 lists the main parameters for the simulations of the single-rod tests. For the boundary conditions we have applied a) the simplified thermo-hydraulic boundary conditions (BC) derived from a parabolic fit and extrapolation of the measured cladding temperatures in the Halden reactor and (b) the axially and time-dependent cladding outside temperatures calculated by means of the SOCRAT code (agreed as common basis for all participants of FUMAC). The other boundary conditions used in the LOCA test simulations is the inner rod pressure, which has been inferred directly from the on-line measurements as for the QUENCH-LOCA cases.

For simulating both IFA 650.10 and IFA 650.11 with the TRANSURANUS code, the combined stress-strain cladding failure criterion (iclfail = 4) was used. The results with the pure stress-dependent failure criterion (iclfail=1) are not shown here for the sake of conciseness and because in the previous cases (e.g. QUENCH-LOCA) it was already shown that this criterion leads to (much) larger cladding deformation without affecting the time of burst.

The detailed figures below show the most relevant output quantities as a function of time during the LOCA tests and as a function of the axial position at the end of the LOCA test. All figures refer to the SOCRAT boundary conditions only, since these have been selected as common basis for all FUMAC participants.

The evolution of the cladding deformation as a function of time during the LOCA test is shown in Fig. 16 along with the axial distribution of the cladding at the end of the test. Figure 17 reveals the evolution of the rod inner pressure and the fuel central temperature at rod mid-height during the LOCA test in the reactor. The predicted values of the burst time and the final cladding deformation are in reasonable agreement with the experimental data. The main burst parameters are also summarised in

Table 3 containing the results for using both type of boundary conditions (i.e. inferred from the thermocouple signals, or obtained by means of SOCRAT). The table indicates that the TRANSURANUS predictions are slightly conservative in terms of burst time. As shown in the QUENCH LOCA cases that deal only with cladding or in the uncertainty analysis for IFA-650.10 (see below), this can be explained by the uncertainty pertaining to the coolant temperatures. Figure 16 indicates that the boundary condition has also a strong impact on the axial deformation profile at the end of the test.

Table 3 confirms that the burst elevation is strongly dependent on the boundary condition as well.

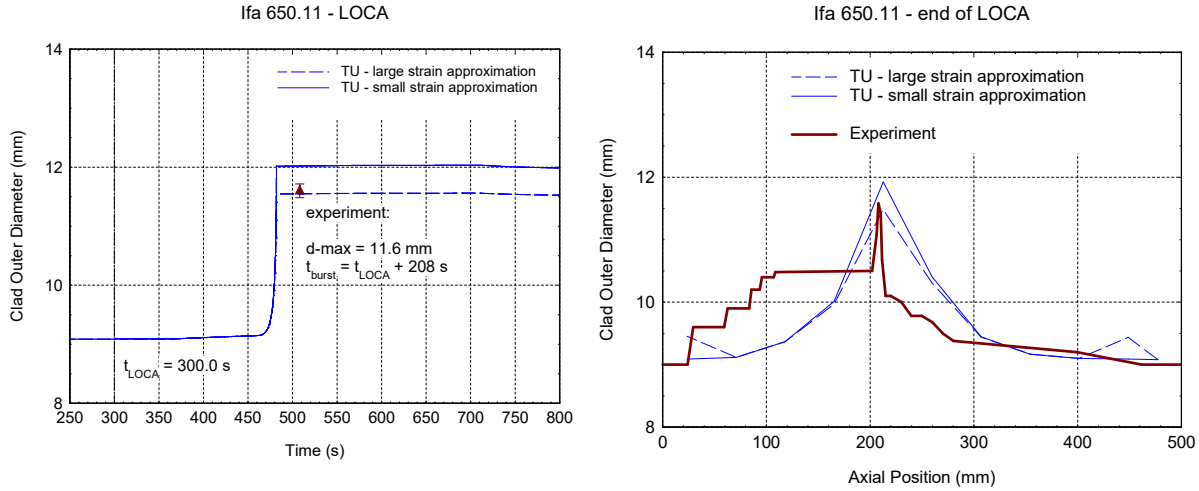

FIG. 16. Cladding outer diameter during the IFA 650.11 LOCA test predicted by TRANSURANUS with its dependence on time (left) and axial position (right).

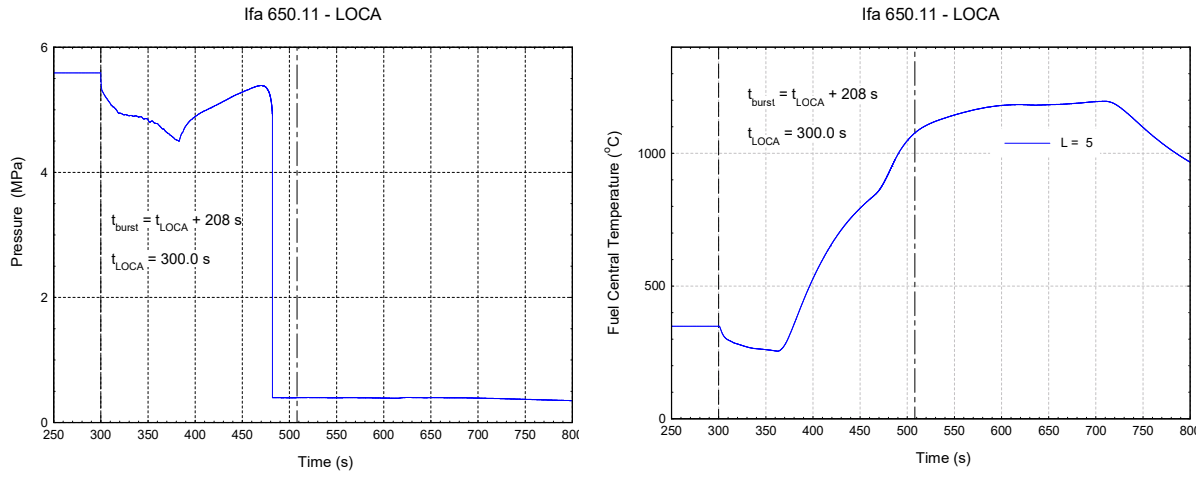

FIG. 17. Rod inner pressure and fuel central temperature during the IFA 650.11 LOCA test predicted by TRANSURANUS.

TABLE 3. MAIN MEASURED AND CALCULATED BURST PARAMETERS FOR THE FUEL SEGMENT IN IFA 650.11

	Experiment	TRANSURANUS with BC Halden	TRANSURANUS with BC SOCRAT	
			Standard strain approximation	Large strain approximation
Burst time (s)	208	186.8	182	182
Burst elevation (mm)	208	165.6	212.6	212.4
Cladding outer diameter at burst (mm)	11.6	12.6	11.9	11.5

In the parametric tests carried out for IFA-650.11, we have also shown that the effect of the large strain deformation is moderate in terms of both the predicted burst time as well as the axial cladding deformation after the experiment as shown in Fig. 16. This plot, along with the results in Table 3, indicates that the cladding deformation could also be improved by application of the boundary conditions obtained from SOCRAT.

The simulated cumulative release fraction in the VVER fuel rod in IFA-650.11 is shown in Fig. 18, applying a local threshold burn-up for the HBS formation of 75 GWd/tU, which corresponds to the value applicable for commercial LWR fuel [14]. There are four different curves shown in the figure, obtained with two different models and two different assumptions:

— Applying the standard fission gas behaviour model of TRANSURANUS with and without the release from the HBS pores;
— Appling the newly developed (more mechanistic) fission gas behaviour model for transient conditions with and without grain boundary cracking.

During the base irradiation there is only athermal release, which is directly proportional with burn-up. After the base irradiation there is a total fractional release about 0.4%, which is in excellent agreement with the measured values.

The effect of the burst release from the HBS during the LOCA test is shown in the right hand-side of Fig. 18 (in the left-hand side the effect cannot be seen as both curves overlap), by comparing the release with and without the HBS burst model. The additional release coming from the HBS pores during the test is around 1.5%, as shown in the right side of Fig. 18.

The small increase in the release curve when disregarding the burst release from the HBS pores stems from a diffusional contribution from the grains. It should be pointed out that as a complement to the burst release model from the HBS also a burst release model based on micro-cracking associated with the grain boundary bubbles has been developed [22] in collaboration with POLIMI and INL. In a future version of the TRANSURANUS code, both burst release models (for the grain boundary bubbles and the HBS pores) will be combined. The additional total cumulative release obtained with consideration of grain boundary cracking at the end of the base irradiation is relatively small as expected. The additional release during the LOCA test is around 0.6%, whereas the mechanistic model that only considers release as a result of bubble interconnection, does not lead to any additional release during the test. This is consistent with the amount of gas being removed from the grains in the central part of the pellets (contributing to diffusion release in the standard model), as shown in Fig. 19. This figure shows the radial distribution of the fission gas release fraction at mid-height at the end of the test. Around 1% release caused by diffusion from the grains is predicted in the central part of the fuel at the end of the test. According to the mechanistic model for fission gas behaviour, this is insufficient to cause bubble interconnection along the grain boundaries, hence there is no additional release predicted during the LOCA test under these conditions.

The other remarkable feature in Fig. 18 is the different time at which the additional burst release occurs according to the two different models. This can be entirely explained on the basis of the temperature evolution. The additional release from the HBS pores during a LOCA is depending on the local temperature only, and therefore starts immediately at the beginning of the test. The additional burst associated with the grain boundary cracking on the other hand depends on both the temperature as well as its rate of change. At the onset of the temperature ramp, not much gas has been transported to the grain boundaries so that cracking does not have an effect. On the other hand, at the end of the test, a fraction of the gas that has been transported to the grain boundaries is released according to the model.

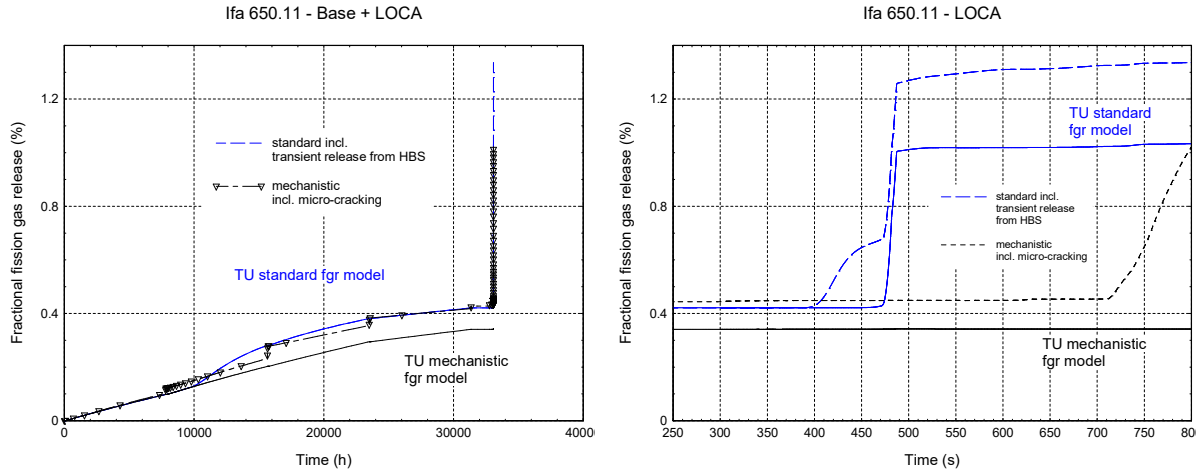

FIG. 18. Incremental fractional fission gas release as a function of time predicted by TRANSURANUS during the entire irradiation (left) and during the IFA 650.11 LOCA test (right).

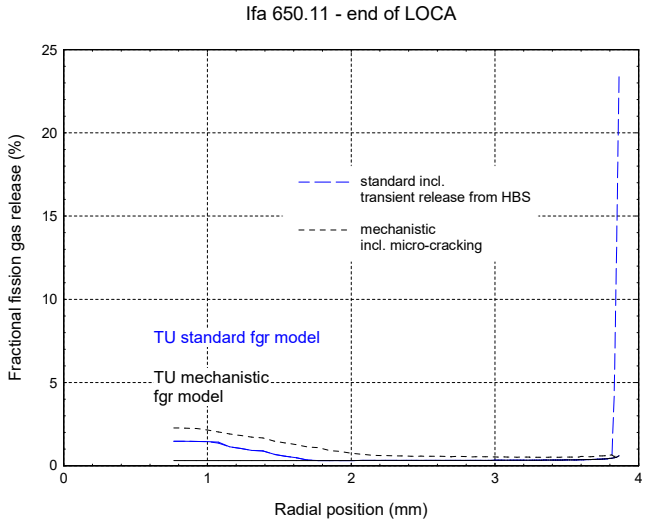

FIG. 19. Radial distribution of the fission gas release fraction at mid-height predicted by TRANSURANUS at the end of the LOCA test in IFA650.11.

5.5. Simulation of IFA-650.10

5.5.1. Base case

The evolution of the cladding deformation as a function of time during the LOCA test is shown in Fig. 20 along with the axial distribution of the cladding at the end of the test. For simulating IFA 650.10, both the inner pin pressure as well as the cladding outer surface temperature were prescribed. The predicted values of the burst time and the final cladding deformation are in reasonable agreement with the experimental data. The main burst parameters are also summarised in Table 4 containing the results for using both type of boundary conditions (i.e. inferred from the thermocouple signals, or obtained by means of SOCRAT). In contrast with the results obtained in IFA-650.11, the table indicates that the TRANSURANUS predictions are slightly non-conservative in terms of burst time. The results obtained with the SOCRAT boundary conditions improved, both in terms of burst time and position. The figure also underlines that the boundary condition has a strong impact on the axial deformation profile at the end of the test.

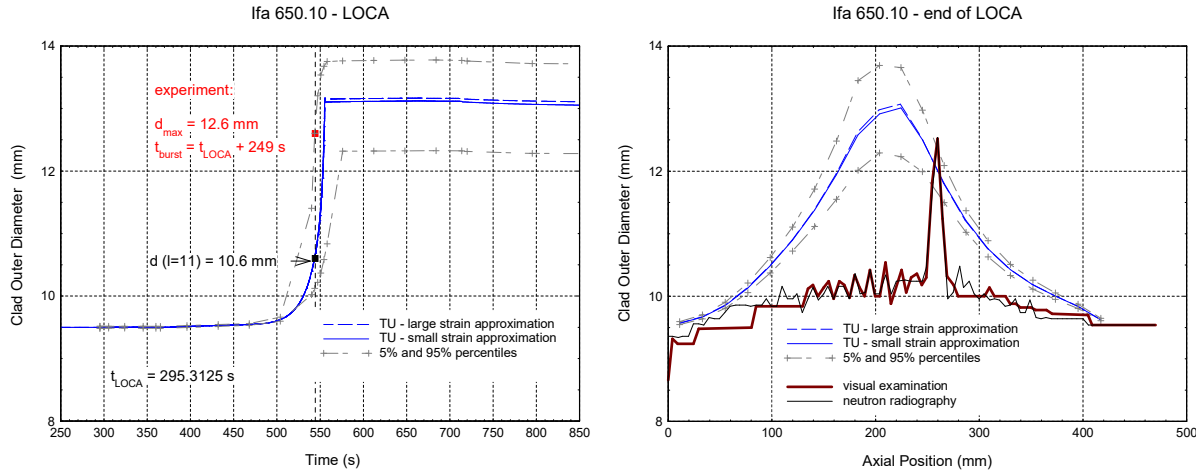

FIG. 20. Cladding outer diameter during the IFA 650.10 LOCA test predicted by TRANSURANUS with its dependence on time (left) and axial position (right). The lower and upper uncertainty limits corresponding to the 5% and 95% percentiles are indicated as well.

Nevertheless, it should be pointed out that the axial deformation at the end of the test deviates in the lower part of the fuel segment, which may indicate an error in the cladding outer temperature in that region (see Fig. 20). This causes a shift in the axial location of the burst as pointed out in Table 4 and is addressed in more detail in the uncertainty/sensitivity analysis below. It is interesting to note that at the (measured) time of burst the cladding at an axial elevation of 224 mm (L=11) was not ruptured in the experiment, while at this time point the calculated deformation is consistent with the measured one.

TABLE 4. MAIN MEASURED AND CALCULATED BURST PARAMETERS FOR THE FUEL SEGMENT IN IFA 650.10

	Experiment	TRANSURANUS with BC Halden	TRANSURANUS with BC SOCRAT	
			Standard strain approximation	Large strain approximation
Burst time (s)	249	285	259.9	260.6
Burst elevation (mm)	259.7	182.8	224.4	223.9
Cladding outer diameter at burst (mm)	12.6	13.0	13.0	13.1

The evolution of the integral fission gas release during the LOCA test is shown in Fig. 21 (left), together with the axial profile of the oxide layers on the cladding at the end of the test (right). The effect of the additional release from the HBS pores in this case is even more reduced in comparison with the results in IFA-650.11, essentially because of the smaller burnup.

Finally, Fig. 21 also reveals that the axial profile of the inner oxide layer — as expected — is predicted to be less pronounced in comparison with the outer cladding oxide, as well as more localised around the burst. For completeness Fig. 22 shows the prescribed cladding outer surface temperature at rod mid-height and the prescribed rod inner pressure during the LOCA test in the reactor.

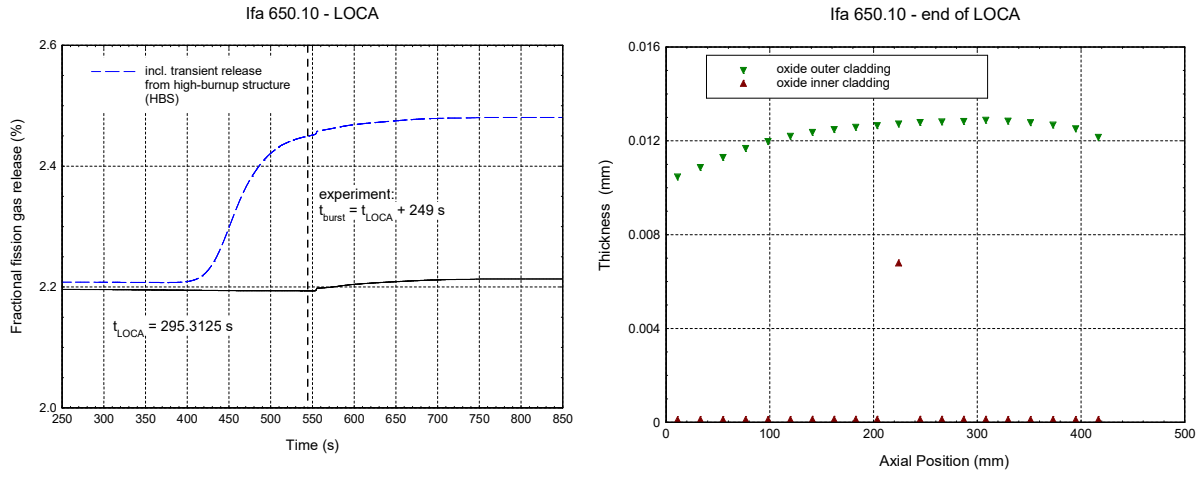

FIG. 21. Fractional fission gas release during the IFA 650.10 LOCA test (left) and cladding oxide layers at the end of the test (right) predicted by TRANSURANUS.

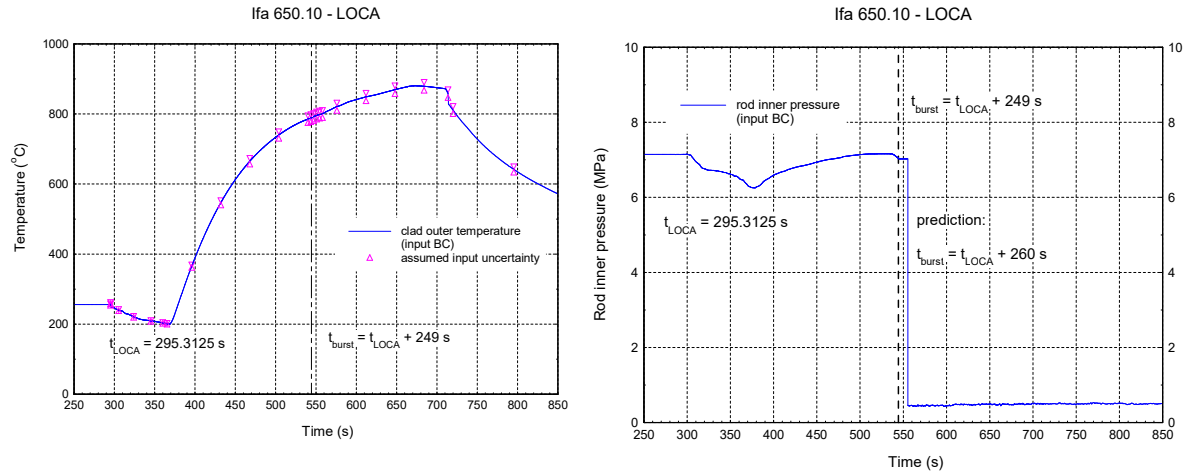

FIG. 22. Cladding outer surface temperature (left) and rod inner pressure (right) during the IFA 650.10 LOCA test given as boundary condition.

5.5.2. Uncertainty analysis

For a first uncertainty analysis of the IFA 650.10 LOCA test, the list of input uncertainties proposed in the final phase of the FUMAC exercise was adopted for matching the available options of the TRANSURANUS fuel performance code (Table 5). Using the Monte-Carlo (MC) event generator of TRANSURANUS two types of probabilistic simulations were run:

- Applying the cladding outer surface temperature as the only input uncertainty as indicated in Fig. 22 (1500 MC runs);
- Applying the complete list of uncertainties as given in Table 5 (2500 MC runs).

The main conclusions can be drawn from Fig. 23, showing the predicted evolution of the cladding outer diameter at the calculated burst node, i.e. at an axial elevation of 224 mm (L=11), together with the lower and upper bounds corresponding to the 5% and 95% percentiles (calculated with simple order statistics). The figure also shows the distribution (histogram) of the simulated burst times. It is interesting to note that

- Applying the complete list of input uncertainties given in Table 5leads to a spread of the simulated burst times in the interval tloca+(240...278 s);
- Depending on the calculated time of burst, the cladding rupture is simulated to occur at different axial elevations of the fuel rod model (corresponding to slices L=9, 10 and 11), which is primarily determined by the boundary condition (i.e. outer cladding temperature);
- The total output uncertainty band considerably broadens for large cladding deformations;
- The input uncertainty of the clad outer temperature dominates the total output uncertainty band of the cladding outer diameter up to large deformations (close to burst);
- After simulated burst (t > tloca+260 s) the impact of the input uncertainty of the cladding outer temperature still makes up at least one third of the total output uncertainty.

TABLE 5. INPUT QUANTITIES SUBJECT TO SIMULATED UNCERTAINTIES FOLLOWING THE PROPOSAL OF THE FUMAC EXERCISE FOR IFA 650.10. COMMENTS IN ITALICS INDICATE DIFFERENCES ARISING FROM THE AVAILABLE INPUT OPTIONS OF TRANSURANUS

Input uncertainty parameter	Distribution				
	Mean	Standard Deviation	Type	Lower bound	Upper bound
1. Fuel rod design/manufacturing data					
Cladding outside diameter (mm)	9.50	0.01	Normal	9.48	9.52
Cladding inside diameter (mm)	8.36	0.01	Normal	8.34	8.38
Pellet outside diameter	8.2	0.01	Normal	8.18	8.22
Fuel theoretical density (kg/m3 at 20 °C)	10457	50	Normal	10357	10557
U^{235} enrichment (%)			n/a		
Filling gas pressure (MPa) - taken as relative variation to the prescribed inner pin pressure	4.0	1.25%	Normal	2.5%	2.5%
2. Operation and test boundary conditions					
Relative power during base irradiation and during test (same distribution parameters taken)	1	0.01	Normal	0.98	1.02
Test rod power profile			n/a		
Cladding temperature (°C) - taken as relative variation to the prescribed outer cladding temperature	1	1%	–	2%	2%
Coolant temperature (°C)			n/a		
Clad-to-Coolant heat transfer coefficient (Same Coef. applied for all flow regimes)			n/a		
3. Physical Properties/Key models (Mult. Coef.)					
Fuel thermal conductivity model	1.00	5%	Normal	0.90	1.10
Clad thermal conductivity model	1.00	5%	Normal	0.90	1.10
Fuel thermal expansion model	1.00	5%	Normal	0.90	1.10
Clad thermal expansion model	1.00	5%	Normal	0.90	1.10
Fuel densification model	1.00	5%	Normal	0.90	1.10
Fuel solid swelling model	1.00	5%	Normal	0.90	1.10
Fuel gaseous swelling model - applied in the same routine as the solid swelling	1.00	5%	Normal	0.90	1.10
Clad Yield stress	1.00	5%	Normal	0.90	1.10
Fuel heat capacity	1.00	1.5%	Normal	0.97	1.03
Cladding heat capacity	1.00	1.5%	Normal	0.97	1.03
Cladding elastic modulus	1.00	5%	Normal	0.90	1.10
Cladding hydrogen pickup fraction during steady-state operation			n/a		
Cladding corrosion model during steady-state operation and at high temperatures - same distribution parameters taken	1.00	15%	Normal	0.7	1.30

Input uncertainty parameter	Distribution				
	Mean	Standard Deviation	Type	Lower bound	Upper bound
Thermal conductivity of the oxide layer Fission gas release (or gas diffusion coefficient)	1.00	25%	Normal	0.50	1.50
Gap gas conductivity	1.00	12.5%	Normal	0.75	1.25
Fuel/cladding emissivity	1.00	5%	Normal	0.90	1.10
Fuel radial relocation			n/a		
Fuel fragment packing fraction (if applicable)			n/a		
Cladding strain threshold for fuel mobility (if applicable)			n/a		
Cladding Meyer hardness			n/a		
Cladding annealing			n/a		
Cladding burst criteria - Burst stress in Transuranus	1.00	10%	Normal	0.80	1.20
Cladding burst strain criteria	1.00	10%	Normal	0.80	1.20
Plenum gas temperature (°C)			n/a		

The lower and upper bounds corresponding to the 5% and 95% percentiles were furthermore calculated for the following output quantities:

- Cladding average tangential stress at calculated burst node;
- Cladding outer oxide layer and equivalent cladding reacted at calculated burst node;
- Fuel central temperature at calculated burst node;
- Fuel axial elongation.

This analysis reveals that the input uncertainty of the cladding outer temperature has a dominating impact - in particular prior to burst – also on the calculated cladding average tangential stress (Fig. 24) and the fuel centre temperature (Fig. 26, left). The situation is somewhat different for the calculated cladding oxidation (Fig. 25) and the calculated axial elongation of the fuel stack (Fig. 26, right). We should note that the equivalent cladding reacted (ECR, Fig. 25 right) includes inner cladding oxidation that is assumed only in case the burst in calculated for the specific axial slice. A more detailed analysis is needed for assessing the different possible causes e.g. the role of the uncertainties of the various fuel and cladding thermo-mechanical properties on one hand and of the uncertainty of the different burst criteria on the other hand. As a follow-up of the FUMAC project a quantitative sensitivity analysis (using e.g. Pearson's or Spearman's correlation coefficients) should be performed but should focus on a few 'priority' input uncertainties (still to be identified in addition to the obviously dominating cladding outer surface temperature).

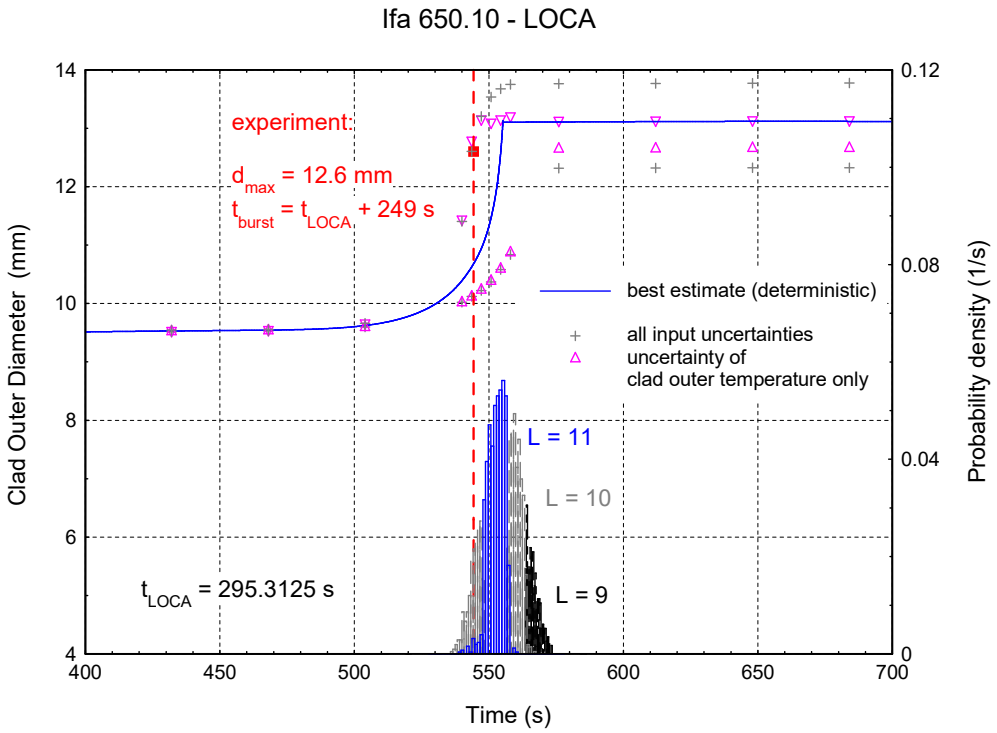

FIG. 23. Cladding outer diameter at calculated burst node during the IFA 650.10 LOCA test and time of burst predicted by TRANSURANUS together with first results of an uncertainty analysis. See text for details.

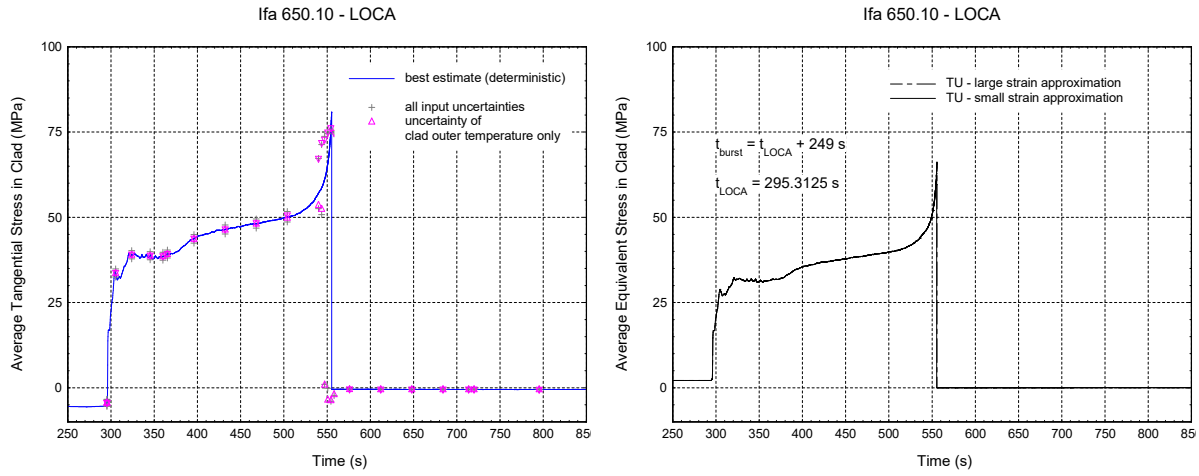

FIG. 24. Cladding average tangential stress (left) and average equivalent stress (right) at calculated burst node during the IFA 650.10 LOCA test predicted by TRANSURANUS together with first results of an uncertainty analysis.

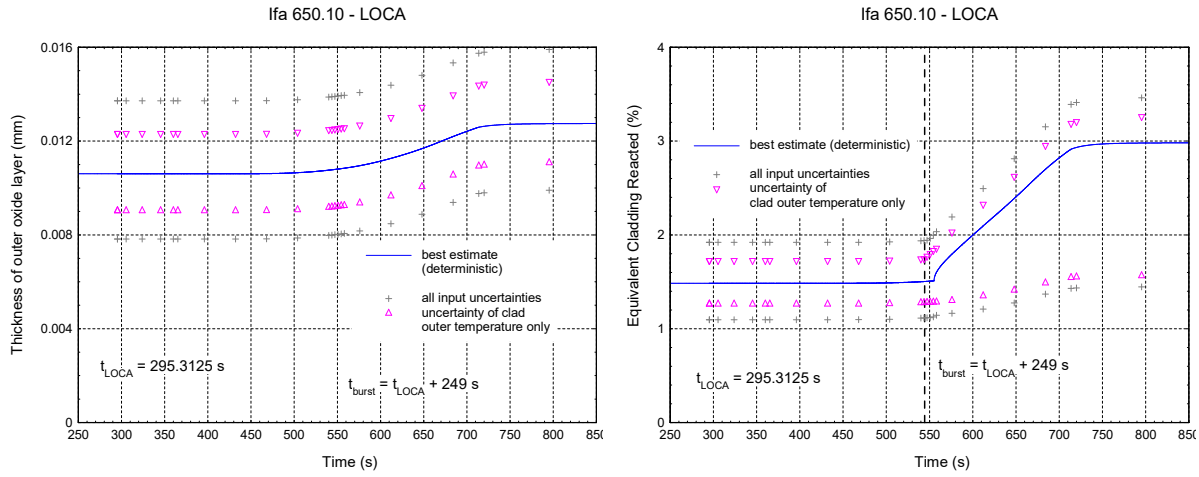

FIG. 25. Thickness of cladding outer oxide layer at calculated burst node (left) and Equivalent Cladding Reacted (right) during the IFA 650.10 LOCA test predicted by TRANSURANUS together with first results of an uncertainty analysis.

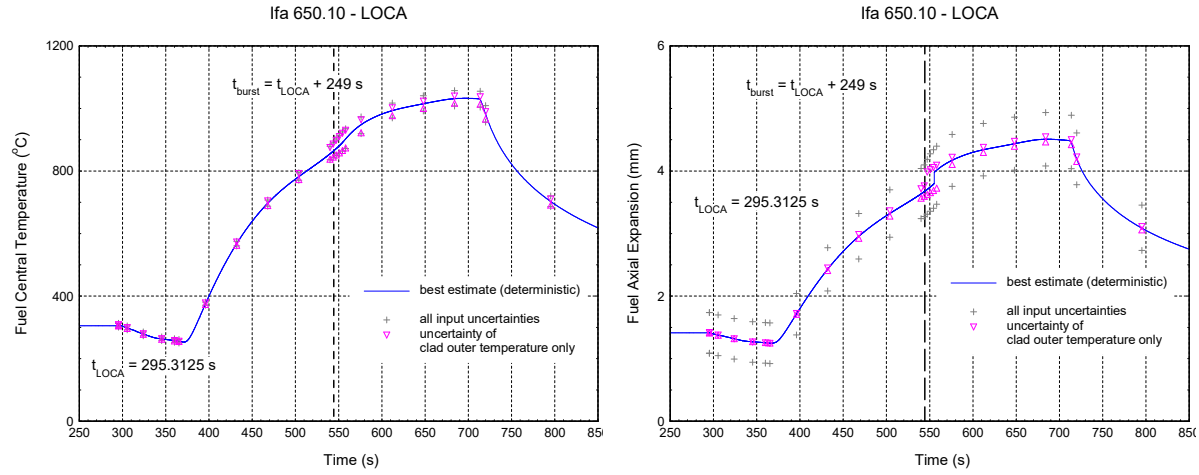

FIG. 26. Fuel central temperature at calculated burst node (left) and fuel axial elongation (right) during the IFA 650.10 LOCA test predicted by TRANSURANUS together with first results of an uncertainty analysis.

6. SUMMARY AND CONCLUSIONS

In this fifth round robin exercise organised by the IAEA for the LWR fuel rod behaviour codes, the focus was on accident conditions in the light of the Fukushima accident. In the frame of the research agreement between the IAEA and JRC for FUMAC, it has been agreed to consider model development, material properties improvements and validation of the TRANSURANUS fuel performance code for assessing fuel behaviour under design basis accidents and the initial phase of severe accidents. To this end the JRC has also co-ordinated some of the efforts of several TRANSURANUS users involved in FUMAC, as well as the ESSANUF project of the EU that ran in parallel. The model improvements considered are in line with the perspectives outlined in the final report of the JRC for FUMEX-III and deal with cladding behaviour such as double sided oxidation, hydrogen production and uptake, and transient fission gas release from the fuel. This report summarised first these code changes and provides references to the relevant publications.

The second and principal part of the report outlines the main results for cases that have been selected by the FUMAC participants at the end of the first research co-ordination meeting, but which had not been simulated before with the TRANSURANUS code.

At first, the out-of-pile single-effect cladding tests of MTA EK have been simulated in order to verify the prediction of cladding failure under LOCA conditions: isothermal tests of cladding tube specimen in a temperature range 800–1200 °C, with linear increasing internal pressure until failure occurred. The results confirmed the outcome of similar tests analysed in the EU funded projects EXTRA (2000–2003) and ESSANUF (2015–2017) for VVER reactors. More precisely, the burst time as well as the decreasing trend of the burst time with increasing temperature could be reproduced well. Nevertheless, the results also pointed out the important uncertainties relating to the cladding strain after burst because of uncertainties pertaining to the burst criterion on one hand and to the uncertainties related to simulations of (very) large strains with the fuel performance codes available.

The second set of data came from the out-of-pile bundle tests with longer cladding tubes in the QUENCH LOCA facility operated by KIT. The simulations not only addressed the cladding deformation and failure during LOCA tests, but also the oxidation by interaction with the steam. The calculation results obtained by means of TRANSURANUS were satisfactory in terms of burst time, burst temperature, burst location and thickness of the cladding affected by the high temperature oxidation. Nevertheless, it also was pointed that since the simulation tool cannot take into consideration the important azimuthal temperature gradients, the cladding bending could not be reproduced. The experimental data further confirmed the reduced cladding strain in bundle tests in comparison with the single rod tests because of these larger tangential temperature gradients, when comparing the cladding deformations obtained in QUENCH LOCA with those of MTA EK.

Due to the lack of available data about the base irradiation, the single rod out-of-pile LOCA tests performed with irradiated fuel rod segments 198 and 192 in Studsvik could not be modelled properly. In particular, only simulations with fresh materials were carried out in order to verify the cladding deformation and failure. The results are also satisfactory, although they pointed out potential room for improvement when applying the proper fuel (fission gas behaviour) and cladding material properties (irradiated opt ZIRLO instead of standard Zry-4), as well as a model that accounts for the kinetics of the axial gas transfer in high burnup fuels.

The final set of experimental data was offered by the OECD Halden Reactor Project. They provided data for in-pile single rod experiments with on-line instrumentation in Instrumented Fuel Assembly (IFA)-650 for both pre-irradiated PWR as well as and VVER fuel. In order to avoid discussions about the boundary conditions applied to the outer fuel rod surface on the basis of some thermocouple signals, and therefore to enable a better (simpler) comparison of the various code predictions, it had been agreed during the second research co-ordination meeting to impose the same boundary conditions at the fuel rod outer surface obtained by means of the SOCRAT code from IBRAE. The simulations obtained by means of the TRANSURANUS code were satisfactory and have enabled to point out the improvements obtained by means of the recent modelling extensions for fission gas behaviour under transient conditions developed in collaboration with POLIMI, INL, HZDR and TUM. More precisely, testing of the new model for dealing with release of fission gas from nuclear fuel containing a high burnup structure (HBS) during design basis accidents such as loss of coolant accident, as well as the more mechanistic model for fission gas behaviour that accounts for the cracking along grain boundaries during temperature variations in a fuel performance code has been verified in these IFA cases. The release from the HBS pores during an accident is essentially assumed to be caused by micro-crack formation. The results of the model are encouraging and are also illustrated by showing the (moderate) impact on the release during a LOCA test of a fuel rod of IFA-650.11 with a moderate discharge burn-up of approximately 55 GWd/tU where the HBS has started to form in the pellet rim region.

During the second co-ordination meeting, it was also agreed to carry out a more detailed uncertainty/sensitivity analysis of the IFA-650.10 test, on the basis of a proposal prepared by ENGIE (and similar to that adopted in the frame of the NEA RIA benchmark phase II) that relies on order statistics and Spearman ranking coefficients. Rather than applying generic statistics software, the JRC has extended and applied the build-in Monte Carlo technique in the TRANSURANUS code. The uncertainty assessment revealed the dominant role played by the cladding (i.e. coolant) temperature during the accident. This constitutes the driving force for coupling of the TRANSURANUS code with system codes like RELAP and ATHLET as developed in the ESSANUF project, for providing the boundary conditions for LOCA simulations as required in licensing.

It is thus fair to conclude that the co-ordinated research project of the IAEA provided an excellent platform to extend the code validation of the TRANSURANUS fuel rod performance code that is applicable to normal operation conditions and has been extended to design basis accident conditions over the recent decade. In addition, in the course of the CRP the TRANSURANUS user group has been extended and includes also partner organisations from countries like P.R. China, Turkey and Brasil. Finally, the uncertainty and sensitivity analysis carried out in the frame of both the FUMAC CRP and the ESSNANUF project of the EU have a strong potential to contribute to the harmonisation of the safety analysis of nuclear fuel.

7. PERSPECTIVES

In the last part of this report, we outline the topics for future work that will be discussed with the other participants during the 3rd and final RCM.

In terms of model developments, the ongoing work on combining the hydrogen uptake during normal and design basis accident conditions in the TRANURANUS code will be completed in collaboration with CIAE, NucleoCon, Westinghouse Sweden Electric and TÜV Nord. Also the extension of the intragranular transient fission gas behaviour model to RIA conditions as well as the coupling with an improved model for helium behaviour will be completed in collaboration with our partners from POLIMI and INL.

Also the model for axial gas flow kinetics under transient conditions, currently available as a standalone model will be implemented and tested in combination with the new model for the plenum temperature (the so-called 2 section model developed in collaboration with NPIC) under transient conditions. If the base irradiation and fuel fabrication data become available, the Studsvik cases of FUMAC could then be re-analysed properly.

In terms of validation, the above mentioned models will be compared with experimental results, while the integral code validation will also be extended in collaboration with TRANSURANUS users via the ongoing OECD-NEA benchmarks for Pellet-Cladding Interaction (with NRI) and the third phase of the fuel behaviour under RIA conditions (with NINE).

In the course of this CRP, agreements have been signed to include new material properties for so-called Accident Tolerant Fuels and materials in the TRANSURANUS code with partners in P.R. China and Brasil. These results will be useful for a potential future code benchmark dedicated to ATF.

As reflected also in FUMAC and the benchmark for fuel behaviour under RIA organised by the NEA, there is a current trend towards reviewing and extending the uncertainty and sensitivity analysis of simulation tools applied in the nuclear safety analysis. The same was observed in the frame of the ESSANUF project. Driven by the users of the TRANSURANUS network the JRC has started analysing the possibilities to extend the current statistical analysis tool of the code. Some of the extensions are being implemented, for example in extending the list of input parameters available for uncertainty analysis by Monte Carlo and for including a sensitivity analysis based on e.g. Pearson's or Spearman's correlation coefficients. Other extensions are required for the tools that are used to analyse and visualise the binary output files

of the TRANSURANUS code. Such extensions must take into considerations the current software developments and needs of the customers of the code. In particular, the requirement to operate both under Windows and Linux operating systems as well as the need to be able to couple the code with other tools in the open source SALOME platform must be considered.

Finally, the JRC is also involved in coupling of simulation tools for improved nuclear safety analysis. After the successful coupling or data transfer between TRANSURANUS with the DYN3D, ATLET, RELAP and SERPENT codes, this will be further extended in the frame of the new McSAFE project funded by the EU and aiming to couple with other codes like PARCS and SUBCHANFLOW as well as to integrate tools like TRANSURANUS in the EU open source platform SALOME for coupling with other codes.

REFERENCES

[1] GYŐRI, C., et al., Extension of Transuranus code applicability with Niobium containing cladding models (EXTRA), Final Report, EVOL-EXTRA-D5 / FIKS-CT2001-00173 (2004).

[2] NUCLEAR ENERGY AGENCY, Nuclear fuel safety criteria technical review, second edition, OECD/NEA, ISBN 978-92-64-99178-1 (2012).

[3] VAN UFFELEN, P., KONINGS, R. J. M., VITANZA, C., TULENKO, J., Analysis of Reactor Fuel Rod Behavior, D.G. Cacuci (Ed.), Handbook of Nuclear Engineering, Springer Science–Business Media, (2010).

[4] C. VITANZA, "RIA failure threshold and LOCA limit at high burnup", J. Nucl. Sci. Technol., Vol. 43, 9, pp. 1074-1079, 2006.

[5] C. GYŐRI, M. JONSON, G. ROBERTSON, P. BLAIR, A. SCHUBERT, P. VAN UFFELEN, Extension and validation of the TRANSURANUS code in the course of the ESSANUF project, in: 12th International conference on WWER fule performance, modelling and experimental support (Bulgarian Academy of Sciences, Nessebar, Bulgaria, 2017).

[6] LIMBÄCK, M., KRAMMEN, M. A., RUDLING, P., PATI, S. R., GARDE, A. M., Corrosion and Hydriding performanceof Zircalloy-2 and Zircalloy-4 cladding materials in PWR's, Topical Meeting on LWR fuel performance, American Nuclear Society, West Palm Beach, Florida, (1994).

[7] ZHOU, G., et al., Corrosion and Hydrogen uptake behavior and modeling for modern BWR cladding materials at high burnup, Top Fuel, Paris, France, (2009).

[8] GYŐRI, CS., et al., Model developments for the simulation of LOCA events by means of the TRANSURANUS Code, 7th Int. Conf. on WWER Fuel Performance, Modelling and Experimental Support, Albena, Bulgaria, (2007).

[9] TULKKI, V., IKONEN, T., Effect of underlying assumptions to the interpretation and presentation of creep experiments, EHPG Meeting, Rorøs, Norway (2014).

[10] Klouzal, J., Matocha, V., Validation and application of TRANSURANUS for the CEZ NPPs, in: Van Uffelen, P., Schubert, A. Van de Laar J., (Eds.), Towards nuclear fuel modelling in the various reactor types across Europe, European Commission, Karlsruhe, Germany (2015).

[11] ROGOZYANOV, A.Y., KOBYLYANSKY, G.P., NUZHDOV, A.A., Behaviour and Mechanisms of Irradiation – Thermal Creep of Cladding Tubes Made of Zirconium Alloys, Journal of ASTM International, Vol. 5, Issue 2, (2008).

[12] PERI, V., TRANSURANUS analyses of VVER-440 fuel in the Loviisa NPP, in: P. Van Uffelen, A. Schubert (Eds.), Towards nuclear fuel modelling in the various reactor types across Europe (European Commission, Lappeenranta, Finland (2017).

[13] LASSMANN, K., O'CARROLL, C., VAN DE LAAR, J., WALKER, C. T., The radial distribution of plutonium in high burnup UO_2 fuels, J. Nucl. Mater., Vol. 208, Issue 3 (1994) 223–231.
[14] HOLT, L., et al., Sensitivity study on Xe depletion in the high burn-up structure of UO_2, J. Nucl. Mater., Vol. 452, (2014) 166–172.
[15] MARCHETTI, M., et al., High Frequency Acoustic Microscopy for the Determination of Porosity and Young's Modulus in High Burnup Uranium Dioxide Nuclear Fuel, in: Advancements in Nuclear Instrumentation Measurement Methods and their Applications (ANIMMA) (IEEE, Lisbon, Portugal, 2015).
[16] CAPPIA, F., et al., Microhardness and local properties of high burnup UO_2 fuel, TOPFuel, Zurich, Switzerland, (2015).
[17] CAPPIA, F., et al., Investigation of mechanical and local properties of high burnup UO_2 fuel with focus on the pellet rim, First Workshop on Research into Nuclear Fuel in Europe and Materials Modeling and Simulation for Nuclear Fuels Workshop, Karlsruhe, Germany (2015).
[18] CAPPIA, F., et al., Microhardness and Young's modulus of high burn-up UO_2 fuel, J. Nucl. Mater., Vol. 479 (2016) 447–454.
[19] CAPPIA, F., et al., Critical assessment of the pore size distribution in the rim region of high burnup UO_2 fuels, J. Nucl. Mater., Vol. 480 (2016) 138–149.
[20] PIZZOCRI D., et al., A semi-empirical model for the formation and depletion of the high burnup structure in UO_2, J. Nucl. Mater., Vol. 487 (2017) 23–29.
[21] BARANI, T., BRUSCHI, E., Extension and validation of a transient fission gas release model for the TRANSURANUS fuel performance code, Master Thesis, Department of Energy, Politecnico di Milano (2015).
[22] BARANI, T., et al., Analysis of transient fission gas behaviour in oxide fuel using BISON and TRANSURANUS, J. Nucl. Mater., Vol. 486 (2017) 96–110.
[23] HOLT, L., SCHUBERT, A., VAN DE LAAR, J., VAN UFFELEN, P., Stand-alone modelling of the high burnup structure formation and burst release during design basis accidents, EHPG Meeting, Rorøs, Norway (2014).
[24] PIZZOCRI, D., Modelling of Burst Release in Oxide Fuel and Application to the Transuranus Code, 11th International conference on WWER fuel performance, modeling and experimental support, Varna, Bulgaria, (2015).
[25] LASSMANN, K., BENK, H., Numerical algorithms for intragranular fission gas release, J. Nucl. Mater., Vol. 280, Issue 2, (2000) 127–135.
[26] VAN UFFELEN, P., SCHUBERT, A., VAN DE LAAR, J., GYŐRI, CS., Development of a transient fission gas release model for TRANSURANUS, Water Reactor Fuel Performance Meeting, Seoul, Korea (2008).
[27] PASTORE, G., LUZZI, L., DI MARCELLO, V., VAN UFFELEN, P., Physics-based modelling of fission gas swelling and release in UO_2 applied to integral fuel rod analysis, Nucl. Eng. Des., Vol. 256, (2013) 75–86.
[28] PIZZOCRI, D., CAPPIA, F., LUZZI, L., PASTORE, G., RONDINELLA, V. V., VAN UFFELEN, P., A semi-empirical model for the formation of the high burnup structure, First Workshop on Research into Nuclear Fuel in Europe and Materials Modeling and Simulation for Nuclear Fuels Workshop, Karlsruhe, Germany (2015).
[29] HIERNAUT, J. P., WISS, T., THIELE, H., WALKER, C. T., GOLL, W., KONINGS, R. J. M., Fission product release and microstructure changes during laboratory annealing of a very high burn-up fuel specimen, J. Nucl. Mater., Vol. 377, (2008) 313–324,.
[30] LI, W., JIAO, Z., CHEN, B., Development of plenum temperature model for accident analysis, in: International Conference on Nuclear Engineering (ICONE24) (2016).

[31] LASSMANN, K., The Statistical Version of the URANUS-Programme, Nucl. Eng. Des., Vol. 56, No.1, (1980) 35–40,.
[32] LASSMANN, K., O'CARROLL, C., VAN DE LAAR, J., Probabilistic fuel rod analyses using the TRANSURANUS code, Technical Committee Meeting on Water Reactor Fuel Element Modelling at High Burnup and Experimental Support, International Atomic Energy Agency, Windermere, UK, 19-23 September 1994, IAEA-TECDOC-957, (1997) 497–506.
[33] SCHUBERT, A., VAN DE LAAR, J., ELENKOV, D., The Statistics Version of TRANSURANUS - Recent Developments and Applications to WWER Fuel, 4th International Conference on WWER Fuel Performance, Modelling and Experimental Support, Albena, Bulgaria, (2001) 293–298.
[34] KILLEEN J., Fuel Modelling at Extended Burnup (FUMEX-II), IAEA-TECDOC IAEA, Vienna (2011).
[35] MARCELLO, V.D., SCHUBERT, A., VAN DE LAAR, J., VAN UFFELEN, P., The TRANSURANUS mechanical model for large strain analysis, Nucl. Eng. Des., Vol. 276, (2014)19–29.
[36] VAN UFFELEN P., GYŐRI, CS., A. SCHUBERT, VAN DE LAAR, J., HOZER, Z., SPYKMAN, G., Extending the application range of a fuel performance code from normal operating to design basis accident conditions, J. Nucl. Mater., Vol. 383, (2008) 137–143.
[37] ERBACHER, F. J., Cladding tube deformation and core emergency cooling in a loss of coolant accident of a pressurized water reactor, Nucl. Eng. Des., Vol. 103, Issue 1, (1987) 55–64.
[38] STUCKERT, J., GROßE, M., RÖSSGER, C., STEINBRÜCK, M., WALTER, M., Results of the LOCA reference bundle test QUENCH-L1 with Zircaloy-4 claddings, Wissenschaftliche Berichte Karlsruher Institut für Technologie, Karlsruhe (2015).

MTA EK ACTIVITIES IN THE IAEA FUMAC CRP

KATALIN KULACSY
Hungarian Academy of Sciences Centre for Energy Research (MTA EK)
1121 Budapest, Konkoly-Thege Miklós út 29-33. Hungary
E-mail: katalin.kulacsy@energia.mta.hu

Abstract

In the framework of the IAEA FUMAC CRP MTA EK provided the PUZRY separate effect dataset of the International Fuel Performance Experiments database to the participants and performed the simulation of the PUZRY dataset, the Halden IFA-650.10 LOCA test and the Studsvik LOCA test No. 192.

1. INTRODUCTION

In the framework of the Research Agreement between the International Atomic Energy Agency (IAEA) and the Hungarian Academy of Sciences Centre for Energy Research (MTA EK), the latter undertook the post-test simulation of LOCA-type experiments within the Coordinated Research Project (CRP) T12028 entitled Fuel Modelling in Accident Conditions (FUMAC). The participation of MTA EK was largely supported by Paks NPP

In accordance with the above, the tasks performed by MTA EK were as follows:

- Simulation of the separate effect ballooning and burst tests performed at the predecessor of MTA EK (KFKI AEKI);
- Simulation of the integral LOCA test IFA-650.10 performed in the Halden Reactor;
- Simulation of the integral LOCA test No. 192 performed in Studsvik;
- Evaluation of fuel fragmentation during the LOCA tests with fuelled test rods;
- Evaluation of the experiments and the relevant models.

The simulations were performed with version 2.0 of the code FRAPTRAN, applying only the finite difference and not the finite elements models available in the code.

The present paper summarises the results of the aforementioned tasks. The detailed descriptions of the experiments were omitted, as the final TECDOC is supposed to include these. The description of the separate effect ballooning and burst tests performed at the predecessor of MTA EK (KFKI AEKI) is not presented here either for copyright reasons, but can be found in Refs [1] and [2].

2. SIMULATION OF THE MTA EK SEPARATE EFFECT BALLOONING AND BURST TESTS

2.1. Main features of the tests

The experiments proposed for benchmarking were ballooning and burst tests performed on unirradiated, unoxidised Zircaloy-4 tubes at constant temperatures and constant pressure increase rates starting from 0 bars. Six cases were selected as closest to real large-break LOCA scenarios:

- PUZRY-26 (700 °C, 0.119 bar/s);
- PUZRY-30 (800 °C, 0.263 bar/s);
- PUZRY-18 (900 °C, 0.115 bar/s);
- PUZRY-8 (1000 °C, 0.076 bar/s);
- PUZRY-10 (1100 °C, 0.071 bar/s);
- PUZRY-12 (1200 °C, 0.072 bar/s).

The test tubes were 50 mm long with inner/outer diameters of 9.3/10.75 mm. The results of the tests are summarised in Fig. 1.

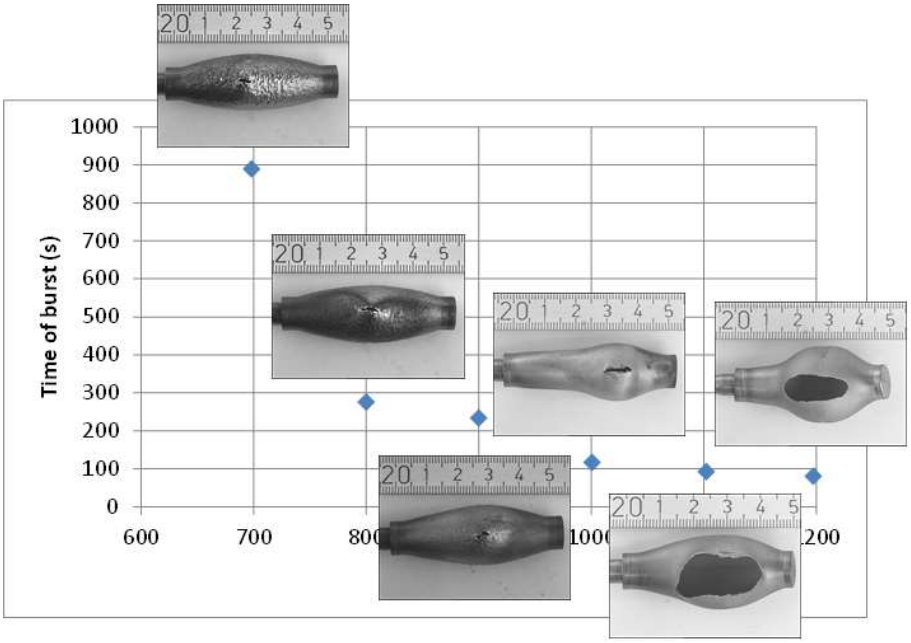

FIG. 1. Times of burst vs. temperature for the proposed 6 tests.

2.2. Input

In order to simulate such a simple setup, the following modelling assumptions were applied:

- The rod length was taken to be 45 mm, as the end plugs took the remaining 5 mm. The length had no effect on the results;
- A fictive fresh fuel stack with a diameter of 2.6 mm, a length of 41.5 mm and a relative density of 0.95 was modelled. This had no effect on the results, as it did not modify the cladding temperature and there was no mechanical contact between the pellets and the cladding;
- The prescribed cladding surface (and average) temperatures were provided by prescribing the same coolant temperature and a very large ($7 \cdot 10^4$ W/m^{2}K) heat transfer coefficient;
- A period of 100 s at room temperature and atmospheric pressure was included to achieve equilibrium before the start of the test;
- Only one axial node was defined, as the code had been tested with three nodes and there was no significant difference in the results;
- The plenum temperature was defined as identical with the cladding temperature at the plenum position (option trise=0 in the code);
- The inner pressure was prescribed as given in the experimental description (applying option prescri=1 in the code);
- After the measured time of burst the pressure history was continued in the input at the same pressure increase rate as previously to allow for calculated burst times longer than the measured ones.

Table 1 summarises the applied data that differed from the default values used by the code.

TABLE 1. INPUT DATA USED FOR THE SIMULATION OF THE MTA EK TESTS

Parameter	Value
Pellet OD (mm)	2.6
Density (%TD)	95
Height (mm)	10
burn-up (MWd/kgU)	0
Cladding material (—)	Zry-4
OD (mm)	10.75*
Rod active length (mm)	41.5
gap thickness (μm)	3350
fill gas (He) pressure at RT (MPa)	0.1
plenum volume (cm^3)	0.239

*Nominal value. The diameters were measured and given for each rod, the measured values were used for the simulation.

2.3. Results

Table 2 summarises the results of the measurements and the calculations. Figs. 2 to 4 show these results for burst pressure, time and tangential strain, respectively.

At low temperatures predicted burst pressures and time are much lower than the measured values. At higher temperatures this difference decreases, but an approx. 25% underestimation still remains. No significant trend can be established for the measured burst strains, the trend of calculated strains increasing with temperature can therefore not be evaluated against the measurements.

TABLE 2. RESULTS OF THE MEASUREMENTS AND THE CALCULATIONS.

No.	T (°C)	dp/dt (bar/s)	p_{burst} (bar)	t_{burst} (s)	$\varepsilon_{t\ avg}$ (%)	p_{calc}	t_{calc}	$\varepsilon_{t\ calc}$ (%)
26	698.4	0.1193	106.05	889	68	45.00	370	26
30	800.4	0.263	72.51	276	64	30.50	113	26
18	900.2	0.1151	26.89	234	40	15.50	127	41
8	1001	0.0763	8.9	117	49	5.20	56	85
10	1102.6	0.071	6.53	92	47	4.76	54	108
12	1197.7	0.0723	5.78	80	46	4.54	50	135

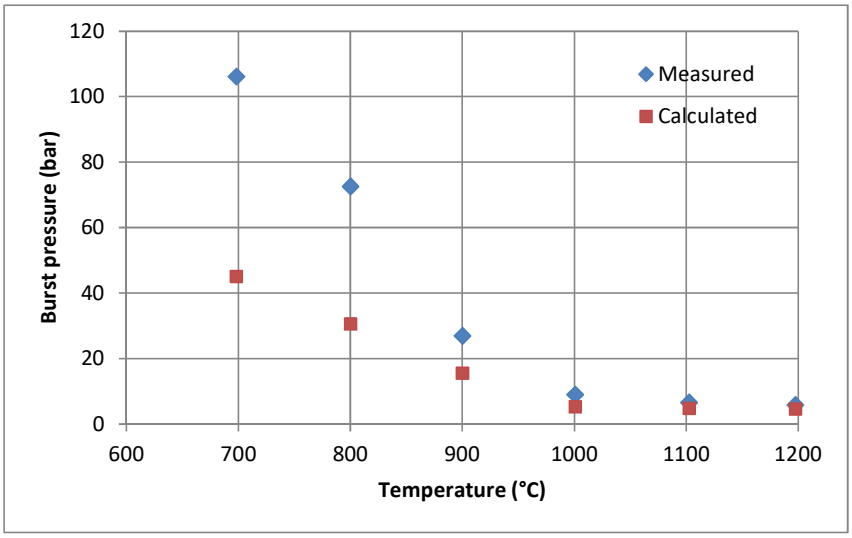

FIG. 2. Measured and calculated burst pressures.

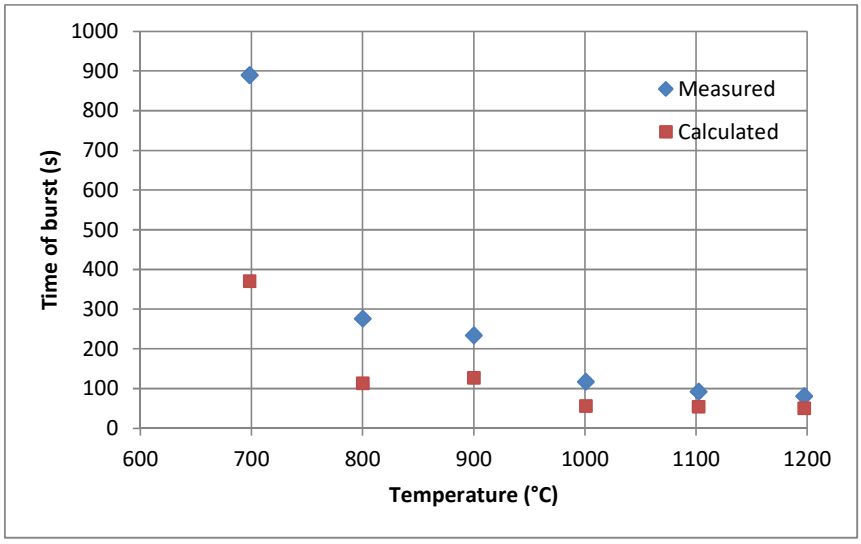

FIG. 3. Measured and calculated burst times.

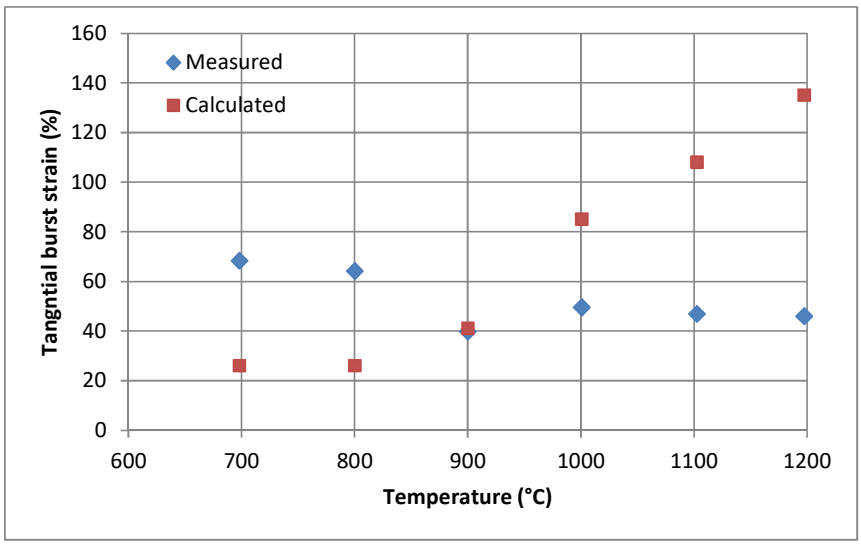

FIG. 4. Measured and calculated tangential burst strains.

3. SIMULATION OF THE HALDEN LOCA TEST IFA-650.10

3.1. Main features of the test

The test was performed on a 61 MWd/kgU section of a commercial PWR rod with an average burn-up of 56.2 MWd/kgU. The active length of the section was 441 mm, the unheated plenum volume was 16 cm^3, the fill gas for the LOCA test consisted of 95% argon and 5% helium.

Cladding temperature was measured on-line at three different heights: below (one thermocouple) and above (two thermocouples at the same height, but different azimuthal positions) the burst position and at the middle of the plenum length. The heater surface temperatures were also recorded at two different heights. Cladding elongation and rod internal pressure were also measured on-line. Neutron detectors were installed at three different heights along the active length.

The rod was surrounded by a heater, which was somewhat longer than the rod, to simulate the heating effect of neighbouring fuel rods. An external shroud surrounded the whole setup.

The rod was pre-conditioned at a linear heat generation rate (LHR) of 12-14 kW/m (similar to the last cycle loading in the power plant) for approx. 200 h to provide decay heat for the test. During this time the external and internal pressures were approximately equal to prevent cladding creep.

After the conditioning period the loop pressure was reduced and the loop was disconnected from the heavy-water loop, achieving natural circulation that was directed upwards next to the fuel rod and downwards between the heater and the containing shroud. The external heating was switched on. After stabilisation the LOCA event was simulated by initiating the blow-down. Cladding temperatures first decreased, then started to increase. Burst occurred after 249 s at 755 °C. According to the pressure curve, ballooning started after 155 s and was relatively slow for 13 s, then accelerated during the last 8 s as the cladding thickness decreased locally. The reactor was scrammed at 417 s.

The burst was rather small in terms of both length and tangential strain. Fuel relocation into the balloon was not significant and only little fuel was dispersed.

3.2. Input

The first simulation was done with boundary conditions interpolated on the basis of those provided by the Halden Reactor Project. The second simulation was done with boundary conditions provided by IBRAE on the basis of calculations performed by the code SOCRAT.

The input consisted of 20 axial sections, 20 fuel rings and 5 cladding layers. Linear heat generation rates provided in the experimental data set were increased by 0.05 kW/m, according to the Halden recommendations. During the LOCA test the axial power profile could be considered as constant and could be derived from the readings of the neutron detectors using spline interpolation. The five values provided by Halden were already obtained by interpolation from the three neutron detectors and one of them was close to the maximum, our interpolation did therefore not introduce any major uncertainty in the LHR values.

Cladding temperatures were only measured below and above, but not at the burst location, some interpolation was therefore necessary. The thermal-hydraulic conditions were rather complicated: at the start of natural circulation the coolant moved upwards between the rod and the heater, but after approx. 70 s an inner circle formed with the steam flowing downwards along the rod and upwards along the heater. This made the interpolation rather difficult and uncertain.

In the first run, different temperature profiles were tested. Fig. 5 shows a spline interpolation along the active length of the fuel rod, between the measured data. The last point is not part of the interpolation and is so low because the plenum temperature was modelled by introducing a last fictive 1 cm thick slice of fuel that had the temperature of the plenum minus

5.6 °C, because this is how the plenum temperature model of FRAPTRAN 1.4 (used initially for the simulation) reproduced the given plenum temperatures. Then the interpolation was modified so that the maximum temperature became 5, 10 and 50 °C lower than the value shown in the figure, to approach estimations provided by the Halden Reactor Project at the HPG meeting held in Antwerp in 2010. The plenum temperatures calculated by the code were tested against those produced by interpolation and the values agreed.

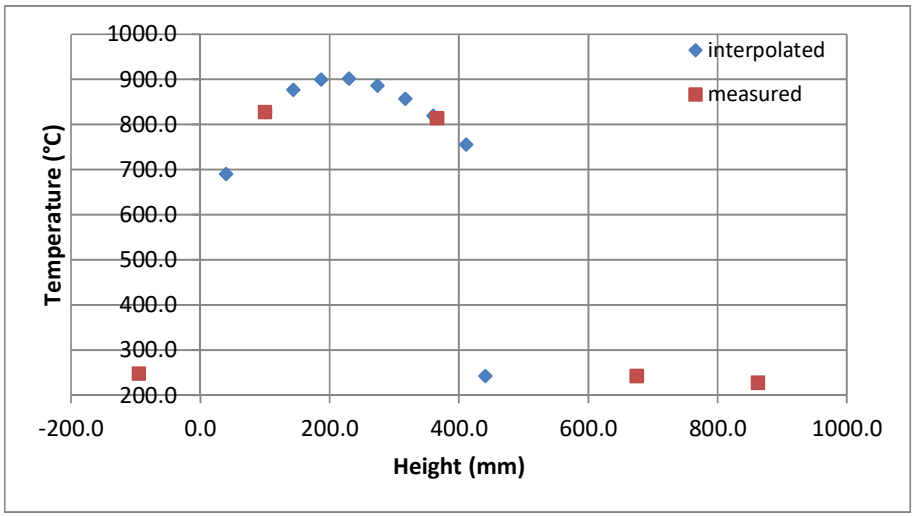

FIG. 5. Interpolated cladding temperatures.

In the second run the boundary conditions provided by IBRAE were used. Unfortunately, the circulation of the steam between the fuel rod and the heater could not be reproduced, moreover, the simulated cladding temperature was significantly higher (the strength of the cladding was lower according to the relevant model) and the plenum temperature was significantly lower in the IBRAE simulations than in the test. On the other hand, the IBRAE calculations could reproduce the double maximum in the axial temperature profile, which explains the double ballooning seen after the test.

FRAPTRAN was initialised with the end-of-life data measured before the LOCA test. Contradicting values were given for the diameter of the pellet and the gap size in the different sources, we could compile two sets of consistent data from these. For the second one the oxide layer thickness of approx. 25 µm was translated into a loss of metal thickness of 22 µm using the cube root of the Pilling-Bedworth ratio (1.16), which yielded a cladding thickness of 0.55 mm. This was combined with the cladding outer diameter of 9.44 mm to obtain a diametral gap of 10 µm when using a pellet diameter of 8.33 mm.

— The pellet outer diameter is 8.21 mm (as stated in the file Description_IFA_650_10.pdf provided in the framework of FUMAC) and the diametral gap is 150 µm as in [3] (referred to as ‘large gap’ in the simulations);
— The pellet outer diameter is 8.33 mm as in [3], but the diametral gap is 10 µm (corresponding to the roughness), according to the pictures that show a closed gap at room temperature (referred to as ‘closed gap’ in the simulations).

We consider the closed gap data as more credible, as the gap is supposed to be closed at such a burn-up.

Fuel density could be calculated on the basis of the initial density and the diameter change. The average fast flux suffered during base irradiation could be estimated from the cycle average LHR data and a conversion factor of $4 \cdot 10^{16}$ $m^{-2}s^{-1}/(kW/m)$ typical of 17×17 PWRs. The input data used for the simulations are summarised in Table 3.

TABLE 3. INPUT DATA FOR THE LOCA SIMULATION

Parameter	Value (large gap)	Value (closed gap)
Pellet OD (mm)	8.21	8.33
Density (% TD)	94	94
Height (mm)	13.78	13.78
Grain size (μm)	9.3	9.3
Burn-up (MWd/KgU)	61	61
Claddingmaterial (—)	Zry-4	Zry-4
OD (mm)	9.44	9.44
Average fast neutron flux (n/m^2s)	8.15×10^{17}	8.15×10^{17}
Oxide thickness (m)	20 – 30	20 – 30
H content (ppm)	220	220
Rod active length (mm)	441	441
Gap thickness (μm)	75	5
He in fill gas (%)	5	5
Ar in fill gas (%)	95	95
Fill gas pressure at RT (MPa)	4	4
Plenum volume (cm^3)	16	16

3.3. Results

Figs. 6 and 7 show the evolution of the rod internal pressure during the test for the interpolated (50 °C lower maximum) and the IBRAE boundary conditions, respectively, both for the closed gap geometry. The pressure in the interpolated case follows the measured values, however, burst is predicted too early. The low plenum temperature in the IBRAE case yields a low pressure in the rod, which is overcompensated by the cladding temperature higher in the IBRAE simulations than in the measurements. As a result, the burst occurs too early as well. We believe that the interpolation as suggested at the 2010 HPG meeting in Antwerp yields a physically more realistic evolution of the pressure and temperatures than the IBRAE boundary conditions. However, without accurately following the measured pressure and temperature history up to the beginning of the ballooning, nothing can be said about the goodness of the models implemented in the code.

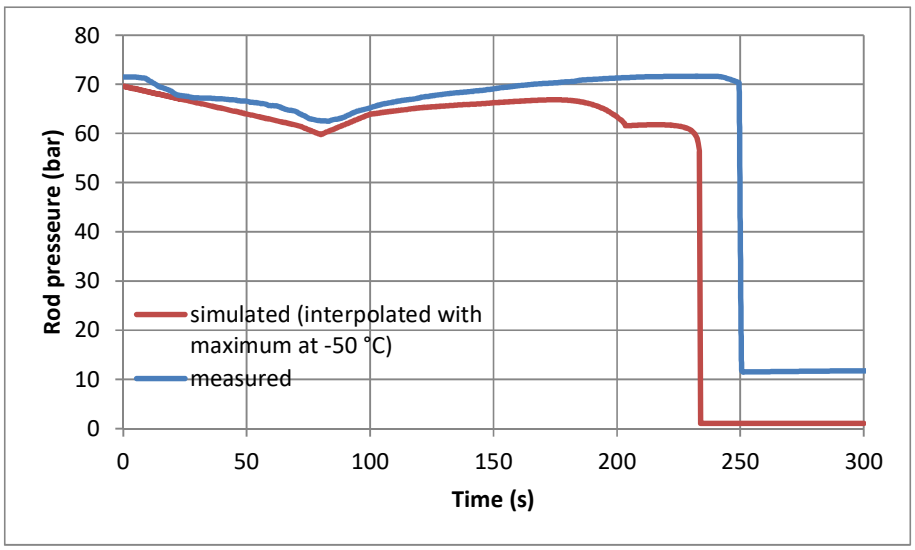

FIG. 6. Evolution of the rod internal pressure with the interpolated boundary conditions corresponding to the profile presented at the 2010 HPG meeting in Antwerp.

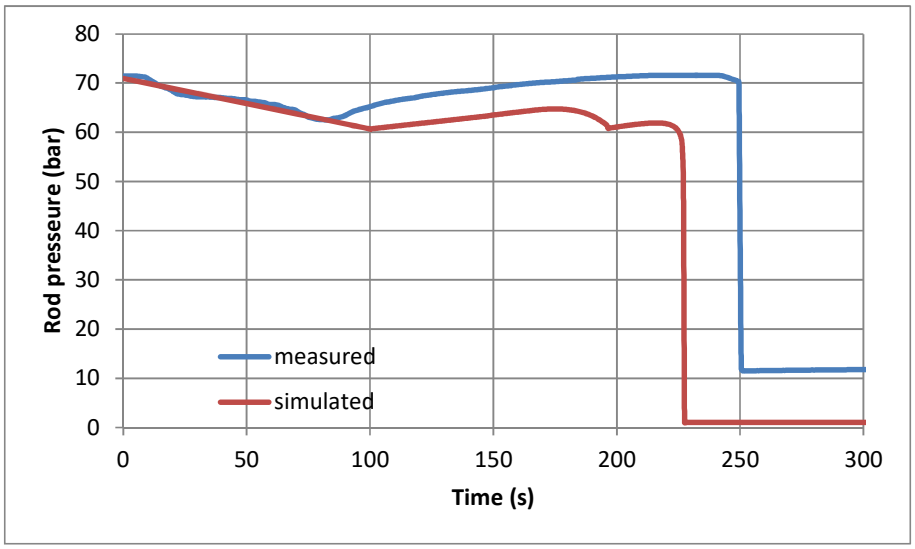

FIG. 7. Evolution of the rod internal pressure with the IBRAE boundary conditions.

Burst times and pressures were compared for all the different runs. Table 4 summarises the burst times calculated using interpolated cladding temperatures and using temperatures calculated by IBRAE, with the open and closed gap initial geometries.

The calculated burst height was 190 mm for the interpolated temperatures and 231 mm for the IBRAE boundary conditions, whereas the measured height was 260 mm. The reason for this discrepancy is unknown.

On the basis of the burn-up a rim layer of 100 µm can be estimated at the end of base irradiation. According to the temperature-dependent model used at MTA EK, where first fragmentation occurs at 600 °C, this layer suffers fragmentation during the test, which can be considered to be in accordance with the experimental results (‘little fragmentation’).

TABLE 4. RESULTS OF SIMULATION RUNS

Run	Burst pressure large gap (bar)	Burst time large gap (s)	Burst pressure no gap (bar)	Burst time no gap (s)
Interpolated T	62.3	199	59.4	203
Interpolated T with 5 °C lower maximum	62.7	201	59.4	205
Interpolated T with 10 °C lower maximum	63.4	203	59.4	208
Interpolated T with 50 °C lower maximum	56.5	228	56.4	234
IBRAE	57.9	221	50.5	228
Measurement	70.3	249.5	70.3	249.5

4. SIMULATION OF THE STUDSVIK LOCA TEST NO. 192

4.1. Main features of the test

A 300 mm section (mother rod burn-up: 68 MWd/kgU; test section burn-up: 78 MWd/kgU) of a commercial PWR fuel rod was filled with helium, welded and heated in a furnace in a steam atmosphere until burst. Heating started at 300 °C and continued at a rate of 5 °C/s up to 1200 °C. Cladding temperature was measured 50 mm above the middle of the rod by means of a thermocouple clamped to the fuel rod. Fill gas pressure was 82 bar at 300 °C. The test section had a lower and an upper plenum with identical pressure transducers in both of them.

4.2. Input

Base irradiation data were rather poor, so end-of-life measured data were used for the simulation. These were not very rich either.

The cladding outer diameter was measured. Assuming that the cladding thickness did not change during base irradiation and that the gap was closed, the pellet outer diameter could be estimated, which also yielded the change of density during base irradiation.

Fast neutron flux was estimated using the rough cycle lengths and cycle average LHRs, together with the same conversion factor as for the IFA-650.10 test, $4 \cdot 10^{16}$ $m^{-2}s^{-1}$/(kW/m).

The options explenumv and explenumt were used to simulate the piping running outside the furnace with unknown temperatures. The temperature of the external plenum was set in such a way that the pressure history within the rod matched the measured data as closely as possible up to the beginning of the ballooning (i.e. as long as only thermal expansion had to be taken into account). This way the behaviour of the cladding (the stresses in it) was the closest possible to the real situation.

Table 5 summarises the input data. The axial nodalisation was determined to match the profilometry data presented in the file NRC Studsvik LOCA test 192.xlsx provided in the framework of FUMAC.

The axial temperature profile was not measured during the test, but several profiles were provided. Unfortunately these contradicted to each other and often to physics as well. The distances below are taken from the centre of the furnace. The thermal centre is the position of the maximum temperature.

— There were measured data at 1200 °C central temperature [4] (measured probably shortly after reaching the required central temperature);

— There were approx. equilibrium axial data with a central temperature of 1205 °C and the profile fitted to these [4] (valid between +/–75 mm from the middle, around 1200 °C, calculated from oxidation; thermal centre at +9 mm);
— There was only a fitted profile (without measured data) valid during heat-up [5] (valid between a distance of +/–75 mm from the middle, between 600 °C and 1200 °C, for a heating rate of 5 °C/s; thermal centre at +4.5 mm), with parameters independent of temperature, which is unphysical;
— There were measured data and a fitted profile at the edge of the furnace for a central temperature of 1200 °C [5] (valid beyond +/–100 mm from the middle; thermal centre at 0 mm).[7] Note that for a central temperature of 300 °C this fit yields frozen edges.
— Figure 8 shows the above profiles.

TABLE 5. INPUT DATA FOR THE FRAPTRAN SIMULATION

Quantity	Unit	Value
Pellet		
OD	mm	8.38
Relative density	%	89
Height	mm	10
Grain size	µm	10
BU	MWd/kgU	78
Cladding		
material	–	ZIRLO
OD	mm	9.512
Average fast flux	n/m^2s	$7 \cdot 10^{17}$
Time of fast flux	s	$2 \cdot 10^{8}$
Oxide layer thickness	µm	25 (bottom) – 30 (top)
Hydrogen	ppm	176 (bottom) – 288 (top)
Rod		
Active length	mm	300
Gap thickness	µm	1
He^* fill gas pressure at 300 °C	MPa	8.2
Upper plenum volume	cm^3	1.2
Upper plenum T	K	373
Lower plenum volume	cm^3	0.7
Lower plenum T	K	373
External gas volume	cm^3	8.5
T of external gas volume	K	530

[7] Studsvik LOCA test machine data sheet.xlsx (provided in the framework of FUMAC).

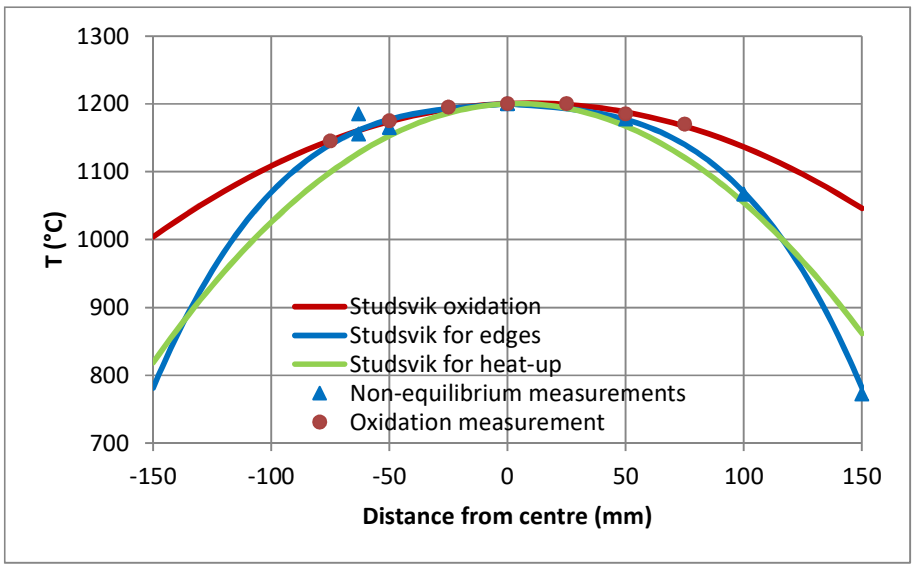

FIG. 8. Axial temperature profiles proposed by Studsvik.

Note that the heated length of the furnace was 267 mm [5], 15 mm at each end of the sample were therefore outside this section.

- The different positions of the thermal centres are problematic, especially when switching from one profile to the other;
- There is a large jump at the end of the heat-up phase to switch to the equilibrium profile.
- The equilibrium profile is in fact the average of heat-up, short-term and long-term hold profiles;
- All the profiles are independent of the central temperature, whereas axial thermal gradients are much higher for higher central temperatures than for lower ones.

We decided to fit our own temperature profile. Considering the short hold time, the heat-up profile was acceptable during all the test between +/–75 mm from the middle. At 1200 °C this reads in Kelvins as

$$T(x) = -0{,}016(x - 4{,}5)^2 + 1473 \quad (1)$$

At the edges (beyond +/–100 mm from the middle) we re-fitted the cubic curve so that the thermal centre be at 4.5 mm:

$$T(x) = -1{,}4 \cdot 10^{-4}|x - 4{,}5|^3 + 10^{-3}|x - 4{,}5|^2 - 0{,}1|x - 4{,}5| + 1473 \quad (2)$$

We assumed that

$$\nabla T = cT|_{x=4{,}5} \quad (3)$$

i.e. all the coefficients are proportional to the temperature in Kelvins. The resulting profiles can be seen in Fig. 9.

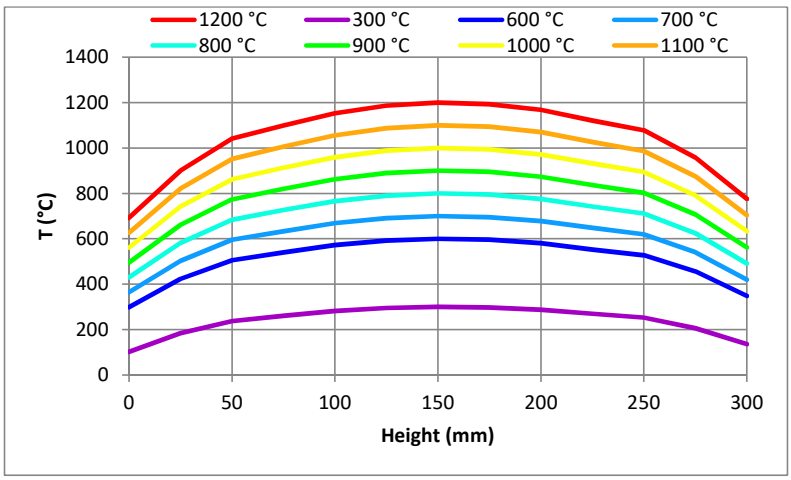

FIG. 9. Fitted axial temperature profiles for different central temperatures.

The axial temperature profile was defined in the input in such a way that the thermal centre be at the middle of one of the nodes and the thermocouple at another one.

5. RESULTS

The calculated pressure can be compared to the measured values in Fig. 10. Before ballooning starts the pressures correspond well, the calculated burst parameters correspond therefore to the real circumstances to which the rod was subjected. As ballooning occurs, the cladding mechanical models come into play in the overall pressure prediction with good results.

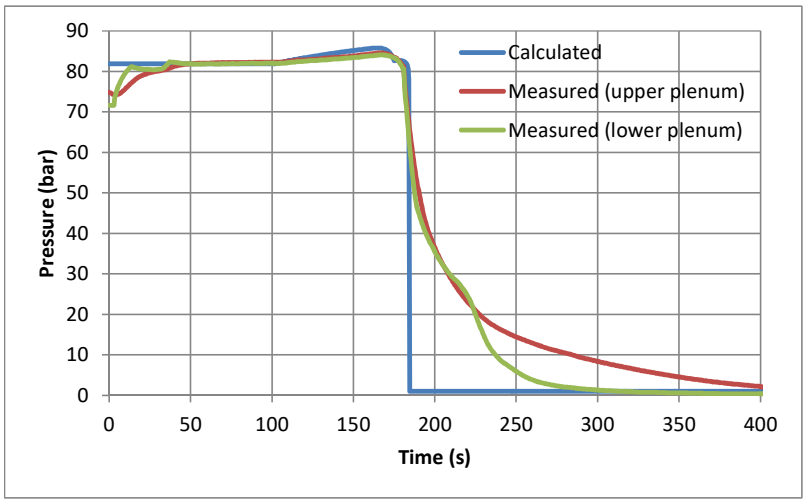

FIG. 10. Calculated and measured pressure histories during the test.

Table 6 summarises the results of the calculations as compared to the measurements. The agreement is excellent.

TABLE 6. MEASURED AND CALCULATED BURST PARAMETERS

Quantity	Measured	Calculated
Time (s)	82	85
Pressure (bar)	77	78
Temperature (°C)	700	738
Maximum strain (%)	80	74

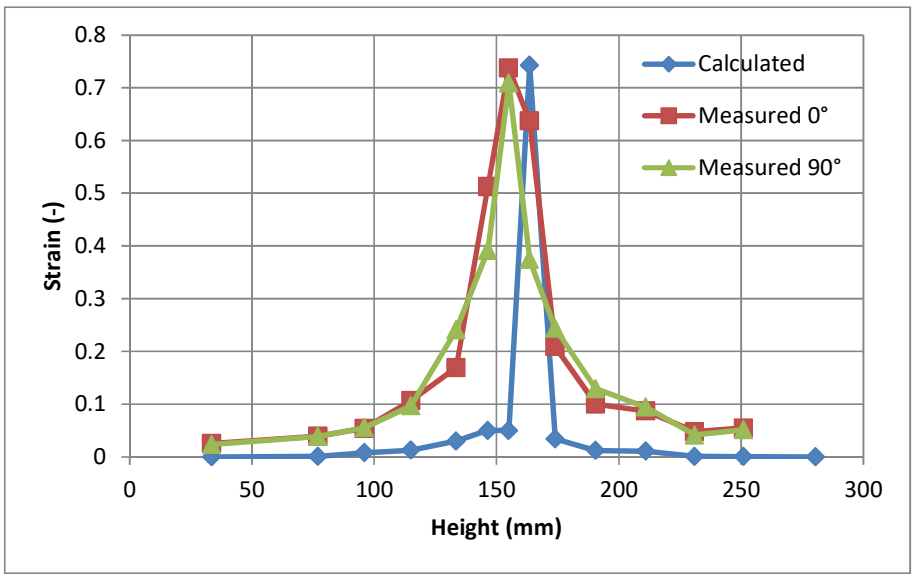

FIG. 11. Calculated and measured axial profiles after the test.

Figure 11. presents the calculated and measured axial profiles after the test. The agreement is very good. The calculated burst falls within the burst opening, but not at the position of the largest strain. Since the temperature profile is perfectly flat in this region, the position of the burst is where the hydrogen content was higher.

Unfortunately the rim width was not known at the beginning of the test. However, such a burn-up corresponds to a rim layer of approx. 190 µm. As the rim reached 600 °C in all its length, it is expected to fragment, which corresponds to 9% of the total fuel mass and means a total of 14 g of fine fragmentation. The amount of the finest fragments published in [6] is 23 g, which is a fair agreement, not to mention that the measured powder may contain fragmented fuel from the dark zone of the fuel as well.

6. CONCLUSIONS

During the co-ordinated work, the following conclusions could be drawn as regards the experimental datasets:

- It is very important to provide accurate boundary conditions, otherwise neither the simulation of the experiments, nor the inter-code comparisons can be meaningfully performed;
- For irradiated rods detailed base irradiation data are necessary;
- The consistency of geometrical data needs to be ensured;
- Measurements need to be meaningful (i.e. the rupture opening should not be included in the strain measurements).

The simulations were done using customised boundary conditions. For the Halden LOCA test IFA-650.10 the best results could be obtained using boundary conditions measured or proposed by the Halden Reactor Project. The results obtained using the boundary conditions calculated with the code SOCRAT were less good and it is somewhat questionable whether they reflect the processes that really occurred in the cladding, considering the significant differences between measured and calculated cladding temperatures.

The Studsvik LOCA test No. 192 was simulated using adjusted boundary conditions, as those provided for the exercise were consistent neither with physics, nor with each other. The temperatures and pressures of the external volumes (of pipes running outside the furnace) were set in such a way that the pressures inside the sample be similar to the measured values as long

as basically only thermal expansion was in play. This ensured that the cladding experienced the same stresses in the simulation as in reality. The results of the simulations were very good.

The inter-code comparisons did not reveal any specific advantages or shortcomings of the code FRAPTRAN 2.0. The code performed less well for very old Zircaloy-4 cladding specimens, which may be due to material properties significantly different from those of more recent batches, but other codes gave similar results. The two LOCA simulations performed with fuel rods clad in more recent versions of Zircaloy-4 gave good results.

REFERENCES

[1] Zoltán H., et al., Ballooning Experiments with VVER Cladding, Nuclear Technology Volume 152, Issue 3 2005 (273–285).

[2] Erzsébet P.F., et al., Experimental database of E110 claddings exposed to accident conditions, J. Nucl. Mater. Volume 397, Issues 1–3 (2010) 48–54.

[3] Lavoil A., LOCA Testing at Halden, the Tenth Experiment IFA-650.10, HWR-974 (2010).

[4] Helin, M., Flygare, J., NRC LOCA tests at Studsvik, Design and construction of test train device and tests with unirradiated cladding material, STUDSVIK/N-11/130.

[5] Flanagan, M. E., Askeljung, P., Post-Test Examination Results from Integral, High-Burnup, Fueled LOCA Tests at Studsvik Nuclear Laboratory, NUREG-2160 (2013).

MODELLING OF THE BEHAVIOUR OF INERT GASES IN OXIDE AND MIXED OXIDE NUCLEAR FUEL UNDER DESIGN BASIS ACCIDENT CONDITIONS

LELIO LUZZI, TOMMASO BARANI, LUANA COGNINI AND DAVIDE PIZZOCRI
Politecnico di Milano, Department of Energy,
Nuclear Engineering Division,
Via La Masa 34, 20156, Milan, Italy

Abstract

This final report summarizes the work performed by Politecnico di Milano (POLIMI) in the FUMAC Project. The objective is the development, implementation in fuel performance codes (FPCs), and validation of models for the behaviour of inert gas in UO_2 nuclear fuel during transients, together with their fundamental parameters. The introduction of these modelling capabilities intends overcoming current limitations of FPCs for the simulation of transients, such as (but not limited to) design basis accidents.

The activity of POLIMI focused on developing/improving three aspects of fission gas behaviour modelling in fuel performance codes, namely: the modelling of inter-granular gas behaviour, by the addition of a burst release model; the modelling of helium behaviour, by the proposal of improved correlations for its diffusivity; and the modelling of intra-granular fission gas behaviour, by the development of a new model describing intra-granular bubble evolution.

Each of these models embodies peculiar physical phenomena (e.g., intra-granular bubble nucleation, grain-boundary micro-cracking) which all together participate in the proper representation of the complete evolution of inert gas behaviour (IGB) during transients and design basis accidents (e.g., LOCAs). This represents a significant step forward with respect to the state of art, in which some of these phenomena are represented by fully empirical correlations (with none or very limited transient capabilities) and others are completely not represented despite their huge impact on the fuel performance.

The models have been implemented, tested, and verified in SCIANTIX (0D stand-alone code, developed by POLIMI), as well as in the fuel performance codes TRANSURANUS [1] (grain-boundary micro-cracking model) and BISON [2] (grain-boundary micro-cracking, intra-granular bubble evolution). The results were compared against available separate effect experiments and against integral irradiation experiments, showing a better predictive capability of the developed models compared to state-of-the-art ones.

As far as inert gas in oxide fuels is concerned, the extension of the work on helium is crucial (e.g., introducing in FPCs correlations for helium solubility in oxide fuel) due to the important role played by this gas in MOX fuels and in storage conditions. More in general, the following items are of interest, in perspective: the extension to other fuel materials (e.g., MOX) and other reactor conditions (i.e., fast reactors), the extension to include other non-inert fission products (e.g., caesium and iodine), and the inclusion of the description of collateral physical phenomena (e.g., restructuring of MOX fuels in fast reactor conditions).

1. INTRODUCTION

Among several aspects of nuclear fuel rod performance analysis, modelling of fission gas behaviour has a crucial role [3]. This is especially true during power/temperature transients (both heating and cooling transients, as those occurring in accident scenarios, e.g., LOCA).

POLIMI activity focused on the development of a model for burst release in oxide fuel, representing an extension of a previously developed diffusion-based model [4]. In fact, a purely diffusion-based model cannot account for the rapid kinetics of fission gas release (FGR) observed in temperature transients (burst release). For a complete and detailed description of

the new model, see Barani et al. [5]. In this report, only the main model assumptions and the main results are summarized, for the sake of brevity.

The model we propose derives from experimental observations relative to both in-reactor irradiation and post-irradiation annealing of UO_2 fuel [6]–[10]. In particular, several micrographs demonstrate the presence of micro-cracks in transient-tested fuel. This indicates micro-cracking as one of the basic mechanism of burst release. Clearly, other mechanisms could be involved in the process, and several models exist that explain release during transients in different way (as in Ref. [11]). A review of these models is out of the scope of this work. The proposed burst release model extends the diffusion-based model previously developed by Pastore et al. [4] by including the description of micro-cracking. This is modelled empirically as a reduction of the grain-face gas inventory and storing capacity during transients.

In the present activity, the basic diffusion-based model developed and validated in Pastore et al. [4] (available in TRANSURANUS and BISON) is generalized by the description of micro-cracking as causing a loss of the gas inventory and storing capacity of a fraction of the grain faces. Compared to the existing models, the proposed one:

— Reproduces the temperature dependence of burst release as observed experimentally; and
— Allows for the characteristic of the phenomenon as occurring in a limited range of conditions, yet allowing for continuity of the calculated fission gas release and swelling.

The resulting extended model (diffusion-based fission gas behaviour together with burst release) is overall semi-empirical, but the burst release capability notably maintains the continuity in both time and space as well as the consistent coupling of the calculated fission gas release and swelling. The burst release model is implemented in the TRANSURANUS fuel performance code, and validated through the simulation of fifty LWR fuel rod irradiation experiments of the OECD/NEA International Fuel Performance Experiments (IFPE) database [12] (Table 1). The results (Fig. 1) show a significant increase in the accuracy (considered the intrinsic uncertainty of fission gas release modelling in FPCs), confirming the improvement introduced by the application of the new burst release model.

The value of the measured FGR is the one obtained from puncturing at the end of the ramp test. All the experiments are from the OECD/NEA IFPE database [12]. In particular, experiments 1–18 are from the Super-Ramp PWR program, 19–25 are from the Super-Ramp BWR program, 26–36 are from the Inter-Ramp BWR program, 37–48 are from the Risø-3 program, 49 is from the REGATE program, and 50 is form IFA 597.3.

TABLE 1. SUMMARY OF THE EXPERIMENTS USED FOR THE VALIDATION OF THE BURST RELEASE MODEL

No.	Experiment	FGR, measured (%)	No.	Experiment	FGR, measured (%)
1	PK1-1	8.5	26	LR1	9.4
2	PK1-2	13.6	27	TR1	3.3
3	PK1-3	22.1	28	LS2	9.7
4	PK1-4	13	29	LS3	4.5
5	PK2-1	28	30	DR1	11.3
6	PK2-2	32.1	31	HR2	7.1
7	PK2-3	44.9	32	HR4	20.0
8	PK2-4	9.5	33	HR5	29.9
9	PK2-S	10.4	34	HS1	12.8
10	PK4-1	10.8	35	HS2	6.9
11	PK4-2	16.2	36	BR1	53.8
12	PK4-3	29.0	37	AN1	36.5
13	PK4-S	28.4	38	AN2	29.7
14	PK6-2	3.5	39	AN3	35.5

No.	Experiment	FGR, measured (%)	No.	Experiment	FGR, measured (%)
15	PK6-3	6.7	40	AN4	40.9
16	PK6-S	6.1	41	AN8	13.7
17	PW3-2	4.3	42	AN10	26.9
18	PW3-3	3.7	43	AN11	5.1
19	BK7-3	1.6	44	II1	16
20	BK7-4	0.8	45	II3	17.4
21	BK7-5	5.2	46	GE2	24.6
22	BK7-6	7.0	47	GE4	27
23	BG8-2	4.8	48	GE7	14.4
24	BG8-4	4.4	49	L10	10.2
25	BG9-1	7.4	50	Rod 8	15.8

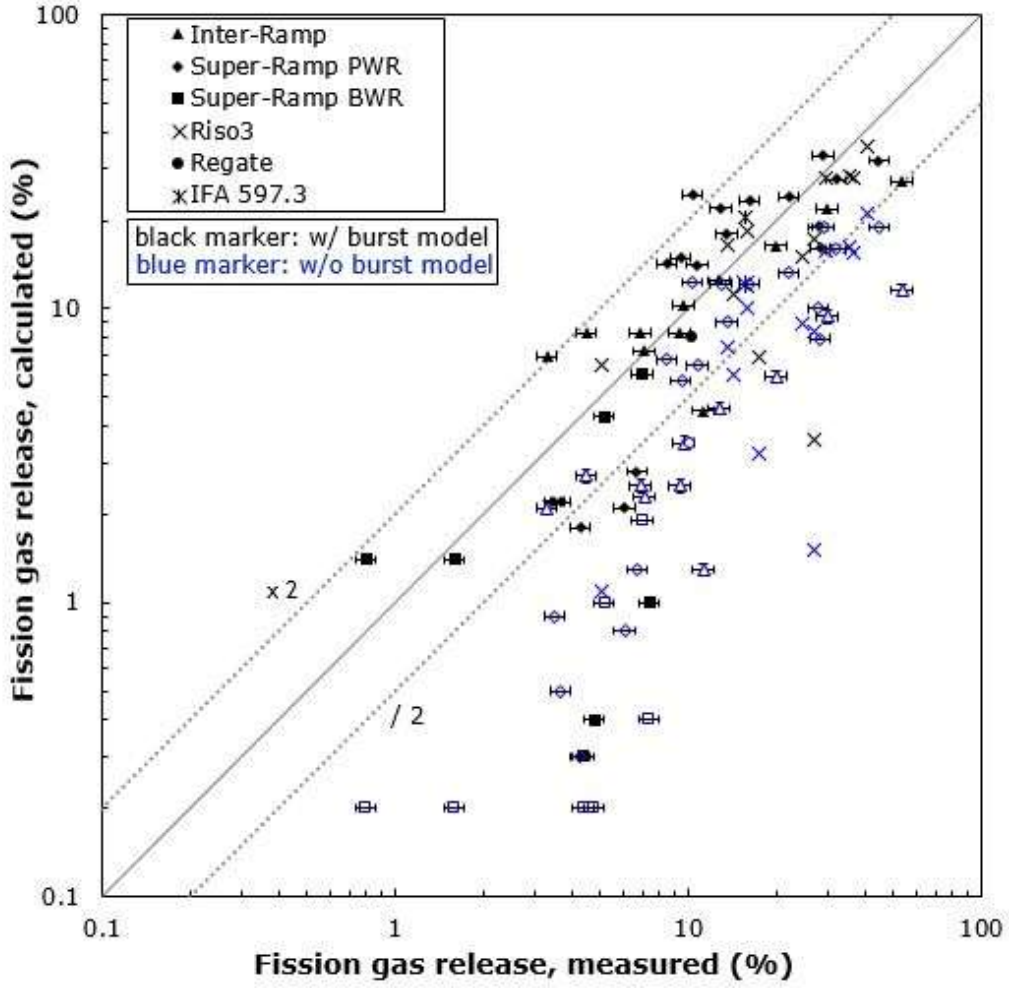

FIG. 1. Summary of the validation results of the burst release model in TRANSURANUS against fifty experiments from the IFPE database [12]. *Each point corresponds to a simulation.*

The distance of each point from the 45° line is a measure of the accuracy. The reported uncertainty bands are in agreement with Pastore et al. [13].

2. MODELLING OF HELIUM RELEASE DURING TRANSIENTS

Helium behaviour is one of the fundamental aspects in determining nuclear fuel performance, both in operation and during storage [3]. The production ways of helium in

nuclear fuel are ternary fissions, (n,α)-reactions and α-decay [14, 15]. Helium then precipitates into intra- and inter-granular bubbles and can be absorbed (or released) from (or to) the nuclear fuel rod free volume [16]. Helium thus contributes to the fuel gaseous swelling and to the pressure in the fuel rod plenum.

Helium diffusivity and solubility are the properties governing the transport and absorption/release mechanisms [17]–[19]. In particular, helium diffusivity determines its kinetics during transients, and is thus the fundamental property to be considered in simulation of design basis accidents. For this reason, POLIMI activity focused on the evaluation of helium diffusivity, in order to improve the description of helium behaviour in FPCs. In particular, POLIMI worked on the derivation of new and less uncertain correlations for helium diffusivity considering all the available literature data, after a critical analysis of the data themselves (for details, see Luzzi et al. [20]). The analysis evaluates three introduction techniques used experimentally, namely: infusion, ionic implantation, and doping. A considerable amount of experiments has been performed with the goal of determining the diffusivity of helium in nuclear fuel by means of these techniques [17]–[19], [21]–[31]. Table 2 collects all the diffusivity data available in the open literature. Fig. 2 shows the experimental data reported in Table 2. Two clusters of data emerge from Fig. 2: the measurements performed with the infusion technique (in the lower region), and those performed with the ion implantation and doping techniques (in the upper region). The overall spread of available diffusivities is extremely large. Therefore, we propose two distinct empirical correlations for the helium diffusivity.

By fitting independently the two clusters of data, the fitting quality results improved compared to a fit of the all data together. Nevertheless, the correlations for the helium diffusivity currently implemented in TRANSURANUS, as well as those available in the open literature, are derived from rough data fitting, or are intended to be engineering upper/lower boundaries to the data [14, 28].

The best estimate correlations derived are:

$$D = 2.0 \cdot 10^{-10} \exp[-2.12/kT] \tag{1}$$

in (m^2 s^{-1}), for the cluster of data from infusion, and

$$D = 3.3 \cdot 10^{-10} \exp[-1.64/kT] \tag{2}$$

in (m^2 s^{-1}), for the cluster from doping and ionic implantation.

For a more extensive discussion (and the related uncertainty analysis) of the derived correlation, see Luzzi et al. [20].

TABLE 2. SUMMARY OF THE EXPERIMENTAL HELIUM DIFFUSIVITIES IN OXIDE FUEL[8]

Sample	Diffusivity (m^2 s^{-1})	Temperature (K)	Ref.
	Infusion		
UO_2 powder (0.16 μm)	9.05×10^{-22}	968	[21]
UO_2 powder (0.16 μm)	1.01×10^{-20}	1070	[21]
UO_2 powder (0.16 μm)	4.08×10^{-20}	1166	[21]
UO_2 powder (0.16 μm)	1.86×10^{-19}	1268	[21]
UO_2 powder (4 μm)	1.5×10^{-17}	1473	[23], [32]
UO_2 single-crystal (1 μm)	6.14×10^{-18}	1473	[24]
UO_2 single-crystal (1 μm)	9.15×10^{-18}	1623	[24]
UO_2 single-crystal (1 μm)	12.57×10^{-18}	1773	[24]
UO_2 single-crystal (18 μm)	9.50×10^{-10} exp(-2.05/*kT*)	range 1170–2110	[18]
UO_2 single-crystal (18 μm)	4.88×10^{-10} exp(-1.93/*kT*)	range 1390–2070	[18]
	Ion implantation		
UO_2 poly-crystal	$(3.7\pm0.74)\times10^{-18}$	1273	[25]
UO_2 poly-crystal (8 μm)	6×10^{-17}	1373	[26]
UO_2 poly-crystal (10 μm)	8×10^{-9} exp(-(2±0.1)/*kT*)	range 1123–1273	[27]
UO_2 poly-crystal (10 μm)	4×10^{-10} exp(-(2±0.1)/*kT*)	range 1123–1273	[27]
UO_2 poly-crystal (24 μm)	2.25×10^{-17}	1073	[29]
UO_2 poly-crystal (24 μm)	7.6×10^{-17}	1373	[29]
$(U_{0.75},{}^{239}Pu_{0.25})O_2$ poly-crystal	9.2×10^{-18}	1123	[30]
$(U_{0.75},{}^{239}Pu_{0.25})O_2$ poly-crystal	1.6×10^{-16}	1273	[30]
UO_2 poly-crystal	5×10^{-10} exp(-(1.4±0.2)/*kT*)	range 973-1373	[31]
	Doping		
$(U_{0.9},{}^{238}Pu_{0.1})O_2$ poly-crystal	$(8\pm2)\times10^{-7}$ exp(-(2.00±0.02)/*kT*)	N/A	[28]
$(U_{0.999},{}^{238}Pu_{0.001})O_2$ poly-crystal (10 μm)	10^{-7} exp(-2.59/*kT*)	range 1320–1800	[33]

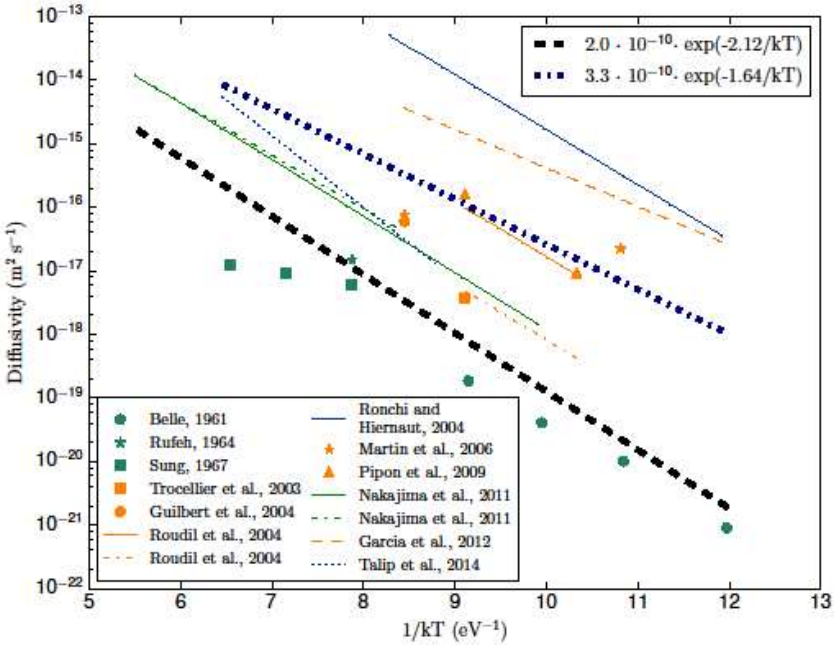

FIG. 2. Plot of the experimental helium diffusivity in oxide fuel.

[8] Available in the open literature, categorized depending on the technique used to introduce the helium in the samples.

The measurements performed via the infusion technique (dark green), those measurements performed via the ion implantation (orange) and doping (navy blue) technique. Each cluster is fitted by a distinct correlation (black dashed and blue dot-dashed).

3. MODELLING OF INTRA-GRANULAR FISSION GAS BEHAVIOUR DURING TRANSIENTS

The transport of inert gas from within the fuel grains to the grain boundaries (intra-granular FGR) is a fundamental controlling mechanism of FGR and gaseous swelling in nuclear fuel. In transient conditions, up to half of the gaseous fuel swelling can be ascribed to the volume of intra-granular fission gas bubbles [34]. Detailed modelling of the bubble evolution coupled with diffusion is hence required in FPCs.

The modelling of the intra-granular bubble evolution involves the description of three processes, namely:

- The nucleation of bubbles, which in UO_2 occurs 'heterogeneously' in the wake of fission fragments;
- Re-solution of gas bubbles caused by interaction with fission fragments and recoil atoms; and
- Diffusion-controlled trapping of atoms into existing bubbles [35, 36].

The state of the art of modelling intra-granular IGB still traces back to the formulation of Speight [37]. Such formulation represents the process mathematically as pure diffusion, with trapping/re-solution assumed in equilibrium and lumped within an effective diffusion coefficient. One-off nucleation is assumed, with empirical correlations accounting for the number density and radius of bubbles. This approach considerably simplifies the mathematical/numerical treatment, but is inherently based on the hypothesis of slowly varying temperature, thus failing to describe fast transients.

The new model for the evolution of intra-granular bubbles presented in this work physically describes the nucleation, re-solution and trapping processes (for detailed description of the model, see Pizzocri et al. [38]). This model is derived directly from the master equations of cluster dynamics [39]. Since the solution of these (thousands of coupled) master equations is impractical for engineering applications, the model considers a Fökker-Planck expansion in the phase space of the problem, and a subsequent average [39, 40].

The comparison of the results of the intra-granular fission gas model with the experimental data from Baker [41] in terms of bubble concentration and of radius of intra-granular bubbles provided satisfactory results, especially when compared to other models available in the open literature (Table 3, see the review of Olander and Wongsawaeng, [36]). This intra-granular IGB model has been implemented in the BISON code [38].

TABLE 3. SIMULATION RESULTS COMPARED TO THE DATA OF BAKER [41]. THE RESULTS OF OLANDER AND WONGSAWAENG [36] MODEL ARE REPORTED FOR COMPARISON.

Intra-granular bubble radius (nm)				
Temperature (K)	Baker, 1977	Olander and Wongsawaeng, 2006		Present model
		Heterogeneous	Homogeneous	
1273	0.55	0.4	1.0	0.45
1373	0.60	-	-	0.53
1473	0.65	-	-	0.59
1573	0.70	-	-	0.63
1673	0.80	-	-	0.66
1773	0.88	-	-	0.67
1873	0.98	1.6	5.1	0.68
1973	1.10	-	-	0.68
2073	1.25	-	-	0.68
Bubble number density (10^{23} bubbles m^{-3})				
Temperature (K)	Baker, 1977	Olander and Wongsawaeng, 2006		Present model
		Heterogeneous	Homogeneous	
1273	8.7	7	3	6.33
1373	7.8	-	-	5.69
1473	7.0	-	-	5.24
1573	6.4	-	-	4.97
1673	5.7	-	-	4.82
1773	5.3	-	-	4.75
1873	4.8	2	0.03	4.72
1973	4.4	-	-	4.71
2073	3.8	-	-	4.71

ACKNOWLEDGMENTS

This work has been carried out as part of a collaboration between POLIMI, the BISON team at Idaho National Laboratory, and the TRANSURANUS team at Joint Research Centre - Karlsruhe. The authors are grateful to Alessio Magni (POLIMI) for his contribution to the modelling of intra-granular fission gas behaviour.

REFERENCES

[1] LASSMANN, K., SCHUBERT, A., VAN UFFELEN, P., GYORI, C., VAN DE LAAR, J., TRANSURANUS Handbook. Karlsruhe, Germany: Institute for Transuranium Elements, (2014).

[2] J. D. HALES et al., BISON Theory Manual: the quations behind nuclear fuel analysis. Tech. Rep. INL/EXT-13-29930, Rev. 1, Idaho Falls (2014).

[3] OLANDER, D.R., Fundamental Aspects of Nuclear Reactor Fuel Elements Fundamental Aspects of Nuclear Reactor Fuel Elements. (1976).

[4] PASTORE, G., LUZZI, L., MARCELLO, V.D., VAN UFFELEN, P., Physics-based modelling of fission gas swelling and release in UO2 applied to integral fuel rod analysis, Nucl. Eng. Des., Vol. 256, (2013) 75–86.

[5] BARANI, T., et al., Analysis of transient fission gas behaviour in oxide fuel using BISON and TRANSURANUS, J. Nucl. Mater., Vol. 486, (2017) 96–110.

[6] ROTHWELL, E., The release of Kr85 from irradiated uranium dioxide on post-irradiation annealing, J. Nucl. Mater., Vol. 5, (1962) 241–249,.

[7] NOTLEY, M. J. F. and MacEwen, J. R., Stepwise release of fission gas from UO_2 fuel, Nucl. Appl., Vol. 2, (1966) 477.

[8] HASTINGS, I. J., SMITH, A. D., FEHRENBACH, P. J., CARTER, T. J., Fission gas release from power-ramped UO2 fuel, J. Nucl. Mater., Vol. 56 (1986) 233–256.
[9] WALKER, C. T., KNAPPIK, P., MOGENSEN, M., Fission gas release from power-ramped UO_2 fuel, J. Nucl. Mater., Vol. 161, (1988) 531–543.
[10] KASHIBE, S., UNE, K., NOGITA, K., Formation and growth of intragranular fuels with burnup of 6-83 GWd/t fission gas bubbles in UO_2, J. Nucl. Mater., Vol. 206, (1993) 22–34.
[11] VESHCHUNOV, M. S., TARASOV, V. I., Modelling of irradiated UO2 fuel behaviour under transient conditions, J. Nucl. Mater., Vol. 437, No. 1–3, (2013) 250–260.
[12] SARTORI, E., KILLEEN, J., TURNBULL, J. A., International Fuel Performance Experiments (IFPE) database, (2010).
[13] PASTORE G., et al., Uncertainty and sensitivity analysis of fission gas behavior in engineering-scale fuel modeling, J. Nucl. Mater., Vol. 456, (2015) 398–408.
[14] FEDERICI, E., COURCELLE, A., BLANPAIN, P., COGNON, H., Helium production and behavior in nuclear oxide fuels during irradiation in LWR, Proc. Int. LWR Fuel Perform. Meet. San Fr. Calif., (2007) 664–673.
[15] BOTAZZOLI, P., Helium Production and Behaviour in LWR Oxide Nuclear Fuels, PhD Thesis, Politec. di Milano, Italy (2011).
[16] MATZKE, H., Gas release mechanisms in UO_2 - a critical review, Radiat. Eff., (1980).
[17] E. MAUGERI et al., Helium solubility and behaviour in uranium dioxide, J. Nucl. Mater., Vol. 385, No. 2, (2009) 461–466.
[18] NAKAJIMA, K., SERIZAWA, H., SHIRASU, N., HAGA, Y., ARAI, Y., The solubility and diffusion coefficient of helium in uranium dioxide, J. Nucl. Mater., Vol. 419, no. 1–3, (2011) 272–280.
[19] TALIP, Z., et al., "Helium behaviour in stoichiometric and hyper-stoichiometric UO2," J. Eur. Ceram. Soc., vol. 34, no. 5, pp. 1265–1277, 2014.
[20] LUZZI, L., et al., Helium diffusivity in oxide nuclear fuel: Critical data analysis and new correlations, Nucl. Eng. Des.
[21] BELLE, J., Uranium Dioxide: properties and nuclear applications, Library (1961) 569–589.
[22] HASKO S., SZWARC, R., Noble gas solubility and diffusion in UO_2, AEC, Div. React. Dev. Washingt., (1963).
[23] RUFEH, F., Solubility of helium in uranium dioxide, M. S. Thesis, Univ. Calif., (1964).
[24] SUNG, P., Equilibrium solubility and diffusivity of helium in single-crystal uranium dioxide, PhD Thesis, Univ. Washingt., (1967).
[25] TROCELLIER, P., et al., Application of nuclear reaction geometry for 3He depth profiling in nuclear ceramics, Nucl. Instruments Methods Phys. Res. Sect. B Beam Interact. with Mater. Atoms, Vol. 206 (2003) 1077–1082.
[26] GUILBERT, S., et al., He migration in implanted UO2 sintered disks, J. Nucl. Mater., Vol. 327, (2004) 88–96.
[27] ROUDIL, D., "Helium thermal diffusion in a uranium dioxide matrix," J. Nucl. Mater., vol. 325, no. 2–3, pp. 148–158,
[28] RONCHI, C.,. HIERNAUT, J. P., Helium diffusion in uranium and plutonium oxides, J. Nucl. Mater., Vol. 325, no. 1, (2004) 1–12.
[29] MARTIN, G. et al., A NRA study of temperature and heavy ion irradiation effects on helium migration in sintered uranium dioxide, J. Nucl. Mater., Vol. 357, no. 1–3, (2006) 198–205.
[30] PIPON, Y., RAEPSAET, C., ROUDIL, D., KHODJA, H., The use of NRA to study thermal diffusion of helium in (U,Pu)O2, Nucl. Instruments Methods, Vol. 267, no. 12–13, (2009) 2250–2254.

[31] GARCIA, P., et al., “A study of helium mobility in polycrystalline uranium dioxide,” J. Nucl. Mater., vol. 430, no. 1–3, pp. 156–165, 2012.
[32] RUFEH, F., OLANDER, D. R., PIGFORD, T. H., The solubility of helium in uranium dioxide, Nucl. Sci. Eng., 1965.
[33] TALIP, Z., et al., Thermal diffusion of helium in 238Pu-doped UO2, J. Nucl. Mater., Vol. 445, no. 1–3, (2014) 117–127.
[34] WHITE, R. J., CORCORAN, R. C., BARNES, P. J., A Summary of Swelling Data Obtained from the AGR/Halden Ramp Test Programme, (2006).
[35] TURNBULL, J. A., The distribution of intragranular fission gas bubbles in UO2 during irradation, J. Nucl. Mater., Vol. 38, no. 2, (1971) (203–212).
[36] OLANDER D. R., WONGSAWAENG, D., Re-solution of fission gas - A review: Part I. Intragranular bubbles, J. Nucl. Mater., Vol. 354, no. 1–3, (2006) 94–109.
[37] SPEIGHT, M. V., A Calculation on the Migration of Fission Gas in Material Exhibiting Precipitation and Re-solution of Gas Atoms Under Irradiation, Nucl. Sci. Eng., vol. 37, (1969) 180–185.
[38] PIZZOCRI, D., et al., A model describing intra-granular fission gas behaviour in oxide fuel for advanced engineering tools, J. Nucl. Mater.
[39] FELL, M., MURPHY, S. M., The nucleation and growth of gas bubbles in irradiated metals, J. Nucl. Mater., Vol. 172, no. 1(1990) 1–12.
[40] CLEMENT, C. F., WOOD, M. H., The principles of nucleation theory relevant to the void swelling problem, J. Nucl. Mater., Vol. 89, no. 1, (1980) 1–8.
[41] BAKER, C., The fission gas bubble distribution in uranium dioxide from high temperature irradiated SGHWR fuel pins, J. Nucl. Mater., Vol. 66, (1977) 283–291.

SIMULATION OF FUEL BEHAVIOR DURING LOCA CONDITION USING FRAPCON/FRAPTRAN AND THE COUPLED MARS-KS CODE:

HYOCHAN KIM, CHANGHWAN SHIN, YONGSIK YANG, YANGHYUN KOO
Nuclear Fuel Safety Research Division,
Korea Atomic Energy Research Institute (KAERI),
111, Daedeok-daero 989beon-gil, Yuseong-gu, Daejeon, 34057,
Republic of Korea
E-mail: hyochankim@kaeri.re.kr (corresponding author)

Taewan Kim
Incheon National University (INU),
119 Academy-ro, Yeonsu-gu, Incheon
Republic of Korea

Abstract

KAERI and INU are participating in the FUMAC project with FRAPCON/FRAPTRAN and MARS-KS, which is a system analysis code for the Korean regulatory body. Therefore, IFA650-2, 9 and 10 were selected for the evaluation because the IFA650 series take into account the thermal hydraulic conditions. KAERI has been developing the fully coupled MARS-KS/FRAPTRAN code system to simulate the fuel behavior and to evaluate safety criteria. Simulation cases were distinguished along the T/H conditions, such as CASE1/2/3/4 for IFA650.2/9/10, respectively.

1. INTRODUCTION

KAERI participates in FUMAC with FRAPCON/FRAPTRAN and MARS-KS, which is system analysis code used as an audit code in Korea. For FUMAC contribution, IFA 650.2, 650.9, and 650.10 were chosen for the simulation. Recently, KAERI and INU (Incheon National University) have been developing a fully coupled MARS-KS/FRAPTRAN code system to simulate the fuel behavior during LOCA [1, 2].

Therefore, fuel of the IFA650 series as well as T/H (thermal hydraulic) of the Halden loop were modelled and simulated to obtain the dedicated T/H conditions during testing. The experiments other than Halden (Studsvik, MTA and QUENCH) do not take into account the thermal hydraulic behavior.

Depending on the T/H boundary conditions, CASES are distinguished as follows:

- CASE1: FRAPTRAN Stand Alone With the measured data (Surface Temperature);
- CASE2: FRAPTRAN Stand Alone With the cladding surface Temperature calculated by MARS-KS;
- CASE3: MARS/FRAPTRAN fully coupled calculation;
- CASE4: FRAPTRAN Stand Alone With the cladding surface Temperature calculated by SOCRAT.

Table 1 shows the modelling and simulation of the experiments with T/H boundary conditions. To evaluate the thermal hydraulic model with a minimized fuel effect, IFA650.2, which conducts tests with fresh fuel, was simulated using FRAPTRAN, MARS, and the coupled code. Based on the IFA650.2 T/H model, IFA650.9 and IFA650.10 were simulated. The results of CASE1, CASE2, CASE3, and CASE4 were compared and studied in terms of the T/H condition. In particular, the T/H results of MARS were compared against those of SOCRAT, which includes the fuel model and fuel relocation model.

TABLE 1. SIMULATION CASES

Database				
IFA650.2	CASE1	CASE2	CASE3	
IFA650.9	CASE1	CASE2	CASE3	CASE4
IFA650.10	CASE1			CASE4

2. DEVELOPMENT OF MARS-KS/FRAPTRAN FULLY COUPLED CODE SYSTEM

2.1. FRAPTRAN and MARS-KS

The Fuel Rod Analysis Program Transient (FRAPTRAN) is a Fortran language computer code that calculates the transient performance of light-water reactor fuel rods during reactor transients and hypothetical accidents such as loss-of-coolant accidents, anticipated transients without a scram, and reactivity-initiated accidents. FRAPTRAN calculates the temperature and deformation history of a fuel rod as a function of the time-dependent fuel rod power and coolant boundary conditions. Although FRAPTRAN can be used in "standalone" mode, it is often used in conjunction with, or with input from, other codes. The phenomena modeled by FRAPTRAN include

- Heat conduction;
- Heat transfer from the cladding to coolant;
- Elastic-plastic fuel and cladding deformation;
- Cladding oxidation;
- Fission gas release; and
- Fuel rod gas pressure.

FRAPTRAN is programmed for use on Windows-based computers but the source code may be compiled on any other computer with a Fortran 2008 and newer compiler. The burnup-dependent parameters may be initialized from the FRAPCON steady-state single rod fuel performance code [3].

The MARS-KS (Multi-dimensional Analysis of Reactor Safety) code has been developed by KAERI for a multi-dimensional and multi-purpose realistic thermal-hydraulic system analysis of light water reactor transients. The backbone of the code has been built by unifying and restructuring the RELAP5/MOD3 and COBRA-TF1 codes [4]. The MARS-KS code has the capability of analyzing a one-dimensional and three-dimensional thermal-hydraulic system as well as the fuel responses of light water reactor transients. The thermal hydraulic modeling capability of the MARS code has been continuously improved and extended for an application, not only to light and heavy water reactors but also to research reactors and to many advanced reactor types. Many improved models and capabilities were added to the code, and the latest version of the series is the MARS-KS 1.4. Notable upgrades include 3-dimensional simulation capabilities incorporated into the latest version in order to treat a turbulent mixing model and a conduction model. MARS-KS has been mainly used for regulatory activities by Korea Institute of Nuclear Safety (KINS).

2.2. Coupling methodology

To develop the MARS-KS/FRAPTRAN code system, the coupling methodology should be defined because each code system was already used and validated with their own methodology. As shown in Fig. 1, we proposed a coupling methodology of two codes for a steady state and transient maintaining each calculation flow and I/O (Input/Output) system.

At the beginning of a fully coupled calculation, MARS-KS performs a steady state calculation with an input file. For this calculation, MARS-KS employs its heat structure instead of a fuel rod. We call the 1st SS (steady state) calculation, which performs a null transient

calculation without FRAPCON/FRAPTRAN. Once MARS-KS completes the 1st SS, it calls S-fraptran (simplified-fraptran) which is modulized FRAPTRAN to be implemented into MARS-KS. For the first calling, S-fraptran initiates the input variables and stores the FRAPCON result file to apply burnup dependent variables. The s-fraptran starts the fuel stabilization, which gradually increases the power to stabilize the fuel thermo-mechanical behavior. We call the 2nd SS for fuel stabilization. Once the fuel stabilization is completed, fully coupled MARS-KS/FRAPTRAN is ready to start the transient calculation for LOCA.

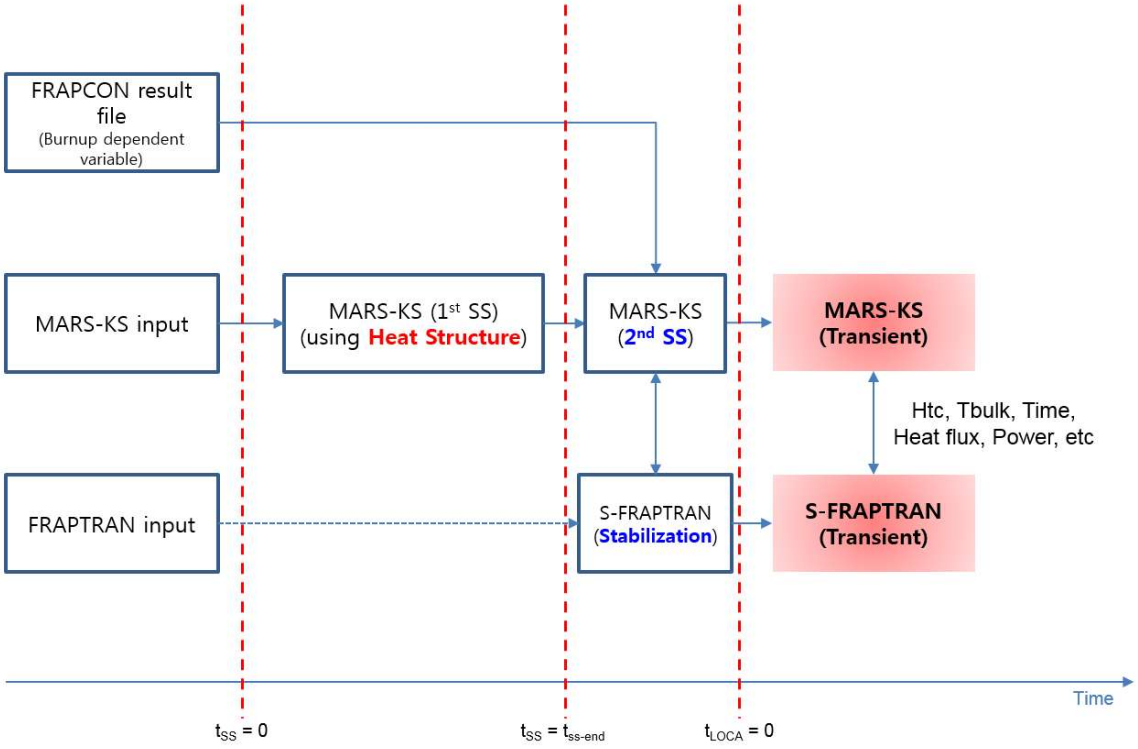

FIG. 1. Coupling methodology of fully coupled MARS/FRAPTRAN.

TABLE 2. COUPLED VARIABLES OF MARS/FRAPTRAN CODE SYSTEM

Calling module	Variable name	Content
S-fraptran	Timeincrement	Size of Time step
	Power	Linear Heat Generation Rate (LHGR)
	CoolPress	Coolant pressure
	Htc	Heat transfer coefficient of cladding surface
	Tbulk	Coolant T
MARS-KS	Outdia	Cladding outer diameter (incl. oxide thickness)
	Heatflux	Cladding heat flux
	Tsurf	Cladding surface T

Coupling variables between MARS-KS and FRAPTRAN were defined as shown in Table 2. For the current time step, MARS-KS calculates the time increment, LHGR, coolant pressure, heat transfer coefficient, and coolant temperature. All variables are stored for S-FRAPTRAN calculation. Subsequently, S-FRAPTRAN calculates the deformed cladding diameter, heatflux, and cladding surface temperature. Those variables are also stored for MARS-KS calculation for next time step.

The fuel module requires power and thermal hydraulic boundary conditions at the surface of the outer cladding to calculate the thermo-mechanical behavior of fuel during LOCA. In addition, the coolant pressure affects the cladding deformation. The system code requires the

outer diameter of the cladding and heatflux considering the radial burnup distribution, gap conductance, and metal water reaction energy. All variables are stored in the module and updated at each time step.

2.3. Modulization of FRAPTRAN (S-FRAPTRAN)

FRAPTRAN2.0 code was modulized as S-fraptran to implement FRAPTRAN into MARS-KS. Basically, FRAPTRAN was modernized to F90. Its environment should be identical to MARS-KS V1.4 as Intel Visual Fortran Composer XE2013 Update2.

To couple the variables of two codes, a new module (MARSLINK) was created in S-fraptran. When the subroutine uses this module, the subroutines are able to access the coupled variables. In addition, new subroutines were added into S-fraptran to obtain new variables from MARS-KS. Some of the subroutines were eliminated because the thermal hydraulic calculations were carried out in MARS-KS. However, the I/O system was maintained to easily use the I/O file for a fuel code user and MARS-KS code user.

When MARS-KS calls S-FRAPTRAN for the current time step, the fuel calculation begins with the input file. If it is the first call, S-FRAPTRAN initializes the variables with the input file and FRAPCON file to take into account the burnup dependent effects. Unlike FRAPTRAN Stand Alone, MARS-KS controls the time increment. Therefore, the time increment from MARS-KS is added for calculation. The procedure of S-FRAPTRAN is identical to that of FRAPTRAN except for the thermal hydraulic calculation. In addition, LHGR and the coolant pressure of all nodes are given from MARS-KS. Once the fuel calculation ends, the main subroutine of MARS-KS begins.

3. MODELLED CASES AND MODELLING DETAILS

3.1. IFA 650.2

The main purpose of IFA-650.2 was to practice the test case with ballooning and a fuel failure to find out how to run the later experiments with the pre-irradiated rods. The test was carried out using a fresh pressurized PWR rod and low fission power to achieve the desired conditions for ballooning and oxidation. The target peak cladding temperature (PCT) of 1050°C was reached, and a clad ballooning and rupture occurred at ~800°C [5].

Due to fresh fuel, FRAPCON simulation is not required. To simulate the transient behavior of a fuel rod, the FRAPTRAN input was generated as follows: fresh conditions (0 MWD/t); gap gas, 100 % He; 40 bar@Room Temperature; simulation time, 0 ~ 250s (time step of 0.01s); ALHR/axial power shape provided in the DB (database); Plenum T, TOA(Coolant Outlet Temperature) + 5.6 K; coolant pressure provided in DB; HT oxidation, C-P model; and deformation, Balon2 model.

The plenum temperature mainly determines the plenum pressure, which affects the burst strain and time. For this simulation, the plenum temperature is assumed as the coolant outlet temperature plus 5.6 K because the plenum void is extended to the upper flask channel for the pressure measurement. Therefore, the plenum temperature and time were prescribed as input with ‘prestmp=1’ option. The fill gas mole in the test rod is calculated using the void volume and pressure as 0.02726.

For CASE2, T/H conditions at each axial node were calculated using MARS-KS. The plenum temperature of CASE2 was determined as the coolant outlet temperature to follow the same methodology as CASE1. For CASE2, T/H conditions at each axial node were generated using MARS-KS. The plenum temperature of CASE2 was determined as the coolant outlet temperature to follow the same methodology of CASE1. Except for the T/H input sequence, the Halden loop model for MARS-KS is identical to the IFA650 series. For CASE3, the fully coupled MARS-KS/FRAPTRAN was simulated with MARS-KS S.A. input and FRAPTRAN S.A. input. However, the prescribed plenum temperature in FRAPTRAN input was eliminated,

and the default option of FRAPTRAN (T_bulk@topnode + 5.6K) was applied. To simulate the T/H system, the Halden loop was also modelled, as shown in Fig. 2.

For a steady state condition, the flow rate through the section, the power of the fuel rod, and the electric heater were obtained from the measured data. For the transient calculation, the sequence is as follows: the flow valves close 1 s before the blowdown valve opens: When the maximum cladding temperature reaches 1143.15 K, the coolant mass flow of 0.019 kg/s to simulate the spray cooling is inserted into the top region of the fuel channel. The spray cooling model in MARS-KS is not prepared, and thus we assumed the spray as having a continuous flow rate. The amount of spray coolant is assumed to match the measured data.

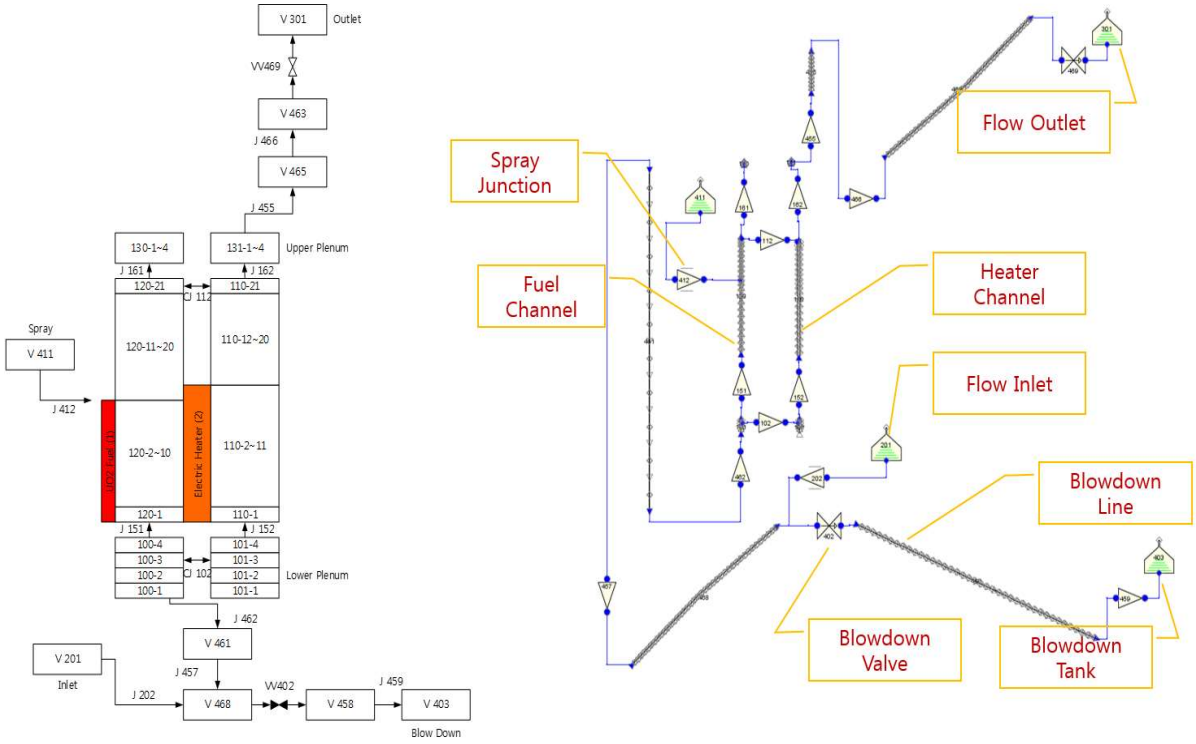

FIG. 2. Nodalization and MARS-KS model for Halden loop.

3.2. IFA650.9

A high burnup (89.9 MWd/kgU) PWR fuel rod was used in the 9th LOCA test IFA-650.9. The test segment was cut from a standard PWR fuel rod between spacers 2 and 3. This segment was a sibling rod to the one used for the previous test, IFA-650.4. It had been irradiated in the PWR Gösgen (Switzerland) during seven cycles (average cycle powers 325, 265, 290, 185, 175, 165 and 155 W/cm) and discharged in June 1998, as shown in Fig. 3. The length of the fuel stack was ~ 480 mm and no end pellets were inserted. The rod was filled with a gas mixture of 95 % argon and 5 % helium at 40 bars (RT) [6].

Because the cladding of the IFA650.9 test is a duplex type, which suppresses the amount of corrosion and hydrogen, the hydrogen content and oxide thickness in spite of high burnup fuel are 30 ppm and 7 um, respectively. The hydrogen content affects the mechanical properties of the cladding, which determines the burst time and strain. Therefore, a hydrogen pickup model was modified in FRAPCON to simulate the duplex cladding behavior during a steady state. Fig. 5 shows the LHGR, which was the given and calculated burnup by FRAPCON. Fig. 6 shows the hydrogen contents that the modified hydrogen pickup model calculates. The results shows good agreement against the measurement data.

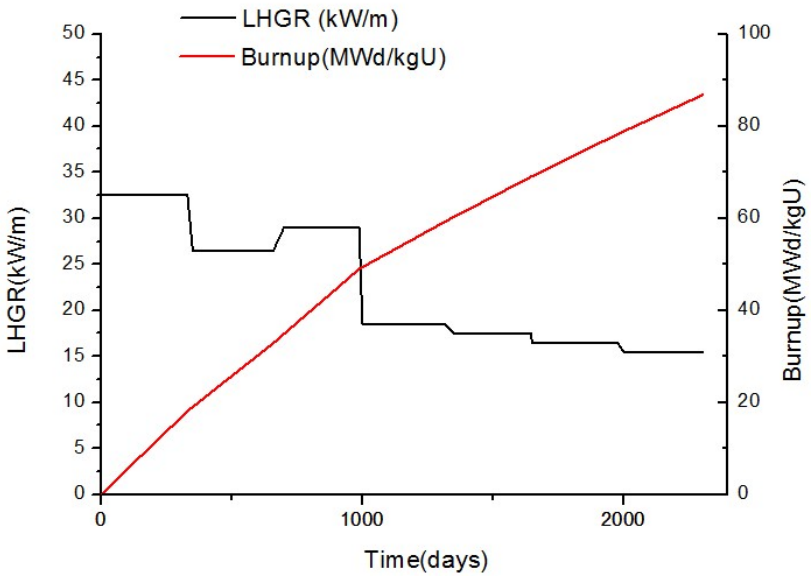

FIG. 3. LHGR and burnup build-up of IFA650.9 rod.

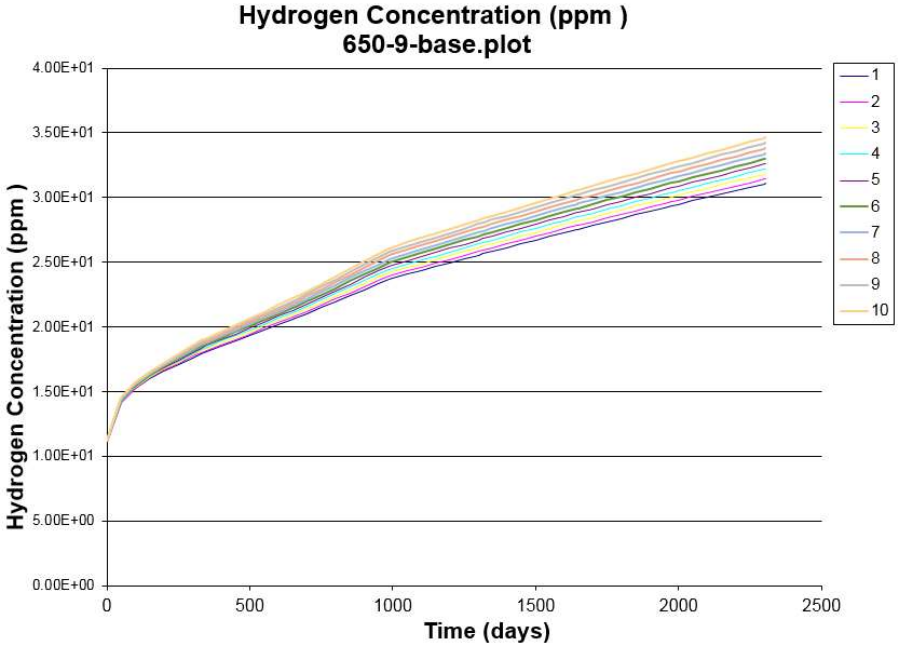

FIG. 4. Calculated hydrogen concentration of IFA650.9.

For the fuel simulation, the following assumptions have been made:

- The axial fuel relocation model was NOT applied for FRAPTRAN;
- The plenum temperature is set as TOA plus 5.6 K;
- The initial free volume is 19 cm^3 and the filled gas mole in the rod is calculated as 0.03066.

To simulate the transient behavior, the FRAPTRAN input is generated as follows: Burnup file requiring (FRAPCON file); gap gas, 95 % Ar; 5%He/ 40 bar@Room Temperature; simulation time, 0 ~ 500s (time step, 0.01s); ALHR/Axial power shape, provided in DB; coolant pressure, provided in DB; HT oxidation, C-P model; and deformation, Balon2 model.

In the same manner as IFA650.2, the plenum temperature and time were prescribed as input with 'prestmp=1' option. For CASE1, the measured temperatures were applied to the T/H conditions. The calculated results show good agreement against the measured data. In the case

of IFA650.9, the temperature difference between the upper and lower parts become bigger after a rod burst because a fuel relocation occurs during the test. Despite the fuel relocation model not being taken into account in this simulation, the fuel behavior can be predicted correctly as long as the surface temperatures are measured. However, the fuel relocation model should be required to evaluate the fuel safety for LOCA.

Because the cladding of IFA650.9 experienced a large deformation as a single rod, a 'pitch' was defined as 0 mm. However, the cladding deformation can be restricted owing to the inner surface of the heater

For CASE2, the T/H conditions at each axial node were generated by MARS-KS. The plenum temperature of CASE2 was determined as the coolant outlet temperature to follow the same methodology as CASE1. Except for the T/H input sequence, the Halden loop model for MARS-KS is identical to the IFA650 series.

Except the transient sequence, the Halden loop model for MARS-KS is identical to the IFA650 series. The steady state condition is decided from the measured data in the same manner as IFA650.2. The transient sequence for IFA650.9 is similar to that of IFA650.2 except for the fuel relocation as follows: the flow valves close one second before the blowdown valve opens: When the maximum cladding temperature reaches 1217.15 K, the coolant mass flow used to simulate the spray cooling is assumed to be 0.01 kg/s: At 133 s after the blowdown valves open, the heat generation from fuel above the ballooning location is reduced by 40%, whereas the heat generation in the bottom region is continuously maintained.

For CASE3, the fully coupled MARS-KS/FRAPTRAN was simulated using the MARS-KS S.A. and FRAPTRAN S.A. inputs. However, the prescribed plenum temperature in the FRAPTRAN input was eliminated and the default option (T@topnode + 5.6K) was applied.

3.3. IFA650.10

The father rod is a UO_2 rod with a SRA Zircaloy-4 cladding, irradiated during five annual cycles up to 57 MWd/kgU (rod average) under moderate power conditions (average liner heat rate used without taking into account the gamma power generated in the coolant: 175 W/cm, 219 W/cm, 214 W/cm, 184 W/cm, and 145 W/cm). At the end of the irradiation on the tested part of the rod, the corrosion layer thickness calculated is around 30 to 40 μm, and the calculated hydrogen content is around 250 ppm. Fig. 5 shows the calculation results for the base irradiation of IFA650.10.

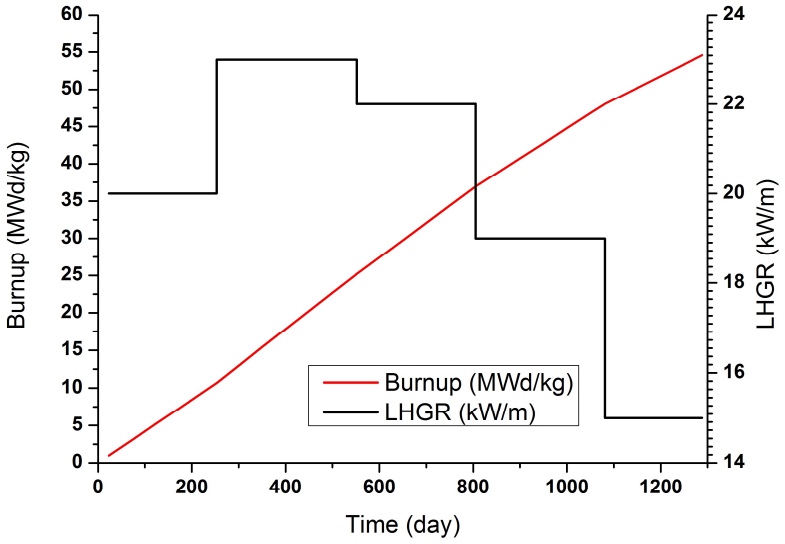

FIG. 5. LHGR and burnup build-up of IFA650.10 rod

This experiment was performed using an IFA650 device, and the HWR report presents the experiment:

For the simulation, the following assumptions were made:

— The plenum temperature was set as TOA plus 5.6 K;
— The initial free volume is 17 cm^3 and the filled gas mole in the rod is calculated as 0.02997.

To simulate the transient behavior, a FRAPTRAN input is generated as follows: Burnup file required (FRAPCON file); gap gas, 95 % Ar; 5%He/ 40 bar (room temperature); simulation time, 0 to 500s (time step, 0.01s); ALHR/Axial power shape, provided in the DB; coolant pressure, provided in DB; HT oxidation, C-P model; and deformation, Balon2 model.

In the same manner as IFA650.9, the plenum temperature and time were prescribed as an input with the 'prestmp=1' option. For CASE1, the measured temperatures were applied into the T/H conditions. The calculated results show a good agreement against the measured data, as shown in Fig. 6. In CASE4, the surface temperatures of the fuel rod at each node calculated by SOCRAT were applied into the T/H conditions for FRAPTRAN.

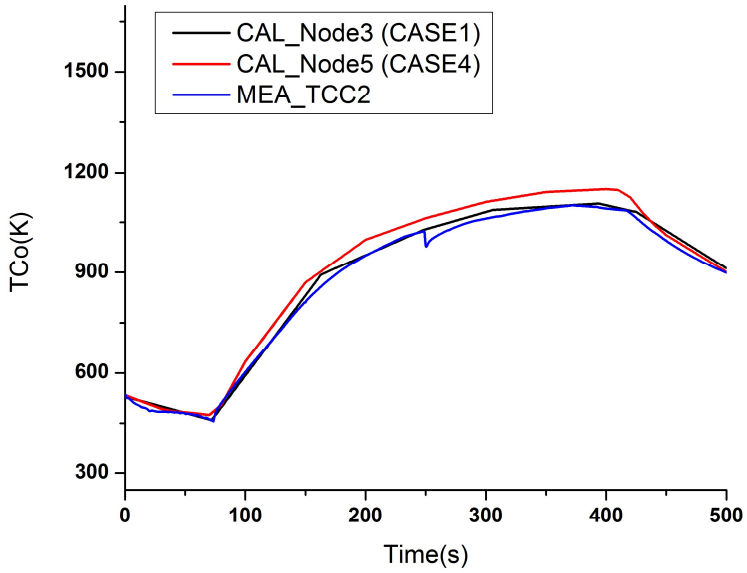

FIG. 6. Comparison between measured data and calculated results (CASE1, CASE4).

4. RESULTS AND DISCUSSION

4.1. T/H calculation

The thermal hydraulic system was simulated using MARS-KS to obtain the T/H boundary conditions as well as evaluate the MARS/FRAPTRAN fully coupled code system. To minimize the fuel burnup effect, IFA650.2 was simulated, as shown in Fig. 10. Owing to absence of a spray model in MARS, the calculated coolant pressure does not match the measured pressure after a blowdown. In view of the temperature behavior of the fuel surface, the results of MARS SA shows a good agreement against that of the measurement. However, the power of MARS SA was tuned with the measurement. When we take a full look at the coupled results, the fuel affects the thermal hydraulic conditions. In particular, the results of the coupled codes is slightly lower than MARS SA because the heat flux of the deformed fuel is smaller than that of the undeformed heat structure, which MARS SA takes into account. When a burst occurs, air flashing from the inner rod cools down the cladding. However, because the fuel code does not take into account this behavior, the temperature profile does not match them. After a burst, the

flow diameter is changed a lot. However, MARS cannot simulate the thermal hydraulic conditions when the flow area is changed. Therefore, the temperature of fully coupled code is lower than that of the measurement (a burst occurs at 99 s after a blowdown).

In the case of IFA650.9, the measurement data, MARS-KS data, and SOCRAT data were compared. A burst occurs at 133 s after a blowdown. Cladding thermocouples were attached 100 mm above the lower end (TCC1) and 80 mm below the upper end (TCC2, TCC3). If the elevation of the active fuel bottom is set to '0 mm', TCC1 and TCC2 are placed at 100 mm and 400 mm elevations, respectively.

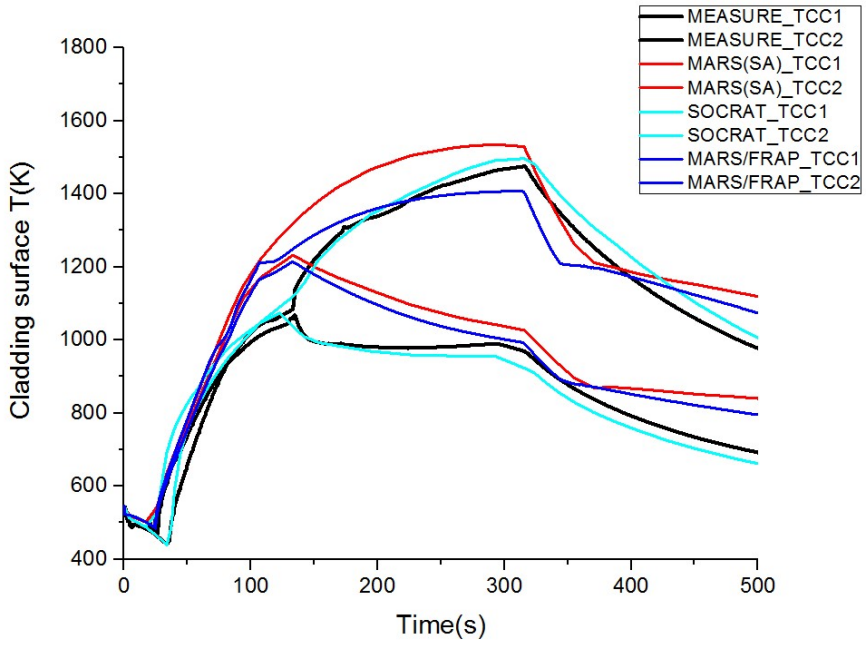

FIG. 7. Comparison between measured data, MARS-KS Stand Alone, MARS/FRAP coupled, and SOCRAT calculation (Surface temperature TCC1 and TCC2) of IFA650.9.

Fig. 7 shows a comparison between the measurement, MARS S.A., MARS/FRAP coupled, and SOCRAT. To take into account the fuel relocation behavior of IFA650.9, the axial power of MARS is adjusted. Therefore, the temperature profile does not match the measurement well despite SOCRAT considering the fuel relocation. When the results calculated by MARS S.A and MARS/FRAP are compared, the temperature of the coupled code is lower than that of MARS owing to a low heat flux. In the same manner as IFA650.2, MARS cannot take into account the thermal hydraulic behavior for the deformed flow zone.

4.2. IFA650.2

Fig. 8 shows the calculation results (rod internal pressure, plenum temperature, cladding temperature of burst node, cladding elongation and cladding diameter in hoop direction) depending on the T/H conditions.

The burst time is as follows: Experiment (99s) / CASE1(77s) / CASE2(71s) / CASE3(68s). The calculated burst time is earlier than the measurement owing to its criterion (that is, the general trend of FRAPTRAN). RIP of CASE3 is up to 8.77 MPa, which is the highest because the plenum temperature is the highest. Because the default option of FRAPTRAN was applied, the plenum temperature of CASE3 is high. In the default option of FRAPTRAN, the plenum temperature is set to the bulk temperature of the top node plus 5.6 k. For validation with the Halden data, the S-FRAPTRAN should take the extra plenum temperature from the MARS calculation. The maximum diameter of the cladding for CASE2

is up to 17.21 mm (181%). According to the Halden report, the measured maximum diameter is up to 190%. The results of CASE2 shows a good agreement against the measurements.

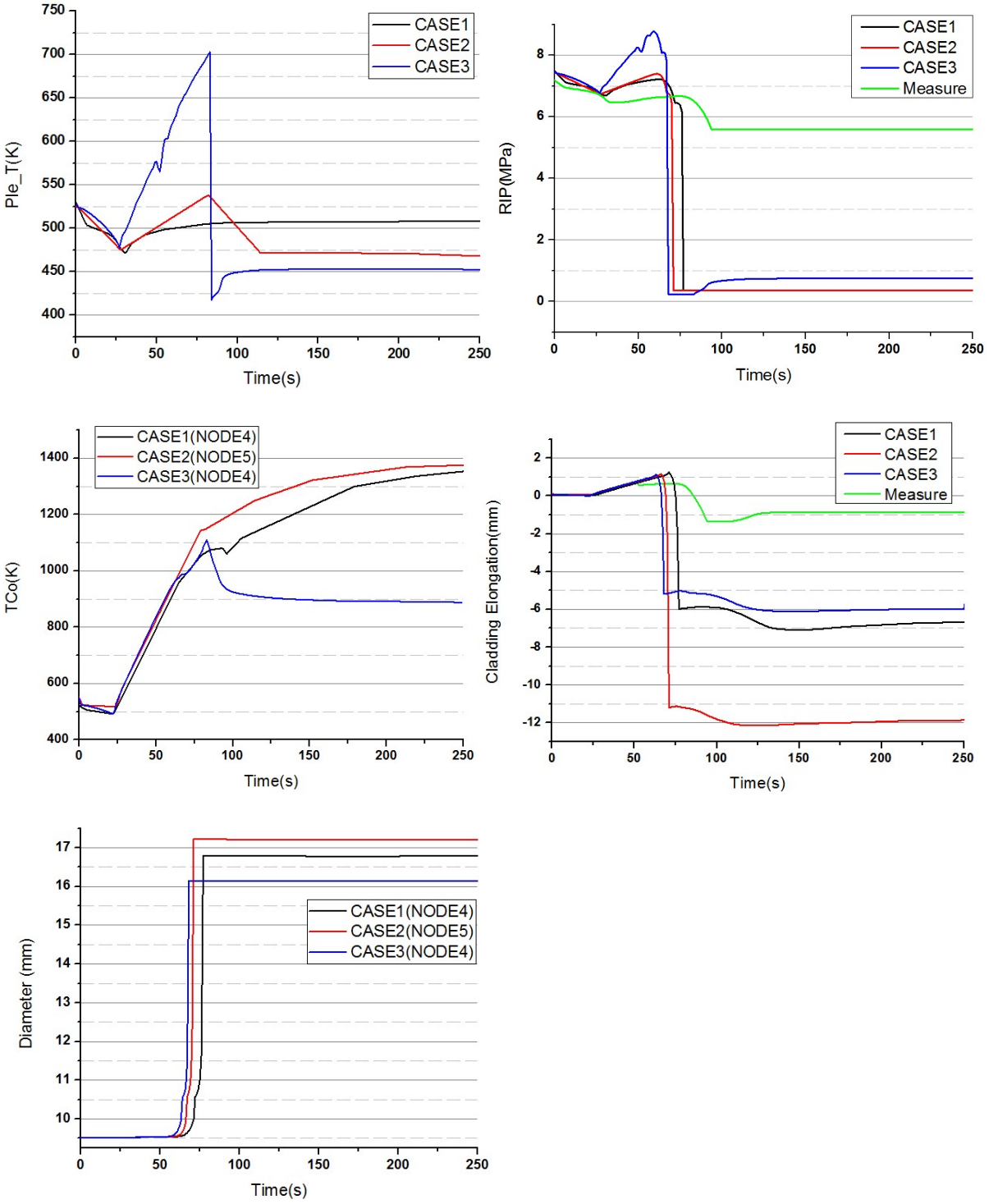

FIG. 8. Calculation results (IFA650.2) of internal rod pressure, plenum temperature, outer cladding temperature, cladding elongation, and cladding diameter for CASE1, CASE2, and CASE3.

II–4.1. IFA650.9

In the case of IFA650.9, the fuel relocation occurs owing to a high burnup fuel and large deformation in burst node. It has been reported that extra space in the rod owing to a deformation leads to a fuel relocation.

Figure 9 shows the calculation results (rod internal pressure, plenum temperature, cladding temperature of burst node, cladding elongation and cladding diameter in hoop direction) depending on the T/H conditions (measured data, T/H calculated by MARS, MARS/FRAPTRAN coupled, SOCRAT). The simulation results of CASE4 are plotted up to 200 s because FRAPTRAN cannot simulate the thermal behavior after a fuel relocation. The cladding tube of IFA650.9 experiences double ballooning in the lower and upper zones, as shown in Fig. 15. Eventually, a cladding burst occurs in the upper zone. SOCRAT is able to simulate the double ballooning because the deformation model is based on the creep behavior. However, the deformation model of FRAPTRAN (Balon2) is limited to simulate double ballooning owing to its methodology.

As the simulation results show, the burst time is as follows: Experiment (133s) / CASE1(128s) / CASE2(86s) / CASE3(85s) / CASE4(117s). The calculated burst time is earlier than the measurement owing to its criterion (that is, the general trend of FRAPTRAN). The low hydrogen content of IFA650.9 cladding postpones the burst time whereas strain in burst node is remarkably high. The RIP of CASE3 is up to 7.83 MPa, which is the highest because the plenum temperature is defined as the bulk temperature at the top node (node #10).

The plenum temperature of CASE1 is close to that of CASE4. When a fuel relocation occurs severely, it is difficult to predict the temperature and strain profile with the fuel relocation model. The maximum hoop strain of the burst node is determined as a function of the pitch. In this simulation, we do not take into account the transient fission gas behavior, which may affect the cladding temperature and internal rod pressure.

The burst time are as follows: Experiment (250s)/CASE1(243s)/CASE4(226s). The calculated burst time is earlier than the measurement owing to its criterion (that is general trend of FRAPTRAN) as shown in Fig. 10. The high cladding temperature of CASE4 results in an earlier burst time. The maximum RIP of the tests cases was 6.86 MPa, 6.81 MPa, and 7.16 MPa for CASE1, CASE4, and the measured value, respectively. When the time is close to the burst time, the trend of the internal rod pressure measured is flat because the amount of ballooning is not big. The burst strain of CASE1 is larger than that of CASE4 because the burst time is delayed.

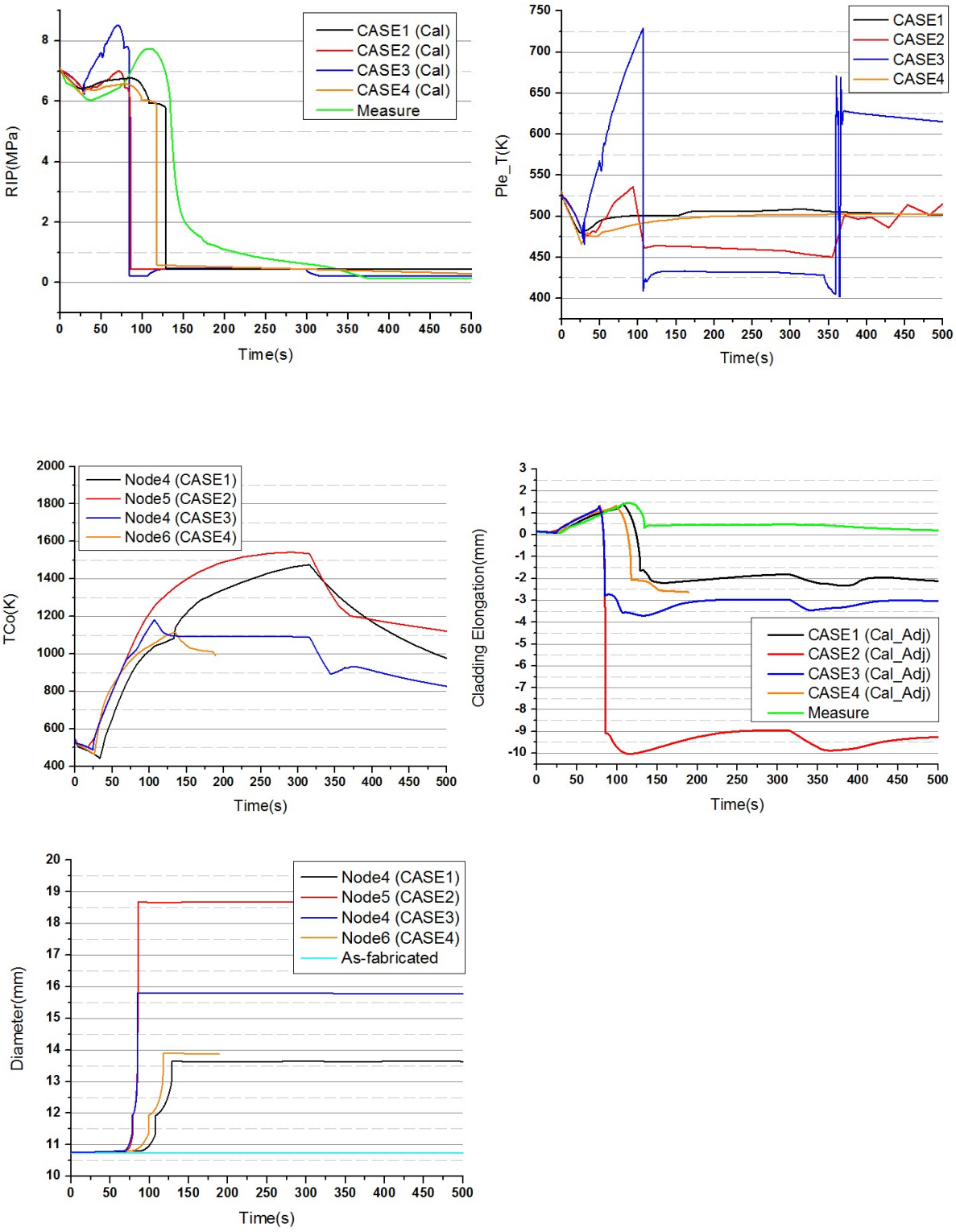

FIG. 9. Calculation results (IFA650.9) of internal rod pressure, plenum temperature, outer cladding temperature, cladding elongation, and cladding diameter for CASE1, CASE2, CASE3, and CASE4.

II–4.2. IFA650.10

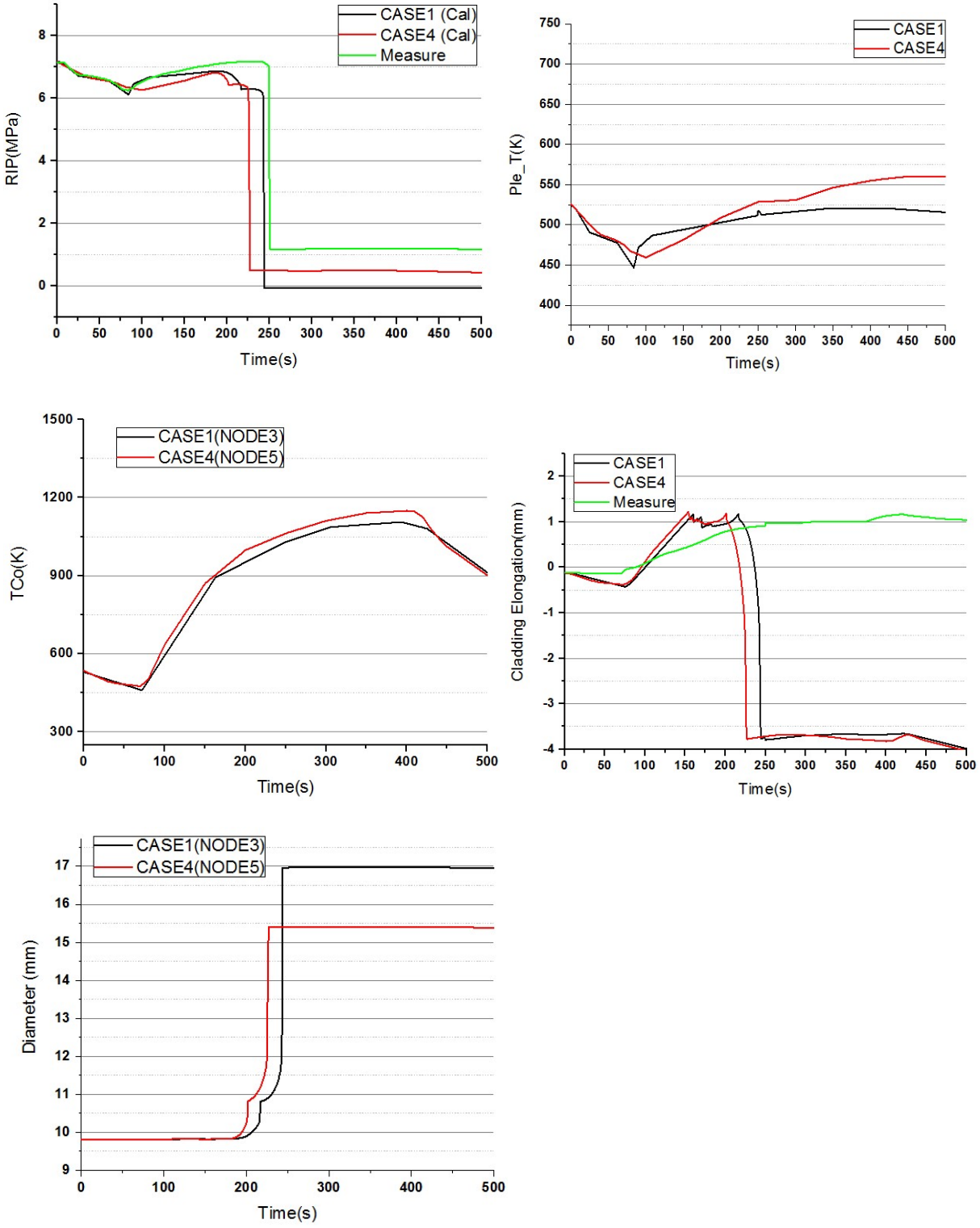

FIG. 10. Calculation results (IFA650.10) of internal rod pressure, plenum temperature, outer cladding temperature, cladding elongation, and cladding diameter for CASE1 and CASE4.

5. SUMMARY AND CONCLUSIONS

The Halden loop was modelled to calculate the thermal hydraulic conditions of the IFA650 test series. Except for IFA650.2, FRAPCON calculated the fuel behavior for a steady state. In particular, the cladding of the IFA650.9 specimen is a duplex, which suppresses the

oxidation during normal operation. Therefore, the model of FRAPCON was modified for IFA650.9.

Large ballooning and fuel relocation were investigated in the IFA650.9 test in spite of high burnup fuel (~89.9 GWd/t). The IFA650.2 test used fresh fuel and a target cladding temperature of 1050°C. The IFA650.9 test using high BU fuel, low corrosion (7 um oxide, 30 ppm hydrogen content), and FFRD was investigated.

As simulation results, T/H calculations of MARS-KS, MARS-KS/FRAPTRAN and SOCRAT were compared. For IFA650.2, the results of MARS-KS/FRAPTRAN is lower than MARS-KS stand alone because heat flux of the deformed fuel is smaller than that of undeformed heat structure which MARS SA take into account. For IFA650.9, lower surface temperatures of the coupled code were also investigated. While results of SOCRAT matched those of measurement, MARS-KS cannot follow the measurement. It is because fuel relocation model and deformation model for simulation of fuel behavior were not taken into account. In addition, spray model in MARS-KS should be implemented to simulate the halden experiment.

The burst time of IFA650.2 for each case is as follows; Experiment (99s) / CASE1(77s) / CASE2(66s) / CASE3(73s). Burst time of IFA650.9 for each case is as follows: Experiment (133s)/ CASE1(129s) /CASE2(85.8s) / CASE3(89.6s). Burst time of IFA650.10 for each case is as follows; Experiment (250s) /CASE1(244s)/CASE4(227s).

Basically, the burst times of simulations are earlier than those of experiment due to burst criterion in the FRAPTRAN. For MARS-KS/FRAPTRAN code, plenum temperature should be the coupling variable to simulate the halden test because the plenum temperature of the coupled code is higher than the others. As a default option, plenum temperature of rod is defined as the bulk temperature plus 5.6K at top node.

REFERENCES

[1] BANG Y.S. et al., Technical Basis for the Revision of ECCS Acceptance Criteria of Domestic PWR Plants, KINS/RR-1686, (2017).

[2] KIM H.C. et al., Development of fully coupled MARS-KS/FRAPTRAN code system for simulation of fuel behavior during LOCA, Transactions of the Korea Nuclear Society Autumn meeting, Gyeongju, Korea (2017).

[3] Geelhood, K.J., Luscher, W.G., Beyer, C.E., Cuta, J.M., FRAPTRAN 1.4: A Computer Code for the Transient Analysis of Oxide Fuel Rods, NUREG/CR-7023, Vol.1, 2011.3.

[4] MARS Code manual (Volume I: Code Structure, System Models, Solution Methods), KAERI/TR-2812, (2004).

[5] HWR-813, LOCA TESTING AT HALDEN; THE SECOND EXPERIMENT IFA650.2. Ek.

[6] HWR 917, LOCA Testing experiment at Halden. The nineth experiment IFA650-9. Chomont.

[7] HWR 974, LOCA Testing experiment at Halden. The tenth experiment IFA650-10. A. Lavoil.

NUMERICAL ANALISYS OF CORA-15 TEST BY SOCRAT CODE

DOLGANOV K.S., KISELEV A.E., TARASOV A.E., TOMASHCHIK D.YU., YUDINA T.A.
Nuclear Safety Institute (IBRAE),
Russian Academy of Sciences,
52, B. Tulskaya, Moscow, 115191,
Russian Federation
E-mail: ksv@ibrae.ac.ru (corresponding author)

Abstract

Numerical modeling of the CORA-15 test was performed with SOCRAT code. In the test, the behavior of the PWR type fuel assembly consisted of 23 fuel rods with 2 absorber rods was investigated under the severe LOCA conditions. An important feature of the experiment was a high overpressure inside the fuel rods. As a result, the fuel rods underwent ballooning and rupture. It is shown that the SOCRAT code adequately reproduces the cladding temperatures evolutions, its ballooning and rupture, hydrogen production, the blockage formation due to melt relocation.

1. INTRODUCTION

CORA-15 test was offered to IAEA FUMAC CRP participants to check the codes capability to model the cladding ballooning and burst parameters of the fuel rods in the bundle. The test was performed with a bundle made up of 23 fuel rods and 2 Ag/ln/Cd - steel absorber rods in out-of-pile CORA facility. The material and radial dimensions of the fuel and absorber rods were identical to those in a PWR bundle. The fuel rods were pressurized to 6.0 MPa while the system pressure was 0.22 MPa to provoke a pronounced cladding ballooning and burst. The bundle was heated up by Joule heat power. The test scenario comprised the bundle heating in a steam-argon flow up to a temperature of ~2000°C followed by its cooling down in an argon flow. The temperature scenario simulates anticipated severe accident conditions in LWR core during small break LOCA [2].

The aims of CORA-15 modeling by integral SOCRAT code are twofold: one is to investigate the ballooning effect on the bundle degradation, and the second is to validate CROX model to predict cladding ballooning and burst parameters, PROF and LIQF models to predict Zr oxidation and hydrogen release, DROG model to predict melt relocation and blockage formation, and their interaction. Description of the SOCRAT code can be found in [3].

2. DESCRIPTION OF THE CORA-15 TEST SECTION AND TEST BUNDLE

The CORA-15 test was performed in CORA facility, its main components are shown schematically in Fig. 1 [2]. The test section with the CORA-15 bundle is given in the Fig. 2[3]. The CORA-15 bundle was made up of 23 fuel rods (16 heated rods and 7 unheated rods) and 2 Ag/In/Cd absorber rods. The material and radial dimensions of the fuel and absorber rods were identical to those in a PWR bundle, more details are presented in Table 1. The fuel rods were filled with UO_2 pellets. A central hole was drilled in each pellet inside the heated fuel rods (for heater insertion) whereas the unheated rods contained full UO_2 pellets of the same outer diameter. Sixteen fuel rods were electrically heated by using tungsten heaters, the heated length was 1000 mm. All fuel rods were pressurized to 6.0 MPa before the test.

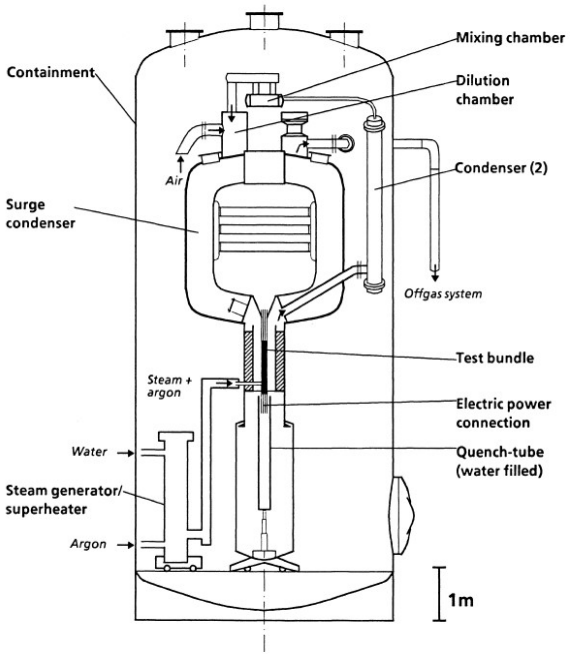

FIG. 1. Main components of CORA facility [2].

The rods were arranged within the bundle with three grid spacers as shown schematically in the cross section in Fig. 3. The bundle was inserted in a shroud made of Zircaloy-4, the latter one was surrounded by a thermoinsulation.

During the experiment both superheated steam, generated by the steam generator and superheater, and argon entered the bundle at a lower unheated elevation and then flowed upwards through the heated part of the test bundle. As steam-argon mixture passed the bundle, it was enriched with the hydrogen produced due to steam-zirconium interaction and finally left the test section.

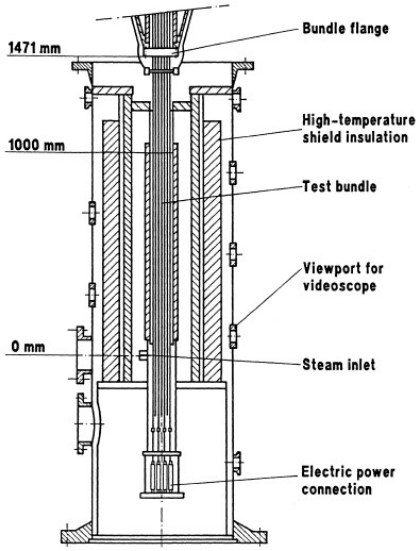

FIG. 2. Test section of CORA facility [2].

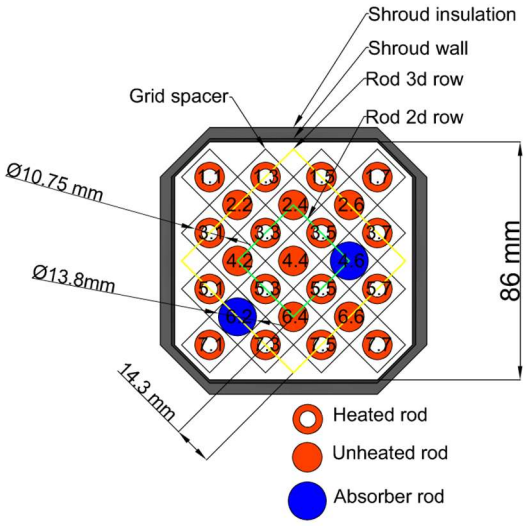

FIG. 3. Schematic cross section of CORA-15 bundle.

TABLE 1. DESIGN CHARACTERISTICS OF THE CORA-15 TEST BUNDLE [2]

Bundle size:		25 rods
Number of heated rods:		16
Pitch:		14.3 mm
Rod outside diameter:		10.75 mm
Cladding material:		Zircaloy-4
Cladding thickness:		0.725 mm
Rod length:		2175 mm
Heated length:		1000 mm
Fuel pellets		
Heated rods:		UO_2 annular pellets
Unheated rods:		UO_2 full pellets
U^{235} enrichment		0.2 %
Pellet outer diameter (nominal)		9.1 mm
Heater material:		Tungsten (W)
Heater diameter:		6 mm
Grid spacer		
Material:		Zircaloy-4, Inconel 718
Length:	Zry	42 mm
	Inc.	38 mm
Location*:	lower (Zry)	- 5 mm
	center(Inc.)	+ 496 mm
	top (Zry)	+ 880 mm
Shroud		
Material		Zircaloy-4
Wall thickness		1.2 mm
Outside dimensions		86 x 86 mm
Elevation		36 mm – 1236 mm
Insulation material		ZrO_2 fiber
Insulation thickness		20 mm
Absorber rod		
Number of rods		2
Material and composition		80Ag, l5In, 5Cd (wt.%)
Cladding		Stainless steel
Cladding OD		10.2 mm
Cladding ID		8.85 mm
Length		1489 mm
Elevation		189 mm to + 1300 mm
Absorber rod guide tube		
Material		Zircaloy-4
OD		13.8 mm
Wall thickness of tube		0.8 mm

*Elevations are meant for the top of the grid spacers and are referred to the bottom of the heated zone.

To measure the cladding and shroud temperature, high temperature W/Re (C-type) thermocouples (TC) located at elevations between 600 and +1300 mm, and low temperature NiCr/Ni (K-type) thermocouples at elevations between 0 and 500 mm were used. Their positions are shown in Fig. 4[4]. Thermocouples as well as pressure sensors chosen for the comparison with the calculated data are given in Table 2.

Six videoscopes were utilized to observe the materials behavior and the relocation of material during the transient.

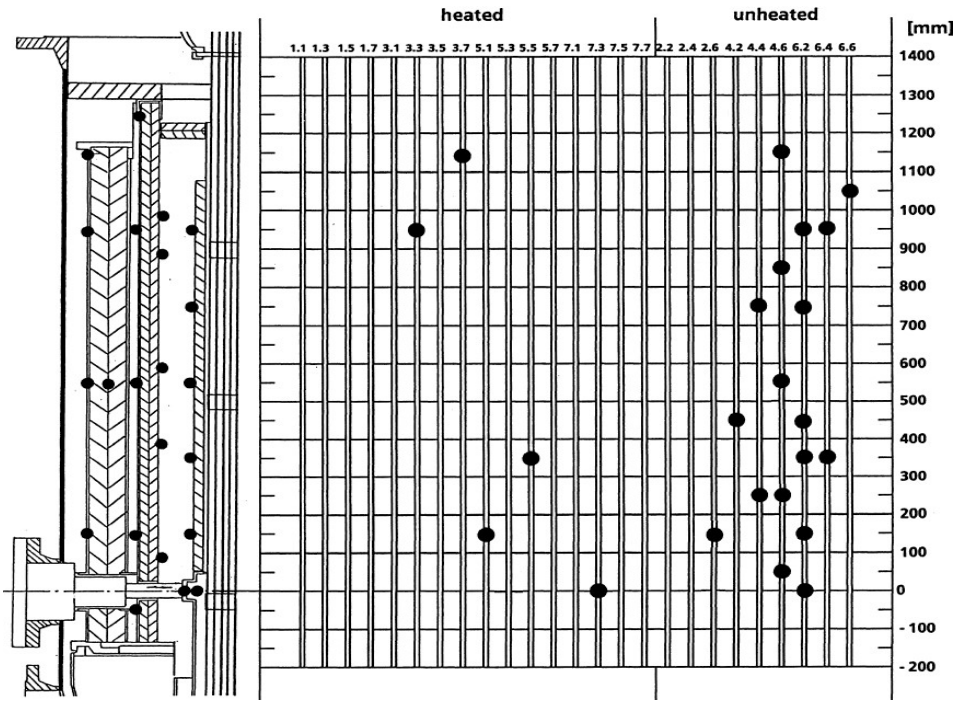

FIG. 4. Positions of thermocouples [4].

TABLE 2. LIST OF INSTRUMENTATION USED FOR COMPARISON WITH THE CALCULATED DATA IN CORA-15

No.	Chann. No.	Name	Unit	Description	Elevation, mm
1	1	T101	°C	Unheated rod 4.4	750
2	2	T102	°C	Unheated rod 6.4	950
3	3	T103	°C	Unheated rod 6.6	1150
4	5	T105	°C	Heated rod 3.3	950
5	6	T106	°C	Heated rod 3.7	1150
6	8	T108	°C	Unheated rod 4.2	450
7	9	T109	°C	Unheated rod 6.4	350
8	10	T110	°C	Unheated rod 4.4	250
9	11	T111	°C	Unheated rod 2.6	150
10	14	T114	°C	Heated rod 5.5	350
11	15	T115	°C	Heated rod 5.1	150
12	17	T117	°C	Absorber rod 4.6	1150
13	18	T118	°C	Absorber rod 6.2	750
14	45	T206	°C	Shroud	550
15	48	T209	°C	Absorber rod 4.6	550
16	49	T210	°C	Absorber rod 6.2	350
17	50	T211	°C	Shroud	350
18	51	T212	°C	Shroud	150
19	52	T213	°C	Shroud	950
20	53	T214	°C	Shroud	750
21	54	T215	°C	Shroud	1150
22	89	P 305	bar	Internal pressure of a rod 6.6	

TABLE 2. LIST OF INSTRUMENTATION USED FOR COMPARISON WITH THE CALCULATED DATA IN CORA-15

No.	Chann. No.	Name	Unit	Description	Elevation, mm
23	90	P 306	bar	Internal pressure of a rod 4.4	
24	91	P 307	bar	Internal pressure of a rod 1.1	
25	92	P 308	bar	Internal pressure of a rod 3.3	
26	93	P 309	bar	Internal pressure of a rod 7.7	
27	94	P 310	bar	Internal pressure of a rod 2.2	

The CORA-15 test scenario is schematically shown in Fig. 5, the main events are presented in Table 3. The scenario comprised pre-heating, heat-up, escalation and cool down phases.

TABLE 3. CORA-15 TEST SEQUENCE

Time, s	Event
0 - 3000	Pre-heating of the bundle by argon flow (a flowrate of about 8 g/s). The electric power is maintained at a constant low level
3000	Start of electric power increase
3300	Start of feedwater supply (a flowrate of about 6 g/s) in the steam generator. The steam-argon mixture enters the bundle
3900 – 4900	Temperature escalation
4900	The feedwater supply is turned off along with the shutoff of the electric power
4900-10000	Cool-down by argon flow (a flowrate of about 8 g/s)

The test started with the bundle pre-heating by a flowing argon (the preheating phase). The argon temperature was about 500°C, the flow rate was 8 g/s. At the heat up phase that lasted from 3000 s to 3900 s, the bundle was heated up with an initial rate of 1 K/s due to increase of the electrical power. At 3300 s the feedwater with a constant flow of 6 g/s was supplied in the steam generator, and the produced steam started to enter the bundle in addition to argon. At 3900 s the temperature escalation phase started. The test was terminated by the cool-down phase. The feedwater supply was turned off along with the shutoff of the electric power. The bundle was slowly cooled down by a flowing argon. The system pressure was about 2.25 bar during the experiment. The measured electrical power, system and internal pressure together with the feedwater and argon flowrate evolutions are shown in Fig. 5.

3. NODALIZATION SCHEME. INITIAL AND BOUNDARY CONDITIONS

Nodalization scheme of the CORA-15 test section developed for modeling the experiment with SOCRAT code is shown in Fig. 6. The test section is represented by the following thermal structures:

- Central rod (group 1);
- 3 unheated rods in inner row and 3 unheated rods in outer row (group 3);
- 4 heated rods in inner row (group 2);
- 2 absorber rods in inner row;
- 12 heated rods in outer row (group 4);
- Shroud (multilayered structure that represents shroud and surrounding thermoinsulation);
- Two spacer grids.

Hydraulic resistance in the central part of the test section (with the rods) is higher than in the peripheral one due to a large gap between the shroud and the peripheral rods (Fig. 3). The cladding ballooning that occurs in the test enhances this effect so that one can expect significant

flow redistribution across the bundle. To predict this phenomenon, gas domain is modeled with two channels – central and peripheral. Special equations were implemented in the SOCRAT code to model the mass exchange between the central and peripheral zones with the cross-flow junctions (2D flow model).

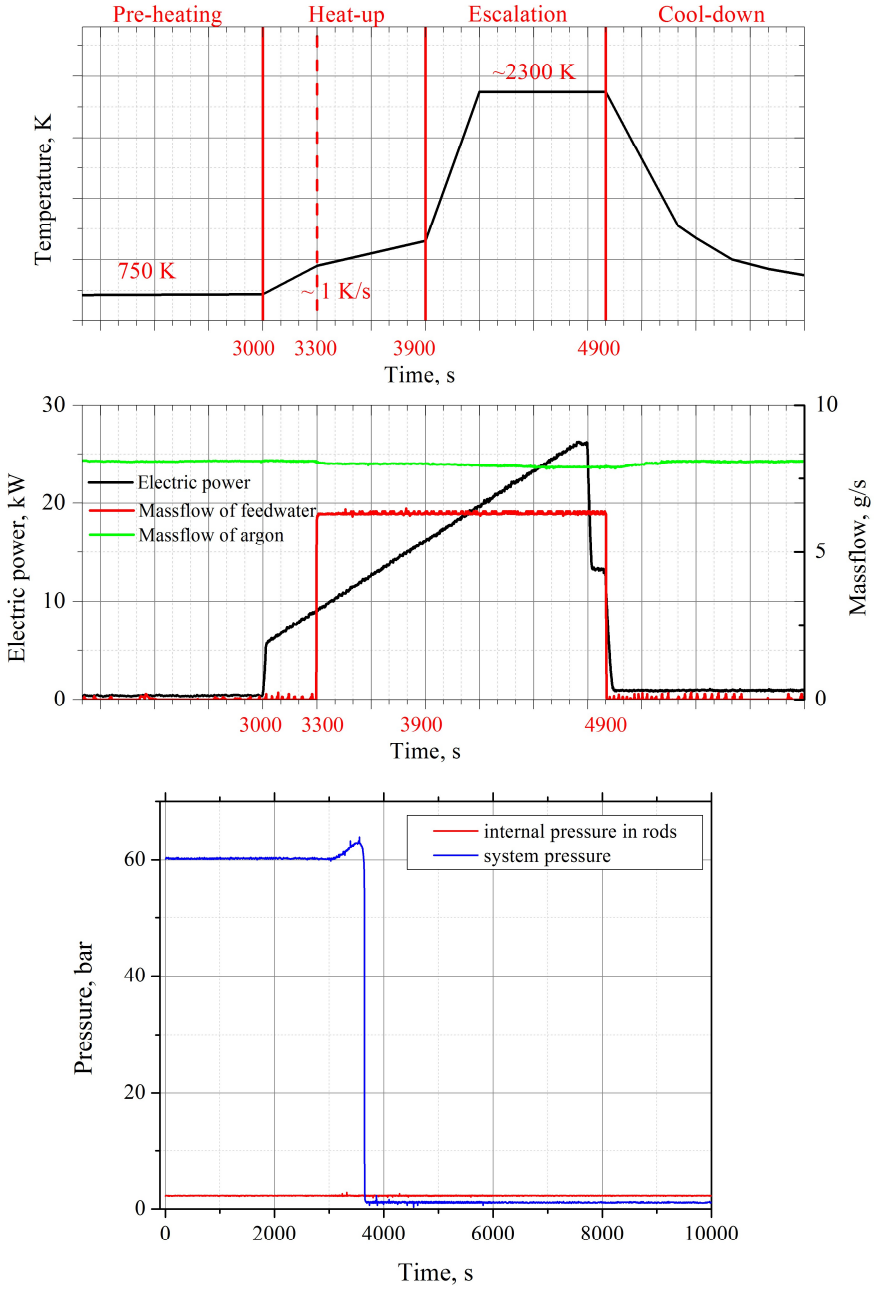

FIG. 5. Scenario of the experiment.

The simulation of the experiment starts at a time moment of 2000 s. The prescribed initial vertical temperature profiles for thermal structures were derived from the TC readings at t=2000 s. The internal pressure in the rods, electric power, argon mass flowrate were set the same as in the test. The imposed steam flowrate at heat up and escalation phases was equal to the measured water flowrate that was feeding the steam generator. At the beginning of the cool down phase, the steam injection was retained in the calculation for 600 s after feedwater switch off (4900 s), with a flowrate linearly decreasing from 0.9 g/s to 0 g/s This simulated the steam production during steam generator drying out. The inlet argon and steam temperatures were set to 745 K.

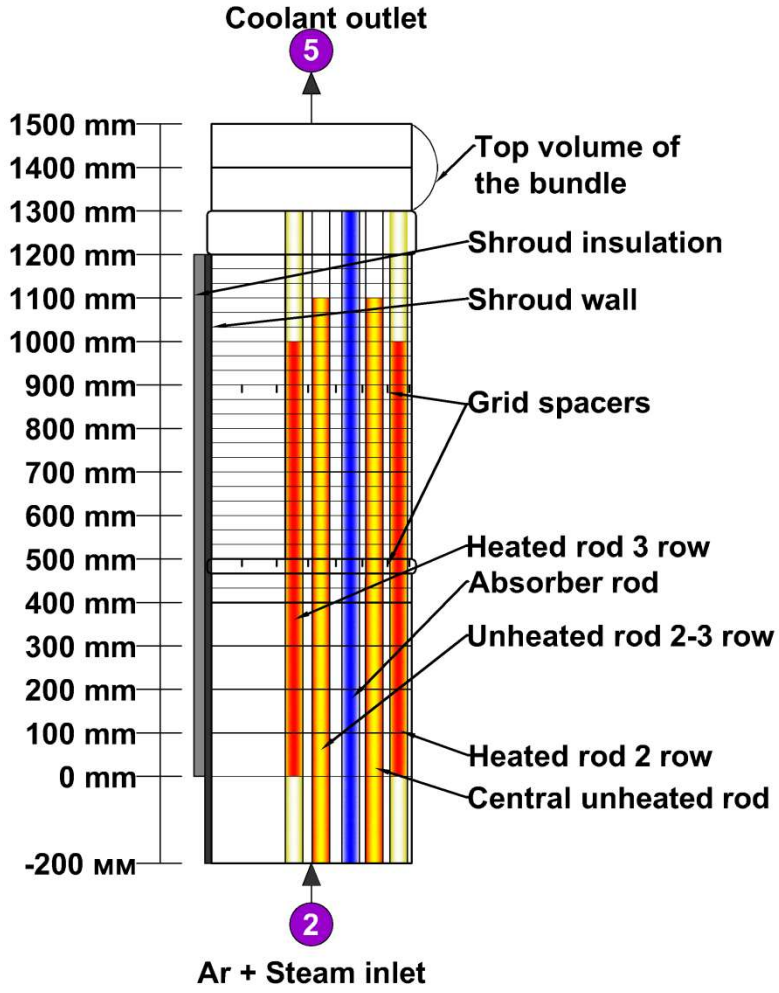

FIG. 6. Nodalization scheme of CORA-15 bundle

4. RESULTS OF THE SIMULATIONS

The following main phenomena are predicted in CORA-15 test:

- The cladding ballooning and rupture at the heat up phase;
- The absorber rod failures due to eutectic material interaction at the escalation phase;
- An extensive melt formation due to the cladding melting and its relocation down at the escalation phase;
- A massive blockage formation at elevations of around 500 mm.

A quantitative comparison of the calculated and measured data is presented below.

4.1. CLADDING BALLOONING AND RUPTURE

The cladding rupture due to its ballooning is predicted and is detected at the heat up phase. Fig. 7presents a comparison of the calculated and measured internal pressure evolutions for all groups of the rods. Overall one can find a good agreement on the burst time:

- 3494 s – 3645 s (measured);
- 3480 s – 3663 s (predicted).

Comparison of the calculated and measured burst times for the individual rods is given inTable 4. Average biases are 54 s for the unheated and 44 s for the heated claddings.

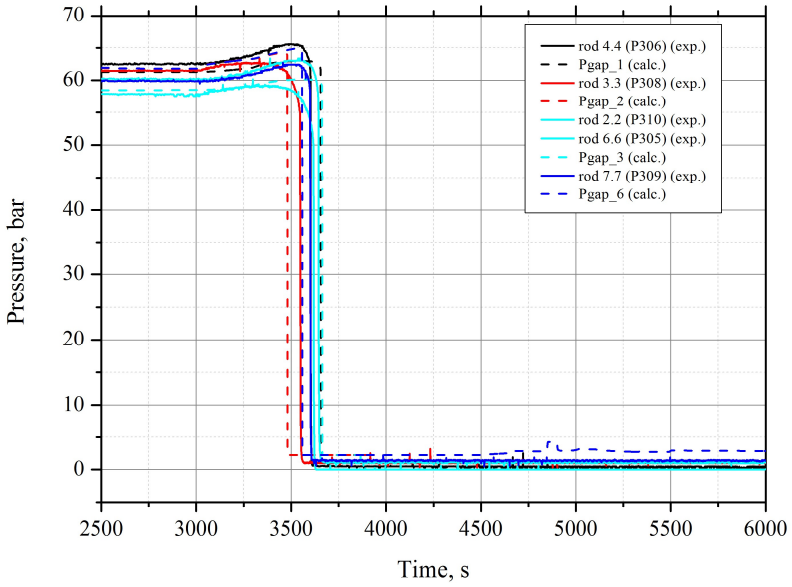

FIG. 7. Internal pressure in the rods.

The first cladding rupture is predicted in the heated fuel rods of the groups 2 and 4 at elevations 633–666 mm and at elevations 733–766 mm respectively (Fig. 7). The rupture elevations correspond to the hottest zone locations at the burst times in the calculation. The burst elevations of the heated fuel rods and related temperatures are unknown in the test since the bundle got melted in its upper half and the heated rods were not instrumented by the thermocouples in the expected rupture zone (Fig. 4).

TABLE 4. COMPARISON OF THE BURST TIME FOR THE INDIVIDUAL RODS

Group	No. of rod	Measured [2], (s)	Predicted, (s)	Δ, (s)
		Unheated rods		
Group 1	(4.4)	3601	3655	54
Group 3	(4.2)	3604.0	3663	59
	(2.4)	3565.1	3663	97.9
	(6.4)	3602.2	3663	60.8
	(2.2)	3616.3	3663	46.7
	(2.6)	3624.8	3663	38.2
	(6.6)	3644.5	3663	18.5
Average $\|\Delta\|$, s				53.5
		Heated rods		
Group 2	(3.3)	3547.8	3480	-67.8
	(3.5)	3561.5	3480	-81.5
	(5.5)	3562.7	3480	-82.7
	(5.3)	3564.2	3480	-84.2
Group 4	(1.1)	3579.4	3558	-21.4
	(1.3)	3562.1	3558	-4.1
	(1.5)	3588.7	3558	-30.7
	(1.7)	3617.8	3558	-59.8
	(3.7)	3602.0	3558	-44
	(5.7)	3588.9	3558	-30.9
	(7.7)	3593.9	3558	-35.9
	(7.5)	3579.5	3558	-21.5

TABLE 4. COMPARISON OF THE BURST TIME FOR THE INDIVIDUAL RODS

Group	No. of rod	Measured [2], (s)	Predicted, (s)	Δ, (s)
	(7.3)	3585.1	3558	-27.1
	(7.1)	3600.8	3558	-42.8
	(5.1)	3493.8	3558	64.2
	(3.1)	3570.2	3558	-12.2
Average $\|\Delta\|$, s				44.4

Cladding rupture of the unheated fuel rods (groups 1 and 3) is calculated about 100 s after the last cladding burst in the heated groups and at a little bit higher at elevations of 766-800 mm since the hottest zone shifts up as the bundle heats up. The temperature was not measured at the burst elevations for the unheated groups, but the thermocouple reading at a lower elevation of 750 mm attached to the central rod (group 1) seems to be suitable for the comparison due to rather low temperature gradient, expected at this zone at this time. It is illustrated by the predicted temperature profile at 3650 s, i.e. 10 s before the burst, in the Fig. 8. Assuming that the hot spot locations are the same in the test and in the calculation, the burst temperature of the central rod is overpredicted by 60 K.

Absorber failure is simulated at a temperature of 1430 K at the hottest elevation of 833 mm – 866 mm at 4044 s. The temperature profile features a sharp temperature gradient by this time. It is illustrated by the predicted temperature profile at 4000 s in the Fig. 8. 10 s later, fuel rod cladding reached zirconium melting point here, giving a start of extensive melt formation.

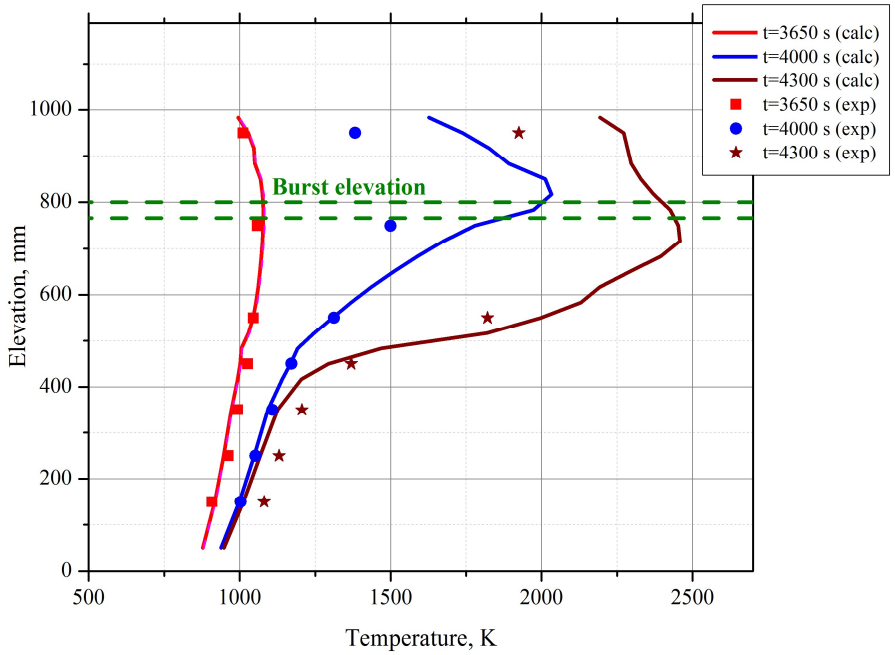

Evolution of temperature profiles for the unheated group 3.

4.2. Local temperature evolutions

The central rod cladding and shroud temperatures at an elevation of 750 mm – just below the predicted burst elevation of the unheated fuel rods - are shown in Fig. 9. One can see a good agreement on temperature behavior at the pre-heating, heat-up and escalation phases, though one can find a tendency to a slight overestimation at the transient phase (till TC failures). Temperature escalation starts here at 4050 s due to zirconium oxidation. By 4075 s, the central channel at an elevation of 833 mm is blocked partially by an extensive melt formation, the coolant escapes the central zone between elevations of 750 mm (ballooning region) to 950 mm

and starvation conditions come here in the calculation. The decrease of the heat up rate at 4075 s, observed in the temperature evolution of the central rod at 750 mm (Fig. 9), results from the reduction of the oxidation due to the starvation conditions. The TC failure occurs at ~1890 K at 4080 s at 750 mm, the maximal predicted temperature is about 2630 K.

Fig. 10 displays the shroud and cladding temperatures of the unheated rods above the hottest zone, at an elevation of 950 mm. The temperatures at the transient phase are overestimated, but the temperature trend is reproduced well – the temperature escalation starts at around 4000 s. At 4250 s when the measured temperature was of ~ 1943 K, TC failure occurred. The calculated temperature at this elevation reaches zirconium melting point somewhat later than in the hottest zone; melt formation, its oxidation relocation downwards is predicted. The calculated maximum temperature is about 2520 K.

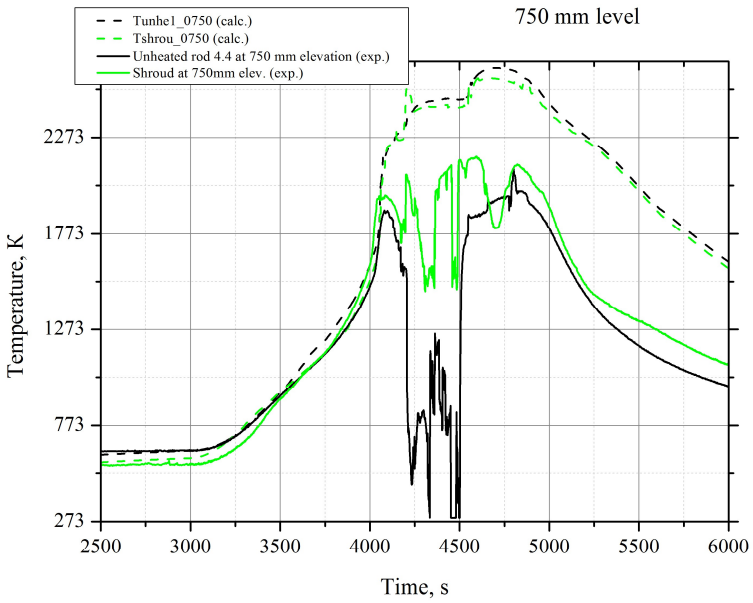

FIG. 8. Central rod cladding and shroud temperatures at 750 mm.

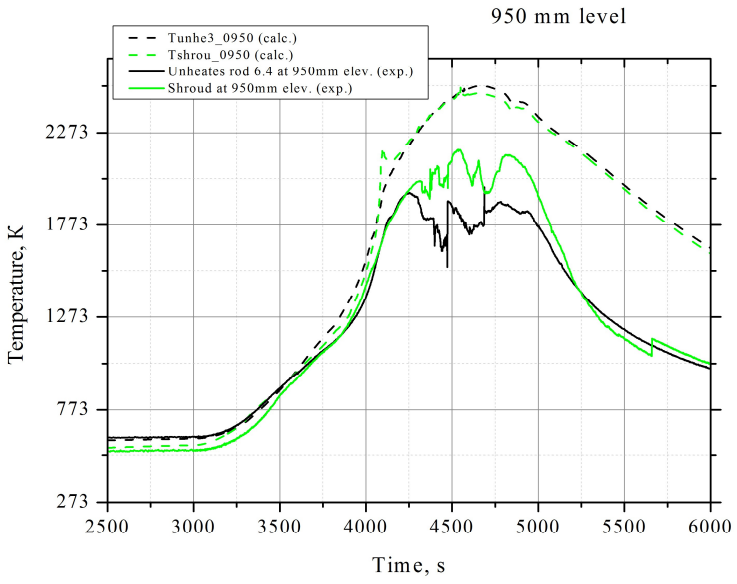

FIG. 9. Cladding temperature of unheated rods in inner and outer rows and shroud temperature at 950 mm.

The shroud temperature evolution at an elevation of 550 mm is shown in Fig. 11(a) (no TC at the fuel rods). An extensive cross-section blockage is predicted and observed here (Figs. 11(b) and 13). Both measured and predicted data show the temperature escalation after 4050 s and zirconium melting point is reached. In the calculation, it is due to melt relocation. Because of rather low initial temperature, the relocated melt cools down and solidifies there.

At a lower elevation of 350 mm (Fig. 12 (a), the predicted and measured temperatures are essentially lower. Some different trends can be found at 4500 s, fast heating up in the calculation results from the melt relocation. That behavior is not observed in the TC reading, likely due to asymmetrical melt relocation in the test (Fig. 12(b)).

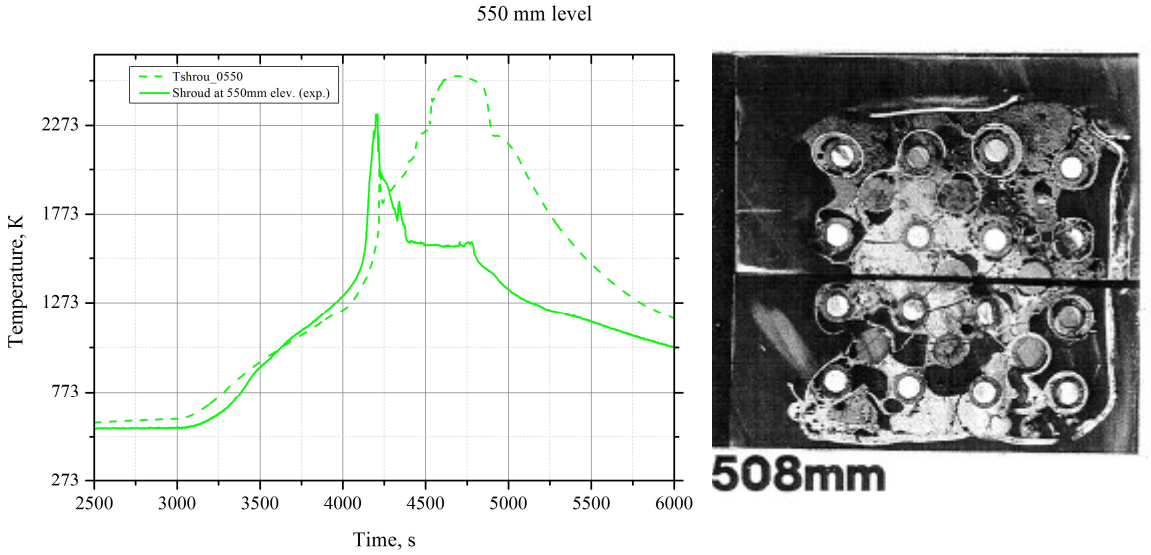

(a) (b)

FIG. 10. Shroud temperatures (a) and cross-section [2] *(b) at 550 mm.*

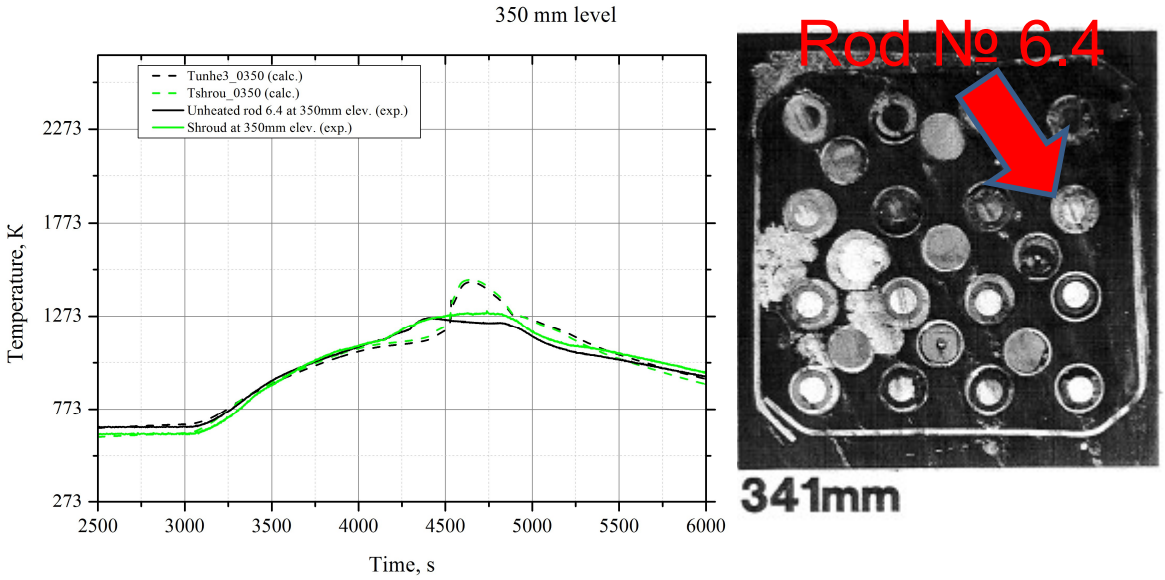

(a) (b)

FIG. 11. Cladding temperature of unheated rods in inner and outer rows and shroud temperature (a) and cross-section [2] *(b) at 350 mm.*

4.3. Blockage profile

The blockage profile of cross-section area is shown in Fig. 13. The location and extension of the blockage in the calculation agree with the posttest investigation results. The predicted maximum blockage at elevation from 466 to 500 mm matches the data well:

— 0,00582 m^2 at an elevation of 512 mm – measured;
— 0,00555 m^2 at elevations of 466 to 500 mm – predicted.

Above an elevation of 600 mm, material relocates downwards both in the calculation and in the test.

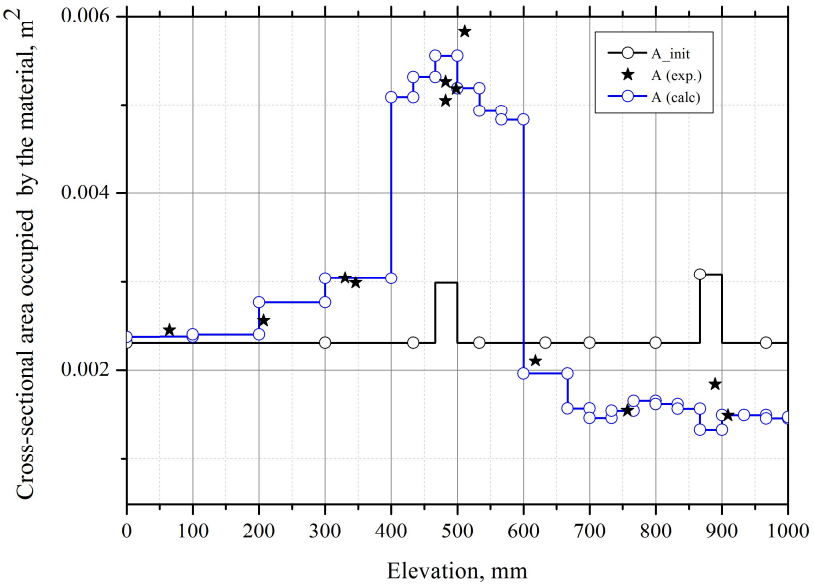

FIG. 12. Blockage profile of cross-section area.

4.4. Hydrogen production

The calculated hydrogen production complies with the experimental data well as one can see in Fig. 14. The measured hydrogen production after 4900 s, that is 1000 s after the water feeding the steam generator was switched off, could be explained by the continuation of steam production due to the boiling of some remaining water mass in the steam generator. This observation suggested to keep a steam flowrate at the cool down phase in the modelling, as discussed earlier (I&B conditions).

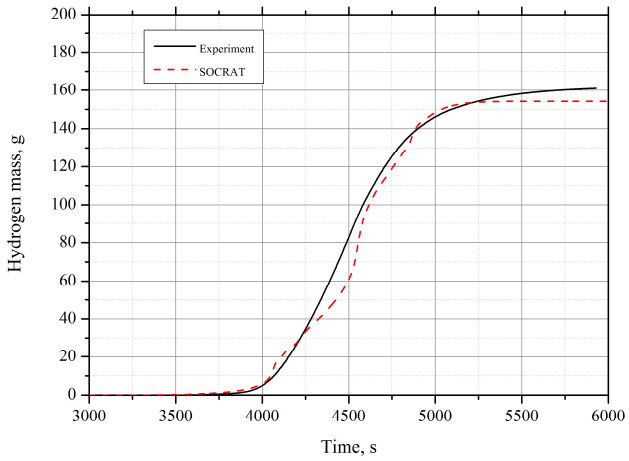

FIG. 13. Hydrogen release.

4.5. Ballooning effect

One more run with an imposed internal pressure being equal to the system pressure was made to recognize an impact of the ballooning on the bundle degradation. Comparison of the calculated cladding temperatures with the pressurized and non-pressurized fuel rods is given in Fig. 15.

The cladding temperature profiles at 3600 s in Fig. 15a illustrate that before the ballooning onset the temperatures in both calculations are the same. Later, the heating up of the pressurized claddings is faster as one can see in the plots with cladding temperature evolutions (Fig. 15b). Higher heat up rate is observed in the ballooning region (600 mm to 800 mm) and above (Fig. 15a, t = 4050 s). It could be explained as follows.

On the one hand, the ballooning enhances the flow redistribution across the bundle. The degradation of the local convective heat exchange due to the decreased local coolant flowrate results in a higher local cladding temperature.

On the other hand, the decreasing local heat exchange between the cladding and fuel due to larger gap width in the ballooning region promotes higher local fuel and heater temperatures. Electrical resistance is temperature dependent, Joule heat power at this zone increases as a feedback to the higher heater temperature.

As a result of both mechanisms, the claddings are heated up faster, and the start of the temperature escalation in the calculation with the pressurized fuel rods becomes earlier (4050 versus 4150 s, Fig. 15b).

Slight differences between two runs were found in later times but the bundle degradations are in general similar.

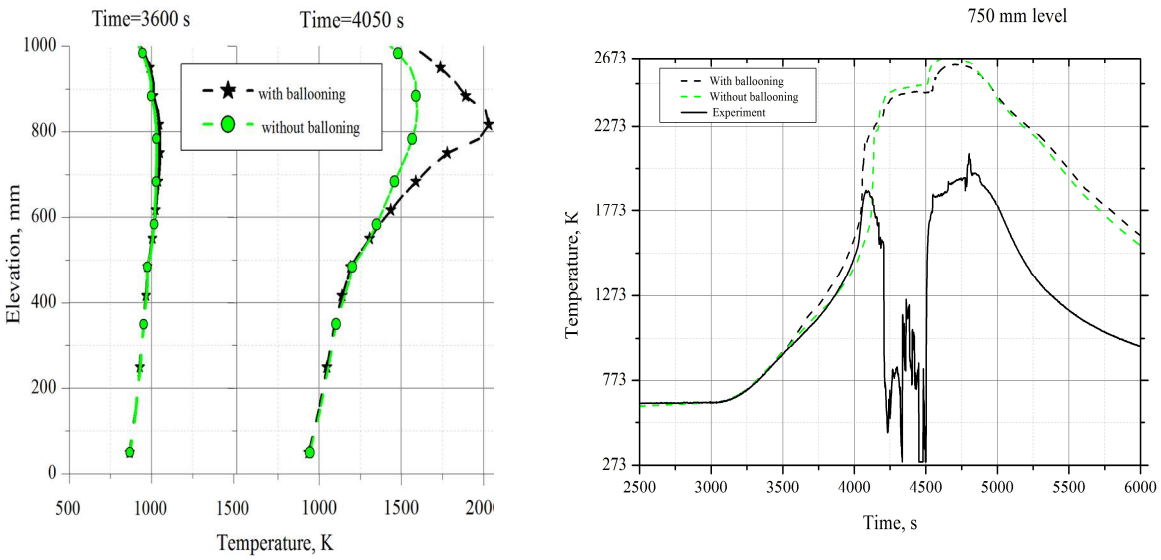

(a) (b)

FIG. 14. Comparison of the cladding temperature profiles (a) and the cladding temperature evolutions at 750 mm (b).

5. CONCLUSIONS

The numerical analysis of the CORA-15 test with the pressurized fuel rods allows drawing the following conclusions:

— SOCRAT code adequately reproduces the claddings temperature evolution and claddings rupture due to ballooning, the hydrogen production, the blockage formation due to melt relocation and solidification (within the uncertainties of the measured data);
— The ballooning effect was recognized based on the comparison of modeling results with and without pressurization of the fuel rods.

REFERENCES

[1] SEPOLD, L., HAGEN, S., HOFMANN, P., SCHANZ. G., Behavior of AgInCd Absorber Material in Zry/UO_2 Fuel Rod Simulator Bundles Tested at High Temperatures in the CORA Facility, FZKA 7448 (2009).
[2] DOLGANOV K.S., KISELEV A.E., TOMASHCHIK D.YU., YUDINA T.A., Simulation of Initial and Boundary Conditions with SOCRAT code for benchmarks based on IFA-650.10 and IFA-650.11 tests, this publication.
[3] STUCKERT. J., Results of the CORA-15 bundle test with pressurized rods, this publication.

SIMULATION OF INITIAL AND BOUNDARY CONDITIONS WITH SOCRAT CODE FOR BENCHMARKS BASED ON IFA-650.10 AND IFA-650.11 TESTS

DOLGANOV K.S., KISELEV A.E., TOMASHCHIK D.YU., YUDINA T.A.
Nuclear Safety Institute (IBRAE),
Russian Academy of Sciences,
52, B. Tulskaya, Moscow, 115191,
Russian Federation
E-mail: ksv@ibrae.ac.ru

Abstract

This paper summarizes results of simulations of HALDEN IFA-650.9, IFA-650.10, and IFA-650.11 tests performed with the integral code SOCRAT/V3 to predict initial and boundary conditions of benchmark exercises that are being prepared for the fuel performance codes in the framework of IAEA FUMAC Project.

1. INTRODUCTION

Several IFA-650 Halden experiments with a single fuel rod (IFA-650.9, 650.10, and 650.11) were provided to the IAEA FUMAC Project participants to check and improve models of fuel behaviour (cladding balloning and burst, fuel fragmentation and relocation) under LOCA conditions. In these tests, short segments of the irradiated fuel rods were explored in the IFA-650 test rig. Scenarios of the tests reproduced the main phases of LOCA: normal operation, blowdown and heating up of the core[9] [1]

A refabricated fuel rod was placed inside a high pressure flask connected with a separate high pressure loop and a blowdown system. The high pressure loop was filled with heavy water. These elements of the test rig allow simulation of natural and forced circulation of coolant, and dry out of the rod in the tests. The flask was inserted in the HALDEN reactor, so that heat release in the fuel pellets due to nuclear fission was controled by the reactor power during the experiments. Given that in real LOCA the isothermal boundary conditions are expected outside the rod cladding because of heat exchange between the neighboring rods, the fuel rod in the test was surrounded by a heater.

IFA-650.9 test with PWR rod (burn-up of 89.9 MWd/kgU) featured a strong fuel fragmentation and relocation that impacted on the cladding temperature. Therefore an axial relocaton model is needed for the simulation of temperature evolution of the cladding. In two other tests, IFA-650.10 test with PWR rod (burn-up of 61 MWd/kgU) and IFA-650.11 test with VVER rod (burn-up of 56 MWd/kgU), effect of fuel fragmentation was not pronounced.

These tests were chosen by the FUMAC Project Participants as a technical basis for benchmark exercises for the fuel performance codes, and IFA-650.10 and IFA-650.11 tests were selected as cases for uncertainty and sensitivity analysis. Integral code SOCRAT/V3 was used to predict the boundary conditions for the code benchmarks. IFA-650.10 and IFA-650.11 tests were analysed with well validated sophisticated models of SOCRAT/V3 code. To reproduce behaviour of the fuel rod in IFA-650.9 test, a simple fuel relocaton model was developed based on the information derived from the IFA-650.9 data.

[9] Notes of the 2nd Research Coordination Meeting on Fuel Modelling in Accident Conditions (CRP T12028 “FUMAC”), Room M3, Vienna International Centre, May 30 – June 2, 2016.

2. BRIEF DESCRIPTION OF SOCRAT/V3 CODE

SOCRAT/V3 (System Of Codes for Realistic Assessment of severe accidents) is a computer code intended for a coupled modeling of a wide range of thermohydraulic, physicochemical, thermomechanical and aerosol processes at all stages of accident progression, starting from initial event and up to corium release following the reactor vessel failure and consequent ex-vessel processes in containment. The code is essentially developed to model VVER NPPs but it was also applied to simulate the severe accidents at integral-type reactors, RMBK, BWR and PWR reactors. SOCRAT/V3 is widely validated on experimental data gotten from Integral and Separate effect tests, including International standard problems and benchmarks and national experiments.

SOCRAT/V3 field of application includes licensing support, design of safety systems, planning of experiments, PSA support, SAMG development and verification, crisis centers support, education. The SOCRAT/V3 is the extended version of SOCRAT/V1 code and maintains all its possibilities to simulate severe accident progression, including the hydrogen source inside the containment, and source of corium (mass, energy and composition) from reactor pressure vessel after its melt-through. These data were used for safety system design (hydrogen recombiners, core catcher). Extended SOCRAT/V3 version allows estimating the source term during severe acctidents that is used in deterministic support of PSA-2 analysed. During the Fukushima accident in 2011 SOCRAT/V3 was used as one of numerical tools in support to decision making on the need for protection of Russian population at Far-East coast.

SOCRAT/V3 as SCORAT/V1 has a modular structure. Each module contains the realistic models of a separate set of physical processes, and interaction between different processes is assured by coupling of modules through the common interface standards. Some of these modules are computer codes developed by different Russian scientific organisations. SOCRAT/V3 contains the data base on the thermo-physical properties of different materials.

Two modules were used for the modeling of HALDEN tests in this work, RATEG and SVECHA.

RATEG module is intended for simulation of thermal hydraulic behavior of the primary and secondary circuits. It contains models for different elements such as channels, chambers, pumps, valves, etc., and models for control and instrumentation systems allowing development of the full scale nodalization schemes for complex thermal hydraulic systems. Modeling of the coolant flow in RATEG is realized with a two-fluid two-phase hydraulic heterogeneous approach. The coolant is assumed to be in a liquid or gaseous phases. Each phase is characterized by its own volume, velocity and temperature, and may include several components. For example liquid phase may contain water and dissolved boric acid or non-condensable gases, and gaseous phase contains steam and non-condensable gases. Interactions of phases (heat and mass transfer, friction) and heat transfer to solid structures depend upon flow regime. The basic thermal hydraulic variables are pressure, void fraction, phasic enthalpies, non-condensable qualities (nitrogen, hydrogen, oxygen), and phasic velocities.

Heat transfer in solid structures (fuel rods, control rods, SG tubes, barrel, shrouds etc.) can be modeled either in one-dimensional or two-dimensional approaches. All heat structures in RATEG module have cylindrical or conic geometry.

SVECHA module package is intended for modeling of core degradation during initial stage of the severe accident and allows modeling of the following processes:

- External and internal oxidation of cladding by steam;
- Cracking of oxide layer and enhancement of cladding oxidation rate;
- Steam starvation conditions when thickness of oxide layer decreases until its complete disappearance;
- Eutectic interactions of UO_2 with Zr cladding in solid state;

— Dissolution of UO_2 and outer ZrO_2 layer by molten zirconium;
— Oxidation of liquid U-Zr-O mixture and formation of ceramic $(U,Zr)O_{2-x}$ corium during oxidation;
— Change of core configuration due to the relocation of molten materials;
— Formation of blockages during relocation of the melt;
— Failure of fuel elements during accident progression, including FP release;
— Oxidation of steel structures;
— Hydrogen release as a result of metal oxidation reactions;
— Thermal effect of oxidation reactions;
— Heat transfer through the gap between fuel and cladding;
— Radiative heat transfer between cladding, in-vessel structures and reactor walls with account for changes in configuration of the core and in-vessels.

Validation of SOCRAT/V3 models simulating the processes of fuel assemblies degradation has a large experimental basis (CORA, PHEBUS, PBF, QUENCH, PARAMETER-SF) and covers a wide range of conditions.

The modeling of mechanical strain and rupture of fuel rod cladding is based on the self-consistent solution of a set of equations that describe the elastic and plastic strain of cladding with account for different materials that form inside the cladding as a result of its heat-up and oxidation. Thus, the model considers the cladding oxidation and formation of multi-layer structures, evolution of thermal and mechanical properties of corresponding material layers.

The thermomechanical model can describe the following important phenomena:

— Change in fuel rod cladding geometry; disappearance/reappearance of the pellet-cladding gap;
— Evolution of pressure drop at fuel rod cladding as a result of cladding strain and burst;
— Effect of cladding hardening during oxygen enrichment of zirconium;
— Effect of cladding strength decrease due to generation of longitudinal cracks in the external layer of zirconium dioxide;
— Acceleration of oxidation process due to additional oxygen access to bearing metal through the cracks in zirconium dioxide layer;
— Failure of zirconium dioxide film by the "flowering" mechanism and the beginning of downward relocation of U-Zr-O melt.

It is assumed that each of the material layers constituting the fuel rod cladding can be described with a thin-walled cylinder having average radius, thickness and height. Each layer has its thickness and temperature. The layer temperature is considered to be constant along the layer height. It is assumed that the loads applied to the layer do not change along the height and in the azimuthal direction. A full distortion of the layer along any coordinate axis can be presented as the sum of elastic deformation, creep deformation and thermal deformation. At a loading stage the field of strain within the protective cladding shall be continuous, i.e. neither gaps nor overlapping between the adjacent layers shall appear. The external pressure is a boundary condition and is determined in thermal hydraulic module RATEG. The internal pressure is calculated from the ideal gas law, with account for fuel rod design, axial temperature distribution in the gas gap, and release of fission gases from fuel.

The mechanism of cladding failure depends on the load applied. The following mechanisms of failure are modeled:

— Cladding break-through owing to ballooning. This failure is accompanied by significant plastic deformations. It is assumed that the cladding burst owing to ballooning occurs if plastic deformation accumulated in the azimuthal direction exceeds the limiting value.

The limiting deformation depends on rod bundle geometry, oxidation conditions, loading or heating rates, phase composition, etc. and may be changed by the user. In this work the value of 0.55 was used, that corresponds to maximal possible strain of the cladding in VVER assembly before contact with a neighbouring rod;

— Brittle fracture occurs without significant plastic deformations owing to formation of several axial through cracks or a net-like population of the axial and azimuthal through cracks. It is assumed that this failure occurs if the alpha-layer stresses reached a critical value, and plastic beta-layer is too thin to arrest the through crack propagation. Brittle fracture is observed at the late stages of the simulated LOCA accident, when the cladding failure owing to balloning has already occurred, and the pressure difference at cladding wall has disappeared;
— Failure of zirconium dioxide film by the "flowering" mechanism. It occurs at high temperatures when the metal layers of the partly oxidized cladding get molten. Formation and opening of through cracks in oxide results in flowing out of the molten metal and the beginning of its intensive oxidation accompanied by temperature escalation. The cause of the stresses resulting in crack formation is assumed to be radial temperature gradient in oxide layer and internal melt pressure. Local dissolution of oxide layer with liquid zirconium is also affecting the cladding deformation by causing stress concentration;
— Melting of protective layer in fuel rod cladding. If no failures have occurred due to the above mechanisms, the further temperature increase causes the melting of external oxide film or its complete dissolution by liquid zirconium.

The build-up, intragranular and intergranular transport and release of FP from fuel are modelled in RELEASE module (based on MFPR code) of SOCRAT/V3. Evolution of FP state is considered self-consistently with the change of fuel defect structure (porosity, swelling), together with its physical-chemical and phase composition. The main object of simulation is a fuel fragment considered as an ensemble of identical grains. The chemical model of RELEASE module considers irradiated fuel, including FP and dissolved oxygen, as a heterogenic system containing several multi-component phases.

In the problem of transport of FP atoms in the UO_2 matrix, the grain is considered to be an isotropic sphere. The problem is formulated separately for two subsystems:

— Atoms of noble gas dissolved in the matrix and located in intragranular bubbles;
— Atoms of chemically active elements and molecules of their compounds.
— SOCRAT/V3 models consider the following physical processes of FP transport:
— Formation and transport of xenon and other fission gas bubbles in the fuel matrix;
— Formation of intergranular porosity and intergranular channels;
— Processes of intergranular transport and release of FP from the fuel, accompanied with chemical interaction between the FP and dissolved oxygen;
— Production of secondary solid phases (precipitates) and gaseous substances;
— Oxidation of the fuel in gas mixtures of various composition.

3. PARAMETRIC CALCULATIONS OF IFA-650.9, 650.10, AND 650.11 WITH SOCRAT/V3 CODE

Reports [1]–[3] and data from section 2.2 was used were used as a the technical basis for the test simulations with SOCRAT/V3 code. Some missing information on the rig loop was derived from the file related to IFA-650.1 and IFA-650.2 tests. The IFA-650 rig geometry was used for the development of a nodalisation scheme which was unified for all three FUMAC tests (IFA-650.9, 650.10, and 650.11). The geometrical model comprised the test flask, blowdown system, and some part of high-pressure heavy water loop connected to the flask

(both hot and cold legs). The nodalization of the test flask was furher completed for each test in order to account for some spesific details of the test section (for example, fuel rod geometry).

Modeling of all three FUMAC tests (IFA-650.9, 650.10, and 650.11) by SOCRAT/V3 code using experimental data as the boundary conditions revealed quite a good agreement between the measured and calculated data in two tests, IFA-650.9 (before onset of the fuel relocation, i.e. before t=100 s) and 650.10 (Fig. 1). But the cladding and heater temperatures in the IFA-650.11 test were overestimated (Fig. 2).

Parametric calculations were made to understand the possible reasons of observed differences in the IFA-650.11 test. Acceptable agreement was achieved in the runs with 15% lower total power (34 W/cm instead of 40 W/cm). Since we give credit to heater power measurement much more than the fuel power measurement, we choose a parametric run where the total power was reduced by reduction of linear heat generation rate (LHGR) in the fuel (75% of the experimental value). The corresponding plots for this case are provided in Fig. 3..

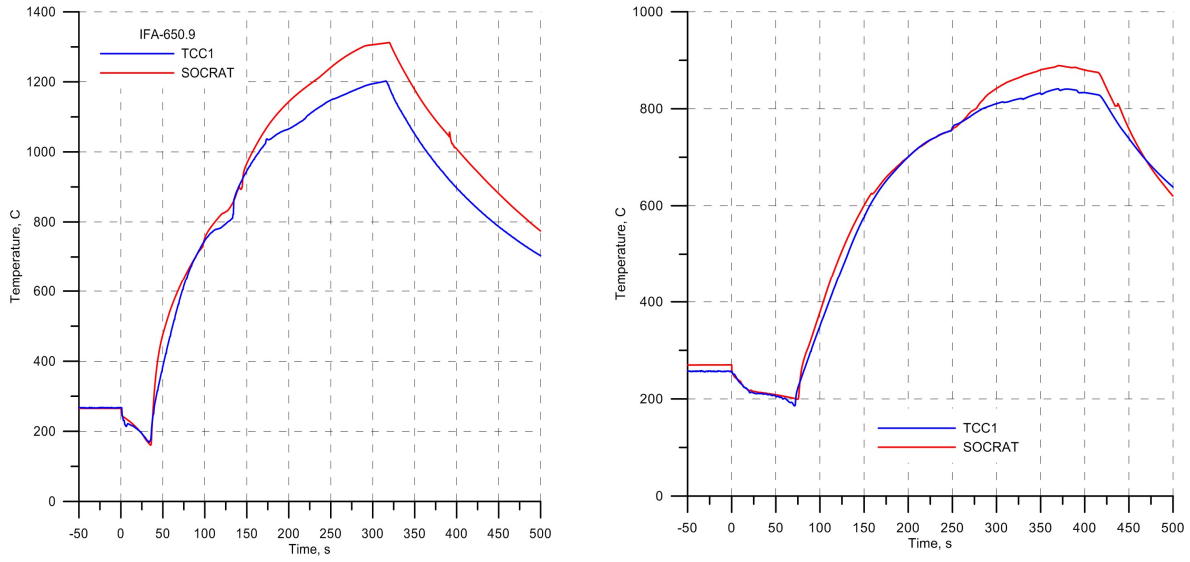

IFA-650.9 IFA-650.10

FIG. 1. Cladding temperature. Calculations with the experimental LHGR (linear heat generation rate in the fuel) and LHR (linear heat rate in the heater).

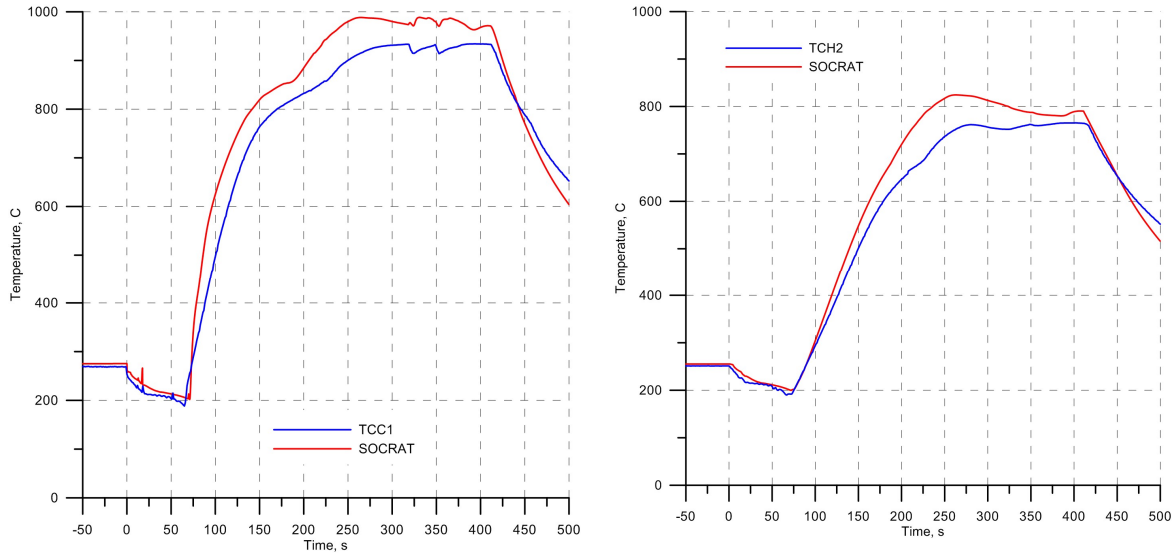

FIG. 2. Cladding (left) and heater (right) temperature IFA-650.11. Calculations with the experimental LHGR and LHR.

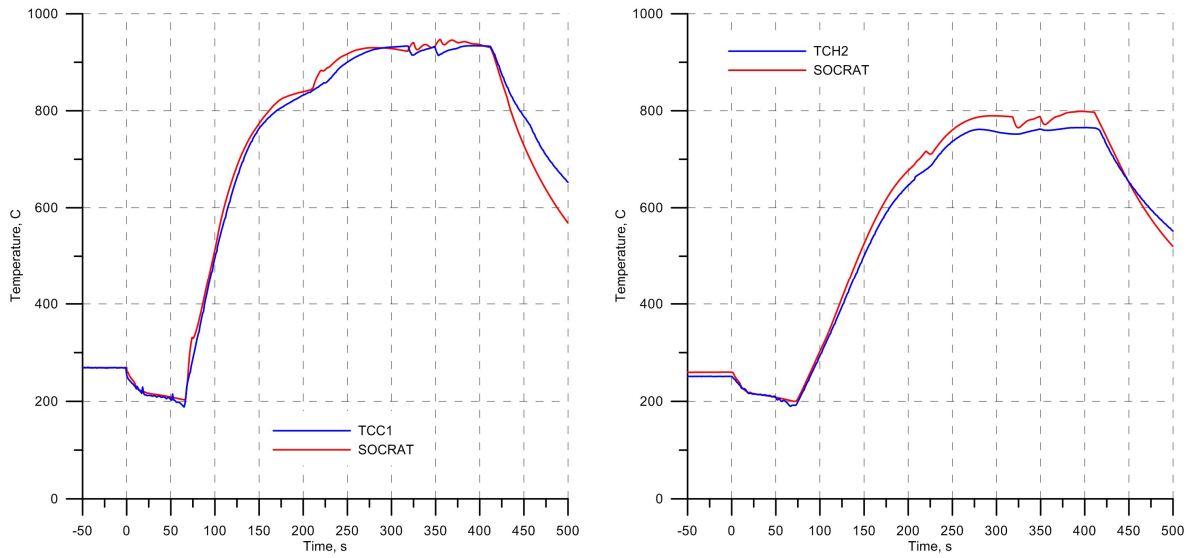

FIG. 3. Cladding (left) and heater (right) temperature IFA-650.11 (75% of experimental LHGR and 100% of experimental LHR).

Comparison of the measured evolutions of the heater temperature in the tests (we consider the heater TCs as much more credible than the cladding TCs because they are embedded in the heater body) supports our assumption about the lower LHGR in IFA-650.11. Indeed, total heat release is the same in the IFA-650.11 and IFA-650.9 tests but the measured heater temperatures are different (Fig. 4, left). Calculated curves (Fig. 4, right, solid lines) demonstrate how close would be the heater temperatures in IFA-650.11 and IFA-650.9 tests if the LHGR value in IFA-650.11 was set in accordance with initial specification. A dashed line to the right side of Fig. 4 shows the heater temperature evolution for the parametric run with the reduced LHGR (75%) in IFA-650.11 which is now much closer to the measured one presented in Fig. 3, right.

These results gave rise to the power recalibration for IFA-650.11 test, and the remommended reduction of rod power to 71% was accepted by the experimentalist team [10].

The parametric calculations indicated also that the IFA-650.11 results are sensitive to the gap width variation.

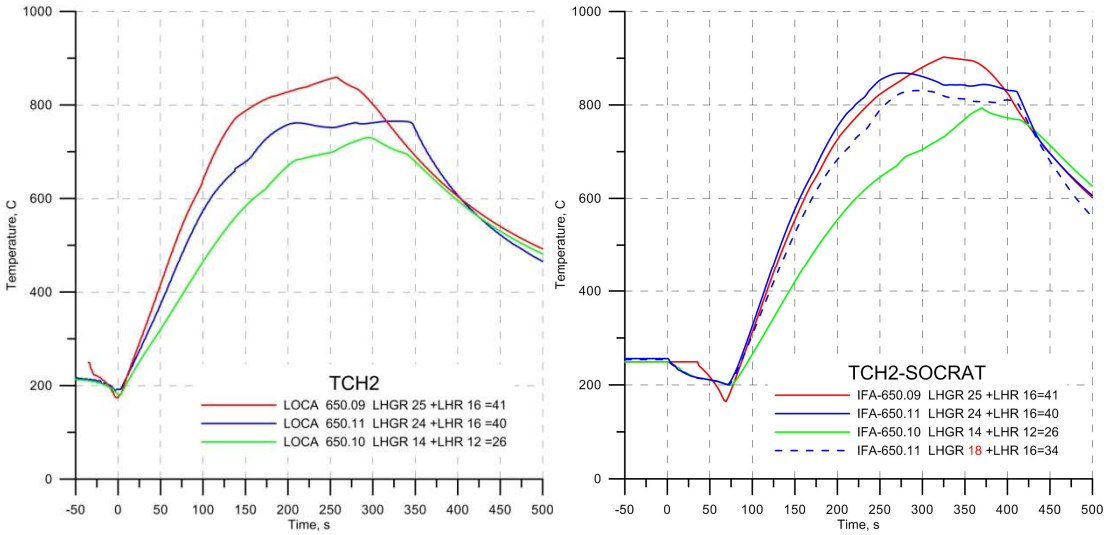

(a) measured (b) calculated

FIG. 4. Heater temperature evolution: effect of total power.

4. REFERENCE CALCULATIONS WITH SOCRAT/V3 CODE

4.1. Main features of the reference calculations

Reference calculations of all three FUMAC tests (IFA-650.9, 650.10, and 650.11) with SOCRAT/V3 code were performed with the unified nodalization scheme of the test rig. To get the initial and boundary conditions for the code benchmarks, IFA-650.10 and IFA-650.11 tests were simulated with sofisticated models of SOCRAT/V3 code. To calculate behaviour of the fuel rod in IFA-650.9 test, a parametric model for the fuel relocaton was developed and implemented in SOCRAT/V3 code based on the information derived from the IFA-650.9 data. Reduction of the nominal fuel-cladding gap width due to fuel swelling at high burnup was modeled by increasing of the gap thermal conductivity in IFA-650.10 and IFA-650.11 tests. In all tests, an extra decay heat due to the reactor operation at a higher steady state power (recommended value of 0.5 W/cm) was taken into account. In IFA-650.11, LHGR was set equal to 71% of nominal values based on the rod power recalibration, i.e. LHGR=(24+0.5)·0.71 W/cm. In IFA-650.10, the 4% uncertainty of LHGR measurement was taken into account as well, i.e. LHGR=(14+0.5)·0.96 W/cm.

Comparison of the predicted and measured data in IFA-650.10 suggests that some additional heat sink starts at the end of the blowdown. A leakage of D_2O was assumed to occur from the spray line into the flask. It was simulated by extra spay injection at the blow-down and transient phases with a mass flowrate of 0.005 g/s (started 50 s after Valve 6333 opening).

To account for thermal properties of heavy water in SOCRAT/V3, the light water properties were modified. Heavy water was simulated as light water with 20% higher density. Also, several modifications were made to take into account the transport properties of D_2O. The other properties (for example, specific heat, saturation line) were kept the same as for H_2O.

4.2. Initial and boundary conditions used in IFA-650.10 and IFA-650.11 simulations

The simulation starts at the time moment t= 300 s according to the experimental timing. The following initial conditions (which are common for both tests) have been used to match the test data:

- Temperature of the rod was set to 27°C;
- Gas mixture of 95% (vol.) Ar and 5% (vol.) He at a pressure of 3 MPa/4MPa (IFA-650.11/IFA-650.10) and a temperature of 27°C was set in the rod free volume;
- Temperature and pressure of the coolant in the loop and the flask were set to 235°C and 7 MPa, respectively;
- Environment outside the flask was specified as heavy water at a temperature of 229°C and a pressure of 3.4 MPa.

The following boundary conditions for the heat source were used in calculations. In the heater, the time history of the Joule heat supply was imposed the same as the measured one, assuming a uniform axial power distribution. Time moments of the rod power supply in the calculations correspond to the experimental data. The shapes of the simulated axial power distribution along the fuel stack are set the same as in the tests. These were extracted from the plots of neutron flux distribution in the experimental fuel rods and are tabulated in Tables 1 and Table 2. In radial direction, the heat sources are assumed to be distributed uniformly. LHGR values of 13.92 W/cm and 17.395 W/cm were used in IFA-650.10 and IFA-650.11 calculation, respectively.

TABLE 1. NORMALIZED VALUES FOR THE AXIAL HEAT GENERATION RATE THAT ARE USED IN THE CALCULATION OF IFA-650.11 TEST

Node	1	2	3	4	5	6	7	8	9
K	0.897	0.934	0.971	1.001	1.019	1.033	1.044	1.053	1.059
Node	10	11	12	13	14	15	16	17	18
K	1.059	1.054	1.043	1.026	1.005	0.983	0.962	0.941	0.920
Node	19	20	21	22	23	24	25	26	
k	0.900	0	0	0	0	0	0	0	

TABLE 2. NORMALIZED VALUES FOR THE AXIAL HEAT GENERATION RATE THAT ARE USED IN THE CALCULATION OF IFA-650.10 TEST

Node	1	2	3	4	5	6	7	8	9
K	0.897	0.934	0.971	1.001	1.019	1.033	1.044	1.053	1.059
Node	10	11	12	13	14	15	16	17	18
K	1.059	1.054	1.043	1.026	1.005	0.983	0.962	0.941	0.920
Node	19	20	21	22	23	24	25	26	
K	0	0	0	0	0	0	0	0	

The boundary conditions at the flask walls in both tests were applied as follows:

— Environment outside the flask is heavy water at a temperature of 229°C and a pressure of 3.4 MPa;
— Heat transfer coefficient is 500 W/m^2K assuming the boiling regime at the external surface of the flask wall.

The following boundary conditions were imposed in the pipe lines in IFA-650.11:

— Phase 1, forced circulation, time period -300 s….-180 s: valves VA6305 and VA6304 are opened, water flowrate is 0.03 kg/s and coolant temperature is 235°C at the end of the cold leg, pressure is 6.9 MPa at the end of the hot leg;
— Phase 2, natural circulation, time period -180 s….0 s: valve VA6305 is closed, valve VA6304 is opened; water flowrate is 0 kg/s and pressure is 6.9 MPa at the end of the cold leg;
— Phase 3, blow-down, time period 0 s…about 70 s (the time moment when the cladding temperature starts to increase): valve 6333 is opened, valve VA6304 is closed, pressure is 0.4 MPa at the end of the blow-down line;
— Phase 4, transient, time period about 70 s …. 411 s: steam temperature is 300°C, 3 pulses were modeled at the end of the spray line 10, 108 and 139 s after the cladding burst, each pulse corresponding to injection of a steam mass of 0.5 g.

The following boundary conditions were set in the pipe lines in IFA-650.10:

— Phase 1, forced circulation, time period -300 s….-180 s: valves VA6305 and VA6304 are opened, water flowrate is 0.03 kg/s and coolant temperature is 235°C at the end of the cold leg, pressure is 6.9 MPa at the end of the hot leg;
— Phase 2, natural circulation, time period -180 s….0 s: valve VA6305 is closed, valve VA6304 is opened, pressure is 6.9 MPa at the end of the cold leg;
— Phase 3, blow-down, time period 0 s…about 70 s (the time moment when the cladding temperature starts to increase): valve 6333 is opened, valve VA6304 is closed, pressure is 0.5 MPa at the end of the blow-down line. At the end of the spray line, steam temperature is 230°C, spray injection starts 50 s after Valve 6333 opening with an average spray mass flowrate of 0.005 g/s;

— Phase 4, transient, time period about 70 s …. 415 s: steam temperature is 230°C, spray injection starts at the phase 3 and continues at the phase 4 with an average spray mass flowrate of 0.005 g/s at the end of the spray line.

4.3. Results of the IFA-650.11 and IFA-650.10 simulations

At the blow-down phase, the system and rod pressures, cladding and heater temperatures are reproduced well (Fig. 5 to Fig. 27). Some differences between the calculated and measured inlet coolant temperatures can be related to a simplified modeling of a region between the inlet tube and the heated region. Besides, using several thermal properties of light water instead those of heavy water could also have some effect on the results. The predicted blow-down times, estimated by the onset of the cladding and heater temperature increase, are about 75 s in IFA-650.11 test and 70 s in IFA-650.10 test, that is in a good compliance with the experimental values.

At transient Phase 4, the cladding heat up, ballooning and burst are simulated reasonably well. Maximal deviations of the predicted cladding temperature from the measured one are 30°C in IFA-650.11 and 15°C in IFA-650.10 at the time span before the cladding burst. The coolant, plenum and heater temperatures in the simulations differ from the measured one no more than 30°C at this time period. Single cladding ballooning is predicted at the hottest zone. Calculated burst parameters match data well as one can see from the Table 3.

After the cladding burst, the argon and helium are released from the rod and fill the flask very quickly. The mixture of steam, hydrogen, argon and helium is further transported to the cold leg and then to the blow-down line. It enters the blow-down line before spray initiation.

At the spray operation sub-phase, the water injected in the spray line interacts with the hot pipe wall in IFA-650.11 test. This produces intensive boiling, and the steam-water mixture enters the flask. In the IFA-650.10 test, steam was assumed to be injected. The cooling effect of spray operation was not observed in the calculations, but the generated/injected steam displaces argon from the flask promoting the cladding oxidation and heat transfer enhancement. Maximal differences between the calculated and measured cladding temperatures are 50°C in IFA-650.11 and 40°C in IFA-650.10 at this time span.

TABLE 3. BURST PARAMETERS

Value	IFA-650.10		IFA-650.11	
	Measured	SOCRAT/V3	Measured	SOCRAT/V3
Burst time, s	249	250	207	206.7
Burst level*, mm	255	200÷250	209	200÷225
Burst pressure, bar	72.5	66.5	55.7	52.1
Burst local (maximal) strain,%	10(31)	12	15(26)	15
TCC1, °C	755	766	839	843

*levels are referred to the bottom of the fuel stack

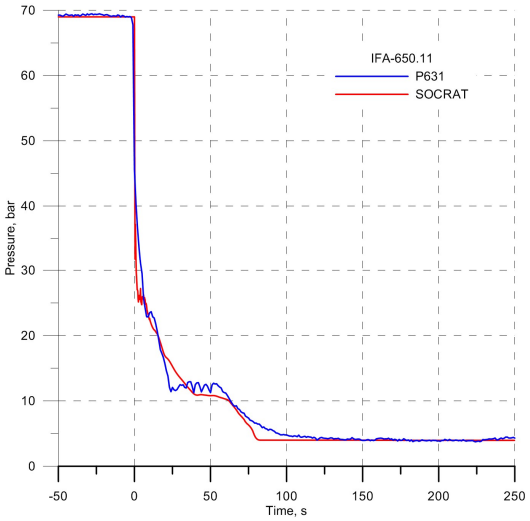

FIG. 5. Pressure evolution in the cold leg. IFA-650.11.

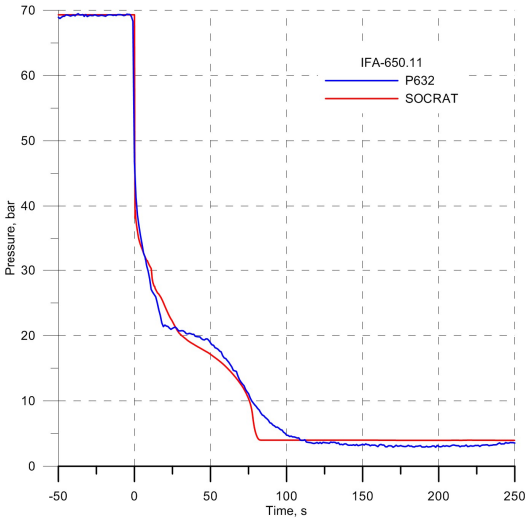

FIG. 6. Pressure evolution in the hot leg. IFA-650.11.

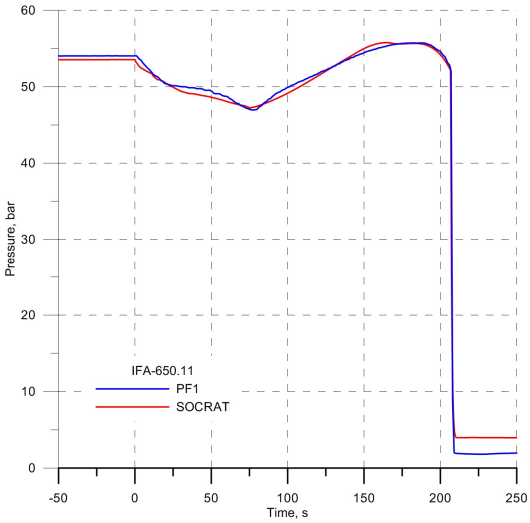

FIG. 7. Pressure evolution in the rod. IFA-650.11.

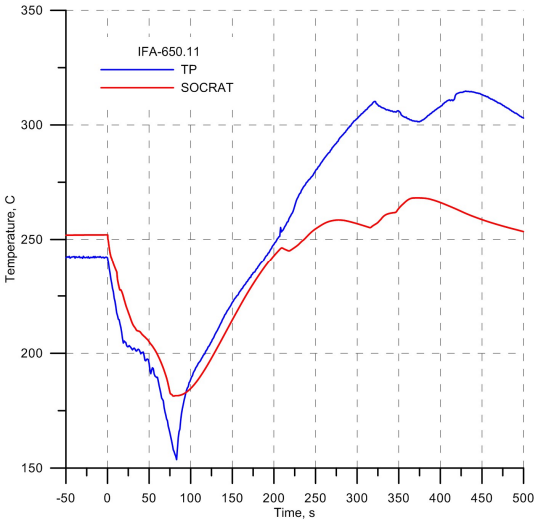

FIG. 8. Plenum temperature evolution. IFA-650.11.

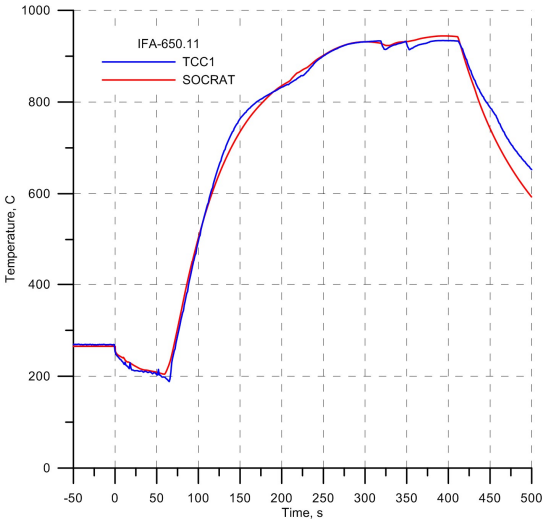

FIG. 9. Cladding temperatures at the lower elevation. IFA-650.11.

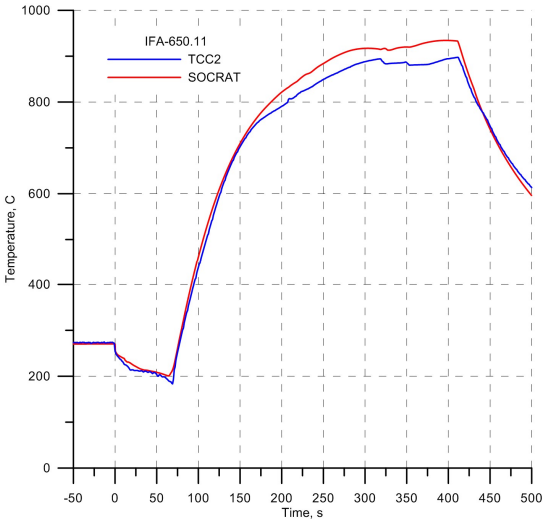

FIG. 10. Cladding temperatures at the upper elevation. IFA-650.11.

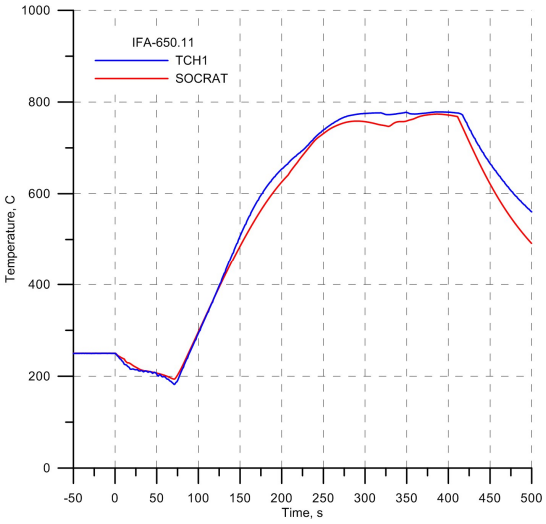

FIG. 11. Heater temperature at the lower elevation. IFA-650.11.

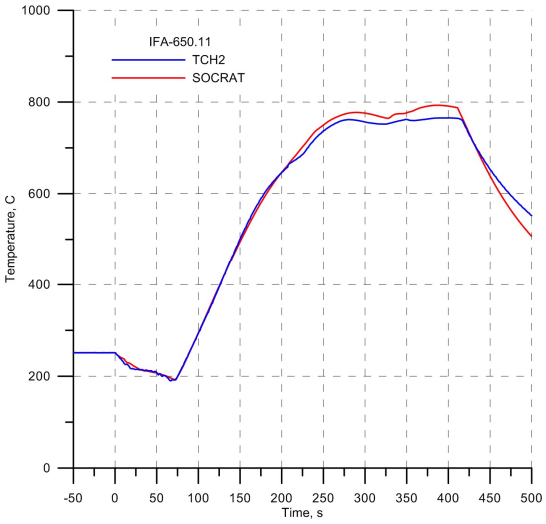

FIG. 12. Heater temperature at the middle elevation. IFA-650.11.

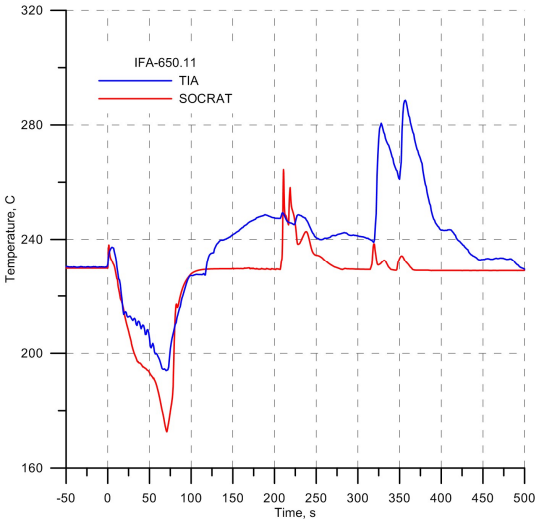

FIG. 13. Inlet coolant temperature. IFA-650.11.

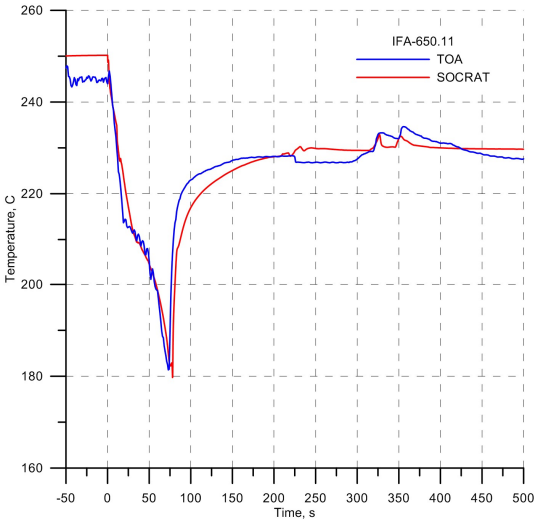

FIG. 14. Outlet coolant temperature. IFA-650.11.

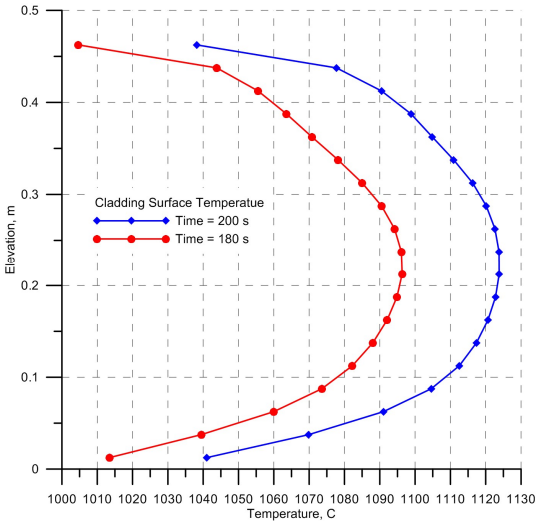

FIG. 15. Vertical cladding temperature profiles at 180 s and 200 s. IFA-650.11.

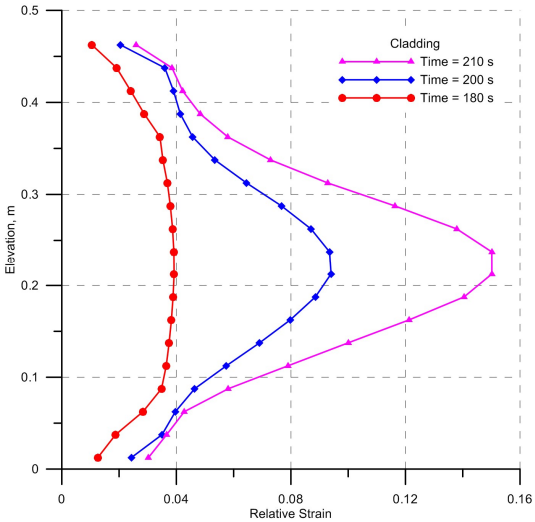

FIG. 16. Cladding strain evolution. IFA-650.11.

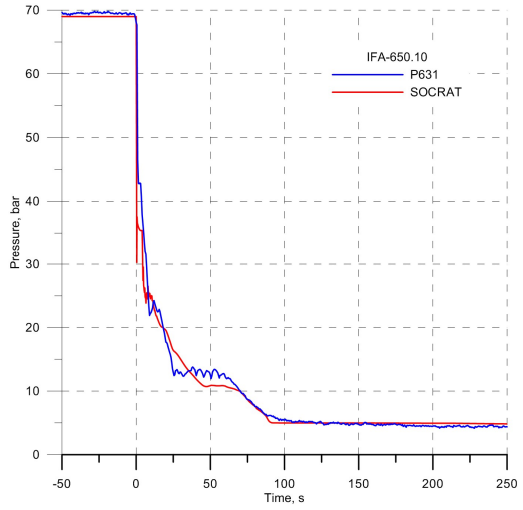

FIG. 17. Pressure evolution in the cold leg. IFA-650.10.

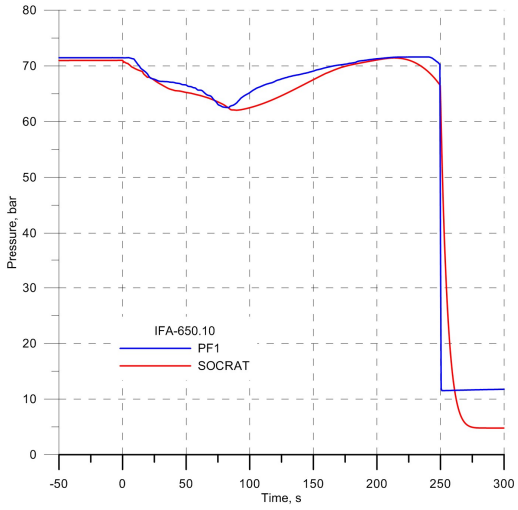

FIG. 18. Pressure evolution in the rod. IFA-650.10.

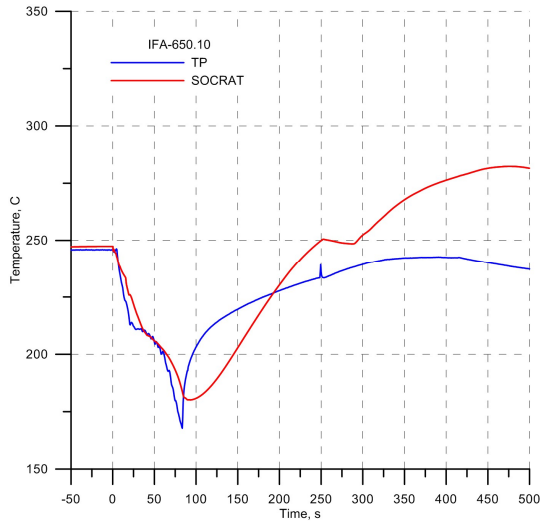

FIG. 19. Plenum temperature evolution. IFA-650.10.

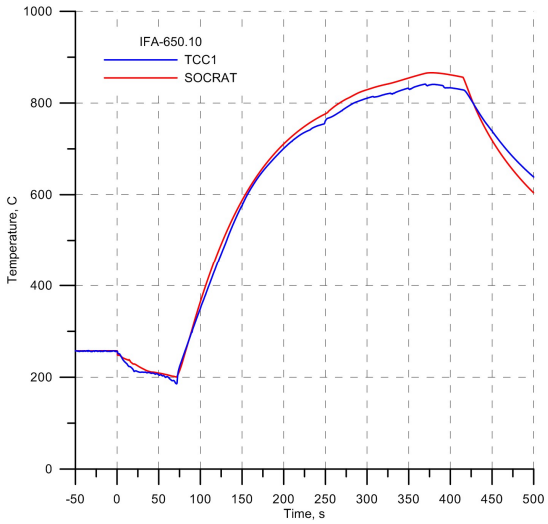

FIG. 20. Cladding temperature at the lower elevation. IFA-650.10.

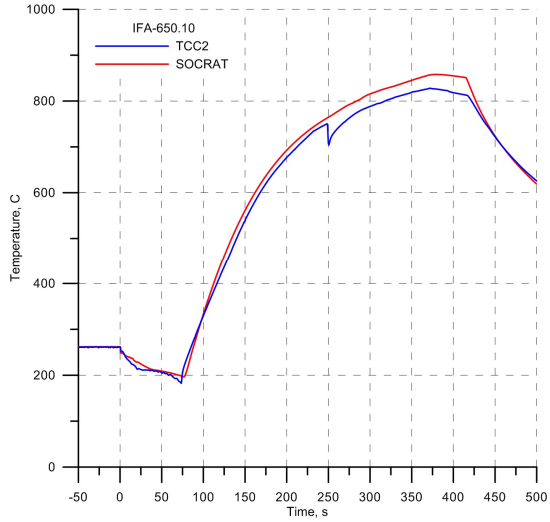

FIG. 21. Cladding temperature at the upper elevation. IFA-650.10.

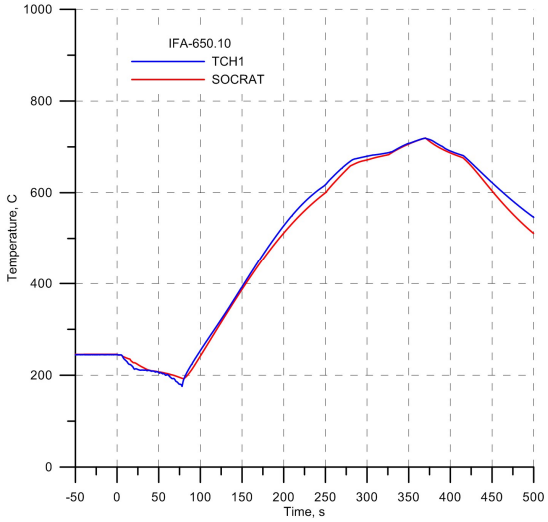

FIG. 22. Heater temperature at the lower elevation. IFA-650.10.

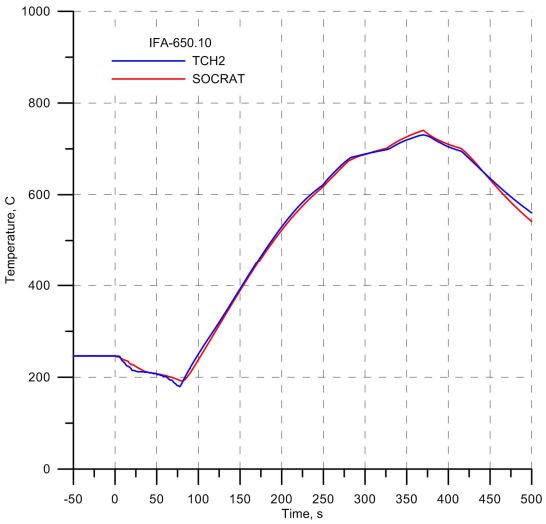

FIG. 23. Heater temperature at the middle elevation. IFA-650.10.

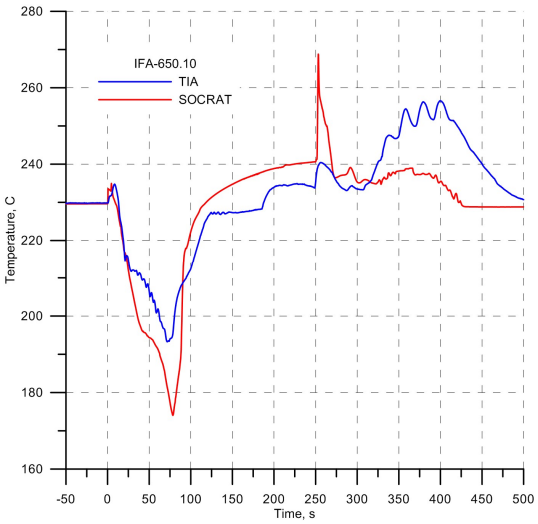

FIG. 24. Inlet coolant temperature. IFA-650.10.

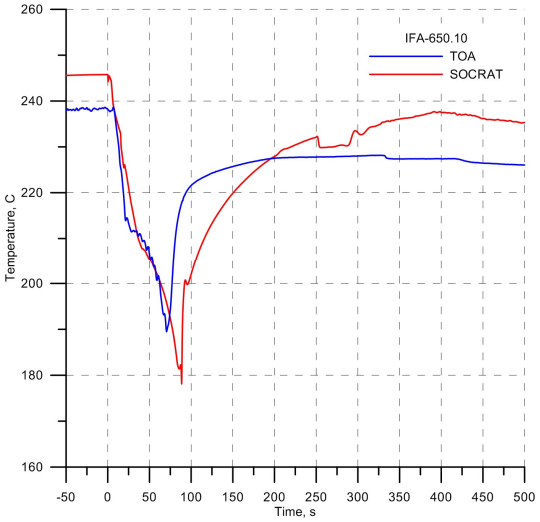

FIG. 25. Outlet coolant temperature. IFA-650.10.

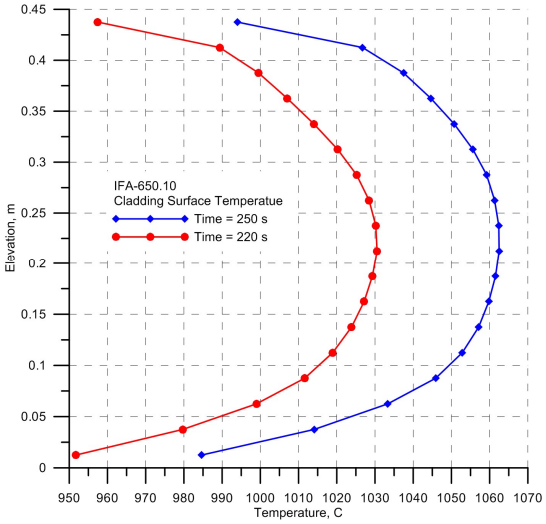

FIG. 26. Vertical cladding temperature profiles at 220 s and 250 s. IFA-650.10.

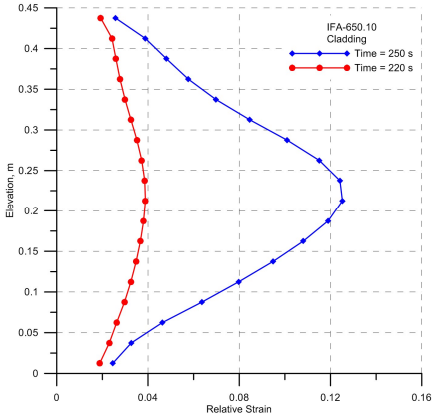

FIG. 27. Vertical cladding relative strain profiles at 220 s and 250 s (at the calculated burst). Burst at level 237.5 mm (1137.5 mm). IFA-650.10.

5. CONCLUSION

Assessment of IFA-650.9, IFA-650.10 and IFA-650.11 tests was performed through the test simulations with SOCRAT/V3 code. Some discrepancies between the measured and calculated temperatures, observed in IFA-650.11 test, indicated too high value of the rod power, and the power recalibration was done by the experimentalists for this test. A good agreement between the predicted and measured data on the set of interrelated parameters in IFA-650.10 and IFA-650.11 in the final calculations with SOCRAT/V3 code allows recommending the use of the calculated data as the initial and boundary conditions for the fuel performance code benchmarks. The results of IFA-650.9 test modeling are presented in Appendix 1 for information. Double ballooned cladding in IFA-650.9 test in comparison with single ballooned cladding in IFA-650.10 and IFA-650.11 tests is explained by a pronounced fuel relocation in IFA-650.9 test.

APPENDIX I:

INITIAL AND BOUNDARY CONDITIONS USED IN IFA-650.9 SIMULATION

The simulation starts at the time moment t= 300 s according to experimental timing. The following initial conditions have been used to match the test data:

- Temperature of the rod was set to 27°C;
- Gas mixture of 95% (vol) Ar and 5% (vol) He at a pressure of 4MPa and a temperature of 27°C was set in the rod free volume;
- Temperature and pressure of the coolant in both the loop and the flask were set to 235°C and 7 MPa, respectively;
- Environment outside the flask specified as heavy water at a temperature of 229°C and a pressure of 3.4 MPa.

Prescribed boundary conditions on the heat source were as follows. The average linear heat generation rate (LHGR) of 25.5 W/cm was set in the fuel stack. The shape of the simulated axial power distribution was extracted from the plot of neutron flux distribution shown in Fig. 7 [3]. The normalized values (k_i) for each node i are given in Table 1. The heat generation rate Q_i^0 in an axial node i before the fuel relocation was calculated as:

$$Q_i^0 = LHGR \cdot (L_{exp}/L_{mod}) \cdot h_i \cdot k_i,$$

where LHGR – average linear heat generation rate, L_{exp} – real fuel stack length (480 mm), L_{mod} – fuel stack length in the model (475 mm), h_i - node height (2.5 cm), k_i – normalized value (Table 8). The heat generation rate Q_i in an axial node i after the fuel relocation onset (105 *s)* was calculated as:

$$Q_i = Q_i^0 \cdot M_i / M_i^0 \cdot M^0 / \sum_i M_i k_i,$$

where M_i – fuel mass in node i, M_i^0 – initial fuel mass in node i, M^0– total fuel mass.

TABLE 1. NORMALIZED VALUES FOR AXIAL HEAT GENERATION RATE AS USED IN THE CALCULATION OF IFA-650.9 TEST

Node	1	2	3	4	5	6	7	8	9
K	0.907	0.944	0.981	1.012	1.030	1.041	1.051	1.057	1.061
Node	10	11	12	13	14	15	16	17	18
K	1.060	1.054	1.043	1.027	1.008	0.987	0.966	0.945	0.924

Node	19	20	21	22	23	24	25	26
k	0.903	0	0	0	0	0	0	0

The time history of the Joule heat supply to the heater was set equal to the measured one: 16 W/cm for the first 168 s and 12.5 W/cm thereafter (Table 2). Uniform axial power distribution was assumed.

TABLE 2. EVOLUTION OF TOTAL HEATER POWER

Time (s)	-300	168	168.02	290	290.02
Q_{heater} (W)	832	832	650	650	0

The boundary conditions at the flask walls in IFA-650.9 were applied as follows:

— Environment outside the flask is heavy water at a temperature of 229°C and a pressure of 3.4 MPa;
— Heat transfer coefficient is 500 W/m2K assuming the boiling regime at the external surface of the flask wall.

The following boundary conditions were imposed in the pipe lines:

— Phase 1, forced circulation, time period -300 s – -180 s: valves VA6305 and VA6304 are opened, water flowrate is 0.03 kg/s and coolant temperature is 235°C at the end of the cold leg, pressure is 6.9 MPa at the end of the hot leg;
— Phase 2, natural circulation, time period -180 s – 0 s: valve VA6305 is closed, valve VA6304 is opened, water flowrate is 0 kg/s and pressure is 7 MPa at the end of the cold leg;
— Phase 3, blow-down, time period 0 s – about 35 s (the time moment when the cladding temperature starts to increase): valve VA6333 is opened at 0 s and closed at 35 s, valve VA6304 is closed at 0 s, valve VA6334 is opened at 5 s, pressure is 0.23 MPa at the end of the blow-down line;
— Phase 4, transient, time period 35 s – 320 s: steam temperature is 140°C, pressure is 0.5 MPa at the end of the spray line. Time moments of spray onset and trip are set to be the same as in the experiment. The prescribed pulse duration (except the first one) is 0.5 s.

1. RESULTS OF IFA-650.9 SIMULATION

In the IFA-650.9 test, the fuel relocation impacts on the fuel rod behavior at the transient phase. Since SOCRAT/V3 code has no dedicated models to treat the fuel fragmentation, relocation and dispersion, the numerical simulation with the sophisticated models covers a time span before the fuel relocation that would start in the experiment at about 100 s. The calculated blow-down time, estimated as the time when cladding started to heat up, matches the experimental value well (Figs 5 to 6). The blow-down phase in IFA-650.9 test is shorter in comparison with IFA-650.10 and IFA-650.11 tests because in IFA-650.9 test it resulted from double-sided discharge of coolant, in contrast to one-sided discharge in IFA-650.10 and IFA-650.11 tests. By the time when fuel relocation started, the cladding heated up to about 750°C both in the test and in the calculation.

Additional efforts were made to understand the further fuel rod degradation. With this aim several trial calculations were made with SOCRAT/V3 code. To model the fuel relocation, a parametric approach was used. The simulations used the following information derived from the experimental data:

— comparison of the cladding and heater heat up rates derived from the thermocouple readings in the IFA-650.9, IFA-650.10 and IFA-650.11 tests before the cladding burst allows estimation of the onset and duration of the fuel relocation, mass of the relocated fuel and a new heat generation rate at the elevations with thermocouples in the IFA-650.9 test;
— the posttest gamma scans of the rod and cladding diameter profile demonstrate that the fuel pellets are missing in the upper zone while the relocated fuel was found at the lower elevations where a large cladding ballooning occurred;
— the rod depressurization slows down at 130 s (Fig. 3) in comparison with IFA-650.10 and IFA-650.11 tests (Figs 7, 8).

The main results of the simulation with the parametric model of fuel relocation are presented in Figs 1 to 3. In the simulation, the cladding ballooning is first appearing at 90 s at an elevation of 252 mm (the elevations are referred to the bottom of the fuel stack), where the maximum cladding temperature is predicted by that time. Local collapse of the fuel pellet column is simulated at this region starting from 105 s. The crumbled fuel moves radially outwards to fill a void volume in the ballooned region and further falls in the gap downwards. In its turn, the fuel above the crumbled fuel relocates down by gravity to occupy the formed free volume. The cladding at the upper elevations, where the fuel relocated from, starts to cool down (Fig. 6).

The maximum of the cladding temperature shifts from the mid-height to the lower region of the fuel rod (Fig. 12), where the relocated fuel accumulates. Here the second and major ballooning starts (Fig. 13). The cladding rupture is predicted to occur at 133 s at elevations of 100-125 mm. The ballooning at elevation of 75-100 mm continues for 10 s after the burst due to rather high internal pressure and high temperature.

Fast depressurization of the rod is prevented by the fuel plug that has formed in the burst region and above it. Fuel relocation stops at 145 s. By this time almost all fuel mass relocates from upper elevations of 470-240 mm downward. From the beginning of the transient phase till the end of fuel relocation and cladding ballooning the difference between the measured and predicted temperatures of the cladding and the heater does not exceed 40 K, except a short time interval around t=50 s, when the difference is 80°C (Figs 5 to 8). Higher temperature differences after 150 s (100°C for the cladding and 200°C for the heater) could be explained by a forcedly simplified simulation of the spray sub-phase (that starts at 149 s), given that the spray mass injected in the flask was not measured in the test. The calculated burst parameters are presented in the Table 3 in comparison with the measured data.

TABLE 3. COMPARISON OF THE CALCULATED AND MEASURED BURST PARAMETERS.

Value	IFA-650.9	
	Measured	SOCRAT/V3
Burst time, s	133	133
Burst level*, mm	54	75-125
Burst pressure, bar	62,7	54,8
Burst local (maximal) strain, %	83(86)	55(65)
TCC1/TCC2, C	810/784	853/787

*levels are referred to the bottom of the fuel stack

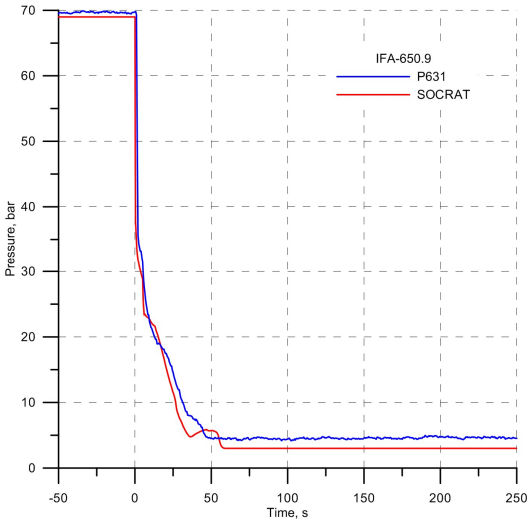

FIG. 1. Pressure evolution in the cold leg. IFA-650.9.

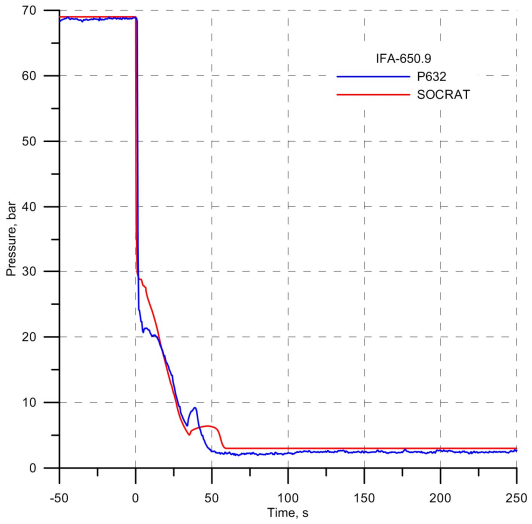

FIG. 2. Pressure evolution in the hot leg. IFA-650.9.

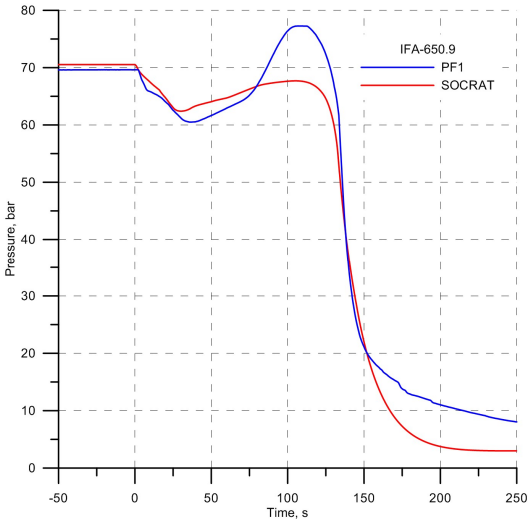

FIG. 3. Pressure evolution in the rod. IFA-650.9.

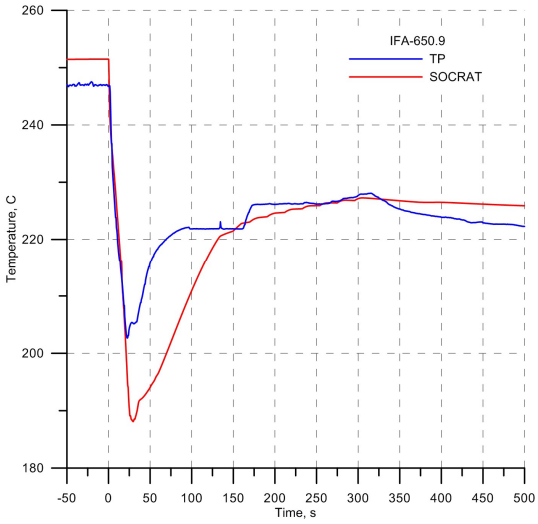

FIG. 4. Plenum temperature evolution. IFA-650.9.

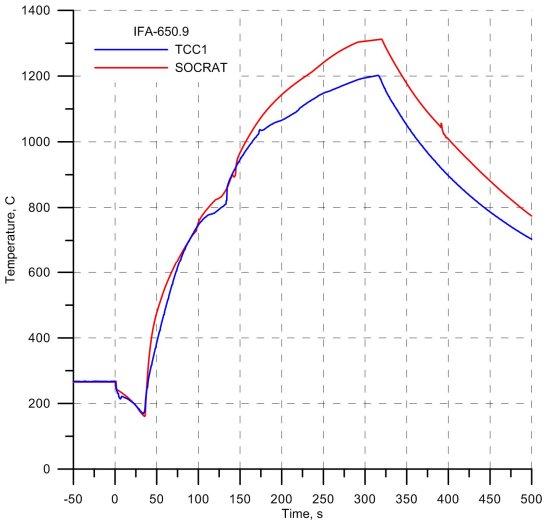

FIG. 5. Cladding temperatures at the lower elevation. IFA-650.9.

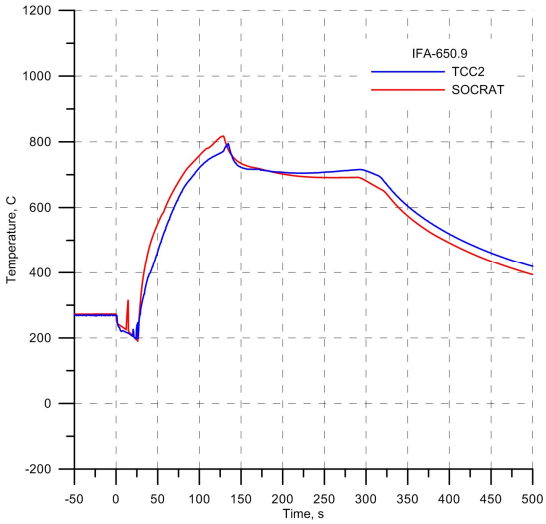

FIG. 6. Cladding temperatures at the upper elevation. IFA-650.9.

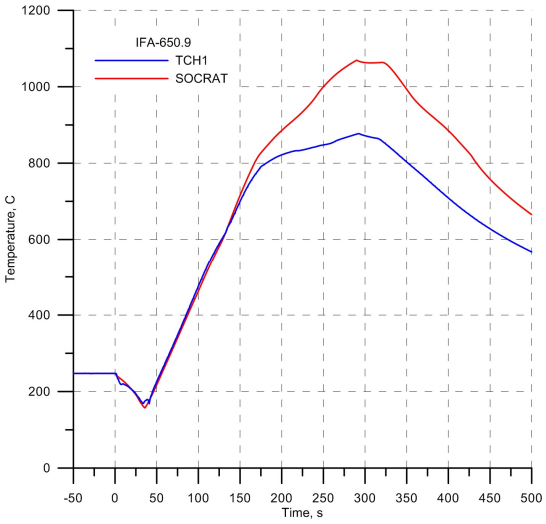

FIG. 7. Heater temperature at the lower elevation. IFA-650.9.

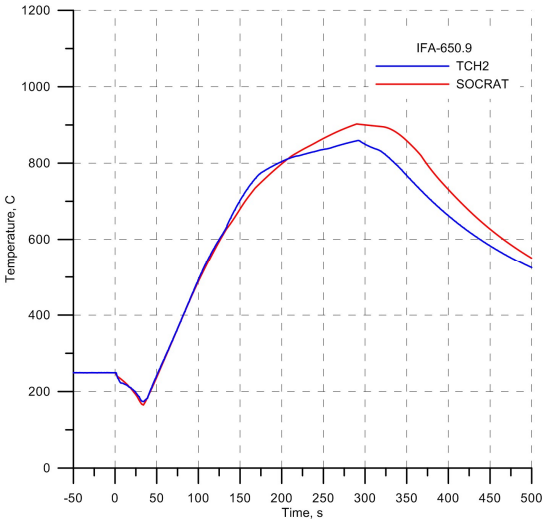

FIG. 8. Heater temperature at the middle elevation. IFA-650.9.

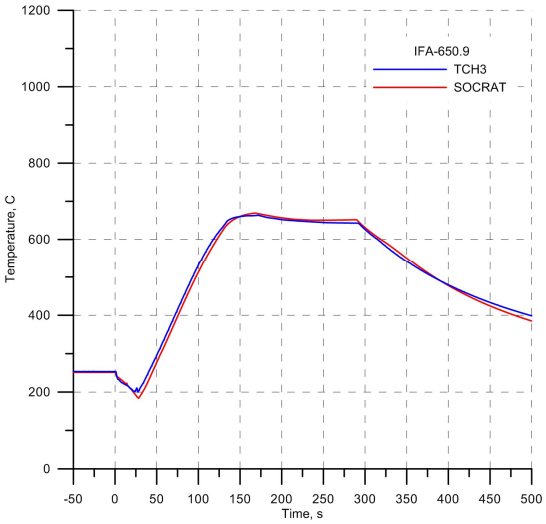

FIG. 9. Heater temperatures at the upper elevation. IFA-650.9.

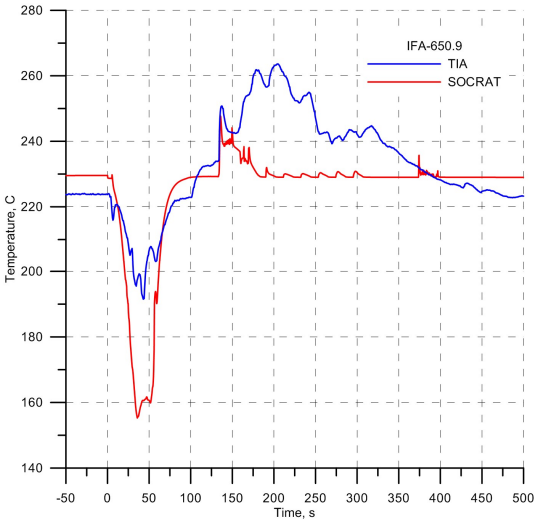

FIG. 10. Inlet coolant temperature. IFA-650.9.

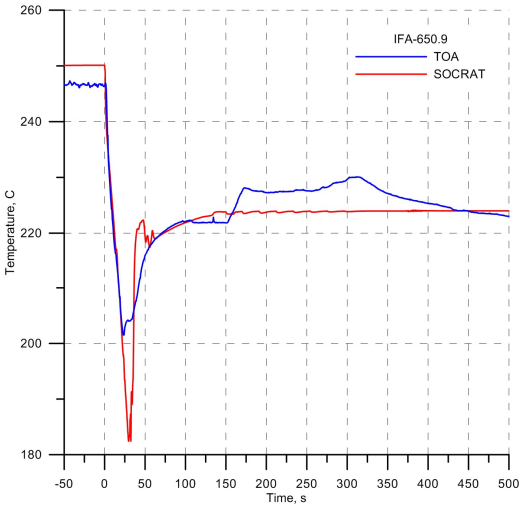

FIG. 11. Outlet coolant temperature. IFA-650.9.

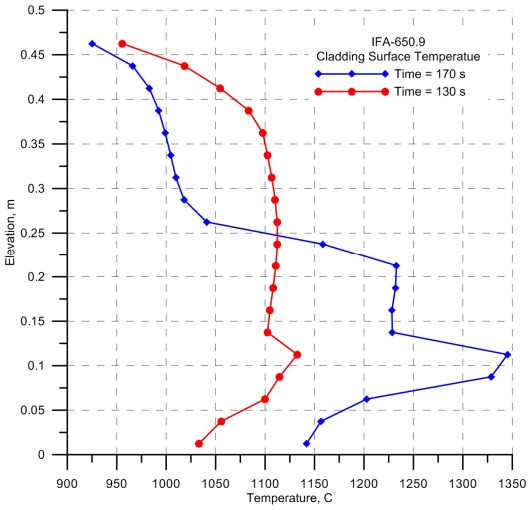

FIG. 12. Vertical cladding temperature profiles at 130 s and 170 s (3 s before and 37 s after the calculated burst). IFA-650.9.

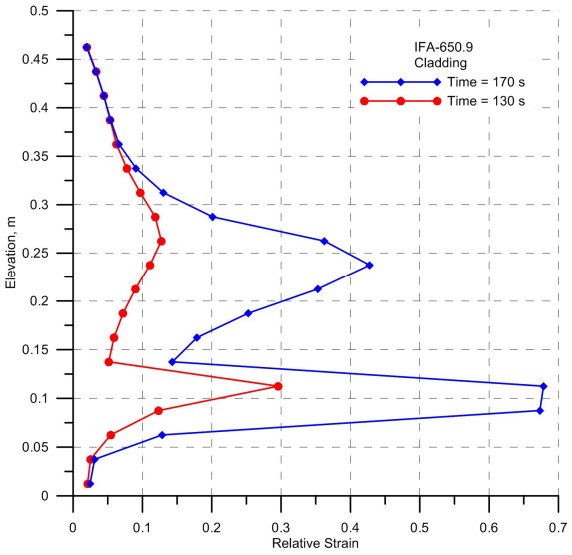

FIG. 13. Cladding strain evolution. IFA-650.9.

REFERENCES

[1] LAVOIL, A., LOCA Testing at HALDEN, the VVER Fuel Experiment IFA-650.11, Report on OECD HALDEN Reactor Project No. HWR-976 (2010).

[2] LAVOIL, A., LOCA Testing at HALDEN, the Tenth Experiment IFA-650.10, Report on OECD HALDEN Reactor Project No. HWR-974 (2010).

[3] DU CHOMONT F.B.,, LOCA Testing at HALDEN, the Ninth Experiment IFA-650.9, Report on OECD HALDEN Reactor Project no. HWR-917 (2009).

CALCULATION MODELING OF THERMOMECHANICAL BEHAVIOR OF FUEL RODS IN IFA-650.9, IFA-650.10 AND IFA-650.11 EXPERIMENTSUSING RAPTA-5.2 CODE

KUZNETSOV V.I., KUMACHEV A.V., NOVIKOV V.V., SALATOV A.V., FEDOTOV P.V.
Stock Company High-technology Research Institute of Inorganic Materials (SC "VNIINM")
5a, Rogova str., Moscow, 123098, Post Box 369
Russian Federation
E-mail: PVFedotov@bochvar.ru (corresponding author)

Abstract

After-testing calculations of the thermomechanical behavior of fuel rods studied in the 650.9, IFA-650.10 and IFA-650.11 experiments were carried out using RAPTA-5.2 code and additional models: special model of heat transfer in the test rig, model of axial displacement of fragmented fuel. In addition, the IFA-650.10 and IFA-650.11 experiments were calculated using the boundary condition of the first kind generated by SOCRAT code. Comparative analysis of calculated and measured parameters of thermomechanical and corrosion behavior of the fuel rod had shown that calculated values for the time of failure, cladding strain, oxide thickness are in good agreement with the experiment.

1. RAPTA-5.2 CODE

The goal for the post-testing calculations with the RAPTA-5.2 code [1] is to determine the thermomechanical and corrosion parameters of the fuel rods, studied in the IFA-650.9, IFA-650.10 and IFA-650.11 experiments, and their comparison to the experimental data.

1.1. General Information

The destination of RAPTA-5.2 code is the calculation of thermomechanical and corrosion behavior of the fuel rod of VVER, PWR and RBMK under accident conditions, accompanied by the increase of cladding and/or fuel temperatures as the result of disturbance of the thermal balance of the fuel rod (loss of coolant accidents, reactivity initiated).

The code is written in FORTRAN-90 and compiled for Intel PC. The code is autonomous and uses only the built-in functions of the FORTRAN. There are no special requirements for the computers. Operating system - MS DOS, version not below 3.3, Windows. The executable module has a capacity of 1 MB, the memory capacity for recording of results vary widely depending on task parameters, the characteristic amount of output files of one task is a few Mb.

RAPTA-5.2 code is used by Chief designer-technologist of VVER fuel rods (SC "VNIINM") to justify the fuel rods behavior in design basis accidents in frame of the development of technical projects within the fuel rods and fuel cycle studies of VVER. Using the RAPTA-5.2 code criterial characteristics of fuel rods are determined. The fuel safety criteria are verified on the base of following characteristics: maximum temperature of the fuel, peak fuel enthalpy, maximum cladding temperature, equivalent cladding reacted fraction of oxidized zirconium, number of depressurized fuel rods.

In accordance with the requirements of normative documents of the Russian Federation NP-082-07 [1] RAPTA-5.2 code passed the software certification procedure used in the justification of the safety of nuclear facilities in the Federal Environmental, Industrial and Nuclear Supervision SERVICE of Russia (Rostechnadzor), which is prescribed in ‘Regulations on certification of software...’ [2] and the ‘Requirements for the composition and content of the report on the verification and justification of software used to support the safety of nuclear facilities’ [3]. RAPTA-5.2 code was certified in 2011 [4].

1.2. Problem Statement

The object of the simulation is fuel element of rod-type with fuel based on uranium dioxide, including fuel with integrated absorber (Gd_2O_3), and with a cladding made of zirconium alloy.

Following interrelated processes are modeled:
(a) Heat transfer in fuel rod taking into account:

- Non-stationary volume power rate in the fuel (input data) taking into account of its radial distribution as the function of burnup;
- The thermal effect of the zirconium oxidation in the steam;
- Transient boundary conditions on a cladding surface (input data);
- Changes of cross-sectional geometry of the fuel rod;
- Cependences of thermodynamic material properties against temperature and burnup taking into account radial distribution;
- Change of the gas content in a fuel rod as the result of additional (compared with the initial state at the accident initial time) FGR from fuel due to the temperature change against the initial steady-state temperature condition.

(b) Fuel rod geometry change taking into account:

- Initial state at the accident initial time taking into account fuel burnup (input data);
- Thermo-elastic deformations of fuel and cladding;
- Additional (compared to the initial state at the accident initial time) fuel swelling and FGR from fuel due to the temperature change against the initial steady state condition;
- Cladding plastic deformations due to of transient difference between internal and external pressures (coolant pressure history is specified in the input file), taking into account fuel-cladding mechanical interaction;
- Cladding depressurization as the result of the accumulation of plastic deformation;
- Zirconium oxide layer growth on the outer and inner cladding surfaces.

c) Cladding oxidation under non-isothermal conditions, accompanied by the heat release and the hydrogen generation.

Properties of the simulated environment (fuel, cladding, a gas mixture) are determined depending on the temperature and taking into account the effect of irradiation during normal operation prior to accident beginning.

It is assumed that the fuel rod always retains rod-type geometry, geometry changes are only quantitative (changes in radial dimensions of layers). Melting phenomena of the fuel rod components, fuel and cladding fragmentation are not considered.

1.3. Solution method

Nodalization scheme of the fuel rod is formed by the specification of the arbitrary number of axial sections (nodalization may be optional) and radial cylindrical layers having the same thickness or the same volumes in both fuel and cladding.

In the course of solution of interrelated problems of thermal conductivity and thermal mechanics at each moment of computational time the temperatures and nodal point coordinates of nodalization grid are determined. Task is solved in axisymmetric formulation.

The scheme of radial ring layers from the fuel rod axis to the periphery may be as follows:

- Central hole (which may be absent), filled with a gas (helium + fission gas products);

— Fuel pellet (UO_2, $UO_2 + Gd_2O_3$) is divided in a specified number of ring layers of equal area;
— Gap between fuel and cladding that is filled with helium and the fission gases and/or steam after cladding depressurization;
— Oxide film (ZrO_2) on the inner surface of cladding;
— Cladding is nodalized in a specified number of ring layers of equal thickness;
— Oxide film (ZrO_2) on on the outer surface of cladding.

In each axial section the nodal points are located on the boundaries of cylindrical layers or sub-layers. In frame of nodalization scheme the maximum number of axial sections - 51, the maximum number of radial grid points in the axial section - 40. The radial structure of the axial layers is the same.

Numerical solution of axisymmetric transient thermal task is organized in the following way. At each time step of integration in each axial cross-section of the fuel rod the system of non-stationary equations of heat balance for cylindrical layers which are adjacent to the nodal points is solved in r-geometry. System of heat balance equations for each of the axial section is a system of quasi-linear algebraic equations (coefficients depend on temperature) relatively to the nodal temperatures with a tridiagonal matrix whose. The sweep method is used to obtain solution.

When carrying out calculations of design basis accidents, on the outer cladding surface the boundary conditions of 1st type (axial distribution of cladding outer surface temperature as the function of time) or 3d type (time dependent heat transfer coefficient and coolant temperature axial distributions) are specified as the input data. For this purpose the results of thermal-hydraulic calculations with special integral thermal-hydraulic codes are used.

Axial heat transfer is accounted by solution of a system of equations for transient heat balance with zero-sources in z-direction. In most tasks the axial heat transfer is negligible compared with the radial heat transfer.

Consideration of temperature dependences of thermal-physical properties of materials is carried out in iterative calculations by temperature.

Fuel-cladding gap thermal conductance is determined taking into account the thermal conductivity of gas mixture, temperature jumps at the "gas-solid" boundaries, radiation heat transfer between fuel and cladding surfaces, the contact component due to fuel-cladding mechanical interaction.

Pressure of the gas mixture in a fuel rod is calculated taking into account the changes in the free volume and its volume average temperature according to the state equation for the ideal gas. Free volume consists of plenum volume, gap between fuel and cladding, the central hole of the fuel (which may be absent) and the fuel open porosity. Initially, the free volume is filled with pressurized helium. During base-irradiation the gas fission products are released from fuel to fuel rod free volume.

Contribution from additional FGR (xenon and krypton) as the result of fuel overheating compared with the initial steady-state condition is taken into account. For this purporse the FGR phenomenological model in dependence on fuel temperature under accident conditions is used.

The coolant pressure is specified by the input data.

Stress-strain state (SSS) of cladding considers: on the outer surface - coolant pressure, on the inner surface - gas mixture and/or steam pressure and the fuel-cladding contact pressure (after fuel-cladding gap closure). The following assumptions are used: the cladding is thin-walled, one-layer, the cladding material is characterized by plastic orthogonal anisotropy and isotropic dynamic and strain-hardening, the volume change is characterized by elasticity, the components of stress deviator and components of plastic strain increments deviator are proportional.

For the calculation of kinetics of cladding SSS under transient temperature-forced loading the model based on the dependence of zirconium alloy flow stress on the value of plastic strain rate, temperature, fast neutron fluence, time, oxygen concentration, as well as taking into account the impact of the allotropic transition accumulation and annealing of irradiation defects, strain hardening and dynamic strain aging.

The Hook rule for the calculation of elastic deformations and the Prandtl-Reuss relation, combined with the Hill function of flow-ability for orthotropic material are used for the calculation of plastic deformations.

Calculation of cladding SSS in a case of ballooning is accompanied by the analysis of the possibility of cladding rupture. Cladding rupture parameters – time-to-rupture and hoop plastic strain at the moment of rupture – are determined using the principle of linear summation of damages. Damage increment is determined as the ratio between the deformation increment on the time step to the strain value during rupture at temperature and pressure stationary conditions corresponding to this time step (deformation criterion). The code uses the dependence of deformation at rupture on temperature and pressure based on the array of experimental data obtained as a result of testing cladding samples and fuel rod simulators on rupture due to inner pressure at high temperature.

Steam-zirconium reaction is calculated with the use of kinetic dependence of oxygen specific weight gain on time under isothermal conditions. Conservative and realistic dependencies derived for electrolytic and sponge based E110 alloy can be used and Cathcart-Pawel or Baker-Just correlations optionally as well. The integral weight gain of oxygen is determined taking into consideration the cladding deformation. The ECR value and fraction of the reacted Zr of a cladding are determined assuming that all the locally absorbed oxygen serves to generate stoichiometric zirconium dioxide. The oxidation of the cladding inner surface is taken into account. The calculation envisages the determination of the mass of hydrogen released.

The time of problem calculation depends on the number of grid points, the estimated duration of the process and the degree of unsteadiness (integration step is calculated automatically based on the rates of change of temperature and geometry). The time of problem calculation is varied from a few tens of s to several tens of minutes.

Initial data for the code are:

- Initial fuel rod geometry;
- Features of the fuel and cladding materials used;
- Filling gas (He) pressure;
- Fuel initial density;
- Inner gas composition and fuel-cladding gap at specified steady-state load as a result of pre-accident irradiation;
- Time-dependent power axial distribution;
- Coolant pressure history;
- Time dependent cladding outer surface temperature or heat transfer coefficients and coolant temperature axial distribution.

Fuel rod state at the initial time of the accident is simulated using the results of calculation of fuel rod behavior during a base-irradiation.

General flow chart of RAPTA-5.2 code is presented in Fig. 1.

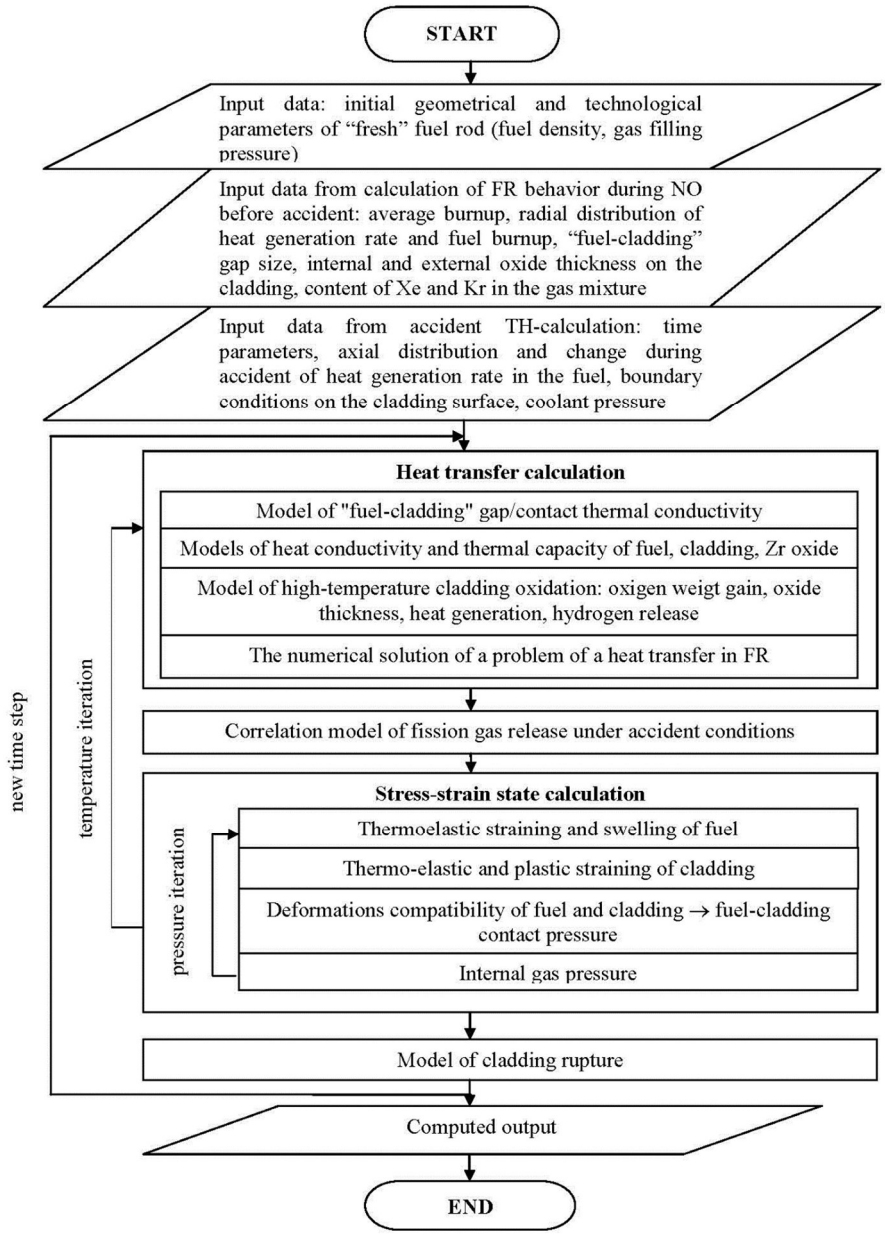

FIG. 1. General flow chart of RAPTA-5.2 code.

1.4. The additional models for IFA-650 experiments calculation

Calculations with the RAPTA-5.2 code were carried out using the additional models:

— Special model of heat transfer in the test rig;
— Model of axial displacement of fragmented fuel.

The model of heat transfer is intended for approximate modeling of heat transfer from the fuel rod in the high-temperature phase of the experiment. The model takes into account:

— Heat transfer through radiation to the inner walls of shroud tube;
— Convective and radiant heat transfer from the fuel rod to the stream of overheated steam.

The key parameter of the model is the temperature of the shroud tube, which is set based on the thermocouple readings. Another key parameter is steam flow. The value for the flow was selected in a way that would provide the closest value of the calculated cladding temperature to the thermocouple readings.

Model of the axial displacement of the fragmented fuel uses the following assumptions:

- Fragmentation and axial relocation of the fuel occurs at the moment of cladding rupture;
- The size of the fuel fragments are small enough to assume that heat transfer is homogenous and axisymmetric.

The model takes into account:

- Changes of density of the fragmented fuel is homogenous;
- Axial redistribution of fuel mass under the gravity forces depending on the cross-section area, limited by the deformed cladding;
- Axial redistribution of the linear heat rate according to the axial distribution of the fuel mass.

The key parameters for the model of the axial displacement of fragmented fuel are:

- Minimal value of the cladding circumferential strain, exceeding which the fuel displacement occur;
- Changed density of the fragmented fuel (reduction factor);
- Ejection of fuel fragments into the coolant through the cladding rupture is not modeled yet (it is assumed that all fuel remains behind the cladding).

2. IFA-650.11

2.1. Short description

Experimental fuel rod tested in the IFA-650.11 experiment was fabricated from the plateau area of J13 fuel rod of the 73856629 fuel assembly which operated for 4 cycles at Unit 1 of NPP 'Loviisa'. Main parameters of the fuel rod tested in the IFA-650.11 experiment are similar to the parameters of the fuel rod tested in the IFA-650.6 experiment [6, 7]:

- Average fuel burnup is 55.5 MW·day/kgU;
- Hydrogen content in the cladding is about 37 ppm;
- Oxide thickness on the internal and external surfaces of the cladding are 10 and 3 μm respectively;
- Gas filling pressure is 3 MPa at room temperature;
- Gas plenum volume is 16 cm^3.

Height profile and changes in the fuel rod linear heat generation rate during the experiment are shown in the Fig. 2.

The fuel rod was equipped with three thermocouples on the cladding surface and a pressure gage. Thermocouples were positioned in the cross-sections 100 mm and 400 mm (2 pieces) from the bottom of the fuel. The IFA-650.11 experiment implemented the fuel rod loading parameters as shown in the Fig. 3 [8].

Maximum temperature according to the readings of TC installed on the cladding in the cross-section 100 mm from the bottom of the fuel was 935 °C. Temperature according to the readings of the TC installed on the cladding in the 400 mm cross-section is about 50 °C lower.

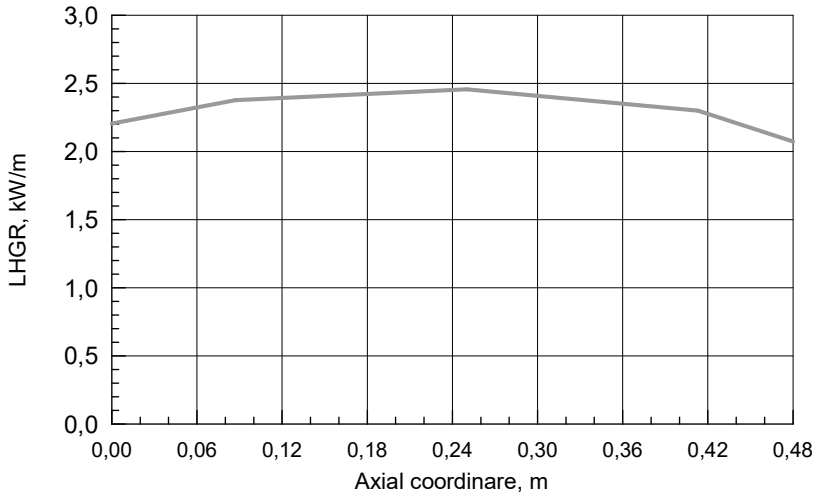

(a)

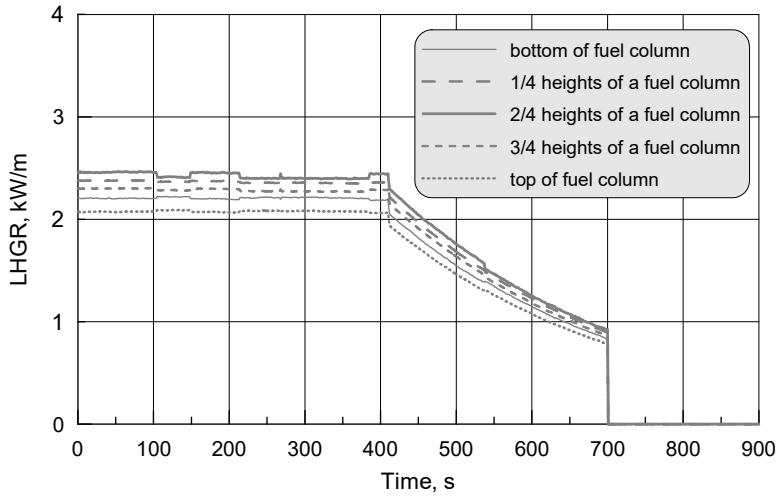

(b)

FIG. 2. Linear heat generation rate in fuel rod of IFA-650.11 experiment.

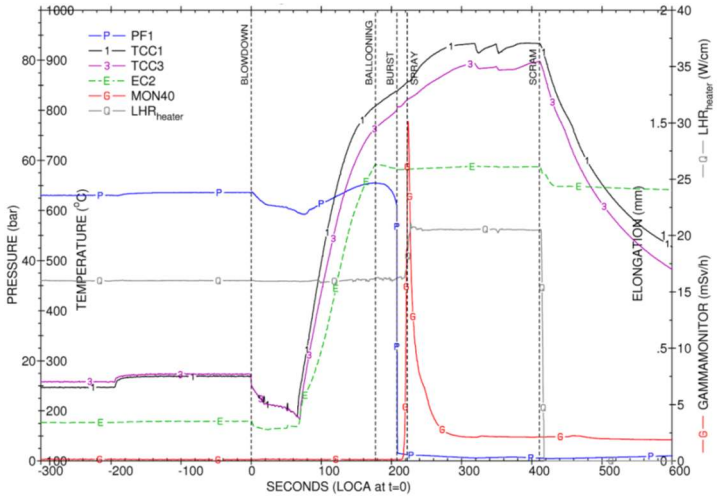

FIG. 3. Basic parameters of fuel rod loading during IFA-650.11 experiment.

According to the pressure gage in the fuel rod the moment of the cladding failure was established as 207 s since the beginning of the transient mode of the experiment.

As a result of the post-test examinations the data, characterizing the strain and corrosion conditions of the cladding, condition of the fuel stack, was obtained [9].

Fuel rod cladding has a rupture 5 mm long and 1 mm wide in the 210 mm cross-section from the bottom of the fuel stack. Cladding ballooning, characterized by the increase in diameter from 9 to 10.5 mm, is positioned above the 100 mm cross-section and has a length of more than 100 mm (see Fig. 4). Cladding diameter in the rupture point amounted to about 11.6 mm, which corresponds to the true hoop strain of 0.254 (see Fig. 5). In the cladding rupture area there is some displacement of large fragments of fuel pellets.

Oxide thickness increment on the cladding internal surface in the LOCA experiment in the hot area (155 – 175 mm) in the places with oxide radial cracking has average values of (10 ± 3) μm, oxide thickness at a distance from the radial cracks is (9.4 ± 3.2) μm. Oxide thickness on the cladding internal surface amounted to (10 ± 3.5) μm.

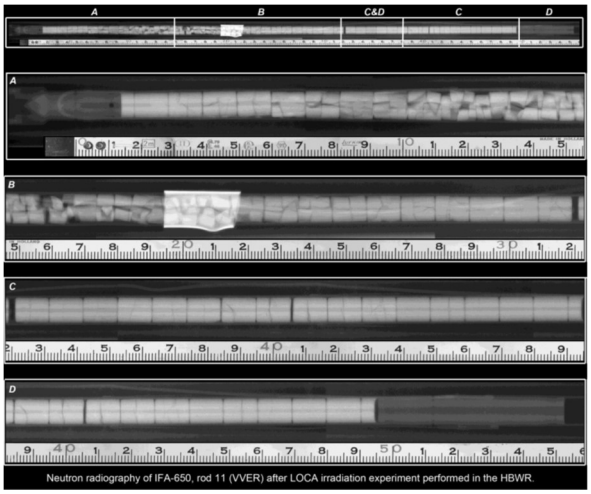

FIG. 4. Neutron radiography of the fuel rod after IFA-650.11 experiment.

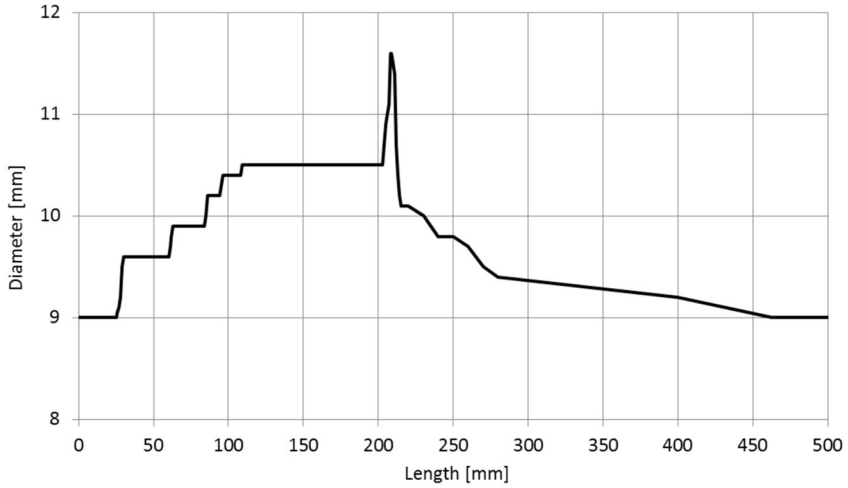

FIG. 5. Axial distribution of the fuel rod diameter after IFA-650.11 experiment.

2.2. Calculation results

The calculation was performed without the fuel relocation model. Calculation results are shown in Figs 6 to 9. Figure 6 shows the change of cladding temperature during the experiment in the cross-sections of installed thermocouples TCC1 and TCC2 and in the cladding rupture section. Fig. 7 shows the changes in fuel rod internal pressure during the experiment. Figs 8 and 9 show axial distribution of cladding strain and oxides thickness.

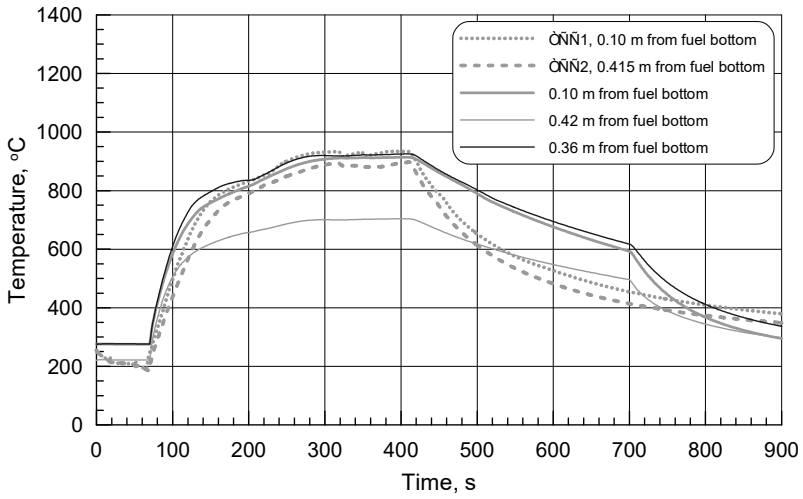

FIG. 6. Cladding temperature in the field of the TCC1 and TCC2 installation.

Table 1 shows the calculated values for the key parameters of thermomechanical and corrosion behavior of the IFA-650.11 fuel rod in comparison to the measured values.

Analyzing the obtained results, the following could be noted. The use of special heat transfer model in conjunction with the RAPTA-5.2 code allowed to accurately enough reproduce the high-temperature phase of the experiment in the middle area of the fuel rod. However, calculated maximum for the temperature was displaced to the upper part of the fuel rod, since the model assumes the steam flow is bottom up. Accordingly, cladding rupture point is shifted up as well. At the same time, a satisfactory agreement between the calculated and experimental parameters of cladding failure were obtained – time of rupture, temperature, pressure, hoop strain. The use of the SOCRAT boundary conditions made it possible to refine the calculation of the axial distribution of cladding deformation.

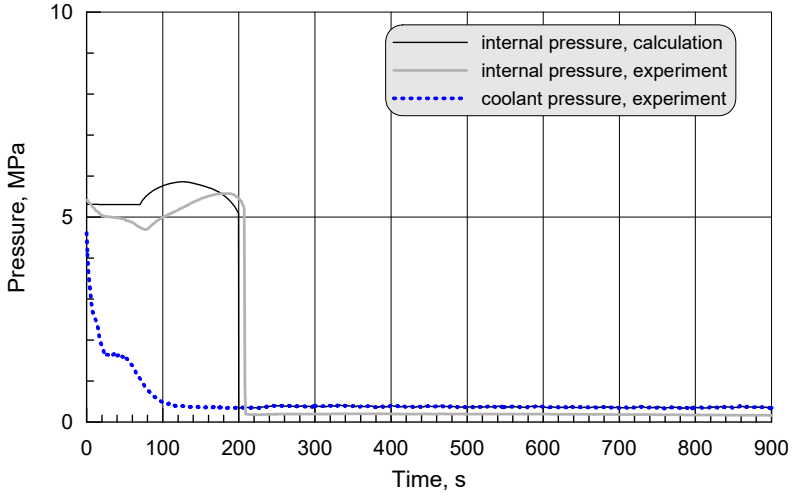

(a)

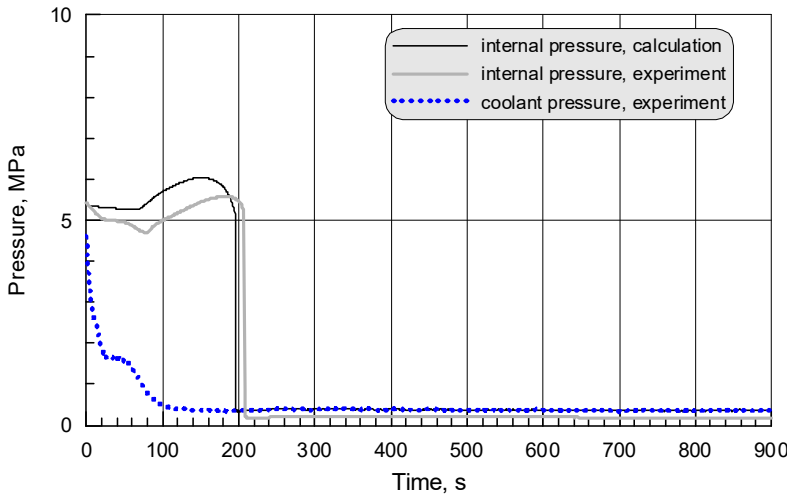

(b)

FIG. 7. Change of internal fuel rod pressure during experiment (a) RAPTA-5.2; (b) RAPTA-5.2 with boundary condition of the first kind generated by SOCRAT code.

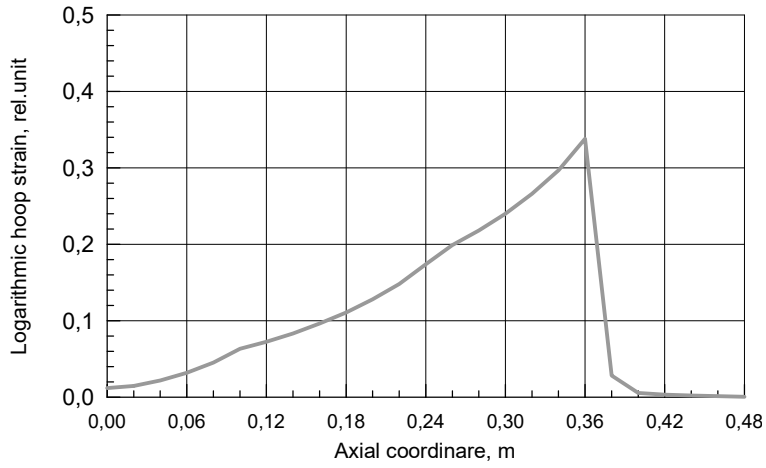

(a)

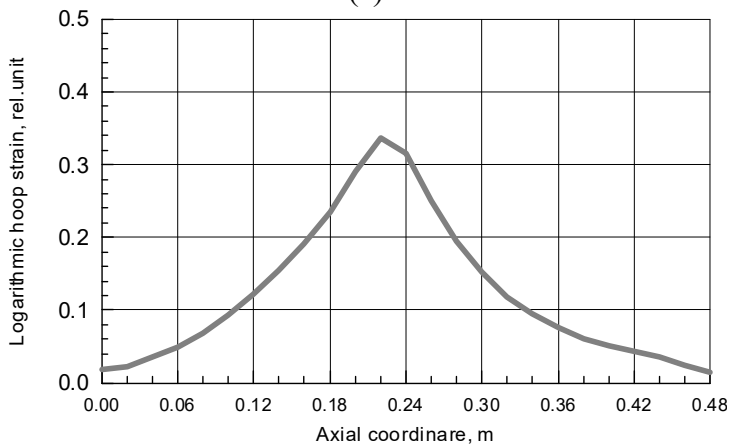

(b)

FIG. 8. Axial distribution of cladding hoop strain (a) RAPTA-5.2; (b) RAPTA-5.2 with boundary condition of the first kind generated by SOCRAT code.

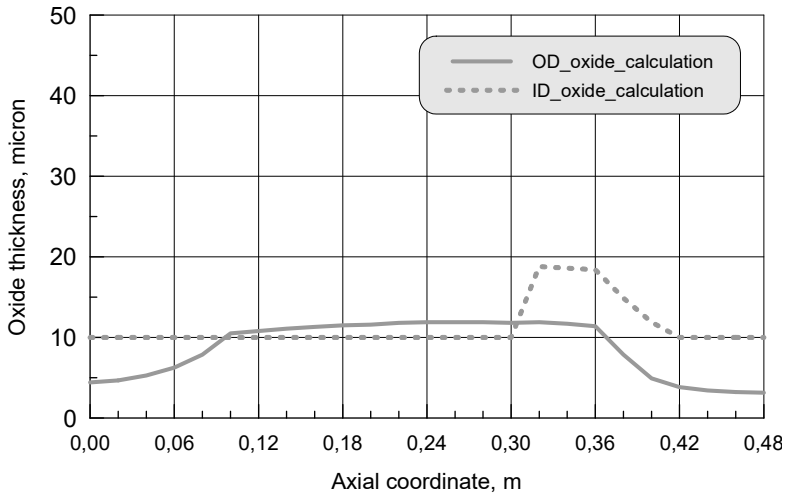

FIG. 9. Axial distribution of oxide thickness.

TABLE 1. CALCULATED AND MEASURED VALUES OF PARAMETERS OF IFA-650.11 FUEL ROD

Parameter		Experiment	RAPTA-5.2	RAPTA-5.2+ SOCRAT BC
Time of cladding failure, s		207	199.9	196.1
Rupture coordinate, mm		210	360	220
Cladding temperature at the rupture time, °C	100 mm	839	815	831
	360 mm	–	835	847
	400 mm	808	712	815
Maximum cladding temperature, °C	100 mm	934	914	944
	220 mm	–	–	954
	240 mm	–	935	954
	360 mm	–	920	944
	400 mm	897	775	934
Cladding diameter, mm / logarithmic hoop strain	100 mm	10.4 / 0.145	9.62 / 0.063	9.89 / 0.093
	210 mm	11.6 / 0.254	–	–
	220 mm	–	10.38 / 0.148	12.33 / 0.337
	360 mm		12.32 / 0.338	9.74 / 0.075
	400 mm	–	9.16 / 0.056	9.54 / 0.051
Oxide thickness on the cladding external surface, μm	155-175 mm	10.0±3	11.3	12.2
	235-250 mm	7.7±3	11.9	12.3
	360 mm	–	11.4	11.4
Oxide thickness on the cladding internal surface, μm *)	155-175 mm	10±3.5	10	10-19.3
	235-250 mm	3.1±1	10	19.3
	360 mm	–	18.4	10
Maximum internal pressure, MPa		5.57	5.86	6.05

* Calculation assumed initial oxide thickness on the cladding internal surface equal to 10 μm.

3. IFA-650.10

3.1. Short description

The fuel was supplied by EDF/FRAMATOME and had been irradiated in the French Graveline 5 PWR to 61 MWd/kgU [10]. The rod characteristics are compiled in Table 2.

Height profile and changes in the fuel rod linear heat rate during the experiment are shown in Fig. 10. The principal measurements i.e. cladding and heater temperatures, rod pressure and cladding elongation, are shown in Fig. 11 and Fig. 12, respectively. Cladding thermocouples were attached 100 mm above the lower end (TCC1) and 74 mm below the upper end (TCC2, TCC3). Cladding burst: detected by PF1, and TCCs at ~249 s. Scram: at 316 s. Figures 13 and 14 show the results of profilometry and the fuel rod appearance in the cladding rupture area.

TABLE 2. ROD CHARACTERISTICS OF IFA-650.10

Items	Value
Fuel - as fabricated and irradiated	
Length fuel (mm)	440
UO_2 density (% of th. d.)	95.32
Pellet diameter (mm)	8.21
Cycles	4
Burnup (MWd/kgU)	61
Cladding - as fabricated and irradiated	
Type	Zry-4
Outer diameter (mm)	9.50
Thickness 9mm)	0.57
Oxide thickness, irradiated (μm)	20 - 30
Hydrogen content, irradiated, (ppm)	150 - 220
After refabrication	
Fill gas / pressure (bar)	95% Ar + 5% He / 40
Free volume (cm^3) as designed into the experiment. Does not include possible free volumes in the fuel (dishing, chamfer, open porosity)	17
Cladding TC positions (mm)	TCC1 = 1000 TCC2 / TCC3 = 1266

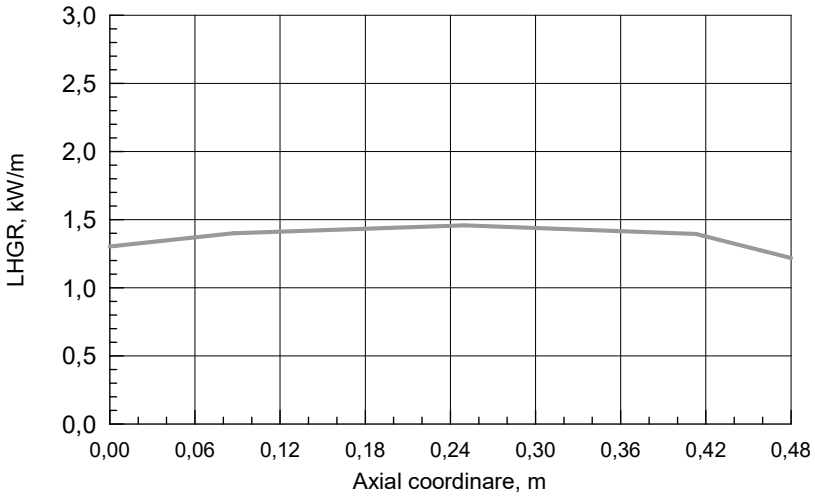

(a)

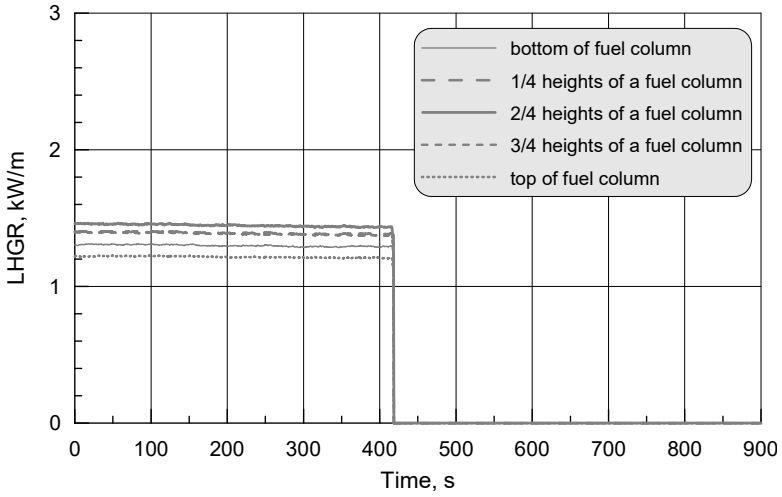

(b)

FIG. 10. Linear heat generation rate in fuel rod of IFA-650.10 experiment.

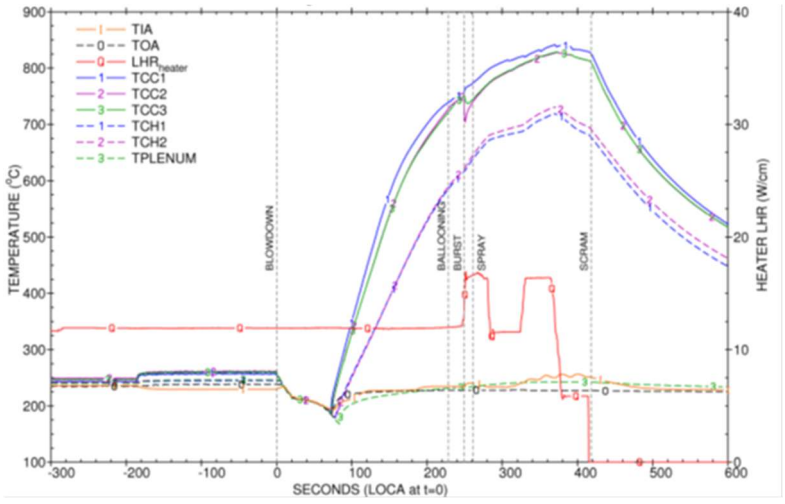

FIG. 11. Cladding and heater temperatures, IFA-650.10.

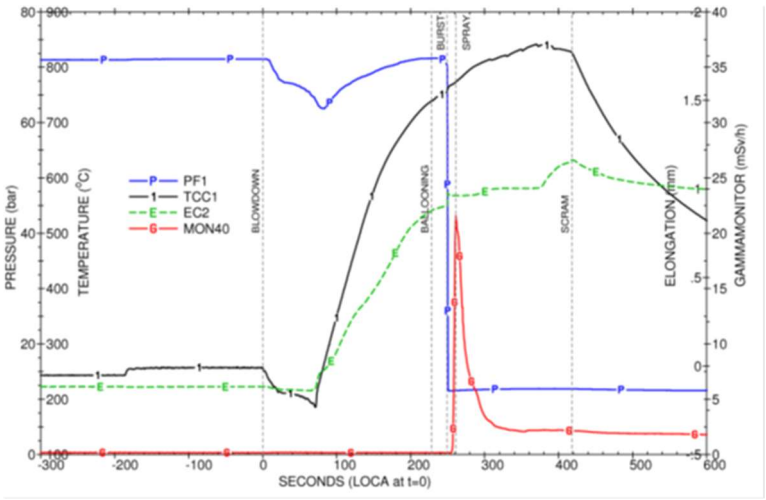

FIG. 12. Rod pressure and cladding elongation, IFA-650.10.

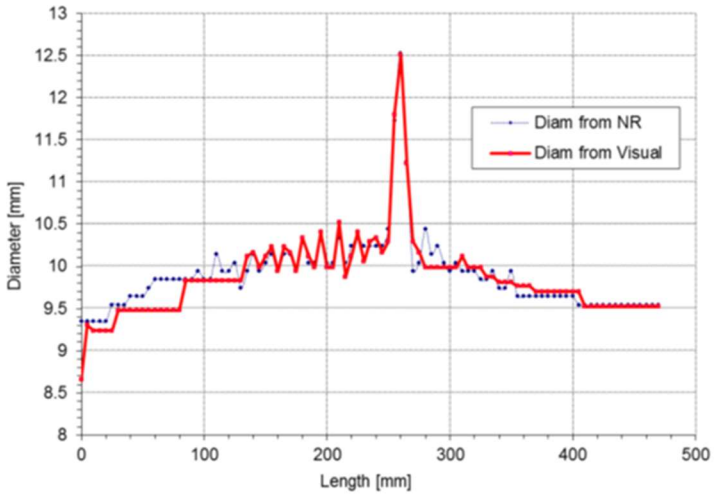

FIG. 13. Diameter profile, IFA-650.10.

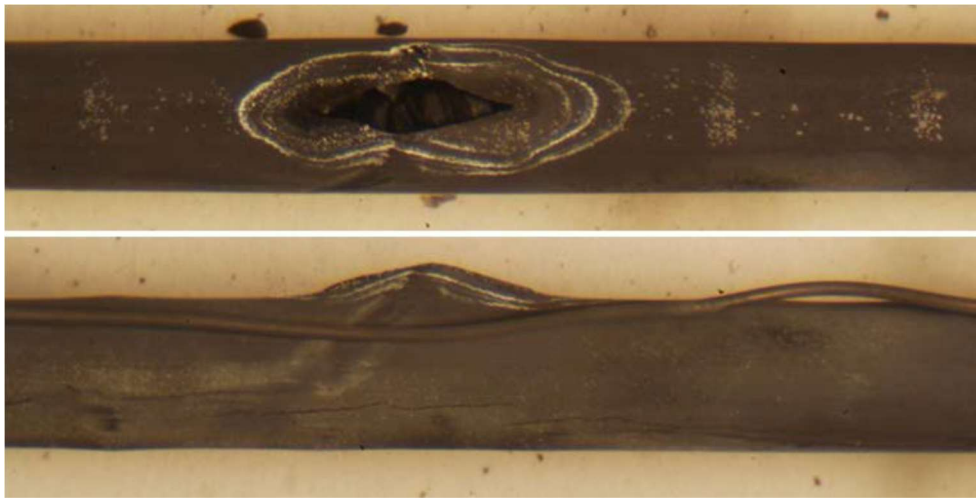

FIG. 14. Burst opening, two orthogonal orientations, IFA-650.10.

3.2. Calculation results

The calculation was performed without the fuel relocation model. Calculation results are shown in Figs 15 to 18. Figure 15 shows the change of cladding temperature during the experiment in the cross-sections of installed thermocouples TCC1 and TCC2 and in the cladding rupture section. Figure 16 shows the changes in fuel rod internal pressure during the experiment. Figures 17 and 18 show axial distribution of cladding strain and oxide thickness on the cladding internal and external surfaces.

Table 3 shows the calculated values for the key parameters of thermomechanical and corrosion behavior of the fuel rod in comparison to the measured values.

Analyzing the obtained results, a significant difference in the axial distribution of cladding hoop strain could be noted – see Figs 13 and 17 Calculated area of cladding ballooning (strain above 0.1) has greater length height-wise (~ 300 mm), while at the same time in the experiment ballooning was contained to the area ~ 30 mm. Calculation used the model for E110 alloy cladding strain and did not take into account the initial corrosion on the plasticity. At the same time, a satisfactory agreement between the calculated and experimental parameters of cladding failure were obtained – time of failure, temperature, pressure, hoop strain. The use of the SOCRAT boundary conditions made it possible to refine the calculation of the axial distribution of cladding deformation.

TABLE 3. CALCULATED AND MEASURED VALUES OF PARAMETERS OF IFA-650.10 FUEL ROD

Parameter		Experiment	RAPTA-5.2	RAPTA-5.2+ SOCRAT BC
Time of cladding failure, s		249	242	252
Rupture coordinate, mm		260	360	200
Cladding temperature at the time of failure, °C	100 mm	755	760	782
	200 mm	–	–	791
	360 mm	–	782	791
	366 mm	749	–	–
Maximum cladding temperature, °C	100 mm	841	866	870
	200 mm	–	–	880
	260 mm	–	890	879
	360 mm	–	891	862
	366 mm	829	–	–
Cladding diameter, mm / logarithmic hoop strain	100 mm	9.8 / 0.031	10.62 / 0.121	11.3 / 0.187
	200 mm	–	–	12.83 / 0.324
	260 mm	12.5 / 0.274	12.28 / 0.279	12.04 / 0.256
	360 mm	9.75 / 0.026	12.80 / 0.324	10.7 / 0.126
	366 mm	9.7 / 0.021	–	–
Maximum internal pressure, MPa		7.16	7.20	7.05

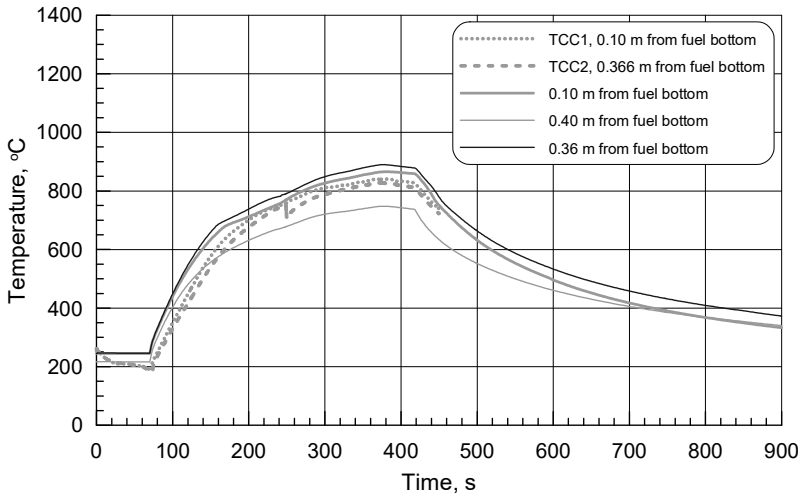

FIG. 15. Cladding temperature in the field of the TCC1 and TCC2 installation.

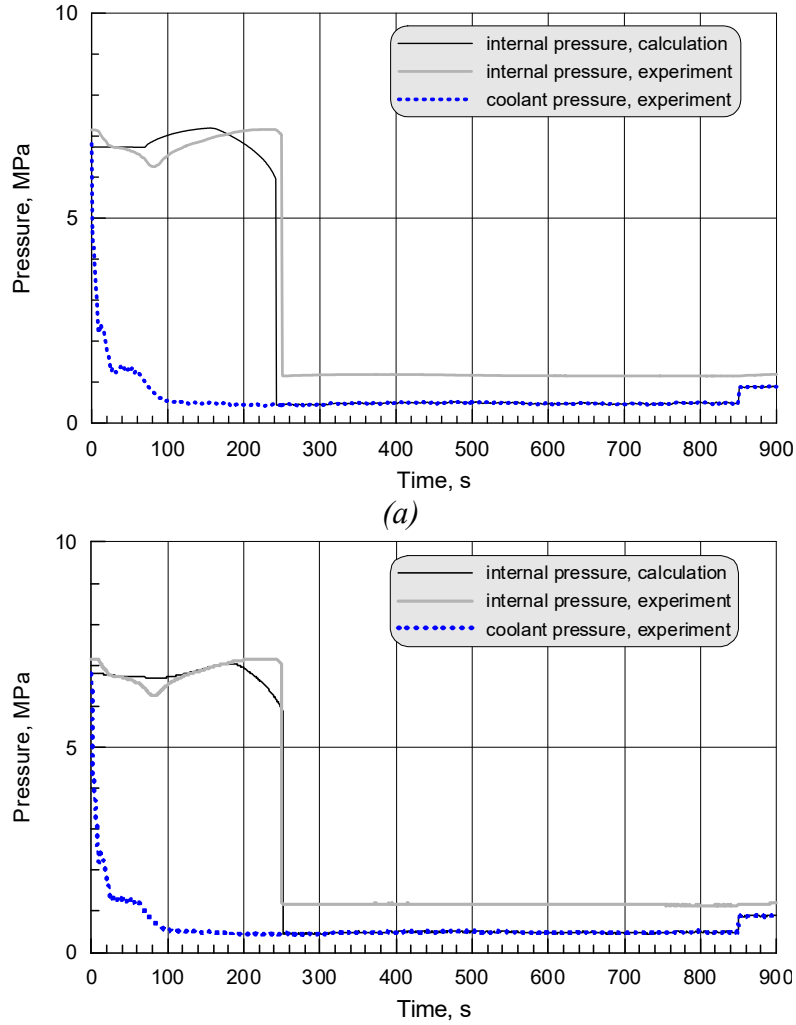

FIG. 16. Change of internal fuel rod pressure during experiment (a) RAPTA-5.2; (b) RAPTA-5.2 with boundary condition of the first kind generated by SOCRAT code.

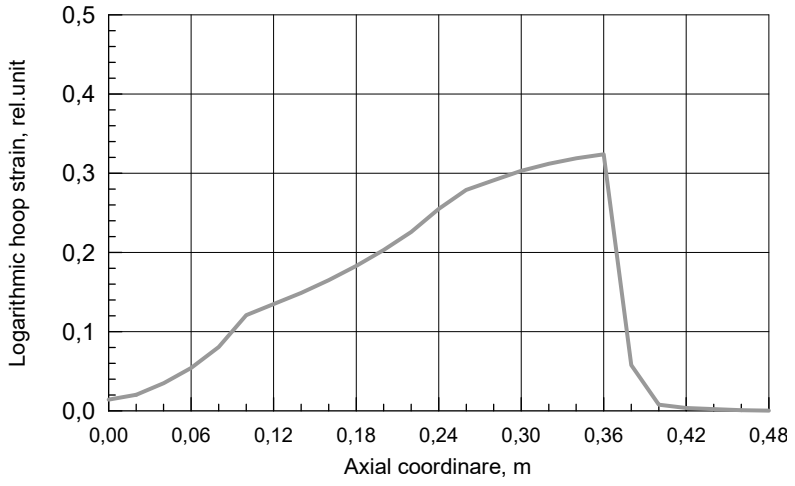

(a)

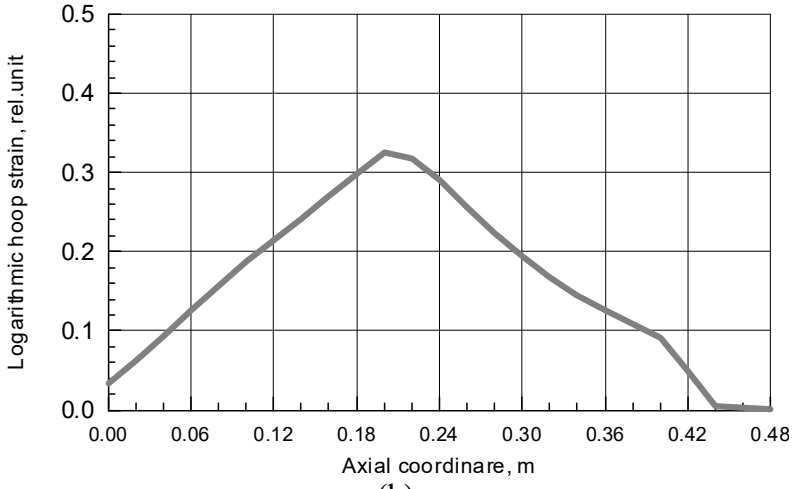

(b)

FIG. 17. Axial distribution of cladding hoop strain (a) RAPTA-5.2; (b) RAPTA-5.2 with boundary condition of the first kind generated by SOCRAT code.

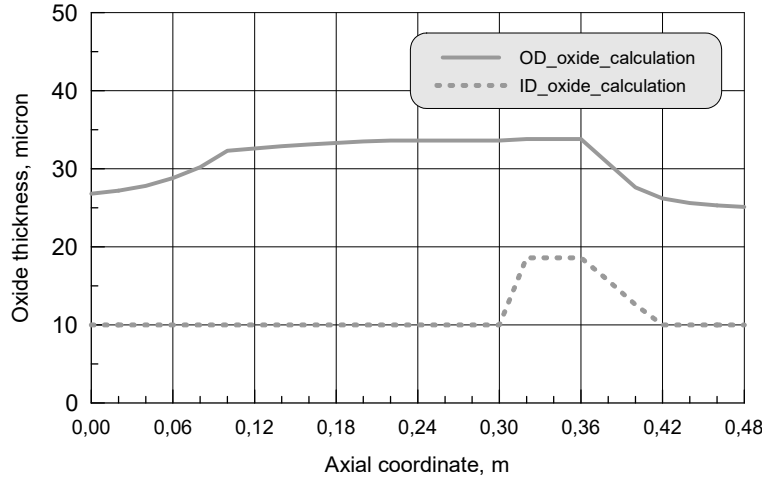

FIG. 18. Axial distribution of oxide thickness.

4. IFA-650.9

4.1. Short description of experiment

The fuel, irradiated in the Swiss NPP Gösgen to 89.9 MWd/kgU, was provided by Framatome ANP [11]. The rod characteristics are compiled in Table 4.

Height profile and changes in the fuel rod linear heat rate during the experiment are shown in Fig. 19. The principal measurements, i.e., cladding and heater temperatures, rod pressure and cladding elongation, are shown in Fig. 20 and Fig. 21, respectively. Cladding thermocouples were attached 100 mm above the lower end (TCC1) and 80 mm below the upper end (TCC2, TCC3). Cladding burst: detected by PF1, and TCCs at ~133 s. Scram: at 316 s. Fig 22 and 23 show the results of profilometry and macrophotography of the rupture cross-section.

TABLE 4. ROD CHARACTERISTICS OF IFA-650.9

Items	Value
Fuel - as fabricated and irradiated	
Length fuel / cladding (mm)	480 / 496
UO_2 density (g/cm^3)	10.43
Pellet diameter (mm)	9.131
Dishing volume (total of both sides) (mm^3)	16
Cycles	7
Burnup (MWd/kgU)	89.9
Cladding - as fabricated and irradiated	
Type	DX Zr2.5Nb (duplex)
Outer diameter (mm)	10.75
Thickness (mm)	0.725
Outer liner (mm)	0.100
Chemical composition of base material (%)	Zry-4, Sn 1.53, Fe 0.22, Cr 0.11, O 0.14
Chemical composition of the liner 9%)	O 0.13, Nb 2.6
Oxide thickness, irradiated, mean (μm)	7
Hydrogen content, irradiated, (ppm)	30
After refabrication	
Fill gas / pressure (bar)	95% Ar + 5% He / 40
Free volume (cm3) as designed into the experiment. Does not include possible free volumes in the fuel (dishing, chamfer, open porosity)	19
Cladding TC positions (mm)	TCC1 = 1000 TCC2 / TCC3 = 1300

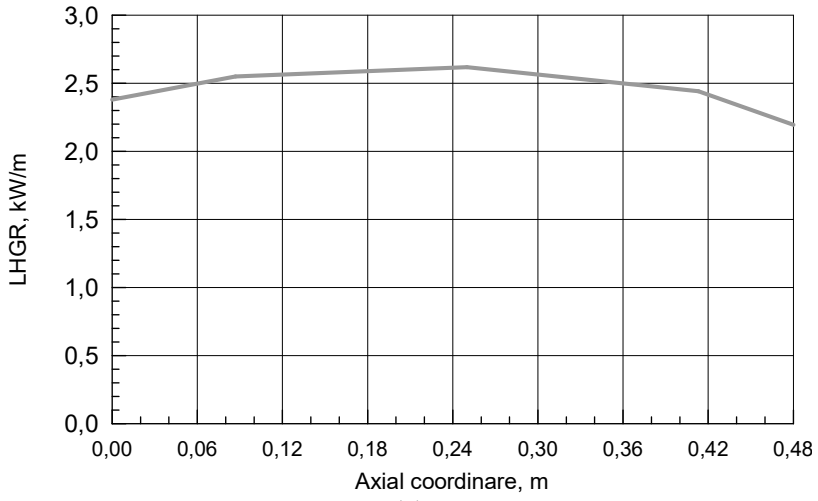

(a)

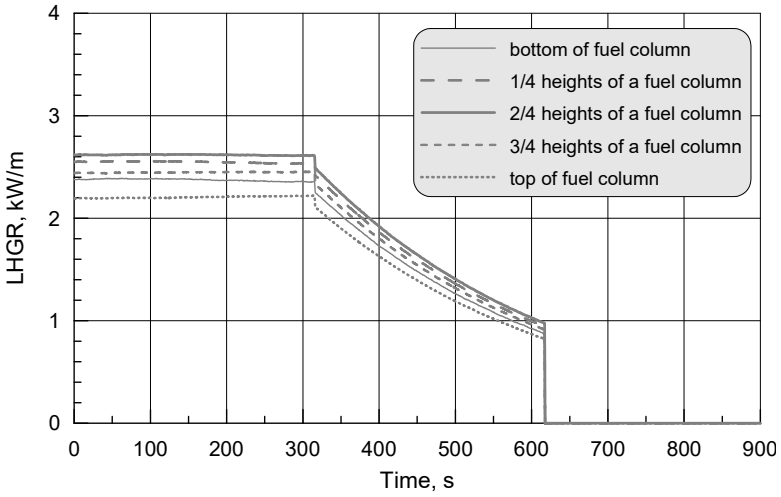

(b)

FIG. 19. Linear heat generation rate in fuel rod of IFA-650.9 experiment.

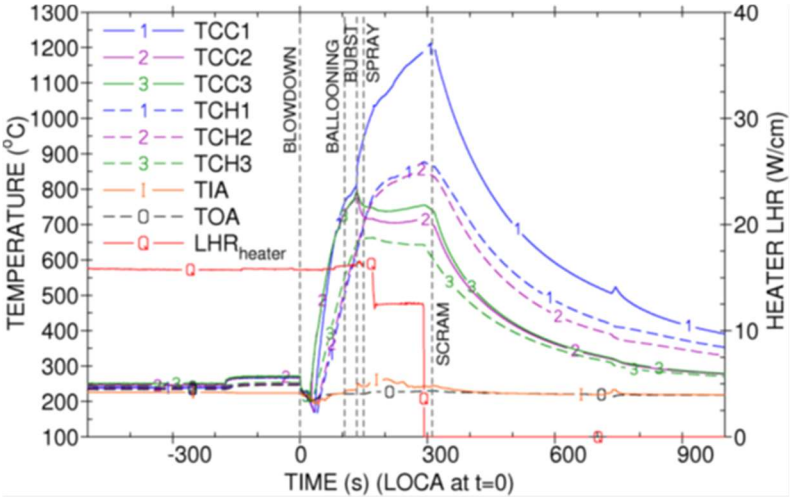

FIG. 20. Cladding and heater temperatures, IFA-650.9.

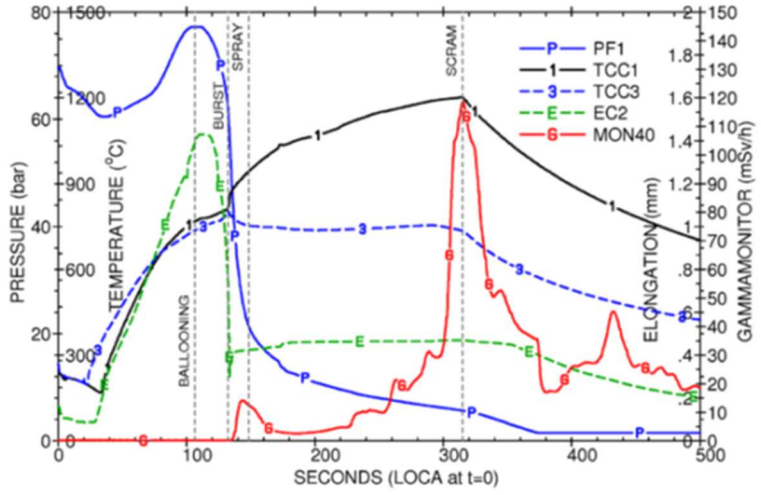

FIG. 21. Rod pressure and cladding elongation, IFA-650.9.

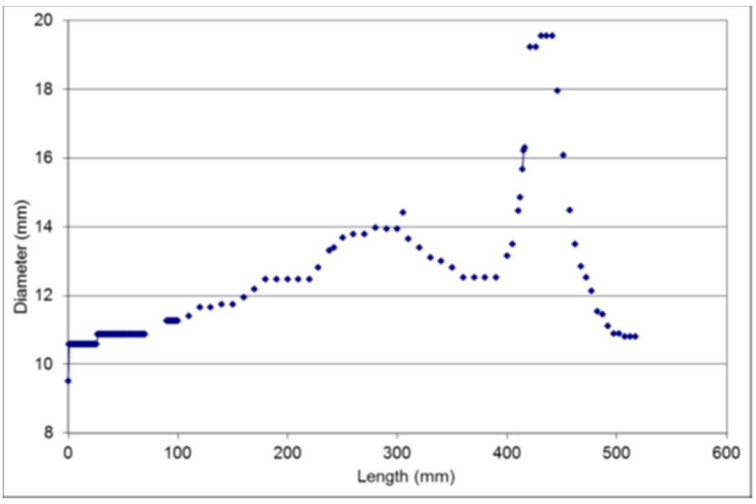

FIG. 22. Diameter profile 90/270 degrees orientation, IFA-650.9 (a reference mark of axial coordinate - the upper V-groove of a cladding).

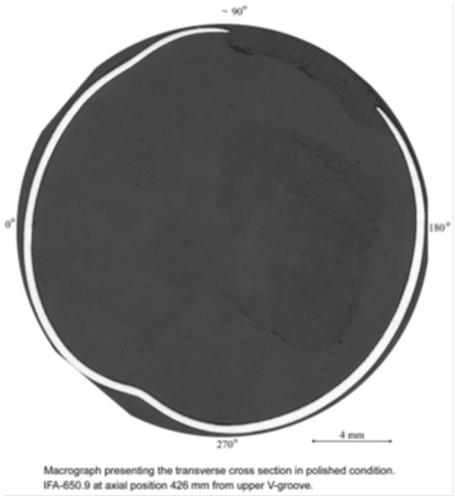

FIG. 23. Cross section macrograph at position of maximal ballooning, IFA-650.9.

4.2. Calculation results

The calculation was performed with the fuel relocation model using. Calculation results are shown in Figs 24 to 29. Fig. 24 shows the change of cladding temperature during the experiment in the cross-sections of installed thermocouples TCC1 and TCC2 and in the cladding rupture section. Fig. 25 shows the changes in fuel rod internal pressure during the experiment. Figures 26, 27 show axial distribution of axial cladding strain and oxide thickness on the cladding internal and external surfaces. Figures 28, 29 show axial distribution of linear fuel mass and linear heat rate before and after the relocation moment (moment of cladding rupture).

Table 5 shows the calculated values for the key parameters of thermomechanical and corrosion behavior of the fuel rod in comparison to the measured values.

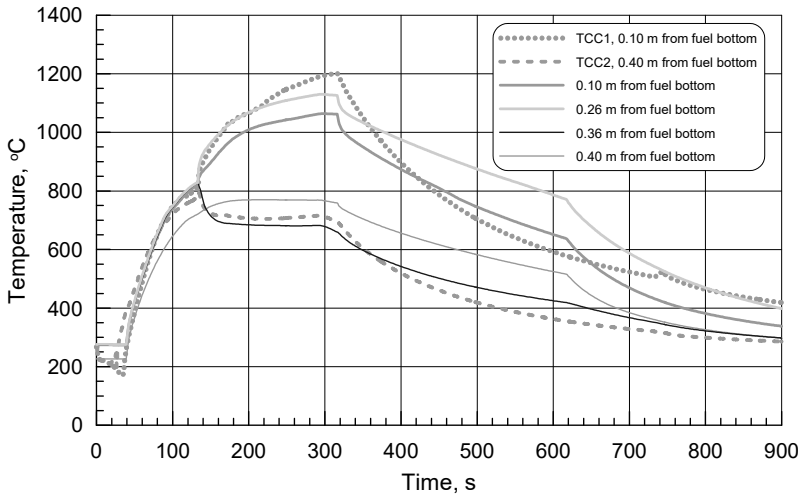

FIG. 24. Cladding temperature in the field of the TCC1 and TCC2 installation.

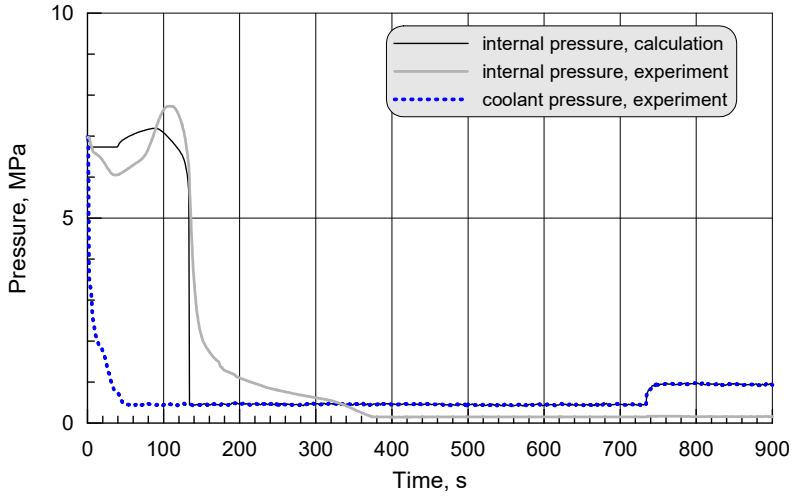

FIG. 25. Change of internal fuel rod pressure during experiment.

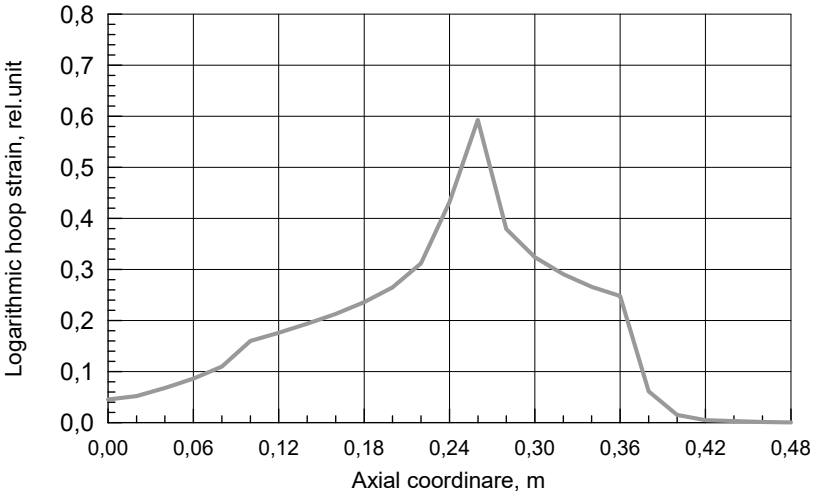

FIG. 26. Axial distribution of oxide thickness.

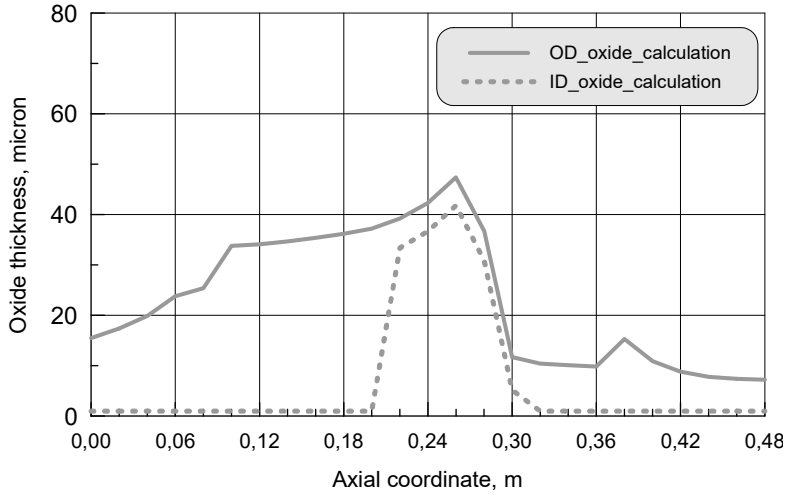

FIG. 27. Axial distribution of oxide thickness.

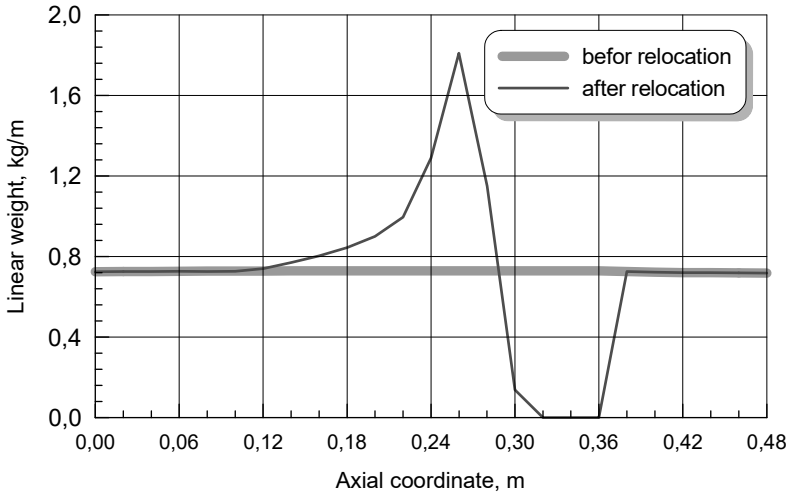

FIG. 28. Axial distribution of oxide thickness.

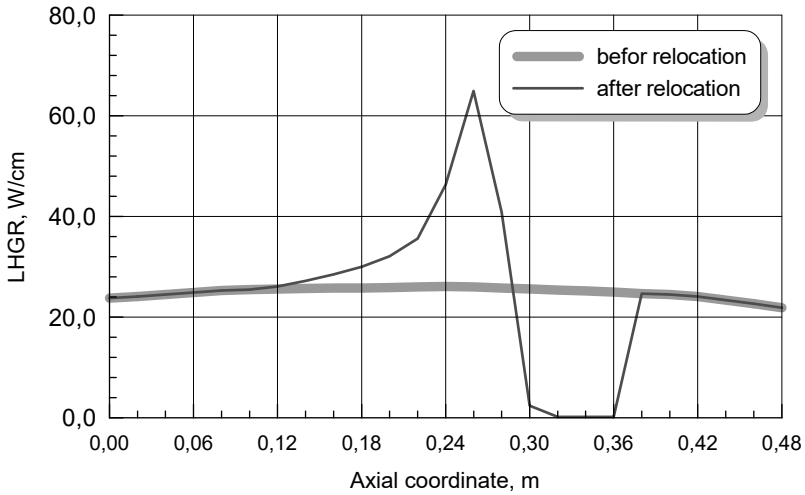

FIG. 29. Axial distribution of LHGR.

TABLE 5. CALCULATED AND MEASURED VALUES OF PARAMETERS OF IFA-650.9 FUEL ROD

Parameter		Experiment	Calculation
Time of cladding failure, s		133	133
Rupture coordinate, mm		450	260
Cladding temperature at the time of failure, °C	100 mm	810	823
	260 mm	–	829
	400 mm	793	721
Maximum cladding temperature, °C	100 mm	1202	1064
	400 mm	801	770
Cladding diameter, mm / logarithmic hoop strain	60 – 80 mm	19.5 / 0.596	11.86 / 0.098
	260 mm	14.0 / 0.264	19.45 / 0.593
	360 mm	11.8 / 0.093	12/80 / 0.324
	400 mm	11.7 / 0.085	10.92 / 0.015-
Maximum internal pressure, MPa		7.73	7.19
Boundaries of the area without fuel after the relocation, mm		330 – 455	300 –360

A satisfactory agreement between the calculated and experimental parameters of cladding failure were obtained – time of failure, temperature, pressure, hoop strain. The effect of axial fuel relocation on the cladding temperature behavior should be noted. As a result of displacement of the fragmented fuel in the cladding ballooning area a significant growth in temperature occurred. Calculated estimation of the effect of axial fuel relocation on the cladding temperature behavior is qualitatively consistent with the experiment.

5. SUMMARY AND CONCLUSIONS

Post-testing calculations using the RAPTA-5.2 code of thermomechanical behavior of the fuel rods in IFA-650.9, IFA-650.10 and IFA-650.11 experiments were conducted. Calculations were carried out using the additional models:

— Special model of heat transfer in the test rig;
— Model of axial displacement of fragmented fuel.

Usage of the aforementioned models in conjunction with the RAPTA-5.2 code allowed to closely enough reproduce the cladding temperature behavior in the high-temperature phase of the experiments. Comparative analysis of the calculated and experimental parameters of the thermomechanical and corrosion behavior of the fuel rods showed, that calculated values for time of failure, temperature and gas pressure at the moment of failure, cladding strain are in good agreement with the experimental data. The use of the SOCRAT boundary conditions made it possible to refine the calculation of the axial distribution of cladding deformation. During the calculation of the IFA-650.9 experiment an estimation of the fuel axial relocation effect on the cladding temperature was obtained, which is qualitatively consistent with the experiment.

REFERENCES

[1] Nuclear safety rules for reactor plants of nuclear power plants; NP-082-07. Effective from 01.07.2008. In Russian. (Правила ядерной безопасности реакторных установок атомных станций. НП-082-07. Введены с 01.07.2008.)

[2] Regulations on the software certification used in the nuclear facilities safety justification. RD–03–17–2001, FIR NRS (Federal Nuclear and Radiation Safety Authority of Russia). Effective from 01.01.2002. In Russian. (Положение об аттестации программных средств, применяемых при обосновании безопасности объектов использования атомной энергии. РД–03–17–2001. ФНР ЯРБ Госатомнадзора России. Введено с 01.01.2002 г.)
[3] Requirements to the composition and content of the verification and justification of program codes report used to justify the safety of nuclear facilities. RD–03–34–2000, FIR NRS (Federal Nuclear and Radiation Safety Authority of Russia). Effective from 29.12.2000. In Russian. (Требования к составу и содержанию отчета о верификации и обосновании программных средств, применяемых для обоснования безопасности объектов использования атомной энергии. РД–03–34–2000. ФНР ЯРБ (Госатомнадзор России). Введено в действие с 29.12.2000).
[4] RAPTA-5.2 software tool. ROSTECHNADZOR (Federal Environmental, Industrial and Nuclear Supervision Service), SEC NRS (Scientific and Engineering Centre of Nuclear and Radiation Safety), Certificate of Computer Code # 299 of 29.09.2011. In Russian. (Программное средство РАПТА-5.2. НТЦ ЯРБ Ростехнадзора, паспорт аттестации ПС № 299 от 29.09.2011).
[5] START-3A software tool. ROSTECHNADZOR (Federal Environmental, Industrial and Nuclear Supervision Service), SEC NRS (Scientific and Engineering Centre of Nuclear and Radiation Safety), Certificate of Computer Code # 328 of 18.04.2013. In Russian. (Программное средство СТАРТ-3А. ФБУ «НТЦ ЯРБ» Ростехнадзора, регистрационный номер 328 паспорта аттестации программного средства от 18.04.2013).
[6] KITANO, K., GRIGORIEV, S., BLOMBERG, G., Destructive Pie For Fuel Cladding From LOVIISA 1, STUDSVIK Nuclear AB Report N-06/065 (2006).
[7] Blomberg, G., Losin, C., Examinations Of Rods Irradiated In LOVIISA 1, STUDSVIK Nuclear AB Technical note, N-04/036 (2004).
[8] Lavoil, A., LOCA Testing At Halden, The VVER Fuel Experiment IFA-650.11, HWR-976 OECD Halden Reactor Project Report (2010).
[9] Oberländer, B.C., Jenssen, H.K., Balak, J., LOCA IFA-650.11 : PIE of a 48 MWd/kgU VVER rod subjected to LOCA testing in the HBWR, EHPG-Meeting, Sandefjord, Norway (2011).
[10] Lavoil, A., LOCA Testing At Halden, The Tenth Experiment IFA-650.10. HWR-974. (2010).
[11] Florian Bole du Chomont. LOCA Testing At Halden, The Ninth Experiment IFA-650.9. HWR-917 (2009).

ANALYSIS OF FUEL CLAD DOUBLE-SIDE OXIDATION AND SECONDARY HYDRIDING UNDER LOCA CONDITIONS IN IFA-650.2 TEST

V.E. SHESTAK
Nuclear Safety Institute (IBRAE),
Russian Academy of Sciences,
52, B. Tulskaya, Moscow, 115191,
Russian Federation
E-mail: sve@ibrae.ac.ru (corresponding author)

B.C. OBERLÄNDER
Institutt for Energiteknikk,
2027 Kjeller, Norway

M.S. VESHCHUNOV
International Atomic Energy Agency,
Vienna International Centre,
PO Box 100, 1400 Vienna,
Austria

Abstract

The effect of secondary hydriding of fuel cladding under LOCA conditions, earlier observed in out-of-pile tests, was confirmed experimentally for the first time in the in-pile experiment, the Halden Reactor Project test IFA-650.2. The modified version of the SVECHA/QUENCH (S/Q) code was applied to simulation of the fuel rod behaviour under LOCA conditions in the IFA 650.2 test. The code reasonably describes evolution of cladding deformation and predicts cladding internal oxidation and secondary hydriding with extremely high hydrogen uptake, in a reasonable agreement with observations.

1. INTRODUCTION

In the high temperature steam environment at a postulated loss-of-coolant accident (LOCA) in light-water-cooled nuclear power reactors (LWR), a fuel rod might undergo ballooning and burst due to the rise of pressure difference between two sides of the Zr cladding. Once the fuel rod rupture is expected, the steam flowing into the ruptured fuel rod interior will oxidize the inner surface of Zr cladding. Besides, the conditions at the cladding inner surface define the high content of hydrogen absorbed in the cladding under a postulated LOCA transient, which may cause embrittlement of the Zr alloy cladding at relatively low temperatures (< 300°C) [1].

The embrittlement of Zircaloy-4 (Zry-4) cladding due to oxidation and hydriding of the inner surface was examined for the first time at Japan Atomic Energy Research Institute (JAERI, Japan) [2], through the simulation of LOCA conditions by heating specimens of Zircaloy cladding. Later these investigations were continued with fresh (including pre-hydrided) and pre-irradiated fuel claddings at JAERI/JAEA (Japan Atomic Energy Agency) [3]–[5], with as-fabricated Zry-2 cladding at ANL (Argonne National Laboratory) [6], in the bundle tests with non-irradiated Zry-4 cladding at KIT (Karlsruhe Institute of Technology) [7] and more recently, with non-irradiated M5 cladding at CEA (France) [8].

It was observed in these tests that, in most cases, secondary hydriding was characterized by the formation of non-axisymmetric highly hydrogenated bands (with hydrogen concentrations ranging from ~1000 wt. ppm up to 3000-4000 wt. ppm) away from the burst location, resulting in strong embrittlement of claddings at these positions. This result becomes especially important taking into account results of additional tensile tests of KIT [7]

demonstrating that fuel rods can break at these positions during post-accident handling, if the local hydrogen concentration exceeds the threshold value of ≈ 1500 wt. ppm. This correlates also with observations of [3]–[5], which evidenced that fuel rods may break at these brittle positions also during quenching. For these reasons, it seems important to take this threshold effect in consideration, elaborating new safety criteria for postulated LOCA accidents.
These observations elucidate an importance of the secondary hydriding effect studies under more representative in-reactor conditions. For this reason, the LOCA experiment IFA-650.2 test was carried out in the Halden reactor using a fresh, tight-gap and pressurised PWR rod with Zry-4 cladding, and was focused on effects that are different from those studied in out-of-reactor tests. The test was carried out using small fission power (23 W/cm) to achieve the desired conditions for ballooning and oxidation. The main objective was to produce ballooning, to determine the time to burst and to assess the material oxidation and hydriding kinetics.

2. EXPERIMENTAL

The LOCA test run IFA-650.2 [9] was carried out in the Halden reactor in May 2004, using a fresh pressurized PWR rod. The target peak cladding temperature (PCT) of 1050°C was reached and clad ballooning and rupture occurred at ~800°C.

The length of the fuel rod was 500 mm and the outer diameter of the pellets 8.29 mm. The fuel pellets were 8 mm long and dished at both ends. The density of the fuel was 95% of the theoretical density and the enrichment was 2 wt. % U^{235}. The diametric clearance between the fuel and cladding was 0.070 mm. The outer diameter of the cladding was 9.50 mm and its thickness 0.57 mm. The cladding material was low tin Zry-4 and the rod was filled with helium at 40 bar (RT). The rod plenum volume (free gas volume) was made relatively large to be able to maintain stable pressure conditions also during ballooning. The total free gas volume was 17.4 cm^3, of which 15.8 cm^3 was located outside the heated region.

The fuel rod was located in a standard high-pressure flask in the IFA-650 test rig, which was connected to a high-pressure heavy water loop and a blow-down system. The test was carried out using small fission power of 23 W/cm. The heater was used to simulate the isothermal boundary conditions, i.e heat from adjacent fuel rods during a LOCA. Cladding temperature is influenced by both rod and heater power. The rod power can be controlled by changing the reactor power.

The target cladding temperature level 1050°C was reached and held for ~4.5 minutes (315 s TCC1), Fig. 1. Cladding failure occurred at 100 s after blow down evidenced by rod elongation, pressure and cladding temperature measurements as well as the gamma monitor on the blowdown line to the dump tank. Photographs taken of the IFA-650.2 rod in the PIE (Post Irradiation Examination) are shown in Fig. 2. The burst was ~35 mm long and situated 2 cm below the rod middle point and downward. In addition to local ballooning, the rod experienced some uniform deformation over the fuel length, more strongly in the lower part. The increase in cladding diameter was ~ 40 % in the vicinity of the burst (up to 90% in burst area), ~ 22 % at 10 cm distance from the lower end, and ~ 7 % at 10 cm from the upper end of the rod.

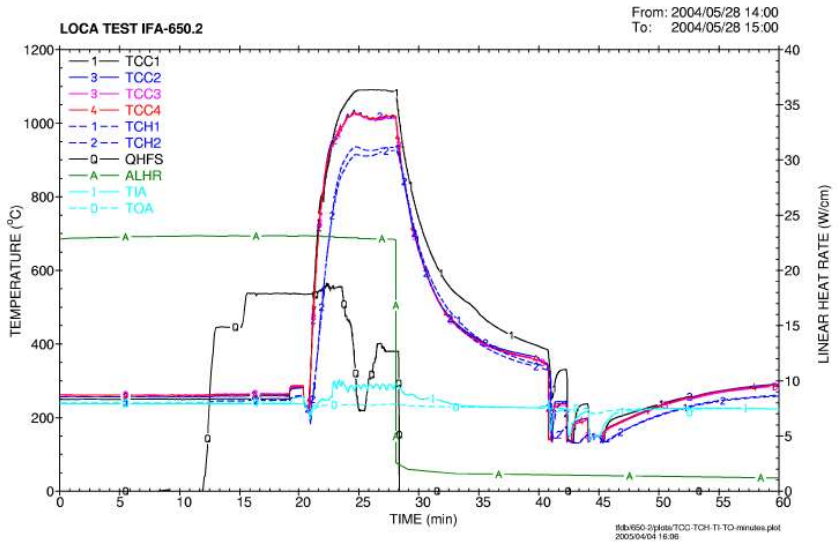

FIG. 1. Cladding (TCC), heater (TCH), coolant inlet (TIA) and outlet (TOA) temperatures, heater power (QHFS) and fuel power (ALHR) in IFA-650.2.

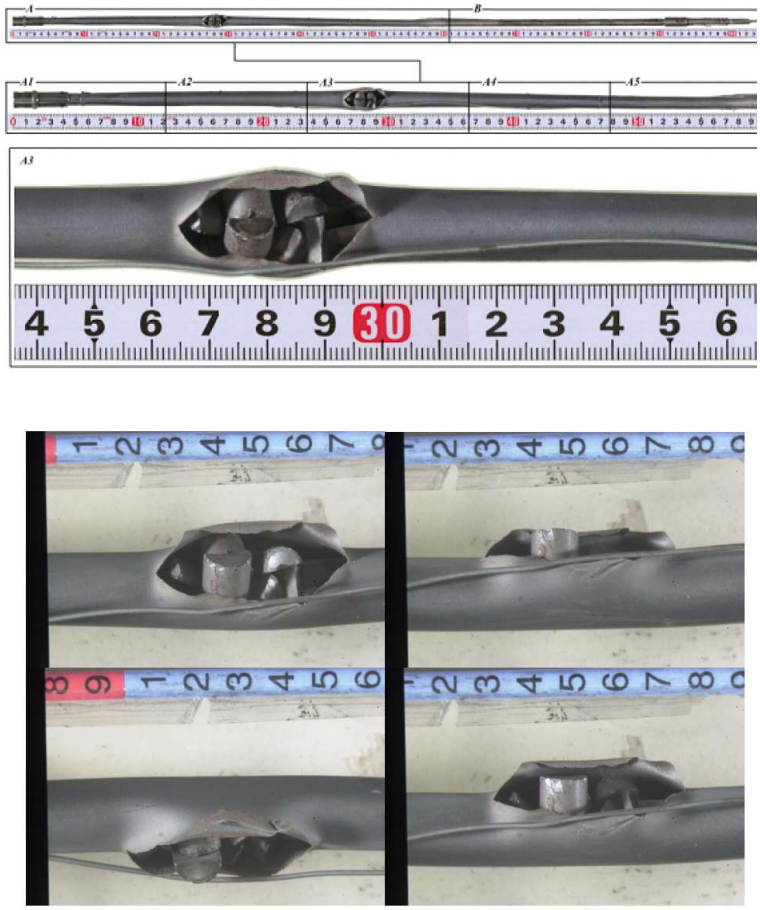

FIG. 2. Photographs of the rod and burst area.

Large pieces of cracked pellets, mainly pellet halves, can be seen in the burst hole. The pellets probably moved to this position during the transport of the rig. It is also possible that some relocation happened during the test, but this cannot be proved.

2.1. Metallography

Metallography was conducted at several axial elevations of the rod between 175 (at the lower thermocouple) and 463 mm (just below the upper thermocouple). The goal of the metallography examination was to document deformations, such as clad wall thickness reduction, clad outer diameter increase (ballooning), oxide layer thickness, hydrides, the grain morphology, and cracks.

2.1.1. Cladding oxidation

The entire rod was covered with black oxide layer. No oxide spallation was found. Below and above the wide burst the continuous oxide layer is 40 to 50 µm thick and developed, both on the water and fuel side of the clad. The waterside oxide thickness at the upper and lower cladding thermocouples was in the range of 24–27 µm. In the balloon region the oxide thickness shows a correlation to the local level of strain/deformation found. The highest oxide thickness values are found where the wall thickness was smallest and the deformation largest at about 0° angular orientation, Fig. 3.

2.1.2. Hydrogen analysis

Cladding samples from various axial elevations were analysed, using a Ströhlein analyser, by melt extraction with respect to the total amount of hydrogen. Prior to hydrogen analysis the samples were acid washed and ultrasonically cleaned in both water and ethanol. The hydrogen content seems to increase from the max split opening in the max balloon zone (56 ppm) to the ends of the rod near the (2460 ppm) upper and (115 ppm) lower thermocouple support. In the max balloon zone the hydrogen content is decreasing from about 100 ppm at the start of the wide burst split to 56 ppm at the max split opening. Secondary hydriding (2460 ppm) is found about 35 mm below the burst zone.

Since hydrogen analysis was carried out only in a few axial positions, Fig. 3, the highest measured value (2460 ppm) can be considered only as the lower limit for the real maximum in the hydrogen distribution peak; however, the peak position can be determined from the measurements with a good accuracy, taking into account that the peak width is normally relatively small.

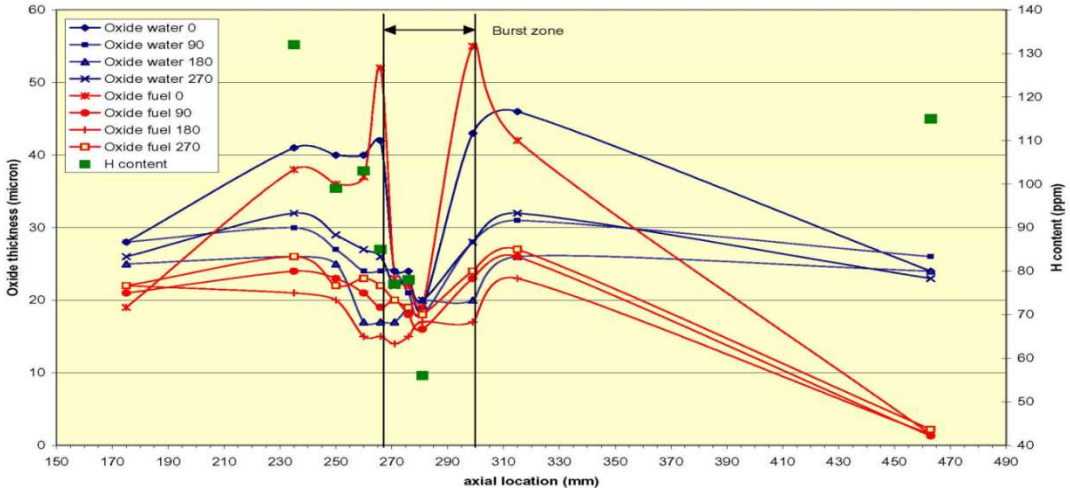

FIG. 3. Oxide thickness and hydrogen content at defined axial positions.

3. MODELLING TOOL

The single-rod SVECHA/QUENCH (S/Q) code, that is a submodule of the fuel performance and safety code SFPR [10], was recently extended to detailed mechanistic modelling of the secondary hydriding phenomenon [11], by implementation of the refined model for Zr alloy cladding oxidation and hydriding [12]. In this model the hydrogen uptake kinetics in various hydrogen-steam mixtures is taken into account and two mechanisms are included as the limiting cases: (i) direct reaction with molecular hydrogen, and ii) absorption of hydrogen liberated by the decomposition of water or steam during the oxidation process and absorbed as part of the oxidation mechanism.

For consideration of mass transport phenomena in the fuel-cladding gap in a burst fuel rod, the gas kinetics module of the S/Q code was modified and coupled with the refined module for internal cladding oxidation and hydriding, Fig. 4. The code was modified to take into consideration the competitive propagation of steam and hydrogen into the pellet-cladding gap due to steam leakage through the burst opening, which is resisted by the counter flow of the filling gas (in the heat up stage) and by the intensive pickup of these species by the cladding inner-metal surface.

The model reasonably reproduces the internal wall oxidation in a narrow axial zone of a few cm around the breach, following Olander's approach [13]; besides, the generalized model additionally predicts the moderate hydrogen uptake in this oxidation zone and the enhanced hydrogen uptake in narrow bands (also of a few cm width) upward and downward the oxidation zone. In accordance with the model calculations, the steam penetration into the gap after the cladding rupture is strongly suppressed owing to counter-flow of the inert gas during the heat up stage and a strong consumption of steam during oxidation of fresh Zr internal surface. In turn, the hydrogen generated by this oxidation process tends to penetrate further into the gap; however, owing to counter-flow of the inert gas and strong consumption of hydrogen by non-oxidized Zr surface outside the oxidation zone, the hydrogen penetration into the gap is also strongly suppressed, resulting in the formation of narrow, heavily hydrogenated bands around the oxidation zone, in accordance with the experimental observations.

The code was applied to simulate the burst of fuel rods in the above mentioned JAERI and ANL single-rod tests and KIT bundle tests under postulated LOCA conditions. The code predicted the typical for those tests distributions of oxygen (narrow oxidation zone near the burst opening) and hydrogen (narrow peaks up to ≈ 3000 wt. ppm outside the oxidation zone) in the Zry cladding, observed in the tests, with a good accuracy.

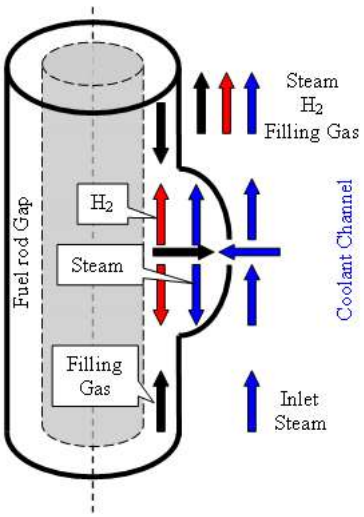

FIG. 4. Schematic representation of the gas mass transfer in the gap and coolant channel in the S/Q code (from [11]*).*

4. CALCULATION RESULTS

The S/Q input file for LOCA IFA-650.2 calculations included 200 axial meshes. Cladding temperature was prescribed according to the measured cladding temperature axial distribution from thermocouples TCC1–TCC4. The plenum temperature was constant and was determined as the inlet channel gas temperature 520 K.

The cladding temperature time history at different axial positions and axial distribution at different moments, used in calculations, are presented in Fig. 5.

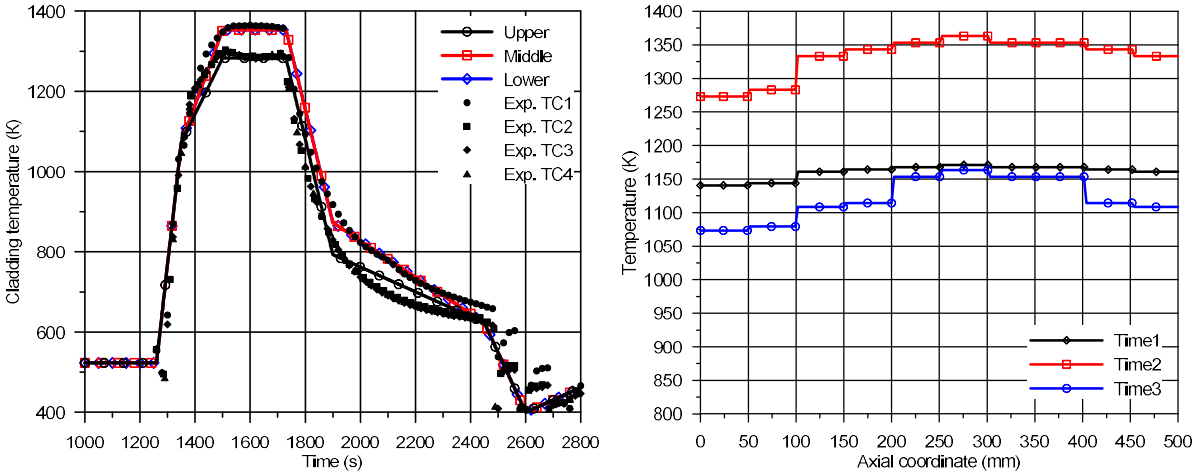

FIG. 5. Cladding temperature time history (left) at three axial positions from the top of the sample - upper (99 mm), middle (249 mm) and lower (399 mm), and axial distribution (right) at different moments 1400, 1500 and 1800 s, used in calculations.

The calculated axial distribution of the cladding outer diameter increase at the end of simulation in comparison with experimental data is plotted in Fig. 6 (left). A reasonable agreement of calculations with experimental measurements was achieved in the axial zone close to the burst position. Underestimation of experimental data is observed in the burst position (due to limitations of the deformation model) and some over predictions are observed in the upper and lower parts of the cladding. Calculated axial distributions of the cladding inner and outer hoop strains at the end of simulation in comparison with the measurements in the ballooned region are shown in Fig. 6 (right).

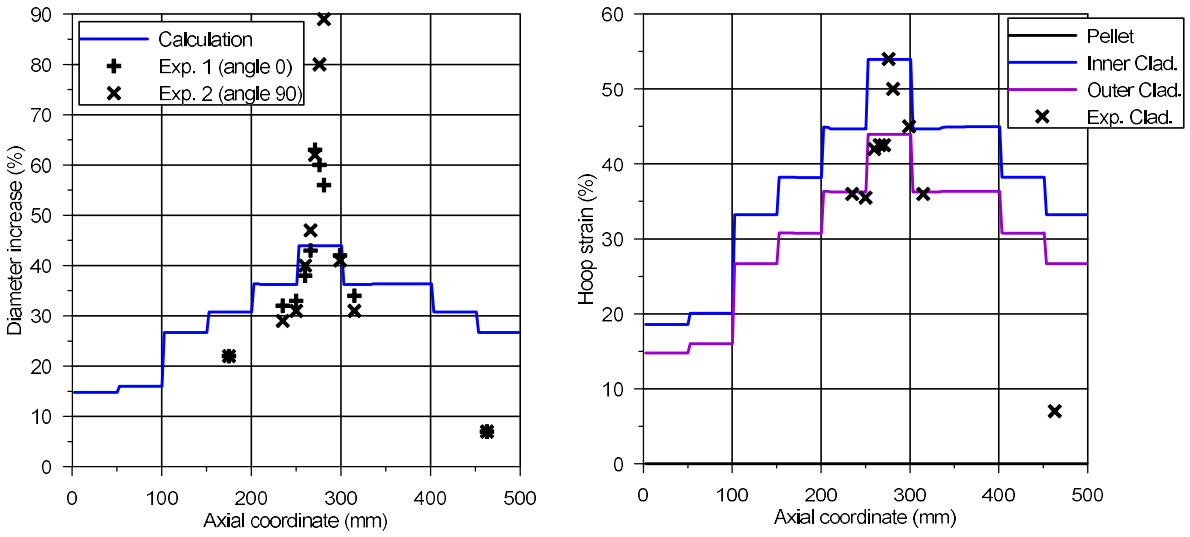

FIG. 6. Calculated axial distribution of the cladding outer diameter increase (left) and inner and outer hoop strains (right) at the end of simulation in comparison with experimental data.

The calculated total gap pressure is plotted in Fig. 7 (left). Gap pressure can be used as an indicator of the commencement of the cladding ballooning and burst. The measured time of the cladding burst is 100 s after the blow down and the calculated burst time is 1383 s, i.e. some seconds after the measured burst time. The calculated internal partial pressures of different gas components in the gap are presented in Fig. 7 (right), which illustrates propagation of steam and hydrogen in the gap in the counter flow of the filling gas.

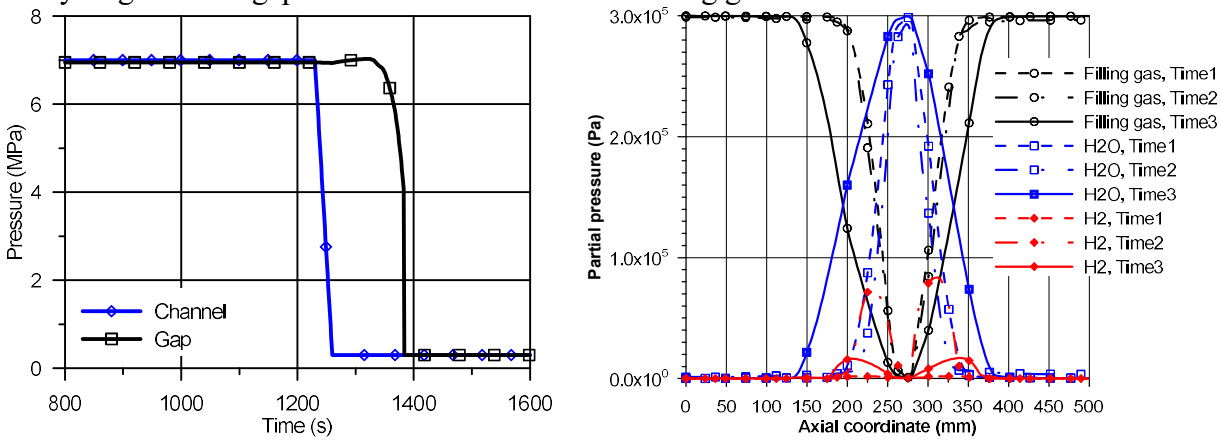

FIG. 7. Calculated gap pressure as the function of time (left) and axial distributions of partial pressures of gas components in the gap at the moments 1400, 1500 and 1800 s (right).

The calculated axial distributions of the cladding outer and inner oxide thickness in comparison with experimental data are plotted in Fig. 8. Taking into account a wide scattering of experimental measurements in the vicinity of the burst position, a reasonable agreement of these calculations with observations may be assumed.

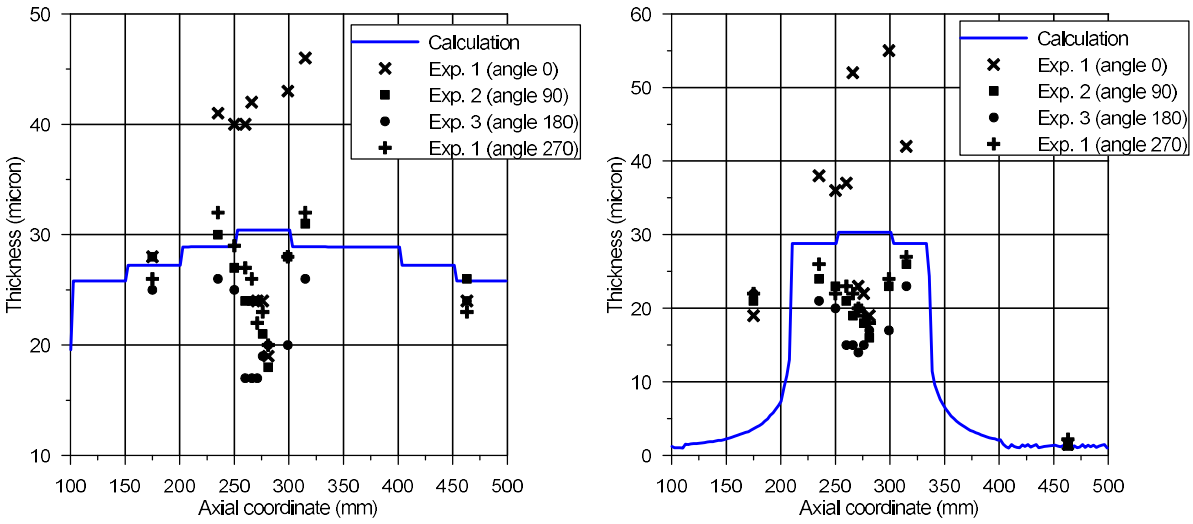

FIG. 8. Calculated axial distribution of the cladding outer (left) and inner (right) oxide thickness in comparison with experimental data.

The calculated axial distribution of the cladding hydrogen absorption at the start (1400 s), mid (1500 s) and end of the oxidation period (1800s) in comparison with experimental data are shown in Fig. 9. One can see two peaks with maximum hydrogen content increasing with time in the regions outside the oxidation zone in the vicinity of the burst opening axial position. Calculations demonstrate a rather good prediction for the peak position, but approximately two-fold overestimation of the hydrogen content in this zone. However, as explained in Section 2.1.2, the highest measured value (2460 ppm) can be considered only as the lower limit for the real maximum in the hydrogen distribution peak; this can be explained by an insufficient number of the hydrogen measurement axial positions in the narrow peak zone.

Comparing Figs. 8 and 9, one can see that the hydrogen peak position corresponds to the periphery of the cladding inner oxidation zone. This is explained by an important assumption of the S/Q hydrogen uptake model [12] on some critical thickness Δ of a few μm of the growing oxide layer, which is transparent for direct penetration of neutral hydrogen atoms, derived from the analysis of various experimental tests on Zr alloy oxidation in the steam/hydrogen mixtures under steam starved conditions [14, 15] (which are also realised in the gap of the of the burst fuel rod in the LOCA test).

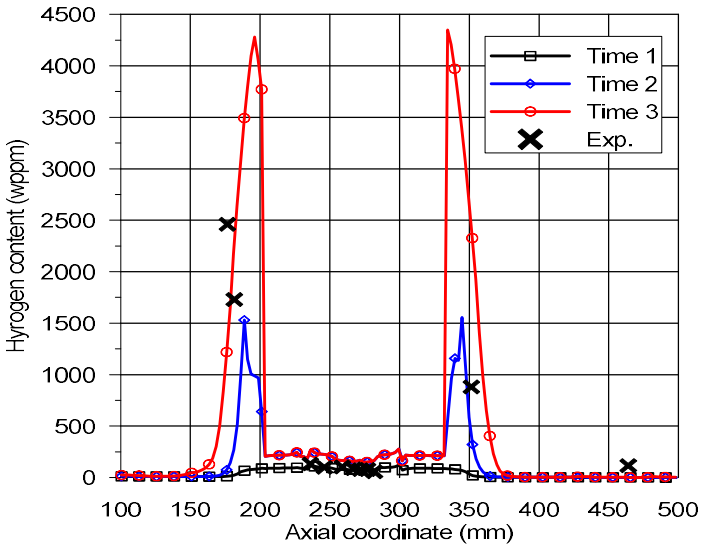

FIG. 9. Calculated axial distribution of the cladding hydrogen absorption at the start (1400 s), mid (1500 s) and end of oxidation period (1800 s) in comparison with experimental data.

5. SUMMARY AND CONCLUSIONS

The effect of secondary hydriding of fuel cladding under LOCA conditions, earlier observed in out-of-pile tests, was confirmed experimentally for the first time in the in-pile experiment, the Halden Reactor Project test IFA-650.2.

The SVECHA/QUENCH (S/Q) code, the submodule of the fuel performance and safety code SFPR modified for modelling of burst cladding, taking into consideration steam/hydrogen penetration in and filling gas release from the fuel rod gap, double-side oxidation and secondary hydriding, was further developed in the framework of the IAEA CRP FUMAC. The modified version of the S/Q code, earlier verified against the JAERI, ANL and KIT out-of-pile tests, was applied to simulation of the fuel rod behaviour under LOCA conditions in the in-pile test IFA 650.2. The code reasonably describes evolution of the cladding deformation and predicts the cladding internal oxidation (~ 2 cm-width zone above and below the breach) and secondary hydriding (~ 1 cm-width zones above and below the oxidized zone) with extremely high hydrogen uptake (up to 4500 wt. ppm), in a reasonable agreement with observations.

This allows utilising the developed secondary hydriding model to justification and practical applications of the new cladding embrittlement criteria, related to the threshold hydrogen concentration of ≈ 1500 wt. ppm in the heavily hydrided bands of internally oxidised claddings during LOCA accident scenarios, revealed in the KIT tests.

REFERENCES

[1] HACHE, G., CHUNG, H. M., The History of LOCA Embrittlement Criteria, NUREG/CP-0172, pp. 205–237 (2001).

[2] UETSUKA, H., FURUTA, T., KAWASAKI, S., Zircaloy-4 cladding embrittlement due to inner surface oxidation under simulated loss-of-coolant condition, J. Nucl. Sci. Tech. 18 (1981) 705–717.

[3] NAGASE, F., FUKETA, T., Effect of Pre-Hydriding on Thermal Shock Resistance of Zircaloy-4 Cladding under Simulated Loss-of-Coolant Accident Conditions, J. Nucl. Sci. Tech. 41 (2004) 723–730.

[4] NAGASE, F., FUKETA, T., Behavior of Pre-hydrided Zircaloy Cladding under Simulated LOCA Conditions. J. Nucl. Sci. Tech. 42 (2005) 209–218.

[5] NAGASE, F., FUKETA, T., Fracture Behavior of Irradiated Zircaloy-4 Cladding under Simulated LOCA Conditions, J. Nucl. Sci. Tech. 43 (2006) 1114–1119.
[6] BILLONE, M., YAN, Y., BURTSEVA, T., DAUM, R., Cladding Embrittlement During Postulated Loss-of-Coolant Accidents, NUREG/CR-6967 (July 2008).
[7] STUCKERT, J., GROSSE, M., RÖSSGER, C., KLIMENKOV, M., STEINBRÜCK, M., WALTER, M., QUENCH-LOCA program at KIT on secondary hydriding and results of the commissioning bundle test QUENCH-L0. Nucl. Eng. Des. 255 (2013) 185–201.
[8] BRACHET, J.C., HAMON, D., LE SAUX, M., VANDENBERGHE, V., TOFFOLON-MASCLET, C., ROUESNE, E., URVOY, S., BÉCHADE, J.L., RAEPSAET, C., LACOUR, J.L. BAYON, G., Study of secondary hydriding at high temperature in zirconium based nuclear fuel cladding tubes by coupling information from neutron radiography/tomography, electron probe micro analysis, micro elastic recoil detection analysis and laser induced breakdown spectroscopy microprobe, J. Nucl. Mater. 488 (2017) 267–286.
[9] OBERLÄNDER, B.C., JENSSEN, H.K., ESPELAND, M., SOLUM, N.O., PIE of the second fuel rod from the LOCA experiment (IFA-650.2), Enlarged Halden Programme Group Meeting, Lillehammer, Norway (2005), Session: F2, Paper: 5.
[10] VESHCHUNOV, M.S., BOLDYREV, A.V., OZRIN, V.D., SHESTAK, V.E., TARASOV, V.I., A new mechanistic code SFPR for modeling of single fuel rod performance under various regimes of LWR operation, Nucl. Eng. Des. 241 (2011) 2822–2830.
[11] VESHCHUNOV, M.S., SHESTAK V.E., Modeling of Zr alloy burst cladding internal oxidation and secondary hydriding under LOCA conditions, J. Nucl. Mater. 461 (2015) 129–142.
[12] VESHCHUNOV, M.S., SHESTAK, V.E., Models for Hydrogen Uptake and Release Kinetics by Zirconium Alloys at High Temperatures, Nucl. Eng. Des. 252 (2012) 96–107.
[13] OLANDER, D.R., Materials chemistry and transport modeling for severe accident analyses in light-water reactors II: Gap processes and heat release, Nucl. Eng. Des. 148 (1994) 273-292.
[14] SCHANZ, G., LEISTIKOW, S., ADELHELM, CH., Zur konkurrierenden Sauerstoff- und Wasserstoff-Aufnahme des Zircaloy-4 bei hohen Temperaturen. In: Gase in Metallen, Ed. by D. Hirshfeld (1984).
[15] MOALEM, M., OLANDER, D.R., Oxidation of Zircaloy by steam, J. Nucl. Mater. 182 (1991) 170–194.

IMPLEMENTATION OF THE MOLTEN U-ZR-O SLUG (BLOCKAGE) RELOCATION MODEL INTO THE SFPR CODE

V.E. SHESTAK, A.V. BOLDYREV
Nuclear Safety Institute (IBRAE),
Russian Academy of Sciences,
52, B. Tulskaya, Moscow, 115191,
Russian Federation
E-mail: sve@ibrae.ac.ru (corresponding author)

M.S. VESHCHUNOV
International Atomic Energy Agency,
Vienna International Centre,
PO Box 100, 1400 Vienna,
Austria

Abstract

The numerical module HTLQ, simulating (U-Zr-O) melt blockage (or slug) physico-chemical interactions (molten corium oxidation, fuel pellets dissolution) during its downward relocation, was implemented in the fuel performance and safety code SFPR. Validation of the modified SFPR code was successfully performed against the bundle CORA-W1 experiment and demonstrated that the core degradation phenomena can be adequately modelled by fuel performance codes.

1. INTRODUCTION

The code package SVECHA for numerical modelling of thermomechanical and physico-chemical degradation phenomena under severe accident conditions in the water cooled reactor was developed at IBRAE [1]–[3] in collaboration with IRSN (Cadarache, France). SVECHA models were further developed and integrated into the single-rod code SVECHA/QUENCH (or S/Q) in collaboration with KIT (Karlsruhe, Germany) [4]–[6]. By coupling of S/Q with the code MFPR, developed for mechanistic modelling of irradiated UO_2 fuel behaviour and fission products release in collaboration with IRSN [7, 8], the fuel performance and safety code SFPR for various regimes of LWR reactor operation (normal and off-normal, including severe accidents) was developed at IBRAE [9]–[11].

The SVECHA model describing massive melt blockage (slug) relocation and physico-chemical interactions with steam and surrounding fuel rods of a bundle [12] was developed on the base of the observations in the CORA bundle tests. Mass exchange owing to slug oxidation and fuel rods dissolution is described by the previously developed 2D model for the molten pool oxidation [13, 14]. Heat fluxes in oxidizing melt along with the oxidation heat effect at the melt relocation front are counterbalanced by the heat losses in the surrounding media and the fusion heat effect of the Zr claddings attacked by the melt. As a result, the slug relocation velocity is calculated from the heat flux matches at the melt propagation front. Model demonstrates a reasonable capability to simulate the main features of the massive slug behaviour observed in the CORA-W1 test [15].

Implementation of the molten U-Zr-O slug (blockage) relocation model into the SFPR code is presented in the current paper.

2. SFPR SINGLE FUEL ROD PERFORMANCE CODE

The SFPR code calculates the following basic processes in fuel rods:

— Simplified heat exchange with water/steam flow and gas dynamics**:** axial distributions of gas mixture components concentration, accounting hydrogen source due to Zr cladding oxidation, gas mixture temperature and velocity;
— Heat conductance: 2D temperature distribution evolution in the fuel rod, accounting heat sources in the fuel pellets and oxidising cladding, and heat exchange with the coolant and shroud;
— Gap conductance: heat conductance in the gas gap, accounting gas content and possible fuel-pellet contact;
— Cladding oxidation and hydrogen absorption**:** oxidation kinetics up to the Zr melting temperature under transient (heat-up) conditions, formation of multi-layered structure β-Zr/α-Zr(O)/ZrO_2 of oxidised cladding, and hydrogen absorption during oxidation;
— Deformation behaviour: deformation of multi-layered structure of oxidised cladding and failure, with different thermomechanical properties of the layers;
— Dissolution/oxidation**:** simultaneous molten Zr oxidation and ZrO_2 scales and UO_2 fuel pellets dissolution kinetics above the Zr cladding melting temperature;
— UO_2 fuel swelling and fission products release.

The corresponding numerical modules are included in the SFPR code:

— Channel mass balance and heat exchange module;
— Fuel rod heat conductance module;
— Cladding oxidation and hydrogen absorption module;
— Fuel rod thermomechanical module;
— UO_2 fuel swelling and fission products release module.

The SFPR code fuel rod calculation scheme is presented in Fig. 1:

— SFPR code simulates single cylindrical fuel rod behaviour under normal and accident conditions;
— Fuel rod is divided into a number of meshes along axial and radial directions;
— Each axial mesh consists of the UO_2 fuel pellet and the multi-layered oxidised Zr cladding.

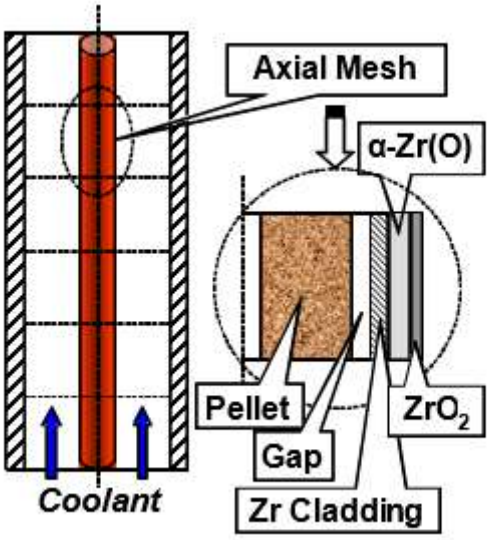

FIG. 1. Fuel rod calculation scheme.

3. MOLTEN U-ZR-O SLUG (BLOCKAGE) RELOCATION MODEL

Melt blockage calculation scheme is presented in Fig. 2. Complicated melt blockage shape is simplified by a cylindrical volume with some vertical length L_{slug} and radius R_{slug}. UO_2 fuel rods are imbedded in the slug melt. Coolant channel is not completely blocked by the melt, which increases its volume (axially and radially) in the course of melt relocation and dissolution of solid materials.

Real bundle structure of a few fuel rods in the slug relocation model is simplified by one effective fuel rod, Fig. 3. Under this assumption the number N of fuel rods with diameters D_{rod} is replaced by one effective fuel rod of diameter $D_{eff} = D_{rod}\sqrt{N}$. This provides conservation of the melt oxidation surface and thus correct description of the melt oxidation kinetics. In order to describe correctly the kinetics of fuel rods dissolution, an additional factor $\sqrt{N}$ is introduced in the mass fluxes from the effective to the melt (see details and justification in [12]).

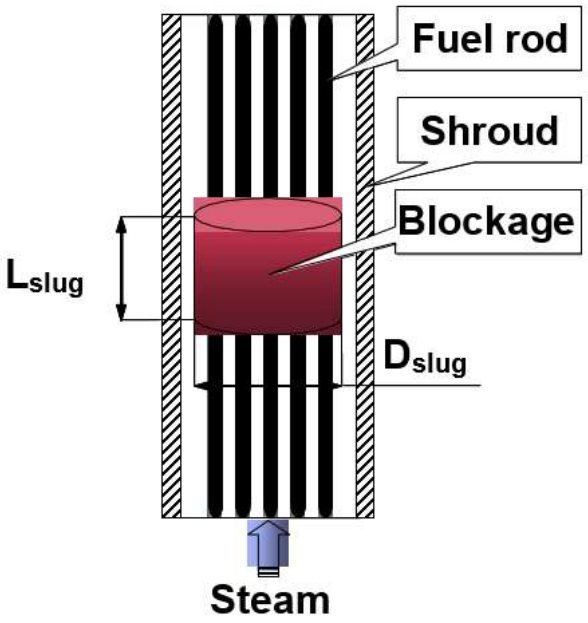

FIG. 2. Melt blockage calculation scheme.

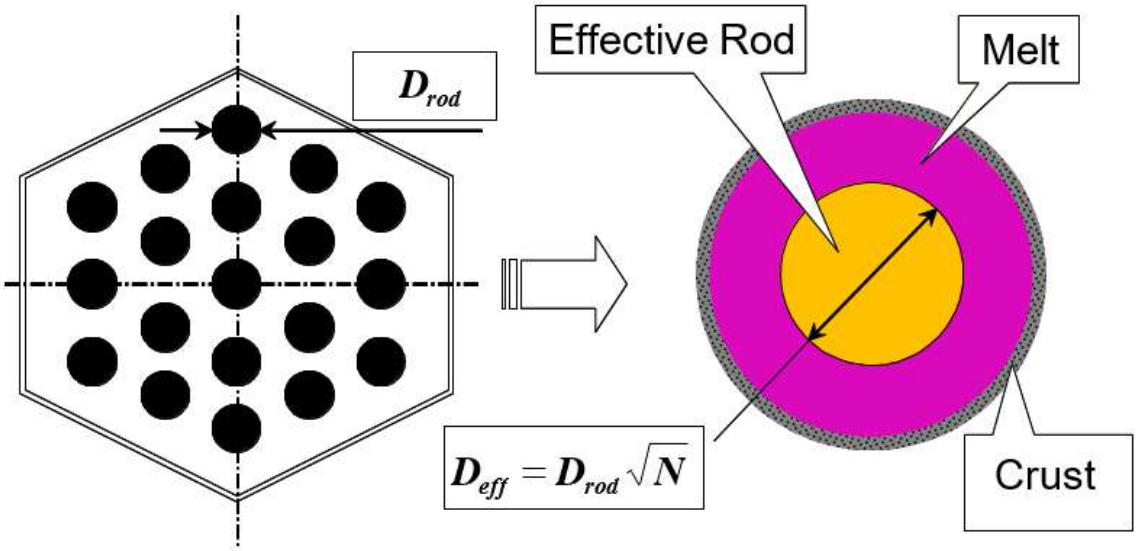

FIG. 3. Effective fuel rod transformation.

The slug consists of the (U-Zr-O) liquid part and the solid scales – $(Zr,U)O_2$ crusts at the lateral, upper and lower surfaces of the slug, Fig. 4.

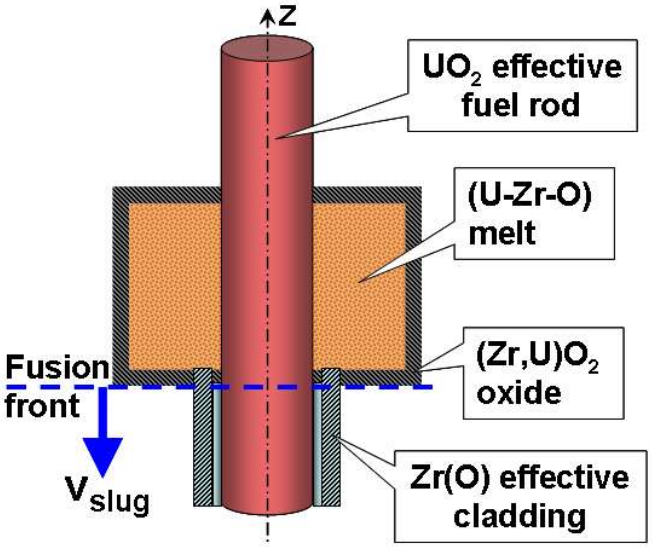

FIG. 4. Melt blockage structure.

The basic equations of the slug relocation model are presented in [12], where the molten corium oxidation model [13, 14] was extended to simulation of the molten pool (or slug) physico-chemical interactions during its relocation.

Mass balance in the melt blockage is considered taking into account external oxygen flux, solid phases dissolution or growth and underlying fuel claddings fusion in the course of melt relocation.

Heat balance in the melt blockage is considered taking into account heat exchange with surroundings, heat sources due to oxidation and phase transformations, heat losses due to the metal cladding fusion during relocation.

Temperature distribution in the melt blockage is approximated by the melt bulk average value, T_{melt}, and linear profiles inside the oxide scales, T_{int},T_{ext}.

The sum of the axial heat flux from the melt bulk and the heat release rate due to melt oxidation is matched at the slug front to the sum of the heat removal from the front (including heat conduction flux along the claddings and heat exchange with the environment below the front) and the heat losses due to metal claddings fusion at the melt progression front, this allows calculating the relocation velocity, v_{slug}.

Oxide crust formed at the progression front (due to steam interaction), has to prevent slug from further relocation. However, mechanical instability of thin oxide crust (supporting the massive slug) results in its local breaching and rapid downward relocations of droplets and rivulets, their refreezing and accumulation at lower (and cooler) elevations, oxidation and formation of a new crust, until it fails again (at some critical thickness), and so on. This provides slow stepwise motion of the slug front and intensive oxidation of fresh relocated portions of melt at the front, represented in the model as continuous motion of slug front with the critical oxide crust thickness as adjusting model parameter (evaluated from a simple physical consideration in [12] as ~100 μm).

On this base, the stand-alone slug relocation module HTLQ was developed and tested in [12].

4. SLUG MODEL IMPLEMENTATION INTO THE SFPR CODE

The HTLQ code consists of two blocks: heat exchange and mass exchange (dissolution/oxidation). Numerical solution of the above described system of equations at each local time step is found by consistent calls of the heat exchange and mass exchange blocks.

Calculations with automatic convergence and accuracy control at each local time-step are performed in the dissolution/oxidation and heat exchange blocks separately.

Coupling between dissolution/oxidation and heat exchange blocks is realized in the module HTLQ at the time step, determined as the minimum value of the local time steps of the two blocks.

Properties of the melt and solid phases (enthalpy, density, specific heat capacity, thermal conductivity) are determined from the SCDAP/RELAP5 MATPRO data base [15].

For the purpose of the slug model implementation into the SFPR code, the solver and database parts of the HTLQ stand-alone module were extracted. Initialization of the new object and calling of the HTLQ module at the global time step were realized in the SFPR head routine. Interconnections of the SFPR code modules (channel heat exchange, rod heat conduction, cladding mechanical deformation and cladding oxidation-dissolution) with HTLQ were realized.

At each global time step necessary inputs for modelling of the blockage heat exchange with surrounding media (average temperature of fuel rods, internal shroud temperature, channel gas temperature at the blockage elevation, and also upper and lower parts of the bundle temperatures, channel gas heat conductivity and velocity) are transferred from the channel heat exchange and rod heat conduction modules of the SFPR code.

In the stage before melt blockage formation, the oxidation/dissolution module of the SFPR code simulates behaviour of U-Zr-O melt in each axial mesh of the representative fuel rod, if melting of cladding takes place in these meshes. The first call of the melt blockage oxidation/dissolution module is performed when the total volume of the melt (in several axial meshes) is sufficient to embed several fuel rods at these axial elevations.

An interface for new output files of the HTLQ module was organized. New input files for verification of the SFPR+HTLQ code were developed. Validation of the modified SFPR code using the test matrix of the HTLQ stand-alone module was performed.

5. VALIDATION OF SLUG MODEL AGAINST CORA-W1 TEST

The SFPR code with the implemented HTLQ numerical module was validated against experimental observations of the melt blockage relocation, oxidation and interaction with the fuel pellets in the CORA-W1 test [16].

In this test the VVER type bundle containing 19 fuel rods was examined under conditions of severe accident (steam oxidation and temperature escalation). On the base of the post-test examination data, it was concluded that after Zr cladding melting at some elevation ≈ 900 mm in the moment ≈ 4200 s, accumulation of relocating materials and formation of the coolant channels blockage commenced; this blockage subsequently relocated downward very slowly (~1 mm/s) in comparison with rather quick relocations of separate droplets and rivulets. The lowest position of the blockage was observed in the moment ≈ 4800 s (i.e. melt relocation time interval is approximately equal to 600 s) at the elevation ≈ 400 mm (Fig. 5) [16].

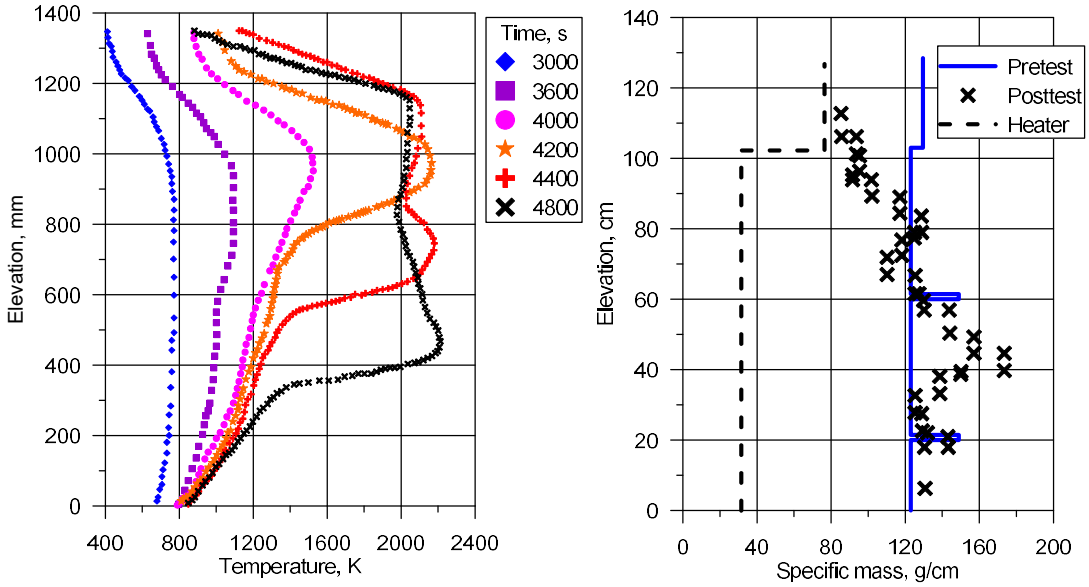

FIG. 5. Evolution of axial temperature distribution during the transient and post-test axial mass distribution in CORA-W1 test [16].

Measured temperature axial distribution inside the CORA-W1 test bundle (Fig. 5) was used in the calculations as the initial and boundary conditions defined on the enclosure surfaces, for simulation of the melt blockage temperature evolution. Mean temperature of the upper enclosure surface, ≈ 2000 K, was set higher than that of the lateral environment (bundle shroud internal surface), ≈ 1800 K, and of the lower environment (intact part of the bundle at lower elevations), ≈ 1400 ‑ 1500 K. Heat source in the melt blockage due to the bundle electrical heating was varied in calculations in the range evaluated from the test data. A series of calculations was performed to adjust the mean oxide crust thickness at the relocation front. A reasonable agreement with observations of blockage relocation was attained with the values in the range from 100 to 300 μm with somewhat different boundary and initial conditions; however, the best fit was attained with 200 μm. For this reason, only results with this option will be presented. After implementation of the slug model in an integral code with an interface between the new model and the thermal hydraulic block of the code for more self-consistent

calculation of the heat exchange with the surroundings, the oxide crust thickness can be determined more definitely using an iteration procedure for calculation of the slug relocation velocity.

An initial gap between the lateral external surface of the blockage and the shroud internal surface was chosen large enough to allow further expansion of the slug in radial direction during relocation. An initial height of the slug was in the range from 60 to 80 mm. An initial position of the slug front was set at 900 mm. Results of calculations are presented in Figs. 6-9.

Calculated temperatures are shown in Fig. 6. The melt bulk average temperature increases from 2250 K when relocation starts, to ≈ 2430 K when the power is switched off (calculation time 600 s) and then decreases up to the moment of melt solidification when calculations are ceased. Calculated temperatures of the upper, lower and lateral oxide scales presented in Fig. 6 well correspond to temperatures measured in the experiment (2200-2300 K, as seen in Fig. 5). The temperature of the bottom crust corresponds to the melting temperature of the α-Zr(O) phase of the cladding.

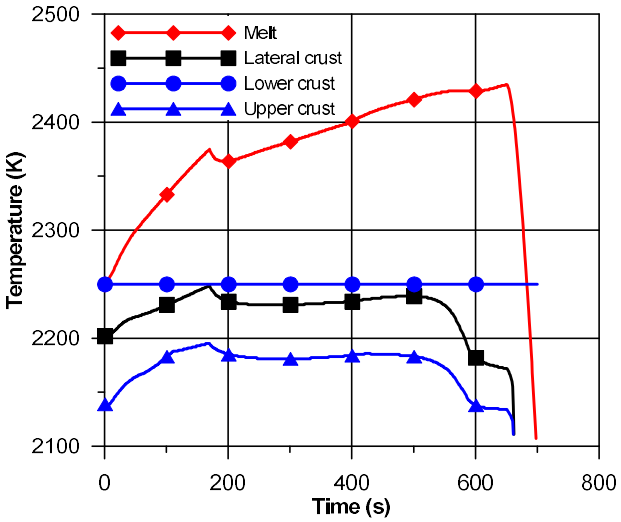

FIG. 6. Simulation results for the mean temperatures evolution during slug relocation.

The calculated relocation velocity attains the value of ~2.5 mm/s and then on the bundle cool down rapidly decreases. The final slug position is calculated at elevation ≈ 400 mm (Fig. 6), in a good agreement with observations (Fig. 5).

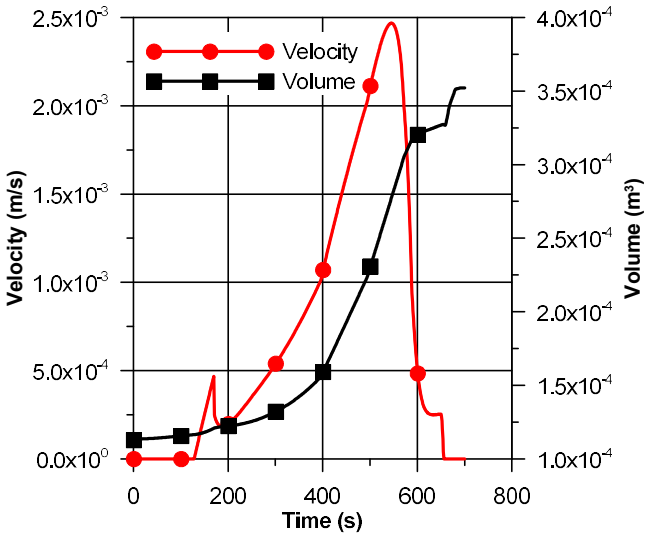

FIG. 7. Simulation results for the slug downward relocation velocity and volume evolution during relocation.

In calculations the molten mixture initially contains: 0% mole fraction of uranium, 73% of zirconium and 27% of oxygen (Fig. 8). During downward relocation new portions of melted claddings are accumulated, slug melt oxidizes and simultaneously dissolves UO_2 pellets. The simulated final slug chemical composition represents 12‑17% mole fraction of uranium, 42‑50% of zirconium and 38‑41% of oxygen, which were not directly measured in the tests.

Lateral and upper oxide scales thicknesses in calculations grow up and attain 1.5-3 mm (Fig. 9), whereas the bottom oxide is stable and corresponds to the fixed mean oxide crust thickness 200 μm (as above explained).

The slug expands in the axial and radial directions, owing to accumulation of fresh portions of dissolved materials (Fig. 10). Noticeable precipitation of mixed ceramic $(U,Zr)O_{2-x}$ phase (> 20%) occurs on cool down, in a qualitative correspondence with observations (Fig. 11).

A rather satisfactory agreement with experimental observations is attained for the fuel pellets dissolution profile presented in Fig. 12: a realistic axial profile of the pellets cross-section area decrease in the range from 20 to 25% is calculated.

Therefore, validation of the modified SFPR code against experimental data of the CORA-W1 test generally demonstrates a reasonable capability of the code to simulate the main features of the massive slug behaviour, such as the relocation velocity and final position of the blockage, its chemical composition and fuel pellets dissolution depth. The calculation results are also similar to those obtained in [12] with the stand-alone module slug relocation module HTLQ; however, do not exactly reproduce them.

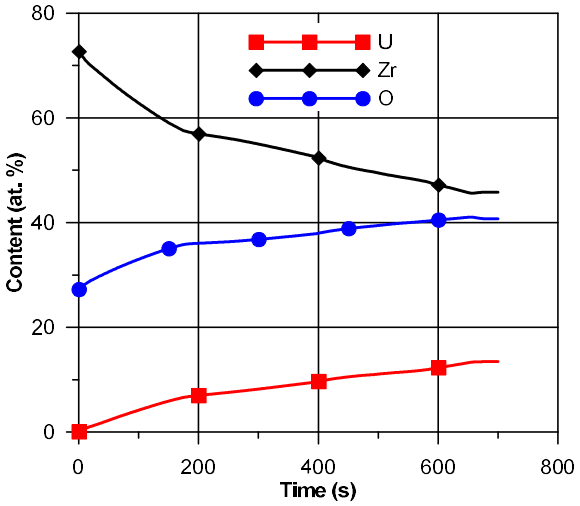

FIG. 8. Simulation results for the melt content during slug relocation.

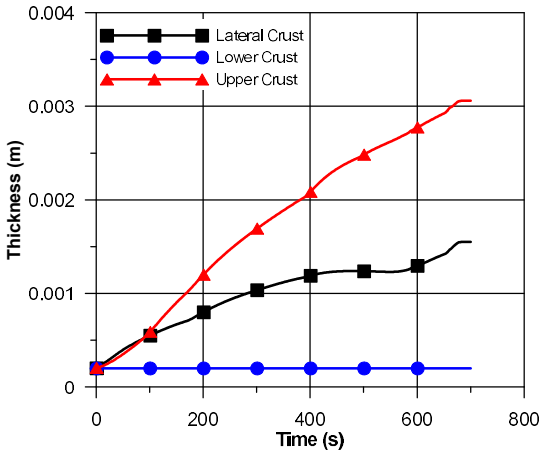

FIG. 9. Simulation results for evolution of the crusts thicknesses during slug relocation.

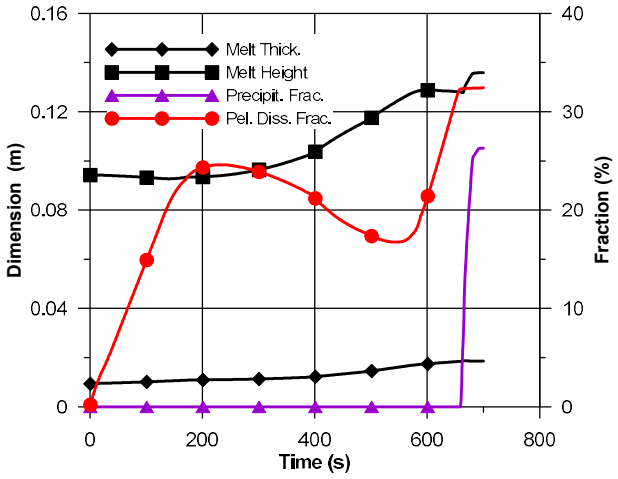

FIG. 10. Simulation results for the volume fraction of solid precipitates, slug melt radius and vertical length during slug relocation.

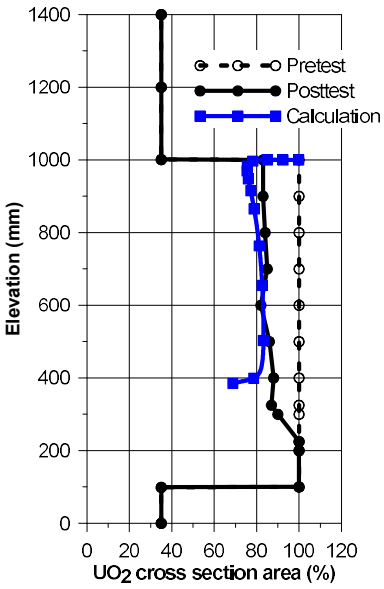

FIG. 11. Calculated axial profile of the pellet cross-section area in comparison with measurements in the CORA-W1 test.

6. SUMMARY AND CONCLUSIONS

The mechanistic modelling of melt relocation and oxidation during core degradation under severe accident (SA) conditions is considered. The earlier developed module HTLQ, simulating (U-Zr-O) melt blockage (or slug) simultaneous relocation, oxidation and fuel dissolution, was implemented in the single fuel rod performance and safety code SFPR. The coupled SFPR+HTLQ code allows complete description of molten slug relocation and oxidation and in particular calculates evolution of the slug relocation velocity. Validation of the modified SFPR code was successfully performed against the CORA-W1 experimental results.

Extension of SFPR to consideration of core degradation processes allows direct implementation of the fuel performance code (as a stand-alone module) in the new generation integral SA codes, preserving their “multi-physics” modular structure (Neutronics - Thermal Hydraulics – Fuel Rod Thermomechanics). This extension also benefits to the goals of the FUMAC Project on extension of fuel performance code to severe accident conditions, initiated in the light of the Fukushima accident.

REFERENCES

[1] VESHCHUNOV, M.S., PALAGIN, A.V., VOLCHEK, A.M., YAMSHCHIKOV, N.V., BOLDYREV, A.V., GALIMOV, R.R., KURCHATOV, S.YU., Code package SVECHA: Modeling of core degradation phenomena at severe accidents, Transactions of SMiRT-13 Conference, Vol. 1, (1995) 159–163.

[2] VESHCHUNOV, M.S., KISSELEV, A.E., YAMSHCHIKOV, N.V., BOLDYRV, A.V., GALIMOV, R.R., KURCHATOV, S. YU., Code package SVECHA: Modeling of core degradation phenomena at severe accidents, in: Proc. 7th Int. Meeting on Nuclear Reactor Thermal-Hydraulics NURETH-7, Vol. 3, (1995) 1914–1929.

[3] BERDYSHEV A. V., BOLDYREV, A. V., PALAGIN, A. V., SHESTAK, V. E., VESHCHUNOV, M. S., SVECHA/QUENCH Code for the Modeling of Reflooding Phenomena in Severe Accidents Conditions, in: Proceedings of the Ninth International Topical Meeting on Nuclear Reactor Thermal Hydraulics (NURETH-9), paper Log_19 (CD-ROM edition), San Francisco, California, USA (1999).

[4] BERDYSHEV A. V., BOLDYREV, A. V., PALAGIN, A. V., SHESTAK, V. E., VESHCHUNOV, M. S., Development of SVECHA/QUENCH Code for Modeling Fuel Cladding Degradation in QUENCH tests, in: Transactions SMiRT 16, Washington DC, Paper # 2028 (2001).

[5] HOFMANN, P., NOACK, V., VESHCHUNOV, M.S., BERDYSHEV, A.V., BOLDYREV, A.V., MATWEEV, L.V., PALAGIN, A.V., SHESTAK, V.E., Physico-Chemical Behavior of Zircaloy Fuel Rod Cladding Tubes During LWR Severe Accident Reflood, Report FZKA 5846, Karlsruhe, Germany (1997).

[6] HOFMANN, P., MIASSOEDOV, A., STEINBOCK, L., STEINBRUECK, M., BERDYSHEV, A.V., BOLDYREV, A.V., PALAGIN, A.V., SHESTAK, V.E., VESHCHUNOV, M.S., Quench Behavior of Zircaloy Fuel Rod Cladding Tubes. Small-Scale Experiments and Modeling of the Quench Phenomena. Report FZKA 6208, INV-COBE(98)-D018, Karlsruhe, Germany (1999).

[7] VESHCHUNOV, M.S., OZRIN, V.D., SHESTAK, V.E., TARASOV, V.I., DUBOURG, R., NICAISE, G., Development of the mechanistic code MFPR for modelling fission products release from irradiated UO_2 fuel. Nucl. Eng. Des. 236, (2006) 179–200.

[8] VESHCHUNOV, M.S., DUBOURG, R., OZRIN, V.D., SHESTAK, V.E., TARASOV, V.I., J. Nucl. Mater. 362, 327 (2007).

[9] VESHCHUNOV, M.S., BOLDYREV, A. V., OZRIN, V.D. , SHESTAK, V.E. , TARASOV, V.I., SFPR: an Advanced Mechanistic Code for Modeling of Single Fuel Rod Performance under Various Regimes of LWR Reactor Operation". Proceedings of Top Fuel 2009, Paris, France, Paper 2011 (2009).

[10] VESHCHUNOV, M.S., BOLDYREV, A. V., OZRIN, V.D., SHESTAK, V.E. , TARASOV, V.I., A new mechanistic code SFPR for modeling of single fuel rod performance under various regimes of LWR operation, Nucl. Eng. Des. 241, (2011) 2822– 2830.

[11] VESHCHUNOV, M.S., BOLDYREV, A. V., KUZNETSOV, A.V., OZRIN, V.D., SERYI, M.S., SHESTAK, V.E., TARASOV, V.I., NORMAN, G.E., KUKSIN, A.Y., PISAREV, V.V., SMIRNOVA, D.E., Development of the advanced mechanistic fuel performance and safety code using the multi-scale approach. Nucl. Eng. Des. 295, (2015) 116–126.

[12] VESHCHUNOV, M.S., SHESTAK, V.E., Model for Melt Blockage (Slug) Relocation and Physico-Chemical Interactions during Core Degradation under Severe Accident Conditions, Nucl. Eng. Des. 238, (2008) 3500–3507.

[13] VESHCHUNOV, M.S., MUELLER, K., BERDYSHEV, A.V., Molten corium oxidation model, Nucl. Eng. Des. 235, (2005) 2431–2450.

[14] VESHCHUNOV, M.S., BOLDYREV, A. V., SHESTAK, V.E., MUELLER, K., Analysis of Molten Pool Physico-Chemical Interactions in PHEBUS FP tests, Nucl. Eng. Des. 238, 1728-1742 (2008).

[15] ALLISON, C.M., BERNA, G.A., CHAMBERS, R., CORYELL, E.W., DAVIS, K.L., HAGRMAN, D.L., HAGRMAN, D.T., HAMPTON, N.L., HOHORST, J.K., MASON, R.E., MCCOMAS, M.L., SCDAP/RELAP5/MOD3. 1 code manual, volume IV: MATPRO–A library of materials properties for light-water-reactor accident analysis, DT Hagrman, NUREG/CR-6150, EGG-2720 (1993).

[16] HAGEN, S., HOFMANN, P., NOACK, V., SCHANZ, G., SCHUMACHER, G., SEPOLD, L., Test Results of Experiment CORA W1, KfK 5212 (1994).

FRAPTRAN CAPABILITIES TO MODEL LOCA THERMO-MECHANICS

L.E. HERRANZ, S.B. PELÁEZ
Unit of Nuclear Safety Research
CIEMAT
Avda Complutense 40, 28040 Madrid, Spain

Abstract

Safety criteria for Loss Of Coolant Accidents (LOCA) are based on experiments conducted in the 70's. Current fuel designs, materials and burnups, though, are noticeable different, so that new experimental campaigns have been launched to investigate the thermo-mechanical response of the new materials under the new conditions and to assess the predictability of the existing analytical tools. FUMAC (FUel Modeling in Accident Conditions) has been a coordinated research project of the IAEA targeted specifically to assess the capability of fuel performance codes to LOCA conditions based on experimental data coming from several laboratories. This paper synthesizes the CIEMAT's contribution to FUMAC on FRAPTRAN-1.5 modeling of experiments from three different facilities: Halden (IFA-650.9 and .10), Studsvik (192, 198) and MTA-EK (PUZRY-8, 10, 12, 18, 26 and 30). Whenever needed, the irradiation previous to the test has been modeled with FRAPCON-3.5. The results show that, despite the enhancement achieved through input deck and model modifications (large strain deformation), the FRAPTRAN mechanical response to the transients simulated should be still improved, although a major constraint to do so is the huge uncertainty existing in the strain and stress failure criteria. Additionally, the paper includes an uncertainty and sensitivity analysis (UASA) carried out with DAKOTA-6.4 on the IFA-650.10 estimates. The outcome of the exercise highlights the cladding outer diameter (*od*) and the base irradiation cladding corrosion model (*oxx*), as the two elements affecting most the mechanical response predicted, although the uncertainties are in no case responsible for the deviations noted with respect to data.

1. INTRODUCTION

The recent changes in fuel design, new cladding materials and the move towards higher fuel burnups raise the concern about applicability of current LOCA safety criteria. Some laboratories have launched experimental campaigns in order to gain a deeper understanding of the phenomena occurring during the LOCA transient in the new fuel materials once submitted to more demanding operation. The IAEA-FUMAC project covers some of the tests executed at facilities such as Halden, Studsvik, MTA-EK and QUENCH.

CIEMAT, as a FUMAC partner, has performed a fuel rod behavior assessment using the FRAP codes: FRAPCON-3.5 to characterize the initial state of the rod (when needed) submitted to the transient, and FRAPTRAN-1.5 to model the LOCA-like scenarios. The tests studied by CIEMAT are the IFA-650.9 and IFA-650.10 from Halden, the 192 and 198 tests from Studsvik, and the PUZRY-8, 10, 12, 18, 26 and 30 from MTA-EK.

CIEMAT modeling, though, is not merely the default one resulting from applying FRAPTRAN. Some modifications in the thermal modeling (mostly through a "wise" use of user input deck options) and in the mechanical modeling (by modifying even the governing equations of strain), gives an individual nature to the results that will be presented below. In addition, an UASA (Uncertainty Analysis and Sensitivity Analysis) has been carried out for the IFA-650.10 test with DAKOTA-6.4 and its results are also compiled below.

2. HALDEN

The Halden research reactor operates under the framework of the OECD-NEA Halden Reactor Project. One of its experimental series, IFA-650, has been specifically aimed at testing fuel rodlets under LOCA conditions; the IFA-650.9 and .10 tests have been opened to the FUMAC participants and modeled by CIEMAT.

2.1. Facility and device

A short description of the facility and the experimental device is given next [1]–[4].

The IFA-650 tests are in general preceded by the respective steady state irradiation. Then, the mother rod is refabricated into the test rodlet. The test rodlet is surrounded by an electrical heater (acting as flow separator and simulating sibling rods), and placed in a high-pressure flask. This device contains instrumentation for measuring rod internal pressure, cladding fuel and coolant temperatures at specific location, rodlet elongation, and other relevant variables (depending on the test, the instrumentation used may vary). During the normal operation prior to the LOCA transient, the coolant comes in at the lower part of the rig and goes out from the upper part. The general sketch of this device is shown in Fig. 1.

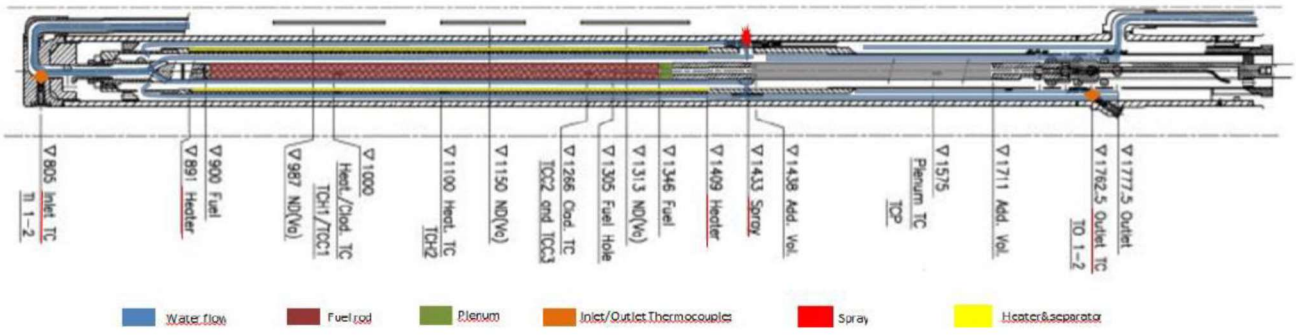

FIG. 1. Sketch of the rig used for the Halden LOCA tests (left-inlet, right-outlet).

The device is connected to a high-pressure loop and to a blowdown system. Each experiment is structured in five test phases:

- Forced circulation (about 10 days). Steady state operation during a few days that allows short-lived fission products generation in the rodlet;
- Natural circulation (few minutes). The outer loop is disconnected and rodlet temperature gets steady under the new flow regime;
- Blowdown (tens of seconds). The valves connecting the test device with the blowdown tank open and the rig is emptied; the channel pressure decreases to about blowdown tank pressure;
- Heat-up and hold at PCT (hundreds of seconds). Fuel temperature increase due to cooling degradation (stagnant superheated steam); under these conditions cladding can ballooned and eventually fail. Then sprays are usually operated to further oxidize the cladding and transport fission products towards blowdown tank, and the reactor is scrammed;
- Cooling. In some tests the sprays are also used for the cooling phase, and finally the rig is filled with helium to secure dry storage.

2.2. Modeling

The IFA-650 tests had been previously simulated with different versions of FRAPTRAN by other researchers. Some of them [5] concluded that a proper modeling required coupling FRAPTRAN to a thermal-hydraulic code, to make sure that the thermal behavior is adequately described. Other authors [6] used FRAPTRAN-1.3 with its own thermal models and noted substantial disagreement between data and estimates, both thermal and mechanical ones, as shown in Fig. 2.

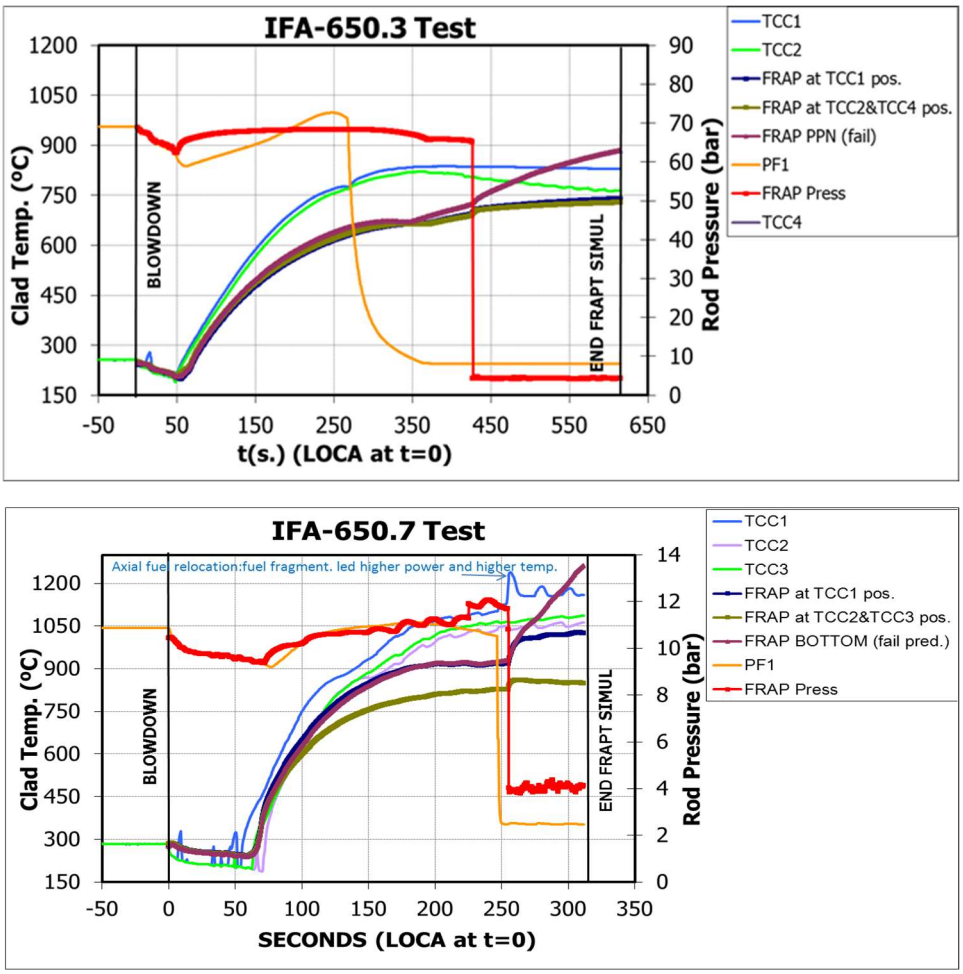

FIG. 2. FRAPTRAN-1.3 modeling of IFA-650.3 and -650.7 [6].

By further studying the experimental set-up and an optimized use of FRAPTRAN-1.5 for this particular facility, an enhanced thermal model has been achieved and the results are reported next. Once a reasonably consistent thermal behavior is achieved, the mechanical predictions by FRAPTRAN have been analyzed in depth and also here reported.

In order to enhance the thermal modeling, the attention was initially paid to capturing the right HTC (clad-to-coolant heat transfer coefficient) by using the available options in the code. To do so, some hypotheses and approximations have been made [7]:

— Whenever no specific fuel rod information was available for the modeling (spring dimensions and turns, for instance), general design values have been assumed [8];
— Upper and extra plena are simulated as just one node with an equivalent volume at the temperature defined below in Eq. (3);
— Wherever duplex cladding applies, the liner thickness is added to the base material, and the oxidation law and hydrogen uptake are modified correspondingly to match measurements at the end of base irradiation.

Regarding the thermal assumptions:

— The 'heat' option in FRAPTRAN is used to model clad-to-coolant heat transfer, which requires HTC as input, and it has been obtained from the Dittus-Boelter correlation (water as fluid) (see Table 1)

$$h = 0.0265 \cdot \frac{k_f}{L} \cdot Re^{4/5} \cdot Pr^{0.3} \quad (1)$$

and, once the rig is empty, the McAdams correlations applies (steam natural convection)

$$h = \frac{k_f}{L} \cdot C \cdot \left(\frac{g.\beta}{v.\alpha}(T_s - T_\infty) \cdot L^3\right)^n \quad (2)$$

— Clad-to-heater radiation heat transfer is considered during the heat-up phase;
— Meaning of 'inlet' and 'outlet' temperatures are reversed given the leak location at the bottom of the rig (modeling conceptually turned upside-down);
— The algorithm to calculate plenum temperature has been modified by assuming that the axial heat conducted from the nearest fueled node through the cladding is absorbed by the plenum gas. This assumption has been initially made to be more consistent with data trends observed, but it is known to lead to overpredict plenum temperature to some extent;

$$T_{plen}(t) = T_{plen}(t-1) + \frac{q}{m \cdot c_p} = T_{plen}(t-1) = \frac{A \cdot k \frac{(T_1 - T_p)}{\Delta x}}{m \cdot c_p} \cdot \Delta t \quad (3)$$

— Whenever a noticeable fuel axial relocation occurred (IFA-650.9), an adapted power profile is set.

By adopting these approximations, the thermal behavior predicted has been brought notably closer to data than earlier estimated [6], as shown in Fig. 3 for the IFA-650.9 and IFA-650.10 tests. In the Fig. there are two sets of calculation, one resulting from the modeling previously describes (CIEMAT) and other based on the thermal boundary conditions that were estimated with the SOCRAT code and set as a reference within the FUMAC CRP (hereafter denoted as FUMAC). It is observed that CIEMAT estimates are acceptable and, in any case, comparable to those of FUMAC.

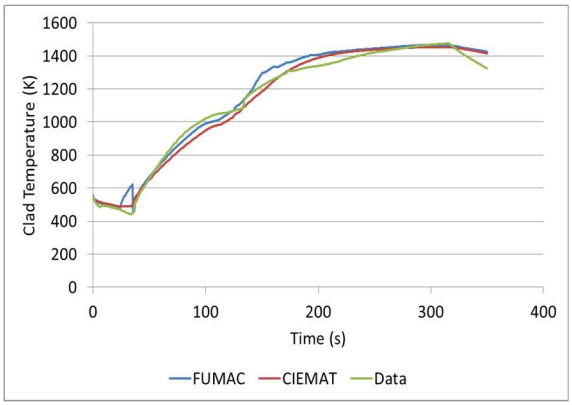

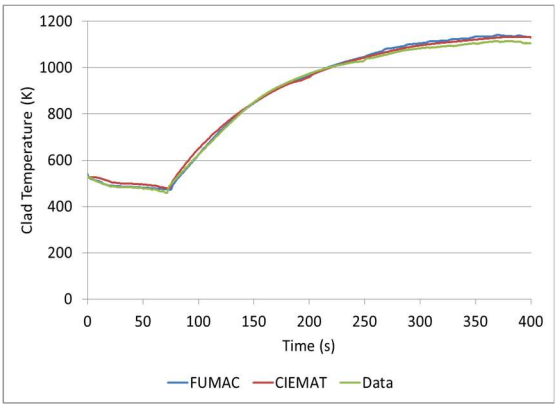

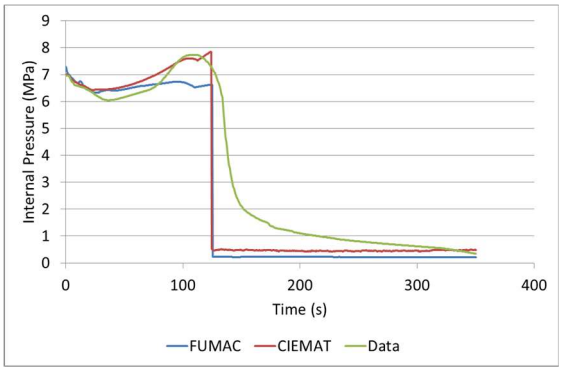

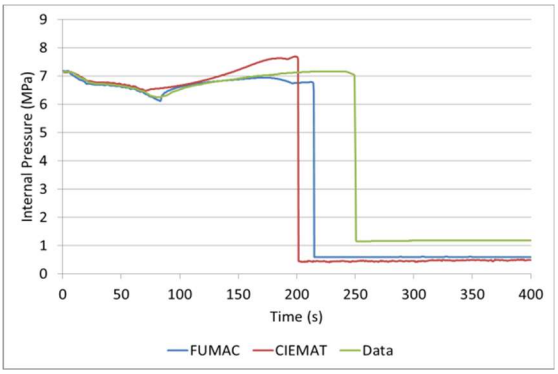

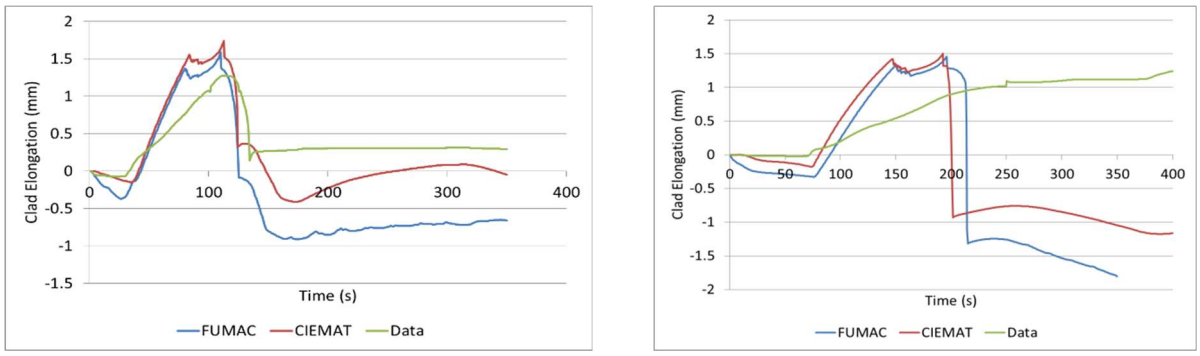

FIG. 3. FRAPTRAN predictions of cladding temperature (top), internal pressure (centre) and clad elongation (bottom) for IFA-650.9 (left) and IFA-650.10 (right).

From these studies some insights have been gained. Despite the observed enhancement of thermal estimates, mechanical discrepancies persist, so that their origin should not be straightforward related to deviations in cladding temperature. Among all the thermal hypotheses, there are three that made a significant impact: the clad-to-heater radiation heat transfer, the plena modeling and the adoption of 'ad-hoc' axial profiles to model fuel axial relocation (profiles which should be input).

In order to assess this mechanical mismatch additional studies have been performed [9]. Taking the IFA-650.9 test as a basis, the internal pressure discrepancies observed in Fig. 3 can be divided into two periods. The first one (50–100s), even though following the experimental trends, a few bar difference is noted, likely due to FRAPTRAN over-prediction of the plenum temperature. During the second period (100-130 s) data and estimates draw a reverse trend: whereas data progressively decrease as a result of the rod ballooning and eventual failure, estimates grow up until the failure is predicted.

This last mentioned mismatch has been postulated to be driven by straining deviations. Data suggests that large strains occur during the ballooning phase and, finally, clad fails. However, FRAPTRAN predicts ballooning with an approximately constant strain, which only increases at failure. Therefore, some alternatives to enhance the mechanical rodlet behavior have been explored. A study was undertaken to check the results sensitivity to variations in the coefficients governing the creep law in FRAPTRAN (BALON2 subroutine). According to the results obtained, the source of discrepancies were not rooted in the uncertainties underneath the creep law used (i.e., none of the variations intended brought the results closer to data available even qualitatively).

Then, an alternative modeling is proposed by extending the FRACAS-I model to the large strains domain. To do so, the Prandtl-Reuss flow law was modified to include a correction term [10] corresponding to large strains. The results obtained with this approach are the ones in the next section. It is worth mentioning that, in accordance to the FUMAC guidelines, the boundary conditions provided by SOCRAT are considered for these calculations.

TABLE 1. NOMENCLATURE USED IN EQS. (1–3).

A	clad cross section (m^2)	C	constant of the free circulation
C_p	gas heat capacity at constant pressure (J/mol·K)	g	gravitational acceleration (m/s^2)
h	average heat transfer coefficient ($W/m^2 \cdot K$)	k_f	thermal conductivity of fluid (W/m·K)
k	clad thermal conductivity (W/m·K)	L	characteristic length (hyd. diam.) (m)
m	number of moles in the plenum (mol)	n	constant of the free circulation
Pr	Prandtl number	q	heat rate from Node 1 to Node p (W)
Re	Reynolds number	T_1	clad Node 1 temperature (K)
Tp	clad Node p temperature (K)	T_{plen}(t	plenum temperature at the time t (K)

TABLE 1. NOMENCLATURE USED IN EQS. (1–3).

$T_{plen}(t-$	plenum temperature at the time t-1 (K)	T_s	clad surface temperature (K)
T_∞	coolant temperature (K)	α	thermal diffusivity of fluid (m^2/s)
β	volumetric thermal expansion coeff. of fluid (K^-	ν	kinematic viscosity (m^2/s)
Δx	length between Node 1 and Node p (m)	Δt	time step (s)

2.3. Results

2.3.1 IFA-650.9

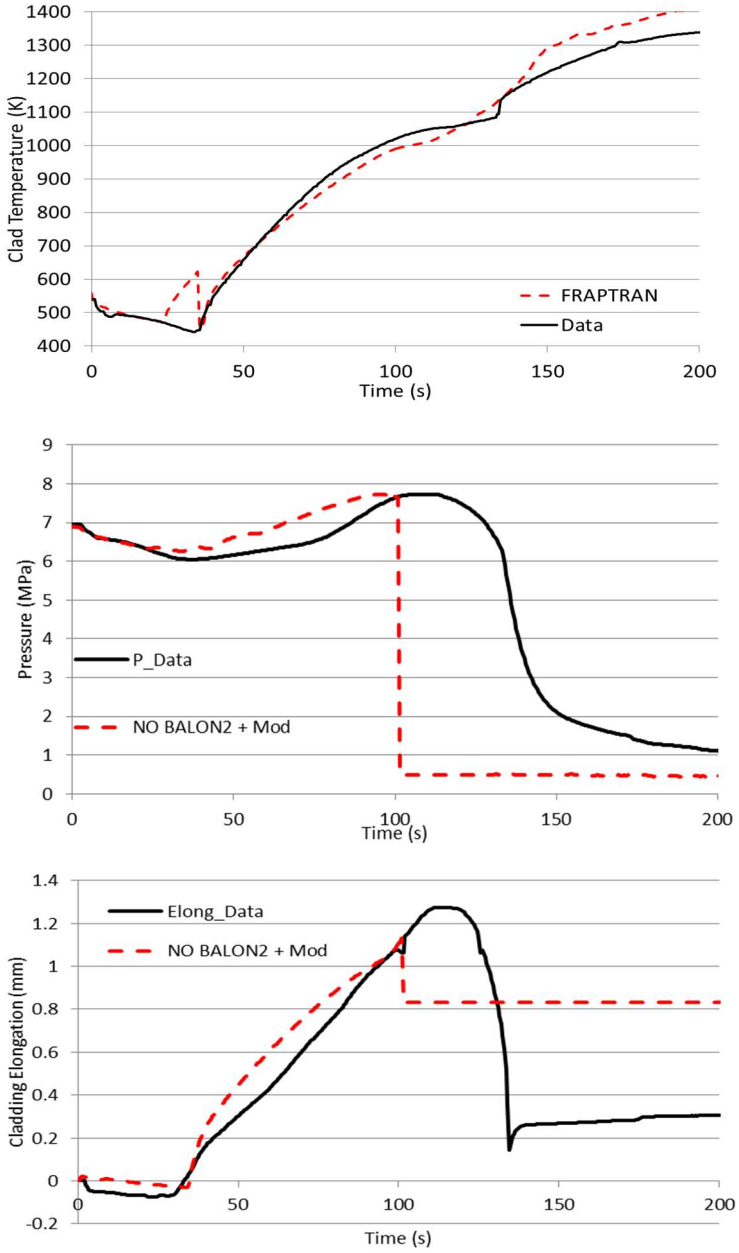

FIG. 4. IFA-650.9 results. Cladding temperature (top), internal pressure (center), cladding elongation (bottom).

As observed in Fig. 4, the straining process occurs faster than expected and eventually leads to a rodlet failure some 30 s earlier than predicted, although at a similar level of elongation (higher than 1.1 mm predicted vs. less than 1.3 measured). This approach notably improves the mechanical response with respect to the initial calculations (Fig. 3), even by avoiding the second

internal pressure rise before failing, but it seems that it overestimates clad straining and, as a consequence, the failure is estimated earlier than observed. It is worth noting that, due to the current code formulation, the pressure decrease once the cladding has failed is always sharp. Besides, the elongation values predicted and measured after failure are not relevant, due to the physical restrictions imposed to the experimental rod.

2.3.2. IFA-650.10

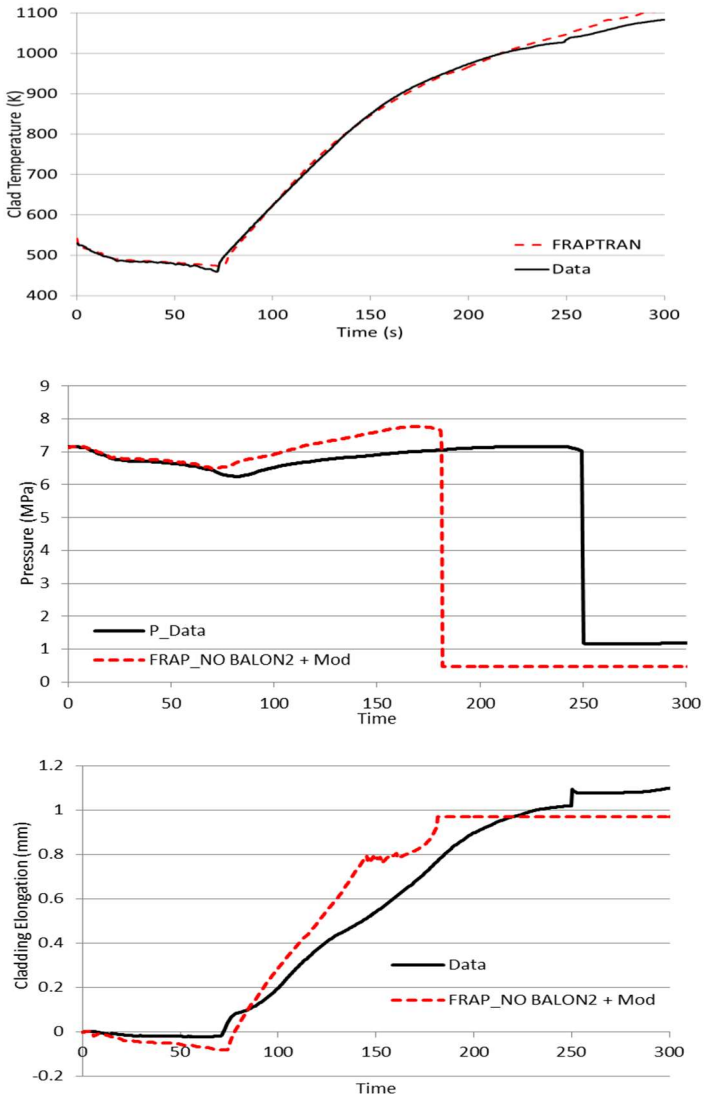

FIG. 5. IFA-650.10 results. Cladding temperature (top), internal pressure (center), cladding elongation (bottom).

Similar insights may be gained from the IFA-650.10 test results: good match of pressure evolution and elongation, but with a substantially earlier prediction of clad failure. From both sets of results it might be concluded that a better modeling of rodlets plena could mean a substantial reduction of discrepancies before attaining the pressure maximum. It is worth remembering that plena modeling mean two major assumptions: a single plenum equivalent to the two real ones and an overheating of the gas due to clad axial conduction.

As a brief summary of the results obtained so far, the thermal predictions of the Halden LOCA tests considered by CIEMAT for FUMAC are noticeably improved by adopting some defendable approximations. Also the mechanical behavior has been enhanced by adding a new term in the Prandtl-Reuss equation to account for large strains. Discrepancies still persist,

though, but they might be better estimated by a more refined definition of the rod plenum, less uncertain failure criteria (strain and stress) and possibly a better definition of the large strain term.

2.3.3. IFA-650.10 Uncertainty Analysis

An UASA (Uncertainty And Sensitivity Analysis) has been performed using simplified thermal-hydraulic boundary conditions. This is aimed to verify that the quantified uncertainties on key physical parameters bound the measured data, and it is optional to identify the relevant input parameters through GSA (Global Sensitivity Analysis). The test chosen was the IFA-650.10 for PWR analysis. The specifications for these analyses in the case of CIEMAT are:

— An input uncertainty propagation method has been used;
— Sampling size set to 200;
— List of input parameters as requested;
— List of output uncertainties as requested;
— The DAKOTA analytical tool used for the UASA.

For the sensitivity analysis the PRCC (Partial Rank Correlation Coefficient) has been used as the indicator, as it helps to readily identify parameters and variables with stronger impact on results.

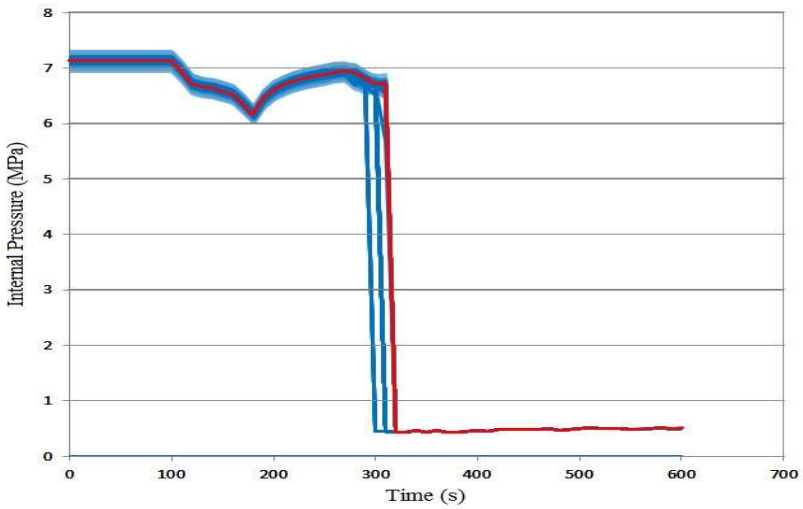

FIG. 6. IFA-650.10 uncertainty analysis. Rod internal pressure (200 runs (blue), reference case (red)).

Fig. 6 presents the uncertainty analysis results. It is observed that similar behavior occurs in all the 200 runs. The uncertainty of the input parameters impacts the internal pressure value at the beginning of the transient and mostly keeps the same behavior during the transient until the failure time. Nevertheless, there is not a single case which predicts cladding failure later than observed (at around 300 s considering that LOCA starts at 100s).

The heatmap with the sensitivity analysis results is provided in Fig. 7 (see also Table 2). The PRCC is presented for each input parameter versus each output variable. Accordingly, a general PRCC is obtained for three major behaviors: fuel thermal, cladding thermal and mechanical (3 rows in the upper part of the heatmap).

From Fig. 7 it is observed that the uncertainties in clad-to-coolant heat transfer coefficient (htcua), coolant temperature (refrit) and relative power during test (pott) input parameters, govern the fuel thermal behavior (FT) uncertainty. Nevertheless, fuel gaseous swelling model

(fgsm), fuel thermal conductivity model (fcd) and cladding annealing (clan) uncertainties also affect.

Regarding the cladding thermal behavior (CT), the most influencing parameter in addition to those governing fuel behavior (htcua, refrit and pott), is the clad corrosion model during steady state operation (oxx). Besides, relative power during base irradiation (pobi) and fuel gaseous swelling model (fgsm) also produce some effect on outputs.

Finally, the mechanical behavior (M) is mainly affected by the cladding outer diameter (od) and base irradiation cladding corrosion model (oxx), and with a noticeably lower impact, filling gas pressure (nm) and coolant temperature (refrit).

TABLE 2. NOMENCLATURE USED IN SENSITIVITY ANALYSIS (FIG. 7).

fd	pellet outside diameter	od	cladding outside diameter correlation
id	cladding inside diameter	td	fuel theoretical density
nm	filling gas pressure	pott	relative power during test
perfil	test rod power profile	pgat	plenum gas temperature
refrit	coolant temperature during test	htcua	clad-to-coolant heat transfer coefficient (test)
en	U^{235} enrichment	pobi	relative power during base irradiation
oxx	cladding corrosion model during base irr.	hpf	clad hydrogen pickup fraction during b.i.
fcd	fuel thermal conductivity model	ccd	clad thermal conductivity model
ftex	fuel thermal expansion model	ctex	clad thermal expansion model
cys	clad Yield stress	hec	fuel heat capacity
clelm	cladding elastic modulus	cheh	cladding heat capacity
oxxi	clad oxidation model at high temp.	oxxt	thermal conductivity of the oxide layer
lgfi	FGR (or gas diffusion coefficient)	fdem	fuel densification model
fssm	fuel solid swelling model	fgsm	fuel gaseous swelling model
cmey	cladding Meyer hardness	clan	cladding annealing
ggco	gap gas conductivity	fcem	fuel/cladding emissivity
frr	fuel radial relocation	cbc	cladding burst strain criteria
cbc0	cladding burst criteria	FT	fuel thermal behavior
CT	cladding thermal behavior	M	mechanical behavior
RIP	rod internal pressure	TFc	fuel centreline temperature
TFo	fuel Surface temperature	PCTi	cladding inner side temperature
PCTo	cladding surface temperature	TOL	clad outsider oxidation layer thickness
ECR	equivalent cladding reacted	DCo	cladding outside diameter
CES	cladding effective stress	ECT	cladding elongation
EFT	fuel elongation		

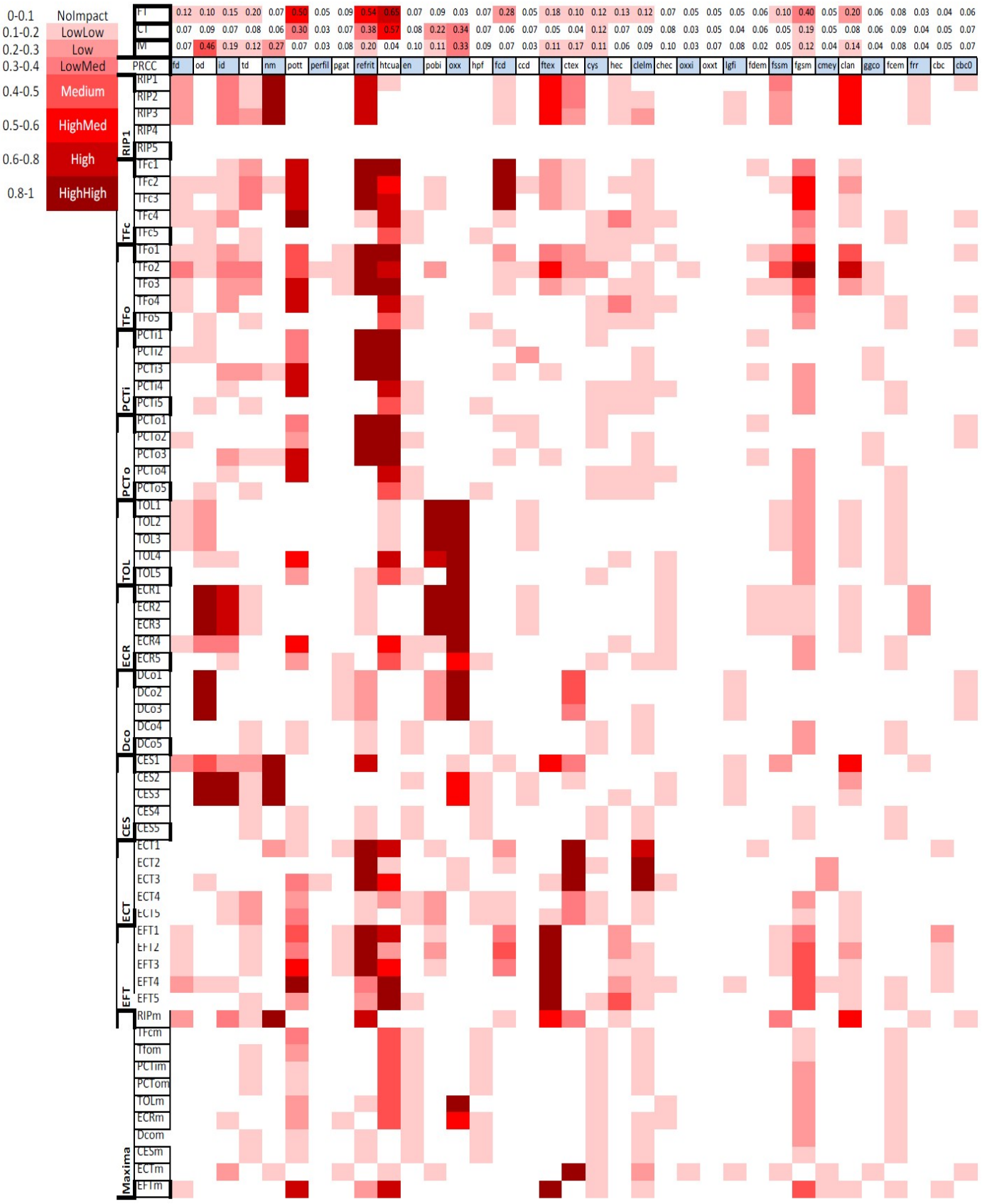

FIG. 7. Sensitivity analysis results. PRCC for each input (column) versus each output (row).

3. STUDSVIK

The US NRC program for LOCA integral tests at the Cell Laboratory of Studsvik Nuclear AB in Sweden included six experiments. The objective of this experimental campaign was to assess the mechanical behavior of ballooned and ruptured high-burnup fuel rods. Among these six experiments, the ones considered under the FUMAC framework by CIEMAT are the 192 and 198 tests [11].

3.1. Facility and device

Once the mother rod had been irradiated a certain number of cycles in a nuclear reactor until high burnup was reached, it was refabricated into a rodlet of about 30 cm. The rodlet was then pressurized and subjected to a temperature transient in a steam environment, as shown in Fig. 8. By doing so, ballooning, cladding failure and high-temperature steam oxidation were induced. In contrast with the Halden reactor facility, in this case there is no fission heat, but just a furnace to set the desired environmental temperature by infrared radiation. Instrumentation for clad temperatures (thermocouples) and pressure (transducers) were used.

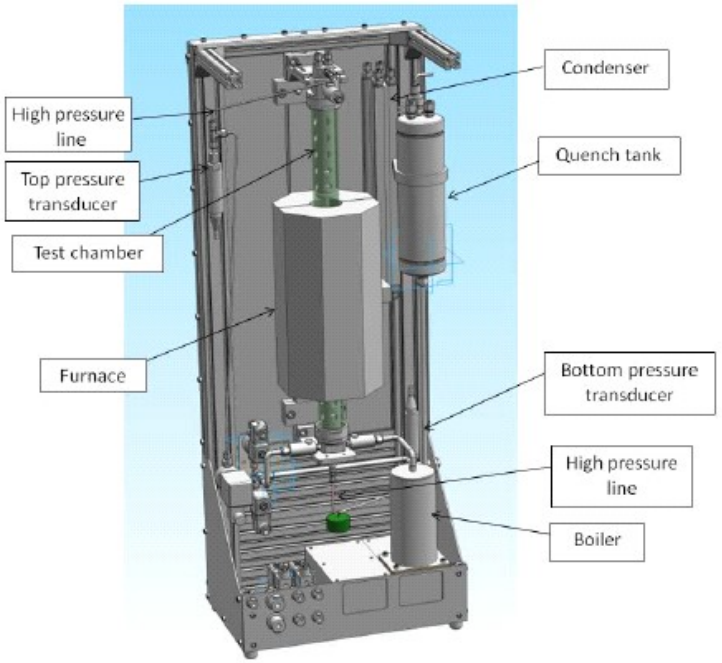

FIG. 8. Schematic view of the test facility [11].

The test procedure was as follows:

— Conditioning phase (several hundreds of seconds), in which the rodlet was brought to about 82 bar and 300 ºC;
— Checking phase (about 200 s), in which readings from pressure transducers located at low and high positions were compared to know about potential gas communication between these locations;
— Heat-up phase (about 200 s), in which temperature ramped from 300ºC to PCT ad ballooning and cladding failure occurred;
— Quenching phase (hundreds of seconds), in which heaters were turned off and temperature decreased.

3.2. Modeling

The steady-state irradiation has been simulated with FRAPCON-3.5 to obtain the restart file for FRAPTRAN. At the end of the base irradiation, some variables have been checked out before simulating the transient and estimates have been compared to data:

- The burnup reached has been confirmed to agree with data in both father rod (68.2 vs. 68.15 MWd/kgU estimated for 192 test; 55.2 vs. 55.23 MWd/kgU estimated for the 198 test) and rodlet (72 vs. 72.9[10] MWd/kgU estimated for the 192 test; 55 vs. 55 MWd/kgU estimated for the 198 test) whenever power got reduced about 8% with respect to the one prescribed[11] (192 test). The in-clad hydrogen has been well estimated by FRAPCON (176-288 vs. 300 wtppm estimated for 192 test; 225 vs. 200 wtppm estimated for 198 test);
- The oxide thickness has been also consistently predicted by FRAPCON (25-30 vs. 30 microns estimated for 192 test; 20 vs. 20 microns estimated for 198 test);
- The internal pressure and temperature at EOL has been reasonably predicted (about 81 bar at 300 ºC predicted and 82 bar at 307 ºC as data).

It is worth noting that no axial power profiles are available, so that a generic one [8] has been adopted for the 192 test and a flat one for the 198 (due to the fact that the same burnup value was found in the mother rod and the rodlet).

After the mother rod has been simulated, another run is performed for the rodlet base irradiation with FRAPCON, and finally FRAPTRAN-1.5 has been used for the transient modeling.

The number of axial nodes is 14 and 25 and 5 for the radial direction in the fuel and cladding, respectively. Besides, since there is not heat generated by fissions, it has been simulated a zero power history and the desired cladding temperature has been reached by setting that specific temperature as the coolant one and imposing a very high HTC ($9 \cdot 10^6$ W/m^{2}K). In other words, test modeling has been based on a nearly perfect thermal match to data. The coolant temperatures at different heights have been calculated using the information provided in the Excel file containing axial temperature profiles.

A key modeling aspect concerns deformation. The mechanical modeling of fuel rod in the Studsvik tests was similar than in the Halden cases; that is, large deformation term introduced in the Prandtl-Reuss equation in the FRACAS-I model.

3.3. Results

The data to be compared to predictions are: cladding temperature evolution (and rupture temperature), internal pressure evolution (and rupture pressure), ECR, maximum plastic hoop strain. Fuel dispersal is not compared because FRAPTRAN does not model it. It is worth mentioning that the cladding thermocouple is placed 5 cm above the axial mid plane (nodes 9 and 10 in the modeling), so the data-code comparison will be accordingly performed.

3.3.1. The 192 test

The predicted cladding temperature is presented for comparison to data in Fig. 9.

---

[10] For the 192 test, an average rodlet burnup of 78 MWd/kgU was estimated according to the information provided by NRC. Nevertheless, a value of 72 MWd/kgU was found in *'Observations of Fuel Fragmentation, Mobility and Release in Integral, High-Burnup, Fueled LOCA Tests'* (M.Flanagan and P.Askeljung)

[11] For the 192 test, the linear heat rate history has been taken from N-05/133 Rev1 Studsvik-SCIP-22 rather than from the information provided by NRC.

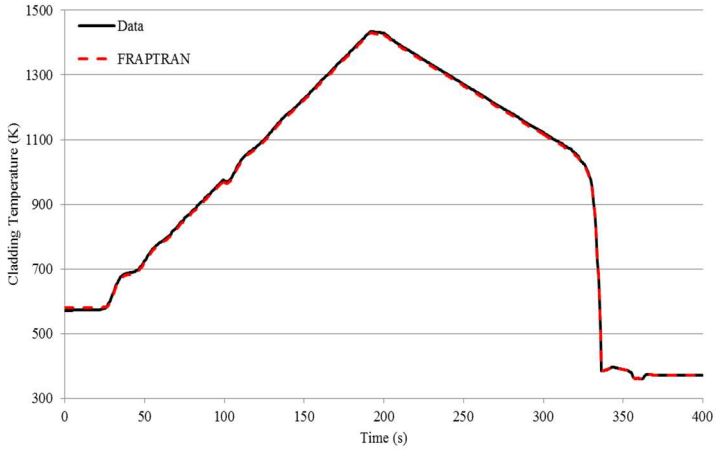

FIG. 9. Cladding temperature in the Studsvik 192 test.

As said above, the measured cladding temperature has been used to calculate the coolant temperatures at different heights and have been input together with a HTC high enough to allow a perfect heat transfer. As a result, the predicted cladding temperature perfectly matches measurements, as expected.

Fig. 10 shows the internal pressure prediction and data for the 192 test.

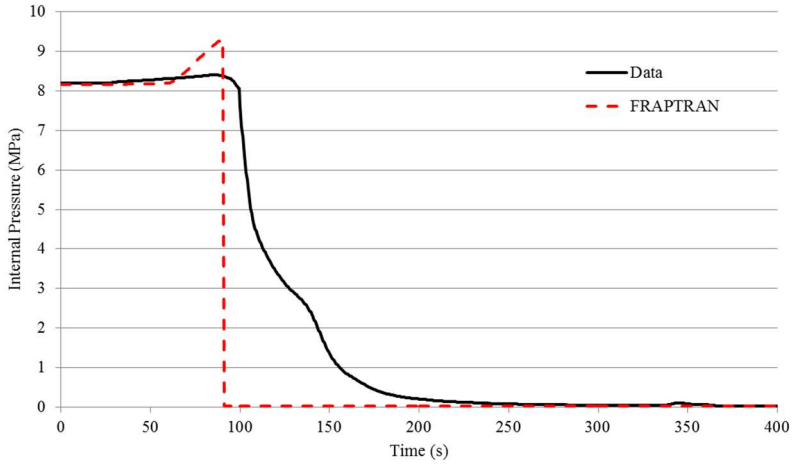

FIG. 10. Internal pressure in the Studsvik 192 test.

It is observed that the pressure trend shows a noticeable discrepancy with respect to data from 60 to 100s (fail). Calculations estimate a fast pressure rise (0.3 MPa/s), while data indicate a soft increase (0.025-0.05 MPa/s); failure time, though, are not too different. From that point on, the cladding has failed and FRAPTRAN does not model the gas leakage through the burst hole. Thus, just the 60-100 s discrepancy is relevant for this analysis and not after failure (as in the Halden tests). Going deeper in data analysis, one may observe that the internal pressure remains at nearly constant value from 60 to 90s. In other words, either the plenum temperature experienced just a slight variation with furnace heat up or any temperature rise is compensated by a free volume growth. Given that temperature measurement slope hardly changed from 25 s till some 90 s, it has been postulated that plenum temperature change during this period was certainly slow. This insight is contrary to what FRAPTRAN predicted through the thermal hypotheses described above. Thus, a second FRAPTRAN calculation was intended in which plenum heat up from 25 s on has been imposed by changing the FRAPTRAN algorithm to estimate the plenum temperature by:

$$T(t) = T(t-1) + \frac{dP}{dT} \cdot \Delta t \quad (4)$$

where *T(t)* is the plenum temperature at time *t*, *T(t-1)* is the plenum temperature at time *t-1*, *dP/dT* is the pressure slope found in the measurements and *Δt* is the time step used by FRAPTRAN. This equation assumes that pressure variation is just driven thermally; in other words, no significant volume change from 25 s to 90 s, roughly. The result when doing so in terms of pressure can be seen in Fig. 11. This means that the deviation in pressure observed with the initial thermal modeling was an artefact of the thermal modeling and a better one would produce a pressure signature rather similar to the experimental one, except that failure time seems not to improve significantly with respect to earlier predictions (worth mentioning that no FGR is estimated by FRAPTRAN). This observation is interpreted as a consequence of the fast deformation and subsequent failure of the rodlet that is not too affected by the internal pressure on the cladding and it is much more dependent on the local temperature at the spot at which failure occurs.

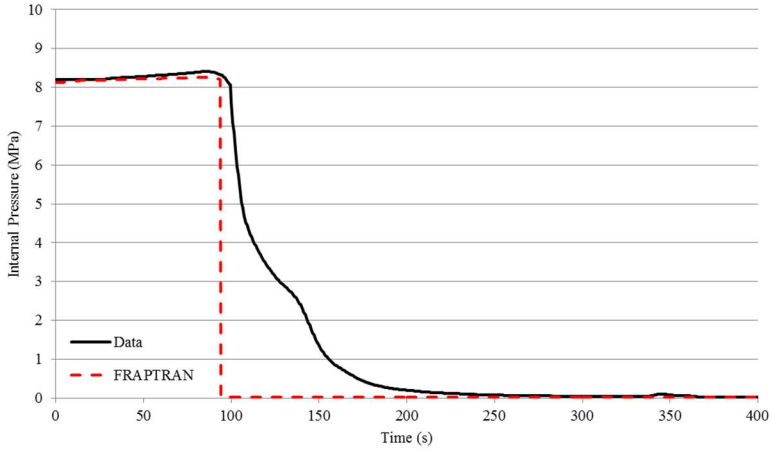

FIG. 11. Internal pressure in the Studsvik 192 test with plenum temperature assumption.

Fig. 12 shows how FRAPTRAN estimates the clad deforms circumferentially: less than about 5 s till reaching the failure strain; the fast deformation to failure is consistent with the form of internal pressure data in terms of the short time period in which clad deformationstarts (approximated as the pressure maximum time) and the clad failure time.

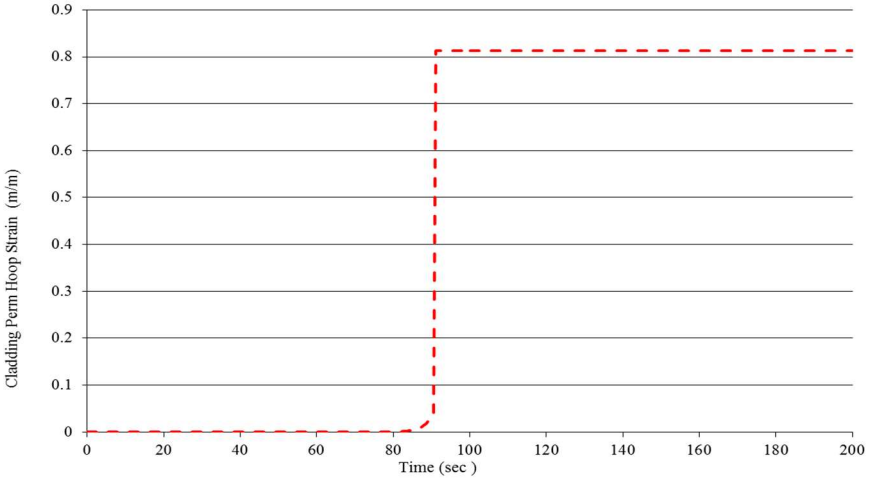

FIG. 12. Estimated cladding hoop strain in the Studsvik 192 test.

Table 3 below summarizes the 192 results. It is worth noting that the difference in the burst time leads to the cladding temperature discrepancy observed.

TABLE 3. 192 TEST RESULTS.

	Data	Prediction
Cladding temp evolution	✓	✓
Cladding temp at fail	973 K	947 K
Pressure evolution	✓	✓
Pressure at fail	8.4 MPa	8.2 MPa
ECR	11 %	12 %
Maximum strain	53 %	

FIG. 8

3.3.2. The 198 Test

The predicted cladding temperature is sown in Fig. 13. As in the 192 test, it accurately follows measurements. Fig. 14 presents internal pressure predictions and data.

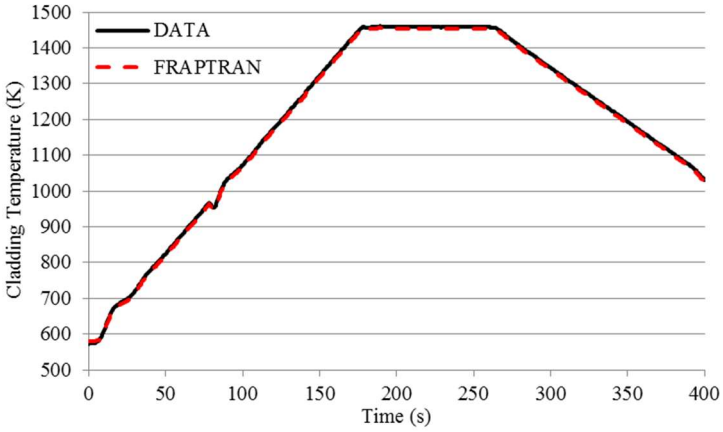

FIG. 82. Cladding temperature in the Studsvik 198 test.

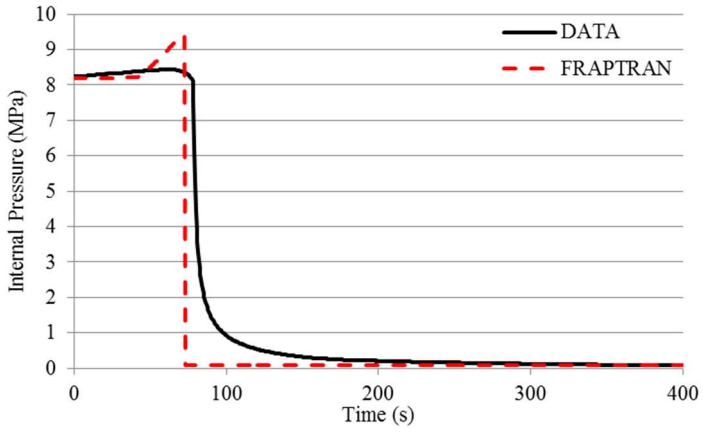

FIG. 83. Internal pressure in the Studsvik 198 test.

Again, by applying the same approximation for the plenum temperature as the one described in the previous section, FRAPTRAN consistently follows pressure data (Fig. 15), which confirms that most of pressure evolution is governed thermally and just at the end of the transient volume transients through cladding deformation plays a role.

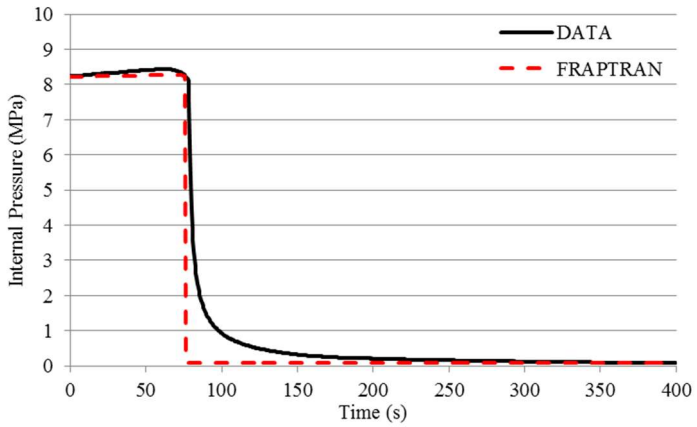

FIG. 84. Internal pressure in the Studsvik 198 test with plenum temperature assumption.

Finally, the strain deformation predicted by FRAPTRAN (Fig. 16) also looks consistent with what might be derived from the pressure data evolution, as discussed above.

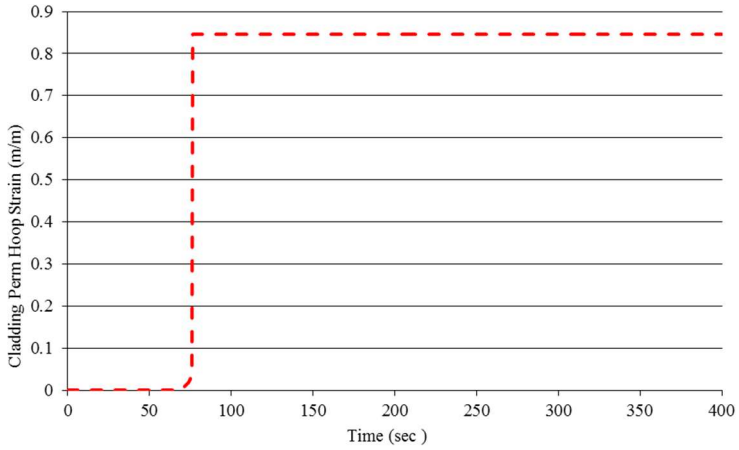

FIG. 85. Cladding hoop strain at the ballooning node in the Studsvik 198 test.

The results for this 198 Studsvik test are presented in Table 4.

TABLE 4. 198 TEST RESULTS.

	Data	Prediction
Cladding temp evolution	✓	✓
Cladding temp at fail	967 K	952 K
Pressure evolution	✓	✓
Pressure at fail	8.5 MPa	8.3 MPa
ECR	15 %	16 %
Maximum strain	25 %	84 %

Note that the temperature difference at failure is a consequence of the shifting to longer times of rodlet failure.

As a brief summary for the Studsvik tests modeling, it has been observed that the thermal modeling in FRAPTRAN mostly govern the transient evolution and that clad deforms and fails in quite a short time period. Thus, this emphasizes that traditional FRAPTRAN assumptions for plenum temperature (i.e., $T_{plenum}(t) = T_{coolant}(t) + 5.6\text{K}$) are not applicable to experimental scenarios in which coolant is an unpressurized quiescent gas heated up in a furnace. However, a more reasonable thermal modeling allows a transient description good enough.

— MTA EK

The Hungarian Academy of Sciences Centre for Energy Research (MTA EK) performed a ballooning studies campaign. It consisted of 7-bundle tests and single rod (integral) tests [12, 13]. Among the integral ballooning tests, the PUZRY series has been released in the FUMAC framework.

4.1. Facility and device

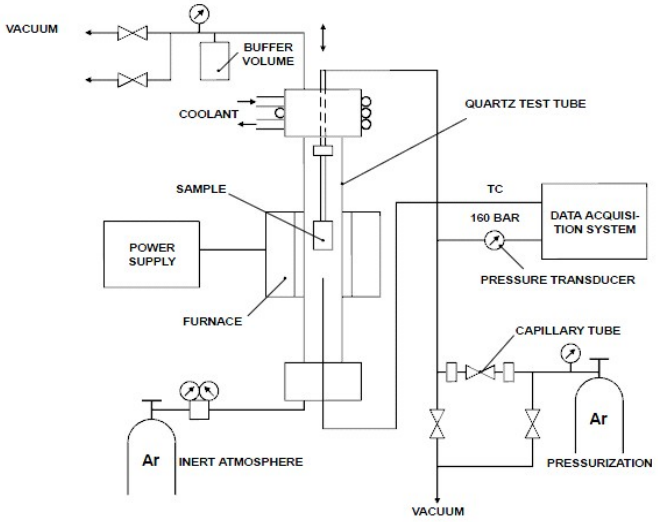

FIG. 86. Cladding hoop strain at the ballooning node in the Studsvik 198 test [12, 13].

The PUZRY series was performed with 31 PWR Zr-4 tubes to provide data for comparative analyses. The test entailed a linear operator-defined pressure ramp under isothermal conditions for each test. The included instrumentation is a pressure sensor and a temperature sensor (Fig. 17).

Six PURZY tests have been simulated by CIEMAT, temperatures ranging from 700 to 1200 ºC. The selected tests, in ascending temperature order, are:

— PUZRY 26 – 700 ºC – 0.119 bar/s;
— PUZRY 30 – 800 ºC – 0.2663 bar/s;
— PUZRY 18 – 900 ºC – 0.115 bar/s;
— PUZRY 8 – 1000 ºC – 0.076 bar/s;
— PUZRY 10 – 1100 ºC – 0.071 bar/s;
— PUZRY 12 – 1200 ºC – 0.072 bar/s.

4.2. Modeling

Since these tests are conducted without a previous steady-state irradiation, FRAPTRAN is the only code used.

The number of radial nodes is 25 and 5, respectively, for fuel and clad (the same as in the Studsvik cases). Nine axial nodes are considered axially. The cladding tubes (5 cm high, 10.75 mm diameter and 0.725 mm thick) do not contain fuel pellets inside. In order to accommodate this in FRAPTRAN, two major approximations are necessary: on one side, a small enough pellet diameter (0.2 mm) has been set in the input deck, so that the pellet did not affect the results; on the other, zero power has been set and the test temperature and internal pressure ramping have been imposed as it occurred in the test. The same strategy has been adopted with springs, providing values as low as 8 mm for the outer spring diameter and 0.2 mm for wire diameter. The results sensitivity to these two assumptions has been tested through a set of parametric cases changing the diameters given and no remarkable change has been found.

4.3. Results

Given the instrumentation in these tests, comparisons set are restricted to internal pressures (temperature is set in the input deck) and similarities and/or differences discussed in terms of failure time.

4.3.1. PUZRY 8, 10, 12, 18, 26, 30

Fig. 18 presents the results for all the PUZRY tests. It is observed that the cladding is estimated to fail always earlier than observed. It is observed that, the larger pressurization velocity is, the higher pressure is reached. Besides, the lower temperature test is, the longer time takes for the cladding to fail and higher pressure is reached. As in the tests from the Halden and Studsvik facilities, the predicted cladding failure is earlier than observed for all PUZRY tests.

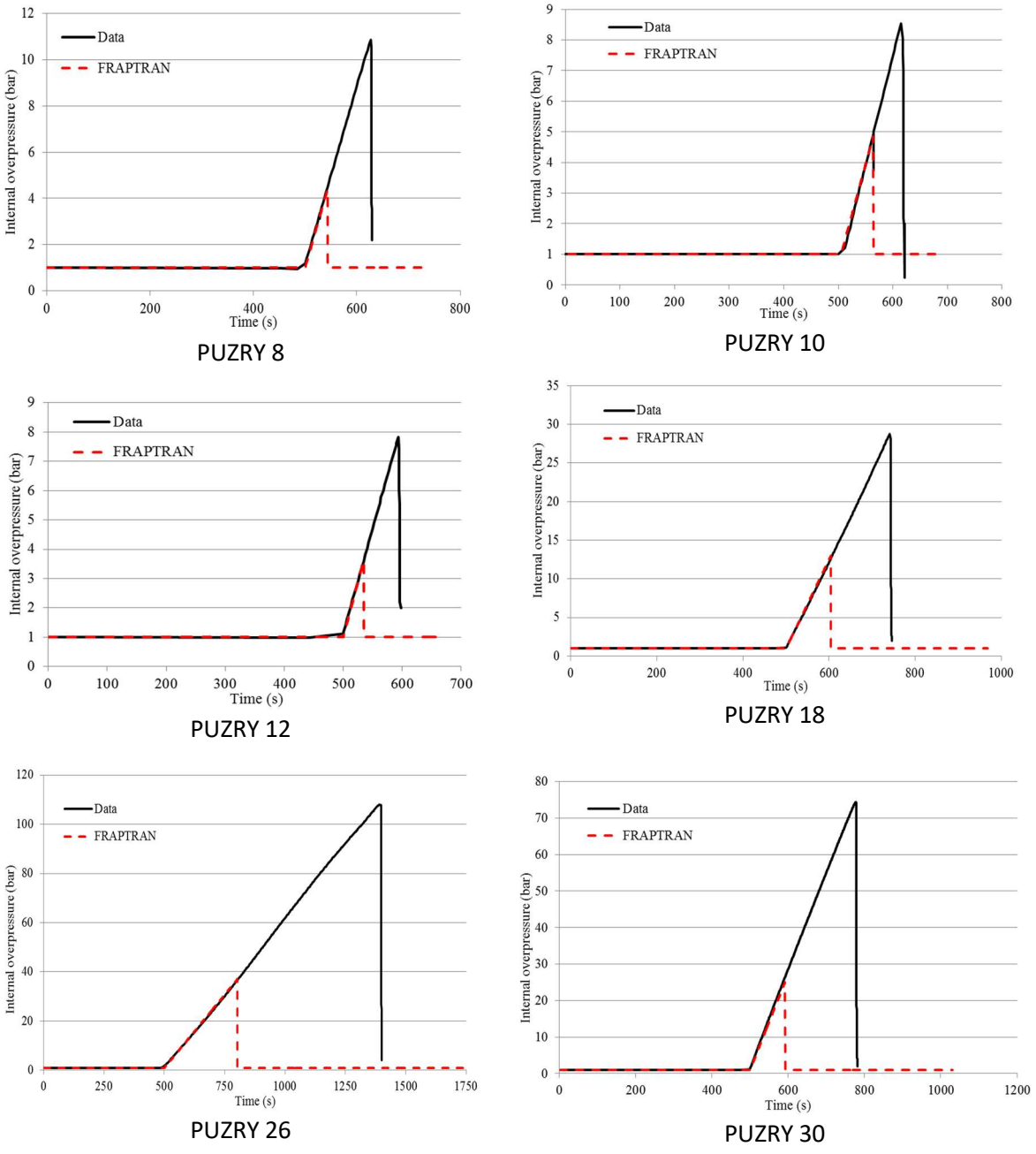

FIG. 87. Internal pressure for the different PUZRY tests simulated.

In order to assess the differences in terms of failure times, Fig. 19 presents the burst time for each test (the first steady 500 s are not considered as transient).

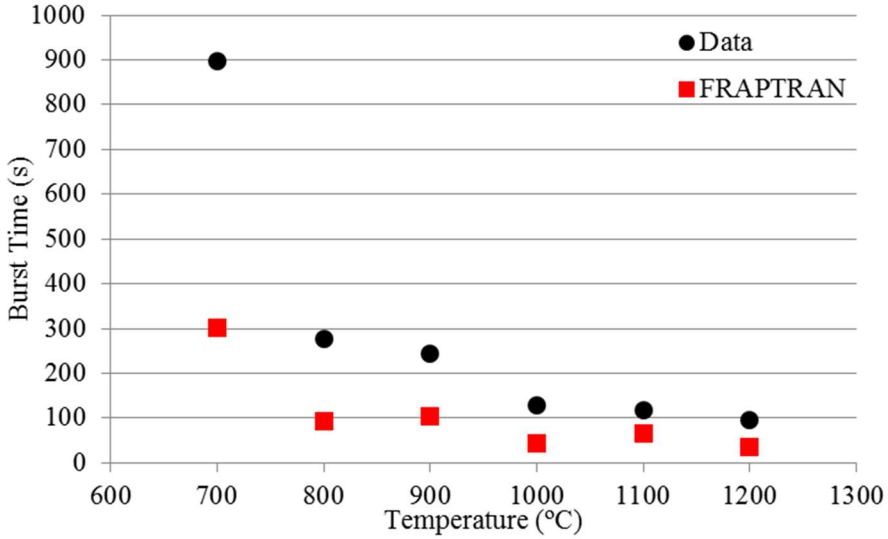

FIG. 88. Cladding hoop strain at the ballooning node in the Studsvik 198 test.

As in the case of Studsvik tests, PUZRY experiments pose a scenario far from the design bases of the FRAPTRAN heat transfer modeling, so that a parametric exercise was conducted to explore the results sensitivity to the internal thermal state of the rodlet. In other words, what if for any unknown reason the gas in the rodlet hadn't reached a thermal equilibrium with the furnace? The study scope was restricted to tests 12 and 26 and it yielded the results shown in Fig. 20. As observed, the time to failure is sensitive to temperature, particularly in the case of Test 12 in which at some point failure time doubles at a certain temperature; in both cases, below 60-80 ºC from the thermal equilibrium with the furnace temperature, the rodlet is not even predicted to fail (i.e., $t_{fail} \rightarrow \infty$)e. This fact might be related to several factors from the thermal state of the clad on the spot to the failure criterion that is poorly correlated with temperature.

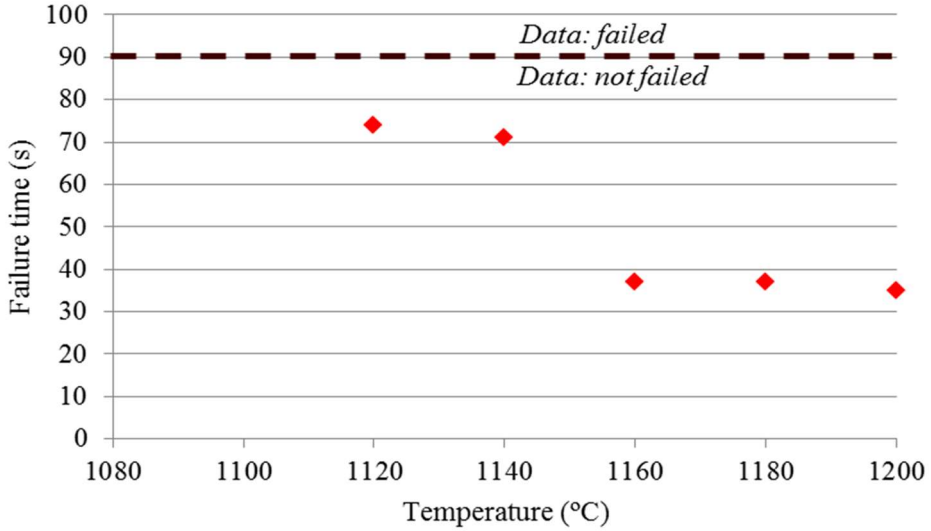

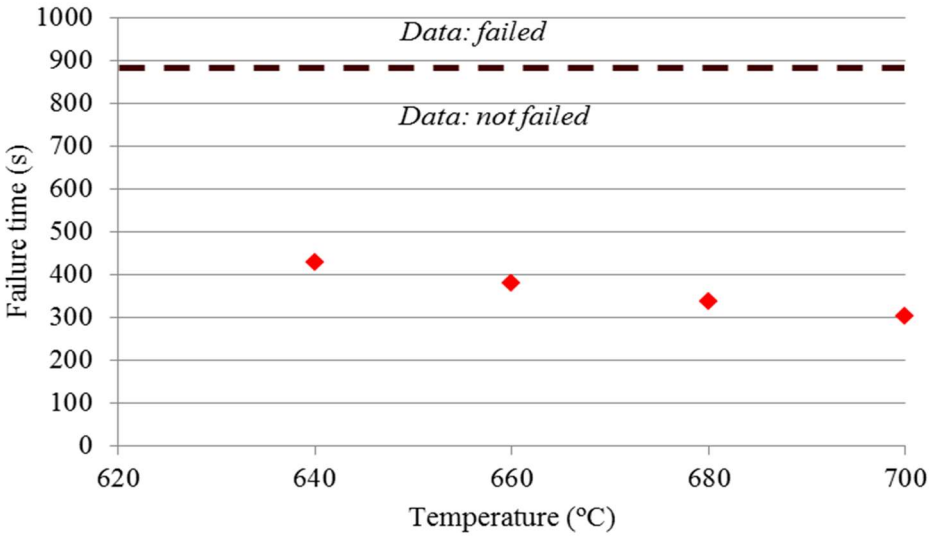

FIG. 89. Parametric cases for PUZRY 12 (top) and 26 (bottom).

4. FINAL REMARKS

This report presents the modeling and analysis results with FRAPCON-3.5 and FRAPTRAN-1.5 for the Halden LOCA tests IFA-650.9 and .10, the Studsvik tests 192 and 198, and the MTA EK tests PUZRY 8, 10, 12, 18, 26 and 30.

Thermal modeling plays a key role for different reasons in all the simulated scenarios. As a common feature, a deep knowledge of the test protocol, the code architecture and major hypotheses underneath are mandatory to properly use the code flexibility, either by adapting the input deck or by modifying the source code. In short, sometimes experimental setups pose challenges that the modeller should be aware of and that require skills beyond systematic running of the tool. Adoption of the right hypotheses may enhance notably FRAPTRAN performance, as shown in the case of IFAs, and can highlight results sensitivity that can to some extent explain discrepancies found, as in the case of the Studsvik's and MTA's tests.

FRAPTRAN mechanical modeling may require some revision leading to the inclusion of large cladding strain in the Prandtl-Reuss equation, according to the findings got in the IFAs modeling. Nonetheless, the work done is just in an initial state and should be further developed before extending the comparison to other LOCA experiments. On the other hand, experimental analyses have shown that large strains might happen in rather short time periods (5 to few tens of seconds) and would be strongly dependent on local temperature, so that with the modifications made in the mechanical model the time-to-failure estimates might be considered good enough for such a purpose. In addition, the uncertainty associated to the failure limits (stress and strain) used by FRAPTRAN makes potential rod failure quite sensitive to such thresholds, although it does not strongly affect time-to-failure because of the fast transient from large deformation to rod failure.

Despite what said in the previous paragraphs, further validation would be needed to soundly confirm the statements made

REFERENCES

[1] EK, M., 2005. 'LOCA testing at Halden, the second experiment IFA-650.2' HWR-813 (OECD Halden Reactor Project).

[2] DU CHOMONT, F.B., 2009 'LOCA testing at Halden, the ninth experiment IFA-650.9' HWR-917 (OECD Halden Reactor Project).

[3] LAVOIL, A., 2010. 'LOCA testing at Halden, the tenth experiment IFA-650.10' HWR-974 (OECD Halden Reactor Project).
[4] WIESENACK, W., 2013. 'Summary of the Halden Reactor Project LOCA Test Series IFA-650' OECD HRP report HRP-380.
[5] MANNGÅRD, T., MASSIH, E., STENGRD, J-O., 2014. 'Evaluation of the Halden IFA-650 loss-os-coolant accident experiments 2, 3 and 4' report number 20104:18 ISSN:2000-0456.
[6] VALLEJO, I. AND HERRANZ, L.E., 2014. 'Halden LOCA Tests: Simulations of IFA-650.3, .5 and .10 with FRAP Serie Codes. Preliminary results and Comparison to experimental Data' EHPG 2014 (OECD).
[7] HERRANZ, L.E. AND PELÁEZ, S.B., 2016. 'Assessment of FRAPTRAN-1.5 Capabilities for Clad-to-Coolant Heat Transfer under Loss of Coolant Accidents' EHPG 2016 (OECD).
[8] O'DONNELL, G.M., SCOTT, H.H., MEYER, R.O., 2001. 'A New Comparative analysis of LWR Fuel Designs' NUREG-1754.
[9] PELÁEZ, S.B. AND HERRANZ, L.E., 2017. 'Assessment of FRAPTRAN Modeling of Large Strains under Loss of Coolant Accidents' WRFPM 2017.
[10] DI MARCELLO, V. et al, 2014. 'The TRANSURANUS mechanical model for large strains analysis', Nucl. Eng. Des., 276, (2014) 19–29.
[11] FLANAGAN, M.E., Askeljung, P., Puranen, A., 2013. 'Post-Test Examination Results from Integral, High-Burnup, Fueled LOCA Tests at Studsvik Nuclear Laboratory', U.S. Nuclear Regulatory Commission report NUREG 2160.
[12] HÓZER, Z., GYÓRI, C., HORVÁTH, M., NAGY, I., MARÓTI, L., MATUS, L., WINDBERG, P., FRECSKA, J., 2005. 'Ballooning experiments with VVER cladding', Nuclear Technology 152 (2005) 273–285.
[13] PEREZ-FERÓ, E., GYÓRI, C., MATUS, L., VASÁROS, L., HÓZER, Z., WINDBERG, P., MARÓTI, L., HORVÁTH, M., NAGY, I., PINTÉR-CSORDÁS, A., NOVOTNY, T., 2010. 'Experimental database of E110 cladding exposed to accident conditions', J. Nucl. Mater. Volume 397, Issues 1–3 (2010) 48–54.

IMPROVING THE FRAPTRAN PROGRAM FOR FUEL ROD LOCA ANALYSES BY NOVEL MODELS AND ASSESSMENT OF RECENT DATA

LARS OLOF JERNKVIST, ALI MASSIH
Swedish Radiation Safety Authority (SSM),
Solna strandvag 96,
17116 Stockholm, Sweden.

Quantum Technologies AB
Uppsala Science Park
SE-75183 Uppsala, Sweden
Email: loje@quantumtech.se

Abstract

This report summarizes work conducted by Quantum Technologies from 2014 to 2017 within the IAEA Coordinated Research Project FUMAC – Fuel Modelling in Accident Conditions. The main objective of the work is to improve an in-house version of the FRAPTRAN computer program, henceforth referred to as FRAPTRAN-QT-1.5, for thermal-mechanical analyses of light water reactor nuclear fuel rods under loss-of-coolant accident (LOCA) conditions.

1. INTRODUCTION

The work was carried out by Quantum Technologies under contract with the Swedish Radiation Safety Authority (SSM) and can be divided into three tasks:

The first task involves development, implementation and verification of a set of models for axial relocation of fuel fragments and its effects on the fuel rod heat load and failure processes during LOCA. The fuel relocation is calculated on the basis of estimated fuel fragment size distributions and the calculated cladding distension along the fuel rod, and its effects on the axial redistribution of stored heat and power are accounted for in thermal-mechanical analyses of the fuel rod. Hence, the new models are integrated with FRAPTRAN-QT-1.5 and make it possible to consider thermal feedback effects from the fuel relocation.

In the second task of the project, a number of existing criteria for cladding high temperature rupture, combined with high-temperature material models that are specific to FRAPTRAN-QT-1.5, are assessed against a large data base of high temperature burst tests on various cladding materials. The objective is to review and systemise burst test data that are available in open literature and, by use of these data, identify suitable rupture criteria that work well together with the aforementioned set of cladding material models in FRAPTRAN-QT-1.5.

In the third task, integral LOCA simulation tests on short-length fuel rodlets with high burnup are used to validate FRAPTRAN-QT-1.5, including the newly developed models. The considered tests are the Halden IFA-650 LOCA tests number 4, 9, 10 and 14, as well as the NRC-Studsvik LOCA test number 192. Three of these tests exhibited significant axial relocation of fragmented fuel and four of them resulted in cladding failure by high temperature ballooning and burst. Hence, the selected tests are particularly well suited for validating the aforementioned relocation models and the cladding rupture criteria.

The report summarizes the work in the aforementioned tasks and the main results are presented and discussed. We also address the transferability of the results, i.e. the relevance of findings from the experiments as well as the computer analyses to the behaviour of prototypical, full-length, fuel rods under conditions expected in light water reactor LOCA.

Suggestions are also made for future experiments, model improvements and further computational analyses.

1.1. Background

Loss-of-coolant accidents (LOCAs) in light water reactors (LWRs) may lead to over-heating of the fuel rods, which in turn may lead to distension of the internally overpressurized cladding tubes and to loss of cladding ductility by high temperature oxidation of the material. To maintain structural integrity of the fuel and to ensure that the reactor core remains coolable, the cladding temperature and oxidation should not transgress certain limits [1]. Specifically designed computer programs are used for confirming that these acceptance criteria are met for postulated accident scenarios. A widely used program for thermal-mechanical analysis of LWR fuel rods under accident conditions is FRAPTRAN [2], developed and maintained by the Pacific Northwest National Laboratory (PNNL), USA.

Since 2010, Quantum Technologies has been contracted by the Swedish Radiation Safety Authority (SSM) for various research tasks on the behaviour of LWR fuel under LOCA conditions. These tasks involved development of high-temperature material models for analysis of the fuel rod thermal-mechanical behaviour under LOCA conditions [3, 4], implementation of the models in an extended version of FRAPTRAN, and application of this computer program for evaluation of recent in-reactor LOCA tests, carried out within the IFA-650 test series in the Halden Reactor, Norway [5]–[7].

1.2. Objectives and scope

The research project summarized in this report is a continuation of the aforementioned work for SSM. The project is aimed to further improve the capacity of our extended version of FRAPTRAN, henceforth referred to as FRAPTRAN-QT-1.5, for analysing the behaviour of LWR fuel rods under LOCA conditions. The objectives will be reached by introducing novel models in the computer program, followed by extensive assessment of the program against experimental data.

More specifically, the project focuses on some poorly understood aspects of the thermal-mechanical behaviour of high burnup fuel under LOCA. Phenomena of particular interest are the fine fragmentation ("pulverization") observed in LOCA simulation experiments on high burnup fuel [8], the axial relocation of finely fragmented fuel and the thermal effects that this relocation may bring about. Another objective is to elucidate differences between the Halden and Studsvik experiments with regard to testing conditions, and how these differences may affect the phenomena observed in the experiments. Understanding of these issues is important, not least for assessing to what extent the experiments are representative of conditions expected in commercial light water reactors under LOCA.

The contemplated extensions of the FRAPTRAN-QT-1.5 computer program include newly developed models for fuel pellet fine fragmentation, for axial relocation of the fuel fragments, and for cladding high temperature rupture. The program, including the aforementioned models, will be assessed and calibrated against separate effect tests as well as integral single rod LOCA tests. For the latter kind of tests, emphasis will be placed on recent experiments on high burnup fuel rods in the Halden IFA-650 series. Apart from improving the capacity of FRAPTRAN-QT-1.5, the project is expected to produce a number of models, firmly based on theory and available data, which can be implemented in other fuel rod performance programs as well.

1.3. Original work plan and summary of achieved results

The project comprises three different tasks. According to the original work plan, the tasks were scheduled to be carried out sequentially in the course of FUMAC, with about one year allotted to each task. In the sequel, we summarize the original work plan and the results actually achieved. It should be remarked that each task has been thoroughly documented in public research reports issued by the Swedish Radiation Safety Authority [9]–[11]. The reader is referred to these sources for a more thoroughgoing presentation of the work.

1.3.1. Task 1 (first year): Models related to fuel axial relocation

Original work plan: During the first year of the project, models for fuel fragmentation, pulverization and axial relocation will be formulated and implemented in FRAPTRAN-QT-1.5. The work can be divided into three subtasks, where the first subtask involves formulation of a submodel for fuel fragmentation and pulverization. Existing models will be reviewed, and available data on fuel fragment size-frequency distributions obtained after LOCA tests as well as annealing tests will be evaluated. Attempts will be made to provide a theoretical explanation to the pulverization phenomenon, with the aim to calculate fuel fragment size-frequency distributions based on the pre-LOCA operating history of the fuel. Of particular importance is the influence of fuel burnup.

The second subtask involves the formulation of a submodel for axial relocation of fuel fragments in ballooned fuel rods. This submodel will be linked to the fuel rod temperature calculations in FRAPTRAN-QT-1.5, since the relocation changes the axial distributions of decay power and stored heat during the LOCA. This, in turn, affects the cladding temperature distribution, with subsequent effects on cladding oxidation, deformation and rupture. A few models for fuel axial relocation have been proposed over the years, but these models do not fully consider the aforementioned consequences on the fuel rod temperature distribution. Moreover, they do not consider effects of fuel fragment size-frequency distribution on the relocation phenomenon, e.g. that small fuel fragments are more easily relocated than large fragments and that non-uniform size distributions may lead to higher packing fractions (less void) in regions where fragments accumulate than obtained with uniform size distributions.

In the third subtask, the implemented submodels will be verified with regard to correctness and numerical stability. A preliminary validation of the models against the Halden IFA 650.4 LOCA experiment is also foreseen.

Achievements: The work outlined in the original work plan has been completed and presented at international conferences [12, 13]. A comprehensive research report of the model development has been issued by the Swedish Radiation Safety Authority [9]. The work is summarized in section 2.2.

1.3.2. Task 2 (second year): Criteria for cladding high temperature rupture

Original work plan: During the second year, work will be focussed on criteria for predicting cladding high temperature rupture during LOCA. Several criteria of this kind were proposed in the late 1970's and early 1980's, based on data available at that time from separate effect tests. There is a need for reappraisal of these criteria in light of more recent findings, among other things the effects of pre-LOCA hydrogen concentration in the cladding, which are important for high burnup fuel rods. Moreover, some experimental data are now available for modern cladding alloys. These data may also call for revisions of existing rupture criteria, which are based entirely on data for Zircaloy-2 and Zircaloy-4 cladding. The objective is to systemise data available from separate effect tests on zirconium alloy cladding high temperature rupture, and from that, identify suitable rupture criteria for application in FRAPTRAN-QT-1.5.

Achievements: Existing rupture criteria have been assessed against an extensive experimental data base, comprising both out-of-reactor separate effect tests and integral, in-reactor LOCA tests. The work has been made available to the public through a research report, issued by the Swedish Radiation Safety Authority [10]. Based on the findings of this work, several ways of improving the existing rupture criteria have been identified, and a continuation of the research along these lines has been proposed. However, the task has been discontinued. The work performed so far is summarized in section 2.3.

1.3.3. Task 3 (third year): Model assessment against integral LOCA tests

Original work plan: Work during the third year of the project will be devoted to assessment and validation of the extended FRAPTRAN-QT-1.5 program against integral single rod LOCA tests. In particular, the fuel rods tested in the Halden IFA-650 LOCA experiments 9 to 12 will be evaluated by analyses and simulations with FRAPTRAN, provided that documentation of the tests and their results is made available by the Halden Reactor Project. Since three of these tests have been identified as potential verification cases in the FUMAC coordinated research program, much of the planned work will hopefully be done in cooperation with other FUMAC participants. For example, the sensitivity/uncertainty analysis suggested as part of FUMAC could be an important part of our work. The proposed assessment will be a continuation of earlier work of this kind, carried out jointly by the Swedish Radiation Safety Authority, the Technical Research Centre of Finland (VTT) and Quantum Technologies.

Achievements: An extended version of FRAPTRAN-QT-1.5, which includes the models for fuel fragmentation, pulverization and axial relocation that were developed during the first two years, has been validated against LOCA simulation tests in Halden and Studsvik. More precisely, the tests 4, 9, 10 and 14 from the Halden IFA-650 series and the NRC-Studsvik LOCA test 192 have been used for model validation [11]. Three of these tests belong to the experiments identified within FUMAC as particularly valuable for model validation. Part of the results have been presented at an Enlarged Halden Programme Group Meeting [14]. The contemplated sensitivity and uncertainty analyses have, however, not been pursued. The considered LOCA tests and the applied methodology for simulating them with FRAPTRAN-QT-1.5 are described in section 3, and the results of the model validation against the tests are summarized in section 4.

1.4. Organization of the report

This report summarizes the work in the aforementioned tasks, and the main results are presented and discussed. Section 2 of the report summarizes Tasks 1 and 2 of the project, i.e. the development of computational models related to axial relocation of fuel pellet fragments and the assessment of existing criteria for high temperature cladding rupture against data from separate effect tests. Sections 3 and 4 are devoted to Task 3, i.e. the assessment of integral LOCA simulation tests by use of the computational models. The most important results of the project are finally summarized in section 5, where we also draw some general conclusions from the study and make suggestions for further work.

2. COMPUTATIONAL MODELS

2.1. Applied computer programs

The most important computer program used in this work is FRAPTRAN-QT-1.5, which is an in-house version of FRAPTRAN-1.5 that we have extended with additional and alternative models. In comparison with the standard version of FRAPTRAN-1.5 [2], our extended version of the program contains the following:

- A set of models that treat cladding high temperature metal-water reactions, solid-solid phase transformation, creep and failure in a unified fashion [3, 15];
- A set of models that treat fine fragmentation of high burnup fuel, axial relocation of the fragmented material and thermal feedback effects caused by the relocation. These models, which were developed as part of this research project, are described in section 2.2;
- An extended set of criteria for high temperature rupture of the cladding tube. Three different strain based rupture criteria are available in the standard version of FRAPTRAN-1.5. These criteria are in FRAPTRAN-QT-1.5 supplemented by four stress

based criteria, taken from literature. The criteria are presented and assessed against data from separate effect tests in section 2.3.

In addition to these model extensions, several errors observed in the standard version of FRAPTRAN-1.5 have also been fixed in our version of the program [16]. These errors have been reported to PNNL and corrected in the latest version (2.0) of FRAPTRAN [17].

Since FRAPTRAN is intended for thermal-mechanical analyses of fuel rods under transient conditions only, the computer analyses of the considered Halden IFA-650 and NRC-Studsvik LOCA tests in this report were carried out in two steps.In the first step, the pre-irradiation of each fuel rod segment that was later re-fabricated into a test rodlet was modelled by use of FRAPCON-3.5. More precisely, the pre-irradiation in the relevant nuclear power plant was modelled with the standard version of the program [18], as delivered by Pacific Northwest National Laboratory (PNNL), without introducing any modifications or extensions to the program. The procedure is described in section 3.2.1.

Calculated results from FRAPCON-3.5, defining the pre-test conditions for each test fuel rodlet, were used as input to the second analysis step. This step involved simulations of the LOCA test with FRAPTRAN-QT-1.5. The procedure is described in section 3.2.2.

2.2. Models related to axial relocation of fragmented fuel

2.2.1. Background

Axial relocation of oxide fuel fragments inside distending cladding tubes of LWR fuel rods was first observed about 35 years ago in early in-reactor experiments on fuel rod behaviour during LOCA [19, 20]. Post-test examinations revealed that significant amounts of fuel fragments could relocate downwards by gravity and accumulate in ballooned regions of the test rods, provided that the cladding distension was sufficiently large. These findings raised concern that the relocation would increase the local heat load in ballooned parts of fuel rods, which would then result in higher temperature and faster cladding oxidation than normally considered in safety analyses. However, in a seminal modelling work on axial fuel relocation, Siefken [21] stated that ballooning in most cases would lower the cladding temperature.
The reason is that disorderly stacked, mm-sized, fuel fragments in the ballooned part of the fuel rod have a fairly low packing fraction, which means that the cladding tube diameter has to increase significantly to accommodate additional fuel. As a result, the increase in coolable area caused by the large cladding distension more than compensates for the locally increased amount of hot fuel within the cladding.

Although axial fuel relocation remained an issue among regulators, little attention was paid to the phenomenon until 2006, when a LOCA test (IFA-650.4) on a very high burnup fuel rod in the Halden reactor, Norway, resulted in cladding rupture with concomitant dispersal of a large amount of fuel fragments into the coolant. Subsequent post-test examinations revealed that a large part of the fuel pellet column had been “pulverized” into very fine (< 0.2 mm) fragments, which had relocated axially and been ejected into the coolant through the fairly small rupture opening. This kind of very fine fragments had not been observed in earlier tests, which were limited to fuel rods with burnups lower than 35 MWd/kgU. Later integral LOCA tests [22, 23] as well as separate effect tests [24] have shown that the aforementioned pulverization may occur when UO_2 fuel with a local burnup in excess of about 70 MWd/kgU is overheated. The fine fuel fragments formed by this process seem to have a higher potential for axial relocation and subsequent dispersal into the coolant than the fairly large fuel fragments typically observed in early LOCA tests on low to medium burnup fuel. There is also a concern that the fine fragments may increase the packing fraction of crumbled and relocated fuel in ballooned regions of the fuel rod, which may lead to higher local heat loads than for the coarse fragments typically seen in low burnup fuel.

The observed difference in behaviour between low and high burnup fuel during LOCA has revived interest in the fuel fragmentation, relocation and dispersion phenomena among regulators [8, 25, 26]. In comparison with the 1980s, the regulatory focus has somewhat shifted from the effects of axial fuel relocation on the local heat load to its effects on fuel dispersal upon cladding rupture. The fuel dispersal is a potential issue with regard to radiological consequences and long-term coolability of the material ejected into the coolant.

Along with the recent LOCA tests on high-burnup fuel, computational models have been proposed for the observed fuel relocation [27]–[29]. All these relocation models estimated the extent of fuel fragment relocation based on the cladding distension along the fuel rod, as calculated with fuel rod analysis programs. However, the models were not integrated with these programs, and the effects of relocation on the axial redistribution of fuel mass, stored heat and power were not accounted for in the thermal-mechanical analyses of the fuel rods. In contrast, the computational model for axial fuel relocation presented in this work is implemented as an integral part of FRAPTRAN-QT-1.5, and the model is closely integrated with the solution methods for radial heat transfer in this program. Hence, in contrast to earlier relocation models [27]–[29], our model considers thermal feedback effects from the fuel relocation. Another essential feature of the presented model is that it uses submodels to calculate the packing fraction and effective thermal conductivity of the particle bed formed by crumbled fuel in ballooned regions of the fuel rod, based on the estimated state of fragmentation and pulverization of the fuel pellets. The submodels involved are summarized below. A more complete presentation of the models, including results from verification and assessment, is given in [9].

2.2.2. Axial relocation of fragmented fuel

The submodel for axial relocation of fragmented fuel inside the cladding tube is based on two postulated prerequisites for the relocation. Firstly, a sufficient pellet-cladding gap is required for fuel fragments to detach from the surrounding cladding and move downward. This threshold radial gap size, g^{th}, is set to 0.2 mm in our model, based on results from recent LOCA simulation experiments in Studsvik, Sweden, and Halden, Norway. Post-test examinations of test rodlets used in these experiments show that the local cladding hoop strain must exceed about 5 % to allow fuel fragment separation and axial movement [25, 30]. No observable dependence on fuel pellet burnup is reported for this threshold strain over the investigated burnup range (44–92 MWd/kgU). The threshold pellet-cladding gap size used in our model corresponds to a cladding hoop strain of about 4.5–5.0 %, depending on the cladding tube dimensions. More experiments are needed to determine whether the threshold gap size g^{th} depends on fuel burnup or any other parameter, e.g. the axial gradient in internal gas pressure.

Secondly, the cladding distension along at least one axial segment of the discretized fuel rod must be sufficient to accommodate relocated fuel fragments in a disordered (crumbled) configuration, which is assumed to contain a lot more void volume than the original, pellet-like configuration. In a specific axial segment of the fuel rod, henceforth referred to by subscript *k*, the fuel configuration is defined by the packing fraction of fuel fragments,

$$\phi_k = V_k^f / V_k \tag{1}$$

Here, V_k^f is the volume occupied by fuel fragments and V_k is the total volume enclosed by the cladding tube in the k:th segment. In an axial segment of length L_k, this volume is $V_k = \pi\, L_k R_{cik}^2$, where R_{cik}^2 is the cladding inner radius. Under normal reactor operation, ϕ_k is close to unity, since the fuel fragments are then densely packed and retained in the original, cylindrical configuration of the pellets, where the void volume is made up essentially of pellet dishes, cracks and possibly a narrow pellet-cladding gap. When the cladding tube distends

under LOCA, the gap gradually widens and may reach a size that makes the fuel pellet column collapse. The fuel fragments then move radially outward and turn into a disordered pattern with ϕ_k significantly lower than unity. Here, we make the assumption that local collapse of the fuel pellet column in an axial segment occurs when more fuel can be accommodated in a crumbled configuration than in the original, pellet-like, configuration. This condition on fuel pellet column collapse can be written as:

$$m_k^M = m_k^i \tag{2}$$

where, with $m_k^M = \phi_k \rho_f V_k$, ρ_f being the density of the fuel material, is the fuel mass in the k:th axial segment in case it is completely filled with crumbled fuel, and m_k^i is the initial (as-fabricated) fuel mass in the segment.

The condition defined by Eq. (2) will preclude axial relocation until the cladding tube in some axial segment reaches a threshold deformation, roughly given by $\phi_k R_{cik}^2(t) \approx R_{cik}^2(0)$, where the right-hand-side quantity is the as-fabricated cladding inner radius. In terms of cladding hoop logarithmic (true) strain, $\varepsilon_{\theta\theta}(t) \approx \ln(R_{cik}(t)/R_{cik}(0))$, the condition in Eq. 2 can thus be written

$$\varepsilon_{\theta\theta}(t) > \varepsilon_{\theta\theta}^{th}(t) \approx -\ln(\phi_k)/2 \tag{3}$$

where $\varepsilon_{\theta\theta}^{th}$ can be interpreted as a cladding threshold strain (logarithmic) for fuel pellet column collapse and onset of fuel fragment relocation. This threshold strain is plotted in Fig. 1. It is clear that it is sensitive to the value assumed for the packing fraction of crumbled fuel. We treat the packing fraction of crumbled fuel as a model parameter, which is correlated to the fragment size distribution; see section FIG. 2 below.

Once it occurs, the axial fuel relocation is calculated by a fairly simple algorithm, which comprises two loops over the N axial segments of the discretized fuel rod; see Fig. 2. Henceforth, the segment numbering is assumed to run bottom-up, and subscript k refers to the k:th segment from the bottom. We consider a time step that starts at time t_o, and assume that the fuel mass in each axial segment is known for this point in time. This mass is henceforth denoted m_k^o, whereas m_k denotes the sought fuel mass at end of the time step. In the first loop, the aforementioned requirement on a minimum pellet-cladding gap size for fuel mobility is used for calculating the amount of fuel, m_k^r, that each axial segment may receive from higher elevation segments.

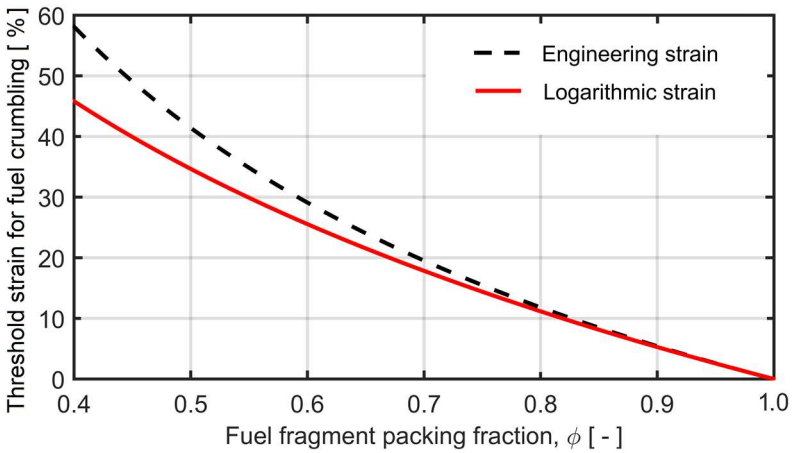

FIG. 1. Cladding hoop logarithmic strain for fuel pellet column collapse and onset of axial fuel relocation, as defined by Eq. 3 For comparison, the relocation threshold is also plotted in terms of engineering strain (relative elongation).

All fuel in an axial segment, except for a small residual fraction x^r, is allowed to fall down if $g_k > g_k^{th}$. The residual fraction represents small fuel fragments that are bonded to the cladding inner surface. Next, the condition from Eq. (3) is applied in the second loop to "fill" ballooned axial segments, according to the calculated crumbled fuel packing fraction and cladding deformation that applies to the segment. Filling is possible only if sufficient moveable fuel is available above the segment, as determined in the first loop. Conditions are also imposed so that the total fuel mass in the rod is conserved and upward relocation precluded. The upper and lower limits for the sought end-of-timestep fuel mass m_k in Fig. 2 are given by:

$$m_k^L = \sum_{j=1}^{k} m_j^o - \sum_{j=1}^{k-1} m_j \tag{4}$$

$$m_k^U = m_k^r + \sum_{j=1}^{k} m_j^o - \sum_{j=1}^{k-1} m_j \tag{5}$$

The cladding deformation, calculated with FRAPTRAN-QT-1.5, is essential input to both loops in Fig. 2, and the relocation model is applied at the end of each time step taken by FRAPTRAN. The calculated results from the relocation model are used by FRAPTRAN-QT-1.5 for modifying the fuel rod temperature calculations in the next time step. Firstly, the changes caused by fuel relocation on the axial distributions of fuel mass, stored heat and power along the fuel rod are accounted for. Secondly, when the fuel pellet column collapses in ballooned segments of the fuel rod, we consider the changes in geometrical configuration as well as effective material properties. The pellet-cladding gap is significantly reduced, while gas-filled voids open up between the disorderly stacked fuel fragments. Since the volume fraction of gas is typically 20–30 %, the macroscopic thermal conductivity of the crumbled fuel in the balloon may be much lower than that of solid fuel material. This conductivity degradation is accounted for in the model, as described in Section 2.2.4.

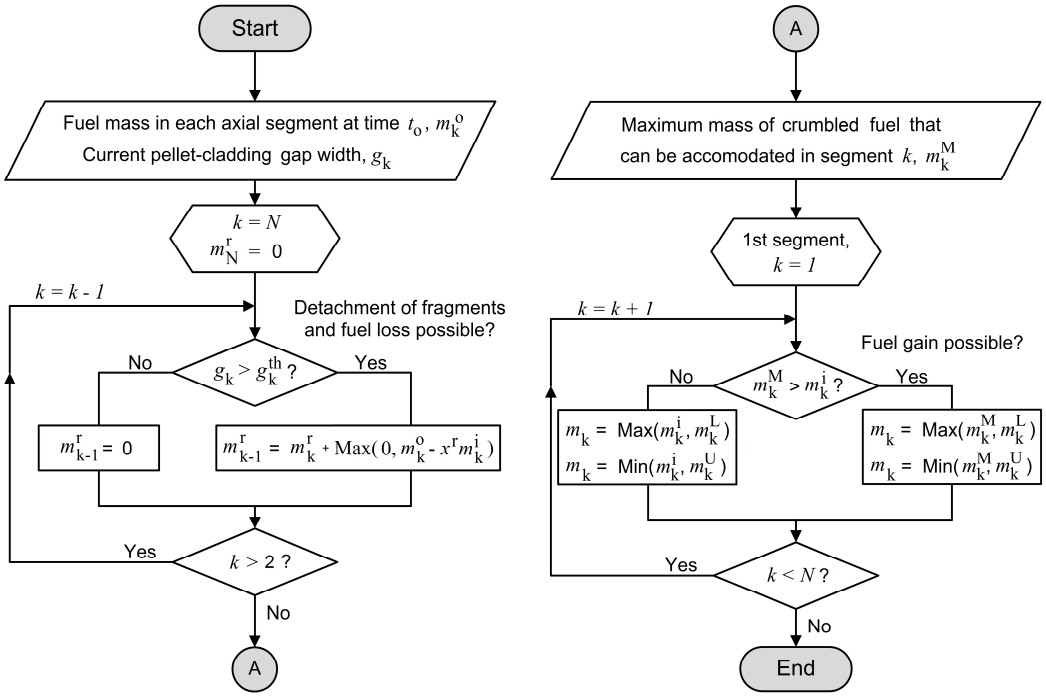

FIG. 2. Computational algorithm. First loop (left) over the N axial segments determines mass of relocatable fuel, m_k^r. Second loop (right) updates local fuel mass, m_k. All variables are defined in the running text.

2.2.3. Packing fraction of crumbled fuel

The packing fraction of crumbled fuel is in our model calculated by use of a simple semi-empirical model, which rests on the assumption that the crumbled fuel consists of two different size classes of fragments: The first class includes mm-size fragments, created by thermal stresses in the fuel during normal operation, whereas the second class comprises fine (< 0.2 mm) fragments, created during the LOCA by overheating high burnup fuel. The second fragment class thus exists only under certain conditions, and a recently proposed empirical 'pulverization threshold' [31] is in our model used for estimating the mass fraction of small fuel fragments, based on the calculated distributions of burnup and temperature in the fuel. The fine fuel fragments are important, since they may effectively fill up voids between the mm-size fragments and thereby significantly increase the overall fragment packing fraction.

Data on the packing fraction of large (mm-size) fuel fragments are available from the early work of Siefken [21], who used gamma scanning and photomicrography to determine the packing fraction of the collapsed fuel pellet column in ballooned parts of eight low burnup fuel rods after in-reactor LOCA tests. The measured packing fractions ranged from 0.62 to 0.79, with an average value of 0.69. Consequently, we use $\Phi^L = 0.69$ in our model, where Φ^L denotes the packing fraction of large fuel fragments that are formed under normal reactor operation. The size of these fragments is typically 2–3 mm, depending on burnup and peak power experienced by the fuel during operation. We use the aforesaid parameters for estimating the characteristic size of large fragments through an empirical correlation [9].

As to the packing fraction of small (< 0.2 mm) fuel fragments, experimental data are currently unavailable. Pulverization by overheating of high burnup fuel is reported to produce fragments over a fairly wide size range; observed fragment sizes typically range from 20 to 200 μm [24]. For this reason, it is likely that the fragment packing fraction is higher than obtained for beds with more uniformly sized particles. Pending reliable data, we use $\Phi^S = 0.72$, where

Φ^Sdenotes the packing fraction of small fuel fragments that are formed by pulverization of overheated high burnup fuel.

The overall packing fraction of a mixture containing both large (L) and small (S) fuel fragments is calculated through Westman's relation for binary particle mixtures [32]

$$a^2 + 2Gab + b^2 = 1 \tag{6}$$

Where,

$$a = \frac{\Phi^S(\Phi^L - x^L\Phi)}{\Phi\Phi^L}$$

$$b = \frac{\Phi^S\Phi^L - \Phi\Phi^L(x^S + x^L\Phi^S)}{\Phi\Phi^S(II - 1 - \Phi^L)} \tag{7}$$

and G is a parameter that depends on the differences in particle shape and size between the two components of the mixture. Here, $x^S$and x^L are the mass fractions of small and large fragments, and Φ is the sought overall packing fraction of the binary mixture. The parameter G in Eq. 6 can be fitted empirically to a specific binary mixture, but some general expressions for estimating G based on the particle characteristics also exist; see [9] and references therein. For our applications, G ranges from about 40 to 150, depending mainly on the relative difference in fragment size between the large and small fragment class. Figure 3 shows the calculated fuel fragment packing fraction as a function of x^S, assuming five different sizes for the small fragments, while the large fragments are assumed to be 2.0 mm in size. Obviously, the binary mixture has a peak packing fraction for $0.25 < x^S < 0.35$. The peak value, as well as the location of the peak, depends on the difference in size between the large and small fragments. In our model, we set the characteristic size of the small fragment class to 0.1 mm, which means that the overall fragment packing fraction can reach values above 0.85.

By combining the calculated curve for the 0.1 mm fragment size in Fig. 3 with Eq. 3 , we may calculate the threshold cladding strain for fuel pellet column collapse and onset of fuel fragment relocation as a function of the relative amount of small fuel fragments. The results, which are presented in Fig. 4, show that the threshold strain decreases rapidly as the mass fraction of small fragments increases from zero to about 30 %, and then increases again. Experimental data in support of the cladding strain threshold in Fig. 4 are available only for low and medium burnup fuel with $x^S = 0$. For example, Siefken [21] evaluated 18 test rods with burnup < 35 MWd/kgU and concluded that no axial fuel relocation occurred for cladding strains < 17 %. Likewise, Raynaud [25] reported a threshold cladding strain of 13–17 % for two Halden IFA-650 test rods with burnups of 56 and 61 MWd/kgU.

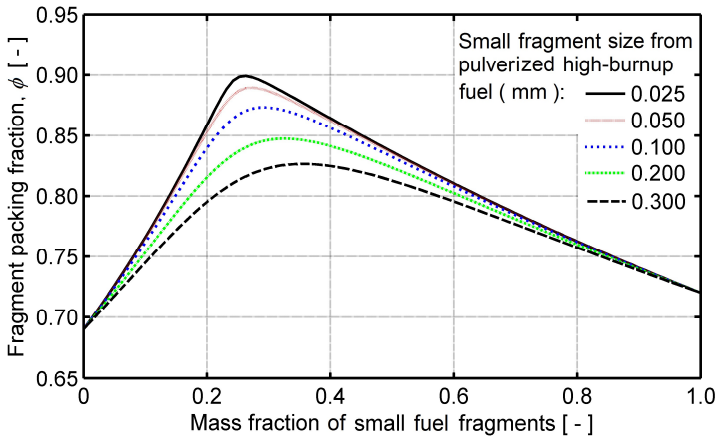

FIG. 3. Fuel fragment packing fraction (ϕ_k) vs. relative amount of small fragments (x^S) from pulverized high burnup fuel, calculated through Eqs. 6 and 7.

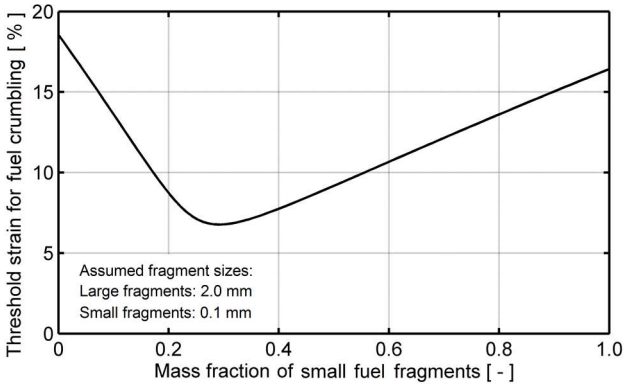

FIG. 4. Cladding threshold hoop logarithmic strain for onset of axial fuel relocation vs. mass fraction of small fragments (x^S), calculated through Eqs. 3, 6 and 7.

2.2.4. Thermal effects of fuel crumbling and axial relocation

Calculated results from the relocation model are used for modifying the fuel rod temperature calculations in FRAPTRAN-QT-1.5. Firstly, the changes caused by fuel relocation on the axial distributions of fuel mass, stored heat and power along the fuel rod are accounted for. Secondly, when the fuel pellet column collapses in ballooned segments of the fuel rod, we consider the changes in geometrical configuration as well as effective material properties. The pellet-cladding gap is significantly reduced, while gas-filled voids open up between the disorderly stacked fuel fragments. Since the volume fraction of gas is typically 20–30 %, the macroscopic thermal conductivity of the crumbled fuel in the balloon is much lower than that of solid fuel material. Consequently, the net outcome of fuel crumbling on the fuel radial temperature distribution is a lower fuel temperature close to the cladding surface (due to a reduced pellet-cladding gap) and a steeper radial temperature gradient (due to a low macroscopic thermal conductivity of the solid-gas mixture). To account for these effects, we modify the radial heat conduction equation in the fuel:

$$\rho_f c_{pf} \frac{\partial T}{\partial t} - \frac{1}{r}\frac{\partial}{\partial r}\left(\lambda_f r \frac{\partial T}{\partial r}\right) = q'''(t,r) \tag{8}$$

which is solved in FRAPTRAN-QT-1.5 for each axial segment of the fuel rod separately. Here, T is temperature, r is the radial coordinate, q'''denotes the volumetric heat source, and ρ_f, λ_f and c_{pf} are the density, thermal conductivity and specific heat capacity of the fuel material. The modified equation reads

$$\Phi\rho_f c_{pf}\frac{\partial T}{\partial t} - \frac{1}{\tilde{r}}\frac{\partial}{\partial \tilde{r}}\left(\lambda_{eff}\tilde{r}\frac{\partial T}{\partial \tilde{r}}\right) = \Phi q'''(t,\tilde{r}) \quad (9)$$

Hence, the fuel density and volumetric heat source are scaled with the fuel fragment packing fraction and the fuel thermal conductivity is replaced with an effective thermal conductivity for the crumbled fuel. This property, λ_{eff}, depends on the thermal conductivities of the solid fuel fragments and the surrounding gas, and on the packing fraction of the fuel fragments. It is calculated through a model by Chiew and Glandt [33], which has been successfully validated against experimental data [9]. Moreover, the positions of the nodes used for solving the heat conduction equation by the finite difference technique in FRAPTRAN-QT-1.5 are scaled ($r \rightarrow \tilde{r}$), such that the collapsed pellet surface comes into contact with and follows the distending cladding.

2.3. Criteria for high temperature rupture of the cladding tube

2.3.1. Background

In anticipated scenarios for LOCA in light-water reactors, the combination of overheating and internal overpressure in the fuel rods may cause excessive outward expansion (ballooning) of the cladding tube, primarily by creep mechanisms, which may lead to rupture of the cladding. Cladding ballooning will also reduce the subchannel area available for flow of the coolant water, or may cause coolant blockage in the refilling and flooding stages of the LOCA [1].

The cladding behaviour during the accident is governed by phase transformation, Zr-H_2O reactions (oxidation and hydrogen uptake), creep deformation, and rupture, processes that act within a time span of a few minutes [34]. Computational models that consider these processes, explicitly or implicitly, are needed in the LOCA safety analysis. It is important that the models play together, i.e. that the complex interaction between different phenomena is adequately considered by the applied set of phenomenological submodels.

Over the last decade, Quantum Technologies has developed a set of models for the Zircaloy cladding behaviour at high temperature, applicable to LOCA conditions, and implemented them in FRAPTRAN-QT-1.5. The set consists of submodels for the following phenomena in a variety of cladding materials [15]:

- Steam oxidation;
- Solid-solid ($\alpha \leftrightarrow \beta$) phase transformation;
- High temperature creep deformation;
- High temperature rupture.

The key quantities calculated by these models are:

- Oxygen parameters, which can be either the total amount of oxygen picked up by the cladding during the oxidation process, the oxide layer thickness or the oxygen concentration in the cladding metal layer;
- The volume fractions of α-phase and β-phase in the zirconium alloy,
- The cladding creep deformation; and
- The cladding burst hoop stress or hoop strain.

In FRAPTRAN-QT-1.5, the evolution of the first three quantities during the accident is calculated through a set of interconnected kinetic equations, whereas the cladding burst stress or burst strain is calculated through empirical functions of cladding temperature and oxygen concentration; see section 2.3.2. below. The background to the models is given in [3, 35, 36] and their implementation in FRAPTRAN-QT-1.5 is described in [15].

The aforementioned models have been implemented for use with the finite element (FE) based mechanical module in FRAPTRAN-1.5 [37]. This module was introduced as an option in the standard versions of FRAPCON and FRAPTRAN in 2006, but has not been further developed or maintained by PNNL since that time. However, over the years, Quantum Technologies has corrected, modified and extended this FE-based module. The reason is that it provides more versatility, higher numerical stability and more sophisticated modelling than the standard thin-shell (FRACAS-I) mechanical module in FRAPTRAN-1.5 [2]. For example, pellet-cladding interaction is modelled with friction between the contacting surfaces, and cladding non-elastic deformation by combined creep and plasticity can be modelled in a consistent manner.

Unfortunately, the FE-based module and the high-temperature material models that we have implemented in it do not work well together with the default criterion for high temperature cladding rupture in FRAPTRAN-1.5. The reason is that this criterion is designed and validated for use together with the FRACAS-I mechanical module and the BALON2 ballooning model in FRAPTRAN-1.5 [2]. Consequently, we have assessed a number of alternative rupture criteria, combined with the set of high-temperature material models in the FE-based module, against a large data base of high temperature burst tests on various cladding materials. The objective is to identify suitable rupture criteria that work well together with the FE-based mechanical module and our particular set of cladding material models. The assessed rupture criteria and the experimental data base are briefly described in Section 2.3.2. and Section 2.3.3. below, and the results are summarized in Section 2.3.4. A complete presentation of the work is given in [10].

2.3.2. Assessed rupture criteria

Four different rupture criteria are assessed. All of them are taken from open literature, and they all have similar form. More precisely, cladding rupture is assumed to occur when the cladding true (Cauchy) hoop stress σ_θ exceeds the burst stress σ_b. The latter is calculated through empirical correlations with the form

$$\sigma_b(T, x_{Tot}) = A_b e^{-B_b T} e^{-x_{Tot}^2/9.025\times10^{-7}} \tag{10}$$

where T is the cladding absolute temperature, x_{Tot} is the total weight fraction of oxygen picked up by the cladding in high temperature metal-water reactions, and A_b and B_b are material dependent coefficients that depend strongly on the phase composition of the material. In practice, A_b and B_b are defined as temperature dependent functions that are specific to a certain cladding material.

Two of the assessed burst stress correlations are well-known and based on data for Zircaloy-4 cladding. They are due to Rosinger [38] and Erbacher and co-workers [39], respectively. The other two correlations apply to Zr-Nb type cladding, and they are based on burst stress data presented for M5 and E110 cladding by Forgeron et al. [40] and van Uffelen et al. [41], respectively. Fig. 5 is a comparison of σ_b, calculated for unoxidized cladding (x_{Tot}=0) with the four different correlations. A more detailed description of the four rupture criteria, including expressions for the coefficients A_b and B_b in Eq. 10, is given in [10, 15].

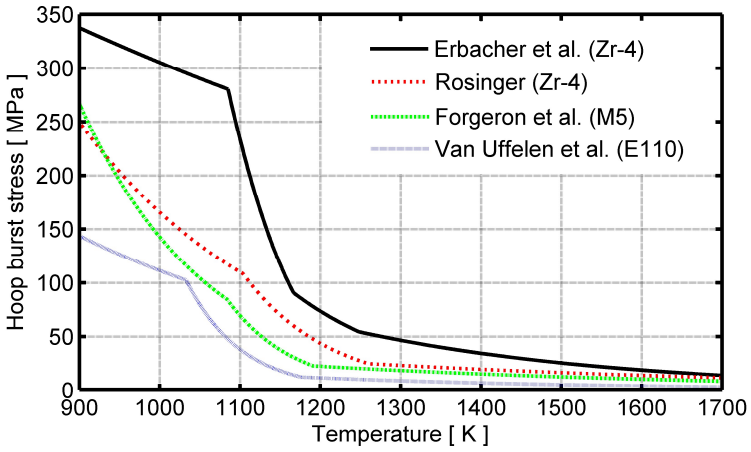

FIG. 5. Hoop burst stress for unoxidized cladding (x_{Tot}=0), according to the four different rupture criteria assessed in Task 2 of the project [10].

2.3.3. Assessed data base

The data base used in our assessment consists of cladding rupture data, obtained under simulated LOCA conditions from various experimental programs conducted from about 1980 to present. Most of the experiments are out-of-reactor heating tests, conducted with internally pressurized cladding samples in steam environment. In most of the tests, the internal overpressure is kept (nearly) constant, while the cladding temperature is increased at a controlled rate. Some tests are done with constant temperature, using either a constant or an increasing overpressure. Table 1 summarizes the considered experiments. A more complete summary of them and a review of the test results is given in [10].

Early experimental data on Zircaloy-4 cladding are from burst tests performed in the former Kernforschungszentrum Karlsruhe (KfK) [19, 39, 42] in Germany and those made available by Oak Ridge National Laboratory (ORNL) [43, 44] in the USA. More recent data include those produced at Commissariat á l'ènergie atomique et aux ènergies alternatives (CEA), France, the former AEKI Institute, Hungary, Argonne National Laboratory (ANL) USA, Studsvik Nuclear, Sweden, and the Halden reactor IFA-650 LOCA experiments in Norway. Most of the data are for un-irradiated cladding materials. The exceptions are the Studsvik tests, the Halden IFA-650 tests, and some of the KfK tests [19, 45]. The latter two test series were conducted in-reactor; all other tests were made out-of-reactor.

It should be remarked that the testing conditions and/or the results for some of the experiments in Table 1 have only been partly reported in the open literature. This make it impossible to model the tests in detail and/or to make quantitative comparisons between calculated and measured results. However, these experiments, which are marked with a P in Table 1, are still useful for making qualitative comparisons and for detecting trends in the data [10]. Experiments marked with a W in Table 1 are reported with well-defined testing conditions and results. These experiments, comprising 153 tested samples, have been used for evaluating the relative deviations between calculated and measured values for burst time, burst temperature, burst strain and stress, and for assessing the rupture criteria quantitatively. The results are reported and discussed in Section 2.3.4. below.

Table 1: Data Base on Fuel Cladding Burst Experiments Performed in LOCA Conditions. (Note: Some studies are well reported (W) in open literature, whereas data for other experiments are only partially available (P)).

TABLE 1. DATA BASE ON FUEL CLADDING BURST EXPERIMENTS PERFORMED IN LOCA CONDITIONS.

Experiment (data set ID)	Cladding material	Data source	Heating method	Heat rate (K/s)	Reference, source
ORNL-79	Zr-4	W	Internal	5–31	[43, 44, 46]
KfK-79	Zr-4	P	Internal	1–31	[46]
KfK-82	Zr-4	P	Induction	1–35	[39]
KfK-83	Zr-4	W	Internal/nuclear	7–19	[19, 45]
KfK-85	Zr-4	P	Internal	7	[42, 47]
KfK-87	Zr-4	P	Induction	0–80	[48]
KfK-88	Zr-4	W	Internal	1	[49]
CEA-02	Zr-4	P	Induction	0–NA	[50]
CEA-00	M5	P	Induction	0–100	[40]
AEKI-00	E110	W	Furnace	6–14	[51, 52]
W-EDF-09	ZIRLO	P	NA	3–28	[53]
ANL-10	ZIRLO	W	Furnace	5	[54, 55]
Studsvik-12	ZIRLO	W	Furnace	5	[23, 56]
IFA-650	Various	P	Furnace/nuclear	2–9	[7, 11]

2.3.4. Results and discussion

The main results of our assessment are the relative differences between calculated and measured cladding burst time, burst temperature and burst strain or stress. Two measures were used to quantify these differences, namely, the mean of the relative deviation and the root mean square deviation (RMSD), between the calculated and measured values.

The mean relative deviation between the calculated and measured quantity in a data set is:

$$\langle R_n \rangle = \frac{1}{n}\sum_{i=1}^{n}\left|\frac{\hat{y}_i - y_i}{y_i}\right| \tag{11}$$

where $\hat{y}_i$ and y_i is the i:th calculated and measured instance of the quantity, respectively, and n is the number of measurements in the data set. The RMSD is defined by:

$$\langle S_n \rangle = \sqrt{\frac{1}{n}\sum_{i=1}^{n}\left(\frac{\hat{y}_i - y_i}{y_i}\right)^2} \tag{12}$$

The RMSD can be considered as an uncertainty (1σ-level) in the computed quantity relative to the measured value, if a sufficient number of data points are taken into account.

Table 2 summarizes the calculated mean relative deviations for each evaluated data set, whereas Table 3presents the calculated root mean square deviations. For the tests on Zircaloy-4 and ZIRLO cladding, a comparison is made between Rosinger's [38] and Erbacher's [39] rupture criteria.

Table 2: Mean Relative Deviation Between Calculated and Measured Burst Variables. (Note: The burst criteria are A: Rosinger [38], B: Erbacher et al. [39] and C: Van Uffelen et al. [41]).

TABLE 2. MEAN RELATIVE DEVIATION BETWEEN CALCULATED AND MEASURED BURST VARIABLES

Cladding tube material	Data set	# tests n	Burst criterion	Cladding burst variable: Time $\langle R_n \rangle$	Temperature $\langle R_n \rangle$	Hoop stress $\langle R_n \rangle$
Zircaloy-4	ORNL-79	34	A	0.071	0.036	0.263
			B	0.050	0.025	0.720
	KfK-83	41	A	0.128	0.027	0.246
			B	0.123	0.026	0.649
	KfK-88	45	A	0.116	0.036	0.333
			B	0.119	0.034	0.447
ZIRLO	ANL-10	21	A	0.043	0.019	0.117
			B	0.046	0.021	0.972
	Studsvik-12	6	A	0.165	0.067	0.196
			B	0.166	0.068	1.238
E110	AEKI-00	12	C	0.149	0.096	0.654

Table 3, RSMD Between Calculated and Measured Burst Variables. (Note: The burst criteria are A: Rosinger [38], B: Erbacher et al. [39] and C: Van Uffelen et al. [41]).

TABLE 3. RSMD BETWEEN CALCULATED AND MEASURED BURST VARIABLES

Cladding tube material	Data set	# tests n	Burst criterion	Cladding burst variable: Time $\langle R_n \rangle$	Temperature $\langle R_n \rangle$	Hoop stress $\langle R_n \rangle$
Zircaloy-4	ORNL-79	34	A	0.082	0.043	0.319
			B	0.062	0.032	0.820
	KfK-83	41	A	0.154	0.033	0.298
			B	0.149	0.034	0.788
	KfK-88	45	A	0.123	0.043	0.368
			B	0.125	0.040	0.520
ZIRLO	ANL-10	21	A	0.048	0.021	0.155
			B	0.050	0.023	1.088
	Studsvik-12	6	A	0.176	0.072	0.246
			B	0.177	0.072	1.379
E110	AEKI-00	12	C	0.244	0.151	0.664

We note that the burst time and burst temperature are calculated with fair accuracy for all the data sets, but that the deviations between calculated and measured burst hoop stress are large. This is also evident from Fig. 6 and Fig. 7, in which comparisons are made between the calculated and measured time to burst and burst stress, respectively. The two rupture criteria calculate the time to burst with similar accuracy, but Rosinger's criterion give higher accuracy for the calculated burst stress. This is also illustrated by Fig. 8, which shows the relative errors, $\hat{y}_i - y_i/y_i$, in calculated burst time and burst stress for the two criteria, when applied to all 147 tests on Zircaloy-4 and ZIRLO cladding. It is clear that the criterion by Erbacher et al. overestimates the cladding burst stress, when the stress exceeds about 50 MPa.

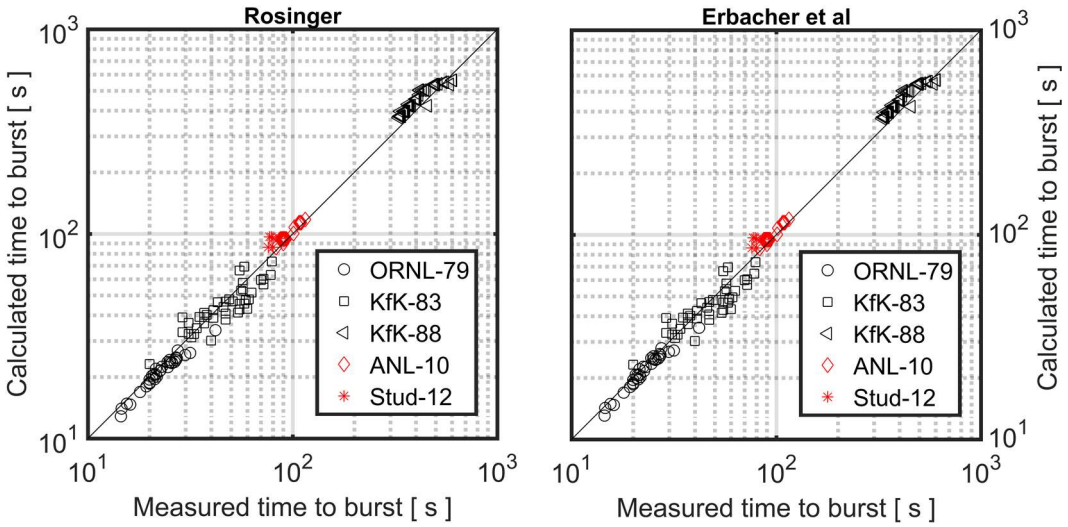

FIG. 6. Calculated versus measured time to burst for tests on Zircaloy-4 (black symbols) and ZIRLO (red symbols) cladding samples.

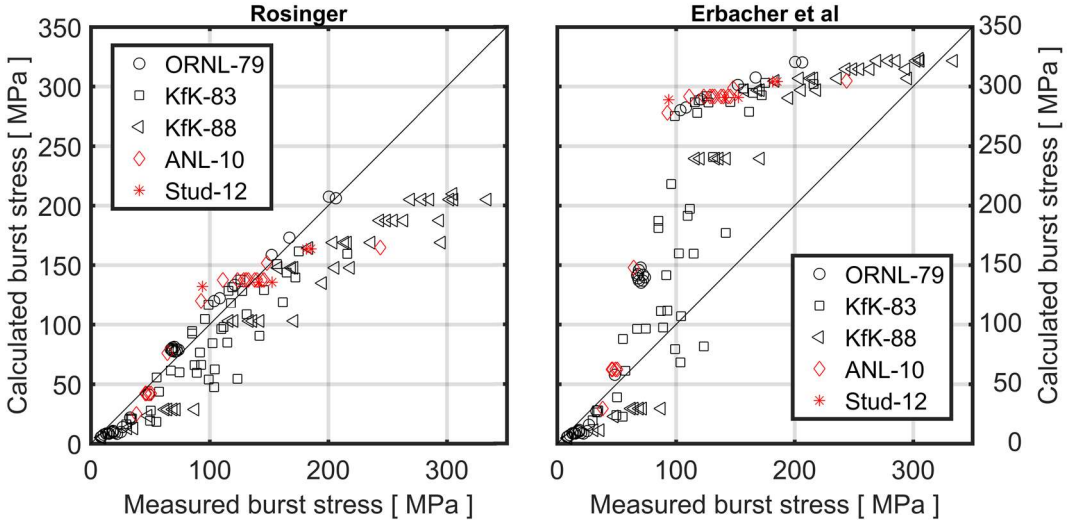

FIG. 7. Calculated versus measured true (Cauchy) hoop burst stress for tests on Zircaloy-4 (black symbols) and ZIRLO (red symbols) cladding samples.

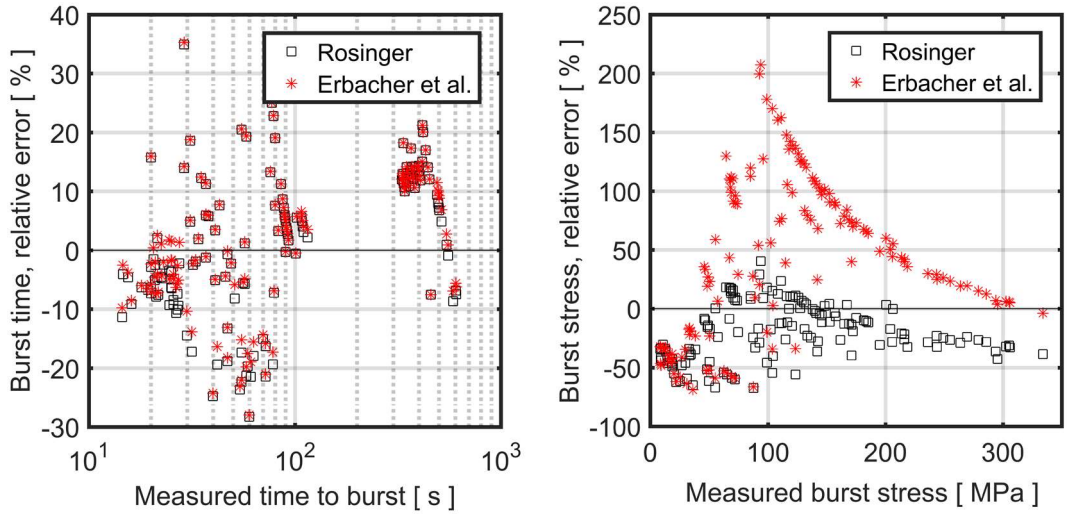

FIG. 8. Relative errors in burst time (left) and true hoop burst stress (right), calculated with Rosinger's [38] *and Erbacher's* [39] *burst criteria for all Zircaloy-4 and ZIRLO samples.*

To quantitatively compare Rosinger's and Erbacher's burst criterion, we have calculated $\langle R_n \rangle$ and $\langle S_n \rangle$ with regard to the total number of tests on Zircaloy-4 and ZIRLO samples in the data base. The results are presented in Table 4. The difference between the overall levels of uncertainty for these criteria is obviously very small as regard to the burst time and burst temperature, but Rosinger's criterion gives less deviation from measurements regarding the burst stress, viz. roughly by a factor 2. We should recall that these burst stress criteria were originally developed from Zircaloy-4 data; here we have used them also for ZIRLO cladding. Our analysis guides us to use Rosinger's burst criterion for Zircaloy and ZIRLO until additional data on modern cladding materials become accessible for analysis. Table 4: Overall Differences Between Calculated and Measured Burst Variables.

TABLE 4. OVERALL DIFFERENCES BETWEEN CALCULATED AND MEASURED BURST VARIABLES.

Cladding material	# tests n	Burst criterion	Cladding burst variable		
			Time	Temperature	Hoop stress
			$\langle R_n \rangle$	$\langle R_n \rangle$	$\langle R_n \rangle$
Zircaloy-4 and ZIRLO	147	A	0.101	0.032	0.255
		B	0.095	0.029	0.673
E110	12	C	0.149	0.096	0.654
			$\langle S_n \rangle$	$\langle S_n \rangle$	$\langle S_n \rangle$
Zircaloy-4 and ZIRLO	147	A	0.120	0.040	0.309
		B	0.116	0.037	0.812
E110	12	C	0.244	0.151	0.664

3. ASSESSMENT OF INTEGRAL LOCA SIMULATION TESTS

3.1. Considered tests

The integral LOCA simulation tests considered in our assessment are summarized below. The Halden IFA-650 LOCA tests number 4, 9, 10 and 14 are presented in Section 3.1.1. and Section 3.1.2. deals with the NRC-Studsvik LOCA test number 192. Details on the results of these tests are given in [11].

3.1.1. The Halden LOCA tests IFA-650.4/9/10/14

The IFA-650 series of tests are conducted since 2003 in the Halden heavy water test reactor, Norway. To date, fifteen tests on short fuel rodlets have been carried out under simulated loss-of-cooling accident conditions. Twelve of the tests have been made on pre-irradiated fuel rods [22, 57]. One of the primary objectives of the tests is to quantify the extent of fuel fragment axial relocation into the ballooned regions of the rods, and to study possible effects of fuel relocation on cladding temperature and oxidation. Several tests have exhibited axial relocation of fuel fragments; the most notable relocation resulted from tests 4 and 9.

3.1.2. Design and operation of the IFA-650 test rig

The design of the IFA-650 test rig is shown in Fig. 9, and a schematic cross-sectional drawing of the heated part of the rig is given in Fig. 10. In each test, a single test rodlet with an active (fuelled) length of 360–480 mm is instrumented and placed in the centre of the rig, which in turn is placed in one of the experimental channels of the test reactor. The rodlet is surrounded by an electrically heated shroud and a pressure flask. The heated shroud is part of a flow separator, which separates the coolant into a central channel adjacent to the fuel rod and an outer annulus. The heated shroud provides boundary conditions that resemble the heating

effects of nearby fuel rods with similar power. The temperature of the test rodlet is controlled both by nuclear heating of the rodlet itself and the electrical heating of the shroud. The power for the heated shroud is uniformly distributed along the test section, while the axial power profile for the rodlet is peaked to the rodlet midplane; see Fig. 9. The inner/outer diameters of the heated shroud and pressure flask are 20/26.2 mm and 34/40 mm, respectively.

The pressure flask is connected to a water loop. During the precondition phase before the test, the loop is filled with heavy water at a pressure and temperature of about 7 MPa and 515 K, which is circulated by pumps through the loop. Shortly before the test, the pressure flask is isolated from the loop and the test rodlet is cooled only by natural circulation within the flask. The LOCA simulation test is then initiated by opening valves to a blowdown tank, which causes a sudden pressure drop in the flask. The coolant flashes to steam, which flows to the blowdown tank and condensates. The flashing lowers the temperature of the remaining coolant. At the end of this blowdown phase, the coolant pressure in the flask stabilizes at 0.2–0.3 MPa [57]. The duration of the blowdown phase differs between tests, since some tests are done by evacuating the test rig through flow lines from the bottom part only (referred to as one-sided blowdown), while others are done by evacuating the rig from both the bottom and top (two-sided blowdown). The typical duration of the blowdown phase is 65–70 s for the former case and about 30–35 s for the latter.

After the blowdown phase, the test rodlet heats up with a rate that depends on the predetermined power levels of the rodlet and the electrically heated shroud. In most of the tests, small amounts of water are periodically sprayed into the upper part of the rig during this high temperature phase to maintain a sufficient amount of steam for cladding oxidation, but otherwise, no actions are taken until the test is terminated by switching off the electrical heater and scramming the reactor. The test rod is then left to cool down slowly, without quenching, in order to minimize any disturbances that could influence the fuel fragmentation and relocation that may have occurred during the high temperature phase.

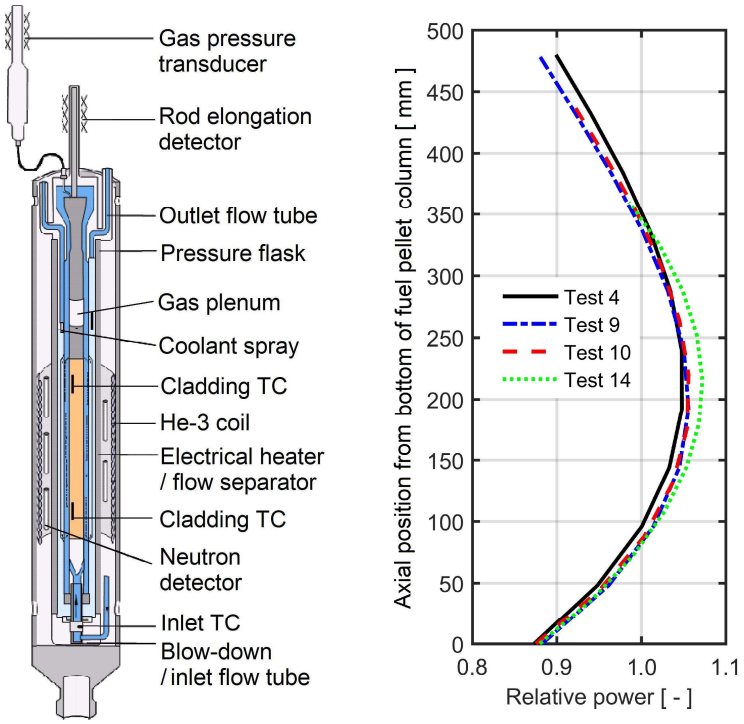

FIG. 9. Design of the IFA-650 test rig (left) and rodlet axial power profiles for the four considered test rodlets in the IFA-650 series (right) [57, 58].

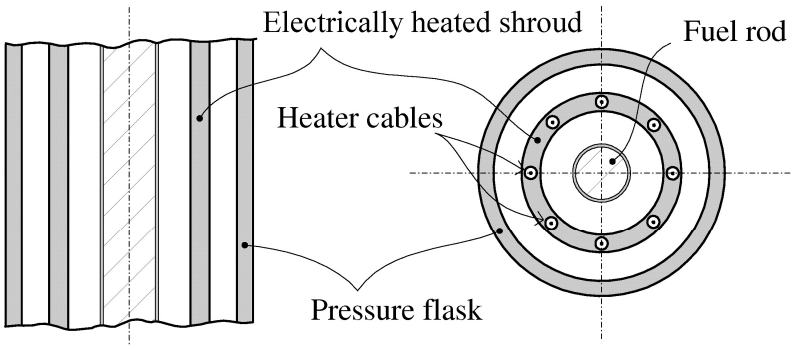

FIG. 10. Schematic drawing of the heated section of the IFA-650 test rig [5].

The general test procedure includes a preconditioning period of 7–8 hours, during which the test rodlet is operated at a linear heat generation rate (LHGR) around 8.5 kWm^{-1}. The reactor and rod power is decreased prior to the test. During the test, the rod power is held nearly constant, typically at 1–3 kWm^{-1}, depending on the target peak cladding temperature. The axial power profile in the rodlet during the test is nearly symmetric, with an axial peak to average power ratio of 1.04–1.08. Fig. 9 shows the axial power profiles for the IFA-650 LOCA tests considered in this report. The variation from one test to another is fairly small.

As indicated in Fig. 9, the IFA-650 test rig instrumentation consists of a fuel rod elongation detector, a fuel rod gas pressure transducer, and coolant thermocouples at the inlet and outlet of the rig. For most tests, there are also 2–4 cladding surface thermocouples, three vanadium neutron detectors and 2–3 heater surface thermocouples. All of these are axially distributed along the rod. Tests 4 and 10 were also equipped with thermocouples at the axial level of the rod gas plenum; the gas plenum is located about 250 mm above the top of the fuel pellet column, away from the heated section.

3.1.3. Test rodlets IFA-650.4, 9 10 and 14

The considered test rodlets were sampled and re-fabricated from full-length light water reactor UO_2 fuel rods that had been operated in commercial power reactors to high burnup. All samples were taken from axial segments between spacer grids, except for the IFA-650.14 rodlet. The length of the samples differed, and the active length of the re-fabricated test rodlets varied between 360 and 480 mm. The design and pre-test material conditions of the considered IFA-650 test rodlets are summarized in Table 5, and the pre-irradiation histories for the re-fabricated short length segments are shown in 11.

In Table 5, design Data and Pre-test Conditions for the Considered IFA-650 Test Rodlets are given. (Note: Data are compiled from [57], [59]–[64]. It should be remarked that these sources are not always consistent.)

TABLE 5. DESIGN DATA AND PRE-TEST CONDITIONS FOR THE CONSIDERED IFA-650 TEST RODLETS

Parameters		650.4	650.9	650.10	650.14
Rodlet active length	(mm)	480	480	440	360
Cold free volume	(cm^3)	21.5	19.0	17.0	1.9
Fill gas pressure at 295 K	(MPa)	4.0	4.0	4.0	2.0
As-fabricated enrichment of U^{235}	(wt%)	3.5	3.5	4.49	3.71
As-fabricated fuel pellet density	(kgm^{-3})	10 421	10 443	10 457	10 550
As-fabricated fuel pellet diameter	(mm)	9.13	9.13	8.19	8.19
As-fabricated fuel pellet height	(mm)	11.00	8.00	13.78	8.70
As-fabricated dish volume per pellet	(mm^3)	16.0	16.0	11.3	3.8
Pre-test average fuel burnup	($MWd(kgU)^{-1}$)	92.3	89.9	61.0	70.8
Cladding tube design		Duplex	Duplex	Monotube	Liner
Cladding tube base material		Zircaloy-4	Zircaloy-4	Zircaloy-4	Zircaloy-2
Inner surface liner material		–	–	–	Zr-0.3%Sn
Outer surface liner material		Zr-2.6wt%Nb	Zr-2.6wt%Nb	–	–
Heat treatment		SRA	SRA	SRA	RX
Inner surface liner thickness (nominal)	(μm)	–	–	–	70
Outer surface liner thickness (nominal)	(μm)	100	100	–	–
As-fabricated cladding outer diameter	(mm)	10.75	10.75	9.50	9.62
As-fabricated cladding wall thickness	(mm)	0.725	0.725	0.570	0.630
Pre-test oxide thickness (mean)	(μm)	10	7	27	32
Pre-test oxide thickness (max)	(μm)	11	8	30	40
Pre-test hydrogen concentration	(wppm)	50	30	150-220	180
Pre-test fast neutron fluence (> 1 MeV)	(m^{-2})	1.52×10^{26}	1.47×10^{26}	1.01×10^{26}	1.18×10^{26}

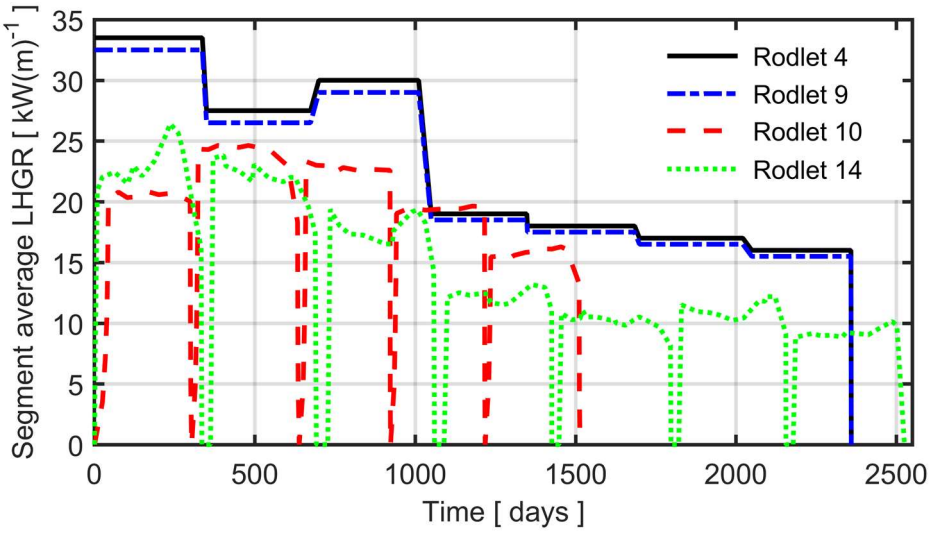

FIG. 11. Pre-irradiation histories for the considered IFA-650 test rodlet.

As part of the re-fabrication process, the test rodlets were filled with a gas mixture consisting of 95 vol% argon and 5 vol% helium to a pressure of either 2 or 4 MPa at room temperature. Argon was used to mimic the low conductivity fission product gases Xe and Kr, while a small amount of helium was needed to leak test the rodlet. Except for the IFA-650.14 rodlet, the gas plenum volume of each rodlet was made large, in order to maintain a stable internal gas pressure until cladding rupture. The IFA-650.14 rodlet, on the other hand, was fabricated with a very small plenum volume, since this test was intended to be interrupted before cladding rupture. The small plenum volume helped to achieve this objective, since it resulted in a declining internal pressure as the cladding tube ballooned.

The test rodlets for IFA-650.4 and IFA-650.9 were re-fabricated from one or two full-length PWR fuel rod(s)[12], manufactured by Framatome ANP and operated in the Gösgen nuclear power plant, Switzerland, to very high burnup [59, 60]. The IFA-650.4 rodlet was sampled from the span between the fifth and sixth spacer grid, whereas the IFA-650.9 rodlet was sampled between the second and the third spacer. The active length of both rodlets was 480 mm, and the sampled sections had reached a burnup of 92.3 and 89.9 MWd(kgU)$^{-1}$, respectively, during seven reactor cycles of operation in the Gösgen reactor. The irradiation histories were very similar, but the IFA-650.4 segment had somewhat higher power than IFA-650.9, as shown in Fig. 11. The mother fuel rod(s) to the IFA-650.4 and 650.9 rodlets had an experimental, Duplex-type Zircaloy-4 stress relieved annealed (SRA) cladding, with an outer layer of Zr-2.6wt%Nb. This cladding had a good corrosion resistance, which explains the low hydrogen concentration and thin oxide layer, in spite of the long operating life of the mother fuel rod. The variation in pre-test oxide layer thickness along the rodlets was insignificant.

The mother rod to the IFA-650.10 rodlet was a 17×17 PWR fuel rod of standard Framatome design; it had UO_2 fuel pellets with fairly high enrichment and standard stress relieved annealed Zircaloy-4 cladding. The mother rod was irradiated in the Gravelines 5 PWR, France, during five reactor cycles [61, 62]. The average burnup of the sampled fuel rod segment was 61.0 MWd(kgU)$^{-1}$, and the irradiation history is shown in Fig. 11.

The IFA-650.14 rodlet was re-fabricated from a boiling water reactor (BWR) mother rod of SVEA-96 design (AEB072-J9), manufactured by Westinghouse Electric Sweden [64, 65]. The

[12] It is not clear from the available documentation wether the rodlets were sampled from the same mother rod, or from two sibling mother rods in the same fuel assembly.

cladding material was recrystallized (RX) Zircaloy-2 with an internal zirconium liner with low concentrations of Sn and Fe. The mother fuel rod was irradiated in the Leibstadt BWR, Switzerland, during seven reactor cycles. The average burnup of the sampled fuel rod segment was 70.8 MWd(kgU)$^{-1}$, and the irradiation history is shown in Fig. 11. It should be remarked that the sampled segment contained the fourth spacer grid, and that there were local variations in cladding oxide layer thickness and crud thickness along the part of the segment where the spacer had been positioned [64]. The IFA-650.14 rodlet differed from the other rodlets also by having a lower fill gas pressure and a much smaller fission gas plenum; see Table 5. The plenum was made small to better control the ballooning of the cladding tube and to make it possible to terminate the test before cladding rupture.

3.1.4. Summary of test conditions and test results

The most important test parameters for the considered Halden IFA-650 LOCA tests are summarized in Table 6. All tests resulted in local ballooning of the cladding tube, and except for IFA-650.14, the cladding tube failed. Gamma emission scanning shortly after each test, as well as later neutron radiography of the rodlets, revealed significant axial fuel relocation in all tests except for IFA-650.10. Further details on the tests and results of post-test examinations are given in [11]. Table 6: Summary of Test Parameters for the Considered IFA-650 Tests [59]–[61], [63].

TABLE 6. SUMMARY OF TEST PARAMETERS FOR THE CONSIDERED IFA-650 TESTS [59]–[61],[63].

Parameter:	650.4	650.9	650.10	650.14
Rodlet LHGR (kWm^{-1})	0.93	2.60	1.37	0.97
Heater LHGR (initial) (kWm^{-1})	1.5	1.6	1.2	1.5
Peak cladding temperature (K)	1075	1475	1114	1065
Blowdown type (one/two sided)	1	2	1	1
Blowdown duration (s)	58	35	71	75
Timing of events (after start of blowdown):				
Cladding tube failure (s)	336	133	249	None
First spraying (s)	566	149 (175)	261	None
Reactor scram (s)	617	316	417	274

3.1.5. The NRC-Studsvik LOCA test 192

A series of six out-of-reactor LOCA simulation tests were performed from 2011 to 2012 by Studsvik Nuclear AB, Sweden, under contract with the U.S. Nuclear Regulatory Commission (U.S. NRC). The tests were done on fuel rodlets that had been sampled from full-length mother rods with average rod burnups ranging from 55 to 72 MWd(kgU)$^{-1}$. All the mother rods were of Westinghouse PWR design and had UO_2 fuel pellets and first generation ZIRLO (Zr-1.03Nb-0.98Sn by wt%) cladding. The tests were designed to assess the mechanical performance of ballooned and ruptured high burnup fuel rods under typical LWR LOCA conditions, and they have provided useful information on fuel fragmentation, axial relocation and dispersal [23, 66].

3.1.6. Design and operation of the Studsvik LOCA test rig

The design of the Studsvik LOCA test rig is shown in Fig. 12. A single test rodlet with an active length of about 0.30 m is centred inside a quartz tube and externally heated by infrared radiation from a clamshell furnace. There is no nuclear heating in the tests, and the rig is placed in a hot cell. The rodlet is heated in flowing steam with atmospheric pressure, and the test may be terminated by quenching the rodlet with room temperature water.

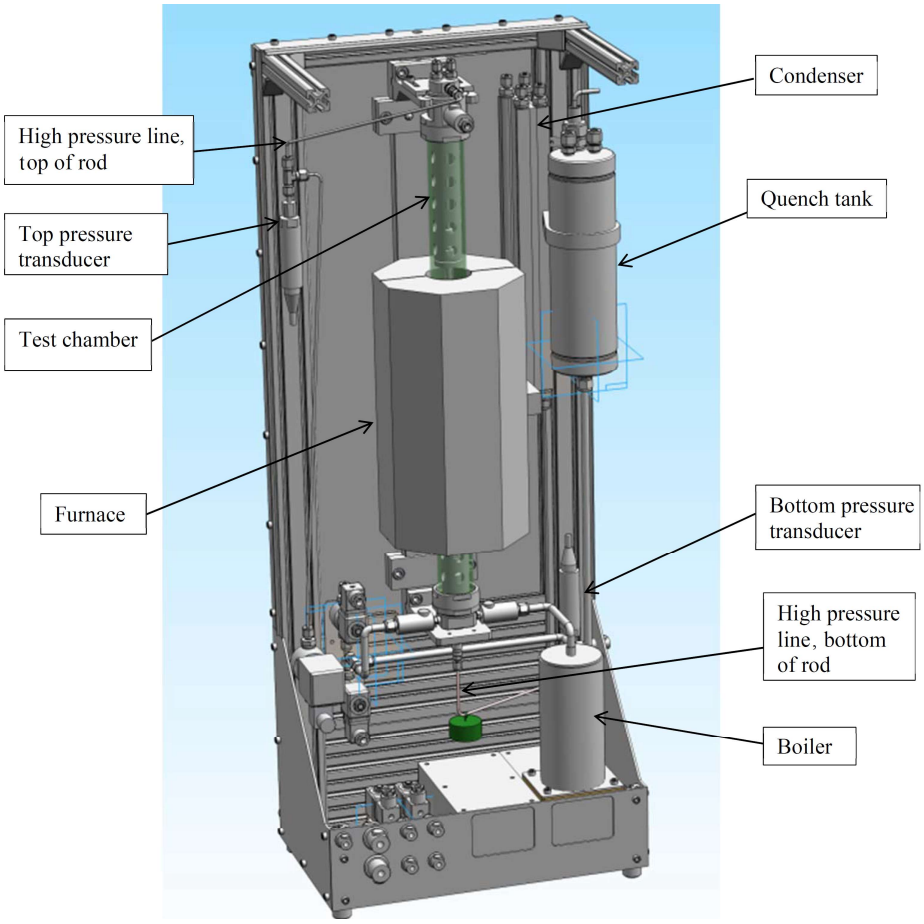

FIG. 12. Design of the Studsvik LOCA test rig [56].

A typical test starts at a temperature of 573 K by heating the rodlet such that a nearly constant heating rate of 5 Ks^{-1} is attained for the cladding tube. The cladding temperature is monitored by a single thermocouple, attached by a metal clamp about 50 mm above the axial midplane of the rodlet. The peak cladding temperature ranged from about 1220 to 1430 K for the six tests, and the rodlets were held at the peak temperature for 0, 5, 25 or 85 s to achieve various degrees of oxidation. Following the high temperature hold, two of the tests (189 and 196) were terminated by switching off the furnace and letting the rodlets cool slowly. In the other four tests, the rodlets were first cooled with an average rate of -3 Ks^{-1} to 1073 K, after which they were quenched by rapidly filling the quartz tube with room temperature water [23, 56].

The test rodlets were filled with helium to pressures between 8.2 and 11.0 MPa at 573 K. These pressures, which are consistent with high-end end-of-life internal pressures in PWR fuel rods, where chosen to induce cladding ballooning and rupture with hoop rupture strains in the range of 30–50 %. Rupture typically occurred at cladding temperatures around 950–1000 K, i.e. significantly below the peak cladding temperatures reached in the tests.

During the tests, the rod internal pressure was monitored by pressure transducers connected to the top and bottom ends of the rodlet; see Fig. 12. The internal free volume of the pressure lines to the transducers was fairly large; about 7.3 cm^3 in the upper end and about 3.1 cm^3 in the lower end of the test rodlet. Most of this gas volume remained near room temperature during the tests; see Section 2, Appendix II.

After each LOCA simulation test, the rodlet was subject to a four-point bend test at room temperature to measure the residual mechanical strength and ductility of the ballooned and ruptured region. The two broken halves of the rodlet were then inverted and gently shaken to dislodge loose fuel pellet fragments. Mass measurements were made before and after the LOCA

simulation test, after the bend test and after the shake test to determine the fuel release at each stage. After the final stage, the size distribution of the dislodged fuel fragments was measured for five of the six rodlets [23, 66].

3.1.7. Test rodlet NRC-Studsvik-192

The rodlet used in the NRC-Studsvik LOCA test 192 was sampled from the middle section of a full-length Westinghouse 17×17 PWR UO_2 fuel rod with first generation ZIRLO cladding that had been operated to a rod average burnup of 68.2 MWd(kgU)$^{-1}$ during four reactor cycles at a twin-unit plant in the USA. The first three cycles took place in the first unit from 1987 to 1994 with a two year interruption between the first and second cycle. After the third cycle, the mother fuel rod was extracted from the discharged fuel assembly and inserted into a new assembly, which was operated for an additional reactor cycle in the second unit of the plant from 1999 to 2001. This procedure was applied for altogether ten rods in the original fuel assembly, and some of the sibling high burnup rods have been refabricated into rodlets and used for other tests by Studsvik Nuclear [67, 68]. The design and pre-test material conditions for test rodlet 192 are summarized in Table 7, and the pre-irradiation history for the re-fabricated short length segment in the two PWR units is shown in Fig. 13.

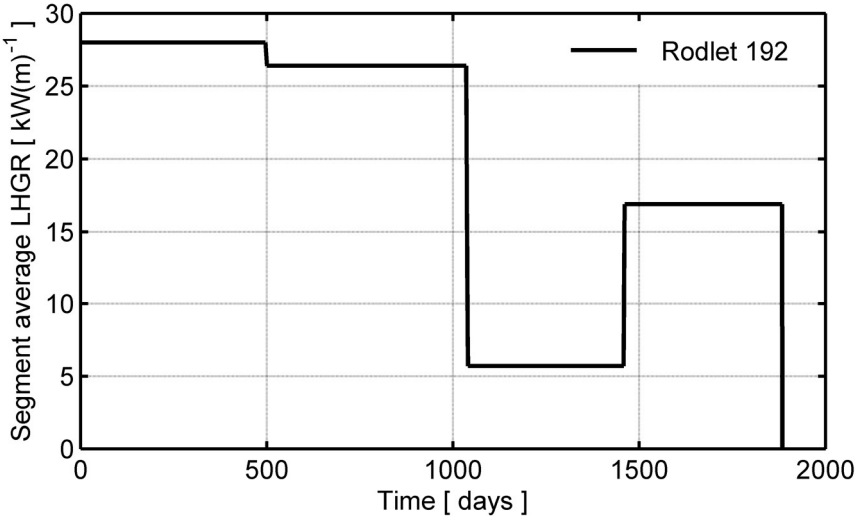

FIG. 13. Pre-irradiation history for the NRC-Studsvik-192 LOCA test rodlet [69].

Table 7: Design Data and Pre-test Conditions for the NRC-Studsvik-192 Test Rodlet [23], [67]–[69]. (Note that data for the rod design are taken from open literature reports on sibling fuel rods that have been used in earlier tests by Studsvik Nuclear AB.)

TABLE 7. DESIGN DATA AND PRE-TEST CONDITIONS FOR THE NRC-STUDSVIK-192 TEST RODLET

Parameter	Value
Rodlet active length (mm)	300
Cold free volume (cm^3)	10.4
Fill gas pressure at 573 K (MPa)	8.2
As-fabricated enrichment of U^{235} (wt%)	3.99
As-fabricated fuel pellet density (kgm^{-3})	10 440
As-fabricated fuel pellet diameter (mm)	8.192
As-fabricated fuel pellet height (mm)	9.830
As-fabricated dish volume per pellet (mm^3)	4.2

TABLE 7. DESIGN DATA AND PRE-TEST CONDITIONS FOR THE NRC-STUDSVIK-192 TEST RODLET

Parameter	Value
Pre-test average fuel burnup (MWd(kgU)$^{-1}$)	78
Cladding tube design	Monotube
Cladding tube material	ZIRLO
Heat treatment	SRA
As-fabricated cladding outer diameter (mm)	9.500
As-fabricated cladding wall thickness (mm)	0.571
Pre-test oxide thickness (mean) (μm)	27
Pre-test oxide thickness (max) (μm)	30
Pre-test hydrogen concentration (wppm)	235
Pre-test fast neutron fluence (> 1 MeV) (m^{-2})	1.31×10^{26}

3.1.8. Summary of test conditions and test results

The most important test parameters for the NRC-Studsvik LOCA test 192 are summarized in Table 8. Further details on the test and the results of post-test examinations are given in [11].

TABLE 8. SUMMARY OF TEST PARAMETERS FOR THE NRC-STUDSVIK LOCA TEST 192 [23, 69]

Parameter	Value
Initial temperature (K)	574
Initial rod pressure (at 574 K) (MPa)	8.21
Cladding temperature at failure (K)	981
Peak cladding temperature (PCT) (K)	1446
Hold time at PCT (s)	5
Steam mass flow (kgs^{-1})	1.8×10^{-4}
Timing of events (after start of heating):	
Cladding tube failure (s)	81
Hold at PCT (s)	173-178
Quenching (s)	297

3.2. Methodology applied in computer analyses

As already mentioned in section 2.1, the computer analyses of the considered Halden IFA-650 and NRC-Studsvik LOCA tests were carried out in two steps. In the first step, the pre-irradiation of each fuel rod segment that was later re-fabricated into a test rodlet was modelled by use of the standard version of FRAPCON-3.5 [18], as delivered by PNNL. The procedure is described in Section 3.2.1. below.

Calculated results from FRAPCON-3.5, defining the pre-test conditions for each test fuel rodlet, were then used as input to the second analysis step. This step involved simulations of the LOCA test with FRAPTRAN-QT-1.5, our extended version of FRAPTRAN-1.5, as described in section 2. The procedure and assumptions made for the calculations are described Section 3.2.2. below.

Both FRAPCON and FRAPTRAN are best-estimate computational tools, and the presented analyses should be considered as best-estimate; no uncertainty or sensitivity analyses were carried out. However, the analysis of each LOCA test was done twice: with and without the fuel relocation model. Except for this difference, the two calculations were done with identical models and input data.

It should be remarked that no computer program was used for calculating the transient thermal-hydraulic boundary conditions that are needed for fuel rod analyses with FRAPTRAN. These boundary conditions were derived from measured temperatures and pressures in the considered test rigs; the applied methodology and assumptions are described in Section 3.2.2. and Appendices I and II.

3.2.1. Simulations of pre-irradiation

The pre-irradiation of each fuel rod segment that was later re-fabricated into a test rodlet was simulated by use of the standard version of FRAPCON-3.5 [18]. Input for the simulations, in terms of fuel pellet and cladding design data and power histories, are given in 3.1.3. and 3.1.7. The linear heat generation rate during the pre-irradiation was assumed to be uniform along each segment. Nominal core average thermal-hydraulic conditions for each PWR were used in the simulations, but the coolant inlet temperature was increased to represent the local conditions at the axial elevation pertinent to the considered segment of the full length mother fuel rod.

Recommended default models and options for FRAPCON-3.5 were used in the calculations. In particular, the thin-shell mechanical model was used for the cladding tube, rather than the finite element based model. The Duplex-type cladding material of the IFA-650.4 and IFA-650.9 rodlets was represented by models for M5 cladding, which are available in FRAPCON-3.5 [18]. These models were selected, since the M5 alloy has similar performance with regard to waterside corrosion as the Zr-2.6wt%Nb surface liner in the Duplex cladding.

In all calculations with FRAPCON-3.5, the fuel rod samples were discretized axially into 20 mm long axial nodes. Hence, the number of axial nodes ranged from 15 to 24, depending on the length of the considered sample. The radial discretisation of the fuel pellet stack consisted of 44 annuli.

3.2.2. Simulations of LOCA tests

The Halden IFA-650 and NRC-Studsvik LOCA tests were simulated with our extended version of FRAPTRAN-1.5, using previously developed high temperature models for the cladding tube [15] in combination with a slightly modified version of the finite element based mechanical solution module [37]. All tests were simulated twice, with and without consideration of axial fuel relocation, in order to assess the importance of the relocation to the thermal-mechanical behaviour and high temperature degradation of the tested fuel rodlets.

All calculations were done with an axial discretisation consisting of 20 mm long axial segments for the active part of the test rodlet, i.e. the same discretisation as was used for the simulations of the rodlet pre-irradiation with FRAPCON-3.5. Likewise, the radial discretisation comprised 44 annuli in the fuel pellet and one element across the cladding thickness. A constant time step length of 10 ms was used in the calculations, and the simulations covered the heat-up phase, the high temperature phase and most part of the cooling phase in each test.

For the Halden IFA-650 tests, the rodlet LHGR was held constant at the values defined in Table 6 until reactor scram, after which the LHGR was reduced to 0.05 kWm^{-1} to simulate decay heating. The axial power profiles used in the simulations of the Halden tests are shown in Fig. 9. No nuclear heating was modelled for the NRC-Studsvik-192 out-of-reactor test.

The NRC-Studsvik-192 test rodlet was filled with helium, whereas the Halden IFA-650 test rodlets were filled with a low-conductivity gas mixture, consisting of 95 vol% Ar and 5

vol% He; see 3.1.3. and 3.1.7. These gas compositions were postulated for the calculations with FRAPTRAN. In the calculations, the amount of fill gas in each rodlet was adapted, such that the calculated 'hot' pre-test pressure matched the measured value for each test.

Other pre-test conditions of the rodlets were defined by the end-of-life fuel rod conditions after operation in the commercial power reactors, as calculated with FRAPCON-3.5. Calculated results for the permanent deformations of fuel and cladding, cladding oxide layer thickness and hydrogen content, as well as the radial distributions of fuel burnup and power, were imported to FRAPTRAN input from FRAPCON output. Most of these data are presented and discussed in section 4.1. It should be remarked that any axial variation in the pre-test conditions calculated by FRAPCON-3.5, such as the cladding oxide layer thickness, was neglected when using them as input to FRAPTRAN-QT-1.5.

Transient fission gas release from the high burnup fuel was not considered in the calculations, except for test Halden IFA-650.14. As mentioned in Section 3.1.3. this test was performed on a rodlet with an exceptionally small gas plenum volume, which means that the amount of fill gas was much less than the amount of fission gas released during the test. More precisely, there was 1.56×10^{-3} mole fill gas in the rod before the test, and 4.72×10^{-3} mole gas after the test, as a result of transient fission gas release [70]. The amount of gas released during the test corresponds to about 18 % of the gas produced during the lifetime of the fuel [70].

For reasons described above, modelling of transient fission gas release was necessary for the Halden IFA-650.14 test. The FRAPTRAN-1.5 computer program has no proper model for fission gas release, but the user may prescribe the fractional fission gas release as time dependent input to the program [2]. In our simulations of the IFA-650.14 test, we prescribed the transient fission gas release fraction, x_f, by use of a smooth ramp function with respect to time:

$$x_f(t) = \frac{0.18}{2}\left(1 + \tanh\left(\frac{t-t_c}{t_s}\right)\right) \tag{13}$$

Here, t is the time from start of blowdown in the IFA-650.14 test, while t_c = 225 s and t_s = 50 s are parameters that were empirically fitted so that the calculated and measured time histories of rod internal gas pressure matched. Eq. (13) is shown graphically in Fig. 38 and will be further discussed in Section 4.2.4. .

Possible restrictions of rod internal gas flow during the tests were neglected. Hence, the internal gas was assumed to have uniform pressure and composition along the rod, in the rod plena, and in connected gas-containing systems. For the tests in which transient fission gas release was not modelled, the gas composition remained unchanged until cladding rupture was calculated to occur. By default in FRAPTRAN-1.5, steam is assumed to completely and immediately replace the rod internal gas from the time of cladding rupture [2]. Since the inflowing steam has higher thermal conductivity than argon, cladding rupture resulted in improved pellet-to-cladding heat transfer and a rapid rise in cladding temperature along the entire rodlet in our simulations of the Halden IFA-650 tests. This rather unrealistic behaviour is further discussed along with the calculated results in section 4.2. The steam entering the fuel rod after cladding rupture is in FRAPTRAN-1.5 assumed to cause oxidation of the cladding inner surface. However, the inner surface oxidation is restricted to axial segments that are within a distance of 3 inches from the cladding breach [2].

All the test rodlets considered in this report had internal gas plena that differed from the typical design of LWR fuel rods. The IFA-650 series of rodlets had a single gas plenum that was located about 200 mm above the top of the fuel pellet column, outside the heated zone. The plenum gas temperature therefore remained fairly low during these tests. In the IFA-650.4 and IFA-650.10 tests, thermocouples were attached to the cladding and shroud at the axial position of the plenum. Figure 14 shows the measured temperatures from the IFA-650.4 test, together

with the approximation used for the plenum gas temperature in our simulations of the test. During the blowdown phase, the temperature is equal to the saturation temperature of the flashing steam. After blowdown, the gas plenum heats up and approaches a temperature somewhat above the moderator temperature in the Halden reactor (510 K); the temperature difference depends on the combined power of the rodlet and heater. The discontinuity of the measured temperature histories in Fig. 14 is due to the outflow of hot gas upon cladding rupture.

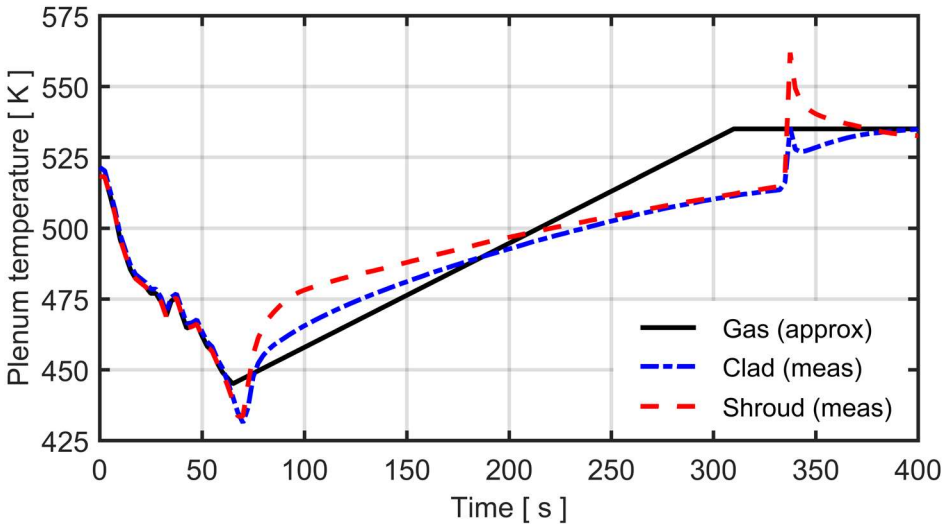

FIG. 14. Measured temperatures at the gas plenum position for the IFA-650.4 rodlet, together with the approximation for plenum gas temperature used in calculations.

In our simulations of the Halden IFA-650 tests, we used approximations to the plenum gas temperature, similar to the one shown in Fig. 14. For each rod, the gas temperature was assumed to follow the steam saturation temperature during the blowdown phase, which was then followed by a phase with linear heat up to a final gas temperature of 515–535 K. As for the NRC-Studsvik-192 test rodlet, it had a more complex design than the IFA-650 rodlets with regard to internal gas volumes. The modelling of these volumes and their temperature evolution is described in Section 2 of Appendix II.

The time dependent thermal-hydraulic boundary conditions required by FRAPTRAN for calculating the fuel rod behaviour during the LOCA simulation tests were derived from temperatures and pressures measured in different parts of the test rigs. The procedure for deriving the boundary conditions for the Halden IFA-650 tests is fairly complex. It is described in detail in Appendix I.

The thermal-hydraulic boundary conditions for the NRC-Studsvik-192 test were simpler, since the test was performed in steam at atmospheric pressure and the heating was by a furnace that surrounded the rodlet. The boundary conditions for this test were derived from the measured cladding temperature close to the midplane of the rodlet, in combination with measured data for the typical axial temperature variation, obtained during conditioning of the test rig [56]. The thermal boundary conditions applied for the NRC-Studsvik 192 test are described in detail in section II.1 of Appendix II.

The NRC-Studsvik-192 test rodlet had ZIRLO cladding, in contrast to the Halden IFA-650 rodlets that had Zircaloy cladding. Since our extended version of FRAPTRAN-1.5 lacks specific material models for ZIRLO, we used generic Zircaloy models also for the NRC-Studsvik-192 rodlet. More precisely, in all calculation presented in this report, we used the Cathcart-Pawel high temperature oxidation model [71], and the Zircaloy-4 high temperature creep model by Rosinger [38, 72]. The latter was used without any specific creep model for the mixed $\alpha+\beta$ phase region.

None of the temperature dependent criteria for cladding high temperature rupture that are available in FRAPTRAN-QT-1.5 [15] worked well for the considered tests: For the IFA-650.4 and IFA-650.9 tests, the calculations resulted in contact between the distending cladding tube and the surrounding heater before cladding rupture was calculated to occur. Once in contact, the heater acted as a die, forcing the cladding balloon to grow in the axial direction until it finally ruptured. Since this behaviour was not observed in the tests, we postulated an ad-hoc threshold for the effective creep strain, at which the cladding was assumed to fail. This threshold effective strain (logarithmic) was set to 0.75 for the IFA-650.4 and IFA-650.9 tests, since this value resulted in cladding failure just before the cladding came into contact with the surrounding heater; see Figs 18 and 24. We adopted the same methodology for the IFA-650.10 and the NRC-Studsvik-192 test, for which the threshold effective strain for cladding failure was set to 0.30 and 0.70 respectively.

The cladding creep rate in FRAPTRAN-QT-1.5 had to be scaled, in order to match the calculated and measured time to cladding rupture. A scale factor of 0.40 was found to give a good match for the considered Halden IFA-650 tests, when fuel relocation was included in the calculations. To allow meaningful comparisons between tests and also between the calculated cases with and without fuel relocation, this scale factor was used in *all* calculations presented in this report. Except for the scaled creep rate and the ad-hoc rupture criterion described above, models in FRAPTRAN-QT-1.5 were not modified or tuned. The model parameters used in our relocation model were those used in earlier work [9], unless otherwise stated; $g^{th} = 0.20$ mm, $g^{r} = 5.0$ μm, $x^{r} = 0.01$, $\Phi^{L} = 0.69$, and $\Phi^{S} = 0.72$.

4. RESULTS AND DISCUSSION OF SIMULATED TESTS

4.1. Pre-irradiation

Key results of the simulated pre-irradiation of the considered test rodlets with the FRAPCON-3.5 computer program are summarized in **Error! Reference source not found.**9. Measured data are included for comparison, when available. The calculated cladding corrosion (hydrogen pickup and oxide layer thickness) is in fair agreement with measurements. We recall from Section 3.2.1. that the non-standard Duplex-type cladding material of the IFA-650.4 and IFA-650.9 rodlets was represented by models for M5 in our calculations with FRAPCON-3.5 [18], in order to reproduce the corrosion performance.

TABLE 9. PRE-TEST CONDITIONS OF THE TEST RODLETS CALCULATED WITH THE FRAPCON-3.5 COMPUTER PROGRAM *(Measured data are given in brackets for comparison)*

Parameter	650.4	650.9	650.10	650.14	192
Rodlet average burnup (MWd(kgU)$^{-1}$)	91.9 (92.3)	89.5 (89.9)	60.7 (61.0)	70.8 (70.8)	78.4 (78)
Pellet centre burnup (MWd(kgU)$^{-1}$)	77.9	76.1	54.5	61.6	68.0
Pellet surface burnup (MWd(kgU)$^{-1}$)	257.0	248.5	128.2	174.6	194.9
Fuel fraction with local BU > 70 MWd(kgU)$^{-1}$	1.0	1.0	0.11	0.32	0.74
Radial power peaking factor (–)	3.53	3.53	3.06	3.34	3.395
Fuel fragment average size (mm)	1.87	1.90	2.05	1.93	1.85
Fission gas release (%)	11.1	7.6	2.5	3.6	11.1
Cladding hydrogen concentration (wppm)	67–76 (50)	57–65 (30)	172–225 (150–220)	415 (180)	213–256 (176–288)
Cladding outer oxide layer thickness (μm)	14–16 (6–8)	11–13 (6–8)	20–27 (20–30)	29 (32–35)	22–27 (25–30)

Table 9 includes calculated values for the local fuel burnup at the pellet centre and surface (rim). The calculated distribution of fuel burnup is of interest, since it is used in our version of

FRAPTRAN-1.5 to estimate the amount of fuel material that may pulverize when overheated during the LOCA test. More precisely, a local burnup of at least 70 MWd(kgU)$^{-1}$ is required for the fuel to pulverize, according to our model [9]. As can be seen from Table 9, the fuel fraction exceeding this threshold, and thus susceptible to pulverization at high temperature, ranges from 11 to 100 % among the considered test rods.

Figure 15 shows the distributions of power and burnup across the fuel pellets after pre-irradiation of the IFA-650.4 and IFA-650.10 test rodlets, according to our calculations with FRAPCON-3.5. The radial distributions of power are fairly similar in these two test rods, but the distributions of burnup are much different. The calculated distributions are assumed to be valid for the entire length of the test rodlets, since the irradiation conditions were fairly uniform along the sampled rod segments.

The radial distributions of fuel burnup and power, calculated with FRAPCON-3.5, are used in subsequent analyses of the LOCA simulation tests with our extended version of FRAPTRAN-1.5. It is assumed that the distributions do not change with time during the tests – not even when fuel crumbling and axial fuel relocation occurs [9]. Finally, from Table 9, we note that the estimated average size of fuel fragments in the considered rodlets range from 1.87 to 2.05 mm before the LOCA tests. These fragment sizes are calculated through an empirical model, based on the fuel pellet average burnup and the peak power experienced by the fuel during its lifetime [9].

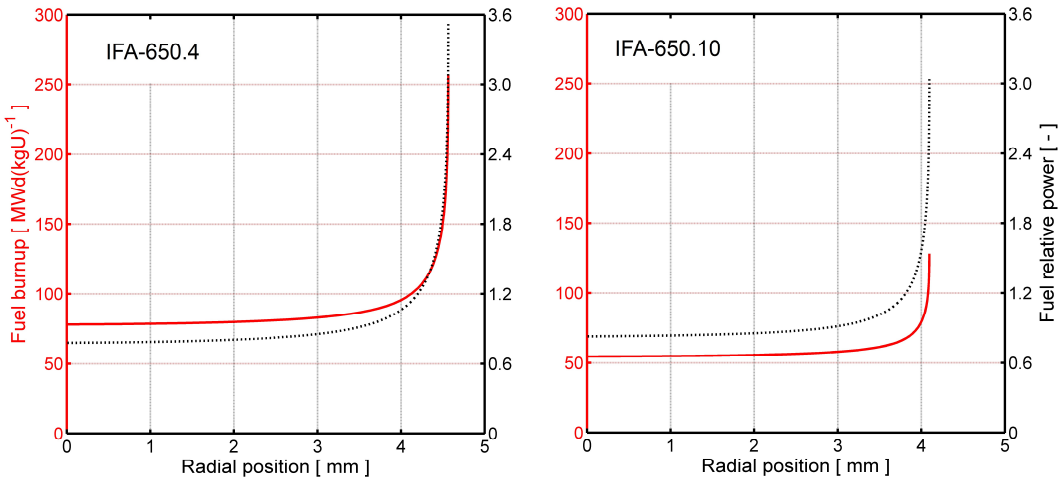

FIG. 15. Calculated distributions of burnup (full red line) and power (dashed black line) across the fuel pellets in the IFA-650.4 and IFA-650.10 test rodlets.

4.2. Halden IFA-650 LOCA tests

Here, we consider the results of our simulations of the Halden IFA-650 LOCA tests. For each test, calculated results are presented graphically for the cases with and without fuel relocation considered in the analyses with our extended version of FRAPTRAN-1.5. Measured data are included in the graphs for comparison, whenever data are available. Throughout the presentation, time zero refers to the start of the LOCA test, defined by the opening of valves between the in-core pressure flask and the blowdown tank; see Section 3.1.2.

4.2.1. IFA-650.4

Figure 16 shows the calculated and measured evolution of rod internal gas pressure in the upper plenum during the Halden IFA-650.4 test. From Section 3.2.2. we recall that the gas pressure is calculated on the basis of calculated temperatures and deformations along the active length of the rodlet, together with a postulated temperature history for the gas within the rod

plenum. We also recall that the initial cold pressure was reduced from its reported value of 4.0 MPa to 3.86 MPa in our calculations, in order to match the calculated "hot" pre-test gas pressure to the measured value (6.95 MPa). The calculated gas pressure is in close agreement with measurements for $t < 290$ s, but overestimated for the remaining 46 s preceding cladding rupture. A likely explanation to this deviation is that ballooning of the cladding starts earlier and progresses more gradually than calculated with our version of FRAPTRAN-1.5.

In Fig. 16 the calculated curves for the cases with assumed relocation ("relo") and without relocation ("norelo") coincide up to $t = 326$ s. This is the time at which fuel fragments start to relocate axially, according to our calculations. The calculated time of cladding failure is 334.2 s for the case with fuel relocation and 348.2 s without. These results suggest that cladding ballooning, collapse of the fuel pellet column, and axial relocation of fuel take place in a fairly short (7–8 s) period before cladding rupture, but that the thermal feedback effects are still strong enough to affect the rupture process. For the considered test, the calculated time to rupture was shortened by no less than 14 s, as a result of thermal feedback effects from fuel crumbling and relocation. As already mentioned, the deviation between the calculated and measured gas pressure time histories in Fig. 16 suggests that the ballooning and relocation in test IFA-650.4 may actually have occurred over a longer period than in our calculations. If so, the impact of thermal feedback effects on the rupture process would have been even more important.

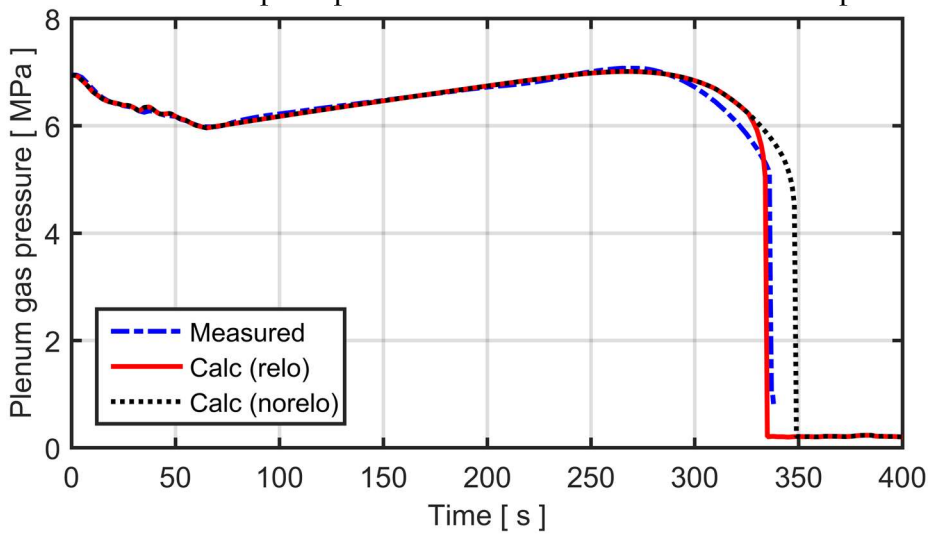

FIG. 16. Calculated evolution of plenum gas pressure in comparison with measurements. Calculations were done with (relo) and without (norelo) assumed axial fuel relocation.

Fig. 17 shows the calculated evolution of cladding deformation and axial fuel relocation during the last seven seconds before cladding rupture. The thick red line shows the calculated state at the time of cladding rupture. This is also the state expected after the test is completed, since no further deformation or relocation is supposed to take place after rupture and depressurization of the rodlet. The family of thinner black lines represent the calculated conditions 1, 2, 3,..,7 s before cladding rupture. The leftmost curve thus shows the conditions about the time when the balloon starts to grow and fuel starts to relocate.

The calculations suggest that the local fuel mass is increased by about a factor of three in the most distended cross section of the test rodlet. The relocated fuel originates from the uppermost, 120 mm long, part of the fuel pellet column, which has disappeared completely. This is well in line with the results reported from the test: Gamma scan (see insert in Fig. 17) as well as ceramography showed that the uppermost part of the fuel pellet column was completely missing after the test; no remaining fuel fragments were detected. The length of the missing fuel part was 190 mm, which is 70 mm longer than calculated with our model. The

difference is understandable, since a significant amount[13] of fuel had been expelled through the cladding breach and was found just above the balloon and at the bottom of the pressure flask after the test [73]. This dispersal of fuel fragments, which is not accounted for by our model, most certainly increased the amount of fuel lost from the upper part of the fuel rod.

Finally, we note that the calculated fuel temperature is in the range of 1100 to 1159 K, when relocation starts at t = 326 s. This means that, according to our model, the entire fuel column has been pulverized into fine (< 0.2 mm) fragments, and that the crumbled fuel has an assumed packing fraction of 0.72 everywhere in the ballooned region; see the description of the applied models for fuel fragmentation and pulverization in [9].

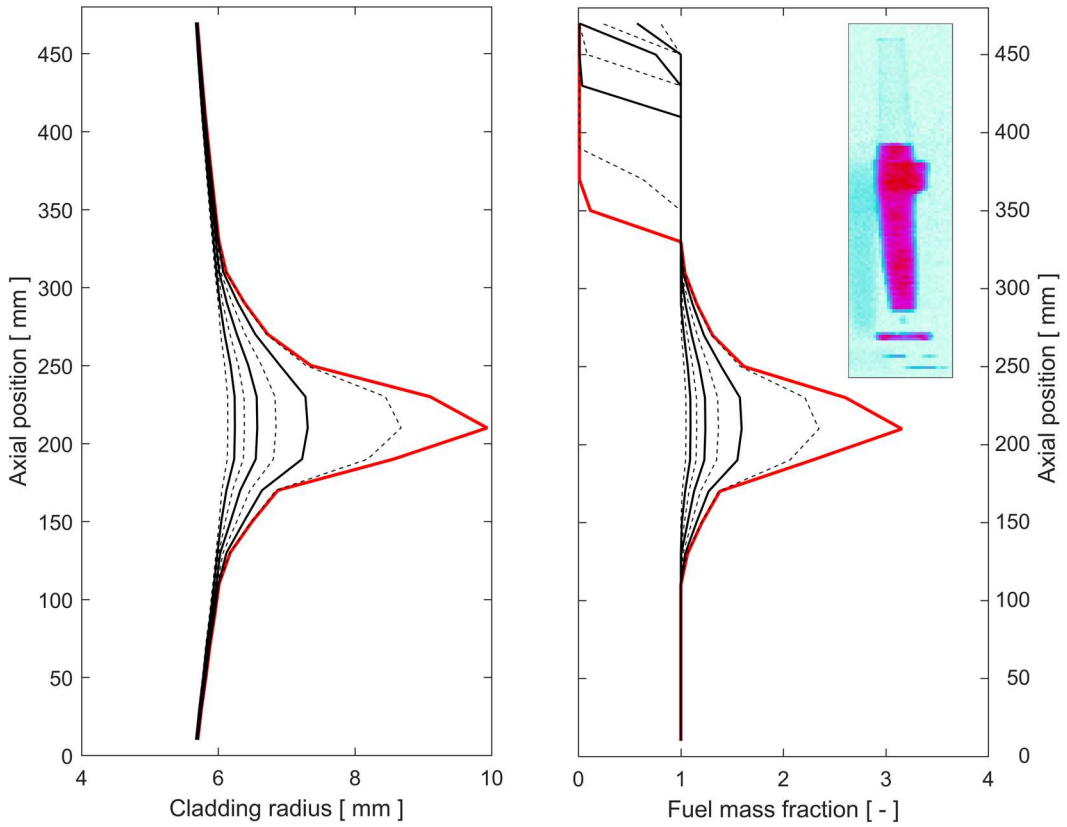

FIG. 17. Calculated evolution of cladding deformation (left) and fuel relocation (right) during the last seven seconds before cladding rupture. The rightmost curve (red) represents the conditions at time of rupture, while the seven curves to the left of it show the calculated state 1, 2,...,7 s before rupture. A post-test gamma scan image of the IFA-650.4 test rig is included for comparison [73].

Figure 18 shows the calculated post-test diameter profile of the IFA-650.4 rodlet in comparison with measurements. The latter were obtained by metallography of thirteen cross sections, for which the cladding tube diameter was measured in two perpendicular directions. Hence, the data also provide some information on the degree of cylindrical symmetry for the deformation. The calculated peak deformation is the same for the two considered cases, since the same failure criterion in terms of a threshold for the local effective strain was used for both of them. However, the calculated deformation profiles differ. As expected, the fuel relocation tends to concentrate, or localize, the cladding deformation. The reason is the concentrated heat

[13] The weight of dispersed fuel in the IFA-650 series of tests was not determined. Only qualitative assessments of the dispersal in each test, based on post-test gamma scan results and visual inspections, are available [30, 57].

load, resulting from fuel crumbling and accumulation of fuel fragments in the ballooned region of the rod.

Consequently, we next consider the thermal effects of fuel relocation and their impact on the cladding failure behaviour. Figure 19 shows a comparison of the calculated cladding surface temperature with measured data from thermocouples TCC1 and TCC2, which were located 80 mm below the top of the fuel pellet column, i.e. in the part that was completely emptied of fuel upon cladding rupture. The two thermocouples give very similar results, which suggests that the azimuthal temperature difference along the cladding circumference was insignificant at this axial position. It is clear from Fig. 19 that the cladding temperature is slightly underestimated during the heat-up phase ($65 < t < 250$ s): the maximum difference between calculated results and measured data is about 20 K. The most likely explanation to the deviation is our simplified modelling of the clad-to-coolant heat transfer; see Appendix I.

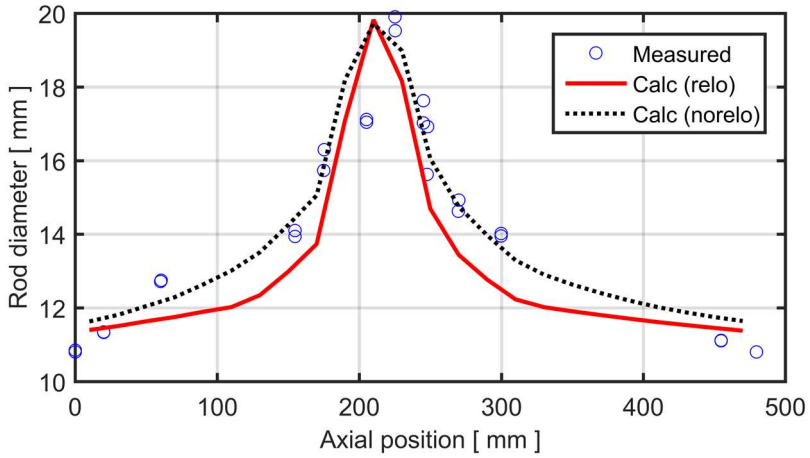

FIG. 18. Calculated and measured post-test diameter profiles for the IFA-650.4 rodlet [73].

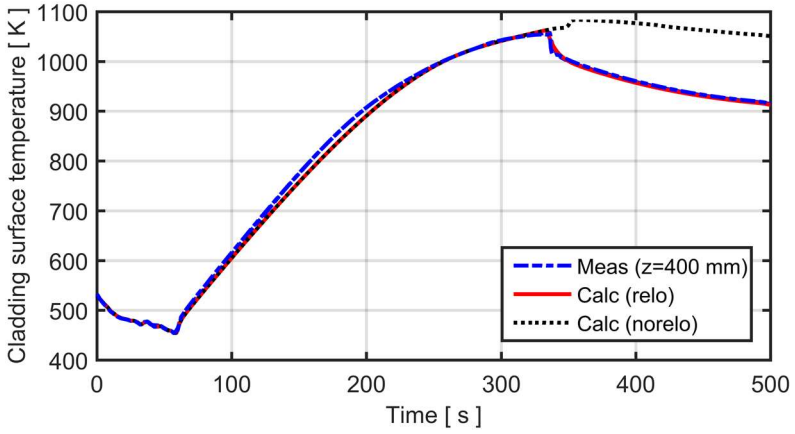

FIG. 19. Calculated and measured cladding surface temperature versus time. The temperature refers to the position of thermocouples TCC1 and TCC2, which were attached 400 mm above the bottom of the fuel pellet column.

Figure 20 is a close-up of Fig. 19, showing the calculated and measured temperature variation about the time of cladding rupture (336 s in experiment, 334 and 348 s in calculations with and without fuel relocation, respectively). The calculated curve for the case with axial fuel relocation is very close to the measured data. This confirms that thermal feedback effects due to the complete fuel loss from the upper part of the rodlet are accurately captured by our model. When the fuel is lost, the cladding temperature approaches that of the surrounding coolant and heater; this is why the calculated and measured curves virtually coincide for $t > 345$ s.

For the calculated case without axial fuel relocation, the cladding temperature increases just after the calculated time of cladding rupture at t = 348 s. The temperature rise is a result of improved pellet-cladding heat transfer, since FRAPTRAN by default models instantaneous and complete ingress of steam from the coolant channel to the pellet-cladding gap upon cladding rupture. The steam has higher thermal conductivity than the initial fill gas, which consisted of 95 vol% argon and 5 vol% helium.

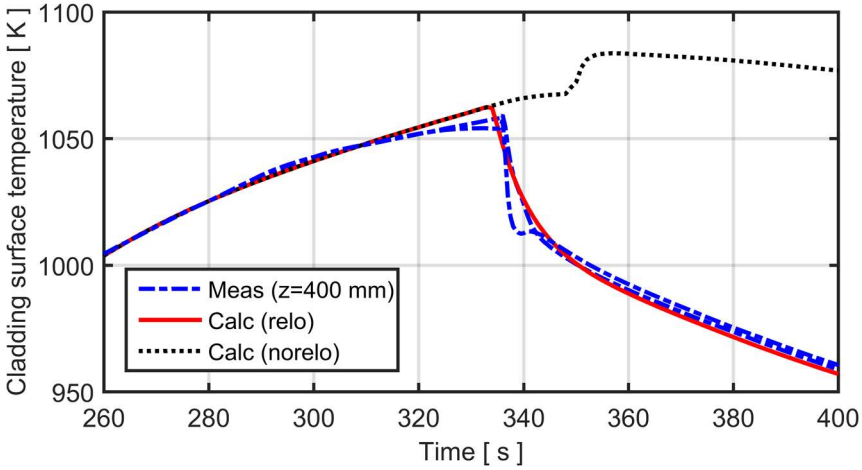

FIG. 20. Calculated and measured cladding surface temperature about the time of cladding rupture (336 s); close-up of Fig. 19.

The long term effect of fuel crumbling and axial relocation on the cladding temperature and oxidation is illustrated by Fig. 21, which shows the calculated cladding outer surface temperature and equivalent cladding reacted (ECR) versus axial position at time t = 500 s. The ECR is a cladding degradation parameter that is widely used in acceptance criteria for emergency core cooling systems. It is defined as the percentage of the cladding thickness that would be oxidized, if all the oxygen from the cladding-water reactions stayed in the oxide layer as ZrO_2. At t = 500 s, transient effects from the collapse of the fuel pellet column into the balloon have decayed and the temperature distribution reflects a quasi-steady condition. It is obvious that the calculated temperature field for the case with axial fuel relocation is governed by the axial distribution of fuel mass and power; compare the right panel of Fig. 17. We note that the case without axial fuel relocation in Fig. 21 shows the opposite trend; the calculated cladding temperature has a minimum in the ballooned region, due to the local increase in coolable surface area. It should be remarked that the case calculated without fuel relocation in Fig. 21 is in fact affected by relocation: the low temperature calculated for the upper part of the fuel rod for the case without relocation is due to the decline in heater temperature, which is caused by the fuel relocation that occurs in the test. The measured space-time variation of the heater temperature is used for defining the thermal-hydraulic boundary conditions in all calculations with FRAPTRAN, both with and without the relocation model, so this effect is inevitable.

As can be seen from the calculated post-test ECR in the right panel of Fig. 21, the long-term change in temperature distribution caused by the axial fuel relocation has a noticeable effect on the post-failure oxidation of the cladding. The calculated pre-test ECR from low temperature oxidation in Gösgen was about 1.6 %; this pre-test oxidation is included in the curves presented in Fig. 21.From the Fig., it is clear that the calculated contribution to the peak post-test ECR from the IFA-650.4 LOCA test is about 70 % larger when axial fuel relocation is considered.

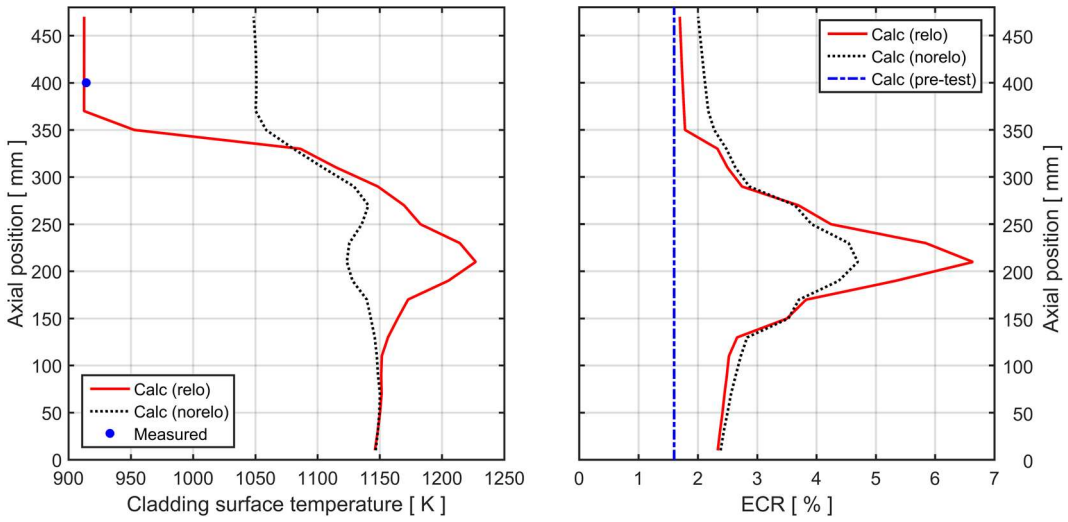

FIG. 21. Calculated cladding outer surface temperature and equivalent cladding reacted (ECR) versus axial position at time t = 500 s, with and without consideration of axial fuel relocation.

The calculated results presented for the ECR in the right panel of Fig. 21 cannot be directly verified against experimental data, since no post-test measurements were made of the axial variation in cladding oxide thickness or metal oxygen concentration. However, the outer surface oxide layer thickness was measured at some positions in the ballooned region after the test. It ranged from about 10 to 13 μm, and the thickest oxide was found at the lower end of the balloon [73]. These results indicate that the peak post-test ECR would be around 3.3 %, i.e. significantly lower than our calculated results for the cases with and without fuel relocation. This is not surprising, considering that fuel fragments were ejected from the failed balloon into the coolant during the test. The fuel ejection, which is not accounted for in our simulations of the test, lowered the fuel fragment packing fraction in the balloon. More precisely, the post-test area fraction covered by fuel fragments was estimated to be no more than 0.4–0.5 in the balloon, based on image analyses [73]. The low fragment packing fraction that resulted from the fuel ejection most certainly limited the thermal feedback effects of axial fuel relocation in the post-failure part of the experiment.

4.2.2. IFA-650.9

The design and pre-irradiation conditions for the IFA-650.9 rodlet were nearly identical to those of the sibling IFA-650.4 rodlet. However, the IFA-650.9 rodlet was tested at much higher power and reached significantly higher temperatures than its sibling IFA-650.4 [11].

Figure 22 shows the calculated and measured evolution of rod plenum gas pressure during the Halden IFA-650.9 test. In the calculations, the initial cold pressure was reduced from its reported value of 4.0 MPa to 3.78 MPa, to match the calculated “hot” pre-test gas pressure to the measured value (6.96 MPa). It is clear that the calculated plenum pressure deviates significantly from the measurements in this test, both before and after cladding rupture, which occurred at t = 133 s. The slow equilibration with the external (rig) pressure after cladding rupture suggests that the axial gas flow between the upper plenum and the cladding breach at the bottom part of the rodlet was significantly restricted. This is not captured in the calculations, since axial pressure gradients are neglected by FRAPTRAN-1.5; see Section 3.2.2.

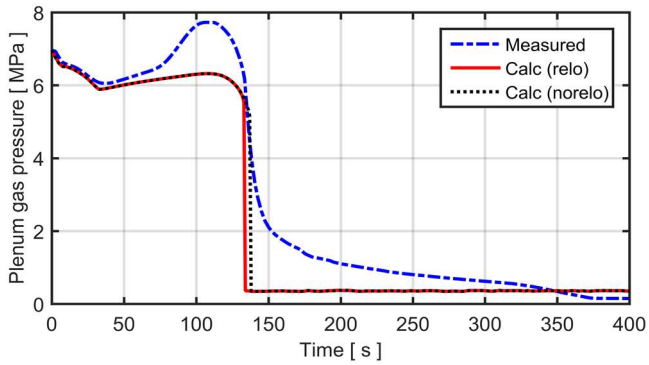

FIG. 22. Calculated evolution of rod plenum gas pressure in comparison with measurements for the IFA-650.9 test rodlet.

Restricted axial gas flow has been observed also in a few other Halden IFA-650 test rodlets (3 and 5), and the behaviour observed in these rodlets has been analysed by use of computer models [74]. The same computer models were then applied to analyse the internal gas flow in a full length PWR fuel rod, having a cladding breach far away from its gas plenum. The results suggest that the flow restrictions in a full length fuel rod are significant, and that the restrictions may delay cladding rupture by limiting the amount of gas available in the ballooned region [74].

In Fig. 22, the calculated curves for the cases with and without assumed fuel relocation coincide up to t = 130 s, which is the time when fuel fragments start to relocate axially, according to our calculations. The calculated time of cladding failure is 133.5 s for the case with fuel relocation and 137.8 s without. These results suggest that cladding ballooning, collapse of the fuel pellet column, and axial relocation of fuel take place within 3–4 s before cladding rupture.

Figure 23 shows the calculated evolution of cladding deformation and axial fuel relocation during the last four seconds before cladding rupture. The thick red line shows the calculated state at the time of cladding rupture, and the leftmost curve shows the conditions about the time when the balloon starts to grow and fuel starts to relocate.

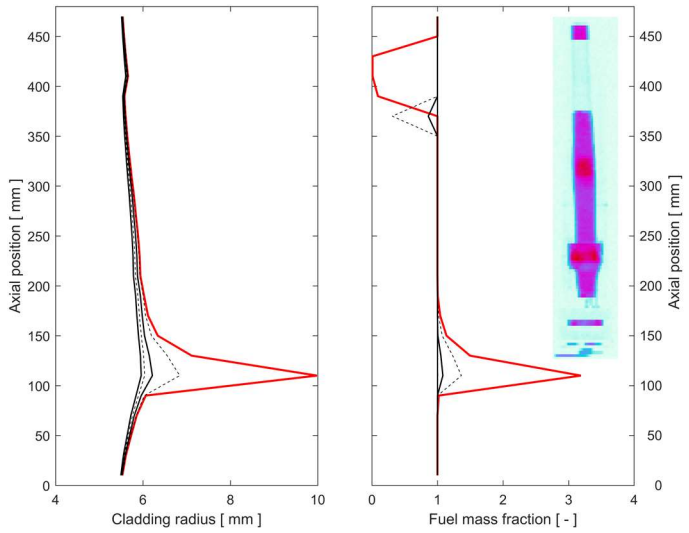

FIG. 23. Calculated evolution of cladding deformation (left) and fuel relocation (right) during the last four seconds before cladding rupture. The rightmost curve (red) represents the conditions at time of rupture, while the four curves to the left of it show the calculated state 1, 2, 3 and 4 s before rupture. A post-test gamma scan image of the IFA-650.9 test rig is included for comparison [60].

The calculations suggest that the local fuel mass is increased by a factor of 3.2 in the most distended cross section of the test rodlet. The relocated fuel originates from a 50 mm long part of the fuel pellet column, which has disappeared completely. Above this emptied part, there is a "plug" of remaining fuel pellets at the very top of the fuel pellet column. This is well in line with the results reported from the test: Gamma scan (see insert in Fig. 23) showed that there were in fact a few remaining fuel pellets above the missing part of the fuel pellet column after the test. The length of the missing fuel part was 120–130 mm, which is about 70 mm longer than calculated with our model. Similar to the IFA-650.4 test, a significant amount of fuel had been expelled through the cladding breach and was found at the bottom of the pressure flask after the test [60, 75]. This dispersal of fuel fragments, which is not accounted for by our model, most certainly increased the amount of fuel lost from the upper part of the IFA.650.9 rodlet. The gamma scan results also show that there is a secondary hot spot, caused by fuel accumulation about the axial midplane of the rodlet. This is not captured by our model, since the secondary balloon is not reproduced; see below.

According to our calculations, the entire fuel column had been pulverized into fine (< 0.2 mm) fragments at time of cladding rupture, which means that the crumbled and relocated fuel had an assumed packing fraction of 0.72 everywhere in the ballooned region; see the description of the applied models for fuel fragmentation and pulverization in [9].

Figure 24 shows the calculated post-test diameter profile of the IFA-650.9 rodlet, in comparison with data that were obtained by analysing visual inspection photos [75]. The calculated results differ from the measurements in two respects: the position of the primary balloon at the bottom part of the rod is a little bit too high, and the secondary balloon at the midplane of the rodlet is not captured at all. As with the IFA-650.4 test, the calculations suggest that axial relocation of hot fuel tends to localize the cladding deformation to the primary balloon.

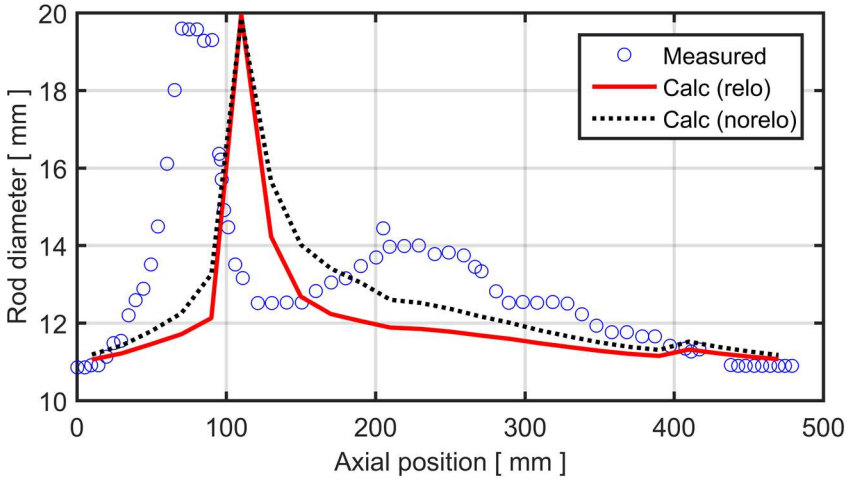

FIG. 24. Calculated and measured post-test diameter profiles for the IFA-650.9 rodlet [75].

Figure 25 and Fig. 26 show comparisons of the calculated cladding surface temperature with measured data at different axial positions of the IFA-650.9 rodlet. The measured data clearly show that, at time of cladding rupture, the cladding temperature suddenly increases in the lower part of the rodlet, whereas it decreases in the upper part. This is a consequence of axial fuel relocation, and our calculations with the relocation model activated captures the observed thermal feedback effects fairly well. Figure 27 and Fig. 28 are close-ups, showing the calculated and measured temperature variations about the time of cladding rupture (133 s in experiment, 133.5 s and 137.8 s in calculations with and without fuel relocation, respectively).

We note from Fig. 25 and Fig. 27 that the cladding temperature at the primary balloon is overestimated after cladding rupture, when fuel relocation is considered in the calculations. This difference may be due to fuel ejection, possibly leading to a lower fuel fragment packing fraction and cladding temperature in the balloon than in our calculations, where fuel ejection into the coolant is not considered.

Two comments should also be made on Fig. 26 and Fig. 28: Firstly, the temperatures measured by TCC2 and TCC3 differ by up to 30 K after cladding rupture. This azimuthal temperature difference is probably due to bending of the rodlet [60, 75]. Secondly, the temperature drop caused by the fuel loss from the upper part of the rodlet is overestimated by our model. This may be explained either by the fact that axial heat conduction in the cladding tube is not considered in FRAPTRAN-1.5, or by the fact that some fuel actually remained in the upper part of the rodlet for some time after cladding rupture.

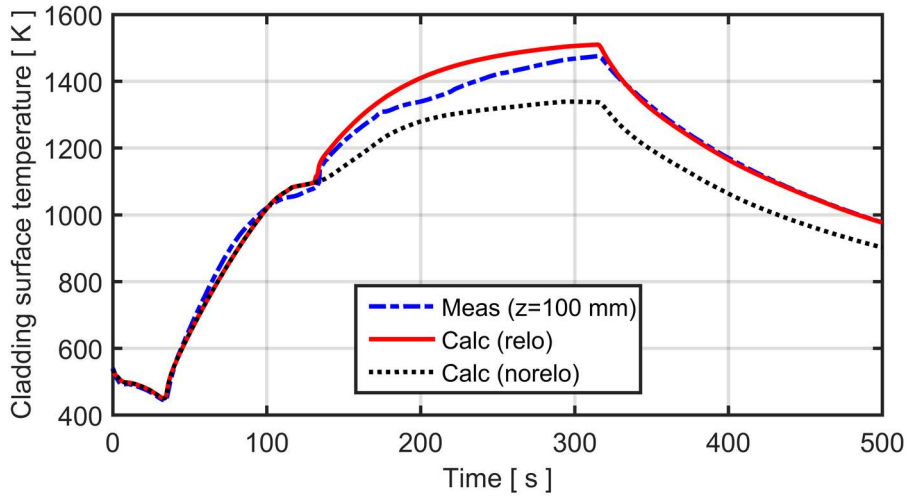

FIG. 25. Calculated and measured cladding surface temperature versus time. The presented temperature refers to the position of thermocouple TCC1, which was attached 100 mm above the bottom of the fuel pellet column.

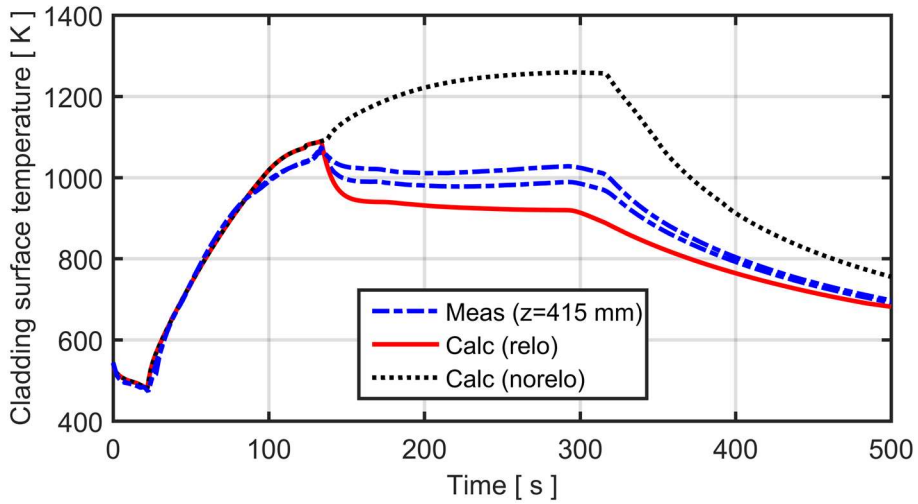

FIG. 26. Calculated and measured cladding surface temperature versus time. The temperature refers to the position of thermocouples TCC2 and TCC3, which were attached 415 mm above the bottom of the fuel pellet column.

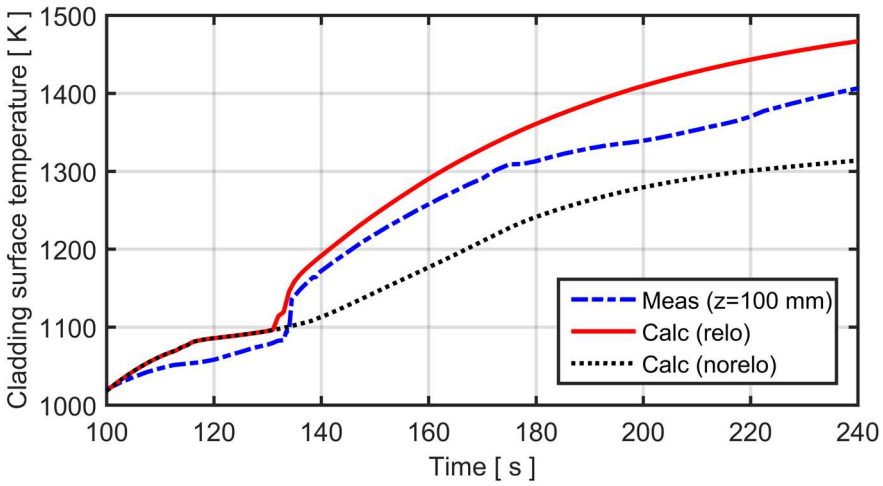

FIG. 27. Calculated and measured cladding surface temperature about the time of cladding rupture (133 s); close-up of Fig. 25.

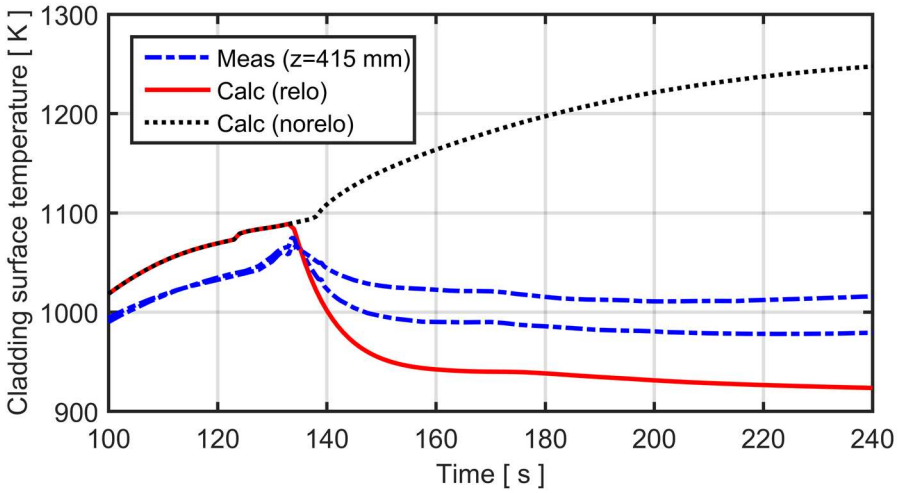

FIG. 28. Calculated and measured cladding surface temperature about the time of cladding rupture (133 s); close-up of Fig. 26.

The long term effect of fuel crumbling and axial relocation on the cladding temperature and oxidation for the IFA-650.9 test is illustrated by Fig. 29, which shows the calculated cladding outer surface temperature and equivalent cladding reacted versus axial position at time t = 500 s. As with the IFA-650.4 test, it is obvious that the calculated temperature field for the case with axial fuel relocation is governed by the axial distribution of fuel mass and power; compare the right panel of Fig. 23. The measured cladding surface temperatures are in perfect agreement with the calculated results for the case with fuel relocation.

As can be seen from the calculated post-test ECR in the right panel of Fig. 29, the long-term change in temperature distribution caused by the axial fuel relocation has a very strong effect on the post-failure oxidation of the cladding for test IFA-650.9. The reason is that the cladding was exposed to high temperature for a fairly long time, following axial fuel relocation and cladding rupture. The calculated pre-test ECR from low temperature oxidation in Gösgen was about 1.3 %; this pre-test oxidation is included in the curves presented in Fig. 29.

Since no systematic post-test measurements were made of the axial variation in cladding oxide thickness or metal oxygen concentration, the calculated axial distribution presented for the ECR in the right panel of Fig. 29 cannot be assessed against experimental data. However, metallography was carried out on three cross sections of the cladding tube, two of which were

directly at the failed (primary) balloon in the lower end of the rodlet [75]. The thickness of the outer and inner oxide layer at the balloon was about 20 and 5 µm, respectively [75]. The corresponding values calculated with the Cathcart-Pawel oxidation model in FRAPTRAN-1.5 are 78 and 66 µm, respectively.

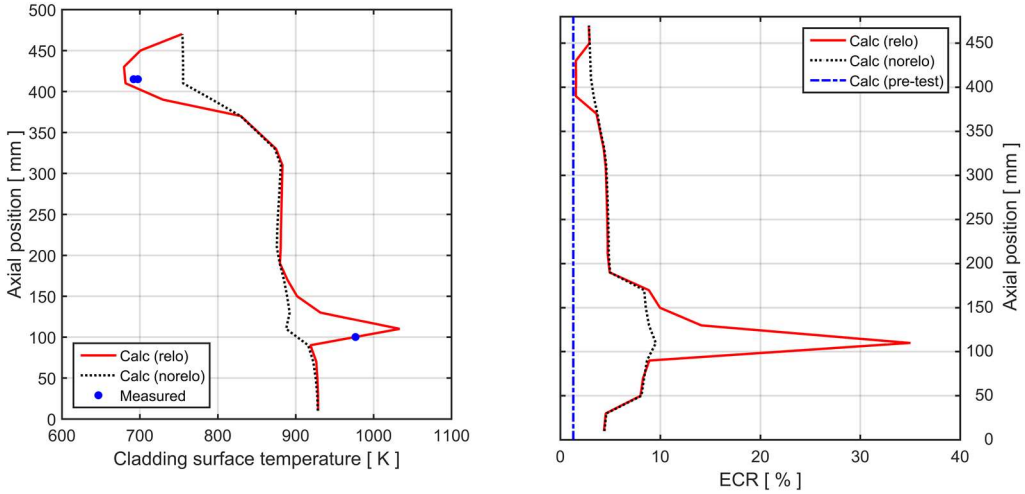

FIG. 29. Calculated cladding outer surface temperature and equivalent cladding reacted (ECR) versus axial position at time t = 500 s, with and without consideration of axial fuel relocation.

These large differences between calculated and measured oxide layer thicknesses cannot be explained by differences between calculated and measured cladding temperatures: as shown by Fig. 25, the local temperature at the primary balloon is fairly well reproduced by our extended version of FRAPTRAN. The only reasonable explanation to the differences is that local oxidation in the lower part of the fuel rod was limited by steam starvation, i.e. the cladding oxidation may have reduced the partial pressure of oxygen and created a gas enriched in hydrogen. This hypothesis is supported by the very high post-test hydrogen concentration, 1570 ±600 wppm, which was measured in the ballooned region of the cladding tube [75].

4.2.3. IFA-650.10

Figure 30 shows the calculated and measured evolution of rod plenum gas pressure during the Halden IFA-650.10 test. In the calculations, the initial cold pressure was reduced from its reported value of 4.0 MPa to 3.98 MPa, to match the calculated "hot" pre-test gas pressure to the measured value (7.15 MPa). The calculated gas pressure is in close agreement with measurements for $t < 160$ s, but underestimated for the remaining period up to cladding rupture, which occurred at $t = 249$ s in this test. We also note that, upon cladding failure, the measured plenum pressure dropped instantaneously to about 1.2 MPa, according to Fig. 30. In reality, the gas pressure fell to that of the coolant (0.3–0.4 MPa), but mechanical constraints in the pressure transducer limited the measuring range.

In Fig. 30, the calculated curves for the cases with and without assumed fuel relocation coincide up to $t = 247$ s, which is the time when fuel fragments start to relocate axially, according to our calculations. The calculated time of cladding failure is 249.9 s for the case with fuel relocation and 259.1 s without. These results suggest that cladding ballooning, collapse of the fuel pellet column, and axial relocation of fuel take place within three seconds before cladding rupture.

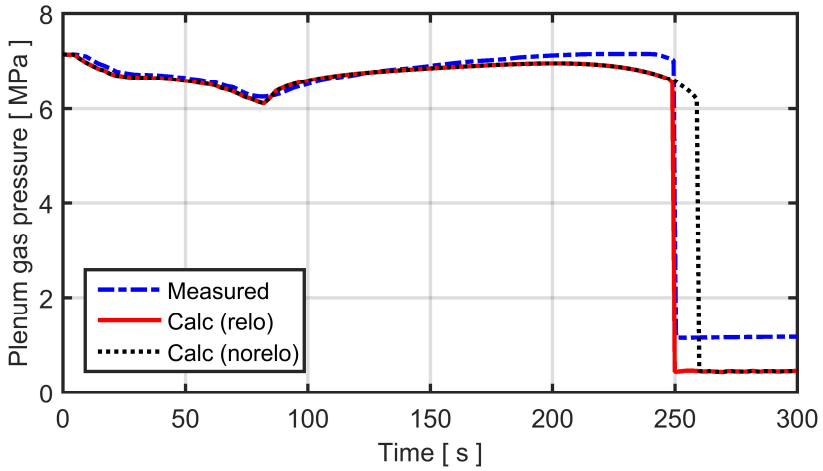

FIG. 30. Calculated evolution of rod plenum gas pressure in comparison with measurements [61] *for the IFA-650.10 test rodlet.*

Figure 31 shows the calculated evolution of cladding deformation and axial fuel relocation during these last three seconds before cladding rupture. The thick red line shows the calculated state at the time of cladding rupture, and the leftmost curve shows the conditions about the time when the balloon starts to grow and fuel starts to relocate. The calculations suggest that the local fuel mass is increased by a factor of 1.3 in the most distended cross section of the test rodlet. The relocated fuel originates from the upper part of the balloon and the region just above the balloon. Hence, our relocation model does not calculate any long range axial fuel relocation in the upper part of the rodlet, in contrast to the other IFA-650 tests considered in this report. As can be seen from the inserted gamma scan image in Fig. 31, this result agrees with the relocation pattern observed in the test [76]. Axial fuel relocation was observed only within the ballooned region of the rodlet, where fuel fragments were missing from the upper part. As seen from the inserted gamma scan image in Fig. 31, a small quantity of fuel had been ejected through the rupture opening and was found at the bottom of the test rig after the test [76].

The IFA-650.10 rodlet had an average fuel burnup of 61 $MWd(kgU)^{-1}$, which is significantly lower than other test rods considered in this report. As can be seen from Table 9, only 11 % of the fuel had a calculated local burnup in excess of 70 $MWd(kgU)^{-1}$, which is a necessary condition for fuel pulverization in the applied models for fuel fragmentation and pulverization [9]. Consequently, according to our calculations, 11 % of the fuel in the region where cladding ballooning and fuel relocation took place had been pulverized into fine (< 0.2 mm) fragments at time of cladding rupture. This result seems to agree qualitatively with findings from the post-test examinations [76], but the post-test fuel fragment size distribution was unfortunately not measured for this test. The calculated mixture of large and small fuel fragments leads to an estimated packing fraction of 0.77 everywhere in the ballooned region [9]. This packing fraction is slightly higher than that calculated for the IFA-650.4 and IFA-650.9 rodlets (0.72), in which the entire fuel inventory was assumed to pulverize during the tests.

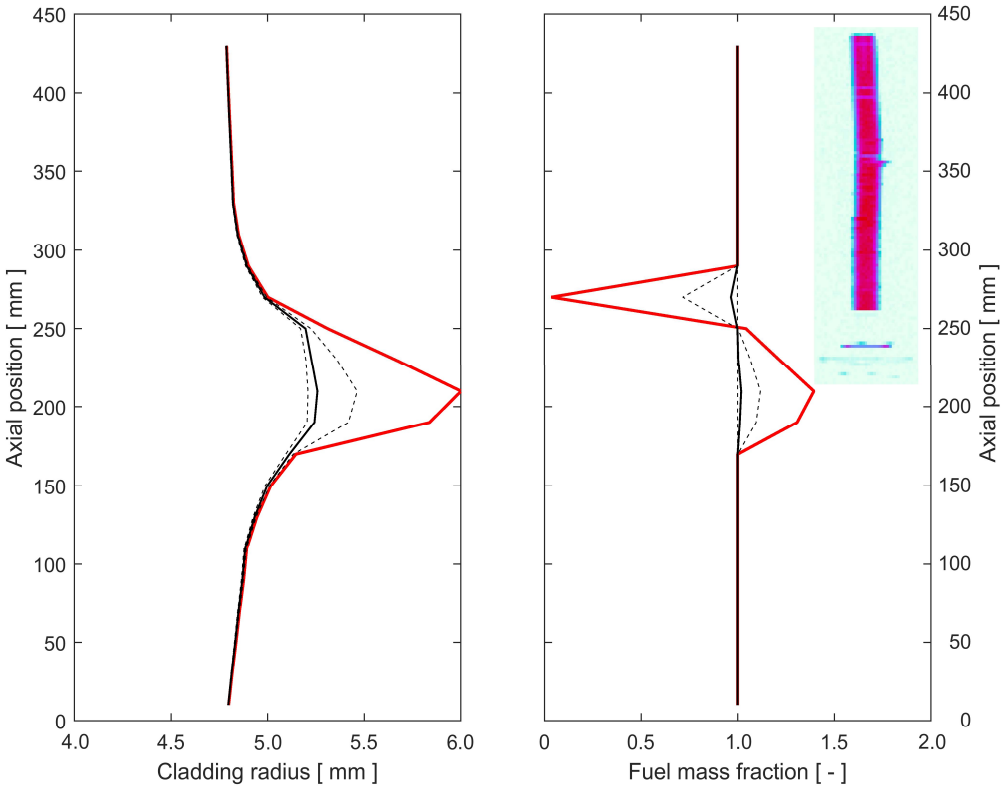

FIG. 31. Calculated evolution of cladding deformation (left) and fuel relocation (right) during the last three seconds before cladding rupture. The rightmost curve (red) represents the conditions at time of rupture, while the three curves to the left of it show the calculated state 1, 2 and 3 s before rupture. A post-test gamma scan image of the IFA-650.10 rig is included for comparison [76].

Figure 32 shows the calculated post-test diameter profile of the IFA-650.10 rodlet in comparison with data that were obtained by analysing visual inspection photos and neutron radiographs [76]. It is clear from Fig. 32 that the length of the ballooned region is overestimated, and the calculated axial position of the balloon is slightly lower than actually observed. As seen also for the other IFA-650 tests in this report, the calculated results presented in Fig. 32 suggest that axial relocation of hot fuel tends to localize the cladding deformation to the balloon.

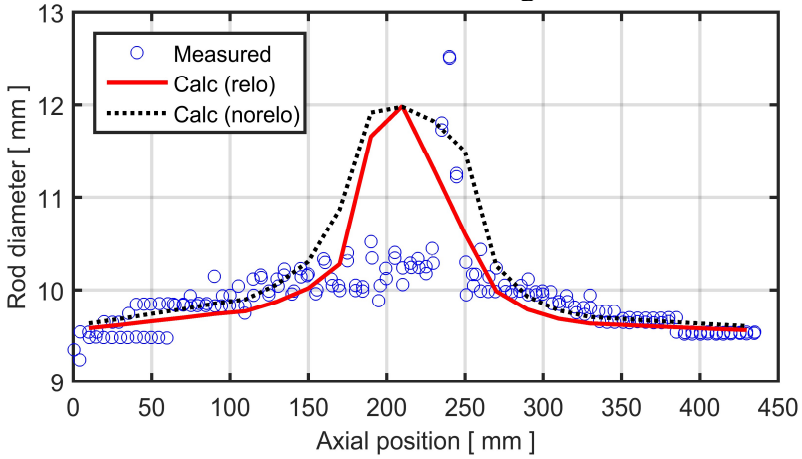

FIG. 32. Calculated and measured post-test diameter profiles for the IFA-650.10 rod [76].

Figure 33 and Fig. 34 show comparisons of the calculated cladding surface temperature with measured data at different axial positions of the IFA-650.10 rodlet. In addition, Fig. 35 and Fig. 36 are close-ups, showing the calculated and measured temperature variations about

the time of cladding rupture (249 s in experiment, 249.9 and 259.1 s in calculations with and without fuel relocation, respectively). The measured data show that, at time of cladding failure, the cladding temperature dropped temporarily for a few seconds in the upper part of the rodlet. This is attributed to cooling from the rod internal gas, which flowed from the relatively cool gas plenum towards the cladding breach [61]. As shown by the data in Fig. 30, the axial gas flow from the plenum was fast in the IFA-650.10 rodlet.

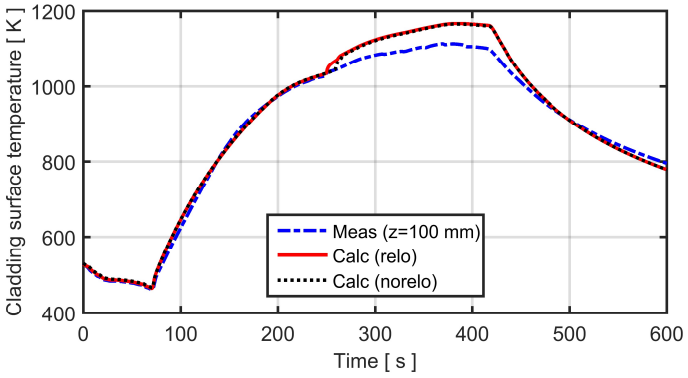

FIG. 33. Calculated and measured cladding surface temperature versus time. The presented temperature refers to the position of thermocouple TCC1, which was attached 100 mm above the bottom of the fuel pellet column.

Effects of cooling from flowing gas in the pellet-cladding gap are not considered in FRAPTRAN-1.5 [2], and the temperature dip measured by TCC2 and TCC3 is therefore not captured in our calculations. The calculations in fact suggest that the cladding temperature increases by 10–15 K immediately upon cladding failure. This calculated temperature rise is an artificial effect, caused by the assumption made in FRAPTRAN-1.5 that steam completely and immediately replaces the rod internal gas from the time of cladding rupture [2].

From Fig. 33 and Fig. 34, it is clear that the cladding surface temperature is overestimated by 40–50 K at both ends of the IFA-650.10 rodlet after cladding failure. The difference is larger than observed for the other IFA-650 tests considered in this report, and the reason is unclear. A possible explanation is that the water spraying cooled the cladding to a larger extent than in the other considered IFA-650 tests [11]. Direct cooling effects from water spraying would not be captured in our calculations, since they are not addressed by the applied thermal-hydraulic boundary conditions; see Appendix I.

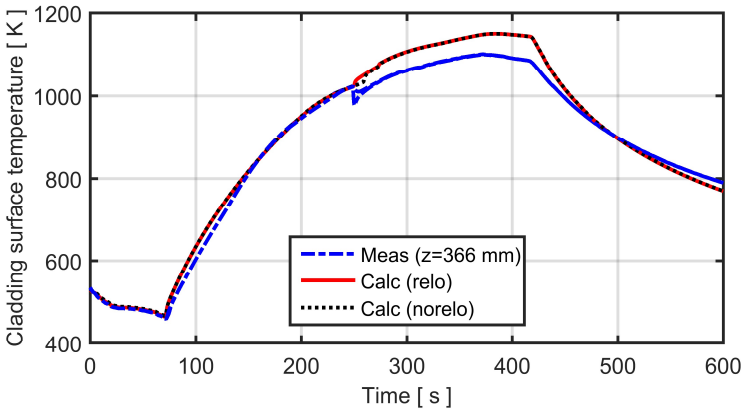

FIG. 34. Calculated and measured cladding surface temperature versus time. The temperature refers to the position of thermocouples TCC2 and TCC3, which were attached 366 mm above the bottom of the fuel pellet column.

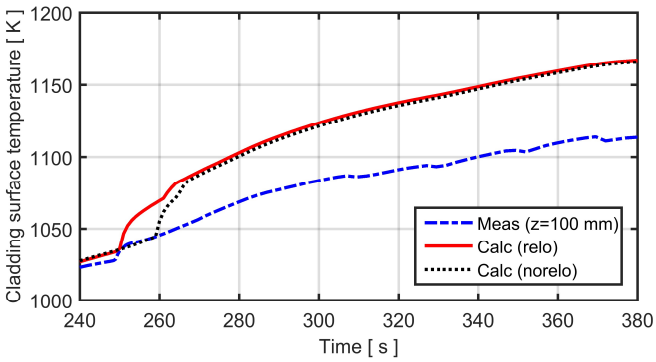

FIG. 35. Calculated and measured cladding surface temperature about the time of cladding rupture (249 s); close-up of Fig 33.

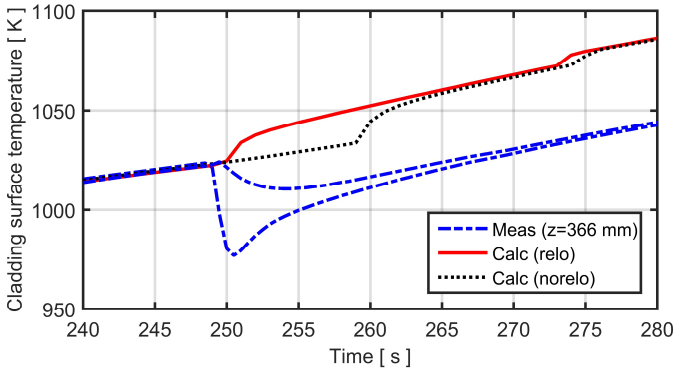

FIG. 36. Calculated and measured cladding surface temperature about the time of cladding rupture (249 s); close-up of Fig. 34.

Figure 37 shows the calculated cladding outer surface temperature and equivalent cladding reacted versus axial position at time t = 600 s. Similar to the results presented previously for IFA-650.4 and IFA-650.9, the calculated temperature field for the case with axial fuel relocation is governed by the axial distribution of fuel mass and power. However, the calculated temperature changes caused by the relocated fuel are moderate. The reason is that the calculated amount of relocated fuel is fairly small in the IFA-650.10 test; compare the right panel of Fig. 31. The cladding surface temperature at t = 600 s is underestimated by about 20 K, which is more than for the IFA-650.4 and IFA-650.9 tests.

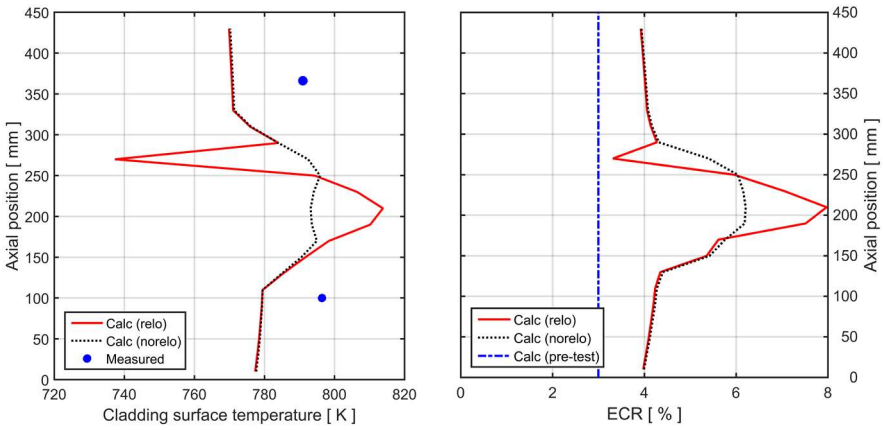

FIG. 37. Calculated cladding outer surface temperature and equivalent cladding reacted (ECR) versus axial position at time t = 600 s, with and without consideration of axial fuel relocation.

As can be seen from the calculated post-test ECR in the right panel of Fig. 37, the long-term change in temperature distribution caused by the axial fuel relocation has a moderate effect

on the post-failure oxidation of the IFA-650.10 cladding. The calculated pre-test ECR from low temperature oxidation in Gravelines 5 was about 3 %; this pre-test oxidation is included in the curves presented in Fig. 37.

The thickness of the oxide layer at the cladding inner and outer surfaces was measured in post-test metallographic investigations [76]. Measurements were made over a 120 mm long section of the cladding, which was centred at the failed balloon. Mean values of the inner surface oxide thickness at various axial positions were in the range of 9–15 μm, while the outer surface oxide was 34–39 μm thick [76]. The calculated results from our extended version of FRAPTRAN-1.5 agree very well with these measurements: the best-estimate peak values for the post-test inner and outer surface oxide layer thickness in the balloon were 12.6 and 35.9 μm when fuel relocation was considered in the calculations, and 8.6 and 31.8 μm when the relocation model was deactivated. The cladding high temperature oxidation is thus accurately reproduced for the IFA-650.10 test, in contrast to the IFA-650.4 and IFA-650.9 tests. This suggests that the water spraying in the IFA-650.10 test was sufficient to maintain cladding oxidation (no steam starvation as suspected for the IFA-650.9 test). The cladding temperature, and thus the oxidation rate, was fairly low in the IFA-650.10 test.

4.2.4. IFA-650.14

The IFA-650.14 test rodlet had an average fuel burnup of 70.8 MWd(kgU)$^{-1}$. According to our calculations, about 32 % of the fuel reached a local burnup above 70 MWd(kgU)$^{-1}$, which is a necessary condition for fuel pulverization in our applied model for fuel fragmentation and pulverization [9]. However, since the fuel temperatures remained low in the test, only 22 % of the fuel pulverized, according to our simulations. The resulting mixture of small and large fuel fragments that relocated into the ballooned region of the cladding tube had a calculated packing fraction of 0.84, which is much higher than for the other tests considered in this report.

The calculated fraction of pulverized fuel, 22 %, disagrees with the results from post-test sifting of the fragmented fuel [70]. According to these measurements, only 0.6 % of the dislodged fuel fragments were smaller than 0.25 mm. Because of the large difference between calculated and measured fractions of pulverized fuel for the IFA-650.14 test, we used the measured rather than the calculated fraction in calculations with our relocation model. More precisely, we postulated that the maximum value for the fuel fragment packing fraction of crumbled fuel, ϕ_m, is 0.69. This value is based on measured data from LOCA tests on low-burnup fuel, in which no fuel pulverization was observed [9]. In addition, we also considered a case with ϕ_m = 0.72, which corresponds to the fuel fragment packing fraction used for analyses of the IFA-650.4 and IFA-650.9 rodlets in this report. The purpose was to illustrate the sensitivity of the calculated results to the packing fraction assumed for the crumbled fuel.

In addition, we considered transient fission gas release in our analyses of the Halden IFA-650.14 test. As mentioned in Section 3.2.2., the transient fission gas release must be modelled for this test, since it resulted in a threefold increase of the amount of free gas within the rodlet. For lack of a transient fission gas release model in FRAPTRAN-1.5, we postulated a smooth ramp function for the fission gas release, as defined by Eq. 13 in Section 3.2.2. This function is shown in Fig. 38, together with the calculated evolution of fuel pellet temperature at the peak power axial position of the rodlet. It is clear that significant transient fission gas release is assumed to occur at fuel temperatures above 900 K.

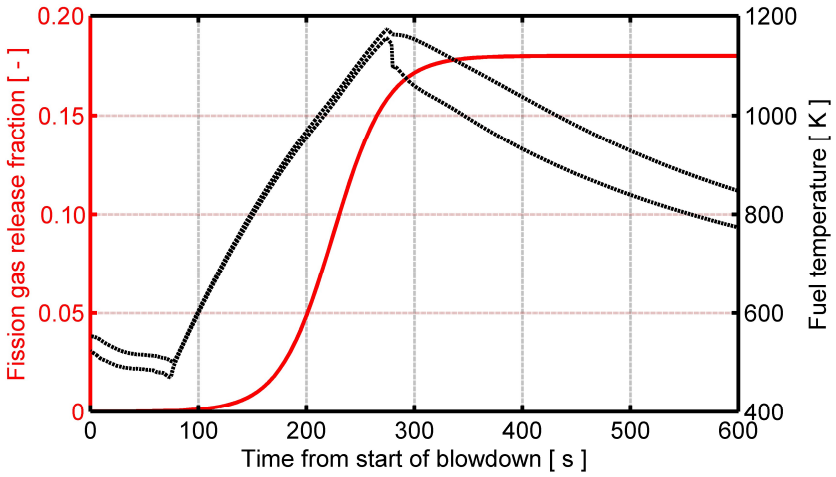

FIG. 38. The red full line shows the assumed time history for the transient fission gas release; see eq. 13. The black dashed lines show the calculated fuel temperatures for the pellet centre and surface at the peak power axial position of the IFA-650.14 test rodlet.

Fig. 39 shows the calculated and measured evolution of rod plenum gas pressure during the Halden IFA-650.14 test. In the calculations, the initial cold pressure was reduced from its reported value of 2.0 MPa to 1.66 MPa, to match the calculated "hot" pre-test gas pressure to the measured value (3.49 MPa). The calculated gas pressure is in close agreement with measurements throughout the test. The best agreement is obtained for the case with ϕ_m = 0.72, but the influence of axial fuel relocation and assumed fuel fragment packing fraction is moderate.

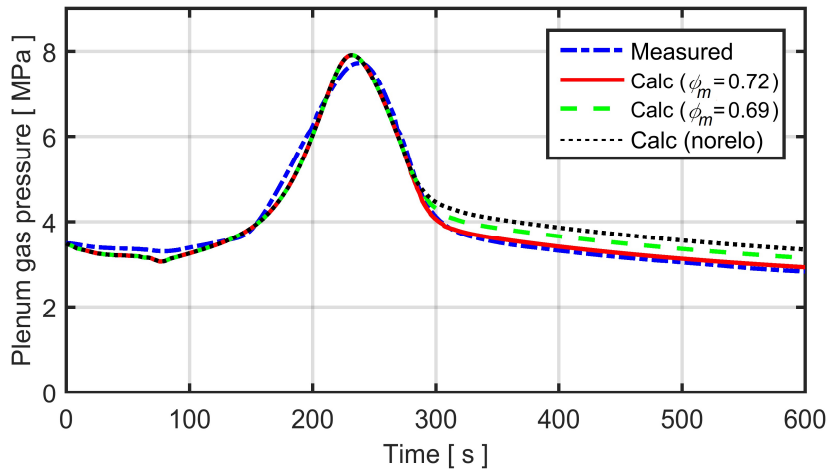

FIG. 39. Calculated evolution of rod plenum gas pressure in comparison with measurements [63] *for the IFA-650.14 test rodlet. Here, ϕ_m is the postulated max value for the fuel fragment packing fraction in the relocation model.*

Fig. 40 and Fig. 41 show the evolution of cladding deformation and axial fuel relocation, calculated with ϕ_m = 0.72 and ϕ_m = 0.69, respectively. The results pertain to the time interval from 280 to 340 s, in which a cladding balloon is calculated to form just above the axial midplane of the rodlet. The calculations suggest that the local fuel mass is increased by a factor of 1.50 or 1.25 in the most distended cross section of the test rodlet, depending on the value assumed for the fuel fragment packing fraction in the balloon. The relocated fuel originates from the very top of the fuel pellet column, according to our calculations. This is not fully consistent with results from post-test neutron radiography of the rodlet, which showed that a 35 mm long section ('plug') of the fuel pellet column remained at the very top [70].

It is interesting to compare the fairly long (~60 s) period under which the balloon develops in the IFA-650.14 test with the very much shorter ballooning times calculated for the other IFA-650 tests in this report. The difference is caused by the exceptionally small free internal gas volume in the IFA-650.14 rodlet; see Table 5. This effect of internal gas volume is significant to the expected burst behaviour of full-length LWR fuel rods under LOCA; see Section 5.3.2.

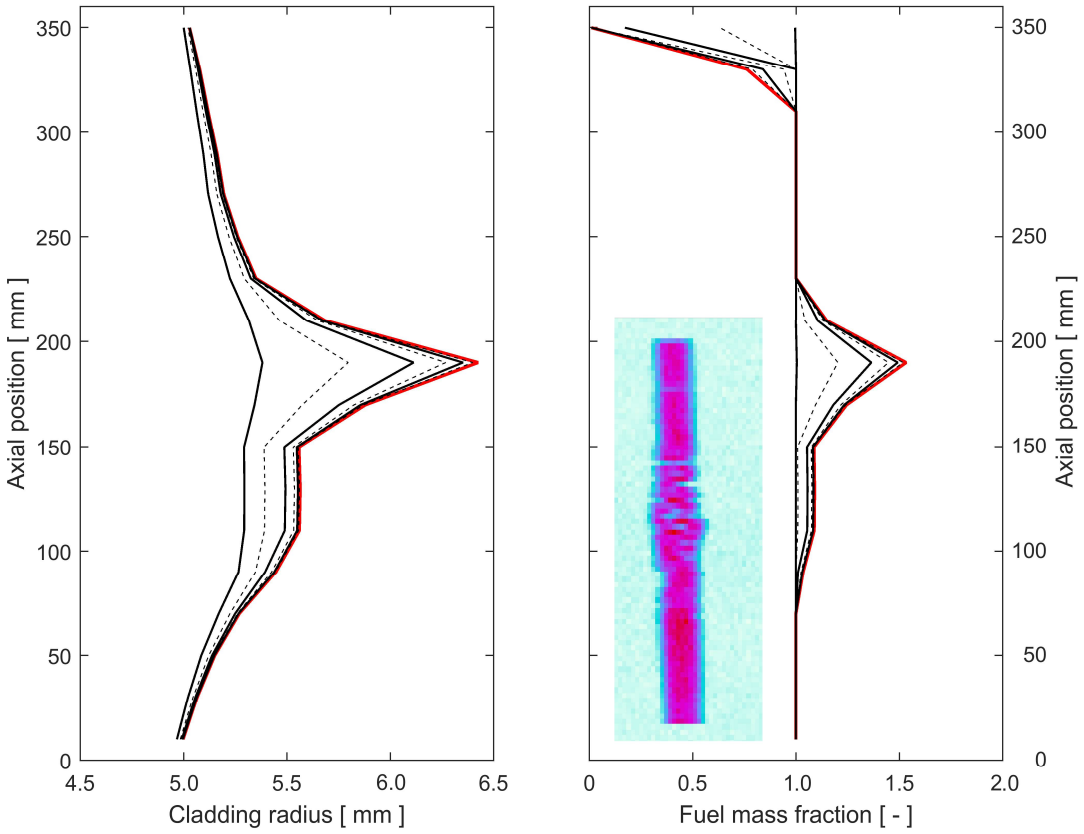

FIG. 40. Calculated evolution of cladding deformation (left) and fuel relocation (right) during the time interval from 280 to 340 s. The calculations were done with a postulated max fuel fragment packing fraction (ϕ_m) of 0.72. A post-test gamma scan image of the IFA-650.14 rodlet is included for comparison [63].

Figure 42 shows the calculated post-test diameter profile for the IFA-650.14 rodlet in comparison with data that were obtained by contact profilometry [70]. The position of the primary balloon is accurately reproduced, but the local cladding deformation at the balloon is underestimated. The calculated peak deformation depends strongly on the assumed packing fraction of the fuel fragments.

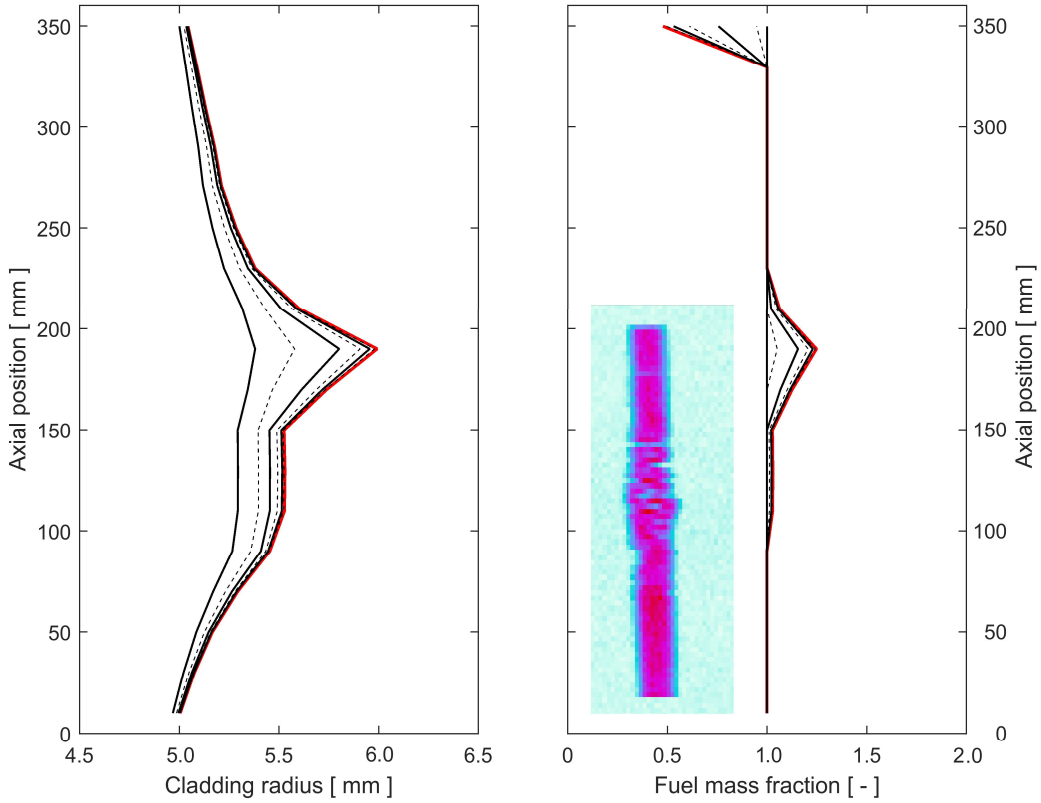

FIG. 41. Calculated evolution of cladding deformation (left) and fuel relocation (right) during the time interval from 280 to 340 s. The calculations were done with a postulated max fuel fragment packing fraction (ϕ_m) of 0.69. A post-test gamma scan image of the IFA-650.14 rodlet is included for comparison [63].

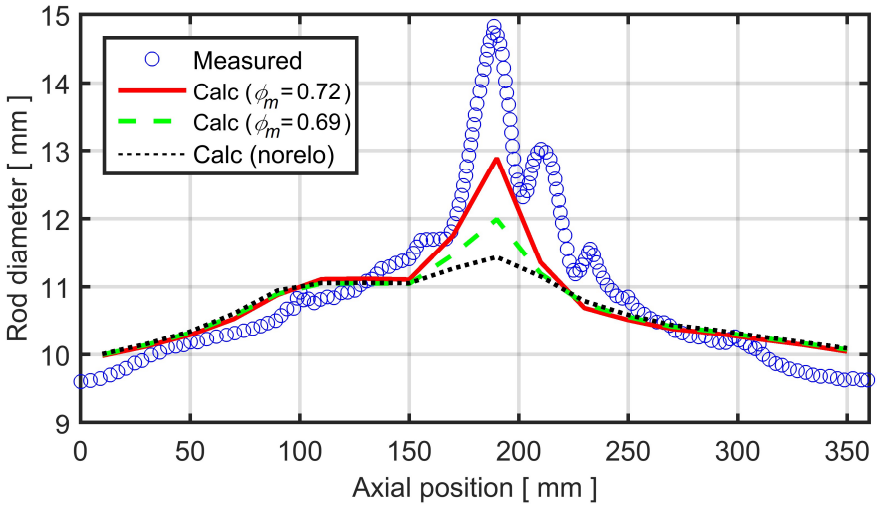

FIG. 42. Calculated and measured post-test diameter profiles for the IFA-650.14 rod [70].

Figure 43 and Fig. 44 show comparisons of the calculated cladding surface temperature with measured data at different axial positions of the IFA-650.14 rodlet. In addition, Fig. 45 and Fig. 46 are close-ups, showing the calculated and measured temperature variations about the time of reactor scram (275 s). It is clear that the cladding surface temperature is reproduced quite well by our extended version of FRAPTRAN-1.5, both in the lower and upper part of the rodlet. The largest differences between calculated and measured temperatures, about 20 K, are found in the upper part of the rodlet, following reactor scram.

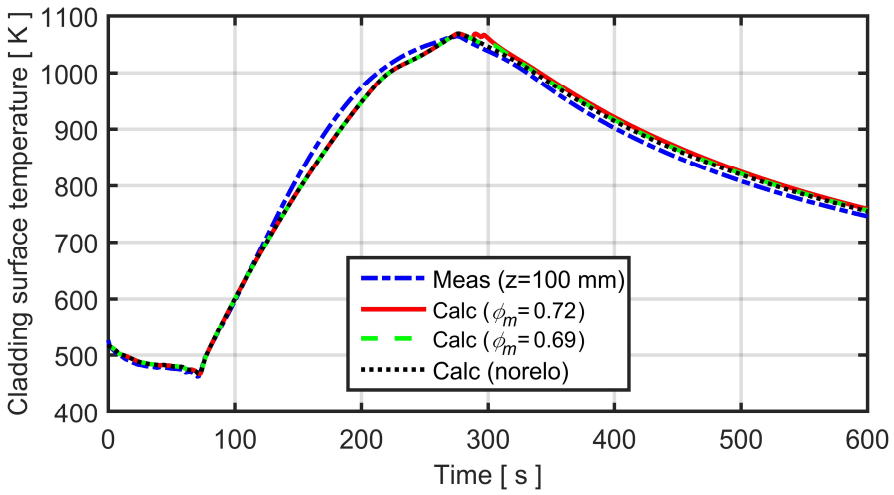

FIG. 43. Calculated and measured cladding surface temperature versus time. The temperature refers to the position of thermocouple TCC1, which was attached 100 mm above the bottom of the fuel pellet column.

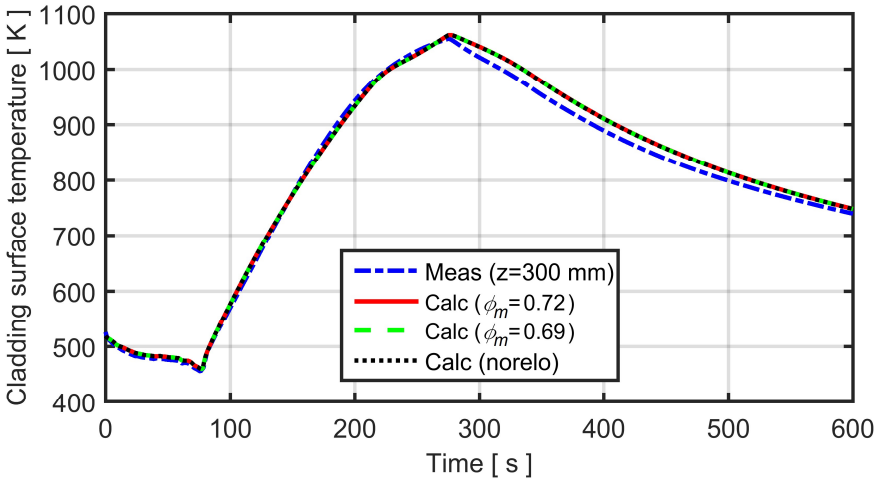

FIG. 44. Calculated and measured cladding surface temperature versus time. The temperature refers to the position of thermocouple TCC2, which was attached 300 mm above the bottom of the fuel pellet column.

There is no evidence of axial fuel relocation in the measured histories for the cladding surface temperature in IFA-650.14. From Fig. 45, it is clear that the calculated cladding surface temperature at z = 100 mm is increased by a few kelvin as a result of calculated fuel relocation. As can be seen from Fig. 40 and Fig. 41, the fuel mass fraction at z = 100 mm is somewhat increased by fuel relocation, according to our calculations.

The calculated effect of the relocation on cladding surface temperature is transitional; as can be seen from Fig. 45, the calculated temperature increase drops from 10–15 K just after the relocation has occurred to less than 5 K within about 30 s. The temperature increase depends on the packing fraction assumed for the fuel fragments.

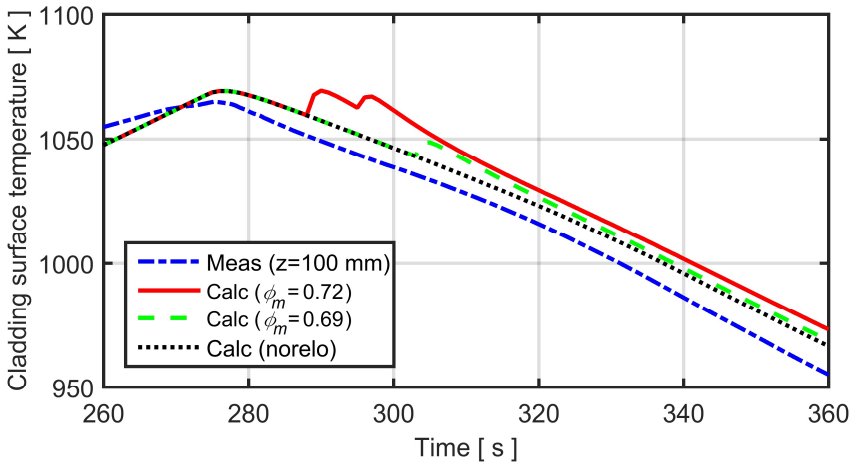

FIG. 45. Calculated and measured cladding surface temperature about the time of reactor scram (275 s); close-up of Fig. 43.

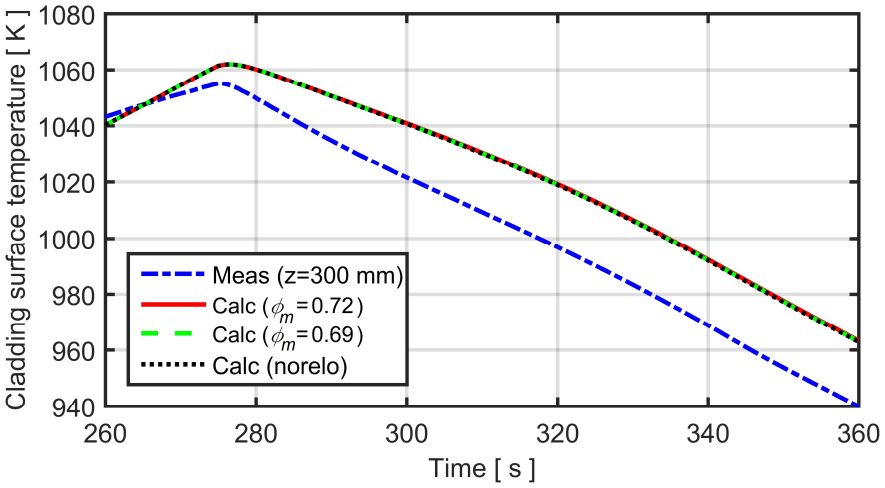

FIG. 46. Calculated and measured cladding surface temperature about the time of reactor scram (275 s); close-up of Fig. 44.

Figure 47 shows the calculated cladding outer surface temperature and equivalent cladding reacted versus axial position at time t = 600 s. Similar to the calculated results for other tests in the Halden IFA-650 series, the calculated temperature fields for the cases with axial fuel relocation are governed by the axial distribution of fuel mass and power. However, the temperature increase in the ballooned region, caused by the relocated fuel, is less than 25 K. The reason is that the calculated amount of relocated fuel is small in the IFA-650.14 test.

As can be seen from the calculated post-test ECR in the right panel of Fig. 47, the long-term change in temperature distribution caused by the axial fuel relocation has a moderate effect on the post-failure oxidation of the IFA-650.14 cladding. The calculated pre-test ECR from low temperature oxidation in Leibstadt was about 3.2%; this pre-test oxidation is included in the curves presented in Fig. 47.

It should be remarked that the calculated post-test ECR in the uppermost part of the IFA-650.14 rodlet is apparently not affected by the temperature drop caused by the fuel loss. This peculiarity is due to the fact that FRAPTRAN-1.5 uses a cut-off temperature of 1073 K for the cladding metal-water reactions [2]. In the late part of the test, when fuel relocation occurred, the calculated cladding temperature in the upper part of the rodlet was below this temperature, which means that further cladding oxidation was neglected.

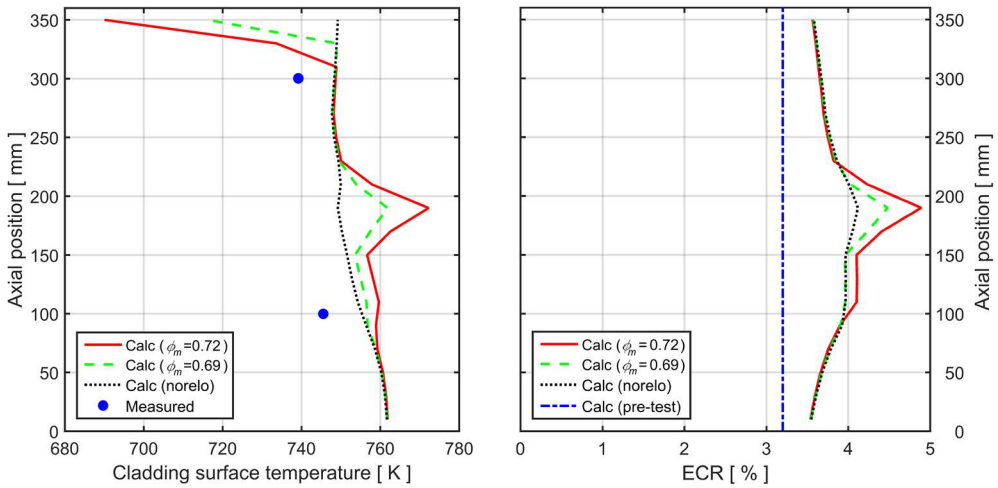

FIG. 47. Calculated cladding outer surface temperature and equivalent cladding reacted (ECR) versus axial position at time t = 600 s, with and without consideration of axial fuel relocation.

4.3. NRC-Studsvik-192 test

A major difference between the NRC-Studsvik LOCA simulation tests and the Halden IFA-650 tests is that the former are done out-of-reactor, i.e. without nuclear heating of the test rodlets. This means that effects of axial fuel relocation on the concentration of heat load to ballooned regions of the rodlets are negligible in the NRC-Studsvik tests: For example, our simulations of test 192 show that axial relocation of the cold fuel delays cladding rupture by 0.13 s, since the cladding tube is slightly cooled by the relocated and crumbled fuel in the balloon. This delay is practically insignificant, and so are all other calculated differences between the cases with and without axial fuel relocation for the NRC-Studsvik tests. In the following, we therefore present calculated results only for the case with fuel relocation considered in the simulations.

Figure 48 shows the calculated evolution of rod internal gas pressure in comparison with data from the pressure transducers connected to the lower and upper ends of the NRC-Studsvik-192 test rodlet. Henceforth, time zero refers to the beginning of heating from the initial temperature of 573 K; see Section 2.2.6. From Section 3.2.2., we recall that the gas pressure is calculated on the basis of calculated temperatures and deformations along the active length of the rodlet, together with an estimated temperature history for the gas within rod plena and connected gas lines; see Section 2 in Appendix II. The initial amount of free gas in the rodlet and its connected gas lines was adjusted in the calculations, such that a good match was obtained between the calculated and measured initial gas pressures.

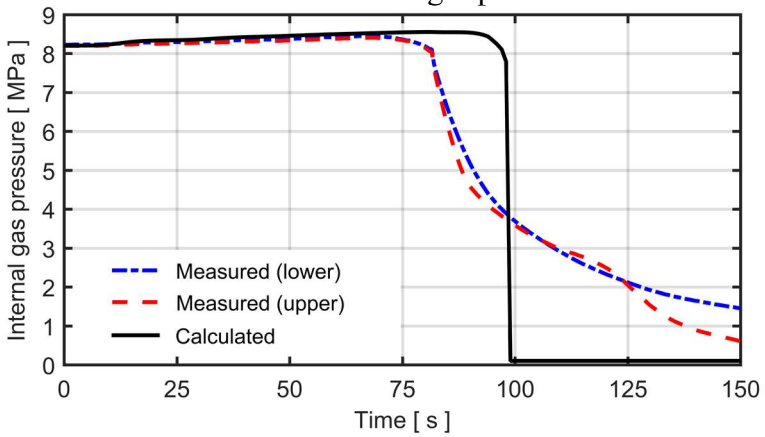

FIG. 48. Calculated evolution of rod internal gas pressure in comparison with data from the upper and lower end pressure transducer in the NRC-Studsvik-192 test rodlet [69].

It is clear from Fig. 48 that the internal gas pressure is fairly constant up to the point of cladding rupture. This is due to the large (12.58 cm^3) gas volume, and that most of the gas (10.60 cm^3) is held at nearly constant temperature during the test; see section II.2 in Appendix II. The two pressure transducers record a significant pressure drop, starting at t = 81 s, which is indicative of cladding rupture. Depressurization of the failed rodlet is fairly slow; the time constant for the pressure equilibration is about 20s, which indicates that the flow path for the gas is restricted. This conclusion is supported by post-test examinations of the rodlet, which showed that about 48 % of the fuel pellet inventory remained within the cladding tube, even though the rodlet was broken in two halves and gently shaken to dislodge as much fuel as possible [23]. The fuel pellets at both ends of the rodlet thus remained in firm contact with the cladding tube. This explains the restricted flow path for the gas towards the cladding breach, which was slightly above the axial midplane of the rodlet.

From Fig. 48, it is also clear that the time to cladding rupture is overestimated; the calculated rupture time is 98.1s, while the reported value is 81s. This is a large difference, considering that the calculated rupture times for the three Halden IFA-650 tests are within seconds of the measured values; see 4.2.1. to 4.2.3. The most important reason for the large difference between the measured and calculated rupture time for the NRC-Studsvik test is that generic high-temperature material models for Zircaloy were used to represent the ZIRLO cladding in the calculations with our extended version of FRAPTRAN-1.5. This conclusion is based on a recent assessment of the aforementioned models against a large number of high temperature burst tests and LOCA simulation tests, which comprised both Zircaloy and ZIRLO cladding [10]. This assessment showed that the models reproduce rupture times for tests on Zircaloy cladding without bias, while rupture times for tests on ZIRLO cladding are systematically overestimated; see Figs 25 and 27 in [10].

Figure 49 shows the calculated evolution of cladding deformation and axial fuel relocation during the last five seconds before cladding rupture. The thick red line shows the calculated state at the time of cladding rupture, and the leftmost curve shows the conditions about the time when the balloon starts to grow and fuel starts to relocate. The calculations suggest that the local fuel mass is increased by a factor of 3.2 in the most distended cross section of the test rodlet. This value is comparable to the calculated results for the Halden IFA-650.4 and IFA-650.9 tests; see 4.2.1. to 4.2.3. The relocated fuel originates from the upper part of the balloon and the region just above the balloon, where a ~50 mm long section is completely emptied of fuel. Above this emptied section, there is a 60 mm long "plug" of remaining fuel pellets at the very top of the fuel pellet column. This is well in line with the results reported from the test: Wire probe measurements through the cladding breach just after the LOCA simulation test showed that fuel was missing from a 110 mm long segment of the rodlet. The missing part started about 120 mm and ended about 230 mm above the bottom of the fuel pellet column [23]. Later wire probe measurements and axial gamma scans, which were carried out after breaking and shaking the rodlet, revealed further fuel loss, mostly from the lower end [23].

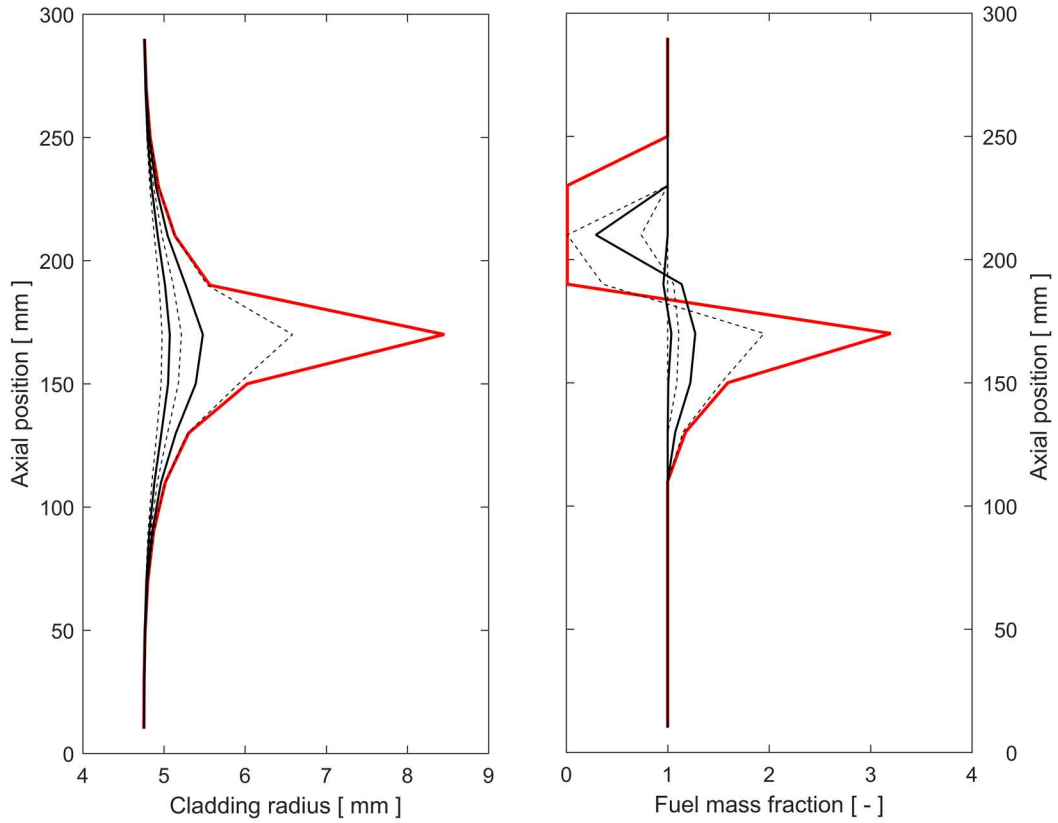

FIG. 49. Calculated evolution of cladding deformation (left) and fuel relocation (right) during the last five seconds before cladding rupture. The rightmost curve (red) represents the conditions at time of rupture, while the five curves to the left of it show the calculated state 1, 2, 3, 4 and 5 s before rupture.

According to our calculations, about 22 % of the fuel within the hot, central, part of the test rodlet had been pulverized into fine (< 0.2 mm) fragments at time of cladding rupture. The calculated degree of pulverization at the ends of the rodlet, where the temperature is significantly lower, was 11–14 %; see the description of applied models for fuel fragmentation and pulverization in [9]. After cladding rupture, the fuel temperature continued to increase, which according to our model led to further pulverization of the fuel. The calculated post-test mass fraction of pulverized fuel was 73 %. This value can be compared with results from post-test size distribution measurements, carried out by sifting of recovered fuel fragments [23]. These measurements showed that about 43 weight% of the fuel fragments collected from the NRC-Studsvik-192 rodlet were smaller than 0.25 mm. Hence, our model overestimates the fuel pulverization also for this test; compare with the similar results obtained for the IFA-650.14 test in Section 4.2.4.

Figure 50 shows the calculated post-test diameter profile of the NRC-Studsvik-192 test rodlet in comparison with measured data. The latter were obtained at thirteen axial positions, where the cladding tube diameter was measured in two perpendicular directions. This means that the data also provide some information on the degree of cylindrical symmetry for the deformation. It is clear from Fig. 50 that the calculated position of the cladding balloon is about 10 mm above the observed position. This is an acceptable difference, considering that the calculations were done with an axial discretization consisting of 20 mm long segments (nodes); see Section 3.2.2. It is likely that a closer match would be obtained with a finer axial discretization.

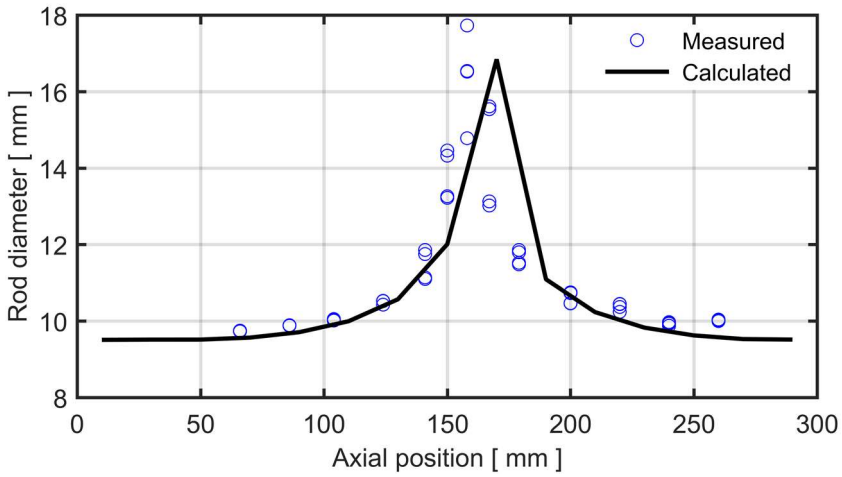

FIG. 50. Calculated and measured post-test diameter profiles for the NRC-Studsvik-192 test rodlet [69].

We also note that the cladding deformation outside the ballooned region is reproduced with fair accuracy. Very limited cladding deformation is obtained towards the ends of the rodlet, due to the axial temperature gradient in the test; see section II.1 in Appendix II, and Fig. 52 below.

Temperature gradients exist both in the radial and axial direction of the NRC-Studsvik-192 test rodlet. The radial temperature gradient, calculated at an axial position of 170 mm above the bottom of the fuel pellet column and at four different times during the test, is illustrated in Fig. 51. The considered times correspond to the conditions just after cladding rupture (99 s), attainment of peak cladding temperature (173 s), start of final quenching (297 s) and 30 s into the quenching (327 s). The results suggest that significant temperature gradients exist across the crumbled fuel in the balloon, particularly during quenching. It should be remarked that the calculations were done without considering possible cooling effects of water entering into the balloon through the cladding breach; the modelled heat removal was only by cooling at the cladding outer surface.

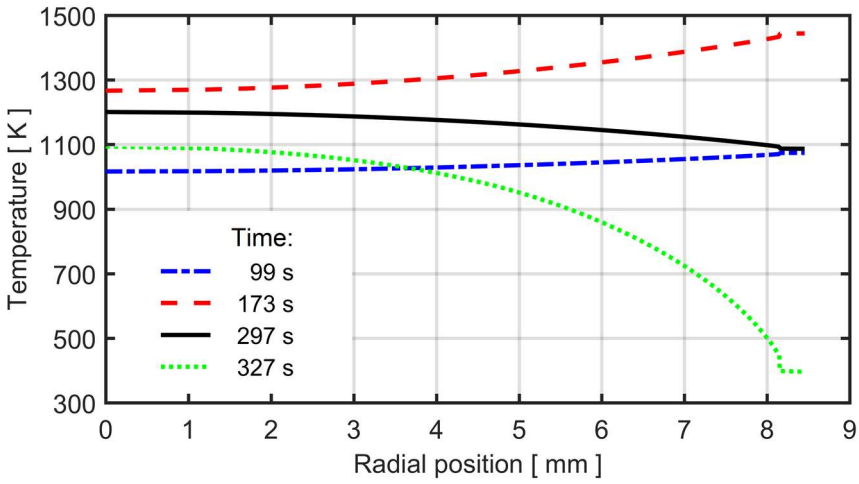

FIG. 51. Radial temperature distributions, calculated at an axial position 170 mm above the bottom of the fuel pellet column for four stages of the NRC-Studsvik-192 test.

The calculated axial temperature gradient, evaluated at the cladding outer surface, is shown in the left panel of Fig. 52. The difference between the peak temperature position and the lower end of the rodlet is nearly 250 K, when the peak cladding temperature is attained (t =

173 s); see section II.1 in Appendix II. The axial temperature gradient leads to large differences in the cladding oxidation rate, which is illustrated by the post-test ECR in the right panel of Fig. 52. The marked peak at z = 170 mm is a result not only of the temperature peak, but also of substantial thinning of the cladding wall at the rupture position.

The calculated post-test ECR presented in the right panel of Fig. 52 can unfortunately not be compared with measurements, since no quantitative data regarding the ECR or the cladding inner and outer oxide layer thicknesses are reported for the NRC-Studsvik LOCA test rods. However, metallographic examinations of the oxidized cladding were done at a few axial positions of the rodlets, and quantitative information in the form of micrographs is available [23].

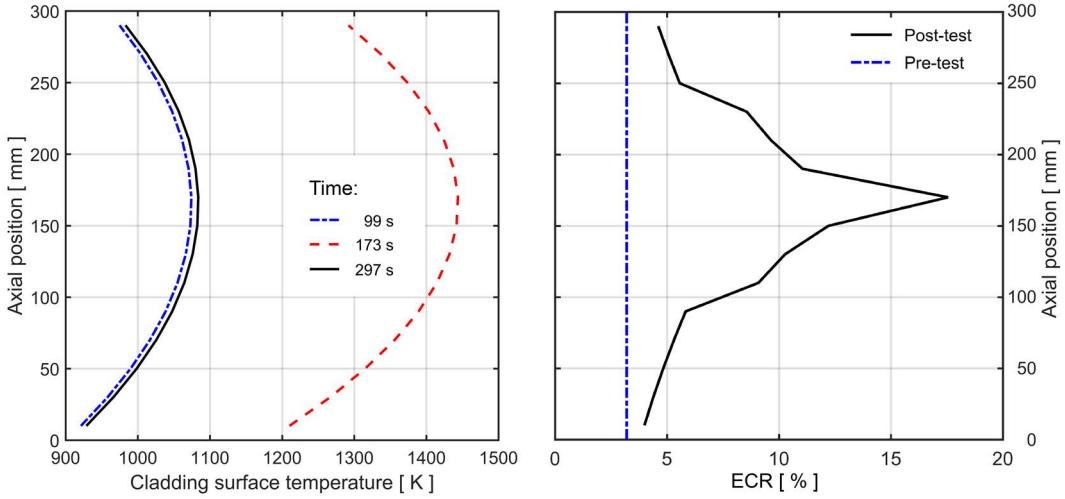

FIG. 52. Calculated cladding outer surface temperature at different times during the NRC-Studsvik-192 test (left) and calculated equivalent cladding reacted (right).

5. SUMMARY AND CONCLUSIONS

5.1. Task 1: models related to axial relocation of fuel pellets

The model for axial relocation of fuel pellet fragments presented in Section 2.2.2. is based on the same assumptions as in all models hitherto proposed for the phenomenon, namely, that the relocation is essentially controlled by the cladding distension along the fuel rod and the fragment packing fraction attained by crumbled fuel in ballooned regions of the rod. The cladding distension is normally calculated by a suitable computer program for thermal-mechanical fuel rod analyses, in our case FRAPTRAN-QT-1.5, an extended version of FRAPTRAN-1.5 [2], while the packing fraction is treated as a model parameter. Nonetheless, our model has a number of features that make it stand out from earlier relocation models.

First and foremost, our relocation model is integrated with the equations used for calculating the space-time variation of fuel and cladding temperature in FRAPTRAN-QT-1.5. This means that thermal feedback effects from the axial redistribution of power and stored heat that axial fuel relocation brings about are fully accounted for in the transient fuel rod analysis. Earlier relocation models [27]–[29] have been designed and used as post-processors to various computer programs for fuel rod analysis, meaning that the programs have calculated the fuel rod thermal-mechanical behaviour with no or only partial consideration of fuel relocation.

Secondly, we consider in our model the state of fuel fragmentation and pulverization when estimating the packing fraction of crumbled fuel in ballooned regions of the fuel rod; see section FIG. 2. The packing fraction is a key parameter that controls the degree of fuel relocation, given the deformed configuration of the cladding tube. We have taken the novel approach of estimating the fuel fragment packing fraction from a simple semi-empirical model, which is based on the assumption that the crumbled fuel consists of two different size classes

of fragments: The first class includes mm-size fragments, created by thermal stresses in the fuel during normal operation, and the second class comprises fine (< 0.2 mm) fragments, created during LOCA by overheating high burnup fuel. The second fragment class thus exists only under certain conditions, and a recently proposed empirical 'pulverization threshold' [31] is used in our model for calculating the mass fraction of small fuel fragments, based on the distributions of burnup and temperature in the fuel.

Thirdly, when solving the radial heat conduction equation in our extended version of FRAPTRAN-1.5, we account not only for the changes in local fuel mass and heat load caused by axial fuel relocation, but also for the changes in fuel column geometry and material properties caused by fuel crumbling in ballooned regions of the rod; Section 2.2.4. For example, the thermal conductivity of the particle bed of crumbled fuel in the balloon is calculated through an effective medium model for solid particles surrounded by stagnant gas. According to this model, which has been verified against thermal conductivity data for UO_2 particle beds in various gases, the effective thermal conductivity of the particle bed depends on the thermal conductivities of the fuel fragments and the surrounding gas, and on the packing fraction of the fuel fragments.

5.2. Task 2: Criteria for cladding high temperature rupture

In Task 2 of the project, we assessed a number of existing stress-based criteria for cladding high temperature rupture, combined with the set of high-temperature material models that are specific to FRAPTRAN-QT-1.5 [15], against a large data base of high temperature burst tests on various cladding materials. The objective was to identify a suitable rupture criterion that works well together with the FE-based mechanical module and our particular set of cladding material models.

The assessment showed that all the rupture criteria, when combined with the high temperature material models in FRAPTRAN-QT-1.5, exhibit systematic errors (bias). Hence, the rupture criteria should be calibrated, such that their performance together with the high temperature models in FRAPTRAN-QT-1.5 is improved. From our assessment, it is also clear that the calculated time to cladding rupture depends more heavily on the models for cladding high temperature creep and plasticity than on the rupture criterion. The reason is that cladding high temperature rupture is triggered by excessive local deformation (ballooning) of the cladding, and this deformation must be accurately calculated by the creep and plasticity models. Consequently, it is important to calibrate also these models against available burst test data. This conclusion is also corroborated by our evaluation of integral LOCA tests; see Section 5.3.1.

While the cladding high temperature creep and plasticity models are important for calculating the time to cladding rupture, the rupture criterion is essential for accurate prediction of the cladding strain and stress at burst. We note that Rosinger's criterion [38] reproduces the burst strain and burst stress data for Zircaloy-4 and ZIRLO with higher fidelity than the criterion proposed by Erbacher and co-workers [39]. However, Rosinger's criterion has some bias that could be removed by calibration. This can be easily done by the information gained from our assessment of burst test data; see for example Fig. 53.

Finally, we note that the extent of background information and the quality of experimental data vary between the burst test series in the data base used for our assessment of rupture criteria. For many of the test series, particularly those on modern ZrNb-type cladding materials, open literature publications do not provide sufficient information that one-to-one comparisons of calculated and measured results can be made. For all cladding materials, there is also a notable lack of burst tests with heating rates in the range of 1–5 Ks^{-1}. This is obvious from Table 1, and manifests itself as a lack of data with time to cladding burst in the range of 100–300 s; see Fig. 53.

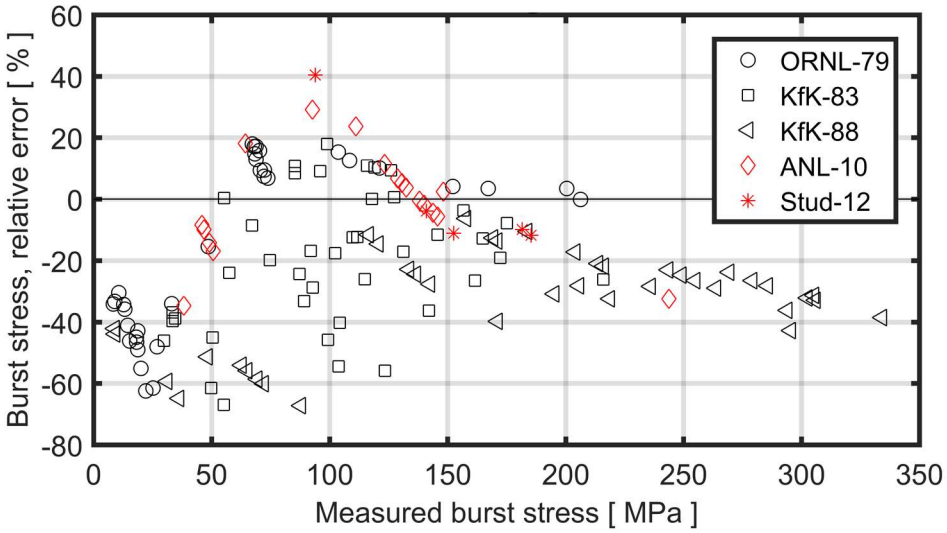

FIG. 53. Relative error in cladding burst stress, calculated with Rosinger's rupture criterion [38]*, for Zircaloy (black symbols) and ZIRLO (red symbols) samples. See Table 1 for explanations to the legend.*

5.3. Task 3: Model assessment against integral LOCA tests

5.3.1. Summary and interpretation of results

The assessment of Halden and Studsvik LOCA simulation tests in sections 3 and 4 was done by best-estimate computational analyses of the experiments, using FRAPTRAN-QT-1.5. Since the objective was partly to validate this computer program, we deliberately refrained from matching the calculated and measured results by tuning model parameters. The only exceptions are the cladding creep rate, for which we used a constant scaling factor of 0.40 in all calculations, and the ad-hoc criteria for cladding rupture; see Section 3.2.2. It should also be remarked that the thermal-hydraulic boundary conditions used in the analyses were approximations, based on measured data for each test, simplifying assumptions regarding the heat transfer, and fitting procedures; see Appendices I and II.

Let us first examine the agreement/disagreement between measured and calculated results for key properties: Disagreements indicate that the involved phenomena are inadequately modelled, and possibly, poorly understood. In summary, we get good or even very good agreement between measured and calculated results for the cladding temperature and the time to cladding rupture for the Halden IFA-650 tests. In particular, the calculations seem to capture the thermal effects of axial fuel relocation well. Poor agreement between measured and calculated results is on the other hand seen for the time to cladding rupture in the NRC-Studsvik-192 test, and in some of the considered tests, for the dynamics of gas depressurization after rupture. In addition, the degree of fuel pellet fine fragmentation ('pulverization') is overestimated for the tests where the fragment size distribution has been reported.

The disagreement between calculated and measured time to cladding rupture for the NRC-Studsvik-192 test is due to the lack of high temperature models for ZIRLO cladding in our extended version of FRAPTRAN-1.5; as explained in Section 3.2.2., generic models for Zircaloy were used in simulations of all the tests. Our assessment of these models against burst test data in section 2.3 shows that they reproduce rupture times for tests on Zircaloy cladding without much bias, while rupture times for tests on ZIRLO cladding are systematically overestimated; see e.g. Fig. 6.

The slowly decreasing internal gas pressure after cladding rupture in the IFA-650.9 and the NRC-Studsvik-192 tests gives evidence of impeded axial gas flow, and a few other tests in the same series exhibit similar behaviour [23, 57]. This phenomenon, which is seen in high

burnup fuel rods that usually have a tightly closed pellet-cladding gap, is not modelled by FRAPTRAN-QT-1.5, where unrestricted gas flow and mixing are assumed in all internal cavities. Impeded axial gas flow will reduce the driving force for cladding ballooning, burst and subsequent ejection of fuel fragments through the cladding breach. More precisely, the gas inventory in fuel rod plena becomes less important for driving the local deformation in the ballooning region, whereas transient fission gas release in the same region becomes relatively more important [74]. In this context, we recall from Section 4.2.2. that the IFA-650.9 test rodlet exhibited not one, but two balloons, which were separated by a ~40 mm long axial section with fairly small cladding distension. The fact that this deformation pattern occurs in a short rodlet with fairly peaked power and temperature profiles suggests that growth of multiple balloons, controlled by local fission gas release, is likely in full-length fuel rods where the axial gradients are moderate; see Section 5.3.2.

The importance of transient fission gas release to the internal pressure loading in high burnup fuel rods is also illustrated by the IFA-650.14 test rodlet, which had an exceptionally small gas plenum. Transient fission gas release therefore accounted for most (67 %) of the post-test internal free gas in this rodlet, and in contrast to the other tests considered in this report, the IFA-650.14 test could not be reproduced without considering transient gas release in the computer simulations; see sections 0 and 0. The calculated results and the experimental data for test IFA-650.14 suggest that the cladding ballooned gradually for more than a minute, concurrent with fission gas release caused by the increasing fuel temperature. This is much different from the other IFA-650 tests, where the cladding ballooned rapidly, typically within 3–5 s, and failed by plastic instability. This difference has importance to the transferability of the test results to LWR LOCA conditions; see Section 5.3.2.

The post-test size distribution of fuel pellet fragments was determined by sifting all dislodged fragments in two of the considered tests. The measured mass fractions of small (< 0.25 mm) fragments in these tests are compared with our calculated results in Table 10. The table also includes information on differences between the two tests and the test rods, which may explain the fairly large difference in their fragmentation behaviour. Table 10: Measured and Calculated Mass Fractions of Small (< 0.25 MM) Fuel Fragments, Collected After LOCA Simulation Test IFA-650.14 [70] and NRC-Studsvik-192 [23].

TABLE 10.MEASURED AND CALCULATED MASS FRACTIONS OF SMALL (< 0.25 mm) FUEL FRAGMENTS, COLLECTED AFTER LOCA SIMULATION TEST IFA-650.14 [70] AND NRC-STUDSVIK-192 [23].

Parameter:	Halden IFA-650.14	NRC-Studsvik 192
Measured mass fraction of small fragments (wt%)	0.6	43
Calculated mass fraction of small fragments (wt%)	22	73
Fuel pellet average burnup ($MWd(kgU)^{-1}$)	70.8	78
Average LHGR during final operating cycle (kWm^{-1})	9	17
Peak fuel temperature during LOCA test (K)	1180	1430
Final quenching of test rodlet	No	Yes

In summary, the NRC-Studsvik-192 test was performed on a rodlet with higher burnup, the fuel had been operated at higher power during end of life, it reached higher temperature during the test, and after the test, the rodlet was rapidly cooled by quenching. All these factors are known to promote fine fragmentation (pulverization) of the fuel [31, 77]. However, our computational model for the pulverization accounts only for two of these factors: burnup and peak fuel temperature [9]. The measured post-test mass fraction of small fragments for the IFA-650.14 test rodlet is surprisingly small, considering that the transient fission gas release measured in the test was no less than 18 % [70]. Such a high release fraction is difficult to reach

within minutes, unless virtually all fuel grain boundaries are broken and all gas residing in grain boundary pores is released [78]. The grain boundary rupture, if it occurred, did in any case not lead to much observable fuel pulverization in the IFA-650.14 test.

The fact that our model for fuel pulverization seems to overestimate the fraction of small fuel fragments is problematic, since the calculated fraction is used for estimating the packing fraction of crumbled fuel. The packing fraction, which is a key parameter in our relocation model [9], has a very limited data base. Some data for the packing fraction of crumbled fuel with burnup below 16 MWd(kgU)$^{-1}$ are available [19, 21], while data for higher burnup fuel are unavailable. However, recent post-test investigations of the latest rodlet tested in the Halden IFA-650 series, with a burnup around 64 MWd(kgU)$^{-1}$, provide valuable information on this matter [79]. More precisely, high resolution gamma emission scans along the rodlet show that the fuel mass increased locally by a factor 2.7–2.8 in the most distended part of the rodlet, as a consequence of axial fuel relocation [79]. This value is marginally lower than the calculated results from our simulations of the IFA-650.4 and IFA-650.9 tests, where 0.72 was used as an approximation for the fuel fragment packing fraction in the ballooned regions; see Fig 17 and 23. Hence, we conclude that fragment packing fractions around 0.7 are realistic, and that the best-estimate value of 0.69, presented more than thirty years ago by Siefken [21], is relevant also for high burnup fuel. It should be remarked that a cursory sensitivity analysis with regard to the fuel fragment packing fraction was done for the IFA-650.14 test in Section 4.2.4. The analysis shows that a slight variation of the packing fraction, from 0.69 to 0.72, has a fairly large impact on some parameters, such as the peak cladding deformation and oxidation.

Our simulations of tests 4, 9 and 10 in the Halden IFA-650 series suggest that ballooning of the cladding, and the fuel relocation that resulted from it, occurred over a short (3–5 s) period, just before cladding rupture. The close agreement between the calculated and measured changes in cladding temperature that suddenly occurred in the IFA-650.4 and IFA-650.9 rodlets just before cladding rupture corroborates that the time of fuel relocation is accurately reproduced by the model. The results are interesting, and it should be remarked that there has been some dispute in the past as to whether axial fuel relocation during LOCA occurs before or after cladding rupture. Today, there is clear experimental evidence from two in-reactor LOCA tests that fuel relocation may precede cladding rupture. These are test E5, conducted in the German FR2 reactor [19], and the Halden IFA-650.14 test [63, 70]. The cladding did not rupture in either of these tests, but post-test neutron radiography revealed that extensive axial relocation had nevertheless taken place inside the ballooned cladding during the tests.

Our simulations also suggest that thermal feedback effects from fuel relocation are strong enough to influence the dynamics of cladding ballooning and rupture, notwithstanding the short duration of these processes. As shown in Table 11, the calculated time to cladding rupture in the considered IFA-650 tests was shortened by 4–14 s, as a result of thermal feedback effects from the fuel relocation. According to our calculations, the most important thermal feedback effect during the short period from onset of axial fuel relocation to cladding rupture is caused by the collapse of the fuel pellet column, which makes hot fuel fragments come into direct contact with the expanding cladding. The local increase of fuel mass in ballooned regions results in minor thermal feedback effects before cladding rupture, but as can be seen from Table 11, it has significant effects on the local cladding temperature and oxidation rate *after* rupture. These results are interesting with regard to LOCA licensing analyses, since they indicate that conservative assumptions have to be made in the analyses, unless fuel relocation and its consequences to cladding local temperature and oxidation are accounted for in the computational evaluation models.

TABLE 11.CALCULATED IMPACT OF AXIAL FUEL RELOCATION ON KEY PARAMETERS IN THE CONSIDERED HALDEN IFA-650 LOCA SIMULATION TESTS

Parameter (calculated results)		650.4	650.9	650.10	650.14
Peak cladding temperature (K)	With relocation	1230	1646	1244	1095
	Without relocation	1149	1400	1180	1071
	Difference	81	246	64	24
Peak post-test ECR (%)	With relocation	6.64	35.0	7.97	4.89
	Without relocation	4.69	9.55	6.21	4.12
	Difference	1.95	25.4	1.76	0.77
Time to cladding rupture (s)	With relocation	334.2	133.5	249.9	–
	Without relocation	348.2	137.8	259.1	–
	Difference	-14.0	-4.3	-9.2	–

5.3.2. Transferability of results to LWR LOCA conditions

As shown in Table 11, most of the Halden IFA-650 tests considered in this report give evidence of strong thermal feedback effects from the axial fuel relocation. However, it should be borne in mind that the tests were deliberately designed to amplify axial fuel relocation, and they are therefore not fully representative of actual conditions under LOCA in commercial power reactors [26]. The most important differences in design and operating conditions between the considered test rodlets and typical LWR fuel are:

— The fuel burnup of the rodlets is higher than today's typical discharge burnup of commercial fuel;
— The cladding distension is not limited by contact with neighbouring fuel rods, as it would be in a real fuel assembly;
— Except for the IFA-650.14 rodlet, the ratio of the gas plenum volume to the rod active length is an order of magnitude larger than in commercial LWR fuel designs;
— The axial gradients in fuel rod power and/or temperature are larger than those expected in the high temperature phase of an LWR LOCA.

These differences accentuate fuel fragmentation and localized cladding deformation in the test rodlets, and thus, they contribute to the axial fuel relocation.

Based on these observations and the results of parametric studies in the Halden IFA-650 tests, the NRC-Studsvik tests and similar LOCA test programs [19, 80, 81], it is reasonable to expect that the fuel behaviour in an LWR LOCA will be somewhat different than observed in the aforementioned tests. For example:

— The local increase in fuel mass caused by axial fuel relocation within the fuel rods will most likely be lower, since cladding ballooning is limited by contact with neighbouring fuel rods, and since the fuel fragment packing fraction is supposedly lower for the lower-burnup fuel;
— Once a fuel rod fails, fuel fragments ejected through the cladding breach may accumulate at the spacer grid below and contribute to the local heat load of neighbouring, yet unfailed, rods. The possibility of thermal feedback from axial fuel fragment relocation outside the fuel rods is currently unexplored;
— The cladding ballooning is expected to be slower, since it will be controlled mainly by the rate of transient fission gas release, as in the IFA-650.14 test.

In fuel rods with high burnup, impeded axial gas flow will make the occurrence of multiple balloons likely. Multiple balloons, separated by spacer grids, have been observed in LOCA simulation tests on longer test rods than those used in Halden and Studsvik [80, 81]. It is also expected that the axial positions at which the balloons develop will be difficult to predict by computational models, since these positions will depend on local pellet-cladding gap conditions and transient fission gas release. Also, the aforementioned possibility of axial fuel relocation of dispersed fuel to lower spacer grid positions will contribute to the complexity.

Further experiments, model development and computational analyses are needed to elucidate the fuel behaviour under more realistic LWR LOCA conditions. Of particular concern is the behaviour of high burnup fuel rods, for which the data base is restricted to single-rod LOCA simulation tests on short rodlets.

5.4. Suggestions for further work

5.4.1. Model development

The results presented in this report indicate that there are certain models in our extended version of FRAPTRAN-1.5 that could be improved. Firstly, the results of our assessment of burst test data in section 2.3 and the fact that we needed to scale the cladding high temperature creep rate by a factor of 0.40 in all simulations of the integral LOCA tests (see Section 2.3.) suggest that the current models for cladding high temperature creep in FRAPTRAN-QT-1.5 can be improved by calibration against relevant experiments. The models also need to be adapted to ZIRLO cladding, since they are not calibrated against this material. For modelling cladding rupture, we believe that the stress-based criterion by Rosinger [38] is the best suited for Zircaloy and ZIRLO cladding. However, this criterion needs some calibration to reduce the bias discussed in sections 2.3.4. and 5.2. More elaborate rupture criteria, utilizing life-fraction concepts, are reviewed and discussed in [10]. These criteria are interesting for the future, but would require substantial validation and calibration before they can be applied to fuel rod LOCA analysis.

Secondly, some submodels used in our newly developed set of models for calculating fuel axial relocation need improvement. For example, the mass fraction of fine fuel fragments is currently calculated by use of an empirical threshold for pulverization of high burnup fuel during temperature excursions [24, 31, 82]. The results put forth in Table 10 show that this empirical model significantly overestimated the degree of fuel pulverization for two of the considered tests. The threshold should therefore be replaced with a refined, mechanistically based, model for fuel pulverization, which accounts for more parameters than just the fuel local burnup and temperature. Of particular interest is the impact of mechanical constraint from the cladding and effects of pre-LOCA operating history for the fuel. Models of this kind, which link pulverization to the local fuel porosity and distribution of gaseous fission products in the fuel, are currently being studied by Quantum Technologies in a separate research project for SSM [83, 84]. The aim of the new project is to calculate the degree of pulverization and the associated transient fission gas release, based on the thermal-mechanical loading subjected to the fuel during the LOCA, as well as the pre-LOCA operating history. Ongoing and planned separate effect tests on high burnup fuel in the third phase of the Studsvik Cladding Integrity Project (SCIP-III) will provide useful data for setting up an improved pulverization model [8].

Moreover, the model used for estimating the fuel fragment packing fraction from the calculated state of fuel fragmentation and pulverization predicts very high packing fractions for fuel that contains about 30 wt% fine (< 0.2 mm) fragments [9]. According to the aforementioned threshold for fuel pulverization, this mass fraction of fine fragments is typically obtained when overheating fuel pellets with an average burnup around 70–75 $MWd(kgU)^{-1}$. In this burnup range, the packing fraction predicted by the model may exceed 0.80–0.85. At present, there are no experimental data for UO_2 fuel that directly support such high values, but supporting data

exist for other granular materials with binary size distributions [9]. This is further discussed in Section 5.4.3. below.

Our relocation model provides, for each axial segment of the fuel rod, an upper bound of the fuel mass that may be ejected into the coolant, should the cladding fail within the considered axial segment [9]. The calculated amount of dispersed fuel is based on the assumption that all fuel above the cladding breach that is free to move downward will be ejected through the breach. This is a crude upper bound estimate, since the fuel dispersal will most likely be limited by the rupture opening and by choke points for the axial relocation at spacer grid positions. Considering the observed effects of spacers [80], it is probably realistic to assume that no relocation will take place past spacer grids. Hence, fuel located above the spacer grid that is nearest above the cladding breach may be precluded from the amount of fuel that could be ejected through the breach. Moreover, it would be possible to correlate the estimated amount of ejected fuel to the fuel fragment size distribution and to the expected area of the rupture opening. It is known that this area depends on the phase composition of the cladding metal at the time of rupture [85]. The area of the rupture opening is also known to increase with the internal overpressure in the fuel rod [49] and to decrease with the cladding hydrogen concentration [57]. In conclusion, it would be possible to extend our relocation model such that it provides more realistic estimates of fuel dispersal. To this end, a submodel for axial gas flow, induced by pressure gradients along the pellet-cladding gap, should be introduced in FRAPTRAN-1.5. This is because the dynamics of pressure equilibration will affect both the cladding rupture size (through the magnitude of the local overpressure at time of ballooning and burst) and the propensity for fuel ejection (through the magnitude and duration of axial pressure gradients after burst that may entrain fuel fragments in the flowing gas).

Thirdly, the lack of models for transient fission gas release and restricted axial gas flow in our extended version of FRAPTRAN-1.5 is clearly one of the main reasons for the observed differences between calculated and measured results in this work. Transient fission gas release and restricted axial gas flow within the rod are phenomena with importance to the internal pressure loading of high burnup fuel rods. As already mentioned in Section 5.3.2., the phenomena are expected to be more important for full-length LWR fuel rods than for the short rodlets typically used in LOCA simulation tests. Models for transient fission gas release from high burnup fuel in LOCA conditions are currently being studied by Quantum Technologies in the aforementioned research project on fuel pulverization, since pulverization and transient fission gas release are related phenomena. The aim is to formulate a combined model for pulverization and transient gas release, suitable for implementation in FRAPTRAN-QT-1.5. For completeness, a model for axial gas flow is also needed, in particular for analysing full-length fuel rods.

Finally, we note that local mesh refinement is necessary for analyses of cladding ballooning and burst in full-length fuel rods with our extended version of FRAPTRAN-1.5. In the calculations presented in this report, we used a fixed axial discretisation, consisting of 20 mm long axial segments (nodes), along the entire active length of the rodlets. To carry out analyses of a full length (3.6 m) LWR fuel rod with such a discretisation is impracticable. Computer programs used for analyses of ballooning must therefore allow local refinement of the discretisation at axial positions of particular interest. FRAPTRAN-QT-1.5 has this capacity [2], but the program would be significantly improved if the refinement could be done adaptively, i.e. automatically in the course of the calculation.

5.4.2. Computational analyses

As already mentioned, the fuel behaviour observed in LOCA simulation tests on single test rods with an active length of 0.3–0.5 m may depart from that of real full-length fuel rods in a commercial fuel assembly under LWR LOCA conditions. Some of the expected differences

were discussed in section 5.3.2. where it was also stated that further experiments, model development and computational analyses are needed to elucidate these differences.

Computational analyses of the thermal-mechanical behaviour of full-length fuel rods under conditions expected in LWR LOCAs with our extended version of FRAPTRAN-1.5 are therefore recommended. The current version of the program is adequate for analyses of low to medium burnup fuel; analyses of high burnup fuel should preferably wait until the model improvements proposed in section 5.4.1. have been made. Of particular importance are the models for restricted axial gas flow, fuel pulverization and transient fission gas release.

The calculations carried out so far with our model for axial fuel relocation suggest that the results are sensitive to two model parameters, namely the fuel fragment packing fraction, ϕ, and the minimum pellet-cladding gap size needed for fuel fragments to detach from their original, close-packed configuration and relocate downwards, g^{th}. These parameters, as well as the experimental data base in support of the values used for them, are presented in [9].

A cursory sensitivity study for the fuel fragment packing fraction, pertinent to the IFA-650.14 test, is presented in section 4.2.4. of this report. A more comprehensive sensitivity study, including both ϕ and g^{th}, is desirable. Any of the IFA-650 tests considered in this report would be a suitable baseline case for such a study.

5.4.3. Tests and experiments

From the assessment of cladding rupture criteria in section 2.3, we recall that there is a lack of useful high temperature burst test data for modern ZrNb-type cladding materials, such as ZIRLO and M5, in open literature. Likewise, the public data base is scarce for samples with high pre-test hydrogen concentrations, irrespective of the cladding material. For all cladding materials, there is also a notable lack of burst tests with heating rates in the range of 1–5 Ks^{-1}. Further tests, or publication of existing proprietary data, would be valuable to bridge these gaps.

Computer analyses presented here and elsewhere [86]–[88] suggest that the effects of axial fuel relocation on peak cladding temperature and ECR under a loss-of-coolant accident would depend strongly on the fuel fragment packing fraction in the ballooned region of the fuel rod. As already mentioned, some data on the packing fraction exist for fuel with low (< 16 $MWd(kgU)^{-1}$) burnup [19, 21], but there are currently no open literature data at all for higher burnup fuel. Such data can be produced by combining high resolution gamma scans, carried out on the rodlets shortly after the LOCA tests, with axial scans of the cladding radial deformation. A first step in this direction has been taken in Halden [79], and similar experimental techniques is used in the third phase of the Studsvik Cladding Integrity Project (SCIP-III) [8].

The model used for estimating the fuel fragment packing fraction in our calculations predicts particularly high packing fractions for fuel that contains about 30 wt% fine (< 0.2 mm) fragments [9]. Unfortunately, there are currently no measured data on the fuel fragment packing fraction versus mass fraction of fine fragments that can confirm or refute this modelling result. Such data can be produced in connection with post-test sifting of collected fuel fragments from failed test rods, simply by measuring the mass and bulk (effective) volume of the fragments. Although these measured packing fractions would not be representative of fuel accumulated within the balloon of a distended fuel rod, they would still be valuable for identifying and determining possible relationships between the packing fraction and the fragment size distribution.

Finally, we suggest some modifications of the LOCA testing procedures in Halden and Studsvik, in order to ease the interpretation of the tests. With regard to the Halden IFA-650 tests, we suggest that water spraying into the upper part of the test rig is conducted with constant flow instead of intermittent pulses: When liquid water is injected into the rig, the water flashes to steam and expands by a factor ~550. The volume expansion forces much of the steam out of

the test rig, into the evacuation line to the blowdown tank; see Section 3.1.2. Hence, only part of the injected water remains in the rig to feed the zirconium-water reactions.

This amount was obviously insufficient for the IFA-650.9 test; as mentioned in Section 4.2.2. there is clear evidence that the local cladding oxidation in the lower part of the IFA-650.9 rodlet was limited by steam starvation. The pulse-wise flow caused by the intermittent spray procedure is difficult to model, which leads to large uncertainties regarding the actual amount of water locally available in the rig for oxidation of the cladding. A constant water spray would be easier to model, and thus, reduce some of this uncertainty.

As for the LOCA simulation tests in Studsvik, we request that more than one thermocouple should be used for measuring the cladding temperature during the test, in order to reduce the uncertainty that currently exists regarding axial temperature gradients. One thermocouple at each end of the active length, in addition to the more centrally placed thermocouple, would provide the information needed. If possible, the heated zone of the rig should also be lengthened, to reduce the unrealistically steep axial gradients in cladding temperature.

It would also be interesting to carry out a pair of tests to investigate the effect of final quenching on fuel pulverization. Early investigations on fresh UO_2 fuel suggest that the thermal shock experienced by the fuel during quenching leads to formation of micro cracks [89]. The response of high burnup fuel is unclear, since open literature reports on this issue are unavailable. Ideally, two identical rodlets with high burnup fuel should be tested under identical conditions, except for the final cooling, i.e. quench or no quench. Two of the six tests in the NRC-Studsvik series were done without quenching, but unfortunately, the fuel burnup and/or peak temperature in these two tests were such that comparisons with the other four tests become inconclusive [23].

ACKNOWLEDGEMENTS

The work was supported by the Swedish Radiation Safety Authority (SSM) under contract numbers SSM2014-2355 and SSM2015-3357. We thank Mrs. Anna Alvestav at SSM for managing these projects and for her contribution to the work. Thanks are also due to the OECD Halden Reactor Project for providing data from the four Halden IFA-650 LOCA tests considered in this report. We are also indebted to the U.S. Nuclear Regulatory Commission and Studsvik Nuclear AB, who kindly placed experimental data for the NRC-Studsvik LOCA test 192 at our disposal.

REFERENCES

[1] OECD–NUCLEAR ENERGY AGENCY, Nuclear fuel behaviour in loss-of-coolant accident (LOCA) conditions: State-of-the-art report, 2009, Report NEA No. 6846, OECD Nuclear Energy Agency, Paris, France.

[2] GEELHOOD, K.J., ET al., FRAPTRAN-1.5: A computer code for the transient analysis of oxide fuel rods, 2014, Report NUREG/CR-7023, Vol. 1, Rev. 1, Pacific Northwest National Laboratory, Richland, WA, USA.

[3] MANNGÅRD, T. AND A.R. MASSIH, Modelling and simulation of reactor fuel cladding under loss-of-coolant accident conditions. J. Nucl. Sci. Technol., 2011. 48(1): 39–49.

[4] MANNGÅRD, T. AND A.R. MASSIH, Modelling of nuclear fuel cladding under loss-of-coolant accident conditions, 2013, Report SSM 2013:24, Swedish Radiation Safety Authority, Stockholm, Sweden.

[5] MANNGÅRD, T., et al., Evaluation of the Halden IFA-650 loss-of-coolant accident experiments 2, 3 and 4, 2014, Report SSM 2014:18, Swedish Radiation Safety Authority, Stockholm, Sweden.
[6] MANNGÅRD, T. AND J.-O. STENGÅRD, Evaluation of the Halden IFA-650 loss-of-coolant accident experiments 5, 6 and 7, 2014, Report SSM 2014:19, Swedish Radiation Safety Authority, Stockholm, Sweden.
[7] MANNGÅRD, T., et al. Evaluation of Halden IFA-650 loss-of-coolant accident experiments 2, 3, 4, 5, 6 and 7, 2013. In: Enlarged Halden Programme Group Meeting, March 10-15, 2013, Storefjell, Norway: OECD Halden Reactor Project, Halden, Norway.
[8] Report on fuel fragmentation, relocation and dispersal, 2016, Report NEA/CSNI/R(2016)16, OECD Nuclear Energy Agency, Paris, France.
[9] JERNKVIST, L.O., MASSIH, A.R., Models for axial relocation of fragmented and pulverized fuel pellets in distending fuel rods and its effects on fuel rod heat load, 2015, Report SSM 2015:37, Swedish Radiation Safety Authority, Stockholm, Sweden.
[10] MASSIH, A.R., JERNKVIST, L.O., Assessment of data and criteria for cladding burst in loss-of-coolant accidents, 2015, Report SSM 2015:46, Swedish Radiation Safety Authority, Stockholm, Sweden.
[11] JERNKVIST, L.O., Computational assessment of LOCA simulation tests on high burnup fuel rods in Halden and Studsvik, 2017, Report SSM 2017:12, Swedish Radiation Safety Authority, Stockholm, Sweden.
[12] JERNKVIST, L.O., MASSIH, A.R., Modelling axial relocation of fragmented fuel pellets inside ballooned cladding tubes and its effects on LWR fuel rod failure behaviour during LOCA, 2015. In: 23rd International Conference on Structural Mechanics in Reactor Technology (SMiRT-23), Manchester (2015).
[13] JERNKVIST, L.O., et al. Axial relocation of fragmented and pulverized fuel and its effects on fuel rod heat load during LOCAs, 2015. In: Reactor Fuel Performance 2015 (TopFuel-2105), September 13-17, 2015, Zürich, Switzerland: European Nuclear Society, (2015) 401–410.
[14] JERNKVIST, L.O., et al. Computational assessment of axial fuel relocation in Halden IFA-650 LOCA tests, 2016. In: Enlarged Halden Programme Group Meeting, May 8-13, 2016, Sandefjord/Fornebu: OECD Halden Reactor Project.
[15] JERNKVIST, L.O., Implementation of models for cladding high temperature metal-water reactions, phase transformation, creep and failure in the FRAPTRAN-1.4 computer program, 2012, Report TR10-005V2, Quantum Technologies AB, Uppsala, Sweden.
[16] JERNKVIST, L.O., Observed and corrected errors in source code and algorithms of FRAPTRAN-1.5, 2015, Report TR15-002, Quantum Technologies AB, Uppsala, Sweden.
[17] GEELHOOD, K.J., et al., FRAPTRAN-2.0: A computer code for the transient analysis of oxide fuel rods, 2016, Report PNNL-19400, Vol. 1 Rev2, Pacific Northwest National Laboratory, Richland, WA, USA.
[18] GEELHOOD, K.J., LUSCHER, W.G., FRAPCON-3.5: A computer code for the calculation of steady-state, thermal-mechanical behavior of oxide fuel rods for high burnup, 2014, Report NUREG/CR-7022, Vol. 1, Rev. 1, Pacific Northwest National Laboratory, Richland, WA, USA.
[19] KARB, E.H., et al., LWR fuel rod behavior in the FR2 in-pile tests simulating the heatup phase of a LOCA, 1983, Report KfK-3346, Kernforschungszentrum Karlsruhe, Karlsruhe, Germany.

[20] BROUGHTON, J.M., et al., PBF LOCA test series: Test LOC-3 and LOC-5 fuel behavior report, 1981, Report NUREG/CR-2073, U.S. Nuclear Regulatory Commission, Washington, DC, USA.
[21] SIEFKEN, L.J., Axial fuel relocation in ballooning fuel rods, 1983. In: 7th International Conference on Structural Mechanics in Reactor Technology (SMiRT-7), Chicago, IL, USA (1983)
[22] KOLSTAD, E., et al. High burn-up fuel behaviour under LOCA conditions as observed in Halden experiments, 2011. In: IAEA Technical Meeting on Fuel Behaviour and Modelling under Severe Transient and Loss-of-Coolant Accident (LOCA) Conditions, October 18-21, 2011, Mito, Japan: International Atomic Energy Agency, IAEA-TECDOC-CD-1709.
[23] FLANAGAN, M., et al., Post-test examination results from integral, high-burnup, fueled LOCA tests at Studsvik Nuclear Laboratory, 2013, Report NUREG-2160, U.S. Nuclear Regulatory Commission, Washington, DC, USA.
[24] YAGNIK, S., et al. An investigation into fuel pulverization with specific reference to high-burnup LOCA, 2014. In: 2014 Water Reactor Fuel Performance Meeting (WRFPM 2014), September 14-17, 2014, Sendai, Japan.
[25] RAYNAUD, P.A.C., Fuel fragmentation, relocation and dispersal during the loss-of-coolant accident, 2012, Report NUREG-2121, U.S. Nuclear Regulatory Commission, Washington, DC, USA.
[26] WIESENACK, W., Safety significance of the Halden IFA-650 LOCA test results, 2010, Report NEA/CSNI/R(2010)5, OECD Nuclear Energy Agency, Paris, France.
[27] AOUNALLAH, Y., et al. Simulations of the Halden IFA-650.3/.4 high burnup LOCA tests with TRACE and FALCON; A preliminary study on axial relocation, 2006. In: 2006 International Meeting on LWR Fuel Performance (TopFuel 2006), October 22-26, 2006, Salamanca, Spain: European Nuclear Society, pp. 305-311.
[28] KHVOSTOV, G., et al. Modeling the effects of axial fuel relocation in the IFA-650.4 LOCA test, 2007. In: Enlarged Halden Programme Group Meeting, March 12-15, 2007, Storefjell, Norway: OECD Halden Reactor Project, Halden, Norway.
[29] GOVERS, K. and M. Verwerft. Simulation of ballooning and relocation in the Halden LOCA tests with FRAPTRAN, 2014. In: Enlarged Halden Programme Group Meeting, September 7-12, 2014, Røros, Norway: OECD Halden Reactor Project, Halden, Norway
[30] OBERLÄNDER, B.C. and W. Wiesenack, Overview of Halden reactor LOCA experiments (with emphasis on fuel fragmentation) and plans, 2014, Report IFE/KR/E-2014/001, Institute for Energy Technology, Kjeller, Norway.
[31] TURNBULL, J.A., et al., An assessment of the fuel pulverization threshold during LOCA-type temperature transients. Nuclear Science and Engineering, 2015. 179: pp. 477-485.
[32] WESTMAN, A.E.R., The packing of particles: Empirical equations for intermediate diameter ratios. Journal of the American Ceramic Society, 1936. 19: pp. 127-129.
[33] CHIEW, Y.C. and E.D. Glandt, The effect of structure on the conductivity of a dispersion. Journal of Colloid and Interface Science, 1983. 94(1): pp. 90-104.
[34] CHUNG, H.M., Fuel behavior under loss-of-coolant accident situations. Nucl. Eng. Technol. , 2005. 37(4): pp. 327-362.
[35] MASSIH, A.R., JERNKVIST, L.O., Transformation kinetics of alloys under non-isothermal conditions. Modelling and Simulation in Materials Science and Engineering, 2009. 17(Paper ID 055002).
[36] MASSIH, A.R., High-temperature creep and superplasticity in zirconium alloys. J. Nucl. Sci. Technol., 2013. 50(1): pp. 21-34.

[37] KNUUTILA, A., Improvements on FRAPCON3/FRAPTRAN mechanical modelling, 2006, Research report VTT-R-11337-06, VTT Technical Research Centre of Finland, Helsinki, Finland.
[38] ROSINGER, H.E., A model to predict the failure of Zircaloy-4 fuel sheating during postulated LOCA conditions. J. Nucl. Mater., 1984. 120: 41–54.
[39] ERBACHER, F.J., et al. Burst criterion of Zircaloy fuel claddings in a loss-of-coolant accident, 1982. In: Zirconium in the Nuclear Industry: Fifth Conference, Philadelphia, PA, USA: D.G. Franklin, Editor American Society for Testing and Materials, ASTM STP-754, 271–283.
[40] FORGERON, T., et al. Experiment and modeling of advanced fuel rod cladding behavior under LOCA conditions: alpha-beta phase transformation kinetics and EDGAR methodology, 2000. In: Zirconium in the Nuclear Industry: Twelfth International Symposium, West Conshohocken, PA, USA: G.P. Sabol and G.D. Moan, Editors, American Society for Testing and Materials, ASTM STP-1423, 256–278.
[41] VAN UFFELEN, P., et al., Extending the application range of a fuel performance code from normal operating to design basis accident conditions. J. Nucl. Mater., 2008. 383(1–2): 137–143.
[42] ERBACHER, F.J., LEISTIKOW, S., Zircaloy fuel cladding behavior in a loss-of-coolant accident: A review, 1987. In: Zirconium in the Nuclear Industry: Seventh International Symposium, Philadelphia, PA, USA: R.B. Adamson and L.F.P. van Swam, Editors, American Society for Testing and Materials, ASTM STP-939,. 451–488.
[43] CHAPMAN, R.H., et al. Zirconium cladding deformation in a steam environment with transient heating, 1979. In: Zirconium in the Nuclear Industry: Fourth Conference, Philadelphia, PA, USA: J.H. Schemel and T.P. Papazogiou, Editors, American Society for Testing and Materials, ASTM STP-681, pp. 393-408.
[44] CHAPMAN, R.H., et al., Effect of creep time and heating rate on deformation of Zircaloy-4 tubes tested in steam with internal heaters, 1978, Report NUREG/CR-0343, U.S. Nuclear Regulatory Commission, Washington, DC, USA.
[45] KARB, E.H., et al., LWR fuel rod behavior during reactor tests under loss-of-coolant conditions: Results of the FR2 in-pile tests. J. Nucl. Mater., 1982. 107(1): 55–77.
[46] POWERS, D.A. and R.O. MEYER, Cladding swelling and rupture models for LOCA analysis, 1980, Report NUREG-0630, U.S. Nuclear Regulatory Commission, Washington, DC, USA.
[47] ERBACHER, F.J., LEISTIKOW, S., A review of Zircaloy fuel cladding behavior in a loss-of-coolant accident, 1985, Report KfK 3973, Kernforschungszentrum Karlsruhe, Karlsruhe, Germany.
[48] LEISTIKOW, S., SCHANZ, G., Oxidation kinetics and related phenomena of Zircaloy-4 fuel cladding exposed to high temperature steam and hydrogen-steam mixtures under PWR accident conditions. Nucl. Eng. Des., 1987. 103: pp. 65-84.
[49] MARKIEWICZ, M.E., ERBACHER, F.J., Experiments on ballooning in pressurized and transiently heated Zircaloy-4 tubes, 1988, Report KfK 4343, Kernforschungszentrum Karlsruhe, Karlsruhe, Germany.
[50] BRACHET, J.C., et al. Influence of hydrogen content on the alpha/beta phase transformation temperatures and on the thermal-mechanical behavior of Zy-4, M4 (ZrSnFeV), and M5 (ZrNbO) alloys during the first phase of LOCA transient, 2002. In: Zirconium in the Nuclear Industry: Thirteenth International Symposium, West Conshohocken, PA, USA: G.D. Moan and P. Rudling, Editors, American Society for Testing and Materials, ASTM STP 1423, pp. 673-701.

[51] HÓZER, Z., et al., Ballooning experiments with VVER cladding. Nuclear Technology, 2005. 152: pp. 273-285.
[52] PEREZ-FERO, E., et al., Experimental database of E110 cladding under accident conditions, 2007, Report AEKI-FRL-2007-123-01/01, AEKI KFKI Atomic Energy Research Institute of the Hungarian Academy of Sciences, Budapest, Hungary.
[53] CHAPIN, D.L., et al. Optimized ZIRLO qualification program for EDF reactors, 2009. In: TopFuel-2009, September 6-10, 2009, Paris, France: European Nuclear Society, pp. 60-65.
[54] YAN, Y., et al., Argonne results for ANL-Studsvik benchmark tests, 2010, ANL letter report to the U.S. NRC ADAMS accession no. ML111380445, U.S. Nuclear Regulatory Commission, Washington, DC, USA.
[55] YAN, Y., et al., Update of LOCA-integral and post-LOCA bend test results for fresh ZIRLO cladding, 2010, ANL letter report to the U.S. NRC ADAMS accession no. ML111380437, U.S. Nuclear Regulatory Commission, Washington, DC, USA.
[56] HELIN, M., FLYGARE, J., NRC LOCA tests at Studsvik: Design and construction of test train device and tests with unirradiated cladding material, 2012, Report STUDSVIK/N-11/130, Studsvik Nuclear AB, Studsvik, Sweden.
[57] WIESENACK, W., Summary of the Halden Reactor Project LOCA test series IFA-650, 2013, Report HPR-380, OECD Halden Reactor Project, Halden, Norway.
[58] Kolstad, E. LOCA experiments with high burnup fuel in the Halden programme, 2010. In: Swedish Radiation Safety Autority Research Seminar on Reactor Safety, April 22-23, 2010, Stockholm, Sweden.
[59] KEKKONEN, L., LOCA testing at Halden: The fourth experiment - IFA-650.4, 2007, Report HWR-838, OECD Halden Reactor Project, Halden, Norway.
[60] BOLE DU CHOMONT, F., LOCA testing at Halden: The ninth experiment IFA-650.9, 2009, Report HWR-917, OECD Halden Reactor Project, Halden, Norway.
[61] LAVOIL, A., LOCA testing at Halden: The tenth experiment IFA-650.10, 2010, Report HWR-974, OECD Halden Reactor Project, Halden, Norway.
[62] NISHI, M., LEE, B. H. Summary of pre-irradiation data on fuel segments supplied by EDF/Framatome and tested in IFA-610, 629 and 648, 2001, Report HWR-664, OECD Halden Reactor Project, Halden, Norway.
[63] TRADOTTI, R., LOCA testing at Halden: The BWR fuel experiment IFA-650.14, 2014, Report HWR-1084, OECD Halden Reactor Project, Halden, Norway.
[64] LEDERGERBER, G., Characterisation of KKL BWR fuel for test series in IFA-610, IFA-629 and IFA-650, 2014, Report HWR-1033 Rev. 1, OECD Halden Reactor Project, Halden, Norway.
[65] LEDERGERBER, G., et al., Characterization of high burnup fuel for safety related fuel testing. J. Nucl. Sci. Technol., 2006. 43(9): 1006–1014.
[66] FLANAGAN, M., ASKELJUNG. P., Observations of fuel fragmentation, mobility and release in integral high-burnup, fueled LOCA tests, 2012. In: OECD Halden Reactor Project LOCA Workshop, May 29-30, 2012, Lyon, France: OECD Halden Reactor Project, Halden, Norway.
[67] ZWICKY, H.U., Re-fabrication of ramp rodlet Z-3 from Westinghouse father rod irradiated in North Anna, 2006, Report N-05/131 Rev. 1, Studsvik Nuclear AB, Nyköping, Sweden.
[68] ZWICKY, H.U., Re-fabrication of ramp rodlet Z-4 from Westinghouse father rod irradiated in North Anna, 2006, Report N-05/133 Rev. 1, Studsvik Nuclear AB, Nyköping, Sweden.
[69] RAYNAUD, P.A.C., NRC Studsvik LOCA test 192, 2014, MS Excel data file contributed to the IAEA CRP FUMAC on December 8, 2014, U.S. Nuclear Regulatory Commission, Washington, DC, USA.

[70] OBERLÄNDER, B.C., JENSSEN, H.K., PIE on the rod from the LOCA test IFA-650.14 on high burn-up BWR fuel, 2014, Report HWR-1096, OECD Halden Reactor Project, Halden, Norway.
[71] CATHCART, J.V., et al., Zirconium metal-water oxidation kinetics, IV: reaction rate studies, 1977, Report ORNL/NUREG-17, Oak Ridge National Laboratory, Oak Ridge, TN, USA.
[72] ROSINGER, H.E., et al., The steady-state creep of Zircaloy-4 fuel cladding from 940 to 1873 K, 1978, Report AECL-6193, Atomic Energy of Canada, Pinawa, MB, Canada.
[73] OBERLÄNDER, B.C., et al. PIE results from the high burnup (92 MWd/kgU) PWR segment after LOCA testing in IFA 650-4, 2008. In: Enlarged Halden Programme Group Meeting, May 18-23, 2008, Loen, Norway: OECD Halden Reactor Project.
[74] KHVOSTOV, G., et al., Some insights into the role of axial gas flow in fuel rod behaviour during the LOCA, based on Halden tests and calculations with the FALCON-PSI code. Nucl. Eng. Des., 2011. 241: pp. 1500-1507.
[75] OBERLÄNDER, B.C., JENSSEN. H.K., LOCA IFA-650.9: PIE of the 90 MWd/kgU PWR rod subjected to a high temperature transient, 2010. In: Enlarged Halden Programme Group Meeting, March 14-19, 2010, Storefjell, Norway: OECD Halden Reactor Project.
[76] OBERLÄNDER, B.C., JENSSEN. H.K., LOCA IFA-650.10: PIE of a PWR rod with a burn-up of 61 MWd/kgU after LOCA testing in the HBWR, 2011. In: Enlarged Halden Programme Group Meeting, October 3-6, 2011, Sandefjord, Norway: OECD Halden Reactor Project.
[77] BIANCO, A., et al., Experimental investigation on the causes for pellet fragmentation under LOCA conditions. J. Nucl. Mater., 2015. 465: pp. 260-267.
[78] GUERIN, Y., In-pile and out-of-pile burst release of fission gases, 2012. In: Enlarged Halden Programme Group Meeting, September 8-13, 2002, Storefjell, Norway: OECD Halden Reactor Project.
[79] ANDERSSON, P., et al., Inspection of LOCA test rod IFA-650.15 using gamma emission tomography, 2016, Report HWR-1164, OECD Halden Reactor Project, Halden, Norway.
[80] FRESHLEY, M.D., HESSON, G.M., Summary results of the LOCA simulation program conducted in NRU, 1983, Conference paper presented at the Eleventh NRC Water Reactor Safety Meeting, Gaithersburg, MD, USA, October 14-28, 1983, Report PNL-SA-11536, Pacific Northwest Laboratory, Richland, WA, USA.
[81] FEDOTOV, P.V., et al. LOCA test with high burnup VVER fuel in the MIR reactor, 2015. In: Reactor Fuel Performance 2015 (TopFuel-2015), September 13-17, 2015, Zürich, Switzerland: European Nuclear Society, pp. 335-344.
[82] TURNBULL, J.A., et al. An investigation into fuel pulverization with specific reference to high burnup LOCA, 2014. In: Enlarged Halden Programme Group Meeting, September 7–12, 2014, Røros, Norway: OECD Halden Reactor Project, Halden, Norway.
[83] Utveckling av modeller för fissionsgasinducerad fragmentering av högutbränt kärnbränsle, 2015, Research project agreement SSM-2015-4050-2, (In Swedish), Swedish Radiation Safety Authority, Stockholm, Sweden.
[84] Utveckling av modeller för fissionsgasinducerad fragmentering av högutbränt kärnbränsle, fortsättning, 2016, Research project agreement SSM2016-3944-2, (In Swedish), Swedish Radiation Safety Authority, Stockholm, Sweden.
[85] CHUNG, H.M., KASSNER, T.F., Deformation characteristics of Zircaloy cladding in vacuum and steam under transient-heating conditions: summary report 1978,

Report NUREG/CR-0344, U.S. Nuclear Regulatory Commission, Washington, DC, USA.
[86] BERGQUIST, P., A parameter study concerning the impact on the calculated peak clad temperature of a redistribution of the fuel after cladding swelling and rupture, 1979, Report FV-79-0017/2, AB Fjärrvärme, Trosa, Sweden.
[87] ROUTLEDGE, K.T., et al. Calculations of the effects of fuel pellet fragment axial relocation on the peak clad temperature during a loss-of-coolant accident in a pressurized water reactor, 1988. In: Second UK National Conference on Heat Transfer, September 14–16, 1988, Glasgow, UK: Institution of Mechanical Engineers, Mechanical Engineering Publications, London, UK, 2, pp. 1531-1540.
[88] GRANDJEAN, C., et al. High burnup UO2 fuel LOCA calculations to evaluate the possible impact of fuel relocation after burst, 2001. In: OECD Topical Meeting on LOCA Fuel Safety Criteria, March 22-23, 2001, Aix-en-Provence: OECD Nuclear Energy Agency, Committee on the Safety of Nuclear Installations, Report NEA/CSNI/R(2001)18, Paris, France, 239–266.
[89] OGUMA, M., Integrity degradation of UO2 pellets subjected to thermal shock. J. Nucl. Mater., 1985. 127: 67–76.
[90] BESTION, D. System code models and capabilities, 2008. In: OECD-NEA/UNIPI Seminar on the Transfer of Competence, Knowledge and Experience Gained through CSNI Activities in the Field of Thermal Hydraulics (THICKET 2008), May 5-9, 2008, Pisa, Italy: OECD Nuclear Energy Agency, 81–106.
[91] MODEST, M.F., Radiative Heat Transfer. 3rd ed. 2013, Oxford, UK: Academic Press.
[92] STUCKERT, J., et al., On the thermo-physical properties of Zircaloy-4 and ZrO2 at high temperature, 2002, Report FZKA 6739, Forschungszentrum Karlsruhe, Karlsruhe, Germany.
[93] KARLSSON, J., Studsvik LOCA test machine data sheet, 2016, MS Excel data file contributed to the IAEA CRP FUMAC on March 24, 2016, Studsvik Nuclear AB, Nyköping, Sweden.

TESTING OF THE TRANSURANUS COMPUTER CODE BY JOINT SOLUTION OF TEST PROBLEMS WITHIN FUMAC PROJECT

M. IEREMENKO
State Scientific and Technical Centre for Nuclear and Radiation Safety
Kyiv, Ukraine
e-mail: ml_eremenko@sstc.com.ua

Abstract

This report describes the testing and validation of the TRANSURANUS computer code against tests performed in MTA-EK, Halden and Studsvik in the framework of IAEA's FUMAC project. FUMAC - Fuel Modelling in Accident Conditions - IAEA's Coordinated Research Activities (CRP), Code T12028. Main objective of project is support the Member States in their efforts to analyse and better understand the behaviour of water-cooled power reactor fuel in the LOCA accident conditions through sharing of experimental data and best practices in application of fuel modelling computer codes. Loss of Coolant Accidents (LOCA) are among the most demanding accidents that can happen in a Light Water Reactor (LWR). The lack of cooling and the drop in pressure impose large stresses on the nuclear fuel which would increase the risk of fuel rod damage and the subsequent release of active material. But LOCA is also an accident that the nuclear power plant is designed to withstand with a limited release of radioactivity to the surroundings.

1. INTRODUCTION

Loss-of-coolant accidents (LOCAs) in light water reactors (LWRs) may lead to overheating of the fuel rods, which in turn may lead to distension of the internally overpressurized cladding tubes and to loss of cladding ductility by high temperature oxidation of the material. To maintain structural integrity of the fuel and to ensure that the reactor core remains coolable, the cladding temperature and oxidation should not transgress certain limits 0. These regulatory safety criteria for LOCA are based primarily on experimental studies from the 1970s and 1980s, which were carried out on low burnup fuel of the design and materials of that time. The introduction of new fuel designs, most importantly new cladding materials, and the move to higher discharge burnups have prompted a need to verify that the existing safety criteria remain valid and appropriate. To this end, both separate effect tests and integral LOCA simulation tests have been carried out on modern fuel designs and fuel with high burnup over the last decade. Examples of the latter are the IFA-650 series of in-reactor tests in Halden, Norway 0, the outof- reactor tests done in Studsvik, Sweden 0, and the recent MIR-LOCA inreactor test in Dimitrovgrad, Russia 0.

Along with the LOCA experiments on high burnup fuel, computational models and computer programs for analyses of LOCA are being modified and refined to capture the experimentally observed phenomena. An example of international cooperation in this field is the IAEA coordinated research project FUMAC – Fuel Modelling in Accident Conditions. This international project, which is running from 2014 to 2018, brings together 27 organisations, including SSTC NRS, with a common interest in improving their computational tools and experience. Organisations participating in FUMAC are given access to detailed data on experiments deemed particularly valuable for computer program validation. Another benefit from FUMAC is the possibility to compare models and computational tools used among the participants, and to share knowledge and best practices within the group. A final report on the activities in FUMAC is planned to be issued by the IAEA in 2018. To date, SSTC NRS has contributed to the project by modelling of MTA-EK, Halden (IFA 650.10, IFA 650.11) and NRC-Studsvik (192, 198) experimental data. All modelling are carried out by TRANSURANUS computer code 0–0.

2. USED CODE AND IMPROVEMENTS

All modelling are carried out by following versions of TRANSURANUS code:

- TRANSURANUS version - v1m1j11 (Software Licensing Agreement No. 3176), MTA-EK data;
- TRANSURANUS version - v1m1j17 (Software Licensing Agreement No. 33955), Halden (IFA 650.10, IFA 650.11) and Studsvik (192, 198) experimental data.

3. MODELLED CASES

According FUMAC RCM1 0 for modelling following data sets was chosen:

- MTA-EK 0–0;
- IFA 650.10 0;
- IFA 650.11 0;
- Studsvik 192–198 0, 0–0.

4. MODELLING DETAILS

All modelling are carried out by TRANSURANUS code in LOCA mode. For this possibility main following keys was used 0, 0:

- ILOCA. Control variable for LOCA simulation. =1;
- IPHASEZR. Control variable for Zr-based cladding crystallographic phase transition model for Zircaloy and for Zr1%Nb;
- IBMECH. Option for the mechanical analysis;
- ICORRO. Option for the outer cladding corrosion model;
- IFBA. Option for the selection of a IFBA-model (NRC-Studsvik LOCA test 198);
- TTRANS, TLOCA. Time of LOCA initiation;
- IKUEHL, IALPHA. For input of cladding temperature;
- IPLNUM. Option for average temperature in the plenum;
- ICLFAIL. Control variable for the cladding failure model in the LOCA simulation.

Options for specific correlations of material properties of the cladding from different alloys (PWR, WWER) are shown in Table 1.

TABLE 1. TRANSURANUS OPTIONS FOR SPECIFIC CORRELATIONS OF MATERIAL PROPERTIES OF THE CLADDING

	Items	Subprogram	Zircaloy	Zry-4	Zr1Nb
1	Creep anisotropy coefficients	Anisotrp	18		25, 26, 27
2	Elasticity constant	ELOC	20		25
3	Poisson’s ratio	NUELOC	20		25
4	Strain due to swelling	SWELOC	19, 20, 21	17, 18	25, 26, 27
5	Thermal strain	THSTRN	19, 20		25
6	Thermal conductivity	LAMBDA	19, 20, 21, 22		25
7	Creep strain	ETACR	18, 20		25, 26, 27, 28
8	Yield stress	SIGSS	19, 20		25
9	Rupture strain	ETAPRR	20		25
10	Burst stress	SigmaB	18		25
11	Crystallographic Phase Transition	ZrBeta	18		28
12	not used				
13	Specific heat at constant pressure	CP	20		25

TABLE 1. TRANSURANUS OPTIONS FOR SPECIFIC CORRELATIONS OF MATERIAL PROPERTIES OF THE CLADDING

	Items	Subprogram	Zircaloy	Zry-4	Zr1Nb
14	Density	RO	20		25
15	Not used				
16	Solidus–liquidus melt temperature	SOLIMT	19, 20		25
17	Heat of melting	FH	19, 20		25 (25->20)
18	Emissivity	EMISS	19, 20		25 (25->20)
19	Not used	RUPSTR		18	25
20	Not used				

4.1. MTA-EK

Analyses of tests MTA-EK series using the TRANSURANUS (v1m1j11) code are presented in this section. The results from the calculations are compared with measured data for the following parameters:

— Pressure of cladding rupture;
— Cladding diameter at rupture.

Modeling of all sets of experimental data (31 experiments) was carried out. At the first stage of modeling pre-processing of experiment data was carried out (delete or smoosing wrong measurements - negative absolute pressures, non-realistic pressure drops, etc. Fig. 1). At the second stage calculation of each experiment was carried out.

Input data – cladding geometry and alloy, cladding temperature and inner pressure during experimental.

— Axial layers – 10×5 mm;
— Calculation mode – LOCA. Cladding behaviour + Clad Failure model;
— Output – maximal pressure (Fig. 2) and geometry (Fig. 3) at cladding fail.

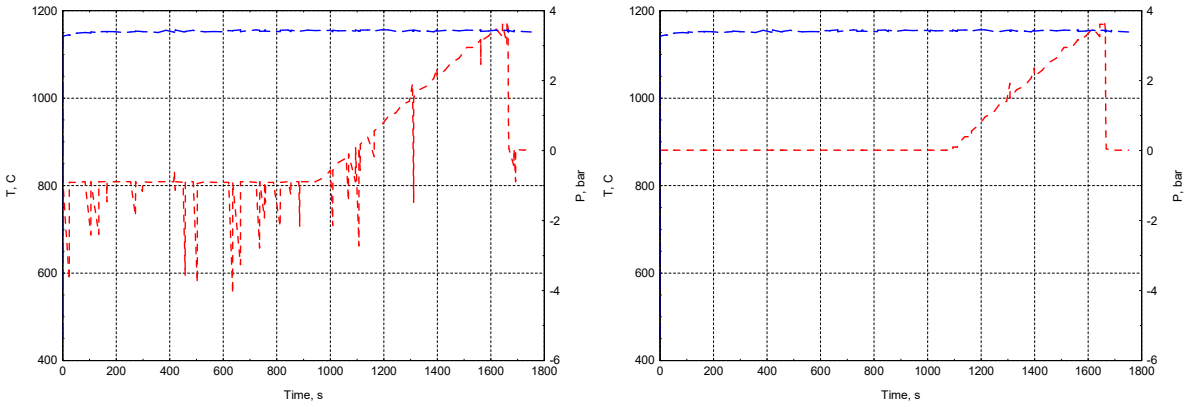

FIG. 1. Experimental data before and after pre-processing.

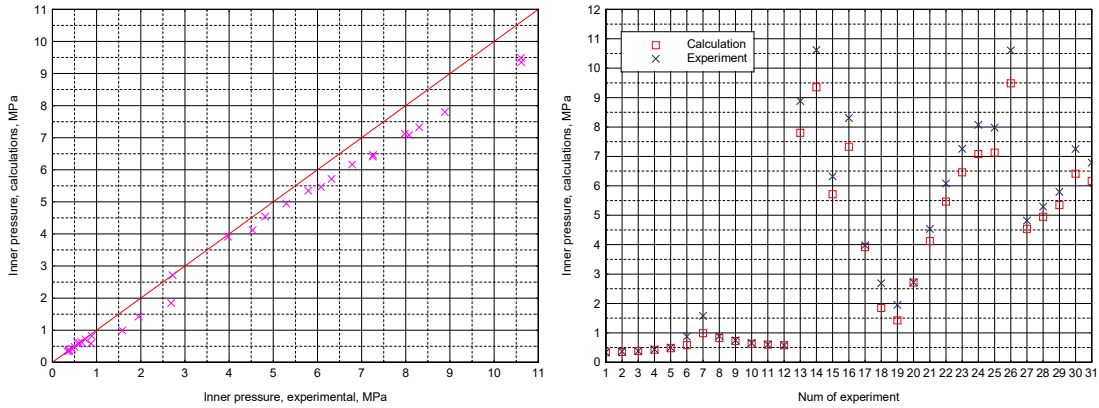

FIG. 2. Calculation result. Maximal pressure at cladding fail.

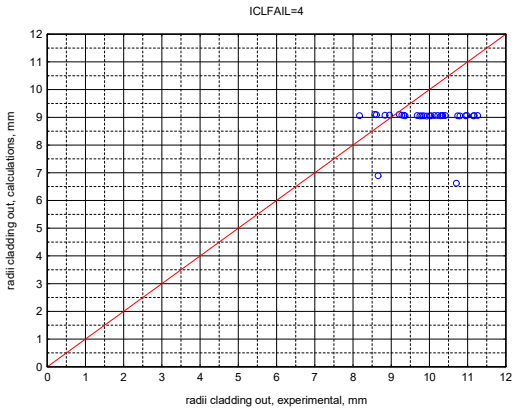

FIG. 3. Calculation result. Cladding out radius at fail.

4.2. IFA 650.10

Analyses of test IFA 650.10 series using the TRANSURANUS (v1m1j17) code are presented in this section. The results from the calculations are compared with measured data for the following parameters:

- Time of cladding rupture;
- Pressure of cladding rupture;
- Cladding diameter at rupture;
- Cladding elongation.

4.2.1. Simulations of pre-irradiation

The computer analyses of the considered Halden IFA 650.10 tests were carried out in two steps. In the first step, the pre-irradiation of full (or father) fuel rod that was later re-fabricated into a test rodlet was modelled by use of TRANSURANUS (v1m1j17). Calculated results from TRANSURANUS, defining the pre-test conditions for test fuel rodlet, were used as input to the second analysis step. Storage of spent fuel in a water pool practically doesn't influence characteristics of a cladding and fuel pellets.

Input for the simulations, in terms of fuel pellet and cladding design data and power histories, are given in 0. General reactor data are used from 0. The axial profile of linear heat generation rate during the pre-irradiation was assumed as profile for WWER-1000 reactor for middle cycle moment, Fig. 4(a). Core dimension of WWER-1000 and PWR (Gravelines-5, 900 MWe, fuel 17×17) are similar (∅≈3 m, h≈3.5 m) and this assumption is acceptable.

Nominal core average thermal-hydraulic conditions for PWR were used in the simulations 0. In calculations the full fuel rod were discretized axially into 20x183 mm long axial nodes.

Input data – cladding geometry and alloy, initial (factory) inner pressure, power during operation, power axial profile like for PWR (Gravelines 5, 900 MWe, fuel 17×17) core.

Axial layers – 20x183 mm.

Calculation mode – fuel pin behaviour during operation.

Output – fuel pin characteristics during operation and at the end of operation.

Result – Burnup – 61 MWd/kgU experimental value, 59.8 MWd/kgU result of calculation.

Oxide thickness – 20…30 μm experimental value, ≈17 μm result of calculation.

Fuel rod linear power and inn-cladding pressure during full rod pre-irradiation history modelling are present in Fig. 4(b).

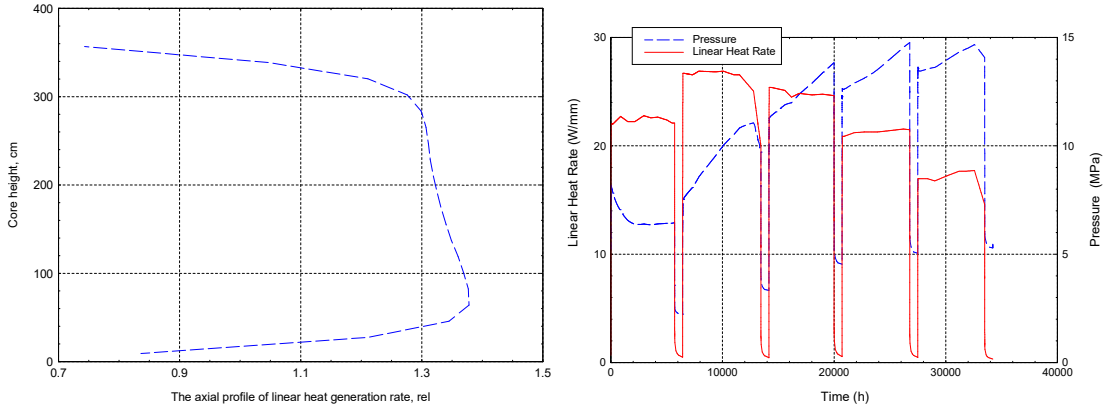

(a) (b)

FIG. 4. The axial profile of linear heat generation rate (a) and fuel rod linear power and inside cladding pressure (b) during full rod pre-irradiation history modelling. IFA 650.10.

4.2.2. Simulations of LOCA tests

This step involved simulations of the LOCA test with TRANSURANUS code too. No uncertainty or sensitivity analyses were carried out. Using full (father) rod pre-irradiation history modelling the input data for the test rodlet was prepared. From father rod are used the following parameters: linear power, inn-cladding pressure, temperature of cooling. Using restart option of TRANSURANUS code change of inn-cladding gas composition before LOCA experiment was simulated (not for all calculations, part of tasks was done with inn-cladding gas pressure as boundary conditions). All calculations were done with an axial discretisation consisting of 20x22 mm long axial segments for the active part of the test rodlet.

It should be remarked that no computer program was used for calculating the transient thermal-hydraulic boundary conditions that are needed for fuel rod analyses with TRANSURANUS. These boundary conditions were derived from measured temperatures or from pre-calculated data distributed through FUMAC participants (calculated by SOCRAT code). For axial profiles of cladding temperatures the following possibility was used:

— Flat profile;
— Profile from prediction of boundary conditions of the Halden LOCA IFA-650, tests 3 by ATHLET-CD 0;
— Profile calculated by SOCRAT code 0, 0.
— Input data – Cladding data from core operation + experimental data: outer pressure, power. Cladding temperatures and power axial profile – flat, ATHLET-CD for IFA-650.3,

SOCRAT for IFA-650.10. Part of calculations with experimental rod inner pressure (no inn pressure drop after experimental cladding fail).

— Axial layers – 20x22 mm;
— Calculation mode – LOCA. Cladding behaviour + Clad Failure model;
— Output – Moment of fail, cladding geometry, rod inner pressure;
— Result – Time of cladding fail – 250 s experimental value, 204…305 s result of calculation. Maximal diameter at fail – 12.5 mm experimental value, ≈13 mm result of calculation.

Time of cladding fail for different variants of calculations are present in Table 2.

TABLE 2. TIME OF CLADDING FAIL FOR THE IFA-650.10 TEST RODLET

		Time of cladding fail (s)
	Experimental	250
Calculations variant	Profile 650.3	224
	ProfileSOCRAT(profile+Tmeasured)	218
	Profile SOCRAT (Tsocrat)	205
	Profile SOCRAT (Tplenum=SOCRAT)	262
	Pinn mesured, profile flat	305
	Pinn mesured, profile 650.3	286

Figure 5(a), shows the calculated and measured evolution of rod plenum gas pressure during the Halden IFA-650.10 test. The calculated gas pressure is a little more then measurements for t>≈80 s. It can be explained by same indeterminacy in pin free volume (volume of connected measurement lines, temperature). In calculations characteristic of free volume gas was predict by TRANSURANUS code. In calculations the characteristic of free volume gas was predict by TRANSURANUS code. In additional for understanding influence of inn-gas uncertainties the part of calculations are carried out with gas pressure as boundary conditions (used measured value).

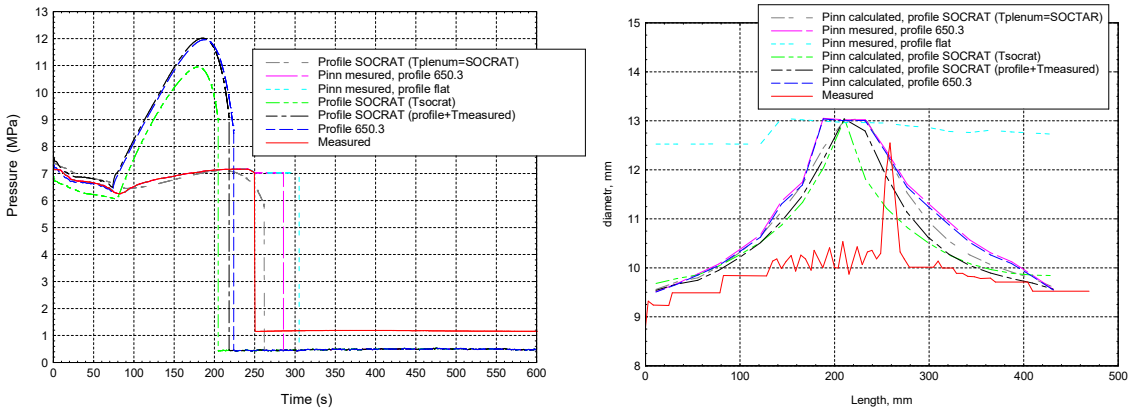

(a) (b)

FIG. 5. Calculated evolution of rod plenum gas pressure (a) and diameter profiles (b) in comparison with measurements for the IFA-650.10 test rodlet.

Fig. 5(b), shows the calculated post-test diameter profile of the IFA-650.10 rodlet in comparison with data that were obtained by analysing visual inspection photos and neutron radiographs. It is clear from Fig. 5(b), that the length of the ballooned region is overestimated, and the calculated axial position of the balloon is slightly lower than actually observed.

Fig. 6 shows the calculated and measured evolution of rod cladding elongation during the Halden IFA-650.10 test. The calculated elongation is overestimated then measurements value.

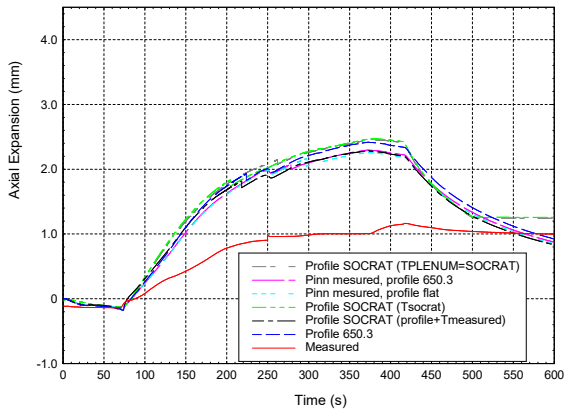

FIG. 6. Calculated evolution of rod cladding elongation in comparison with measurements for the IFA-650.10 test rodlet.

4.3. IFA 650.11

Analyses of test IFA 650.11 series using the TRANSURANUS (v1m1j17) code are presented in this section. The results from the calculations are compared with measured data for the following parameters:

- Time of cladding rupture;
- Pressure of cladding rupture;
- Cladding diameter at rupture;
- Cladding elongation.

4.3.1. Simulations of pre-irradiation

The computer analyses of the considered Halden IFA 650.11 tests were carried out in two steps. In the first step, the pre-irradiation of full (or father) fuel rod that was later re-fabricated into a test rodlet was modelled by use of TRANSURANUS (v1m1j17). Calculated results from TRANSURANUS, defining the pre-test conditions for test fuel rodlet, were used as input to the second analysis step. Storage of spent fuel in a water pool practically doesn't influence characteristics of a cladding and fuel pellets.

Input for the simulations, in terms of fuel pellet and cladding design data and power histories, are given in 0. General reactor data are used for WWER-440. The axial profile of linear heat generation rate during the pre-irradiation was assumed as profile for WWER-440 reactor for middle cycle moment, Fig. 7(a). In calculations the full fuel rod were discretized axially into 20×122 mm long axial nodes.

- Input data – cladding geometry and alloy, initial (factory) inner pressure, power during operation, power axial profile for WWER-440 core;
- Axial layers – 20×122 mm;
- Calculation mode – fuel pin behaviour during operation;
- Output – fuel pin characteristics during operation and at the end of operation.
- Result – Burnup – 56 MWd/kgU experimental value, 60 MWd/kgU result of calculation. Oxide thickness – 5 μm experimental value, ≈ 6 μm result of calculation.

Fuel rod linear power and inn-cladding pressure during full rod pre-irradiation history modelling are present in Fig. 7(b).

4.3.2. Simulations of LOCA tests

This step involved simulations of the LOCA test with TRANSURANUS code too. No uncertainty or sensitivity analyses were carried out. Using full (father) rod pre-irradiation history modelling the input data for the test rodlet was prepared. From father rod are used the following parameters: linear power, inn-cladding pressure, temperature of cooling. Using restart option of TRANSURANUS code change of inn-cladding gas composition before LOCA experiment was simulated (not for all calculations, part of tasks was done with inn-cladding gas pressure as boundary conditions). All calculations were done with an axial discretisation consisting of 20×24 mm long axial segments for the active part of the test rodlet.

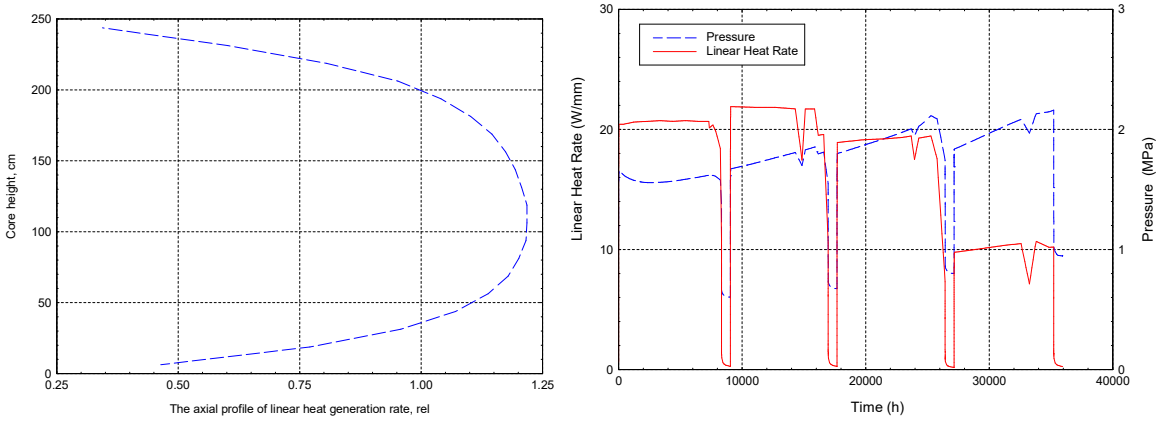

(a) (b)

FIG. 7. The axial profile of linear heat generation rate (a) and rod linear power, inn-cladding pressure (b) during full rod pre-irradiation history modelling. IFA 650.11.

It should be remarked that no computer program was used for calculating the transient thermal-hydraulic boundary conditions that are needed for fuel rod analyses with TRANSURANUS. These boundary conditions were derived from measured temperatures or from pre-calculated data distributed through FUMAC participants (calculated by SOCRAT code). For axial profiles of cladding temperatures the following possibility was used:

- Flat profile;
- Profile fro;m prediction of boundary conditions of the Halden LOCA IFA-650, tests 3 by ATHLET-CD 0;
- Profile calculated by SOCRAT code 0, 0.
- Input data – Cladding data from core operation + experimental data: outer pressure, power. Cladding temperatures and power axial profile – flat, ATHLET-CD for IFA-650.3, SOCRAT for IFA-650.11. Part of calculations with experimental rod inner pressure (no inn pressure drop after experimental cladding fail).
- Axial layers – 20×24 mm.
- Calculation mode – LOCA. Cladding behaviour + Clad Failure model.
- Output – Moment of fail, cladding geometry, rod inner pressure.
- Result – Time of cladding fail – 208 s experimental value, 168…220 s result of calculation. Maximal diameter at fail – 11.5 mm experimental value, ≈ 11.5 mm result of calculation.

Time of cladding fail for different variants of calculations are present in Table 3.

TABLE 3. TIME OF CLADDING FAIL FOR THE IFA-650.11 TEST RODLET

		Time of cladding fail (s)
	Experimental	208
Calculations variant	Profile 650.3	183
	ProfileSOCRAT(profile+Tmeasured)	172
	Profile SOCRAT (Tsocrat)	168
	Profile SOCRAT (Tplenum=SOCRAT)	186
	Pinn mesured, profile flat	220
	Pinn mesured, profile 650.3	207

Figure 8(a) shows the calculated and measured evolution of rod plenum gas pressure during the Halden IFA-650.11 test. The calculated gas pressure is a little more then measurements for t>≈70 s. It can be explained by same indeterminacy in pin free volume (volume of connected measurement lines, temperature). In calculations characteristic of free volume gas was predict by TRANSURANUS code. In calculations the characteristic of free volume gas was predict by TRANSURANUS code. In additional for understanding influence of inn-gas uncertainties the part of calculations are carried out with gas pressure as boundary conditions (used measured value).

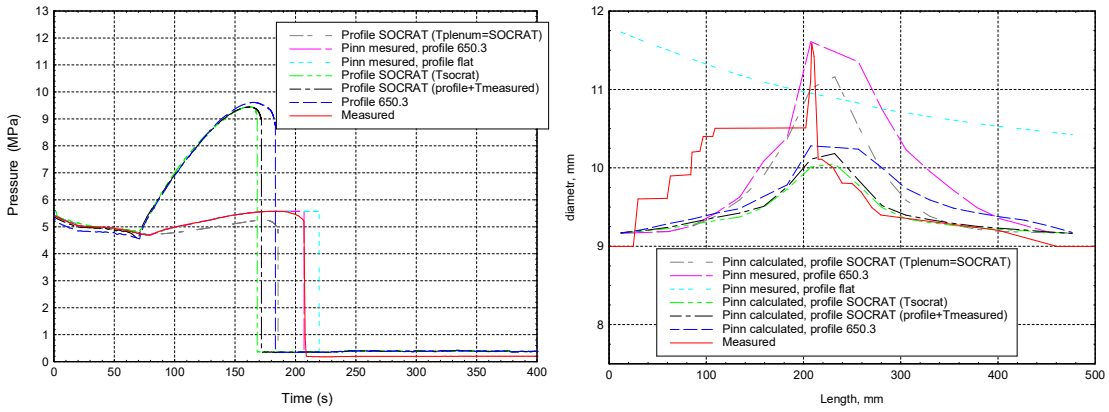

(a) (b)

FIG. 8. Calculated evolution of rod plenum gas pressure (a) and diameter profiles (b) in comparison with measurements for the IFA-650.11 test rodlet.

Fig. 8(b) shows the calculated post-test diameter profile of the IFA-650.11 rodlet in comparison with data that were obtained by analysing visual inspection photos and neutron radiographs. It is clear from Fig. 8(b) that the length of the ballooned region is overestimated, and the calculated axial position of the balloon is slightly lower than actually observed.

Fig. 9 shows the calculated and measured evolution of rod cladding elongation during the Halden IFA-650.11 test. The calculated elongation is overestimated then measurements value.

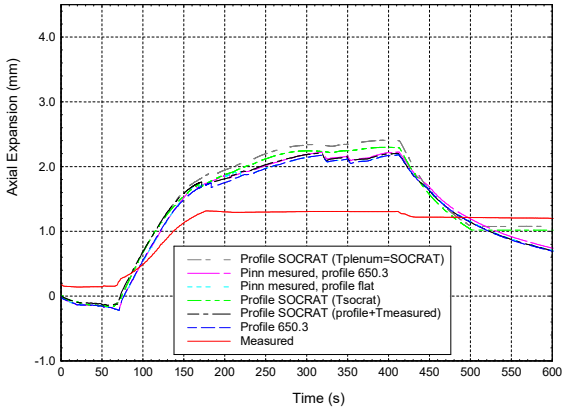

FIG. 9. Calculated evolution of rod cladding elongation in comparison with measurements for the IFA-650.11 test rodlet.

4.4. NRC-Studsvik LOCA test 192

Analyses of NRC-Studsvik LOCA test 192 using the TRANSURANUS (v1m1j17) code are presented in this section. The results from the calculations are compared with measured data for the following parameters:

- Time of cladding rupture;
- Pressure of cladding rupture;
- Cladding diameter at rupture.

4.4.1. Simulations of pre-irradiation

The computer analyses of the considered NRC-Studsvik LOCA test 192 were carried out in two steps. In the first step, the pre-irradiation of full (or father) fuel rod that was later re-fabricated into a test rodlet was modelled by use of TRANSURANUS (v1m1j17). Calculated results from TRANSURANUS, defining the pre-test conditions for test fuel rodlet, were used as input to the second analysis step. Storage of spent fuel in a water pool practically doesn't influence characteristics of a cladding and fuel pellets.

Input for the simulations, in terms of fuel pellet and cladding design data and power histories, are given in 0, 0–0. General reactor data are used from 0. The axial profile of linear heat generation rate during the pre-irradiation was assumed as profile for WWER-1000 reactor for middle cycle moment, Fig. 4(a). Core dimension of WWER-1000 and PWR (Westinghouse 3-loop PWR, fuel 17×17) are similar (∅≈ 3 m, h≈ 3.5 m) and this assumption is acceptable. Nominal core average thermal-hydraulic conditions for PWR were used in the simulations 0. In calculations the full fuel rod were discretized axially into 20×183 mm long axial nodes.

- Input data – cladding geometry and alloy, initial (factory) inner pressure, power during operation, power axial profile like for PWR (Westinghouse 3-loop PWR) core.
- Axial layers – 20x183 mm.
- Calculation mode – fuel pin behaviour during operation.
- Output – fuel pin characteristics during operation and at the end of operation.
- Result – Burnup – 68.2 MWd/kgU experimental value, 67.7 MWd/kgU result of calculation. Oxide thickness – 27…30 μm experimental value, ≈20 μm result of calculation.

Fuel rod linear power and inn-cladding pressure during full rod pre-irradiation history modelling are present in Fig. 10.

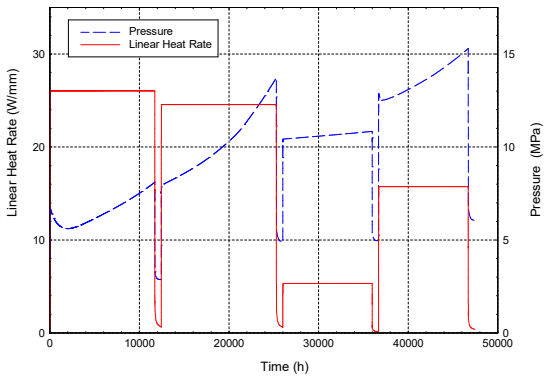

FIG. 10. Fuel rod linear power and inn-cladding pressure during full rod pre-irradiation history modelling. NRC-Studsvik 192.

4.4.2. Simulations of LOCA tests

This step involved simulations of the LOCA test with TRANSURANUS code too. No uncertainty or sensitivity analyses were carried out. Using full (father) rod pre-irradiation history modelling the input data for the test rodlet was prepared. From father rod are used the following parameters: linear power, inn-cladding pressure, temperature of cooling. Using restart option of TRANSURANUS code change of inn-cladding gas composition before LOCA experiment was simulated (not for all calculations, part of tasks was done with inn-cladding gas pressure as boundary conditions). All calculations were done with an axial discretisation consisting of 20×15 mm long axial segments for the active part of the test rodlet.

It should be remarked that no computer program was used for calculating the transient thermal-hydraulic boundary conditions that are needed for fuel rod analyses with TRANSURANUS. These boundary conditions were derived from measured temperatures. For axial profiles of cladding temperatures the following possibility was used:

- Flat profile;
- Profile by expression $T = -0.0078 \cdot z^2 + 0.1429 \cdot z + Tm$ (°C), 0. Profile_A;
- Profile by expression $T = -0.016 \cdot z^2 + 0.1429 \cdot z + Tm$ (°C), 0. Profile_B.
- Experiment started form t=0 s, LOCA part of experiment (test rodlet heating) from t≈1080 s.
- Input data – Cladding data from core operation + experimental data: outer pressure. Cladding temperatures axial profile – flat, expression “Profile_A”, expression “Profile_B”. Part of calculations with experimental rod inner pressure (no inn pressure drop after experimental cladding fail).
- Axial layers – 20×15 mm.
- Calculation mode – LOCA. Cladding behaviour + Clad Failure model.
- Output – Moment of fail, cladding geometry, rod inner pressure.
- Result – Time of cladding fail – 77 s experimental value, 74…98 s result of calculation. Maximal diameter at fail – 16.5 mm experimental value, ≈13 mm result of calculation.

Time of cladding fail for different variants of calculations are present in Table 4.

TABLE 4. TIME OF CLADDING FAIL FOR THE NRC-STUDSVIK 192 TEST RODLET.

		Time of cladding fail (from start of experiment), (s)	Time of cladding fail (from start LOCA), (s)
	Experimental	1157	77
Calculations variant	Pinn calculated, Profile_B, T upper, lowert plenum calculated	1154	74
	Pinn calculated, Profile_B, T upper, lowert plenum =const	1173	93
	Pinn mesured, profile flat	1178	98
	Pinn mesured, profile_A	1175	95
	Pinn mesured, profile_B	1172	92

Figures 11(a) and (b), shows the calculated and measured evolution of rod plenum gas pressure during the NRC-Studsvik 192 test. The calculated gas pressure is a little more then measurements for t>≈5 s. It can be explained by some indeterminacy in pin free volume (volume of connected measurement lines, temperature). In calculations characteristic of free volume gas was predict by TRANSURANUS code. In additional for understanding influence of inn-gas uncertainties the part of calculations are carried out with gas pressure as boundary conditions (used measured value) and with the constant temperature of gas of upper and lower plenum.

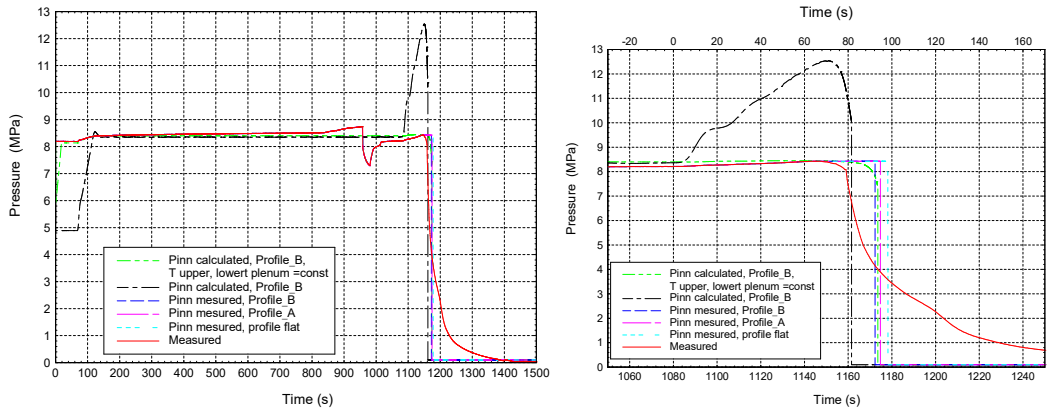

(a) (b)

FIG. 11. Calculated evolution of rod plenum gas pressure ((b)-LOCA time) in comparison with measurements for the NRC-Studsvik 192 test rodlet.

Figure 12 shows the calculated post-test diameter profile of the NRC-Studsvik 192 rodlet in comparison with data that were obtained by analysing visual inspection photos and neutron radiographs. It is clear from Fig. 12 that the length of the ballooned region is overestimated and the cladding diameter of failed area is underestimated. The calculated axial position of the balloon has a good correlation with experimental data.

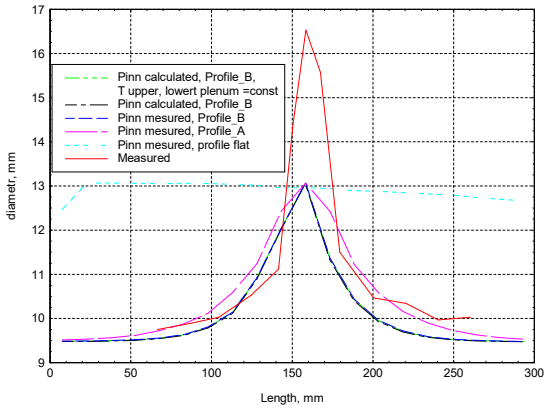

FIG. 12. Calculated and measured post-test diameter profiles for the NRC-Studsvik 192 rod.

4.5. NRC-Studsvik LOCA test 198

Analyses of NRC-Studsvik LOCA test 198 using the TRANSURANUS (v1m1j17) code are presented in this section. The results from the calculations are compared with measured data for the following parameters:

- Time of cladding rupture;
- Pressure of cladding rupture;
- Cladding diameter at rupture.

4.5.1. Simulations of pre-irradiation

The computer analyses of the considered NRC-Studsvik LOCA test 198 were carried out in two steps. In the first step, the pre-irradiation of full (or father) fuel rod that was later re-fabricated into a test rodlet was modelled by use of TRANSURANUS (v1m1j17). Calculated results from TRANSURANUS, defining the pre-test conditions for test fuel rodlet, were used as input to the second analysis step. Storage of spent fuel in a water pool practically doesn't influence characteristics of a cladding and fuel pellets.

Input for the simulations, in terms of fuel pellet and cladding design data, are given in 0, 0, 0–0. The pre-irradiation history for the re-fabricated short length segment (history of father rod) was not present in 198 test specifications 0. For modelling of father rod the hypothetical power history was used. Time of cycles (4 cycles) was chosen for achieving of the rod burnup value (55.2 MWd/kgU). General reactor data are used from 0. The axial profile of linear heat generation rate during the pre-irradiation was assumed as profile for WWER-1000 reactor for middle cycle moment, Fig. 4(a). Core dimension of WWER-1000 and PWR (Westinghouse 3-loop PWR, fuel 17×17) are similar (∅≈3 m, h≈3.5 m) and this assumption is acceptable. Nominal core average thermal-hydraulic conditions for PWR were used in the simulations 0. In calculations the full fuel rod were discretized axially into 20×183 mm long axial nodes.

- Input data – cladding geometry and alloy, initial (factory) inner pressure, power during operation, power axial profile like for PWR (Westinghouse 3-loop PWR) core.
- Axial layers – 20×183 mm.
- Calculation mode – fuel pin behaviour during operation.
- Output – fuel pin characteristics during operation and at the end of operation.
- Result – Burnup – 55.2 MWd/kgU experimental value, 55.9 MWd/kgU result of calculation. Oxide thickness – 20 μm experimental value, ≈16 μm result of calculation.

Fuel rod linear power and inn-cladding pressure during full rod pre-irradiation history modelling are present in Fig. 13(a).

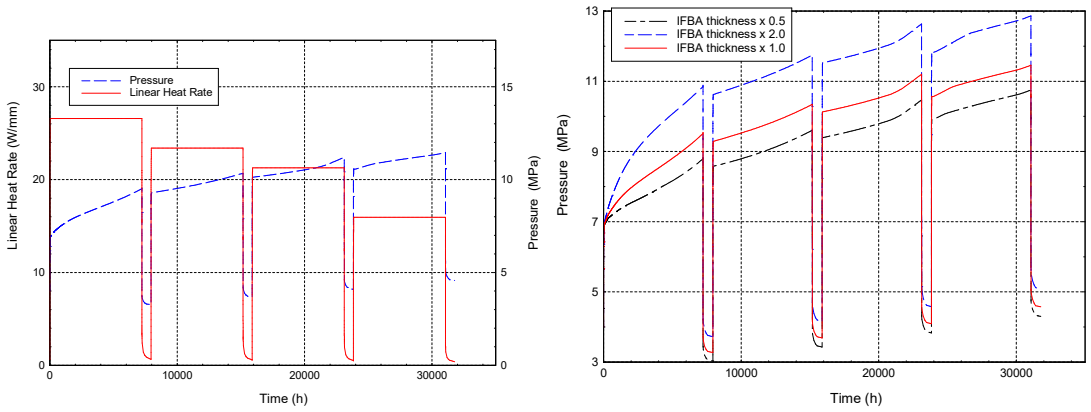

(a) (b)

FIG. 13. Fuel rod linear power and inn-cladding pressure during full rod pre-irradiation history modelling. NRC-Studsvik 198.

It should be noted that for NRC-Studsvik 198 test the Westinghouse IFBA fuel rod was used. Fuel pellets of this rod was coated by burnable absorber - zirconium diboride ZrB_2. But characteristics of this burnable absorber was not present in 198 test specifications 0. For modelling of this IFBA rod the Westinghouse's WWER-1000 fuel data was used (first 6 LTA FA for Ukrainian NPP had IFBA). This burnable absorber in the form of a thin layer works through the (n, α) reaction, e.g. He is produced that is accounted for in the gas composition in the free volume of fuel rod. As a result inn-cladding pressure are depend from characteristics of zirconium diboride layer (thickness or mass pro length of fuel) and geometry of cladding for test rodlet is depend too. Fig. 13(b) shows the calculated inn-cladding pressure during full rod pre-irradiation history modelling for two additional cases: thickness of ZrB_2 multiplied or divided by 2.

4.5.2. Simulations of LOCA tests

This step involved simulations of the LOCA test with TRANSURANUS code too. No uncertainty or sensitivity analyses were carried out. Using full (father) rod pre-irradiation history modelling the input data for the test rodlet was prepared. From father rod are used the following parameters: linear power, inn-cladding pressure, temperature of cooling. Using restart option of TRANSURANUS code change of inn-cladding gas composition before LOCA experiment was simulated (not for all calculations, part of tasks was done with inn-cladding gas pressure as boundary conditions). All calculations were done with an axial discretisation consisting of 20×15 mm long axial segments for the active part of the test rodlet.
It should be remarked that no computer program was used for calculating the transient thermal-hydraulic boundary conditions that are needed for fuel rod analyses with TRANSURANUS. These boundary conditions were derived from measured temperatures. For axial profiles of cladding temperatures the following possibility was used:

— Flat profile;
— Profile by expression T = -0.0078*z^2 + 0.1429*z + Tm (°C), 0. Profile_A;
— Profile by expression T = -0.016*z^2 + 0.1429*z + Tm (°C), 0. Profile_B.
— Experiment started form t=0 s, LOCA part of experiment (test rodlet heating) from t≈1138 s.

— Input data – Cladding data from core operation + experimental data: outer pressure. Cladding temperatures axial profile – flat, expression “Profile_A”, expression “Profile_B”. Part of calculations with experimental rod inner pressure (no inn pressure drop after experimental cladding fail).
— Axial layers – 20×15 mm.
— Calculation mode – LOCA. Cladding behaviour + Clad Failure model.
— Output – Moment of fail, cladding geometry, rod inner pressure.
— Result – Time of cladding fail – 78 s experimental value, 85…101 s result of calculation.
— Maximal diameter at fail – 12.4 mm experimental value, ≈12.5 mm result of calculation.

Time of cladding fail for different variants of calculations are present in Table 5.

TABLE 5. TIME OF CLADDING FAIL FOR THE NRC-STUDSVIK 198 TEST RODLET

		Time of cladding fail (from start of experiment), (s)	Time of cladding fail (from start LOCA), (s)
	Experimental	1138	78
Calculations variant	Pinn calculated, Profile_B, T upper, lowert plenum calculated	1144	85
	Pinn calculated, Profile_B, T upper, lowert plenum =const	1156	96
	Pinn mesured, profile flat	1161	101
	Pinn mesured, profile_A	1157	97
	Pinn mesured, profile_B	1154	94

Figure 14(a) and (b) shows the calculated and measured evolution of rod plenum gas pressure during the NRC-Studsvik 198 test. The calculated gas pressure is a little more then measurements for t>≈10 s. It can be explained by some indeterminacy in pin free volume (volume of connected measurement lines, temperature). In calculations characteristic of free volume gas was predict by TRANSURANUS code. In additional for understanding influence of inn-gas uncertainties the part of calculations are carried out with gas pressure as boundary conditions (used measured value) and with the constant temperature of gas of upper and lower plenum.

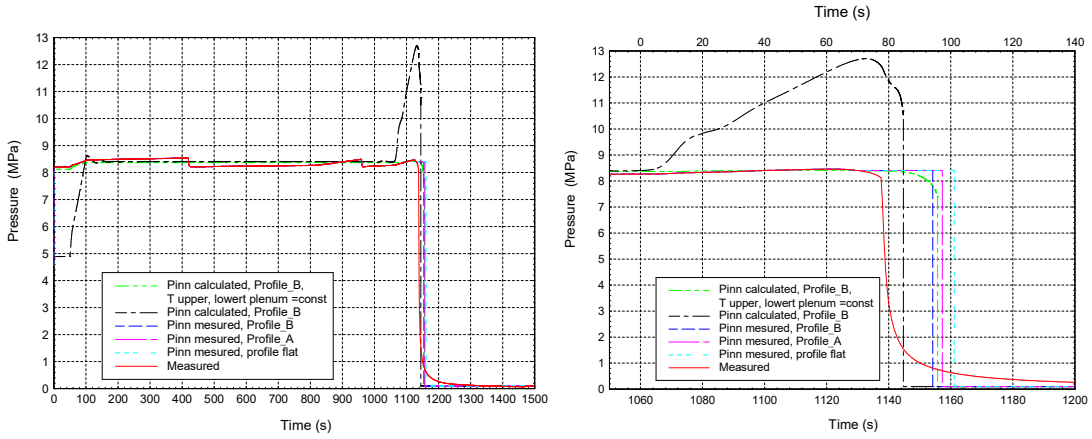

FIG. 14. Calculated evolution of rod plenum gas pressure (b)-LOCA time) in comparison with measurements for the NRC-Studsvik 198 test rodlet.

Figure 15 shows the calculated post-test diameter profile of the NRC-Studsvik 198 rodlet in comparison with data that were obtained by analysing visual inspection photos and neutron radiographs. It is clear from Fig. 15 that the length of the ballooned region is overestimated and

the cladding diameter of failed area is underestimated. The calculated axial position of the balloon has a good correlation with experimental data.

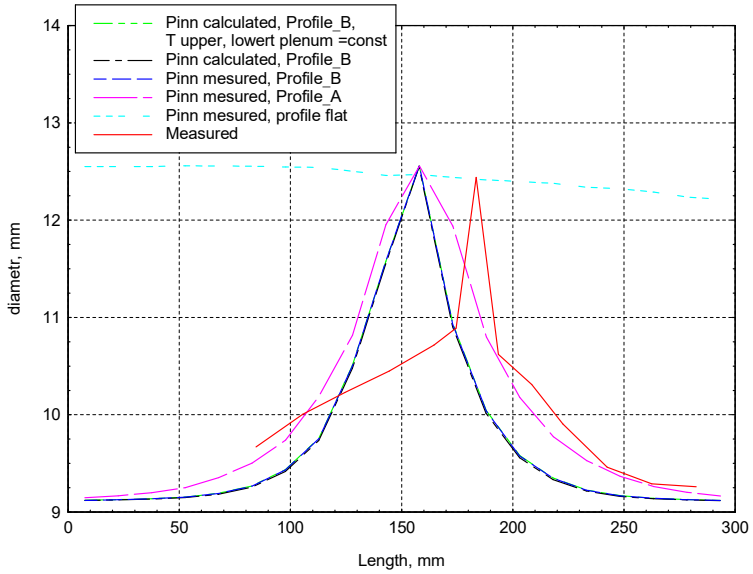

FIG. 15. Calculated and measured post-test diameter profiles for the NRC-Studsvik 198 rod.

5. RESULTS AND DISCUSSION

The modelling of the MTA-EK, IFA 650.10, IFA 650.11, NRC-Studsvik-192 and 198 cases allowed to formulate some overall issues and conclusions.

5.1. Experimental data

At the first stage of modelling pre-processing of experiment data is needed (delete or smoosing wrong measurements - negative absolute pressures, non-realistic pressure drops, etc. Mostly for MTA-EK test series).

The axial profile of linear heat generation rate during the not presented for cases IFA 650.10, IFA 650.11, NRC-Studsvik-192 and 198.

For cases IFA 650.10 and IFA 650.11 not presented burnup value separately for full (‘father’) rod and for test rodlet.

There are is some indeterminacy in pin free volume (volume of connected measurement lines, temperature) for cases NRC-Studsvik-192 and 198.

For case NRC-Studsvik-198 not specified pre-irradiation power history and characteristics of burnable absorber (IFBA rod).

Only one case (IFA 650.11) for WWER fuel rod cladding was chosen for FUMAC project. It isn't enough for code full-scale testing for WWER fuel.

5.2. Results of modelling

5.2.1. Time of burst

Predicted time of cladding burst for both general types of cladding (PWR and WWER) show good correlations with experimental data for such type of regimes.

5.2.2. Cladding geometry at burst moment

Diameter of cladding after burst for both general types of cladding (PWR and WWER) show good correlations with experimental data for such type of regimes.

Predicted elongation of cladding during the IFA-650.10 and IFA-650.11 tests is slightly overestimated then measurements value for both general types of cladding (PWR and WWER).

5.2.3. Inside-cladding pressure

Due some differences in fuel rod plenum design in test rodlet and fuel rod for commercial nuclear reactors the temperature of plenum gas in TRANSURANUS model have been described as boundary conditions from measurement data or from calculations by other code.

Considering this moment the inn-cladding gas pressure predicted by TRANSURANUS can be compared with measurement value with some limitations.

6. CONCLUSIONS AND RECOMMENDATIONS

TRANSURANUS code demonstrated good possibility to predict behaviour of nuclear fuel rod cladding. Predicted geometry of cladding and time of burst for both general types of cladding (PWR and WWER) show good correlations with experimental data for such type of regimes.

For modelling of nuclear fuel rod in LOCA by TRANSURANUS code the boundary conditions should be predicted by thermal-hydraulic codes.

TRANSURANUS's model for prediction of the fuel for plenum temperature in LOCA mode should be additional tested from point of view fuel rod design for commercial nuclear reactors.

SSCT NRS improved the possibility for modelling nuclear fuel rod in LOCA for both types of cladding: typical WWER cladding and cladding for the Westinghouse fuel design.

REFERENCES

[1] OECD–NUCLEAR ENERGYAGENCY, Nuclear fuel behaviour in loss-of-coolant accident (LOCA) conditions: Stateof-the-art report, Report NEA No. 6846, OECD Nuclear EnergyAgency, Paris, France (2009)

[2] KOLSTAD, E., et al. High burn-up fuel behaviour under LOCA conditions as observed in Halden experiments, 2011. In: IAEA Technical Meeting on Fuel Behaviour and Modelling under Severe Transient and Loss-of-Coolant Accident (LOCA) Conditions, October 18-21, 2011, Mito, Japan:International Atomic Energy Agency, IAEA-TECDOC-CD-1709

[3] FLANAGAN, M., et al., Post-test examination results from integral, high-burnup, fueled LOCA tests at Studsvik Nuclear Laboratory, 2013, Report NUREG-2160, U.S. Nuclear Regulatory Commission, Washington, DC, USA

[4] FEDOTOV, P.V., et al. LOCA test with high burnup VVER fuel in the MIR reactor, 2015. In: Reactor Fuel Performance 2015 (TopFuel-2015), September 13-17, 2015, Zürich, Switzerland: European Nuclear Society, pp. 335-344

[5] LASSMANN K., TRANSURANUS: a Fuel Rod Analysis Code Ready for Use, J. Nucl. Mater. 188 (1992) 295

[6] TRANSURANUS HANDBOOK. Document Number Version 1 Modification 1 Year 2011 ('V1M1J11'). January 2011. European Commission. Joint Research Centre. Institute for Transuranium Elements, Karlsruhe

[7] TRANSURANUS HANDBOOK. Document Number Version 1 Modification 1 Year 2017 ('V1M1J17'). January 2017. European Commission. Joint Research Centre. Directorate G - Nuclear Safety & Security. Karlsruhe

[8] JERNKVIST, L.O.,. Computational assessment of LOCA simulation tests on high burnup fuel rods in Halden and Studsvik. Technical Report. March 2017. Report number: 2017:12 ISSN: 2000-0456. Available at www.stralsakerhetsmyndigheten.se
[9] KARLSRUHE INSTITUTE OF TECHNOLOGY, 1st Research Coordination Meeting on Fuel Modelling for Accident Conditions (CRP FUMAC). 11-14 November 2014, Germany (2014).
[10] ZOLTÁN H., CSABA G., MÁRTA H., IMRE N., LÁSZLÓ M., LAJOS M., PÉTER W., JÓZSEF F., Ballooning Experiments with VVER Cladding, Nuclear Technology Volume 152, Issue 3, (2005) 273–285.
[11] ERZSÉBET P.F.,, CSABA G., LAJOS M., L.V., ZOLTÁN H., PÉTER W., LÁSZLÓ M., MÁRTA H., IMRE N., ANNA P.C., TAMÁS N., Experimental database of E110 claddings exposed to accident conditions, J. Nucl. Mater. Volume 397, Issues 1–3, 48–54, (2010)
[12] PEREZ-FERÓ, E., et al. Experimental Database Of E110 Claddings Under Accident Conditions EK-FRL-2011-744-01/04 Budapest, April (2012)
[13] ALEXANDRE L., LOCA Testing At Halden, The Tenth Experiment IFA-650.10. HWR-974. OECD Halden Reactor Project. December (2010)
[14] ALEXANDRE L., LOCA Testing At Halden, The VVER Fuel Experiment IFA-650.11. HWR-976. OECD Halden Reactor Project (2010).
[15] HELIN, M. AND J. FLYGARE, NRC LOCA tests at Studsvik: Design and construction of test train device and tests with unirradiated cladding material, 2012, Report STUDSVIK/N-11/130, Studsvik Nuclear AB, Studsvik, Sweden
[16] NRC-Studsvik LOCA test 192 data sheet. FUMAC's website shared documents. (https://nucleus.iaea.org/sites/nefw-projects/fumaccrp/Shared%20Documents)
[17] Studsvik LOCA test machine data sheet.xlsx. FUMAC's website shared documents. (https://nucleus.iaea.org/sites/nefw-projects/fumaccrp/Shared%20Documents)
[18] FLANAGAN, M., "NUREG-2160: Post-Test Examination Results from Integral, High-Burnup, Fueled LOCA Tests at Studsvik Nuclear Laboratory," August 2013. U.S. Nuclear Regulatory Commission
[19] FLANAGAN, M., ASKELJUNG, P., Observations of Fuel Fragmentation, Mobility and Release in Integral, High-Burnup, Fueled LOCA Tests. Halden Workshop on LOCA. Lyon, France 29-30 May, 2012
[20] NRC-Studsvik LOCA test 198 data sheet. FUMAC's website shared documents. (https://nucleus.iaea.org/sites/nefw-projects/fumaccrp/Shared%20Documents)
[21] The Westinghouse pressurized water reactor nuclear power plant. Westinghouse Electric Corporation. 1984. (www4.ncsu.edu/~doster/NE405/Manuals/PWR_Manual.pdf)
[22] TRAMBAUER, K., SONNENBURG, H., LERCHL G., Prediction of boundary conditions of the Halden LOCA IFA-650 tests 3 with ATHLET-CD for ballooning benchmark. GRS, Germany
[23] SOCRAT code application for FUMAC. 2nd Research Coordination Meeting on "Fuel Modelling in Accident Conditions" (CRP T12028 "FUMAC"). Vienna International Centre. May 30 – June 2, 2016
[24] Final TH boundary conditions_IFA 650.9-11_SOCRAT. FUMAC's website shared documents. (https://nucleus.iaea.org/sites/nefw-projects/fumaccrp/Shared%20Documents)

CONTRIBUTION OF IDAHO NATIONAL LABORATORY TO THE CRP FUMAC

PASTORE G., WILLIAMSON R., HALES J., GAMBLE K., GARDNER R., TOMPKINS J.
Fuel Modeling and Simulation Department,
Idaho National Laboratory,
Idaho Falls, USA

Abstract

This report summarizes the contribution of Idaho National laboratory (INL) to the IAEA Coordinated Research Project on Fuel Modeling under Accident Conditions FUMAC. In line with the original research agreement between INL/US DOE/Battelle and IAEA, work at INL has focused on both development of INL's fuel performance code BISON for the analysis of loss-of-coolant accidents (LOCA) and simulation of selected FUMAC priority cases. With reference to code development efforts, models were implemented in BISON for high temperature cladding oxidation, Zircaloy solid-solid phase transformation, Zircaloy high temperature creep, cladding burst failure and axial fuel relocation. BISON, analyses were performed of the FUMAC cases: MTA EK tests PUZRY; QUENCH L1 rods 4 and 7; Halden IFA-650.2; and Halden IFA-650.10. In addition, the REBEKA separate effects tests were analyzed, including an effort to investigate 3D cladding response in presence of azimuthal temperature variations. In general, BISON predictions of burst temperature, pressure and time to burst are very reasonable. Predictions of cladding hoop strain are less satisfactory and require additional investigation. Finally, results of 3D simulations indicated that 3D effects are potentially important in fuel rod analysis during LOCAs. BISON results are made available to the FUMAC project as a contribution to the FUMAC benchmark exercise.

1. INTRODUCTION

To coordinate and support research on nuclear fuel modeling under accident conditions in member countries following the Fukushima accident, the International Atomic Energy Agency (IAEA) sponsored the Coordinated Research Project (CRP) on Fuel Modeling under Accident Conditions (FUMAC).

The US Department of Energy (DOE) has been developing state-of-the-art capabilities to simulate of nuclear fuel behavior within the Nuclear Energy Advanced Modeling and Simulation (NEAMS) and Consortium for Advanced Simulation of Light Water Reactors (CASL) programs. The result is the BISON code [1], a multidimensional, finite-element based fuel performance code developed at Idaho National Laboratory (INL). Validation work for BISON has focused initially on Light Water Reactor (LWR) fuel during normal operating conditions and power ramps [2]. More recently, significant work has been performed on BISON development and validation for the analysis of accident scenarios such as loss of coolant accidents (LOCA) [3, 4] and Reactivity Insertion Accidents (RIA) [5, 6].

This report gives an account of INL's accomplishments in the framework of the CRP FUMAC. The proposal of INL for participation in FUMAC [7] included

- Development of the BISON fuel performance code to include models for phenomena relevant to fuel rod behavior during LOCAs;
- Simulation of some of the FUMAC cases using BISON, with results being made available to the project.

The work has been performed along the lines outlined in the proposal, with the BISON code having been extended to simulation of LOCA accident scenarios and applied to the analysis of several FUMAC cases. In this report we provide a description of BISON developments for LOCA analysis carried out throughout the project and present and discuss the

BISON simulations. As agreed upon during the First Research Coordination Meeting (RCM1), the FUMAC cases that have been analyzed with BISON are:

— MTA EK tests PUZRY;
— QUENCH L1 rods 4 and 7;
— Halden IFA-650.2; and
— Halden IFA-650.10.

In addition, simulations of the ballooning tests REBEKA were performed and are included in this report, in view of the potential interest to the FUMAC project. This additional work included 3D simulations accounting for azimuthal temperature variations.

The work on BISON development and validation for LOCAs, including INL's contribution to FUMAC, has benefited from collaboration between INL and the Halden Reactor Project. This collaboration has been strengthened by having BISON developers working onsite in Norway.

The structure of this report is as follows. In Section 2 we summarize BISON enhancements for the analysis of LOCA behavior. In Section 3 we present BISON simulations of the FUMAC cases, as well as additional calculations of potential interest to the project. For each of the considered cases, we include a description of the experiment, details of the BISON setup for the simulations, and a report and discussion of the results. Results are made available to FUMAC for the benchmark exercise. A final chapter provides conclusions and recommendations from the INL activities within FUMAC.

2. BISON DEVELOPMENTS FOR LOCA ANALYSIS

From the beginning, BISON has incorporated a large-strain mechanics formulation, essential to correctly analyze cladding ballooning during LOCAs. In order to capture the complex material response during accident situations, however, it is also necessary to incorporate in the code specific models dealing with the high-temperature, transient phenomena involved. For this purpose, dedicated material models have been incorporated in the thermo-mechanics analysis framework of BISON. Models are overviewed in this section.

BISON's capability enhancements for accident analysis performed during this work and applied to the simulations presented in Section 2 include models for high-temperature steam oxidation of Zircaloy cladding, crystallographic phase transformation of Zircaloy, high-temperature cladding creep and cladding failure due to burst [3, 4].

In addition, BISON's model of fission gas swelling and release in UO_2 was extended to include a specific treatment of the burst release effect during transients. This transient model was originally developed based on power ramp data [8, 9] and has not been re-calibrated and validated yet for LOCA transients. However, it has been applied with some success to RIA design basis accident simulations [6], and can potentially be adapted and applied to the improved simulation of FGR during LOCA transients. In view of its potential for the modeling of fission gas behavior during DBAs, this development is deemed relevant to the FUMAC project and has been included in this report. The development of the transient fission gas behavior model was carried out in collaboration with POLIMI (Italy) and JRC-Karlsruhe (European Commission, Germany).

Also, two recent BISON developments for LOCA analysis, i.e., cladding oxidation energy deposition and axial fuel relocation, have not yet been applied to the simulations described in Section 3. However, these are new BISON capabilities that are in place and relevant to LOCA analysis, thus they are deemed of potential interest to the FUMAC project and included in this report as an additional contribution. These capabilities will be applied in future LOCA simulations with BISON.

2.1. High-temperature cladding oxidation

The process of oxidation of Zircaloy through an exothermic reaction with the coolant affects both thermal and mechanical performance of the cladding. In the high temperature range (e.g., LOCA) the coolant has become steam, and oxidation proceeds much more rapidly than at normal LWR operating temperatures. Under these conditions, the kinetics of oxide scale growth and oxygen mass gain can be described by a parabolic law, with the reaction rate constant defined as a function of the temperature through an Arrhenius relation [10]:

$$\frac{d\xi}{dt} = A \cdot exp\left(-\frac{Q}{RT_I}\right) \quad (1)$$

where ξ is either the oxide scale thickness, $\xi = s$ (m), or the oxygen mass, $\xi = g$ (kg·m^{-2}), t (s) the time, A (m or kg·m^{-2}) the pre-exponential factor, Q (J/mol) the activation energy, R (J/mol-K) the universal gas constant, and T_I (K) the metal-oxide interface temperature. Following the recommendations in [10], the BISON model includes correlations for oxide scale growth and oxygen mass gain rates in Zircaloy-2/4 appropriate to different temperature ranges. In particular, the following approach is adopted:

- For metal-oxide interface temperatures from 673 K up to 1800 K, the Leistikov [11] correlation is used. The Cathcart-Pawel correlation [12] is also available and can be chosen as an option. The Leistikov correlation has been selected as reference in view of the larger underlying database, the availability of experimentally determined mass gain for all tests, and the better fit for lower temperature relative to the Cathcart-Pawel correlation [10];
- Above 1900 K, the Prater-Courtright correlation [13] is used;
- Between 1800 and 1900 K, a linear interpolation is made. Linear interpolation between two correlations of Arrhenius type is obtained by a third correlation of the same type [10].

The values of the parameters in Eq. 2 relative to the different correlations are given in Table 1.

2.2. Phase transformation of the cladding material

An increase in the cladding temperature above ~1000–1100 K, which may occur during a LOCA, involves time and temperature dependent phase transformation of the Zr alloy from hexagonal (α-phase) to cubic (β-phase) crystal structure. Modeling the kinetics of crystallographic phase transformation is needed for the assessment of the mechanical properties essential for fuel rod integrity (deformation and burst) during a postulated LOCA.

TABLE 1. PARAMETERS OF THE CORRELATIONS FOR CXIDE SCALE (S) AND OXYGEN MASS GAIN (G) AT HIGH TEMPERATURE [10]

Correlation	A_S (m^{2}s^{-1})	Q_S/R (K)	A_g (kg·m^{-2})	Q_g/R (K)
Leistikov	$7.82 \cdot 10^{-6}$	20214	52.42	20962
Cathcart-Pawel	$2.25 \cdot 10^{-6}$	18062	36.22	20100
Prater-Courtright	$2.98 \cdot 10^{-3}$	28420	$3.3 \cdot 10^{3}$	26440

The crucial parameter for the transformation kinetics is the evolution of the volume fraction of the new phase as a function of time and temperature. A model has been implemented in BISON for calculation of the volume fraction of β-phase in Zircaloy-4 as a function of time and temperature during phase transformation in non-isothermal conditions. The model is based on [14]–[16]. The phase transformation rate is expressed by

$$\frac{dy}{dt} = k(T)[y_s(T) - y] \tag{2}$$

where y is the volume fraction of β-phase, y_s (/) the steady-state or equilibrium value of y, and k (s^{-1}) the rate parameter. The β-phase equilibrium fraction is a sigmoid function of temperature

$$y_s = \frac{1}{2}\left[1 + tanh\left(\frac{T - T_{cent}}{T_{span}}\right)\right] \tag{3}$$

where T_{cent} and T_{span} are material specific parameters related to the center and span of the mixed-phase temperature region, respectively. For Zircaloy-4, $T_{cent} = 1159 - 0.096w$ (K) and $T_{span} = 44 + 0.026w$ (K) [14] are used, with w being the hydrogen concentration in the range $0 \leq w \leq 1000$ wppm (weight parts per million hydrogen). The rate parameter is expressed in the form

$$k = k_0 exp\left(-\frac{E}{k_b T(t)}\right) + k_m \tag{4}$$

where k_0 is a kinetic factor, E an effective activation energy, $k_b$the Boltzmann constant, and k_m a constant. For Zircaloy-4, $k_0 = 60457 + 18129|q|$ (s^{-1}) and $E/k_b = 16650$ (K) [14,16] are used, where $q = dT/dt$ (Ks^{-1}) is the heat rate in the range $0.1 \leq |q| \leq 100$ Ks^{-1}. The $\alpha \rightarrow \beta$ transformation is purely diffusion controlled, while the $\beta \rightarrow \alpha$ transformation is partly martensitic. This is represented by the constant k_m given in the form [16]

$$\begin{cases} k_m = 0 & \alpha \rightarrow \beta \\ k_m = 0.2 & \beta \rightarrow \alpha \end{cases} \tag{5}$$

The starting temperatures for the onset of $\alpha \rightarrow \alpha + \beta$ and $\beta \rightarrow \alpha + \beta$ phase transformations are calculated as (in kelvin) [14]

$$T_{\alpha \rightarrow \alpha+\beta} = \begin{cases} 1083 - 0.152w & for\ 0 \leq q < 0.1\ Ks^{-1} \\ (1113 - 0.156w)Q^{0.0118} & for\ 0.1 \leq q \leq 100\ Ks^{-1} \end{cases} \tag{6}$$

$$T_{\beta \rightarrow \alpha+\beta} = \begin{cases} 1300 & for -0.1 < q \leq 0\ Ks^{-1} \\ 1302.8 - 8.333|Q|^{0.477} & for -100 \leq q \leq -0.1\ Ks^{-1} \end{cases} \tag{7}$$

for $0 \leq w \leq 1000$ wppm. Note that $w = 0$ is considered in BISON at this time.

The β-phase volume fraction as a function of time is calculated by numerical integration of Eq. 2.2. The calculated volume fractions of β phase as a function of temperature at equilibrium and for temperature variation rates of ±10 Ks^{-1} are shown in Fig.1.

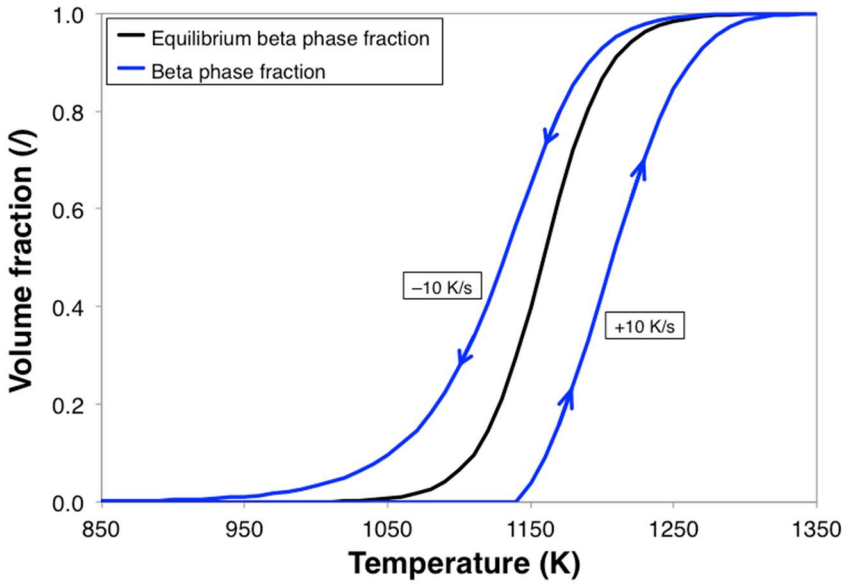

FIG. 1. Calculated volume fraction of β-phase as a function of temperature. Equilibrium conditions (slow temperature variation) and temperature variation rates of ±10 Ks^{-1} are considered.

2.3. High-temperature creep of Zircaloy cladding

During a LOCA, outward creep deformation of the cladding tube under the effect of internal pressure and high temperature drives cladding ballooning and eventual failure due to burst. For LOCA analysis, the large creep deformation of the cladding is defined by a strain rate correlation in the form of a Norton power equation [17]–[19]:

$$\dot{\varepsilon}_{eff} = A\, exp\left(-\frac{E_a}{RT}\right)\sigma_{eff}^{n} \tag{8}$$

where $\dot{\varepsilon}_{eff}$ (s^{-1}) is the effective creep strain rate, A ($MPa^{-n}\,s^{-1}$) the strength coefficient, E_a (J mol^{-1}) the activation energy for the creep deformation, T (K) the temperature, σ_{eff} (MPa) the effective (Von Mises) stress, and n (-) the stress exponent. The material parameters (Table 2) used in the model were obtained from tension tests on Zircaloy-4 tubes [18, 19]. In the mixed phase ($\alpha + \beta$) region (Section 2.2), interpolations are made to calculate the Norton parameters. Depending on the strain rate, different approaches are adopted [18]:

TABLE 2. MATERIAL PARAMETERS USED TO CALCULATE CREEP OF ZIRCALOY-4 [19, 20]

Phase	$\dot{\varepsilon}_{eff}$ (s^{-1})	A ($MPa^{-n}\,s^{-1}$)	E_a (J mol^{-1})	n (-)
α	any	8737	$3.21\cdot10^{5}$+24.69 (T-923.15)	5.89
50% α–50% β	≤$3\cdot10^{-3}$	0.24	102366	2.33
	>$3\cdot10^{-3}$	LI of ln(A)	LI	LI
β	any	7.9	141919	3.78

Note: LI stands for linear interpolation

— For $\dot{\varepsilon}_{eff} \leq 3\cdot10^{-3}$ s^{-1}, linear interpolation of $\ln(A)$, n and E_a is made between the values for pure α and middle of $\alpha + \beta$ (50% α–50% β) phase, and between 50% α–50% β and pure β phase.

— For $\dot{\varepsilon}_{eff} > 3 \cdot 10^{-3}$ s^{-1}, it is assumed that the values of $\ln(A)$, n and E_a vary linearly between the values for pure α and pure β phase.

To perform the interpolation, the fraction of each phase calculated from a dedicated model as described in Section 2.2 is used.

2.4. Cladding burst failure model

For determining the conditions for failure due to burst of Zircaloy-4 cladding during LOCA accidents, the following criteria have been implemented in BISON:

An overstress criterion, which assumes that the time of burst is reached when the local hoop stress equals a limiting burst stress [19]:

$$\sigma_\vartheta \geq \sigma_b \tag{9}$$

where σ_ϑ is the hoop stress and σ_b is the burst stress. The burst stress is calculated following Erbacher et al. [19] and depends on the temperature and oxygen concentration. Details can be found in [19] and are not given here for brevity.

A plastic instability criterion, which considers cladding burst at the attainment of a limiting value for the effective plastic strain rate:

$$\dot{\varepsilon}_{pl,eff} \geq \dot{\varepsilon}_b \tag{10}$$

where $\dot{\varepsilon}_{pl,eff}$ is the effective plastic (creep + plasticity) strain rate and $\dot{\varepsilon}_b$ is the limiting value. Following [21], in BISON we use $\dot{\varepsilon}_b$=100 h-1 ≅ 2.78·10-2 s-1.

A combination of the above criteria, which establishes that cladding burst occurs when either condition 1.9 or 1.10 is fulfilled.

As the overstress criterion may lead to unsafe predictions in low-stress situations [21], either the plastic instability or the combined criterion are used in our calculations (Section 3).

2.5. Transient fission gas behavior in oxide fuel

Fission gas release (FGR) and gaseous swelling in UO_2 fuel are computed in BISON by a physically based model from [22, 23]. This model has been recently extended to allow for the rapid FGR (burst release) during transients [8, 9]. This new transient capability was originally developed and validated based on annealing and power ramp tests, but can be potentially adapted and applied to DBA transient analysis. Initial application to RIA calculations has led to promising results [6].

In this model, burst release is interpreted as driven by fuel micro-cracking, which is associated with gas depletion of the cracked grain faces during transients and with a corresponding increase in FGR. Gas depletion of a fraction of the grain faces is modeled as a reduction of the fractional grain-face bubble coverage, f. In particular, f is scaled by a factor, f, corresponding to the fraction of non-cracked (intact) grain faces. The reduction of the fractional coverage effectively leads to a decrease of the amount of gas retained in the fuel – consequently, of fission gas swelling – and to a corresponding increase of FGR.

We simplify the micro-cracking process into a temperature-dependent behavior, characterized by a micro-cracking parameter, m. We also observe that the process can only affect intact grain faces, and write

$$\left[\frac{df}{dt}\right]_c = -\frac{dm}{dt} f \tag{11}$$

Based on the available experimental evidence, the functional form of m is chosen as a temperature-dependent sigmoid function

$$m(T) = 1 - \left[1 + D\ exp\left(s\frac{T - T_{infl}}{B}\right)\right]^{-\frac{1}{D}} \quad (12)$$

where T_{infl} (K) is the value for the temperature at the inflection point of the function $m(T)$ (inflection temperature, or temperature of maximum micro-cracking rate), and B (K) and D (-) are parameters related to the temperature-domain width of the phenomenon and the deviation from symmetric behavior during heating/cooling transients, respectively. The value of s (-) is set to +1 during heating transients and to –1 during cooling transients, so that m increases during both heating and cooling. Combination of Eqs. (11) and (12) leads to a FGR contribution that activates only during temperature variations (transients). In particular, the FGR during a temperature transient will result from the time integral of Eq. (11) during the transient.

Model's characteristics are based on the available experimental evidence of transient FGR (e.g., [24]–[27]). The inflection temperature corresponds to what has been observed experimentally as a critical temperature for the onset of burst release, and T_{infl}~1773 K above 20-30 GWd/tU burnup (e.g., [27]). Rather than adopting a discrete temperature threshold for the onset of burst release, we interpret the observations as a continuous but peaked micro-cracking (hence, gas release) rate as a function of temperature. Burnup dependence of micro-cracking, and micro-crack healing, are also accounted for, although details are not given here for brevity. A more extensive description of the model is given in [8]–[9].

2.6. Cladding oxidation energy deposition

During a LOCA the exothermic zirconium oxidation reaction in high temperature steam may lead to significant heat deposition in the cladding. This section describes the addition of an oxidation energy deposition model to capture this effect in BISON.

The conversion of zirconium to zirconium oxide follows the following simple chemical equation [28]:

$$2H_2O + Zr \rightarrow 2H_2 + ZrO_2 + \mathrm{Q} \quad (13)$$

The model uses the incremental oxide layer thickness calculated in BISON (Section 2.1) to calculate the energy added to the cladding. In particular, the energy from the zirconium oxidation reaction is calculated as [28]:

$$P = \left(\frac{0.74}{0.26}\right)\left(\frac{\Delta W}{\Delta t}\right)(2\pi R_0)\ 6.45 \cdot 10^6 \quad (14)$$

where P ($\mathrm{Wm^{-1}}$) is the linear power from the oxidation reaction, ΔW ($\mathrm{kg \cdot m^{-2}}$) the mass gain per unit surface due to oxidation during the time step Δt (s), R_0 (m) the initial cladding outer radius, $6.45 \cdot 10^6$ ($\mathrm{J \cdot kg^{-1}}$) the heat of reaction, and $0.74/0.26$ is the ratio of Zr reacted to O added:

$$\frac{\Delta Zr}{\Delta W} = \frac{1 - 0.26}{0.26} = \frac{0.74}{0.26} \quad (15)$$

where ΔZr ($\mathrm{kg \cdot m^{-2}}$) is the mass of zirconium per unit surface area consumed by oxidation during a given time increment, and 0.26 is the weight fraction of oxygen in ZrO_2. Eq. (15) underlies the assumption that all oxygen forms stoichiometric zirconium oxide.

2.7. Axial fuel relocation

Axial relocation of fuel fragments during a LOCA is a phenomenon that causes redistribution of heat within the rod potentially accelerating cladding failure. As the cladding balloons, fragmented and pulverized fuel pellets can fall from upper regions of the rod into the

ballooned region. The reduced thermal conductivity of the crumbled fuel and plenum gas mixture, in addition to the increased heat load due to a larger mass of fuel in the ballooned region, results in higher cladding temperatures further exacerbating the cladding distention. The ability to model this complex phenomenon using fuel performance codes is of great importance to ensure accurate predictions of cladding temperature, cladding strain, and the mass of fuel available for dispersal.

Recently, an empirical model was added to BISON to account for the axial relocation phenomenon during LOCAs. In particular, the model developed by Jernkvist and Massih [29] has been incorporated into BISON. The BISON implementation includes:

— The fuel fragmentation and pulverization model to quantify the number and size of fuel fragments and pulvers, the mass fractions of both fragments and pulvers, and an effective packing fraction of the fuel particles;
— The axial mass redistribution of the fuel;
— The thermal conductivity of the crumbled fuel; and
— The radial heat transfer in the fuel rod in presence of crumbled fuel and axial fuel relocation.

Details of this model can be found in [29], and are not given here for brevity. The current implementation is based on the 1.5-dimensional capability of BISON. Plans are in place to extend modeling of axial relocation to 2D and 3D calculations.

Jernkvist and Massih [29] propose two test cases denoted as single balloon and twin balloon. These test cases were analyzed with BISON in order to verify the implementation of the axial relocation model. The single balloon verification test is to simulate cladding distention that is maximum at the midplane of the active length. The twin balloon verification test is to simulate the effect of having a spacer-grid at the midplane of the active length. The BISON results of these test cases are compared to the digitized results from the Jernkvist and Massih's report [29] in Fig. 2. Three panels are shown for each case representing different times through the duration of the simulation corresponding to 40, 60, and 100 s (final time). The plots show the mass fraction of fuel as a function of axial position. A mass fraction >1 indicates that mass has accumulated in this region and a mass fraction <1 corresponds to a region partially (or completely) void of fuel. As expected, in the regions near the maximum cladding ballooning the mass fractions are largest. It should be noted that at the very top of the fuel rod the mass fraction remains as 1. This is because the cladding distention is not large enough in this top layer to allow fuel to relocate out of it. As is evident in both test cases, the BISON implementation has been verified to be correct as the results match Jernkvist and Massih's results extremely well. This model will allow first BISON simulations of LOCA experiments that exhibited significant axial fuel relocation, such as the Halden IFA-650.9 test considered in FUMAC.

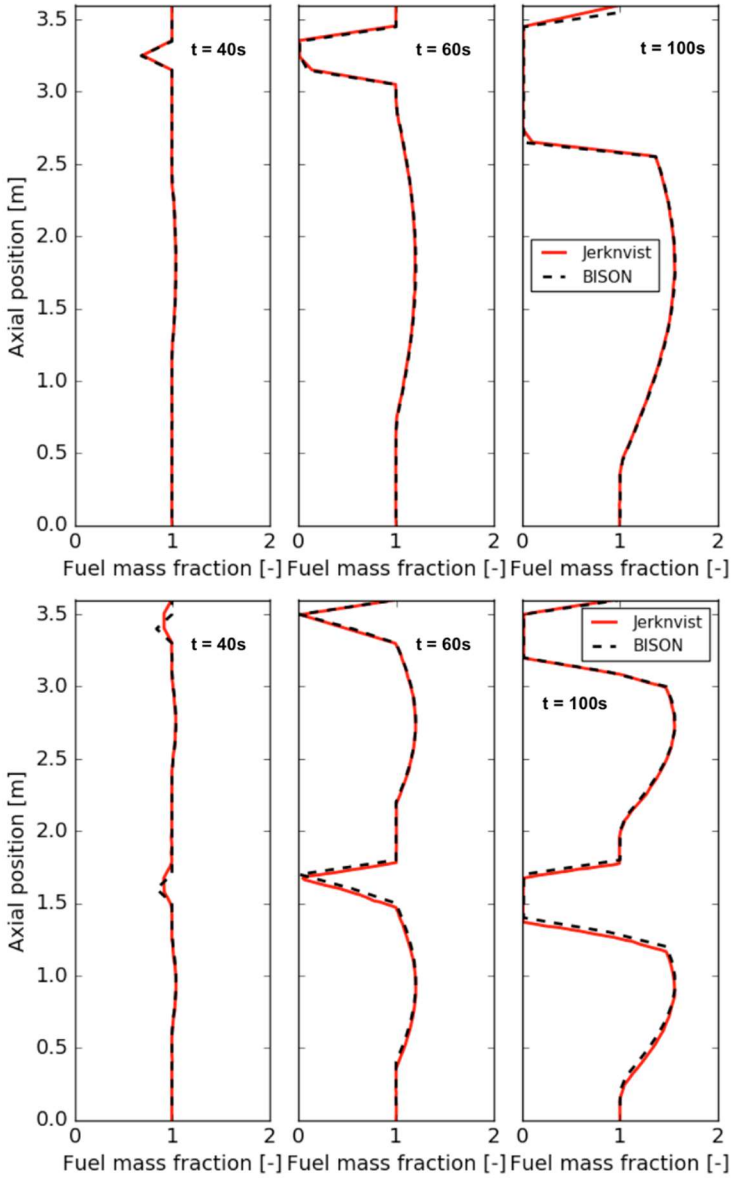

FIG. 2. Mass fraction as a function of axial position at 40, 60, and 100 s for single balloon (top) and twin balloon (bottom) test cases. Jernkvist data obtained from [29].

3. BISON SIMULATIONS OF LOCA EXPERIMENTS

The BISON code, extended with the modeling capabilities described in Section 2, was applied to simulations of LOCA experiments, including several FUMAC priority cases. In particular, BISON analyses for the following cases are presented in this chapter:

- MTA EK separate effects tests PUZRY;
- Separate effects tests REBEKA;
- QUENCH L1 rods 4 and 7;
- Halden test IFA-650.2;
- Halden test IFA-650.10.

These are all of the cases agreed upon by INL during the FUMAC RCM1. Although the REBEKA tests were not included in FUMAC, they were analyzed as part of the LOCA validation database for BISON. They are included in this report as part of the INL contribution to FUMAC for completeness and also, for one of the REBEKA cases the 3D capability of BISON was applied to investigate 3D cladding response in presence of azimuthal temperature

variations. This produced initial insights into 3D effects during LOCAs, which can be of interest to FUMAC, as discussed during the RCM2 [30]. 3D BISON simulations are presented in Section 3.2.

The case EON – Segment 2 was also modeled with BISON [36, 31]. However, because this case was later excluded from the FUMAC project, the relative BISON results are not included in this report. More recently, other LOCA cases (not included in FUMAC) were analyzed with BISON. These include the Hardy separate effects experiments [32] and the NRU-MT4 and MT6A fuel rod tests [33, 34]. These simulations are also not included in this report. Details can be found in [35].

In the following sections, the analyzed experiments are described and the results of the BISON simulations are presented and discussed.

3.1. MTA EK separate effects tests PUZRY

INL considered the PUZRY experimental series of isothermal ballooning tests on Zircaloy-4 claddings [36, 37]. All of the 31 PUZRY cases were modeled with BISON, although only 6 cases were selected for FUMAC. In this section, we present the overall results for the full set of 31 cases for completeness. We also provide detailed tabulated results for the 6 FUMAC cases.

3.1.1. Description of the tests

The PUZRY experimental series [36, 37] was performed in order to study the mechanical behavior (ballooning and burst) of Zircaloy-4 cladding subject to inner pressure transients at high temperature. In particular, the effects of temperature and pressurization rate on the deformation and the failure (burst) pressure were investigated.

The samples were tested in a resistance furnace providing isothermal conditions in the temperature range of 700–1200°C. The inner pressure of the test tube was increased linearly until the burst of the sample. After an approximately 1000 s heat-up period the sample was pressurized with Ar gas at a constant pressure increase rate. Table 3 summarizes temperature and pressure conditions for the PUZRY cases selected for FUMAC.

TABLE 3. CONDITIONS OF THE 6 MTA EK PUZRY CASES SELECTED FOR FUMAC [36, 37]

Test number	Temperature (K)	Pressure ramp rate (MPa/s)
8	1274.15	0.00763
10	1375.75	0.00710
12	1470.85	0.00723
18	1173.35	0.01151
26	971.55	0.01193
30	1073.55	0.02630

The specimens were 50 mm long Zircaloy-4 tubes. The specimens' inner / outer diameters of 9.3 / 10.75 mm corresponded to the parameters of PWR fuel cladding. Since the experiments were performed in Ar, cladding corrosion was not investigated.

3.1.2. Setup of the BISON simulations

Details of the BISON setup adopted for the calculations are as follows:

— Finite-element 2D axisymmetric models of the cladding tubes were used;

— Taking advantage of the symmetry of the problem, only the lower half of the heated cladding length was modeled;
— End plugs were considered by preventing radial motion (i.e., applying zero radial displacement boundary conditions) to the tube inner surfaces in correspondence of the plugs. These correspond to the 5 mm end sections of the cladding;
— Time-dependent pressures were simulated by Dirichlet pressure boundary conditions applied to the tube inner and outer walls;
— The furnace heating was simulated by a Dirichlet temperature boundary condition applied to the tube outer wall. In the PUZRY database, tubes temperature profiles along the axial direction are not given. However, applying a perfectly uniform temperature axially would lead to a distributed ballooning along the tube, while several experiments showed localized ballooning with maximum strain and burst occurring near the tube's mid-plane. This can be interpreted as associated with axial temperature variations that, albeit small, lead to significant strain axial variations by virtue of the strong (exponential) temperature dependence of the creep rate (see Section 2.3). To account for this, we included a slight axial temperature variation in the BISON simulations. Within FUMAC, Katalin Kulacsy communicated that axial temperature variations of 5-6 K along the central 50 mm section of the furnace can be expected, based on measurements performed in another furnace [38]. On this base, in the BISON simulations we applied a linear temperature profile (simplest possibility in absence of detailed indications) with the maximum temperature applied at the mid-plane. The overall (tube end to tube mid-plane) variation was made equal to 6 K, with the average (tube quarter-length) temperature being equal to the experimental value;
— Prior to the pressure transient, we considered the initial heat-up period by applying atmospheric (0.1 MPa) pressure to both sides of the tube and ramping the temperature up from ambient (300 K) to the test temperature over 1000 s. The inner pressure transient from 0.1 MPa at the experimental rate was applied afterwards, under isothermal conditions. Outer tube pressure was kept constant at 0.1 MPa;
— The combined overstress and plastic instability criterion for cladding burst failure (Section 2.4) was used.

3.1.3. Results

We present comparisons of the BISON simulation results for the 31 PUZRY cases to the experimental data. Figures 3 and 4 show the comparisons of cladding inner pressure at cladding burst and time to burst, respectively. Note that the axes in these plots have a logarithmic scale. The accuracy of BISON predictions appears reasonable.

We also present the BISON results in terms of maximum engineering hoop strain at the cladding outer surface at the time of burst. Comparisons of calculated strains to experimental data for the 31 PUZRY cases are shown (on a linear scale) in Fig. 5. Predictions deviate from experimental data by up to a factor of ~2.6. Average deviation is of a factor of ~1.7. Prediction of cladding strains is notoriously difficult for fuel performance codes, even more for LOCA calculations whereby very high strain rates are reached as cladding burst is approached. This implies that the maximum strain reached in the calculation is very sensitive to the specific criterion adopted to determine the time of rod burst (thus, the final time of the calculation and the time at which strain is considered), since small differences in the final time may correspond to large differences in the maximum strain. This has been clearly demonstrated by a previous study by JRC-Karlsruhe where different failure criteria were tested in cladding ballooning and bust simulations with the TRANSURANUS code [21].

Further investigation and sensitivity analysis of the dependence of calculated strains upon the choice of the burst criterion (e.g., in line with [21]) and the relative uncertainties is of

interest in perspective. Besides this, further developments of the cladding creep model (e.g., considering anisotropic creep) may also improve strain predictions.

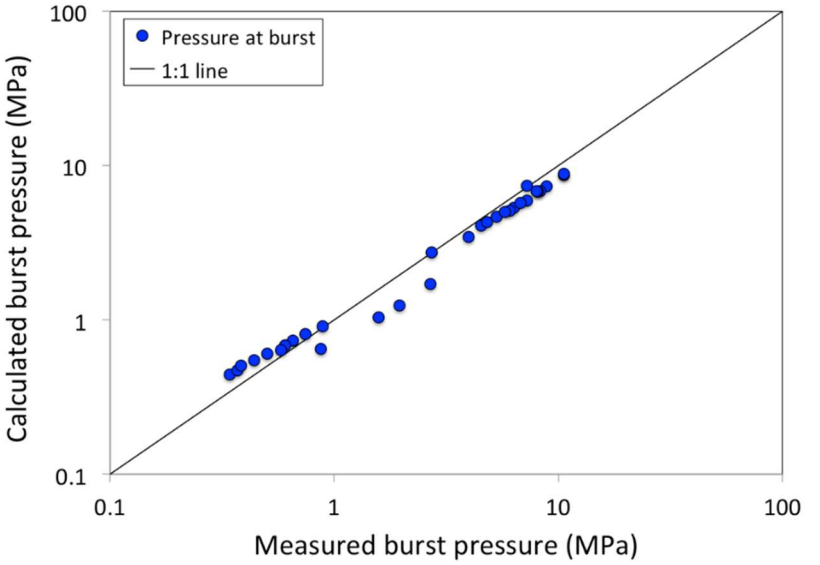

FIG. 3. Comparison of calculated and measured tube inner pressures at burst for the PUZRY cases.

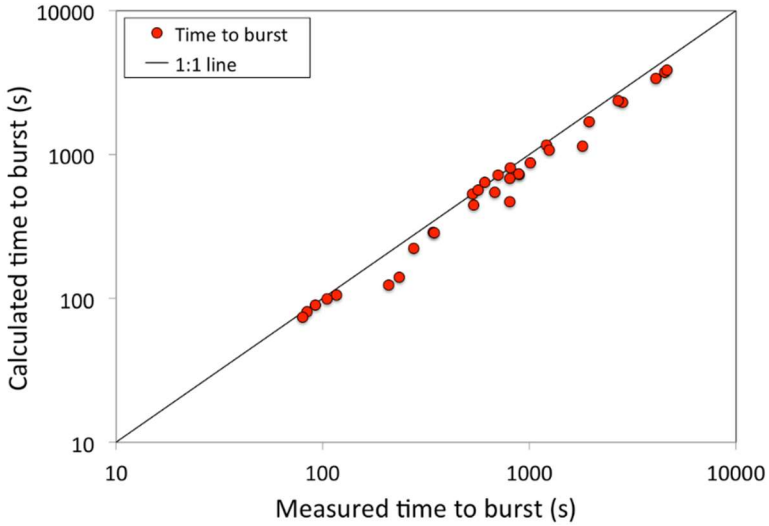

FIG. 4. Comparison of calculated and measured time to burst for the PUZRY cases.

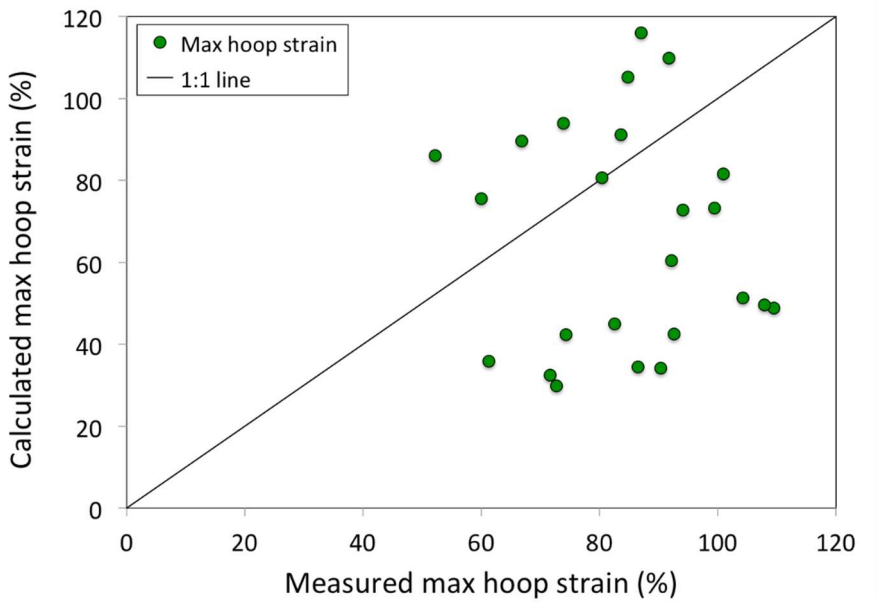

FIG. 5. Comparison of calculated and measured maximum engineering hoop strain at the cladding outer surface at the time of burst for the PUZRY cases.

Calculated and experimental burst times are plotted as a function of test temperature in Fig. 6. The reduction of the burst time as a function of the temperature is reproduced. Deviations of predictions from the experimental data appear to increase at the lower test temperatures.

In Fig. 7 and 8 we present comparisons between BISON predictions and experimental data of burst pressure and time to burst as a function of test temperature, for the 6 FUMAC cases only. Again, accuracy is very good for the higher temperature cases and grows worse at lower temperatures.

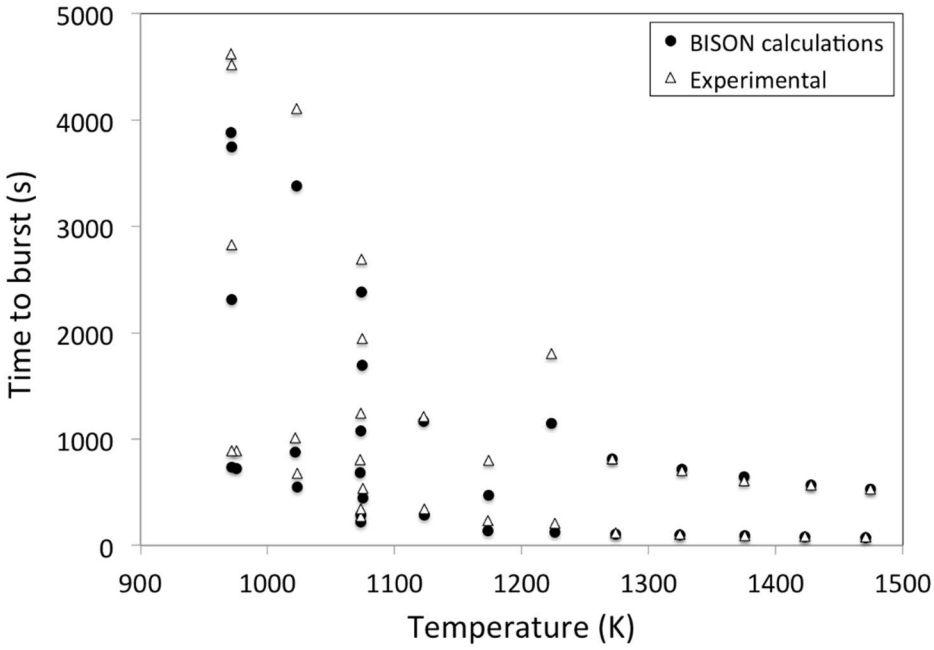

FIG. 6. Calculated and measured time to burst as a function of test temperature for the PUZRY cases.

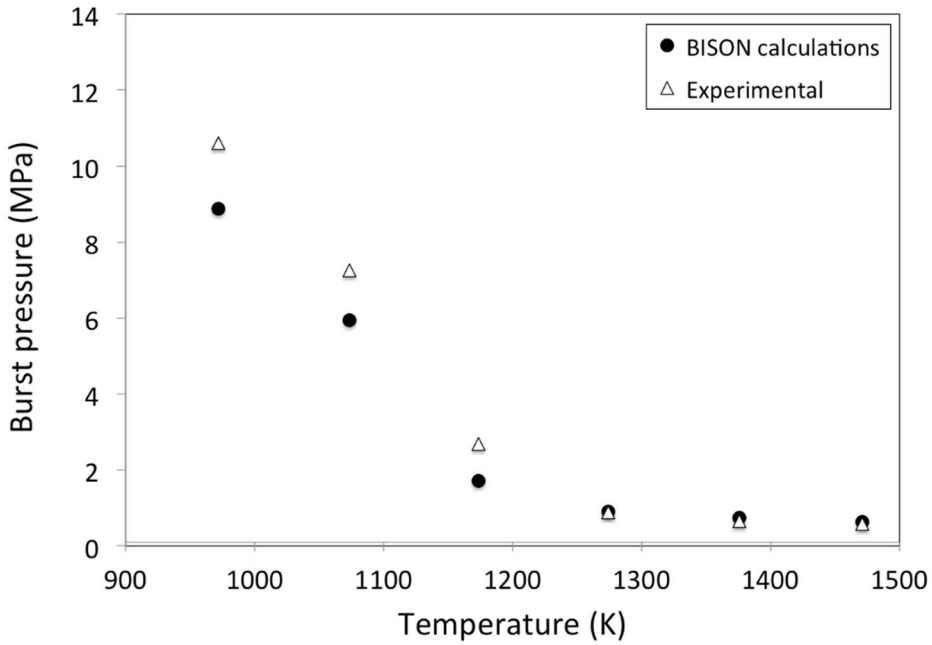

FIG. 7. Calculated and measured tube inner pressures at burst as a function of test temperature for the 6 PUZRY cases included in FUMAC.

Higher discrepancies between calculations and experiments at the lower temperatures indicate that deviations may be partly due to anisotropic creep behavior, which is not considered in the BISON model at this time and characterizes alpha-Zr (i.e., in absence of phase transition to beta-Zr at high temperature, see Section 2.2) [18, 19].

Detailed BISON results and experimental data for the 6 PUZRY cases included in FUMAC are tabulated in Table 4.

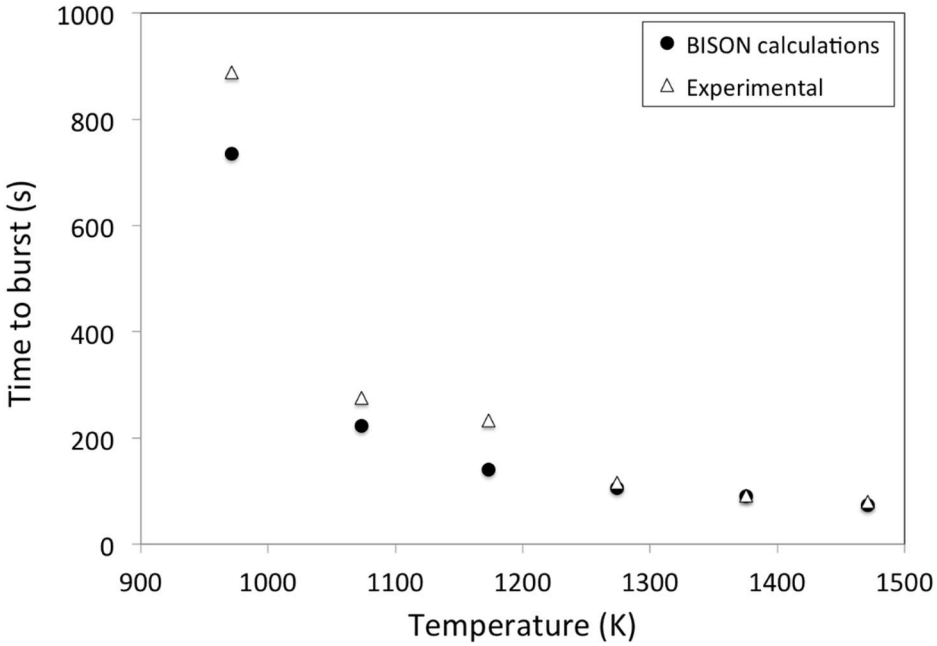

FIG. 8. Calculated and measured time to burst as a function of test temperature for the 6 PUZRY cases included in FUMAC.

Table 4: Experimental Data and BISON Predictions for the 6 FUMAC Cases from the.

TABLE 4. PUZRY EXPERIMENT. TIME TO BURST IS FROM THE BEGINNING OF THE TRANSIENT

Rod	Temperature (K)	Burst pressure (MPa)		Time to burst (s)		Max hoop strain (%)	
		Experiment	BISON	Experiment	BISON	Experiment	BISON
8	1274	0.890	0.906	116.7	105.7	80.37	80.7
10	1376	0.653	0.737	92.0	89.8	72.76	29.9
12	1471	0.578	0.636	80.0	74.1	71.62	32.5
18	1173	2.689	1.717	233.7	140.5	74.29	42.3
26	972	10.605	8.874	888.8	735.4	100.97	81.6
30	1074	7.251	5.951	275.7	222.5	104.28	51.3

3.2. Separate effects cladding tests REBEKA

The REBEKA separate effects tests [19, 20, 39] are temperature transient tests in steam performed on single PWR-size Zircaloy-4 tubes at a variety of internal pressures and heating rates. The purpose of the tests was to establish data of cladding ballooning and burst with reference to LOCA conditions.

As mentioned before, although the REBEKA tests were not originally included in FUMAC, BISON simulations are presented here for completeness and including a 3D analysis demonstration, which is of potential interest to the project.

3.2.1. Description of the tests

The cladding tubes had a fabricated inner/outer diameter of 9.30/10.75 mm, with a 325 mm heated length, and were heated indirectly by conduction heating from the inside, using an electrically insulated heater rod. A stack of alumina annular pellets (Al_2O_3) was used to simulate the fuel column. The diametral clearance between the cladding inner diameter and the pellet outer diameter was 0.15 mm. The test parameters covered a range of 1 to 14 MPa for the internal rod (He) pressure and 1 to 30 K s^{-1} for the heating rate. The test atmosphere was almost stagnant steam at atmospheric pressure and at a temperature of 473 K. The cladding temperatures were measured by thermocouples spot-welded on the outer surface of the cladding. More details on the experimental apparatus and conditions are given in [19, 20, 39].

3.2.2. Setup of the BISON simulations

The considered cases are modeled considering only the cladding, while the alumina pellets are taken into account by imposing a proper temperature boundary condition at the cladding inner radius, which accounts for the heat transfer through the inner components. For simplicity, only the heated portion of the rods was simulated. The internal electric heating was simulated by a time-dependent Dirichlet temperature boundary condition applied to the tube inner wall and consistent with the experimental conditions. In particular, a parabolic temperature profile symmetric with respect to the tube mid-plane was considered, which results from the uniform axial power generation in the heater rod [39]. To estimate the temperature variation over the heated length of the cladding, simplified calculations of axial heat conduction within the rod and convection to the outer steam atmosphere were performed. Pressure equal to the experimental value was applied at the tube inner wall. A 2-dimensional axisymmetric quadratic (Quad8 elements) mesh was used to model the geometry of the considered rods. In addition, to investigate inherently three-dimensional aspects, such as the effect of azimuthal temperature differences, 3D simulations were conducted employing hexahedral elements

(Hex20 elements). Taking advantage of the symmetry of the problem, only the lower half of the heated cladding length was modeled in the 2D simulations. For the 3D simulations, a quarter of the cladding circumference was modeled.

The combined overstress and plastic instability criterion for cladding burst failure (Section 2.4) was used for the REBEKA simulations with BISON.

3.2.3. Results for 2D simulations

Using the 2D axisymmetric model, simulations were conducted of the REBEKA experiments with a heating rate of 1 Ks^{-1}, considering the full range of 1 to 14 MPa for the internal cladding pressure. As for the 3D model, only one case is reported here, in order to demonstrate BISON's ability to assess the impact of azimuthal temperature variations on cladding ballooning and burst.

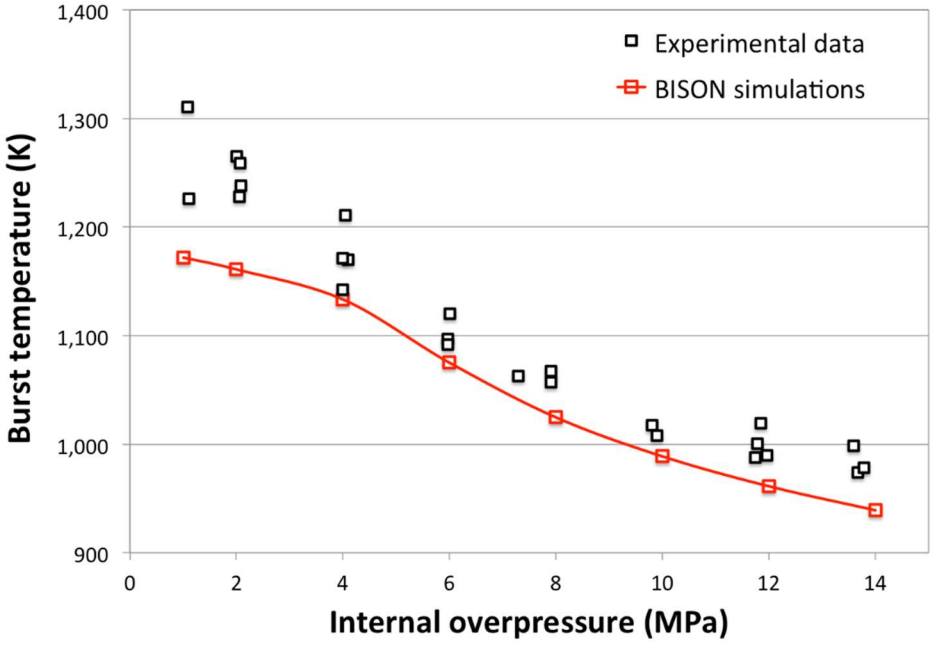

FIG. 9. Comparison between BISON predictions and experimental data of cladding burst temperature for the simulations of the REBEKA tests with a heating rate of 1 Ks^{-1}.

The predictions of burst temperature at the various internal cladding pressures are compared to the available experimental data in Fig. 9. The trend of increasing burst temperature with decreasing internal pressure is reproduced, and the quantitative accuracy of predictions is reasonable. Nevertheless, a moderate but systematic under-prediction is observed. Such discrepancies may be due to uncertainties inherent in the cladding mechanics, burst, oxidation and phase transformation modeling, and 3D effects (azimuthal temperature differences) that cannot be captured by 2D modeling.

3.2.4. Results for 3D simulation

In addition to the above-mentioned boundary conditions applied to the 2D simulations, in the 3D simulation an azimuthal temperature gradient was applied. A maximum azimuthal temperature variation of 30 K was considered, in conformity with the experimental indications from thermocouple measurements [20]. The results are presented for the exemplifying case of 10 MPa internal pressure at the time of cladding burst. Fig. 10 shows contour plots of temperature, creep strain magnitude, and locations where the local stress reached the limiting burst stress. The 3D simulation reproduces the non-uniform cladding ballooning and a localized

burst on the hottest side of the cladding, which is consistent with the experimental observations [20]. Note that the predicted burst temperature is higher (by about 10 K) than for the corresponding 2D simulation, thus indicating that capturing 3D aspects such as the effect of azimuthal temperature differences is of importance for fuel analysis during LOCA accidents. Further investigation of 3D effects in fuel rod analysis during LOCAs with BISON will be pursued in the future.

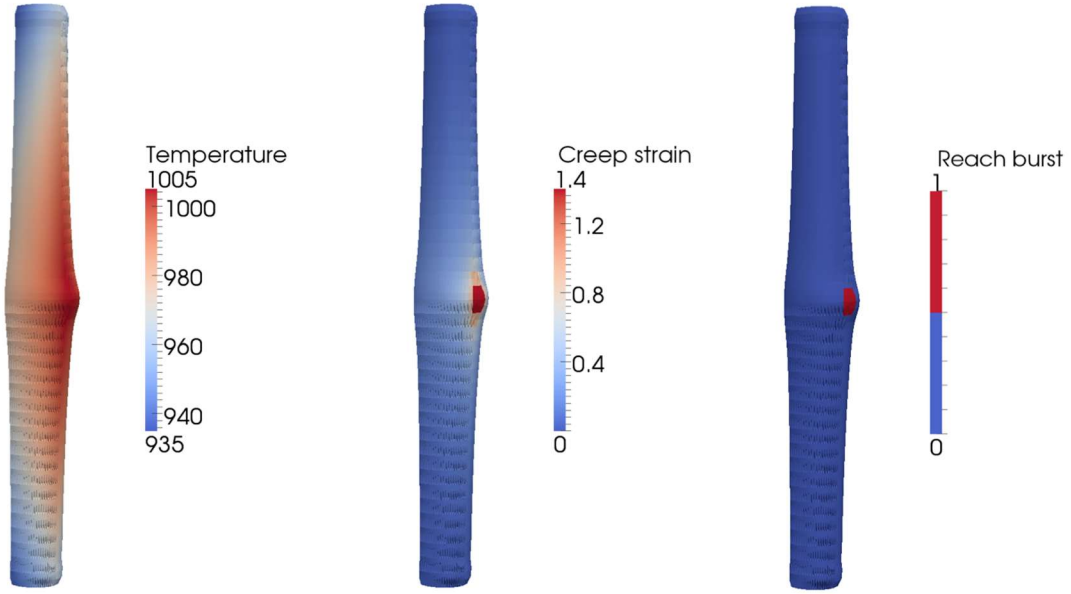

FIG. 10. Contour plots for the BISON 3D simulation of the REBEKA test with 10 MPa internal pressure at the time of cladding burst. The results for the lower quarter of the heated cladding are mirrored to obtain a full-length, half circumference view. The view is magnified 3 times in the radial direction for improved visualization.

3.3. QUENCH-L1

BISON simulations for the QUENCH-L1 experiment [40] were carried out for rods 4 and 7. Experimental data was used as much as possible to develop accurate boundary conditions for the simulations.

3.3.1. Description of the test

During the QUENCH-L1 test, superheated steam and argon enter a test rod bundle at the bottom of the assembly and flow upward. Quenching water is injected from the bottom of the assembly. The test bundle consists of 21 fuel rod simulators and four corner rods. Each fuel rod simulator is approximately 2.5 meters in length. The heated length of the rod begins at 692.5 mm from the bottom of the rod, and consists of a central tantalum heater with a diameter of 6 mm surrounded by 1.575 mm thick ZrO_2 pellets. The plenum separating the heater/pellet combination meant to simulate fuel pellets is filled with krypton gas with a gap between the outer radius of the ZrO_2 pellets and the cladding of 0.075 mm. The Zircaloy-4 clad of 0.725 mm thickness encases this system. The heated length is 1024 mm long.

Thermocouples along the surface at axial locations ranging from -250 mm to 1250 mm in increments of 100 mm as well as those in the plenum of instrumented rods collect temperature data throughout the experiment. Pressure sensors in the plenum as well as the inlet and outlet record internal rod and system pressures respectively.

The experiment began by applying a total power of 3.5 kW to the electrical bundle. Fuel rod simulators were then individually backfilled to 55 bar and electrical power was rapidly increased to 43 kW to initiate the transient. This initial power increase was followed by a steady

increase to 59 kW over the next 87 s. The power was then rapidly decreased back to 3.5 kW with water injection at a rate of 100 g/s beginning at 207 s. The quench progressed toward the top of the coolant channel (bundle bottom at 246 s, ballooned region at 266 s, whole bundle at 293 s).

3.3.2. Setup of the BISON simulations

Rods 4 and 7 were chosen for consideration since they had the largest number of axial thermocouples. Results from the instrumentation were used as applicable to define boundary conditions in the model. The aim of the calculation was to simulate the fuel rod behavior up to burst and compare to measured burst conditions.

A 2D axisymmetric finite element mesh was developed considering only the headed portion of the rods. The Ta heater was included along with the ZrO_2 pellets as hollow cylindrical pellets fitting around the heater, and the Zy-4 cladding. Material properties of the ZrO_2 pellets were obtained from [40].

The plastic instability criterion for cladding burst failure (Section 2.4) was used for the QUENCH-L1 simulations with BISON.

3.3.3. Development of the boundary conditions

Pressure and temperature data from the experiment were used to build boundary conditions for BISON. Provided instrument data begins at –100.6 s before the initial power ramp begins the transient, but a ramp of temperature and pressure for the system initial conditions is necessary. In addition, the pressure ramp begins well before –100.6 s so is digitized directly from the plots in [40] to provide accurate plenum conditions. Boundary conditions on the outside of the cladding depend upon axial position and must be interpolated in a way that both preserves the original data but predicts the data shape accurately between experiment collection points as BISON linearly interpolates between provided data points.

Power provided to the inner and outer rod groups over the course of the experiment is detailed in the collected data and is kept generally the same (3.5 kW total) before the transient occurs. A ramp from zero power is included before the pressure ramp to stabilize the system. This ramp, along with the recorded power, is read into the input as a function, and applied as a heat source.

The gas gap pressure is given from -100.6 s through rod bursts and subsequent quenching. The initial rod backfill data are digitized from [40], and obtained values are used as the internal pressure boundary condition from approximately –3000 s to –911 s at which point the pressure recorded for each rod at -100.6 s is held steady. A sudden drop in pressure for each rod at around 50 s indicates the point at which the cladding fails via the burst mechanism. Informing the simulation from experimental pressure data is problematic around this point, as providing the experiment pressure values to the simulation in cases where the burst time prediction is later than experiment burst time reduces the pressure on the cladding prematurely. To address this, pressures from the beginning of the transient until the burst are fitted to a linear regression model, and this pressure model is used as the plenum pressure boundary condition from t = 0 s until predicted burst. Employing this modeling scheme does remove perturbations and the larger the difference between experimental and simulation burst times, the more the model departs from collected data. However, this is viewed as the most viable method to predict extended plenum pressure behavior, as the difference between model and experimental pressure data up until the burst is minimal. By way of example, rod inner pressure experimental data and linear regression model that is used to inform the BISON calculation for rod 4 are shown in Fig. 11.

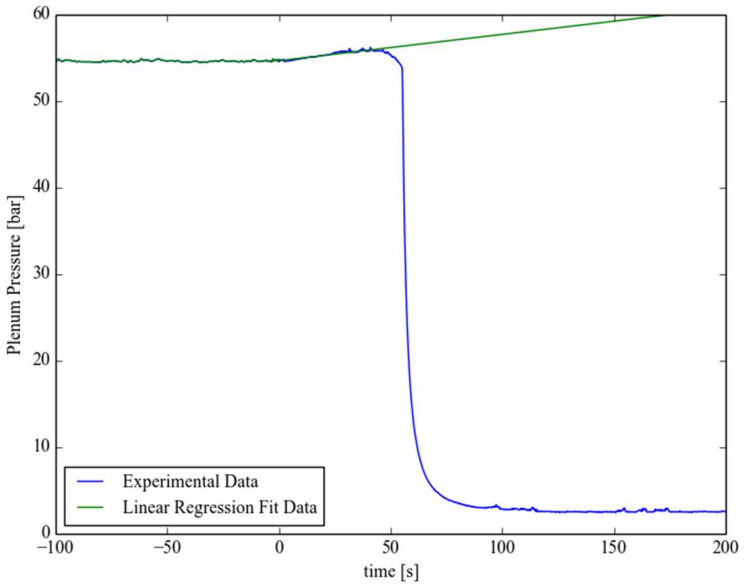

FIG. 11. Plot of plenum pressure vs. time for Rod 4.

To build the outer cladding temperature boundary conditions, the sampled cladding surface thermocouple data is conditioned using cubic spline interpolation. Note that the lowest temperature collection point for rod 4 is at 25 mm while the bottom of the simulated fuel rod begins at 0 mm. To remedy this gap in the data, we assume system conditions are likely to be similar before flowing past the heated length of the fuel rod simulators, and data from one thermocouple recording temperatures from below the heated length of rod 7 is added to the rod 4 data. By way of example, the data and the interpolated values for rod 4 are plotted in Fig. 12 at several points during the power ramp.

The final boundary condition the simulation requires is the system pressure along the cladding. Pressures are collected from the inlet and outlet of the cooling loop and values recorded over time are given in [40]. Pressure along the heated length is linearly interpolated as the pressure condition along the heated length.

3.3.4. Results

Comparison of metrics between the experiment and calculated models are provided in Tables 5 and 6. Cladding burst is predicted to occur at 55.8 s and 68.4 s after beginning the transient heating phase for rods 4 and 7, respectively. The experimental failures were observed at 55.2 and 54.4 s for rods 4 and 7, respectively. The hoop strain is under-predicted in both cases by about a factor of 3. Temperature and pressure calculations are very close to the measured values at the time of failure. Both predicted burst elevations are higher than the experimental locations but are consistent with the experiment in that burst elevation occurs at the upper end of the fuel rod simulators.

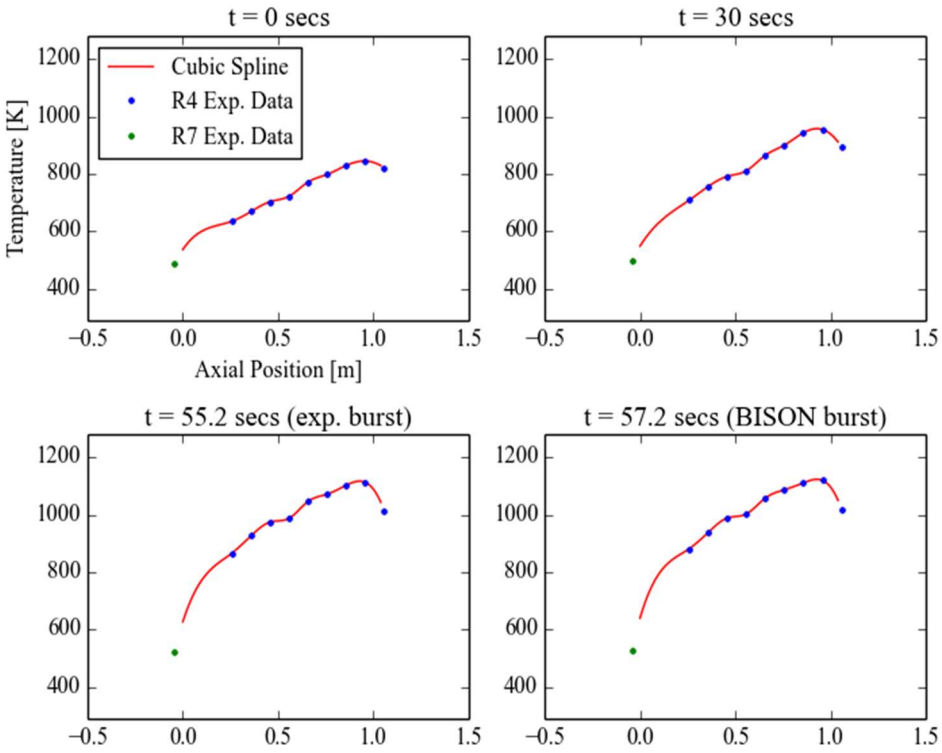

FIG. 12. Rod 4 Temperature vs. axial location on outside of clad.

TABLE 5. EXPERIMENTAL AND SIMULATION RESULTS FOR QUENCH-L1 ROD 4

	Experiment	BISON
Burst time (s)	55.2	55.8
Burst elevation (mm)	979	927
Burst inner pressure (bar)	53.9	56.4
Temperature at 950 mm (K)	1154	1117
Max hoop strain (%)	28.9	8.9
Max rod diameter (mm)	15	11.6
Min rod diameter (mm)	13	10.8

TABLE 6. EXPERIMENTAL AND SIMULATION RESULTS FOR QUENCH-L1 ROD 7

	Experiment	BISON
Burst time (s)	54.4	68.4
Burst elevation (mm)	953	800
Burst inner pressure (bar)	55.1	56.6
Temperature at 950 mm (K)	1074	1077
Max hoop strain (%)	24.8	8.1
Max rod diameter (mm)	14.7	11.5
Min rod diameter (mm)	12.5	10.8

3.4. Halden IFA-650.2

LOCA tests at Halden (IFA-650 series) are integral in-pile single rod tests. Relative to separate effects tests, they also provide information on the integral behavior of a fuel rod during a LOCA accident. The second trial test IFA-650.2 [41] was modeled with BISON.

3.4.1. Description of the test

The test was carried out using a fresh, pressurized PWR rod and low fission power to achieve the desired temperature conditions. The rod plenum volume was made relatively large to be able to maintain stable pressure conditions during ballooning. The fabrication characteristics of the IFA-650.2 fuel rod are reported in Table 7.

The fuel rod was located in a standard high-pressure flask in the IFA-650 test rig in the Halden reactor. A heater surrounding the rod was used to simulate the heat from adjacent rods. The flask was connected to a high-pressure heavy water loop and a blowdown system. During normal operation prior to the LOCA test, the rig was connected to the loop and forced circulation flow conditions existed. Then, the rig was disconnected. A natural convection phase began, with water flowing up between the fuel rod and flow separator (with heater) and down between flow separator and flask wall. Full pressure still existed in the rig. LOCA was initiated by opening the valves leading to the blowdown tank (blowdown phase). The initial pressure in the loop was ~7 MPa and the counterpressure in the blowdown tank was ~0.2 MPa. The channel pressure decreased to 3–4 bars, and the rig was practically emptied of water within 30–40 s. Stagnant superheated steam surrounding the rod provided inadequate cooling and the cladding temperature increased quickly (heat-up phase). A low fission power of 2.3 kW/m was used to simulate decay heat and achieve the desired temperature conditions. Cladding ballooning and burst rupture occurred during the heat up phase. Measured cladding temperature at burst was ~815 C. The test was ended by a reactor scram.

TABLE 7. DESIGN DATA OF IFA-650.2 FUEL ROD [41]

Fuel material		UO_2
Fuel density	%TD	95.0
U^{235} enrichment	wt%	2.0
Active stack length	mm	500
Pellet OD	mm	8.29
Pellet ID	mm	0
Cladding material		Zy-4
Cladding ID	mm	8.36
Cladding OD	mm	9.50
Diametral gap	μm	70
Free volume	cm^3	17.4
Fill gas		He
Fill gas pressure	MPa	4.0

3.4.2. Setup of the BISON simulation

The rod geometry was modeled following the design specifications from [41] (Table 7).The enriched fuel pellet column was represented with a smeared fuel column. Natural UO_2 pellets at the top and bottom of the fuel stack were also included. A single rod upper plenum was considered, whose volume is the sum of the various plenum volumes in the more complex real geometry [41]. A 2D axisymmetric quadratic finite element mesh was used.

The combined overstress and plastic instability criterion for cladding burst failure (Section 2.4) was adopted for the IFA-650.2 simulation.

The boundary conditions (BCs) in terms of linear heat rate and rig pressure were derived from the raw data from provided by the Halden Project and tabulated for usage in BISON. Temperature BCs at the cladding outer surface were evaluated based on cladding outer

temperatures, which were measured at two axial positions during the experiment. In particular, axial temperature profiles at the clad outer surface were obtained using some simplifying assumptions and imposing coincidence with the measured temperatures at measurement axial locations. The obtained profiles were used as outer cladding temperature BCs in absence of detailed thermal-hydraulics calculations. The procedure and assumptions adopted for the calculation of the temperature BCs used for the BISON simulations of IFA-650.2 at INL was first discussed on the FUMAC website in advance of the RCM2 [42]. A detailed description is given hereinafter.

3.4.3. Determination of the thermal boundary conditions

Clad outer temperature axial profiles are obtained based on the following assumptions:

— The effect of radiation is lumped into an "effective" heat transfer coefficient. This simplification is based on linearizing the radiative heat transfer law $q'' \propto (T_1^4 - T_2^4)$ to $q'' \propto h_{rad}(T_1 - T_2)$. Here q'' is the heat flux and $h_{rad} \propto T_{average}^3$ and has units of a heat transfer coefficient. The linearized equation is accurate if T_1 and T_2 are close enough. Under this assumption, the axial clad temperature profile can be written in a form as if heat transfer were purely convective

$$T(z) = T_{cool}(z) + q''(z)/h_{eff}(z) \tag{16}$$

where z is the axial coordinate, T_{cool} the coolant temperature, and h_{eff} is the "effective" heat transfer coefficient (convection + radiation).

— The coolant temperature is approximated as the heater temperature at the axial position z. This is estimated based on the Halden data of measured heater temperature at two axial locations and a linear interpolation.

— The heat flux is proportional to the local linear heat rate, i.e., $q''(z) \propto q'(z)$. This is reasonable provided that the coolant channel conditions are reasonably uniform along the rod and that no significant axial fuel relocation takes place during the test. From this assumption and Eq. 3.1, it follows:

$$T(z) = T_{cool}(z) + q'(z)/h^*(z) \tag{17}$$

where $h^*(z) = k\, h_{eff}(z)$ and k is a constant. The local linear heat rate, $q'(z)$, is obtained from the Halden data.

— $h^*(z)$ is determined based on the measured cladding temperatures. For this purpose, h^* is assumed to vary linearly along z

$$h^*(z) = Az + B \tag{18}$$

— The two equations needed to determine the coefficients A and B are the conditions of $T(z)$ Eq. (17) being equal to the measured temperatures at the two measurement locations (thermocouples at clad outer wall).

The strongest simplification in the above approach is taking a linear fit of the heat transfer coefficient along the axial direction. When radiation is dominant, $h^*(z) \propto T_{average}^3$, approximately, which likely has a maximum at peak power position. However, the above approach based on measured temperatures may be accurate enough in view of the uncertainties involved in determining thermal-hydraulic boundary conditions.

Figs 13 to 16 show the estimated clad outer temperature profiles at selected instants during different phases of the experiment. Using the measured temperatures and an axially varying heat transfer coefficient, actually, allows one to capture effects such as the higher temperature in the lower part of the rod during the blowdown phase, which are difficult to explain [41] or reproduce through thermal-hydraulics calculations.

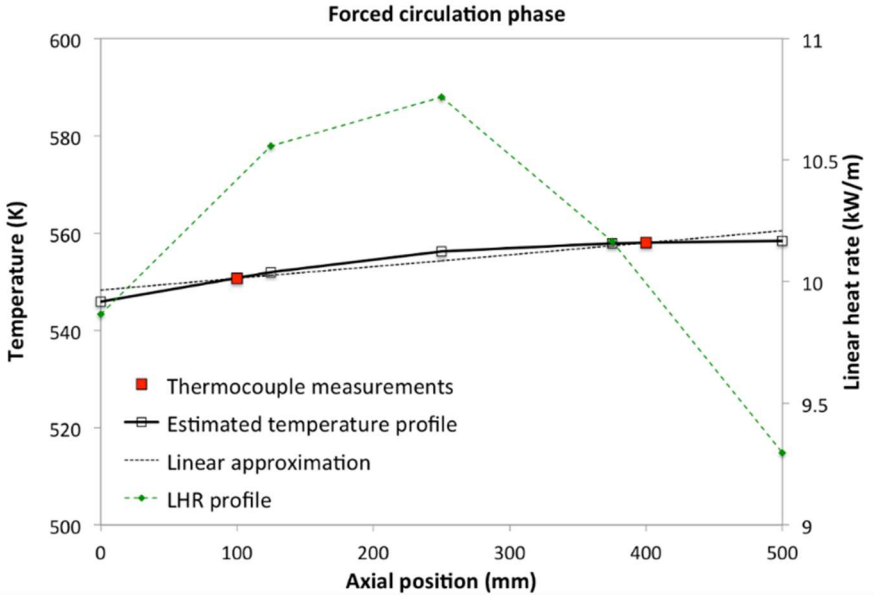

FIG. 13. Estimated axial temperature profile at cladding outer surface at an instant during the forced circulation phase of the IFA-650.2 experiment. The measured temperatures at the thermocouple locations and the linear heat rate (LHR) profile interpolated from Halden data are also shown.

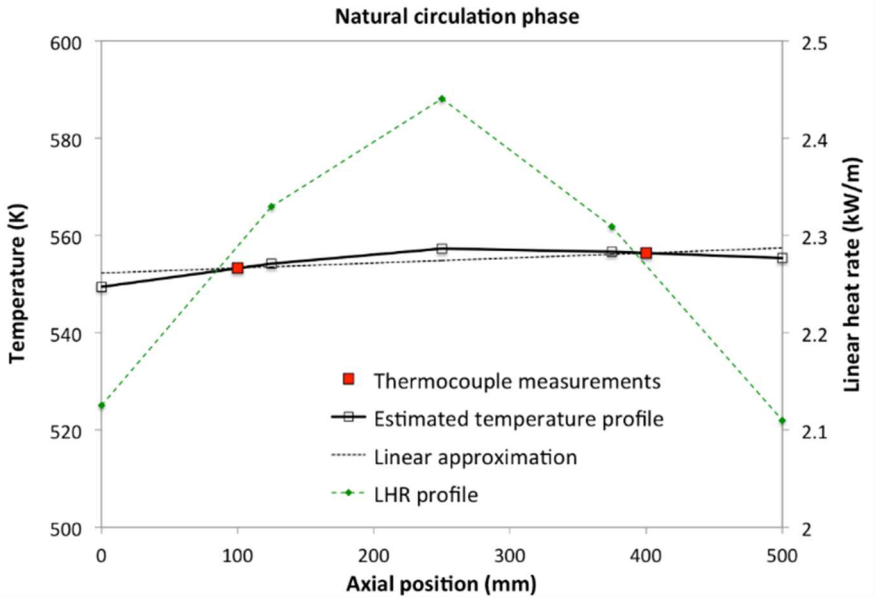

FIG. 14. Estimated axial temperature profile at cladding outer surface at an instant during the natural circulation phase of the IFA-650.2 experiment. The measured temperatures at the thermocouple locations and the linear heat rate (LHR) profile interpolated from Halden data are also shown.

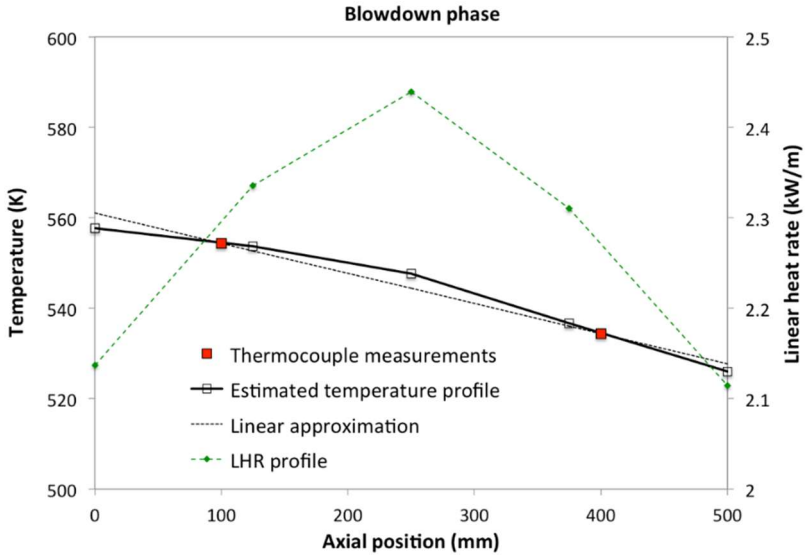

FIG. 15. Estimated axial temperature profile at cladding outer surface at an instant during the blowdown phase of the IFA-650.2 experiment. The measured temperatures at the thermocouple locations and the linear heat rate (LHR) profile interpolated from Halden data are also shown.

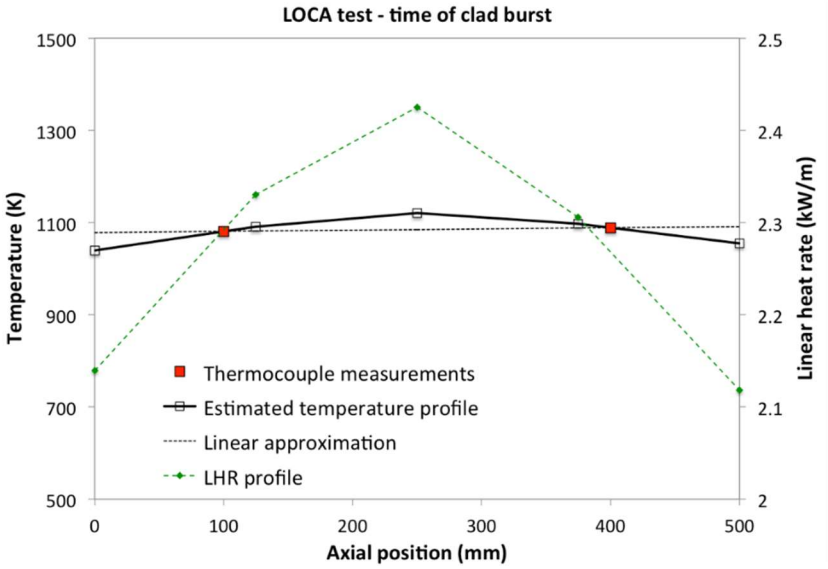

FIG. 16. Estimated axial temperature profile at cladding outer surface at the time of cladding burst for the IFA-650.2 experiment. The measured temperatures at the thermocouple locations and the linear heat rate (LHR) profile interpolated from Halden data are also shown.

3.4.4. Results

In Fig. 3.15, calculated inner pin pressure during the LOCA transient is compared to the on-line experimental measurement, with predicted and experimental time to burst being also illustrated. The comparison points out that both quantities are predicted reasonably well by BISON. Rod pressure is moderately over-predicted during the heat-up phase of the test, which may be ascribed to discrepancies in the calculated plenum temperature and/or evolution of fuel rod inner volume during ballooning.

In this work, cladding temperature boundary conditions are determined based off the measured cladding outer temperatures, as detailed above. Clearly, temperature BCs at the cladding also affect plenum temperature and in turn, plenum pressure. The small “dip” in the calculated pressure shown in Fig. 17 at a time of around 30 s is due to a corresponding dip in

the measured cladding outer temperatures (in particular, from the thermocouples at the upper axial position) from the Halden data. This behavior will require further investigation.

Fission gas release is very low due to the test being performed with a fresh fuel rod and is not expected to affect rod pressure significantly.

Calculated time to burst is ~91.1 s after blowdown, i.e., about 7 s before the experimental time to burst (~98.5 s after blowdown).

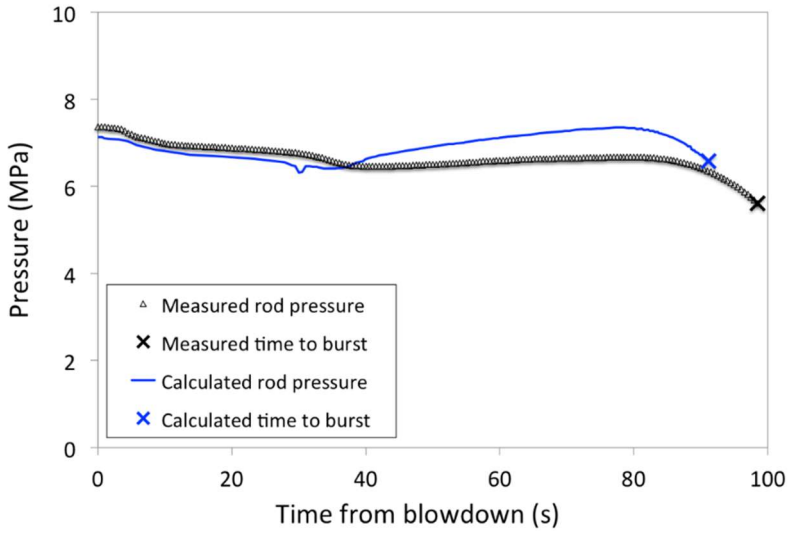

FIG. 17. Comparison between measured and calculated fuel rod inner pressure and time to cladding bust for the Halden IFA-650.2 test. Time zero corresponds to the beginning of the blowdown phase.

3.5. Halden IFA-650.10

The FUMAC priority case Halden IFA-650.10 [43] has been simulated with BISON. The developed BISON computational model included a 2D geometric representation of the IFA-650.10 rod, consistent with the design specifications provided by the Halden Project, power histories and coolant conditions from the beginning of life through the commercial base irradiation and the LOCA test. Furthermore, the simulation was informed with the thermal boundary conditions calculated with the SOCRAT code and provided through FUMAC [44]. We exercised this computational model to obtain a BISON simulation of IFA-650.10 through all the phases of the experiment and up to cladding burst failure.

3.5.1. Description of the test

The tenth Halden LOCA test, i.e., IFA-650.10 [43] was carried out using a segment of a PWR rod that had been irradiated in a commercial PWR (Gravelines 5, 900 MWe, EDF, France) up to a burn-up of 61 MWd/kgU. During the test a low fission power (25 W/cm) was used to achieve the desired conditions for high cladding temperatures, ballooning and oxidation. A heater surrounding the rod and operating at 12 W/cm was used for simulating the heat from adjacent rods. The average cladding temperature increase rate during the heat-up was around 8 K/s. Cladding failure occurred ~249 s after blowdown at a cladding temperature of ~1025 K. The fabrication characteristics of the IFA-650.10 fuel rod are reported in Table 8.

The fuel rod was located in a high-pressure flask in the IFA-650 test rig, which was connected to a high-pressure heavy water loop and a blowdown system. Cladding temperature is influenced by both rod and heater powers. The flask was surrounded by a shroud and was placed inside the Halden reactor. The annulus between the shroud and the flask is filled with moderator (heavy water) at a pressure of 34 bar and a temperature of 235 °C.

TABLE 8. DESIGN DATA OF THE IFA-650.10 FUEL ROD [43, 45]

Fuel material		UO_2
Fuel density	%TD	95.32
^{235}U enrichment	wt%	4.487
Active stack length	mm	440
Pellet OD	mm	8.21*
Pellet ID	mm	0
Pellet length	mm	10
Cladding material		Zy-4
Cladding ID	mm	8.36
Cladding OD	mm	9.50
Diametral gap	μm	150
Free volume	cm^3	17
Fill gas		95% Ar, 5% He
Fill gas pressure	MPa	4.0

* For consistency with the fuel-cladding gap width [43, 45].

One cladding surface thermocouple was located 9.5 cm above the fuel stack bottom, and the other two were attached 8 cm below the top of the stack. The rig instrumentation also included a fuel pressure sensor and thermocouples at the inlet and outlet of the rig to measure the coolant temperatures.

The experimental procedure for the IFA-650.10 test is detailed below [43]. Note that we refer here to the LOCA test performed in the Halden reactor on the pre-irradiated, refabricated PWR fuel rod. In the BISON simulation, we also considered the commercial base irradiation preceding the test.

The general test scheme of IFA-650.10 consisted of the following phases:

— Preparatory phases. The test started with a preparatory irradiation with effective water cooling, consisting of a forced circulation phase followed by a natural circulation phase. The forced circulation phase started with steady state operation at a linear heat generation rate (LHGR) of 120-130 W/cm, with the outer loop connected and the pressure in the loop set to ~70 bar. Then the LHGR was decreased to ~25 W/cm. The power levels were chosen based on the previous test runs and pre-calculations to achieve the target peak cladding temperature (PCT) of 850 C during the heat-up phase of the test. Then the flow regime was switched to natural circulation by disconnecting the rig from the outer loop. Full pressure still existed in the rig. Temperatures in the rig were left to stabilize for three minutes before blowdown.
— Blowdown phase. Valves to the dump tank were opened (blowdown). The channel pressure decreased rapidly to ~4 bar as water flew out of the pressure flask. The rig was practically emptied of water in ~71 s, which corresponds to the end of the blowdown phase (beginning of the dry phase).
— Dry or heat-up phase. Stagnant superheated steam surrounding the test rod provided inadequate cooling and the fuel cladding temperature increased quickly. Much of the heat removal from the test rod is by radiation to the surrounding heater. Ballooning and burst occurred during the heat-up phase and were detected from pressure and temperature signals (burst at ~1025 K, ~249 s after blowdown). The test was ended by a reactor scram 418 s after blowdown.

3.5.2. The BISON computational model for IFA-650.10

A 2D BISON model of the IFA-650.2 fuel rod was constructed. The fuel pellet stack was meshed as a smeared column. The plenum length was adjusted such that the initial rod inner volume was consistent with the rod data [43, 45]. For simplicity, the base irradiation was simulated on the geometry of the refabricated IFA-650.10 rod rather than on the geometry of the original commercial mother rod. Refabrication in BISON was accounted for by specifying the temperature, pressure, and volume of the rod filling gas at refabrication.

The plastic instability criterion for cladding burst failure (Section 2.4) was chosen for this simulation, as it was found to be the most appropriate for the analysis of pre-irradiated fuel rod experiments.

3.5.3. Time-dependent boundary conditions

Simulation of the commercial base irradiation was included in the BISON analysis of IFA-650.10. The power history for the base irradiation was digitized from the chart provided within FUMAC [46] and tabulated for usage as input to BISON. For the coolant conditions during the base irradiation, typical PWR parameters were adopted, i.e., water at a pressure of 15.5 MPa, an inlet temperature of 580 K and an inlet mass flux of 3800 kg/m^2-s was considered. The heat transfer from the cladding to the coolant was modeled using BISON's internal coolant channel model for convective heat transfer under PWR conditions.

The Halden test began with preparatory phases of fuel rod irradiation under coolant conditions of forced circulation, first, and natural circulation, afterwards. Since the SOCRAT calculations do not cover these preparatory phases fully [44], to determine the thermal boundary conditions we adopted a pragmatic approach in which we used the measured temperatures available from the Halden data. In particular, for these initial phases of the experiment, we considered an axially flat temperature profile, with the (time dependent) temperature value being the average of the temperature data measured at two different axial locations. The temperature profile along the plenum length is also considered as flat, with the temperature value being equal to the temperature measured by the plenum thermocouple. This approach guarantees good accuracy as the temperature values are derived directly from the measurements. The downside of this approach is that axial temperature peaking (which is associated with power peaking) is not allowed as an axially flat profile is used. This makes such an approach less suitable for the post-blowdown phases of the test, when cladding ballooning occurs that presents an axial dependence (localized ballooning and burst in correspondence of the hottest axial position). This is a consequence of the axial temperature peaking in the cladding and the strong temperature dependence of Zircaloy thermal creep and the associated cladding ballooning. Hence, more detailed thermal boundary conditions are needed for the post-blowdown phases.

The SOCRAT calculated cladding outer temperatures were used from a time 280 s before the beginning of blowdown onwards (i.e., for the time period where SOCRAT calculated temperatures are available [44]). Fig. 18 shows the comparison of the cladding outer temperatures compared to the Halden measurements at the axial locations where the measurements were performed. Temperatures are the same as shown in [44] and confirm that the SOCRAT data were supplied correctly to BISON.

As for the linear heat generation rate (LHGR) history for the rod, this was obtained from the Halden raw data and tabulated for usage in BISON. As data are provided at different axial locations, axial linear interpolation was used.

Note that the experimental transient continued beyond the time of burst, but we stop the simulation at burst time. After burst, factors such as the geometry of the burst opening, fuel rod depressurization, and possible fuel dispersal all affect fuel rod behavior, and are not accounted

for in BISON. In this work, we rather focus on predicting pre-burst fuel rod behavior (temperatures, ballooning) as well as the time to burst.

3.5.4. Results

Figure 19 shows contour plots of calculated fuel temperatures in the fuel rod at the time of predicted cladding burst failure. Besides the full rod, separate plots for the fuel and cladding are shown with specific color scales. The cladding reaches very high temperatures compared to normal PWR operation values of around 600 K because of the degraded heat transfer to the coolant during a LOCA that ultimately causes cladding heat-up and ballooning due to thermal creep.

Figure 20 shows a contour plot of calculated hoop strain at the time of predicted burst. The Fig. demonstrates how cladding ballooning, with large cladding strain and a maximum localized near the axial mid-plane of the fuel stack, is reproduced by BISON.

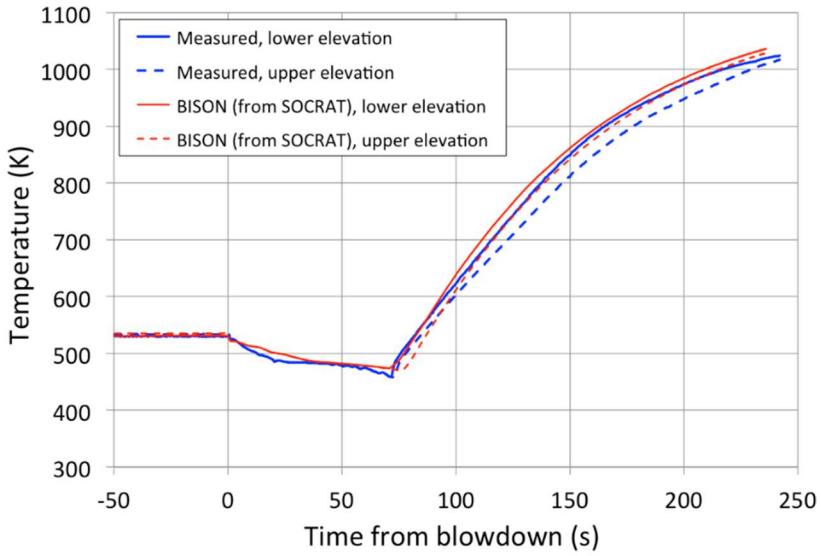

FIG. 18. Measured cladding outer temperatures at two different axial locations in the IFA-650.10 rod during the post-blowdown phases of the test and corresponding temperatures in BISON (prescribed, from the SOCRAT calculations [44]).

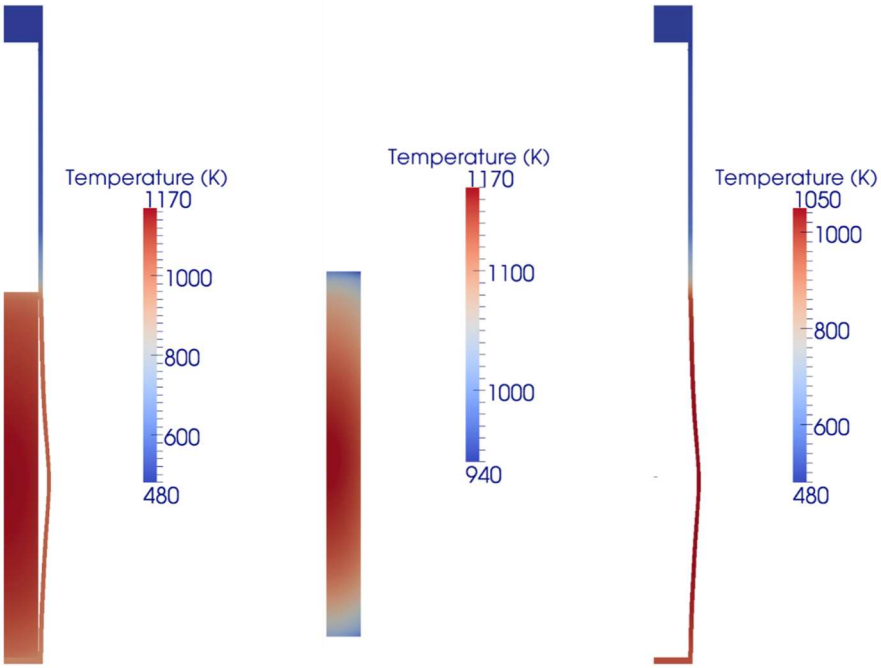

FIG. 19. Contour plots of calculated temperature in the IFA-650.10 fuel rod at the time of cladding burst failure. Full rod (left), fuel only (center) and cladding only (right). The view is magnified 10 times in the radial direction for improved visualization.

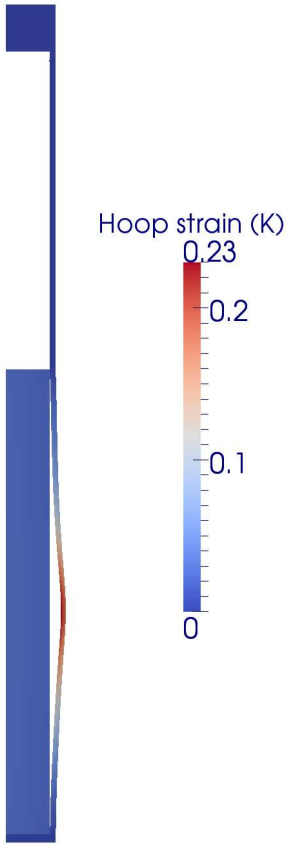

FIG. 20. Contour plot of calculated hoop strain in the IFA-650.10 fuel rod at the time of cladding burst failure. Cladding ballooning as reproduced in the simulation is evident. The view is magnified 10 times in the radial direction for improved visualization.

Figure 21 shows the axial profile of the cladding diameter at the end of the simulation compared with the experimental data from post-irradiation examinations. BISON is able to predict cladding ballooning with a physically meaningful profile and with the position of maximum strain being reasonably close to the experimental observation. However, an over-prediction of cladding outward strain along the rod is observed.

As already noted in Section 3.1, the accurate prediction of maximum cladding strains reached during LOCA tests is extremely difficult. In particular, very high strain rates are attained as cladding burst is approached, which implies that the maximum strain reached in the calculation is very sensitive to the specific criterion adopted to determine the time of rod burst (i.e., the time at which the simulation ends and strain is considered), since small differences in the final time may correspond to large differences in the maximum strain. In order to potentially improve cladding strain predictions with BISON, further investigation and sensitivity analysis of the dependence of calculated strains upon the choice of the burst criterion, as well as further developments of the cladding creep model (e.g., considering anisotropic creep), are of interest in perspective.

In Fig. 22, the calculated time evolution of rod inner pressure during the post-blowdown phases of the IFA-650.10 experiment is compared to the experimental (pressure transducer) data from Halden. BISON reproduces the experimental behavior with a good accuracy. Deviations of the calculation from the experimental data may be partly due to a discrepancy between the calculated and actual plenum temperature (which together with rod inner volume and gas content determines the plenum pressure) in consequence of the uncertainties in the temperature calculation and boundary conditions, and the assumptions in the plenum temperature calculation itself.[14]

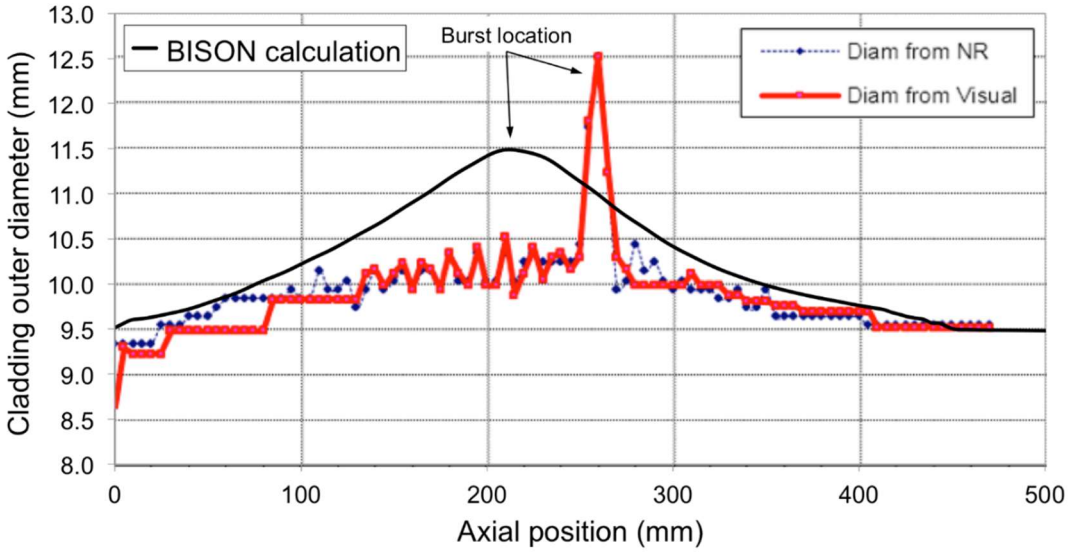

FIG. 21. Calculated cladding outer diameter profile for IFA-650.10 at the end of the simulation compared to the Halden experimental data.

Also, the calculated pressure as burst time is approached decreases more rapidly than experimentally observed. This is expected to be a consequence of calculated cladding outward deformation (ballooning) and the associated increase in rod inner volume being more rapid than

[14] Plenum temperature in the BISON model of IFA-650.10 is calculated as the average cladding inner temperature, with only the plenum height considered. Outer fuel temperature, and cladding inner temperature below the plenum (i.e., along the gap) are neglected. This assumption is deemed reasonable for an experiment such as IFA-650.10 where the plenum length and volume are high compared to standard plenum/fuel column ratios [43], so that the gas temperature is predominantly determined by the inner cladding temperature along the plenum.

occurred experimentally. This is confirmed by the calculated cladding diameter profile at the end of the simulation shown in Fig. 21. An improved treatment of cladding creep that allows for anisotropic behavior, and a refined calculation of the plenum temperature, may improve our results.

Cladding burst is predicted to occur ~236 s after blowdown, i.e., ~13 s before time observed experimentally (249 s after blowdown). Furthermore, BISON's prediction is conservative as the cladding is predicted to fail before it was experimentally observed.

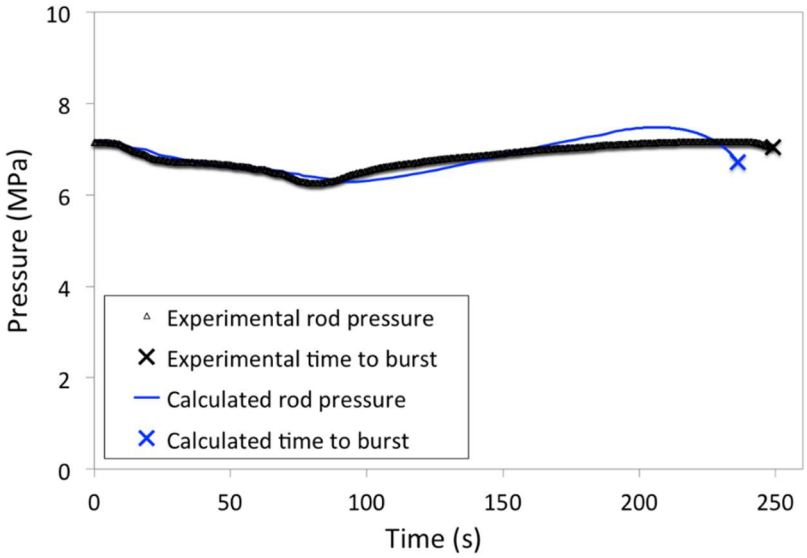

FIG. 22. Rod inner pressure evolution during the post-blowdown phase of IFA-650.10 and time to cladding burst. BISON results are compared to the Halden experimental data.

4. CONCLUSIONS

In this report we summarized the contribution of Idaho National laboratory (INL) to the FUMAC project. In line with the original research agreement, work at INL has focused on both:

- Developments of INL's fuel performance code BISON for the analysis of LOCAs; and
- Simulation of selected FUMAC priority cases.

As for code developments, BISON extensions relevant to FUMAC included the incorporation into the code of the key material and behavior models required to address transient high-temperature phenomena occurring during LOCAs. In particular, models were implemented in BISON for high temperature cladding oxidation, Zircaloy solid-solid phase transformation, Zircaloy high temperature creep, cladding burst failure and axial fuel relocation.

With reference to the simulation of the FUMAC cases with BISON, as originally agreed several cases were considered, including both separate effects and integral fuel rod tests. In particular, BISON simulations were performed for the FUMAC cases:

- MTA EK tests PUZRY;
- QUENCH L1 rods 4 and 7;
- Halden IFA-650.2; and
- Halden IFA-650.10.

In addition, simulations of the ballooning tests REBEKA were performed and are included in this report, in view of the potential interest to the FUMAC project. This additional work included 3D simulations accounting for azimuthal temperature variations.

All of the 31 MTA EK separate effects ballooning and burst tests PUZRY were simulated with BISON. Results were reasonable in terms of cladding burst times and pressures. It was noted that discrepancies between calculations and experimental data may be partly due to anisotropic creep behavior, which is not considered in the BISON model at this time. Predictions of maximum cladding strain were less satisfactory, indicating an area of potential future improvement. It was emphasized that the accurate prediction of cladding strains reached during LOCA tests is extremely difficult, because very high strain rates are attained as cladding burst is approached, making the maximum strain reached during the calculation very sensitive to the specific burst criterion adopted and the associated uncertainties.

Additional separate effects simulations were performed for the REBEKA tests, which also pointed out a reasonable accuracy of BISON burst predictions (burst temperatures). Moreover, using BISON's 3D capability, one of the REBEKA cases was simulated in 3D, to investigate cladding response in presence of azimuthal temperature variations. Results indicated 3D effects are potentially important to accurate fuel rod analysis during LOCAs.

BISON simulations of the QUENCH L1 rods 4 and 7 confirmed a good predictive capability of the code for cladding burst temperatures and pressures, and less satisfactory predictions of cladding strains. In particular, maximum cladding hoop strains were under-predicted. As noted above, this is expected to be, to a significant extent, related to the high sensitivity of calculated maximum strains to the choice of and uncertainties in the cladding burst criterion.

Simulation of the Halden test IFA-650.2 involved determination of the thermal boundary conditions at the cladding outer wall following an approximate calculation procedure based on the Halden thermocouple data. Results were compared to experimental data of rod inner pressure evolution during the test and time to cladding burst. Both quantities were reasonably well predicted by BISON. Rod pressure was moderately over-predicted during the heat-up phase of the test, which may be ascribed to discrepancies in the calculated plenum temperature and/or evolution of fuel rod inner volume during ballooning. Calculated time to burst was ~7 s before the experimental one.

Finally, we presented the BISON simulation of the Halden IFA-650.10 case. The calculation included all of the phases of the experiment from the beginning of life through the commercial base irradiation and the LOCA test. The analysis of the LOCA test was informed with the thermal boundary conditions calculated with the SOCRAT code and provided through FUMAC. The time to cladding burst failure was predicted with a good accuracy, the calculated time being within 13 s of the experimental one. Furthermore, the calculation was conservative, the predicted failure time being slightly earlier than experimentally observed. Also, a comparison of the cladding diameter profile at the end of the test was shown, pointing out significant discrepancies between experimental and calculated profiles. However, cladding ballooning was reproduced, with a physically meaningful profile. Finally, BISON was able to reproduce the experimental evolution of rod inner pressure during the test with a good accuracy.

The BISON results are made available to the FUMAC project as a contribution to the FUMAC benchmark exercise.

In perspective, further developments of BISON for LOCA analysis are of interest in order to enhance the code's predictive capability for LOCAs. In particular, further investigation and sensitivity analysis of the dependence of calculated maximum cladding strains upon the choice of the burst criterion is deemed useful. Also, improvements in predictions of cladding strain as well as cladding burst may be achieved by considering the anisotropic creep behavior of alpha-Zr under LOCA conditions. This will require modifying the mechanics models in the code to consider anisotropic creep strain. Another potential source of discrepancy is the 2D representation of fuel rod behavior that involves inherently 3D effects such as localized ballooning and burst associated with azimuthal temperature variations. As demonstrated by

initial 3D simulations with BISON, 3D effects are important for LOCA analysis. Additional simulations in 3D with BISON to further investigate such effects are of interest in perspective.

Currently, BISON does not consider the thinning of the cladding metal wall during oxidation, which can be of importance to cladding mechanical behavior at the high oxidation rates that can be attained during LOCAs. This could be considered in a finite element code using the Extended Finite Element Method (X-FEM) to simulate a moving material interface (metal, oxide). Moreover, internal cladding oxidation is not considered at this time and is of interest for future developments. Also, a model for hydrogen production and uptake during oxidation is available in BISON and has been applied to fuel rod lifecycle simulations including spent fuel storage [47]. However, this model has not been applied yet to LOCA simulations with BISON, which represents a potential future application. Finally, coupling to thermal-hydraulics system codes developed at INL is of potential interest for an improved multiphysics coupling that could result in improved boundary conditions for the BISON fuel rod calculations under accident conditions.

ACKNOWLEDGMENTS

This work was funded by the U.S. DOE Nuclear Energy Advanced Modeling and Simulation (NEAMS) program, the U.S. DOE Consortium for Advanced Simulation of Light Water Reactors (CASL) project, and the INL Laboratory Directed Research and Development (LDRD) program.

The submitted manuscript has been authored by a contractor of the U.S. Government under Contract DE-AC07-05ID14517. Accordingly, the U.S. Government retains a non-exclusive, royalty free license to publish or reproduce the published form of this contribution, or allow others to do so, for U.S. Government purposes.

The work fits in the framework of the Coordinated Research Project (CRP) on Analysis of Fuel Modeling under Accident Conditions (FUMAC) of the IAEA and benefited from the discussion within the CRP. Travel funding from IAEA is also acknowledged. INL participated in FUMAC under the IAEA Research Agreement No: 18464/R0.

Katalin Kulacsy (Hungarian Academy of Sciences) and Juri Stuckert (KIT) are graciously acknowledged for the discussions and information about the PUZRY and QUENCH experiments.

REFERENCES

[1] WILLIAMSON, R.L., HALES, J.D., NOVASCONE, S. R., TONKS, M.R., GASTON, D.R., PERMANN, C.J., ANDRS, D., MARTINEAU. R.C., Multidimensional multiphysics simulation of nuclear fuel behavior. J. Nucl. Mater., 423:149–163, (2012).

[2] WILLIAMSON, R.L., GAMBLE, K.A., PEREZ, D.M., NOVASCONE, S.R., PASTORE, G., GARDNER, R.J., HALES, J.D., LIU, W., MAI. A., Validating the BISON fuel performance code to integral LWR experiments. Nucl. Eng. Des., 301:232–244, (2016).

[3] PASTORE, G., NOVASCONE, S.R., WILLIAMSON, R.L., HALES, J.D., SPENCER, B.W., STAFFORD. D.S., Modelling of fuel behaviour during loss-of-coolant accidents using the BISON code. In Proc. of the LWR Fuel Performance Meeting, Zurich, Switzerland (2015).

[4] PASTORE, G., WILLIAMSON, R.L., NOVASCONE, S.R., SPENCER, B.W., HALES, J.D., Modelling of LOCA tests with the BISON fuel performance code. In Enlarged Halden Programme Group Meeting, Fornebu, Norway (2016).

[5] WILLIAMSON R.L., FOLSOM, C.P., PASTORE, G., VEEARAGHAVAN, S., Reactivity insertion accident (RIA) capability status in the BISON fuel performance code. Technical Report CASL-X-2016-1104-000, (2016).
[6] PASTORE, G., FOLSOM, C.P., WILLIAMSON, R.L., HALES, J.D., LUZZI, L., PIZZOCRI, D., BARANI, T., Modelling fission gas behaviour with the BISON fuel performance code. In Enlarged Halden Programme Group Meeting, Lillehammer, Norway (2017).
[7] US DOE Participation in the FUMAC Coordinated Research Project on Fuel Performance Modeling. Proposal for research agreement between Battelle Energy Alliance and International Atomic Energy Agency for the FUMAC Coordinated Research Project (2014).
[8] PASTORE, G., PIZZOCRI, D. NOVASCONE, S.R., PEREZ, D.M., SPENCER, B.W., WILLIAMSON, R.L., VAN UFFELEN, P., LUZZI, L., Modelling of transient fission gas behaviour in oxide fuel and application to the BISON code. In: Enlarged Halden Programme Group Meeting, Røros, Norway, September 7–12, 2014.
[9] BARANI, T., BRUSCHI, E., PIZZOCRI, D., PASTORE, G., VAN UFFELEN, P., WILLIAMSON, R.L., LUZZI, L., Analysis of transient fission gas behaviour in oxide fuel using BISON and TRANSURANUS. J. Nucl. Mater., 486 (2017) 96–110.
[10] SCHANZ, G., Recommendations and supporting information on the choice of zirconium oxidation models in severe accident codes. Technical Report FZKA 6827, SAM-COLOSS-P043, Forschungszentrum Karlsruhe, Germany, 2003.
[11] LEISTIKOW, S., SCHANZ, G., BERG H.V., ALY, A.E., Comprehensive presentation of extended Zircaloy-4/steam oxidation results 600-1600 C. In CSNI/IAEA specialists meeting on water reactor fuel safety and fission product release in off-normal and accident conditions, Risø National Laboratory, Denmark (1983).
[12] CATHCART, J.V., PAWEL, R.E., MCKEE, R.A., DRUSCHEL, R.E., YUREK, G.J., CAMPBELL, J.J., JURY, S.H., Zirconium metal-water oxidation kinetics, IV. Reaction rate studies. Technical Report ORNL/NUREG-17, Oak Ridge National Laboratory (1977).
[13] PRATER, J.T., COURTRIGHT, E.L., Zircaloy-4 oxidation at 1300 to 2400 C. Technical Report NUREG/CR-4889, PNL-6166, Pacific Northwest National Laboratory, 1987.
[14] MASSIH. A.R., Transformation kinetics of zirconium alloys under non-isothermal conditions. J. Nucl. Mater., 384:330–335, (2009).
[15] MASSIH A.R., JERNKVIST, L.O., Transformation kinetics of alloys under non-isothermal conditions. Modelling and Simulation in Materials Science and Engineering, 17:055002 (2009) 15.
[16] MASSIH, A.R., Evaluation of loss-of-coolant accident simulation tests with the fuel rod analysis code FRAPTRAN-1.4. Technical Report TR11-008V1, Quantum Technologies AB, (2011).
[17] VAN UFFELEN, P., GYŐRI, C., SCHUBERT, A., VAN DE LAAR, J., HOÓZER, Z., SPYKMAN, G., Extending the application range of a fuel performance code from normal operating to design basis accident conditions. J. Nucl. Mater., 383:137–143, (2008).
[18] NEITZEL, H. J., ROSINGER, H., The development of a burst criterion for zircaloy fuel cladding under LOCA conditions. Technical Report KfK 4343, Kernforschungszentrum Karlsruhe, Germany, (1980).
[19] ERBACHER, F. J., NEITZEL, H. J., ROSINGER, H., SCHMIDT, H., WIEHR, K., Burst criterion of Zircaloy fuel claddings in a loss-of-coolant accident. In Zirconium in the Nuclear Industry, Fifth Conference, ASTM STP 754, D.G. Franklin Ed., American Society for Testing and Materials (1982) 271–283.

[20] MARKIEWICZ M. E., ERBACHER F.J., Experiments on ballooning in pressurized and transiently heated Zircaloy-4 tubes. Technical Report KfK 4343, Kernforschungszentrum Karlsruhe, Germany (1988).
[21] Di Marcello, V., Schubert, A., Van de Laar, J., Van Uffelen, P., The TRANSURANUS mechanical model for large strain analysis. Nucl. Eng. Des., 276: (2014).
[22] PASTORE, G., LUZZI, L., DI MARCELLO, V., VAN UFFELEN P., Physics-based modelling of fission gas swelling and release in UO_2 applied to integral fuel rod analysis. Nucl. Eng. Des., 256: (2013) 75–86.
[23] PASTORE, G., SWILER, L.P., HALES, J.D., NOVASCONE, S.R., PEREZ, D.M., SPENCER, B.W., LUZZI, L., VAN UFFELEN, P., WILLIAMSON, R.L., Uncertainty and sensitivity analysis of fission gas behavior in engineering-scale fuel modeling. J. Nucl. Mater., 465 (2015) 398–408.
[24] CARROLL, R. M., MORGAN, J. G., PEREZ, R. B., SISMAN, O., Fission density, burnup, and temperature effects on fission-gas release from UO_2. Nuclear Science and Engineering, 38 (1969) 143–155.
[25] HASTINGS, I. J., SMITH, A. D., FEHRENBACH, P. J., CARTER, T. J., Fission gas release from power-ramped UO_2 fuel. J. Nucl. Mater., 139 (1986) 106–112.
[26] WALKER, C. T., KNAPPIK, P., MOGENSEN, M., Concerning the development of grain face bubbles and fission gas release in UO_2 fuel. J. Nucl. Mater., 161: (1988) 10–23.
[27] UNE, K., KASHIBE, S., Fission gas release during post irradiation annealing of BWR fuels. J. Nucl. Sci. Technol., 27 (1990) 1002–1016.
[28] SCDAP/RELAP5-3D Code Manual. MATPRO a library of materials properties for light-water-reactor accident analysis. Technical Report INEEL/EXT-02-00589, Idaho National Engineering and Environmental Laboratory, Vol. 4. (2003).
[29] JERNKVIST, L. O., MASSIH, A., Model for axial relocation of fragmented and pulverized fuel pellets in distending fuel rods and its effects on fuel rod heat load. Technical Report SSM-2015, 37, (2015).
[30] PASTORE, G., WILLIAMSON, R. L., HALES. J. D., Status Report on INL Contribution to FUMAC with the BISON Code. Presentation given at the Seconds Research Coordination Meeting of the FUMAC Project, Vienna, Austria, May 30 – June 2, 2016. Available at https://nucleus.iaea.org/sites/nefw-projects/fumaccrp/SitePages/ Home.aspx.
[31] WILLIAMSON, R. L., PASTORE, G., HALES J. D., Status Report on US DOE/INL Participation in the Coordinated Research Project FUMAC. Technical report, May 2016. Submitted in support of the Second Research Coordination Meeting of the FUMAC Project.
[32] HARDY D.G., High Temperature Expansion and Rupture Behaviour of Zircaloy Tubing. In CSNI Proceeding of the Specialist Meeting on Safety of Water Reactor Fuel Elements, Saclay, France (1973).
[33] WILSON C. L., et al. LOCA simulation in NRU program: Data report for the fourth materials experiment (MT-4). Technical Report NUREG/CR-3272 (PNL-4669), Pacific Northwest Laboratory (1983).
[34] WILSON C. L., et al. Large-break LOCA in-reactor fuel bundle materials test MT-6A. Technical Report PNL-8829, Pacific Northwest Laboratory, September 1993.
[35] WILLIAMSON, R. L., Pastore, G., Gamble, K. A., Gardner, R. J., Tompkins, J., Liu, W., Development of a LOCA Experimental Benchmark for BISON. Technical Report CASL-U-2017-1422-000, Consortium for Advanced Simulation of LWRs (2017).

[36] HÓZER, Z., GYŐRI, C., HORVÁTH M.,, NAGY, I., MARÓTI, L., MATUS, L., WINDBERG, P., FRECSKA J., Ballooning Experiments with VVER Cladding. Nuclear Technology, 152:273–285 (2005).
[37] PEREZ-FERÓ, E., GYŐRI, C., MATUS, L., VASÁROS, L., HÓZER, Z., WINDBERG, P., MARÓTI, L., HORVÁTH, M., NAGY, I., PINTÉR-CSORDÁS, A., NOVOTNY T., Experimental database of E110 claddings exposed to accident conditions. J. Nucl. Mater., 397: (2010) 48–54.
[38] KULACSY. K., Communication within the FUMAC Project, (2015).
[39] ERBACHER, F.J., NEITZEL, H.J., WIEHR, K., Technical Report KfK 4781, Kernforschungszentrum Karlsruhe, Germany, (1990).
[40] STUCKERT, J., GROBE, M., ROSSGER, C., STEINBRUCK, M., WALTER, M., Results of the LOCA reference bundle test QUENCH-L1 with Zircaloy-4 cladding. Technical Report KIT-SR 7651, Karlsruhe Institute for Technology, Germany (2015).
[41] EK, M., LOCA Testing at Halden; The Second Experiment IFA-650.2. Technical Report HWR-813, OECD Halden Reactor Project, (2005).
[42] FUEL MODELLING IN ACCIDENT CONDITIONS (FUMAC) CRP, https://nucleus.iaea.org/sites/nefw-projects/fumaccrp/SitePages/Home.aspx.
[43] LAVOIL, A., LOCA Testing at Halden; The Tenth Experiment IFA-650.10. Technical Report HWR-974, OECD Halden Reactor Project (2010).
[44] Short Information on the Results of IFA-650.10 and IFA-650.11 Calculations with SOCRAT code. Technical note, version 1. Technical report, 2016. Released to the FUMAC project. Available at https://nucleus.iaea.org/sites/nefw-projects/ fumaccrp/SitePages/Home.aspx.
[45] LAVOIL, A., LOCA Experiments IFA-650.10. Technical Report EP-1650.10, OECD Halden Reactor Project, 2010.
[46] Extract from Technical Report HWR-664, OECD Halden Reactor Project. Fuel modelling in accident conditions (FUMAC) CRP, At https://nucleus.iaea.org/sites/nefw-projects/fumaccrp/SitePages/Home.aspx
[47] STAFFORD. D.S., Multidimensional simulations of hydrides during fuel rod lifecycle. J. Nucl. Mater., 466: (2015) 362–372.